TR92 - 46

PETROGENESIS OF THE UPPER CRITICAL ZONE IN THE WESTERN BUSHVELD COMPLEX WITH EMPHASIS ON THE UG1 FOOTWALL AND BASTARD UNITS.

THESIS

Submitted in fulfilment of the
requirements for the Degree of
DOCTOR OF PHILOSOPHY

by

WILLIAM JOHAN DE KLERK
B.Sc. (Hons), M.Sc. (Rhodes)

September, 1991

PREFACE

I first developed an interest in the layered rocks of the Bushveld Complex during my first appointment, after graduation, as a mine geologist at the Rustenburg Platinum Mines (RPM) in the western sector of the Bushveld Complex at the beginning of 1976. Initially I was based at Rustenburg and later at Union Section, spanning a period of five years. This mining experience was followed by a transfer to the company's (JCI) Fundamental Research Unit (Bushveld Section). It was at this time that my data, collated while on the mines, was written up on a part-time basis, and submitted for an MSc degree (1982). Most of the descriptive geology relating to this study was subsequently published in Viljoen et al. (1986a). Here data on the geochemistry and cryptic variations of a sequence through the Upper Critical Zone in the central part of RPM Union Section was compiled and a component of this work is embodied in Eales et al. (1986). Although my career path moved away from the Bushveld Complex for some time, the fascination of these enigmatic layered magmatic rocks still remained with me and, with a move to the Albany Museum in Grahamstown (1985), I was once again able to pursue my research on the Bushveld Complex at Rhodes University under the guidance of Prof. H.V. Eales. Data and concepts in this thesis build on the studies mentioned above as well as on other published works: Scoon and de Klerk (1987), de Klerk (1989), Eales et al. (1988) and Eales et al. (1990a and b).

ABSTRACT

This study is an account of the stratigraphic sequence, the petrography, mineralogy (microprobe investigations of orthopyroxene, clinopyroxene, olivine and plagioclase feldspar), and whole-rock major- and trace-element geochemistry of the silicate cumulates of the Upper Critical Zone in the western Bushveld Complex. Two parts of the study - an investigation of a 350m column incorporating the MG3 and UG1 Footwall Units, and a comparison of two additional Upper Critical Zone profiles with a previously compiled profile between the UG1 and Bastard Units - are focused on RPM Union Section in the northwestern sector of the Complex. The third part is a detailed vertical and lateral investigation of the Bastard Unit at the top of the Critical Zone, which draws on sampling and data compilation from seventeen profiles in the western limb of the Complex.

The MG3 Unit (45m) is made up of a lower chromitite layer overlain by a norite-pyroxenite-anorthosite sequence while the UG1FW Unit (295m) is composed of a related series of lower chromitite layers (MG4) overlain by a pyroxenite-norite-anorthosite sequence capped by the UG1 chromitite layer. These mafic cumulates display a distinctive pattern of oscillating cryptic variation in whole-rock Mg/(Mg+Fe), FeO/TiO_2, Cr/Co and Ni/V ratios through the sequence. Sympathetic oscillations are recorded for compositions of orthopyroxene and plagioclase feldspar and eight sub-cycles are recognised through the UG1FW Unit. The entire sequence is characterised by the presence of small, spheroidal, embayed and irregularly shaped plagioclase grains which are poikilitically enclosed in cumulus orthopyroxene grains of both pyroxenites and norites. This texture is indicative of partial resorption of pre-existing feldspar primocrysts within the melt prior to their being incorporated into the host orthopyroxene grains. Textural, geochemical and isotopic data suggest that this sequence was built up by periodic additions of fresh, relatively primitive liquid into fractionated resident liquid, and subsequent mixing within the magma chamber.

The Bastard Unit sequence, described in Chapter 4, is the last and most complete cyclic unit (c. 60m) of the Critical Zone, and its upper contact defines the boundary between the Critical and Main Zones of the Complex. This Unit can conveniently be sub-divided into a lower part, where orthopyroxene occurs as a cumulus phase, and the upper part which is composed entirely of anorthosite (Giant Mottled Anorthosite). The basal part of the Unit ($\leq$ 18m) comprises a thin chromitite layer ($<$ 0.5cm) overlain by a pyroxenite-melanorite-norite-leuconorite sequence. The basal pyroxenite is orthocumulate in character and rapidly gives way to

norites and leuconorites. A distinct threefold subdivision emerges within the Giant Mottled Anorthosite which is predominantly an adcumulate which becomes orthocumulate in character at its top. Apart from minor deviations in thicknesses these lithologies are recorded over the entire strike-length covered in this study. Profiles of cryptic variation are compiled for orthopyroxene, plagioclase and whole-rock data and show that the Bastard Unit displays a characteristic pattern which is maintained throughout the western Bushveld Complex. A minor yet distinctive reversal in cryptic variation is revealed at a level which is stratigraphically variable within the lower Giant Mottled Anorthosite, and results in a double cuspate pattern. A remarkable feature of the basal Bastard pyroxenites is that although the modal proportion of mafic to felsic constituents varies systematically away from the northwestern sector, the Mg/(Mg+Fe) ratio of orthopyroxenes remains constant at 0.804 over a lateral strike distance of 171km. Within the upper part of the Unit the orthopyroxene is markedly Fe-rich and it is here that inverted primary pigeonite appears for the first time as a cumulus phase. In addition, K-feldspar, oscillatory zoned plagioclase grains and high levels of incompatible trace elements are noted at this level.

On the basis of the data presented it is concluded that the Bastard Unit represents the crystallisation of a final, relatively large influx of hotter primitive liquid, with upper Critical Zone affinities, and subsequent mixing with a column of cooler (less dense) supernatant liquid which had in part hybridized with the overlying Main Zone magma. It is hypothesised that this new liquid was emplaced as a basal flow beneath supernatant liquid and that it initiated the deposition of mafic cumulates at its base. The supernatant liquid is interpreted as representing the fractionated residuum produced by crystallisation of earlier cyclic units, with plagioclase on the liquidus, and that it contained an abundance of small plagioclase primocrysts in suspension.

Development of the Unit can be viewed as a two-stage process. In the lower half of the unit, chemical and physical parameters typical of the new magma dominated the crystallisation process, and resulted in cumulates very similar to other relatively complete Upper Critical Zone units. In the upper, leucocratic sequence, above a minor reversal, crystallisation was from a liquid which was the product of mixing of a minor pulse of primitive liquid with the reservoir of hybridized supernatant liquid. Although the Bastard Unit is not continuous around the entire Western limb of the Complex, it is concluded that it developed in a single, or connected, magma chamber and that its irruptive feeder zone was located in the proximal northwestern facies of the Complex.

ACKNOWLEDGEMENTS

I would like to express my sincere thanks and appreciation

- to Professor Hugh Eales for his continued encouragement, assistance and guidance throughout this study and for criticism offered on earlier drafts of this thesis. From the date of my first employment on the platinum mines in 1976, Professor Eales took an active interest in my work on the Bushveld Complex and I would like to thank him for the many stimulating discussions and field trips that we have shared - long may they continue.
- to my wife Vivian, for cheerfully doing time on a mine at the start of our marriage, and for her unwavering encouragement and patience during this period of research. In particular I appreciate the many stoic hours of proofreading she put in towards the end of this study.
- to my patient and understanding children, Jennifer, Andrew and Christopher, who have, inevitably, had to make sacrifices in order to enable me to complete this overdue magnum opus.
- to the Management and Board of Trustees of the Albany Museum for allowing me to pursue my research on a part-time basis, and for granting me an extended period of study leave to write up this thesis. I would like to extend a special word of thanks to my good friends Brian Wilmot and Wouter Holleman, Director and Deputy Director respectively, who spurred me on.
- to the members of staff of the Geology Department at Rhodes University who assisted me in various ways and who were alwaysamenable to having their "ears bent" - especially Professors Roger Jacob, Goonie Marsh and Norton Hiller and Dr Alan Butcher. A special word of thanks to Goonie for his guidance in XRF analytical techniques. My thanks also go to the technical staff of the Geology Department, especially Mr Rob Skae for his patience and guidance during my stints on the microprobe and John Hepple, Vumile (Bennett) Bongwana and Mlungisi (Wilberforce) Hashe for their contribution in the cutting of microprobe and thin sections.

- to my fellow Bushveld researchers Bernd Teigler, Mike Botha, Roger Scoon, Matthew Field, Wolfgang Maier and Sue Haikney who all provided stimulating and friendly discussion.
- to Piet Coetzer and John Barry (on the mines) and Chris Lee, Morris Viljoen, Richard Viljoen, and Ronny Hieber (at the JCI - FRU) for all they did in contributing to my understanding of the Bushveld Complex while in the employ of the JCI Platinum Division over a period of 7½ years.

I would also like to thank the management of the mining companies who provided access to underground workings and borehole cores: Johannesburg Consolidated Investment Co. (JCI), Impala Platinum Mines (Genmin) and Crocodile River Platinum Mine (previously Lefkochrysos now controlled by Rand Mines). Without the logistical and indirect financial support of these mining companies this type of study would be almost impossible to accomplish in the western Bushveld Complex.

The financial assistance of the CSIR during the execution of the National Geoscience Programme (Sub-programme: Bushveld Complex) is gratefully acknowledged. I am also indebted to the Commission for Administration for having granted me a one-year Public Service Bursary.

DECLARATION

All work in this thesis is the original work of the author, except where specific acknowledgement is made to the work of others.

Signed:

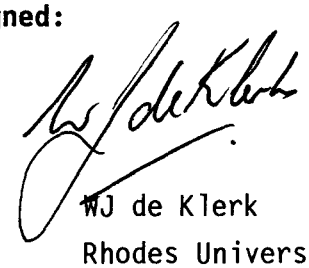

WJ de Klerk
Rhodes University
Grahamstown
September, 1991.

CONTENTS

CHAPTER 3 : THE INTERVAL BETWEEN THE UG1 CHROMITITE AND THE BASTARD UNIT AS SEEN IN TWO PROFILES AT RPM UNION SECTION.

CHAPTER 4 : THE BASTARD UNIT ALONG 171 KM OF STRIKE IN THE WESTERN BUSHVELD COMPLEX.

LIST OF FIGURES

LIST OF TABLES

LIST OF PLATES

CHAPTER 1

INTRODUCTION AND OVERVIEW

"The wonders of nature and the frailties of the human mind are perhaps nowhere more strikingly juxtaposed than in the study of layered intrusions." Morse (1988a)

1.1 General

Hypotheses regarding magmatic processes are varied and controversial and a brief review of thinking in this field is in order as a preliminary to a more detailed discussion on specifics of the Critical Zone in the Bushveld Complex.

The pioneering work dealing with layered intrusions by Wager and Deer (1939), Jackson (1961), Wager and Brown (1968) and others, interpreted these rocks as being the result of crystal settling within a magma chamber. Workers in the 1970's, notably McBirney and Noyes (1979), questioned this model and argued that crystal settling would be unlikely, especially for plagioclase, because the nucleating crystals would be small and unable to overcome the yield strength of the liquid. Calculations by Bottinga and Weill (1970) indicated that crystallising plagioclase in the Skaergaard intrusion would be less dense than its parental liquid during the formation of the Layered Series, and the crystals were thus more likely to float.

The view that all crystal growth in magmatic systems took place in situ was in vogue for a time but a number of geologists (Campbell, 1978; Irvine, 1980a) recognised that certain features (and textures) could not easily be explained by in situ crystal growth and had to be explained by other mechanisms. However, experimental work on crystal settling and in situ growth by Martin (1990) has now convincingly demonstrated that both mechanisms are valid processes during crystallisation. Irvine (1978 and 1980b) also recognised the importance of postcumulus metasomatic processes that can take place in a crystallising sequence and introduced the concept of infiltration metasomatism. In his study of the Muskox Intrusion, Irvine (1980b) convincingly showed with that the primary composition of cumulus phases becomes reset by reaction with intercumulus

liquids squeezed out from below by the compacting crystalline sequence. This work emphasised that the features now seen in layered rocks (cryptic variation, recrystallisation, reaction etc.) may frequently obscure the original features of slowly cooled layered intrusions.

The igneous layering of the Bushveld Complex and other intrusions is now widely accepted as being largely the result of the combined processes of *in situ* crystal growth, limited crystal settling, deposition by density currents, soft-sediment deformation and post-cumulus processes which all contribute to what we now see in such layered rocks.

Within the last decade two stimulating concepts have contributed to a new approach in the understanding of mafic layered complexes. The first is the application of fluid dynamic models to magma chambers (Huppert and Sparks, 1980; Rice, 1981; Irvine et al. 1983; Campbell and Turner, 1986) and the second is the concept of mixing of magmas of different compositions (Irvine, 1977; Irvine et al., 1983; Campbell, 1986; Naldrett et al., 1987). Persuasive evidence to support these concepts has been accumulated for magmatic bodies around the globe and in many studies specific to the Bushveld Complex these concepts have found strong support (Kruger and Marsh, 1982; Campbell et al., 1983; Harmer and Sharpe, 1985; Sharpe, 1985; Campbell, 1986; Eales et al., 1986, 1990a; Eales, 1987; Hatton and von Gruenewaldt, 1987; Naldrett et al., 1987; Hatton, 1988),

It is now generally accepted that at least two isotopically distinct magma types were responsible for the development of the layered sequence of the Bushveld Complex which is made up of the Lower, Critical, Main and Upper Zones. Initially a more "primitive" liquid (Sharpe's 1985 "U-type") was intruded into the magma chamber, with periodic additions, to produce the Lower and Critical Zones of the Complex. This magma had an initial strontium isotope ratio of between 0.703-0.705. It was also rich in incompatible elements and Cr (900-1600ppm) as well as being SiO_2- and MgO-rich, similar to olivine boninites (Sharpe, 1985). Rocks produced by the second magma had a tholeiitic lineage (Sharpe's "A-type") with higher initial strontium isotope ratios (c. 0.7065-0.7087) and low incompatible trace-element and Cr values (Cr = 250ppm).

Modelling the crystallisation of the Bushveld layered sequence on these two end-member parental magmas may be an oversimplification. Liquids with intermediate strontium isotopic ratios are recognised as being parental to the Upper Critical Zone. Eales et al. (1986) pointed out that because Sr-isotope ratios are unaffected by crystal fractionation, the overall trend of the initial Sr-isotope profile through the Upper Critical Zone and the Main Zone lends support to the hypothesis that mixing occurred between magmas with initial ratios of c. 0.7064 and c. 0.7087 respectively. The hypothesised existence of a parental liquid intermediate between the "U-" and "A-types" of Sharpe (1985) with an initial ratio of 0.7068 is supported by data presented for the Upper Critical Zone between the Middle and Upper Group chromitite layers by Eales et al. (1990a).

This study and others (Kruger and Marsh 1985; Naldrett et al, 1986; Eales et al. 1986 and 1990a) suggest that in the initial stages the Bushveld magma was intruded as a multiple series of pulses rather than as a massive single influx, which seems to have characterised the introduction of the "A-type" liquid which produced the bulk of the Main Zone.

1.2 The Bushveld Complex - overview and geological setting

The Bushveld Complex, situated in the central part of Transvaal, forms a large lobate mass which underlies an area of approximately 65000 km^2 (Tankard et al., 1982). In outcrop (and sub-outcrop) it appears as a series of connected lobes and Willemse (1964 and 1969) recognised five distinctive magmatic phases in the development of the Bushveld Magmatic Province (Irvine, 1982):

1) **A volcanic phase** during the deposition of the Transvaal Supergroup. Rb/Sr age determinations of the Hekpoort Andesite Formation yielded 2224 ± 21 My (Burger and Coertze, 1973).
2) **A sill phase** comprising a diverse group of sills which were intruded into the Transvaal Supergroup sediments.
3) **An epicrustal phase** involving extrusion and injection of felsites, granophyres, and related rock types of the Rooiberg Felsite Group.

4) **The main plutonic phase** during which the diorites, gabbros, and ultramafic rocks of the Rustenburg Layered Suite (RLS) were emplaced and differentiated. Geochronological studies done on rocks from different zones within the RLS have yielded an average Rb/Sr-age of 2050 ± 22 My (Vermaak and von Gruenewaldt, 1986, report recalculated determinations of Hamilton, 1977).
5) **A later plutonic phase** during which the Bushveld Granite (Lebowa Granite Suite) was intruded. Ages reported in Vermaak and von Gruenewaldt (1986) vary between 1670 ± 30 My (Makhutso Granite) and 2010 ± 20 My (Nebo Granite).

The regional distribution of the mafic rocks of the RLS can broadly be subdivided into five areas. A regional map of the Bushveld Complex depicting these areas is presented in Willemse (1969, p.3) and Vermaak and von Gruenewaldt (1986, p.1026).

a) Far Western Transvaal limb with exposures to the west of the Pilanesberg Alkaline Complex. These rocks represent only the lower part of the RLS (Marginal and Lower Zone successions).
b) Western Bushveld limb - exposed in an arc extending from Pretoria through Brits, Rustenburg, Union and Amandelbult Sections of Rustenburg Platinum Mines (Figure 1.1).
c) Potgietersrus - Villa Nora limb in central northern-Transvaal.
d) Eastern Bushveld limb which forms an arc extending both to the north and south of Steelpoort.
e) Bethal lobe of the Eastern Bushveld which is overlain by younger sediments of the Karoo Sequence.

The eastern and western limbs of the RLS, although widely separated (± 300 km from Rustenburg to Steelpoort), show remarkably similar stratigraphic and lithological characteristics. This factor suggests that both limbs of the Complex shared a common magma source and that these widely separated magma chambers experienced similar sequences of magmatic events. These factors ultimately led to the formation of not only similar sequences of layered rocks, but also the chromitite and platiniferous ore-bodies.

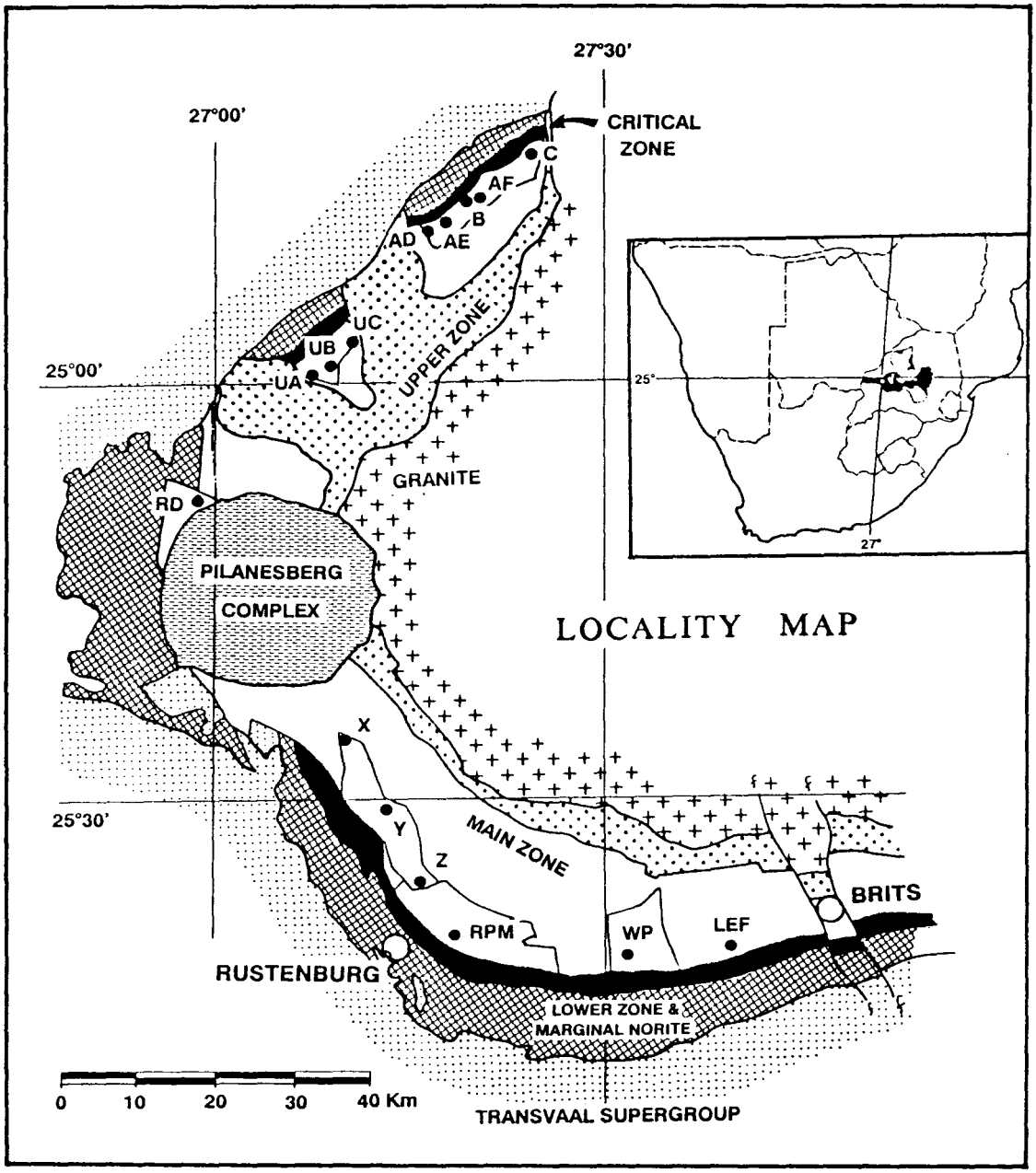

Figure 1.1 Locality map of the western limb of the Bushveld Complex showing the extent of the layered sequence and the four major zones in relation to the floor and roof rocks. Positions of the various profiles are indicated by solid circles while open circles are for the major towns. Approximate mining lease boundaries are shown for Amandelbult (**AD**, **AE**, **B**, **AF**, C), Union (**UA**, **UB**, **UC**), Impala (**X**, **Y**, **Z**), Rustenburg (**RPM**) and Western Platinum Mines (**WP**).

Geophysical models of the Bushveld Complex have evolved a great deal from the model proposed by Cousins (1959). He suggested that the mafic exposures in the eastern and western Bushveld were not part of a lopolith but represent rather two deep curved troughs of mafic rocks having an arcuate, superficially synclinal structure, with dyke-like central feeders. The modern, more widely accepted model, is one of **dipping terminated sheets** which was proposed by du Plessis and Kleywegt (1987) - derived from gravity data and substantiated by deep electrical sounding data (Meyer and de Beer, 1987). This model of the magma chamber's geometry suggests that the mafic sequence in both these parts of the Complex occurs as segments of inward-dipping sheets transgressing the layering of the Transvaal Sequence sedimentary rocks into which they intruded. The model also predicts that there is very little or no mafic Bushveld material in the central part of the Complex and that here the Bushveld Granite lies directly on Transvaal or Archaean gneiss.

The Bushveld Complex has, over the past sixty years, been subjected to intensive exploration and mining directed mainly at the platinum- and chromium-bearing ore bodies which occur as discrete layers in the Critical Zone. Unlike the good exposures of the layered sequence which make up the Marginal, Lower and Critical Zones in the eastern Bushveld Complex, the surface expression of these zones in the western limb is poor. The layered sequence here underlies a flat, rather featureless plain which is rimmed on one side by resistant meta-sediments of the Transvaal Supergroup forming the floor, and on the other by the gabbro and gabbronorite hills (colloquially called the "Pyramid hills") of the Main Zone in the hangingwall. Regional dip of the Critical Zone succession to the north of the Pilanesberg is taken as 19° while that to the south is between 10° and 12°. Exploration boreholes and mining activity directed towards the platinum-bearing layers of the Complex usually only expose the hangingwall succession and the immediate footwall of the platiniferous ore bodies - the Merensky Reef and the UG2 chromitite. Mining development on these two layers requires the development of footwall haulages and cross-cuts (usually no more than 50m below the stopes) and it is only in long tramming and ventilation crosscuts from a production shaft that the deeper footwall is exposed.

It is for these reasons that the bulk of earlier research, which has focused on features and the origin of the Upper Critical Zone and Main Zone, has been coloured by the characteristics of these exposures. Relatively little attention has been paid to the deeper succession below the UG1 chromitite, particularly in the western limb of the Complex. Only in the past three years have researchers (Teigler, 1990; Eales et al., 1990a) documented the succession and geochemistry of the Lower and Lower Critical Zone rocks in any detail in an attempt to gain additional insight into the genesis of the complete layered sequence in the western Bushveld Complex.

1.3 Stratigraphic succession of the Upper Critical Zone

The Bushveld Complex is broadly divided into the Marginal, Lower, Critical, Main and Upper Zones with their combined thickness being some 7000m in the western limb (Figure 2.1). The first appearance of cumulus plagioclase feldspar within the column is used as a marker to separate the ultramafic dunites, harzburgites, pyroxenites and chromitites of the Lower and Lower Critical Zones from rocks of the Upper Critical Zone (predominantly harzburgites, pyroxenites, norites, chromitites and anorthosites). The overlying Main Zone essentially comprises gabbronorites and anorthosites while the Upper Zone is made up of magnetite gabbros, magnetitites and evolved gabbros containing fayalitic olivine and cumulus apatite. More detailed stratigraphic descriptions of the Upper Critical Zone under consideration are available in the literature (de Klerk, 1982; Viljoen et al., 1986a; Eales, et al., 1986; and Eales et al., 1990a) and no more than a summary is necessary here. Stratigraphic detail on the Bastard Unit is presented in section **4.5**.

The UG1 Footwall Unit (UG1FW) underlying the UG1 chromitite is unusually thick when compared with other Upper Critical Zone units. At Union Section it is c. 290m thick and is divided lithologically into two main parts: (a) a lower pyroxenitic sequence (c. 135m thick), floored by the MG4 chromitite layer, and overlain by (b) 150m of an essentially noritic sequence. The norites become more leucocratic and finely layered towards the top of the unit. The immediate footwall of the UG1 chromitite consists of anorthosite which has abundant disseminated and layered

chromite. This part of the succession, and the data pertaining to the UG1FW Unit, are discussed in detail in section **2.2.**

Overlying the UG1FW Unit are the UG1 and UG2 Units which are composed essentially of feldspathic pyroxenites floored by robust chromitite layers. The UG2 chromitite is now being mined as a major economic source of PGE, beneath the Merensky Reef, at several localities around the Complex. The Pseudoreef Unit, above the UG2 Unit, is an association of feldspathic harzburgites of two differing textural types at Union Section, designated the Lower and Upper Pseudoreefs (Scoon and de Klerk, 1987). Leuconorites, norites, troctolites and feldspathic harzburgites are more commonly developed in the Pseudoreef Multicyclic Unit at Amandelbult Section. The attenuation of this unit at Union Section has been attributed by Eales et al. (1988) to progressive resorption of leucocratic components by "thermal erosion", which was most pronounced in the region postulated to have been in close proximity to a feeder system. Overlying the Pseudoreef Unit is the Merensky Footwall Unit which forms the floor on which the economically important, PGE-enriched Merensky Reef rests. This unit may be characterised largely as a leucocratic sequence of mottled anorthosite overlying norites with only a small amount of pyroxenite and harzburgite (sometimes pegmatoidal) at the base of the unit, reaching a thickness of one metre. A characteristic feature of the Footwall Unit is that it may locally be absent, in which case the anorthosite - and in some cases the norite - is missing, beneath the so-called "pothole structures" which cause the overlying Merensky Reef to transgress across progressively lower layers (see Viljoen et al., 1986a). The Merensky Reef is located at the base of the Merensky Unit which is in turn overlain by the Bastard Unit.

The Bastard, Merensky, and possibly the Footwall Unit, are ostensibly "complete" cyclic units with ultramafic lithologies (feldspathic pyroxenites, with or without accompanying feldspathic harzburgites) at the base, grading upwards through melanorites, norites and leuconorites to anorthosites at the top. Plagioclase is of intercumulus habit within the ultramafic rocks, but adopts a cumulus habit and becomes more calcic within the melanorites and overlying layers of each unit. The formal definition of the contact between the Critical and Main Zones is still

being debated in the literature but for the purpose of this discussion the top of the Critical Zone is defined as the top of the Giant Mottled Anorthosite of the Bastard Unit (SACS, 1980).

1.4 Scope and aim of the study

This study concentrates on the petrology, geochemistry and mineralogy of the **silicate** layered sequence in the Upper Critical Zone that has been exposed by mining and exploration activities in the western Bushveld Complex.

Initially the study was seen as an extension of part of the writer's M.Sc. thesis (de Klerk, 1982), aiming to continue the documentation of cryptic variations and geochemistry in selected profiles at RPM Union Section in the northwestern Bushveld Complex. The Bushveld Complex is of such a size and thickness that detailed studies of variation in the succession along strike constitute an essential prerequisite to any understanding of the genesis of the Complex. To extend the data provided (de Klerk, 1982) by a stratigraphic profile in the centre of Union Section (**UB**), additional boreholes were sampled in the SW (**UA**) and NE (**UC**) sectors of the mine (see Figures 1.1, 1.2 and 1.3).

The stratigraphic interval covered in these profiles extends from just below the UG1 chromitite layer upward through the UG2, Pseudoreef, Footwall, Merensky and Bastard Units, totalling some 100m (Figure 1.2). As an expansion of this sampling exercise at Union Section, data relating to an additional 14 profiles from the western limb of the Complex were compiled for the Bastard Unit. This cyclic unit was selected to investigate the processes that were operative at the junction between the Critical and Main Zones, and to establish whether any marked spatial geochemical variation occurs along strike in the western Bushveld Complex. The analysis of lateral variation is based primarily on seven sampled profiles of the Bastard Unit, supplemented by additional data available in published and unpublished reports (See section **4.5**).

Most of the stratigraphic and geochemical studies that have been done on the layered sequence of the Bushveld Complex, particularly within the

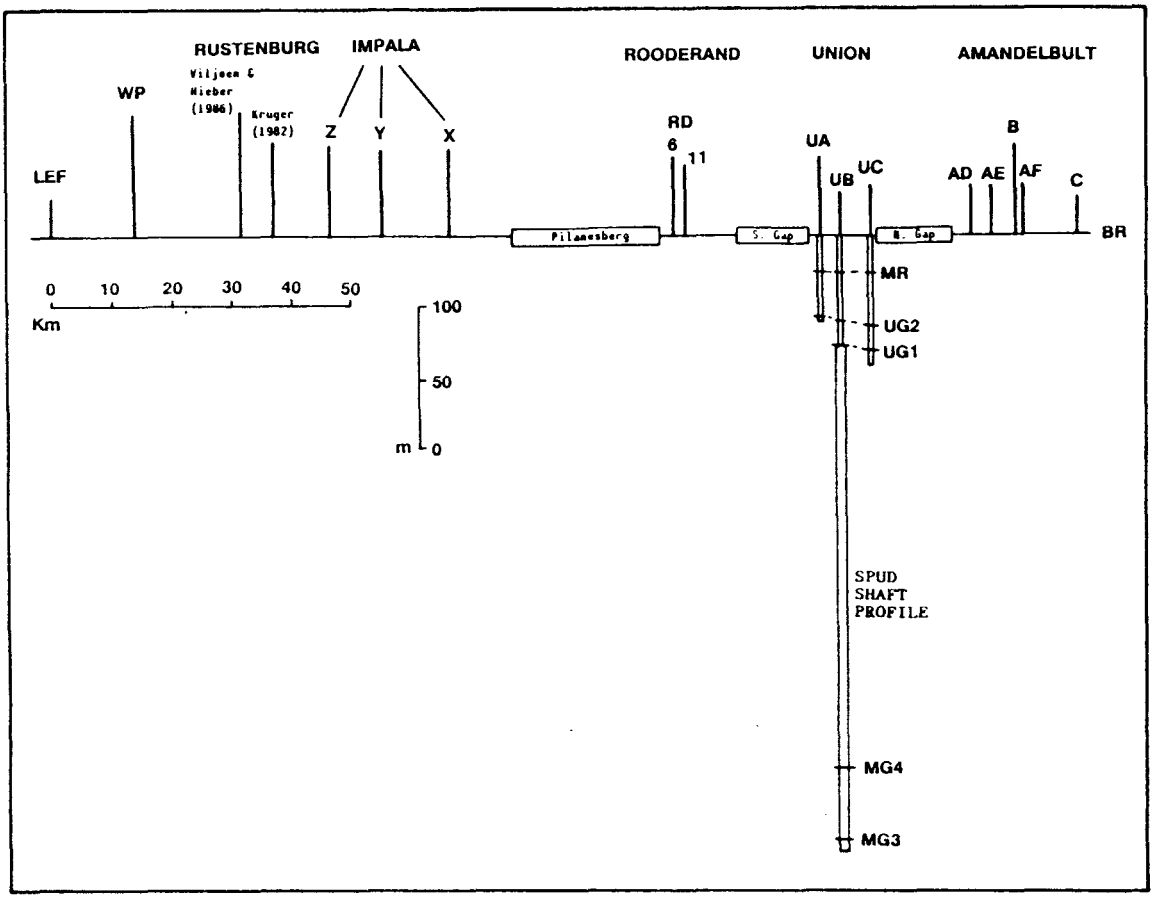

Figure 1.2 Schematic diagram illustrating the spatial distribution of sampled and compiled profiles around the western limb of the Bushveld Complex with the main focus of the study being at RPM Union Section. The datum line is taken as the base of the Bastard Unit (BR - Bastard Reef) and shows the profiles from Lefkochrysos (**LEF**) and Western Platinum Mines (**WP**) in the Brits area through to RPM Rustenburg Section (2 profiles) and Impala (**Z**, **Y** and **X**) to the south of the Pilanesberg. North of the Pilanesberg are the three Critical Zone "islands" at Rooderand, Union and Amandelbult Sections separated by the Southern and Northern Gap Zones respectively.

Critical Zone, have focused on the economic ore-bearing horizons (Merensky Reef and UG2 chromitite) and their hangingwall and footwall layers. Only a cursory account and synthesis of the layered sequence away from the platinum- and chromium-bearing layers have been published to date. With this in mind the sequence between the Middle Group (MG) chromitites and the UG1 Unit was also selected for study - a sequence some 350m thick.

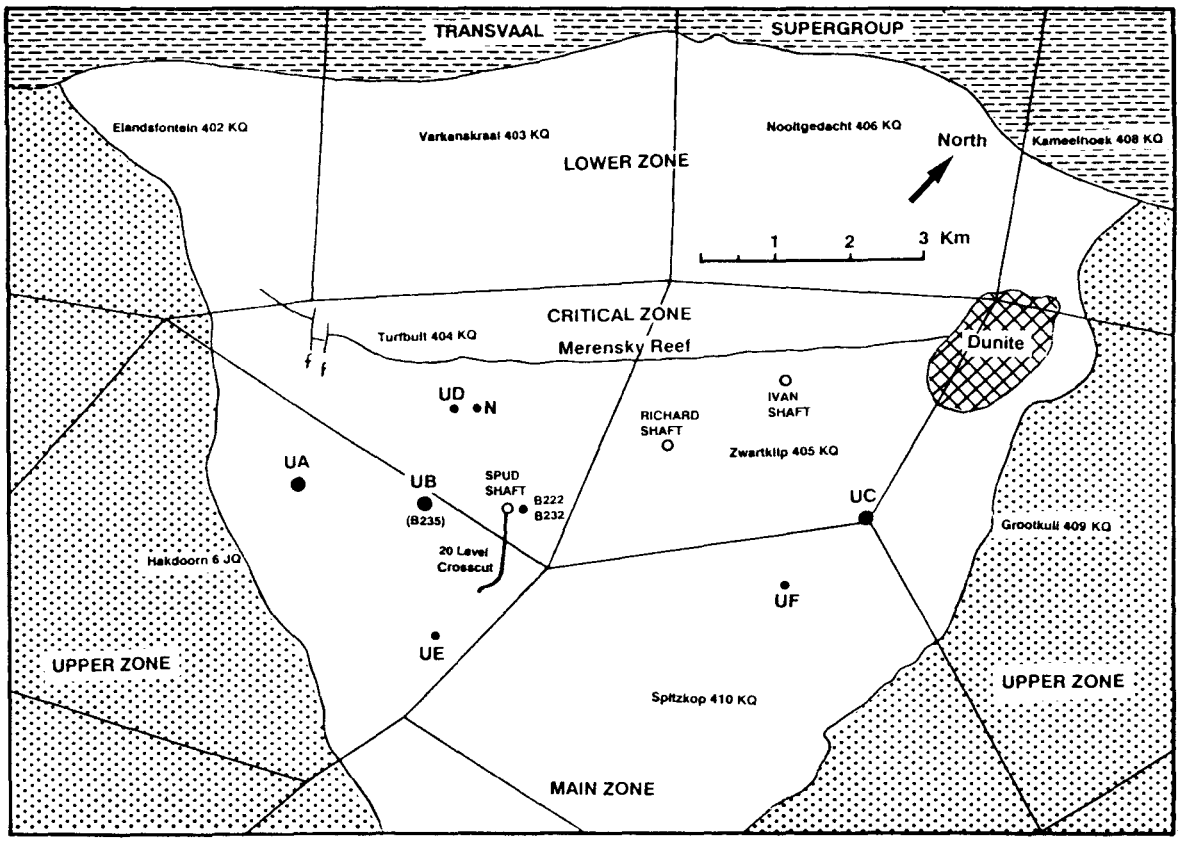

Figure 1.3 Locality map of RPM Union Section showing the positions of the various borehole and underground profiles used in this study; N is the position of the profile used by Naldrett et al. (1984). The Spud shaft crosscut was used to sample the MG3 and UG1FW Unit. This map is based on that indicating the regional geological setting of Union Section in Vijoen et al. (1986a, p.1065).

In essence the objectives of this study are thus fourfold:

* to document the cryptic variation of the entire Upper Critical Zone at RPM Union Section (from the MG chromitites to the Main Zone boundary) with emphasis on the UG1FW and Bastard Units;
* to establish whether lateral geochemical variations are evident along strike within a selected single cyclic unit, the Bastard Unit;
* to test various hypotheses that have been proposed to account for the layered sequence of the Upper Critical Zone, and
* to attempt to reconstruct the sequence of magmatic events that gave rise to this layered sequence.

The study falls naturally into two main sections: the examination of the interval between the MG3 and UG1 chromitite layers at Spud Shaft, Union Section (**Chapter 2**), and the investigation of a single laterally persistent cyclic unit in the Upper Critical Zone at various localities spread across the western Bushveld Complex (**Chapter 4**)(see Figure 1.2). **Chapter 3** constitutes a supporting section in which new whole-rock data are presented for a number of additional profiles in the Union Section area and provides continuity between the UG1FW Unit and the Bastard Unit.

This work has in effect produced a composite stratigraphic and geochemical profile spanning some 460m through the Upper Critical Zone at Union Section (Middle Group chromitite layers to the top of the Bastard Unit).

1.5 Nomenclature, classification and conventions used

The nomenclature and classification of the cumulate rocks in this study are broadly based on the recommendations of the IUGS Subcommission on the systematics of igneous rocks (Streckeisen, 1976; Le Maitre, 1989). Part of Shand's (1943) colour-index classification has been retained, with the prefixes mela- and leuco- being used to describe the more mafic and felsic variants of norites (see Figure 1.4).

In any rock assemblage, such as in the Upper Critical Zone at Union Section, which shows every gradation between anorthosite and pyroxenite, rock nomenclature is subjectively influenced by field terms, textural features, and tradition. Usage of terms such as melanorite, norite and leuconorite is not consistent. The scheme of classification for **plagioclase - pyroxene** cumulates which is adopted here is the same as that proposed by Eales et al. (1988, p.64). Briefly, the range of compositional variation between anorthosites and pyroxenites is defined by the CIPW normative composition of or + ab + an (total feldspar) plotted against whole-rock $\%Al_2O_3$ (Figure 1.5) and the subdivisions are as close as is practicable to those advocated by Streckeisen (1973). The justification for adopting this convention lies in a remarkably good correlation obtained between point-counted modes and the calculated CIPW norms for some 33 samples in the Bastard Unit (See **4.7.6**). Simple linear

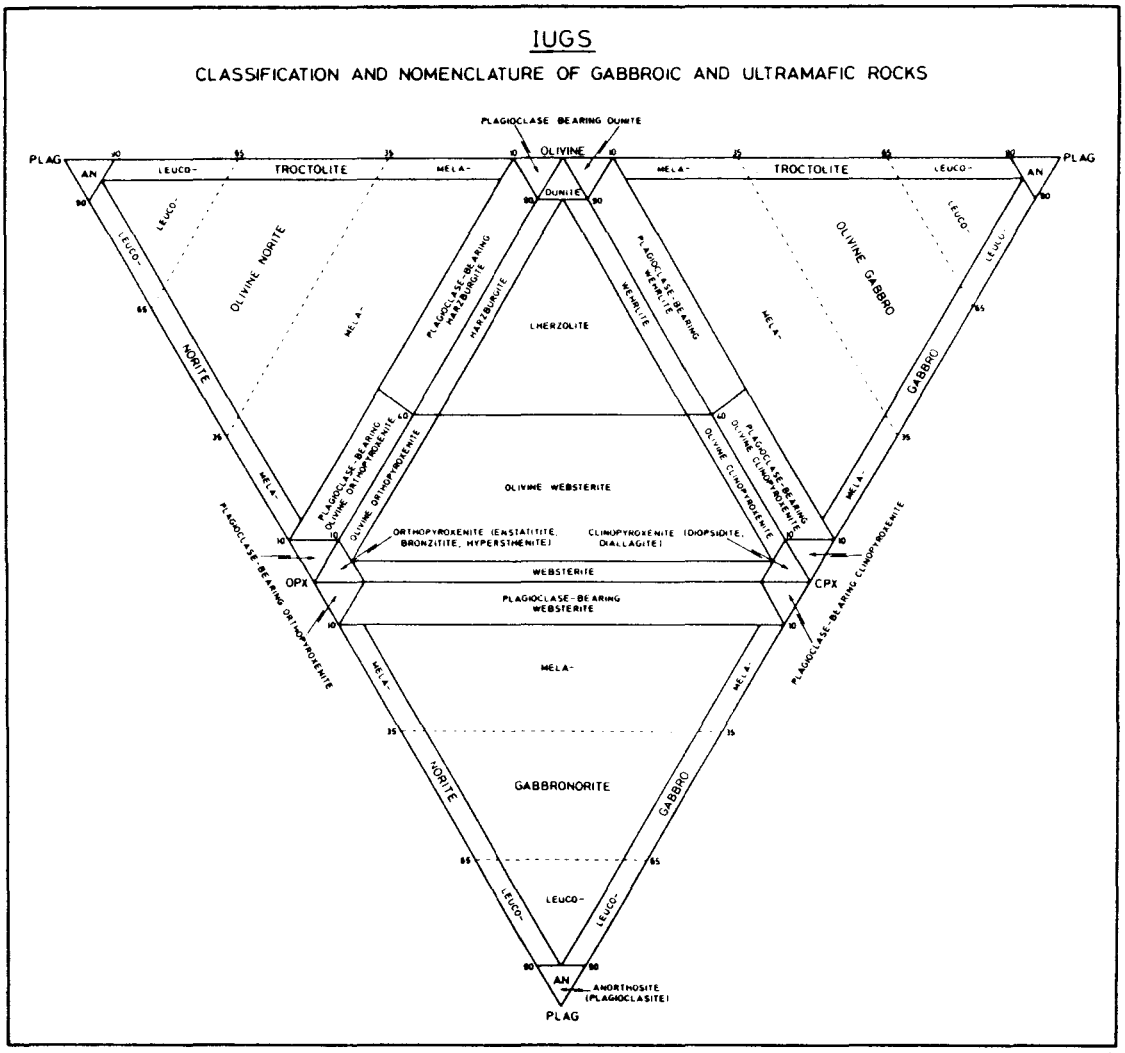

Figure 1.4 Nomenclature of gabbroic and ulramafic rocks recommended by IUGS (Streckeisen, 1976).

regression analysis of 124 samples from the Bastard Unit (similar to that displayed in Figure 1.5) yields the expression:

Total feldspar = 3.0 Al_2O_3 + 1.28 (corr. coef. 0.998) (see **4.7.6**).

Whereas Streckeisen's (op. cit.) definition requires anorthosite to have >90% feldspar, the classification above adopts a value of 85% in order to avoid controversial re-definition of entrenched terms such as "Giant Mottled Anorthosite" as "Giant Mottled Leuconorite". In view of the fact that pyroxenites of the Upper Critical Zone contain appreciable intercumulus feldspar, the division between melanorite and feldspathic pyroxenite is placed at 6.5% Al_2O_3 in this study. Synonymous or

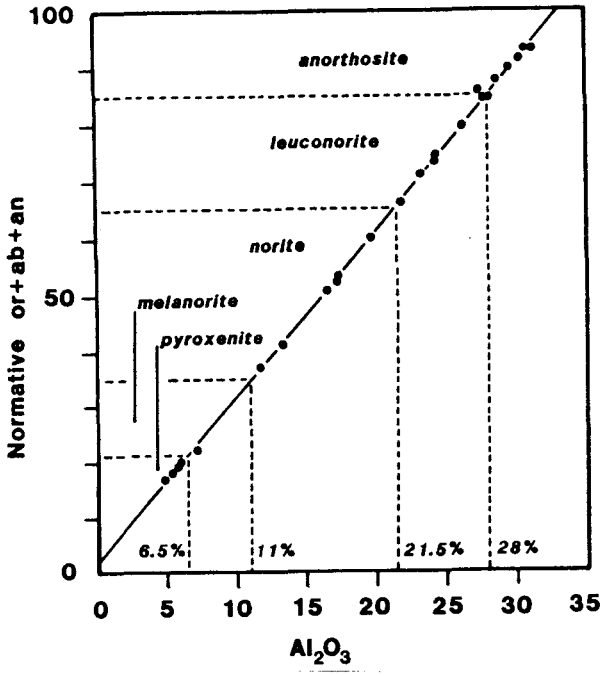

Figure 1.5 Nomenclature adopted for orthopyroxene - plagioclase rocks, based on a plot of normative or + ab + an against whole-rock Al_2O_3. Simple linear regression of these data yield the expression: Total feldspar = 2.95 Al_2O_3 + 2.22 (correlation coefficient 0.9995)(After Eales et al., 1988, p.65).

equivalent rock names using cumulate terminology and conventional names are presented in Table 1.1.

The original cumulus terminology proposed by Wager, Brown and Wadsworth (1960) was largely genetic in character, the underlying tenet being that the crystals accumulated (by gravitational settling) to form a cumulate. The terms ortho-, meso- and adcumulate were given to cumulates differing in the amount of postcumulus material they contained. This terminology was later questioned when the validity of gravity settling was queried by workers like Campbell (1978), McBirney and Noyes (1979) and Morse (1979a). One of their objections was that the density of plagioclase is too low for it to settle in basaltic liquids. In a review paper on the terminology of layered rocks, Irvine (1982) pointed out that the cumulus terminology introduced by Wager et al. (op. cit.) was so well entrenched in the literature that he recommended it be retained but used in a non-genetic sense. Wadsworth (1985) defended the original definitions and strongly recommended that these definitions of orthocumulate,

Table 1.1: Comparison of different schemes of terminology.

Bushveld Complex (This study)	$\%Al_2O_3$	Cumulate type (Irvine 1982)		General petrographic terminology (Streckeisen, 1976)
Olivine pyroxenite		orthopyroxene-olivine	boC	Olivine orthopyroxenite
Harzburgite*		olivine-orthopyroxene	obC	Harzburgite
(with poikilitic opx)				
Pyroxenite*	< 6.5	orthopyroxene	bC	Orthopyroxenite
(feldspathic)				
Melanorite	6.5 - 11	orthopyroxene-plagioclase	bpC	
Norite	11 - 21.5	orthopyroxene-plagioclase	bpC	Norite
			or pbC	
Leuconorite	21.5 - 28	plagioclase-orthopyroxene	pbC	
Anorthosite	> 28	plagioclase	pC	Anorthosite
(mottled)				
Chromitite		chromite	cC	Chromitite

* In the more ultramafic rocks like harzburgites and pyroxenites the adjective "feldspathic" is used to indicate an abundance of postcumulus material.

mesocumulate and adcumulate, using the full complement of fractionated residual material, be retained. He did, however, point out that some advantage may be gained by the more precise quantification of these categories as proposed by Irvine (1982). The cumulus terminology used in this study adheres to the definitions of Wager, Brown and Wadsworth (op. cit.) but also takes cognisance of Irvine's quantifications. A generalised account of the three cumulate types mentioned above is summarised in Figure 1.6.

A) <u>Orthocumulates:</u> Wager, Brown and Wadsworth (1960) defined an orthocumulate as consisting essentially of one or more cumulus minerals together with the products of crystallisation of the intercumulus liquid, which had a composition similar to that of the contemporary magma. Postcumulus material (mostly interstitial) is abundant and relatively easy to identify, as the overgrowths are zoned towards lower temperature compositions and the associated interstitial minerals are quite distinctive. Irvine (1982) suggested that the cumulus minerals should ideally exhibit much of their original crystal forms and postcumulus minerals comprise c. 25-50% of the rock.

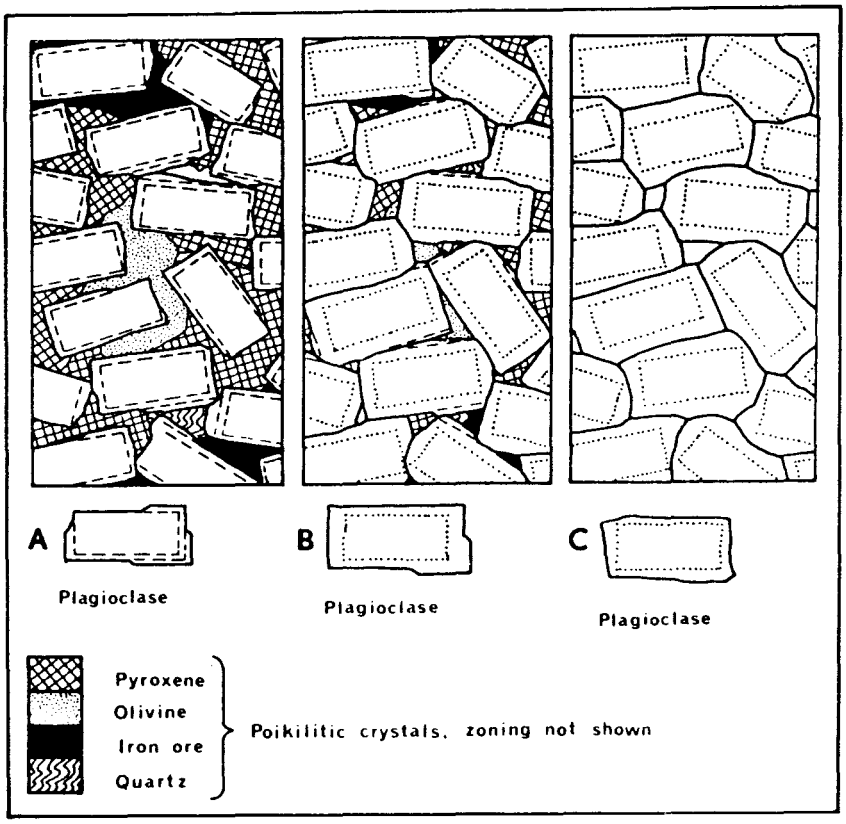

Figure 1.6 Diagrammatic representation of plagioclase cumulates formed from basaltic magmas (after Wager, Brown and Wadsworth, 1960), reproduced from Irvine (1980). For explanation see text. A = orthocumulate; B = mesocumulate; C = adcumulate.

B) **Mesocumulates:** these rocks have less postcumulus material, and the cumulus grains should adjoin in part along mutual interference grain boundaries developed through overgrowth (c. 7-25% postcumulus minerals).

C) **Adcumulates:** here the overgrowths are similar in composition to the cumulus cores and it is difficult to identify the relative proportion of cumulus and intercumulus material. Irvine (1982) suggested that adcumulates can be recognised by the presence of minor discrete postcumulus materials and that mutual interference boundaries are the norm for the cumulus phase (c. 0-7% postcumulus minerals).

The term **primocryst**, used in this study, refers to any crystal which nucleates at an early stage from the parent liquid and may subsequently settle under gravity or be retained in suspension. The term specifically excludes intercumulus phases.

Mineral names

A recent study by the International Mineralogical Association (Morimoto, 1989) has recommended that the nomenclature of the orthorhombic Mg-Fe pyroxenes be simplified and that only the two end-member mineral names be retained: Enstatite (En) and Ferrosilite (Fs), the division being taken at the 50% mark. Mineral names which have been entrenched in Bushveld and other layered complex literature, like bronzite and hypersthene, have been placed on the obsolete list and their recommendation is that these minerals be called **enstatite**. In this study the term **orthopyroxene** is synonymous with enstatite and has been used throughout.

LIST OF ABBREVIATIONS

Lithologies

UZ - Upper Zone
MZ - Main Zone
CZ - Critical Zone
LZ - Lower Zone

UGMA - Upper Giant Mottled Anorthosite
GMM - Giant Mottled Middling
LGMA - Lower Giant Mottled Anorthosite
GMA - Giant Mottled Anorthosite
BU - Bastard Unit
BR - Bastard Reef
MU - Merensky Unit
MR - Merensky Reef
UG2 - Upper Group Chromitite layer 2
UG1 - Upper Group Chromitite layer 1
UG1FW - Upper Group Chromitite 1 footwall
MG4 - Middle Group Chromitite layer 4
MG3 - Middle Group Chromitite layer 3
MG2 - Middle Group Chromitite layer 2

Standard Conventions and Symbols

Rock type		Whole-rock* % Al_2O_3
Pegmatoidal pyroxenite/harzburgite		
Olivine pyroxenite		
Harzburgite		
Pyroxenite	Px	< 6.5
Melanorite	Mn	6.5 - 11
Norite	N	11 - 21.5
Leuconorite	Ln	21.5 - 28
Anorthosite (mottled)	An	> 28
Chromitite		
Chromitite layer or dissemination		
Data point off scale		

* Eales et al. (1988)

Profile Localities

LEF - Lefkochrysos Mining Company (now controlled by Rand Mines and called Crocodile River Platinum Mine).
WP - Western Platinum Mine.
RPM - Rustenburg Platinum Mines (RPM) - Rustenburg Section.
Z - Impala Platinum Mines (South) - Wildebeestfontein Mine.
Y - Impala Platinum Mines (Central) - Bafokeng South Mine.
X - Impala Platinum Mines (North) - Bafokeng North Mine.
RD - Rooderand 46 JQ - farm on the NW flank of the Pilanesberg.
UA - RPM Union Section, SW sector.
UB - RPM Union Section, central sector.
UC - RPM Union Section, NE sector.
AD - RPM Amandelbult Section, far west.
AE - RPM Amandelbult Section, west.
AF - RPM Amandelbult Section, central.
B - RPM Amandelbult Section, central.
C - RPM Amandelbult Section, east.

Petrological, Mineralogical and Geochemical

ol - Olivine
opx - Orthopyroxene
cpx - Clinopyroxene
plag - Plagioclase
Sr_i - Initial strontium isotope ratio ($^{87}Sr/^{86}Sr$)
MMF - Atomic ratio of $Mg/(Mg + Fe^{2+})$ in pyroxene
MMF_{WR} - Whole-rock $Mg/(Mg + Fe)$ atomic ratio where all Fe is expressed as Fe^{2+}
ΣC_{WR} - Sum of major elements compatible in pyroxenes (Fe_2O_3 + FeO + MnO + MgO)
PGE - Platinum group elements (Pt, Pd, Os, Ru, Rh and Ir)
PGM - Platinum group metals

Statistical

sd - Standard deviation
cc - Coefficient of correlation
r^2 - Coefficient of determination (it defines the portion of total sum of squares accounted for by regression).
$r^2 = Q_R/Q$ where Q_R = model sum of squares
$Q = Q_R + Q_{Error}$
= total sum of squares

Figure 1.7 Abbreviations and conventions used thoughout the thesis.

CHAPTER 2

THE UG1FW UNIT - CASE STUDY OF A CYCLIC UNIT

2.1 Introduction.

This chapter describes the texture, mineralogy and geochemistry of a section extending c. 350m beneath the UG1 chromitite at Rustenburg Platinum Mines (RPM), Union Section. It illustrates the complexities that emerge from detailed study (at close sampling intervals) of a single unit changing, with stratigraphic height, from ultramafic to leucocratic rocks. The model which evolves becomes relevant to the interpretation of other sequences within the Upper Critical Zone. The text and accompanying diagrams in this chapter, include substantial extracts from Eales, de Klerk, Butcher and Kruger (1990a), but additional data which were not included in that paper are added here. A reprint of this paper is included in Appendix E.

The interval between the UG1 and the MG4 chromitites (291m), here termed the UG1 Footwall Unit (**UG1FW Unit**), provides convincing evidence of hybridisation through the mixing of fresh inputs of magmatic liquid with partially crystallised resident liquids bearing abundant plagioclase feldspar. The unique significance of the section lies in the preservation of incompletely resorbed small plagioclase inclusions within host orthopyroxene grains of pyroxenites and norites. This evidence is also used to support the view that mixing may also have operated within other cyclic units where the plagioclase primocrysts have been destroyed by more complete reaction.

2.2 Stratigraphy.

The stratigraphic interval between the UG1 and MG3 chromitite layers, and the various lithologies and sample positions, are illustrated in Figure 2.1 while more detail of the MG4 and MG3 chromitites is shown on Figure 2.3.

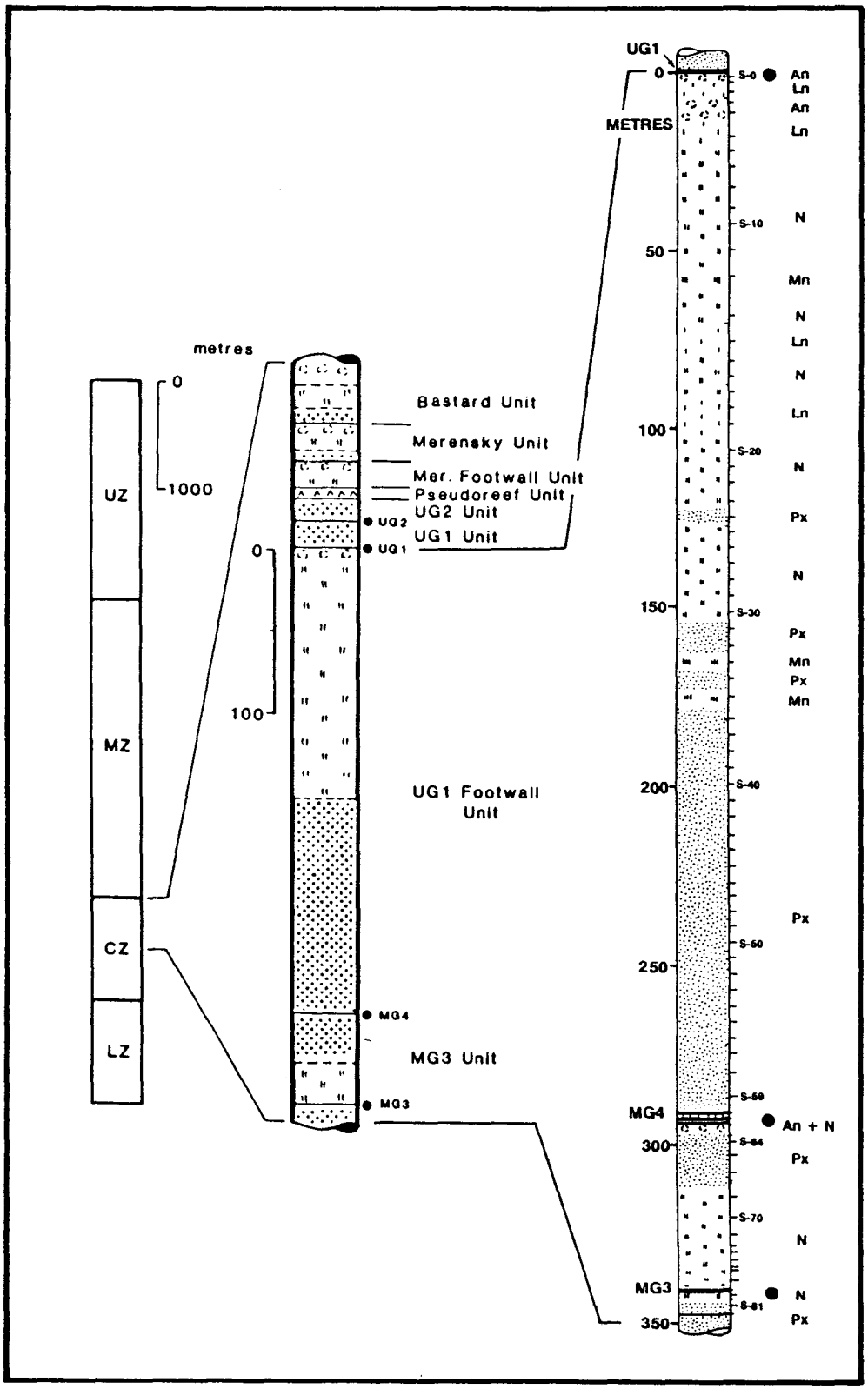

Figure 2.1 Generalised stratigraphic succession through the western Bushveld Complex with detail for the Upper Critical Zone and UG1 Footwall Unit at Union Section. Significant chromitite layers at the bases of units are indicated by solid circles. Sample positions and rock types are indicated on the right of the column (An - anorthosite; Ln - leuconorite; N - norite; Mn - melanorite; Px - pyroxenite). Symbols are the same as those used in Figure 1.7. LZ - Lower Zone; CZ - Critical Zone; MZ - Main Zone; UZ - Upper Zone.

The contact between the UG1 Unit and the underlying UG1FW Unit is one of the more prominent and distinctive features of the Critical Zone succession. Undisturbed UG1 chromitite at Union Section is the exception rather than the norm and at infrequent exposures of undisturbed regular layering the UG1 chromitite package consists of two robust chromitite layers, the upper 50-60cm thick and the lower c. 30cm thick, separated by c. 30cm of pyroxenite. These well-defined layers rest concordantly on white to pale grey anorthosite, and the basal contact of the lower chromite is taken to be the boundary between the UG1 Unit and UG1FW Unit (Plate 2.1a).

More commonly, the contact between these two units is complex and displays the same features that are seen at the well known Dwars River exposures in the eastern Transvaal. An upper group of regular chromitite and pyroxenite layers overlies 3-4m of anorthosite within which thin chromitite layers (commonly 1-200mm thick) converge and diverge to yield an anastomosing system (Plate 2.1b). This gross structure may in turn give way along strike, or in depth, to an irregular system of contorted, discontinuous stringers, lenses and pods of chromitite (and in some instances pyroxenite) which display distinctive, soft-sediment deformation features (Plate 2.2 and 2.3). These textures are suggestive of disruptive movement within the crystalline mush prior to solidification. Textural evidence in some areas suggeststhat at least two disruptive events took place prior to final solidification (Plate 2.3b). Lenticular pods of chromitite and/or pyroxenite with an oblate-spheroid shape (diameters up to 0.5m) appear to have subsided within the anorthosite, depressing and disrupting the layering beneath and around the pods (Plates 2.2b, 2.3a & b). The pyroxenitic pods are charged with a high concentration of disseminated chromite. These structures have been attributed by various authors to intrusion into the anorthosite of a chromite-bearing residual magma (Sampson, 1932), intrusion of anorthosite into chromitite (Coertze, 1958), deposition of chromitite accompanied by turbulent mixing with plagioclase crystals (Vermaak, 1976), and emplacement of a chromitite mush as a result of fracturing (Cameron, 1964) or a process akin to that which produces sandstone dykes and sills in sediments (Lee, 1981).

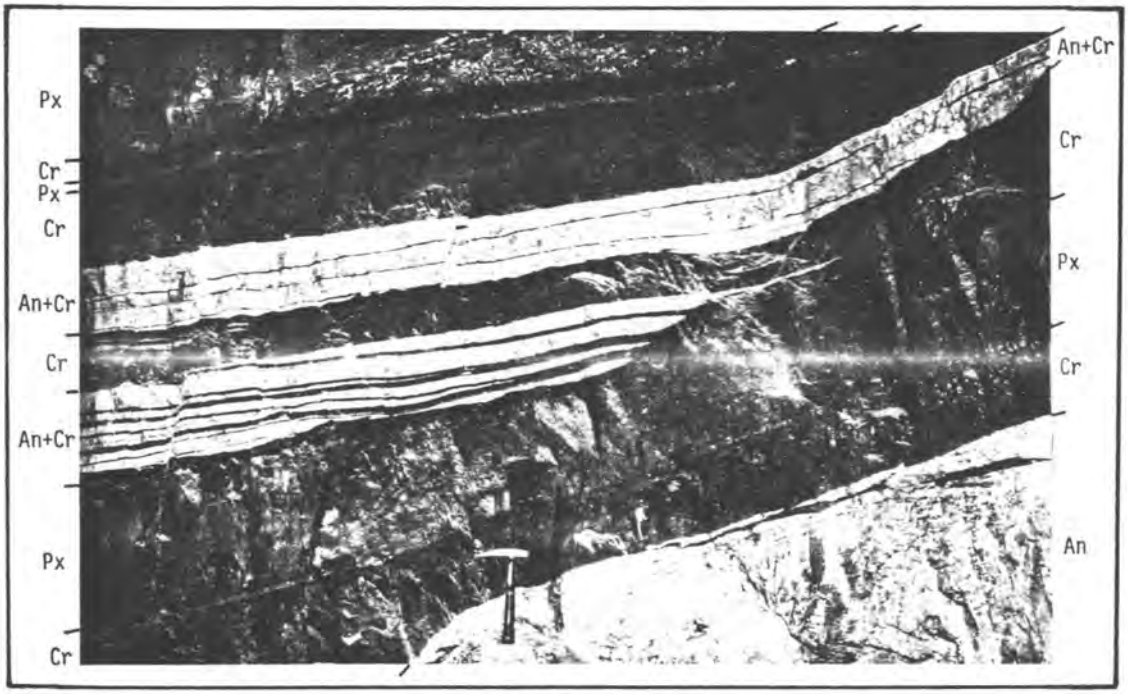

Plate 2.1a Contact between the UG1 chromitite layer and the top of the UG1FW Unit (anorthosite). Here the UG1 chromitite shows the typical pattern of bifurcation which, in this case, is concentrated in the upper chromitite above the pyroxenite parting. Locality - Union Section, Spud shaft 15 haulage south.

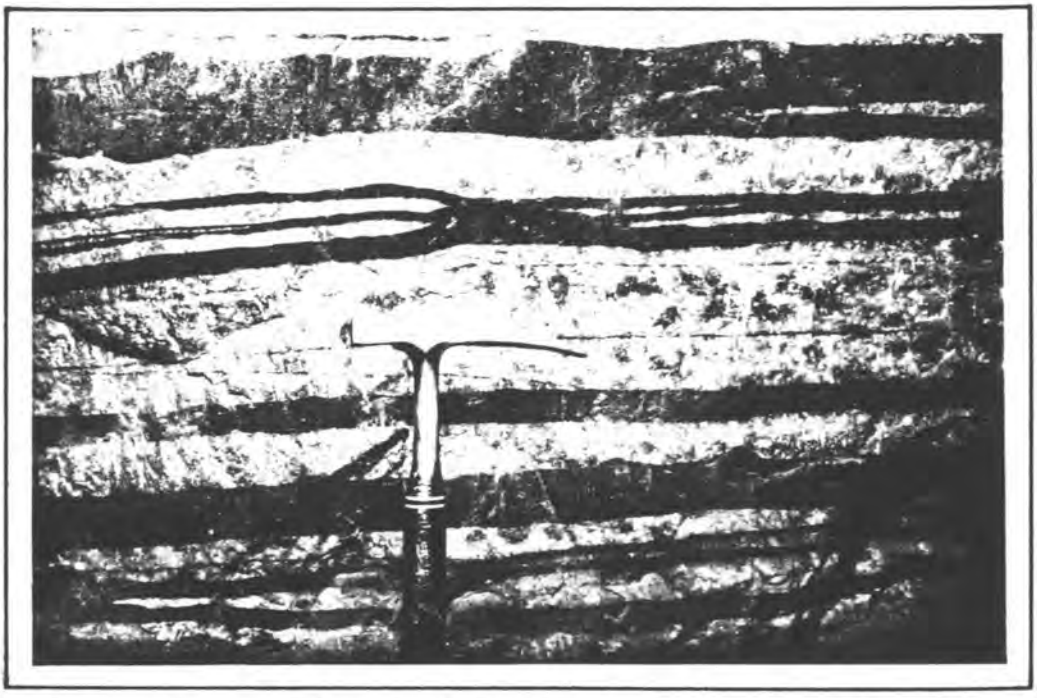

Plate 2.1b Continuous UG1 chromitite layers in the footwall anorthosite showing typical bifurcation, convergence and variable thickness of individual layers. Note the upward dimpling on the top contact of some chromitite layers. Locality - Union Section, Spud shaft 15 haulage south.

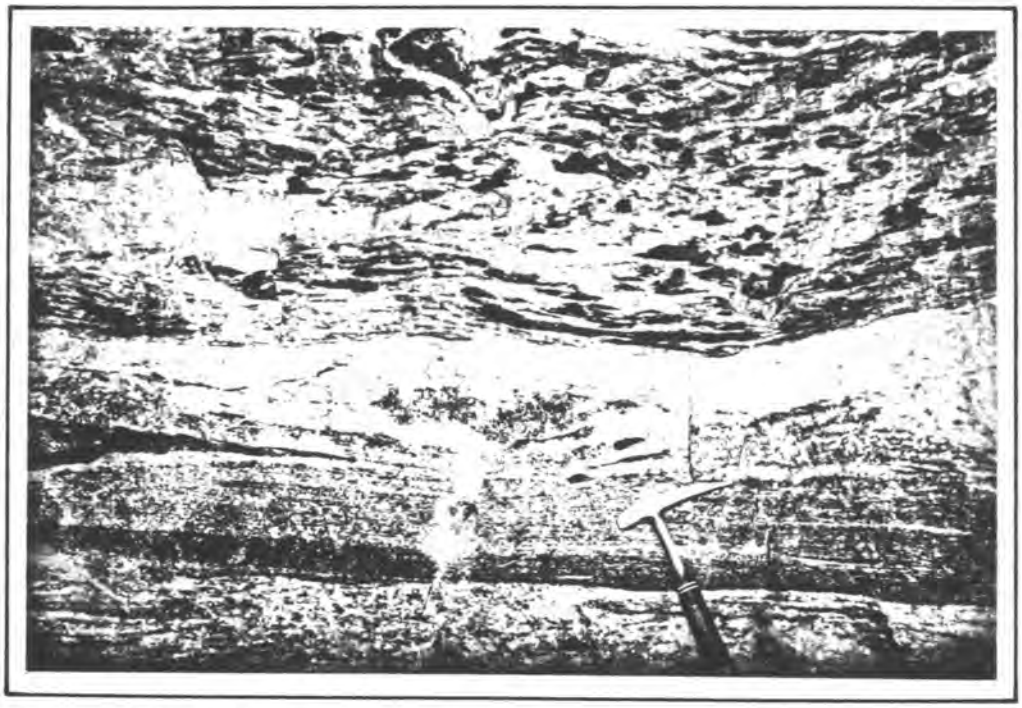

Plate 2.2a Discontinuous UG1 chromitite stringers, blebs and lenses within the anorthosite overlying fine-scale layered leuconorite. Locality - Union Section, Spud shaft 15 haulage south.

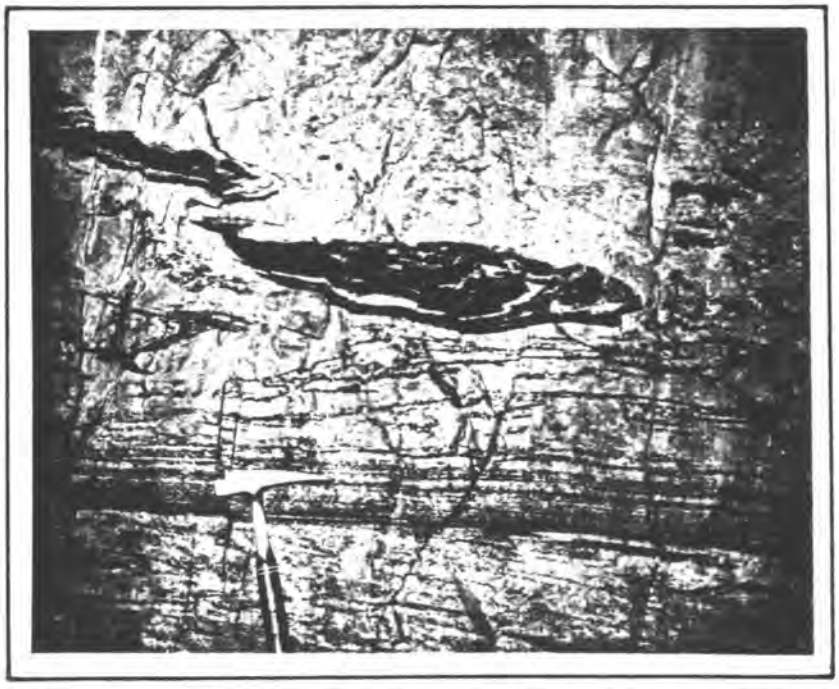

Plate 2.2b Slumping and flow-folding of discontinuous UG1 chromitite through the anorthosite. A zone of distorted layering, above well-layered leuconorite, occurs below the chromitite slump structure. Locality - Union Section, Spud shaft 15 haulage south.

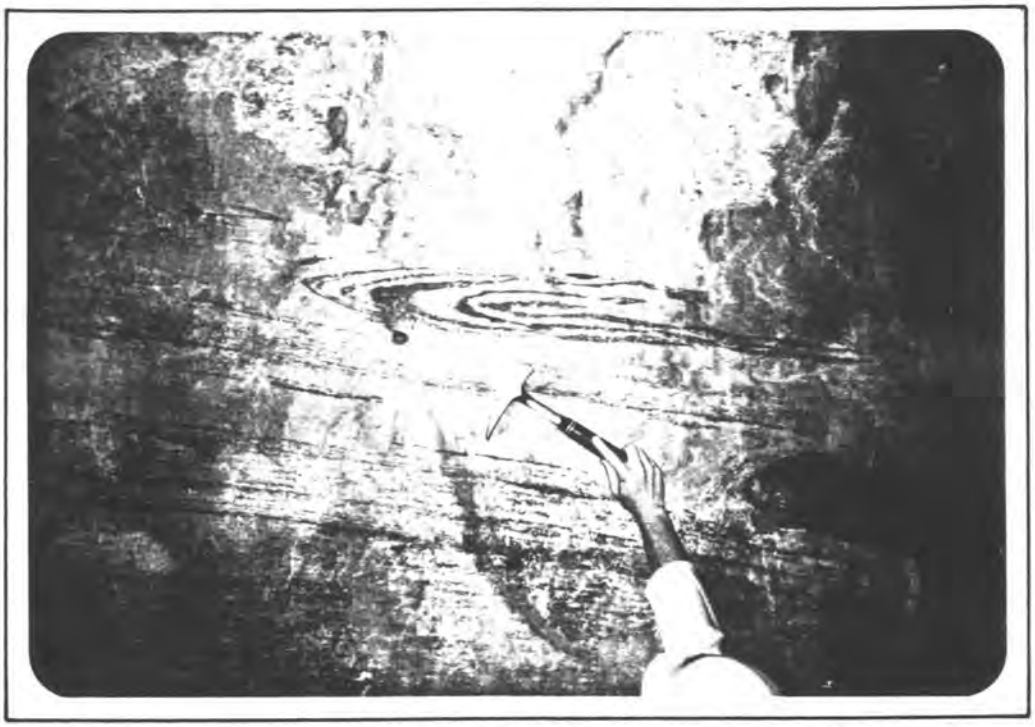

Plate 2.3a Overturned layer of cumulus orthopyroxene and chromite within the UG1 footwall anorthosite. Note the larger chromitite fragment above well-layered leuconorite on the right of the picture. Locality - Union Section, Richard shaft, 20 level station crosscut.

Plate 2.3b Fragmented xenoliths of continuous UG1 chromitite layers juxtaposed with contorted discontinuous chromitite layers within anorthosite. This texture suggests that at least two stages of deformation took place after crystallisation of the chromitite. Locality - Union Section, Richard shaft, 20 level station crosscut.

Plate 2.4a Chromitite pod (with a high concentration of orthopyroxene) rimmed by anorthosite (white). This pod has disrupted and truncated the regular mm-scale layering of the uppermost UG1FW Unit leuconorite (4m below the UG1 chromitite layer). Note the flow-fold in the lower left of the picture. Locality - Union Section, Spud shaft 15 haulage south.

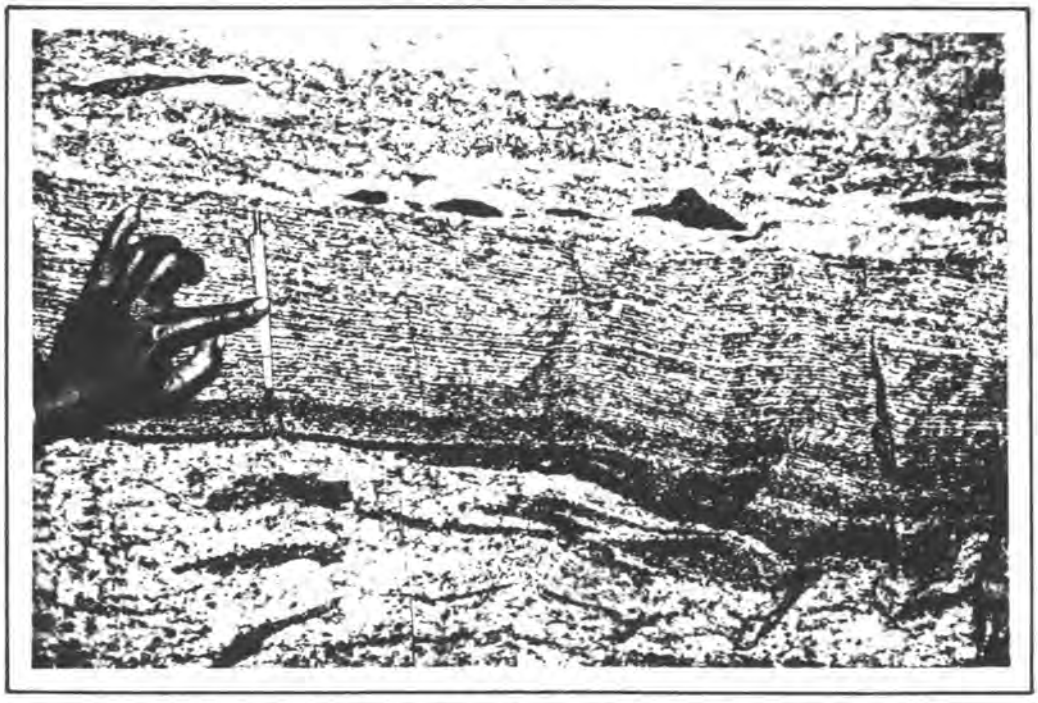

Plate 2.4b Fine mm-scale layering of cumulus orthopyroxene in the uppermost leuconorite of the UG1FW Unit (4m below the UG1 chromitite). Note the small irregular lenses and blebs of chromitite in a more anorthositic layer above the well-layered leuconorite. Locality - Union Section, Spud shaft 15 haulage south.

Plate 2.5a Norite c. 20m below the UG1 chromitite showing trough and cross-bedding features within the layering. Locality - Union Section, Richard shaft, 10 level station crosscut.

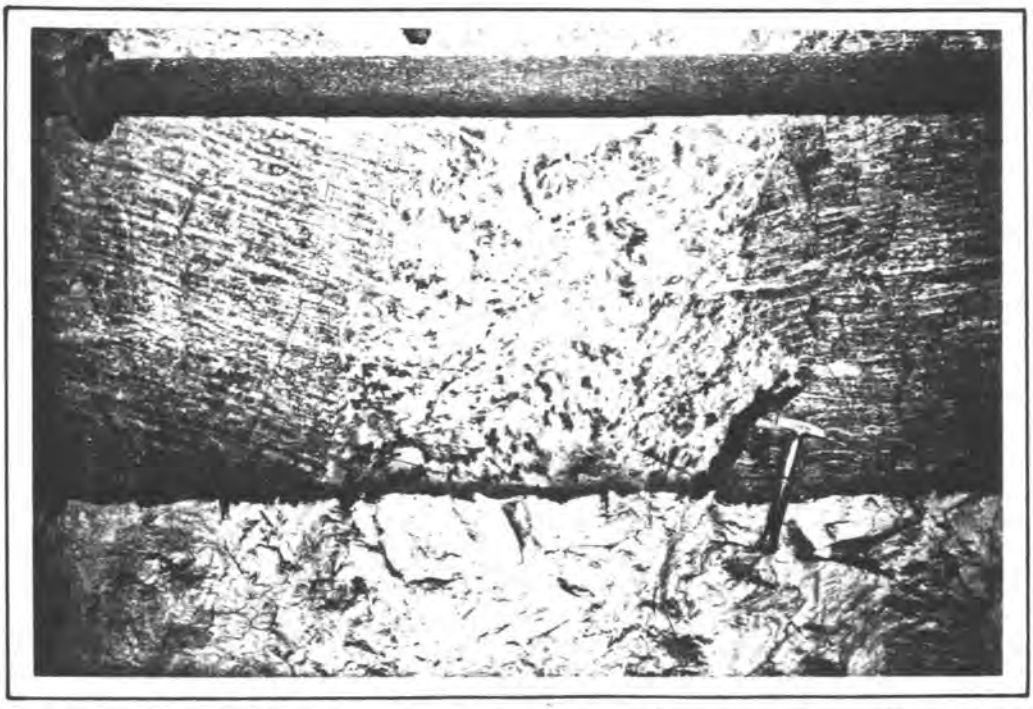

Plate 2.5b Layered norite 30m below the UG1 chromitite disrupted by the introduction of mottled anorthosite. Locality - Union Section, Spud shaft 20 level crosscut east.

The upper half of the UG1FW Unit comprises a leucocratic suite of rocks, mainly leuconorites, norites and anorthosites. An upper layer of chromitiferous anorthosite (2-3m thick) rests upon some 5m of what is locally known as the "Streaky Norite", displaying mm-scale layering (Plates 2.2, 2.3a and 2.4). Beneath this is a second couplet of Cr-poor anorthosite (c. 31% Al_2O_3) and leuconorite resting on approximately 130m of norite alternating with leuconorite and minor pyroxenite. This norite is well layered, although not on the fine scale illustrated in Plate 2.4b, and also displays trough and cross-bedding features (Plate 2.5a). Irregular, discordant mottled anorthosite bodies occasionally disrupt this layered norite as well (Plate 2.5b). The norite grades downwards via c. 20m of pyroxenite alternating with melanorite (7-10% Al_2O_3) to a 115m-thick sequence of pyroxenite (<6.5% Al_2O_3) which is floored by the MG4 chromitite. In this part of the Complex the total thickness of this UG1FW Unit (285m) is appreciably greater than that of other cyclic units such as the Footwall, Merensky and Bastard Units, which are 18, 25 and 63m thick respectively.

Some of the field characteristics of this sequence are implicit in the variations in whole-rock Al_2O_3 and normative mineral levels shown in Figure 2.2. These are:-

* the existence of a continuum of compositions between pyroxenite and anorthosite, but with a dominance of pyroxenites (<6.5% Al_2O_3) and norites (11-21% Al_2O_3);
* gradations from one horizon to another, as from pyroxenite to norite (160m to 130m), pyroxenite to leuconorite (125m to 94m) and melanorite to anorthosite (57m to 8m); and
* gradual but sustained increases in proportions of pyroxenes with stratigraphic height within parts of the sequence, e.g. between 330m (norite) and 300m below datum (pyroxenite), or between 94m (leuconorite) and 57m (melanorite).

The sequence between the top of the MG3 and the base of the MG4 chromitites is essentially an upward gradation from norite (27.5m thick) to pyroxenite (16.0m thick) followed by a rapid transition to anorthosite within the uppermost 1.2m. This forms the immediate footwall to the MG4

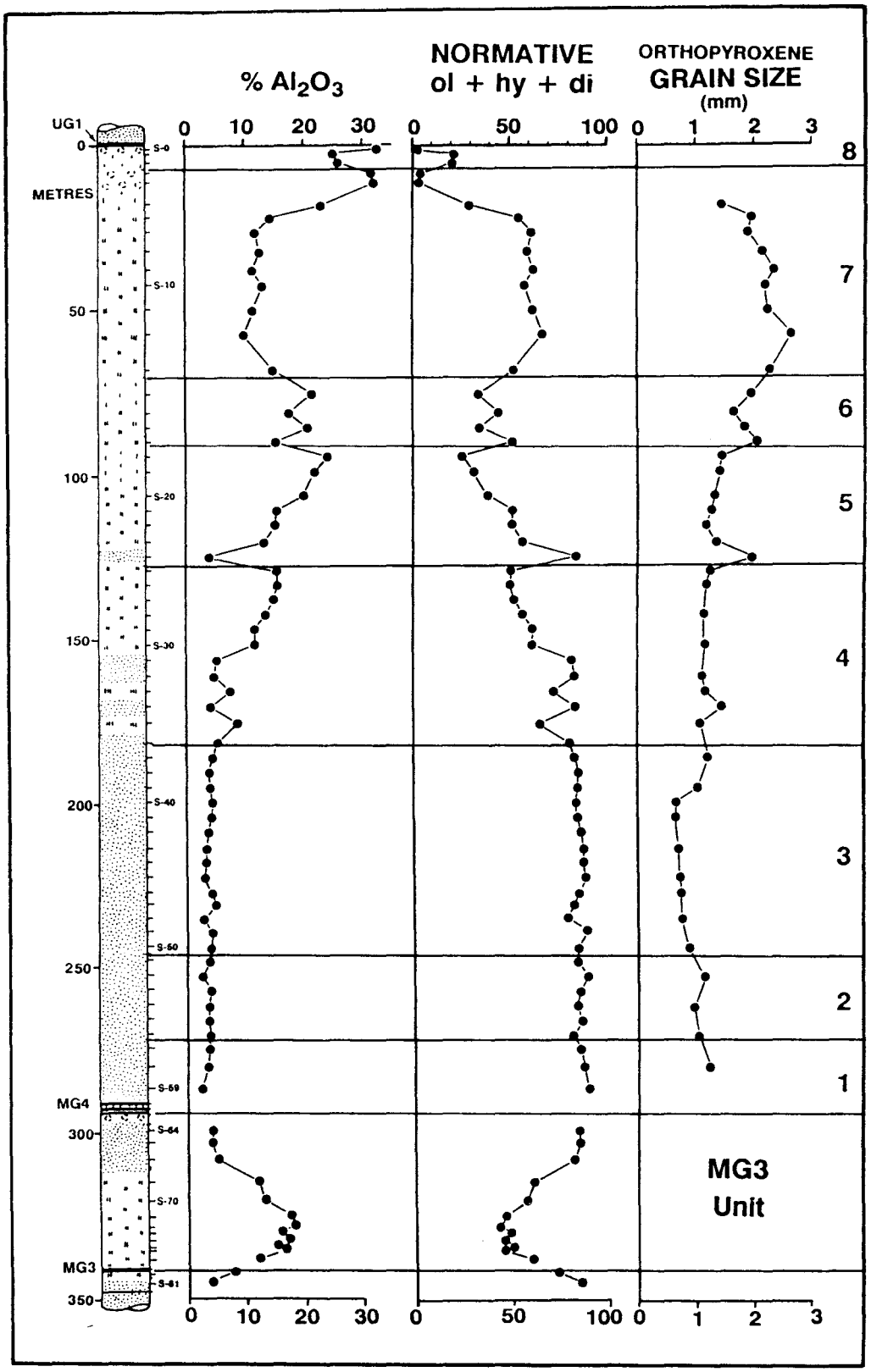

Figure 2.2 Variations in Wt. $\%Al_2O_3$, normative ol + hy + di, and grain size of orthopyroxene from below the MG3 through the MG3 and UG1FW Units. Subdivisions of the UG1FW Unit are based on data presented later and stratigraphic height is given in metres below the UG1 chromitite layer. Redrawn, with additions, from Eales et al. (1990a).

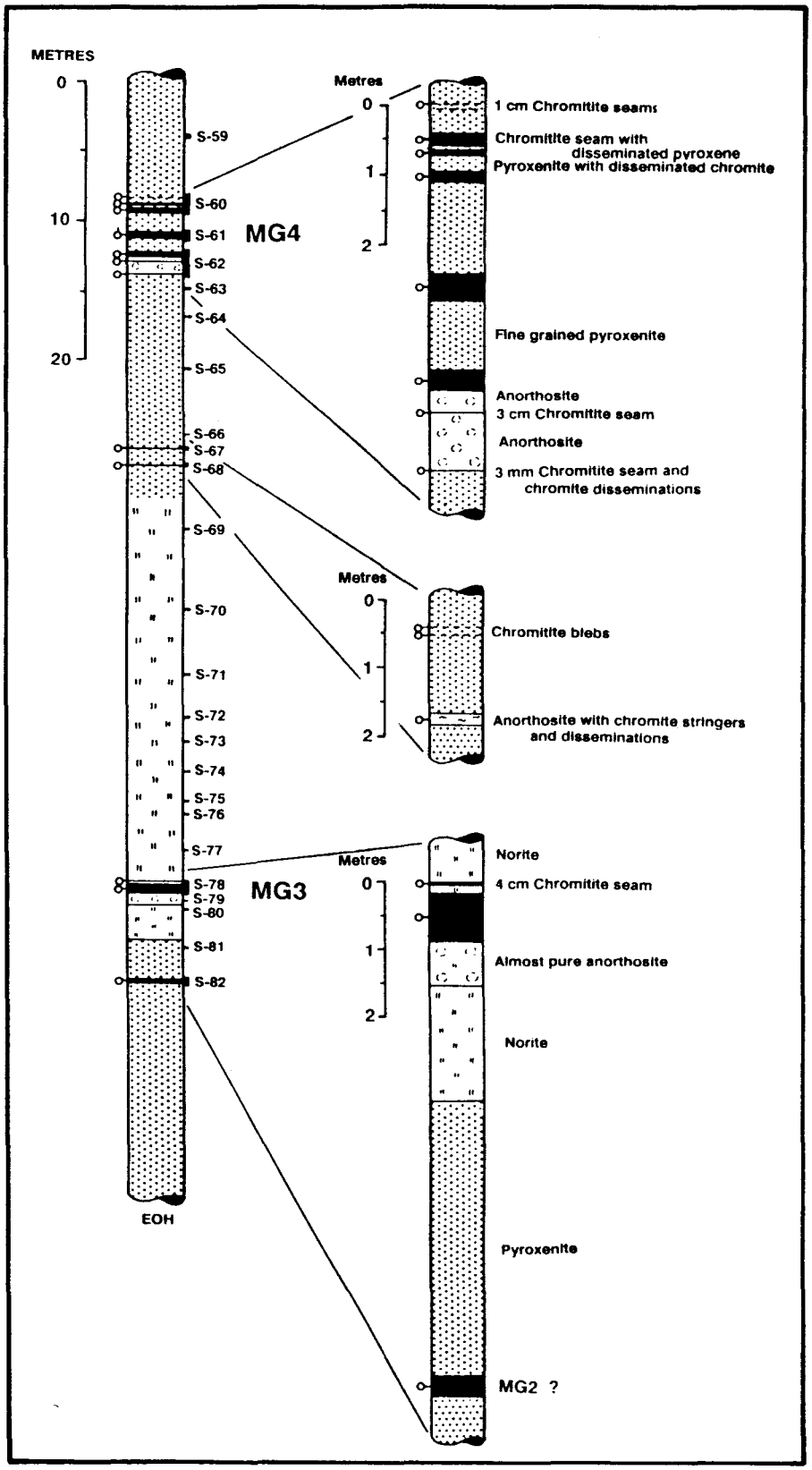

Figure 2.3 Stratigraphic detail of the Middle Group chromitite layers exposed in underground workings at Spud shaft (20 level). Additional information was obtained from two underground boreholes in the same vicinity. Sample positions are indicated on the right of the column while open circles on the left indicate chromite occurrences - either robust layers or less compact disseminations.

chromitite (Figure 2.3). The entire sequence from the base of the MG3 chromitite to the base of the MG4 constitutes the **MG3 Unit.** The sequence of rock types in this unit is anomalous in terms of the normal succession one finds in other Upper Critical Zone units where mafic lithologies at the base becomes more leucocratic upward. A more detailed account of this part of the succession is presented in Eales, de Klerk and Teigler (1990b).

A similar rapid transition (see Figure 2.3) occurs immediately beneath the MG3 chromitite where pyroxenites grade upward into norites and anorthosites which form the footwall of the MG3 chromitite. A thin (32cm) chromitite with sharp upper and lower contacts occurs within the pyroxenite 6.4m below the base of the MG3 chromitite. It is not known whether this chromitite constitutes all or part of the MG2 chromitite layer as the underground borehole was terminated at this point.

Justification for treating the entire sequence between the MG4 and UG1 chromitite as a single unit, despite its great thickness of 285m, lies, first, in its correspondence with the sequence chromitite-pyroxenite-melanorite-norite-leuconorite-anorthosite which is so characteristic of cyclic units elsewhere, and, second, in the internal coherence of geochemical parameters which distinguish it from units above and below. These parameters include the difference in V and Cr concentrations in the MG3 and the UG1FW Units (Figure 2.17) and the marked breaks in the trends of whole-rock $Mg/(Mg+Fe^{2+})$ atomic ratio (hereafter abbreviated to the MMF_{WR} ratio), and Ni/V, Cr/Co and Ni/Sc ratios which also occur at the level of the MG4 chromitite layer (Figures 2.10 and 2.16).

The following reasons are given for defining the interval between the MG3 and the MG4 chromitites as a single unit.

a) There is a steady decline in Al_2O_3 with a concomitant increase in the MMF_{WR} ratio up to the MG4 chromitite (Figures 2.2 and 2.10). With this is coupled essentially uniform levels of Ni/V ratios (Figure 2.16) which span a range of values that does not overlap with that found in the UG1FW Unit.

b) Significant shifts in Cr_2O_3 levels in orthopyroxene and values of whole-rock MMF_{WR}, FeO/TiO_2, Ni/V and Cr/Co ratios occur across the MG4 chromitite layer (Figures 2.4, 2.10 and 2.16).

c) Regression analysis of whole-rock V against MgO (Figure 2.17) yields different linear models for the rocks above and below the MG4 chromitite; the UG1FW Unit is clearly enriched in V relative to the MG3 Unit. A similar effect is seen in the plot of Cr against MgO which indicates a relative Cr depletion within the UG1FW Unit. These differences are seen in samples with less than 3000ppm Cr, indicating that the effect cannot be attributed to disseminated chromite.

The MG3 Unit, thus defined, ends with a norite-anorthosite layer (1.2m thick) and the UG1FW Unit therefore commences with a chromitite layer.

2.3 Petrography.

Rock types within the MG3 and UG1FW Units have a relatively simple mineralogy with orthopyroxene and plagioclase feldspar being the dominant minerals. Clinopyroxene, chromite and magnesian biotite, in various modal proportions, are less common. Olivine is absent. High concentrations of chromite at the bases of both units yield the MG3 and MG4 chromitite layers. These chromitites have varying proportions of silicate minerals present. The upper and lower contacts of individual chromitite layers (with either pyroxenite or anorthosite) are commonly gradational where the concentration of disseminated chromite decreases away from the chromitite layer. Within the pyroxenites, poikilitic clinopyroxene may form dark spots up to 0.5cm in diameter which enclose all older phases (Plate 2.6a), and in some instances replace orthopyroxene.

Clinopyroxene may partially rim orthopyroxene in the norites and be optically continuous with exsolved blebs within the cumulus orthopyroxene. Mica is invariably intercumulus. Accessory chromite is absent throughout most of the UG1FW Unit in contrast with its ubiquitous occurrence in the overlying UG1, UG2, Merensky Footwall and Merensky Units. Only between 210-250m, and immediately above the MG4 chromitite are traces of chromite found. Thin layers of disseminated chromite are also found in the norites above the MG3 chromitite (Figure 2.3).

Grain-size measurements for cumulus orthopyroxene crystals plotted against stratigraphic height are presented in Figure 2.2 (after Eales et al., 1990a). Here the mean value of the long intercept of between 30-60 orthopyroxene grains, intersected on a rectilinear grid in each thin section, is used in the plot. A range of 0.63-2.65mm is displayed. The more fine grained rocks, i.e. those with a grain-size of 0.6-1.25mm, are pyroxenite adcumulates with well developed 120° triple junctions and low feldspar contents. The overlying noritic rocks are distinctly coarser grained (1.15-2.65mm) and have poorly developed crystal shapes. Geochemical evidence for subdividing the UG1FW Unit into sub-cycles is presented later, but Eales et al. (1990a) note that there is a relative depression of grain sizes within those sections (260-270m, 200-230m, 130-165m, 100-115m and 20-50m) where geochemical ratios have more primitive values.

Leuconorites and anorthosites constitute the upper 20m of the UG1FW Unit. Here the cumulus orthopyroxene is clearly visible in hand specimens of leuconorites ("spotted anorthosites") but the true anorthosites with >28% Al_2O_3 only have minor amounts of intercumulus pyroxene. Where present, the intercumulus pyroxene displays a poikilitic habit that typifies "mottled anorthosite". The grain size of these rocks is normally 0.5-3mm and a preferred orientation of feldspar laths, parallel to the layering, may be adopted.

A most significant feature of the entire column is the ubiquitous occurrence of small plagioclase inclusions within orthopyroxenes of both pyroxenites (Plates 2.6 and 2.7) and norites (Plate 2.8). These inclusions are commonly 0.02-0.25mm in diameter and spheroidal, ovoid or irregularly embayed. The number of inclusions within any one host orthopyroxene grain is variable between 0 and 20 with no sample being free of these inclusions. Occasionally the inclusions form small clusters (Plates 2.6 and 2.6a) and the distribution and orientation of the inclusions is random within the host grain. Rare grains of orthopyroxene have cores which are devoid of inclusions (Plate 2.9a). The shapes of the inclusions are atypical of plagioclase within noritic rocks and the intergrowth cannot be compared with ophitic texture or with the fabric adopted by intercumulus pyroxenes within anorthosites. The texture seen here implies

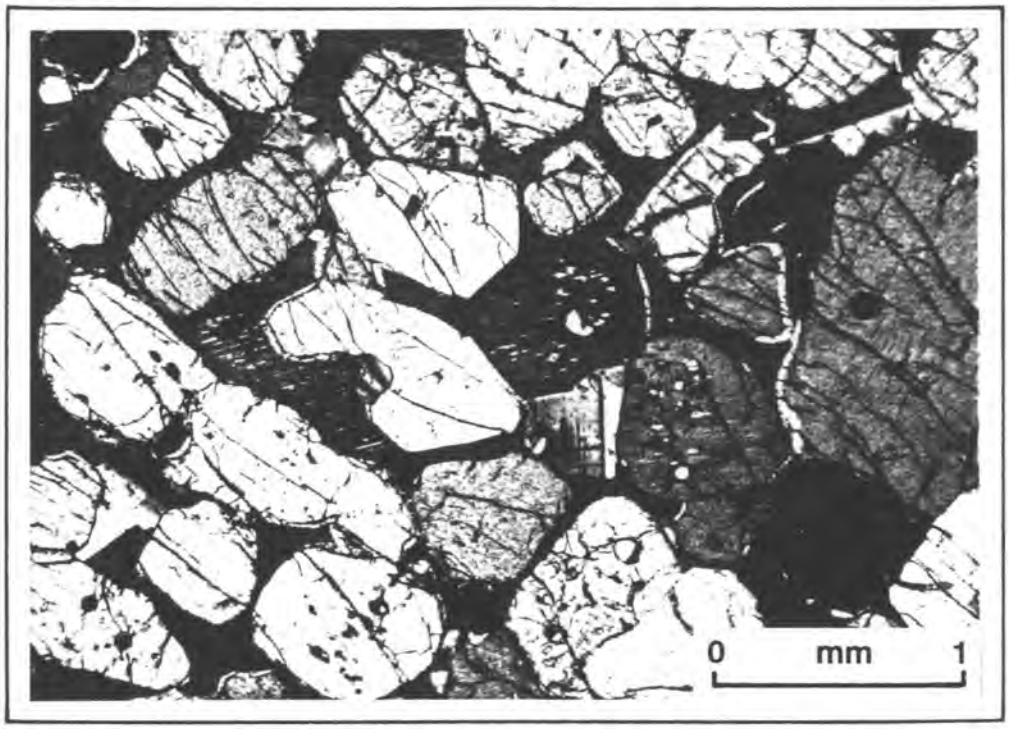

Plate 2.6a A large optically continuous crystal of intercumulus poikilitic clinopyroxene in a pyroxenite (S-52). This oikocryst of clinopyroxene encloses cumulus orthopyroxene and intercumulus plagioclase grains. Note the numerous small plagioclase inclusions within the orthopyroxene grains.

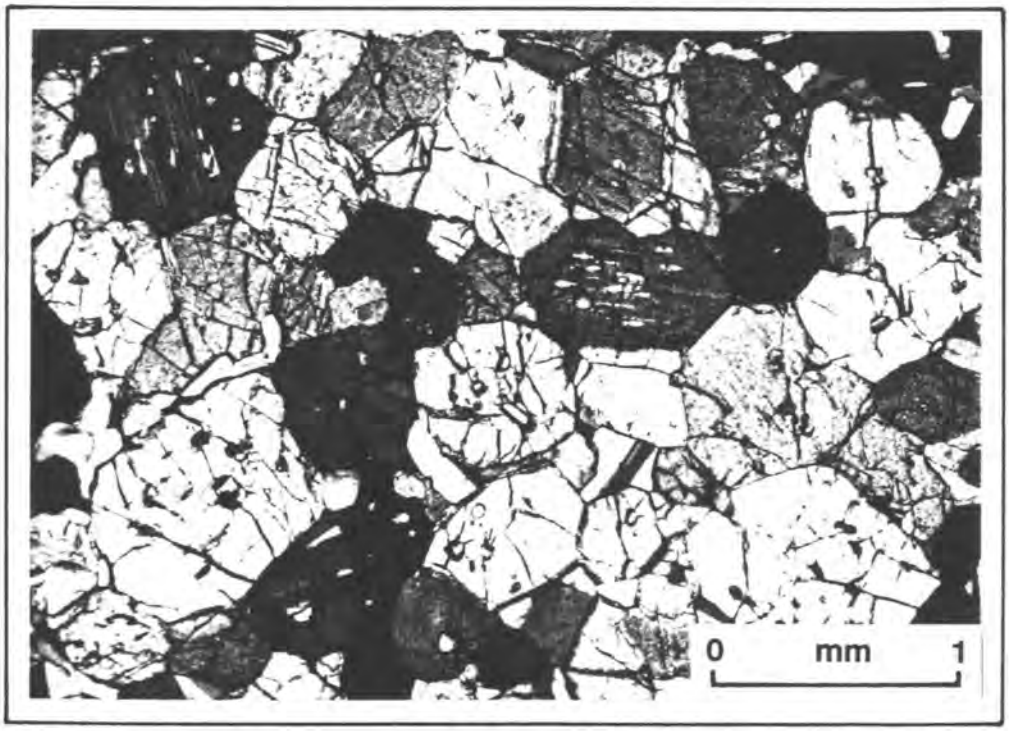

Plate 2.6b Adcumulus pyroxenite (S-40) showing the numerous irregularly shaped plagioclase feldspar inclusions in orthopyroxene. These inclusions are quite distinct from the larger intercumulus plagioclase grains and they tend to occur in small clusters.

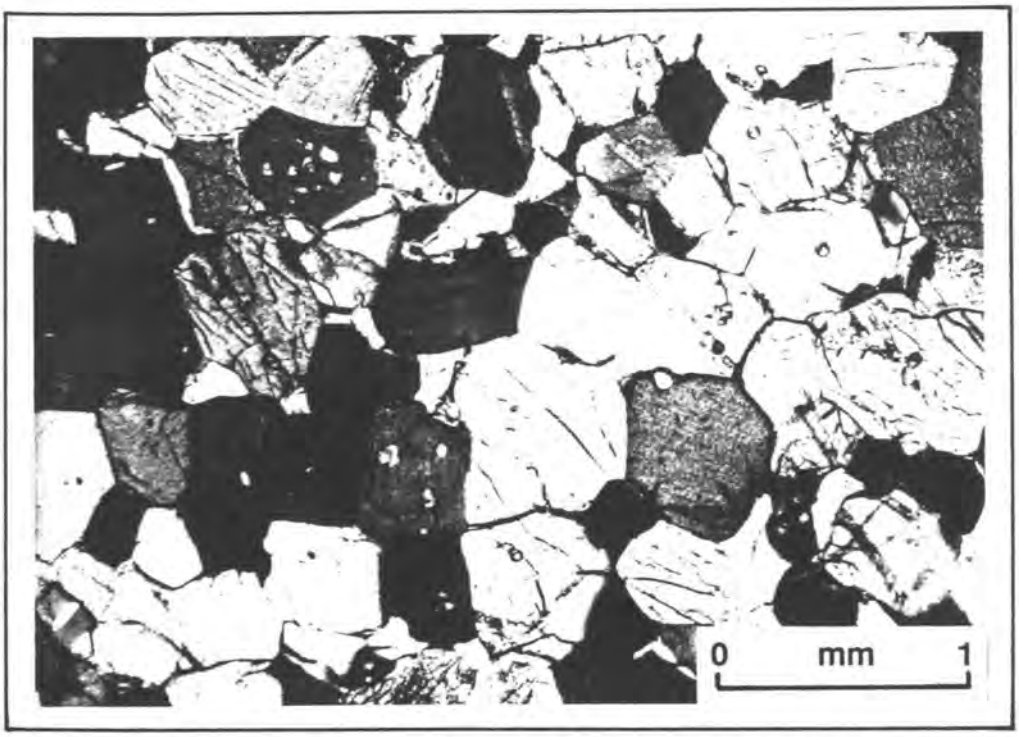

Plate 2.7a Pyroxenite adcumulate (S-44) showing advanced resorption of relict plagioclase feldspar. Inclusions are small and, in adcumulates, single inclusions may indent adjacent orthopyroxene grains.

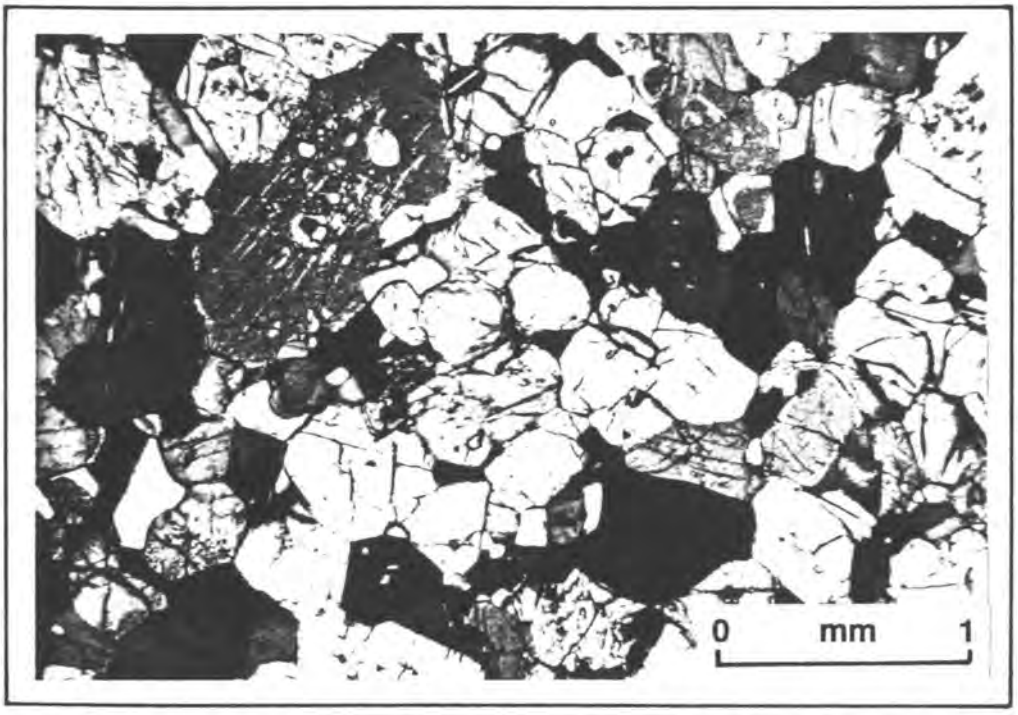

Plate 2.7b Orthocumulus pyroxenite (S-41) showing the typically high density of plagioclase inclusions and exsolved clinopyroxene lamellae in the cores of orthopyroxene grains, surrounded by a clear zone devoid of inclusions.

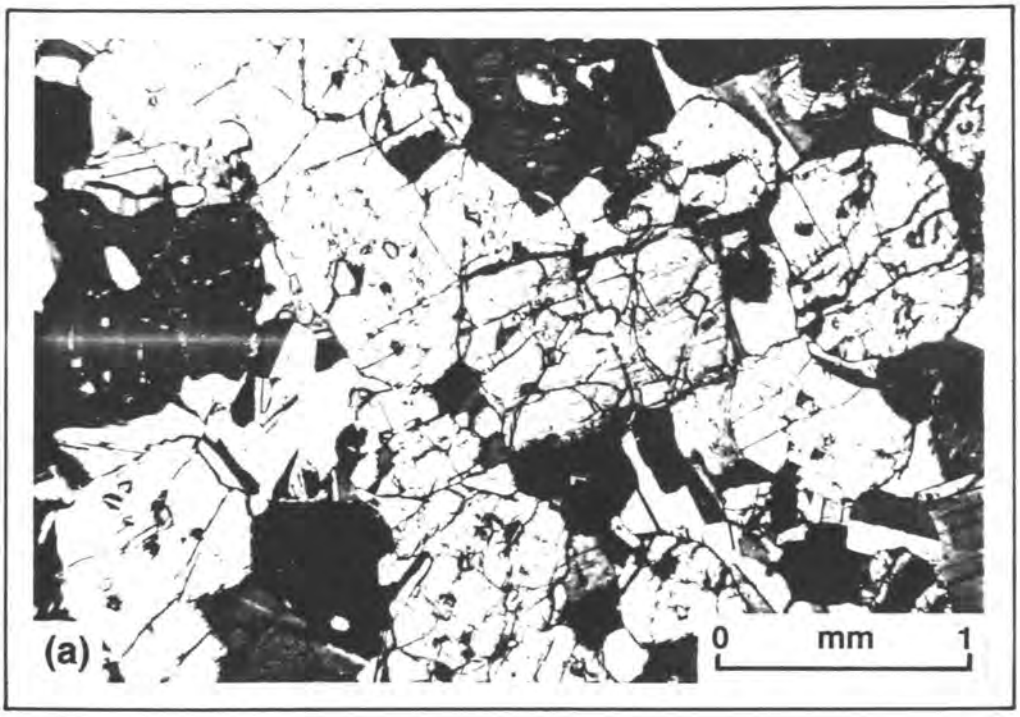

Plate 2.8 Cumulus orthopyroxene grains enclosing numerous ovoid and embayed plagioclase inclusions in (a) melanorite, S-33 and (b) norite, S-21 (uncrossed nicols).

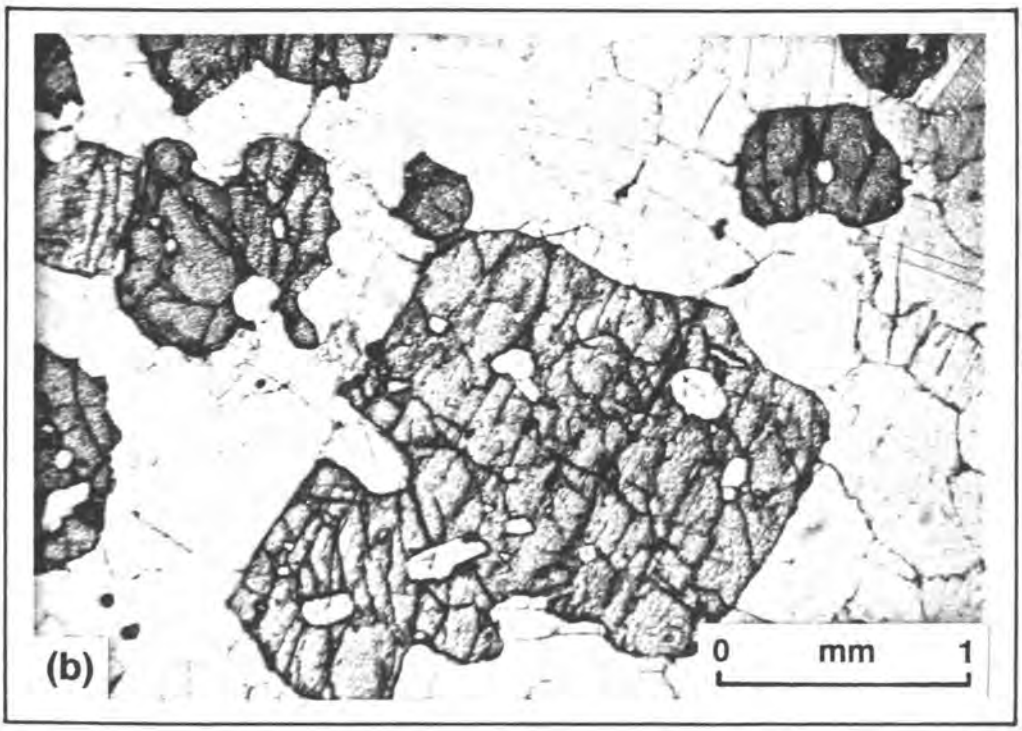

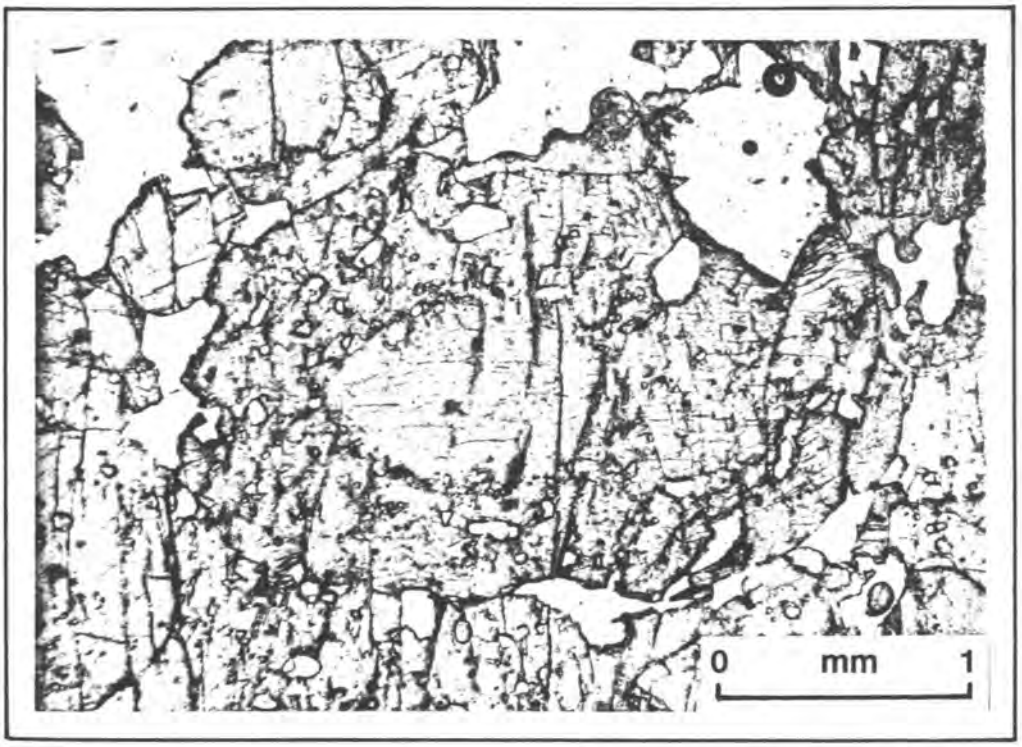

Plate 2.9a An unusual type of zoned orthopyroxene grain with a clear core surrounded by a zone containing c. 80 partially resorbed plagioclase inclusions of various sizes (pyroxenite S-37; uncrossed nicols).

Plate 2.9b Pyroxenite (S-40) enclosing a cluster of cumulus plagioclase feldspar grains. These cumulus feldspar clusters yielded Sr-isotope signatures which are different to other single large plagioclase grains and to the pyroxene fraction.

partial resorption of feldspar within a melt which subsequently crystallised orthocumulus and adcumulus pyroxenites. Plausible mechanisms whereby these relict plagioclase grains became incorporated within ultramafic assemblages are discussed in **2.4.3.**

A further variety of plagioclase occurs in the form of rare laths up to 1.5mm in length or clusters up to 2.5mm embedded in some pyroxenites (Plate 2.9b). Isotopic evidence presented in Eales et al. (1990a) has established that these larger grains and clusters are cumulus xenocrysts. The pyroxenites, therefore, have three textural varieties of plagioclase present (a) inclusions within cumulus orthopyroxene (intragranular); (b) cumulus xenocrysts (intergranular) and (c) intercumulus plagioclase. This texture is interpreted as unequivocal evidence for nucleation of pyroxenes, leading to accumulation of pyroxenites, within melts containing partially resorbed, earlier-generation feldspar.

2.4 Mineral chemistry.

Electron microprobe analyses of the three main silicate phases - orthopyroxene, clinopyroxene and plagioclase feldspar were performed on selected samples taken from below the MG3 chromitite to the footwall of the UG1 Unit.

2.4.1 Pyroxenes.

A total of 460 microprobe analyses through the profile were made (Figure 2.4). Zonation between the crystal margins and cores is subdued throughout the profile. MMF ratios at crystal margins within the leucocratic upper part of the unit, i.e. above 180m level are, with few exceptions, lower than core values. Reversed zoning is absent in the norites of the UG1FW Unit but not uncommon in pyroxenites and samples within the MG3 Unit.

Orthopyroxenes of the UG1FW Unit do not follow the normal fractionation sequence of cryptic variation where magnesium enrichment at the base of the unit gives way to more Fe-rich varieties towards the top. Between 180m and datum the pattern observed is one of cyclical variation from a

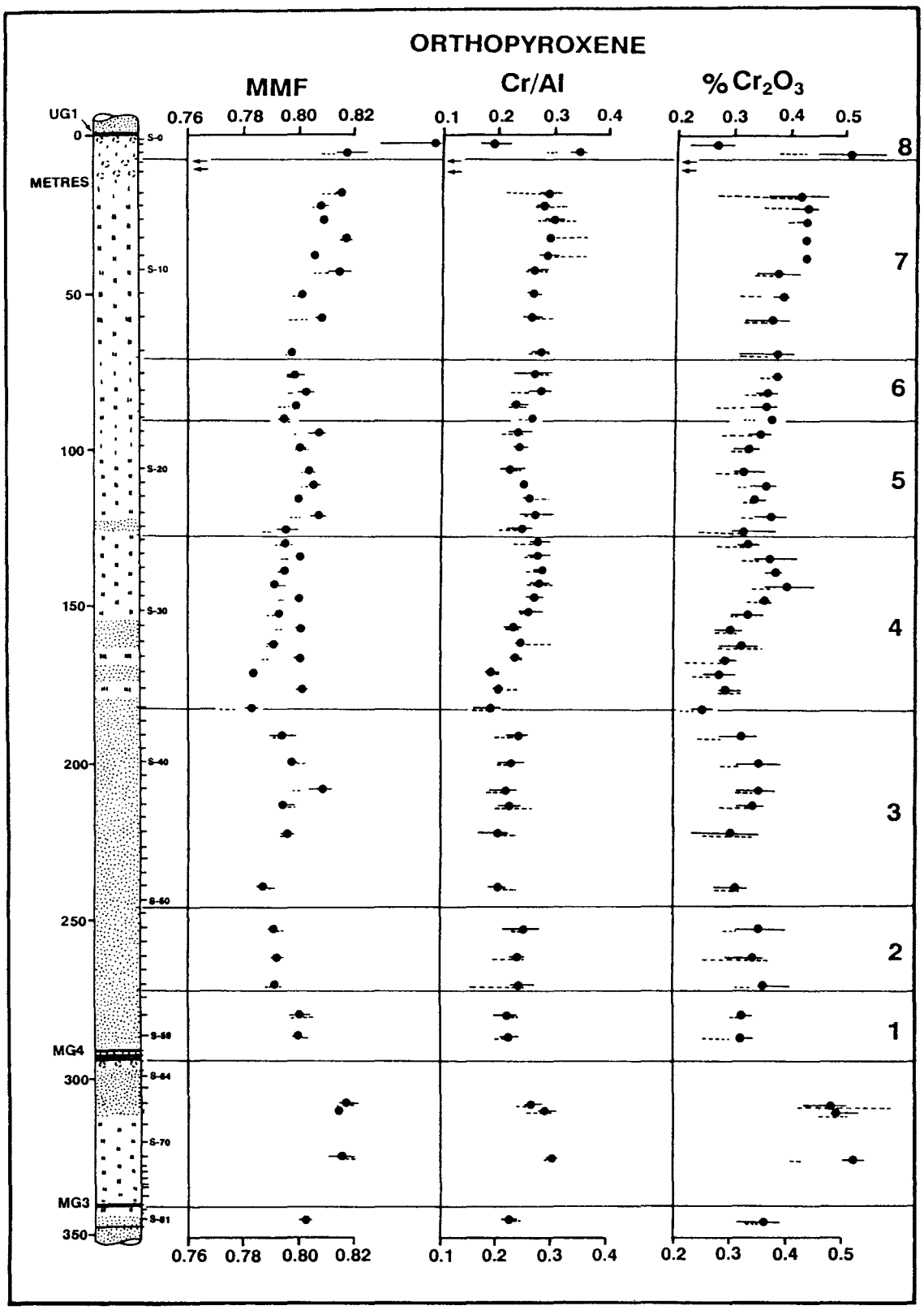

Figure 2.4 Compositional trends for orthopyroxene. Dots indicate the average compositions for grain cores while the solid bars represent the range (290 core analyses). Dashed lines indicate the range in composition for analyses done on grain margins (170 analyses). Each point represents the average of a minimum of 3 analyses; in some cases between 5 and 10 analyses have been done for each sample.

minimum average MMF of 0.783 (S-36) within the pyroxenites, increasing through the overlying norites to a peak value of c. 0.849 (S-1) below the UG1 in the leucocratic roof zone. The mean MMF ratio in norites is thus 0.800 ± 0.007, and 0.794 ± 0.007 in the underlying pyroxenites. Within the interval designated "4" in Figure 2.4, an element of bimodality is seen in the MMF ratios of orthopyroxene. This is suggestive of two populations - a more magnesian population stemming from a noritic lineage, or pyroxenitic cumulates derived from it, and a less magnesian population characterising the top of the thick, underlying, pyroxenitic suite.

MMF values within the MG3 Unit are clearly offset to higher values when compared to those above the MG4 chromitite. Here the average core MMF ratios for three samples (S-66, S-68 and S-71) are 0.816, 0.814 and 0.815 respectively. One sample below the MG3 yielded an average value of 0.802 which is similar to sample values at the base of the UG1FW Unit.

Levels of Cr_2O_3 in orthopyroxene (Figure 2.4) increase from 0.25% at 180m below the UG1 Unit to 0.43% near the top of the norite column. The average in noritic pyroxenes is 0.347 ± 0.043%, and 0.310 ± 0.028% in pyroxenites. Grain cores are in almost all cases Cr-enriched relative to the margins. The Cr_2O_3 values for orthopyroxenes in the MG3 Unit are clearly much higher (>0.45%) than those in the UG1FW Unit. Only sample S-2 at the top of the UG1FW Unit has a Cr_2O_3 value (average 0.51%) comparable to those in the MG3 Unit. Figure 2.5 shows a plot of Cr_2O_3 against MMF ratios for all samples of the UG1FW and MG3 Units and no discontinuity in trend is apparent here. Irrespective of whether the trend is due to fractionation or crystallisation from hybridised liquids, Figures 2.4 - 2.5 emphasise the anomalous increase in both Cr and Mg in orthopyroxene through the norites towards the top of the unit.

The atomic Cr/Al ratios closely follow the observed trend of the MMF ratio and the Cr_2O_3 levels in orthopyroxene. A clear pattern of oscillation is seen within the pyroxenites above the MG4 chromitite up to the 180m level where a low average of 0.19 is recorded for the Cr/Al ratio. From this point there is a distinct upward increase in the Cr/Al ratio to the top of the noritic sequence, accompanied by well defined

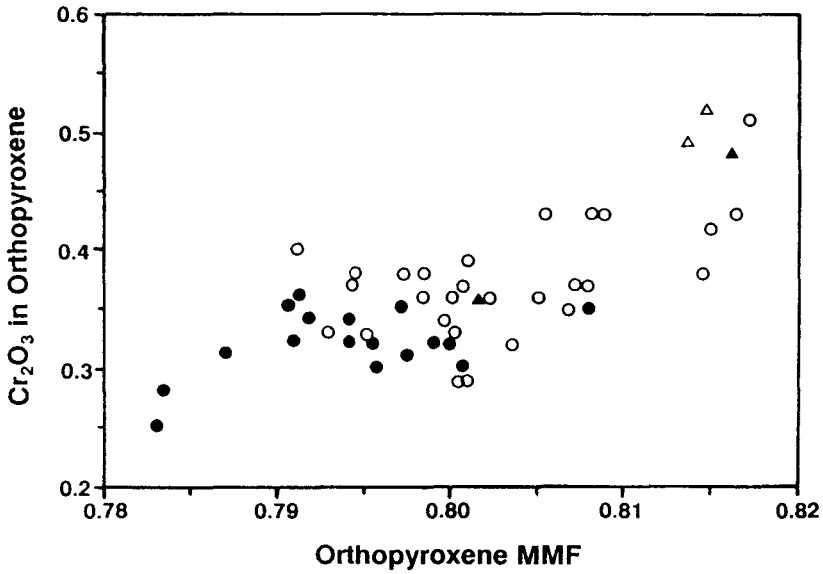

Figure 2.5 Cr_2O_3 levels in orthopyroxene within the UG1WF and MG3 Units based on averaged analyses for individual samples (total 460 analyses). Simple linear regression analysis of the data yields the linear model Cr_2O_3 = 4.92 MMF - 3.58 (cc. = 0.734, r^2 = 53.9). UG1FW Unit - circles, MG3 Unit - triangles. Solid symbols - pyroxenites: open symbols - norites.

cyclical oscillations. The general pattern through the UG1FW Unit is one of an upward increase in Cr/Al ratio. The orthopyroxene Cr/Al ratios in the MG3 Unit are marginally higher (>0.25) than those above the MG4 chromitite (<0.25).

A sharp drop in MMF ratio (to 0.62) and Cr_2O_3 levels (averaging 0.02%) occurs within the first anorthosite overlying the noritic sequence (Figure 2.4, S-3 and S-4). This follows the trends which are typical of whole-rock MMF ratios in the anorthosites of the Footwall, Merensky and Bastard Units (see Figure 3.3 and Eales et al., 1986). The uppermost leuconorite-anorthosite couplet (S-1 and S-2) is, however, remarkable in that the average MMF ratios are unusually high at 0.849 and 0.817 (Figure 2.4) while Cr_2O_3 in orthopyroxene exceeds 0.5% in the leuconorite and 0.25% in the anorthosite. The uppermost leuconorite (S-2) is thus anomalously Cr-rich but contains no accessory chromite - the overlying anorthosite (S-1) contains chromite as a major modal phase. This disseminated chromite is thought to be the result of contamination from the overlying UG1 chromitite layer. In summary, the UG1FW Unit, although

showing absolute whole-rock Cr-depletion (Figures 2.14 and 2.17) in the major part of the unit, because of modal variations, is characterised by an upward increase in orthopyroxene MMF ratios accompanied by a sympathetic increase in the Cr_2O_3 levels in orthopyroxene (Figure 2.4).

Hatton (1984) showed that reversals in the expected fractionation trend of orthopyroxenes in the eastern and western lobes of the Bushveld Complex are not the result of changes in pressure in the magma chamber. His calculations showed that unrealistically high pressure changes would be required to generate observed changes in the orthopyroxene content and he proposed the emplacement of fresh pulses of magma to account for these reversals.

The discussion above has perhaps not emphasised the fact that although clear cyclicity is seen within the sequence, the compositions of the pyroxene throughout the 350m column have a limited range. A plot of the average compositions of all the samples yields a tight grouping around En_{80} when plotted on a conventional ternary diagram (Figure 2.6). It is only in the upper three samplesof the unit, where orthopyroxene occurs as an intercumulus phase (S-1, 3 and 4), that greater compositional variability is seen.

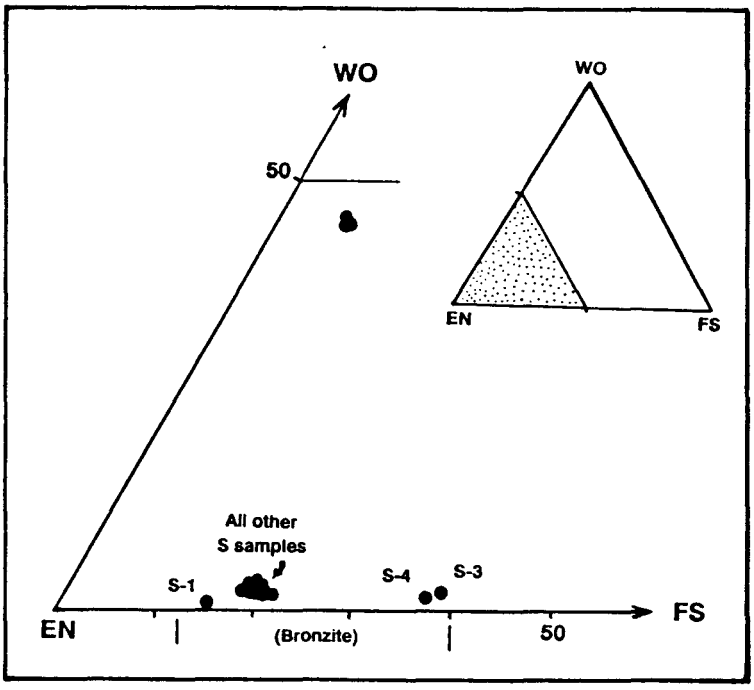

Figure 2.6 Conventional ternary diagram for pyroxene (WO - EN - FS) analyses showing the average composition recorded for both ortho- and clinopyroxenes.

The same observation is true for the clinopyroxenes which also fall in a restricted grouping (average of 12 samples). A limited study of poikilitic clinopyroxenes enclosing orthopyroxenes, and those of intercumulus habit, showed the tie-lines between the ortho- and clinopyroxenes on a conventional triangular plot to match those established for the Lower (Botha, 1987) and Upper (Atkins, 1969) Critical Zones (Figure 2.6).

2.4.2 Plagioclase feldspar.

Analyses of the cores of 448 feldspar grains, summarised in Figure 2.7, show that the range of composition is An_{57-85}. A distinction is made on a basis of plagioclase habits and accordingly analyses of the small partially resorbed inclusions within orthopyroxene are compared with cumulus and intercumulus grains within individual samples. No clear-cut distinction in composition, which would possibly indicate discrete populations, is evident. However, some bias is shown towards more sodic compositions for the inclusions when the average compositions (and the ranges) of the two habits are plotted against each other. In Figure 2.7 21 of the 25 sample pairs within the UG1FW Unit indicate a more sodic composition for the inclusions. A further feature of note is the matching trends of %An between both inclusions and non-included feldspar. Samples with notably sodic inclusions show the associated cumulus/intercumulus grains also shifted to more sodic compositions (Figure 2.8).

In Figure 2.8 the %An of plagioclase is plotted against stratigraphic height. Here the compositions of intercumulus and cumulus plagioclase are distinguished from those of the small plagioclase inclusions within the orthopyroxene. The sympathetic variation established in Figure 2.7 is seen at all levels and a clear cyclicity becomes apparent. Within the basal pyroxenites of the UG1FW Unit, sub-cycles show an upward decline of anorthite content, but above the level where cumulus feldspar enters the paragenesis (at 150m) the trends followed by felsic and mafic phases vary sympathetically. The measurement of extinction angles of the feldspar inclusions indicates that a narrow rim may encircle each inclusion. At the base of sub-cycles where feldspars are calcic this rim displays reversed zoning, but where more sodic compositions dominate zoning is either normal or absent.

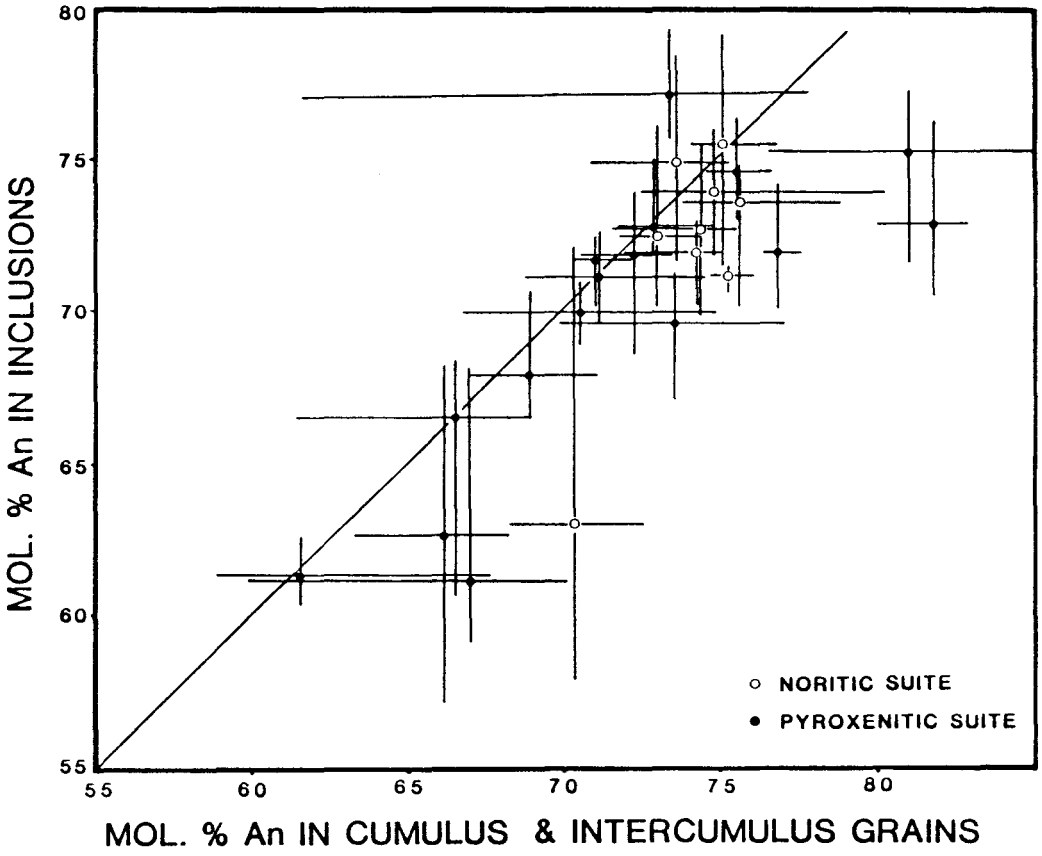

Figure 2.7 Average compositions (dots; by microprobe analysis) of cores of partially resorbed plagioclase inclusions within orthopyroxene hosts, plotted against compositions of cumulus and intercumulus plagioclase grains in the same sample. Bars represent the range in composition.

A feature recognised by Vermaak (1976), Lee (1983), Eales et. al (1986, 1988) and others is that the feldspars of anorthosites and norites at the top of well defined units of the Upper Critical Zone (like the Footwall and Merensky) are more calcic than those of both cumulus and intercumulus habits in underlying rocks. This is also true of the UG1FW Unit (Figure 2.7). Here the mean compositions of the feldspar cores are $An_{76.5-78.5}$ within the upper 25m of the unit (Sample S-1, 2, 3, 4, 5, 6 and 7). Compositions of cumulus feldspar within the underlying norites are $An_{73.5-75.6}$ while that for the intercumulus grains within the pyroxenites is commonly a further 5-10% richer in ab molecule.

An explanation as to how the relict plagioclase inclusions became incorporated within the pyroxenes is important in the interpretation of the UG1FW Unit and the following possibilities exist:

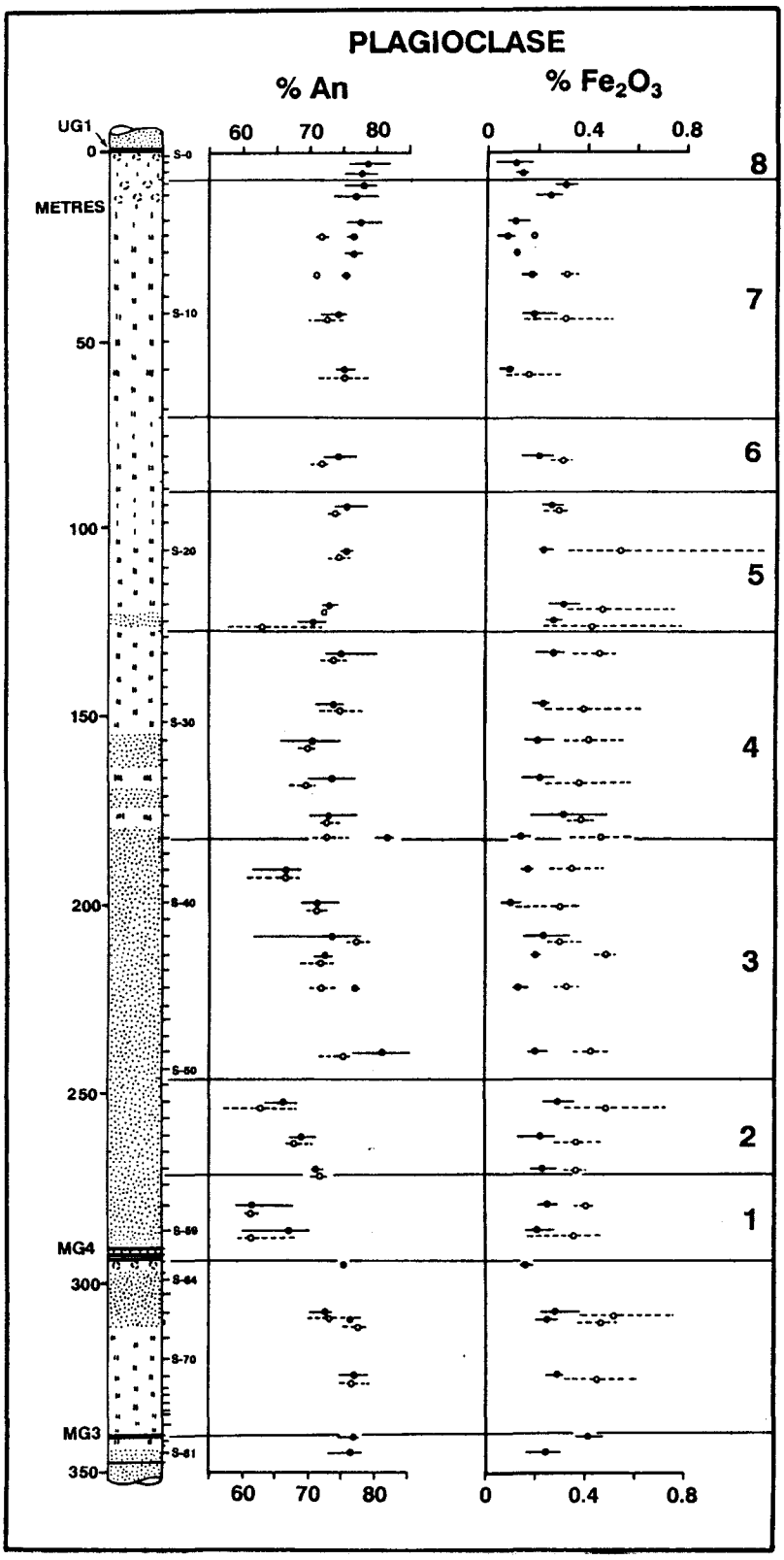

Figure 2.8 Compositional trends for plagioclase feldspars (core analyses only; 448). Solid circles and range bars represent cumulus and intercumulus grains while open circles and dashed bars indicate partially resorbed plagioclase inclusions within cumulus orthopyroxene. Each point represents the average of a minimum of 5 analyses and in many cases 10 analyses have been done per sample.

(a) Inclusions represent aberrations in the normal sequence of crystallisation of the silicate phases. The paragenetic sequence may have been inverted by spatial shifts of primary phase volumes under the influence of pressure, fO_2 or concentration of volatiles.

(b) Plagioclase nucleated within a bottom zone, enriched in the components of feldspar, following in situ crystallisation of pyroxene at or near the floor.

(c) Inclusions are the undigested remains of pre-existing feldspathic layers (anorthositic or noritic) that were disrupted during the emplacement of fresh pulses of primitive liquid.

(d) Inclusions represent plagioclase crystals that have been trapped by pyroxene crystals settled from higher liquid layers in a stratified liquid column controlled by double diffusive convection.

(e) The texture is the result of mixing of evolved (fractionated) residual liquid bearing feldspar on the liquidus, with influxes of fresh, relatively primitive mafic liquid into the chamber.

Sr-isotopic, chemical and field evidence suggest rejection of the first three models. Isotopic evidence presented in Eales et al. (1990a) showed that the feldspar population is not homogeneous and that isotopic disequilibrium prevails between the feldspar and pyroxene fractions of the rocks. Alternatives (a) and (b) do not satisfactorily account for the resorption that must necessarily have followed the initial period of growth. Alternative (b) is further weakened by the probability that compositional convection (Tait et al., 1984) would enforce rapid mixing of low-density residua with the overlying column. Inclusions are especially prominent within pyroxene grains of both pyroxenites and norites within which reversals of the MMF ratio, and increasing levels of Cr in orthopyroxene, occur with increasing stratigraphic height. These features support alternatives (d) and (e). It is considered unlikely that the small plagioclase grains would have been able to settle through the liquid. Because of their small size and low density it is unlikely that they would have been able to overcome the yield strength of the liquid. Model (e) appears to be the most plausable.

Eales et al. (1990a) note that inherent properties of the feldspar lattice render volume diffusion and compositional readjustment sluggish

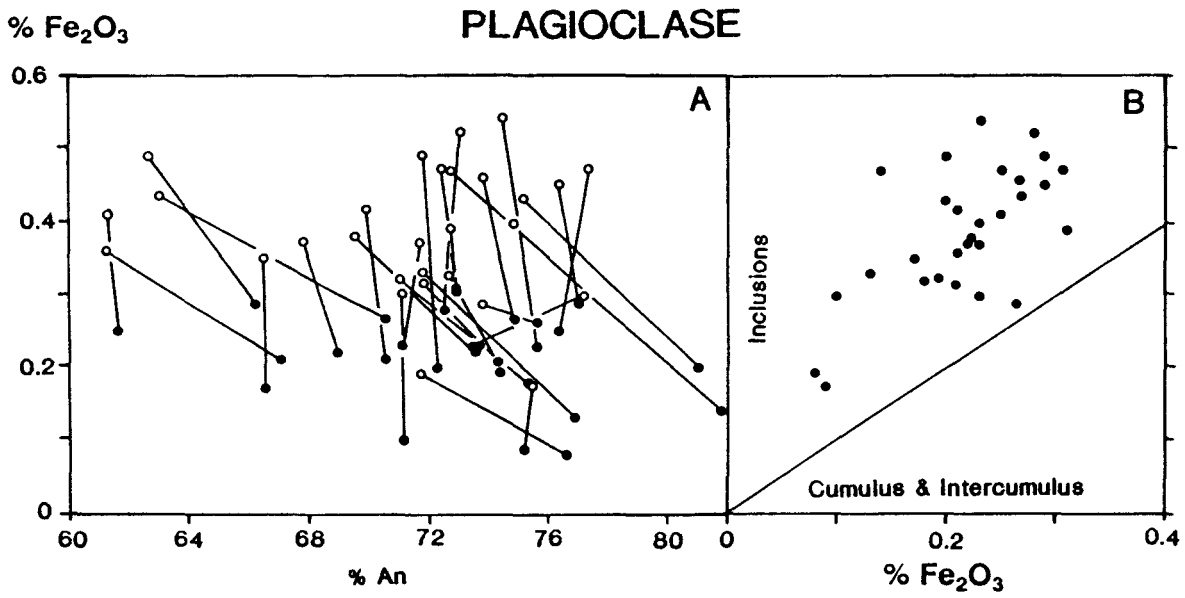

Figure 2.9 A. Plot of average wt. $\%Fe_2O_3$ in plagioclase against mol. %An for inclusions in orthopyroxene (open circles) and cumulus-intercumulus plagioclase (solid dots) in the same sample being connected by tie-lines (29 sample pairs). Note that in all cases the inclusions are iron-enriched and that in 25 sample pairs the inclusions are more sodic than the cumulus/intercumulus plagioclase.

B. Average $\%Fe_2O_3$ in the small, partially resorbed plagioclase inclusions within orthopyroxene hosts plotted against the average wt. $\%Fe_2O_3$ of the cumulus/intercumulus plagioclase grains within the same sample. In all cases (29 samples) the inclusions are iron-enriched and plot above the line representing a ratio of unity.

processes (Smith, 1974), but optimum conditions for the modification of grain compositions would be yielded by the small size of the inclusions and super-liquidus conditions implied by resorption. Consequently, the present composition of the inclusions may not represent their original compositions and the sympathetic variations in composition of feldspar inclusions and intercumulus feldspars are attributed to reaction between the inclusions and surrounding liquid.

The iron content of plagioclase throughout the profile varies between 0.5 and 0.8% Fe_2O_3 and without exception the inclusions within orthopyroxene are enriched in iron relative to associated cumulus and intercumulus plagioclase (Figure 2.9). The range of iron content within the inclusions is also larger than that for the plagioclase external to orthopyroxene.

Two possible explanations for this phenomenon are that the included plagioclase crystallised from a liquid which was iron-enriched (more fractionated), or that the higher iron content is a direct result of contamination and the influence of the host orthopyroxene and other mafic phases.

The adoption of model (e) above would imply that the original plagioclase crystals (before partial resorption) had been crystallising from an evolved fractionated liquid. This liquid by its very nature would have been more Fe-enriched and more Fe would have been partitioned into these plagioclase crystals, now seen as inclusions in orthopyroxene.

2.5 Whole-rock chemistry.

Analyses for major elements and 11 trace elements were run by XRF spectrometry on 74 samples. Whole-rock data are presented in Appendix D, with total Fe represented as Fe_2O_3 (Table D4). The original data were also recalculated to an assumed Fe_2O_3/FeO ratio of 0.1 and normalised to 100%. These data are used throughout the presentation of the results and were used to calculate the CIPW weight percent norms (Table D8). Absolute levels of individual elements are dictated by the mode and the range in composition of individual major element oxides and are best seen in the plots against MgO (Figure 2.12). Recognising that these are cumulus rocks not representative of liquid compositions, interelement ratios are also used to gain a better insight into the geochemical behaviour of these rocks. The stratigraphic variation of the mafic components in the sequence is perhaps best represented by the whole-rock MMF ratios (Figure 2.10). Other whole-rock ratios like FeO/TiO_2, Ni/V and Cr/Co are also used (Figure 2.10 and 2.17). In all cases these ratios utilise a numerator of higher and a denominator of lower bulk distribution coefficient and accordingly measure the chemical "primitiveness" of the rock.

2.5.1 Major element variations.

MMF_{WR} ratios within the sequence extending for 350m beneath the UG1 chromitite show the following features: (Figure 2.10).

a) The least primitive rock in terms of MMF_{WR} ratios is the lower of the two anorthosite layers in the uppermost 20m of the UG1FW Unit. This ratio is decoupled from the trend for feldspar compositions insofar as the most calcic plagioclase within the Unit occurs in these anorthosites.

b) There is no simple trend within the column beneath the anorthosite roof. The highest (or most primitive) MMF_{WR} ratios are encountered immediately beneath the anorthosite roof of the UG1FW Unit where values in excess of 0.80 are recorded (S-9, 10 and 11). The lowest MMF_{WR} values are recorded at 50m and 120m above the MG4 chromitite where respective values are 0.770 and 0.769 (S-49 and S-35).

c) Chemical trends through the Footwall, Merensky and Bastard Units in the northwestern limb of the Complex display a saw-tooth pattern (see Figure 3.3 and Eales et al., 1986, 1988), because rocks with primitive chemical signatures at the base of units abruptly overlie more evolved rocks at the top of previous cycles. No such pattern exists within the sub-cycles of the UG1FW Unit or the MG3 Unit.

The general pattern seen in both the MG3 and the UG1FW Unit shows an overall upward increase in the MMF_{WR} ratios. MMF_{WR} values in the immediate hangingwall of the MG3 chromitite are around 0.785-0.790 in the norite and gradually increase through the pyroxenite to 0.796 (S-64) in the footwall of the MG4 chromitite. The pattern of variation is more complex in the UG1FW Unit where a distinctive pattern of cyclicity in MMF_{WR} is observed through the sequence, and a series of partial or complete sub-cycles are defined. Each sub-cycle first shows a gradual increase in primitive character followed by a gradual decline. Eales et al. (1990a) identified eight such sub-cycles which are indicated in Figure 2.10. Sub-cycles 2-5 appear to be complete, with the rise and fall in MMF ratios (whole-rock and microprobe data) being closely matched by trends in FeO/TiO_2 (Figure 2.10), Ni/V and Cr/Co ratios (Figure 2.16), and Cr_2O_3 levels in orthopyroxene (Figure 2.4). This subdivision of the UG1FW Unit

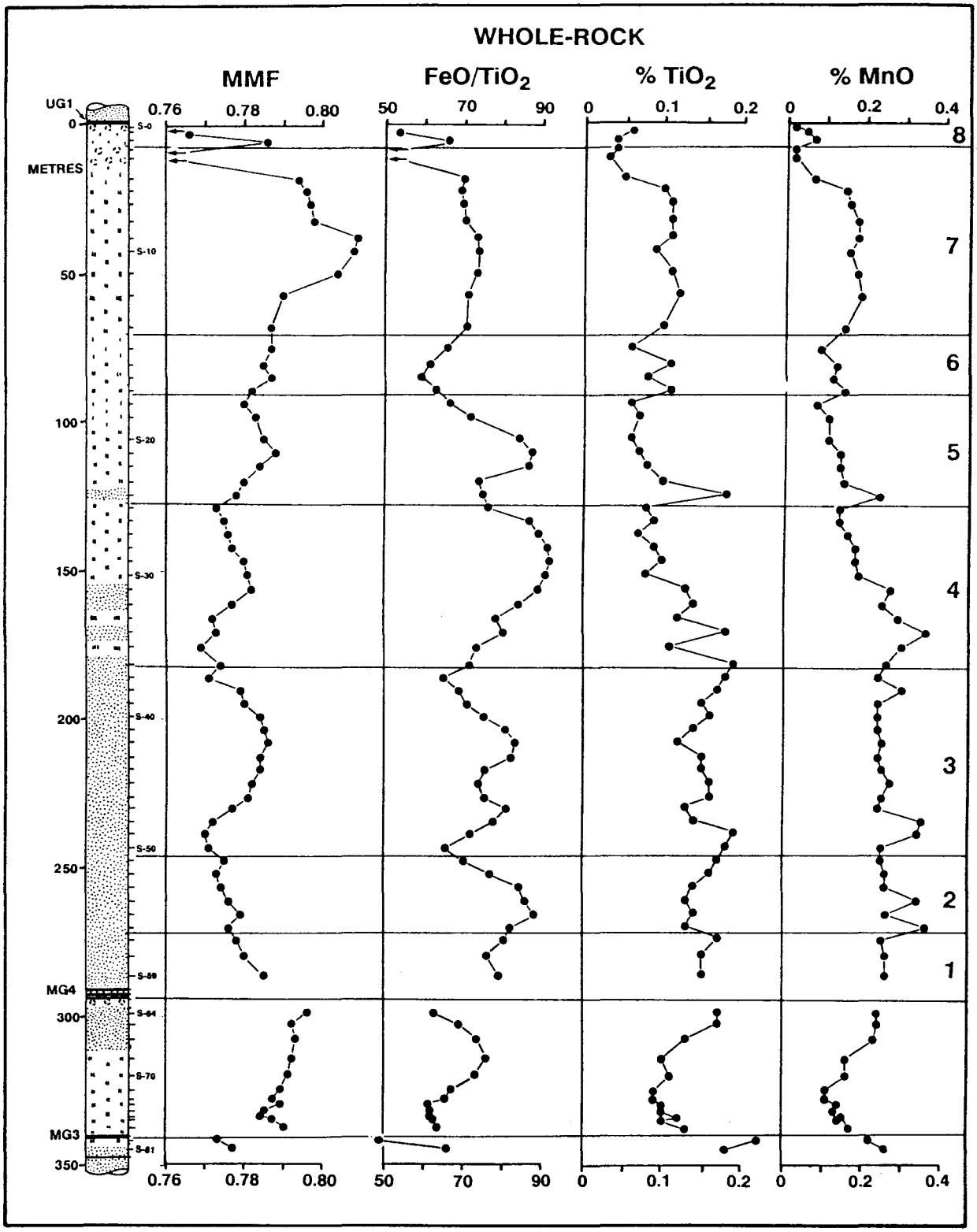

Figure 2.10 Stratigraphic variations of whole-rock data through the MG3 and UG1FW Units. The first two profiles of whole-rock ratios have been smoothed in part by employing three-point moving averages. Here the ratios of MMF_{WR} (atomic Mg/(Mg+Fe) where all Fe is expressed as Fe^{2+}) and FeO/TiO_2 are shown as well as the oxides TiO_2 and MnO (Wt.%). Arrows indicate data points off scale.

conforms with that indicated by cyclic variations in feldspar compositions described earlier, but Ni/V, Cr/Co and FeO/TiO_2 ratios, and feldspar data suggest that sub-cycle 3 is probably composite (see summary Figure 2.20).

Values of TiO_2 in both the MG3 and UG1FW Units never exceed 0.2%, with the pyroxenites all having values in excess of 0.12%. The upper noritic assemblage displays values below 0.12% (Figure 2.10 and 2.12). This level continues to decrease upward in the sequence to c. 0.05% in the leucocratic footwall of the UG1 chromitite. The norite (S-79, 0.22%) and pyroxenite samples (S-81, 0.18%) in the footwall of the MG3 do display marginally higher levels than in the overlying two units. Generally the overall trend is one of increasing TiO_2 in the MG3 and decrease in the UG1FW Unit.

Manganese (MnO) is a minor constituent in the rocks of this profile and rarely exceeds 0.35% (Figures 2.10 and 2.12). Values in the pyroxenitic suite of the UG1FW Unit are c. 0.25%. The highest levels are recorded within the lower parts of each of sub-cycles 2, 3, 4, 5 and 6. MnO concentrations in the noritic sequence once again show a general decrease through the leucocratic sequence and marked inflections in MnO levels are seen close to the base of individual sub-cycles.

Whole-rock Al_2O_3 levels (Figure 2.2) provide a measure of the normative plagioclase in norites and pyroxenites (see also Figure 1.5), where

$\underline{or} + \underline{ab} + \underline{an} = 3.03\ Al_2O_3 + 0.73$ (cc. 0.9996, n = 56 samples).

This linear model over-estimates the normative plagioclase in anorthosites where feldspars are more calcic (aluminous). Variations in Al_2O_3 in the UG1FW Unit show that total feldspar may either increase (160-130m, 125-94m and 57-0m below datum) or decrease (335-30m and 94-57m) with height within the section (Figure 2.2).

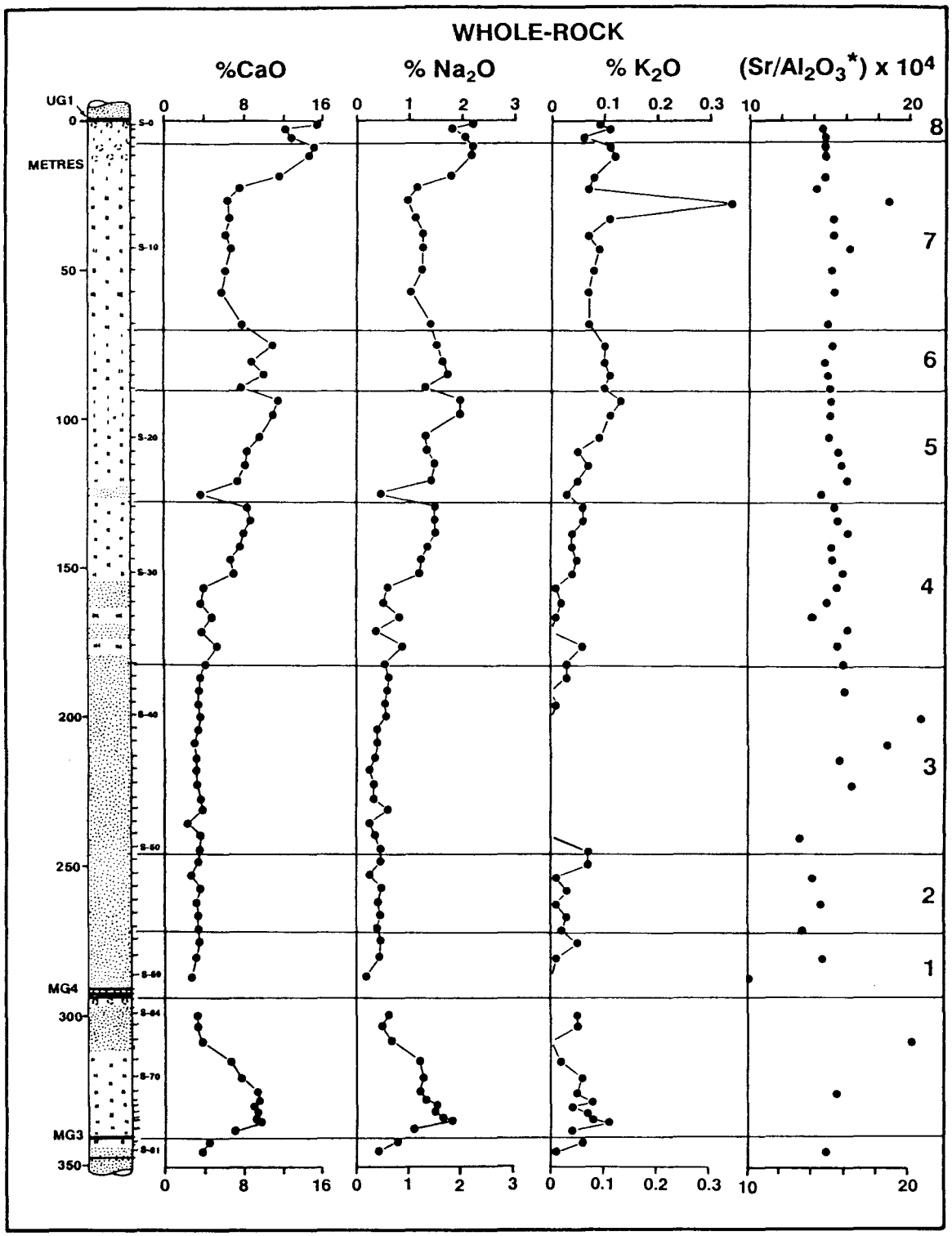

Figure 2.11 Whole-rock variations for CaO, Na_2O and K_2O (Wt.%) for the MG3 and UG1FW Units. The $Sr/Al_2O_3^*$ ratio, in which a small correction is made for the amount of Al contained in pyroxene (Eales et al., 1986), effectively shows the Sr content within plagioclase alone. This profile is a downward extension of the Upper Critical Zone data presented in Eales et al. (op cit). The relatively high values of this ratio and K_2O in sample S-7 are attributed to deuteric alteration close to a younger dyke.

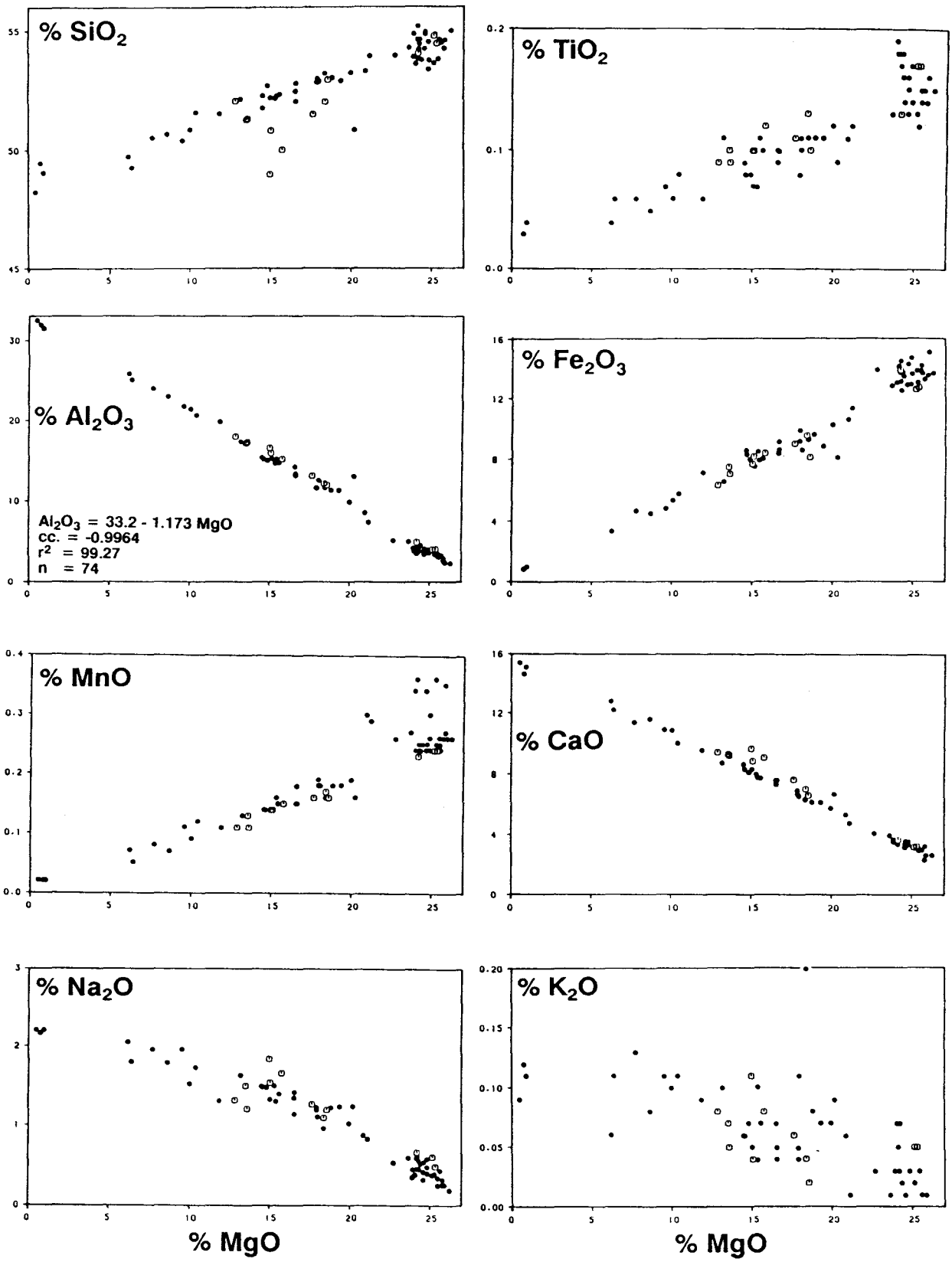

Figure 2.12 Harker-type plots of major elements (Wt.% oxides) vs MgO. Solid points are for the UG1FW Unit while the open circles are for the MG3 Unit.

2.5.2 Trace element variations.

Trace element data are presented in Table D8. Compositional variations of the trace elements are graphically illustrated, first, by means of plots against stratigraphic height (Figures 2.13, 2.14 and 2.15) and, second, in simple plots in which MgO is used as the abscissa (Figures 2.17 and 2.18). A brief discussion of the behaviour of the individual elements, and their affinities for inclusion into particular mineral phases, is presented below. A compilation of distribution coefficients according to various authors is given in Table 2.1.

Strontium (Sr)

This element has an ionic radius of 1.18 Å which is intermediate between that of Ca^{2+} (1.01 Å) and K^{+} (1.33 Å) and which distributes itself between Ca^{2+}- and K^{+}-bearing feldspars. Strontium reflects, almost directly, the modal proportion of plagioclase in these cumulates and the reverse linear relationship between Sr and MgO (Figure 2.17) demonstrates this feature. Experimental studies by Drake and Weill (1975) indicate that the distribution coefficient of D_{Sr}^{plag} is greater than unity. This is in agreement with estimates from natural systems by Griffin and Murthy (1969) and Philpotts and Schnetzler (1970) which indicate that D_{Sr}^{plag} is approximately 1.3 in tholeiitic melts. By contrast, Frey et al. (1978) give D_{Sr} of 0.016 and 0.165 for ortho- and clinopyroxene respectively.

Whole-rock Sr concentrations, which are therefore almost entirely controlled by the amount of plagioclase in the rock, are low in the pyroxenites (30-70ppm) and high in the anorthosite footwall of the UG1 chromitite (465ppm, S-3)(Figure 2.13). Intermediate values are recorded for the norites. By extrapolation, linear regression analysis indicates a value of 494ppm Sr for pure plagioclase (Figure 2.17).

The $Sr/Al_2O_3^*$ ratio, as defined by Eales et al. (1986) is in the upper 50m of the unit (range 14.4-15.2) maintained down to 180m below the UG1 chromitite while more scatter is recorded in the lower pyroxenitic part of the unit (Figure 2.11). A brief description of the $Sr/Al_2O_3^*$ ratio is given in **3.4.**

TABLE 2.1: Partition coefficients for trace elements in plagioclase, orthopyroxene clinopyroxene, olivine and biotite extracted from the literature.

Element	Plagioclase	Orthopyroxene	Clinopyroxene	Olivine	Biotite
Sr	1.3[1+2] 2.2[5] 1.5-2.2[22] 3.06[20] 1.75[23]	0.016[3] 0.018[10] 0.01[5] 0.007[19]	0.165[3] 0.07[5] 0.067[19] 0.1[21] 0.16-0.28[22]	0.003[10] 0.001[5+22] 0.00019[19] 0.01[2] 0.01[20]	0.08[5]
Co	0.1[16] 0.026[4]	2.0[3]	1.2[3] 0.5-2.0[25] 1.7-4.9[11] 1.2[4] 1.2[9]	1-7[10] 3.1[4] 4.8[9]	
Cr	0.01[5] 0.1[15] 0.026[4]	2.0[5]	10[5] 20[9] 40[14] 1.2[4]	0.2[5] 2.7[9] 3.1-10[13] 3.1[4]	7.0[5]
V	0.1[15]	0.3[3] 0.06-3.4[10] 0.5-2.3[11]	1.5[3] 1.3[9] 0.94-4.1[11] 0.06-3.4[17]	0.04[10] 0.09[3] 0.05[9]	
Zn	0.13[4]	0.49[5] 0.49[4]	0.49[4]	1.8[4]	
Ni	0.01[5] 0.2[12]	1.1-3.1[10] 4.0[5] 5-3[3]	2.0[5] 2-4[3] 6.5[11] 4.5[9]	10[5] 3.8-35[3] 4.8-34[8] 23.8[9]	3.5[5]
Sc	0.008[4] 0.01[18] .017-.065[10]	0.53-1.4[10] 1.1[3] 3.3[4]	3.1[3]	0.37[10] 0.33[4] 0.25[3]	
Rb	0.05[1] 0.03[2] 0.07[5] .03-.0002[21]	0.004[10] 0.0006[19] 0.001[5] <0.05[1]	<0.05[1] 0.017[10] 0.0011[19] 0.001[5] 0.03[21]	0.0001[5] 0.00018[19] 0.01[2] 0.01[3] 0.002[21]	3.1[5] 0.94-3.3[2]
Zr	0.01[6]	0.01-0.03[6]	0.1[6] 0.12[10]	0.01[6]	
Y	0.031[10] 0.03[6] 0.014[20] 0.049[24]	0.009[3] 0.2[6]	0.2[3] 0.5[6] 1.65[24]	0.002[3] 0.01[6]	0.03[6]
Cu	0.004[4] 0.24[11]	0.071[4]	0.071[4]	0.47-0.27[10] 0.023[4]	
K	0.2[10] 0.2[5]	0.001[5] 0.001[11]	0.0026[10] 0.002[5] 0.002[19]	0.001[5] 0.0018[19]	2.7[5]
Ti	0.4[6]		0.3[6] 0.34[9]	0.2[6] 0.07[9]	

1. Griffin and Murthy (1969)
2. Philpotts and Schnetzler (1970)
3. Frey et al. (1978)
4. Paster et al. (1974)
5. Cox et al. (1979)
6. Pearce and Norry (1979)
7.
8. Leeman and Lindstrom (1978)
9. Duke (1976)
10. Irving (1978)
11. Ewart et al. (1973)
12. De Long (1974)
13. Flower (1973)
14. Campbell and Borley (1974)
15. Walker (1970)
16. Jensen (1973)
17. Ringwood (1970)
18. Salpas et al. (1983)
19. Hanson (1977)
20. Drake and Weill (1975)
21. Hart and Brooks (1974)
22. Sun et al. (1974)
23. Morse (1982)
24. Morse and Nolan (1985)
25. Lindstrom and Weill (1978)

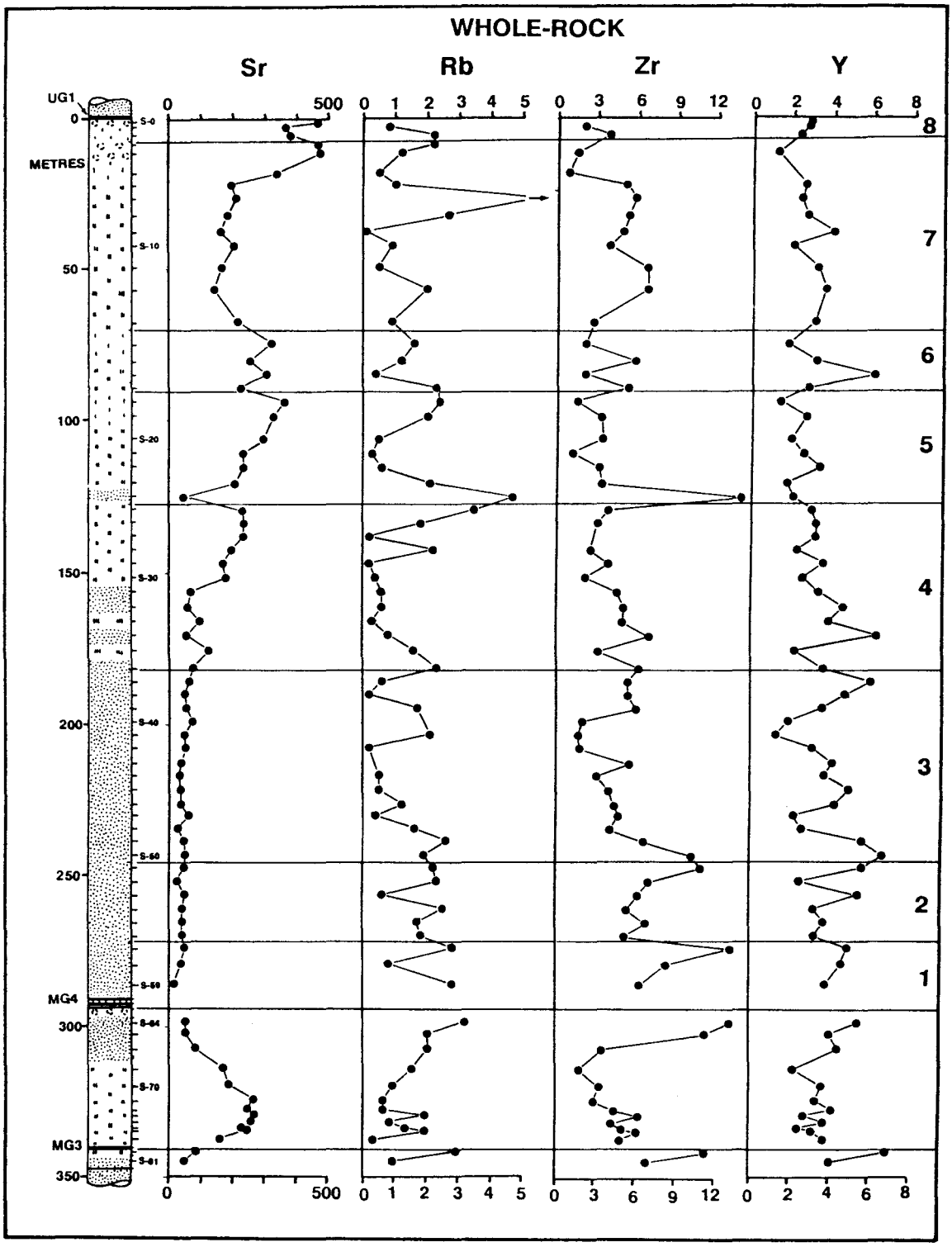

Figure 2.13 Whole-rock trace element variations in ppm for Sr, Rb, Zr and Y through the Spud shaft profile. Stratigraphic height is given in metres below the UG1 chromitite layer and arrows indicate data points off scale.

Cobalt (Co)

This element, together with Cr and V, is a member of the first transition series of the periodic table, and all three elements behave in essentially the same way. Co generally substitutes for Mg (Burns, 1970) and distribution coefficients of 1.2 and 2 were recommended by Frey et al. (1978) for clino- and orthopyroxene respectively. Data of Paster et al. (1974) show D_{Co}^{plag} for plagioclase to be approximately 0.03.

Whole-rock Co values rarely exceed 120ppm in the pyroxenitic sequence (Figure 2.14 and 2.17) though an anomalously high value of 141ppm was recorded for S-34. An overall pattern of decreasing absolute Co is seen through the UG1FW Unit - reflecting the modal composition.

Chromium (Cr)

Cr partitions strongly into pyroxene, particularly clinopyroxene, whilst being almost totally rejected by plagioclase. Distribution coefficients suggested by Cox et al. (1979) are $D_{Cr}^{cpx} = 10$ and $D_{Cr}^{plag} = 0.01$. This implies that in the absence of a spinel phase the proportion of modal pyroxene in the rock will have a strong influence on Cr concentration. The effect of modal mineralogy will, however, be modified by strong fractionation effects due to the high distribution coefficients for Cr, particularly into clinopyroxene.

The presence of disseminated chromite in some samples from both the footwall of the MG3 and the MG3 Unit itself is clearly indicated by the high Cr values recorded in these rocks - in excess of 4000ppm (Figure 2.14). A clear distinction is seen between the Cr values in the MG3 and UG1FW Unit when plotted against MgO (Figure 2.17). Here higher Cr values of the MG3 Unit are offset from those recorded for the UG1FW Unit. Apart from minor disseminations of chromite directly above the MG4 chromitite layer, and more prominently within the anorthosite footwall of the UG1 chromitite, chromite does not occur within the UG1FW Unit pyroxenites and norites. Levels of Cr within the lower pyroxenites are generally above 2500ppm. As for Co, an overall pattern of decreasing Cr is seen throughout the unit. The presence of disseminated chromite in the anorthosite footwall of the UG1 is reflected where Cr values approaching 1000ppm were recorded in samples S-0, S-1 and S-2. These samples were

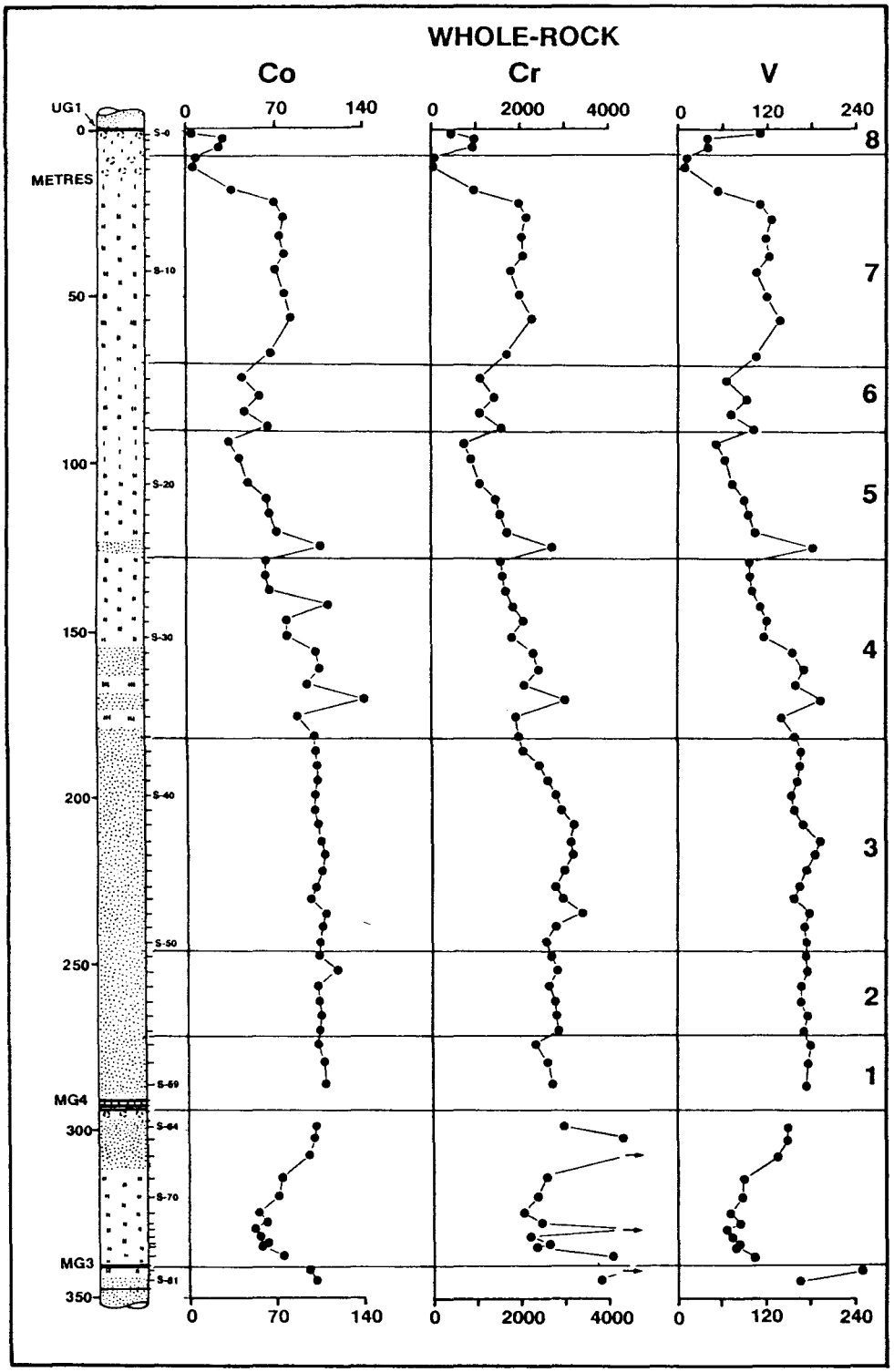

Figure 2.14 Whole-rock trace element variations in ppm for Co, Cr and V through the Spud shaft profile. Stratigraphic height is given in metres below the UG1 chromitite layer and arrows indicate data points off scale.

carefully selected to minimise the amount of chromite, but its ubiquitous presence at this level precluded analysis of chromite-free samples.

Vanadium (V)

This element distributes preferentially into clinopyroxene and Frey et al. (1978) quote a D_V^{cpx} of 1.5. That for orthopyroxene is lower at 0.3. Vanadium is almost completely excluded by plagioclase but partitions very strongly into any magnetite present in the rock.

Vanadium concentrations within the UG1FW Unit pyroxenites are well constrained between 160 and 180ppm and then gradually decrease through the noritic sequence to around 10ppm in the UG1 footwall (Figure 2.14). The lithologies of the MG3 Unit (both norites and pyroxenites), on the other hand, indicate lower levels of V when compared with their counterparts in the overlying UG1FW Unit. The V - MgO plot (Figure 2.17) clearly demonstrates this point where the datasets of each unit are significantly different. A simple regression analysis of the data yielded different linear models for each unit:

UG1FW Unit	V = 7.00 MgO - 4.74 (cc. 0.9829, n = 59); and
MG3 Unit	V = 6.14 MgO - 14.4 (cc. 0.9565, n = 12).

A similar convincing distinction is made in a plot of Sr against V (Figure 7 in Eales et al., 1990a) but no separation is evident when Sr is plotted against MgO (Figure 2.17) or Al_2O_3 for the same samples (Figure 5 in Eales et al. 1990b). Clearly the discrete regression lines in the V plot (Figures 2.17) arise out of a relative V-depletion below the MG4 chromitite.

Zinc (Zn)

Limited quantitative information is available regarding the behavior of zinc. Its behaviour is similar in most respects to that of the compatible elements V, Co, Ni, and Sc. A distribution coefficient of 0.49 for D_{Zn}^{px} (combined ortho- and clinopyroxene) and 0.13 for D_{Zn}^{plag} is used by Paster et al. (1974). Cox et al. (1979) also quote a distribution coefficient of 0.49 for orthopyroxene.

Although some scatter is evident for Zn within the pyroxenites of the UG1FW Unit it would appear that the pattern is one of an upward increase from 80ppm (above the MG4 chromitite) to a high of 100ppm at 225m before a decline to values around 90ppm at the top of the pyroxenitic suite (S-36 in Figure 2.15). From this level the general pattern is one of upward decrease through the rest of the noritic sequence as modal feldspar increases.

Nickel (Ni)

Nickel partitions preferentially into almost all the ferro-magnesian mineral phases and therefore behaves in much the same way as Co and Cr. The data of Frey et al. (1978) suggest that nickel partitions very strongly into both clino- and orthopyroxene, with D_{Ni} being of the order of 4 for both minerals. Nickel partitions strongly into olivine and base-metal sulphides. Plagioclase almost completely rejects this element and the considerations above mean that Ni should vary in a positive and linear way with respect to MgO (Figure 2.17) as no olivine or sulphides are present in the sequence. Concentrations of Ni within the pyroxenites vary between 500 and 600ppm and show much the same decreasing trend through the noritic sequence as Zn, Co, V and Sc.

Scandium (Sc)

Frey et al. (1978) recommended values of D_{Sc} = 3.1 for clinopyroxene, and 1.1 for orthopyroxene. Data from Paster et al. (1974) suggest an extremely low D_{Sc}^{plag} of 0.008 for plagioclase. Scandium values in the leucocratic rocks are generally lower than 10ppm while those for the norites are 10-28ppm (Figure 2.15 and 2.17). Within the lower pyroxenitic sequence of the UG1FW Unit the Sc values remain almost constant at around 32ppm. The distribution pattern of Sc with respect to stratigraphic height is similar in almost all respects to that of Ni, V, Co and Zn.

Interelement ratios

In the discussion above it is obvious that the absolute, whole-rock concentrations of compatible elements are determined largely by the modal composition of the rock. For this reason interelement ratios are used to establish patterns of fractionation. Ratios which best define the sub-

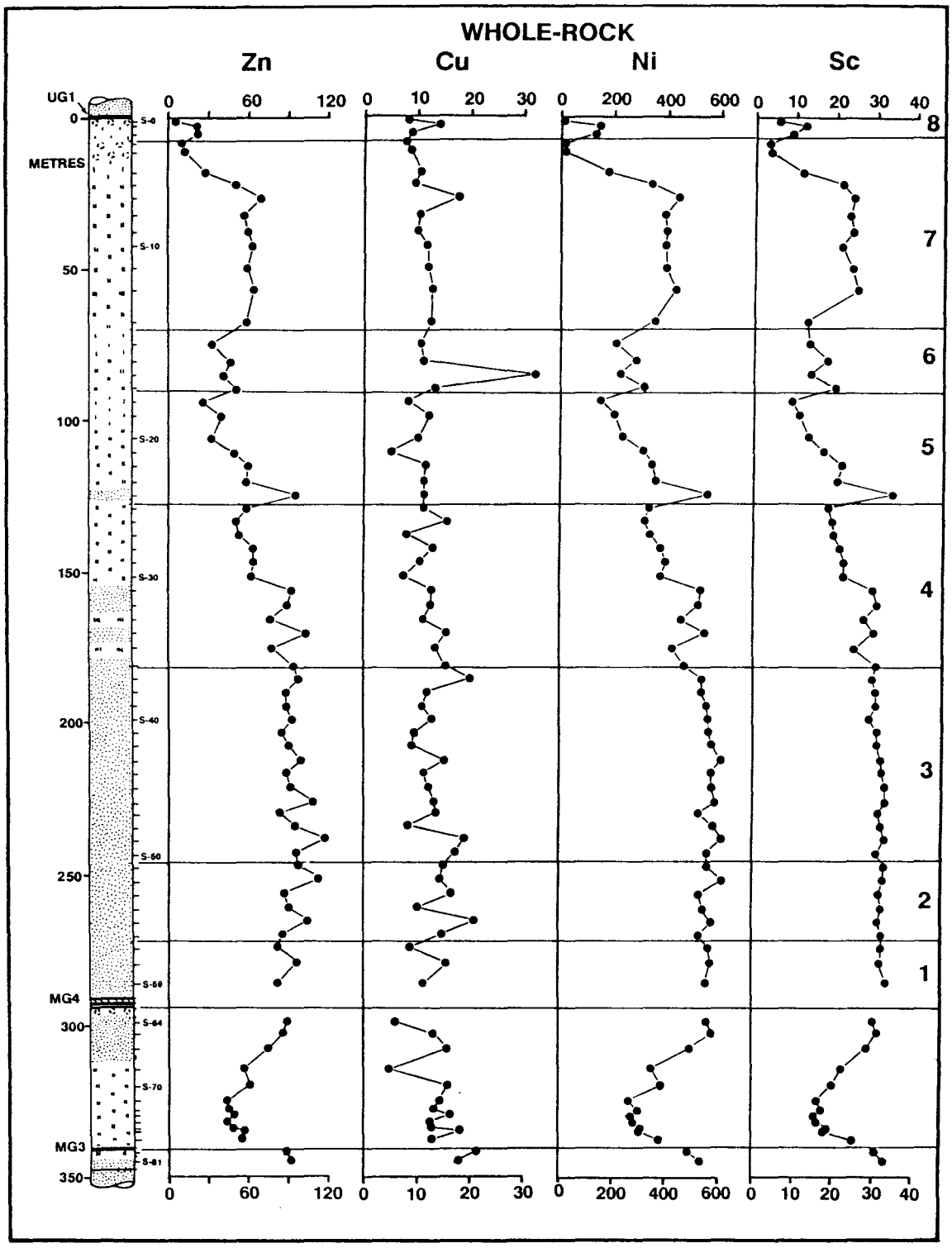

Figure 2.15 Whole-rock trace element variations in ppm for Zn, Cu, Ni and Sc through the Spud shaft profile. Stratigraphic height is given in metres below the UG1 chromitite layer.

cycles within the UG1FW Unit, and the breaks between them, are Ni/V, Cr/Co, Ni/Sc and to a lesser degree V/Sc (Figure 2.16).

The Ni/V ratio clearly indicates the breaks between four Upper Critical Zone units in Figure 2.16, i.e. the unit below the MG3 chromitite, the MG3 Unit, UG1FW Unit and the overlying UG1 Unit.

* samples from the footwall of the MG3 chromitite (S-79 and S-81) have ratios below 3.2.
* The MG3 Unit has Ni/V ratiosbetween3.6 and 4.0.
* A distinctive break to lower values (c. 3.2) occurs above the MG4 chromitite. The rest of the UG1FW Unit is defined by a series of cyclic oscillations between 3.5 and 2.9.
* A break to higher values in excess of 4.0 occurs within the overlying UG1 Unit at Union (de Klerk, 1982).

A clear distinction is also recorded for the Cr/Co ratio between the MG3 Unit and the UG1FW unit (Figure 2.16) and, like the Ni/V ratio, the muted oscillations within the UG1FW Unit support the definition of separate sub-cycles.

Trace elements incompatible in all phases of the UG1FW Unit.

The concentrations of the elements Rb, Zr, Y and Cu through the sequence is shown in Figure 2.13 and 2.15. Levels of these elements are also plotted against MgO in Figure 2.18. No consistent pattern is clearly discernible for these elements through the sequence, although Rb, Zr and Y levels at the bases of some sub-cycles have values akin to those at the top of preceding sub-cycles. For example, the trend of increasing Rb at the top of sub-cycle 4 continues into the base of sub-cycle 5 before dropping off to values below 1ppm. This pattern is again repeated in the overlying sub-cycle 6 and is also indicated for Zr and Y in other sub-cycles. This phenomenon suggests that limited infiltration metasomatism has occurred from below (Irvine, 1980b; Eales et. al, 1988).

Incompatible element abundances ought in general to increase upwards in the intrusion but such trends are wholly subservient to the amount of

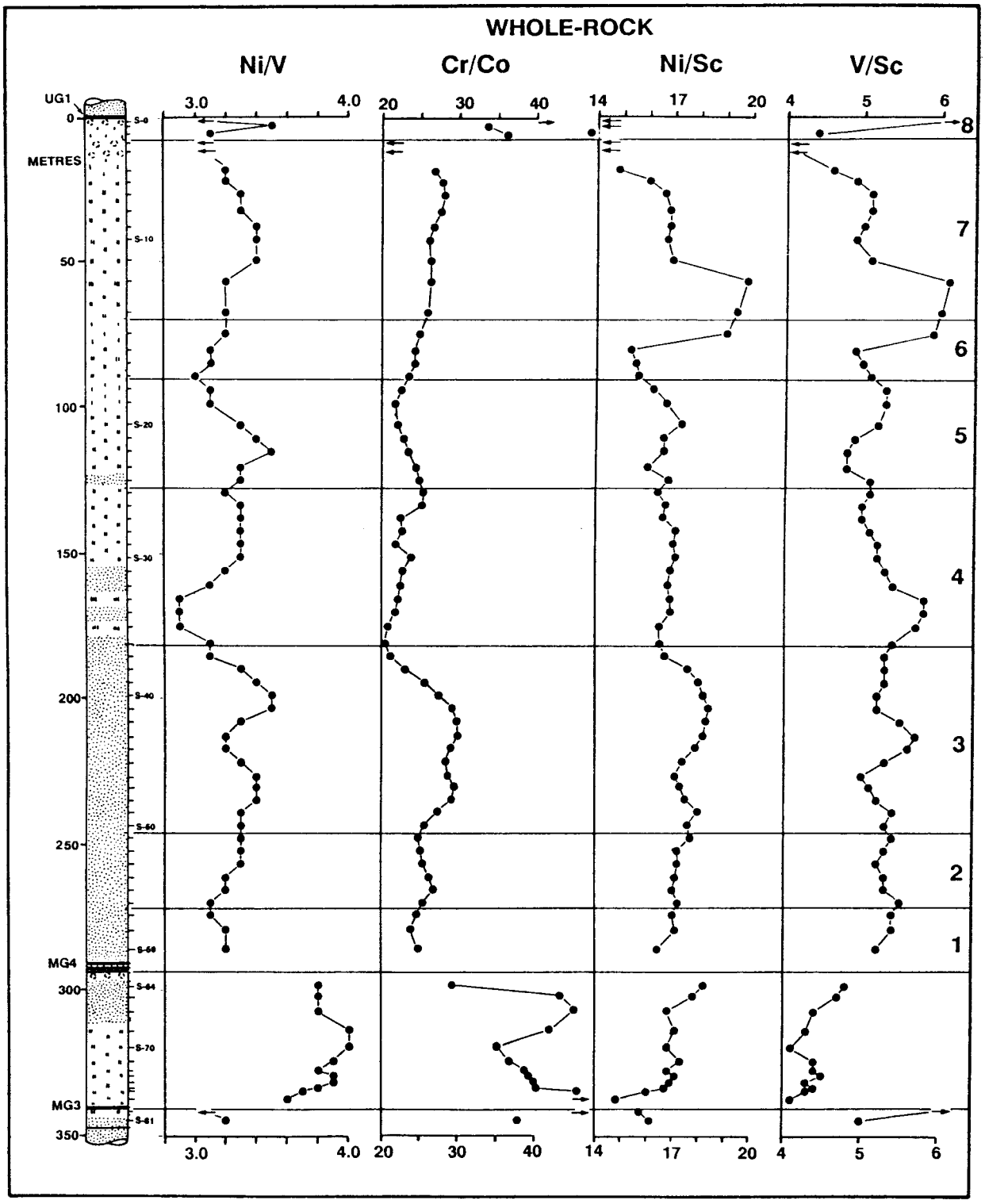

Figure 2.16 Whole-rock trace element ratios for Ni/V, Cr/Co, Ni/Sc and V/Sc through the Spud shaft profile. These profiles have been smoothed in part by employing three-point moving averages. Stratigraphic height is given in metres below the UG1 chromitite layer and arrows indicate data points off scale.

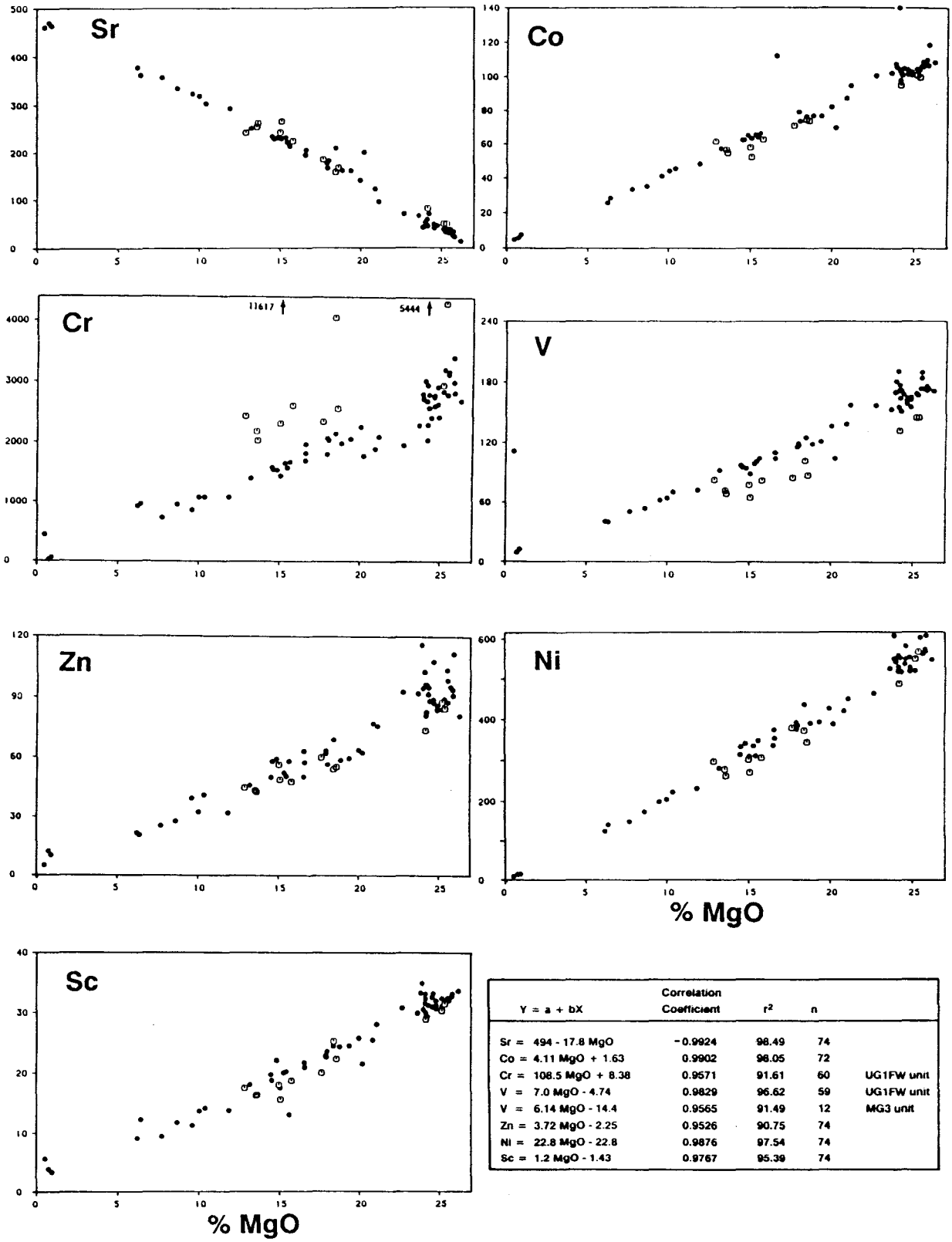

Y = a + bX	Correlation Coefficient	r^2	n	
Sr = 494 - 17.8 MgO	-0.9924	98.49	74	
Co = 4.11 MgO + 1.63	0.9902	98.05	72	
Cr = 108.5 MgO + 8.38	0.9571	91.61	60	UG1FW unit
V = 7.0 MgO - 4.74	0.9829	96.62	59	UG1FW unit
V = 6.14 MgO - 14.4	0.9565	91.49	12	MG3 unit
Zn = 3.72 MgO - 2.25	0.9526	90.75	74	
Ni = 22.8 MgO - 22.8	0.9876	97.54	74	
Sc = 1.2 MgO - 1.43	0.9767	95.39	74	

Figure 2.17 Trace elements (in ppm) vs MgO (Wt.%). Solid dots are for the UG1FW Unit while the open circles represent the MG3 Unit. The two data points off scale for Cr (arrows) are from the MG3 Unit. Note the consistent difference in concentration of Cr and V in the UG1FW Unit and the MG3 Unit.

late-stage liquid that is actually trapped in cumulus rock. Cawthorn (1983), in his study of the trace element behaviour of the Losberg intrusion (a satellite related to the Bushveld Complex), pointed out that if multiple intrusion of magma did occur then it would be reflected in the changes in the composition of the trapped liquid, which is best indicated by the incompatible trace elements.

Rubidium (Rb)

The distribution coefficient D_{Rb}^{plag} is of the order of 0.05 while that for pyroxene is substantially lower than this (Griffin and Murthy, 1969). The ionic radius of Rb (1.47 Å) is larger than that of K (1.33 Å) and Rb will readily enter sites normally filled by K^+ in alkali-feldspars, but shows a marked preference for entry into the micas (Taylor, 1965). Rubidium concentrations in the profile vary from levels below the instrumental lower limits of detection to 5ppm, but are generally below 3ppm. An anomalously high value of 10.6ppm is recorded for sample S-7 and is thought to be the result of partial deuteric alteration (mainly saussuritisation) adjacent to an intrusive dyke of Pilanesberg age. Higher K_2O values were also recorded in this sample (see Figure 2.11).

Zirconium (Zr)

Distribution coefficients reported by Pearce and Norry (1979) for Zr in basic assemblages are 0.01 for plagioclase and orthpyroxene and 0.1 for clinopyroxene. Zr, with an ionic radius of 0.79 Å and a charge of +4, does not enter any of the major cation sites in common cumulus minerals, concentrating itself rather in the residual liquid and ultimately crystallising as zircon. Zr may substitute to a limited extent for Ti in early Ti-Fe oxides (Taylor, 1965; Walker, 1970) or enter clinopyroxene and apatite.

The common range of this element through the profile is 1-12ppm with only 3 samples having values beyond this range. No clear pattern of variation is discernible through the pyroxenite and noritic assemblages of the UG1FW Unit, although breaks to lower values above the MG3 and MG4 chromitites are evident(Figure 2.13).

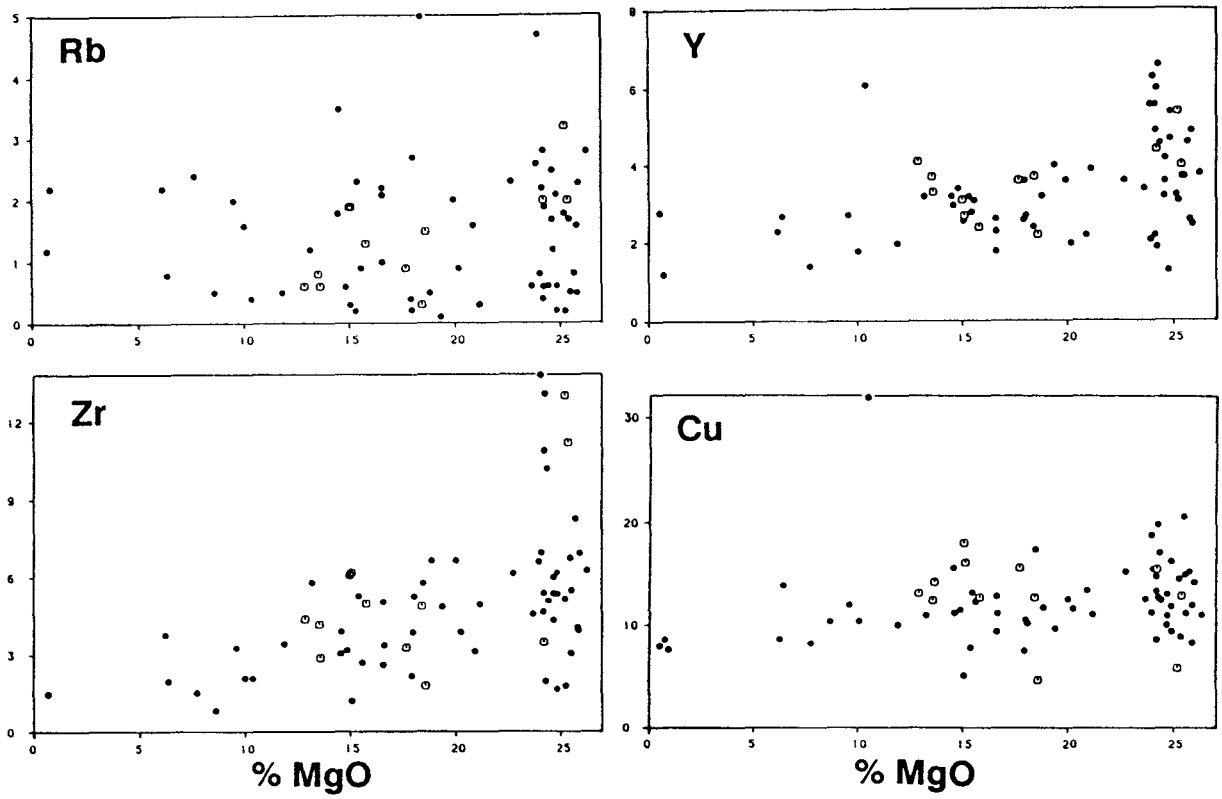

Figure 2.18 Plots of incompatible trace element variations (in ppm) vs MgO (Wt.%). Solid dots are for the UG1FW Unit while the open circles represent the MG3 Unit.

Yttrium (Y)

The distribution coefficient D_Y^{plag} is very much less than 0.1 (Drake and Weill, 1975; Pearce and Norry, 1979). The work of Frey et al. (1978) suggests that D_Y^{opx} for orthopyroxene is also very low (0.009) while that for clinopyroxene is 0.2. The implications of these data are that Y will only be accepted into late-crystallising clinopyroxene and will otherwise behave as an incompatible trace element in the interstitial liquid. Yttrium has an ionic radius of 0.98 Å which lies between Fe^{2+} (0.76 Å) and Ca^{2+} (1.01 Å), though closer to the latter. The behaviour of Y in melts, arising out of its substitution for Ca, has been discussed by Lambert and Holland (1974).

Yttrium does not exceed 6.8ppm throughout the entire profile. A pattern of muted cyclical ocsillation, which mimics other geochemical parameters, is apparent within the UG1FW Unit (Figure 2.13). Once again, clear breaks to lower values are recorded above the MG3 and MG4 chromitite layers.

Copper (Cu)

The distribution coefficients of plagioclase (D_{Cu}^{plag}) and pyroxene (D_{Cu}^{px}) are extremely low and a D_{Cu} value of less than 0.1 is recommended for both these minerals (Paster et al., 1974). Frey et al. (1978) set the bulk distribution coefficient for Cu below 0.01 in basaltic systems. Cu will therefore behave as an incompatible except in the presence of a sulphide liquid. Campbell's (1977) work on the Jimberlana Intrusion suggests that cumulate rocks in which the concentration of Cu is greater than 10ppm contain sulphides.

The copper values throughout the UG1FW sequence (which bears no sulphides) vary between 8 and 20ppm (Figures 2.15 and 2.18) with only one sample showing an anomalously high value of 32ppm (S-16). No opaque phases were identified in this thin section.

2.5.3 Strontium isotope data.

A composite profile showing $^{87}Sr/^{86}Sr$ initial ratios (Sr_i) has been compiled by Eales et al. (1990a) for the central part of Union Section utilising samples taken from above the UG1 in the **UB** profile (boreholes B235, B232) and from the 20-level crosscut through the MG3 and UG1FW Units (Figures 1.2 and 1.3). For illustrative purposes the composite Sr_i profile presented in this publication is reproduced here as Figure 2.19 and a brief summary of the findings of Eales et al. (1990a) pertaining to the MG3 and UG1FW Units is presented below.

1. In all but two samples through the MG3 and UG1FW Units the range of whole-rock Sr_i ratios is 0.7057-0.7063. An anomalously high whole-rock value of 0.7070 was recorded for S-68 in the MG3 Unit while sample S-40, within the UG1FW Unit, yielded a value of 0.7073. A repeat analysis recording 0.7074 confirmed this high ratio.

2. Sr_i values for the lower pyroxenite suite were found to be very similar to those in the overlying noritic rocks. Variations with stratigraphic height were seen to approximate a trend of regular increase through the noritic suite, but they follow a non-systematic and unpredictable pattern in the pyroxenites.

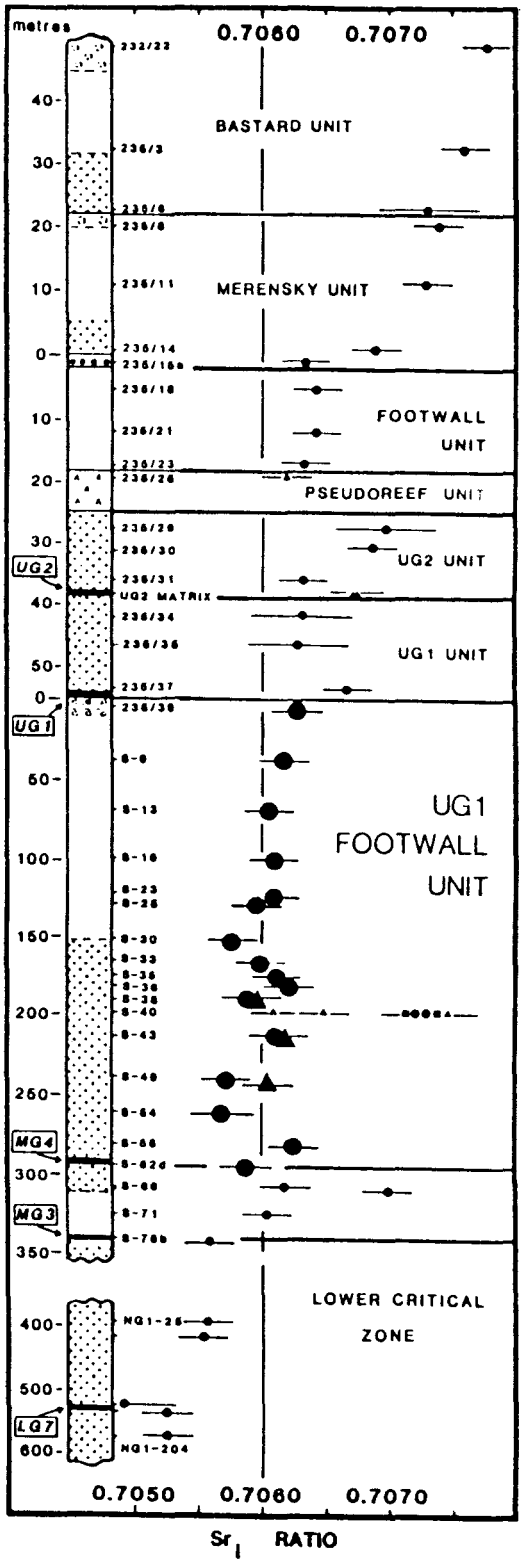

Figure 2.19 Variations in the initial strontium isotope ratio (Sr_i) at 2050 ± 25 Ma. (2 sigma) plotted against stratigraphic height for a 400m section below the Main Zone (from Eales et al., 1990a). Note the changes of vertical scale above the base of the UG1 and below the UG1FW Unit. Solid circles - whole-rock data; triangles - plagioclase separates; squares - orthopyroxene separates. Unshaded areas indicate norites and error bars are given at the 2 sigma level.

3. Seven determinations on sample S-40 yielded values between 0.7061-0.7075. The analyses were executed on two whole-rock fractions, three plagioclase and two orthopyroxene mineral separates. The average of the two whole-rock Sr_i ratios for this sample is 0.70725 which is almost identical to the average of the two values yielded by the orthopyroxene fraction. Two large plagioclase xenocrysts (of the type described in **2.3**) were hand-picked and yielded values of 0.7061 and 0.7075 respectively, but a value of 0.7065 was obtained for a composite plagioclase fraction that contained all three textural types of plagioclase (intercumulus plagioclase, partially resorbed plagioclase inclusions within orthopyroxene, and xenocrystic plagioclase). This extremely wide range in Sr_i values gives some insight into the heterogeneity that can occur within individual samples and the evidence clearly indicates that isotopic disequilibrium occurs between the different minerals in some samples, but not necessarily in all.

Eales et al. (1990a) noted that the isotopic disequilibrium seems to be maintained where the feldspars are large grains, whereas isotopic and major-element compositional equilibrium with liquid are approached when all inclusions are small. Of particular significance is the indication that the feldspar population is a mixed one. Despite the possible complicating effects produced by fractionation, compositional convection and isotopic disequilibrium, all the isotopic data and observations noted above lend support for a model involving mixing of magmas.

2.6 Summary.

Features of genetic significance which have emerged from the preceding sections are summarised below. Seven of these features have been highlighted in Eales et al. (1990a) from which the following extracts (single-spaced text) are taken.

(a) The UG1FW Unit is of exceptional thickness (285m), but is geochemically coherent, and distinguishable from the units above and beneath it. Pyroxenite overlying chromitite is dominant within the lowermost 135m, while norites of varying colour index constitute the succeeding 130m section. The unit is capped by a lower leuconorite-anorthosite couplet displaying evolved

attributes (low MMF ratios and Cr levels in orthopyroxene), which is overlain by a second leuconorite-anorthosite couplet in which MMF ratios of orthopyroxenes are higher than in any underlying member of the unit (Fig. 5) and in which Cr contents are anomalously high for rocks of leucocratic affinity. Chromite appears in abundance within the uppermost anorthosite, which is overlain by the robust UG1 chromitite and its associated hangingwall pyroxenites.

These features are best illustrated in Figures 2.4 and 2.20.

(b) A distinctive texture characterises almost the entire column extending for 350m below the UG1 chromite. Spheroidal or embayed inclusions of partially resorbed plagioclase feldspar are found entrapped in abundance within orthopyroxene hosts. Rare grains of cumulus or xenocrystic feldspar are also entrapped within some pyroxenites (e.g. S-40). Intragranular, cumulus and late intercumulus feldspar species thus exist within pyroxenites, as well as norites. Microprobe analysis shows that the anorthite contents of the included and non-included grains vary in sympathy, with the inclusions being generally more sodic.

This provides evidence for the crystallisation of pyroxenites from modified liquids in which feldspar was previously a phase. If one considers that a single pyroxene grain may contain up to 20 plagioclase inclusions (small, rounded and randomly orientated) then one could perhaps conclude that the concentration (or density) of plagioclase residua in the crystallising liquid must have been fairly high. Eales et al. (1991), who drew not only from this work but from observations made in the Lower Zone, Lower Critical Zone and the Footwall Unit, found that this texture manifested itself only in those parts of the sequence where chemical evidence pointed to the addition of primitive liquid to the crystallising column, causing a reversal of fractionation trends.

(c) Sr_i ratios vary in an unpredictable manner from one sample to another. This indicates that the UG1FW Unit could not have been the derivative of a single, homogeneous column of liquid within which phase or modal layering was controlled by purely physical parameters such as temperature, pressure, rhythmic nucleation or the sorting of crystals settling under gravity, or under the influence of currents.

(d) Sr_i ratios vary independently of stratigraphic height and petrographic features. Separate analysis of feldspar and pyroxene fractions shows that, within the same sample, isotopic signatures may be significantly different in these two fractions. Non-systematic whole-rock Sr_i variations can best be attributed to the feldspar population being a mixed one.

(e) The plotting of peak MMF ratios of orthopyroxenes of the UG1FW, UG1 and UG2 Units, as determined by microprobe analysis, against whole-rock Sr_i ratios (Figure 10) reveals that >80% of the available data points can be regressed. The derivation of this suite of rocks by some form of

mixing between end members S (Sr_i = 0.7054; MMF = 0.78-0.79) and P (Sr_i = 0.7068; MMF = 0.82) is thus a viable hypothesis.

(f) Whole-rock major- and trace-element data indicate at least 8 sub-cycles between the MG4 and the UG1 chromitite layers. These sub-cycles are not demarcated by abrupt reversals of trends which are characteristic of the transition from one unit to another in the three uppermost cycles of the Upper Critical Zone (as shown by Eales et al., 1986). The pattern is, rather, one of gradational change to rocks of more, or of less, primitive type with stratigraphic height.

Indications of sub-cycles are best shown by whole-rock ratios Ti/FeO, MMF, Ni/Sc and Cr/V. Incompatible trace elements (Rb, Zr and Y) do in some instances reinforce the positioning of the sub-cycle boundaries. In these cases the trends of incompatible elements peak above the boundary of the sub-cycles (Figure 2.20).

(g) The unit as a whole shows chemically evolved traits when compared with overlying cyclic units. It is depleted in Cr. Apart from a thin interval immediately above the MG4 chromitite layer, chromite is either absent or present as minute traces only, in contrast with its common occurrence as an accessory phase in norites and pyroxenites of the UG1, UG2, Merensky and Bastard Units. The orthopyroxenes average 0.336% Cr_2O_3 (std. dev. = 0.045%; 43 samples; 393 analyses). By contrast four Union Section borehole intersections of the UG2 pyroxenite show average Cr_2O_3 levels to be 0.492%, 0.463%, 0.417% and 0.412% Cr_2O_3, respectively (averages drawn from 240 microprobe analyses). Similar Cr depletion is noted in Cameron's (1982, Table 2) data pertaining to the equivalent M Unit in the eastern lobe of the Complex. Moderate but consistent Ni depletion is also evident in the UG1FW Unit where 26 whole-rock pyroxenite samples yield an average (Ni/MgO) x 10^4 ratio of 22.23 ± 0.80, within the range of 20.7-23.6. The average value is 24.0 ± 1.5 (range 22.8-27.2) within the overlying UG1 and UG2 Units at Union Section, and 24.20 ± 0.85 (range 23.4-25.9) at Amandelbult Section. A further indication of chemically evolved traits is given by MMF ratios of the orthopyroxenes. A mean value of 0.798 for the entire UG1FW Unit is suggestively lower than values of 0.822 ± 0.005, 0.817 ± 0.009, 0.814 ± 0.009 and 0.805 ± 0.007 determined in four separate intersections through the UG2 Unit (24 samples; 240 analyses) at Union Section.

(h) The occurrence of mm-scale layering (banding) in the top norite (below the anorthosite footwall of the UG1 chromitite) is distinctive and may imply a roof zone in the unit. A parallel can be drawn between this type of fine mm-scale layering and **solute banding** described by Rice (1981, p.408) in his review of similarities in magma chambers and metallurgical systems. He pointed out that this feature is common in the roof and wall zones of magma chambers and is "a manifestation of vigorous nonlaminar convection which seems almost always present in solidifying melts". Rice (op. cit.) suggests that since the convection is

nonlaminar, repetitive temperature variations in the melt at the crystallisation front serve to favour precipitation of first one component then another, which produces a banded structure in the solid.

(i) Structures at the top of the UG1FW Unit in close proximity to the UG1 chromitite (i.e. the basal contact of the UG1 Unit) indicate that the crystal pile was unstable in most localities. The following features are recognised:
- complex deformation of thin chromitite layers in anorthosite below the level at which others bifurcate and re-join to form an anastomosing system;
- associations of plagioclase with disseminations of chromite of varying density; and
- slumping of blocks of chromitite and/or pyroxenite into well laminated leuconorite.

(j) A characteristic $Sr/Al_2O_3^*$ ratio is noted for the UG1FW Unit when compared with the overlying Upper Critical Zone Units. This ratio varies between 14 and 15 in the majority of samples of the upper noritic suite of the UG1FW Unit. This range is the same as that at Amandelbult and Union Sections (Eales et al., 1988). The well constrained range of the $Sr/Al_2O_3^*$ ratio in the norites is not maintained within the lower pyroxenitic suite where a greater degree of scatter is recorded (Figure 2.11).

2.7 Synthesis and conclusion.

The characteristic features of the UG1FW Unit that have been presented and discussed in the preceding sections are unique when compared to other Upper Critical Zone units. The patterns of cryptic variation, petrographic features, isotopic signature and gross geochemical characteristics of the unit support a hypothesis that the UG1FW Unit developed in response to periodic additions of a more primitive magma to a somewhat evolved resident liquid column. The new pulses then blended with the partially fractionated residual liquid which had an abundance of small plagioclase primocrysts in suspension. For a more detailed discussion, and an account of the model, the reader is referred to Eales et al. (1990a) in Appendix E.

A summary diagram illustrating the variation in trends is presented in Figure 2.20 which incorporates data drawn from Figures 2.2, 2.4, 2.8, 2.10, 2.13 and 2.16. This summary diagram emphasises the distinctive cyclicity within the UG1FW Unit and highlights the criteria which have been used in the demarcation of the 8 sub-cycles. Crystallisation of Mg- and Cr-rich cumulates below the MG4 chromitite layer (Sr_i c. 0.7054) produced an Fe-enriched and Cr-, Ni- and Mg-poor supernatant (**S**) liquid residuum which retained the same isotopic signature. This residual liquid then mixed, in different proportions, with new, more primitive (**P**) magma which was periodically injected into the chamber in varying volumes. Alternatively, replenishment of **P-liquid** components may have been achieved by convective overturn. The **P-liquid** is hypothesised to have been akin to the parental magma responsible for the mafic layers of the overlying Upper Critical Zone units, like the UG1 and UG2 Units which have a Sr_i ratio of c. 0.7067 - 0.7070 and are Mg- and Cr-enriched. By extrapolation of the data presented in this chapter the two end-member liquids (**P** and **S**) would have had the potential for crystallising cumulates with the following characteristics.

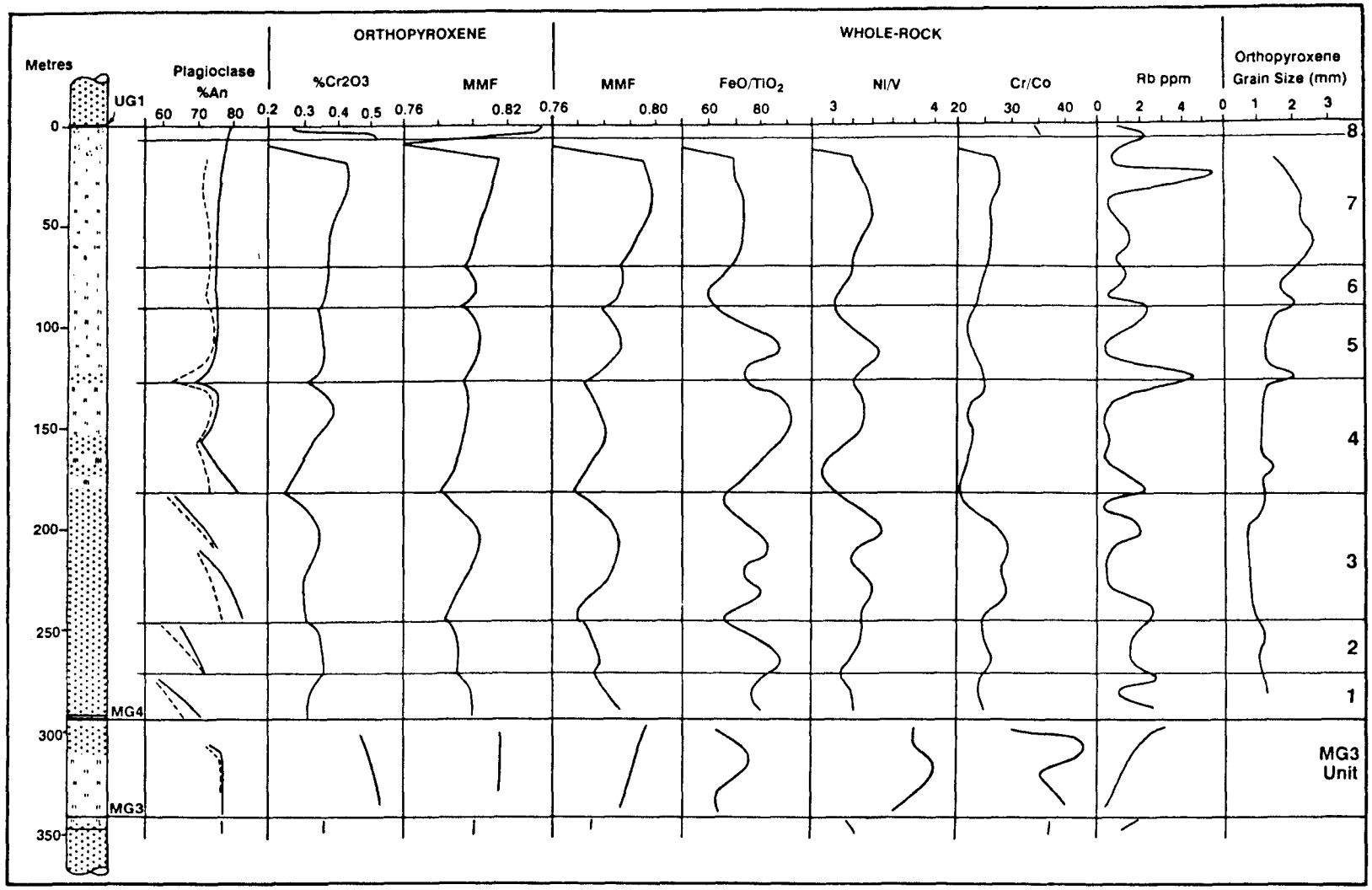

Figure 2.20 Summary diagram showing compositional trends for mineral and whole-rock analyses taken from preceding variation diagrams. Subdivisions of the UG1FW Unit into sub-cycles 1-8, and the limits of the MG3 Unit are also shown. Trends for plagioclase inclusions in orthopyroxene are indicated by dashed lines and those for cumulus and intercumulus cores in solid lines.

S-liquid : Sr_i ratio c. 0.7054
MMF of orthopyroxene c. 0.785
Cr_2O_3 in pyroxene c. 0.25%
Plagioclase c. An_{70}
Whole-rock Ni/V c. 2.9 and Cr/Co c. 20.

P-liquid : Sr_i ratio c. 0.7068
MMF of orthopyroxene c. 0.82
Cr_2O_3 in orthopyroxene c. 0.5%
Plagioclase c. An_{81-85}
Whole-rock Ni/V c. 3.5 and Cr/Co c. 30.

Summary of Model

A genetic model to account for the cyclicity and development of the entire UG1FW Unit has been presented in Eales et al. (1990a, Appendix E - see also Fig. 12) and a brief account is given here. A schematic diagram illustrating the various stages of development in an idealised sub-cycle in the lower pyroxenites of the Unit is presented in Figure 2.21 (stages A - G).

Stage A starts with a column of **S-liquid** overlying a partly crystalline floor. As this **S-liquid** is the residual product of the crystallisation of earlier cumulates it was Cr-, Ni- and Mg-depleted. The Sr_i ratio of the liquid was c. 0.7054 and it was nucleating plagioclase feldspar (An_{70}) and Mg-poor orthopyroxene in cotectic equilibrium.

Stage B. An influx of a hotter and denser **P-liquid** (Sr_i ratio c. 0.7068) was then emplaced between the crystalline floor and the overlying **S-liquid** column with jetting perhaps being important closer to the feeder zone (Campbell et al., 1983). Data presented by Eales et al. (1988), Teigler (1990) and in Chapter 4 of this work suggests that Union Section is perhaps located proximally with regard to a feeder zone. If this is the case then jetting may have been important for the emplacement of the new influx of **P-liquid** at this locality but a basal flow mechanism may have been more important away from Union Section. Mixing between the **S-** and **P-liquids** produced a hybrid layer immediately above the crystalline

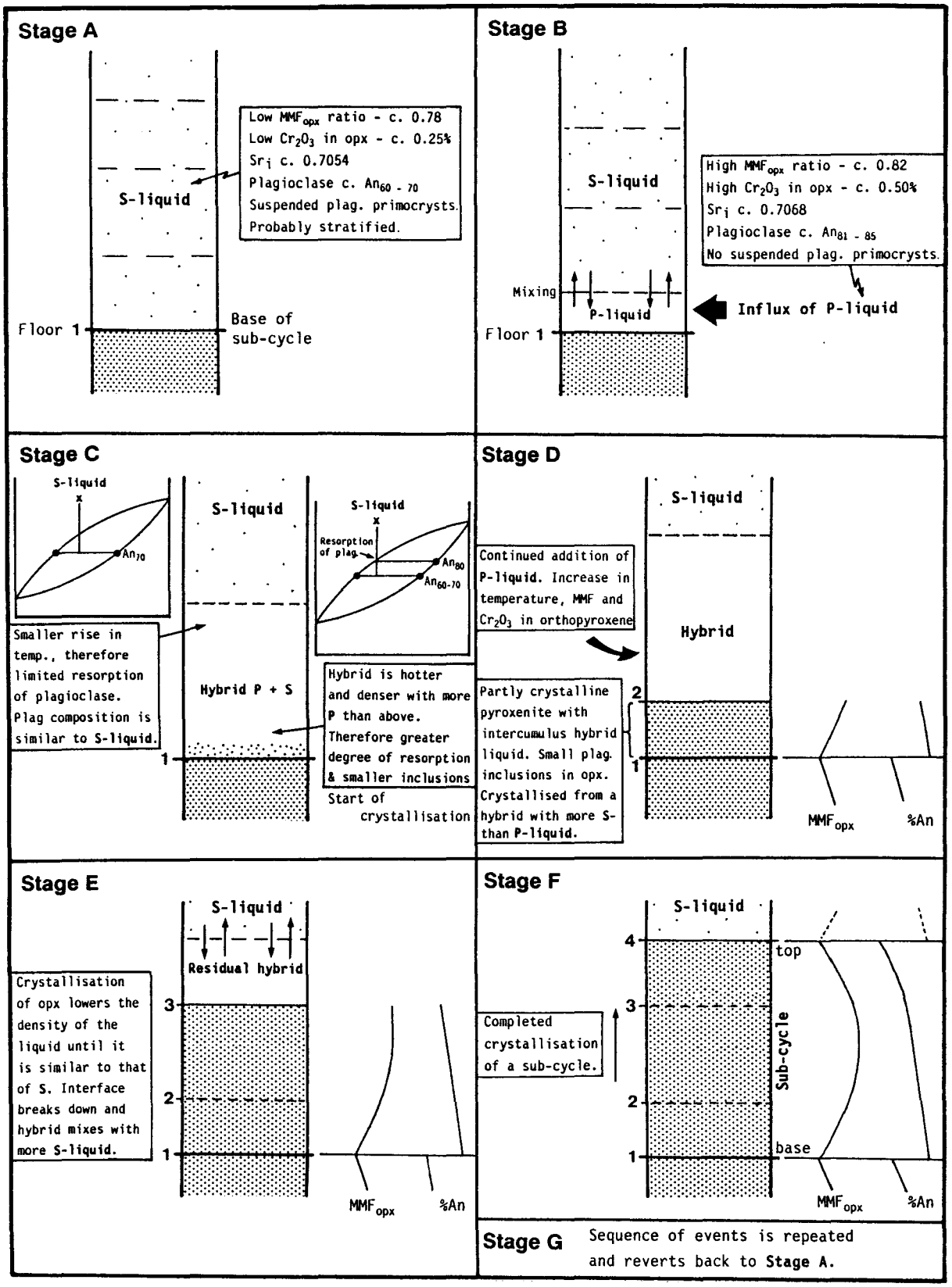

Figure 2.21 Schematic diagram showing the sequence of magmatic events (stages A-G) which were responsible for the development of a typical sub-cycle in the lower (pyroxenitic) part of the UG1FW Unit.

floor and the ratio of **P/S** liquid, and the temperature, were initially highest at the base of the layer.

Stage C. Suspended small primocrysts of plagioclase feldspar were partly resorbed and corroded. Partial equilibration and reverse zoning of these relict crystals within the **S-liquid** also took place. This had the effect of raising the anorthite content of the small corroded feldspar grains. These effects were most pronounced closer to the base of the hybrid layer. At higher levels within the hybrid layer, a more limited temperature rise repressed resorption and re-equilibration. This is confirmed by a contrast between a dense concentration of large feldspar inclusions within orthopyroxene hosts in the upper parts of sub-cycles (20 inclusions per grain, up to 7 volume per cent, in sub-cycle 3) and a sparseness in the lower parts (averaging 1 small inclusion per host grain).

Stage D. Sustained addition of **P-liquid** shifted the system into the primary phase volume of orthopyroxene, and nucleation and growth of orthopyroxene entrapped relict feldspar grains. Adcumulus growth of orthopyroxene in the basal part of the hybrid layer resulted in the formation of pyroxenites with a low incidence of resorbed feldspar inclusions and those which are present are small and show advanced resorption. At the base of the column the ratio of **P-** to **S-liquid** is relatively low in the hybrid liquid. As more **P-liquid** is added to the system its proportion is increased in the hybrid liquid and on crystallisation this yields cumulates with higher Cr levels and orthopyroxene MMF ratios. Occasional reversed zoning of cumulus orthopyroxene from cores to margins is seen but the entrapped plagioclase inclusions are shielded from further reaction, and remain sodic despite the more calcic nature of the hybrid liquid (dominantly **P-liquid**). The resultant cryptic variation trend of orthopyroxene MMF ratios is one of increasing MMF ratios in orthopyroxene and a decrease in the An content of plagioclase.

Stage E. All sub-cycles in the lower pyroxenites of the Unit, and the majority of those in the overlying norites, grade to Mg- and Cr-poor cumulates towards the tops of the sub-cycles (Figure 2.20). This fact

suggests that the inflow of **P-liquid** had temporarily abated and that fractional crystallisation combined with progressive incorporation of evolved **S-liquid** overlying the hybrid layer, produced a normal cryptic variation trend. As crystallisation proceeded, the liquid density of the hybrid layer declined and the diffusive interface with the overlying **S-liquid** column broke down in response to the upward migration low-density residua by compositional convection during the crystallisation of the pyroxenites.

Stage F. Crystallisation of the hybrid liquid, which was now dominated by **S-liquid** characteristics, completed the development of the sub-cycle before the sequence was repeated by the influx of fresh **P-liquid** into the chamber. The plagioclase inclusions incorporated within the orthopyroxenes at this level are more sodic and somewhat larger than those at the base of the sub-cycle.

During the crystallisation and accumulation of the lower pyroxenites of the UG1FW Unit the hybrid liquid remained within the primary phase volume of orthopyroxene by repeated influxes of **P-liquid** and this resulted in a substantial upward migration of low-density residua which were enriched in plagioclase components. The commencement of crystallisation of intercumulus liquid lagged behind that of the cumulus phases. More calcic feldspar would initially have nucleated at the base of the crystal pile, but concurrent compaction by sintering and reduction in primary porosity would have displaced sodic intercumulus residua upwards. Each sub-cycle therefore displays a trend towards sodic feldspar with stratigraphic height (Figure 2.20).

Periodic repetition of stages (A - F), outlined above, resulted in the formation of sub-cycles 1-4 (Figure 2.20). While the composition of these **P-liquid** influxes remained apparently constant (Figures 2.5 and 2.17), the **S-liquid** displayed the cumulative effects of repeated additions of **P-liquid** to the system. Figure 2.20 shows that the starting compositions of both plagioclase inclusions and intercumulus plagioclase become systematically more calcic through cycles 1 to 4. The slopes of the cryptic variation trends in Figure 2.20 do give some indication of the volume and frequency of inputs of **P-liquid** during the inflation of the

chamber. A low average volume and frequency of inputs per unit time resulted in sub-cycles of limited thickness (e.g. cycles 1 and 2 in Figure 2.20) without pronounced reversals in the trend of cryptic variation; larger influxes of **P-liquid** yielded thick sub-cycles within which significant increases in MMF ratio and Cr_2O_3 contents of orthopyroxene are seen (Figure 2.20, sub-cycle 3).

Cumulus plagioclase started to crystallise at a stage which is now recognised as being midway through the development of the UG1FW Unit. Cumulus plagioclase crystallised at the base of sub-cycle 4 producing the first two layers of melanorite within the UG1FW sequence at c. 175m and 165m below the UG1 chromitite, separated by pyroxenites (Figure 2.20). Apart from a thin (3m) layer of pyroxenite at the base of sub-cycle 5, the remainder of the column constitutes a more leucocratic sequence - termed the "Noritic Suite" by Eales et al. (1990a). These rocks are predominantly made up of norites (up to 13m below the UG1 Unit) overlain by interlayered anorthosites and leuconorites. The appearance of cumulus plagioclase in the upper part of sub-cycle 4 marks the stage at which the hybrid liquid reached the orthopyroxene-plagioclase cotectic. Factors which may have aided the hybrid liquid in crystallising cumulus plagioclase would have been:

a. the upward migration of low-density Na-, Ca- and Al-rich residua which were produced during the sustained crystallisation of the 115m sequence of pyroxenites at the base of the Unit, and,
b. possible settling of orthopyroxene out of the **S-liquid** layer.

These two factors above would have aided in producing a liquid within the primary phase volume of plagioclase.

The advent of crystallisation of cumulus plagioclase is generally accepted (Campbell et al., 1983, Sparks et al., 1984; Naldrett et al., 1986) as marking the stage in the evolution of the residual liquid at which its density starts to rise and may eventually exceed that of the parent liquids (**P-liquid**). Eales et al. (1990a) point out that it is significant that the lowest MMF ratios in the UG1FW Unit norites, and the lowest Cr_2O_3 contents of orthopyroxenes, are recorded at the base of sub-

cycle 4, just below the first appearance of cumulus plagioclase in the melanorite (Figure 2.4 and 2.20). They suggest that this implies that the fractionated residua no longer rose within the column above this level, but remained trapped there as intercumulus liquid.

Within sub-cycles 5-7 normal zoning is recorded for cumulus orthopyroxene grains and a drop in MMF and Cr values is recorded between cores and margins of individual grains. Occasional cumulus plagioclase grains display oscillatory zoned growth patterns and these complex crystals are juxtaposed with grains of simpler design. This texture is indicative of a mixed plagioclase population comprising (a) normal cumulus plagioclase with one growth cycle and (b) primocrysts of plagioclase which had nucleated at an earlier stage and grew in response to repeated influxes of new liquid before being incorporated into the crystal pile.

In Figure 2.20 it is noted that there is an overall trend of increasing MMF ratios and Cr_2O_3 content of orthopyroxene, and whole-rock MMF and Cr/Co ratios from the base of sub-cycle 4 to a level some 20m below the UG1 chromitite (near the top of sub-cycle 7). The pattern of repeated cyclicity is still, however, recognised through this enigmatic interval displaying an overall pattern of reversed fractionation as it becomes increasingly leucocratic towards the top. The top of sub-cycle 4 and the base of 5 are well-defined (Figure 2.20) whereas the overlying transitions into sub-cycles 6 and 7 are somewhat less obvious. Eales et al. (1990a) resolve this problem of apparent reversed fractionation in terms of mass balance. Influxes of relatively small proportions of **P-liquid** into a liquid rich in potential feldspar but with a low content of FeO and MgO, would exert a marked influence on MMF ratios without overly increasing the absolute modal proportions of crystallising mafic phases. The variation recorded for the Sr_i ratios in the norite sequence (0.7058-0.7063) falls within the range of values which could be expected as a result of mixing of **S-** (0.7054) and **P-liquids** (c. 0.7068) in differing proportions. Eales et al. (1990a) noted that less fluctuation is displayed by the Sr_i ratios within the noritic sequence than those of the underlying pyroxenites in sub-cycles 1 - 4 (Figure 2.19). They ascribed this feature to the fact that variations in the ratio of **S/P**-type feldspars are more effectively buffered in norites, where feldspars are a major modal constituent.

The layer of leuconorite near the top of sub-cycle 7, which is 12-20m below the UG1 chromitite (Figure 2.2 and Plate 2.5a), has a similar geochemical signature to the underlying norites, but the overlying 6m of anorthosite at the top of sub-cycle 7 is highly evolved. Samples S-3 and S-4, within this anorthosite, yielded Al_2O_3 values of 31.6% and 32.0% respectively. A combined average of 13 analyses from samples S-3 and S-4 (Table C5) yielded an orthopyroxene MMF ratio of 0.621 (sd = 0.012) and a Cr_2O_3 value of 0.03% (sd = 0.01). Whole rock ratios of MMF, FeO/TiO_2, Ni/V and Cr/Co are also significantly depressed (Figures 2.10, 2.16 and 2.20). These data are suggestive of crystallisation of modally insignificant intercumulus mafic phases from a very small volume of depleted liquid that was not flushed away from the crystallising layer or rejuvenated by the influx of a new volume of liquid, as had been the case in underlying sub-cycles.

The uppermost leuconorite of the UG1FW Unit (4-6m below the UG1 chromitite), at the base of sub-cycle 8 (Figure 2.2 and Plates 2.2 and 2.4.), displays higher whole-rock Cr/Co and MMF ratios and Cr_2O_3 content of orthopyroxene than those recorded in the leuconorites at the top of sub-cycle 7. Chromite, however, does not appear as a crystallising phase within this leuconorite. By contrast, the overlying 4m anorthosite layer, which constitutes the footwall of the UG1 chromitite layer, contains abundant chromite as disseminated grains, discontinuous layers, and pods (Plates 2.2, 2.3 and 2.4). Whole-rock chemical data are thus misleading, but microprobe data show that Cr_2O_3 values of orthopyroxene are high in sub-cycle 8 and the MMF ratios now match those of orthopyroxenes in the overlying UG1 Unit (see Eales et al., 1990a, Fig. 5).

It is within the upper part of this anorthosite, at the top of the UG1FW Unit or the immediate footwall of the UG1 chromitite, that the well-known anastomosing and disrupted layers of chromitite occur (see **2.2** and Viljoen et al. 1986a). Eales et al. (1990a, p.41) suggest that these features are the result of the interaction between a feldspathic residue of the UG1FW Unit, almost wholly deficient in ferromagnesian components, and the parent **P-liquid** responsible for the overlying UG1 Unit. They further suggest that

> "The mixing of a chromiferous mafic liquid with feldspathic liquid has the potential to bring hybrids within the primary phase volume of Cr-spinel (Irvine et al., 1983; Hatton and von Gruenewaldt, 1987) and the occurrence of the robust, if structurally complex, UG1 chromitite at this position is not in conflict with theory".

The contention of Irvine et al. (1983) that a significant batch of anorthositic A-type liquid was emplaced at this level is not supported by the geochemical and isotopic data in this study. Data presented in this chapter show that the MG3 and UG1FW Units conform to the general geochemical characteristic of the Upper Critical Zone reported by Eales et al. (1986, Figs. 6, 7 and 8) and no A-type characteristics, typical of the Main Zone, are identified. Upper Critical Zone characteristics recognised in this sequence, which are quite distinct from those of Main Zone (A-type) lineages, include:

* higher whole-rock MMF ratios in mafic (U-type) lithologies
* Zr/Y ratios typical of the Upper Critical Zone lineage. The average Zr/Y ratio calculated for the combined MG3 and UG1FW Units is 1.45 (sd. 0.55) as compared to lower values in the Main Zone which are closer to 1.0 at the level of the Porphyritic Gabbro Marker
* overall Cr-enrichment in U-type lineages (higher atomic Cr/Al in orthopyroxene)
* lower Sr_i ratios of c. 0.7064 of the Upper Critical Zone. These values are significantly lower than those of c. 0.7087 in the Main Zone. The Sr_i ratio in the immediate footwall of the UG1 chromitite (Figure 2.19) is 0.7063 which does not support the view that an A-type liquid had been emplaced at this level.

The precipitation of chromitites by interaction between primitive, chromiferous liquids, and residual, feldspathic liquids (Eales, 1987; Botha, 1987) remains the favoured model. After the precipitation of copious amounts of chromite (UG1 chromitite layer) onto the unconsolidated anorthosite floor, at least two episodes of disruptive movement occurred within the crystal pile prior to final solidification. This is attested by the "brecciated" texture exhibited by the chromitite within the anorthosite seen in Plate 2.3b.

In conclusion, the UG1FW Unit has been built up by the periodic influx of hotter, more primitive **P-liquid** which added to and blended with a cooler, more evolved, supernatant **S-liquid** resting upon the crystal pile. Sub-cycles within the Unit include more mafic cumulates deposited from hybrids with a higher proportion of **P-liquid**, whereas cumulates with more evolved traits reflect supernatant liquid fractions that experienced a lesser degree of rejuvenation, or evolved by subsequent fractionation. The recognition of the abundant, small, spheroidal, ovoid or deeply embayed inclusions of plagioclase within cumulus orthopyroxene grains of both pyroxenites and norites is significant as it implies the existence of plagioclase feldspar in the magma before the development of ultramafic cumulates from these melts. Eales et al. (1991) have noted the occurrence of these inclusions within cumulus orthopyroxene grains of both pyroxenites and norites and they recognise five separate stratigraphic intervals which exhibit this texture within the Lower and Critical Zones, including the MG3, UG1FW and Bastard Units. This texture might be overlooked in other noritic rocks where ophitic enclosure of cumulus plagioclase by orthopyroxene is quite common. It is important to note that this texture is seen only where resorption has been incomplete - complete resorption could have occurred in other parts of the layered sequence without leaving any petrographic evidence at all.

CHAPTER 3

THE INTERVAL BETWEEN THE UG1 CHROMITITE AND THE BASTARD UNIT AS SEEN IN TWO PROFILES AT RPM UNION SECTION.

3.1 Introduction.

An account of the geology of Union Section was presented in de Klerk (1982). In that study the whole-rock geochemistry and cryptic variations of various mineral phases was based on a stratigraphic profile in the central part of the mine (this profile is now termed **UB**). The original geochemical data for the profile, supplemented by additional microprobe and strontium isotope analyses, served as the basis for a number of publications. These include the general geology of the area (Viljoen et al., 1986a), the development of a genetic magmatic model for the Upper Critical Zone (Eales et al., 1986), and studies of regional trends of cryptic variation and lithology (Scoon and de Klerk, 1986; Eales et al., 1988). The geochemistry and genesis of the numerous chromitite layers at Union Section have been covered in detail by Eales (1987) and Eales and Reynolds (1986); these studies refer to sections in close proximity to the **UB** profile.

In this chapter new whole-rock major and trace element data for two additional profiles, covering the same interval as **UB**, are presented. These profiles are located roughly along strike to the southwest and northeast of **UB** and have been designated **UA** and **UC** respectively (Figure 1.3). A further series of close-spaced samples was taken through the UG2 Unit in three additional borehole profiles designated **UD**, **UE** and **UF** (Figure 1.3). Here trace element analyses alone (11 elements) were performed on the pyroxenite and harzburgite samples. Additional whole-rock data for single profiles through the Footwall, Merensky and Bastard Units at Union and Rustenburg Sections have been presented by Naldrett et al. (1984 and 1986) and include MgO, K_2O, P_2O_5, Y, Cr, Cu and Ni (combined in Figure 4.25).

These new whole-rock data in **UA**, **UC** and the three UG2 Unit profiles (**UD**, **UE** and **UF**) show remarkable similarity to the data of **UB** and little geochemical variation along strike is readily apparent.

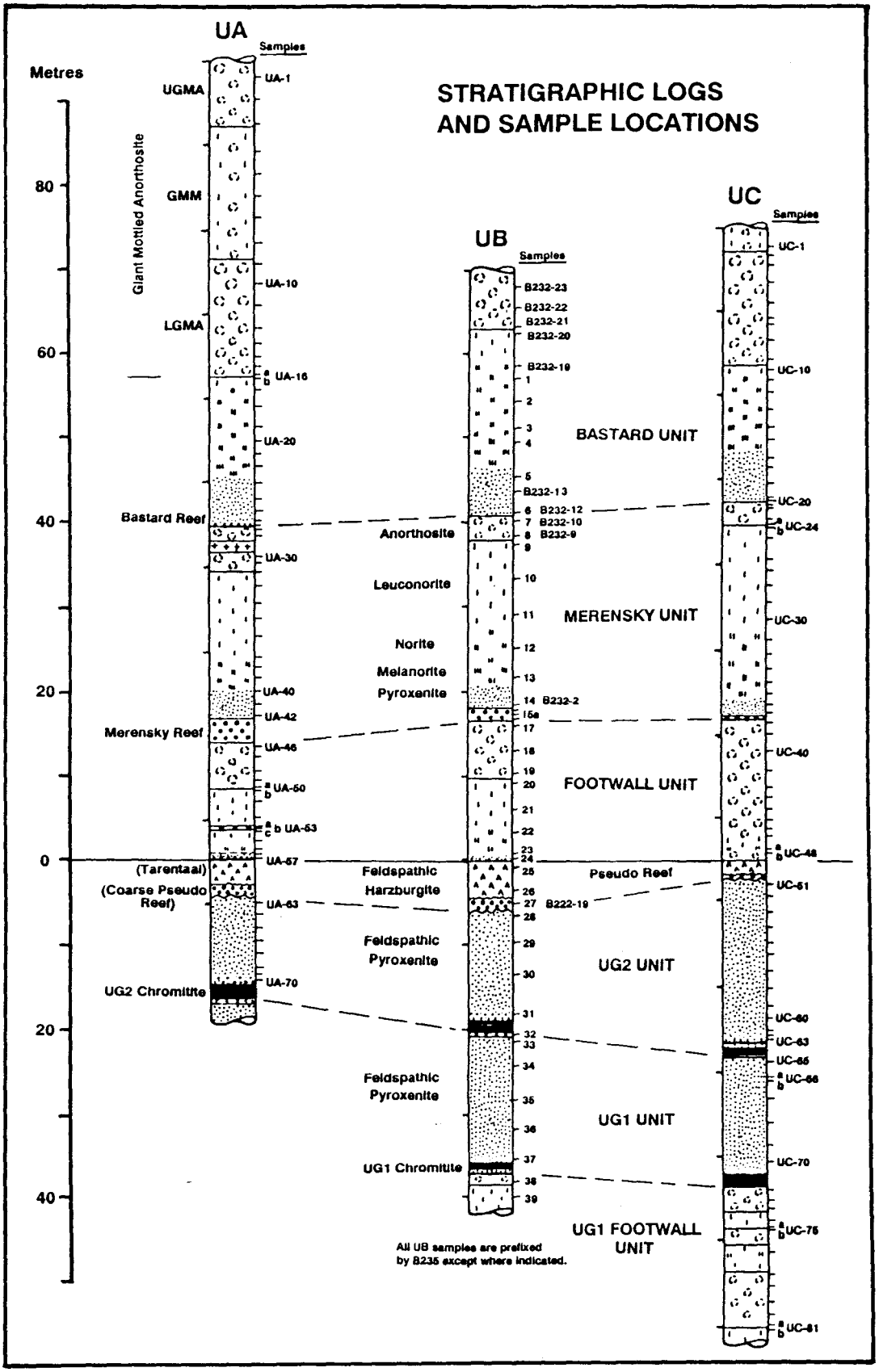

Figure 3.1 Stratigraphic columns of profiles UA, UB and UC showing the relative thicknesses of lithologies and the positions of individual samples.

3.2 Description of profiles.

A summary diagram of the three stratigraphic profiles (**UA**, **UB** and **UC**) showing the sample positions and different lithologies, is presented in Figure 3.1 while that for **UD**, **UE** and **UF**, including the trace element concentrations, is presented in Figure 3.2.

UA

Drilling of borehole **UA** (HN-3) was stopped in the footwall of the UG2 and hence no sample coverage for the pyroxenitic UG1 Unit is available. More complete sample coverage was obtained for the Bastard Unit than in **UB** and **UC**, but no whole-rock samples of the Merensky and Pseudoreefs were taken here.

UB

This sequence was compiled from carefully positioned underground boreholes (B235), supplemented by underground sampling, and two further boreholes (B232 and B222) which were drilled through a pothole sequence 1.2km to the east of B235 in the vicinity of Spud shaft (see de Klerk, 1982, p.60).

UC

This borehole (ZK-10), located in the eastern corner of the farm Zwartklip 405 KQ (Figure 1.3), intersects the normal stratigraphic succession. Sampling of **UC** covered an interval of 130m from 18m below the UG1 chromitite to the top of the Lower Giant Mottled Anorthosite. No whole-rock samples of the Merensky Reef or Pseudoreefs were taken here.

UD, UE and UF.

These three additional UG2 Unit intersections were selected in areas both up- and down-dip of the strike section through **UA**, **UB** and **UC**.

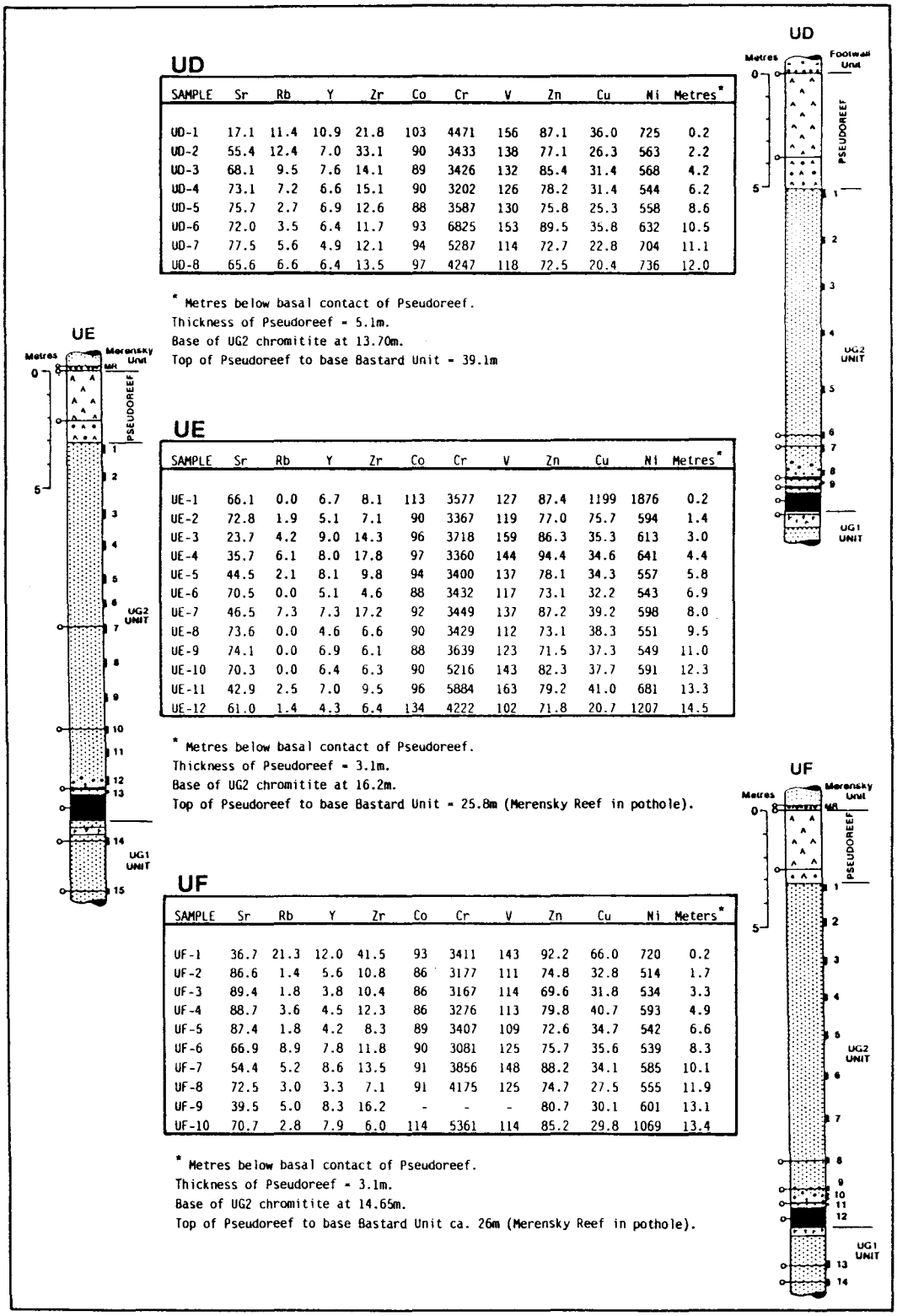

Figure 3.2 Stratigraphic logs and positions of individual samples for the UG2 Unit profiles UD, UE and UF. Results of trace element analyses are also shown. Note that profiles UE and UF have Pothole Merensky Reef overlying the Pseudoreef.

3.3 Stratigraphy.

A generalised account of the stratigraphy of the Upper Critical Zone has been presented in **1.4** and more detail is provided by de Klerk (1982) and Viljoen, et al. (1986a). Comprehensive coverage of the Bastard Unit sequence is presented in section **4.5**. Figure 3.1 also reveals the following facts:

1. There is marked variability in the thickness of the Merensky Reef. The apparent systematic thinning of the Reef along strike, from SW to NE (**UA** - 3.0m; **UC** - 0.64m), is quite misleading. Firstly, it has been shown that on a regional basis the Merensky Reef is much thicker in the NE sector of the mine, and, secondly, the Merensky Reef may locally be much thinner in close proximity to potholes. The location of **UC** close to a pothole explains the anomalously thin Merensky Reef intersection.
2. A notable feature of the Footwall Unit in **UC** is the development of a greater thickness of mottled anorthosite to the virtual exclusion of norite. This leucocratic sequence, dominated by mottled anorthosite, has only a trivial amount of norite developed near its base. In addition, there is no inch-scale layering in the **UC** Footwall Unit. The absence of the bulk of noritic rocks in this intersection is considered to be anomalous and localised, as borehole profiles in the same area (presented in van Zyl, 1970) indicate a normal development of the Footwall Unit (similar to that of profile **UB**).
3. The inch-scale layering, which is well developed in the Footwall Unit norites at **UB**, is pronounced in the **UA** profile. In **UB** stringers of orthopyroxene crystals (which form discrete layers at the position of sample B235/22) are separated by thin layers of anorthosite; the thickness of individual anorthosite layers decreases away from the centre of the layered sequence (see Figure 13 in Viljoen et al., 1986a, p.1071). At **UA** however, the thickness of the anorthosite layers has expanded to the point at which they coalesce and form a discrete anorthosite layer (0.5m thick) with layering in the norites above and below. This anorthosite layer has been correlated by some with the "Footwall Marker" at Rustenburg (Viljoen and Hieber, 1986).

3.4 Whole-rock compositional variations.

All major element data for **UA** and **UC** as well as their CIPW norms are presented in Appendix D (Tables D5 and D6). Here total Fe is represented as Fe_2O_3. The original data for **UA** and **UC** were also recalculated to an assumed Fe_2O_3/FeO ratio of 0.1 and normalised to 100%. These recalculated major element data, together with those of profile **UB** are presented in Tables D12 - D14 and have been used in all graphic representations. Trace element data for the three profiles are shown in these tables. Variations of selected elements and interelement ratios have been plotted against stratigraphic height in Figures 3.3 - 3.11 (MMF_{WR} ratio, Al_2O_3, TiO_2, MnO, K_2O, Ni/Sc ratio, and the trace elements Sr, Rb, Zr, Y, Co, Cr, V, Zn, Cu, Ni and Sc).

Whole-rock MMF_{WR} ratios (atomic ratio of Mg/(Mg+Fe) with all Fe expressed as Fe^{2+}) vary from highs of 0.82 in the pyroxenitic rocks, especially at the bases of units, to values below 0.50 in the leuconorites and anorthosites towards the tops of units (Figure 3.3). Within the Merensky Unit the MMF ratios show little variation below a threshold whole-rock value of 26% Al_2O_3 but rapid decline in the ratio occurs within the overlying leuconorites and anorthosites. A minor reversal in trend occurs in the uppermost samples immediately below the Bastard Unit contact in all three profiles, accompanied by marginally lower MMF ratios at the base of the Bastard Unit (see also **4.9.1**). This suggests that hybridization took place between the fractionated interstitial liquid of the Merensky Unit and a new influx of more primitive magma which initiated the deposition of the Bastard Unit.

This inference is supported by the behaviour of K_2O across the Merensky - Bastard Unit contact (Figure 3.5). K_2O concentrations increase upward through the Merensky Unit and reach values in excess of 0.4% within the anorthosite at the top of the unit. Indications in profile **UA** and **UB** are that the peak values are represented not in the very top of the anorthosite but in the second sample below the contact. Intermediate K_2O values are noted at the base of both the Merensky and Bastard Units. These values then decline to trace levels through the pyroxenite and melanorite before increasing through the upper parts of the unit. Rb shows a similar trend (Figures 3.10).

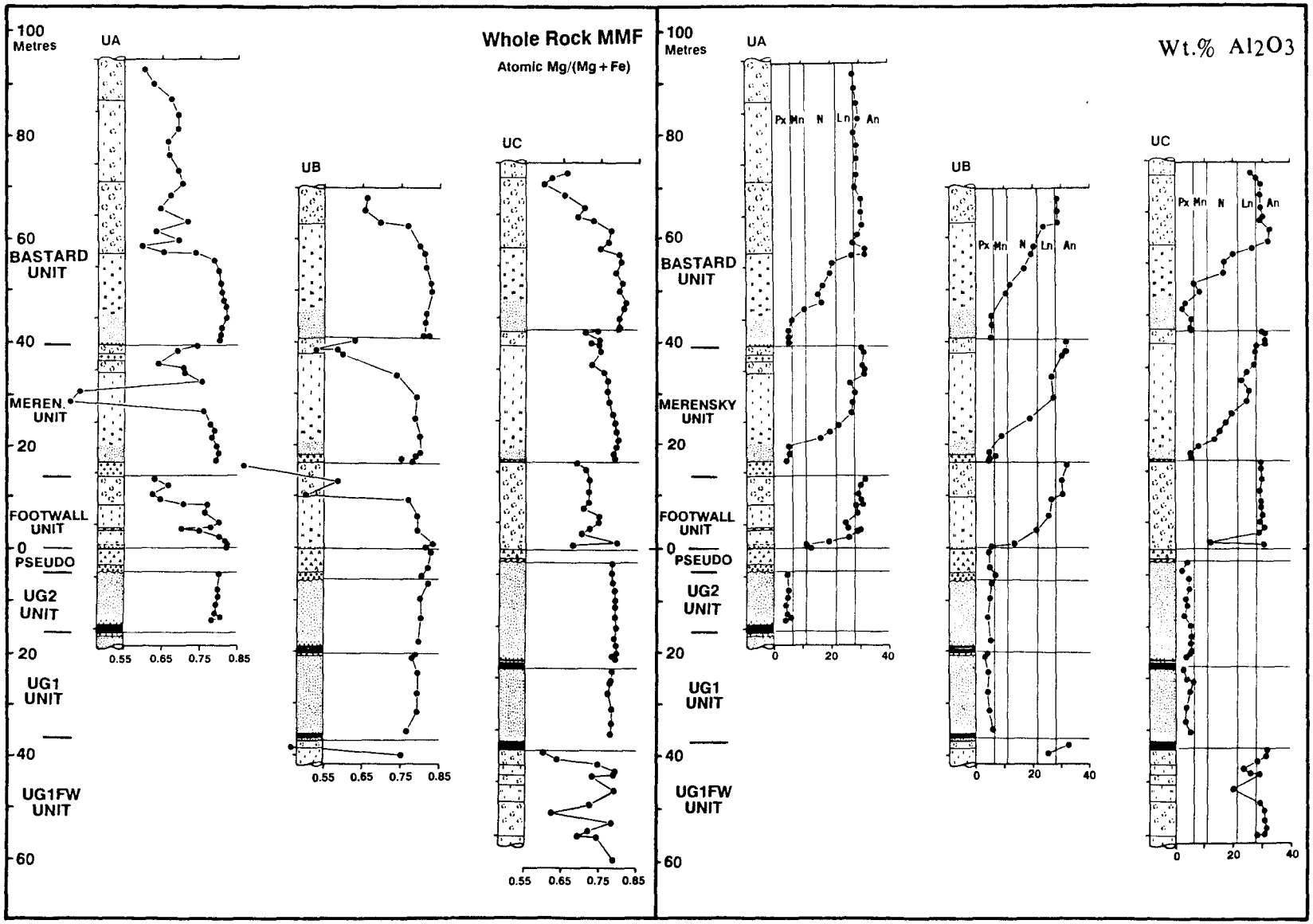

Figure 3.3 Stratigraphic variations of whole-rock MMF_{WR} ratio and $\%Al_2O_3$.

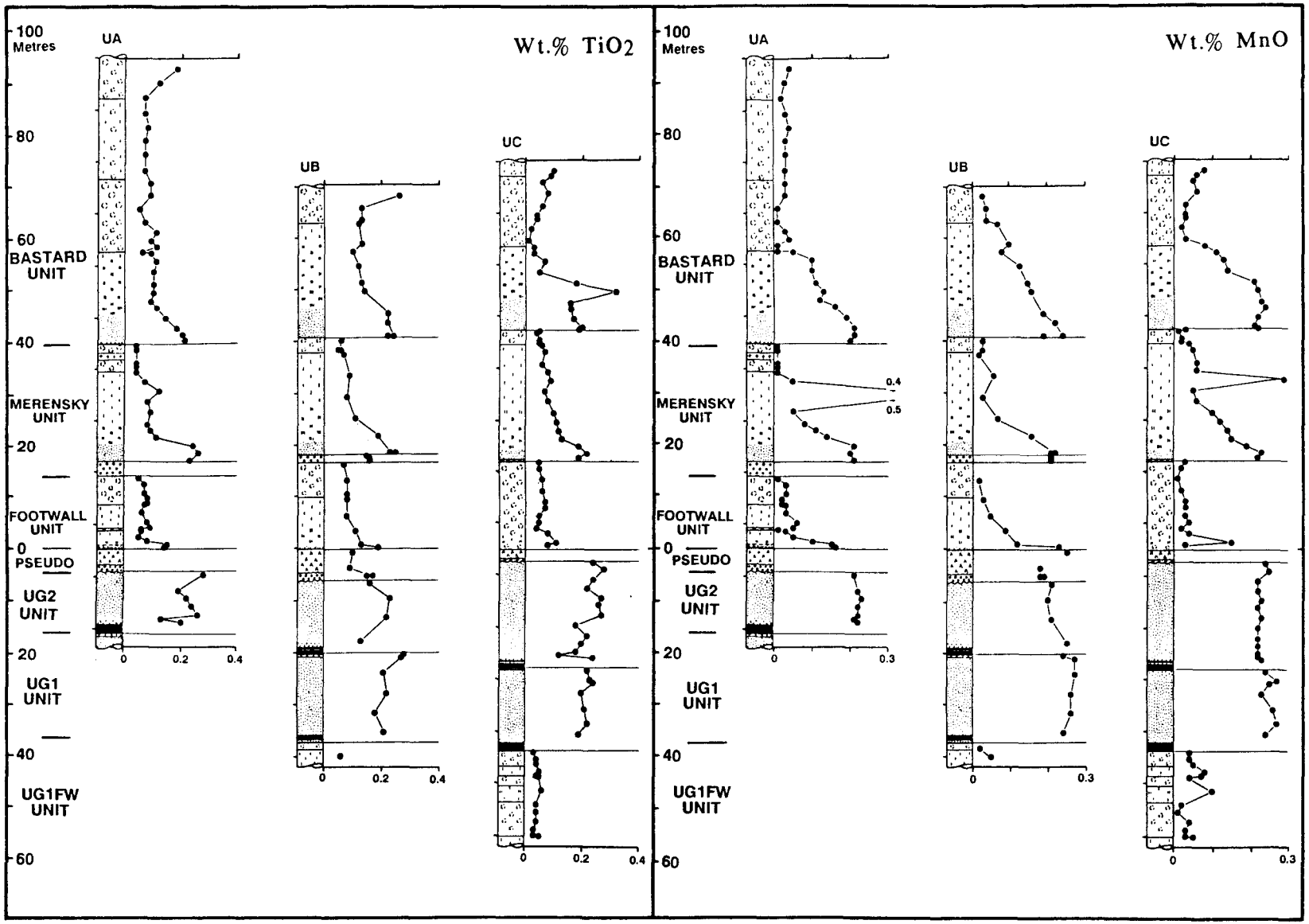

Figure 3.4 Stratigraphic variations of whole-rock $\%TiO_2$ and %MnO.

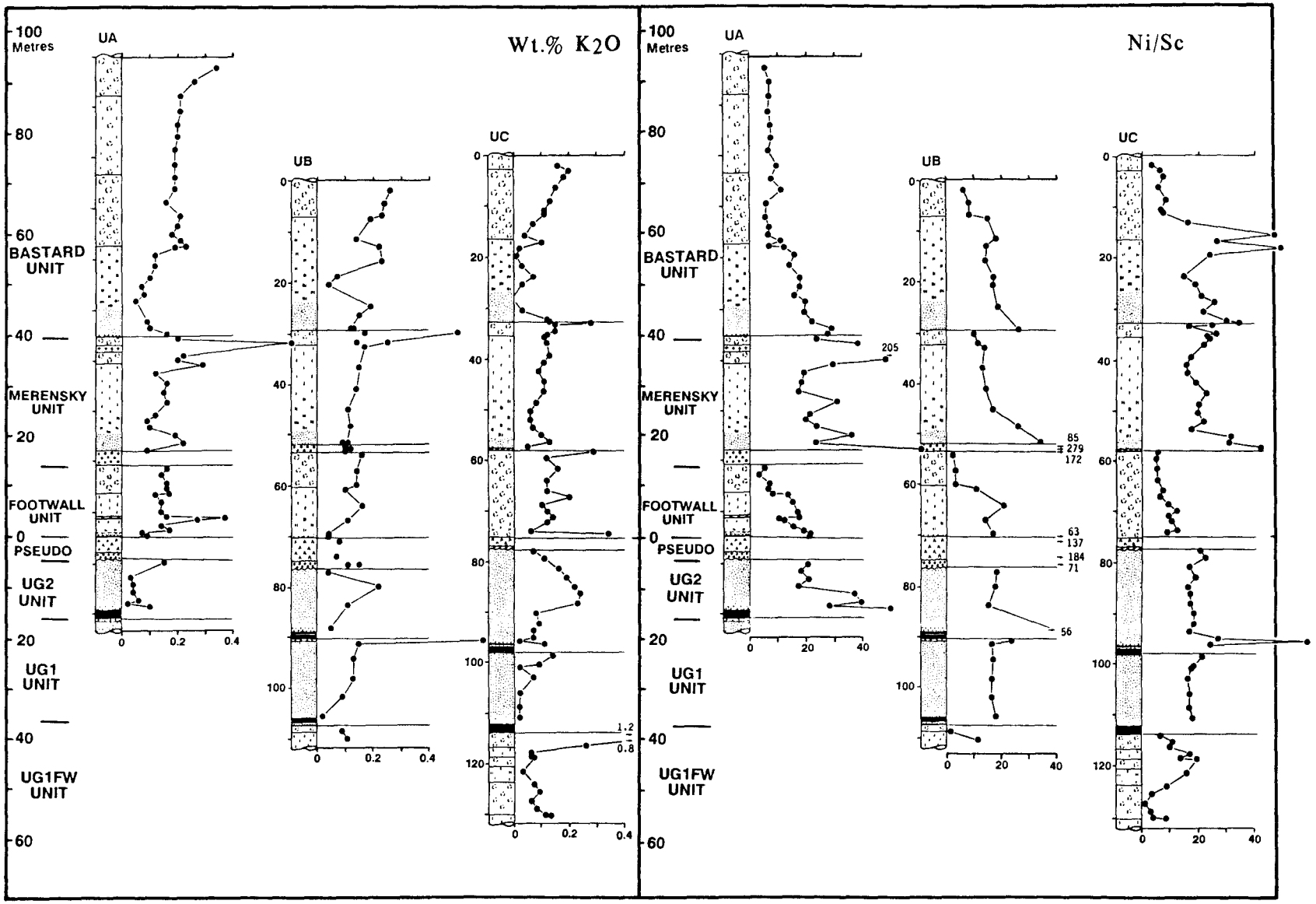

Figure 3.5 Stratigraphic variations of whole-rock $\%K_2O$ and the Ni/Sc ratio.

Strontium (Sr)

The range of Sr levels through the Upper Critical Zone varies from 22 to 560ppm. The lowest value (UC-17, an olivine-melanorite) is anomalous; the common range is 50-400ppm (Figure 3.6).

Sr has been shown to be one of the most useful indicators of cryptic variation and cyclicity in the Upper Critical Zone. Initial work done on profile **UB** (de Klerk, 1982) in which the whole-rock Sr was allocated to total normative feldspar and the calculated value of Sr in feldspar plotted against stratigraphic height, indicated distinctive Sr levels in the feldspars of the individual cyclic units. This feature was also demonstrated by Naldrett et al. (1984) at Union and Rustenburg by plotting whole-rock Sr against %MgO. Simple linear regression of the data from separate units yielded distinctly different regression models.

A refinement of this approach was introduced by Eales et al. (1986 and 1988) by plotting the $Sr/Al_2O_3^*$ ratio against stratigraphic height at Union and Amandelbult Sections. Here the $Al_2O_3^*$ value reflects the residual Al_2O_3 after the Al content of pyroxene has been subtracted from the whole-rock value as follows:

$$Al_2O_3^* = Al_2O_{3\ rock} - \left(\frac{MgO_{rock}}{MgO_{pyroxene}} \times Al_2O_{3\ pyroxene}\right)$$

This correction is used where samples are, effectively, composed of varying proportions of orthopyroxene and plagioclase (pyroxenites, norites and anorthosites). Where olivine is present as a crystallising phase a further correction, detailed by Eales et al. (1986), must be made. The $Sr/Al_2O_3^*$ ratio was used effectively by Eales et al. (1988, Figure 8) at Union (**UB**) and Amandelbult to show the characteristic signature of each unit. A composite diagram utilising data for the Footwall, Merensky and Bastard Units from different localities in the western Bushveld is presented in Figure 4.55.

To illustrate the unique Sr signature that is characteristic of individual units at Union Section the Sr data for the three profiles have been plotted against MgO for each of the Bastard, Merensky, Footwall and UG1FW Units (Figure 3.6). This approach is adopted here because

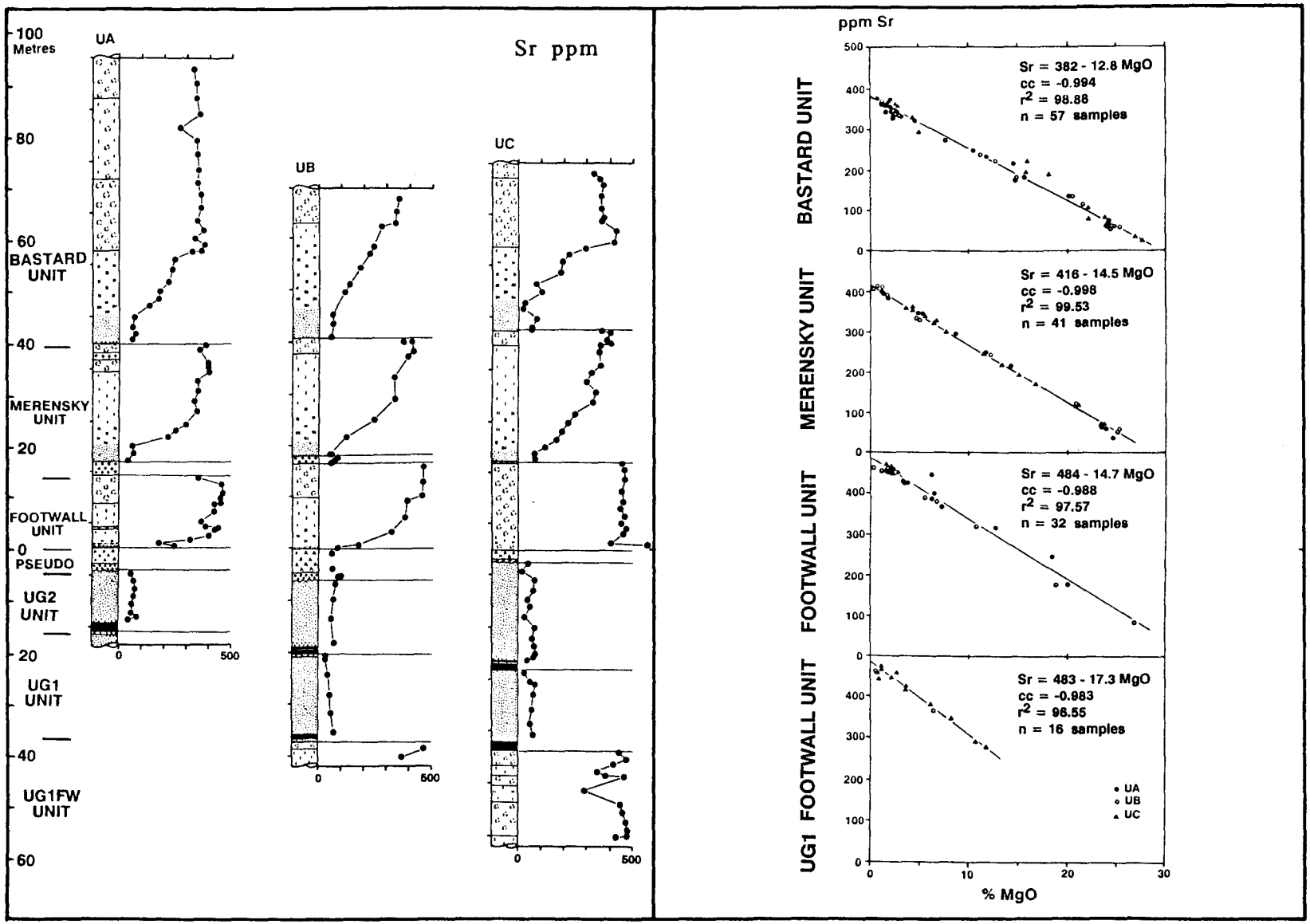

Figure 3.6 A) Stratigraphic variations of whole-rock Sr (ppm). B) Scatter plots of whole-rock Sr against %MgO for the three profiles (**UA**, **UB** and **UC**) in the Bastard, Merensky, Footwall and upper part of the UG1FW Unit. Regression analyses in each unit indicate that each has its own characteristic Sr content which is laterally consistent along strike.

insufficient orthopyroxene analytical data is available through **UA** and **UC**. Data for each unit clearly fall along well defined trends which are essentially controlled by the modal pyroxene content in the samples. A simple regression analysis of the data indicates that the projected Sr content in pure plagioclase is 382, 416 and 484ppm respectively, in each of the upper three Critical Zone Units, while that in the UG1FW Unit (483ppm) is similar to that of the Footwall Unit (Table 3.1). A value of 494ppm was obtained for all S-samples in the UG1FW Unit (Figure 2.17).

Table 3.1: Linear regression analysis of Sr against MgO for some Upper Critical Zone units.

Unit	Linear Model	Correlation Coefficient	Number Samples
Bastard	Sr = 382 - 12.6 MgO	-0.994	57
Merensky	Sr = 416 - 14.5 MgO	-0.998	41
Footwall	Sr = 484 - 14.7 MgO	-0.988	32
UG1FW (UB & UC)	Sr = 483 - 17.3 MgO	-0.983	16
UG1FW (S0 - S36)	Sr = 487 - 17.2 MgO	-0.990	37
UG1FW (All S samples)	Sr = 494 - 17.8 MgO	-0.992	74

Copper - Cu

Clear evidence of high sulphide concentrations at the base of cyclic units is indicated by Cu values generally in excess of 100ppm. If the high sulphide - Cu spikes are excised, characteristic background Cu values are clearly evident for individual units. Average background Cu values were calculated for individual units by pooling data for the three profiles and the results are presented in Table 3.2. The economically important Merensky and UG2 Units clearly have higher background Cu values of 51.6 and 33.6ppm respectively, indicating the ubiquitous presence of small amounts of sulphides throughout these units. Sulphides are less abundant in the Bastard and Footwall Units which results in whole-rock Cu values of c. 14ppm while there is an almost total absence of sulphide in the UG1FW Unit (9.3ppm Cu).

Table 3.2: Average background Cu concentrations in six Upper Critical Zone units as seen in the three profiles **UA**, **UB** and **UC**. High Cu values at the base of units and any anomalous "sulphide" spikes in excess of 100ppm have been excluded from the calculation. The population standard deviation is taken as the square root of the variance where n (the number of values) is used as the denominator rather than n-1.

Unit	Bastard	Merensky	Footwall	UG2	UG1	UG1FW
Mean	14.0	51.6	14.4	33.6	20.9	9.3
Pop. Std. Dev.	4.6	11.2	3.5	5.0	4.7	2.2
Number samples	46	28	29	20	13	19

Ni/Sc Ratio

The bulk distribution coefficients for Ni are greater than for Sc in mafic rocks and the Ni/Sc ratio is therefore a useful index of the increase in primitive character towards the bases of cyclic units. Discrepant values may be introduced by the presence of sulphides, but sulphide-bearing samples are recognised by anomalously high levels of Cu and have accordingly been rejected. These ratios (Figure 3.5) indicate the clear cyclicity of all the units in the Upper Critical Zone at Union Section. The Ni/Sc ratio has also been used to good effect by Eales et al. (1988) at Amandelbult to show the cyclicity between the Footwall and the Pseudoreef Multicyclic Units, which was not indicated by other geochemical parameters. Eales et al. (1986) also showed that Co/V, Cr/Sc and Cr/V ratios behave in much the same way as the Ni/Sc ratio and decline more or less steadily through each successive unit, but with minor reversals at the top of the Merensky Unit.

3.5 Summary.

Generalizations that may be drawn from Figures 3.3 to 3.11 are:-

(a) Levels of trace and minor elements are dominated by the modal composition of the host rock, and care is thus demanded in the interpretation of cryptic variations.

(b) The preferential partitioning of compatible elements into ferromagnesian silicates (Mn, Co, Cr, V, Zn, Ni, Sc) or plagioclase feldspar (Sr) is clearly revealed.

(c) The behaviour of those elements normally regarded as incompatible in basaltic systems is unpredictable, and their absolute levels are controlled not so much by distribution coefficients as by the amount of intercumulus liquid retained in the cumulates (i.e., by texture). Accordingly, no consistent trends are shown between pyroxenites and anorthosites by Rb, Zr and Y.

(d) While Ti behaves incompatibly in basaltic rocks, it is partitioned here into pyroxenes and chromite, leaving leucocratic rocks impoverished in Ti in the absence of appropriate host phases.

(e) K_2O shows enrichment towards the top of cyclic units, particularly in the Merensky and Bastard Units. This enrichment is mainly due to the presence of intercumulus K-feldspar (orthoclase) and partly to an increase in the K_2O levels of the plagioclase (as shown in **4.8.4**).

(f) Interelement ratios like MMF and Ni/Sc clearly illustrate the nature of cyclicity in the Upper Critical Zone. Primitive values at the bases of individual units give way to more evolved levels upward through the sequence. Some cycles are incomplete and do not display upward fractionation (UG1, UG2 and Pseudoreef Units). These units have been "beheaded" either by removal of the upper part of the units, or an interruption of crystallisation due to a new influx of magma into the chamber.

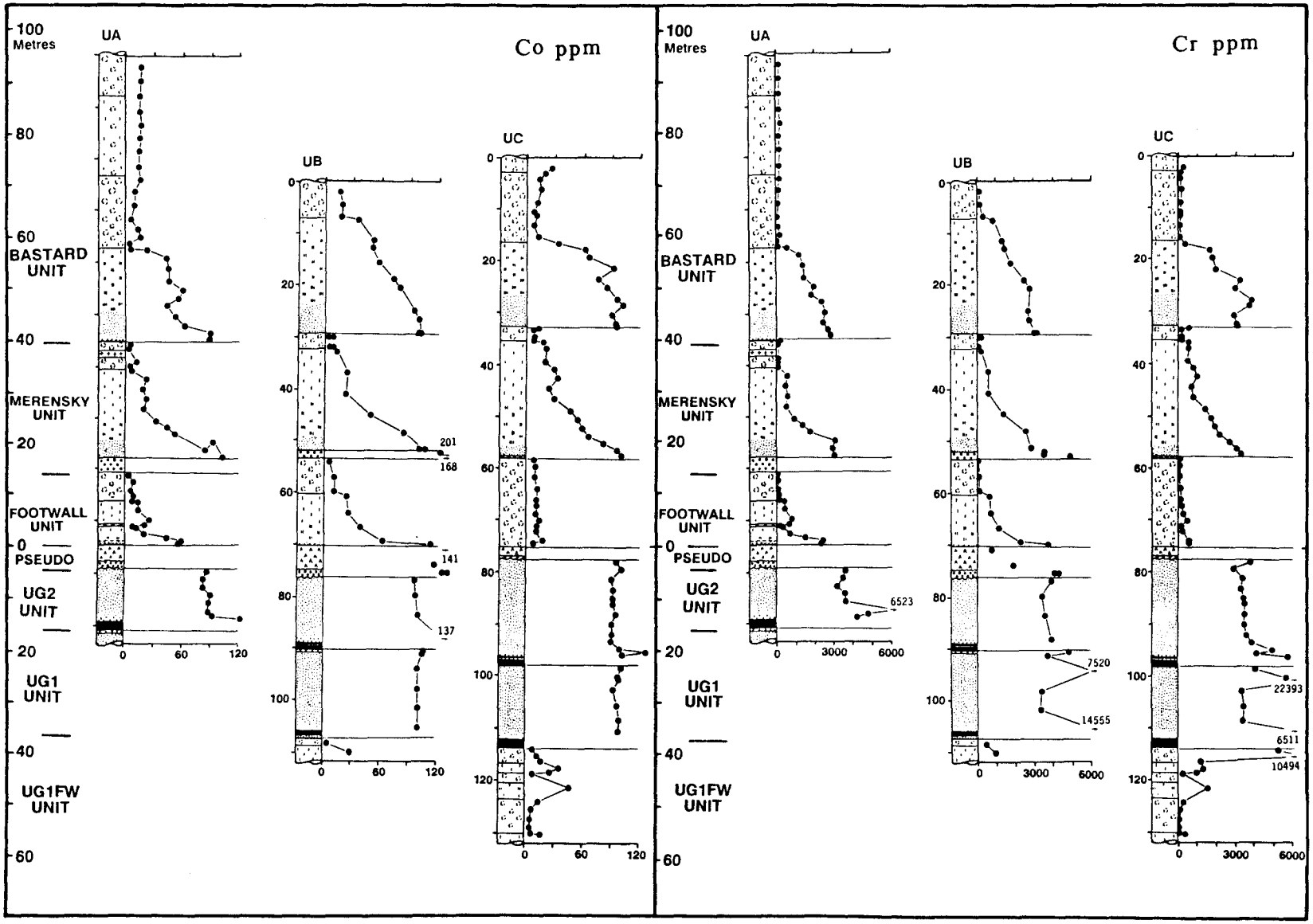

Figure 3.7 Stratigraphic variations of whole-rock Co and Cr (ppm).

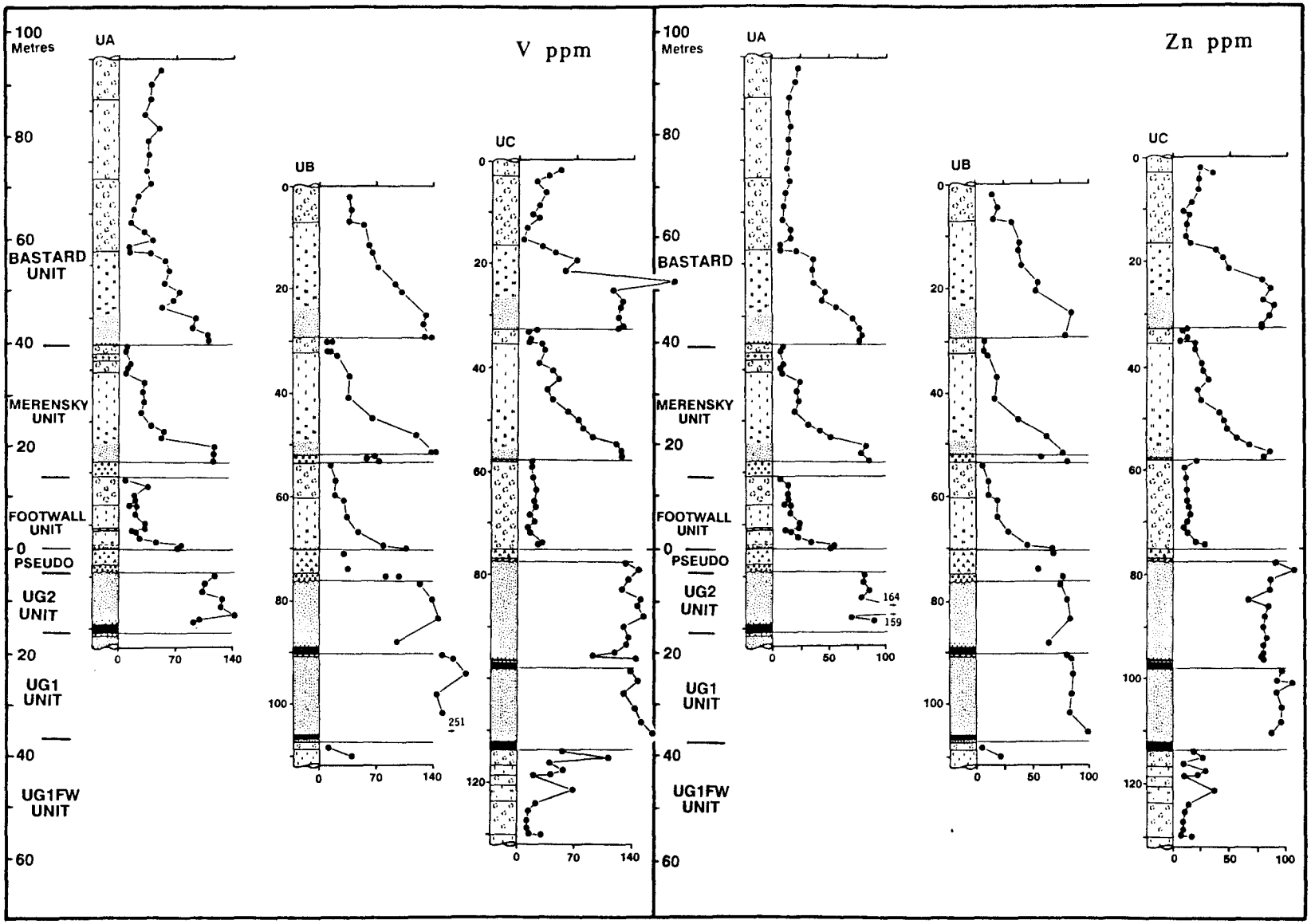

Figure 3.8 Stratigraphic variations of whole-rock V and Zn (ppm).

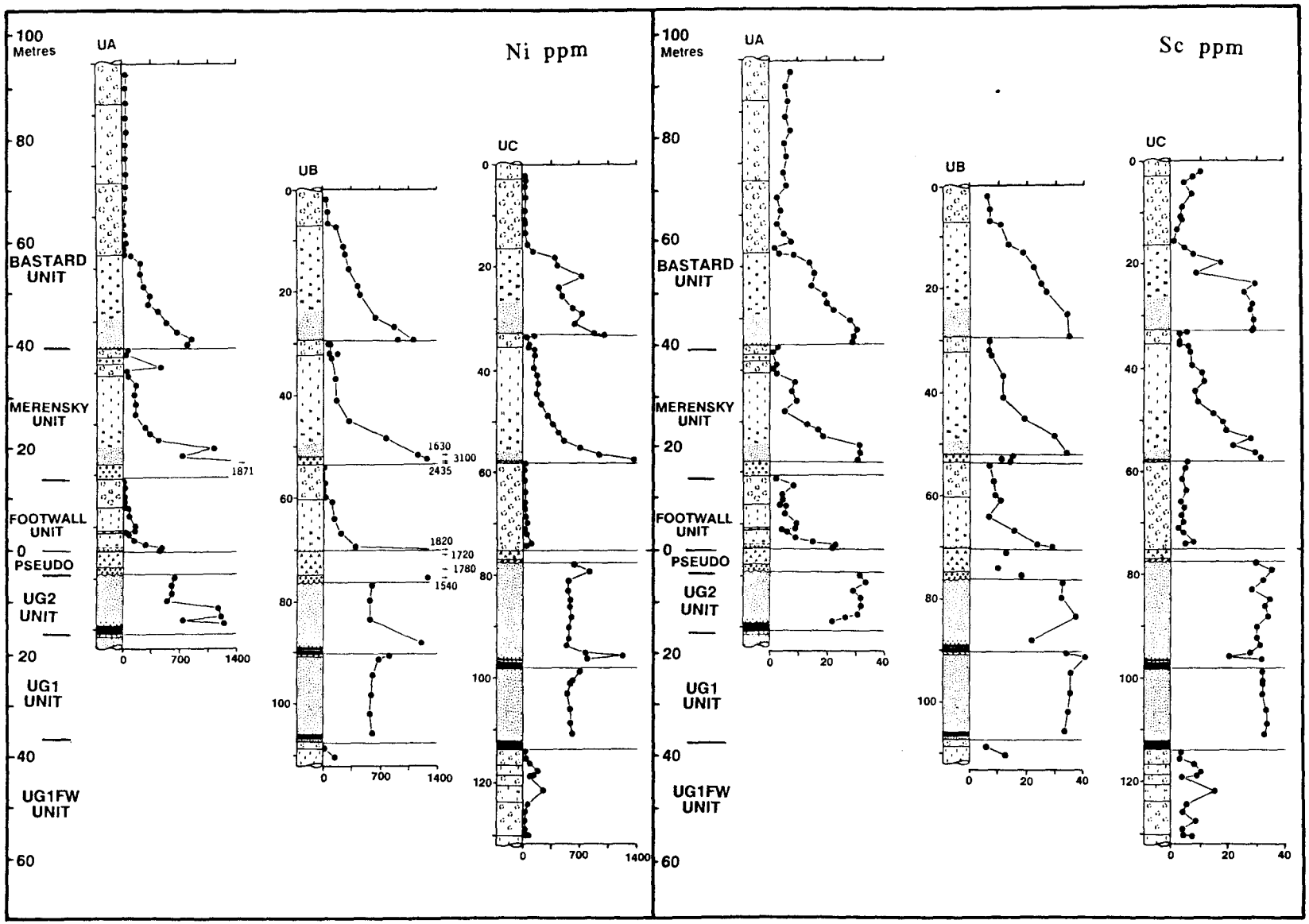

Figure 3.9 Stratigraphic variations of whole-rock Ni and Sc (ppm).

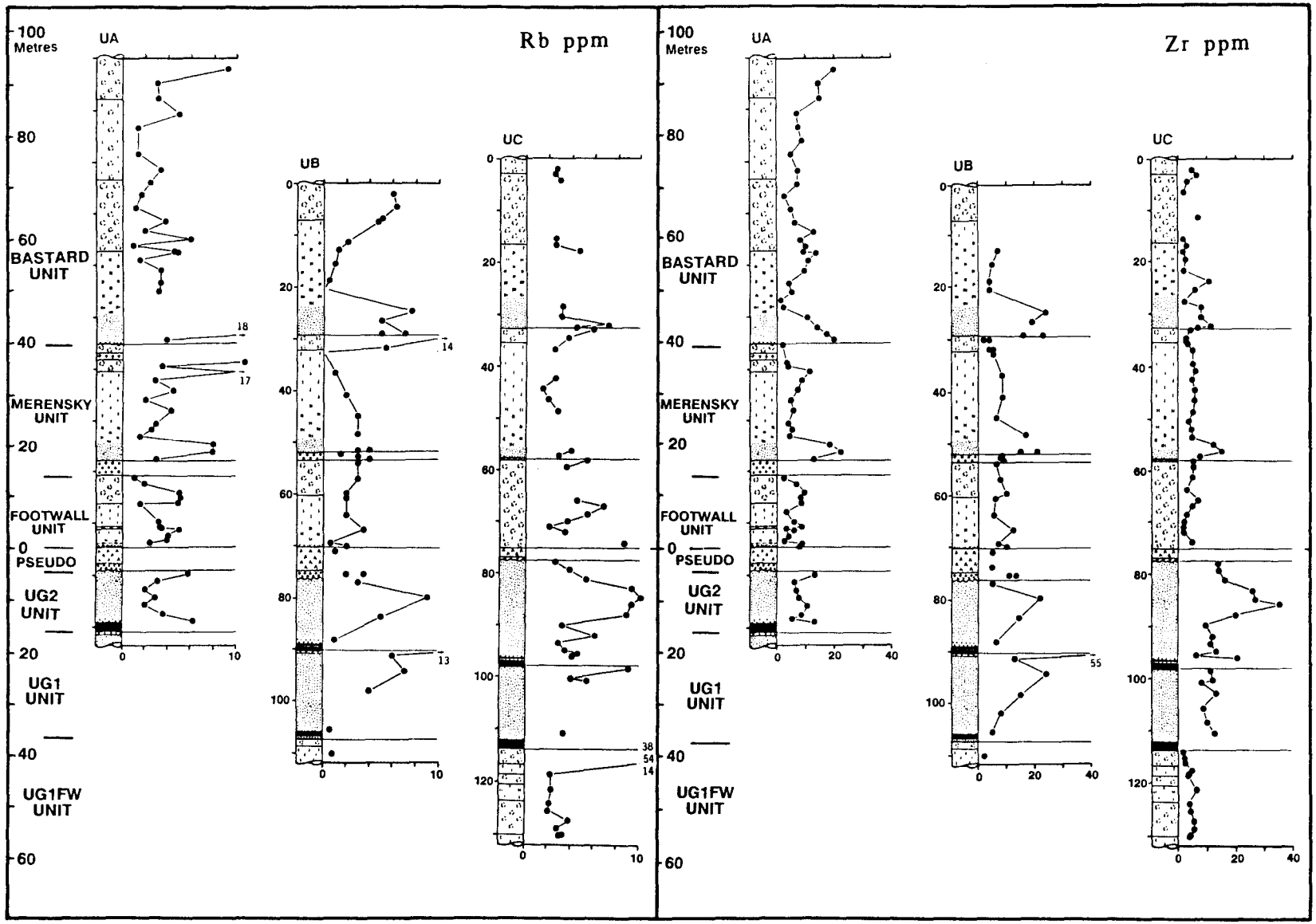

Figure 3.10 Stratigraphic variations of whole-rock Rb and Zr (ppm).

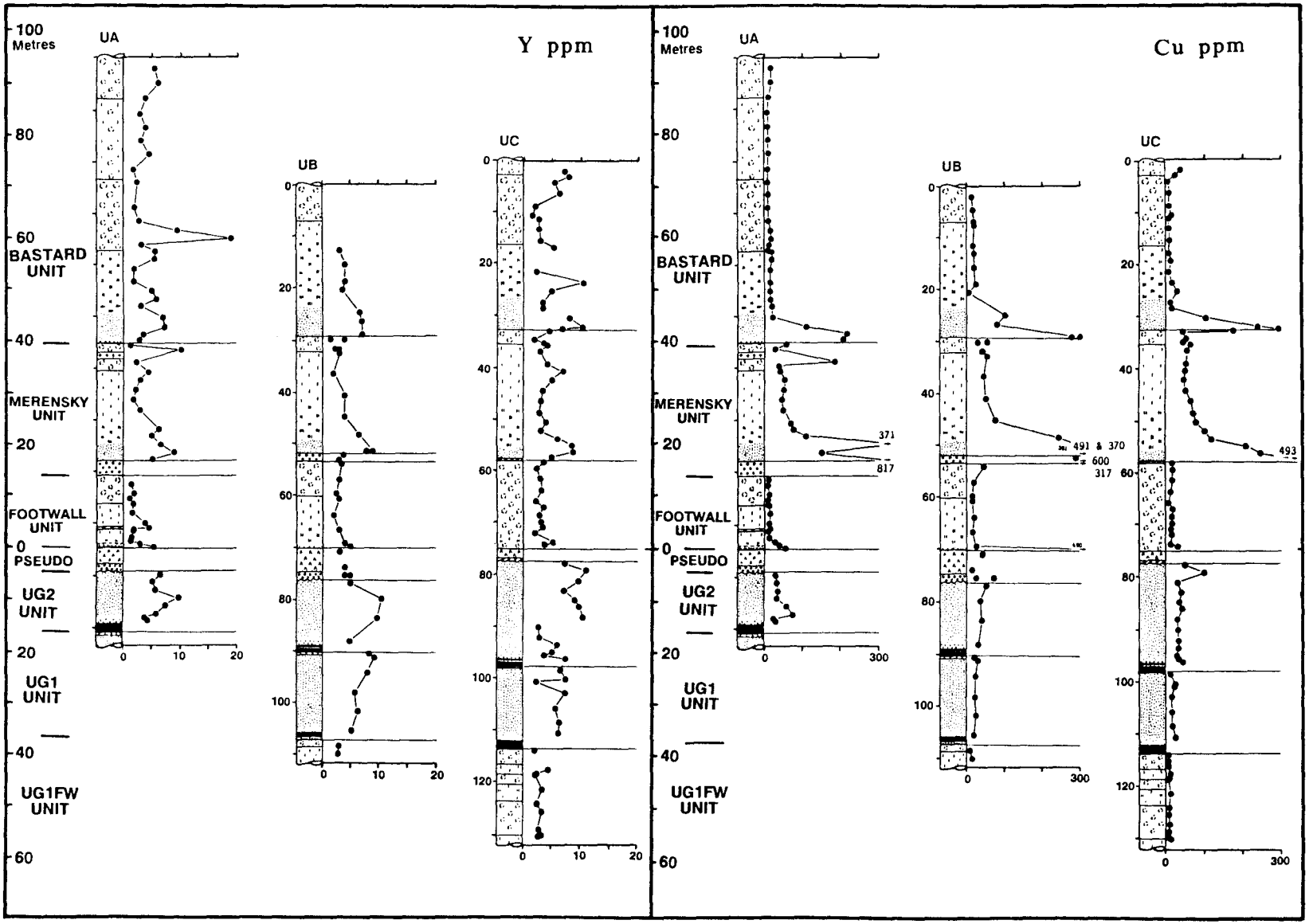

Figure 3.11 Stratigraphic variations of whole-rock Y and Cu (ppm).

CHAPTER 4

THE BASTARD UNIT ALONG 171 KM OF STRIKE IN THE WESTERN BUSHVELD COMPLEX

4.1 Historical note and summary of previous work.

After the initial discovery of the Merensky Reef in the eastern Bushveld by A.F. Lombaard in September 1924 (Cousins, 1969), Dr Hans Merensky and his team traced it for several hundred kilometers along strike both in the eastern and later in the western Bushveld Complex. During this phase of exploration the hangingwall and footwall successions of the Merensky Reef were exposed in surface boreholes and trenches and it was recognised that a very similar sequence of rocks occurred 10-15m higher in the column above the platiniferous "reef". This rock sequence closely resembled the Merensky Reef Unit.

Trenching was by far the most economical and rapid method used to trace the extent and position of the Merensky Reef and was extensively used, especially in the western Bushveld Complex. Here trenches were dug through the black-turf soil cover to a depth of between 1,5 and 6m. The initial trenching target was the mottled anorthosite footwall of the Merensky Reef as it provided a clear marker of the position of the overlying Reef itself. Mottled anorthosites are more resistant to weathering than the more melanocratic rocks and hence the overlying soil profile is not as deep. Occasionally, exploration trenches were inadvertently sited well into the hangingwall of the Merensky Reef, and the exposed sequence was incorrectly identified as the Merensky Reef. This upper "reef" came to be known as the **Bastard Reef** in view of the frustration it caused these pioneers.

The earliest description of the **Bastard Reef** to be found in the literature is that of Wagner (1925) where, in a discussion of "platinum deposits of the **Merensky horizon type** found in the Lydenburg districts" (eastern Bushveld), the following is said (p.107):-

> "Boreholes put down on Forest Hill No.342 and Maandagshoek No.148 prove that there is a so-called "**Bastard Reef**" lying between 40 and 50 feet above the Merensky Horizon. This is identical in petrographical character with the Main Reef but carries only traces of platinum. It is underlain and overlain by spotted anorthosite."

In his discussion of the Rustenburg district (p.108) Wagner states the following.

> "Within the past fortnight ore of the Merensky Horizon type has been opened up under the direction of Dr. H. Merensky ..... Here as in the Lydenburg district, the platinum bearing layer is overlain by a "**Bastard Reef**". This lies from 50 to 70 yards, measured horizontally above it, and is composed of medium grained pseudoporphyritic diallage norite. It carries only traces of platinum. The hangingwall is formed of mottled anorthosite and the footwall of spotted anorthosite. There is much prospecting activity in the area, and further discoveries are to be expected."

Feringa (1959) based his study in the northwestern Bushveld Complex at Union Section and subdivided the Upper Critical Zone (which he called the Differentiated Zone after the terminology of Wagner, 1929) into eight sub-zones on the basis of whether the rocks were dominantly **Pyroxenitic** or **Anorthositic**. Consequently the Bastard Unit was subdivided into two sub-zones only, namely 7 and 8 (Figure 4.1). Sub-zone 7, a feldspathic pyroxenite, represented the Bastard Reef (or Bastard Merensky - a local mining term which is unlikely to have pleased its discoverer!), while sub-zone 8 included the noritic rocks as well as the overlying Giant Mottled Anorthosite (**GMA**). Feringa (1959) recognised a subtle textural variation within the anorthosites and made a three-fold subdivision of the GMA (discussed in **4.5**).

Cousins (1964 and 1969) compiled a series of profiles from around the Complex and correlated individual layers in the Upper Critical Zone between these localities. In his first paper only a preliminary attempt was made at correlation and six profiles were used (two in the east and four in the west). In the second paper more detailed stratigraphic profiles were used (four in the west and six in the east) which included the top of the Critical Zone. He called this the Layered Zone. A number of features of the Bastard Unit were highlighted by this study:-

* It occurs in both the eastern and western limbs of the Bushveld Complex and has the same gross characteristics in both areas.
* At all localities it has a footwall of mottled anorthosite.

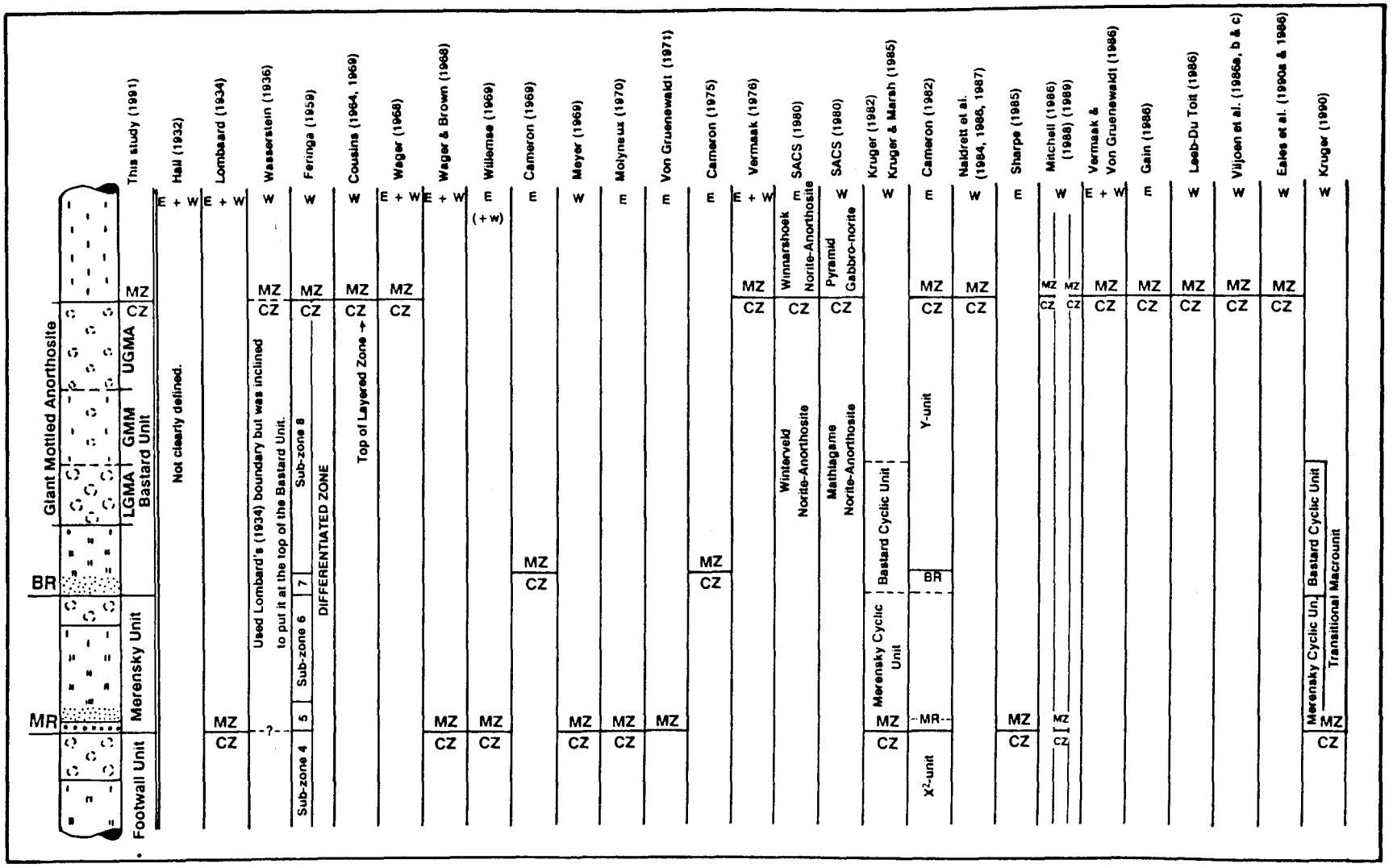

Figure 4.1 Diagram illustrating stratigraphic subdivisions used by various workers on the layered sequence at the top of the Critical Zone and overlying Main Zone of the Bushveld Complex. MZ = Main Zone; CZ = Critical Zone; MR = Merensky Reef; BR = Bastard Reef; W and E = West and East limbs of the Complex.

* Its maximum thickness is attained at Union Section (75m) while the overall thickness throughout the Complex is c. 60m and usually in excess of 40m. The figure of 31m quoted by Cousins for Rustenburg is considered to be too low. An exception to this generalisation is that of profile **LEF** quoted in this study, where the thickness is 2.61m.
* The basal feldspathic pyroxenite is not present in some areas of the eastern Bushveld where only norites are developed (Turfpan and Booysendal).
* The basal pyroxenite appears to be duplicated in certain areas of the eastern Bushveld (Maandagshoek, Eerstegeluk and St.George). This feature was also noted by Vermaak (1976) in the eastern Bushveld. A duplication of the pyroxenite layer in profile **X**, at Impala Platinum Mine, is reported in this study.
* A three-fold subdivision of the GMA is recognised both in the east and west. Cousins (op. cit., p.243) goes on to say that

> "This mottled anorthosite of the Bastard Unit is always characterised by a central portion, in which the mottling is much smaller, and where the pyroxene clusters that form the mottles show sedimentary-like stratification".

This middle layer he called **Banded Anorthosite** and it is equivalent to the present writer's Giant Mottled Middling (**GMM** - see **4.5**).

The first account of the petrology and geochemistry of the Upper Critical Zone rocks at Union Section was that of van Zyl (1960 and 1970). This work was based on the farm Swartklip 988 (Figure 1.3), which now forms the north-eastern part of Union Section Mine. The Merensky Reef on this farm is now largely mined out. Van Zyl (1970) correlated the stratigraphy in five boreholes in the area, and reported on the petrography and limited geochemical studies of selected samples from borehole ZK-9 (3 samples in the Bastard Unit). This borehole is one kilometre west of the profile **UC** and has a stratigraphic sequence similar to it.

Some features of the petrography and mineralogy of the Bastard Unit in the Eastern Bushveld were noted by von Gruenewaldt (1973) in his work on the Main Zone at Roossenekal. Three samples from each of the Merensky and Bastard Units were analysed and both these Units were included in the lower **Subzone A** of the Main Zone. Mitchell (1986) carried out a study of

the Main Zone of the western Bushveld at Union Section. He included the Bastard Unit, at the base, in his study profile and these data provide a record of cryptic variation that is relevant to the present study.

A milestone paper on regional aspects of the Merensky Unit and part of the Bastard Unit was published by Vermaak (1976). Here a detailed description of a number of Upper Critical Zone profiles from around the entire Complex was presented. A feature which Vermaak noted was that "the Bastard Reef [i.e. the pyroxenite] thins rapidly towards the southern extremities of both lobes of the Complex in the eastern and western Transvaal" (1976, p.1286).

Cameron (1982), in his systematic documentation of petrography and cryptic variations in the Critical Zone of the eastern Bushveld Complex, placed the GMA and its noritic footwall into his Y-Unit at the top of the Critical Zone (Figure 4.1). He included the Bastard pyroxenite with the underlying Merensky Unit. Only five samples from the Bastard Unit are described by Cameron (1982) and these were used mainly for petrographic analysis; two silicate mineral analyses were also reported.

Work by Kruger (1982) and Kruger and Marsh (1982, 1985) was focused on Rustenburg Section Mine (**RPM**) and here the cryptic variations of the main mineral phases were studied through the top three cyclic units of the Upper Critical Zone (Footwall, Merensky and Bastard Units). In this work Kruger placed the contact of the Main Zone at the base of the "Merensky cyclic unit". Emphasis in this study (Kruger, 1982) was on the cryptic variations of the main silicate mineral phases - determined mainly by electron microprobe analyses and XRF analyses of mineral separates. The work of Kruger and Marsh (1982) also provided the first profile of initial strontium isotope ratios (Sr_i) through the Upper Critical - Main Zone succession. This work has been widely quoted in the literature in view of the fact that the marked inflection of the ratio to higher values at the level of the Merensky Reef has been interpreted as indicative of a major influx of magma which brought about the platinum enrichment within the Merensky Reef and the crystallisation of the bulk of the Main Zone rocks.

More recent studies on the three upper cyclic units of the Critical Zone in the western Bushveld by Naldrett et al. (1984, 1986 and 1987) and Naldrett (1989) have focused on two stratigraphic profiles at Union (borehole TB-12) and Rustenburg (boreholes RTL-7 and 21). This detailed work on the mineral and whole-rock geochemistry (cryptic variation) of the Footwall, Merensky and Bastard Units was used by Naldrett et al. (op. cit.) to illustrate the geochemical behaviour of these rocks and also to develop a model for the origin of the Merensky-type platinum ore deposits. This model, they argue, is equally applicable to the PGE deposits in other layered complexes.

The studies of de Klerk (1982), Scoon (1985), Mitchell (1986) and Field (1987) focused on aspects of the Bastard Unit. Field (1987) investigated three Upper Critical Zone profiles at Amandelbult Section, which included the lower part of the Bastard Unit. Whole-rock major- and trace-element analyses and microprobe analyses of the main silicate mineral phases were collected for one profile (**AE**) while whole-rock trace element data only were compiled for profile **AF**. These data have been included in the present study.

By utilising this considerable database of field relations, whole-rock data, mineralogical analyses and isotopic information, Eales et al. (1986, 1988, 1990a, 1990b, 1991) have developed a model to explain the sequence of events which resulted in the crystallisation of the Upper Critical Zone. A preliminary account of the present study of the Bastard Unit has also been presented by de Klerk (1989).

4.2 Scope of the present study.

The present regional study of the Bastard Unit was started as an extension of the work done at Union Section on three Upper Critical Zone profiles between the UG1 and the top of the Bastard Unit (**UA**, **UB** and **UC**, Figures 1.3). A further series of Bastard Unit profiles were then selected and sampled from areas south of Union Section at Rooderand (farm 46JQ - on the north-western flank of the Pilanesberg Complex) and from the Impala Platinum Mine lease area north of Rustenburg (Figure 1.1).

elsewhere in this sector of the Complex has been included in Lefkochrysos the synthesis. A further profile in the Brits area, made available by the (**LEF**) Mining Company, is also included in the database (this mining venture is now controlled by Rand Mines and called the Crocodile River Platinum Mine).

Seventeen vertical profiles, with varying densities of sampling, were compiled through the Bastard Unit. For some profiles only the geological log was available whereas in others, where the core has been preserved, samples were taken and analysed for whole-rock major and selected trace elements. Electron microprobe analyses of the main silicate and oxide mineral phases (ortho- and clinopyroxenes, olivine, plagioclase and spinel) were also carried out.

To depict the spatial distribution of the profiles in Figure 4.4 a convention is adopted that assumes that the reader is viewing the western arc of the Complex from a position east of the Pilanesberg. The individual profiles, covering 171km of strike, are thus presented (from left to right) in the following order:

Lefkochrysos (**LEF**)	-	1 profile
Western Platinum (**WP**)	-	1 profile
Rustenburg (**RPM**)	-	2 profiles
Impala (**Z**, **Y** and **X**)	-	3 profiles
Rooderand (**RD**)	-	2 profiles
Union (**UA**, **UB**, **UC**)	-	3 profiles
Amandelbult (**AD**, **AE**, **B**, **AF**, **C**)	-	5 profiles

4.3 The definition of cyclic units.

Cyclicity of cryptic variation and other geochemical parameters in an orderly sequence of layered magmatic rocks has been recognised by numerous workers on layered complexes (Jackson, 1961 and 1970; Irvine and Smith, 1967; Wager and Brown, 1968; Vermaak, 1976; Campbell, 1977; etc.). The repetition of rock layers in layered mafic sequences is generally clear enough in the field, but there is some doubt as to which rock-type should be seen as the first in the cycle. The usual approach, which is certainly both practical and geologically sound, is to define

the start of a unit (cycle) as a chromitite layer, or a layer of ultramafic rock (Wager and Brown, 1968), overlain by lithologies of more leucocratic character. Irvine et al. (1983) and Irvine and Sharpe (1986) have theorised on the basis of their two-magma (U and A-type) concept that for genetic reasons the appropriate starting rock type is anorthosite. They consider that an ideal anorthosite-bearing Bushveld cyclic unit should be, from base to top:

anorthosite - chromitite - pyroxenite - norite,

while that for the Stillwater Complex is

anorthosite - peridotite - troctolite (p.186).

For the Bushveld Complex they cite the MG3, MG4 and especially the UG1 chromitite layers as being typical of the first sequence.

A short review of different criteria used to position the subdivisions of individual cyclic units is presented in Eales et al. (1986). They point out that in any orderly sequence of layers ABCABCABC a cyclic repetition is apparent, but the identity of that layer that starts a cycle is not always obvious (cycles might be ABC, BCA or CAB). Cycles will, however, be defined within a layered sequence by geochemical parameters that are either characteristic of individual cyclic units (Figure 4.2a), or evolve progressively from some primitive value within each cyclic unit (Figure 4.2b).

A typical example of the first pattern would be the distinctive $Sr/Al_2O_3^*$ ratio displayed by the individual units of the Upper Critical Zone at both Union and Amandelbult Sections. An example of the second pattern would be the evolving inter-element ratios within the units (MMF, Co/V, Ni/Sc) which display a distinctive saw-tooth pattern (see Figures 3.3 and 3.5, or Eales et al., 1986 and 1988). The geochemical coherence of the MG3, UG1FW, UG1 and other units discussed in Chapters 2 and 3 clearly argue against the definition proposed by Irvine and Sharpe (1986), and cyclical units of the Upper Critical Zone are thus ideally characterised, in the author's view, by the sequence:

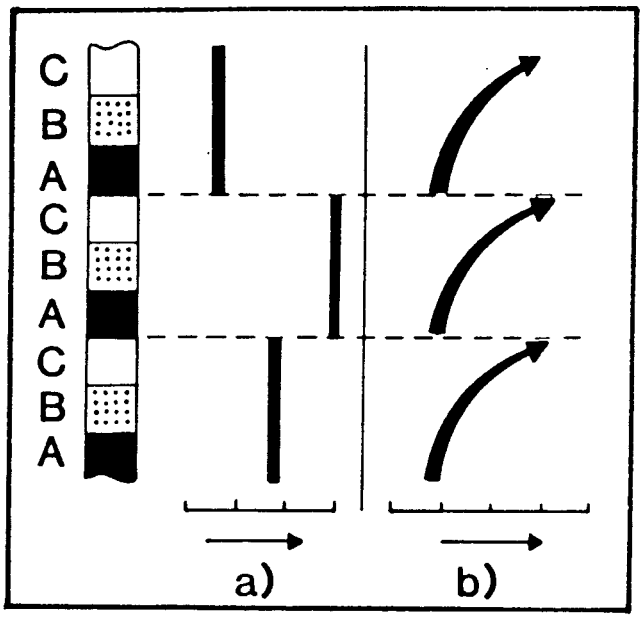

Figure 4.2 Schematic representation of geochemical parameters that (a) are distinctive of individual cyclic units or (b) evolve progressively from some primitive value within each cycle. From Eales et al. (1986).

chromitite - pyroxenite (± olivine) - norite - anorthosite.

Individual cycles are in some cases not complete and are represented by the lowermost lithologies only (UG1, UG2 and Pseudoreef Units). The incomplete development of a cycle might be the result of either the removal at a later stage of the upper lithologies or incomplete development before the onset of renewed crystallisation in response to the introduction of a fresh magma pulse. In summary then a cyclic unit is defined by:

* a distinctive lithological and geochemical break at its base, which contrasts with the rock-type at the top of the underlying unit,
* a similar lithological and geochemical break at the top, and
* coherence or smooth gradation of geochemical parameters <u>within</u> the unit.

The contrast in both lithology and geochemistry is poorly defined at the top of the Bastard Unit, and this has resulted in some ambiguity in the

definition of its top contact (SACS, 1980). The transition is essentially based on a textural change of the minor mafic mineral phases in a predominantly leucocratic sequence - from intercumulus to cumulus habit. Some geochemical parameters which are now described help to resolve this ambiguity.

4.4 Geological setting.

The Bastard Unit of the Upper Critical Zone can be traced from a position some 16km east of Brits to the eastern boundary of RPM Amandelbult Section, south of Thabazimbi, a distance of 200km (Figure 1.1 and 1.2). Because of the poor exposure of the Critical Zone in the western Bushveld, the character of the Bastard Unit is known mainly from borehole intersections directed at the underlying, economically important Merensky Reef and UG2 layers, and to a lesser extent from underground mining development (most mining development is confined to the footwall of the Merensky Reef). The Critical Zone, and hence the Bastard Unit, is not continuous over this distance and gaps occur in four places:-

a) an 11km gap to the south of the Pilanesberg where rocks of the Upper Critical Zone pinch out against the floor of the Complex (in this case metasediments of the Transvaal Supergroup),
b) a 23km gap occurs where the Pilanesberg Alkaline Complex has intruded through the mafic rocks of the Bushveld Complex,
c) a gap to the south of Union Section which is 11km wide, and
d) a further gap between Union and Amandelbult Sections which is 12km wide.

Because of a lack of good exposure, and hence of any reliable detailed information, there is as yet no unanimity on the origin and structure of (c) and (d) above - colloquially known as the "Southern and Northern Gap Areas". A summary of the ideas regarding the origin of these two gaps is presented in de Klerk (1982, p.8-11) and Viljoen et al., (1986a, p.1064-1066). These gaps in the Critical Zone succession do present a problem when interpreting the geochemistry across the gaps as it is not known whether the preserved Critical Zone at Rooderand, Union and Amandelbult represents separate magma chambers (with a common source) or whether it

is a single chamber, in which the Critical Zone (and perhaps the Main Zone) rocks crystallised prior to being isolated along strike by emplacement of the Upper Zone rocks seen in these areas today.

4.5 The Bastard Unit sequence in detail.

The "Bastard Unit" is the last of the cyclic units of the Upper Critical Zone, overlying the Merensky Unit; its upper contact is here taken at the top of the GMA as recommended by SACS (1980, Figure 4.1). The Unit is different from the underlying units for three reasons: it does not have a well-defined top contact (with an overlying unit); it is much thicker than the Merensky and Footwall Units; and it has an unusually thick sequence of mottled anorthosite at its top. From published information it is evident that the Bastard Unit is usually in excess of 2.5 times the thickness of the Merensky Unit (Table 4.1).

Table 4.1: Indicated thicknesses of the Merensky and Bastard Units extracted from the literature (m).

	Merensky	Bastard	Ratio	Source
Western Plats	12	42	3.5	Farquhar (1986)
Rustenburg	10	64	6.4	Viljoen and Hieber (1986)
Impala (mid)	10	56	5.6	Leeb-du Toit (1986)
Boschkoppie	11	40	3.6	Cousins (1969)
Union	29	67	2.3	Feringa (1959)
Amandelbult	22	61	2.8	Cousins (1969)

A generalised stratigraphic column of the Bastard Unit interval in the western Bushveld Complex has the following features from the base upwards (Figure 4.3).

* The footwall of the Bastard Unit is consistently made up of mottled (poikilitic) anorthosite which forms the top of the Merensky Unit. This anorthosite is often devoid of intercumulus mafic minerals (mottles) along the immediate contact (1-2cm) and contains irregular patches of finely disseminated base metal sulphides which appear to have been derived from the overlying Bastard pyroxenite by filtering

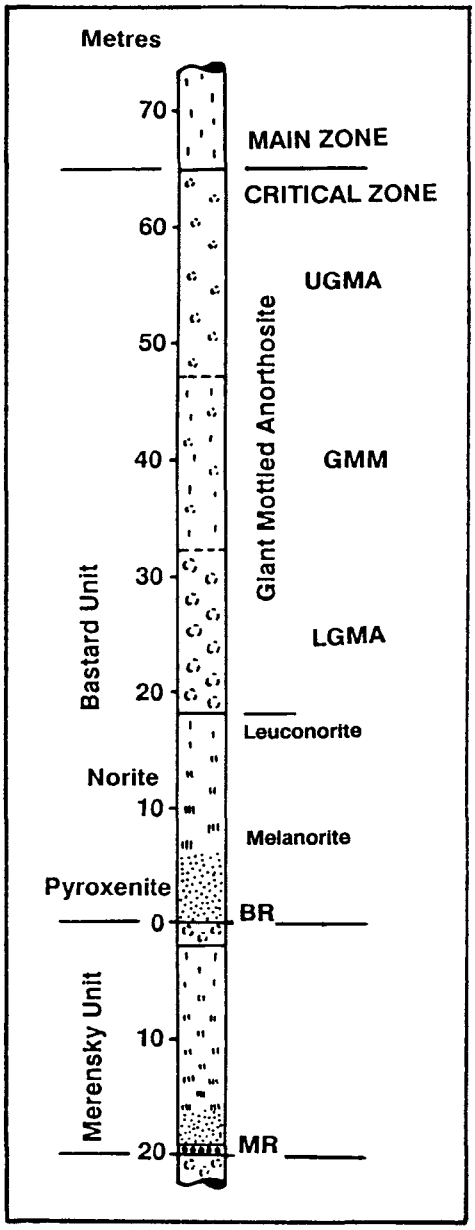

Figure 4.3 Representative stratigraphic column of the Bastard and Merensky Units in the western Bushveld Complex. BR = Bastard Reef; MR = Merensky Reef; UGMA = Upper Giant Mottled Anorthosite; GMM = Giant Mottled Middling; LGMA = Lower Giant Mottled Anorthosite. Thin chromitite seams occur at the top and bottom of the MR and at the base of the BR.

downward into interstitial pore space. This same feature is more pronounced in the footwall of the Merensky Reef.

* At Union Section, where the Merensky Reef is in pothole condition (see **1.4**), the Merensky Unit mottled anorthosite is overlain by a streaky, well-layered leuconorite, usually 1.5m thick - this now forms the footwall of the Bastard Unit. This lens-shaped layer of leuconorite

has a distinctive fabric produced by acicular orthopyroxene crystals and tabular cumulus plagioclase crystals which are randomly orientated in the plane of layering. It also has a high concentration of disseminated sulphides and occasional, isolated chromite grains. This texture is unique to the Bastard Unit footwall and is found only where the underlying Merensky Reef is potholed. This same feature is also recognised at the newly developed Northam Platinum Mine down-dip from Amandelbult Section (M. Botha, pers. comm. 1991).

* The basal contact of the Bastard Unit is characterised by a very thin chromitite layer which is never more than 5mm thick, and often only 1-2mm thick. This layer is rarely preserved, as the contact zone is intersected by a bedding plane shear which often destroys the layer (Plate 4.1a). This feature was also recorded by Cousins (1969), who noted that "movement along the fault has developed a mud seam along the fault plane". No evidence of any significant displacement has been recorded, although slickensides are evident. Hydrothermal alteration of the immediate footwall and hangingwall rocks, in the form of saussuritisation and serpentinisation of the anorthosites and pyroxenites, respectively, is also common. Rare underground exposures where the basal chromite layer has been preserved also display a "dimpled" or undulatory contact with the underlying anorthosite, similar to but less pronounced than that at the base of the Merensky Reef.

* A feldspathic orthopyroxenite, known as the **Bastard pyroxenite**, overlies the thin chromitite layer (Plate 4.1a). A colloquial term, "Bastard Reef" has also been applied to this pyroxenite, but generally refers to the lower (15-30cm) sulphide-bearing, mineralised part of the layer. This pyroxenite (usually 4-5m thick) varies in thickness from 15cm in the Brits area to as much as 5.5m in the **UA** profile. Occasionally, a patchy development of a coarse pegmatoidal texture is seen in the lower 10-15cm of the pyroxenite, as in the Merensky Reef. Larger crystals (oikocrysts) of clinopyroxene, up to 2cm in diameter, which partly or wholly enclose smaller cumulus orthopyroxene grains, are also encountered within the pyroxenite. Fine-grained, disseminated base metal sulphides, with associated low levels of PGM, Cu and Ni mineralisation, are present in this basal portion.

Plate 4.1a Contact between the Bastard pyroxenite and the underlying Merensky Unit (mottled anorthosite). Here the basal chromitite layer of the Bastard Unit has been destroyed by the pronounced bedding plane shear. Locality - Rustenburg Section, Townlands shaft 7 crosscut north.

Plate 4.1b Contact between the leuconorite and the overlying LGMA. Note the distinctive layering and suggestion of penecontemporaneous deformation within the leuconorite (pencil for scale in leuconorite). Locality - Union Section, Richard shaft 11-6S crosscut east.

* With the appearance of cumulus feldspar the pyroxenite gives way to a noritic sequence with the pyroxenite-norite contact being gradational rather than sharp. The noritic package is characterised by melanorite at the base, and the progressive introduction of more cumulus plagioclase feldspar upward through the sequence results in a leuconorite at the top (Plate 4.1b). A characteristic feature of this noritic layer at Union and Amandelbult Sections is a diffuse yet distinctive layering near its top. At Rooderand, and further to the south of the Pilanesberg, the norite and leuconorite contain discrete, thin anorthosite partings. Leeb-du Toit (1986, p.1102) records that between two and three anorthosite layers occur approximately 2m from the top of the norite in the Impala area. Personal observation, as well as information published by Vermaak (1976, p.182, columns 13 & 14) and Kruger (1982, p.16), confirm the existence of a thin but distinctive anorthosite layer within the leuconorite at **RPM**.

* Overlying the leuconorite is a distinctive, composite anorthositic sequence made up of poikilitic anorthosite, generally known as the **Giant Mottled Anorthosite (GMA)**. Examination of underground exposures of the interface between the underlying leuconorite and the GMA indicates that intercumulus pyroxene may sometimes form a continuous layer at this boundary (Plate 4.2a). At other localities the boundary is characterised by distinct layering of cumulus orthopyroxene at the top of the leuconorite (Plate 4.1b). This boundary layer is occasionally characterised by textures which indicate that significant movement took place in the semi-consolidated crystal pile before solidification. "Soft sediment deformation" textures like flow-folding and slumping of the layers are evident (Figure 4.1b). Overturned flow-folds and slump structures, up to 3m in length, are also reported at this level at Northam Platinum Mine (M. Botha, pers. comm. 1991). Similar features have been documented in feldspathic peridotites on the Isle of Rhum (Wadsworth, 1973). The thickness of the entire GMA varies between 25 and 54m, although the **LEF** profile would appear to display an anomalously thin anorthosite of only 2.5m. The GMA layer can broadly be subdivided into three distinct parts. Feringa (1959) and Cousins (1964, 1969) also recognised these sub-divisions.

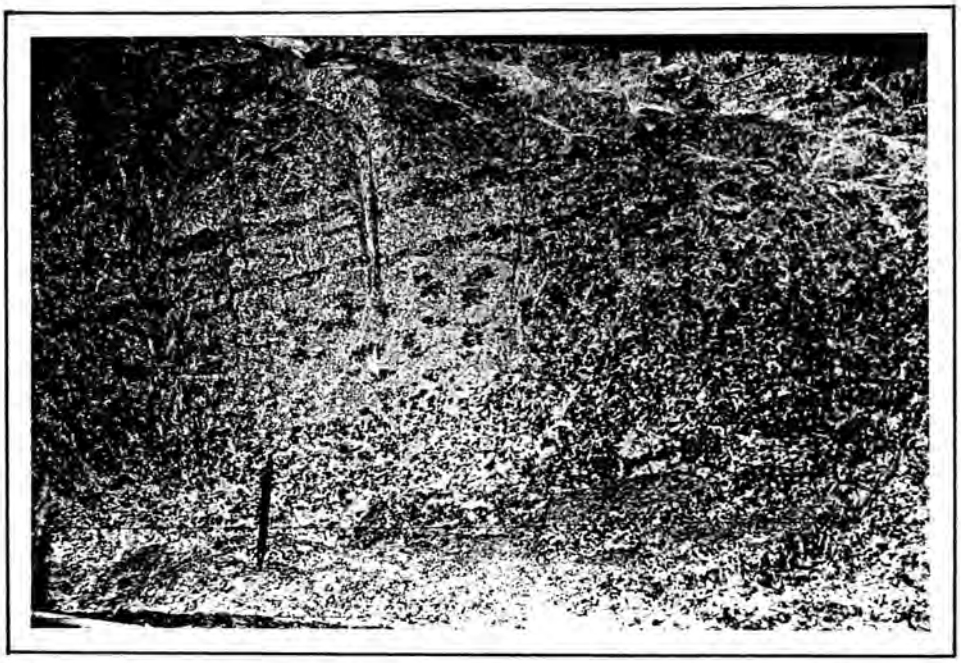

Plate 4.2a Contact between the leuconorite and the overlying LGMA. Here a distinctive layering is developed within the mottled anorthosite c. 20cm above the contact (pencil for scale in leuconorite). Locality - Union Section, Richard shaft 11-6S crosscut east.

Plate 4.2b Contact between the LGMA and the GMM. Note the contrast in size of the mottles between these two lithologies. Locality - Union Section, Richard shaft 11-6S crosscut east. Person in photograph is Dr. C.A. Lee.

a) The Lower Giant Mottled Anorthosite (**LGMA**) is recognised as being quite different in character to the rock types higher up in this sequence. It is characteristically made up of an anorthosite with large, diffuse, grey mottles of ortho- and clinopyroxene (>10cm in diameter) set in an adcumulus anorthosite (Plates 4.1b and 4.2a & b). The anorthosite between the mottles is usually snowy white but does display local subtle variations in colour from white to grey, while in areas of **Pothole Merensky Reef** at Union Section it has a distinctive pinkish hue. The LGMA is readily recognisable throughout the western Bushveld and ranges in thickness between 7.2 and 15.6m. It has an average thickness of 14m in the Union and Amandelbult areas while in the Rooderand area, and southward (Western Platinum Mine) the layer is generally thinner at 6.5-10m.

b) The middle portion, here termed the Giant Mottled Middling (**GMM**), is predominantly a "mixed zone" of leuconorite and anorthosite with **small** mottles, sometimes termed "anorthositic norites" or "spotted anorthosites" in the literature and mining company borehole logs. This lithology has a mixed character, with the leuconorites often displaying subdued mottling and in some cases grading into small-mottled anorthosites (Plates 4.2b and 4.3a & b).

c) The Upper Giant Mottled Anorthosite (**UGMA**) is characterised by an anorthosite in which the mottles are both smaller and not as prominent as those in the LGMA (Plate 4.3b). Leeb-du Toit (1986, p.1102) reports that in the Impala area "the mottles are set in a dirty-grey, needle-like feldspar matrix" and this would aptly describe the other profiles as well.

Kruger (1982, p.29), in his study of the Bastard and Merensky Units at Rustenburg, recognises that there is a distinct difference in lithology and texture between the lower 9m and the rest of GMA package. He proposed that this basal part of the GMA be named the "Bastard Mottled Anorthosite". The description by Viljoen and Hieber (1986) of the same area indicated an identical thickness for the GMA but did not distinguish the three different lithologies described here.

* Overlying the GMA is a zone of leuconorites and norites with occasional small-mottled anorthosite layers. These rocks gradually grade upwards into the gabbronorites of the Main Zone.

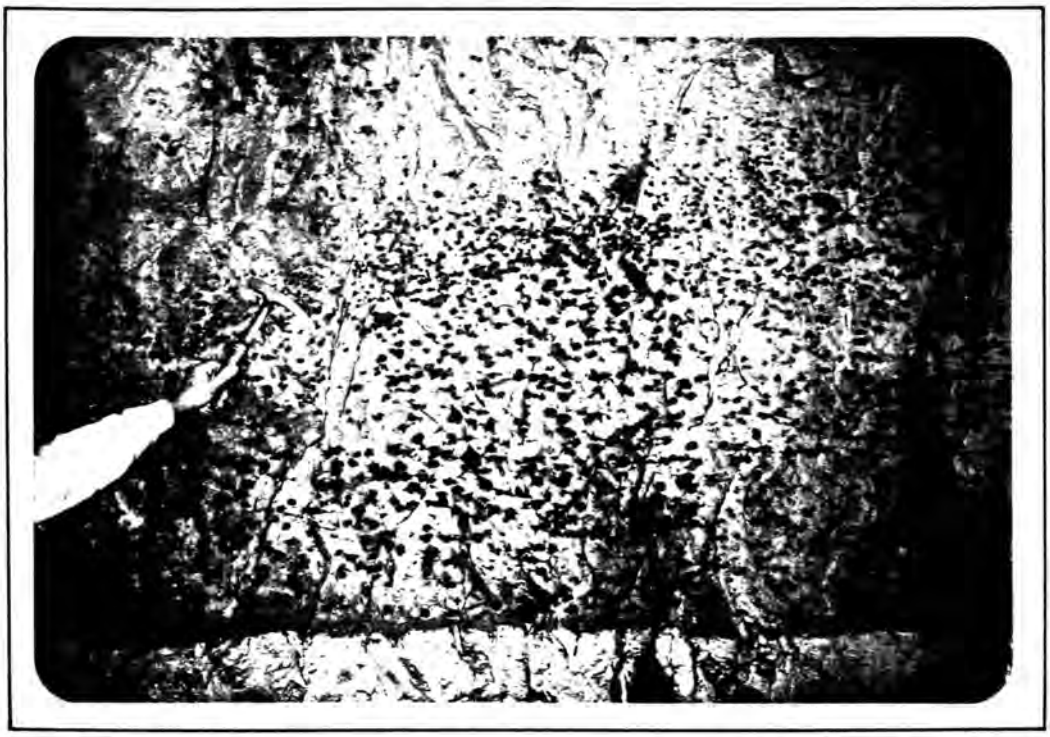

Plate 4.3a Exposure of the Giant Mottled Middling - a small-mottled anorthosite. Locality - Union Section, Richard shaft 11-6S crosscut east.

Plate 4.3b Contact between the GMM and the overlying UGMA. The mottles in the UGMA are more diffuse than those in the underlying GMM and the LGMA (pencil for scale c. 20cm above the contact). Locality - Union Section, Richard shaft 11-6S crosscut east.

4.6 Description of profiles.

The stratigraphic sequence and sample positions in each profile are presented in Figure 4.4 and an account of the individual profiles is presented in Appendix A. Table 4.2 summarises the thicknesses of individual layers as well as the sampling densities, and the number and type of analyses executed within each profile. The data from the work of Naldrett et al. (1984, 1986 and 1987) on single profiles at Rustenburg and Union Sections are integrated with the present compilation.

4.7 Petrography.

The Bastard Unit is made up of a range of lithologies that illustrates extreme variation over a restricted interval of c. 60m. This contrasts with the more uniform sequence in the overlying Main Zone with its characteristically subtle lithological changes. The mineralogy of all the rock types in the Bastard Unit is relatively simple and comprises mainly orthopyroxene, plagioclase feldspar and clinopyroxene with minor chromite, olivine, biotite and some base metal sulphides in varying modal proportions.

Petrographic studies were focused on 212 samples from nine profiles; **LEF**, **RPM**, **Y**, **X**, **RD**, **UA**, **UB**, **UC**, and **AE** (Figure 4.4). The petrography of the different rocks (defined in **4.5**) is described from the base of the Unit upwards.

4.7.1 Basal chromitite layer.

The basal contact of the Bastard Unit, which is rarely observed in underground or borehole exposures (see **4.5**), has fortunately been preserved at three localities which have been sampled - two at Union Section (**UB** sample H232/3 reported in Eales (1987) and **UA**-27) and one at **LEF** (sample H998.1). This contact is characterised by a thin chromite layer of variable thickness (usually no more than 1-2mm), although a more robust (5mm) seam is recorded at **UB** (H232/3; Plate 4.4c). It may locally be discontinuous or absent. At **LEF** (Plate 4.4a) the small subhedral chromite grains form an undulating and sometimes patchy or discontinuous

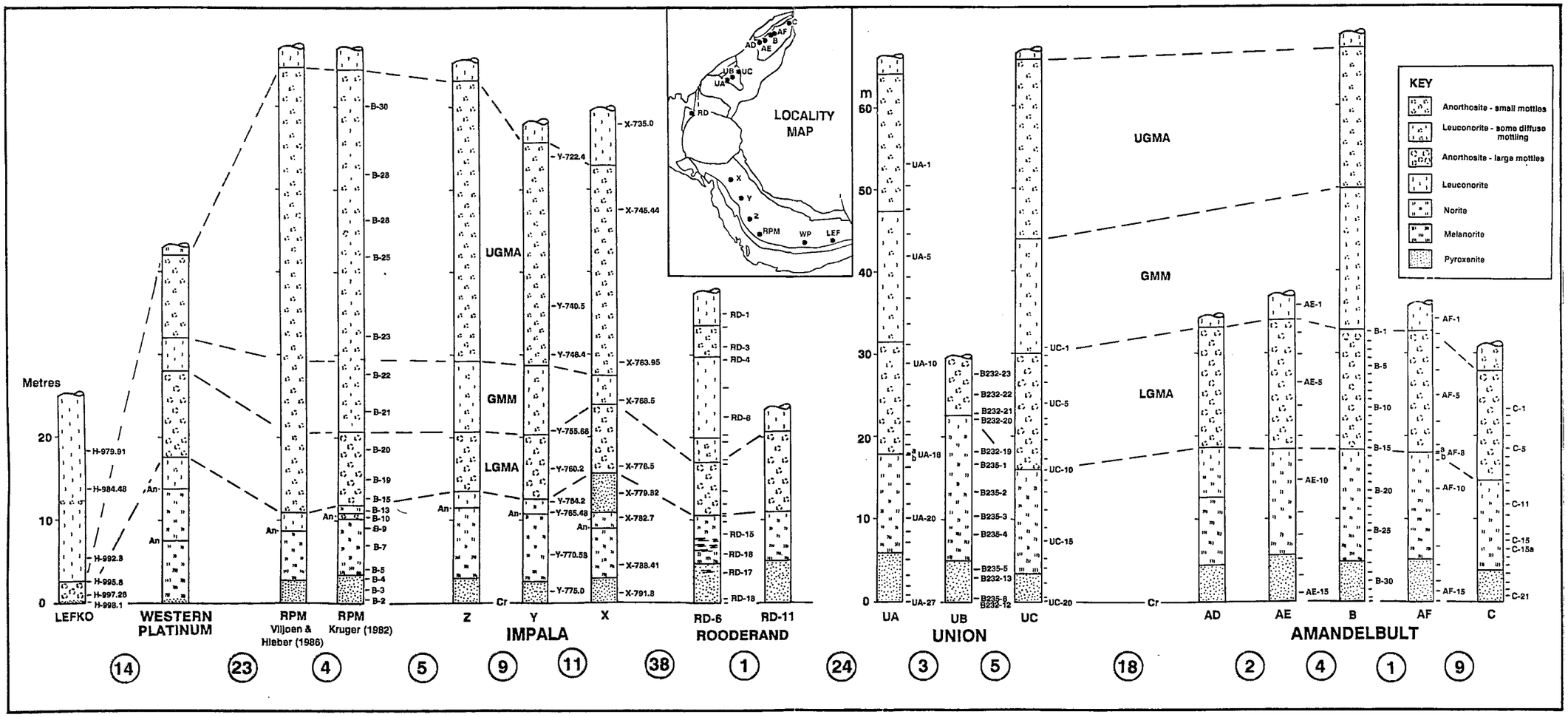

Figure 4.4 Stratigraphic columns of the Bastard Unit profiles in the western Bushveld Complex. Sampling positions and sample numbers are shown on the right of each column. "An" indicates thin anorthosite layers while the ⌐ symbol at Rooderand (RD-6) indicates shearing. LGMA = Lower Giant Mottled Anorthosite; GMM = Giant Mottled Middling; UGMA = Upper Giant Mottled Anorthosite. Inset locality map shows the spatial distribution of the profiles and the circled numbers indicate the map distance (km) between profiles.

TABLE 4.2: Data summary for Bastard Unit profiles, western Bushveld Complex.

	Lefko-chrysos	Western Plats	RPM-Rustenburg Viljoen	RPM-Rustenburg Kruger	Impala Z	Impala Y-1329	Impala X-1512	Rooderand RD-6	Rooderand RD-11	RPM-Union Section UA	RPM-Union Section Naldrett	RPM-Union Section UB	RPM-Union Section UC	RPM-Amandelbult Section AD	RPM-Amandelbult Section AE	RPM-Amandelbult Section B	RPM-Amandelbult Section AF	RPM-Amandelbult Section C
STRIKE DISTANCE (km)																		
From LEF	0	14	37	37	46	55	66	104	106	129	132	132	137	153	157	161	162	171
THICKNESS (m)																		
Pyroxenite	0.15	0.05	2.77	3.52	3.00	2.54	2.95	5.00	5.09	5.90	9.28?	5.00	4.10	4.50	5.65	5.45	5.10	3.91
Norite	NONE	17.10	8.15	8.34	11.5	9.92	7.85*	5.56?	5.93	11.90	10.16	17.50	12.65	14.10	12.75	13.46	12.90	10.73
Giant Mottled Anorth	2.46	24.40	53.76	51.60	49.7	43.26	37.34	22.98?	?	46.30	43.89	43.87	48.50	-	-	48.07	-	-
LGMA	2.46	10.40	?	8.83	7.2	7.83	8.34	6.43?	9.69	13.70	15.17	15.17	14.00	14.5	15.6	14.38	14.7	13.22
GMM	0	4.00	?	?	8.5	8.43	3.52	12.79?	?	16.50	11.39	11.40	13.10	-	-	16.67	-	-
UGMA	0	10.00	?	?	34.0	27.00	25.48	3.77?	?	16.10	17.33	17.30	21.40	-	-	17.02	-	-
TOTAL Bastard Unit	2.61	41.55	64.68	63.46	64.2	55.72	52.89	33.54?	>20.71	64.10	63.33	66.37	65.25	-	-	66.98	-	-
SAMPLING																		
No. Samples	9	NONE	NONE	18	NONE	9	9	19	NONE	27	NONE	13	20	14	15	32	17	19
Sample Prefix	H			B		Y	X	RD		UA		B235 & B232	UC	AD	AE	B	AF	C
WHOLE-ROCK ANALYSES	(No.Samples/No. Elements)																	
Major Elements	6/10			-		9/10	9/10	8/10		27/10		13/10	20/10	-	15/10	-	17/10	-
Trace Elements	6/11			-		9/11	9/11	8/11		27/11		13/11	20/11	-	15/11	32/7	17/11	19/7
MICROPROBE ANALYSES	(No.Samples/No.Analyses)																	
Olivine	-			-		-	-	-		-		-	3/41	-	-	-	-	-
Chromite	1/6			-		-	-	-		-		1/7	-	-	-	-	-	-
Orthopyroxene	9/43			18/96		9/34	9/39	9/38		16/70		-	14/91	-	10/50	-	-	-
Clinopyroxene	-			16/59		4/13	-	1/3		-		-	6/20	-	6/16	-	-	-
Plagioclase	9/55			18/152		9/138	9/140	9/48		11/55		-	14/102	-	11/70	-	-	-

* Additional 4.75m of pyroxenite between Norite and GMA.

Sources of analytical data.
1) Microprobe analyses for RPM - Kruger (1982)
2) Chromite analyses for UB - Eales (1987)
3) All analytical data for AE - Field (1987)
4) Trace element data for AF - Field (1987)
5) Whole-rock data for UB - de Klerk (1982)
6) Trace element data for B and C - Walters (1982, unpubl.) (apart from Sc)

layer at the contact between the underlying mottled anorthosite and overlying pyroxenite. Where the chromitite is thicker, the anorthosite is characterised by a thin selvage of "annealed" plagioclase crystals, almost devoid of interstitial mafic minerals (Plate 4.4c), resulting in an extreme adcumulate. This forms a distinctive layer at the contact (c. 1cm thick) - very similar to that seen at the basal contact of the Merensky Reef. Conversely, where a thinner or discontinuous chromite layer is developed, the areas of mafic mottling in the anorthosite are juxtaposed with the chromitite (Plate 4.4a & b).

The chromite grains are generally small, and at Union Section grains range from 0.05 to 0.15mm in diameter (average 0.1mm). The discontinuous chromitite at **LEF** is even finer grained at between 0.01-0.03mm; here the chromite grains are more euhedral than those at Union Section (Plate 4.4a). At Union the chromite grains are subhedral to anhedral with lobate and cuspate forms (complex amoeboid shapes) sparsely scattered amongst both plagioclase and orthopyroxene (Plate 4.4b). The texture of the chromite at **LEF** is generally one of small discrete grains at the orthopyroxene - plagioclase boundary and in places local coalescence of smaller clusters of grains does occur. This texture is described by Eales (1987, p.152 and Figure 7-4) as being sub-coalescent. The two intersections at Union Section have more subhedral and amoeboid grain morphologies which Eales (op. cit.) describes as being poikilitic or vermiform. Inclusions of silicates are identified within the chromite grains. Some are in optical continuity with the silicate phase enclosing the spinel, indicating a cylindrical embayment in the spinel; others are discrete silicate inclusions. Irregular sulphide blebs are associated with this layer, and also occur within the footwall anorthosites and the overlying pyroxenite.

4.7.2 Bastard (Reef) pyroxenite.

Overlying the chromitite layer is a feldspathic pyroxenite, sometimes also termed poikilitic pyroxenite, which constitutes the "Bastard Reef" (Plate 4.5a, **UA**-27). Its main components are subhedral to euhedral cumulus orthopyroxene, and anhedral intercumulus plagioclase and clinopyroxene. Accessory mineral phases include intercumulus biotite and

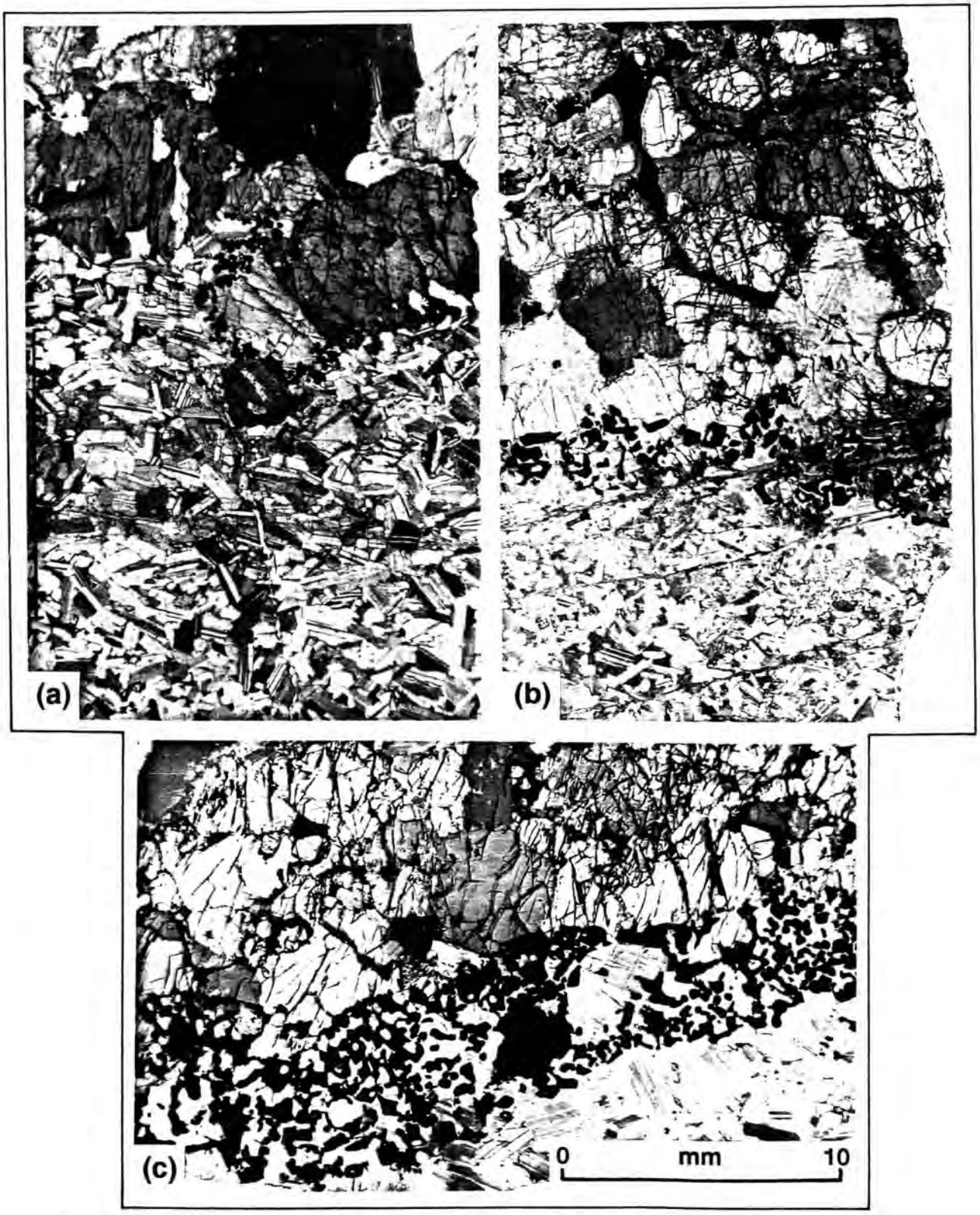

Plate 4.4 Basal contact of the Bastard Unit at (a) **LEF** (H998.1 - microprobe slide), (b) Union Section (**UA**-27) and (c) **UB** (H232/3). In all cases the adcumulate anorthosite Merensky footwall and the overlying coarser grained orthocumulate Bastard pyroxenite are clearly illustrated. These two lithologies are separated by a thin chromitite layer. At **LEF** (a) the chromitite layer is not continuous and is finer grained while at **UA** (b) and **UB** (c) it is more robust with anhedral grain morphologies. Small grains of disseminated (opaque) sulphides are evident in the anorthosite, 1cm below the chromitite at **LEF** (a) and larger intercumulus sulphides are evident within the pyroxenite of all three samples. The false colour is produced by partial rotation of the upper nicol.

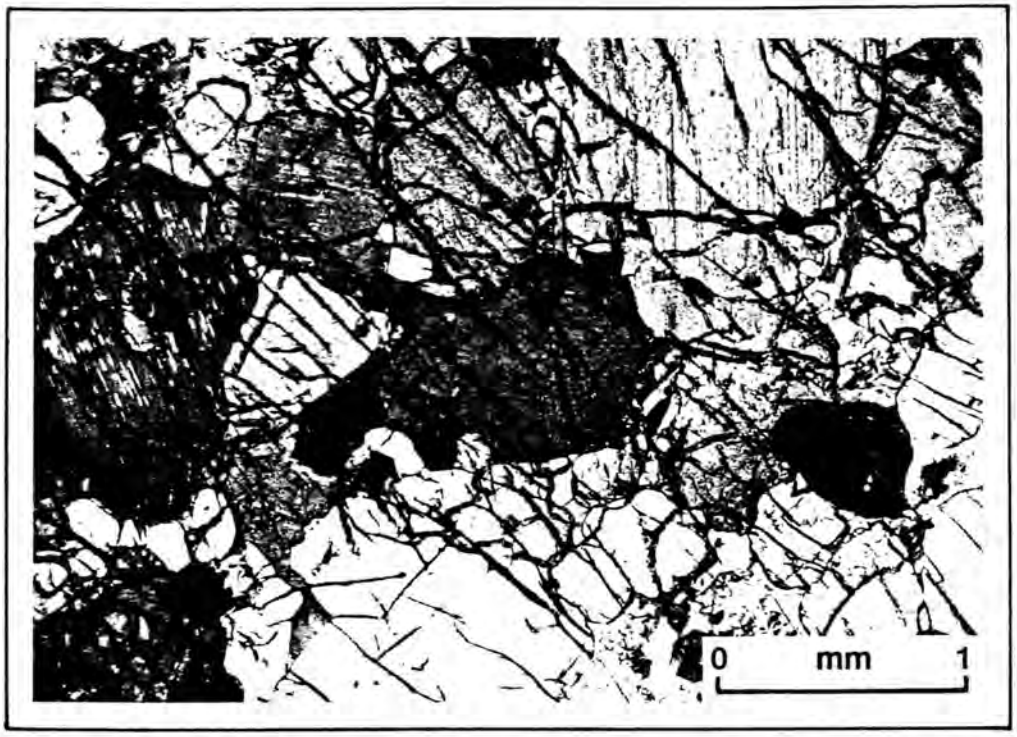

Plate 4.5a Detail of the orthocumulate Bastard pyroxenite (UA-27) showing cumulus orthopyroxene and intercumulus plagioclase, clinopyroxene and some biotite. Note the partial alteration of plagioclase feldspar - lower right of photograph.

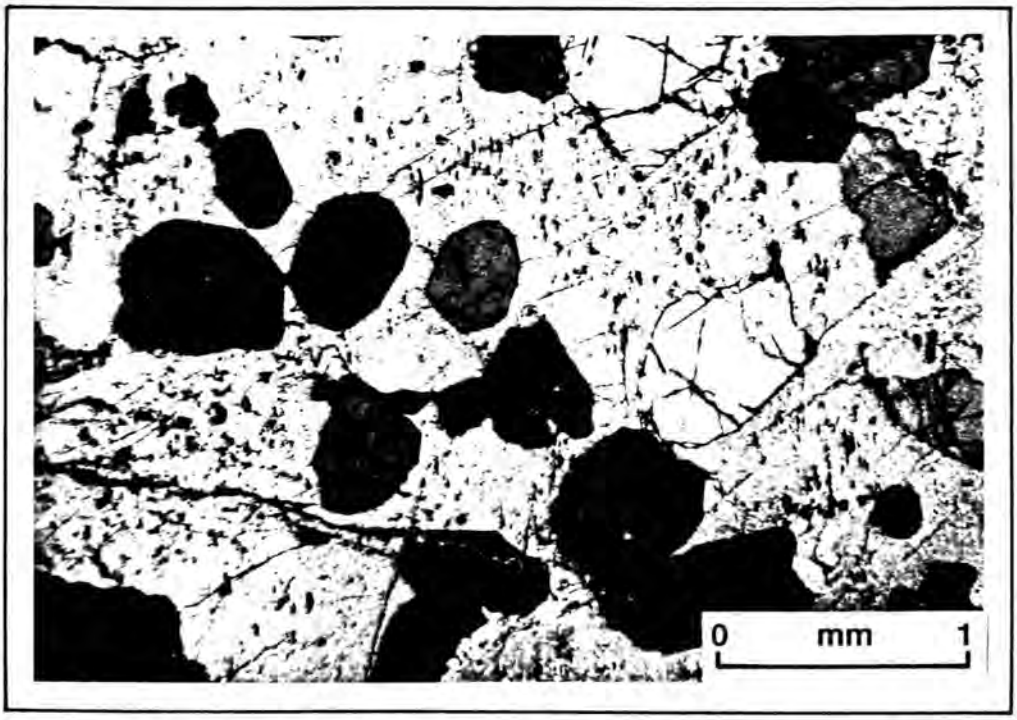

Plate 4.5b Large optically continuous oikocryst of clinopyroxene poikilitically enclosing subhedral cumulus orthopyroxene crystals (melanorite UC-17). These clinopyroxene oikocrysts can be as much as 1cm in diameter.

various opaque base metal sulphides responsible for PGE mineralisation. The basal 2-5cm of the pyroxenite hosts larger grains up to 5mm in diameter (where samples were available - **LEF**, **UB** and **UA**), while the remainder of the sequence has a grain-size between 0.5 and 2mm. These crystals have annealed in places into areas of close-packed orthopyroxene (grain boundaries forming triple junctions), with patches of intercumulus plagioclase (Plate 4.4a, **UA**-27). This intercumulus plagioclase characteristically occurs as large (1cm), optically continuous oikocrysts which poikilitically enclose the more abundant cumulus orthopyroxene. A similar texture is observed where larger postcumulus clinopyroxene oikocrysts poikilitically enclose euhedral orthopyroxene (Plate 4.5b, **UC**-17). Optically (and as shown later by microprobe analysis) the intercumulus plagioclase displays advanced zoning which supports the view that the pyroxenite represents an orthocumulate.

Occasional small irregular plagioclase inclusions are isolated within the cumulus orthopyroxene grains. These inclusions range in size between 0.05 and 0.3mm (Plate 4.6a, **UA**-24). The shape of the inclusions is quite irregular and the frequency of occurrence increases upward in the column. Orthopyroxene grains display fine, closely spaced exsolution lamellae and blebs of clinopyroxene which are arranged parallel to the (100) plane of the host grain.

4.7.3 Melanorite - Norite - Leuconorite.

The contact between feldspathic pyroxenite and the overlying noritic rocks is taken at the level where plagioclase becomes a primary cumulus phase. A progressive modal increase in plagioclase with stratigraphic height, with a concomitant decrease in cumulus orthopyroxene, is seen in the norite. The grain-size of the orthopyroxene is 1-3mm, and that of the cumulus plagioclase 0.5-2.5mm. A significant and distinctive feature of the melanorite and norite is the abundance of small plagioclase inclusions within the orthopyroxene. These inclusions are commonly 0.05-0.35mm in diameter, and are spheroidal, ovoid or irregularly embayed (Plate 4.6b, UA-22 and 4.6c, **X**788.41). In some cases these inclusions form small clusters but generally their distribution and orientation within the host grain is quite random. These inclusions closely resemble those described in the UG1FW Unit (see **2.3**).

Plate 4.6 Small irregularly shaped plagioclase inclusions poikilitically enclosed within (a) pyroxenite, **UA**-24, (b) melanorite **UA**-22 and (c) norite X788.41. Note that there is a low incidence of inclusions within the pyroxenite (a) and that their numbers increase upward through the melanorite (b) and norites (c).

An intriguing texture is displayed by the norites, leuconorites, and, occasionally, the anorthosites. Here cumulus orthopyroxene grains (1-3mm) are surrounded by a zone of smaller subhedral plagioclase primocrysts (0.5mm) set in interstitial orthopyroxene representing an outgrowth of the primary cumulus orthopyroxene grain (Plate 4.7a, **UA**-7). This is in turn surrounded by adcumulus plagioclase which has a larger grain-size (1-2mm). The implication here is that orthopyroxene incorporated the small plagioclase primocrysts after a period of initial growth. Kruger (1982) studied the same texture in the Merensky Unit and established that the inclusion-free orthopyroxene core is strongly zoned with respect to the Cr_2O_3 concentration from centre (0.56%) to margin (0.31%), but where the orthopyroxene becomes interstitial at its periphery the Cr_2O_3 level declines further to 0.22%.

An unusual feature within the noritic rocks of profile **UC** is the occurrence of **olivine** within the Bastard Unit; this phase is not seen in any of the other profiles and this is the first recorded occurrence of olivine above the Merensky Reef in the Upper Critical Zone. Close-spaced sampling in **UC** revealed that three samples contain olivine in excess of 5% (**UC**-11, **UC**-13 and **UC**-17). These samples represent olivine-bearing norite layers separated by olivine-free intervals. The olivine displays an anhedral, almost intercumulus, habit and in places is oikocrystic towards robust plagioclase laths. As with orthopyroxene the olivine grains also enclose small spheroids of plagioclase which appear to have been resorbed to some degree (Plate 4.7b & c, **UC**-13). This kind of texture for olivine has also been recorded in the Upper Critical Zone within the P2 Middling Member (leuco-troctolite) of the Pseudoreef Multicyclic Unit at Amandelbult Section (Field, 1987 and Eales et al., 1988).

4.7.4 Giant Mottled Anorthosite (GMA).

Cumulus plagioclase within the **Lower Giant Mottled Anorthosite (LGMA)** can broadly be sub-divided into clean white plagioclase between the mottles and that which occurs in intergrowth with the intercumulus mafic minerals forming the "mottles", i.e. cumulus plagioclase within the mottles.

Plate 4.7a Leuconorite (UA-7) within the GMM showing a large cumulus orthopyroxene grain with a high density of small plagioclase feldspar inclusions concentrated at its margin. The orthopyroxene core is devoid of inclusions. In hand specimen this texture gives the orthopyroxene grains a distinctive fuzzy appearance.

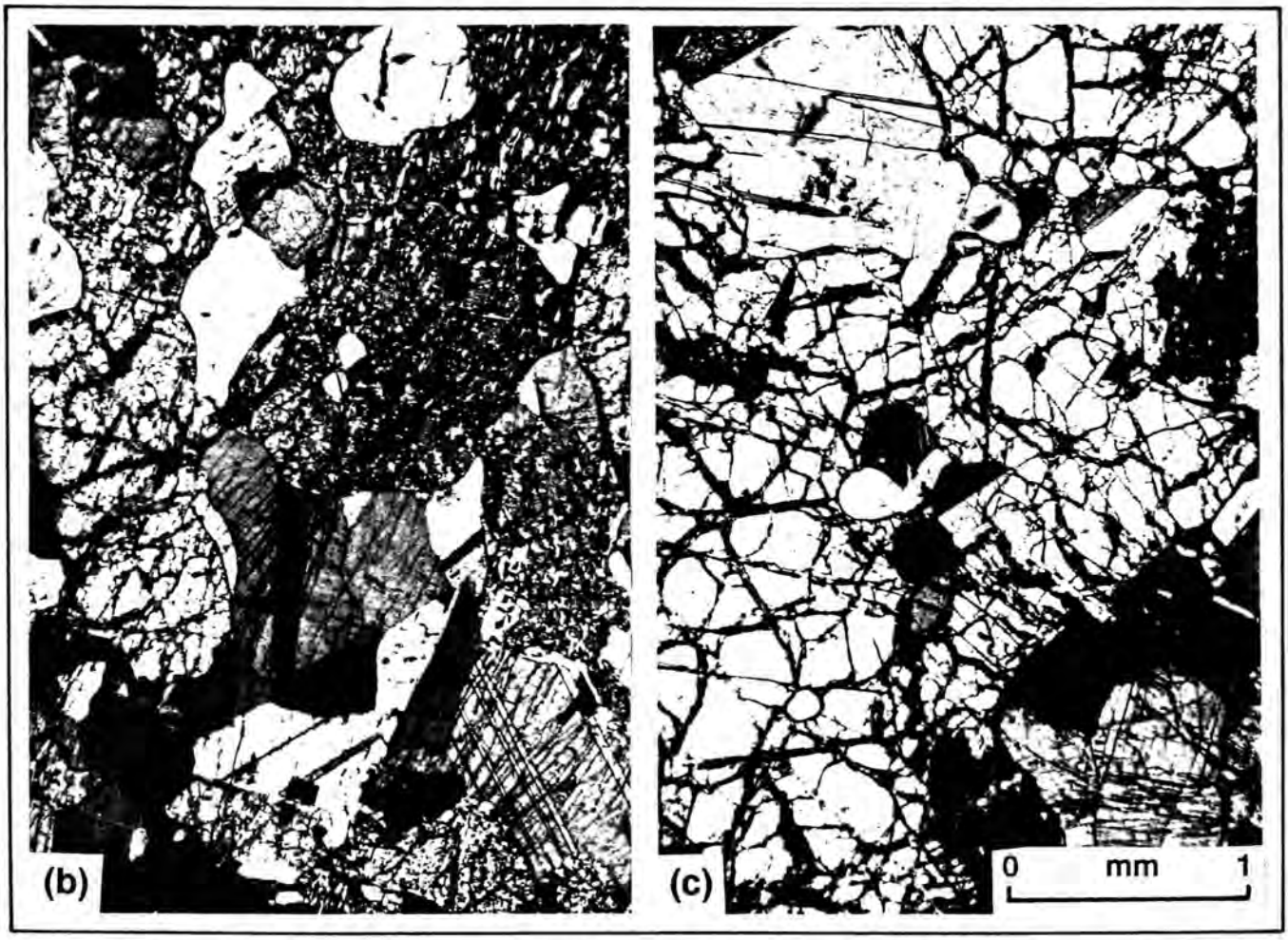

Plate 4.7b & c Olivine-bearing norite (UC-13) showing the anhedral, almost intercumulus, habit of the olivine. Like orthopyroxene the olivine also encloses small rounded inclusions of plagioclase feldspar.

Characteristics of the first of these types are that the plagioclase grains are more uniform in size than those in the UGMA, and somewhat smaller (between 0.5-1.5mm). Zoning within the cumulus plagioclase is not common but where present is not of a complex nature. Cumulus plagioclase crystals within the mottles, however, are subhedral to euhedral in shape with both lath-like and tabular habits (Plate 4.8a, **B**-10 at **RPM**). Post-cumulus growth of plagioclase in this case has been inhibited by the crystallisation of the intercumulus mafic phases. The matrix anorthosite, which makes up the bulk of the LGMA, can be described as a typical adcumulate while feldspar associated with the mottles is more orthocumulus in habit.

The poikilitic habit adopted by pyroxene (both ortho- and clinopyroxene) in the LGMA yields the typical mottles developed within the anorthosite. These mottles are somewhat irregular and form discrete, dark, muffin-shaped areas of intercumulus pyroxene. The texture and mineralogy of individual mottles is quite variable with clinopyroxene and orthopyroxene being the dominant intercumulus phases. Minor biotite and rare opaque phases are also present. The mottles are also quite variable in terms of the proportion of pyroxene and the optical continuity of the intercumulus grains. In some cases the pyroxene forms only a sparse intercumulus lacework (Plate 4.8a, **B**-10 at **RPM**) where the individual grains of cumulus plagioclase are in close proximity to each other. At the other extreme, where pyroxene is more robust (abundant), the ubiquitous subhedral plagioclase grains within the orthopyroxene are widely separated from each other. Mottles can be made up of either large, optically continuous ortho- or clinopyroxene (Plate 4.8b, **AE**-5 and Plate 4.8c, **UA**-7), or discrete, small, intercumulus pyroxene grains (Plate 4.9a & b, **UA**-16a and **UA**-14). A feature of the latter type (optically discontinuous ortho- or clinopyroxene) is that the associated cumulus plagioclase grains appear to have undergone some deformation as they display evidence of bending and secondary twinning (Plate 4.9a & b).

The mottling in the **Giant Mottled Middling (GMM)** resembles that described as "robust" above, but here the mottles are smaller and more dense. This layer has in the past been described as a leuconorite (Cousins, 1969). The GMM layer was examined in profiles **RPM**, **X**, **Y**, **RD** and **UA** and was found

Plate 4.8a Mottle within adcumulus mottled anorthosite (B-10 at **RPM**) showing a connected lace-work of intercumulus orthopyroxene between euhedral to subhedral cumulus plagioclase crystals. These plagioclase grains have distinctive tabular and lath-like shapes (uncrossed nicols).
Plate 4.8b Mottle within adcumulus mottled anorthosite (LGMA, **AE**-5). Here the mottle is made up of optically continuous intercumulus orthopyroxene.
Plate 4.8c Mottle within adcumulus mottled anorthosite (LGMA, **UA**-7). Here the mottle comprises optically continuous intercumulus clinopyroxene.

Plate 4.9a Mottle within adcumulus mottled anorthosite (LGMA, **UA**-16a). Here the mottle is made up of optically discontinuous intercumulus orthopyroxene.

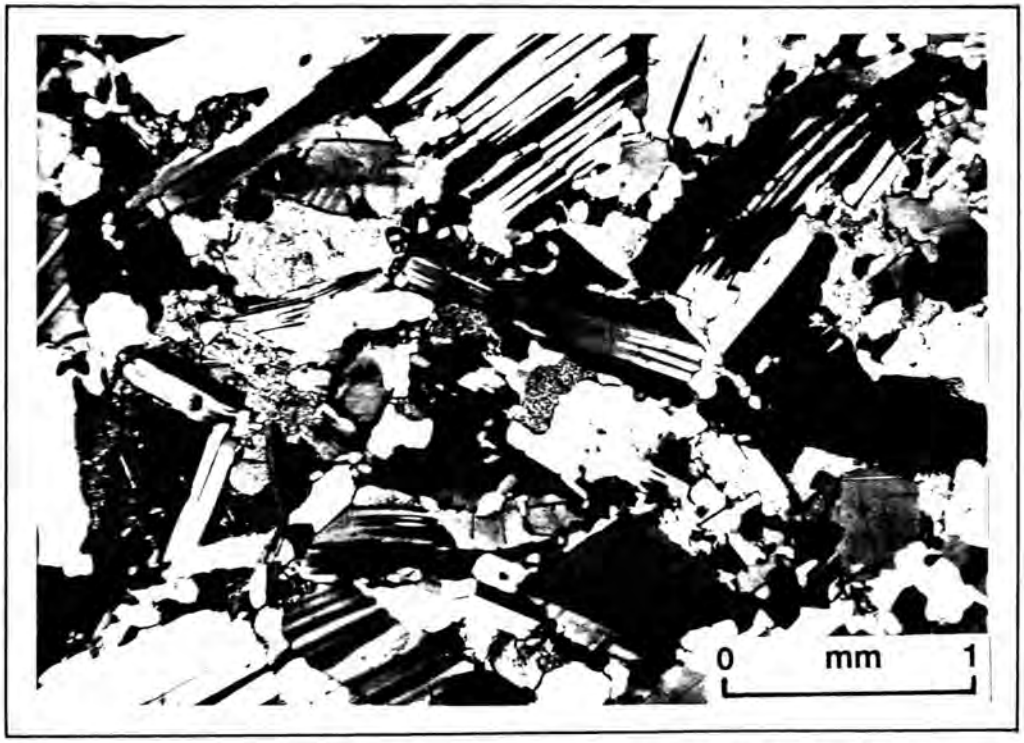

Plate 4.9b Mottle within adcumulus mottled anorthosite (LGMA, **UA**-14). Here the mottle is made up of optically discontinuous intercumulus clinopyroxene. Bending and secondary twinning of feldspar are apparent.

to have cumulus orthopyroxene mottles with an abundance of plagioclase inclusions. Although plagioclase inclusions occur throughout the orthopyroxene oikocrysts there is a tendency for them to concentrate around the margins of the grains (Plate 4.7a, **UA**-7). Small mottles may also be made up of intercumulus clinopyroxene).

The **Upper Giant Mottled Anorthosite (UGMA)** was sampled in four profiles at **RPM**, **X**, **Y**, and **UA**. Here the mottles are smaller and more irregular than those in the LGMA and the cumulus plagioclase is more lath-shaped in habit (especially within the mottles). The plagioclase grain size is variable between 0.5 and 3.5mm with the bulk of larger cumulus grains being in excess of 2.5mm in diameter. This sub-unit also has a distinctive, dull gray colour in hand specimen. Inverted primary pigeonite, now seen as orthopyroxene with its characteristic exsolution lamellae of clinopyroxene, occurs in the UGMA (**B**-26, **B**-28 and **B**-30 at **RPM**; **Y**-722.4, **Y**-740.5; **X**-735, **X**-745.44; **UA**-1, **UA**-2). The inverted pigeonite occurs as an anhedral intercumulus phase which takes up **angular** intercumulus space between lath-like plagioclase crystals (Plate 4.10a, **B**-28 at **RPM**), unlike the irregular anhedral habit seen in the LGMA. The habit of exsolved clinopyroxene varies from plates rigidly parallel to (100) and relict (001) planes of the host (Plate 4.10b, **UA**-1) to more irregular, vermiform intergrowths (Plate 4.10c, **UA**-2), where augite has coalesced to form blebs and irregular, but optically continuous, inclusions within the host. These habits reflect varying degrees of subsolidus mobility of the clinopyroxene. A notable feature of the augite exsolution is that at grain boundaries, against plagioclase, acicular extensions of exsolved augite extend or "penetrate" into the larger cumulus plagioclase grains (Plate 4.11a, **B**-28 at **RPM**).

Oscillatory-zoned, cumulus plagioclase grains are common throughout the GMM and the UGMA. Grains which display several cycles of oscillations are generally larger that those of simpler design. The number of growth zones varies from grain to grain and in many cases a grain with complex zoning, displaying numerous zone cycles, may be juxtaposed with grains of simpler design - displaying little or no zoning at all (Plate 4.11a & b, **B**-28 and **X**735.0). A more detailed study of two zoned grains is presented in **4.7.4.**

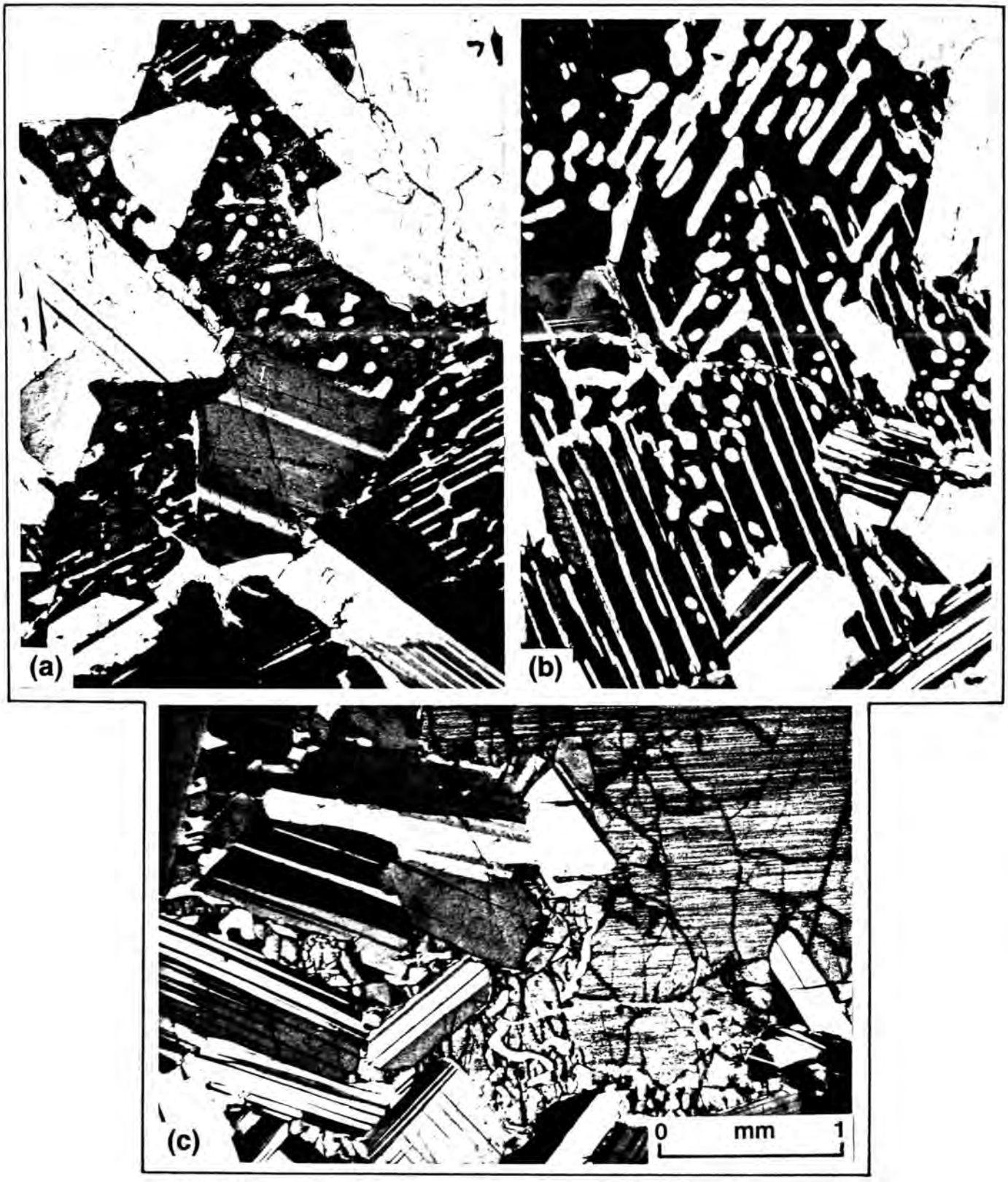

Plate 4.10a Intercumulus inverted primary pigeonite now seen as orthopyroxene and exsolved clinopyroxene in the UGMA (B-28, **RPM**). The clinopyroxene occurs either as (a) discrete intercumulus phases (top right), (b) as irregular exsolved blebs or (c) as exsolved lamellae within the host grain. Note the zoning of the cumulus plagioclase grain at lower right.

Plate 4.10b Intercumulus inverted primary pigeonite in the UGMA (**UA-1**). Here the exsolution lamellae of clinopyroxene are aligned parallel to (100) and relict (001) planes of the host orthopyroxene.

Plate 4.10c Intercumulus inverted primary pigeonite in the UGMA (**UA-2**). Here the exsolved clinopyroxene takes on an irregular, vermiform habit which is optically continuous within the host.

Plate 4.11a Orthocumulus mottled anorthosite (UGMA, B-28 at **RPM**) displaying two zoned cumulus plagioclase feldspar grains with complex growth patterns (dark grains in extinction). The larger grain displays at least 9 separate growth events. Note the acicular extensions of intercumulus clinopyroxene into the adjacent cumulus plagioclase grains.

Plate 4.11b A single large euhedral zoned plagioclase feldspar crystal within the UGMA (**X**735.0). Here up to 10 growth zones are recognised and the crystal is juxtaposed with other feldspar grains which display no zoning at all. Note the intercumulus inverted primary pigeonite.

Plate 4.11c Orthocumulus mottled anorthosite (UGMA, **UA**-1) with small areas of clear white intercumulus K-feldspar (centre and lower left) between cumulus plagioclase feldspar. Note the single large zoned plagioclase grain at centre right.

Potassium feldspar, in the form of orthoclase, appears as an accessory intercumulus phase in the UGMA (Plate 4.11c, **UA**-1). Small (0.2-0.5mm) anhedral grains occupy irregular intercumulus spaces and do not exceed 1% of the rock. There appears to have been some corrosion of plagioclase by the K-feldspar as the grain boundaries are quite irregular. K-feldspar also occurs as irregular intergrowths within abnormally larger plagioclase crystals (sample **B**-28 at **RPM**). No quartz was identified within the UGMA.

The textures of the UGMA are unequivocally characteristic of plagioclase orthocumulates and this observation is supported by the higher concentrations of incompatible trace and minor elements (Rb, Zr, Y, K_2O, TiO_2 and P_2O_5) at this level than in GMM and LGMA (see **4.9.3**). The GMM is taken to be a mesocumulate - transitional between the LGMA with adcumulus affinities and the UGMA orthocumulate.

4.7.5 Alteration.

The degree of late-stage deuteric alteration within the Bastard Unit is variable between individual profiles and between the different lithologies. Alteration generally occurs along, and adjacent to, pervasive veins and cracks which transgress the rock. This alteration usually results in the saussuritisation of plagioclase and the replacement of pyroxene by a felted intergrowth of chlorite and sericite. Olivine, where it is present in the **UC** profile, is most affected, being altered to serpentine, magnetite and bowlingite and/or iddingsite.

The basal Bastard pyroxenite (within the first few centimetres) usually displays the highest degree of alteration and this is attributed to its close proximity to the ubiquitous bedding plane shear at the contact. This shear acted as a channelway for hydrothermal fluids. Here the pyroxenite has numerous irregular cracks along which the orthopyroxene and plagioclase have been altered. A high degree of alteration was observed in the **RD** profile in the lower part of the Giant Mottled Anorthosite (see **4.6.5**).

4.7.6 Modal percentages of main mineral phases.

Modal analyses were compiled for 33 samples in the profiles **LEF**, **X**, **Y** and **RD**, and these results are tabulated in Appendix B. Point-counted modal proportions of 32 samples and their corresponding CIPW weight percent norms are compared in Figure 4.5. Good correlation is established for both plagioclase and orthopyroxene (correlation coefficients of 0.978 and 0.984 respectively). Whole-rock Al_2O_3 levels also provide a measure of normative total feldspar in these rocks, where

$$\underline{or} + \underline{ab} + \underline{an} = 2.997\ Al_2O_3 + 1.284 \quad (\text{corr. coef. } 0.9982$$
$$r^2 = 99.64,\ n = 124 \text{ samples}).$$

Normative and modal data for plagioclase, orthopyroxene and olivine are shown for nine profiles in Figure 4.6.

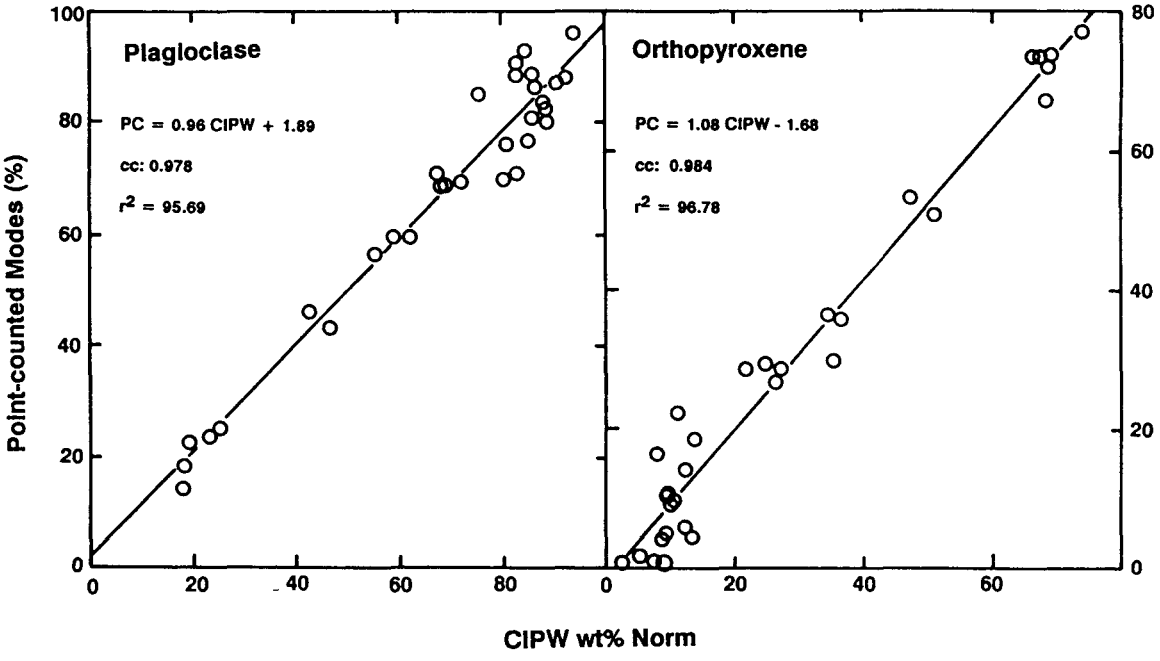

Figure 4.5 Scatter plot of point-counted modes (PC) for plagioclase and orthopyroxene against the CIPW weight percent normative values (CIPW); linear regression line is also shown. A selection of 32 samples from the profiles **LEF**, **X**, **Y** and **RD** is used.

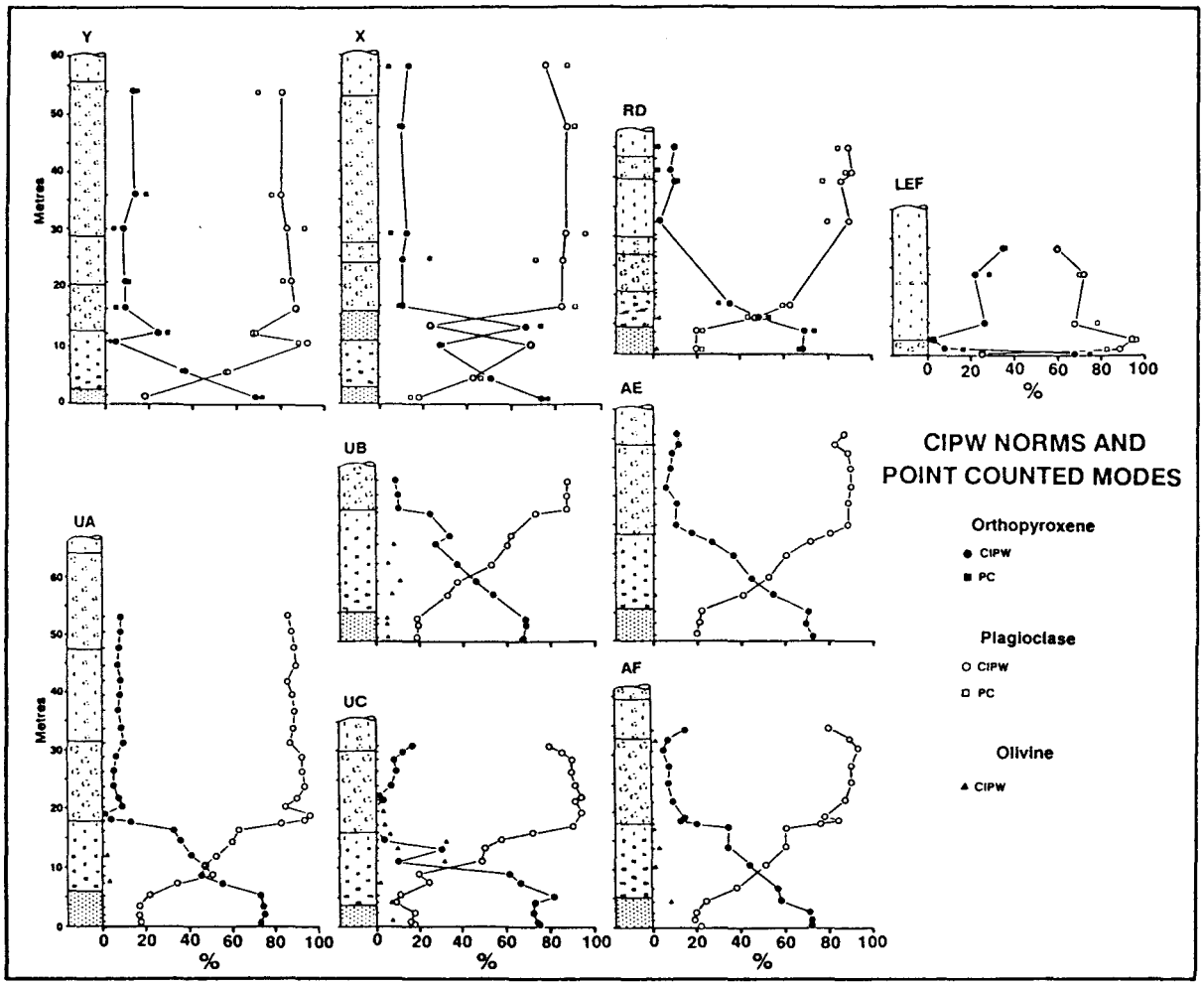

Figure 4.6 CIPW weight percent norms and point counted (PC) modes of orthopyroxene, plagioclase and olivine plotted against stratigraphic height in nine Bastard Unit profiles.

4.8 Mineral chemistry.

Only limited analytical data have been presented in the literature for the main mineral phases of the Bastard Unit. Compositions of pyroxene and plagioclase, in widely-spaced samples, have been reported by von Gruenewaldt (1973) and Cameron (1982) in the eastern Bushveld Complex, while Kruger (1982) presented an account of the cryptic variations in the Bastard Unit at **RPM** Rustenburg Section. Naldrett et al. (1984, 1986) presented microprobe data for samples in single profiles at Union and Rustenburg Sections and an additional profile at Jagdlust in the eastern Bushveld (Naldrett et al., 1987). The work of Field (1987; also published in Eales et al., 1988) and Mitchell (1986 and 1990a) provide further limited data for the western Bushveld Complex.

New electron microprobe data (Appendix C) are presented here for orthopyroxene (315 analyses) and plagioclase (853 analyses) in profiles **LEF**, **Y**, **X**, **RD**, **UA**, and **UC**. Clinopyroxenes (52 analyses) were analysed in selected samples from **Y**, **RD** and **UC**, and olivine in three **UC** samples. Six chromite grains were analysed at the basal contact of the Bastard Unit in the **LEF** profile (Table C30).

4.8.1 Pyroxenes.

The compositional variations of orthopyroxene with stratigraphic height are represented in terms of the atomic ratio $Mg/(Mg+Fe^{2+})$ (**MMF**) (Figures 4.7 and 4.8) and plots of the average atomic Cr/Al and Cr/Ti ratios are presented in Figure 4.9. Variations in Cr_2O_3, TiO_2, Al_2O_3, MnO and NiO are plotted against stratigraphic height and presented in Figures 4.10 - 4.12. Conventional plots of Wo-En-Fs for the pyroxenes are shown in Figure 4.13.

The Orthopyroxene MMF Ratio.

The MMF ratio within the Bastard Unit ranges from a maximum of 0.835 in the leuconorite of **UC**-11 to a minimum of 0.536 in sample **Y**740.5. Cumulus orthopyroxene in the Bastard pyroxenite and the overlying norites shows little variation within individual samples. This variation is rarely in excess of 0.01, although a maximum of 0.018 is attained in **UC**-18 (analyses of both cores and margins). A greater degree of variation is observed where orthopyroxene occurs as an intercumulus phase in the GMA; a range of 0.03 is evident for the majority of GMA samples, but this increases to 0.096 at **RPM** (**B**-26).

Zoning within individual cumulus orthopyroxene grains was investigated in six samples from the lower part of profile **UC** (below the GMA). Although minor differences were observed between cores and margins, no systematic pattern is apparent. The maximum difference found was 0.008 (Figure 4.7). Barnes (1986) pointed out that ferromagnesian phases in cumulates are usually unzoned. This could be due to either (a) equilibrium crystallisation of the trapped liquid and continuous re-equilibration of crystals and melt, or (b) subsolidus removal of the original

compositional gradients. In either case, homogenization of orthopyroxene grains occurs by the mechanism of intragranular diffusion, and the final result is the same. This view may be an oversimplification as these rocks may represent adcumulates, especially in the case of the norites.

MMF ratios within the Bastard Unit display a distinctive pattern of cryptic variation which is repeated in all eight profiles investigated along 170km of strike. The generalised pattern through **all** the profiles of Figure 4.7, and those of Naldrett et al. (1986) presented in Figure 4.8, may be described as follows:

* MMF values within the Bastard pyroxenite are 0.804 at the base and gradually increase upward through the pyroxenite to levels in excess of 0.825 at the pyroxenite - melanorite boundary. This increase in MMF ratio within the first 4-5m of the Unit represents a reversed fractionation trend.

* The basal samples within the first 8cm in **RD** and **UC** have MMF values marginally higher than those in the overlying pyroxenite sample (differences of 0.03 and 0.01 respectively). A larger difference of 0.08 is seen over 10cm at **LEF** but in view of the drastic reduction in the thickness of this layer, the difference is thought to represent the full range of variation within the basal mafic lithologies of the Unit at this locality.

* A decline in MMF, from high values around 0.82, is initiated within the norite in all profiles and becomes more marked in the leuconorites in the footwall of the GMA. This decline continues to values between 0.62 and 0.68 within the LGMA. The only exception to this general pattern is seen at Impala **Y** where a low of 0.70 is recorded in the leuconorite 1.2m below the GMA contact, rather than above it.

  A notable aspect of this decreasing trend is that it is unrelated to the textural habit of the pyroxene (intercumulus or cumulus); the MMF ratio behaves coherently and changes along a **continuous** trend across the lithological and textural boundary at the base of the LGMA.

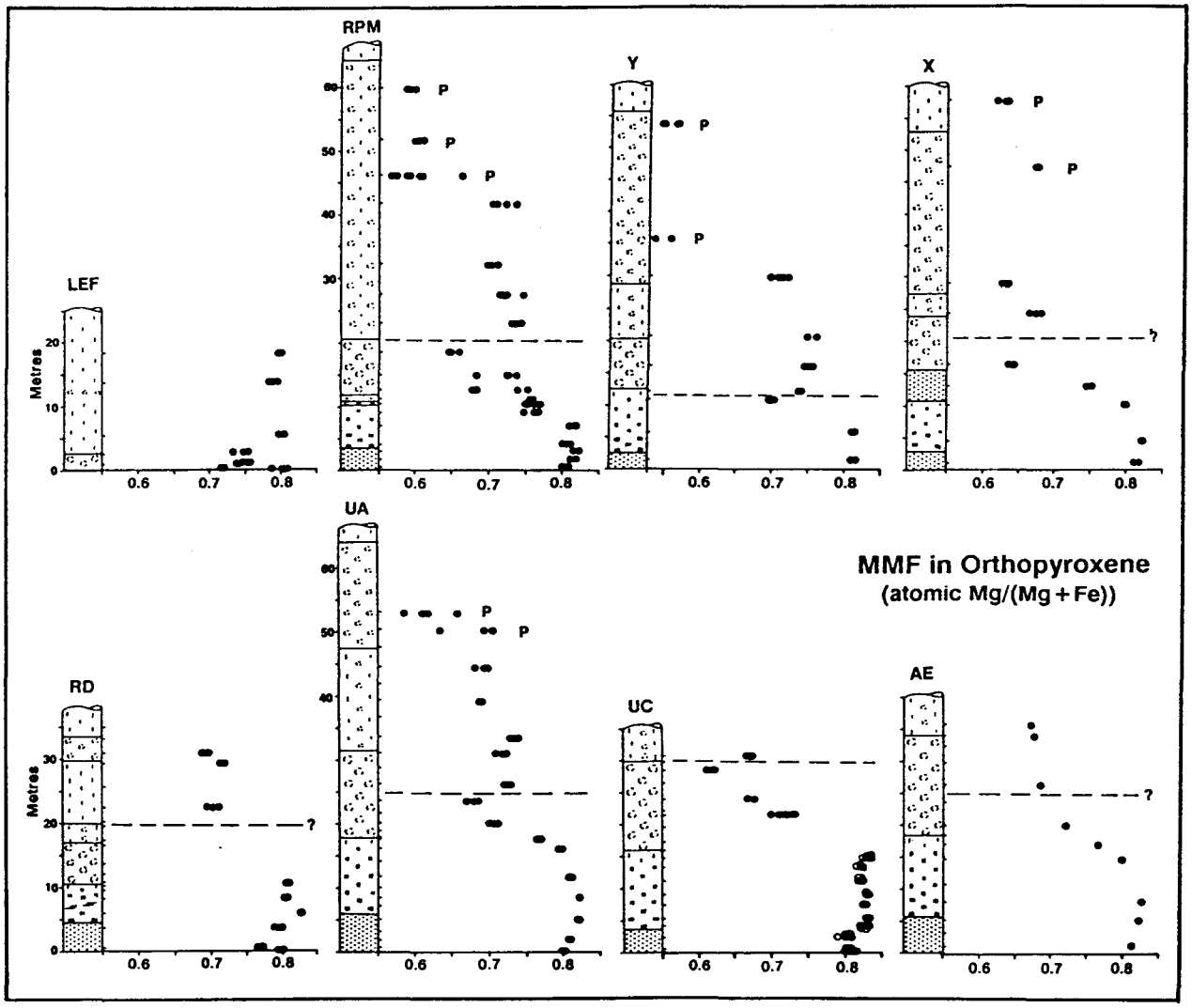

Figure 4.7 MMF ratio (atomic Mg/(Mg + Fe)) for orthopyroxene plotted against height for eight Bastard Unit profiles. Ticks on right of column indicate sample positions. "P" denotes those samples with inverted pigeonite evident in thin section and the dashed line indicates the inferred position of a reversal in trend of MMF. Open circles in profile UC are for analyses of grain margins.

* A marked reversal to higher MMF values of 0.70-0.75 is initiated within the basal part of the GMA. In the case of profile **Y**, the reversal occurs at a lower stratigraphic level.

* The exact position at which this reversal starts is not everywhere well constrained, because of a low sample density in some profiles, and alteration of this part of the sequence in the case of profile **RD**.

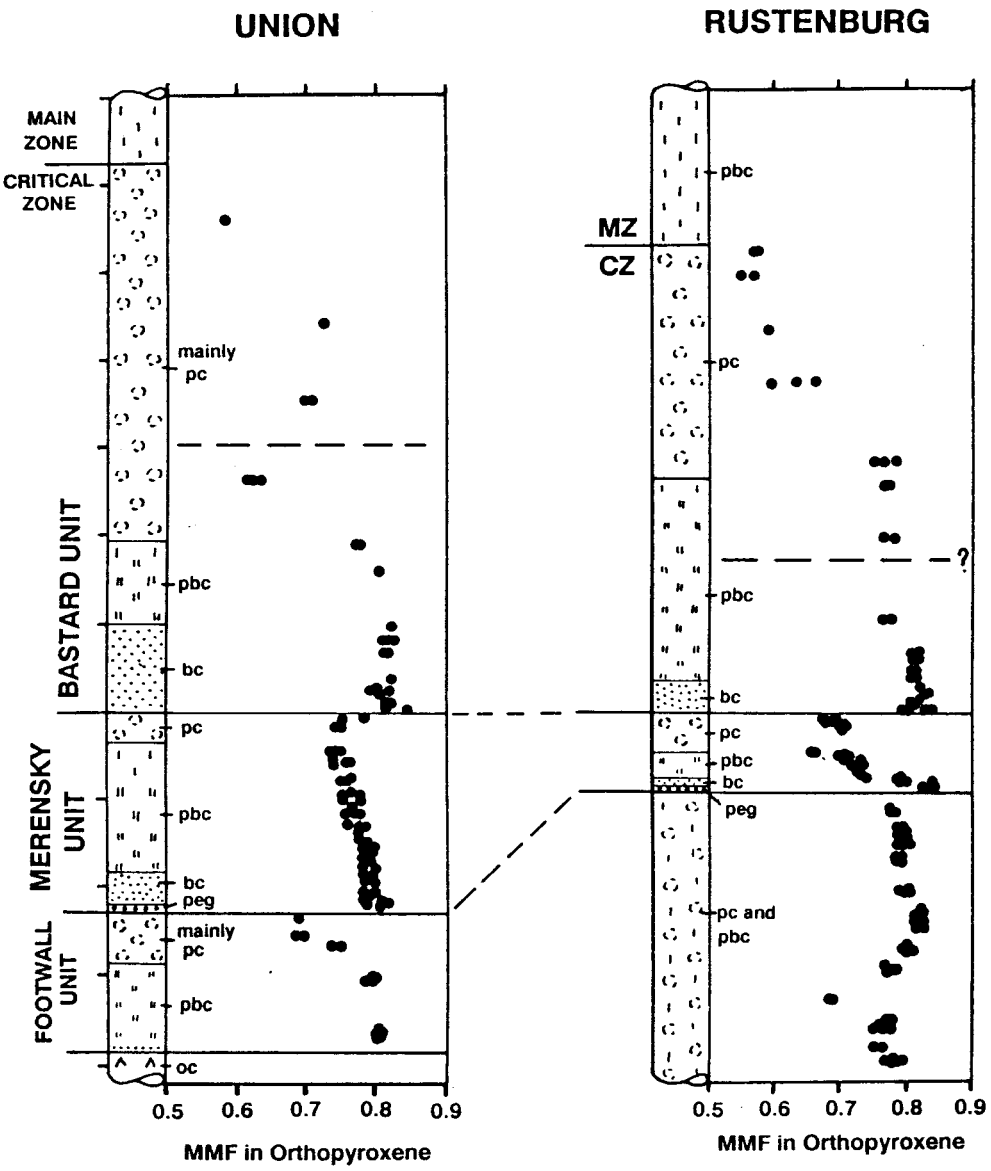

Figure 4.8 Diagram, modified after Naldrett et al. (1986, p.1107), showing the variation in MMF ratio (atomic Mg/(Mg+Fe)) of orthopyroxene with height in the Bastard, Merensky and Footwall Units at Union and Rustenburg Sections. The positions of the contacts have not been altered and lithological abbreviations used by Naldrett et al. (1986) are as follows: peg = pegmatoid, pc = plagioclase cumulate, pbc = plagioclase bronzite cumulate, bc = bronzite cumulate, oc = olivine cumulate. Ticks on left of columns are at 10m intervals. Dashed line in the Bastard Unit indicates the inferred position of a reversal in trend of MMF.

* The reversal is not coincident with any obvious lithological change, nor is it initiated at a uniform stratigraphic level. This level is:

- in profile **Y**: below the GMA,
- in profile **X**, **RD**, **UA** and **AE**: within the LGMA, and
- in profile **RPM** and **UC**: close to the LGMA/GMM contact.

* The reversal is abrupt in profiles where samples are closely spaced (**LEF**, **RPM**, **Y**, **UA** and **UC**) but this cannot be proved where the spacing is wider (**X**, **RD** and **AE**.

* Although the reversal is clearly present in every profile the peak value of MMF ratio attained in the first sample above the break is variable:

LEF	- 0.75	**RPM**	- 0.73
Y	- 0.74	**X**	- 0.66
RD	- 0.71	**UA**	- 0.73
UC	- 0.67	**AE**	- 0.69

* In the layered sequence above the reversal a gradual decline of the MMF ratio is again evident through the middle part of the GMA. The decline becomes pronounced in the UGMA of the profiles at **RPM**, **Y** and **UA**, where values drop below 0.60. This trend may be recognised also in Naldrett's (1986) Rustenburg profile, and is suggested by a single analysis in his Union Section profile (Figure 4.8). The low levels of MMF in the UGMA are representative of inverted pigeonite.

* Low MMF values continue across the upper Bastard Unit contact into the Main Zone for some 30m before gradually reverting back to levels of c. 0.70 (see Figure 4.57).

Basal samples of the Bastard pyroxenite (i.e. the lower 2.3m) indicate little or no variation in MMF ratio over 171km of strike and an average ratio of 0.804 is indicated at this level (Table 4.3). Lateral variation in the MMF ratio is seen only in those samples above the basal pyroxenite.

Table 4.3: Average MMF ratio of orthopyroxenes in the base of the Bastard pyroxenite.

metres	≤2.3	≤1.9	≤1.7	≤1.4	≤1.1	≤0.6	≤0.5
MMF	0.804	0.804	0.804	0.803	0.803	0.801	0.801
sd	0.012	0.012	0.012	0.012	0.012	0.012	0.013
No. analyses	75	67	64	59	56	51	46
No. samples	14	13	12	11	10	9	8
No. profiles	8	8	8	8	7	6	6

The resultant pattern for MMF through the Bastard Unit has a double cuspate form, with the upper cusp being more evolved than that at the base. The distinctive reversal of MMF in the vicinity of the LGMA is suggestive of a final, less robust, influx of parental liquid which was unable to initiate the crystallisation of abundant cumulus orthopyroxene. The volume of new liquid was apparently unable to shift crystallisation into the primary phase volume of orthopyroxene.

A pattern that is remarkably similar to that described above for MMF ratios is seen in the atomic Cr/Al and Cr/Ti ratios of orthopyroxenes, although more scatter is apparent (Figure 4.9). Eales et al. (1986, p.574) showed that a clear break in the atomic Cr/Al ratio of orthopyroxene occurs at the boundary between the Critical and Main Zones. They showed that values in the Lower and Critical Zones vary between 0.15 and 0.28 but that at the top of the Bastard Unit a clear decline to levels of c. 0.1 are found, and further decline is extended through the lower half of the Main sub-zone A. Values below 0.05 are recorded through the rest of the Main Zone. Cr/Al ratios through the Bastard Unit are clearly in accord with this pattern, and transitional between the lows recorded in the Main Zone and those which are characteristic of Critical zone lineages (Figure 4.9).

Minor elements in Orthopyroxene.

For comparative purposes the levels of minor elements in orthopyroxene (Cr_2O_3, MnO, Al_2O_3, TiO_2 and NiO) are plotted in Figures 4.10 - 4.12. Absolute levels of Cr_2O_3 vary from trace amounts to 0.54% and broadly follow the same pattern as MMF ratios with higher values occurring in the more mafic lithologies at the base of the Unit. Levels below 0.25% occur only in the GMA. A marked increase in Cr_2O_3 is recorded in those samples adjacent to the basal contact of the Unit, i.e. close to the basal chromitite layer in **LEF**, **RD**, **UA** and **UC**. The variation within any one sample is usually no more than 0.1% although the ranges within samples at **RPM** are greater (variation within sample B-15 at **RPM** is 0.43%). Levels of MnO (Figure 4.10) show an increasing trend upward through the Bastard Unit and display a more restricted range within individual samples than the ranges for other minor elements in orthopyroxene. The position of the reversal in trend, seen in the MMF ratios is also is clearly evident for

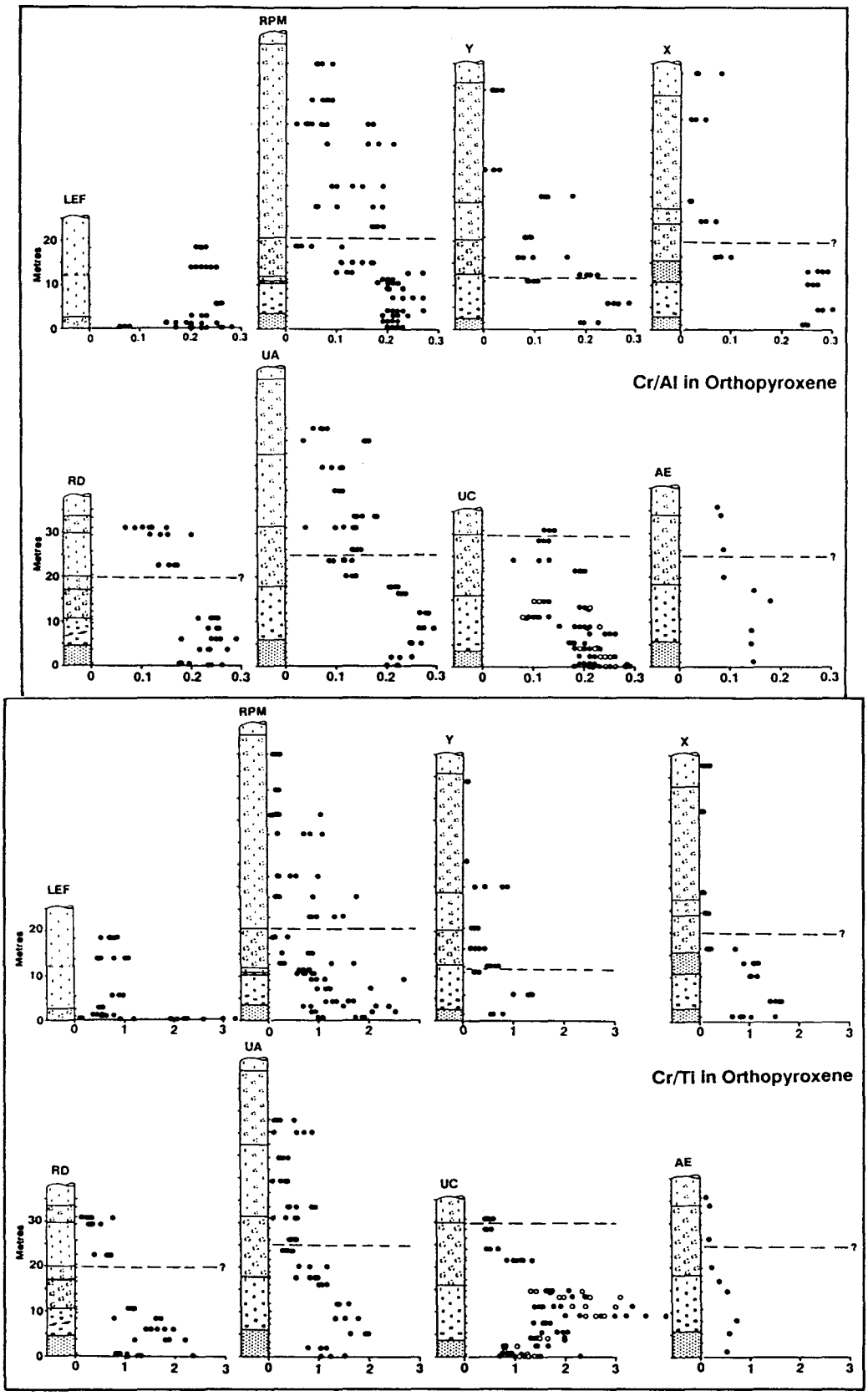

Figure 4.9 The atomic Cr/Al and Cr/Ti ratios for orthopyroxene plotted against height for eight Bastard Unit profiles. Ticks on right of column show sample positions and the dashed line indicates the inferred position of a reversal in trend of MMF taken from Figure 4.7. Open circles in profile UC are for analyses of grain margins.

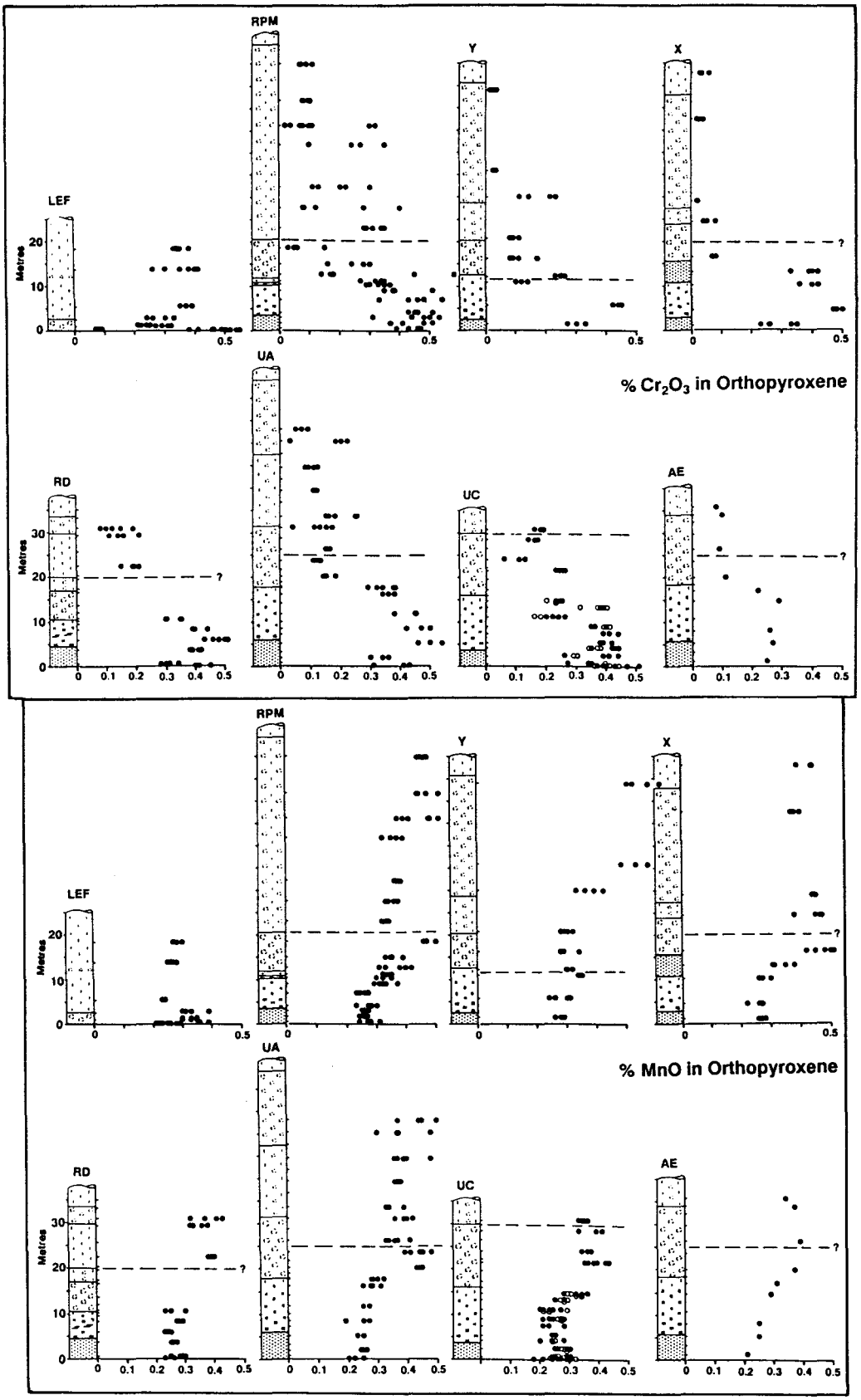

Figure 4.10 Cr_2O_3 and MnO (%) content of orthopyroxene plotted against height for eight Bastard Unit profiles. Ticks on right of column show sample positions and the dashed line indicates the inferred position of a reversal in trend of MMF. Open circles in profile UC are for analyses of grain margins.

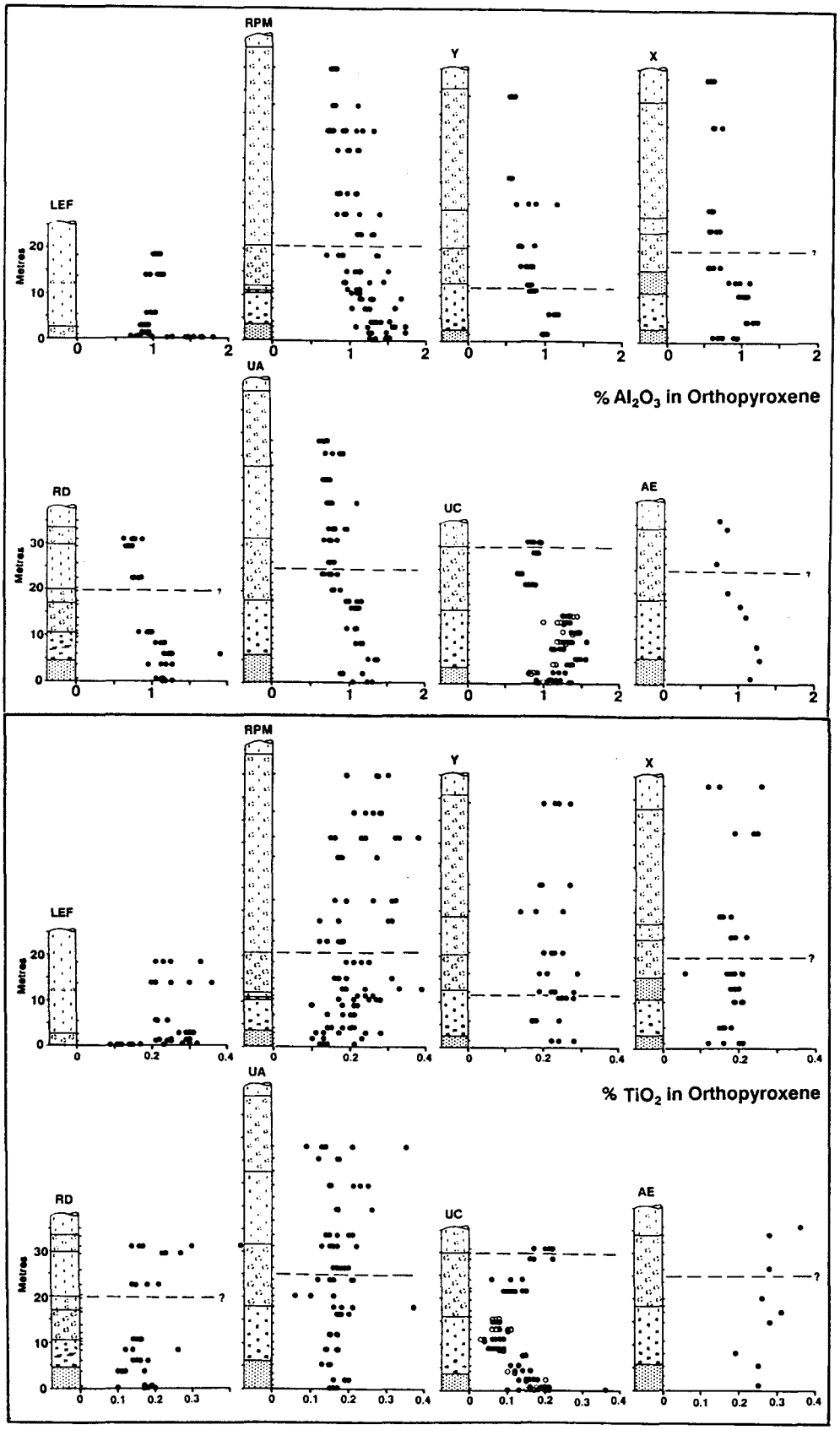

Figure 4.11 Al_2O_3 and TiO_2 (%) content of orthopyroxene plotted against height for eight Bastard Unit profiles. Ticks on right of column show sample positions and the dashed line indicates the inferred position of a reversal in trend of MMF. Open circles in profile UC are for analyses of grain margins.

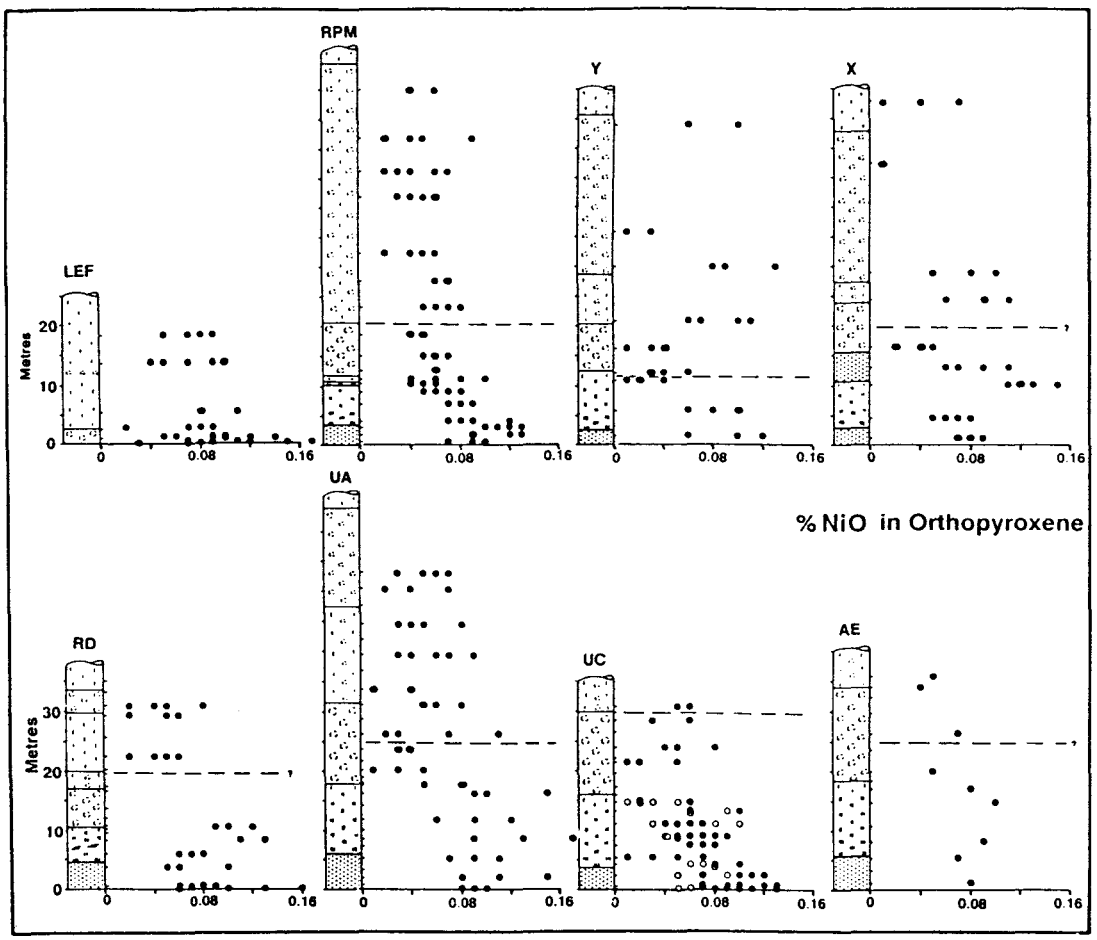

Figure 4.12 NiO (%) content of orthopyroxene plotted against height for eight Bastard Unit profiles. Ticks on right of column show sample positions and the dashed line indicates the inferred position of a reversal in trend of MMF. Open circles in profile **UC** are for analyses of grain margins.

MnO, especially so at **RPM**, **UA** and **X**. Orthopyroxene NiO values in these profiles also clearly show this reversal.

Pigeonite

Inverted primary pigeonite (see **4.7.4**) occurs in the GMM and the UGMA of four profiles and is indicated by "P" in Figure 4.7 (at **RPM** sample B-26, B-28 and B-30; **Y**-722.4, **Y**-740.5; **X**-735, **X**-745.44; and **UA**-1, **UA**-2). These samples are all characterised by higher Fe contents and hence a marked decrease in MMF ratios to levels below 0.65 is noted.

The occurrence of inverted primary pigeonite at the top of the Bastard Unit and the lower part of the Main Zone is a ubiquitous feature of the

entire Bushveld Complex. Pigeonite at this level was first reported by von Gruenewaldt (1973) at Roossenekal in the eastern Bushveld. Here a value of En_{66} was recorded in a sample of the GMA, 58m above the base of the Unit. Von Gruenewaldt (1973) noted that

> ".... from the abundance of thick exsolution lamellae of augite in orthopyroxene, it is concluded that this is the first inverted pigeonite in the sequence. The presence of inverted pigeonite at this level in the intrusion is highly anomalous and no explanation for its presence can be offered at this stage". (von Gruenewaldt, 1973, p.219).

He goes on to say that this zone of inverted pigeonite is only a few metres thick and that the Mg content of orthopyroxene increases gradually to En_{75} at 115m above the base of the Bastard Unit (i.e. into the lower part of the Main Zone). Von Gruenewaldt noted that the An content of cumulus plagioclase changes in sympathy with that of the inverted pigeonite, and that changes in composition from An_{76} to An_{68} occur at this level. A similar trend is recorded in the western Bushveld where values approaching An_{69} are seen at **RPM**, **Y** and **X**. An exception occurs at **UA**, where no decrease in An is evident, but this may be due to insufficient sampling higher in the profile.

Mitchell (1986, p.33) records that "brief occurrences of pigeonite were observed within the Bastard Cyclic Unit, at 30m above the Bastard Reef..." at Union Section. Mitchell (1990a) reported MMF values of 0.602 and 0.613 at this level at Union Section and similar low MMF ratios (c. 0.60) in the Brits area (Mitchell 1990b). He notes that the next appearance of pigeonite in the layered cumulates of the Main Zone occurs in his **Macro-unit VI**, c. 1050m above the Merensky Reef at Union Section.

Clinopyroxene

Representative samples containing clinopyroxene co-existing with orthopyroxene were analysed in profile **Y**, **RD** and **UC**. Data for clinopyroxenes were available for **RPM** (Kruger, 1982) and **AE** (Field, 1987)(see Tables C9, C11, C13, C17 and C19). Average analyses, plotted on conventional triangular diagrams (Wo-En-Fs, Figure 4.16) show that these clinopyroxenes fall within the diopside and augite fields (Morimoto, 1989) and are broadly scattered around the fractionation curves established by Atkins (1969) for the Bushveld Complex.

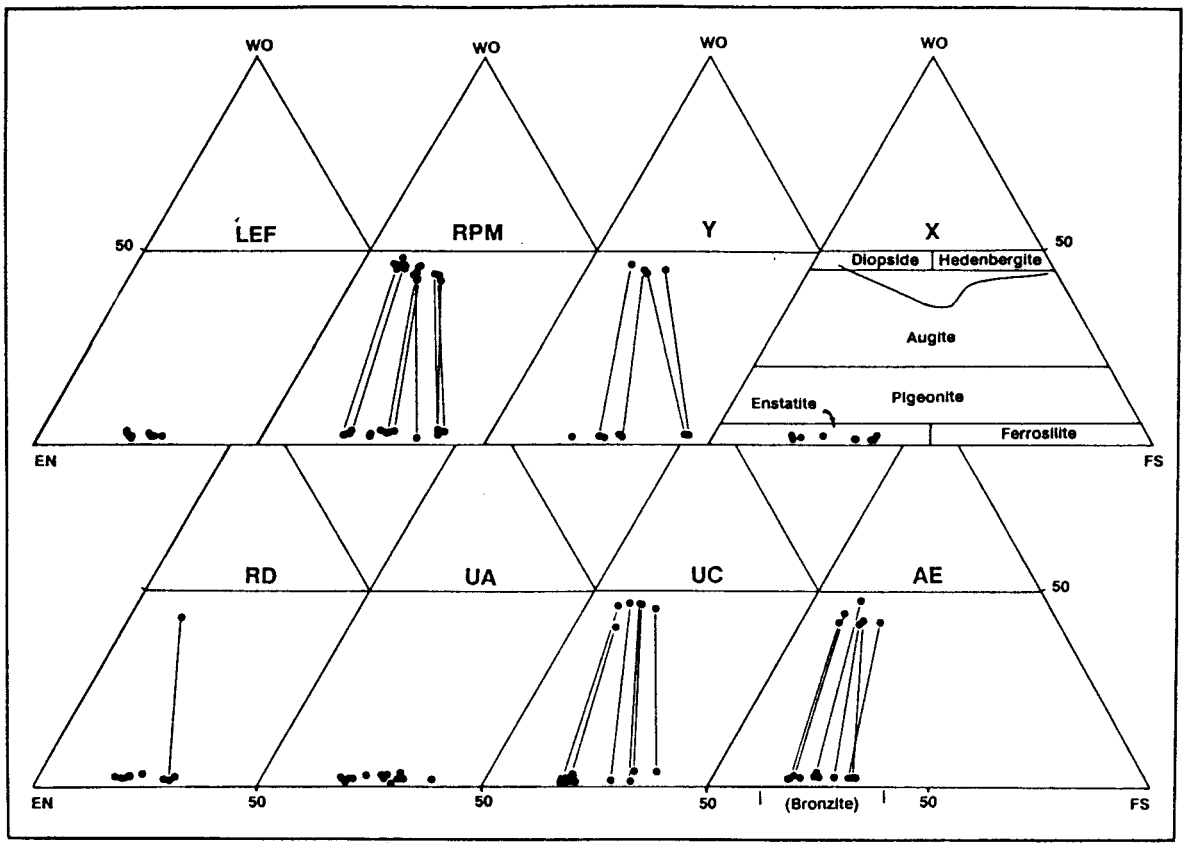

Figure 4.13 Conventional ternary diagrams for all pyroxene analyses in individual Bastard Unit profiles showing tie-lines between co-existing ortho- and clinopyroxenes. The Bushveld fractionation curve of Atkins (1969) as well as the field names of those recomended by Morimoto (1989) are superimposed on X. WO = Wollastonite; EN = Enstatite; FS = Ferrosilite.

4.8.2 Olivine.

The last appearance of olivine in the Critical Zone had, in the past, been reported at the level of the Merensky Reef, where typical values of $Fo_{79.4}$ were recorded at Union Section (de Klerk, 1982). Close-spaced sampling in profile **UC** at Union Section has revealed that three samples contain modal olivine in significant amounts (UC-11 = 32.6%; UC-13 = 32.4%; and UC-17 = 7.3% - see Figure 4.6). Compositions of grain cores range from $Fo_{78.9}$ to $Fo_{81.0}$ (Figure 4.14 and Table C4) and these levels do not differ markedly from those measured in the Merensky ($Fo_{79.4}$) and Pseudoreefs ($Fo_{80.6}$) lower in the sequence. There is a suggestion that weak zonation occurs between grain cores and margins in the upper two samples (UC-11 and UC-13). Analyses of grain margins indicate marginal enrichment of 0.2% in the Fo molecule.

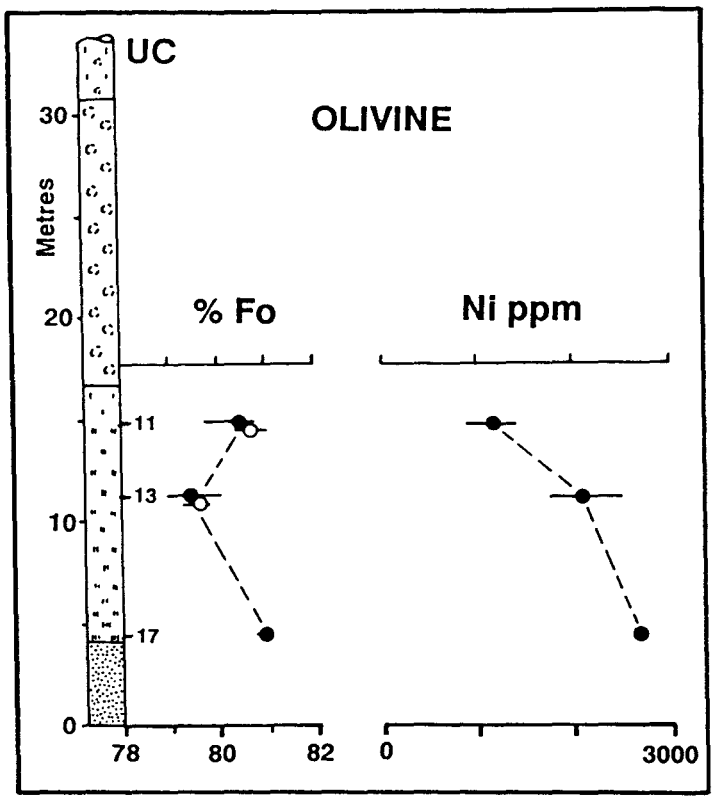

Figure 4.14 Plot of average molecular %Fo and Ni in olivine against height for three samples in profile UC.
Solid circles = core analyses; open circles = analyses on grain margins. Bars indicate the range of composition measured.

Morse (1979b) noted that, in many natural and experimental assemblages, olivine and orthopyroxene in equilibrium obey the approximate rule:

$$MMF_{opx} = 0.85 * MMF_{olivine} + 0.15$$

Scoon (1985, p.168) recorded a similar relationship for the Upper Critical Zone of the Bushveld Complex:

$$(Mg/(Mg+Fe^{2+}))_{opx} = (Mg/(Mg+Fe^{2+}))_{olivine} * 0.875) + 0.125$$

Average analyses of cores of orthopyroxene and olivine in the three UC samples show that they do not deviate significantly from either of these defined relationships (Figure 4.15). Average Ni contents of olivine decrease quite markedly from a high of 2829ppm in the lower sample (UC-17), to a value of 1120ppm (range 864-1366ppm) in the leuconorite (UC-11). These Ni values in olivine are lower than those recorded in the

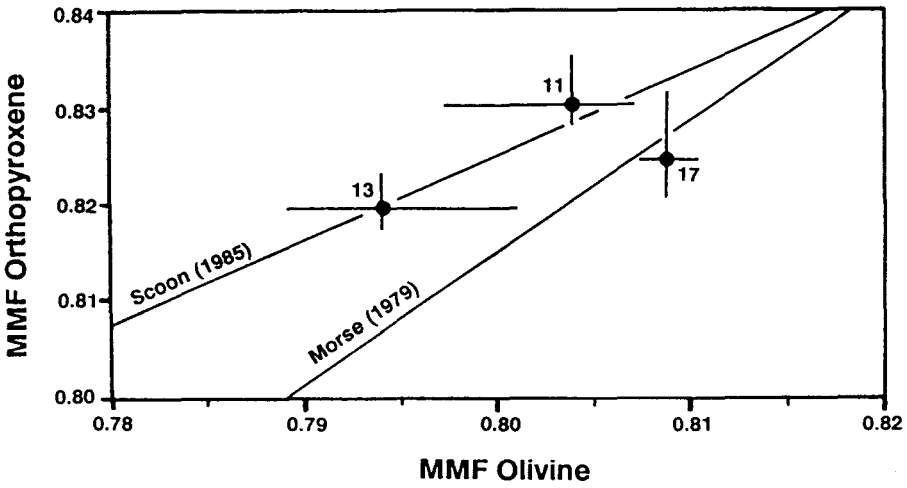

Figure 4.15 Plot of average MMF ratios in orthopyroxene (cores) against the average MMF ratio in olivine in the three UC olivine-bearing samples. Bars indicate the range in composition. The linear relationships established by Morse (1979) and Scoon (1985) are also shown.

Merensky Reef (2762 - 3866ppm) and Pseudoreefs (2525-3235ppm) at Union Section.

It is perhaps noteworthy that CIPW normative olivine only manifests itself in those Bastard Unit profiles north of the Pilanesberg - at RD (one sample), Union (16 samples) and Amandelbult (3 samples) (Figure 4.6). This concentration of olivine in the norm is more conspicuous in the melanocratic rocks and was also noted by van Zyl (1970) at Union Section. Of three Bastard Unit samples which he analysed the lower two indicated olivine in the norm (olivine in norite - 6.14%, and olivine in pyroxenite - 1.46%). The fact that more normative olivine occurs in this northwestern sector indicates that these rocks are more undersaturated than elsewhere in the Complex. This feature supports the contention of Eales et al. (1988) that the northwestern sector of the Complex, and more specifically Union Section, displays more primitive characteristics and represents a "proximal facies" located closer to an irruptive or feeder centre than exposures more distant along strike.

4.8.3 Plagioclase feldspar.

Compositional variations of plagioclase with stratigraphic height are presented in Figure 4.16 and are represented in terms of the end members albite and anorthite (mol. %An). Between 5 and 10 analyses of grain cores were analysed in each sample. Ubiquitous zoning of both cumulus and intercumulus plagioclase in all profiles resulted in a display of wide compositional range within individual samples. A study of plagioclase zoning is presented later. The "within sample" compositional range for **cumulus** plagioclase in the norites and anorthosites is generally between 2 and 6 mol. %An, but can be considerably greater, especially in the UGMA, where a range of 10% An is not uncommon. **Intercumulus** plagioclase in the basal Bastard pyroxenite has a lower An content than that of cumulus habit higher in the sequence. These lower An levels for intercumulus plagioclase display a far greater compositional range of c. 15 mol. %An (a range of 25% is recorded for some samples in profiles **UC** and **AE**) when compared with cumulus plagioclase.

A similar pattern of An content is seen through the succession in all profiles, although some differences are evident where lithologies do not conform to a normal sequence (**LEF**, **X** and **RD**). Profiles which best represent the distribution of %An are **RPM** and **UA**, reinforced by the detailed coverage of **UC** and **AE** in the lower part of the Unit. These data are supported by the work of Naldrett et al. (1986, Figure 2) at Union and Rustenburg. The generalised pattern of An content through the sequence for the 10 profiles is summarised as follows (Figure 4.16):

* Intercumulus plagioclase within the first 30cm of the Bastard pyroxenite has an average composition of An_{61} (range An_{46-74}).
* The average An content of intercumulus plagioclase increases upward through the pyroxenite, to values approaching An_{75} at the contact with the overlying melanorite.
* Cumulus plagioclase makes its appearance within the melanorite and here the An content continues to rise until An_{80} is attained in the central part of the norites. The An content at this level in profile **UC** is anomalously high and levels in excess of An_{85} are recorded.

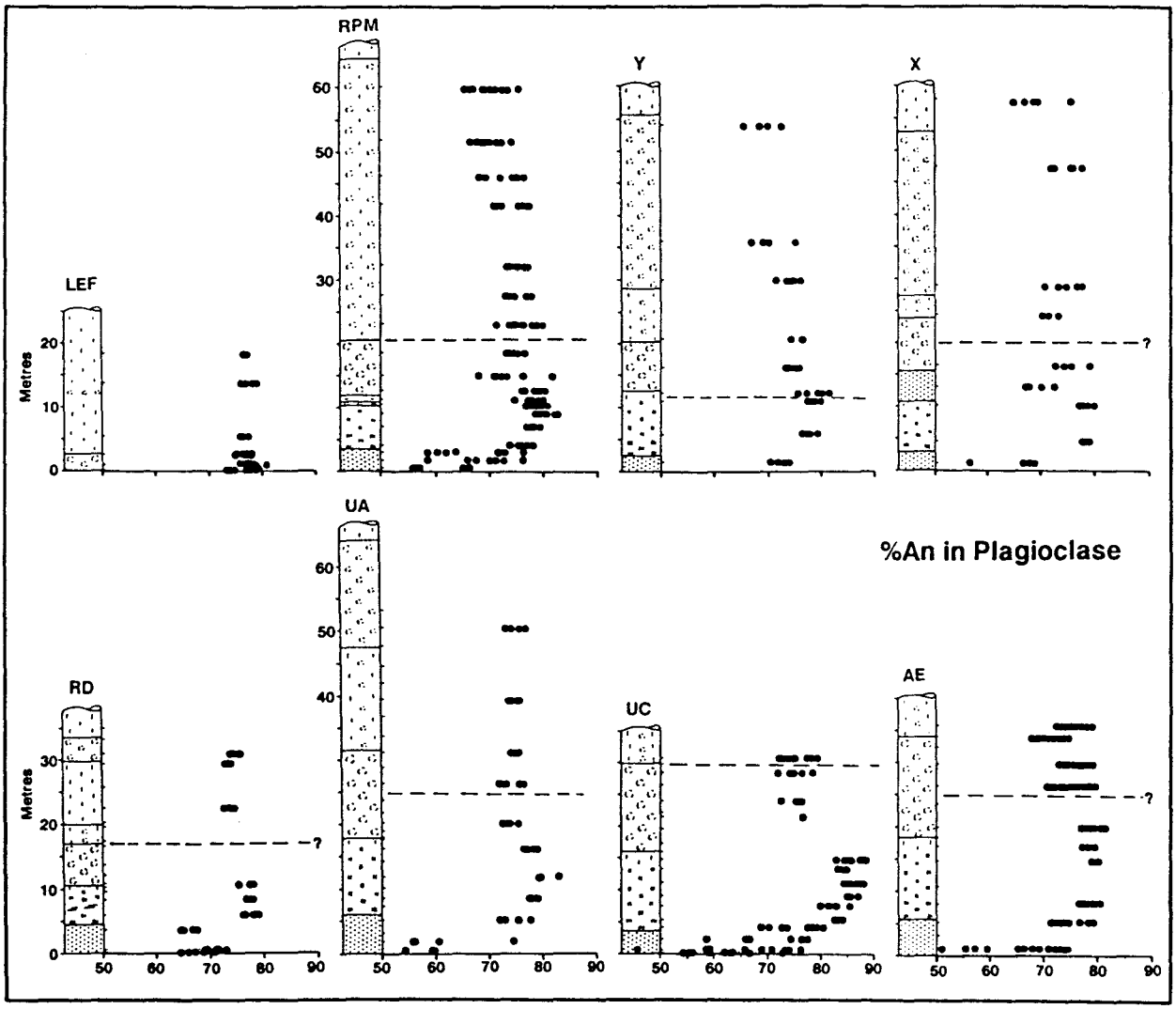

Figure 4.16 Variations of mol. %An in plagioclase plotted against height for eight Bastard Unit profiles. All analyses are of grain cores and intercumulus plagioclase occurs only in the basal pyroxenite (stipple). Ticks on the right of each column show sample positions while the horizontal dashed line indicates the inferred position of a reversal in trend of MMF in orthopyroxene.

* A gradual decline in An content occurs within the leuconorites and continues into the lower part of the GMA. Levels of An_{75} are seen in the middle of the LGMA.
* This level of An_{75} remains fairly constant through the upper part of the LGMA, the GMM and the lower half of the UGMA.
* A further decrease to An_{70} occurs in the UGMA of profile **RPM** and **Y**. The decline in An levels for profile **X** occurs only in the leuconorites above the UGMA. This decrease in An content for the three profiles is accompanied by a concomitant increase in the range of values within individual samples.

The pattern of cryptic variation for cumulus plagioclase does not behave as expected by following a similar trend established for the orthopyroxene MMF ratio. Rather a clear decoupling of cryptic variation is noted between these two phases. No distinctive reversal in An content is seen at the level where the prominent reversal in MMF ratio is recorded for orthopyroxene. Only a suggestion of a possible reversal in the trend of %An content is seen in profiles **RPM**, **UA** and **UC**.

The distribution of the minor elements K_2O and FeO in plagioclase is presented in Figure 4.17 and 4.18. Concentrations of K_2O are shown only for profiles **RPM**, **X** and **UA**, (spuriously low K_2O values were obtained in samples from profile **Y**, **RD** and **UC**, attributed to an incorrect background value being used in the data reduction). K_2O levels range from 0.05% to values seldom higher than 0.35%. A high variation of c. 0.1% is recorded within individual samples, with some pyroxenite samples displaying ranges in excess of 0.25% (**UA**-25). High values of up to 0.45% are seen in two samples at the base of the Bastard pyroxenite (**UA**-25 and 27). The broad distribution pattern of K_2O, in profile **UA** and **RPM**, is a mirror image of that seen for the MMF ratio in orthopyroxene although the double cuspate pattern is not as well defined in profile **X**. Levels of K_2O

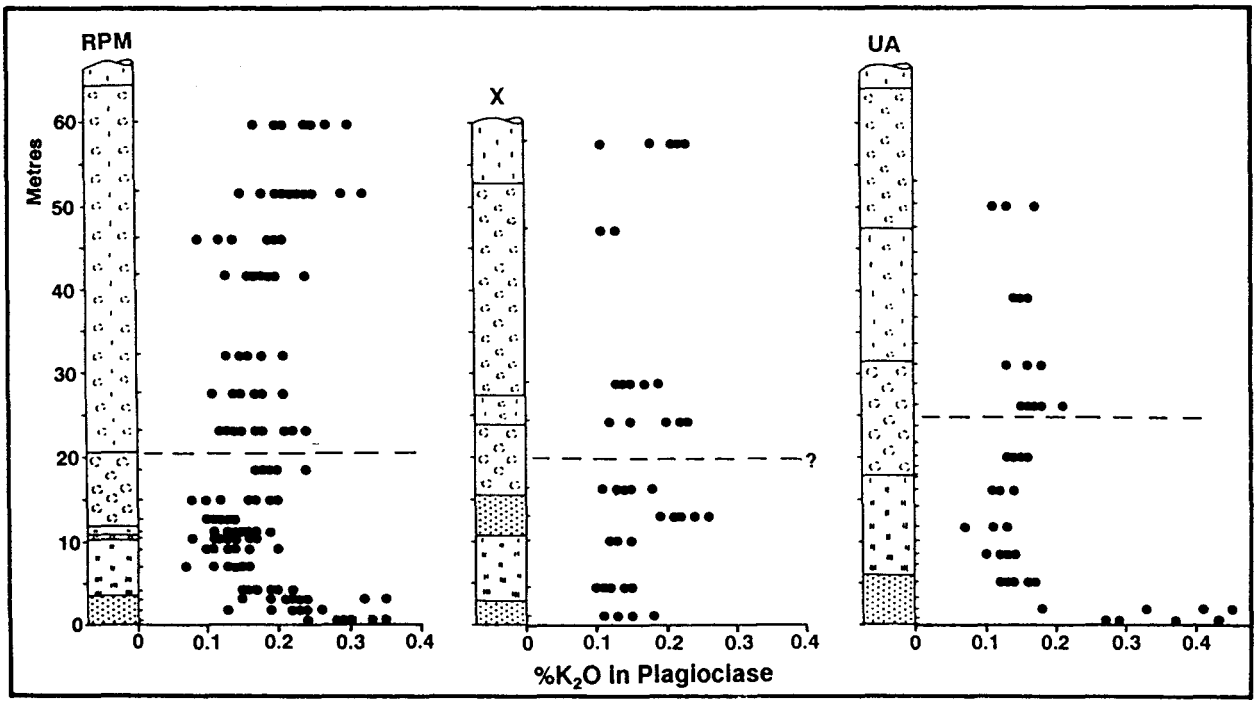

Figure 4.17 Variations of $\%K_2O$ in plagioclase plotted against height for three Bastard Unit profiles. Ticks on right of column show the sample positions while the horizontal dashed line indicates the inferred position of a reversal in trend of MMF in orthopyroxene.

in plagioclase in the UGMA, where K-feldspar occurs as an intercumulus phase (see **4.7.4**), are marginally higher than in the lower parts of the GMA.

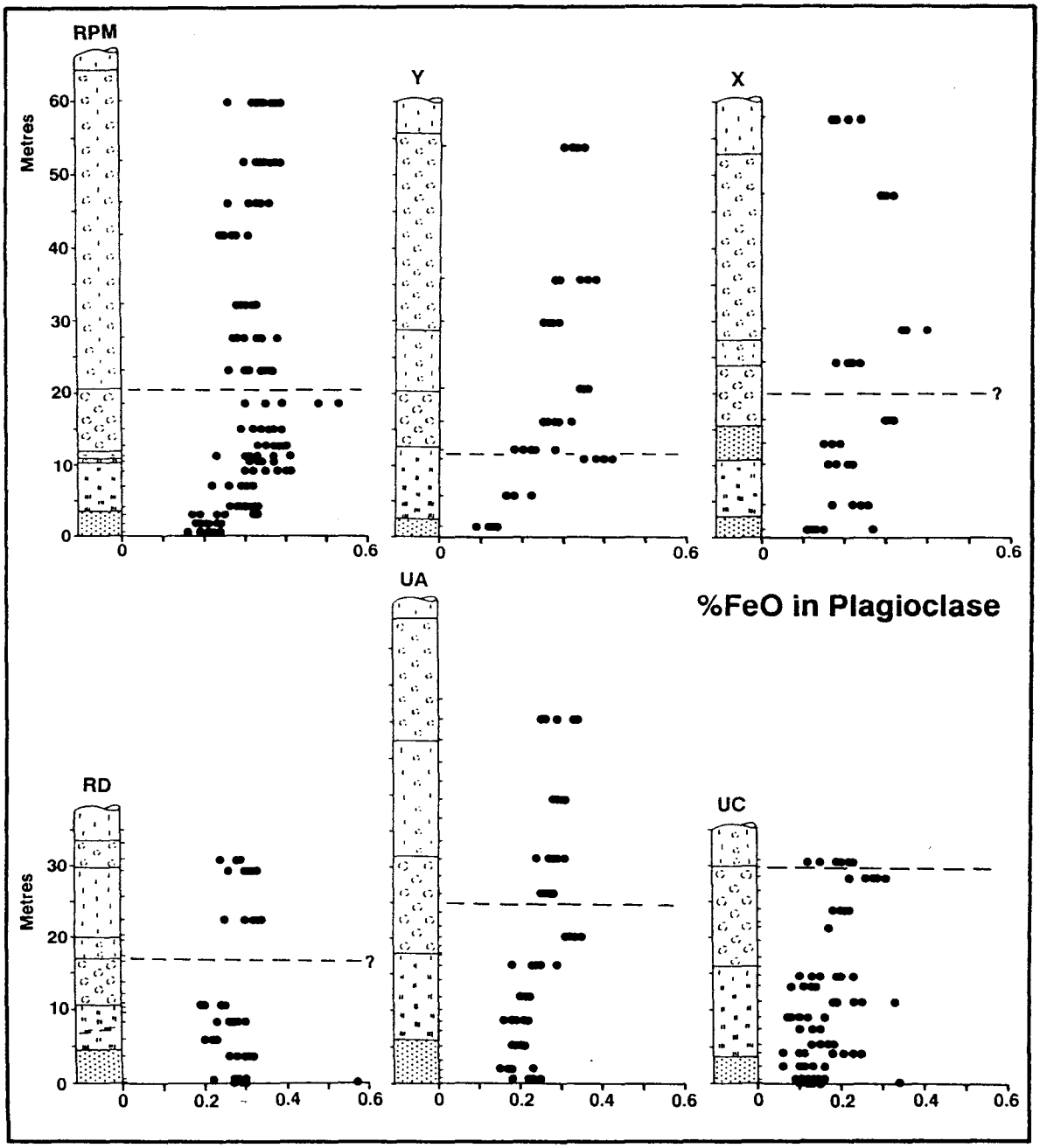

Figure 4.18 Variations of %FeO in plagioclase plotted against height for six Bastard Unit profiles. Ticks on right of column show the sample positions while the horizontal dashed line indicates the inferred position of a reversal in trend of MMF in orthopyroxene.

The content of Fe (reported here as FeO) in plagioclase throughout the Bastard Unit is similar to that reported in the UG1FW Unit (see 2.4.3) and is between 0.10 and 0.54%. As with K_2O, there is wide variation

within individual samples, although data for **UA** show the least scatter. The pattern of FeO values in plagioclase through the sequence strongly supports the postulate of a reversal in the vicinity of the LGMA indicated by the MMF ratio of orthopyroxene. A distinctive reversal in FeO content of plagioclase is seen in profiles **RPM**, **Y**, **X**, **UA** and **UC** (Figure 4.18).

Zoning of Plagioclase

Oscillatory zoned plagioclase crystals are common within the GMA (see **4.7.4**). The majority of grains (1-3mm) display some form of zonal growth. Some grains may have up to eight distinct zones (rare) while others may display only a single oscillation. Two distinctive zoned crystals were selected for detailed microprobe analysis to establish the nature of the zonation seen optically in thin section. These grains were selected from samples **X**-768.5 (GMM) and **Y**-722.4 (UGMA). Analytical results are presented in Table C29.

Sample X-768.5 (GMM)

The grain selected in this sample is 2.3mm in diameter and optically displays more than five distinct zones in thin section (Figure 4.19). Optical zoning is obscured by fine twinning in part of the grain. Four analytical traverses, of varying point density, were executed across the grain. Only a small amount of intercumulus orthopyroxene is present in the sample and the traverses were positioned so as not to be in close proximity to it. The start of each traverse (at the grain boundary) is in contact with adjacent cumulus plagioclase grains.

A gross compositional variation of 10.4% An was recorded within the grain (range $An_{81.2-70.8}$) and an average value of $An_{74.0}$ (std. dev. 2.27, n = 90) was obtained for all analyses. A lower value of $An_{71.5}$ (std. dev. = 1.0, n = 5 analyses) was initially obtained for the sample.

Profile A, from the grain margin to the core, illustrates the general zonal pattern in the crystal while the detail in **Profile B** shows the variation in %An at the grain margin. A strongly reversed rim is observed at the grain boundary where the following values are recorded:

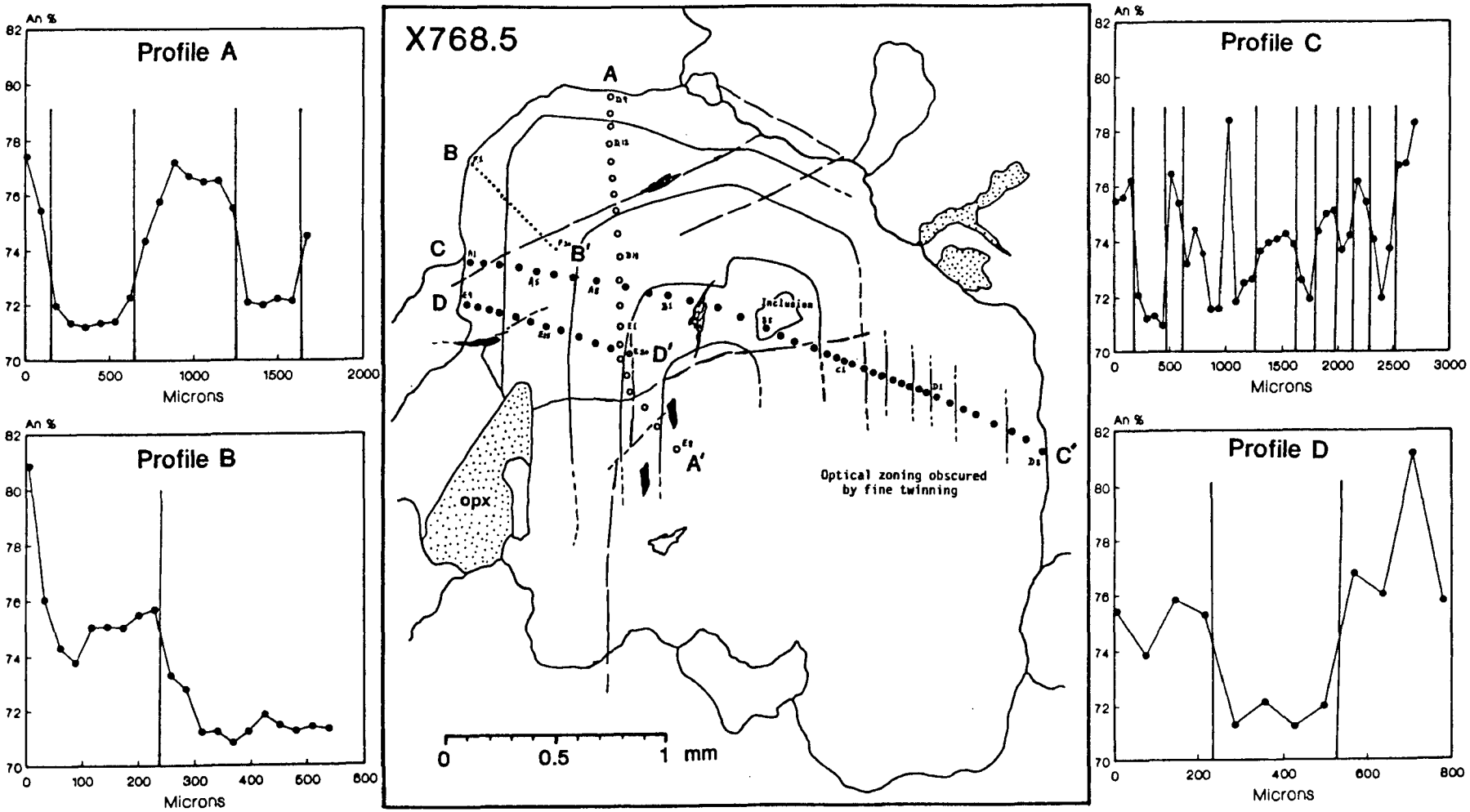

Figure 4.19 Four analytical traverses across the zoned cumulus plagioclase grain in sample X768.5. Variations in An content for each traverse are shown.

Profile A $An_{77.0}$
Profile B $An_{80.9}$
Profile C $An_{75.5}$ and $An_{78.3}$
Profile D $An_{75.4}$

The An levels at the grain margins are generally higher than those seen within the core of the grain. From high An values at the margin the An content drops to values below An_{72} at

Profile A 200-600 microns
Profile B 300-550 microns
Profile C 200-500 microns
Profile D 250-500 microns.

A series of peaks and troughs between An_{76} and An_{72} are recorded through the grain (Figure 4.19, **Profile C**). A notable feature of **Profile C** is the isolated high value of $An_{78.4}$ at 1000 microns from the grain edge. This value is in sharp contrast to the surrounding lower values (c. An_{72}) and is due to a small plagioclase chadacryst within the larger cumulus grain. The shape of the inclusion is clearly seen in thin section. The occurrence of this inclusion supports the view that the population of small, partly resorbed plagioclase grains found elsewhere within cumulus orthopyroxene (see **4.6**) also occurs within rocks where cumulus plagioclase is the dominant cumulus phase (i.e. within the GMA).

Sample Y-722.4 (UGMA)
The grain selected in this sample is c. 1.25mm in diameter and is partly enclosed by intercumulus orthopyroxene. Optically it displays three zonal shells in thin section (Figure 4.20). The start and end of each analytical traverse is adjacent to orthopyroxene. This plagioclase crystal appears to have been partly resorbed before the crystallisation of orthopyroxene as part of the second shell is not preserved at the start of **Profile 1.**

Three traverses, of varying point density, were executed across the grain and the compositional variation recorded for all analyses is 15.2% An (range $An_{60-75.2}$). A range of 9.1% An ($An_{66.1-75.2}$) is indicated if the low value of An_{60}, recorded at the grain margin of **Profile 2**, is excluded.

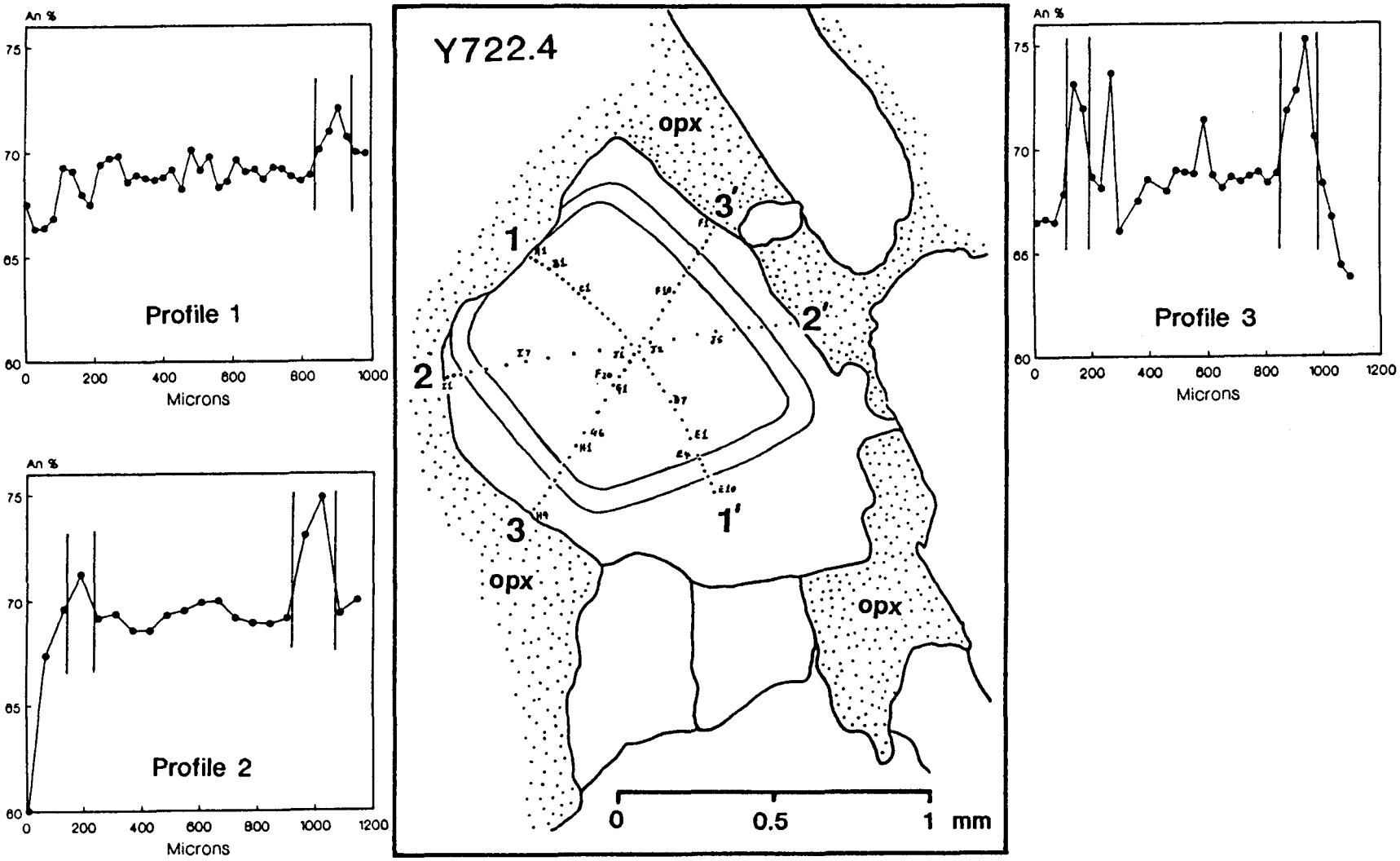

Figure 4.20 Three analytical traverses across the zoned cumulus plagioclase grain in sample Y722.4. Variations in An content for each traverse are shown.

This variation of $An_{9.1}$ is similar to that recorded in **X-768.5** and the average An content for all analyses is $An_{69.1}$ (std. dev. 2.10, n = 91 analyses). This value is in excellent agreement with the average of $An_{69.0}$ obtained for the sample (std. dev. = 2.51 for 4 plagioclase core analyses).

The pattern of zonation displayed in this grain is as follows:

* Values generally below An_{66} are seen at the grain boundaries in contact with orthopyroxene.
* The An content rises to a peak within the prominent second shell ($An_{71.3-75.2}$). A second peak ($An_{73.7}$) is seen at 270 microns in **Profile 3.**
* A rise in An content is seen towards the core of the grain where a subdued high of $An_{70.0-71.1}$ is recorded.

Summary of observations on zoning

This limited study on the zoning of two plagioclase grains within the GMA illustrates their complex nature and the variations of crystal growth that took place at this level of the sequence. The following salient points emerge:

a) A wide range in An content is seen within individual grains. This can be as much as An_{15} but is more commonly c. An_{10}.
b) Grain margins in contact with other plagioclase crystals display a marked reversal to higher An values compared to those in the rest of the grain. This phenomenon has also been documented by Morse and Nolan (1984) in troctolites and olivine gabbros of the Kiglapait intrusion. They report reversals of as much as 32% of An. Analyses of the margins of cumulus plagioclase grains in **UC**-1, 11 and 13 also show this feature where the average An content rises by between $An_{4.5}$ and $An_{1.5}$. Similar reversals were evident in two of the three traverses reported by Field (1987, p.62) across cumulus grains at Amandelbult. Analyses of cumulus grain margins reported by Naldrett et al. (1986) do not have any consistent pattern at either Union or Rustenburg Sections.
c) Where plagioclase grain boundaries are in contact with orthopyroxene the An content at the margins is depleted by up to 6% of An. This

observation is supported by the more detailed work of Field (1987, p.61) in which he reported a marked An depletion of as much as An_{18} at grain margins in contact with orthopyroxene. The data of Naldrett et al. (1986, p.1107) for both Union and Rustenburg confirm this generalization.

Petrographic and analytical evidence indicates that the style of zoning within individual plagioclase grains is variable and does not readily fit any of the zonal classification systems that have been proposed (Homma's classification, p.210 in Smith, 1974). The classification of "Irregular-oscillatory reverse (VIr)" zoning would perhaps best describe the observed pattern of zonation. Ideally, continuous 2 micron step-scan traverses for Na, K and Ca, similar to those done by Smith and Lofgren (1983), would be needed to establish in detail the style of zoning.

This study on plagioclase zonation has highlighted the problem of obtaining a realistic bulk plagioclase composition from a limited number of microprobe analyses. Field (1987), in his study of plagioclase at Amandelbult, pointed out that random analyses throughout a sample were unlikely to be representative and suggested that analytical traverses across whole grains would partly overcome this problem. This technique would at the same time give some idea of the chemical variation within individual grains and within the sample. Another approach would be the analysis of 10 or more grain cores randomly selected through the sample. These methods would only give an approximation to the bulk An content of the plagioclase and ideally an additional XRF analysis of mineral separates would produce the most representative result.

Plagioclase - a summary

Profiles which best represent the chemical variation in plagioclase feldspar are those for **RPM**, **X**, **Y**, **UA**, **UC**, **AE** and to a lesser degree **RD**, as well as two profiles reported by Naldrett et al. (1986). All of these profiles display the following characteristics:

* Intercumulus plagioclase feldspar at the base of the Unit is more sodic than its cumulus counterpart higher in the sequence.
* The range of An content is greater for intercumulus plagioclase than

for the cumulus variety.

* The variable patterns of zoning within individual grains, and the presence of small plagioclase inclusions within larger complex zoned grains suggest that one is dealing with more than one plagioclase population in the sequence. Similarities with the mixed plagioclase population within the UG1FW Unit (see **2.3** and **2.4.2**) are also suggested by the presence of the small resorbed plagioclase inclusions seen in cumulus orthopyroxene grains - especially in the norites.

4.8.4 Chromite.

Analytical data for the thin chromite layer at the base of the Bastard Unit (see **4.6.1**) have been captured at two localities. These are at Union Section (**UB** sample H232/3), where seven chromite grains were analysed by Eales (1987, p.159), and the exposure at **LEF** (H998.1), where 6 chromite grains were analysed in this study (Table C30). The average composition of the chromite at **LEF** is almost identical to that at **UB** in terms of the cations Cr, Al, Fe^{3+} and Ti. The principal difference is that the MMF ratio ($Mg/Mg+Fe^{2+}$ with Fe^{2+} in the octahedral site) at **UB** (c. 0.35) is higher than that recorded at **LEF** (average 0.30). The composition of the Bastard Unit chromite at **LEF** conforms with the general pattern of Cr and Al depletion accompanying enrichment in Fe^{3+} and Ti identified by Eales (1987) for all chromitite layers above the UG2 layer in the Upper Critical Zone.

4.9 Whole-rock chemistry.

Whole-rock major element data have been compiled for 124 samples in nine profiles and trace element data for 179 samples in 11 profiles. All analyses were performed by XRF spectrometry. The analytical methods and conditions, as well as the reliability of the trace element analyses, are discussed in Appendix D. A summary of the number of samples and elements recorded in each profile, together with the sources of data, is presented in Table 4.2.

Naldrett et al. (1984 and 1986) presented some whole-rock data for single profiles at Union and Rustenburg Sections and reported levels of MgO, K_2O, P_2O_5, Y and Cr (in 1984), and Cu and Ni (in 1986). These data have been incorporated in Figure 4.25 and are also included in this discussion. In this study simple linear regression analysis has been used in the synthesis of whole-rock compatible element data and therefore the merits of using this statistical technique are discussed.

4.9.1 Major element variations.

Major element data for the profiles **LEF**, **Y**, **X**, **RD**, **UA**, **UB**, **UC**, **AE** and **AF** are presented in Tables D5 - D7 (Appendix D), with total Fe represented as Fe_2O_3. The original data were recalculated to an assumed Fe_2O_3/FeO ratio of 0.1 and were normalised to 100% (Tables D9 - D14). These recalculated data were used throughout in the graphical presentation of the data and for the calculation of the CIPW norms. Variations of selected major elements in individual profiles are graphically illustrated by means of plots against stratigraphic height and cryptic variation through the sequence is best illustrated through the use of interelement ratios.

The whole-rock MMF_{WR} ratios (atomic ratio of Mg/(Mg+Fe) where all Fe is expressed as Fe^{2+}) closely reflects the pattern seen for the orthopyroxene MMF ratio (**4.8.1**). MMF_{WR} ratios vary between 0.82 in the melanorites and 0.60 in the GMA. The stratigraphic variation of MMF_{WR} through the Unit is summarised as follows (Figure 4.21):

* A reversed fractionation trend is apparent within the lower 4 - 5m of all profiles apart from **LEF** and **Y**. MMF_{WR} values at the base start at 0.800 and increase upward through the pyroxenite and melanorite. Here a maximum value of 0.819 is attained (**UA**-23 and **AF**-12).
* A decrease in MMF_{WR} from these high values (i.e. >0.800) is seen within the norite, and this becomes more marked upward into the leuconorite (0.750). An exception to this general pattern is seen in profile **Y** where an unusually low MMF_{WR} ratio of 0.603 is recorded in the leuconorite.
* MMF_{WR} ratios continue to decline across the basal contact of the GMA into the LGMA where an average value of 0.650 is evident (average 0.676). Considerable variation between 0.597 (**UA**-15) and 0.778 (**UC**-8) is seen within the LGMA. At Union Section minimum values of 0.597 (**UA**-15) and 0.599 (**UC**-3) are recorded.
* The reversal recorded for MMF ratios in orthopyroxene is not as sharply defined in the whole-rock data. Apart from profile **Y**, where the reversal is conspicuous, other profiles like **UA** and **AE** rather display a gradational increase in MMF_{WR} above the inferred reversal level before decreasing again.
* Levels in the GMM and UGMA (in **Y**, **X**, **RD** and **UA**) have variable distribution patterns (range 0.751-0.601). In all cases the overall trend is one of decreasing MMF_{WR}. Variability of the MMF_{WR} ratio between profiles in the upper part of the GMA may in part be due to the relative proportion of clino- and orthopyroxene present in individual samples.
* The pattern of decreasing MMF_{WR} ratio continues upward for a short distance (30m) into the Main Zone before an increasing trend is established in the lower 400m of the Main Zone (Mitchell, 1986).

The absolute compositional ranges recorded for major elements in different lithologies of the Bastard Unit are presented in Table 4.4.

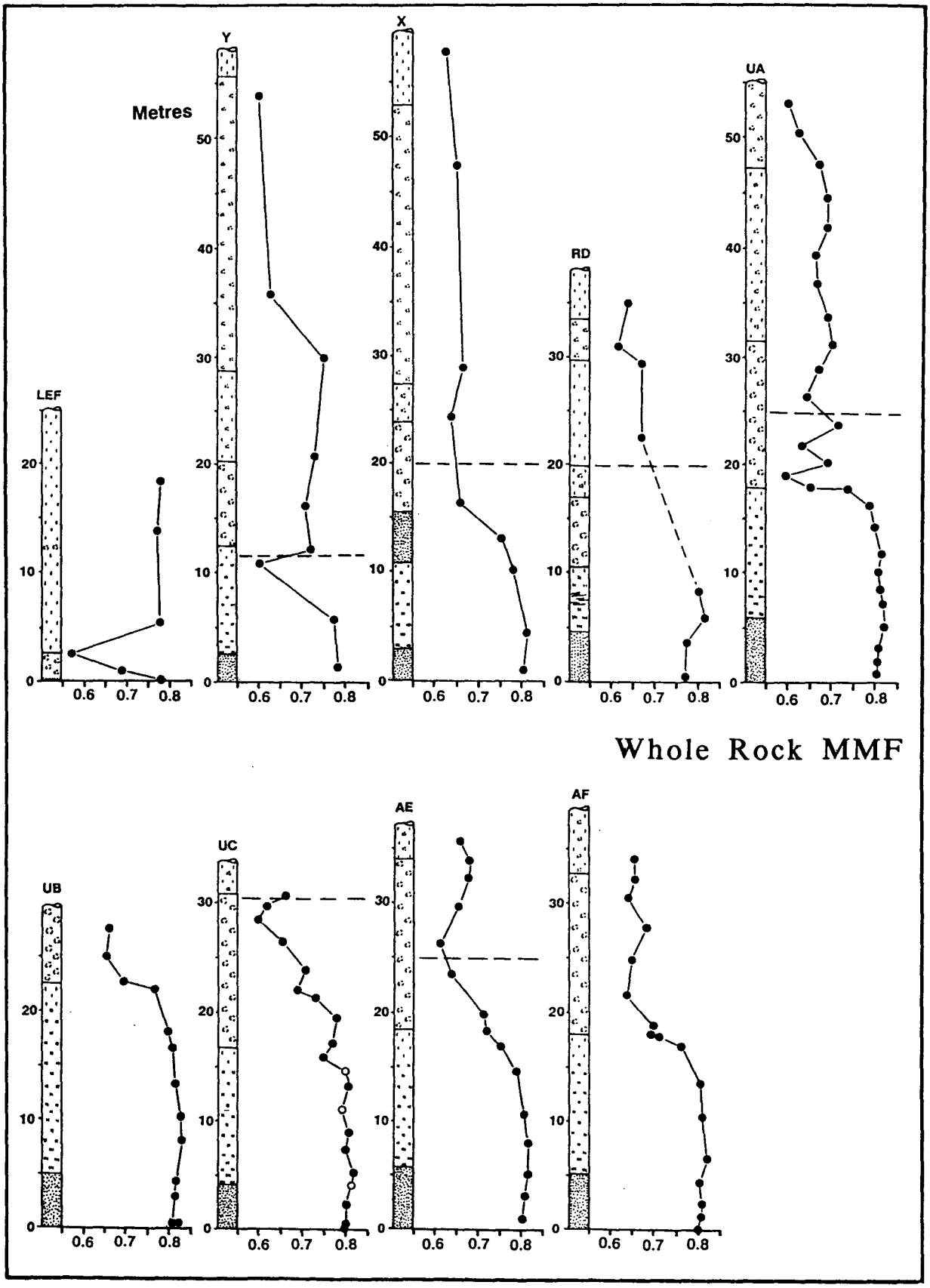

Figure 4.21 Whole-rock MMF_{WR} ratio plotted against stratigraphic height for nine Bastard Unit profiles. Open circles in profile UC are olivine-bearing samples. Horizontal dashed line indicates the inferred position of a reversal in trend of MMF ratio in orthopyroxene demonstrated in Figure 4.7.

Table 4.4: Absolute ranges for whole-rock major and trace elements in different lithologies of the Bastard Unit.

Lithology	Pyroxenite	Norite	Anorthosite
wt.%			
SiO_2	53.9 - 56.0	44.2 - 54.1	45.8 - 51.8
TiO_2	0.14 - 0.25	0.03 - 0.26	0.01 - 0.26
Al_2O_3	4.97 - 6.86	7.15 - 28.3	24.9 - 33.0
Fe_2O_3	0.87 - 1.09	0.19 - 1.09	0.07 - 0.37
FeO	8.75 - 10.9	1.89 - 10.9	0.73 - 3.71
MnO	0.17 - 0.24	0.03 - 0.22	0 - 0.08
MgO	21.9 - 25.4	2.34 - 23.2	0.70 - 4.85
CaO	3.49 - 4.91	4.87 - 17.5	12.2 - 16.8
Na_2O	0.28 - 0.92	0.56 - 2.82	1.79 - 2.78
K_2O	0 - 0.24	0 - 0.29	0.04 - 0.51
P_2O_5	0 - 0.17	0 - 0.08	0 - 0.17
MMF_{WR}	0.770 - 0.821	0.625 - 0.829	0.573 - 0.778
ppm			
Sr	54 - 92	57 - 567	269 - 456
Rb	0 - 18	0 - 7.0	0 - 17
Y	2.8 - 10	0 - 7.3	0 - 19
Zr	6.9 - 28	0 - 21	0 - 39
Co	52 - 107	12 - 92	4.3 - 35
Cr	1850 - 3572	180 - 3459	22 - 372
V	89 - 142	29 - 136	5.9 - 67
Zn	66 - 131	7.4 - 124	7.4 - 72
Cu	23 - 461	4.0 - 258	6.2 - 102
Ni	534 - 1457	46 - 726	15 - 235
Sc	24 - 35	4.9 - 30	1.4 - 11

Note: 1) The basal "pyroxenite" at LEF has been excluded from the Pyroxenite range.
2) Olivine-bearing norites in UC are not included.

Salient features recorded for absolute levels of some whole-rock major elements are as follows. Whole-rock TiO_2 values in the basal pyroxenite generally start at a high of 0.2% and fall off to values of c. 0.1% within the norite and mid- to lower part of the GMA (Figure 4.24). An increase to values in excess of 0.2%, is seen in the UGMA. Mitchell (1986) did not observe this distinctive increase at this stratigraphic level (perhaps because of his wider sampling interval) but rather a steady increase from 0.09% within the Bastard Unit to 0.19% c. 787m above the base of the Bastard Unit. Anomalously high values of TiO_2 are also seen in the LGMA of **UB** (0.26%) and the norite of **UC** (0.18 and 0.32%) (Figure 4.24).

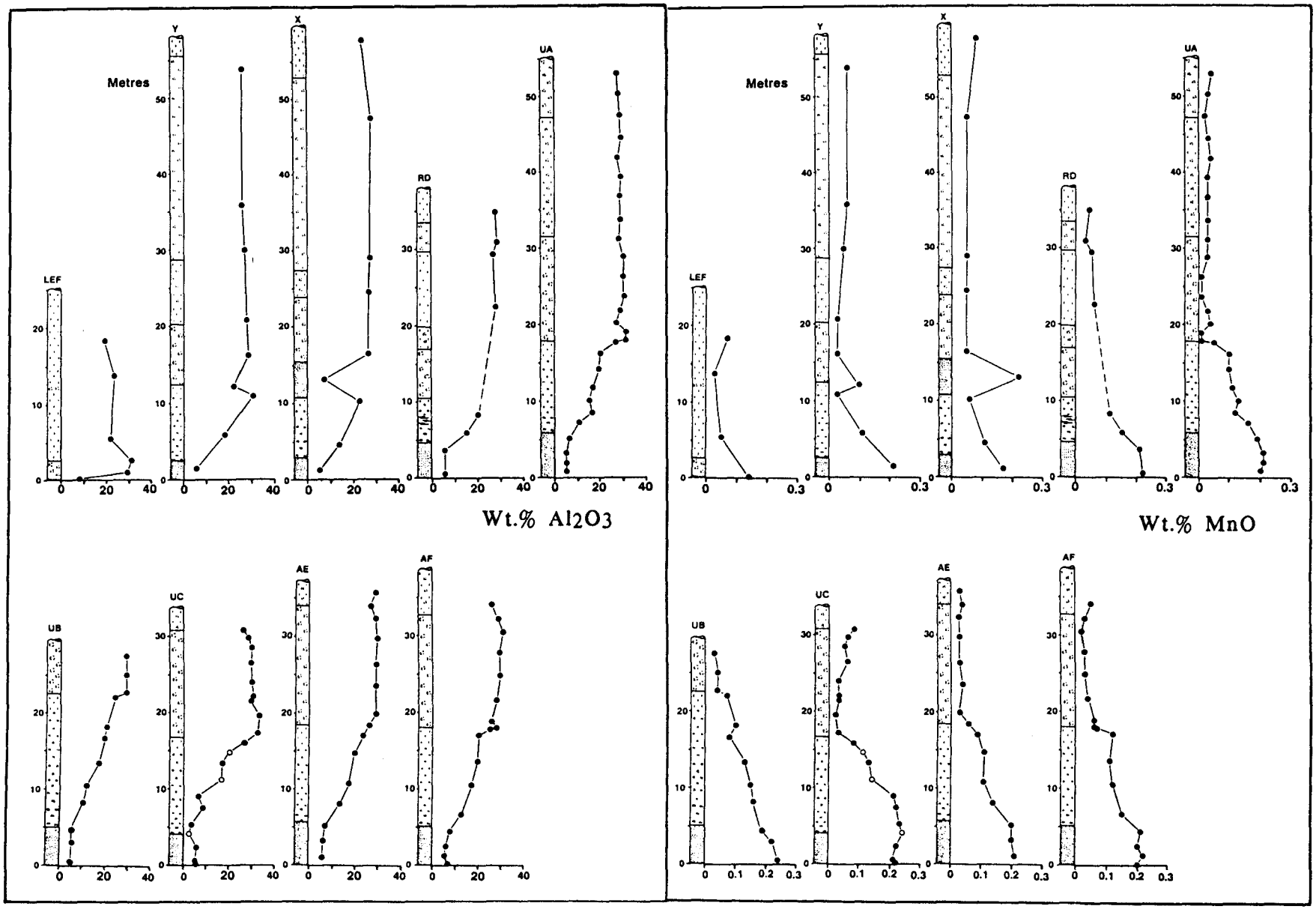

Figure 4.22 Whole-rock Al_2O_3 and MnO (Wt.%) plotted against stratigraphic height for nine Bastard Unit profiles. Open circles in profile UC are olivine-bearing samples.

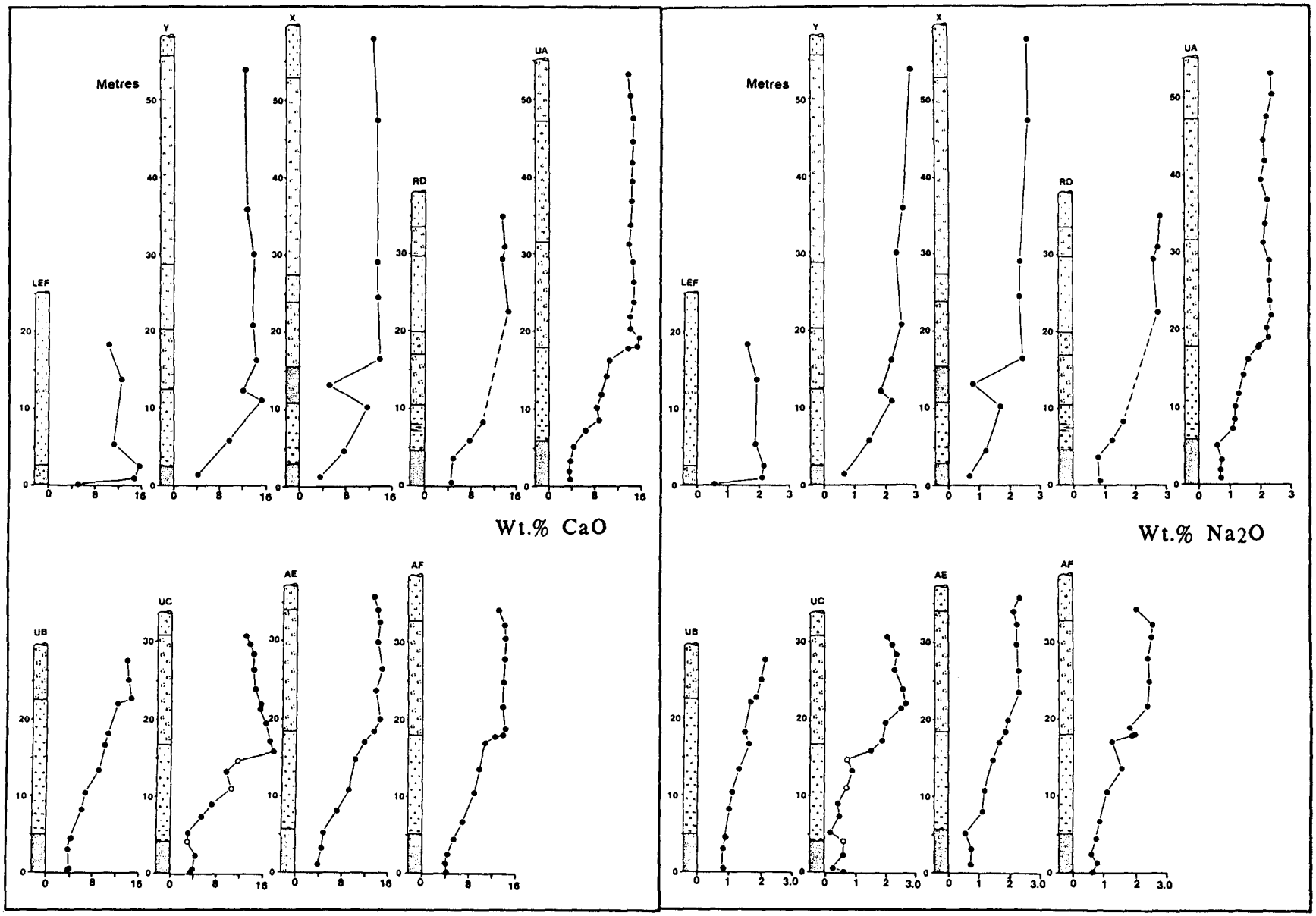

Figure 4.23 Whole-rock CaO and Na_2O (Wt.%) plotted against stratigraphic height for nine Bastard Unit profiles. Open circles in profile UC are olivine-bearing samples.

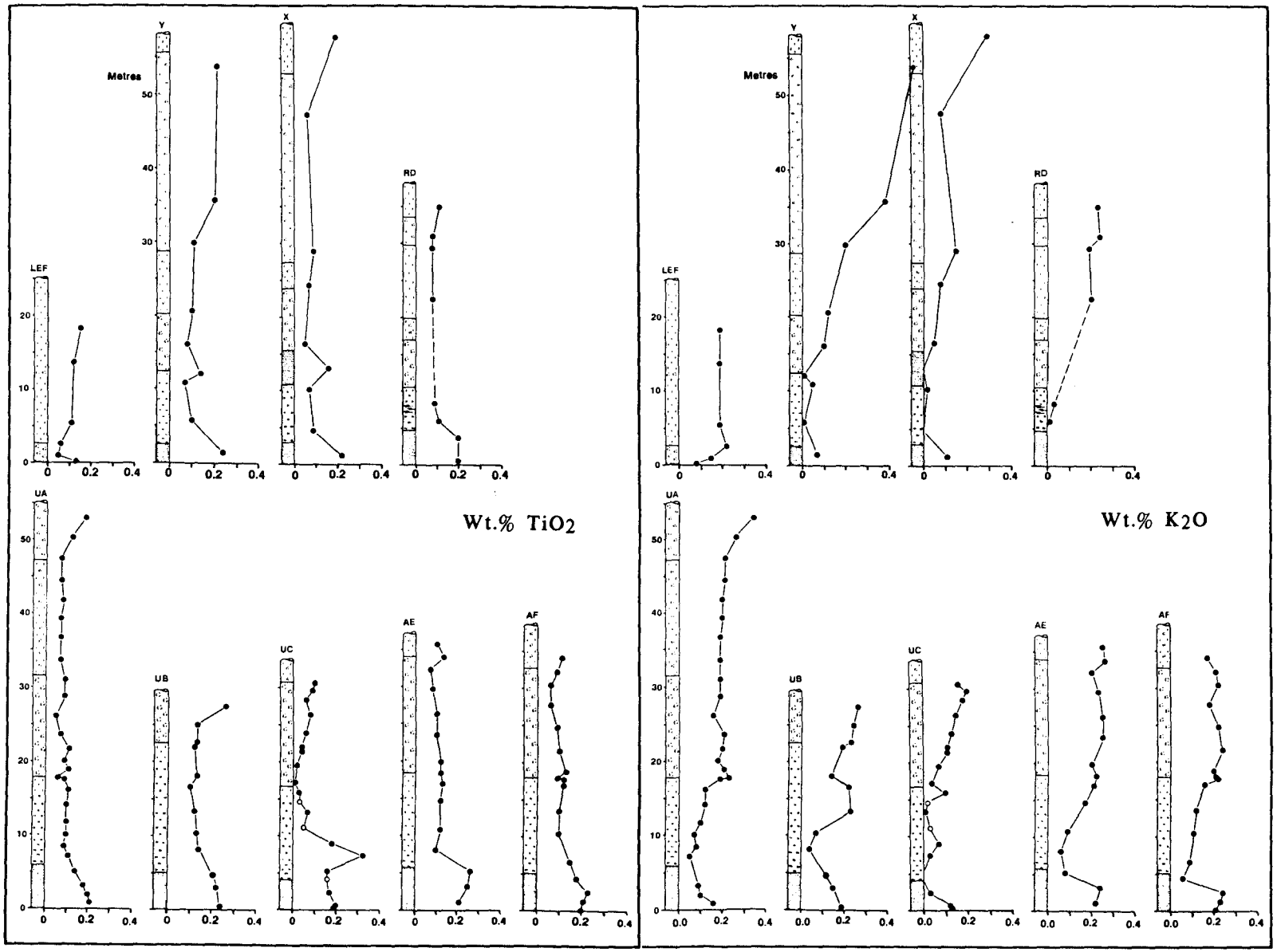

Figure 4.24 Whole-rock TiO_2 and K_2O (Wt.%) plotted against stratigraphic height for nine Bastard Unit profiles. Open circles in profile UC are olivine-bearing samples.

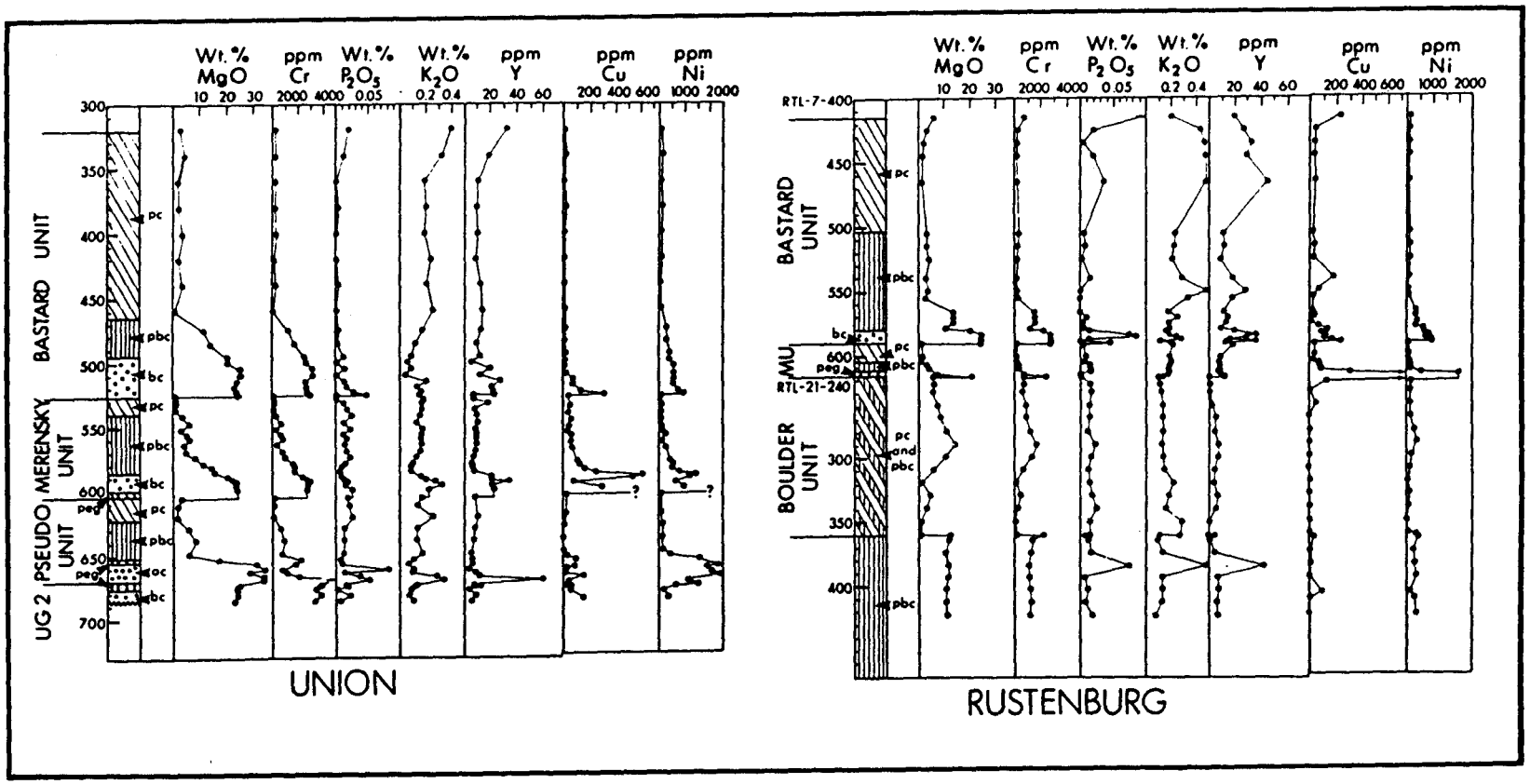

Figure 4.25 Some whole-rock major and trace element data for profiles at Union and Rustenburg Sections in the Pseudo, Boulder (Footwall), Merensky and Bastard Units. From Naldrett et al. (1984) - MgO, Cr, P_2O_5, K_2O, Y; and Naldrett et al. (1986) - Cu and Ni.

K_2O values in all profiles are generally below 0.2%, although a wide range of 0.01% to 0.5% is recorded in profile Y (Figure 4.24). The level of 0.2% is in close agreement with that reported for K_2O in plagioclase (Figure 4.17). In almost all cases the K_2O levels at the base of the Bastard pyroxenite start at 0.2% and fall off to a low of ≤0.05% at the contact with the melanorites. At this level a general trend of increasing K_2O is then recorded through the sequence to values in excess of 0.5% in the UGMA. Samples with values above 0.3% K_2O were found to have significant concentrations of intercumulus K-feldspar in thin section (see **4.7.4** - UGMA).

Linear Regression Analysis.

Because whole-rock compatible element data plotted against MgO (or Al_2O_3) in simple binary diagrams display a marked linear relationship (Figure 4.26) one is inclined to explain this relationship only in terms of the strong modal influence imparted by the dominant mineral phases. However, closer inspection of the data does provide insight into the complexity of these cumulates and the use of the more rigorous linear regression technique has been adopted. This approach is justified on the following basis:

* it attempts to derive a best estimate of the mean minor-element content of particular mineral phases;
* the method uses the data pertaining to all samples within a unit and is therefore statistically representative of that unit;
* electron microprobe analyses may yield considerable error for low-level elements;
* whole-mineral concentrates are never pure and may thus also introduce analytical errors;
* the regression approach allows comparison of the data of one profile with that of another; and
* discrepant samples "stand out" from a good regression line and can be discounted (e.g. sulphide influence in the case of Ni and Cu, or disseminated chromite in the case of Cr).

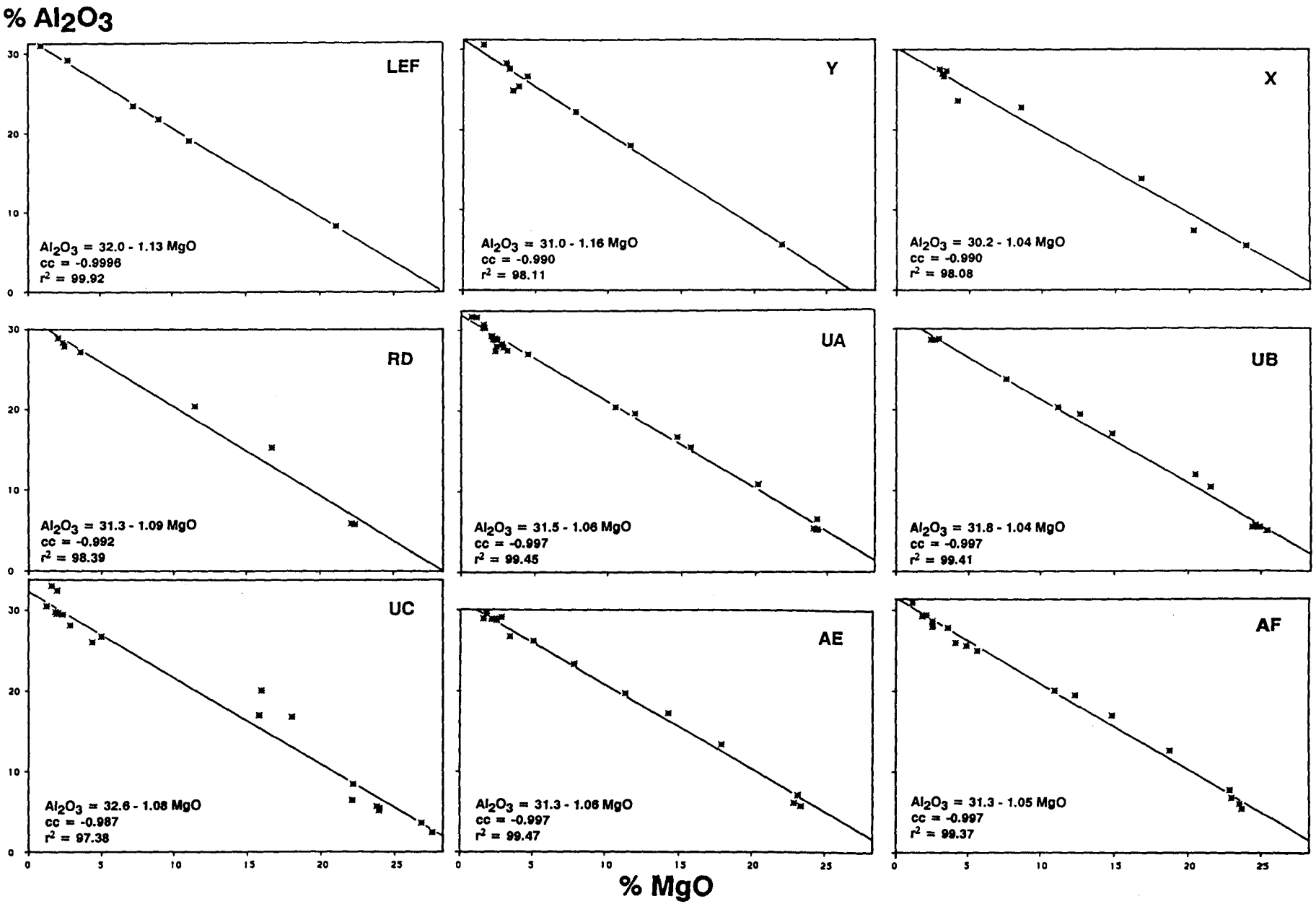

Figure 4.26 Plots of Wt.% Al_2O_3 vs MgO for nine Bastard Unit profiles. Individual regression lines are also indicated. The regression of the combined data (124 samples) yields the relationship Al_2O_3 = 31.42 - 1.05 MgO (cc. = -0.9916).

Simple linear regression analysis is designed to predict one value on the basis of another, within limits, and also to test if two bivariate samples are from the same population. The linear model has the form $y = ax + b$ and is calculated by the method of least squares.

Slope: $a = \frac{\Sigma xy - Nxy}{\Sigma x^2 - Nx^2}$ **Intercept:** $b = y - ax$

Where N = number of data pairs.

It assumes no error in X and implies that all error lies in the Y-term. When conventional regression methods are used, the slope of the regression line is directly dependent on the independent variable (X-axis). The assumption of dependent and independent variates, in the case of most geochemical data, is perhaps without foundation as both variables are invariably dependent on each other. The use of the conventional regression line does suffer from this drawback especially when low correlation coefficients are evident.

Two different regression lines could be generated for a set of two variables, depending on which is chosen as the X-axis. To overcome this problem a single line, called the **reduced major axis**, has been adopted in the analysis of both geological and biological data. This technique takes the error in both terms into account and is carried out by minimising the sum of the areas of triangles rather than minimising the sum of the squares of the deviation in the Y-axis (Miller and Kahn, 1962, p.204).

Slope: $a = \frac{\text{Std.dev. } y}{\text{Std.dev. } x}$ **Intercept:** $b = y - ax$

The results of the **reduced major axis** regression analyses were compared to those obtained for conventional simple regression and are presented in Table 4.5.

Table 4.5: Comparison between the results of simple linear regression and reduced major axis regression for selected variables in different profiles.

Profile	Simple Regression	Reduced Major Axis	cc.
LEF	Sr = 13.4 Al_2O_3 - 13.1	Sr = 13.3 Al_2O_3 - 12.6	0.9986
X	Sr = 12.8 Al_2O_3 - 10.5	Sr = 12.9 Al_2O_3 - 11.7	0.9952
RD	Sr = 19.3 Al_2O_3 - 53.5	Sr = 19.7 Al_2O_3 - 60.6	0.9952
UA	Sr = 374 - 12.5 MgO	Sr = 375 - 12.6 MgO	0.9872
X	Cr = 132 MgO - 230	Cr = 134 MgO - 230	0.9898

From this comparison it is evident that both methods yield similar results which are directly attributable to the particularly good correlation coefficients in all cases. Had there been more scatter of the data the reduced major axis regression method would have been more appropriate, but in view of the good correlations, simple linear regression analysis has been used throughout this study. It is recognised that linear regression analysis is subject to error and cognisance must be taken of the various possible sources of error if meaningful conclusions are to be drawn. Sources of error, some of which may appear to be quite obvious, need to be emphasised and include the following.

1. **Analytical error** of the trace elements under review, i.e. the dependent variable. Here the calibration working curves of the analytical runs must be as accurate as possible and the use of correct mass absorption coefficients (MAC) is of paramount importance.
2. **Analytical error** of the other element used in the regression also influences the result (independent variable - MgO or Al_2O_3). Factors here would include the count rates for major elements and the working curve. Further, the normalisation of the major elements to 100% may also introduce errors if even one element is inaccurately determined. Normalisation to 100% is also influenced by the LOI and the amount of H_2O in the rock, especially where "loss on ignition" appears to be negative (due to oxidation of Fe).
3. An **inadequate number of samples** of the various lithologies in the profiles would also introduce errors. It is generally accepted that

for a reliable regression analysis at least 12 samples are required. With this in mind, the results obtained for profiles **LEF**, **Y**, **X** and **RD** are perhaps suspect, as these profiles are based on only 6, 9, 9 and 8 whole-rock samples, respectively.

4. A good **spread of values** in the data is also desirable to prevent too much reliance being placed on a single datum point at one end of the regression line. For this reason less reliance is again placed on results of the regression in profiles **LEF** and **Y**, where only one pyroxenite sample is represented.
5. The **effect of zoning** within individual mineral phases is that an average result is obtained.
6. **Cryptic variation overprint** may introduce error. Strictly speaking, linear regression analysis assumes that no chemical variation exists in the main mineral phases throughout the suite of samples. Cryptic variation of both the main silicate mineral phases (plagioclase and orthopyroxene) has, however, been demonstrated in section **4.8**. In practice, the effects of cryptic variation on the regression analysis are minimised, because although anorthosites exhibit the most variable MMF ratios, considerable variation in MgO values will here have only a minor effect on the extrapolation to the pyroxenite field (Figure 4.27). The pyroxenites are characterised by much smaller variations in MMF ratios than leucocratic rocks.

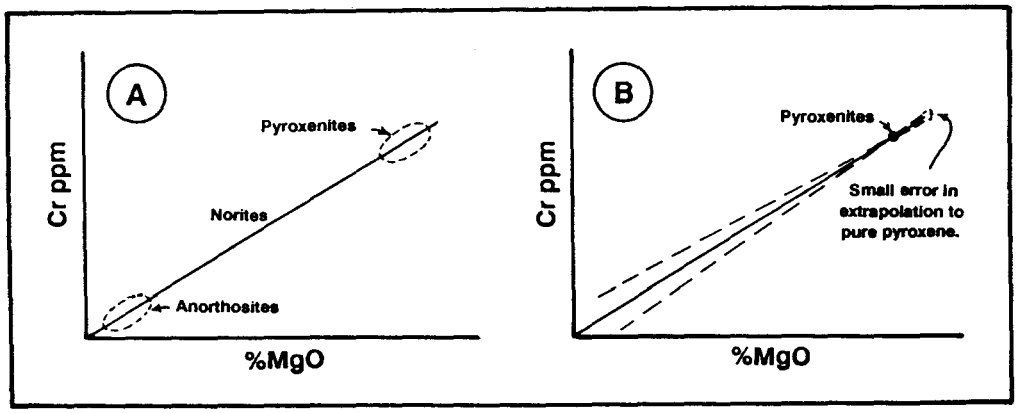

Figure 4.27 Diagram illustrating the minor effects of cryptic variation on the regression line for Cr plotted against MgO. (A) illustrates the fields in which anorthosites and pyroxenites would plot. Considerable variation in MgO in the anorthosite field (B) will have only a minor effect on the extrapolation to the pyroxenite field.

7. **Other mineral phases** in the system would also introduce error in the regression analysis approach.

   Chromite will increase the whole-rock Cr values. The occurrence of disseminated chromite within the Bastard Unit is **rare** and those samples which display anomalously higher Cr values are readily recognised by the presence of disseminated chromite in thin section and are excluded from the regression analysis. The additional Fe and Mg are considered to be trivial.

   Clinopyroxene may hold more Cr but less total MgO than orthopyroxene.

   Mica in the form of biotite holds Al, Ti and Cr in significant amounts. Those samples with an abundance of this phase (particularly some pyroxenites) should perhaps be screened out to give more emphasis to the low-mica samples. The pyroxenites in the Bastard Unit rarely have more than 5% biotite in the mode and usually less than 3%. These low amounts are considered to have very little effect on the regression line.

   Feldspars do have variable Al content but within the ranges of plagioclase compositions seen within the Bastard Unit (An_{60-80}), the variation is a maximum of 4% (30-34% Al_2O_3).

Whole-rock estimates based on the regression analysis of **LEF**, **Y**, **X** and **RD** are not as well constrained as those at Union and Amandelbult. These profiles have a lower sampling density (especially within the more mafic lithologies) and in some cases there is an imbalance in the spread of data (profile **Y**). It is also recognised that regression analysis of samples with < 5% MgO yield different linear models to that for all samples in the profile. Here a marked depletion of Co, V, Sc and Zn is noted in the intercumulus mafic minerals within anorthosites.

4.9.2 Trace element variations.

Trace element data for Sr, Rb, Y, Zr, Co, Cr, V, Zn, Cu, Ni and Sc are presented for the 9 profiles discussed above while data for the latter 7 elements are also included for an additional 2 profiles, **B** and **C**, at Amandelbult Section. These data are all presented in Tables D9 - D15. Trace element variations are plotted against stratigraphic height while Sr, Co, Cr, V, Zn, Ni and Sc have been plotted in binary diagrams against

MgO. Sr is also plotted against ΣC_{WR} for eight profiles (where ΣC_{WR} is the sum of major elements compatible in pyroxene - Fe_2O_3 + FeO + MnO + MgO). Simple linear regression analyses have been performed for these elements in individual profiles and the equations are presented with the binary diagrams.

4.9.2.1 Strontium (Sr)

The range of whole-rock Sr levels seen within the Bastard Unit is between 22ppm in **UC**-17 and 567ppm in **RD**-6 (Figure 4.28). These extremes may be somewhat anomalous as **UC**-17 is an olivine-bearing melanorite, while the whole-rock Sr values in all samples at **RD** appear to be higher than at other localities. This may in part be due to an alteration overprint. A more common range of Sr in all other profiles is from 60ppm in the pyroxenites to 400ppm in anorthosites.

As was shown in **3.4**, whole-rock Sr values have been effectively used to define the cyclic units of the Upper Critical Zone. Both Naldrett et al. (1984) and Eales et al. (1986, 1988) included a lateral dimension in their syntheses of the Bastard Unit by incorporating data from different parts of the Complex. Naldrett et al. (1984) plotted whole-rock Sr against MgO (16 samples at Union and 15 at Rustenburg), while Eales et al. (1988) plotted the $Sr/Al_2O_3^*$ ratio against stratigraphic height at both Union and Amandelbult Sections, and included the Sr/Al_2O_3 ratios of plagioclase separates from Rustenburg analysed by Kruger (1982). Both these studies indicated that comparable Sr concentrations were evident in the Bastard Unit at these widely spaced localities. Only small differences are seen in the $Sr/Al_2O_3^*$ ratio between Union and Amandelbult for both the Bastard and Merensky Units. The mid-value of the envelopes bracketing the data for individual units was compared (Eales et al. 1988, p.72). This minor difference is within error and no real lateral variation in the Sr content of the feldspars in these rocks can be inferred.

An estimate of the amount of Sr in cumulus plagioclase is derived from the Y-intercept of the projected regression line in Figures 4.29 and 4.30. By inspection it is noted that in both figures this Y-intercept in

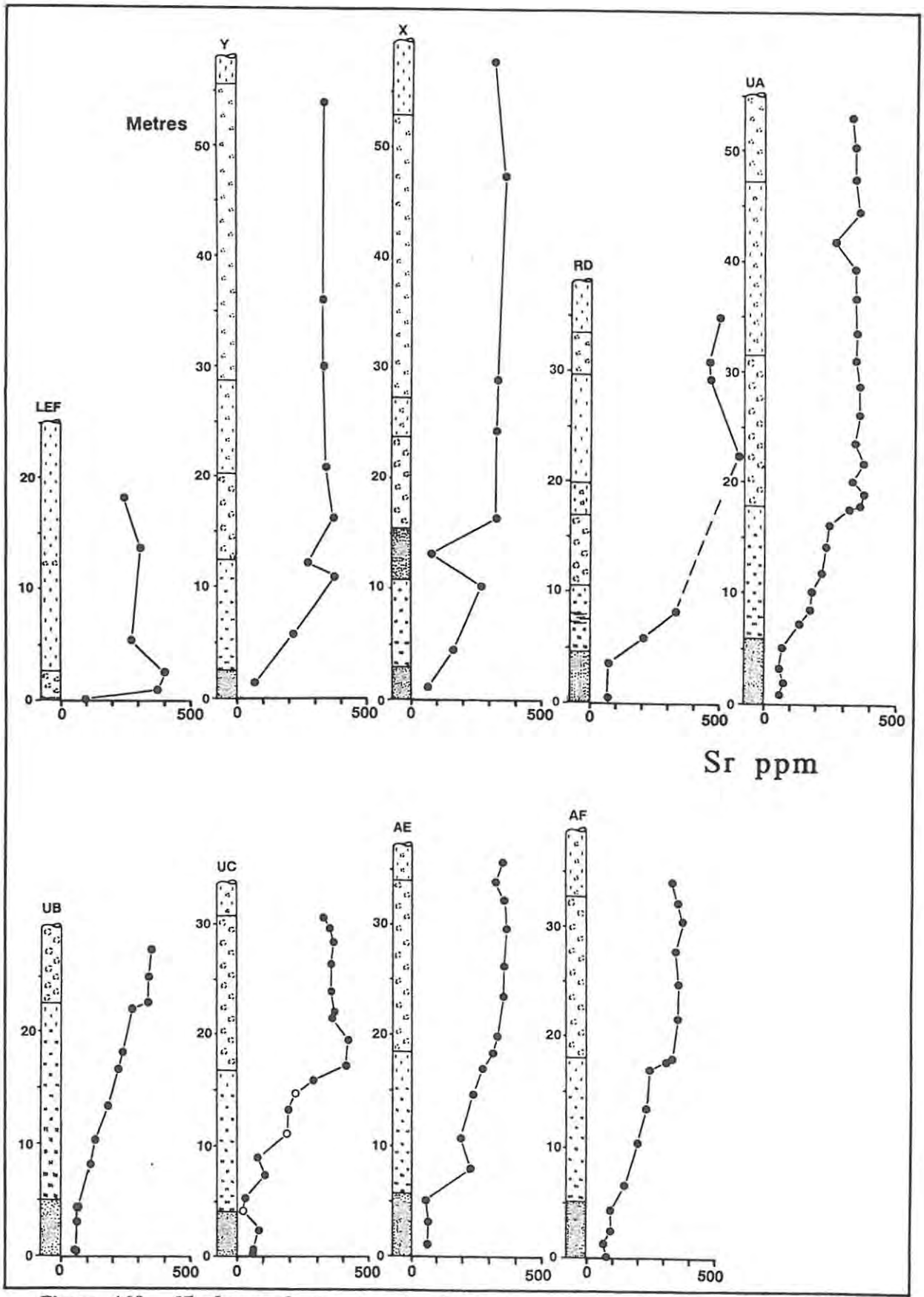

Figure 4.28 Whole-rock Sr (ppm) plotted against stratigraphic height for nine Bastard Unit profiles. Open circles in profile UC indicate olivine-bearing samples.

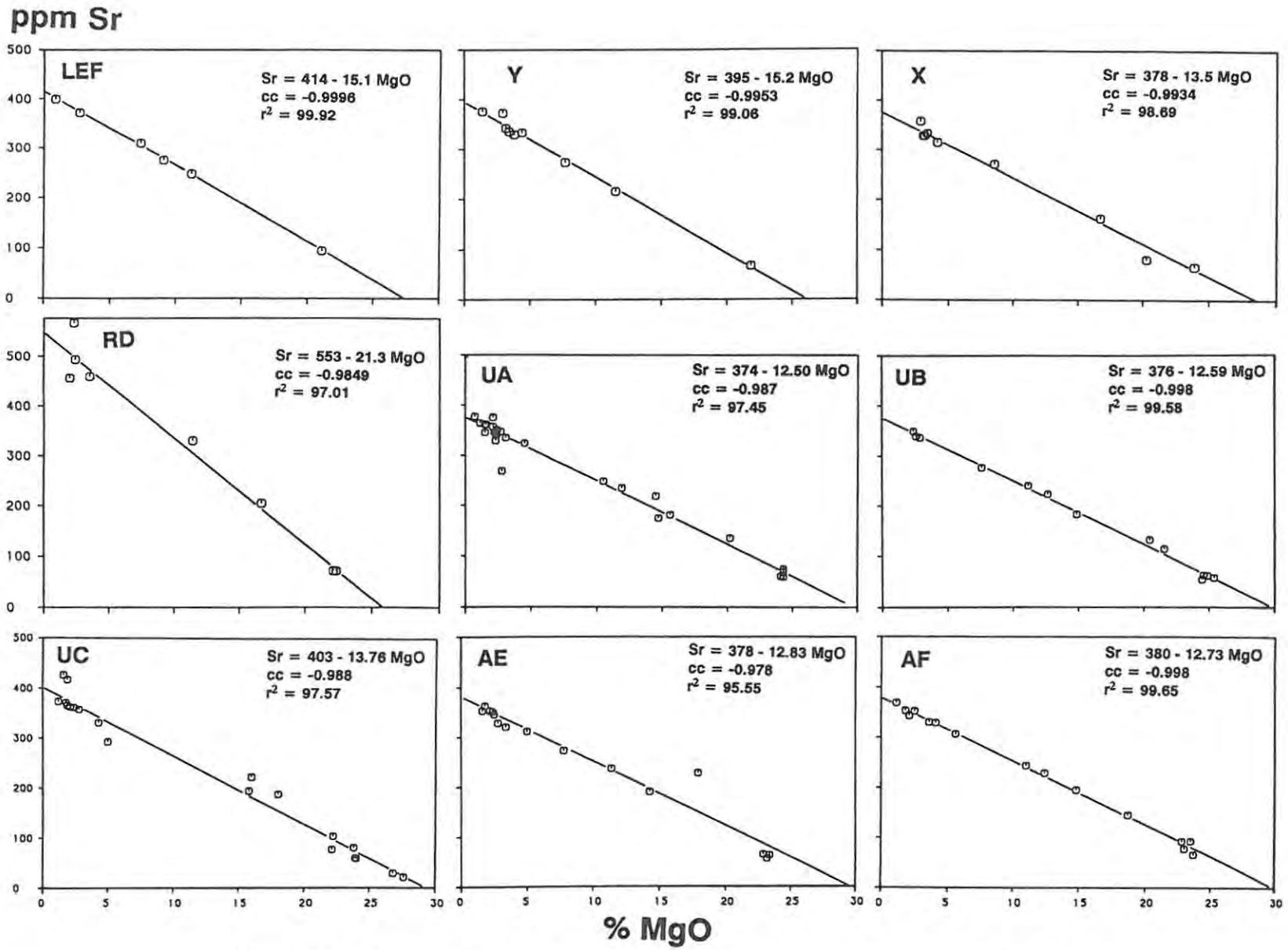

Figure 4.29 Plot of Sr vs Wt.% MgO for nine Bastard Unit profiles, with linear regression data.

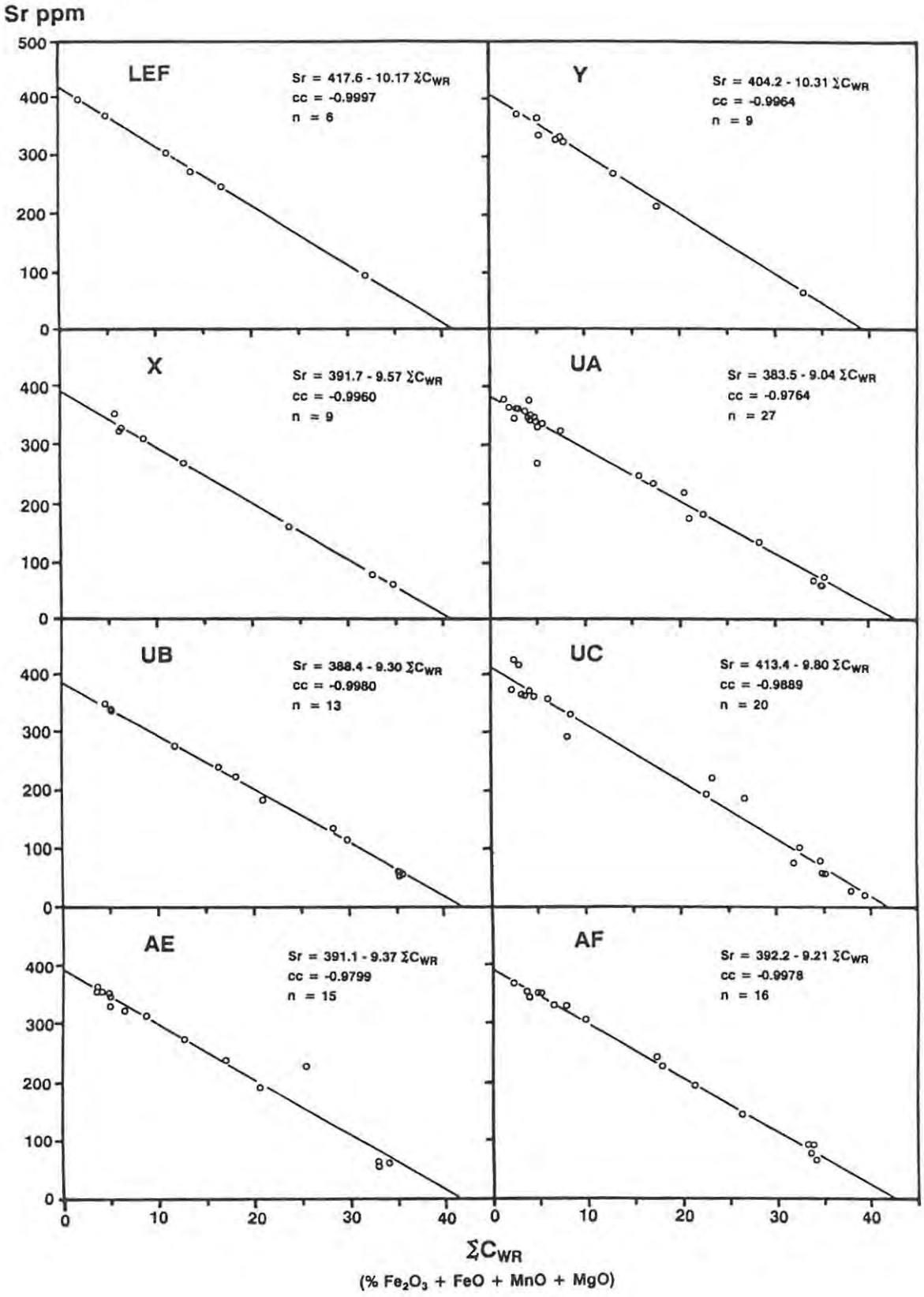

Figure 4.30 Plot of Sr vs Wt.% ΣC_{WR} for eight Bastard Unit profiles, with linear regression data (ΣC_{WR} = Fe_2O_3 + FeO + MnO + MgO).

eight profiles is close to 400ppm while that for **RD** is aberrant, in excess of 550ppm. Furthermore, the slopes of the regression lines are somewhat greater for the four profiles south of Union Section (**LEF**, **X**, **Y** and **RD**) with the X-intercept at Sr=0 occurring below 28% MgO and 41% ΣC_{WR} respectively in these cases. At Union and Amandelbult Sections this intercept is at c. 30% MgO and c. 42% ΣC_{WR}.

The estimated Sr levels in plagioclase in the eight profiles based on the Sr vs ΣC_{WR} regression, as well as the mineral separate data at **RPM** (Kruger and Marsh, 1985), are plotted against strike distance from **LEF** in Figure 4.31. The Sr content of plagioclase at **RD** is anomalously high (562ppm) and this is tentatively attributed to the introduction of Sr during alteration of the layered sequence at the time of intrusion of the Pilanesberg Complex. The indicated level of 418ppm at **LEF** may not be representative as the upper three samples at this locality are considered to be within the Main Zone. If one excludes the results obtained at **RD** and **LEF** then the maximum and minimum limits calculated for Sr in plagioclase occur at Union Section. A difference of 29ppm is seen between

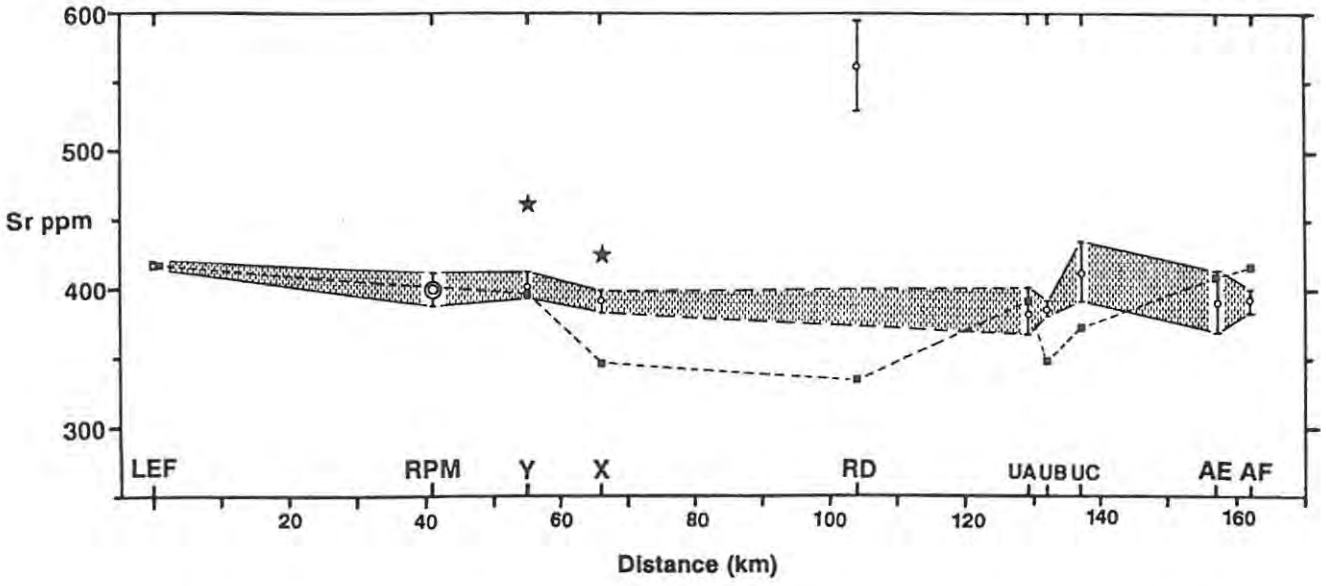

Figure 4.31 Strontium levels for individual profiles indicated by the linear regression models. Open circles represent the Sr contents of plagioclase at ΣC_{WR} = 0, with the bar indicating the standard error of estimate. Double circle at **RPM** denotes the average Sr level in plagioclase separates within the Bastard Unit, with the bar indicating the range of composition at this locality (Kruger, 1982). Calculated levels of Sr in intercumulus plagioclase at 34.9% ΣC_{WR} are indicated by solid circles. Star symbols at **Y** and **X** are the analysed Sr contents of intercumulus plagioclase (see text for details).

UC (413ppm) and **UA** (384ppm). Values in all other profiles, including the average mineral separate data at **RPM**, fall within this narrow envelope. This observation would suggest that no significant difference of Sr content in cumulus plagioclase is apparent along 170km of strike in the Bastard Unit of the western Bushveld Complex.

Intercumulus feldspar

By utilising the regression data, and applying appropriate corrections, an attempt has been made to estimate the Sr content of the intercumulus plagioclase of the Bastard pyroxenites. The approach is best explained if one considers the simple linear regression of Sr vs ΣC_{WR} in profile **UA** (Figure 4.30):

Regression model for **UA**: $Sr = 383.5 - 9.04\ \Sigma C_{WR}$ (cc.-0.9764)

Here the Y-intercept, at $\Sigma C_{WR} = 0$, is at 384ppm Sr while at $Sr = 0$ the X-intercept indicates a value of 42.4% ΣC_{WR}, a value which compares favourably with the average microprobe orthopyroxene ΣC_{opx} content of 41.83% (Table 4.7). If this regression line represents a simple modal mixing line, then it implies that the Sr content of the intercumulus plagioclase is similar to that indicated for cumulus plagioclase. To check this assumption, the following mass balance calculation is presented:

(1) The upper limit of whole-rock Al_2O_3 in feldspathic pyroxenites is taken at 6.5% (Figure 1.5). This value would relate to 23.67% MgO according to the regression relationship between Al_2O_3 and MgO defined for all Bastard Unit samples (Figure 4.26). Therefore, a rock with 24% MgO would be classified as a feldspathic pyroxenite where plagioclase occurs as an intercumulus phase.

(2) Marginally different linear regression models were obtained for the individual profiles where Al_2O_3 is plotted against ΣC_{WR} (Table 4.6).

(3) An average ΣC_{WR} value of 34.9% was obtained for 15 Bastard Unit pyroxenite samples and ΣC_{WR} is made up of the following components:

Fe_2O_3	=	0.97%
FeO	=	9.72%
MnO	=	0.21%
MgO	=	23.99%
ΣC_{WR}	=	34.89%

This value of 34.9% is representative of an average (ideal) Bastard pyroxenite and has been adopted for the purpose of this calculation.

(4) Utilising the linear regression models for Al_2O_3 vs ΣC_{WR} the whole-rock Al_2O_3 content for each profile is determined at ΣC_{WR} = 34.9%. In the case of **UA** this value is 5.75% (Table 4.6).

Table 4.6: Results of simple linear regression analyses for Al_2O_3 plotted against ΣC_{WR} in individual profiles. The Al_2O_3 level at 34.9% ΣC_{WR} is also indicated.

Profile	Linear regression model	Corr. Coef.	Std. error of est.	No. samples n	Indicated Al_2O_3 at ΣC_{WR} = 34.9%
LEF	$Al_2O_3 = 32.46 - 0.767\ \Sigma C_{WR}$	-0.9989	0.42	6	5.69
Y	$Al_2O_3 = 32.16 - 0.800\ \Sigma C_{WR}$	-0.9968	0.64	9	4.24
X	$Al_2O_3 = 31.59 - 0.747\ \Sigma C_{WR}$	-0.9973	0.70	9	5.54
RD	$Al_2O_3 = 32.14 - 0.754\ \Sigma C_{WR}$	-0.9982	0.64	8	5.83
UA	$Al_2O_3 = 32.34 - 0.762\ \Sigma C_{WR}$	-0.9989	0.44	27	5.75
UB	$Al_2O_3 = 32.80 - 0.767\ \Sigma C_{WR}$	-0.9989	0.46	13	6.04
UC	$Al_2O_3 = 33.42 - 0.770\ \Sigma C_{WR}$	-0.9882	1.80	20	6.53
AE	$Al_2O_3 = 32.40 - 0.769\ \Sigma C_{WR}$	-0.9982	0.57	15	5.55
AF	$Al_2O_3 = 32.44 - 0.759\ \Sigma C_{WR}$	-0.9983	0.56	17	5.95
Regression analysis on all 124 Bastard Unit samples yielded					
	$Al_2O_3 = 32.41 - 0.759\ \Sigma C_{WR}$	-0.9950	0.94	124	

The major part of the 5.75% Al_2O_3 in the **UA** pyroxenite is contained within the intercumulus feldspar, while the remainder would be held mainly within the pyroxenes and to a very small degree in the micas (biotite). A close approximation of the amount of Al_2O_3 held within plagioclase can be made by correcting for the alumina content of orthopyroxene:

$$Al_2O_3 \text{ assigned to plag} = Al_2O_3 \text{ whole-rock} - \frac{(\Sigma C \text{ whole-rock} \times Al_2O_3 \text{ opx (probe)})}{\Sigma C \text{ opx (probe)}}$$

$$= 5.75 - \frac{(34.9 \times 1.19)}{41.83}$$

$$= 4.76\% \; Al_2O_3 \text{ plag}$$
in whole-rock (ideal) pyroxenite.

From Figure 4.32 it is noted that orthopyroxenes with higher Fe levels would yield significantly higher ΣC_{opx} values. The restricted range of MMF ratios recorded for the orthopyroxenes in the basal Bastard pyroxenites implies that a further correction would be superfluous.

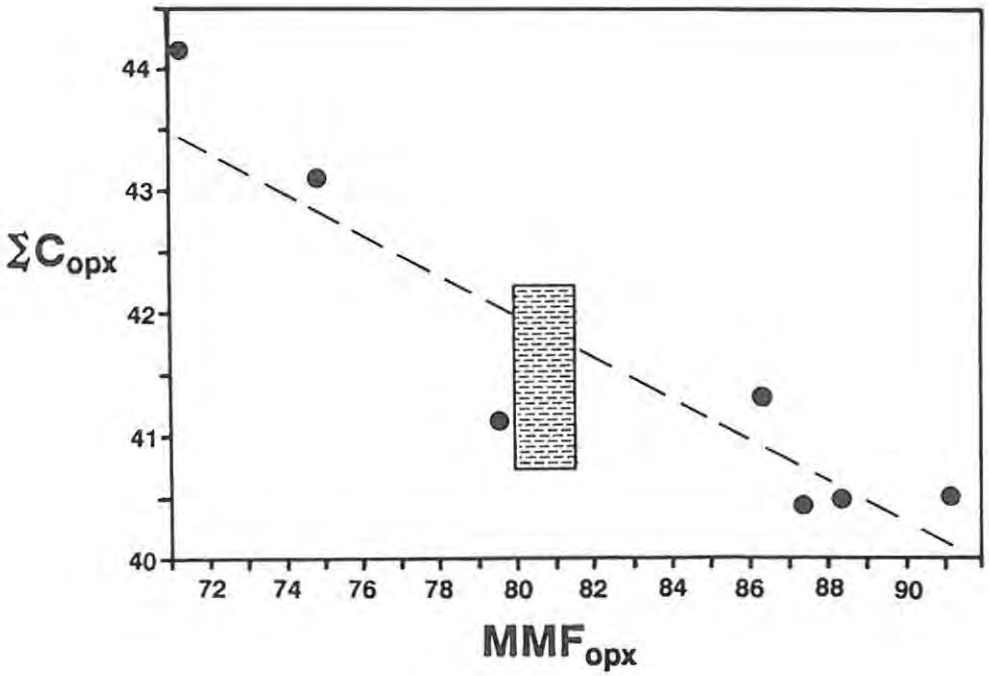

Figure 4.32 Plot of ΣC_{opx} against MMF_{opx} from data of Deer et al. (1967). The full range of orthopyroxene compositions in the Bastard pyroxenites fall within the shaded box.

(5) An approximation of the amount of plagioclase in this ideal pyroxenite is required, i.e. the wt% of plagioclase in the rock. Microprobe data of intercumulus plagioclase cores yielded an average value of 29.2% Al_2O_3 in **UA-27** (Table 4.7). The effect of normal zoning of plagioclase at grain boundaries would be to yield an average intercumulus feldspar composition some 10% lower in **An** molecule (i.e. 1.7% lower in Al_2O_3) than in crystal cores.

The average amount of intercumulus plagioclase in the rock is therefore:

$$\text{Modal \% plag in rock} = \frac{Al_2O_3 \text{ held in plag}}{\text{Average } Al_2O_3 \text{ content of plag}} \times 100$$

$$= \frac{4.76}{29.2 - 1.7} \times 100$$

$$= 17.31\%$$

(6) From the linear regression models of Sr vs ΣC_{WR} a whole-rock Sr value is derived where ΣC_{WR} = 34.9%. In the case of **UA** the whole-rock Sr content is 68ppm at 34.9% ΣC_{WR} (Figure 4.30).
Therefore Sr in intercumulus plagioclase is

$$Sr_{\text{ in intercumulus plagioclase}} = \frac{Sr \text{ whole-rock at } 34.9\%\Sigma C}{\text{Modal \% plag in rock}} \times 100$$

$$= \frac{68}{17.31} \times 100$$

$$= 393 \text{ ppm.}$$

This agrees remarkably well with the estimate of 384ppm Sr yielded by direct extrapolation of the regression line to the Y-intercept. By utilising the appropriate electron microprobe data for the necessary corrections (Table 4.7), similar calculations were made for all profiles and the results are tabulated below (Table 4.8).

Table 4.7: Whole-rock Sr values and selected microprobe data for orthopyroxene and plagioclase in Bastard pyroxenite samples.

	SAMPLE	Whole-rock Sr at ΣC_{WR} = 34.9%	Average $\%Al_2O_3$ in opx	Average ΣC_{opx}	Average $\%Al_2O_3$ in plag	Al_2O_3 correction for zoning
LEF	H998.1/T	62.8	1.38	40.94	31.58	1.58
RPM	B-2	-	1.39	41.46	-	
Y	Y775	44.2	1.00	41.95	32.26	1.66
X	X791.8	57.7	0.94	42.24	30.32	1.67
UA	UA-27	68.0	1.19	41.83	29.20	1.70
UB		64.0	No mineral analyses - assume same as **UA**.			
UC	UC-20	71.5	1.18	40.74	30.44	1.68
AE	AE-15	64.1	1.16	41.01	30.79	1.69
AF		70.9	No mineral analyses - assume same as **AE**.			

Table 4.8: Indicated Sr content of cumulus plagioclase at ΣC_{WR} = 0 from individual Bastard Unit profiles (numbers in brackets are the estimates from the Sr vs MgO regression analyses). These values are compared with the estimated Sr levels of intercumulus plagioclase. The X-intercept values (ΣC_{WR} at Sr = 0) are also shown.

	Sr ppm in cumulus plagioclase (ΣC_{WR} = 0)	Corr. Coef.	Std. error of est.	X or ΣC_{WR} intercept (Sr = 0)	Est. of Sr in intercumulus plagioclase at 34.9% ΣC_{WR}	%Diff. between cumulus & intercumulus plagioclase
LEF	418 (414)	-0.9997	2.7	41.1	417	0.1
Y	404 (395)	-0.9964	10.3	39.2	397	1.8
X	392 (378)	-0.9980	7.7	40.9	347	11.4
UA	384 (374)	-0.9881	17.2	42.4	393	-2.5
UB	388 (376)	-0.9990	5.3	41.8	349	10.3
UC	413 (403)	-0.9889	22.2	42.2	373	9.9
AE	391 (378)	-0.9799	23.4	41.8	409	-4.5
AF	392 (380)	-0.9978	7.9	42.6	416	-6.1
Average and standard deviation.	398 ±11.6				388 ±26.5	

(7) Within errors and approximations inherent to the method of calculation it is concluded that the Sr content of pure anorthosite (idealised) is the same as the Sr levels within intercumulus plagioclase (Figure 4.31 and Table 4.8). Similar calculations, using different abscissae like MgO, atomic proportions of ΣC_{WR}, and ΣC_{WR} where total Fe is expressed as Fe_2O_3 were made. Although similar results were obtained it is considered that the most reliable result is that outlined above.

Four intercumulus plagioclase mineral separates from the Bastard Unit were analysed by Kruger (1982) at **RPM** (B1 - B4) and yielded values of 385, 442, 414 and 481ppm, respectively. These values are similar to those calculated for individual Bastard Unit profiles .

An additional observation drawn from Table 4.8 is that the X-intercept (at Sr = 0) for all the profiles at Union and Amandelbult Sections is c. 42% ΣC_{WR} while in those profiles to the south of Union Section (**RD**, **X**, and **Y**) lower values of c. 40% ΣC_{WR} prevail before rising to 41% ΣC_{WR} at **LEF**. No systematic pattern is, however, seen for the microprobe ΣC_{opx} values of average Bastard pyroxenites (Table 4.7). A factor that could perhaps explain the decrease the ΣC_{WR} regression intercept could be a <u>real</u> reduction in the Sr content of the intercumulus plagioclase, relative to the cumulus phase. An attempt was made to establish whether in fact a reduced Sr content occurs in the intercumulus plagioclase at **Y** and **X**. Plagioclase mineral separates from the pyroxenite samples **Y**775.0 and **X**791,8 were prepared and analysed; the results are tabulated below (see also Appendix D).

Sample	ppm Sr at ΣC_{WR}=34.9%	Calc. Sr in intercumulus plag at ΣC_{WR}=34.9%	Sr in plag. separate
Y775.0	44.2	397	464
X791,8	57.7	347	425

In both cases the directly measured concentrations (Figure 4.31) are above calculated values. It must be emphasised, however, that only a

small (< 2.5gm) and very finely crushed (63-180 micron) sample was available and that the method of crushing, washing and magnetic separation may have concentrated sodic plagioclase, relative to calcic plagioclase in the concentrate.

In summary, the Sr content of the plagioclase in the Unit appears to be the same in both intercumulus and cumulus varieties and, apart from the **RD** profile, there is no marked change in Sr concentration in the Bastard Unit plagioclase feldspar throughout the Western Bushveld Complex.

4.9.2.2 Chromium (Cr)

Whole-rock Cr values in the Bastard Unit reflect the concentration within the mafic silicate phases. Chromite occurs only as a thin selvage at the basal contact of the Unit and occasionally as rare disseminated grains in the basal 10cm of the pyroxenite. The range of Cr values is 20 - 3806ppm (**UA**-14, **UC**-16) (Figure 4.33). Simple regression analyses of the data resulted in a negative Y-intercept of the regression line in all profiles when plotted against MgO (Figure 4.34). The reason for this is that Cr levels in the intercumulus ferromagnesian minerals of the mottled anorthosites are lower than those of the pyroxenites and norites. This feature indicates that the intercumulus pyroxene crystallised from a fractionated and Cr-depleted interstitial liquid.

Where sufficient samples were available, separate regression analyses were done for those rocks with less than 4% MgO (profiles **UA**, **UC**, **AE** and **AF** in Figure 4.34, insets). Clearly these four sub-set regression lines are quite different from the regression lines of the full datasets. The Y-intercept in these four cases is now closer to the origin and has reduced slopes (Table 4.9).

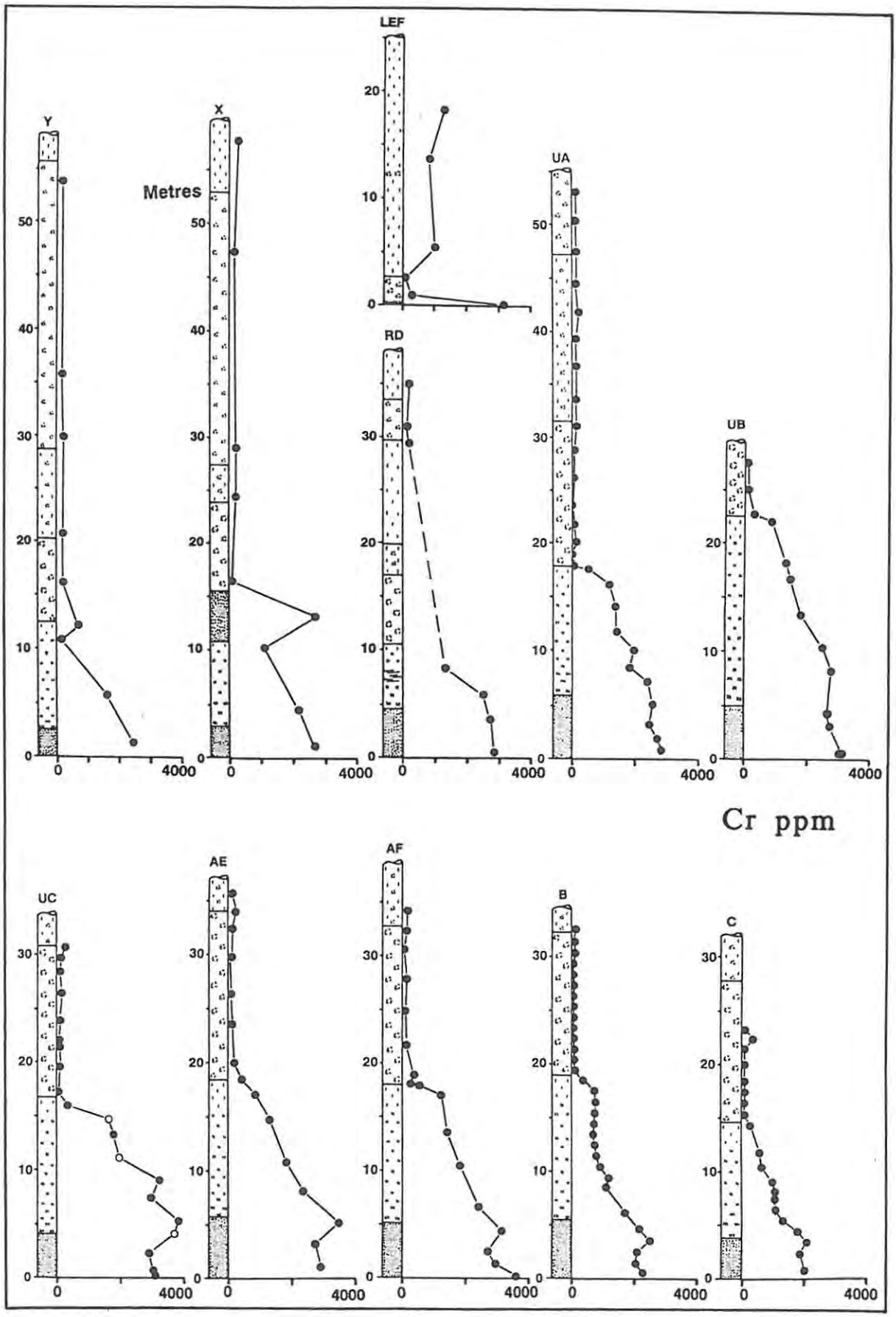

Figure 4.33 Whole-rock Cr (ppm) plotted against stratigraphic height for nine Bastard Unit profiles. Open circles in profile UC indicate olivine-bearing samples.

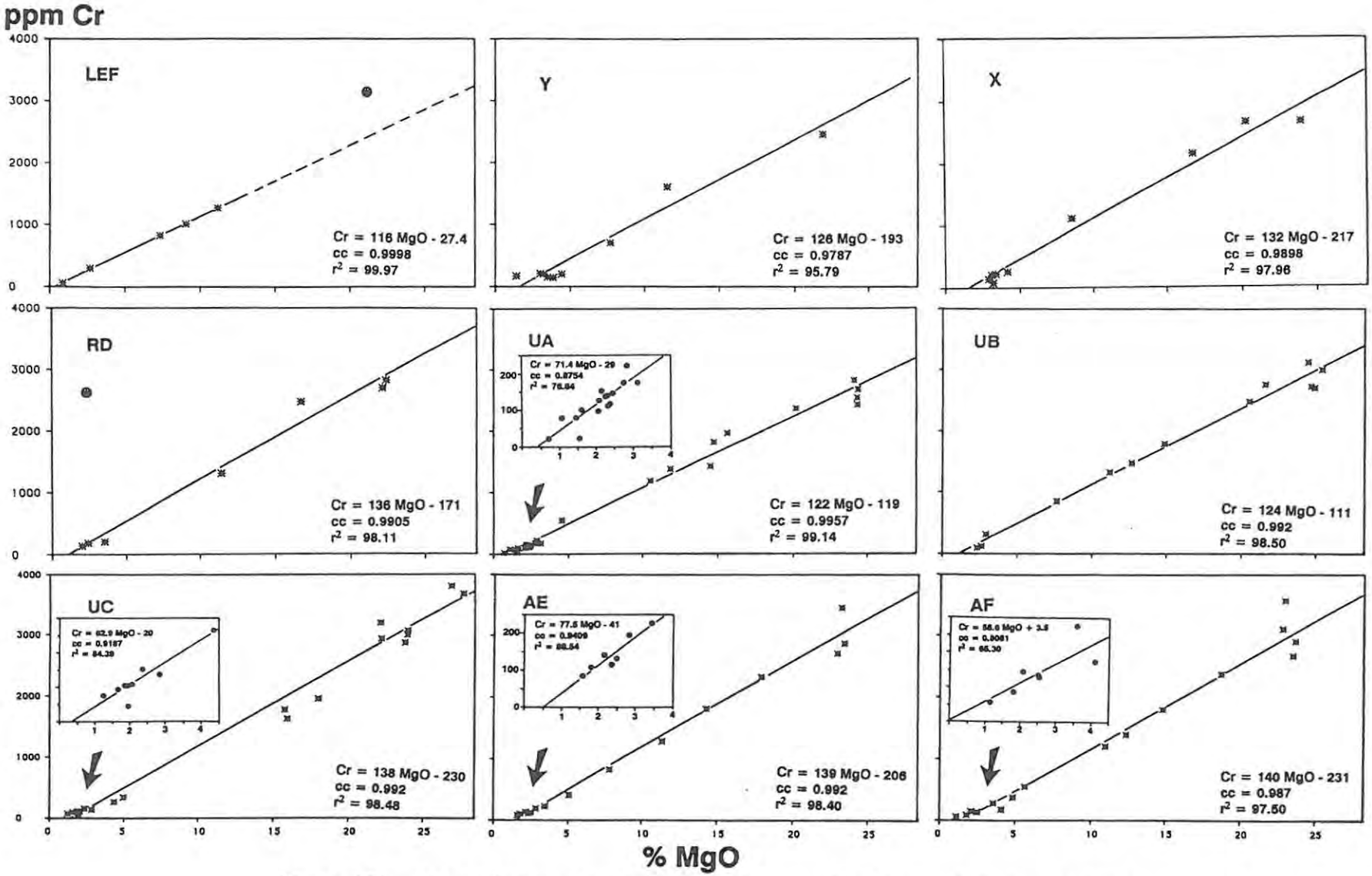

Figure 4.34 Plot of ppm Cr vs Wt.% MgO for nine Bastard Unit profiles, with linear regression data. Circled data points at **LEF** and **RD** were excluded from regression analysis.

Table 4.9: Comparison of linear regression models of samples with less than 4% MgO and those employing all data.

	All Data Linear model	cc.	**Data < 4% MgO** Linear model	cc.
LEF	Cr = 116 MgO -27.4	0.9998		
Y	Cr = 126 MgO - 193	0.9787		
X	Cr = 132 MgO - 217	0.9898		
RD	Cr = 136 MgO - 171	0.9905		
UA	Cr = 122 MgO - 119	0.9957	Cr = 71 MgO - 29	0.8754
UB	Cr = 124 MgO - 111	0.9925		
UC	Cr = 138 MgO - 230	0.9924	Cr = 63 MgO - 20	0.9187
AE	Cr = 139 MgO - 206	0.9920	Cr = 77 MgO - 41	0.9409
AF	Cr = 140 MgO - 231	0.9874	Cr = 56 MgO + 3.5	0.8081

By employing regression analysis, and applying the appropriate corrections, an attempt has been to made to estimate the average bulk Cr concentration of the Mg-bearing phases in the Bastard pyroxenite. Two avenues of approach have been adopted in establishing this estimate. First, the whole-rock Cr - ΣC_{WR} relationship was used and then that of Cr - Al_2O_3.

An indication of the average level of Al_2O_3 in pyroxene is given in Figure 4.35 where whole-rock Al_2O_3 is plotted against Sr for all Bastard Unit samples excluding those in **RD**.

$$\%Al_2O_3 = 0.08 \text{ ppm Sr} + 0.83 \text{ (cc. = 0.9920, n = 115 samples)}$$

Assuming that all Sr is contained within plagioclase the Al_2O_3 content at Sr = 0 would ideally be the residual levels contained within pyroxene. This is not quite the case as a value of 2ppm Sr is indicated within the orthopyroxenes of the Bastard pyroxenite (Kruger, 1982). If this is the case then a value of 0.99% Al_2O_3 is indicated for the Bastard pyroxenites (at Sr = 2ppm). This value is in close agreement with the microprobe values shown in Figure 4.11 and the average values (0.94-1.39%) reported in Table 4.7.

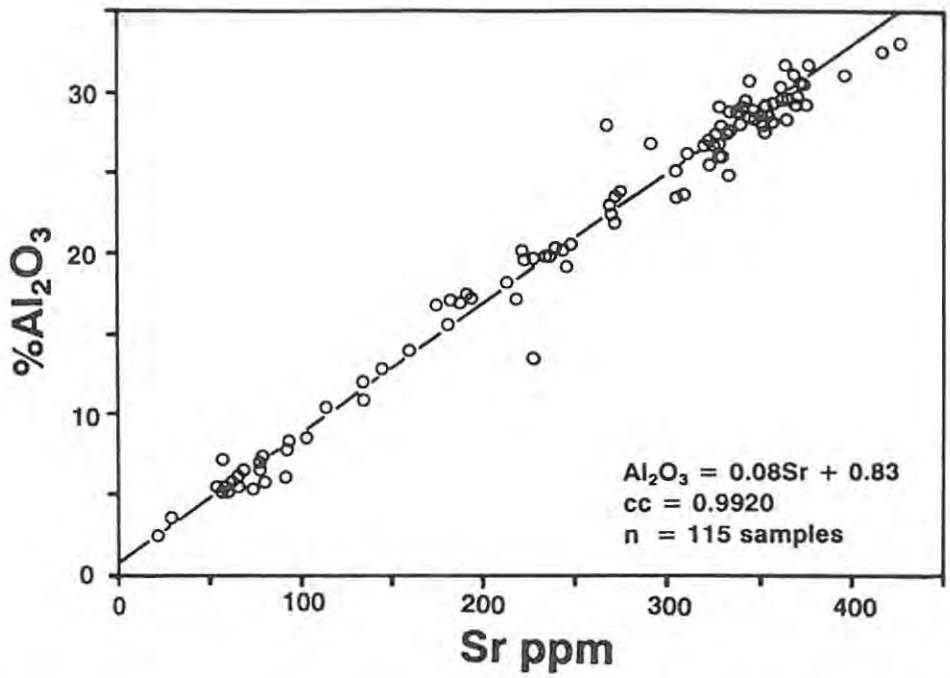

Figure 4.35 Scatter plot of whole-rock Al_2O_3 vs Sr for all Bastard Unit samples except those in profile **RD**. The positive Y-intercept at 0.83% Al_2O_3 is indicative of the alumina contained within orthopyroxenes. Kruger (1982) reported a Sr level of 2ppm in the orthopyroxene fraction of the Bastard pyroxenite at **RPM** and this would suggest that a value of 0.99% Al_2O_3 is contained within orthopyroxene.

If one adopts an average value of 0.99% Al_2O_3 and 41.5% ΣC_{opx} as being representative of the concentrations in orthopyroxene in the Bastard pyroxenite at all localities, then the following estimates can be made:

Consider profile **UA**

a) The linear model for Cr vs ΣC_{WR} at this locality is (Table 4.10)

$$Cr = 83.6\ \Sigma C_{WR} - 184 \quad (cc.\ 0.9923)$$

The Cr concentration at 41.5% ΣC_{WR} would be 3287ppm (std. error of estimate = 127ppm).

b) The regression of Cr - Al_2O_3 in profile **UA** yielded the linear model

$$Cr = 3353 - 109.2\ Al_2O_3 \quad (cc.\ -0.9881).$$

At 0.99% Al_2O_3 the estimated Cr concentration is 3245ppm (std. error of estimate = 159ppm). This value is marginally lower than the estimate at 41.5% ΣC_{WR} (i.e. 3287ppm) but still within error.

The same procedure was adopted for all other profiles and the results are shown in Table 4.11 and Figure 4.36.

Table 4.10: Linear regression models for Cr - ΣC_{WR} and Cr - Al_2O_3.

	Linear model	cc.	Std.error of est.	Linear model	cc.	Std.error of est.
LEF	$Cr = 80.9\Sigma C_{WR} - 97.7$	0.9999	7.2	$Cr = 3163 - 99.2\ Al_2O_3$	-0.9982	24
Y	$Cr = 85.7\Sigma C_{WR} - 304$	0.9694	218	$Cr = 3102 - 105.4\ Al_2O_3$	-0.9569	258
X	$Cr = 93.7\Sigma C_{WR} - 382$	0.9874	191	$Cr = 3550 - 123.8\ Al_2O_3$	-0.9769	258
RD	$Cr = 92.6\Sigma C_{WR} - 252$	0.9798	273	$Cr = 3658 - 120.4\ Al_2O_3$	-0.9690	338
UA	$Cr = 83.6\Sigma C_{WR} - 184$	0.9923	127	$Cr = 3353 - 109.2\ Al_2O_3$	-0.9881	159
UB	$Cr = 91.3\Sigma C_{WR} - 225$	0.9904	164	$Cr = 3670 - 118.4\ Al_2O_3$	-0.9858	200
UC	$Cr = 98.1\Sigma C_{WR} - 326$	0.9897	214	$Cr = 3900 - 125.8\ Al_2O_3$	-0.9896	215
AE	$Cr = 101\ \Sigma C_{WR} - 340$	0.9896	180	$Cr = 3898 - 130.5\ Al_2O_3$	-0.9858	210
AF	$Cr = 101\ \Sigma C_{WR} - 375$	0.9866	211	$Cr = 3941 - 132.7\ Al_2O_3$	-0.9823	243

Table 4.11: Estimation of Cr concentrations in the Mg-bearing phases of the Bastard Unit, utilising the regression analyses on the whole-rock Cr - ΣC_{WR} and Cr - Al_2O_3 relationships. The results in parentheses are those calculated from the Cr - MgO relationship at 29% MgO.

PROFILE	Cr at 41.5% (29%) ΣC_{WR} (MgO)	Std.error of est.	Cr at 0.99% Al_2O_3	Std.error of est.	% Diff.	Probe Sample	Avg. Cr in orthopyroxene (microprobe) ppm Cr	Cr_2O_3%
LEF*	3260 (3334)	7 (11)	3065	24	6.0		3079	0.45
Y	3254 (3461)	218 (182)	2998	258	7.9	Y775	2053	0.30
X	3507 (3620)	191 (172)	3427	258	2.3	X791.8	1984	0.29
RD	3592 (3773)	273 (188)	3539	338	1.5	RD-19	2942	0.43
UA	3287 (3407)	127 (88)	3245	159	1.3	UA-27	2600	0.38
UB	3565 (3485)	164 (145)	3553	200	0.3	-	-	-
UC	3745 (3772)	214 (184)	3775	215	-0.8	UC-20	2874	0.42
AE	3851 (3825)	180 (158)	3769	210	2.1	AE-15	1711	0.25
AF	3833 (3829)	211 (205)	3810	243	0.6	-	-	-

* Note that both regression analyses for **LEF** were done on only 5 samples with ΣC_{WR} values below 17% (12% MgO) and Al_2O_3 values between 15-32%. Projections to 41.5% ΣC_{WR} and 1.2% Al_2O_3 must in this case be somewhat suspect.

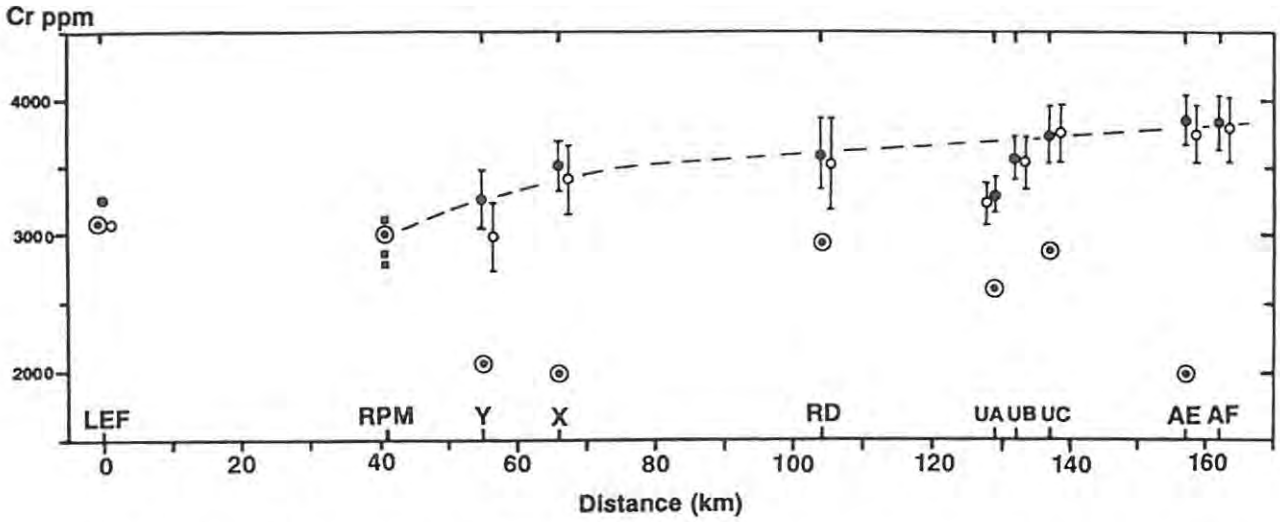

Figure 4.36 Estimations of Cr levels in orthopyroxene for individual profiles indicated by the regression data. Whole-rock Cr estimates at 41.5% ΣC_{WR} are indicated by solid circles while the Cr estimates at 0.99% Al_2O_3 are shown by open circles (bars represent the standard error of estimate). Mineral separate data for three samples from the basal 4m of the Unit at **RPM** are shown by solid squares (Kruger, 1982). Average microprobe Cr values for orthopyroxenes in the Bastard pyroxenites are shown by a circled dot.

Good agreement is evident between the two estimates in individual profiles apart from those at **LEF** and **Y** where the regression lines are not as well constrained. Average Cr values for orthopyroxene obtained by microprobe analysis (Table 4.11) are in all cases lower than the whole-rock estimates. These microprobe Cr values are for orthopyroxene only and other Cr bearing phases could be contributing to the higher whole-rock estimates. It might be noted that as little as 0.2% chromite present in the rock sample could account for this discrepancy. Mineral separate data for Cr in orthopyroxene in three samples from the basal 4m of the Bastard Unit at **RPM** yielded values of 3109, 2855 and 2775ppm (Kruger, 1982, see Figure 4.36).

On a regional basis there appears to be a systematic decrease in Cr levels of orthopyroxene from north to south (exclude **LEF**)(Figure 4.36). Locally, a pronounced systematic increase is seen at Union Section from 3287ppm at **UA** in the south to c. 3745ppm at **UC** in the north. The levels of Cr indicated by ΣC_{WR} fall within a narrow range between 3254ppm (**Y**) and 3851ppm (**AE**) - a 597ppm difference, while the range yielded by the Al_2O_3 estimates is 565ppm (excluding **LEF** and **Y**).

4.9.2.3 Cobalt (Co)

Values of Co in the Bastard Unit range between 4ppm, at the base of the LGMA (**UA**-15), and 107ppm in the Bastard Reef pyroxenite (**AE**-14) (Figure 4.37). Regression lines for individual profiles show a positive Y-intercept at MgO = 0 in all cases (Figure 4.38) and may in part be due to the lower MgO content of orthopyroxene and the presence of clinopyroxene. These factors effectively shift the points, in the anorthosite field, to the left. A marked depletion of Co is evident in the intercumulus ferromagnesian phases of the anorthosites. This feature is illustrated in those profiles which have a sufficient number of anorthosite samples to permit construction of a separate regression line (**UA**, **UC** and perhaps **AF**). A line drawn through those samples with less than 5% MgO projects through the origin (Figure 4.38).

An estimate of the Co content of the Mg-bearing phases was made based on the MgO content of orthopyroxene at an average of 29% and the results are presented in Figure 4.48 and Table 4.13. The indicated average Co content of the pyroxenes in all profiles is 111ppm (range 104 - 116ppm) and no marked systematic regional trend is seen for the Bastard Unit Co content.

4.9.2.4 Vanadium (V)

Levels of V vary from 6ppm (**UC**-9) to values approaching 140ppm in the Bastard pyroxenite. A maximum V content of 190ppm was recorded for **UC**-14 (Figure 4.39). Positive Y-intercepts at c. 30ppm were recorded for all regression lines (Figure 4.40). This is because vanadium concentrations in the anorthosites have a different distribution from that in the norites and pyroxenites. Kruger (1982) showed that V levels in both intercumulus ortho- and clinopyroxenes (in the LGMA) are higher than in the cumulus phases lower in the sequence. This phenomenon is clearly illustrated in **UA** where a sufficient number of samples have been taken in the anorthosites. Here a separate regression analysis for rocks with less than 3% MgO, clearly shows a steeper slope with an intercept close to the origin (Figure 4.40, inset at UA). The reason for this different distribution is that there is proportionately more clinopyroxene, in the form of intercumulus mottles, than orthopyroxene. The reverse is true

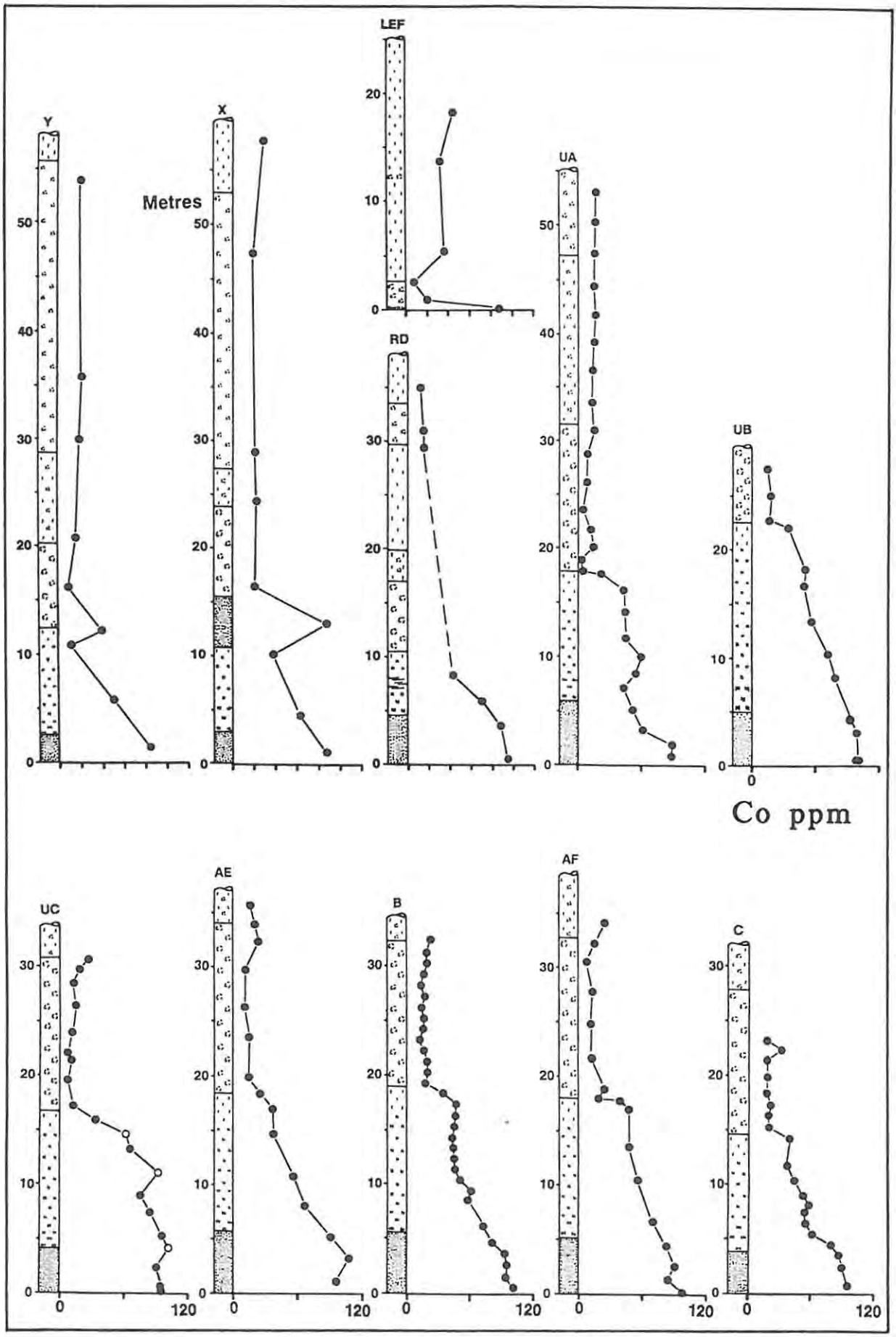

Figure 4.37 Whole-rock Co (ppm) plotted against stratigraphic height for eleven Bastard Unit profiles. Open circles in profile UC indicate olivine-bearing samples.

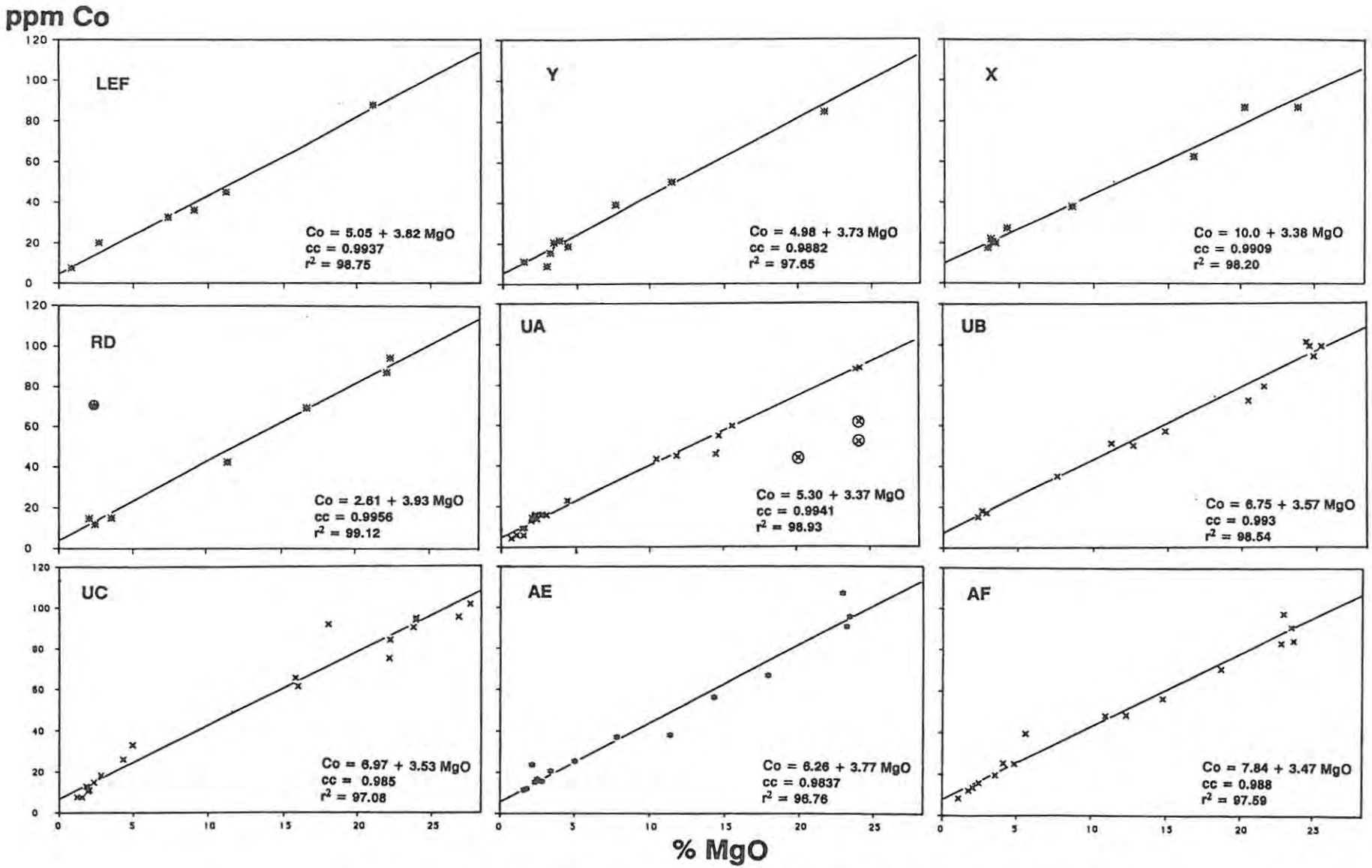

Figure 4.38 Plots of ppm Co vs Wt.% MgO for nine Bastard Unit profiles with the linear regression data. Circled symbols in **RD** and **UA** were excluded from the regression analysis.

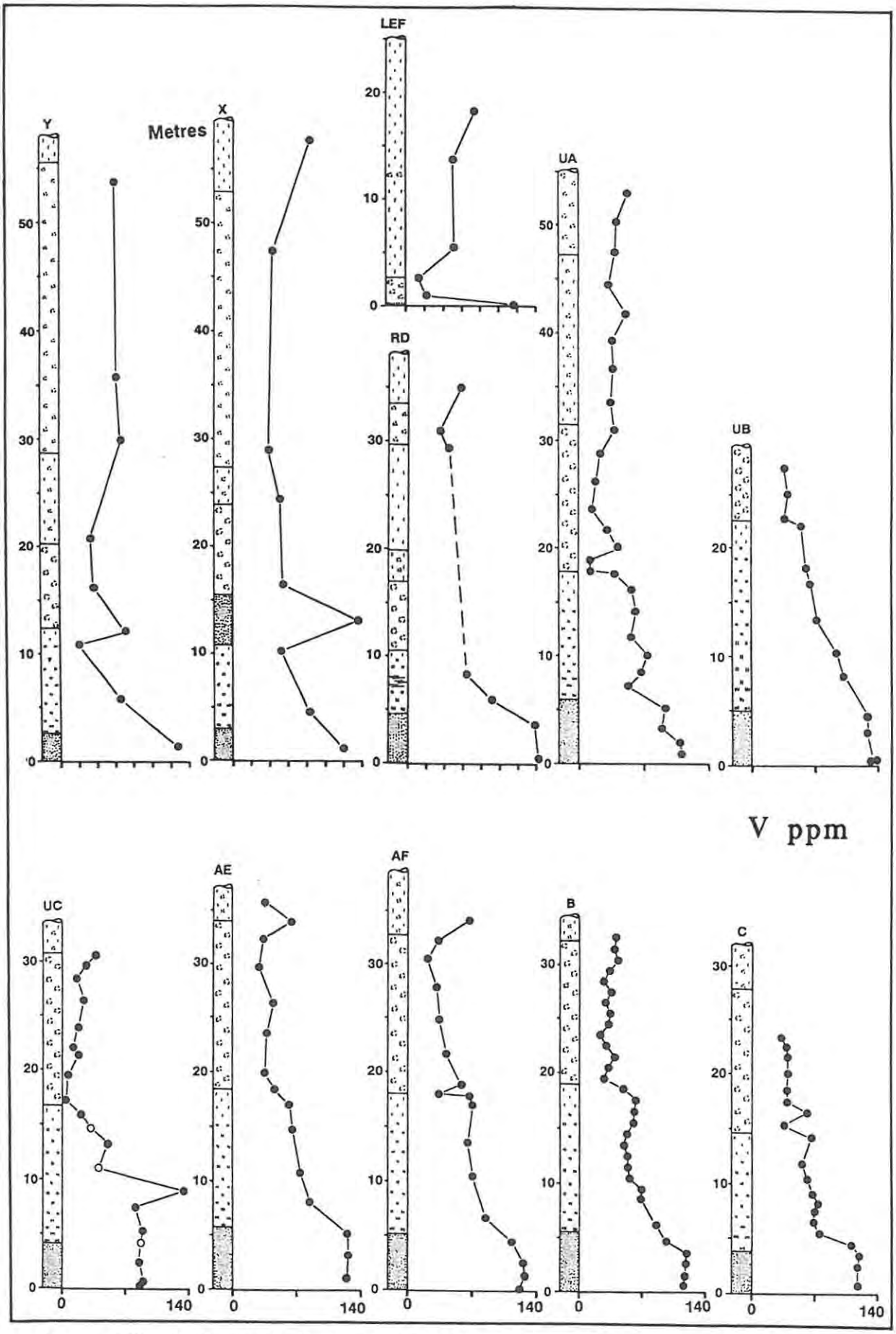

Figure 4.39 Whole-rock V (ppm) plotted against stratigraphic height for eleven Bastard Unit profiles. Open circles in profile UC indicate olivine-bearing samples.

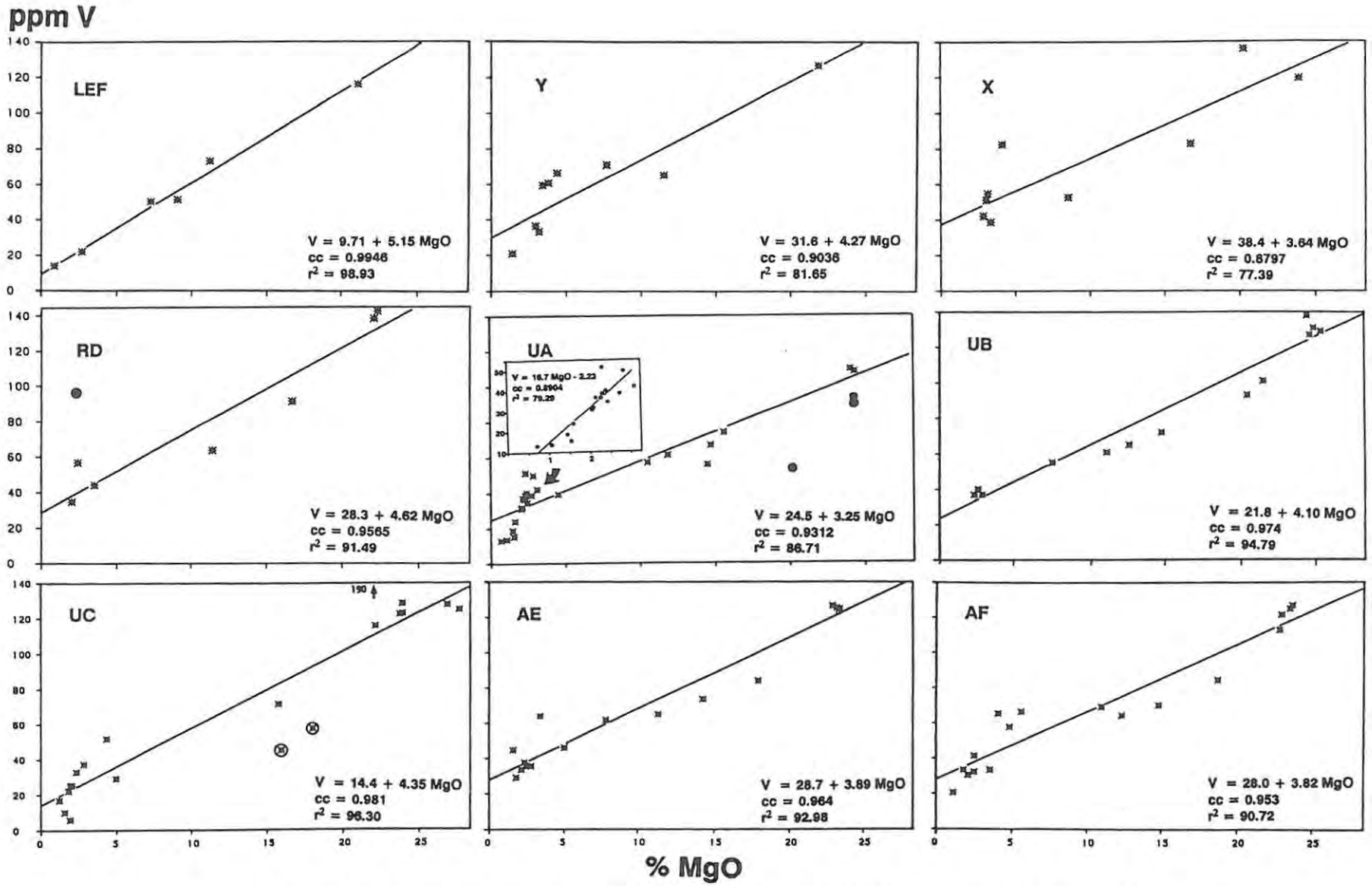

Figure 4.40 Plots of ppm V vs Wt.% MgO for nine Bastard Unit profiles with linear regression data. Circled symbols in RD, UA and the olivine-bearing samples in UC were excluded from the regression analysis.

where pyroxene occurs as a cumulus phase. As was discussed in **2.5.2** vanadium distributes preferentially into clinopyroxene (D_V^{cpx} = 1.5) compared with orthopyroxene (D_V^{opx} = 0.3) and hence a higher V content is expected in the anorthosites with minor amounts of pyroxenes.

The average estimated V content of the Mg-bearing phases at 29% MgO is 145ppm. There is a suggestion of an increase in the V levels in a southerly direction away from the Amandelbult and Union Sections in the northwestern sector of the Complex (Figure 4.48 and Table 4.13).

4.9.2.5 Zinc (Zn)

The stratigraphic distribution of Zn is very similar to that of V. Zn levels vary between 7.4ppm, within the anorthosites (**Y**765.48, **UA**-15 and 16a), and an average high of 90ppm in the basal pyroxenites (Figure 4.41). Two anomalously high values of 124 and 131 are recorded in the Bastard pyroxenite of profile **C** (**C**-16 and 18). Although more scatter is evident in the binary diagrams than that for V, all profiles indicate a positive Y-intercept of the regression line at MgO = 0 (Figure 4.42). The intercept value varies between 2.7ppm (**Y**) and 12.4ppm (**AF**). The presence of sulphide phases at the base of the unit does not have a marked influence on its concentration. Like V, there is a suggestion of increasing Zn values away from the northwest sector of the Complex towards the south.

4.9.2.6 Copper (Cu)

Copper values in the Bastard Unit vary between 4 and 461ppm. As was pointed out in **2.5.2**, this element behaves as an almost perfect chalcophile element; its distribution is directly related to the presence of sulphides and it is incompatible with respect to the other cumulus phases. The low levels of Cu throughout the Bastard Unit (apart from the sulphide-rich basal zone) are attributed in part to microscopic grains of sulphides throughout the column and Cu within plagioclase. Analyses of plagioclase separates of Bastard Unit at **RPM** by Kruger (1982) (excluding the basal pyroxenites) yielded an average value of 17.4ppm (13 samples, sd = 7.31).

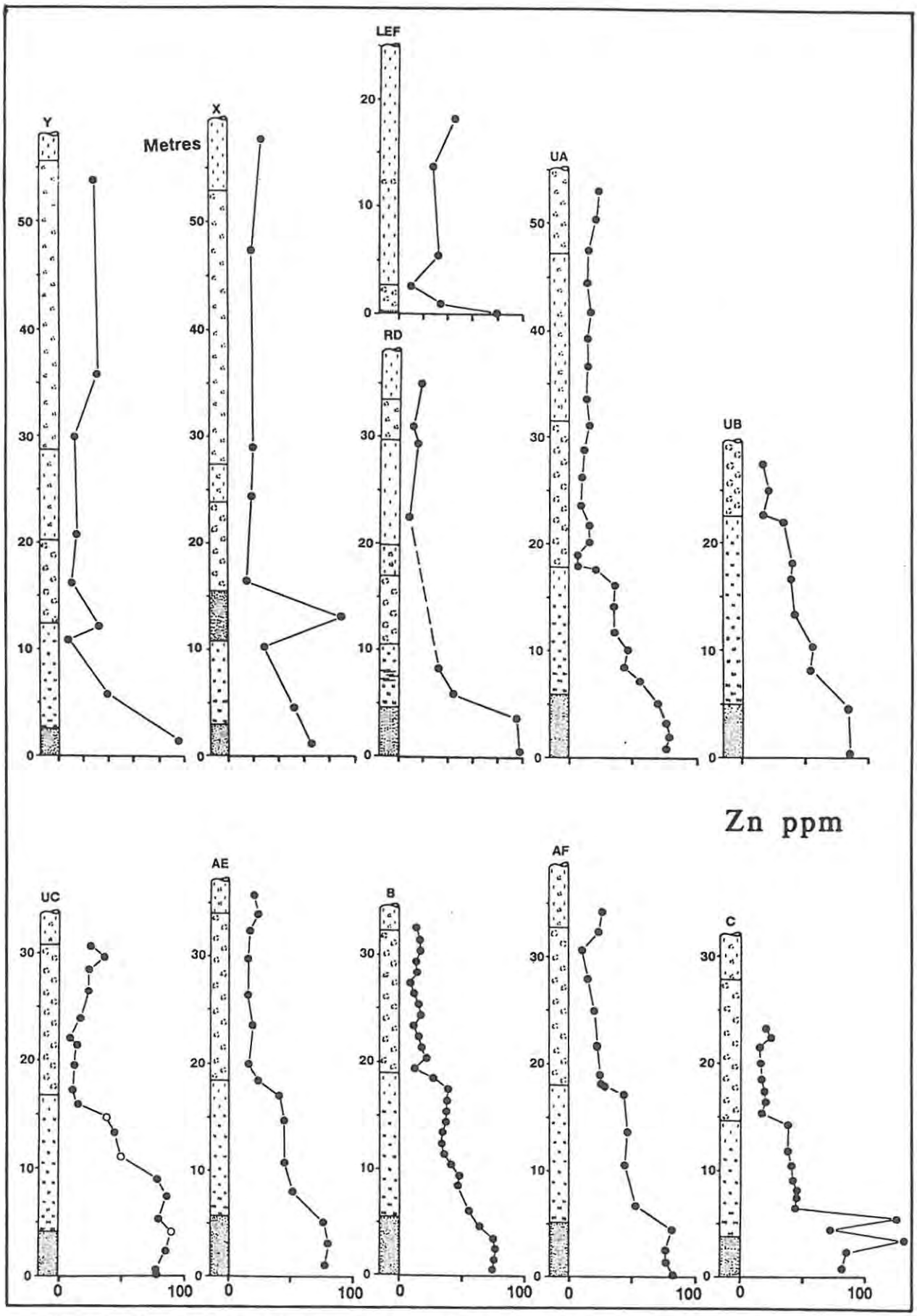

Figure 4.41 Whole-rock Zn (ppm) plotted against stratigraphic height for eleven Bastard Unit profiles. Open circles in profile UC indicate olivine-bearing samples.

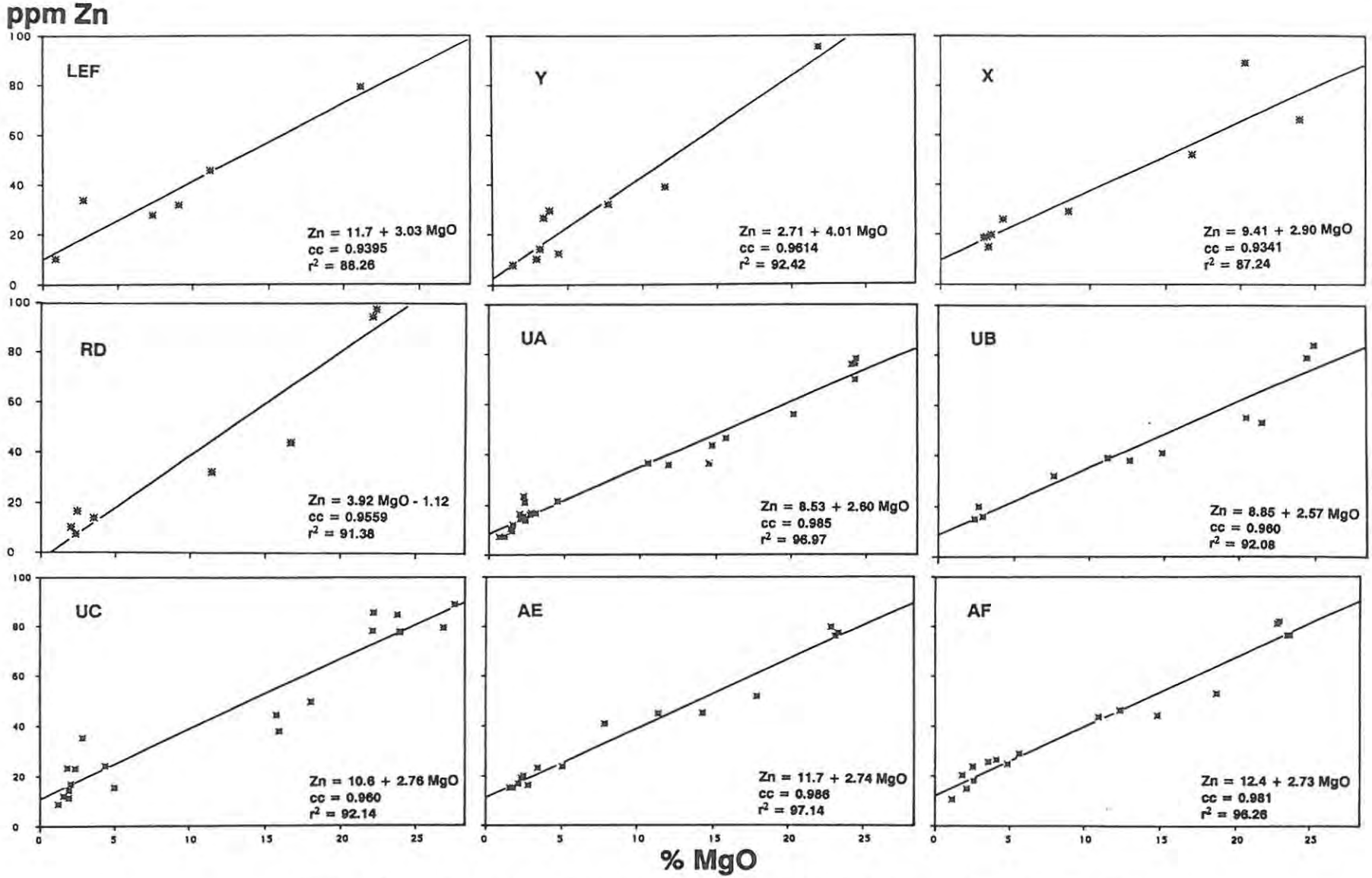

Figure 4.42 Plots of ppm Zn vs Wt.% MgO for nine Bastard Unit profiles with linear regression data.

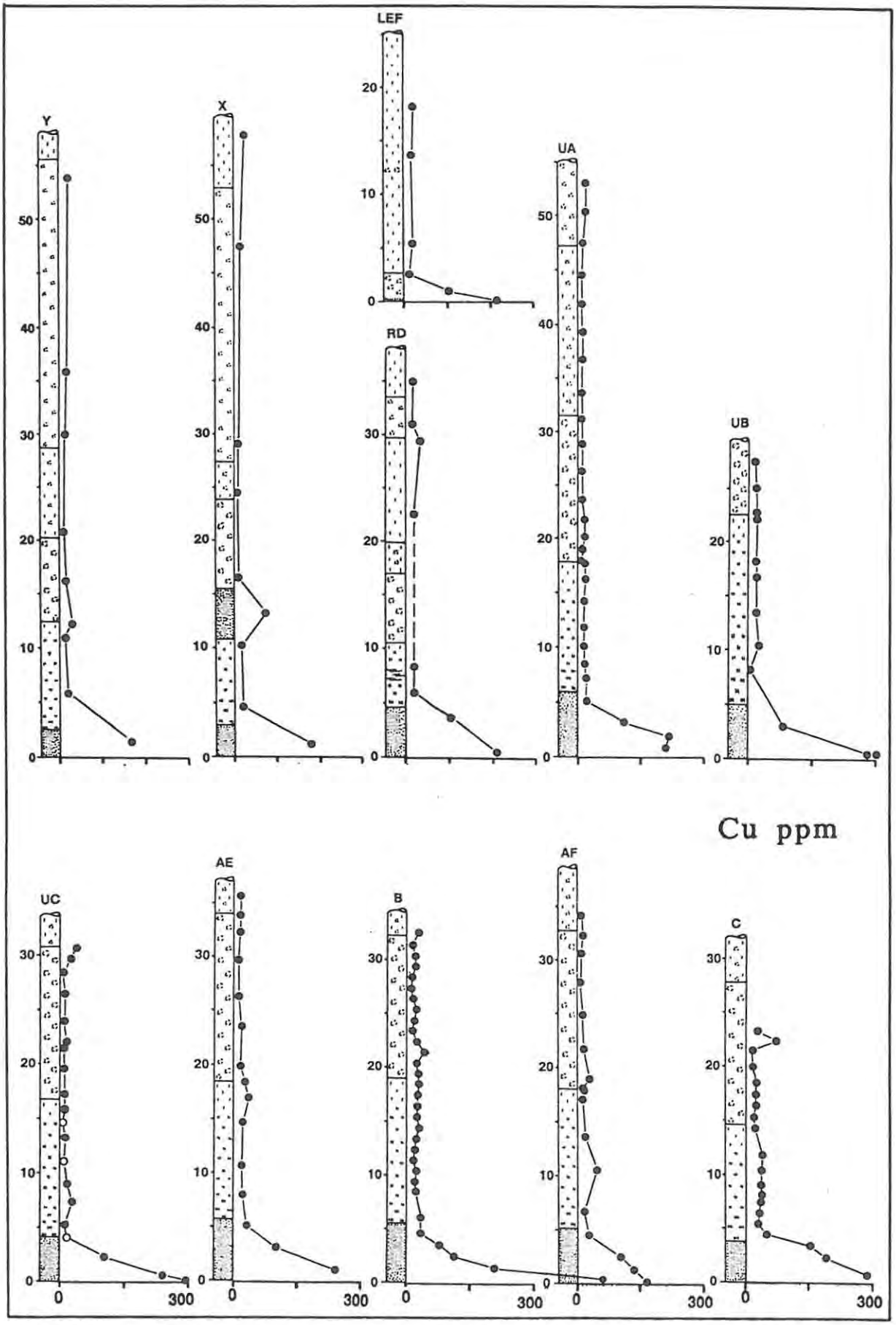

Figure 4.43 Whole-rock Cu (ppm) plotted against stratigraphic height for eleven Bastard Unit profiles. Open circles in profile UC indicate olivine-bearing samples.

The distribution of Cu in all the profiles indicates the presence of abundant sulphides at the base of the Bastard Unit (Figure 4.43). Samples with values in excess of 30ppm were considered to have more than background levels present and were deleted from the total dataset; a background Cu value of 17.4ppm was obtained for the Bastard Unit (128 samples, sd = 6.1). This value is only marginally higher than that mentioned earlier (**3.5.2**) for the Bastard Unit at Union Section (**UA**, **UB** and **UC**) where an average value of 14.0ppm was obtained (Table 3.2).

4.9.2.7 Nickel (Ni)

Ni concentrations vary from 15ppm in the LGMA (**UA**-12) to 1457ppm (**B**-32) in the Bastard pyroxenite (Figure 4.44). High Ni values within the basal pyroxenites are due to the presence of base-metal sulphides. These sulphide-bearing samples are readily recognised in the Ni - MgO plot, as they fall well above the regression line through the sulphide-poor samples. Naldrett et al. (1986, p.1109) suggested that a line could be drawn in such a variation diagram, below which no sample points would fall. This line they defined from the origin to a point represented by 700ppm Ni at 29.5% MgO, corresponding to the expression Ni = 23.729 MgO. This lower limit line they applied to the Bastard, Merensky and Footwall Units at Union and Rustenburg Sections. Naldrett et al. (1986) suggested that those samples falling on or close to the line are sulphide-free and those which plot above the line contain excess Ni due to the presence of sulphides.

This base line has been included in Figure 4.45. The average Ni concentration in the Mg-bearing phases (no sulphides) at 29% MgO is 648ppm (Figure 4.48). This value compares favourably with that of 688ppm calculated from the linear model for the Bastard Unit reported by Naldrett et al. (op cit.) at 29% MgO.

The **(excess Ni)/Cu** ratio was calculated for sulphide-bearing rocks in the Bastard Unit as well as for the Bastard basal sulphide samples and yielded average ratios of 1.11 and 1.37 respectively (Table 4.12). These values compare favourably with those quoted by Naldrett et al. (1986) of 1.12 and 1.77 for the Bastard Unit and are also very similar to the 1.2:1

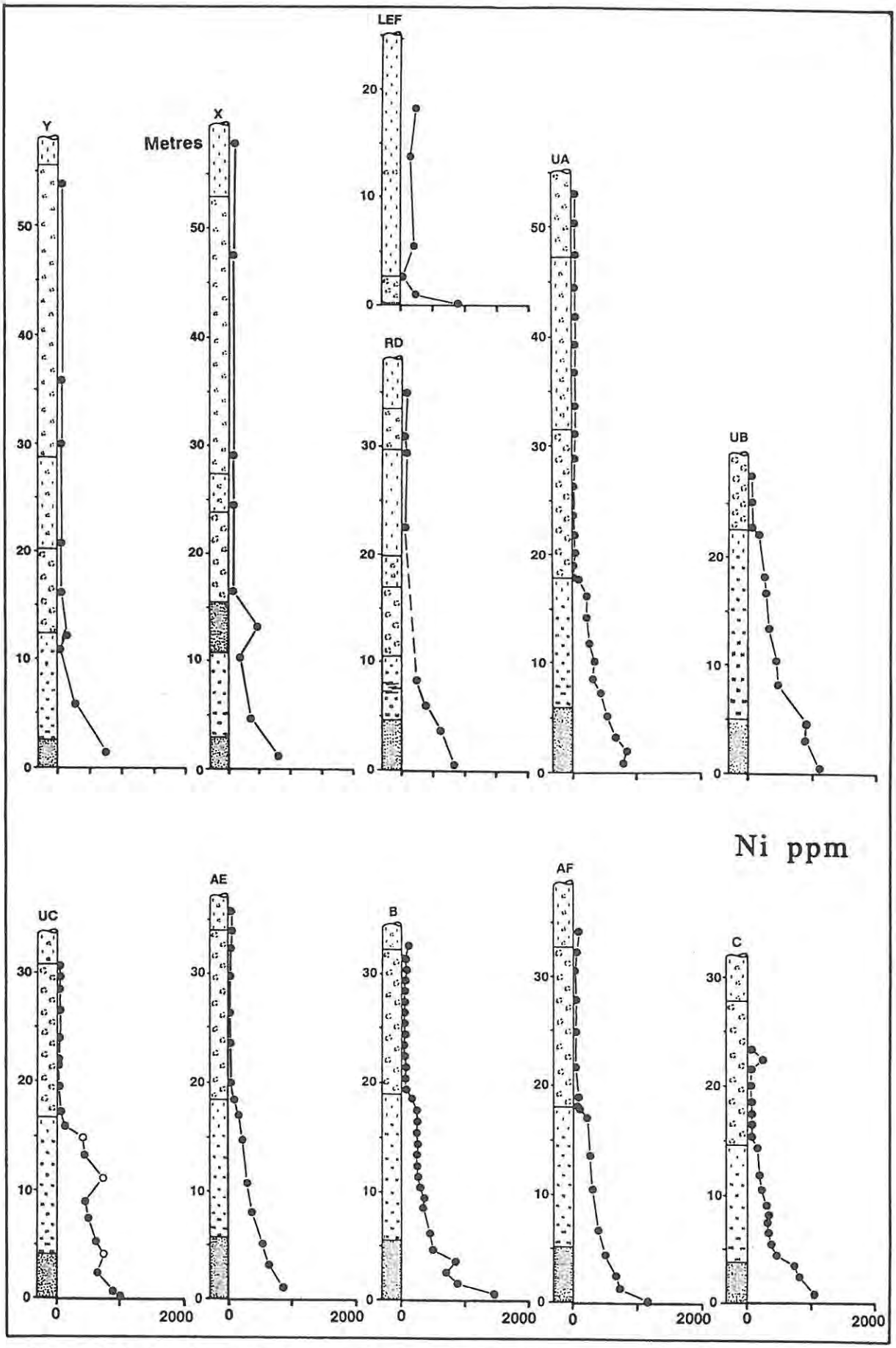

Figure 4.44 Whole-rock Ni (ppm) plotted against stratigraphic height for eleven Bastard Unit profiles. Open circles in profile UC indicate olivine-bearing samples.

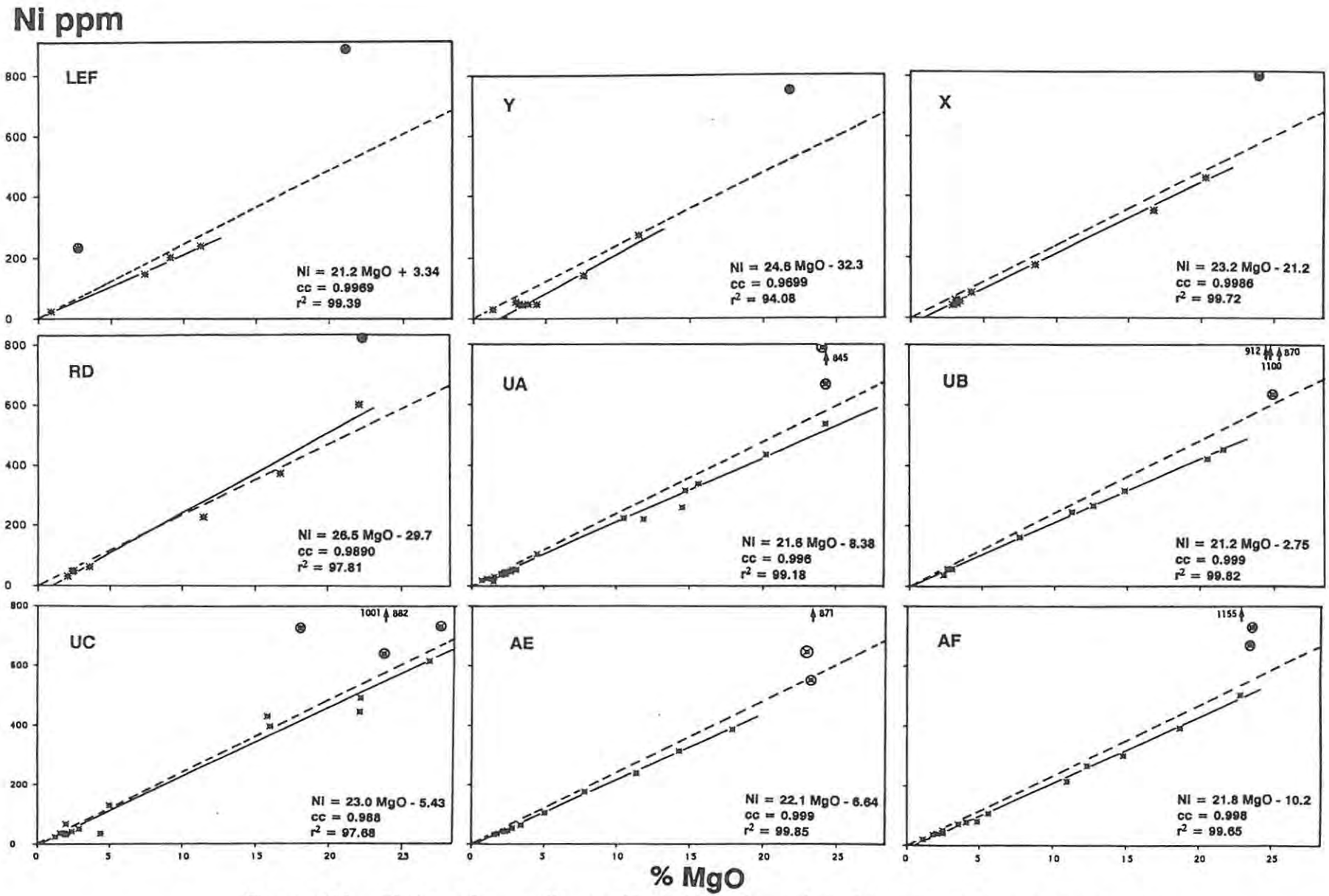

Figure 4.45 Plots of ppm Ni vs Wt.% MgO for nine Bastard Unit profiles with linear regression data. All samples which were identified as being sulphide-rich were excluded from this analysis (circled symbols). In most cases these samples have Ni values in excess of 500ppm. The dashed line represents the expression Ni = 23.729 MgO as suggested by Naldrett et al. (1986) (see text).

value in the Merensky Unit. By contrast, the published Ni/Cu ratio for the Merensky Reef itself is 2.3:1 (Cousins, 1964; and Naldrett et al. 1986).

Table 4.12: Calculated (excess Ni)/Cu ratios for the Bastard Unit and the basal sulphides for all profiles.

Sample	MgO (Wt%)	Cu (ppm)	Ni (ppm)	Ni = 23.7MgO	Excess Ni	Excess Ni/Cu
Bastard Unit						
H997.26	2.70	102.2	231.9	64.2	167.7	1.64
RD-17	22.12	102.9	603.8	524.9	78.9	0.77
UA-24	24.28	109.9	670.4	576.1	94.3	0.86
UC-19	23.94	238.9	881.8	568.0	313.8	1.31
AE-14	22.92	101.6	647.0	543.9	103.1	1.02
AF-14	23.53	103.7	669.0	558.4	110.6	1.07
Average						1.11
Basal sulphide-bearing Bastard Unit samples						
H998.1	21.08	214.2	889.3	500.1	389.2	1.82
Y775	21.86	166.3	749.5	518.7	230.8	1.39
X791.8	23.95	178.3	796.5	568.2	228.3	1.28
RD-18	22.35	208.0	824.2	530.4	293.8	1.41
UA-25	24.33	216.3	845.1	577.2	267.9	1.24
UA-26	24.06	207.6	790.3	570.9	219.4	1.06
B235/6	24.45	278.0	912.0	580.1	331.9	1.19
B232/12	25.40	300.0	1100.0	602.7	497.3	1.66
UC-20	23.97	293.3	1001.4	568.9	432.6	1.48
AE-15	23.40	239.0	871.0	555.3	315.7	1.32
AF-15	23.69	135.0	728.0	562.1	165.9	1.23
Average						1.37
Average for all Bastard Unit samples						1.28

4.9.2.8 Scandium (Sc)

The range of Sc values within the unit is from 2ppm (**UA**-15) in the LGMA to 34.7ppm (**RD**-17) in the Bastard pyroxenite Figure 4.46). Like Co, V and Zn this element shows a positive Y-intercept for the regression line when plotted against MgO (Figure 4.47). Kruger (1982) has shown that very little variation is seen in the Sc concentrations of both ortho- and

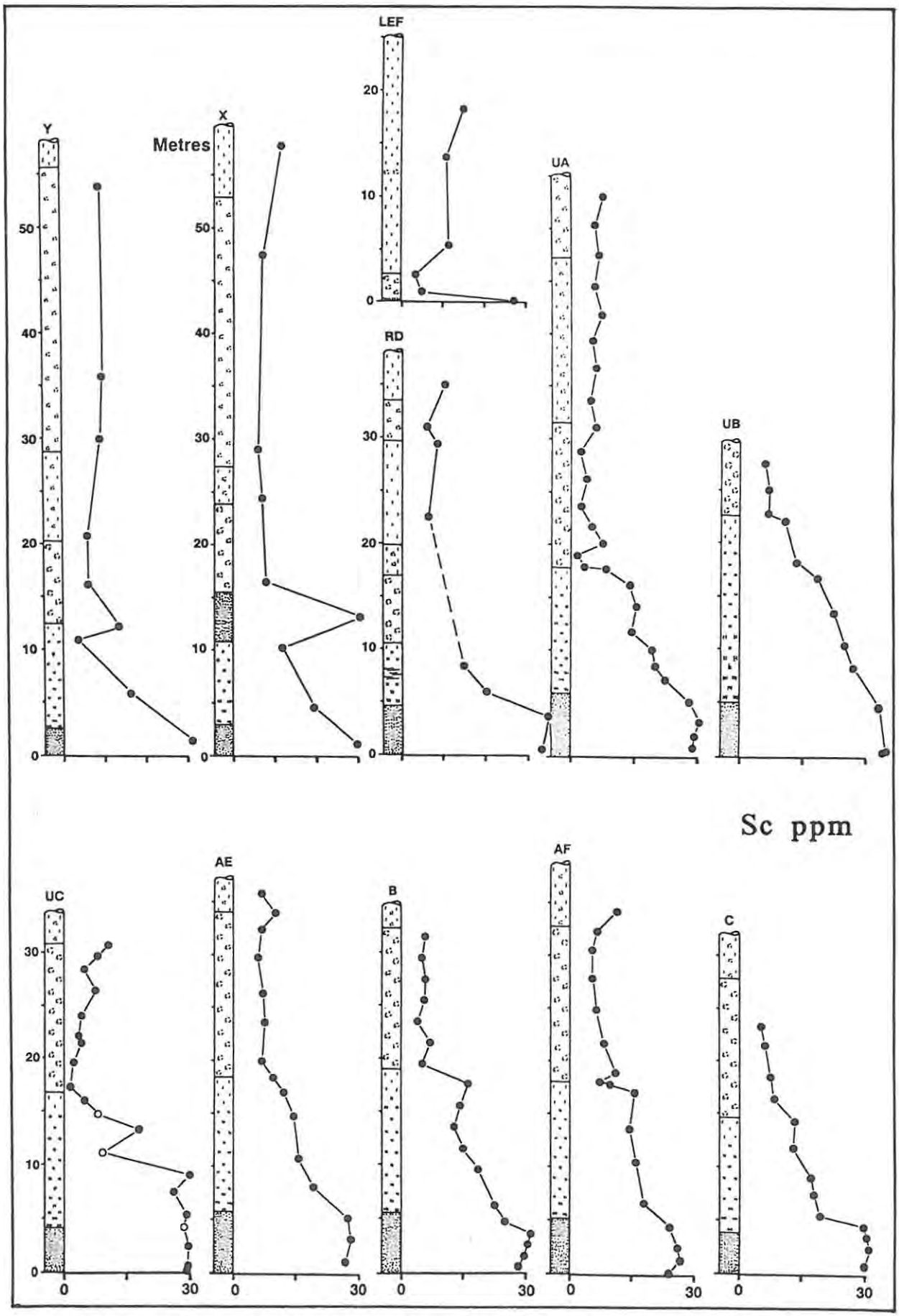

Figure 4.46 Whole-rock Sc (ppm) plotted against stratigraphic height for eleven Bastard Unit profiles. Open circles in profile UC indicate olivine-bearing samples.

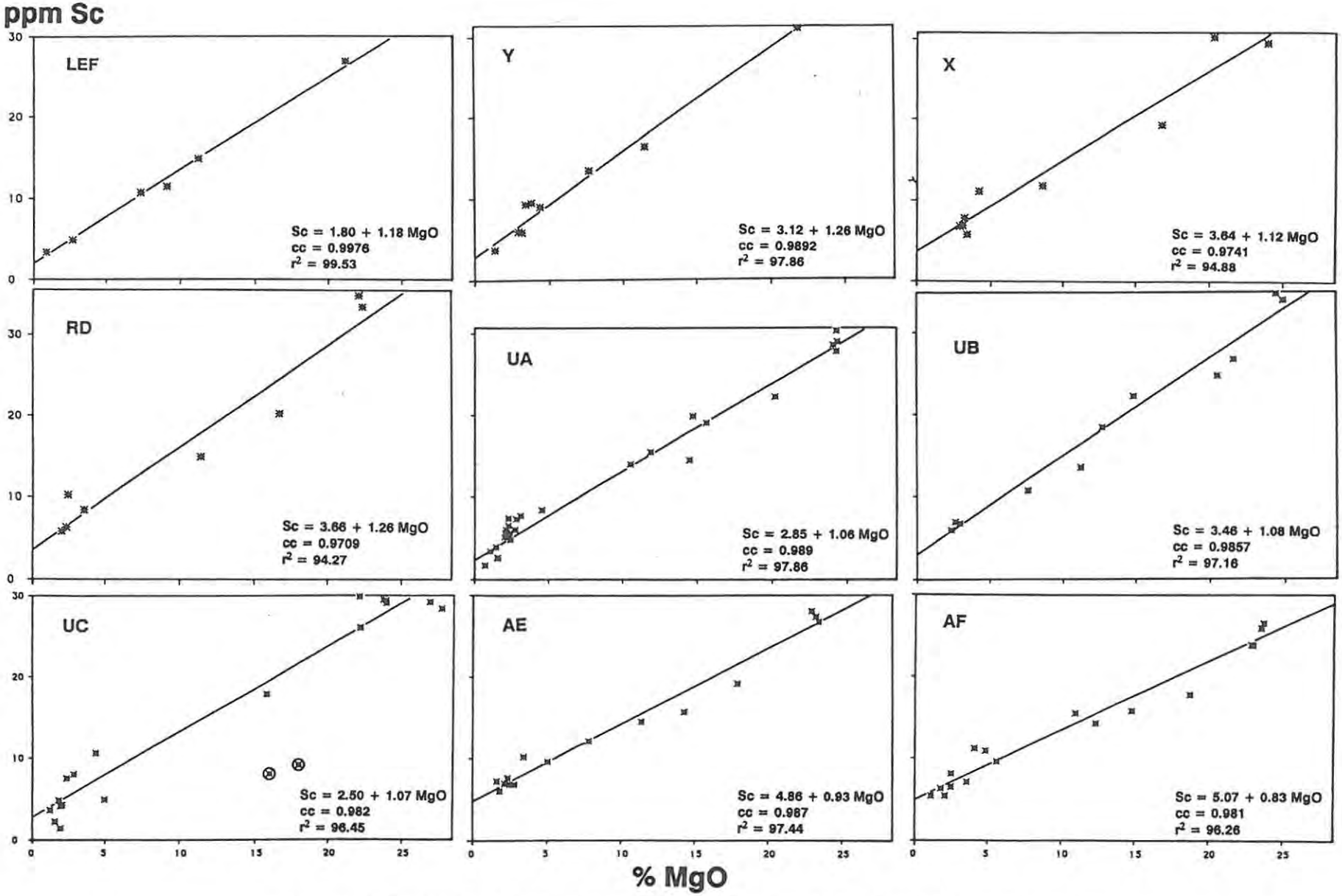

Figure 4.47 Plots of ppm Sc vs Wt.% MgO for nine Bastard Unit profiles with linear regression data. Circled symbols in UC were excluded from the regression analysis.

clinopyroxenes through the Bastard Unit (orthopyroxene 30-40ppm and clinopyroxene 70-80ppm). The average Sc concentrations in the Mg-bearing phases of the Bastard pyroxenites (at 29% MgO) is 35ppm which is 6ppm higher that the 29ppm obtained in two mineral separates of orthopyroxene from the lower 2m of the Unit at **RPM** (Kruger, 1982) (Table 4.13). This discrepancy is accounted for by the presence of clinopyroxene. Clinopyroxene separates of these samples reported by Kruger (op. cit.) yielded values of 80 and 75ppm respectively which is in keeping with the recommended values of D_{Sc} = 3.1 for clinopyroxene, and 1.1 for orthopyroxene (Frey et al., 1978). On a regional basis there is again a suggestion of increasing Sc values away from Amandelbult Section towards Rustenburg in the south.

Table 4.13: Estimated trace element concentrations in the Mg-bearing phases, calculated at 29% MgO from the linear regression model for individual profiles. Standard error of estimates in parentheses. Data for RPM are orthopyroxene mineral separates from the basal 2m of the Unit (Kruger, 1982).

PROFILE	Co	V	Zn	Ni	Sc
LEF	116 (3.5)	159 (4.3)	99 (8.9)	618 (9.1)	37 (0.6)
RPM	101	133	87	743	29
Y	112 (4.0)	155 (14.0)	119 (7.9)	680 (21.7)	38 (1.3)
X	108 (4.1)	144 (17.7)	94 (10.0)	651 (9.2)	36 (2.4)
RD	116 (3.7)	162 (14.0)	113 (11.7)	739 (35.5)	40 (3.0)
UA	104 (2.7)	119 (9.4)	84 (4.1)	618 (13.8)	34 (1.4)
UB	110 (4.1)	141 (9.1)	83 (6.9)	612 (7.0)	35 (1.5)
UC	109 (6.6)	141 (9.6)	91 (8.6)	662 (34.0)	34 (2.3)
AE	116 (6.2)	142 (9.6)	91 (4.2)	634 (5.0)	32 (1.3)
AF	109 (5.0)	139 (11.1)	92 (4.9)	622 (9.5)	29 (1.5)
Average (excluding **RPM**)	111	145	96	648	35

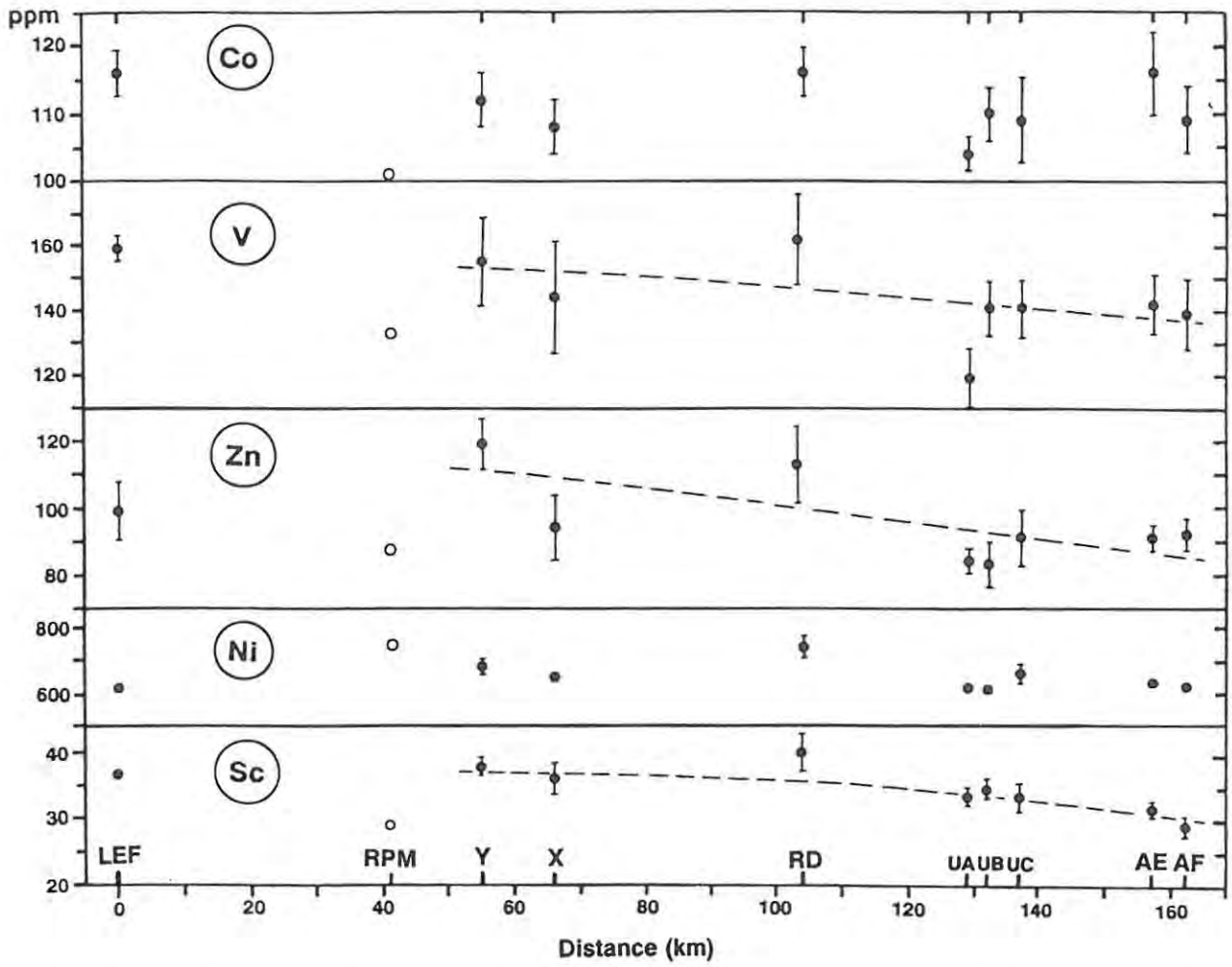

Figure 4.48 Levels of Co, V, Zn, Ni and Sc in pyroxenes in individual profiles indicated by the regression data at a whole-rock MgO content of 29%. Bars show the standard error of estimate. Open circles at **RPM** indicate values in orthopyroxene mineral separates from the lower 2m of the Bastard pyroxenite (Kruger, 1982).

Interelement ratios

From the above discussion it is apparent that there are strong modal controls on the behaviour of individual elements. The use of interelement ratios can to a large degree nullify the modal effects and the variation of interelement ratios can indicate the geochemical evolution that takes place during crystallisation.

Bulk distribution coefficients are greater for Ni than for Sc in mafic rocks and the **Ni/Sc** ratio has been shown to be a useful indicator of increasingly primitive character towards the bases of cyclic units. Anomalous values may be introduced by the presence of sulphides, but

these samples are identified by their anomalously high Cu or Ni values and are accordingly rejected. The pattern for the Ni/Sc ratio through the Upper Critical Zone shows marked cyclicity and has been used to good effect by Eales et al. (1988) to define the limits of individual units, especially when other geochemical parameters do not readily define the unit limits. Figure 4.49 shows the characteristic trend of the Ni/Sc ratio for all the Bastard Unit profiles. Here the Ni/Sc ratio decreases upward through the pyroxenite - norite sequence and into the LGMA. A minor yet distinctive reversal to more primitive values occurs at or near the top of the LGMA - especially in profiles **AE**, **UA**, **X**, **B** and to a lesser degree in **AF** and **Y**. The ratio then remains reasonably constant between 5-10 throughout the remainder of the GMA. This reversal is coincident with that of the reversal in orthopyroxene MMF ratios (see **4.8.1**). Ni/Sc ratios within the **UC** profile are anomalously high and may be a reflection of the generally more primitive character (reflected by the occurrence of olivine) in the area.

The **V/Cr** ratio also displays a distinctive pattern through the Bastard Unit (Figure 4.50) and here the **UA** and **AE** profiles best depict the behaviour of this ratio. Low values (< 0.1) are evident through the pyroxenite - norite sequence. An increase in the ratio is apparent through the lower half of the LGMA to a peak (c. 0.6) before reverting to intermediate values (c. 0.3). The values above the reversal gradually increase through the remainder of the Unit without exceeding 0.5. Mitchell, (1986) has shown that low V/Cr values (below 0.35) persist through the first 500m of the Main Zone before a gradual increase is seen to levels above 12.0 at the top of Subzone B (below the Pyroxenite Marker). The reversal within the LGMA is more pronounced at **UA**, **AE** and **X**. In the absence of magnetite, variations in this ratio are attributable to clinopyroxene.

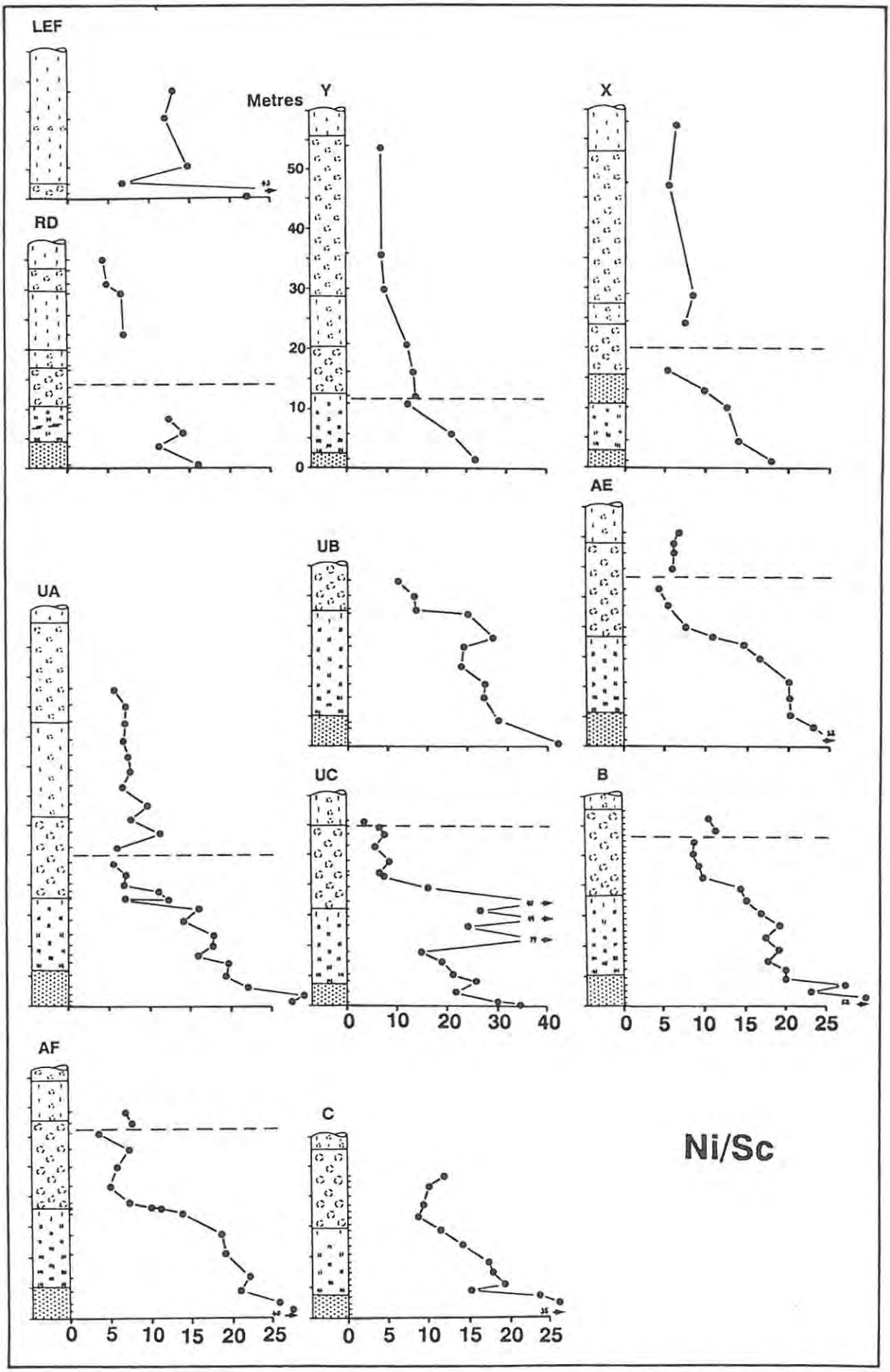

Figure 4.49 Whole-rock Ni/Sc ratios plotted against stratigraphic height for eleven Bastard Unit profiles. The dashed line indicates the position of the inferred reversal of the orthopyroxene MMF ratio. Note scale change for UC. Arrows indicate data point off scale.

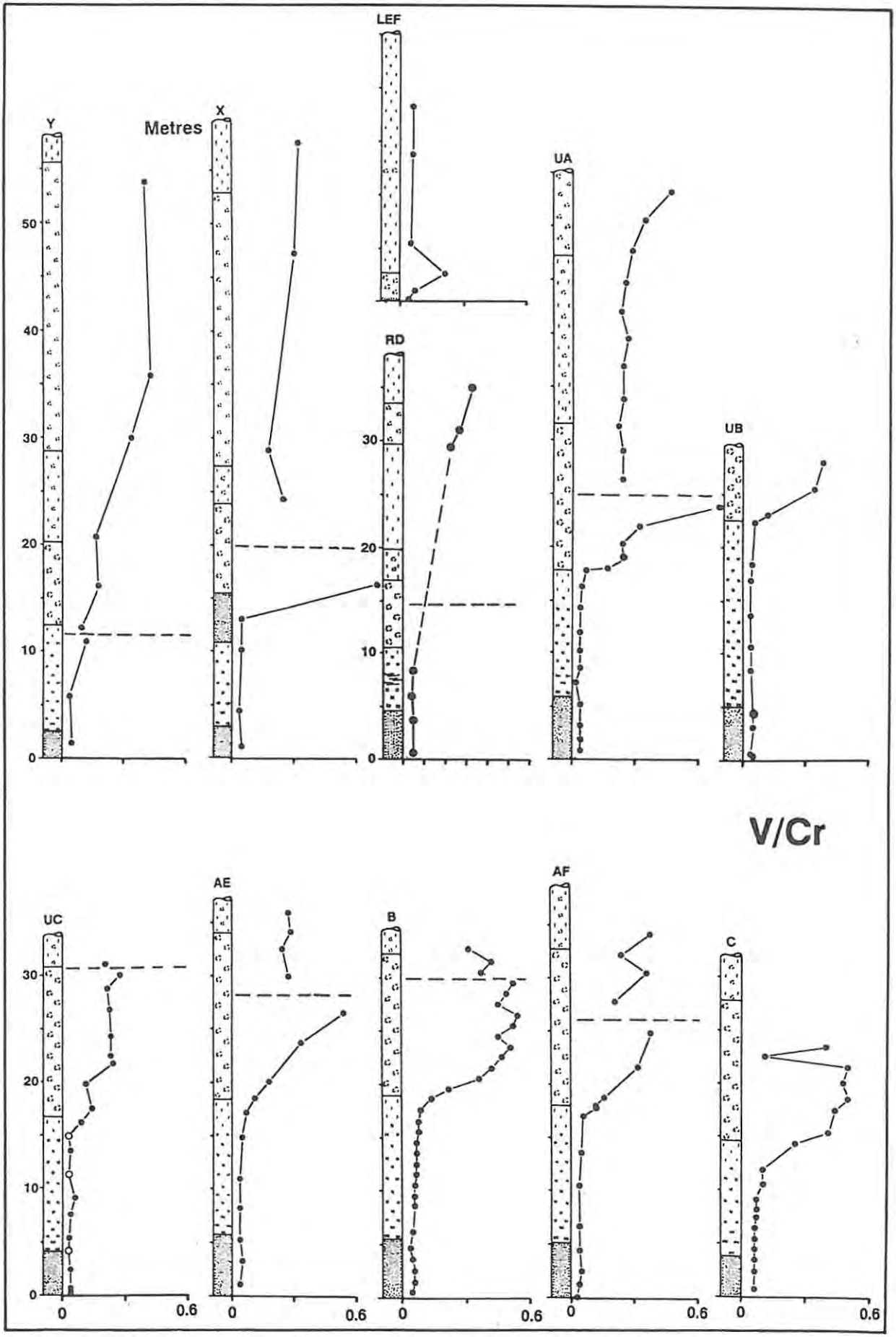

Figure 4.50 Whole-rock V/Cr ratios plotted against stratigraphic height for eleven Bastard Unit profiles. The dashed line indicates the position of a reversal in trend for MMF ratios in orthopyroxene (Figure 4.7).

Trace elements incompatible in all phases of the Bastard Unit.

4.9.2.9 Rubidium (Rb)

Concentrations of Rb in the unit would, at first glance, appear to have a rather erratic distribution (Figure 4.51) with values ranging from a high of 17.6ppm (**UA**-25) to those below detection limits (≤1.3ppm) - mainly in the norites and the LGMA. A generalised pattern of distribution through all the profiles is, however, recognised and is as follows.

* Moderately high values, in excess of 5ppm, occur within the basal Bastard pyroxenite.
* A sharp drop, to notably low values, occurs at the pyroxenite - melanorite contact. Rb values remain low through the norites (< 3ppm).
* A progressive increase is then seen within the leuconorites and upward through the entire GMA. Peak values in excess of 15ppm are recorded at the top of the Bastard Unit.

This distinctive stratigraphic distribution of Rb suggests that a geochemical break, to lower values, occurs 5-10m above the basal contact of the Unit. This geochemical displacement is perhaps explained by late-stage fractionated interstitial liquid being squeezed out from the Merensky Unit below, resulting in a concentration of Rb in the basal part of the Bastard Unit.

The upward increase in Rb from the base of the norites through the remainder of the unit is recognised in all profiles. This trend of increasing Rb was also recognised by Mitchell (1986) and he clearly showed that the pattern continues into the basal part of the Main Zone (**Unit I**), before reverting to values below 5ppm, 50m above the Bastard Unit, and remaining at these levels through the first 500m of the Main Zone.

4.9.2.10 Zirconium (Zr)

An almost identical distribution pattern to that of Rb is seen for this element although values are generally double those of Rb (Figure 4.52). Levels vary between ultra-trace amounts within the norites to 38.6ppm (**Y**-722.4) at the top of the UGMA. Mitchell (1986) reports a similar Zr increase towards the top of the Bastard Unit and upward into the basal

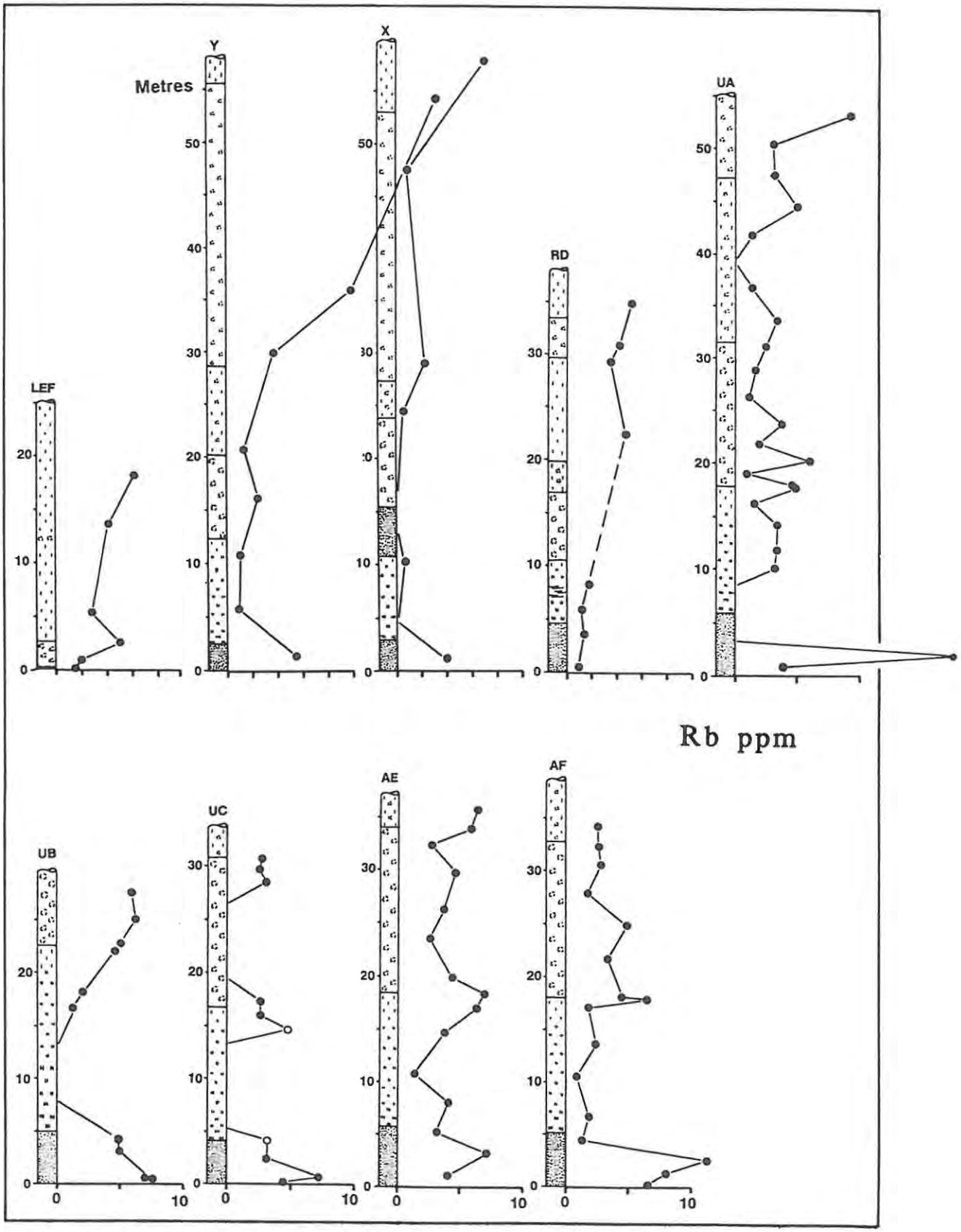

Figure 4.51 Whole-rock Rb (ppm) plotted against stratigraphic height for nine Bastard Unit profiles. Open circles in profile UC indicate olivine-bearing samples.

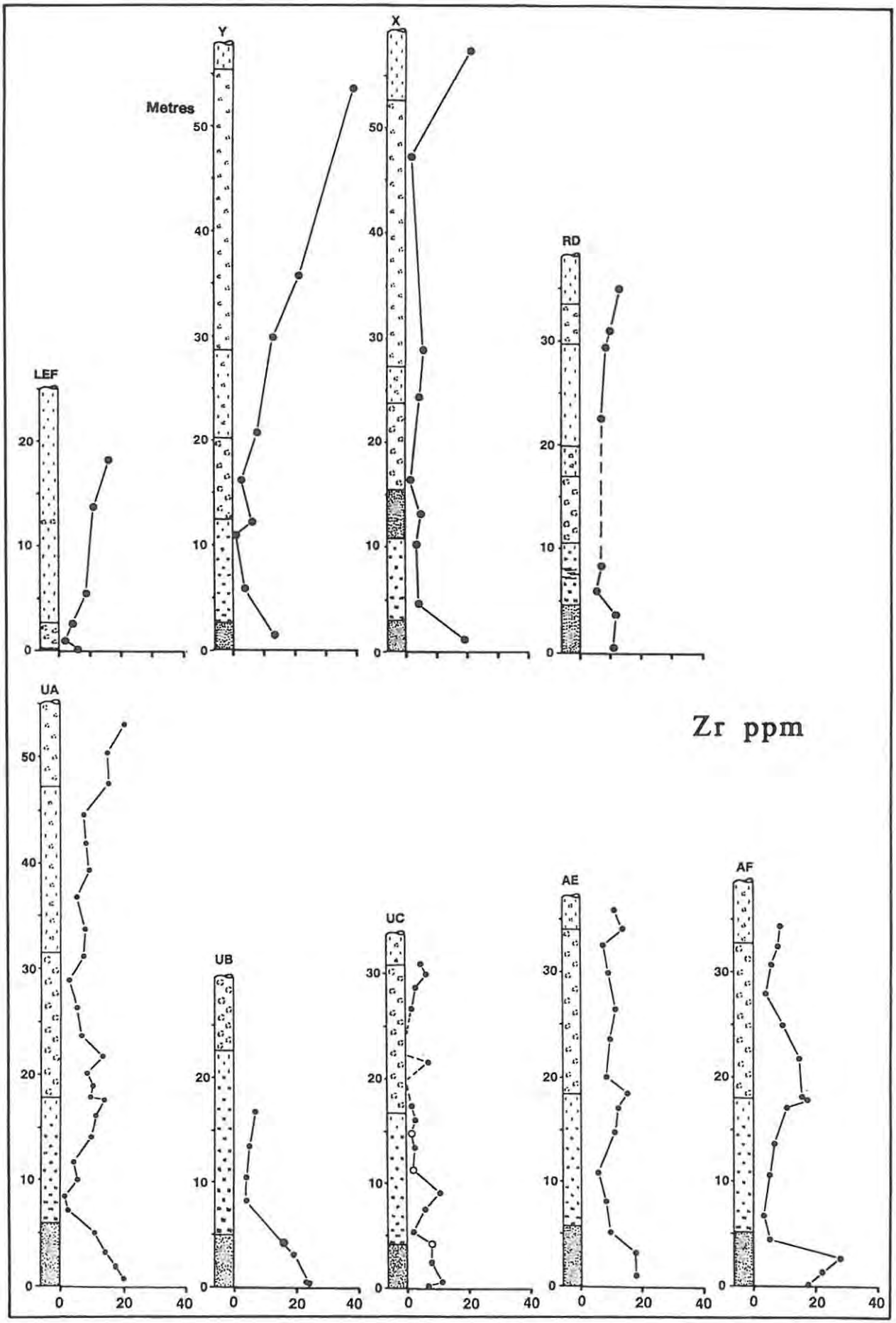

Figure 4.52 Whole-rock Zr (ppm) plotted against stratigraphic height for nine Bastard Unit profiles. Open circles in profile UC indicate olivine-bearing samples.

part of the Main Zone. A reversal to lower values (c. 10ppm) occurs 100m above the base of the Bastard Unit.

4.9.2.11 Yttrium (Y)

Although a wide range of Y is observed (ultra-trace values - 18.9ppm in UA-14), the bulk of samples in all profiles indicate levels below 10ppm which is in agreement with the levels reported by Mitchell (1986) in the Bastard Unit. No obvious systematic distribution pattern is seen through any of the profiles in this study (Figure 4.53). The work of Naldrett et al. (1984, Figure 4.25) does, however, show a marked similarity in distribution to that of Rb, Zr and K_2O and their Y values are generally higher, being in excess of 10ppm. Naldrett et al. (1984) clearly indicate values of 20-30ppm within the Bastard pyroxenite while the norites and the bulk of the GMA have values between 10 and 20ppm. A progressive Y increase is seen at the top of the GMA where values of c. 32ppm are reported. This increase is again similar to that observed for the elements Zr, Rb and K_2O.

4.9.3 Summary of whole-rock data.

Features indicated by the whole-rock data of the Bastard Unit are as follows.

a) Whole-rock $\%Al_2O_3$ is an excellent indicator of the modal feldspar content in the cumulates and has been used effectively in the classification of the different lithologies (Figures 1.5, 4.22 and 4.26).

b) The whole-rock MMF_{WR} ratios in all the profiles closely match the trend of the MMF ratios for orthopyroxene. All Bastard Unit profiles around the western limb of the Complex display a characteristic cryptic variation pattern through the basal pyroxenite - norite sequence (Figure 4.21). Almost no variation is seen for MMF_{WR} ratios within the base of the pyroxenite at different localities (0.80) which is in close agreement with the MMF ratios in orthopyroxene at this level. Generally lower MMF_{WR} values, with a greater degree of variability, are seen within the GMA. MMF_{WR} ratios within the LGMA (c. 0.65 - 0.70) are more primitive than those in the UGMA ($\leq$ 0.6).

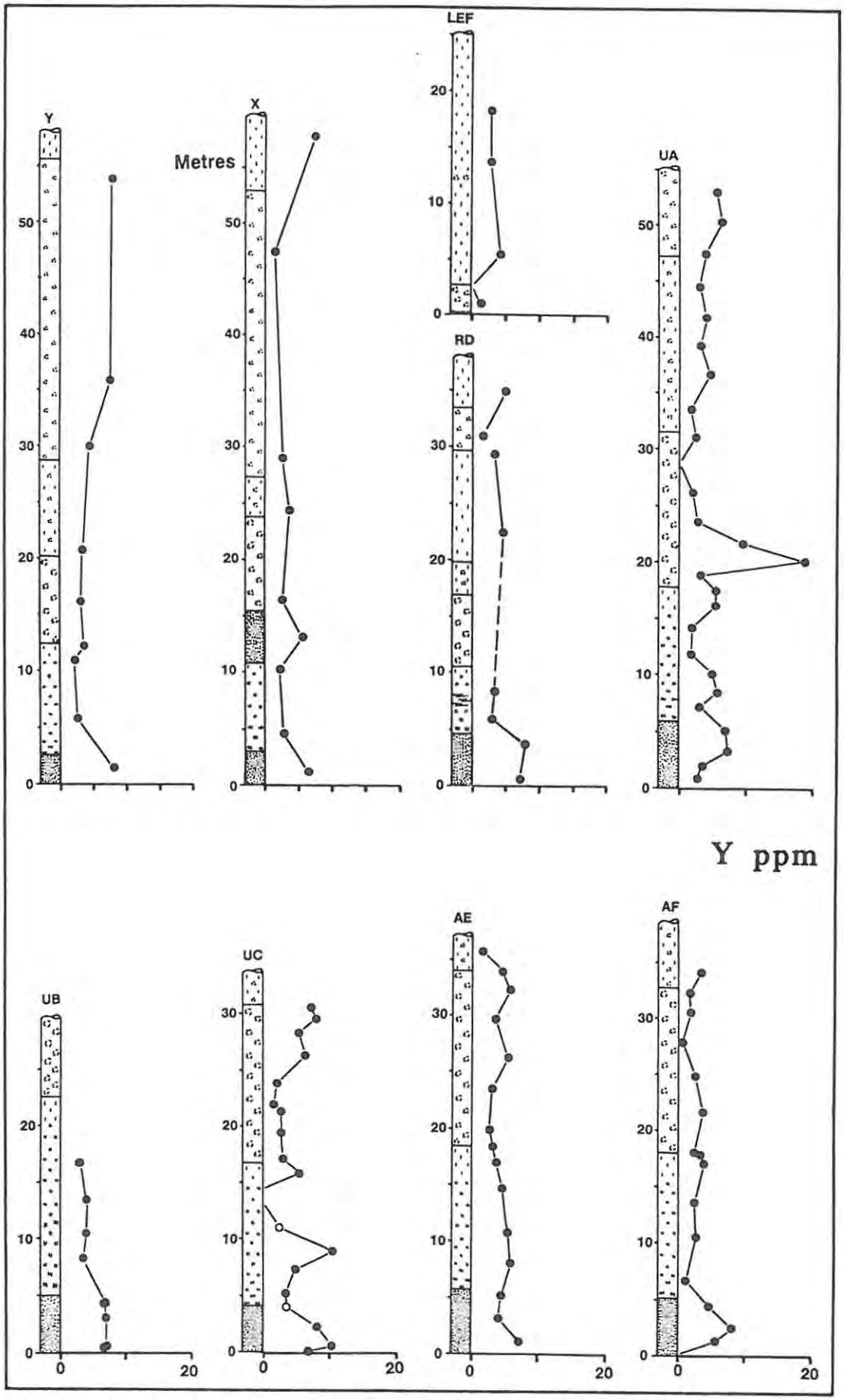

Figure 4.53 Whole-rock Y (ppm) plotted against stratigraphic height for nine Bastard Unit profiles. Open circles in profile UC indicate olivine-bearing samples.

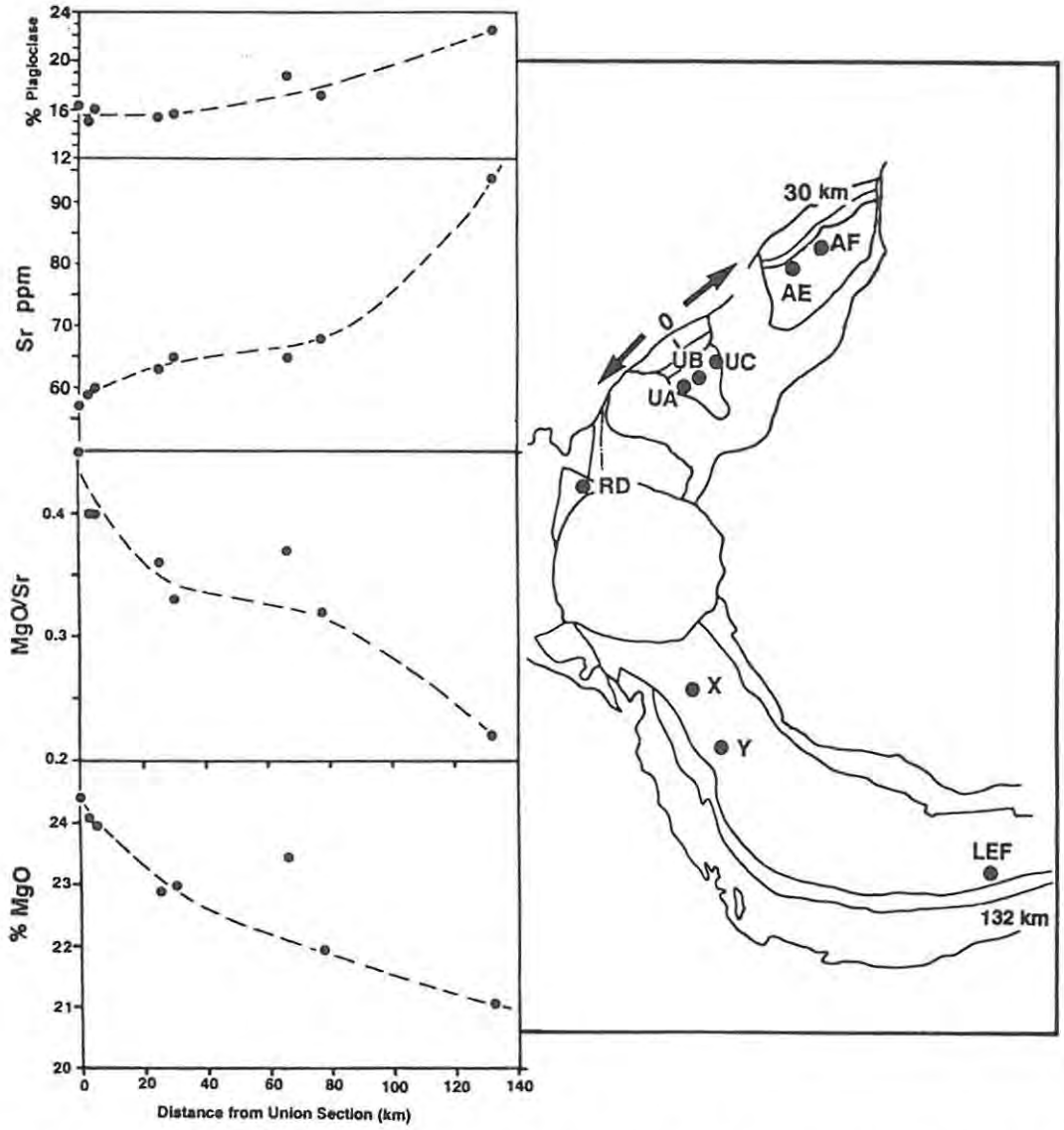

Figure 4.54 Plots of % intercumulus plagioclase, Sr, %MgO and MgO/Sr ratios for the basal Bastard pyroxenites against map distance (km) from the central part of Union Section. Trend lines are drawn in by eye. The map shows the spatial distribution of the various profiles and their distances from Union Section.

c) Absolute %MgO values of the **basal pyroxenite** samples around the western limb of the Complex are not the same at all localities. The highest %MgO contents are recorded at Union Section while the lowest levels are at **LEF** (Figure 4.54). The progressive decrease in %MgO away from Union Section is also reflected by the MgO/Sr ratio and increasing Sr levels - a measure of the amount of intercumulus plagioclase of the rock. It is therefore clear that the basal part of the Bastard Unit becomes progressively less mafic away from Union Section. Whole-rock interelement ratios like MMF_{WR}, $Sr/Al_2O_3{}^*$, Ni/Sc and V/Cr do not vary along strike but display similar values at all localities. However, there

does appear to be an increase in V, Zn and Sc values within the basal pyroxenites in a southerly direction away from Amandelbult and Union Sections. This trend probably reflects an increase in the modal proportion of clinopyroxene at this level.

d) Strontium has been shown to be an effective indicator of cyclicity within the Upper Critical Zone - each unit displaying its own characteristic Sr signature. Two effective measures of Sr signature are the $Sr/Al_2O_3^*$ ratio (Eales et al., 1986) and the linear regression models yielded by individual units when Sr is plotted against MgO or ΣC_{WR} (Figures 3.6, 4.29 and 4.30).

The bulk of the Bastard Unit, excluding the lower pyroxenite, displays the lowest recorded $Sr/Al_2O_3^*$ ratios for a cyclic unit in the Upper Critical Zone and the first 900m of the Main Zone (Figure 4.55). Levels of $Sr/Al_2O_3^*$ can be bracketed by an envelope between 11.3 - 13.0. The mid-value of the Bastard Unit envelope is 12.2 while those of the underlying Merensky and Footwall Units are 13.3 and 14.8 respectively. A value of c. 13.4 is recorded for the first 900m of the Main Zone. It is notable that the $Sr/Al_2O_3^*$ ratios recorded for the GMA match those of the underlying norites. The anorthosites do not therefore appear to be derivatives of a discrete liquid (contrary to the proposal of Irvine et al., 1983) unless this liquid was undergoing continuous contamination.

Apart from the anomalous ratios recorded in the leucocratic lithologies at **RD**, all $Sr/Al_2O_3^*$ values from different localities around the western limb of the Complex fall within the narrow range of 11.3 - 13.0. It is concluded that little or no variation of Sr content occurs in plagioclase over a distance in excess of 170km.

The linear regression model, illustrated in Figure 3.6, for all the Bastard samples at Union Section is

$$Sr = 382 - 12.8\ MgO \quad (cc. = -0.994,\ n = 57\ samples)$$

while all Bastard Unit samples, excluding the **RD** data, yield the expression:

$$Sr = 379 - 12.9\ MgO \quad (cc. = -0.956,\ n = 116\ samples).$$

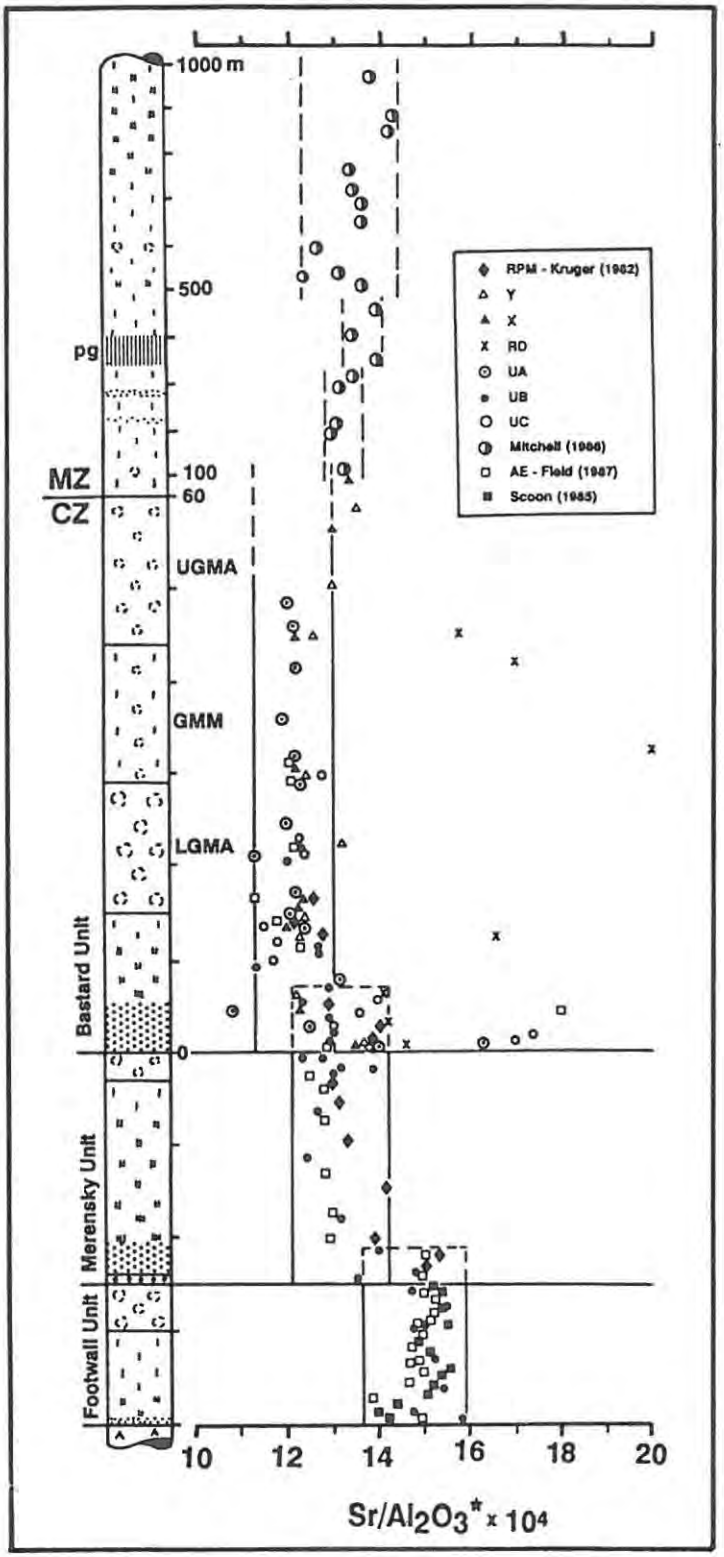

Figure 4.55 Composite plot of $Sr/Al_2O_3^*$ ratios against stratigraphic height for the Footwall, Merensky and Bastard Units of the Critical Zone as well as the first 1000m of the Main Zone in the western Bushveld Complex (see Mitchell, 1986 for a more detailed geological log of the Main Zone). The representative stratigraphic column has a bias towards that in the NW sector of the Complex. Vertical scale is indicated by 10m (CZ) and 100m (MZ) intervals on the right side of the column (note scale change at the top of the Bastard Unit); pg = porphyritic gabbro. Data for **RPM** are for plagioclase mineral separates (Kruger, 1982) and the field envelopes for the Critical Zone as well as the data for **UB** are from Eales et al. (1986). Broken-line boxes at the top of the fields suggest infiltration of residual liquids from underlying units.

Indirect determination of the Sr concentrations in intercumulus plagioclase suggests that no discernible difference is evident between plagioclase of cumulus and intercumulus habit. This observation is mainly based on the profiles in the northwestern sector, where sufficient samples through the Unit were able to define rigidly the regression lines. This is also supported by direct analysis of intercumulus plagioclase separates at **RPM** and to a lesser degree the single analyses at **Y** and **X**. In summary, there is no marked difference in the Sr content of cumulus and intercumulus plagioclase within the Unit and no marked lateral variation is evident over a distance of 171km.

e) Regression analysis of other "compatible" trace elements (Cr, Co, V, Zn, Ni and Sc) indicate that minor variations are evident between profiles (Figures 4.36 and 4.48). The bulk compositions, shown by the regression data of Cr, V, Zn and Sc, show that there is a distinct decrease in composition in a southerly direction away from Amandelbult and Union Sections. No discernible trend is, however, recognised for Co and Ni which display lateral consistency around the western Bushveld Complex. Lateral fractionation within the Bastard Unit is therefore recognised for Cr, V, Zn and Sc.

f) Levels of Cr, V, Co and Sc are different in the mafic phases when the habit changes from cumulus to intercumulus (whole-rock MgO < 4%). This suggests that these elements were preferentially included into the earlier-formed cumulus mafic phases, lower in the sequence, and by the time the intercumulus pyroxene crystallised the liquid was depleted of these components.

g) A number of geochemical parameters suggest that the composition of the basal part of the Bastard Unit has been affected by the infiltration of late-stage fractionated fluids which have been expelled from the underlying Merensky Unit. This phenomenon is described by Irvine (1980b) as postcumulus magmatic infiltration metasomatism. Only some of these parameters display clear geochemical breaks some distance above the base of the Unit, while most others indicate a more subtle influence, or overprint, from the underlying Merensky Unit, and continue the trend established in that Unit. Evidence of infiltration is provided by the following observations:

* Some samples at the base of the Bastard Unit display $Sr/Al_2O_3^*$ ratios which are higher than those in the main body of the unit and are more characteristic of those in the underlying Merensky Unit (Figure 4.55).

* Breaks in the trends of particular incompatible trace elements are not always coincidental with the base of a cyclic unit and it is often noted that a trend established in one cyclic unit continues into the overlying unit before reverting to more primitive values. Evidence of this phenomenon in the Bastard Unit is seen where trace element data are also available for the underlying Merensky Unit (**AE** in Field (1987); **UB**, **UC** and **UA** in Chapter 3; and the two profiles of Naldrett et al. (1984) in Figure 4.25). Incompatible trace elements which best display this feature are K_2O, Rb, Y and possibly Zr. Uninterrupted trends over the basal contact of the Bastard Unit, preceding a reversal to lower values, are indicated in the following profiles:

K_2O - Both Union and Rustenburg profiles of Naldrett et al. (1984) - Figure 4.25.
- **UA**, **UB** and **UC** in Figure 3.5
- **AE** in Field (1987, Figure 5.2). In contrast to all other profiles, there is an increase in K_2O within the first 2 (**AE**) or 3 (**AF**) samples at the base of the Bastard Unit at Amandelbult (Figure 4.25).

Rb - **UA**, **UB** and **UC** in Figure **3.10**. **AE** in Field (1987, Figure 5.5)

Zr - **AE** in Field (1987, Figure 5.5)
AF Figure 4.52

Y - Rustenburg profile of Naldrett et al. (1984) - Figure 4.25 (Not evident in their Union profile).

MnO - **UA** and **UC** in Figure **3.4** and **4.22**.

* The infiltration of late-stage fractionated fluids may also have contributed to the depression of both the whole-rock MMF_{WR} and orthopyroxene ratios at the base of the Bastard Unit.
The orthopyroxene MMF values here could have been depressed by the more evolved ratios (< 0.75) at the top of the Merensky Unit (Figure 3.3 and 4.57) and thus yielded a reversed fractionation trend seen at the base of the Bastard Unit. Conversely, it is possible that the reversed fractionation trend is a primary feature.

h) A progressive increase in the concentration of incompatible trace elements occurs towards the top of the GMA (TiO_2, K_2O, P_2O_5, Rb, Zr and Y). The highest concentrations of these elements, for leucocratic cumulates in the Upper Critical Zone, are recorded at the top of the Bastard Unit (Figure 4.56). Incompatible trace element concentrations in cumulates have been shown to be good indicators of the amount of trapped intercumulus liquid (Henderson, 1968; Naldrett et al., 1984). The higher concentrations of these trace elements within the UGMA would therefore indicate more efficient trapping of intercumulus liquid at this level, related to increased primary porosity.

Note: In Figures 4.56 and 4.57 an idealised, or "average", stratigraphic section was compiled for the Footwall, Merensky and Bastard Units in the western Bushveld Complex. Samples from separate profiles have been incorporated into this idealised column and are proportionately placed according to lithology and relative stratigraphic position.

i) Ni/Sc and V/Cr ratios display distinctive cyclicity within the units of the Upper Critical Zone (Figures 3.5 and 4.56). A suggestion of a reversal in the normal fractionation trend within the LGMA, similar to that seen for MMF ratios in orthopyroxene, is evident for both these parameters. Ni/Sc levels are particularly high at **UC** (Figure 4.49) in comparison with the other profiles and this factor, coupled with the occurrence of olivine in the profile, is perhaps a reflection of the overall increased mafic (or primitive) nature of the sequence at this locality.

j) Background Cu concentrations in the Bastard Unit are lower than those for the Merensky and UG2 Units, indicating an overall depletion in the amount of sulphide available within the unit. This feature indirectly emphasises the minor economic importance of this Unit.

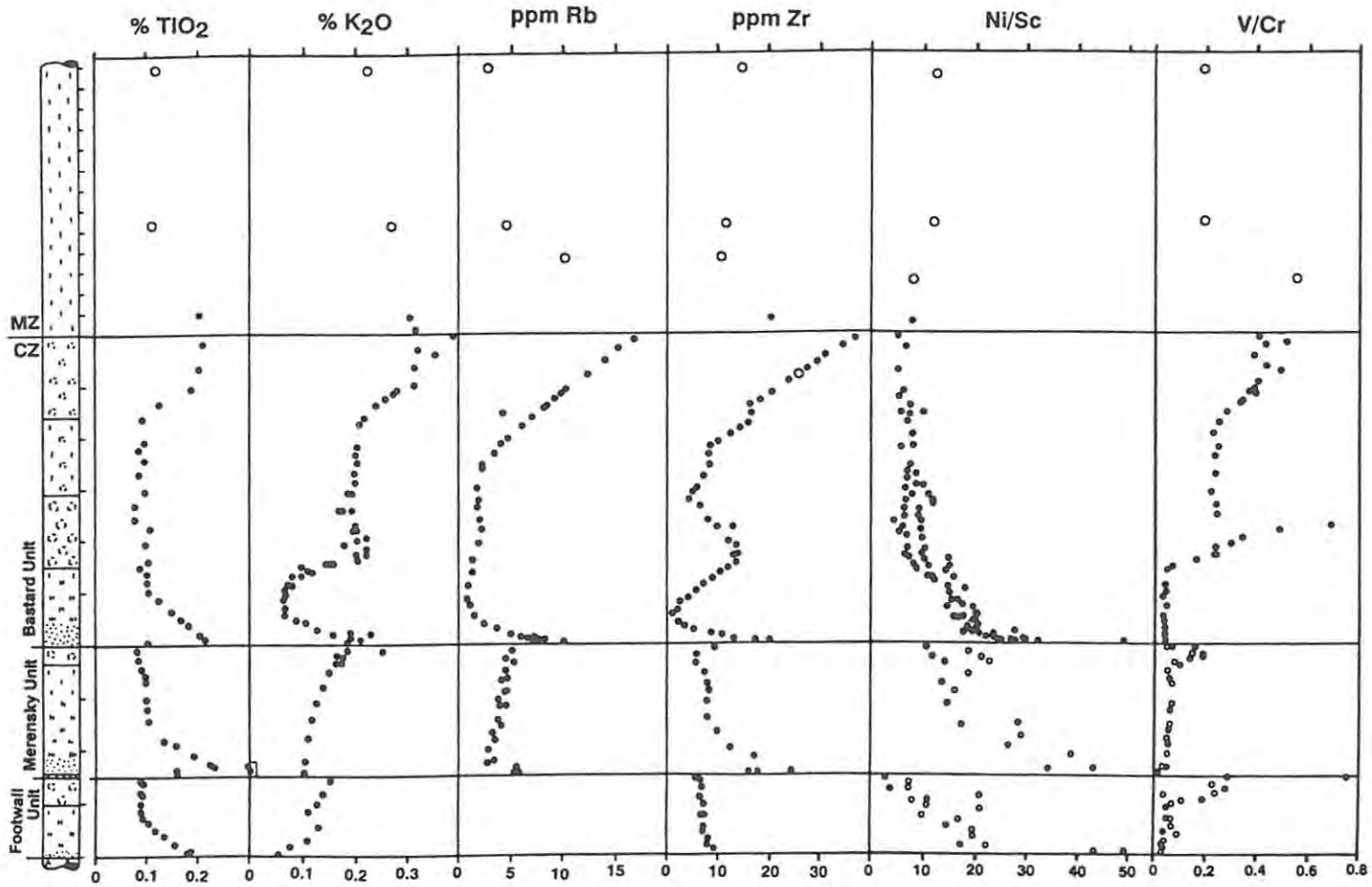

Figure 4.56 Composite plot of four incompatible trace elements and whole-rock Ni/Sc and V/Cr ratios through the Footwall, Merensky and Bastard Units and the lower part of the Main Zone. Additional data for the Footwall and Merensky Units of UB and AE have been extracted from de Klerk (1982; filled circles) and Field (1987; open circles) and for K_2O in the Bastard Unit from Naldrett et al. (1984). Open circles in the Main Zone represent data from Mitchell (1986). Although some scatter is evident within individual profile plots, this diagram illustrates the general trends for these elements. Vertical scale is indicated at 10 m intervals on the right-hand side of the column; note scale change within the Main Zone.

4.10 Diagnostic characteristics of the Bastard Unit.

The detailed cryptic variation pattern of the Bastard Unit is best illustrated in those profiles where a high sampling density has been achieved, best exemplified by **UA** and **RPM**. Other profiles reinforce the trends seen in these two and provide more detailed information about the lower part of the Unit. Any model which is invoked to explain the petrogenesis of the Bastard Unit in the western Bushveld Complex must account for the following characteristic features.

a) The Bastard Unit is the last of the cyclic units of the Upper Critical Zone and is appreciably thicker than those units in its footwall above the UG1 chromitite. The basal 20-25m of the Unit represents an almost exact duplication of the lithological sequence seen in the Footwall and Merensky Units but it differs from other units in having an abnormally thick sequence of leucocratic rocks in its upper half, above the pyroxenite - norite package. The textural characteristics and gross features of the LGMA are akin to those of the mottled anorthosites at the top of the Footwall and Merensky Units. In contrast, however, the overlying GMM and the UGMA, although comprising anorthosites, are quite different in appearance, texture and chemical composition.

b) It differs from units lower in the sequence by not having a lithologically well-defined top contact. This contact between leucocratic rock types of subtly differing textures is rather diffuse over 20cm. It is occasionally difficult to recognise in borehole cores and a degree of confusion has been evident, both in the literature and in exploration borehole logs. The positioning of the upper GMA contact has sometimes been erroneously taken at the more prominent top of the LGMA. It is, however, readily recognisable in underground haulage and crosscut exposures. Well-defined contacts are evident at the base of the Unit, the base of the GMA and the top of the LGMA, while the pyroxenite - melanorite boundary is more gradational. These features and the internal layering of the sequence emphasise the distinctive layering displayed within the Unit, in marked contrast to the more massive character of the Main Zone where layering features are subdued.

c) Apart from the "gap zones" mentioned in **4.4**, the Unit occurs throughout the western limb of the Complex over a strike distance of c. 200km.

d) The thickness of the Bastard Unit is reasonably consistent at c. 60m between Rustenburg and Amandelbult. A thinning of the Unit is apparent in an easterly direction from **RPM** through **WP** (42m) and then further to the east where a particularly thin sequence is encountered at Brits (**LEF** 2.61m). The more common thickness of c. 60m is closely matched in the eastern Bushveld (Cousins, 1969).

e) Footwall rocks of the Unit are in all cases mottled anorthosites. This indicates that, unlike the Merensky Reef, the Bastard pyroxenite has the same footwall lithology throughout the western Bushveld Complex.

f) The basal contact of the Unit is characterised by a pervasive bedding plane shear. Occasional undisturbed exposures of the basal contact are seen where the shear is absent or displaced into the footwall or hanging wall succession. Here the contact is undulatory with a thin chromitite seam developed between the footwall mottled anorthosite and the overlying Bastard pyroxenite.

g) The basal part of the Bastard pyroxenite, within the first 20cm, is characterised by the ubiquitous presence of base metal sulphides and PGE mineralisation and the occasional development of a coarse-grained pegmatoidal texture.

h) There is a change from orthocumulate texture within the pyroxenite (± pegmatoid) to mesocumulate in the melanorites and norites and finally adcumulate texture in the leuconorite and anorthosite (LGMA) in the lower half of the Unit. This is a gradational change. The adcumulate texture then gradually gives way through the GMM to orthocumulates which are dominant within the UGMA. This change is mirrored by the progressive upward increase in plagioclase zoning and higher concentrations of incompatible trace elements towards the top of the Unit.

i) Olivine-bearing lithologies, especially norites and troctolites, are rare in the Upper Critical Zone, particularly above the level of the Merensky Reef. Olivine does, however, occur in the paragenesis within the Bastard noritic sequence of profile **UC**. The olivine composition ($Fo_{79 - 81}$) is characteristic of other Upper Critical Zone occurrences.

j) Abundant small, rounded and embayed plagioclase inclusions (primocrysts) are enclosed within poikilitic cumulus orthopyroxene and anhedral olivine in the norites and to a lesser degree the basal pyroxenites. These plagioclase inclusions are randomly scattered throughout the orthopyroxene grains and are not preferentially concentrated along the margins or in the cores of grains. There is also a suggestion that these small plagioclase inclusions have been incorporated into larger cumulus plagioclase crystals, especially in the GMA (**4.8.3** grain in **X**-768.5).

l) Orthoclase (K-feldspar) appears as a minor intercumulus phase in the upper part of the GMA (see **4.6.4**). This observation is reinforced by the whole-rock data which indicates higher concentrations of K_2O and Rb in the UGMA. A marginal increase in the K_2O concentration of plagioclase is also evident at this level (Figure 4.17, **RPM**).

m) The variation of An content for cumulus plagioclase through the Bastard Unit displays a trend different to that of the fractionation pattern shown by the MMF ratios in orthopyroxene. There is a distinctive decoupling of cryptic variation trends between these two phases.

n) The Bastard Unit displays a particularly wide range of orthopyroxene MMF values (0.536 - 0.835) and the vertical cryptic variation pattern through the Unit has a distinctive double-cuspate form, quite different from the cycles below. The upper is more evolved than that at the base (Figure 4.57). This double-cuspate pattern is recognised in all the studied profiles, though minor deviations do occur (**4.8.1**). A remarkable feature of the basal Bastard pyroxenite samples is that little or no variation occurs in orthopyroxene MMF ratios over a strike distance of 171km - a constant value of 0.804 is indicated at this level. A reversed fractionation trend is evident within the first 4m of the Unit before

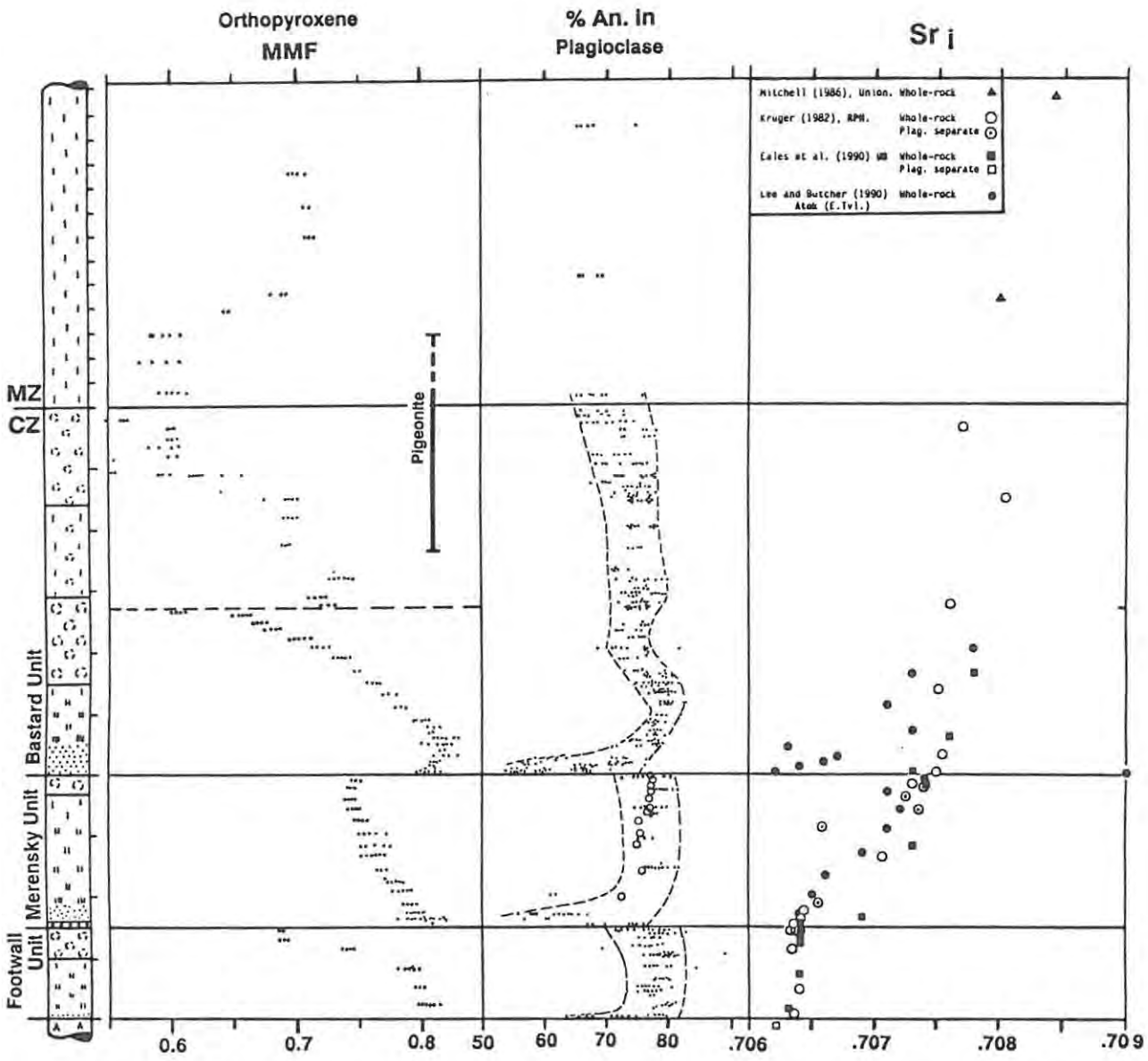

Figure 4.57 Composite plot showing the variations in the orthopyroxene MMF ratio, %An in plagioclase and the initial Sr isotope ratio through the Footwall, Merensky and Bastard Units and the lower part of the Main Zone. Vertical scale is indicated at 10m intervals on the right-hand side of the column; note scale change within the Main Zone.

MMF orthopyroxene. - Main Zone data have been compiled from Union Section and the **LEF** (Brits) area (Mitchell, 1986 and 1989). Merensky Unit data at Union Section has been extracted from de Klerk (1982) and Naldrett et al. (1984) while that for Amandelbult is from **AE** (Field, 1987) and **RPM** (Kruger, 1982). Footwall Unit data are from Naldrett et al. (1984). The occurrence of inverted pigeonite is also indicated at the top of the Bastard Unit and the lower part of the Main Zone.

%An in plagioclase. - Main Zone data from Mitchell (1986). Data for the Bastard Unit have been compiled from **RPM** (Kruger, 1982), **Y**, **X**, **UA**, **UC**, **AE**, and Naldrett et al. (1984). Data for the Merensky and Footwall Units are from **UB** (de Klerk, 1982), **AE** (Field, 1987), and open circles in the Merensky Unit indicate the average composition of cumulus plagioclase (10 - 14 analyses) at **RPM** (Lee, 1983). An envelope indicating the range of composition reported in Naldrett et al. (1986) is shown for the Footwall and Merensky Units.

Initial Sr isotope (Sr_i). This plot incorporates data for both the eastern and western Bushveld Complex.

peak MMF values of 0.82 are recorded at the gradational pyroxenite - melanorite contact. From this level the MMF ratios decrease through the norites and LGMA (to 0.62-0.68) before a marked reversal to higher MMF ratios (0.70-0.75) is seen within, or at the top, of the LGMA. This distinctive reversal is also evident for other geochemical parameters, notably %FeO in plagioclase (Figure 4.18), whole-rock MMF_{WR} (**Y** and **AE** in Figure 4.21), Ni/Sc, and especially V/Cr (Figures 4.56).

The stratigraphic position of the reversal is variable and is not coincident with any marked change in lithology nor is it confined to the mottled anorthosite. The majority of profiles indicate that it occurs either at the top or middle of the LGMA and it is only in profile **Y** that it occurs below the LGMA in the leuconorite. An important facet of this trend is that it does not matter what the textural status of the pyroxene is (intercumulus or cumulus), the MMF ratios behave coherently and lie on a continuous trend across the textural boundary. The pattern above the reversal is one of gradually decreasing MMF through the GMM before a marked drop to values below 0.60 is seen in the UGMA. This decrease is coincidental with the occurrence of inverted pigeonite with its characteristically higher Fe content. Low MMF values ($\leq$ 0.60) continue across the upper Bastard Unit contact into the Main Zone for c. 30m before gradually reverting back to MMF ratios of c. 0.70.

o) Primary inverted pigeonite occurs as a crystallising phase in the upper half of the GMA and remains in the paragenesis for c. 30m into the basal part of the Main Zone.

p) The Bastard Unit is geochemically coherent with regard to Sr and displays its own characteristic signature when compared with other underlying units of the Upper Critical Zone and the overlying Main Zone (see **4.9.3d**). Sr content is the same for both cumulus and intercumulus plagioclase in the same profile and no discernible lateral variation is seen around the western limb of the Complex.

q) Trends for some incompatible elements like K_2O, Rb, Zr, and to a lesser degree Y, indicate a degree of infiltration (metasomatism) within the basal part of the sequence. Geochemical breaks to lower values for

these elements are not at the basal contact of the Unit but are displaced upward into the Bastard Unit and are located at, or near, the pyroxenite - melanorite boundary. Parameters such as the $Sr/Al_2O_3^*$ ratio and possibly the reversed fractionation of MMF ratios (both whole-rock and orthopyroxene) at the base of the Unit support the concept of infiltration of residual liquids from the top of the Merensky Unit.

r) There is a progressive increase in the concentration of incompatible trace elements towards the top of the GMA (see **4.9.3h**).

s) Simple regression analysis of whole-rock data for individual Bastard Unit profiles indicates that little or no lateral variation occurs for Sr, Co and Ni throughout the western Bushveld Complex. A degree of lateral variation does, however occur in the case of Cr, V, Zn, and Sc. A pattern of decreasing Cr levels is observed in the pyroxenes at the base of the Unit from the northwestern sector of the Complex towards the south. V, Zn and Sc levels display an overall increasing trend from north to south and possibly reflects an increase in the amount of clinopyroxene in the system. Some differences between profiles are explained by insufficient sampling densities within the profiles and localised secondary alteration of the succession. There is a general decrease in the absolute whole-rock MgO and increase in Sr contents of the basal pyroxenite samples away from Union Section (see **4.9.3b** and Figure 4.54)

t) Widely spaced samples through the Bastard Unit at **RPM** (Kruger, 1982) and Union Section (Eales et al., 1990a) suggest that the values for initial Sr-isotope ratios lie on a trend which is intermediate between those characteristic of the Merensky Reef and the underlying Upper Critical Zone (c. 0.7063) and those typical of the Main Zone - 0.7087 (Kruger and Marsh, 1982; Mitchell, 1986) (see Figure 4.57).

u). The occurrence of a mafic interval below the LGMA is recorded in profile **X** and has also been reported at several localities in the eastern Bushveld Complex (Cousins, 1969; von Gruenewaldt et al., 1985).

4.11 Discussion.

The basal contact of the Bastard Unit, where preserved, is not as distinctly dimpled as that at the base of the Merensky Reef and can be described as undulatory. These embayments, or "subdued dimples", in the anorthosite footwall, indicate removal of anorthosites before chrome-spinel accumulation. Fine-scale lamination of the cumulus plagioclase has been truncated which indicates that this feature is not due to slumping or loading within the crystal pile. Removal of the anorthosite could have taken place either by resorption, mechanical erosion or replacement. The absence of fragments of anorthosite within the Bastard pyroxenite suggests that resorption, perhaps aided by mechanical loosening, was the dominant erosive process in response to the influx of a hotter, more primitive magma pulse. Experimental studies of natural basalts by Hill and Roeder (1974) indicate that plagioclase appears on the liquidus between 1150° and 1200°C and these temperatures would therefore be a reasonable estimate for the temperature of magma at the time of crystallisation of the Bastard Unit. Further work of Roeder (1975) shows that the liquidus temperature of an olivine-saturated basalt is essentially a function of its MgO content and, with this in mind, Campbell et al. (1983) estimated that the temperature of the parental melt added to the Bushveld magma chamber was about 1325°C - assuming an MgO content of 13%. Campbell et al. (1983) estimated a difference of 100 ±50°C between the temperature of the resident crystallising magma (supernatant liquid) in the chamber and that of a new pulse which formed the cyclic units of the Upper Critical Zone. This temperature difference aided limited resorption of the footwall plagioclase cumulates.

The origin of chrome-spinel at the base of major cyclic units in other intrusions has been the subject of much debate in the literature. Henderson and Suddaby (1971), who worked on the Rhum chromites, proposed that the chromite at the base of the cyclic units was the consequence of the position of chromite on the liquidus of the Rhum parent magma, early-formed chromite being concentrated by settling into layers. They also recognised that post-cumulus reaction of chromite with olivine, plagioclase, and intercumulus liquid had taken place to give a more aluminous chrome-spinel. A subsequent explanation was offered by Huppert and Sparks (1980), who proposed that an influx of picritic liquid into a

magma chamber hybridized with a little evolved liquid already present in the chamber, and that this was able to melt the anorthositic floor, with chrome-spinel resulting from the reaction of floor melt and hybrid liquid.

Limited exposures of the Bastard basal chromitite seam show that it is a more robust layer in the Union Section area and is made up of larger cumulus grains. In contrast, however, the chrome-spinel layer at **LEF** is thinner, patchy and highly irregular with a significantly reduced grain-size. It appears therefore that cumulus chromite settled out of a newly emplaced magma in the Union Section area and that the finer irregular chromite at **LEF** precipitated in situ at the mush-magma interface in response to mixing of liquid expelled from the underlying porous cumulate pile (Irvine, 1980b) with the newly emplaced Bastard magma in the chamber. This mechanism was also proposed by Young (1984) to account for the irregular fine-grained chromitite layer at the Unit 7-8 boundary in the Eastern Layered Series of the Rhum intrusion.

The occasionally coarse-grained pegmatoidal nature of the Bastard pyroxenite, within the first 10 - 15cm of the basal contact, is considered to be the result of recrystallisation of the early- formed orthocumulate by late magmatic fluids. Barnes and Campbell (1988) and Naldrett et al. (1987, p.387) invoked this mechanism to explain the distinctive pegmatoidal nature of the Merensky Reef. The pegmatitic texture in the Olivine-Bearing Zone of the Stillwater Complex (which hosts the J-M Reef) is also ascribed by Campbell et al. (1983) to a generally higher abundance of trapped intercumulus liquid, resulting in localised late-stage recrystallisation.

Lauder (1970) hypothesised that a final volatile-rich fluid was expelled from the floor rocks after the formation of the Merensky Unit and infiltrated the base of the Merensky pyroxenite. Kruger and Marsh (1985) suggest that this caused the otherwise refractory pyroxenite to remain partially molten for an extended period. They attribute the pegmatoidal character, unusual chemistry, and redistribution of the sulphides (noted by Brynard et al. (1976) and Mostert et al. (1982)) to the extended time available for crystallisation and the presence of additional fluid.

Barnes (1986) pointed out that three principal factors must be taken into account when interpreting mineral compositions in cumulate rocks:

1) redistribution of elements due to sub-solidus re-equilibration between minerals.
2) superimposed modification of mineral compositions as a result of crystallisation of trapped intercumulus liquid;
3) changes in the composition of the parent magma due to fractional crystallisation, contamination, magma mixing etc.

The absence of any marked pattern of zoning between the cores and margins of cumulus orthopyroxene grains suggests that diffusion occurred between the cores and the margins within the overgrown cumulus orthopyroxene grains. The final composition is now the weighted average of the original cumulus (i.e. liquidus) composition and that of the postcumulus overgrowth. Subsolidus re-equilibration has also had the effect of smoothing any compositional gradients that may have been present at the time of crystallisation. Barnes (1986) argues that subsolidus redistribution of Fe and Mg in response to changing distribution coefficients with falling temperature is small or even negligible in comparison to the effects of the trapped liquid shift. The data of Sack (1980) show that the olivine/orthopyroxene K_D is virtually independent of temperature in the range 1200 - 800°C for compositions typical of layered intrusions. Measured K_D's between co-existing olivine, orthopyroxene and clinopyroxene from the Stillwater Complex are indistinguishable from experimental values obtained at magmatic temperatures (Barnes and Naldrett, 1986).

Barnes (1986) suggested that the effects of "trapped liquid shifts" from that of the initial precipitated cumulus crystals to the final composition after solidification in orthocumulates would be greater than subsolidus re-equilibration effects. Barnes (op. cit.) modelled the effect of the trapped liquid shift on a typical cyclic unit of the Upper Critical Zone and made use of the data of Kruger and Marsh (1985) at **RPM**. He assumed that the starting composition of the orthopyroxene was En_{84} and, without the benefit of petrography and whole-rock trace element data, assumed that the initial porosity of the cumulate pile was 30%

throughout the sequence from the base of the Bastard Unit to the top of the LGMA. The modelled final composition of orthopyroxene after solidification (Barnes, 1986, p.527) approximates the measured values reported by Kruger and Marsh (1985).

An estimate of the initial porosity in the rock (i.e. the initial proportion of trapped liquid in intercumulus space), based on petrographic evidence and the levels of whole-rock incompatible trace elements, has been made for the Bastard Unit. Levels of incompatible trace elements have been shown to be an effective indicator of the amount of trapped interstitial liquid at the time of crystallisation (see **4.9.3h**), and levels of Rb and Zr (Figure 4.56) indirectly indicate the porosity of the crystal pile. By adopting the 30% porosity estimate used by Barnes (1986) in the basal pyroxenite an **estimated** "porosity index", based on the whole-rock Rb levels in Figure 4.56, was calculated for the **UA** profile. Within the basal pyroxenite the assumption is made that a value of 8ppm Rb would represent a porosity of 30% (% porosity = Rb x 3.75). By assuming the same starting composition of orthopyroxene (En_{84}) and utilising the theoretically calculated curves for final bulk composition of cumulus plus adcumulus orthopyroxene versus initial composition of cumulus grains (Barnes, 1986, p.525, Fig.1a and 1b) the effect of trapped liquid shift was modelled in the **UA** profile (leucocratic rocks above 10m in **UA** were modelled on Barnes' Fig. 1b).

As shown in Figure 4.58 the pattern of the modelled trapped liquid shift compositions approximates the actual measured orthopyroxene compositions. These modelled compositions are in all cases more magnesian than the measured values and this could be attributed to either an inaccurate porosity estimate, an over-estimate of the original Mg-content of the orthopyroxene or a combination of both these factors. The greater divergence between actual and modelled values seen through the GMM and the UGMA (Figure 4.58) is a function of:

1) the use of marginally inaccurate theoretical curves which are based on a 40% concentration of cumulus orthopyroxene (in reality rocks within the GMA contain up to 10% intercumulus orthopyroxene), and
2) progressive fractionation and blending within the last remaining volume of residual (supernatant) Critical Zone liquid.

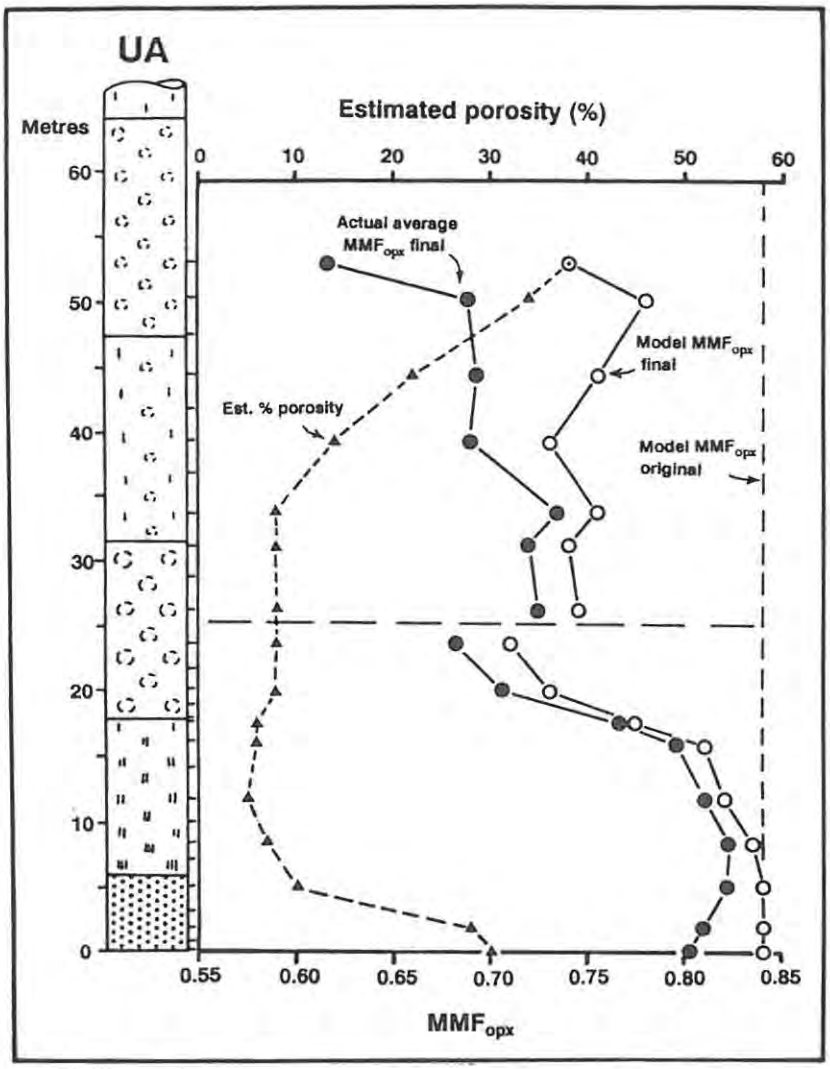

Figure 4.58 Comparison of the average measured orthopyroxene MMF ratios (filled circles) with the modelled "trapped liquid shift" compositions (open circles) in profile **UA**. The layer is assumed to start with a constant orthopyroxene composition of En_{84}. An estimate of the initial porosity, based on Rb concentrations, is indicated by filled triangles (% Porosity = Rb x 3.75).

The adoption of a trapped liquid shift model to account for the observed cryptic variation through the Bastard Unit does at first glance appear to be an attractive one, but is perhaps too simplistic. The model implies that the cumulates completely re-equilibrated with trapped liquid. The stratigraphic significance of cryptic variation would, in this case, be suspect as it must have been modified by intercumulus reactions, and these would depend critically on the mode of the cumulus assemblage and the proportion of the trapped magma. Other reasons for not adopting this approach would include the following:

1) The MMF ratio of the intercumulus liquid is unknown.
2) The shift does not necessarily have to be one of solid to solid but could rather be the result of a mixing of liquids to yield the same trends, i.e. by the primary crystallisation of mixed and fractionated liquids.
3) A trapped liquid shift could not account for the appearance of inverted pigeonite as this would imply that solid orthopyroxene (MMF = 0.84) would shift to pigeonite. It would seem more likely that the pigeonite crystallised directly from a liquid as it is typically intercumulus in habit, occupying "angular" intercumulus space between larger euhedral to subhedral cumulus plagioclase crystals.
4) The %An in plagioclase (Figure 4.57) does not show a shift to sodic compositions when orthopyroxene goes to Fe-rich compositions.
5) The V/Cr ratio (Figure 4.56) shows the highest values in the middle of the LGMA where the indicated porosity is the lowest.
6) It is difficult for the trapped liquid shift to account for the additional pyroxenite below the GMA in profile **X**. Here the Rb content is below detection limits (indicating a low porosity) yet the MMF ratios are low. This would imply a considerable shift and that an enormous porosity, in excess of 60%, would be required to shift a pyroxenite to MMF 0.75.

It is thus evident that the trapped liquid shift model is unconvincing, and that the same results could be achieved by assuming that the effects are primary. It is considered that fractionation linked to mixing with an overlying fractionated supernatant liquid produced the resultant profile of MMF ratios through the Bastard Unit (both whole-rock and orthopyroxene). The trapped liquid shift might have had some influence on the final orthopyroxene composition and was perhaps more significant in the lower part of the Unit where the mafic cumulates are more orthocumulus in character. The minor, yet distinctive, reversal recognised at the level of the LGMA is suggestive of a final, less robust, influx of primitive magma which was unable to initiate the crystallisation of cumulus orthopyroxene. It should be appreciated that the liquid-shift approach represents, in effect, a modification of the broader principle of mixing. What it implies is, effectively, a liquid-solid mixing event. The results of the calculations would not differ

greatly from those relying on liquid-liquid mixing, or the mixing of mushes of crystals and liquids. Hence apparently successful modelling of the process does not yield a definitive answer.

The reversed fractionation trend displayed by increasing orthopyroxene MMF ratios in the basal 4m of the Unit can be attributed to the mode of crystallisation and the amount of trapped interstitial liquid in the cumulate pile. Factors which aided in depressing the MMF ratios towards the base of the Unit could have been the following:

(a) Assimilation (resorption) of the floor rocks with significantly lower MMF ratios (0.75, Figure 4.57) at the time of emplacement of a new magma influx. The "dimpling" of the footwall anorthosite suggests that this is a factor.
(b) A basal flow model for the emplacement of the Bastard magma may account for small amounts of fractionated supernatant liquid that could be incorporated into the base of the flow-front by turbulent mixing. This residual liquid could have become incorporated into the basal part of the flow and would have had the effect of shifting the compositions of cumulus orthopyroxene to more evolved compositions.
(c) Infiltration of residual liquid from the underlying Merensky Unit is considered to have been a continuous yet waning process. After crystallisation of primary cumulus orthopyroxene additional growth from the infiltrated residual liquid occurred in interstitial space. This had the effect of both lowering the MMF ratios and elevating the incompatible trace element concentrations within the basal pyroxenite.

Plagioclase compositions through the Unit vary in a manner inconsistent with normal progressive fractionation of a melt and do not follow the same down-temperature pattern of fractionation established for orthopyroxene. The indicated compositional range of plagioclase in Figures 4.16 and 4.57 is perhaps not representative of the total range, as the majority of analyses in these profiles were done on the cores of grains alone. The two profiles of Naldrett et al. (1986) do, however, highlight the wide range of plagioclase compositions and the extent of the zoning within the orthocumulates at the top and bottom of the Unit. A

more restricted compositional range is evident within the middle part of the Unit where the rocks are more adcumulate in nature. The An content within one cumulus grain alone can vary by as much as 15% but is more commonly c. 10%. Intercumulus plagioclase within the basal pyroxenite (orthocumulate) has a lower An content than that of cumulus habit in the norites and LGMA. Compositional ranges of intercumulus plagioclase are also much greater, being in excess of 15% An. The zoned plagioclase crystals which are evident within the upper part of the GMA (GMM and the UGMA) are considered to be relict cumulus grains which preserve some of the magmatic history of the Upper Critical Zone. These oscillatory zoned crystals, of varying zonal complexity, represent grains that were not incorporated into the cumulus pile for some time but were buoyed upward in the accumulated supernatant liquid before being trapped near the top of the Bastard Unit. The zonal overgrowths therefore represent crystal growth associated with earlier magma pulses that produced the underlying cyclic units of the Upper Critical Zone.

A decoupling of the trends of cryptic variation in feldspars (%An) and pyroxenes (MMF in orthopyroxene) for the Footwall, Merensky and lower part of the Bastard Unit has been well established (Cameron, 1982; Lee, 1983; Naldrett et al., 1984; Kruger and Marsh, 1985; and Eales et al., 1986 and 1988). Within the Bastard Unit the decoupling of trends is especially pronounced through the norite and LGMA succession (Figure 4.57). Pronounced decoupling is also evident through the GMM and the UGMA. Reversals of trend in one need not be matched by reversals in the other, and upward Mg depletion in orthopyroxene may accompany Ca enrichment in plagioclase. Eales (1987, p.160) noted that it is difficult to accept that the decoupling of cryptic variations is in response to the lowering of the liquidus temperatures by accumulation of volatiles, or intracyclic intrusion of new magma. Morse (1979c) pointed out that plagioclase by itself may account for only about a quarter of the total Ca depletion during fractional crystallisation of augite-rich systems. In augite-poor systems, like the Upper Critical Zone, it accounts for most or conceivably all of the Ca depletion.

Evidence for Fe-enrichment at the base of the Main Zone (directly above the Bastard Unit - GMA) has been reported from several parts of the

Bushveld Complex both in the east and west (Meyer, 1969; von Gruenewaldt, 1973; Mitchell, 1986). This study and that of Kruger (1982) also show that iron enrichment, coupled with the presence of inverted primary pigeonite, occurs in the upper part of the Bastard Unit at a number of localities in the western Bushveld Complex. It would thus appear that this phenomenon is not localised but is in fact a fundamental characteristic of the boundary between the Critical and Main Zone throughout the Complex. Mitchell (1990a) suggested that the iron enrichment at the base of the Main Zone is not the result of infiltration metasomatism (Irvine, 1980b) from the underlying GMA, because crystallisation of these leucocratic rocks would have produced a dense rejected solute, which could not have migrated upwards into the overlying magma. He argues that the rejected solute from crystallisation of the leucocratic cumulates at the base of the Main Zone (his **Macro-Unit I**) would be charged with mafic components, particularly iron, and would therefore be relatively dense (Tait et al., 1984: Morse, 1986, 1988b). Tait et al. (op. cit.) showed that the concept of compositional convection need not necessarily apply only to liquids, but also to porous media like a crystal mush. If this were the case in the Main Zone Macro-Unit I, drainage and ponding of dense rejected solute would result in iron-enrichment, or crystallisation of iron-rich minerals, at the crystalline floor of the Main Zone magma chamber. Mitchell cites the presence of intercumulus inverted pigeonite as evidence of ponding of iron-rich liquid at this level.

The relative Fe-enrichment and the occurrence of primary inverted pigeonite within the upper half of the GMA, and upward into the base of the Main Zone, is here considered to be the result of fairly rapid crystallisation of the accumulated and fractionated supernatant liquid enriched in Fe and other incompatible elements.

The concept of a "proximal and distal facies" for the layered sequence, relative to a feeder system, was introduced by Eales et al. (1988, p.77). They noted that a consistent decline in whole-rock MgO values is evident in equivalent basal mafic lithologies of individual Upper Critical Zone units at Union, Amandelbult and Rustenburg Sections. This observation indicated that Union Section may be located closer to an irruptive centre

than are exposures to the north-east, or along the southern limb of the Complex. This hypothesis is supported by the work of Teigler (1990) in which he proposes that the concept of a proximal and distal facies is appropriate to explain the differences along strike of the Lower Zone and the lower Critical Zone in the western limb of the Complex. Eales et al. (1988) noted that particular layers at Union Section are invariably more mafic when compared to equivalent members some distance away from Union Section. The Merensky Reef is rich in olivine at Union Section; the amount is variable at Amandelbult and at Rustenburg the Reef is a pyroxenite with only isolated occurrences of olivine. The Pseudoreef Unit harzburgite declines from c. 36% MgO at Union to 31% at Amandelbult Section. Similar evidence to suggest a more primitive character at Union Section is cited for other units as well (see Table 1 in Eales et al., 1988). They indicate, further, that a good correlation is obtained when the stratigraphic thickness between the top of the UG2 pyroxenite and the Merensky Reef is plotted against the map distance from Union Section. The attenuation of this interval is at its extreme at Union Section and is doubtless due to a complex interplay of a number of factors. The correlation between inferred proximality to a feeder, and the contribution of cumulus plagioclase-bearing rocks to the total thickness of this interval also supports the hypothesis.

Results in this study, for the basal pyroxenites alone, broadly support the findings of Eales et al. (1988). Figure 4.54 shows the progressive decrease in whole-rock MgO and the MgO/Sr ratio with a concomitant increase in the amount of intercumulus plagioclase and whole-rock Sr levels away from Union Section. Some scatter is evident, especially for profile **X** but it must be noted that this point is based on one sample which is not quite at the base of the Unit and may be spurious. Although no whole-rock MgO values are available for the Bastard pyroxenite at **RPM** both the Merensky Reef pegmatoid and the Merensky pyroxenites do display lower MgO values than those reported at Amandelbult and Union Sections (Eales et al., 1988). It is considered unlikely that a deviation from this trend would be evident within the Bastard pyroxenite at **RPM**. The MgO/Sr ratio in Figure 4.54, which is a measure of the proportion of mafic phases to intercumulus feldspar, also reflects a progressive decrease in both directions away from Union Section (the highest ratio of 0.45 is recorded in **UB**).

If an irruptive feeder system is located in the vicinity of Union Section, then the Bastard magma influx would have had to be particularly mobile and remain as a coherent basal flow for a distance in excess of 132km. The more feldspathic nature of the basal pyroxenite towards **LEF** suggests that the Bastard magma influx was charged with a fairly high proportion of primary orthopyroxene crystals which settled out under gravity as the flow advanced through the chamber. The presence of olivine within the Bastard Unit norite at **UC** and the overall elevated Ni/Sc ratios at this locality would also lend support to the hypothesis that Union Section is located proximally to a feeder system and is therefore more primitive in character. Support for this hypothesis is also found in the work of Hartzer (1989, p.123) who reported on the stratigraphy, structure and tectonic evolution of the Crocodile River Fragment of Transvaal sediments (located c. 30km east of Union Section). He concluded that

> "Sedimentation of the Transvaal Sequence was terminated by the intrusion of the mafic magma of the Bushveld Complex through a feeder zone situated between the north-western edge of the basin and the fragment."

The exact nature of the feeder system is at best speculative but it is envisaged that fresh magma was channeled along the base of the cumulate pile in close proximity to the underlying sediments. It is thus postulated that fresh magma influxes entered the chamber, close to its outer flanks, and flowed inward into the arcuate chamber. The resultant cumulate pile of mafic and ultramafic rocks has the general shape of a tapering, inward-dipping sheet (see **1.2**).

The stratigraphic succession of the Unit is much the same at all localities. Profile **X** is anomalous as it includes an additional mafic layer (7.34% Al_2O_3) below the GMA. This additional layer seems, at first glance, to be a duplication of the Bastard pyroxenite, apparently localised in areal extent. Apparent duplications of the Bastard pyroxenite - melanorite sequence have also been recorded in the eastern Bushveld Complex at Maandagshoek, Eerstegeluk and St George (Cousins, 1969); more detail at Maandagshoek was provided by von Gruenewaldt et al. (1985). This apparent duplication could possibly be explained in the following ways:

1) Duplication by reverse faulting.

2) The Bastard pyroxenite was intruded/emplaced as an intact "sill" into a partially crystalline pile, with a coherent anorthosite footwall, and offshoots of the "sill" were developed locally. These secondary sill-offshoots were obliquely transgressive through the proto-norites and were then arrested at the base of the LGMA where they now prevail, parallel to the lower parent pyroxenite.

3) Localised gravitational settling of orthopyroxene, which was cotectically crystallising with plagioclase, resulted in the development of the additional pyroxenitic layer and the overlying LGMA.

The first mechanism is considered unlikely as no shearing was noted in the X borehole core. Reverse faulting in this part of the Complex is not common and where present the vertical displacement is usually no more than 5m (the interval between the two layers at X is 8m).

In its most extreme form the concept of multiple intrusion for the layered sequence of the Bushveld Complex was first proposed by Coertze (1958, 1974). He envisaged that the individual layers of differing rock types were intruded as a series of sills. This type of mechanism has been shown to be highly unlikely for the Bushveld Complex but a similar type of mechanism, on a much smaller scale, was proposed by Bédard et al. (1988) for peridotite sills which they recognised in the Eastern Layered Series (ELS) of the Rhum Complex. The peridotite and allivalite layers were found to be laterally discontinuous and were also seen to vary in both thickness and lithology. Bédard et al. (op.cit.) propose that many of the peridotite layers in the ELS of Rhum formed as thick sills of picritic magma emplaced into a partly solidified, layered troctolite.

If the (apparent) duplication of the Bastard pyroxenite was the result of a sill injection mechanism one would expect that geochemical characteristics of the two pyroxenites would be similar. This is not found to be the case, as the MMF ratios of orthopyroxene determined by microprobe in the upper pyroxenite are significantly lower (0.75) than

those in the basal Bastard pyroxenite (0.82). The sample taken from the upper pyroxenite clearly lies on the orthopyroxene MMF fractionation trend which is also seen in other profiles as well (Figure 4.7). Whole-rock MMF_{WR} ratios also show this phenomenon with a ratio of 0.803 recorded in the Bastard pyroxenite and 0.779 in the upper pyroxenite (Figure 4.21). A further reason why the sill hypothesis is unlikely to be applicable for the origin of the Bastard pyroxenite is that one would expect to see (a) more cross-cutting intrusive relationships, (b) sharp top and bottom contacts (with associated thin chromitite layers) and (c) local thinning and lensing of the pyroxenite. These features are not evident. More importantly, if the Bastard pyroxenite is the result of an intrusive mechanism it is difficult to envisage how such a "sill", of essentially uniform thickness (c. 5m) and constant stratigraphic position, could have been emplaced over such a vast area in this limb of the Complex (200km in length).

The third mechanism is considered to be the most plausible explanation for this duplication but it is difficult to explain why this layer is not more widely developed, as appears to be the case in the eastern Bushveld Complex. Eales et al. (1990a) suggested that the influx of a hot primitive liquid into the base of a column of residual liquid would cause resorption of some of the suspended plagioclase primocrysts in the residual liquid and would allow settling of the pyroxene crystals. On subsequent cooling, the residual liquid would have been in the primary phase volume of plagioclase, in which case anorthosite would have separated as a layer. The stratigraphic position of this pyroxenite layer is unique within the entire column, as it is located within the transition zone between the Critical and Main Zones. The composition of this additional layer may therefore have been influenced by the residual liquids of Critical Zone lineage interacting with the Main Zone liquids; this could possibly explain the lower MMF_{opx} ratios. Other possible reasons for the melanocratic nature of the layer are that

a) there was localised acceleration in the nucleation of orthopyroxene, or conversely, plagioclase nucleation was inhibited.
b) there was localised enrichment in heavy cumulus phases due to either settling processes or density currents. If density currents were responsible then one would perhaps expect MMF ratios which would not necessarily fall on the well-defined fractionation trend in this part of the sequence.

The initial strontium isotope (Sr_i = $^{87}Sr/^{86}Sr$) work of Hamilton (1977) was the first to establish that a significant increase in the Sr_i ratio was evident just above the Merensky Reef (from 0.7066 in the Merensky Reef to 0.7086 in Main Zone). More detailed work by Kruger and Marsh (1982) at **RPM** (Rustenburg), and that of Sharpe (1985) in the eastern Bushveld confirmed this increase to values characteristic of those in the Main Zone. A further Sr_i profile through the Middle and Upper Critical Zone (Eales et al., 1990a) and into the Main Zone (Mitchell, 1986) has been compiled at Union Section and displays a similar pattern to those of Kruger and Marsh (op. cit.) and Sharpe (op. cit.). Kruger and Mitchell (1985) report Sr_i values below the Merensky Reef at Union Section to be 0.7064 and those of the Main Zone to be c. 0.7090. All of the above studies were based on fairly wide-spaced sampling intervals, generally in excess of two metres.

Strontium isotopic data for the Bastard Unit in the western Bushveld <u>per se</u> are rather limited (**UB** - 3 samples; **RPM** - 6 samples) and suggest that the Sr_i ratios (0.7073 - 0.7080) are transitional between those typical of the Critical Zone below the Merensky Reef (c. 0.7064) and the higher values within the Main Zone (c. 0.7087) (Figure 4.57). Eales et al. (1986) point out that as Sr_i ratios cannot be affected by crystal fractionation, a mixing of new liquid (Sr_i = 0.7087) with an older liquid (Sr_i = 0.7064) through a vertical interval of 300m is a feasible hypothesis (i.e. from the base of the Merensky Unit into the Main Zone). An alternative explanation is that the magma influxes which formed the Merensky and Bastard Units had a significantly higher Sr_i signature, the bulk-rock value of which was modified by residual liquid (with a lower signature of c. 0.7064) which moved upward through the crystal pile from below.

A number of authors, including Kruger and Marsh (1982, 1985) and Sharpe (1985) have attributed the isotopic shift to an influx of isotopically distinct magma and have suggested that the presence of the Merensky Reef is related to this influx. Naldrett et al. (1987) concluded that the mixing of two somewhat different magmas can also account for the observed major and trace element compositional variations. Naldrett et al. (1987) do, however, point out that if the change in isotopic composition is

coincident with the change in Sr content of plagioclase in the eastern Bushveld at Jagdlust, it implies that the major influence of the new influx on the cumulate record was felt during formation of the Bastard Unit, not the Merensky Unit. Naldrett et al. (1987) report that the major decrease in the Sr content of plagioclase at Jagdlust occurs in the anorthosite of the Bastard Unit and not in the Merensky Unit. They raise the question as to whether the onset of crystallisation of this isotopically distinct magma is as important to the origin of the Merensky Reef as has been suggested. In addition, if a model is adopted that requires an influx of primitive magma to account in part for the development of the Bastard Unit then the available Sr_i data for the western Bushveld presents a problem as a resetting of the Sr_i ratio to lower values (c. 0.7064) would have been expected at the level of the Bastard pyroxenite.

These questions can perhaps in part be answered by the recently reported detailed isotopic work that was carried out by Lee and Butcher (1990) at Atok Platinum Mine in the eastern Bushveld Complex (Atok is a JCI-managed mine and is now called Lebowa Platinum Mine). Here the Sr_i profile through the Merensky Reef, Merensky Unit and lower part of the Bastard Unit shows a distinctive saw-tooth pattern of variation, quite unlike the simple step-like geometry generally reported (Kruger and Marsh, 1982, 1985; Sharpe, 1985; Eales et al., 1986; 1990a). Here, close-spaced sampling shows that the Sr_i ratios of the entire Merensky Reef are at 0.7064 - a value akin to those reported for the underlying Upper Critical Zone. Lee and Butcher (1990) showed that the increase to higher Sr_i ratios, described by Kruger and Marsh (1982) and Sharpe (1985), starts above the Merensky Reef and reaches 0.7074 at the top of the Merensky Unit (a value approaching those characteristic of the Main Zone). A previously undetected <u>reversal</u> to 0.7064 at the level of the Bastard Reef, before a return to higher Sr_i values with increasing stratigraphic height, is also reported by Lee and Butcher (op. cit.). This reversal supports the hypothesis that the basal part of the Bastard Unit represents the product of a magma influx with Critical Zone characteristics at the time that mixing was occurring between the (newly emplaced) Main Zone liquid (0.7087) and a column of residual supernatant Critical Zone liquid (0.7064) as originally proposed by Eales et al. (1986).

Lee and Butcher (op. cit.) report that this cyclicity is coincident with lithological variation, indicating that the mafic and felsic portions of these units did not form by simple, closed-system fractional crystallisation. More importantly, they report that there is **no** evidence for the mixing of magmas with contrasting Sr-isotopic signatures at the stratigraphic level where concentrations of the platinum element mineralisation occur in the Merensky and Bastard Reefs. The suggestion of Kruger and Marsh (1985), that the Bastard and Merensky Unit crystallised from a single batch of (blended) magma does not therefore receive support. The Atok data now suggests that the simple "mixing-line" trend, established by earlier workers, is in fact a saw-tooth pattern. At present there is no evidence from available Sr_i data in the western Bushveld that such a reversal is evident at the base of the Bastard Unit. The existence of such a reversal is suspected by the author and a detailed series of close-spaced samples over the Merensky - Bastard Unit contact is needed for confirmation.

The degree of geochemical similarity shown by both whole-rock trace element data and mineral compositions within the Bastard Unit profiles spread along strike suggests that there was efficient communication within a single or connected magma chamber at the time of crystallisation. Parts of the Upper Critical Zone sequence have subsequently been removed and the remaining "islands" of Lower, Critical and Main Zones are now separated by the Gap Areas. What is now seen as quite separate exposures of Upper Critical Zone rocks was a connected chamber at the time of crystallisation.

Lateral variations of cryptic and phase layering in cumulate rocks have in the past only received limited attention. As was mentioned in **4.1** the conventional method of investigating a sequence of layered rocks, especially in the Bushveld Complex, has been to collect a suite of samples along one traverse or vertical profile which is accepted as being representative in a particular area and to document phase and cryptic variations through the sequence. Studies involving close-spaced lateral variations in layered intrusions are now being recognised as being vital it the understanding of layered sequences. Wilson and Larsen (1982, 1985) and Wilson et al. (1987) have comprehensively described a two-dimensional study of a layered intrusion, the Fongen-Hyllingen layered mafic complex in Norway. The spatial relationships they report provide new insights

into the complexities of layered rocks. Wilson and his co-workers have, through their very detailed investigation, established that well developed rhythmic layering is markedly discordant with phase and cryptic layering in the southern part of the Fongen-Hyllingen Complex. Here eleven profiles (3-4km long) spaced over a strike distance of 10km of were investigated (an area similar in size to that at Union Section). The apparent angle between cryptic and modal layering was found to be ≤20° and lateral variations in mineral compositions are in some cases as great as those recorded in vertical profiles. Wilson et al. (1987) concluded that in situ crystallisation of a compositionally zoned magma took place along an inclined floor and this resulted in the discordant relationship between modal and cryptic layering. They suggested further that influxes of dense, primitive magma pooled at the floor of the chamber and elevated the compositionally zoned residual magma. Wilson et al. (op. cit.) established that the start of a major regression, reflecting the influx of fresh magma at the floor of the chamber, is concordant with modal layering and implies that the modal layering represents the crystallisation front. They envisaged that crystallisation of compositionally zoned magma took place along an inclined floor, with modal layering representing the crystallisation front and cryptic layering reflecting the composition of the stratified magma (Wilson et al., 1987, Fig. 14).

Other studies incorporating a lateral element in the synthesis include the work by Weibe and Wild (1983) at the relatively small Tigalak layered intrusion in Labrador (dominantly dioritic), while Klemm et al. (1985) investigated the vertical and lateral compositional variations across the Pyroxenite Marker in the upper part of the Main Zone. This latter study was carried out in an area 6km wide by c. 17km along strike in the Roossenekal area of the eastern Bushveld Complex. Like the work done by Wilson and his co-workers, both these studies revealed a degree of discordancy between modal and cryptic layering. The lateral strike-spacing of the profiles in this study was such that the distance between profiles was too great to reveal any subtle variations similar to those reported by the workers mentioned above. Further analysis of profiles both up- and down-dip of existing Bastard Unit profiles may well reveal some form of discordant relationship. Union or Amandelbult Sections, with their relatively close-spaced profiles, may be ideally suited for such a study in the future.

4.12 Upper limit of the Bastard Unit and the Critical - Main Zone boundary.

From Figure 4.1 and the discussion presented in **4.1** it is evident that no final consensus has as yet been reached regarding the position of the Critical - Main Zone boundary. Despite SACS (1980) formally placing this boundary at the top of the Bastard Unit (i.e. top of UGMA), the issue is as yet not resolved, and is still being debated by some (Kruger, 1990). Over the years it has been moved up and down the stratigraphic column, between the base of the Merensky Reef and the top of the Bastard Unit, by various researchers. These moves have, in many cases, been made without any concerted effort by the author concerned to provide supportive evidence for placing the boundary at a particular stratigraphic level, and all too often the exact contact has not been defined.

The early ideas regarding the position of this boundary were based on limited data, as workers on the Bushveld Complex at this time used gross lithological characteristics to sub-divide the layered sequence of the Complex, while mainly lithostratigraphic and petrographic criteria were used by workers between 1960 and 1970. A refinement of the criteria used for demarcating these boundaries, since the 1980's, has been supplemented by an ever-increasing body of geochemical and isotopic data.

A chronological review of the literature has revealed the following sequence of events regarding the definition of this crucial boundary (Figure 4.1):

Hall (1932) appears to have been the first to adopt formally the term **Critical Zone**, but the exact position of this zone, defined by him in the eastern Bushveld, is vague (p.275):

> "The Critical Zone (Critical Level) answers to the upper and greater portion of what P.A. Wagner termed the Differentiated Series south-west of the Pilanesberg in the Western Transvaal. The qualification of "critical" is chosen to emphasise the delicate conditions of adjustment in chemical and physical factors that must have existed in order to lead to the enormous variety of differentiates - some of extreme type - which form such striking features in this zone. ..... The upper limit of the Critical Zone is taken along the base of the overlying Main Zone, which is nowhere far off the eastern foot of the Lulu Range, ... "

Lombaard (1934), whose work was largely based on the Main Zone of the eastern Bushveld Complex, placed the boundary at the **top** of the Merensky Reef. Wasserstein (1936), working on the Critical Zone in the northwestern Bushveld, adopted Lombaard's division, in the vicinity of the Merensky Reef, but noted that the

> "anorthositic rocks which immediately succeed the Merensky Reef should be included in the Critical Zone to which they seem to bear a closer genetic relationship" (loc. cit. p.217).

The views of these two early workers represent the different schools of thought that have persisted regarding the position of the Critical - Main Zone boundary.

Feringa (1959), Cousins (1964, 1969) and van Zyl (1970), all geologists who have worked on the Critical Zone of the western Bushveld, favoured Wasserstein's (op. cit.) approach and placed this boundary at the top of the Bastard Unit. Those working on the Main Zone in the east, namely Willemse (1969), Molyneux (1970, 1974) and von Gruenewaldt (1971, 1973) favoured the base of the Merensky Reef, i.e. the contact between the basal chromitite and the Footwall mottled anorthosite.

Wager (1968) noted this confusion and in his interpretation he placed the contact at the top of the GMA of the Bastard Unit; this position has formally been adopted in the SACS (1980) recommendations (partly modified by Vermaak and von Gruenewaldt, 1986) and has been widely used in the literature (Cameron, 1982; Irvine, 1982; Eales et al., 1986, 1988; Viljoen et al., 1986a, 1986b; Naldrett et al., 1984, 1986, 1989; Gain, 1986; Leeb-du Toit, 1986; and Mitchell, 1986). These authors have not had the final say, for more recently Kruger and Marsh (1982, 1985), Sharpe (1985) and Kruger (1989, 1990) have strongly supported the case for the boundary to be placed at the base of the Merensky Reef, mainly on the basis of strontium isotope systematics.

Kruger (1990) argues that the level of the Merensky Reef marks the position of a major magma influx with the concomitant development of unconformable and transgressive relations with respect to the previously-deposited layered cumulates. He goes further to say that the Merensky and

Bastard Units should be combined into a **Transitional Macro-Unit** of the Main Zone as this would then take into account the intermediate character of the two units with respect to the Critical and Main Zones. In an apparent move from his original (1986) stand, Mitchell (1988) supported Kruger and Marsh (1985) by placing both the Merensky and Bastard Units into their **Transitional Macro-Unit** of the Main Zone at Union Section. In a later paper on additional magma influxes in the Main Zone, however, Mitchell (1989), reversed his position and once again placed the boundary at the top of the Bastard Unit.

The findings of Lee and Butcher (1990) discussed in **4.11** strongly support the view that the basal part of the Bastard Unit represents the product of a magma influx with Critical Zone characteristics at the time that mixing was taking place between the newly emplaced Main Zone magma and a column of residual (supernatant) Critical Zone liquid.

A number of possible stratigraphic alternatives regarding the position of the Bastard Unit can be considered (Figure 4.59).

1. On the basis of initial strontium isotope studies the Merensky and Bastard Units could both be included in the Main Zone, in accordance with Kruger's idea (1989 and 1990) of combining both into a **Transitional Macro-Unit** within the lower part of the Main Zone.
2. Recognising that both Critical and Main Zone characteristics are evident in the Merensky and Bastard Units it could be argued that they should be incorporated into a separate "Hybrid Zone" which is transitional between the Critical and Main Zones.
3. On the basis of geochemical, petrographic and new strontium isotope criteria (Lee and Butcher, 1990) both the Merensky and the Bastard Unit could be viewed as an integral part of the Critical Zone. This would not contradict the formally adopted position at the top of the UGMA (SACS, 1980).
4. The upper limit of the Bastard Unit could be taken at the top of the LGMA and both the GMM and UGMA incorporated into the Main Zone.

Essentially, only two Main Zone characteristics favour option (1) above. These include the elevated initial strontium isotope ratios and the

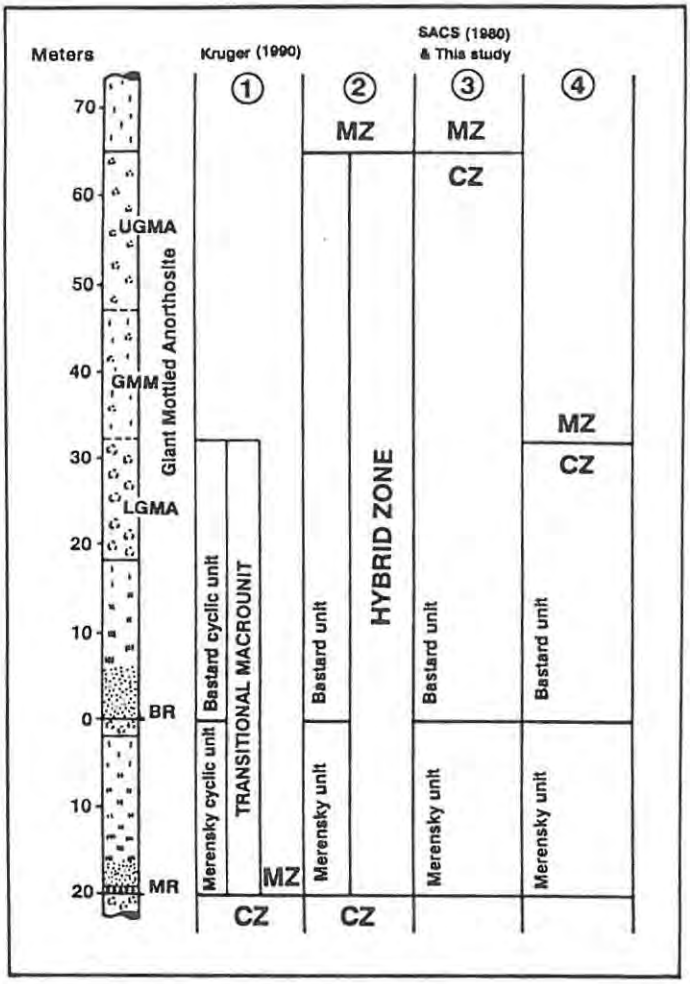

Figure 4.59 Four possible stratigraphic alternatives for the delimitation of both the Bastard Unit and the Critical - Main Zone boundary.

presence of inverted primary pigeonite in the upper part of the Bastard Unit. Mitchell (1986) showed that the occurrence of inverted pigeonite continued for a short distance into the overlying Main Zone leuconorites before reappearing again in the layered cumulates c. 1050m above the Merensky Reef. Inverted pigeonite is characteristic of the Main Zone but this minor occurrence within the Bastard Unit is thought to be an integral part of the final crystallisation of a fractionated supernatant residuum produced by crystallisation of a series of Critical Zone magma pulses.

By introducing a "Hybrid Zone" additional to the layered sequence (option 2), there will no doubt be inevitable objections to yet another name being added to the literature; an added complication which is not

justified in the light of the lack of support for this redefinition. Option (4) has distinct appeal as the contact at the top of the LGMA is well defined. Kruger (1982) re-defined the top of the "Bastard cyclic unit" at **RPM** Rustenburg Section at this level largely on the basis of its distinct lithological break and the fact that a compositional reversal occurred at this level. It was perhaps fortuitous that both these factors coincided at this level at **RPM** as this study has shown that the position of the reversal in cryptic variation is stratigraphically variable. Furthermore, the elevated incompatible trace element levels within the GMM and the UGMA suggest that these layers are an integral part of the Critical Zone as they represent the final crystallisation products of the most extreme fractionate produced by successive pulses of Upper Critical Zone magma.

Factors which favour option (3) include the following:

(a) Both the Merensky and Bastard Units are well developed and have striking petrographic similarities which are more in the style of the underlying UG1, UG2, Pseudoreef and Footwall Units of the Upper Critical Zone than of the overlying Main Zone. They both have mafic lithologies at their bases which become progressively more leucocratic upward through the sequence and, like the underlying Footwall Unit, they are both terminated at the top by mottled anorthosites. An important difference at the top of the Bastard Unit is that no sharp lithological contact (with a further cyclic unit) is seen. The contact is rather one of a textural difference between two leucocratic sequences - mottled anorthosite and leuconorite.

(b) Both Units contain the uppermost chromitite layers in the Bushveld layered sequence. Robust chromitite layers, as well as numerous thin seams and disseminations, typify the Critical Zone, whereas the Main Zone is essentially spinel-free.

(c) There is a high concentration of platinum group element (PGE) and sulphide mineralisation at the base of both the Units. Anomalously high concentrations of PGE mineralisation occur within other units of the Upper Critical Zone, which is a marked characteristic of some

layers (UG2, Pseudoreef, Merensky Reef and Bastard Reef). The Main Zone does not have any known significant PGE mineralisation.

(d) The base of the Merensky Unit, and to a lesser degree the Bastard Unit, typically has a well developed coarse-grained pegmatoidal texture in the pyroxenite. This pegmatoidal texture is also commonly seen in other Upper Critical Zone rocks.

(e) Magnesian olivine-bearing rocks ($>Fo_{76}$), like harzburgites and olivine-bearing norites, are only encountered in the Lower and Critical Zones of the Complex. Abundant magnesian olivine is encountered in the Merensky (Reef) and Bastard Units. The Bastard Unit is generally devoid of olivine but profile **UC**, at Union Section, has an abundance of this phase in the norites (Fo_{79-80}). No olivine is reported from the Main Zone but the iron rich species, fayalite, reappears in the Upper Zone.

(f) Cryptic variation trends established by Naldrett et al. (1984, 1986) and Eales et al. (1986, 1988) through both the Merensky and Bastard Units display distinct Critical Zone characteristics, particularly the decoupling of the An% of plagioclase and the MMF ratio of orthopyroxene. Cyclic variation in interelement ratios such as whole-rock MMF and Ni/Sc from primitive to evolved values, shows that the sequence conforms with the widely held concept of cyclic units.

Eales et al. (1986, p.573) showed that plots of whole-rock ratios MMF, Cr/Co, Co/V and Ni/Sc for the mafic rocks of the Upper Critical Zone (including the Bastard pyroxenite) exhibit ranges of values that are significantly different to the mafic lithologies within the first 1000m of the Main Zone, with virtually no overlap. Whole-rock MMF ratios for the Bastard pyroxenite are akin to those of basal mafic lithologies in other Critical Zone units (c. 0.7), while the MMF ratios of Main Zone mafic rocks are lower (c. 0.6). An abrupt change in geochemical signature occurs immediately above the Bastard Unit. Mafic rocks of the Upper Critical (including the Bastard Unit) and Main Zones thus appear to belong to discrete lineages.

In conclusion, the majority of diagnostic characteristics of both the Merensky and Bastard Units favour option (3) above. It is recognised that both these Units are transitional in nature, with respect to Sr_i, but it is the author's view that both Units display more Critical Zone characteristics than of the overlying Main Zone. Furthermore, the contact at the top of the GMA has already been formally adopted (SACS, 1980) and is well entrenched in the literature. The upper contact of the Bastard Unit, although not glaringly obvious in the field, is nevertheless easily recognisable and can been used as a mappable contact for this important boundary in the layered sequence.

4.13 Synthesis and model for the development of the Bastard Unit.

In the light of an ever-increasing body of knowledge about the physics of magmatic processes, researchers in the field of layered rocks have developed several magmatic models in an attempt to explain the sequence of events which produced these igneous rocks. Because of the economically important platinum deposits in the layered sequence of the Stillwater Complex and that of the Upper Critical Zone in the Bushveld Complex, close parallels have been drawn between them. Genetic models to explain these platinum ores have received considerable attention and they incorporate fundamental principles that have emerged from the work on other layered complexes such as Skaergaard, Rhum, Duke Island, Jimberlana, the Zimbabwean Great Dyke and others. These principles have been used to constrain genetic models which endeavour to explain the layered sequence in the Bushveld Complex. A brief account of some models that have been proposed during the last decade is presented below.

Various magmatic models.

A.) From detailed petrological and geochemical studies of igneous rocks and geophysical investigations of active volcanoes it is known that magma chambers are periodically replenished by influxes of new and generally hotter primitive magma from depth. **Huppert and Sparks (1980)** present a model which is based on the fluid dynamics of an influx of hot, dense, ultrabasic (picritic) magma into a chamber containing lighter, fractionated basaltic magma. This model suggests that the ultrabasic melt

does not immediately mix with the basalt, but spreads out over the floor of the chamber, forming an independent layer. A non-turbulent interface forms between this new layer and the overlying fractionated magma layer across which heat and mass are transferred by a process of molecular diffusion. Both layers convect vigorously as heat is transferred to the upper layer at a rate which greatly exceeds the heat loss to the surrounding country rock; convection continues until the two layers have almost the same temperature.

Huppert and Sparks (1980) propose that the layers remained distinct because of the low diffusivity of mass compared to that of heat. They suggest that for a layer of ultrabasic melt (18% MgO) a few tens of metres thick under a layer of more fractionated basaltic magma (10% MgO), a few kilometres thick, the temperatures of the two layers will approach each other over a period of between a few months and a few years. They suggest that during this time the turbulent convective velocities in the basal primitive layer are far larger than the settling velocities of olivines which crystallise within the layer during cooling. Olivines only settle after the two layers have nearly reached thermal equilibrium. At this stage the residual ultrabasic melt segregates as the olivines sediment in the lower layers and, depending on its density, the released residual ultrabasic melt can either mix convectively with the overlying fractionated basaltic layer, or can continue as a separate layer.

Because of the basic assumptions made regarding the initial starting compositions of the two melts, olivine is the dominant crystallising phase at the base of the new liquid in this model. Huppert and Sparks (1980) did recognise, however, that more complex crystallisation sequences are possible in basic and ultrabasic magmas, depending on pressure, temperature, volatile content and bulk magma compositions. Thus, for example, some ultrabasic magmas can precipitate highly calcic plagioclase. Other types of cumulates, like pyroxenites, could form before the residual magma in the lower layer becomes sufficiently light to mix with the overlying layer.

B.) Irvine, Keith and Todd (1983) and Irvine and Sharpe (1986) propose that the characteristic layering and cyclicity in both the Stillwater and

Bushveld Complexes can be explained by the interaction of two distinctively different magma types, i.e. the magmatic sequence is the product of the interaction between two parental liquids: an ultramafic (U_o) and an anorthositic (A_o) liquid. This model attempts to explain the origin of the J-M Reef (Stillwater) and the Merensky and UG2 Reefs (Bushveld) in terms of the unusual nature of both the Stillwater and Bushveld U-type liquids which they recognise as being boninitic in composition. These two postulated liquids (U- and A-type) had contrasting densities which enabled the two to form separate layers within the magma chamber, and the crystallisation and mixing was controlled by double-diffusive convection. The model has also been invoked to explain the massive chromitite and magnetite layers in both the Critical and Upper Zones respectively (Irvine and Sharpe, 1986).

The modelling of these two liquids requires that an assumed starting composition of each liquid is known. The postulated A-type liquid is calculated to be denser than the U-type liquid and its derivatives, with which it mixed. This then implies that the A-type magma was emplaced below the U-type magma and its derivatives. The fact that the overlying U-type is less dense because it is somewhat hotter than the underlying A-type results in finger mixing between the two magmas.

The field and geochemical evidence presented in this study tends to disprove Irvine et al.'s (1983) model of stratification and onlap transgression of magma. Laterally continuous layers are the norm both along strike and down-dip, and individual Upper Critical Zone units (as defined in this study) have been shown to display their own characteristic geochemical signature. An additional difficulty with Irvine's model is that, although U-type chilled sill phases have been recognised in the floor rock of the Bushveld Complex, no A-type equivalents have as yet been identified.

C.) Campbell et al. (1983) suggest that the PGE-rich sulphide reefs of the Stillwater and Bushveld Complexes were formed by a new pulse of picritic magma which entered the chamber as a jet or plume. During the early stages of fractional crystallisation, when olivine and orthopyroxene are crystallising, the density of the residual magma

decreases. If a new magma pulse enters the chamber it will be denser than the magma within the chamber and it will spread out across the floor as a basal flow. If the new pulse enters the chamber with sufficient momentum it will initially jet upwards into the overlying magma then fall back on itself when negative buoyancy overcomes the jet's initial momentum. During jetting the new pulse mixes with the host magma to form a hybrid melt which collects at the floor of the chamber, producing a gravity stratified layer with warm primitive magma overlain by cooler, more fractionated magma. On cooling the gravity stratified zone breaks up into a number of double diffusive convection cells.

Once plagioclase becomes a cumulus phase the density of the magma increases with increasing crystallisation. Eventually the density of the magma in the chamber becomes greater than that of the parental magma. A new pulse entering the magma chamber at a stage beyond the density crossover point will rise as a plume to the top of the chamber. During ascent the new pulse will mix turbulently with the host magma to produce a density stratified hybrid layer at the top of the chamber. In this case hot primitive magma will overlie cooler, more fractionated magma. Campbell et al. (1983) point out that the mixing of different magmas can produce sulphide liquation and that the turbulence associated with either jets or plumes can produce a very high **R** value (silicate/sulphide mass ratio). They suggest that the most favourable condition for producing a high **R** value is when a new pulse of hot magma is slightly lighter than the resident magma in the chamber. The new pulse will rise to its own density level, then spread laterally to form a density stratified intermediate layer in the form of a plume, which will rapidly lose heat to the cooler overlying host magma.

D.) An elegant model has been developed by **Naldrett et al. (1984, 1986 and 1987)** to account for both the J-M Reef at Stillwater and the Merensky Reef and its associated Upper Critical Zone sequence within the Bushveld Complex. This model is essentially a refinement and modification of that proposed by Campbell et al. (1983). Their contention is that the changes in the MMF ratio of orthopyroxene, Sr content of plagioclase and variations in the Sr_i ratio argue in favour of successive influxes of new magma into the chamber. They report that the rate of upward change in

these compositional variables was inconsistent with the different minerals (or even the different elements in any single mineral) coming from a single body of magma and conclude that fractional crystallisation cannot, by itself, account for the observed compositional variation. They suggest that the resident magma in the chamber was density stratified into a series of doubly diffusive convection cells (McBirney and Noyes, 1979) and that new magma entered the chamber of the intrusion with a density that was lower than that of the residual liquid overlying the crystal pile, but greater than that at the roof of the chamber.

The result of this density contrast was that the new magma rose rapidly as a turbulent plume, drawing within itself and mixing with some of the residual magma through which it was rising. The new influx then spread out laterally at an intermediate level of neutral buoyancy within the chamber. This layer of partially mixed new (hot) magma lost heat to the overlying cooler magma and caused the new layer to convect vigorously at first. As more heat was lost, mafic minerals (orthopyroxene and/or olivine) started to crystallise but remained in suspension while convection was still turbulent. With progressive cooling, the rate of heat loss decreased and convection then became laminar and the suspended crystals (plus sulphides) and some entrained liquid sank through the underlying magma as a series of down-spouts to spread out over the floor of the chamber.

Based on the work of Huppert et al. (1984) they hypothesise that little mixing would occur between the down-spouting crystal/liquid stream and the residual magma. The resultant mixture of mafic crystals, sulphides and liquid then crystallised to form the Merensky Reef. Naldrett et al. (1986) suggest that further cooling of the suspended new layer would increase its density and mixing with the underlying residual magma would occur to form a second, less primitive hybrid liquid which would crystallise orthopyroxene, followed by orthopyroxene plus plagioclase to form a noritic sequence. They further argue that this type of model can also account for the Pseudoreef and Bastard Units, which represent separate influxes of primitive magma. They conclude that the parental magmas have normal PGE contents for flood basalts, and that the platinum ores are due to scavenging by sulphide-laden plumes downspouting through the evolved magma.

E.) On the basis of a detailed study of cryptic variation of the main silicate phase and the strontium isotope signature of the Upper Critical Zone at RPM Rustenburg Section, **Kruger and Marsh (1985)** suggest that both the Merensky and Bastard Units were formed from the blended product of a new magma influx and the residual magma in the chamber. They argue that the Bastard Unit formed from the same batch of magma as the Merensky Unit and suggest that each cyclic unit may not necessarily be associated with a new magma influx but only with the crystallisation of the basal portion of a double-diffusive system. They also conclude that cyclic units are not necessarily associated with influxes of magma that are more dense than the residual liquid already present in the chamber.

F.) Eales et al. (1986, 1988 and 1990a) proposed a model which argues that the Upper Critical Zone at Union Section developed during a period of repeated influxes of primitive magma, emplaced along the interface between the floor and an overlying supernatant column of residual liquid. Largely on the basis of (i) wide variations in the proportions of leuconorites and anorthosites within separate cyclic units, (ii) the decoupling of cryptic variation in pyroxenes and feldspars and (iii) variations of Sr_i ratios between bases and tops of units, Eales et al. (1986) argue that the lower, ultramafic members of units are derivatives of new primitive mafic influxes. The upper, leucocratic members crystallised during progressive hybridization of the fractionated residua of each influx with the supernatant liquid column.

Both the Bushveld and Stillwater complexes are now regarded as the products of crystallisation of high-Mg, high-Si boninitic magmas. The capacity of the primitive liquid to deposit chromite and olivine at the base of Upper Critical Zone units, and their Sr-isotope and other geochemical characteristic led Eales et al. (1986) to link this liquid with a primitive, magnesian, Si-poor facies of the basaltic (tholeiitic) B2 type of marginal rocks defined by Harmer and Sharpe (1985).

The sequence of cyclical units in the Upper Critical Zone has been well documented and there is abundant evidence that individual units have been truncated or "beheaded" at various stages of growth. Eales et al. (1986) point out that units that terminate in pyroxenites in some areas,

continue upward into more feldspathic layers when followed along strike and conclude that a supernatant column of fractionated residua had collected above the crystalline floor. This supernatant liquid was relatively depleted in Mg and elements with high bulk distribution coefficients (Cr, Ni, and Co) which had gone into the formation of the mafic lithologies at the bases of individual units. It also had a depressed MMF ratio and an enrichment in the components of potential feldspar. Incompatible elements as well as H_2O would have been elevated in the supernatant column.

GENESIS OF THE BASTARD UNIT.

The Bastard Unit clearly continues the cyclical pattern of crystallisation recorded in the Upper Critical Zone and any model that is invoked to explain the development of this Unit must also account for the underlying units. Wagner (1929, p.196) was first to speculate on the origin of the Bastard Reef, based on its close similarity to the Merensky Reef ("main horizon"), and he had the following to say:

> "The Bastard Reef thus clearly owes its origin to differentiation of the same type as that which gave rise to the main horizon. It, however, normally carries only traces of platinum. It is to be concluded from this that when the process of differentiation normally accompanied by the magma segregation of platinum came to be repeated in this portion of the norite magma in question, this had been so depleted of that metal that a degree of platinum concentration comparable with that in the main horizon could not be attained."

The model of magmatic events leading to the development of the Upper Critical Zone, which is adopted in this study, is based largely on the genetic model proposed by Eales et al. (1986) and Scoon and de Klerk (1987). This model argues that the cyclic units of the Critical Zone developed in response to numerous influxes of primitive (**P**) magma that were emplaced into the chamber as hot, dense basal flows which reacted and mixed with an overlying less dense supernatant (**S**) liquid. Because it is relatively dense, the new magma remained at the floor of the chamber and elevated the overlying liquid column in a manner similar to that described by Huppert and Sparks (1980) and illustrated in experiments by Huppert et al. (1982).

In this study, the model is extended to account for the observed characteristics of the Bastard Unit which have been enumerated in section **4.10.** The sequence of magmatic events which led to the formation of the Bastard Unit specifically, is schematically portrayed in Figure 4.60. It is perhaps prudent at this stage to summarise some of the salient magmatic events proposed in the Eales et al. (1986) model prior to the development of the Bastard Unit and the reader is referred to the synthesis and schematic diagram in Eales et al. (1986, p.580) for more detail.

UNITS BELOW THE BASTARD UNIT

1. Reconstruction starts with a crystalline floor, made up of the Pseudoreef and UG2 Unit pyroxenite overlain by a column of supernatant (residual) **S-liquid** with a Sr_i ratio of c. 0.7063 - characteristic of the Upper Critical Zone rocks. This liquid represents the accumulation of residual magma which had been partially depleted of mafic components after the crystallisation of successive inputs of a primitive **P-liquid** which produced the underlying UG1, UG2 and Pseudoreef Units; all of these units are considered to be incomplete or "beheaded". The supernatant liquid is considered to be chemically evolved (fractionated) and also H_2O-enriched, with a fairly high concentration of small plagioclase and pyroxene primocrysts in suspension.

2. An influx of hot dense **P-liquid** was emplaced as a basal flow into the chamber and resulted in subsequent limited crystallisation of mafic cumulates at the base. As crystallisation proceeded, the liquid density of this layer declined and the diffusive interface with the overlying supernatant liquid column broke down.

3. Mixing now occurred with the overlying **S-liquid.** This was followed by the crystallisation of norites to form the lower half of the Footwall Unit and the distinctive anorthosites at the top of the Footwall Unit. The Sr_i ratio through the Footwall Unit remains the same as in the floor rocks while the compatible element ratios like MMF, Ni/Sc, Cr/V and Co/V are shifted towards those of the compatible element-depleted supernatant column.

A problem remains with the accumulation of anorthosites, in which there is no cumulus orthopyroxene and which could thus not have crystallised on the orthopyroxene - plagioclase cotectic, without efficient gravitative extraction of the orthopyroxene phase. A solution to this problem was presented in Eales et al. (1990a, p.40) where it was suggested that the influx of the hot primitive liquid into the base of the column of residual **S-liquid** caused resorption of some of the suspended plagioclase, and allowed settling of the pyroxene crystals. Consequently, on subsequent cooling, the **S-liquid** would have been in the primary phase volume of plagioclase, in which case anorthosite would have separated as a layer.

4. At this stage it is hypothesised that a substantial volume of Main Zone liquid was emplaced some hundreds of metres above the crystalline floor and the column of **S-liquid**, at a level where it was stable in terms of its temperature and density characteristics, i.e. commensurate with neutral buoyancy within the stratified liquid column. This new magma had a Sr_i ratio of c. 0.7090 and compatible element ratios characteristic of the composition of the Porphyritic Gabbro Marker in the Main Zone.

5. Subsequent progressive mixing of the Main Zone magma with the older (underlying) **S-liquid** yielded a hybrid liquid with gradational Sr_i ratios between 0.7063 and 0.7090.

6. A pulse of primitive hot, dense **P-liquid** now occurred at the crystalline floor (in this case anorthosite) and produced the mafic cumulates at the base of the **Merensky Unit.** These rocks display the same geochemical characteristics as the underlying Critical Zone lithologies in terms of their Sr_i ratios and various compatible element ratios. Important at this stage is the fact that this primitive liquid was above the feldspar liquidus and resulted in the partial resorption of the mottled anorthosite floor. This produced the distinctive dimpling at the bottom contact of the Merensky Reef. The assimilation products would have been incorporated within the basal liquid layer, changing its bulk composition and lowering its density.

7. Crystallisation of mafic phases within the basal part of the column resulted in the lowering of the density of the liquid and, as in paragraph **3**, the interface with the overlying hybrid liquid layer broke down and mixing between these two liquids occurred. Geochemical attributes now shifted towards those of the hybrid S-liquid layer and it is at this level that the first indication of a shift to higher Sr_i ratios is seen (Figures 4.57 and 4.60A). The liquid entered the primary phase volume of plagioclase by the same mechanism described in paragraph **3**, c. 5 atomic % richer in anorthite than the underlying norites, and mottled anorthosites were crystallised at the top of the Merensky Unit. At this stage the distinctive saw-tooth pattern of cryptic variation is well developed (MMF_{opx}). A cyclical repetition of the events, similar to those which produced the Merensky Unit, now occurred, resulting in the succeeding Bastard Unit.

8. THE BASTARD UNIT

Progressive stages in the development of the Bastard Unit are schematically depicted in Figure 4.60 - stages A to E.

Stage A. Crystallisation of the bulk of the Merensky Unit was almost complete, although the crystal pile had not yet solidified. It is proposed that at this stage fractionated interstitial liquid was still crystallising in intercumulus space within the anorthosite.

Extrapolation from the data embodied in Chapter 4, specifically Figures 4.55, 4.56 and 4.57, suggests the potential of the **S-** and **P-liquids** to deposit cumulates with the following attributes at the time of the development of the Bastard Unit:

S-liquid : - Sr_i ratio c. 0.7075 - a blended product of Main Zone (0.7090) and residual Upper Critical Zone (0.7064) liquids,
- MMF potential orthopyroxene c. 0.75,
- Potential plagioclase c. An_{80} (maximum),
- Whole-rock Ni/Sc < 10 and V/Cr ≥ 0.25,
- $Sr/Al_2O_3^*$ c. 12.1,
- Relatively high concentrations of incompatible trace elements,
- Numerous small plagioclase primocrysts in suspension.

P-liquid : - Sr_i ratio c. 0.7064 - characteristic of Upper Critical Zone lithologies,
- MMF potential orthopyroxene c. 0.84,
- Potential plagioclase c. An_{88} (maximum),
- Whole-rock Ni/Sc > 20 and V/Cr ≤ 0.05,
- $Sr/Al_2O_3^*$ c. 12.6,
- Relatively low concentrations of incompatible trace elements,
- Some primary orthopyroxene crystals (and chromite closer to the feeder) carried in suspension.

Stage B. Crystallisation of the Merensky Unit mottled anorthosite was then interrupted by an influx of hot, dense **P-liquid** into the magma chamber. The adoption of either a "plume" (Campbell et al., 1983; Naldrett et al. 1986) or a "basal flow" model (Eales et al., 1986) for the emplacement of the new magma into the chamber is largely dependent on the density difference between the resident magma in the chamber and the influx of fresh **P-liquid.** It is considered that a convincing case for either the "basal flow" or the "plume" mechanism could be argued for the development of the basal part of the Bastard Unit, as both models could explain the textural and geochemical features observed in the sequence. However, it appears more likely that the new pulse of **P-liquid** had a component of primary mafic crystals in suspension (see **4.11**) and would have included orthopyroxene, and perhaps chromite and olivine closer to the feeder zone. Only a small percentage of crystals within the new magma pulse would have been sufficient to raise the density of the incoming

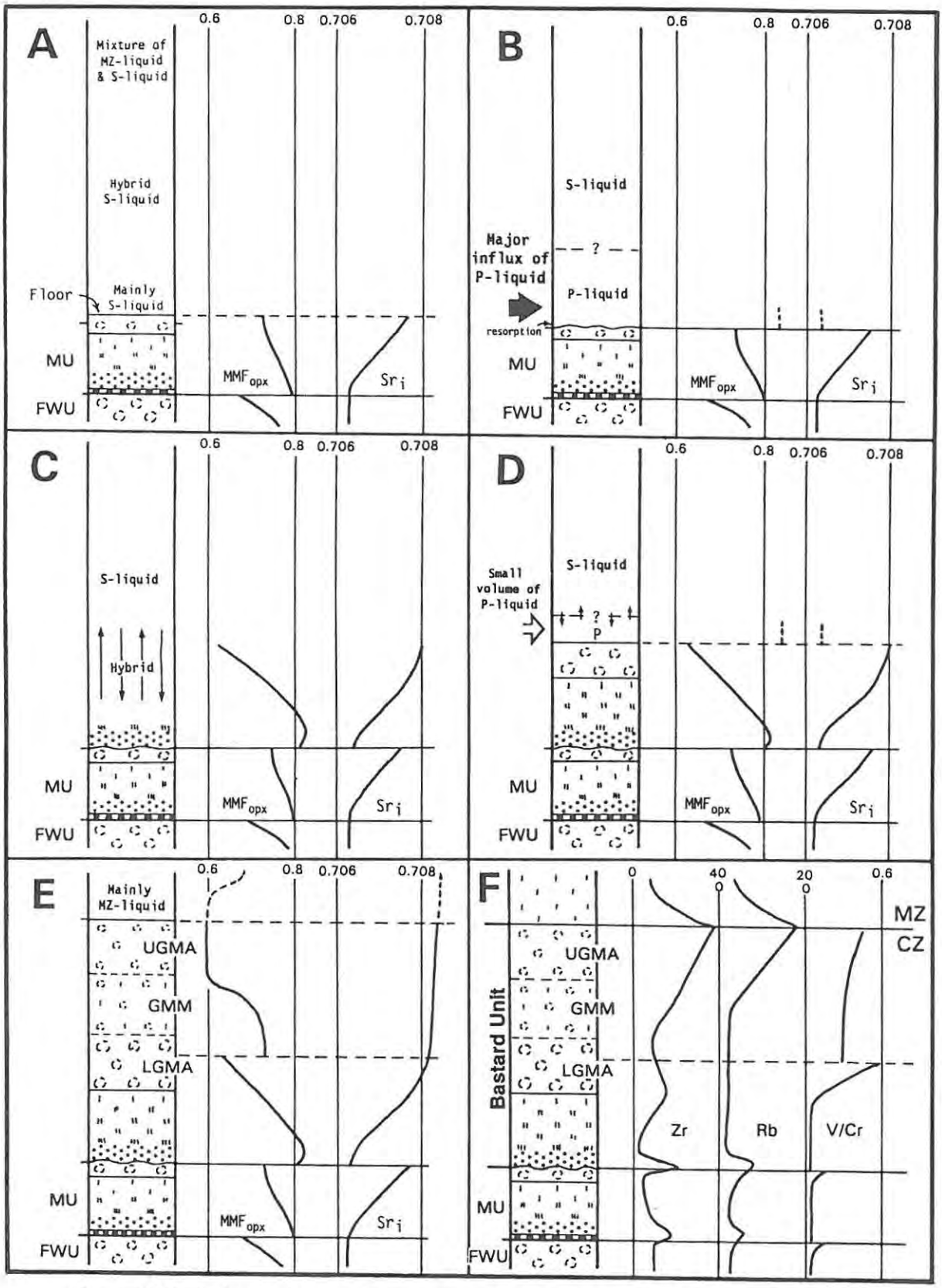

Figure 4.60 Schematic outline of the progressive development of the Bastard Unit through stages A - F (see text for detail).

magma well above that of the residual liquid in the chamber. The resultant effect would be that jetting (Campbell et al., 1983) may have been important at the site of entry but that the newly emplaced magma would have behaved as a basal flow away from the feeder area between the partly crystalline floor and the hybridized **S-liquid** column.

The remarkable degree of consistency displayed by the MMF ratio of orthopyroxene in the basal pyroxenite layer of the Bastard Unit (Table 4.3 and Figure 4.7) suggests that the magma flow maintained its integrity away from the feeder zone and that only limited interaction occurred with the **S-liquid**. It is hypothesised that as the flow advanced through the chamber, a small amount of **S-liquid** was entrained and turbulently mixed into the flow front. Once again this primitive liquid was initially above the feldspar liquidus. The resultant effect was that part of the crystalline anorthosite floor was removed by thermal resorption and mechanical erosion prior to the accumulation of chromite, resulting in an undulatory floor contact. Suspended chromite in the magma settled out in the vicinity of the irruptive feeder and contributed to the development of a more robust chromitite layer in the Union Section area. Additional chromite crystallised in situ on the uneven floor interface in response to mixing of fractionated liquids expelled during compaction of the underlying porous Merensky Unit and the newly emplaced primitive magma.

Stage C. Suspended orthopyroxene settled out of the magma flow and growth of these primary phases continued. Further crystallisation of the new primitive magma resulted in mafic cumulates (orthopyroxene) at the very base of the Unit which poikilitically incorporated the newly crystallised, irregularly shaped chromite crystals. Orthopyroxene MMF ratios recorded at the base of the unit are c. 0.801 while more "primitive" ratios, above 0.820, are recorded a few metres (≥ 5m) higher in the sequence. This apparently anomalous minor reversal here is interpreted as being the result of the combined effect of limited incorporation of **S-liquid** at the flow front and the infiltration of fractionated interstitial liquid from the Merensky Unit below. This resulted in an increase in the iron, and incompatible trace element content of the **P-liquid** at the base of the column. The influence of this type of process only occurs within the basal 5m of the Unit. Progressive

upward crystallisation of mafic phases yielded a reversed cryptic variation trend up to a level where these two factors no longer had any effect.

Continued crystallisation of mafic phases resulted in the lowering of the density of the liquid and the interface with the overlying hybrid **S-liquid** layer broke down and mixing between these two liquids occurred. Geochemical attributes now shifted towards those of the hybrid **S-liquid** layer which produced a gradational composition profile. This then resulted in the crystallisation of the noritic sequence - becoming more leucocratic upward. Here the norites have the distinctive texture of orthopyroxene enclosing small resorbed plagioclase primocrysts. The low incidence of these plagioclase inclusions within the Bastard pyroxenite (Plate 4.6) is indicative of only limited interaction between the **P-liquid** and the hybrid **S-liquid**. Continued fractional crystallisation, coupled with the less pronounced influence of a trapped liquid shift, resulted in the continued decrease in the MMF ratio of orthopyroxene to values below 0.70 within the LGMA. The resultant geochemical profile through the noritic sequence and the LGMA is one of a gradational decrease in the orthopyroxene MMF ratio, from c. 0.8 to <0.7 (Figure 4.57).

The Sr_i ratio at the base of the Unit in the eastern Bushveld (Lee and Butcher, 1990) clearly indicates a reversal to more primitive values (0.7064) before again reverting to progressively higher levels approaching those characteristic of the Main Zone. The fact that no reversal is recorded in the west is here attributed to the inadequate number of samples taken at this level and an added factor may have been that mixing between the hybrid **S-liquid** column and the new influx of **P-liquid** took place sooner in the west than in the east. This earlier mixing event would have effectively suppressed the reversal in the west.

Stage D. The data indicate a final small influx of **P-liquid** at this level to account for the distinctive reversals seen in the MMF ratios of orthopyroxene and in particular the whole-rock ratios of V/Cr, Ni/Sc (Figure 4.56) and to a lesser degree MMF_{WR} (Figure 4.21). This less robust pulse of **P-liquid** was unable to initiate the crystallisation of cumulus orthopyroxene alone but nevertheless had the ability to alter the character of the crystallising liquid. The position of this reversal is

stratigraphically variable and is perhaps a direct consequence of varying rates of nucleation and crystallisation of the cumulates, below the reversal, at different localities.

Stage E. During crystallisation of the GMM a limited amount of cumulus orthopyroxene crystallised and incorporated small plagioclase inclusions. The higher frequency of these inclusions at the margins of the orthopyroxene crystals suggests that as the mafic components were locally depleted during crystallisation the growth rate decreased and more inclusions were captured within the orthopyroxene. The marked zonation of minor elements in orthopyroxene with a similar texture in the Merensky Unit, shown by Kruger and Marsh (1985) (increase in TiO_2 and decrease in Cr_2O_3 and Al_2O_3 content), supports this view. Further crystallisation of the fractionated (and hybridized) **S-liquid** resulted in the first appearance of primary pigeonite in the upper part of the GMA. Once again the level at which pigeonite started to crystallise is not the same at all localities and this is attributed to variability in the progressive concentration of fractionated components in different areas. Where primary pigeonite appears in the paragenesis the MMF ratio of orthopyroxene drops to values below **0.6** before gradually reverting to higher values some 30m into the Main Zone. Crystallisation of interstitial K-feldspar with a concomitant increase in whole-rock K_2O, TiO_2, P_2O_5, Zr and Rb values at this level would also indicate crystallisation from a fractionated liquid. Sr_i values within the upper part of the GMA are at this stage dominated by the Main Zone signature and approach 0.7080.

Stage F represents the crystallisation of the remainder of the hybridized **S-liquid** at the base of the Main Zone. Here the accumulated fractionated products of successive influxes of Critical Zone magma are finally incorporated in the crystallising phases, resulting in the orthocumulates at this level. The UGMA and the lower part (c. 40m) of the Main Zone effectively constitute a "sandwich horizon" between the Critical and Main Zones of the Complex. It is at this level that the highest levels of incompatible trace elements like K_2O, Rb and Zr are recorded for cumulates in the Critical Zone. Sr_i ratios at this level are dominated by the Main Zone magma signature.

4.14 Conclusion.

The development of the Bastard Unit sequence represents the final stage in the crystallisation of a dominantly mafic magmatic event which produced the Critical Zone before the onset of crystallisation of the anorthositic A-type liquid responsible for the development of the Main Zone. The Bastard Unit is considered to be the result of crystallisation of a final influx of primitive liquid, with Upper Critical Zone characteristics, and subsequent mixing with a column of supernatant liquid which had in part hybridized with the newly emplaced overlying Main Zone magma. This Unit is quite unique as it represents the only cyclic unit within the Critical Zone that has crystallised to completion without the interruption of an additional major influx of magma (which would have resulted in yet another cyclic unit). The waning intensity of the periodic influxes of **P-liquid** into the chamber is clearly demonstrated in the Bastard Unit with the recognition of a second minor influx of magma midway through the Unit. It also displays unique characteristics compared with other Upper Critical Zone units; the highest concentrations of incompatible trace elements, in normal cumulates of the Upper Critical Zone, are recorded at the top of the Bastard Unit.

After the influx of fresh **P-liquid** the crystallising sequence of the Bastard Unit can be viewed as a two-stage process:

1) Crystallisation in the lower half of the unit was dominated by properties (chemical and physical) which were introduced by the fresh input of primitive magma. Here the lithologies which have been produced up to the top of (or within) the LGMA are very similar to other (relatively complete) units of the Upper Critical Zone (pyroxenite - norite - anorthosite).

2) Crystallisation of the upper leucocratic sequence, i.e. above the reversal, was from the combined product of the final (minor) influx of **P-liquid** and the reservoir of supernatant liquid which had in part been hybridized with the overlying Main Zone magma. This residuum had built up in response to the crystallisation of the underlying cyclic units.

Scoon and Teigler (1990) report a very similar synthesis in the formation of other units of the Upper Critical Zone. They suggest that each unit reflects two periods of mixing:

- the lower, ultramafic members are derivates of contamination between the new influx and the eroded floor material with minor quantities of entrained residual magma; Scoon and Teigler (1990) call this **MIXING EVENT (A)**. This event accounts for basal chromitite layers.

- the upper, leucocratic members crystallised during hybridization of the fractionated residua of the contaminated influx with the supernatant liquid column; **MIXING EVENT (B)**. They suggest that such an event would explain the juxtaposition of ultramafic and leucocratic cumulates.

The upper leucocratic lithologies (GMM and the UGMA) display geochemical characteristics transitional between the last crystallising phases of the Critical Zone and the overlying Main Zone (see **4.12**) and can be regarded as a mixed **hybrid** or **sandwich layer**. The overall features of the Bastard Unit, however, show a greater number of Critical Zone characteristics than those of the Main Zone and clearly it must be retained as an integral part of the Critical Zone. This interval provides crucial lithological and geochemical evidence which enables a clearer understanding of the processes that were operative at the level of the Critical - Main Zone boundary; the interface between two major styles of magmatism which were responsible in the development of the Bushveld Complex.

If the above synthesis for the development of the Bastard Unit is deemed acceptable then the models of Eales et al. (1986, 1988 and 1990a) and that of Campbell et al. (1983) receive support. It is concluded that fresh influxes of magma were intruded along or near the crystalline floor prevailing at the time and progressively inflated the magma chamber - jetting may have been important at irruptive feeder zones which are indicated to be proximally located in the northwestern sector of the Complex, in the vicinity of Union Section. Emplacement by pluming is not thought to have been important during the formation of the Critical Zone but may have become dominant within the Main Zone.

CHAPTER 5

SUMMARY

1. In **Chapter 2** of this thesis the MG3 and UG1 Footwall Units of the Upper Critical Zone, as exposed in a long tramming crosscut at Union Section, are described and studied. The investigation includes the following aspects:

* Stratigraphy from 22m below the MG3 chromitite to the base of the UG1 chromitite layer - an interval of 350m.

* Documentation of the macroscopic features encountered within the layered sequence in the upper part of the UG1FW Unit, ie. within the norites, leuconorite and anorthosites.

* Petrography of the silicate phases.

* Mineralogical investigations of orthopyroxene, clinopyroxene and plagioclase feldspar by electron microprobe.

* Whole-rock major- and trace-element geochemistry of the silicate cumulates by XRF analysis.

* Sr-isotope variations on whole-rock samples as well as selected mineral separates - investigated by Eales et al. (1990a).

Conclusions which can be drawn from a synthesis of the above investigations are as follows:

1.1 **Stratigraphy.** The MG3 Unit sequence (45m) is somewhat unusual when compared to other Upper Critical Zone Units. Unlike other units which usually have a mafic base and a leucocratic top, the MG3 Unit is essentially an upward gradation from norite to pyroxenite with a thin capping of anorthosite (1.2m) which forms the immediate footwall of the MG4 chromitite. The stratigraphic sequence of the UG1FW Unit (294m), although very much thicker than the MG3 Unit, has a more normal sequence with mafic lithologies at the base giving way to more leucocratic lithologies towards the top. The Unit is divided into roughly equal proportions of an upper noritic and a lower pyroxenitic sequence of layered cumulates. The noritic sequence is

capped by anorthosite, with interlayered leuconorite, which forms the footwall of the UG1 chromitite. It is within this anorthosite that the complex inter-layering of anorthosite and UG1 chromitite occurs.

1.2 **Macro-layering features** throughout the study section are only readily apparent in the upper part of the UG1FW Unit, in the norite, anorthosite and chromitite layers. Here phase layering and modal variations, emphasized by colour differences of the various mineral constituents, are the distinctive features of layering in the sequence (Plates 2.4 and 2.5). The contact between the UG1FW and UG1 Unit is distinctive because of the variety of textures produced by the anorthosite - chromitite associations at this level. The lower pyroxenitic sequence appears more massive in character with only minor, discrete layers and lenses, which contain marginally higher proportions of intercumulus feldspar, being apparent.

1.3 **Petrography.** Although the sequence has a relatively simple mineralogy, the textures displayed by these cumulates vary between extreme adcumulates, usually at the bases of sub-cycles, and meso- to orthocumulates at the tops of sub-cycles. A significant texture recorded though the entire study section is the ubiquitous presence of small plagioclase inclusions within orthopyroxene of both pyroxenites and norites. The texture indicates partial resorption of pre-existing feldspar primocrysts within the melt prior to their being poikilitically incorporated within the cumulus orthopyroxene grains. An additional variety of plagioclase occurs in the form of rare laths and/or clusters within some pyroxenites, and mineral separates of this plagioclase have been shown to have widely differing Sr_i ratios, indicating a mixed feldspar population.

1.4 **Mineralogy.** Cryptic variation trends established for orthopyroxene in the UG1FW Unit (MMF ratios, Cr/Al ratios and Cr_2O_3 content) do not follow an expected normal fractionation trend from Mg-rich species at the base to more Fe-rich varieties at the top of the Unit. There is, rather, a pattern of cyclical variation through the sequence with an overall increase in these parameters towards the top of th UG1FW Unit. Lowest MMF ratios are recorded in the basal pyroxenitic

sequence (0.783) and these values increase through the noritic sequence to a peak value (0.849) in the leuconorite at the top of the Unit. The range of composition of plagioclase cores varies between An_{57-85} and the overall trend through the UG1FW Unit is one of increasing An content. Analysis of plagioclase inclusions within host orthopyroxene grains shows a distinct bias to more sodic compositions when compared to the normal cumulus and/or intercumulus grains of the same sample. In addition, there is sympathetic variation in %An between the inclusions and the non-included feldspar. These trends define a clear cyclical pattern through the UG1FW Unit and this pattern, in conjunction with other geochemical parameters, was used to define the limits of the sub-cycles within the UG1FW Unit.

1.5 Whole rock data. The sequence displays oscillatory fluctuations in whole-rock MMF, FeO/TiO_2, Ni/V, Cr/Co and other ratios with stratigraphic height, and reinforce the demarcation of the eight sub-cycles within the UG1FW Unit. Distinct breaks in the trends are also recognised for these ratios, across the boundary between the MG3 and UG1FW Units and significant differences are evident (especially for V and Cr) between these two units when plotted against %MgO. Regression analysis of whole-rock V and Cr plotted against %MgO (or Sr) indicates that these two units are geochemically quite different and that crystallisation of the MG4 chromitite left the residual liquid depleted of these constituents, a feature now reflected in the lower pyroxenitic sequence of the UG1FW Unit.

1.6 Model. From the textural, geochemical and isotopic evidence it is concluded that the sequence has developed in response to periodic influxes of small volumes of primitive liquid which hybridized with a resident column of supernatant liquid residuum produced by crystallisation of earlier cumulates with a Sr_i ratio of c. 0.7054. This resident S-liquid had abundant plagioclase feldspar primocrysts in suspension and was crystallising plagioclase more sodic and orthopyroxene more Mg-poor compared to those in equilibrium with incoming P-liquid, which is hypothesised to be parental to the cumulates of the Upper Critical Zone (Sr_i c. 0.7064). The

significance of the MG3 and UG1FW Units lies in the preservation of incompletely resorbed small plagioclase inclusions within host orthopyroxene grains of pyroxenites and norites. This evidence is also used to support the view that mixing of new liquids with older residual liquids may be a more general process than is commonly appreciated, and may also have operated within other cyclic units where the plagioclase primocrysts have been destroyed by more complete reaction.

2. **Chapter 3** of this work offers descriptions of two additional Upper Critical Zone sequences along strike at Union Section, between the base of the UG2 and UG1 chromitite respectively, and the Bastard Unit. These two profiles, **UA** and **UC**, compliment an existing centrally located profile (**UB**) which was investigated at an earlier date. New whole-rock major and trace element data, covering the same interval as **UB**, are presented. An additional series of samples were taken through the UG2 Unit in three borehole profiles (**UD**, **UE** and **UF**) which were analysed for trace elements alone. All of these profiles provide a closer-spaced sampling interval through the Upper Critical Zone than **UB** and the study includes the following aspects.

* Stratigraphic sequence of the **UA**, **UC**, **UD**, **UD** and **UE** profiles in relation to the **UB** profile.

* Petrography of the silicate rocks.

* Whole-rock geochemical variations of the silicate cumulates by XRF analysis.

2.1 Close examination of the lithologies and their thicknesses within individual units reveal that only minor variations along strike are evident. This study does, however, emphasise that caution must be exercised when making generalised correlations between strike profiles, as local aberrations of the sequence do occur, especially in close proximity to potholes (see **3.3**). Petrographic investigation has revealed the occurrence of olivine (Fo_{79-81}) in the Bastard Unit, 30m above the level of the Merensky Reef, which had previously been accepted as the level at which Mg-rich olivine left the paragenesis in the Bushveld Complex. This olivine occurs within the noritic

sequence of profile **UC** and displays typical Critical Zone characteristics. A detailed account of these olivine-bearing norites is presented in chapter 4.

2.2 New whole-rock data in **Chapter 3** provide a more comprehensive geochemical database for individual Upper Critical Zone units at Union Section, and constitute the foundation for any future investigation which may be undertaken in this part of the Complex. The whole-rock data in all profiles show remarkable similarity to the data of **UB** and little geochemical variation along strike is readily apparent. The Sr abundance data reinforce the observation that each Upper Critical Zone unit has its own characteristic Sr level in plagioclase.

3. The Bastard Unit. A major section of this thesis is contained within **Chapter 4** which embodies a detailed investigation of the Bastard Unit along 171km of strike in the western Bushveld Complex. This Unit is located at the top of the Critical Zone and constitutes the last of the well-defined cyclic units which are so characteristic of this Zone. Aspects of the investigation included the following:

* Field characteristics and the stratigraphic sequence of the Bastard Unit and correlation with other profiles around the western Bushveld Complex.

* Petrography of all lithologies sampled in profiles at various localities around the western arc of the Complex.

* Mineralogical investigations of the silicate phases olivine, orthopyroxene and plagioclase feldspar (and limited chromite) by electron microprobe.

* Whole-rock major- and trace-element geochemistry of the silicate cumulates by XRF analysis.

The main conclusions reached from a synthesis of the above studies are as follows:

3.1 Stratigraphy. The lithologies which constitute the Bastard Unit are recognisable throughout the western Bushveld Complex. The thickness

and stratigraphic sequence of the Unit remain essentially the same between Amandelbult Section, in the north, and Rustenburg in the south and a thinning of the sequence is recognised towards the east between Rustenburg and Brits. Minor aberrations in the normal sequence of the Unit do occur locally, e.g., an additional pyroxenite is interpolated below the GMA in profile **X**.

3.2 Petrography. Petrographic examination revealed that the base and top of the Bastard Unit are orthocumulate in character while the bulk of the Unit (norite, leuconorite, LGMA and GMM) is essentially an adcumulate. Apart from the dominant cumulus phases (orthopyroxene, plagioclase and clinopyroxene) being recognised, other phases and textures of significance are described. Such include the appearance of cumulus olivine in the noritic sequence of profile **UC**, and intercumulus inverted pigeonite in the GMM and the UGMA at the top of the Unit. K-feldspar also joins the paragenesis at the top of the Unit and occurs both as intercumulus orthoclase and within areas dominated by antiperthite. Complex oscillatory-zoned cumulus plagioclase grains, with varying degrees of zonal complexity, are common in the upper part of the Bastard Unit. These grains are interpreted as records of growth episodes during earlier influxes of magma which were responsible for the development of the underlying cyclic units. The occurrence of abundant small, corroded plagioclase inclusions within cumulus orthopyroxene and olivine is regarded as proof of the presence of plagioclase primocrysts, suspended in a column of supernatant liquid, prior to crystallisation of the mafic phases.

3.3 Mineralogy. Cryptic variations of orthopyroxene compositions define a distinctive pattern through the Unit which is recognisable throughout the western Bushveld Complex. This pattern is described as being double-cuspate in form, with the lower cusp (through the pyroxenite-norite-LGMA) being more primitive in character while the upper cusp displays more evolved traits. A feature of the orthopyroxene MMF ratios within the basal Bastard pyroxenite is that they do not vary over a distance of 171km and remain constant at 0.804 (sd = 0.012) regardless of the overlying stratigraphic variation. The variation of %An content for cumulus plagioclase

through the Unit displays a trend which is inconsistent with that indicated by MMF ratios in orthopyroxene. A pattern of increasing An content is recorded at the base of the Unit through the pyroxenite-melanorite-norite-leuconorite sequence and peak values of c. An_{82} are attained. Profile **UC** exhibits higher maximum values within the leuconorites, in excess of An_{90}. A normal decreasing trend is seen within the LGMA up to the level of the reversal recorded in the orthopyroxene MMF ratios. Above this level the An content remains close to An_{75}, tending to marginally lower values at the top of the Unit. Compositions recorded for olivine in **UC** (Fo_{79-81}) are characteristic of other Upper Critical Zone occurrences.

3.4 Whole-rock data. By utilising the whole-rock data, an attempt was made to estimate the concentrations of "compatible" trace elements within plagioclase and pyroxene in individual Bastard Unit profiles. As long as certain rules are adhered to, the results of applying the linear regression technique for estimating trace element concentrations in these phases compare favourably with direct measurement of mineral separates. Results obtained here indicate that little or no variation is detectable for Sr in plagioclase around the western limb of the Complex, and a similar result was recorded for Co and Ni in pyroxene. Estimates of Cr in pyroxene do, however, show an increase in concentration between Rustenburg and Amandelbult Sections while there is a suggestion that levels of V, Zn, and Sc decrease towards Amandelbult. A progressive increase in the levels of "incompatible" trace (and major) elements is recorded towards the top of the Bastard Unit and the highest levels of Zr and Rb in the Upper Critical Zone are seen at the top of the Unit. This phenomenon is interpreted as indicating the crystallisation of the most extreme fractionates produced during the development of the Upper Critical Zone sequence. This conclusion is in harmony with the first appearance, here, of inverted pigeonite.

Isotopically, the Bastard Unit has been shown to lie within a zone transitional between Sr_i c. 0.7064 at the level of the Merensky Reef and 0.7087 within the basal part of the Main Zone (i.e., 300m above the Merensky Reef). Although no isotopic reversal has yet been recorded at the base of the Bastard Unit here, it is considered, in

the light of the findings of Lee and Butcher (1990) in the eastern Bushveld, that a new magma influx did occur at this level.

3.5 Interpretation. The Bastard Unit is interpreted as representing crystallisation from a final Critical Zone magma influx (**P-liquid**) which entered the chamber as a basal flow beneath a column of residual supernatant (**S-liquid**) that had accumulated in response to earlier crystallisation of underlying cyclic units. It is proposed that the **P-liquid** was progressively blended with the overlying, fractionated, accumulation of a cooler, less dense **S-liquid** which had, itself, partly hybridized with the newly emplaced overlying Main Zone magma. This hybridized **S-liquid** was charged with a high proportion of small plagioclase primocrysts in suspension. Jetting may have been important closer to the feeder zone which is indicated to be proximally located in the Union Section area. It is argued that these processes of mixing, fractional crystallisation and the effects of trapped liquid shift, were responsible for the features of the Bastard Unit recorded in the study.

REFERENCES

Atkins, F.B., (1969), Pyroxenes of the Bushveld intrusion, South Africa. *Jour. of Pet.*, **10**, 222-249.

Barnes, S.J., (1986), The effect of trapped liquid crystallization on cumulus mineral compositions in layered intrusions. *Contrib. Miner. Petrol.*,**93**, 524-531.

Barnes, S.J. and Naldrett, A.J., (1986), Geochemistry of the J-M Reef of the Stillwater Complex, Minneapolis Adit area: II. Silicate mineral chemistry and petrogenesis. *Jour. of Pet.*, **27**, 791-825.

Barnes, S.J. and Campbell, I.H., (1988), Role of late magmatic fluids in Merensky-type platinum deposits: A discussion. *Geology*, **16**, 488-491.

Bédard, J.H., Sparks, R.S.J., Renner, R., Cheadle, M.J. and Hallworth, M.A., (1988), Peridotite sills and metasomatic gabbros in the Eastern Layered Series of the Rhum Complex. *Jour. of the Geological Soc. London*, **145**, 207-224.

Botha, M.J., (1987), Petrology and geochemistry of the lower group chromitites and host rocks on the farm Zandspruit 168 JP, western Bushveld Complex. *MSc Thesis Rhodes University (unpubl.)*, 216 pp.

Bottinga, Y. and Weill, D.F., (1970), Densities of liquid silicate systems calculated from partial molar volumes of oxide components. *Amer. Jour. Sci.*, **269**, 169-182.

Brynard, H.J., de Villiers, J.P.R. and Viljoen, E.A., (1976), A mineralogical investigation of the Merensky Reef at the Western Platinum mine, near Marikana, South Africa. *Econ. Geol.*, **71**, 1299-1307.

Burger, A.J. and Coertze, F.J., (1973), Radiometric age measurements on rocks from Southern Africa to the end of 1971. *Geol. Surv. South Africa*, **Bull. 58**, 0-46.

Burns, R.G., (1970), *Mineralogical Applications of the Crystal Field Theory*. Cambridge University Press. Great Britain, 224 pp.

Cameron, E.N., (1964), Chromite deposits of the eastern part of the Bushveld Complex. *In: Haughton, S.H. (ed.), The geology of some ore deposits in Southern Africa, Volume 2.* Geol. Soc. South Africa, 131-168.

Cameron, E.N., (1969), Postcumulus changes in the eastern Bushveld Complex. *Amer. Min.*, **54**, 754-779.

Cameron, E.N., (1975), Postcumulus and subsolidus equilibration of chromite and co-existing silicates in the eastern Bushveld Complex. *Geochim. et Cosmochim.*, **39**, 1021-1033.

Cameron, E.N., (1982), The upper Critical Zone of the eastern Bushveld Complex - precursor of the Merensky Reef. *Econ. Geol.*, **77**, 1307-1327.

Campbell, I.H., (1977), A study of macro-rhythmic layering and cumulate processes in the Jimberlana intrusion, Western Australia. Part I: The Upper Layered Series. *Jour. of Pet.*, **18**, 183-215.

Campbell, I.H., (1978), Some problems with the cumulus theory. *Lithos*, **11**, 311-323.

Campbell, I.H., (1986), A fluid dynamic model for the potholes of the Merensky Reef. *Econ. Geol.*, **81**, 1118-1125.

Campbell, I.H. and Borley, G.D., (1974), The geochemistry of pyroxenes from the Lower Layered Series of the Jimberlana intrusion, Western Australia. *Contrib. Miner. Petrol.*, **47**, 281-297.

Campbell, I.H., Naldrett, A.J. and Barnes, S.J., (1983), A model for the origin of the platinum-rich sulfide horizons in the Bushveld and Stillwater complexes. *Jour. of Pet.*, **24**, 133-165.

Campbell, I.H. and Turner, J.S., (1986), The influence of viscosity on fountains in magma chambers. *Jour. of Pet.*, **27**, 1-30.

Cawthorn, R.G., (1983), Evidence from trace element geochemistry for multiple magma injection in the Losberg Complex, South Africa. *Trans. Geol. Soc. South Africa*, **86**, 137-141.

Coertzer, F.J., (1958), Intrusive relationships and ore deposits in the western part of the Bushveld Igneous Complex. *Trans. Geol. Soc. South Africa*, **61**, 387-392.

Coertzer, F.J., (1974), The geology of the basic portion of the western Bushveld Igneous Complex. *Geol. Surv. South Africa*, **Memoir 66**, 148p.

Cousins, C.A., (1959), The structure of the mafic portion of the Bushveld Igneous Complex. *Trans. Geol. Soc. South Africa*, **62**, 179-189.

Cousins, C.A., (1964), The platinum deposits of the Merensky Reef. *In: Haughton, S.H. (ed.), The geology of some ore deposits in Southern Africa, Volume 2.* Geol. Soc. South Africa, 225-237.

Cousins, C.A., (1969), The Merensky Reef of the Bushveld Igneous Complex. *Econ. Geol. Monogr.*, **4**, 239-251.

Cox, K.G., Bell, J.D. and Pankhurst, R.J., (1979), *The interpretation of igneous rocks.* George Allen & Unwin. London, 450 pp.

Deer, W.A., Howie, R.A. and Zussman, J., (1967), *Rock forming minerals, Volume 2, Chain Silicates.* Longmans, Green and Co., London, England.

Deer, W.A., Howie, R.A. and Zussman, J., (1972), *An introduction to the rock forming minerals.* Longman Group Limited, London, England (Second Edition), 336 pp.

De Klerk, W.J., (1982), The geology, geochemistry and silicate mineralogy of the upper Critical zone of the north-western Bushveld Complex, at Rustenburg Platinum Mines, Union Section. *MSc Thesis Rhodes University (unpubl.)*, 210 pp.

De Klerk, W.J., (1989), Petrological and geochemical characteristics of the Bastard unit within 170 km of strike in the western Bushveld Complex. *Conference on the origin of Mineralization in Southern African Layered intrusions, Abstract Volume.* University of the Witwatersrand, 46-47.

De Long, S.E., (1974), Distribution of Rb, Sr, and Ni in igneous rocks, central and western Aleutian Islands, Alaska. *Geochim. et Cosmochim.*, **38**, 245-266.

Drake, M.J. and Weill, D.F., (1975), Partition of Sr, Ba, Ca, Y, Eu^{2+}, Eu^{3+} and other REE between plagioclase feldspar and magmatic liquid: an experimental study. *Geochim. et Cosmochim.*, **39**, 689-712.

Duke, J.M., (1976), Distribution of the period four transition elements among olivine, calcic clinopyroxene and mafic silicate liquid: Experimental results. *Jour. of Pet.*, **17**, 499-521.

Du Plessis, A. and Kleywegt, R.J., (1987), A dipping sheet model for the mafic lobes of the Bushveld Complex. *South African Jour. of Sci.*, **90**, 1-6.

Eales, H.V., (1987), Upper Critical zone chromitite layers at R.P.M. Union Section mine, western Bushveld Complex. *In: Stowe, C.W. (ed), Evolution of chromium ore fields.* Van Nostrand Reinhold Co. New York., 144-167.

Eales, H.V., Marsh, J.S., Mitchell, A.A., de Klerk, W.J., Kruger, F.J. and Field, M., (1986), Some geochemical constraints upon models for the crystallization of the upper critical zone-main zone interval, northwestern Bushveld Complex. *Min. Mag.*, **50**, 567-582.

Eales, H.V. and Reynolds, I.M., (1986), Cryptic variations within chromites of the upper Critical Zone, northwestern Bushveld Complex. *Econ. Geol.*, **81**, 1056-1066.

Eales, H.V., Field, M., de Klerk, W.J. and Scoon, R.N., (1988), Regional trends of chemical variation and thermal erosion in the upper Critical zone, western Bushveld Complex. *Min. Mag.*, **52**, 63-80.

Eales, H.V., de Klerk, W.J., Butcher, A.R. and Kruger, F.J., (1990a), The cyclic unit beneath the UG1 chromitite (UG1FW unit) at RPM Union Section platinum mine - Rosetta Stone of the Bushveld upper Critical Zone?. *Min. Mag.*, **54**, 23-43.

Eales, H.V., de Klerk, W.J. and Teigler, B., (1990b), Evidence for magma mixing processes within the Critical and Lower Zones of the northwestern Bushveld Complex, South Africa. *Chem. Geol.*, **88**, 261-278.

Eales, H.V., Maier, W.D. and Teigler, B., (1991), Corroded plagioclase feldspar inclusions in orthopyroxene and olivine of the Lower and Critical Zones, Western Bushveld Complex. *Min. Mag.*, **55**, 479-486.

Ewart, A., Bryan, W.B. and Gill, J.B., (1973), Mineralogy and geochemistry of the younger volcanic islands of Tonga, S.W. Pacific. *Jour. of Pet.*, **14**, 429-465.

Farquhar, J.W., (1986), The Western Platinum Mine. *In: Anhaeusser, C.R. and Maske, S. (eds.), Mineral deposits of Southern Africa Volume II.* Geol. Soc. South Africa, 1135-1142.

Feringa, G., (1959), The geological succession in a portion of the north-western Bushveld (Union Section) and its interpretation. *Trans. Geol. Soc. South Africa*, **62**, 219-233.

Field, M., (1987), The Petrology and Geochemistry of the upper Critical Zone of the Bushveld Complex at the Amandelbult Section of Rustenburg Mines Limited, Northwestern Transvaal, South Africa. *MSc Thesis Rhodes University (unpubl.)*, 128 pp.

Flower, M.J., (1973), Trace element distribution in lava flows from Anjouan and Grande Comore, western Indian Ocean. *Chem. Geol.*, **12**, 81-98.

Frey, F.A., Green, D.H. and Roy, S.D., (1978), Integrated models of basalt petrogenesis: a study of quartz tholeiites to olivine melilites from south eastern Australia utilizing geochemical and experimental petrological data. *Jour. of Pet.*, **19**, 463-513.

Gain, S.B., (1986), The Upper Group chromitite layers at Maandagshoek, eastern Bushveld Complex. *In: Anhaeusser, C.R. and Maske, S. (eds.), Mineral deposits of Southern Africa Volume II.* Geol. Soc. South Africa, 1197-1208.

Griffin, W.L. and Murthy, V.R., (1969), Distribution of K, Rb, Sr and Ba in some minerals relevant to basalt genesis. *Geochim. et Cosmochim.*, **33**, 1389-1414.

Hall, A.L., (1932), The Bushveld Igneous Complex of the central Transvaal. *Geol. Surv. South Africa*, **Memoir 28**, 1-560.

Hamilton, J., (1977), Sr isotope and trace element studies of the Great Dyke and Bushveld mafic phase and their relation to early Proterozoic magma genesis in Southern Africa. *Jour. of Pet.*, **18**, 24-52.

Hanson, G.N., (1977), Geochemical evaluation of the sub-oceanic mantle. *Jour. Geol. Soc. London*, **134**, 235-253.

Harmer, R.E. and Sharpe, M.R., (1985), Field relations and strontium isotope systematics of the marginal rocks of the eastern Bushveld Complex. *Econ. Geol.*, **80**, 813-837.

Hart, S.R. and Brooks, C.J., (1974), Clinopyroxene-matrix partitioning of K, Rb, Cs, Sr and Ba. *Geochim. et Cosmochim.*, **38**, 1799-1806.

Hartzer, F.J., (1989), Stratigraphy, structure, and tectonic evolution of the Crocodile River Fragment. *South African Jour. of Sci.*, **92**, 110-124.

Hatton, C.J., (1984), The effects of pressure, temperature and composition on the distribution of Fe and Mg between olivine, orthopyroxene and liquid; an appraisal of the reversal in the normal fractionation trend in the Bushveld Complex. *Contrib. Miner. Petrol.*, **86**, 45-53.

Hatton, C.J., (1988), Densities and liquidus temperatures of Bushveld parental magmas as constraints on the formation of the Merensky Reef. *Inst. for Geol. Res. on the Bushveld Complex.* University of Pretoria, Report No.73.

Hatton, C.J. and von Gruenewaldt, G., (1987), The geological setting and petrogenesis of the Bushveld chromitite layers. *In: Stowe, C.W. (ed), Evolution of chromium ore fields.* Van Nostrand Reinhold Co., New York., 109-143.

Heinrich, K.F.J., (1966), X-ray absorption uncertainty: *In: McKinley, T.D., Heinrich K.F.J. and Wittry D.B. (eds.), The Electron Microprobe.* John Wiley & Sons Inc., New York, 296-377.

Henderson, P., (1968), The distribution of phosphorus in the early and middle stages of fractionation of some basic layered intrusions. *Geochim. et Cosmochim.*, **32**, 897-911.

Henderson, P. and Suddaby, P., (1971), The nature and origin of the chrome-spinel of the Rhum layered intrusion. *Contrib. Miner. Petrol.*, **33**, 21-31.

Hill, R. and Roeder, P.L., (1974), The crystallization of spinel from basaltic liquid as a function of oxygen fugacity. *Jour. of Geol.*, **82**, 709-729.

Huppert, H.E. and Sparks, R.S.J., (1980), The fluid dynamics of a basaltic magma chamber replenished by influx of hot, dense ultrabasic magma. *Contrib. Miner. Petrol.*, **75**, 279-289.

Huppert, H.E., Sparks, R.S.J. and Turner, J.S., (1984), Some effects of viscosity on the dynamics of magma chambers. *Jour. Geophys. Res.*, **89**, 6857-6877.

Huppert, H.E., Turner, J.S. and Sparks, R.S.J., (1982), Replenished magma chambers: effects of compositional zonation and input rates. *Earth Planet. Sci. Lett.*, **57**, 345-357.

Irvine, T.N., (1977), Origin of chromitite layers in the Muskox intrusion and other stratiform intrusions: A new interpretation. *Geology*, **5**, 273-277.

Irvine, T.N., (1978), Infiltration metasomatism, adcumulus growth, and secondary differentiation in the Muskox intrusion. *Carnegie Inst. Wash. Year Book*, **77**, 743-751.

Irvine, T.N., (1980a), Magmatic density currents and cumulus processes. *Amer. Jour. Sci.*, **280-A**, 1-58.

Irvine, T.N., (1980b), Magmatic infiltration metasomatism, double-diffusive fractional crystallization, and adcumulus growth in the Muskox intrusion and other layered intrusions. *In: Hargraves, R.B. (ed.), Physics of Magmatic Processes.* Princeton University Press, Princeton New Jersey, 325-383.

Irvine, T.N., (1982), Terminology for layered intrusions. *Jour. of Pet.*, **23**, 127-162.

Irvine, T.N. and Smith, C.H., (1967), The ultramafic rocks of the Muskox intrusion Northwestern Territories, Canada. *In: Wyllie, P.J., (ed), Ultramafic and related rocks*. Wiley, New York, p.38-49.

Irvine, T.N., Keith, D.W. and Todd, S.G., (1983), The J-M platinum-paladium reef of the Stillwater complex Montana: II. Origin by double-diffusive convection magma mixing and implications for the Bushveld Complex. *Econ. Geol.*, **78**, 1287-1334.

Irvine, T.N. and Sharpe, M.R., (1986), Magma mixing and the origin of stratiform oxide ore zones in the Bushveld and Stillwater Complexes. *In: Gallagher, R.A., Ixer R.A., Neary, C.R. and Prichard, H.M. (eds.), Metallogeny of basic and ultrabasic rocks*. Inst. of Mining and Metallurgy, 183-198.

Irving, A.J., (1978), A review of experimental studies of crystal/liquid trace element partitioning. *Geochim. et Cosmochim.*, **42**, 743-770.

Jackson, E.D., (1961), Primary textures and mineral associations in the ultramafic zone of the Stillwater Complex Montana. *Geol. Surv. Prof. Paper*, **358**, 1-106.

Jackson, E.D., (1970), The cyclic unit in layered intrusions - a comparison of repetitive stratigraphy in the ultramafic parts of the Stillwater, Muskox, Great Dyke and Bushveld Complexes. *In: Visser, D.J.L. and von Gruenewaldt, G. (eds), Symposium on the Bushveld Igneous Complex and other layered intrusions*. Geol. Soc. South Africa Spec. Pub., **1**, 391-424.

Jensen, B.B., (1973), Patterns of trace element partitioning. *Geochim. et Cosmochim.*, **37**, 2227-2242.

Klemm, D.D., Ketterer, S., Reichhardt, F., Steindl, J. and Weber-Diefenbach, K., (1985), Implications of vertical and lateral compositional variations across the Pyroxenite Marker and its associated rocks in the upper part of the Main zone in the eastern Bushveld Complex. *Econ. Geol.*, **80**, 1007-1015.

Kruger, F.J., (1982), The petrology of the Merensky cyclic unit and associated rocks, and their significance in the evolution of the western Bushveld Complex. *PhD Thesis Rhodes University (unpubl.)*, 123 pp.

Kruger, F.J., (1989), The Sr-isotopic stratigraphy of the western Bushveld Complex. *Conference on the origin of Mineralization in Southern African Layered Intrusions, Abstract Volume*, University of the Witwatersrand.

Kruger, F.J., (1990), The stratigraphy of the Bushveld Complex: a reappraisal and the relocation of the Main zone boundaries. *S. Afr. Jour. Geol.*, **93(2)**, 376-381.

Kruger, K.J. and Marsh, J.S., (1982), Significance of $^{87}Sr/^{86}Sr$ ratios in the Merensky cyclic unit of the Bushveld Complex. *Nature*, **298**, 53-55.

Kruger, F.J. and Marsh, J.S., (1985), The mineralogy, petrology, and origin of the Merensky cyclic unit in the western Bushveld Complex. *Econ. Geol.*, **80**, 958-974.

Kruger, F.J. and Mitchell, A.A., (1985), Discontinuities and variations of Sr-isotope systematics in the Main Zone of the Bushveld Complex, and their relevance to PGE mineralization. *Canadian Min.*, **23**, 306.

Lambert, R.J. and Holland, J.G., (1974), Yttrium geochemistry applied to petrogenesis utilizing calcium-yttrium relationships in minerals and rocks. *Geochim. et Cosmochim.*, **38**, 1393-1414.

Lauder, W.R., (1970), Origin of the Merensky Reef. *Nature*, **227**, 365-366.

Leeb-du Toit, A., (1986), The Impala Platinum Mines. *In: Anhaeusser, C.R. and Maske, S. (eds.), Mineral deposits of Southern Africa, Volume II.* Geol. Soc. South Africa, 1091-1106.

Lee, C.A., (1981), Post-depositional structures in the Bushveld complex mafic sequence. *Jour. Geol. Soc. London*, **138**, 327-341.

Lee, C.A., (1983), Trace and platinum-group element geochemistry and the development of the Merensky unit of the western Bushveld Complex. *Mineral. Deposita*, **18**, 173-190.

Lee, C.A. and Butcher, A.R., (1990), Cyclicity in the Sr-isotopic stratigraphy through the Merensky and Bastard Reef Units, Atok Section, Eastern Bushveld Complex. *Econ. Geol.*, **85**, 877-883.

Leeman, W.P. and Lindstrom, D.J., (1978), Partitioning of Ni^{2+} between basaltic and synthetic melts and olivines - an experimental study. *Geochim. et Cosmochim.*, **42**, 801-816.

Le Maitre (ed.), R.W., (1989), *A classification of Igneous Rocks: Recommendations of the IUGS subcommission on the systematics of igneous rocks.* Blackwell Scientific Publications. Oxford, 192 pp.

Lindstrom, D.J. and Weill, D.F., (1978), Partitioning of transition metals between diopside and co-existing silicate liquids - 1. Nickel, cobalt, and manganese. *Geochim. et Cosmochim.*, **42**, 817-832.

Lombaard, B.V., (1934), On the differentiation and relationships of the rocks of the Bushveld Complex. *Trans. Geol. Soc. South Africa*, **37**, 5-32.

Marsh, J.S., (1979), *A manual for X-ray fluorescence determination of major and trace elements in natural silicate rock materials.* Unpubl. Manual, Rhodes University, 41 pp.

Martin, D., (1990), Crystal settling and in situ crystallization in aqueous solutions and magma chambers. *Earth Planet. Sci. Lett.*, **96**, 336-348.

McBirney, A.R. and Noyes, R.M., (1979), Crystallization and layering of the Skaergaard intrusion. *Jour. of Pet.*, **20**, 487-554.

Meyer, G., (1969), Some petrological aspects of the mafic rocks from borehole sections between the Merensky Reef and the Main zone gabbro in the western and eastern Bushveld Complex. *MSc Thesis Potchefstroom University for C.H.E. (unpubl.).*

Meyer, R., and de Beer, J.H., (1987), Structure of the Bushveld Complex from resistivity measurements. *Nature*, **325**, 610-612.

Miller, R.L. and Kahn, J.S., (1962), *Statistical analysis in the geological sciences*. John Wiley and Sons, New York, 483 pp.

Mitchell, A.A., (1986), The petrology, mineralogy and geochemistry of the Main zone of the Bushveld Complex at Rustenburg Platinum Mines, Union Section. *PhD Thesis Rhodes University (unpubl.)*, 122 pp.

Mitchell, A.A., (1988), The petrology and mineralogy of the Main Zone in the northwestern Bushveld Complex. *Geol. Soc. S.A. Geocongress 1988, Extended Abstracts*, Durban, 439-440.

Mitchell, A.A., (1989), Magma influxes in the Main Zone of the Western Bushveld. *Conference on the origin of Mineralization in Southern African Layered intrusions, Abstract Volume*. University of the Witwatersrand.

Mitchell, A.A., (1990a), The stratigraphy, petrography and mineralogy of the Main Zone in the north-western Bushveld Complex. *Paper in press.*

Mitchell, A.A., (1990b), The Main Zone of the southwestern Bushveld in the vicinity of Brits. *Geol. Soc. S.A. Geocongress 1990, Extended Abstracts*, Cape Town, 419-422.

Molyneux, T.G., (1970), A geological investigation of the Bushveld Complex in Sekhukhuneland and part of the Steelpoort valley, eastern Transvaal, with particular reference to the oxide minerals. *D.Sc. Thesis University of Pretoria (unpubl.).*

Molyneux, T.G., (1974), A geological investigation of the Bushveld Complex in Sekhukhuneland and part of the Steelpoort valley. *Trans. Geol. Soc. South Africa*, **77**, 329-338.

Morimoto, N., (1989), Nomenclature of pyroxenes: Commission on new mineral names: International Mineralogical Association. *Canadian Min.*, **27**, 143-156.

Morse, S.A., (1979a), Kiglapait Geochemistry I: Systematics, sampling and density. *Jour. of Pet.*, **20**, 555-590.

Morse, S.A., (1979b), Reaction constants for En-Fo-Sil equilibria: an adjustment and some applications. *Amer. Jour. Sci.*, **279**, 1060-1069.

Morse, S.A., (1979c), Influence of augite on plagioclase fractionation. *Jour. Geol.*, **87**, 202-208.

Morse, S.A., (1982), Kiglapait geochemistry V: strontium. *Geochim. et Cosmochim.*, **46**, 223-234.

Morse, S.A., (1986), Convection in aid of adcumulus growth. *Jour. of Pet.*, **27**, 1183-1214.

Morse, S.A., (1988a), Book Review of "Origins of Igneous Layering" edited by Parsons, I. (1987). *Jour. of Pet.*, **29**, 523-525.

Morse, S.A., (1988b), Motion of crystals, solute, and heat in layered intrusions. *Canadian Min.*, **26**, 209-224.

Morse, S.A. and Nolan, K.M., (1984), Origin of strongly reversed rims on plagioclase in cumulates. *Earth Planet. Sci. Lett.*, **68**, 485-498.

Morse, S.A. and Nolan, K.M., (1985), Kiglapait geochemistry VII: yttrium and rare earth elements. *Geochim. et Cosmochim.*, **49**, 1621-1644.

Mostert, A.B., Hofmeyr, P.K. and Potgieter, G.A., (1982), The platinum-group mineralogy of the Merensky Reef at the Impala Platinum mines, Bophuthatswana. *Econ. Geol.*, **77**, 1385-1394.

Naldrett, A.J., (1989), *Magmatic Sulfide Deposits*. Oxford Monographs on Geology and Geophysics **No. 14**, 186 pp.

Naldrett, A.J., Gasparrini, C., Barnes, S.J., Sharpe, M.R. and von Gruenewaldt, G., (1984), The petrology of the upper part of the critical zone of the Bushveld complex and its bearing on the origin of the Merensky reef. *Proceedings of the 27th International Geological Congress: Petrology (Igneous and Metamorphic rocks)*, **9**, 373-389.

Naldrett, A.J., Gasparrini, E.C., Barnes, S.J., von Gruenewaldt, G. and Sharpe, M.R., (1986), The upper Critical zone of the Bushveld Complex and the origin of Merensky type ores. *Econ. Geol.*, **81**, 1105-1117.

Naldrett, A.J., Cameron, G., von Gruenewaldt, G. and Sharpe, M.R., (1987), The formation of stratiform PGE deposits in layered intrusions. *In: Parsons, I. (ed.), Origins of Igneous Layering*, D. Reidel Publishing Co., 313-397.

Nesbitt, R.W., Mastings, H., Stolz, G.W. and Bruce, D.R., (1976), Matrix corrections in trace element analyses by X-ray fluorescence: an extension of the Compton scattering technique to long wavelengths. *Chem. Geol.*, **18**, 203-213.

Norrish, K. and Hutton, J.T., (1969), An accurate X-ray spectrographic method for the analysis of a wide range of geological samples. *Geochim. et Cosmochim.*, **33**, 431-453.

Paster, T.P., Schauwecker, D.S. and Haskin, L.A., (1974), The behaviour of some trace elements during the solidification of the Skaergaard layered series. *Geochim. et Cosmochim.*, **38**, 1549-1577.

Pearce, J.A. and Norry, M.J., (1979), Petrogenetic implications of Ti, Zr, Y and Nb variations in volcanic rocks. *Contrib. Miner. Petrol.*, **69**, 33-47.

Philpotts, J.A. and Schnetzler, C.C., (1970), Phenocryst-matrix partition coefficients for K, Rb, Sr, and Ba, with applications to anorthosites and basalt genesis. *Geochim. et Cosmochim.*, **34**, 307-322.

Reynolds, R.C., (1967), Estimation of mass absorption coefficients by Compton scattering: Improvements of the method. *Amer. Min.*, **52**, 1493-1502.

Rice, A., (1981), Convective fractionation: A mechanism to provide cryptic zoning (macrosegregation), layering, crescumulates, banded tuffs and explosive volcanism in igneous processes. *Jour. Geophys. Res.*, **86 No. B1**, 405-417.

Ringwood, A.E., (1970), Petrogenesis of Apollo II basalts and implications for lunar origin. *Jour. Geophys. Res.*, **75**, 6453-6479.

Roeder, P.L., (1975), Thermodynamics of element distribution in experimental mafic silicate-liquid systems. *Fortschr. Miner.*, **52**, 61-73.

Sack, R.O., (1980), Some constraints on the thermodynamic mixing properties of Fe-Mg orthopyroxenes and olivines. *Contrib. Miner. Petrol.*, **71**, 257-269.

Salpas, P.A., Haskin, L.A. and McCallum, I.S., (1983), Stillwater anorthosite: a lunar analogue? *Jour. Geophys. Res.*, **88**, B27-B39.

Sampson, E., (1932), Magmatic chromite deposits in Southern Africa. *Econ. Geol.*, **27**, 113-144.

Scoon, R.N., (1985), Discordant bodies of post-cumulus, ultramafic rock in the upper Critical zone of the Bushveld Complex: iron rich ultramafic pegmatite bodies at Amandelbult and the Driekop platiniferous ultramafic pipe. *PhD Thesis Rhodes University (unpubl.)*, 265 pp.

Scoon, R.N. and de Klerk, W.J., (1987), The relationship of olivine cumulates and mineralization to cyclic units in part of the upper Critical Zone of the western Bushveld Complex. *Canadian Min.*, **25**, 51-77.

Scoon, R.N., Teigler, B., (1990), Platinum-group element mineralization in the Critical Zone of the Bushveld Complex: classification and origin. *Geol. Soc. S.A. Geocongress 1990, Extended Abstracts*, Cape Town, 501-504.

Shand, S.J., (1943), *Eruptive Rocks*. Murby and Co., London. 488 pp.

Sharpe, M.R., (1985), Strontium isotope evidence for preserved density stratification in the Main Zone of the Bushveld Complex, South Africa. *Nature*, **316**, 119-126.

Smith, J.V., (1974), *Feldspar Minerals: Vol. 2, Chemical and Textural Properties*. Springer-Verlag, Berlin, 690 pp.

Smith, R.K. and Lofgren, G.E., (1983), An analytical and experimental study of zoning in plagioclase. *Lithos*, **16**, 153-168.

Sparks, R.S.J., Huppert, H.E. and Turner, J.S., (1984), The fluid dynamics of evolving magma chambers. *Phil. Trans. Roy. Soc. London*, **A310**, 511-534.

South African Committee for Stratigraphy (SACS), (1980), *Stratigraphy of South Africa. Part 1 (Comp. L.E. Kent). Lithostratigraphy of the Republic of South Africa, South West Africa/Namibia, and the Republics of Bophuthatswana, Transkei and Venda*. Geol. Surv. South Africa, **Handbook 8**, 690 pp.

Streckeisen, A.L., (1973), Plutonic rocks: Classification and nomenclature recommended by the IUGS subcommission on the systematics of igneous rocks. *Geotimes*, **October**, 26-30.

Streckeisen, A.L., (1976), To each plutonic rock its proper name. *Earth Sci. Reviews*, **12**, 1-33.

Sun, C.O., Williams, R.J. and Sun, S.S., (1974), Distribution coefficients of Eu and Sr for plagioclase-liquid and clinopyroxene-liquid equilibria in ocean ridge basalt: an experimental study. *Geochim. et Cosmochim.*, **38**, 1415-1433.

Tait, S.R., Herbert, E., Huppert, E. and Sparks, R.S.J., (1984), The role of compositional convection in the formation of adcumulate rocks. *Lithos*, **17**, 139-146.

Tankard, A.J., Jackson, M.P.A., Eriksson, K.A., Hobday, D.K., Hunter, D.R. and Minter, W.E.L., (1982), *Crustal Evolution of South Africa - 3.8 billion years of earth history*. Springer-Verlag. New York, 175-199.

Taylor, S.R., (1965), The application of trace element data to problems in petrology. *Phys. Chem. Earth*, **6**, 133-214.

Teigler, B., (1990), Mineralogy, petrology and geochemistry of the Lower and lower Critical Zones, northwestern Bushveld Complex. *PhD Thesis Rhodes University (unpubl.)*, 247 pp.

Van Zyl, J.P., (1960), Die petrologie van die Merenskyrif en geassosieerde gesteentes in 'n aantal boorgat en mynprofiele op Swartklip 988, Rustenburg. *MSc Thesis Potchefstroom University for C.H.E. (unpubl.)*, 120 pp.

Van Zyl, J.P., (1970), The petrology of the Merensky Reef and the associated rocks on Swartklip 988, Rustenburg district. *In: Visser, D.J.L. and von Gruenewaldt, G. (eds), Symposium on the Bushveld Igneous Complex and other layered intrusions*. Geol. Soc. South Africa Spec. Pub., **1**, 80-107.

Vermaak, C.F., (1976), The Merensky Reef - thoughts on its environment and genesis. *Econ. Geol.*, **71**, 1270-1298.

Vermaak, C.F. and von Gruenewaldt, G., (1986), Introduction to the Bushveld Complex. *In: Anhaeusser, C.R. and Maske, S. (eds.), Mineral deposits of Southern Africa, Volume II*. Geol. Soc. South Africa, 1021-1029.

Viljoen, M.J., de Klerk, W.J., Coetzer, P.M., Hatch, N.P., Kinloch, E. and Peyerl, W., (1986a), The Union Section of Rustenburg Platinum mines limited with reference to the Merensky reef. *In: Anhaeusser, C.R. and Maske, S. (eds.), Mineral deposits of Southern Africa, Volume II.* Geol. Soc. South Africa, 1061-1090.

Viljoen, M.J., Theron, J., Underwood, B., Walters, B.M., Weaver, J. and Peyerl, W., (1986b), The Amandelbult section of Rustenburg Platinum Mines Limited, with reference to the Merensky Reef. *In: Anhaeusser, C.R. and Maske, S. (eds.), Mineral deposits of Southern Africa, Volume II.* Geol. Soc. South Africa, 1041-1060.

Viljoen, M.J. and Hieber, R., (1986), The Rustenburg section of Rustenburg Platinum Mines Limited, with reference to the Merensky Reef. *In: Anhaeusser, C.R. and Maske, S. (eds.), Mineral deposits of Southern Africa, Volume II.* Geol. Soc. South Africa, 1107-1134.

Von Gruenewaldt, G., (1971), A petrographical and mineralogical investigation of the Bushveld Igneous Complex in the Tauteshoogte - Roossenekal area of the eastern Transvaal. *D.Sc. Thesis University of Pretoria (unpubl.).*

Von Gruenewaldt, G., (1973), The Main and Upper Zones of the Bushveld Complex in the Roossenekal area, eastern Transvaal. *Trans. Geol. Soc. South Africa*, **76**, 207-227.

Von Gruenewaldt, G., Hatton, C.J., Merkle, R.K.W.and Gain, S. (1985), Platinum-chromitite associations in the Bushveld Complex. *Inst. for Geol. Res. on the Bushveld Complex.* University of Pretoria, Report No.55.

Wadsworth, W.J., (1973), Magmatic sediments. *Minerals Sci. Engng*, **5**, 25-35.

Wadsworth, W.J., (1985), Terminology of postcumulus processes and products in the Rhum layered intrusion. *Geol. Mag.*, **122**, 549-554.

Wager, L.R., (1968), Rhythmic and cryptic layering in mafic and ultramafic plutons. *In: Hess, H.H. and Poldervaart, A. (eds.), Basalts - Volume 2.* Wiley Interscience, 573-622.

Wager, L.R. and Deer, W.A., (1939), Geological investigation in east Greenland. Part III. The petrology of the Skaergaard intrusion, Kangerdlugssuak. *Medd. Gronland*, **105 No. 4**, 1-352.

Wager, L.R., Brown, G.M. and Wadsworth, W.J., (1960), Types of igneous cumulates. *Jour. of Pet.*, **1**, 73-85.

Wager, L.R. and Brown, G.M., (1968), *Layered Igneous Rocks.* Oliver and Boyd, London, 588 pp.

Wagner, P.A., (1925), Notes on the Platinum deposits of the Bushveld Igneous Complex. *Trans. Geol. Soc. South Africa*, **27**, 83-133.

Wagner, P.A., (1929), *The Platinum deposits and mines of South Africa.* Oliver and Boyd, Edinburgh, 326 pp.

Walker, K.R., (1970), The Palisade sill, New Jersey: a reinvestigation. *Geol. Soc. Amer. Spec. Paper*, **III**, 1-178.

Wasserstein, B., (1936), Some notes on the Critical Zone of the Bushveld gabbro at the Swartkop Chrome Mine in the Rustenburg district. *Trans. Geol. Soc. South Africa*, **39**, 215-222.

Weibe, R.A. and Wild, T., (1983), Fractional crystallization and magma mixing in the Tigalak layered intrusion, the Nain anorthosite complex, Labrador. *Contrib. Miner. Petrol.*, **84**, 327-344.

Willemse, J., (1964), A brief outline of the geology of the Bushveld Igneous Complex. *In: Haughton, S.H. (ed.), The geology of some ore deposits in Southern Africa, Volume 2.* Geol. Soc. South Africa, 91-128.

Willemse, J., (1969), The geology of the Bushveld Igneous Complex, the largest repository of magmatic ore deposits in the world: *Econ. Geol. Monogr.*, **4**, 1-22.

Wilson, J.R. and Larsen, S.B., (1982), Discordant layering relations in the Fongen-Hyllingen basic intrusion. *Nature*, **299**, 625-626.

Wilson, J.R. and Larsen, S.B., (1985), Two-dimensional study of a layered intrusion - the Hyllingen Series, Norway. *Geol. Mag.*, **122**, 97-124.

Wilson, J.R., Menuge, J.F., Pedersen, S. and Engell-Sorensen, O., (1987), The southern part of the Fongen-Hyllingen layered mafic complex, Norway: emplacement and crystallization of compositionally stratified magma. *In: Parsons, I. (ed.), Origins of Igneous Layering*: D. Reidel Publishing Co., 145-184.

Young, I.M., (1984), Mixing of supernatant and interstitial fluids in the Rhum layered intrusion. *Min. Mag.*, **48**, 345-350.

APPENDIX A.

SAMPLING

A1. UG1 Footwall and MG3 Unit at Spud Shaft - S samples.

Spud shaft, at RPM Union Section (Figure 1.3) was collared at a surface elevation of 1030m above mean sea level and intersected the Merensky Reef at a depth of 685m and the UG1 at 728m. Shaft bottom is at an elevation of -105m below mean sea level, effectively exposing a vertical profile of 1135m. The layered sequence exposed below the UG1 is of the order of 385m (ie. normal to the layering) but the lowermost 25m is quite inaccessible as it is used for ore and waste passes and the bottom of shaft loading station. These areas are concrete-lined which precluded any sampling and mapping.

By sampling a combination of underground borehole cores and sidewall samples (the latter making up the bulk of material) an effective column of some 350m, normal to the layering, was sampled below the UG1 chromitite. The uppermost layers of the MG chromitites were exposed in the **20 Level** station crosscut at 1030m below surface. To obtain further detail of the MG chromitite layers not exposed in the crosscut, two underground boreholes (T246 and T247) were drilled to reveal the sequence below this level. Selected sections of these two borehole cores were also used to complete the study column.

Sampling of the sequence between the MG chromitites and the UG1 chromitite was carried out along the **20 Level** twin-tramming crosscut at Spud Shaft which is 1250m long and at right angles to strike (Figure 1.3). This crosscut affords excellent exposures of the sequence with the layering dipping at 21° towards the south-east. Eighty two samples, of c. 3kg each, were taken at intervals of between 20 and 25m along the crosscut effectively providing a vertical sample interval of c. 5m (Figure 2.1).

A2. Union Section profiles UA, UB, UC and other Bastard Unit sequences.

All samples taken in the profiles **UA**, **UB**, **UC**, **LEF**, **Y**, **X** and **RD** consisted of borehole cores approximately 30cm long - in some cases the core had been split. These core, and half-core, samples were broken into roughly three equal parts. The outer two thirds were combined and crushed together to a fine pulp, which was used to make pressed power briquettes and glass fusion discs for XRF whole-rock analyses (see Appendix D). The inner third was retained as a library handspecimen, from which petrographic thin section and electron microprobe sections were prepared. In some cases samples were taken across unusual features and distinctive lithological contacts within the sequence. The above sampling procedure was also adopted at Amandelbult where in 1985 the author and Mr M. Field collected samples of the profiles **AD**, **AE** and **AF**. Mr. B Walters followed the same procedure for the sampling of the two unpublished profiles **B** and **C** at Amandelbult. For a detailed account of the sampling done at **UB** the reader is referred to de Klerk (1982, p.59).

A2.1 Lefkochrysos (Crocodile River) profile (LEF).

This sampled profile was taken from an exploration borehole (**H1/M4**) drilled c. 9km to the west of Brits (Figure 1.1). The base of the Bastard Unit was intersected at a depth of 998.2m and a representative suite of nine samples was selected for electron microprobe analyses. Six of these were used for whole-rock analytical work. Sample numbers, prefixed by **H**, indicate the depth of sampling below collar.

The Bastard Reef pyroxenite is clearly recognised but is anomalously thin, being only 15cm thick. The basal contact and thin chromite layer are well preserved, and no fault plane is evident. The top contact of the pyroxenite is sharp and is immediately overlain by mottled anorthosite (2.46m) which is correlated with the GMA. No noritic interval is evident between the pyroxenite and the anorthosite, unlike the other profiles. Overlying the mottled anorthosite is a 9.46m interval of leuconorite capped by a 20cm thick layer of mottled anorthosite. These two lithologies were initially correlated with the top two subdivisions of the GMA but have subsequently been shown to be of Main Zone affinity in

this study. The entire Bastard Unit is here taken to be only 2.61m thick while only some 4.1km to the west of this profile another borehole (**H4**) exposed a 43.5m Bastard Unit sequence almost identical to that at Western Platinum Mine.

A notable feature in this area is that the interval between the Main Zone Pyroxenite Marker and the Bastard Reef is only 1100m, while the same interval at Union Section is c. 2500m - a reduction in thickness of c. 1400m. It would therefore appear that the entire lower part of the Main Zone and the Bastard Unit are significantly reduced in thickness. The distinctive patterns of compositional variation seen in other profiles are thus obscured.

A2.2 Western Platinum Mine profile (WP).

No sampling was done at this locality and the profile has been constructed from the composite stratigraphic section described by Farquhar (1986). Here the Bastard pyroxenite is only 5cm thick and chromite grains may be present at the base. This anomalously thin pyroxenite appears to be similar to that seen at **LEF**, 14km to the east, although with a different hangingwall assemblage. The pyroxenite is overlain by norite (17.5m) which grades into leuconorite. Two distinctive, thin anorthosite layers occur within the noritic sequence at 7.6 and 13.8m above datum. Thicknesses of other lithologies within the Unit are presented in Table 4.2. Farquhar (1986, p.1137) describes the mottles within the UGMA as being "small, pale and irregular in shape". The overlying leucocratic assemblage (i.e. basal part of the Main Zone) is dominated by norite and leuconorite with occasional thin layers of mottled anorthosite.

A2.3 Two Rustenburg Section profiles (RPM).

Data for this area have been gleaned mainly from the work of Kruger (1982). A second profile published by Viljoen and Hieber (1986) was also used, with minor modifications based on the work of Vermaak (1976). An additional profile from the Rustenburg Townlands area has been discussed in some detail by Naldrett et al. (1984, 1986 and 1987).

Kruger (1982) compiled a composite stratigraphic profile depicting the central part of the Mine by collecting representative samples from underground exposures. These samples have the prefix "B" (not to be confused with profile **B** at Amandelbult). The microprobe data from 18 samples analysed by Kruger have been incorporated in this study. In each sample some eight plagioclase analyses and between four and nine analyses of each of the different pyroxene phases are available. Petrographic thin sections were cut from library specimens lodged by Kruger (see **4.7**).

The basal Bastard pyroxenite is between 2.8 and 3.5m thick and is overlain by a noritic unit, 8.3m thick. A distinctive feature of the norite is that thin anorthosite layers (≤0.5cm) occur c. 2m below the top contact, i.e. below the GMA. Kruger, however, includes a mottled anorthosite layer of 75cm in his composite column at this level. This unusually thick anorthosite layer is considered to be anomalous but nevertheless highlights the fact that discrete anorthosite layers occur near the top of the norite member in most of the profiles south of the Pilanesberg. Overlying the norite is the 53.8m-thick GMA. It is only in the basal 9.1m that large diffuse mottles occur (LGMA). Neither Kruger (1982) nor Viljoen and Hieber (1986) distinguished the upper two sub-divisions of the GMA which are readily recognisable in adjacent profiles.

A2.4 Three Impala profiles (Z, Y and X).

Z - Wildebeestfontein South mine (No. 1 shaft). This profile represents the generalised geological log for the southern part of Impala and is merely used to illustrate the lateral continuity of lithologies between **RPM** and Impala.

Y - Borehole 1329. The geological log of this borehole, drilled in the central part of the Mine, is one of a series along strike used by Leeb-du Toit (1986, p.1093 and 1096 designated E) in his descriptive paper of Impala Platinum Mine. This Bastard Unit profile is almost identical to that at RPM Rustenburg Section. Here the leuconorite interval (GMM) in the middle of the GMA is well defined and called the Hw4 layer by Leeb du-Toit (1986). The entire GMA is 43.5m thick and is subdivided into the Hw3, Hw4 and Hw5 layers (Leeb-du Toit, op. cit.). A total of nine samples

were taken in this profile and used by the present writer for whole-rock major and trace element analyses as well as electron microprobe analyses (see Table 4.2).

X - Borehole 1512. This profile in the extreme northern part of the Mine is somewhat anomalous as there is an additional layer of feldspathic pyroxenite (4.75m thick) at the contact between the norite and GMA. The GMA has also been reduced in thickness to 36.7m. Nine representative samples, including one from the immediate hangingwall of the GMA have been analysed.

A2.5 Two Rooderand profiles (RD).

Borehole RD-6. This Upper Critical Zone borehole was initially selected and sampled because it best represents the normal succession in this area between the UG1 and the top of the Bastard Unit. It was subsequently found that the entire basal part of the GMA, and the first 4m of overlying leuconorite, has been altered (saussuritised) and rendered unsuitable for analysis. This is the reason for a gap in analytical data for this profile.

A further complication is that a number of small shears and a prominent fault zone occur over a core length of 1.8m within the Bastard norite; this faulting appears to have reduced the thickness of the pyroxenite - norite sequence. The contact between norite and the GMA is highly altered and is thought likely to encompass a fault plane along which hydrothermal fluids were introduced. A number of thin, intrusive Pilanesberg sills are also evident within the profile and these younger intrusives contribute to the overall disturbance of this section. Because this profile is in close proximity to the younger intrusive Pilanesberg Alkali Complex it is likely that the Critical Zone country rocks were subjected to hydrothermal activity at the time of this intrusive event.

A total of 19 samples was taken through the Bastard Unit but only eight were suitable for whole-rock analytical work and nine for mineral microprobe analyses (Figure 4.4). Whole-rock samples were selected where the degree of alteration is less than 10% (estimated by point-counting).

The basal pyroxenitic rocks are quite fresh whereas the more leucocratic rocks show alteration.

Borehole RD-11. This borehole was collared 2.9km to the north of the Pilanesberg and the logging indicates an undisturbed Bastard Unit profile. The lower part of the profile is very similar to **Y** at Impala except that a thickening of the Bastard pyroxenite to 5.1m is noted. A thin (1cm) anorthosite layer is also found at the contact between the pyroxenite and the noritic lithologies. This anorthosite layer (or layers) is usually found nearer the top of the norite in the profiles to the south of the Pilanesberg. The basal part of the GMA in both these Rooderand boreholes is well defined, but the logging in the upper part of the GMA fails to define the upper contact of the Bastard Unit.

A2.6 Three Union Section profiles (UA, UB and UC).

Profile UA (borehole HN-3). This borehole profile refers to the southern part of Union Section (Figure 1.3). Here the Bastard Unit has at its base a thin pegmatoidal pyroxenite (6cm) which is overlain by 5.8m of feldspathic pyroxenite and 12m of norite. The three sub-divisions of the GMA (46.3m) are readily recognisable, with the basal LGMA being 13.7m, followed by leuconorite with subdued mottling (GMM - 16.5m) and finally the small-mottled anorthosite (UGMA - 16.1m). A suite of 27 close-spaced samples was taken through the sequence (Figure 4.4).

Profile UB. A composite profile for the central part of Union Section has been built up from two underground boreholes 1,5km apart along strike (**B235** in the 13-30S crosscut and **B232** in 14-21S crosscut). This section was documented by de Klerk (1982) with the emphasis then being placed on the succession between the lower half of the LGMA and an horizon 4m below the UG1. Both these boreholes were drilled at right angles to the layering - all thicknesses are therefore true. Drilling machine limitations on upward drilling precluded the sampling of the upper succession of the GMA and only 7m of the LGMA was cored. Thicknesses of the GMA (Table 4.2) have been extrapolated from a surface borehole (TB-14) 1,4km up-dip from the **UB** profile. A suite of 13 samples was analysed for whole-rock major and trace elements but no microprobe analyses were executed.

Profile UC (borehole ZK-10). This borehole is situated in the northeastern part of Union Section (Figure 1.3) and is almost identical in sequence to **UA** 7.7km to the southwest. The only difference is that the pyroxenite is marginally thinner at **UC** (4m) and the GMA is 48.5m thick - 1.5m thicker than at **UA**. Twenty samples were taken in the lower part of the Bastard Unit (Figure 4.4).

A2.7 Five Amandelbult Section profiles (AD, AE, AF, B and C).

Geological logs and the bulk of analytical data relating to the profiles **AD**, **AE** and **AF** have been taken from Field (1987), while those for profiles **B** and **C** have been taken from unpublished work by B. Walters (1982). Petrographic thin sections of the Bastard Unit samples used in Field's study were re-examined by the author and are discussed in **4.7.**

The Bastard Unit sequence at Amandelbult is remarkably consistent along strike with a thinning of the layers only being observed in the most easterly profile **C** (Table 4.2). Stratigraphic data for the entire GMA are available only in profile **B**, and show it to be similar to that at Union Section.

Profile AD (borehole EL-15). The geological log and a suite of 14 samples were available for this profile.

Profile AE (borehole SKN-19). This profile formed the focus of Field's (1987) study where whole-rock major and trace element analyses were executed on a suite of 15 samples of the Bastard Unit. Selected samples from this unit were also used by Field for microprobe analyses of the silicate mineral phases.

Profile B (borehole 7E/3). Close-spaced samples, at one metre intervals, were taken from the top of the LGMA to the base of the Bastard Unit. These samples were analysed for seven trace elements. No thin sections or library samples were available for petrographic examination.

Profile AF (borehole ML-30). The geological log and a suite of 16 samples were available for this profile. Field (1987) presented the trace element data for this profile. Preparatory work by Field for the major element analyses was taken to completion by the author and available thin sections were used for petrographic study.

Profile C (borehole 60E/3). Detailed sampling, at one metre intervals, was done from the middle of the LGMA to the base of the Bastard Unit and samples were analysed for seven trace elements. Two samples (C-10 and C-20) were excluded from this study as they represent thin lamprophyre sills in pyroxenite and leuconorite. No thin sections were available for petrographic examination.

APPENDIX B.

MODAL ANALYSES

Modal analyses were carried out on 33 samples from the profiles at **LEF**, **X**, **Y** and **RD**. A Swift automatic point-counter and electro-mechanical stage were used. Mineral proportions are calculated as volume percentages and each analysis is based on between 500 and 900 points. No distinction is made in Table B1 for the textural habits of the phases.

TABLE B1: Modal compositions in four Bastard Unit sequences.

Sample Number	plag	opx	cpx	bms	chr	bi	alt	No. Points
LEF profile								
H979.1	59.3	36.1	2.7	0.2	-	0.8	0.8	479
H984.48	69.3	28.5	1.2	0.3	-	0.3	0.3	589
H992.8	70.8	26.7	1.2	0.4	-	0.5	0.4	565
H995.5	67.6	21.1	4.1	0.5	-	0.4	6.4	565
H995.6	96.0	0.6	2.2	0.3	-	0.1	0.7	957
H997.26	82.4	16.2	1.0	0.4	-	-	-	518
H998.1	25.1	73.3	0.8	0.2	0.2	0.4	-	490
Y profile								
Y722.4	69.7	14.1	13.4	0.4	-	1.3	1.1	793
Y740.5	76.0	18.5	1.7	0.4	-	1.5	1.9	745
Y746.4	90.6	4.0	3.8	0.2	-	-	1.4	810
Y755.66	80.5	10.6	6.2	-	-	0.8	1.9	889
Y760.2	86.2	4.9	8.5	0.4	-	-	-	857
Y764.4	68.3	29.3	2.5	-	-	-	-	775
Y765.48	88.0	1.5	10.4	0.1	-	-	-	827
Y770.58	56.1	35.5	7.4	-	-	0.1	0.9	798
Y775.0	18.2	71.8	1.5	0.4	0.2	6.6	1.3	944
X profile								
X735.0	85.0	4.4	9.0	-	0.1	0.6	0.8	789
X745.44	88.6	9.7	0.1	-	-	-	-	667
X763.95	92.9	5.7	0.5	0.6	-	0.1	0.2	814
X768.5	70.9	22.3	5.4	-	-	0.2	1.2	588
X776.5	88.1	9.0	1.9	0.5	-	-	0.5	790
X779.82	23.3	73.3	1.6	1.0	0.5	0.4	-	764
X782.7	68.6	28.5	2.6	0.2	-	0.2	0.0	622
X788.41	46.1	50.7	2.0	0.7	-	0.5	-	881
X791.8	14.1	76.9	3.3	1.4	-	2.7	1.6	789
RD profile								
RD-1	83.5	0.4	4.7	-	-	-	11.4	508
RD-3	86.9	1.0	4.3	-	-	-	7.9	609
RD-4	76.5	10.4	3.5	-	-	0.1	9.5	693
RD-6	79.9	0.4	11.2	0.1	-	-	8.4	735
RD-15	59.4	29.8	1.7	0.1	-	-	9.0	763
RD-16	43.0	53.3	1.4	-	-	-	2.3	570
RD-17	22.6	73.5	3.4	-	-	0.1	0.3	667
RD-18	22.4	67.2	6.3	1.5	-	2.5	0.1	687

plag = plagioclase opx = orthopyroxene cpx = clinopyroxene
chr = chromite bi = biotite alt = alteration products
bms = base metal sulphides

APPENDIX C.

ELECTRON MICROPROBE ANALYSES

The Rhodes University automated **JEOL CXA-733** electron microprobe was used for all mineral analyses, using well tested international standards and pure synthetic crystals for calibration. Most work was done with a defocused 10 micron beam.

This instrument has four crystal spectrometers, two of which are gas flow counters, while the remainder are sealed xenon counters. Samples were prepared as polished thin sections which were carbon coated under vacuum to a thickness of approximately 250 Å. The thickness of the coating was monitored by comparison with the interference colours produced by the carbon on a polished brass plate.

An acceleration potential of 15Kv and a sample current of 25nA was used for all analyses. The beam current was continually monitored by reference to a Faraday cage. The Counting times of 20 seconds on element K-alpha peaks and 10 seconds on background positions on either side of the peak was done for all elements. An electron beam of approximately 10 micron in diameter was used for all analyses except those for the plagioclase analyses used for the determination of zoning - here a focused beam of 1 micron was used.

Data reduction was done using the PACX program supplied by the instrument manufacturers. This program applies the ZAF correction scheme; an Atomic number (Z) correction using Philibert-Tixier's formula, an Absorption correction (A) using Philibert-Heinrich's formula and a Fluorescence correction (F) using Reed's formula (Philibert and Tixier, 1968).

Philibert, J. and Tixier, R., (1968), Brit. Jour. App. Phys., p.1685-1964.

TABLE C1: Instrument settings and standards used for electron microprobe analyses.

Olivine analyses.

Element	Standard	Crystal	Standard CPS
SiO_2	SiO_2 (UK)	TAP	25245
MgO	MgO (UK)	TAP	22338
CaO	Wollastonite (RU)	PET	6310
NiO	NiO (UK)	LiF	3925
FeO	Rhodonite (UK)	LiF	431
MnO	Rhodonite (UK)	PET	8699

Pyroxene analyses.

Element	Standard	Crystal	Standard CPS
SiO_2	SiO_2 (UK)	TAP	25337
TiO_2	TiO_2 (UK)	PET	10852
Al_2O_3	Al_2O_3 (UK)	TAP	26791
FeO	Rhodonite (UK)	LiF	439
Cr_2O_3	Cr_2O_3 (UK)	PET	33516
MnO	Rhodonite (UK)	LiF	1276
NiO	NiO (UK)	LiF	3837
MgO	MgO (UK)	TAP	22560
CaO	Wollastonite (RU)	PET	6227
Na_2O	Jadeite (RU)	TAP	1812

Plagioclase analyses.

Element	Standard	Crystal	Standard CPS
SiO_2	SiO_2 (UK)	TAP	25087
Al_2O_3	Al_2O_3 (UK)	TAP	26595
FeO	Rhodonite (UK)	LiF	431
CaO	Wollastonite (RU)	PET	6301
Na_2O	Jadeite (RU)	TAP	576
K_2O	Orthoclase (RU)	PET	1776

Note: The standards marked (UK) were obtained from Polaron Equipment Ltd., Watford, England, while those marked (RU) are Rhodes University in-house standards which have been acquired from various operating laboratories, and are well used and tested.

ANALYTICAL ERROR

It is recognised that for any single analysis, variation or error could be be introduced by:

1) instrumental drift
2) counting error
3) electron beam diameter
4) thickness of carbon coating
5) suitability of standards compared to unknowns

To account for some of the above factors a series of analyses where carried out on both plagioclase and orthopyroxene. An optically homogeneous grain of each mineral was chosen from sample S-15. The results of analyses under differing conditions are presented in Table C2 and C3. In summary the standard deviation yielded by multiple analyses of single grains was 0.30% An for plagioclase, and 0.002 for MMF in orthopyroxene.

TABLE C2: Plagioclase analyses for sample S-15 (UG1 Footwall Unit).
(c = core of cumulus grain; i = inclusion within orthopyroxene)

	SiO_2	Al_2O_3	Fe_2O_3	CaO	Na_2O	K_2O	Total	%An
Set A - Core of a cumulus grain with 10 micron beam - same spot.								
S-15	49.78	32.05	0.27	15.60	2.81	0.16	100.67	75.41
S-15	49.97	32.18	0.21	15.52	2.92	0.15	100.95	74.61
S-15	50.11	32.11	0.27	15.62	2.90	0.16	101.17	74.86
S-15	49.70	31.97	0.27	15.57	2.85	0.16	100.53	75.13
S-15	49.97	32.13	0.23	15.68	2.91	0.17	101.09	74.84
S-15	49.88	32.14	0.24	15.41	2.90	0.16	100.74	74.61
Mean	49.90	32.10	0.25	15.57	2.88	0.16	100.86	74.91
Std.dev.	0.135	0.068	0.024	0.085	0.039	0.006	0.232	0.285
Set B - Core of same cumulus grain with 20 micron beam. (moved 20 microns away from Set A.)								
S-15	50.13	32.06	0.29	15.20	2.91	0.15	100.73	74.29
S-15	50.20	32.09	0.26	15.32	2.91	0.16	100.95	74.46
S-15	50.12	31.85	0.24	15.24	2.82	0.17	100.44	74.91
S-15	49.94	31.89	0.25	15.30	2.87	0.16	100.42	74.65
S-15	49.98	31.93	0.24	15.31	2.82	0.15	100.42	75.02
S-15	50.07	31.94	0.30	15.28	2.84	0.17	100.60	74.84
Mean	50.07	31.96	0.26	15.27	2.86	0.16	100.60	74.69
Std.dev.	0.090	0.087	0.025	0.043	0.037	0.006	0.195	0.256

	SiO_2	Al_2O_3	Fe_2O_3	CaO	Na_2O	K_2O	Total	%An
Set C - Cores of different cumulus grains - 10 micron beam.								
S-15 c	50.32	31.57	0.20	15.41	2.83	0.02	100.35	75.05
S-15 c	50.74	31.49	0.14	15.08	3.04	0.02	100.52	73.25
S-15 c	50.48	31.83	0.17	15.35	2.88	0.03	100.74	74.66
S-15 c	49.67	32.34	0.19	15.76	2.59	0.02	100.57	77.11
S-15 c	50.35	31.80	0.22	15.16	2.92	0.03	100.47	74.18
S-15 c	50.73	31.78	0.27	15.01	2.97	0.03	100.78	73.65
S-15 c	50.66	31.72	0.24	15.25	2.94	0.02	100.84	74.13
S-15 c	50.88	31.35	0.20	14.80	3.19	0.02	100.44	71.97
S-15 c	50.04	31.73	0.25	15.24	2.89	0.03	100.18	74.46
S-15 c	49.77	31.80	0.21	15.39	2.87	0.03	100.06	74.78
Mean	50.37	31.74	0.21	15.24	2.91	0.02	100.50	74.32
Std.dev.	0.398	0.249	0.036	0.247	0.146	0.004	0.241	1.259
Set D - Cores of different inclusions - 10 micron beam.								
S-15 i	51.17	30.96	0.35	14.45	3.40	0.01	100.33	70.11
S-15 i	50.63	30.82	0.33	14.67	3.34	0.01	99.79	70.82
S-15 i	50.57	30.74	0.32	14.67	3.36	0.02	99.67	70.72
S-15 i	50.18	31.00	0.34	14.95	3.16	0.01	99.63	72.34
S-15 i	50.06	31.03	0.32	15.02	3.22	0.02	99.67	72.04
S-15 i	50.31	31.52	0.26	14.96	3.08	0.03	100.16	72.86
S-15 i	50.54	31.70	0.33	14.90	3.25	0.01	100.74	71.68
S-15 i	50.59	31.63	0.31	14.95	3.21	0.02	100.72	72.02
S-15 i	50.40	31.88	0.32	14.97	3.09	0.02	100.68	72.82
S-15 i	50.52	31.70	0.26	15.05	3.11	0.02	100.66	72.82
Mean	50.42	31.33	0.31	14.91	3.20	0.02	100.19	72.01
Std.dev.	0.287	0.405	0.027	0.185	0.111	0.007	0.454	0.926
Means and Standard deviations for Sets A, B and C.								
Mean	50.16	31.90	0.23	15.34	2.89	0.10	100.62	74.59
Std.dev.	0.344	0.234	0.039	0.222	0.105	0.069	0.272	0.908
Mean and Standard deviations for sets A, B, C and D.								
Mean	50.26	31.71	0.26	15.19	2.99	0.07	100.49	73.72
Std.dev.	0.363	0.409	0.051	0.307	0.187	0.069	0.390	1.572

TABLE C3: Orthopyroxene analyses of sample S-15 (UG1 Footwall Unit). (c = cores, m = margins of grains)

	SiO_2	TiO_2	Al_2O_3	Cr_2O_3	FeO	MnO	NiO	MgO	CaO	Na_2O	Total	MMF
Set E - Core of a cumulus grain - 10 micron beam (all within a 20 micron radius)												
S-15	55.24	0.16	0.96	0.40	13.19	0.24	0.12	28.19	1.34	0.01	99.86	0.792
S-15	55.28	0.17	0.97	0.39	13.03	0.28	0.09	27.93	1.37	0.00	99.51	0.793
S-15	55.07	0.17	0.95	0.39	12.76	0.28	0.12	28.03	1.37	0.00	99.15	0.797
S-15	54.96	0.18	0.96	0.40	12.84	0.26	0.14	27.80	1.35	0.00	98.91	0.794
S-15	54.85	0.15	1.01	0.43	13.05	0.21	0.09	28.15	1.85	0.02	99.81	0.794
S-15	55.02	0.15	1.02	0.42	12.89	0.23	0.06	28.01	1.82	0.02	99.63	0.795
S-15	55.12	0.14	1.02	0.41	12.45	0.24	0.03	27.94	1.84	0.02	99.21	0.800
S-15	54.78	0.13	1.00	0.40	12.91	0.29	0.06	27.88	1.81	0.01	99.27	0.794
S-15	55.18	0.19	0.97	0.37	13.20	0.34	0.07	28.29	1.48	0.02	100.11	0.792
S-15	55.09	0.16	0.96	0.36	13.14	0.29	0.03	28.46	1.47	0.01	99.97	0.794
S-15	54.90	0.17	0.96	0.37	13.12	0.29	0.04	28.43	1.49	0.01	99.79	0.794
S-15	55.14	0.19	0.96	0.38	13.03	0.24	0.02	28.27	1.46	0.01	99.71	0.795
Mean	55.05	0.16	0.98	0.39	12.97	0.27	0.07	28.12	1.55	0.01	99.58	0.794
Std	0.150	0.017	0.025	0.019	0.207	0.034	0.037	0.207	0.199	0.007	0.353	0.002
	SiO_2	TiO_2	Al_2O_3	Cr_2O_3	FeO	MnO	NiO	MgO	CaO	Na_2O	Total	MMF
Set F - Cores of different cumulus grains with 10 micron beam.												
S-15 c	54.77	0.17	0.86	0.35	13.20	0.29	0.05	29.74	1.05	0.00	100.50	0.801
S-15 c	54.86	0.17	0.84	0.35	13.04	0.31	0.07	29.83	0.93	0.00	100.40	0.803
S-15 c	54.88	0.16	0.79	0.35	13.24	0.32	0.05	29.93	0.92	0.01	100.65	0.801
S-15 c	54.88	0.19	0.82	0.36	13.28	0.28	0.05	29.66	0.98	0.01	100.50	0.799
S-15 c	54.99	0.17	0.85	0.34	13.10	0.29	0.04	29.73	1.05	0.00	100.57	0.802
S-15 c	54.75	0.14	0.92	0.38	12.79	0.30	0.07	29.64	1.35	0.02	100.34	0.805
S-15 c	54.73	0.18	0.85	0.35	12.98	0.31	0.06	29.67	1.00	0.00	100.13	0.803
S-15 c	54.69	0.18	0.83	0.37	12.93	0.31	0.07	29.83	1.10	0.01	100.32	0.804
S-15 c	54.96	0.17	0.88	0.35	12.91	0.30	0.04	29.69	1.18	0.00	100.47	0.804
S-15 c	54.74	0.17	0.93	0.36	13.11	0.29	0.06	29.65	1.19	0.01	100.50	0.801
Mean	54.82	0.17	0.86	0.36	13.06	0.30	0.06	29.74	1.07	0.01	100.44	0.802
Std	0.097	0.013	0.040	0.011	0.150	0.010	0.011	0.092	0.126	0.005	0.140	0.002
Set G - Margins of different cumulus grains with 10 micron beam.												
S-15 m	55.23	0.18	0.92	0.36	13.17	0.25	0.08	29.07	0.66	0.01	99.94	0.797
S-15 m	55.56	0.19	0.89	0.33	13.01	0.25	0.05	28.89	0.64	0.01	99.81	0.798
S-15 m	55.66	0.16	0.94	0.32	13.12	0.29	0.09	28.82	0.62	0.02	100.01	0.797
Mean	55.48	0.18	0.92	0.34	13.10	0.26	0.07	28.93	0.64	0.01	99.92	0.797
Std	0.185	0.013	0.020	0.019	0.069	0.017	0.017	0.104	0.019	0.004	0.085	0.001
Means and Standard deviations of Sets E, F and G.												
Mean	55.01	0.17	0.92	0.37	13.02	0.28	0.07	28.86	1.25	0.01	99.96	0.798
Std	0.245	0.016	0.066	0.027	0.181	0.030	0.028	0.774	0.356	0.007	0.479	0.004

In the following pages the compositions of olivine, orthopyroxene, clinopyroxene, plagioclase and chromite are listed. These determinations were all done by the author unless otherwise stated in the table caption.

NOTES:

1. Olivine - Fo = cationic ratio of Mg/(Mg + Fe)

2. Ortho- and clinopyroxene
   MMF = cationic ratio of Mg/(Mg + Fe)
   Wo = cationic ratio of Ca/(Mg + Fe + Ca)
   En = cationic ratio of Mg/(Mg + Fe + Ca)
   Fs = cationic ratio of Fe/(Mg + Fe + Ca)

3. Plagioclase - An = cationic ratio of Ca/(Ca + Na) as a %.

Deer, Howie and Zussman (1972, p.322) note that most iron reported in feldspar analyses is shown to be Fe^{+3}, which replaces some of the Al in the structure. With this in mind the microprobe FeO values were converted to Fe_2O_3 on the basis of stoichiometry and the totals adjusted accordingly.

4. Chromite
   (P) = value from microprobe analysis
   (C) = recalculated value assuming stoichiometry
   Cr/Al = cationic ratio of Cr/Al
   MMF = cationic ratio of $Mg/(Mg + Fe^{2+})$
   FFE = cationic ratio of $Fe^{3+}/(Fe^{3+} + Fe^{2+})$
   Cr/Cr+Al = cationic ratio of Cr/(Cr + Al)

MICROPROBE DATA TABLE C4: Composition of **olivine** in the Bastard Unit - profile **UC**.
Metres given above base of Unit.
* = analyses done at the University of Cape Town.

Sample	UC-11	UC-11	UC-11	UC-11	UC-11	UC-11	UC-11	UC-11	UC-11*	UC-11*	UC-11*	UC-11	UC-11	UC-11	UC-11	UC-11	UC-11*	UC-13	UC-13	UC-13	UC-13	UC-13	UC-13	UC-13	UC-13*	UC-13*	UC-13*
Metres	14.7	14.7	14.7	14.7	14.7	14.7	14.7	14.7	14.7	14.7	14.7	14.7	14.7	14.7	14.7	14.7	14.7	11.1	11.1	11.1	11.1	11.1	11.1	11.1	11.1	11.1	11.1
Position	c = core	c	c	c	c	c	c	c	c	c	c	m = margin	m	m	m	m	m	c	c	c	c	c	c	c	c	c	c
Wt.%																											
SiO_2	39.32	39.09	39.38	39.03	39.10	39.22	39.22	39.11	38.44	38.62	38.36	39.21	39.24	39.24	39.16	39.24	38.68	38.48	38.53	38.65	38.50	38.69	38.42	38.62	38.68	38.60	38.61
FeO	17.77	17.84	18.24	17.88	18.15	17.82	17.97	18.26	18.58	18.81	18.36	18.13	17.77	17.45	18.06	17.77	18.05	19.48	19.06	18.61	18.81	19.17	19.17	19.06	19.51	19.38	19.44
MnO	0.25	0.27	0.29	0.30	0.27	0.27	0.26	0.27	0.31	0.32	0.35	0.29	0.29	0.25	0.27	0.29	0.32	0.21	0.22	0.23	0.22	0.25	0.25	0.23	0.27	0.25	0.29
NiO	0.13	0.14	0.13	0.16	0.14	0.17	0.17	0.13	0.11	0.18	0.17	0.13	0.13	0.15	0.13	0.13	0.17	0.27	0.26	0.31	0.28	0.29	0.31	0.26	0.24	0.24	0.30
MgO	41.72	41.81	41.59	41.85	41.97	41.54	41.79	41.78	41.58	41.46	41.62	41.54	42.09	41.65	41.56	42.09	41.70	41.37	41.61	42.00	41.75	41.56	41.44	41.72	41.04	41.12	41.09
CaO	0.00	0.00	0.01	0.00	0.01	0.00	0.00	0.00	0.00	0.00	0.00	0.00	0.00	0.00	0.00	0.00	0.06	0.08	0.01	0.00	0.00	0.01	0.01	0.00	0.00	0.00	0.02
Total	99.19	99.14	99.64	99.22	99.64	99.01	99.41	99.54	99.02	99.39	98.86	99.29	99.52	98.74	99.18	99.52	98.98	99.89	99.68	99.80	99.55	99.97	99.60	99.89	99.74	99.59	99.75
Cations (based on 4 oxygens)																											
Si	1.0082	1.0039	1.0073	1.0021	1.0006	1.0081	1.0049	1.0023	0.9936	0.9955	0.9929	1.0063	1.0034	1.0095	1.0061	1.0034	0.9977	0.9906	0.9917	0.9915	0.9911	0.9932	0.9908	0.9917	0.9965	0.9955	0.9949
Fe	0.3810	0.3831	0.3902	0.3840	0.3885	0.3831	0.3851	0.3912	0.4016	0.4055	0.3974	0.3891	0.3800	0.3754	0.3880	0.3800	0.3893	0.4194	0.4103	0.3993	0.4049	0.4115	0.4134	0.4093	0.4203	0.4180	0.4189
Mn	0.0054	0.0058	0.0063	0.0065	0.0059	0.0058	0.0056	0.0059	0.0068	0.0070	0.0077	0.0062	0.0064	0.0055	0.0058	0.0064	0.0070	0.0045	0.0048	0.0050	0.0048	0.0054	0.0054	0.0050	0.0059	0.0055	0.0063
Ni	0.0027	0.0029	0.0027	0.0032	0.0029	0.0035	0.0036	0.0026	0.0023	0.0037	0.0035	0.0027	0.0027	0.0031	0.0027	0.0027	0.0035	0.0056	0.0053	0.0065	0.0059	0.0060	0.0065	0.0054	0.0050	0.0050	0.0062
Mg	1.5944	1.6004	1.5857	1.6019	1.6011	1.5914	1.5959	1.5957	1.6020	1.5929	1.6056	1.5893	1.6041	1.5970	1.5913	1.6041	1.6031	1.5872	1.5961	1.6061	1.6021	1.5903	1.5928	1.5970	1.5759	1.5806	1.5782
Ca	0.0000	0.0000	0.0004	0.0000	0.0002	0.0000	0.0000	0.0000	0.0000	0.0000	0.0000	0.0000	0.0000	0.0000	0.0000	0.0000	0.0017	0.0022	0.0002	0.0001	0.0001	0.0003	0.0003	0.0001	0.0000	0.0000	0.0006
Total	2.9918	2.9961	2.9927	2.9979	2.9994	2.9919	2.9951	2.9977	3.0064	3.0045	3.0071	2.9937	2.9966	2.9905	2.9939	2.9966	3.0023	3.0094	3.0083	3.0085	3.0089	3.0068	3.0092	3.0083	3.0035	3.0045	3.0051
Fo	80.71	80.68	80.25	80.66	80.47	80.60	80.56	80.31	79.95	79.71	80.16	80.33	80.85	80.97	80.40	80.85	80.46	79.10	79.55	80.09	79.82	79.44	79.39	79.60	78.94	79.09	79.02
Ni ppm	1038	1102	1029	1220	1120	1320	1366	982	864	1415	1336	1037	1038	1175	1038	1038	1336	2128	2029	2457	2238	2274	2464	2038	1886	1886	2358

Sample	UC-13	UC-13	UC-13	UC-13	UC-13	UC-13	UC-13	UC-13	UC-13	UC-13*	UC-13*	UC-13	UC-17*	UC-17*	UC-17*
Metres	11.1	11.1	11.1	11.1	11.1	11.1	11.1	11.1	11.1	11.1	11.1	11.1	4.1	4.1	4.1
Position	c	c	m	m	m	m	m	m	m	m	m	m	c	c	c
Wt.%															
SiO_2	38.62	38.71	38.71	38.95	38.59	38.46	38.47	38.48	38.47	38.77	38.39	38.95	38.39	38.69	38.73
FeO	19.05	19.01	19.02	19.03	18.80	18.81	18.88	18.90	19.19	18.94	19.28	19.03	17.91	18.14	17.97
MnO	0.20	0.18	0.20	0.22	0.21	0.22	0.22	0.22	0.25	0.23	0.27	0.22	0.26	0.24	0.20
NiO	0.28	0.28	0.26	0.22	0.24	0.27	0.26	0.22	0.27	0.27	0.25	0.22	0.36	0.33	0.33
MgO	41.00	41.24	41.53	41.64	41.55	41.49	41.36	41.54	41.61	41.05	41.31	41.64	42.94	42.63	42.71
CaO	0.09	0.08	0.01	0.01	0.01	0.01	0.02	0.02	0.01	0.05	0.04	0.01	0.00	0.03	0.00
Total	99.25	99.50	99.72	100.06	99.41	99.25	99.20	99.38	99.80	99.32	99.54	100.06	99.86	100.06	99.94
Cations (based on 4 oxygens)															
Si	0.9981	0.9973	0.9951	0.9971	0.9945	0.9932	0.9941	0.9926	0.9898	1.0002	0.9910	0.9971	0.9827	0.9883	0.9894
Fe	0.4117	0.4096	0.4088	0.4073	0.4052	0.4062	0.4080	0.4078	0.4130	0.4086	0.4162	0.4073	0.3834	0.3875	0.3839
Mn	0.0044	0.0040	0.0043	0.0047	0.0047	0.0049	0.0047	0.0048	0.0054	0.0050	0.0059	0.0047	0.0056	0.0052	0.0043
Ni	0.0059	0.0059	0.0054	0.0045	0.0051	0.0055	0.0055	0.0046	0.0057	0.0056	0.0052	0.0045	0.0074	0.0068	0.0068
Mg	1.5792	1.5838	1.5912	1.5890	1.5957	1.5969	1.5932	1.5971	1.5960	1.5789	1.5895	1.5890	1.6383	1.6231	1.6262
Ca	0.0026	0.0022	0.0002	0.0003	0.0003	0.0002	0.0004	0.0006	0.0004	0.0014	0.0011	0.0003	0.0000	0.0008	0.0000
Total	3.0019	3.0027	3.0049	3.0029	3.0055	3.0068	3.0059	3.0074	3.0102	2.9998	3.0090	3.0029	3.0173	3.0117	3.0106
Fo	79.32	79.45	79.56	79.60	79.75	79.72	79.61	79.66	79.44	79.44	79.25	79.60	81.04	80.73	80.90
Ni ppm	2228	2219	2046	1709	1919	2089	2062	1742	2158	2122	1965	1709	2829	2593	2593

MICROPROBE DATA TABLE C5: Composition of **orthopyroxene** in the UG1 Footwall and MG3 Units - all S samples.
Metres given below base of UG1 chromitite.
c = core of grain m = grain margin.

Sample	S-1	S-1	S-1	S-1	S-1	S-2	S-2	S-2	S-2	S-2	S-2	S-2	S-2	S-2	S-2	S-2	S-2	S-2	S-3	S-3	S-3	S-4	S-4	S-4	S-4	S-4	S-4
Metres	2.6	2.6	2.6	2.6	2.6	5.3	5.3	5.3	5.3	5.3	5.3	5.3	5.3	5.3	5.3	5.3	5.3	5.3	8.4	8.4	8.4	11.3	11.3	11.3	11.3	11.3	11.3
Position	c	c	c	c	c	c	c	c	c	c	c	c	c	c	c	m	m	m	c	c	c	c	c	c	c	c	c
Wt. %																											
SiO_2	55.09	55.82	56.24	56.40	55.95	54.79	54.89	54.39	54.31	54.91	54.54	54.75	54.66	54.33	54.20	55.26	55.13	55.15	52.87	52.84	52.51	53.34	53.30	52.56	52.68	52.89	53.25
TiO_2	0.08	0.07	0.08	0.09	0.09	0.13	0.11	0.13	0.12	0.11	0.13	0.12	0.13	0.14	0.12	0.11	0.11	0.10	0.11	0.44	0.15	0.15	0.13	0.16	0.16	0.11	0.19
Al_2O_3	0.94	0.88	1.06	1.08	0.84	1.02	1.04	1.01	1.05	0.98	1.11	0.92	0.97	0.91	0.92	0.88	0.88	0.95	0.62	0.62	0.64	0.63	0.64	0.59	0.58	0.55	0.63
Cr_2O_3	0.30	0.22	0.28	0.29	0.28	0.52	0.54	0.51	0.56	0.49	0.57	0.49	0.51	0.45	0.45	0.38	0.39	0.43	0.01	0.03	0.00	0.03	0.04	0.04	0.03	0.03	0.05
FeO	11.31	10.08	9.13	9.01	11.39	11.80	11.68	12.22	11.90	12.18	12.09	12.21	12.43	12.52	12.20	12.42	12.57	12.60	23.38	23.00	24.41	22.94	23.01	23.62	23.65	23.54	22.62
MnO	0.24	0.20	0.20	0.21	0.27	0.22	0.22	0.27	0.23	0.22	0.27	0.27	0.27	0.27	0.23	0.20	0.21	0.25	0.52	0.48	0.60	0.45	0.45	0.47	0.49	0.51	0.45
NiO	0.05	0.08	0.09	0.10	0.08	0.06	0.08	0.09	0.08	0.05	0.09	0.07	0.08	0.09	0.08	0.12	0.13	0.10	0.00	0.00	0.00	0.04	0.03	0.06	0.03	0.01	0.09
MgO	31.14	32.80	32.98	32.97	30.93	30.30	30.40	30.52	30.13	30.61	30.00	30.44	30.57	30.52	30.73	30.34	30.05	29.90	20.78	20.88	19.59	21.74	21.81	21.46	21.49	21.54	22.01
CaO	0.47	0.35	0.35	0.39	0.52	1.28	1.23	1.14	1.55	0.96	1.65	0.88	0.84	0.89	0.93	0.57	0.49	0.70	0.85	0.71	0.87	0.71	0.69	0.69	0.77	0.55	0.73
Na_2O	0.02	0.01	0.01	0.01	0.00	0.02	0.01	0.01	0.02	0.02	0.01	0.01	0.00	0.01	0.00	0.01	0.00	0.01	0.00	0.00	0.00	0.02	0.00	0.01	0.01	0.01	0.01
Total	99.65	100.50	100.41	100.55	100.35	100.13	100.20	100.30	99.96	100.51	100.45	100.15	100.46	100.13	99.85	100.28	99.97	100.20	99.14	99.01	98.76	100.04	100.09	99.65	99.90	99.75	100.02
Cations (based on 6 oxygens):																											
Si	1.9563	1.9530	1.9594	1.9612	1.9708	1.9472	1.9477	1.9363	1.9381	1.9451	1.9386	1.9472	1.9409	1.9378	1.9358	1.9599	1.9622	1.9603	1.9964	1.9939	2.0015	1.9899	1.9880	1.9787	1.9785	1.9859	1.9856
Ti	0.0022	0.0018	0.0021	0.0024	0.0024	0.0034	0.0029	0.0035	0.0033	0.0030	0.0035	0.0032	0.0035	0.0037	0.0031	0.0028	0.0030	0.0027	0.0032	0.0126	0.0042	0.0041	0.0037	0.0044	0.0045	0.0032	0.0053
Al	0.0395	0.0363	0.0435	0.0443	0.0349	0.0426	0.0433	0.0425	0.0443	0.0409	0.0464	0.0384	0.0404	0.0381	0.0385	0.0367	0.0370	0.0399	0.0277	0.0276	0.0289	0.0278	0.0283	0.0260	0.0259	0.0246	0.0276
Cr	0.0083	0.0061	0.0077	0.0080	0.0078	0.0146	0.0151	0.0145	0.0159	0.0137	0.0160	0.0138	0.0144	0.0128	0.0127	0.0105	0.0110	0.0122	0.0002	0.0009	0.0000	0.0007	0.0011	0.0013	0.0010	0.0010	0.0016
Fe	0.3358	0.2949	0.2661	0.2620	0.3355	0.3508	0.3466	0.3636	0.3550	0.3607	0.3595	0.3633	0.3692	0.3734	0.3643	0.3683	0.3741	0.3745	0.7383	0.7259	0.7780	0.7157	0.7178	0.7437	0.7429	0.7391	0.7054
Mn	0.0073	0.0058	0.0058	0.0062	0.0081	0.0066	0.0067	0.0082	0.0071	0.0067	0.0080	0.0080	0.0081	0.0083	0.0070	0.0060	0.0063	0.0076	0.0167	0.0154	0.0193	0.0142	0.0141	0.0149	0.0156	0.0164	0.0141
Ni	0.0015	0.0023	0.0026	0.0028	0.0023	0.0018	0.0023	0.0027	0.0022	0.0014	0.0026	0.0019	0.0022	0.0027	0.0024	0.0035	0.0038	0.0029	0.0000	0.0000	0.0000	0.0011	0.0008	0.0018	0.0010	0.0002	0.0026
Mg	1.6481	1.7105	1.7125	1.7088	1.6239	1.6048	1.6081	1.6188	1.6027	1.6161	1.5894	1.6140	1.6176	1.6223	1.6359	1.6038	1.5943	1.5838	1.1697	1.1744	1.1127	1.2091	1.2123	1.2043	1.2029	1.2052	1.2230
Ca	0.0180	0.0131	0.0130	0.0145	0.0196	0.0487	0.0469	0.0434	0.0593	0.0364	0.0627	0.0334	0.0320	0.0339	0.0357	0.0216	0.0188	0.0266	0.0342	0.0286	0.0354	0.0283	0.0275	0.0280	0.0310	0.0221	0.0290
Na	0.0014	0.0004	0.0004	0.0003	0.0003	0.0010	0.0008	0.0006	0.0013	0.0010	0.0004	0.0005	0.0000	0.0006	0.0000	0.0008	0.0000	0.0007	0.0002	0.0000	0.0000	0.0014	0.0003	0.0005	0.0006	0.0011	0.0004
Total	4.0183	4.0242	4.0131	4.0105	4.0056	4.0214	4.0206	4.0330	4.0291	4.0251	4.0270	4.0237	4.0283	4.0334	4.0355	4.0141	4.0107	4.0113	3.9866	3.9793	3.9799	3.9924	3.9938	4.0035	4.0039	3.9987	3.9947
MMF	0.8307	0.8529	0.8655	0.8671	0.8288	0.8206	0.8227	0.8166	0.8187	0.8175	0.8155	0.8163	0.8142	0.8129	0.8179	0.8132	0.8099	0.8088	0.6130	0.6180	0.5885	0.6281	0.6281	0.6182	0.6182	0.6199	0.6342
Wo	0.9	0.6	0.7	0.7	1.0	2.4	2.3	2.1	2.9	1.8	3.1	1.7	1.6	1.7	1.8	1.1	0.9	1.3	1.8	1.5	1.8	1.5	1.4	1.4	1.6	1.1	1.5
En	82.3	84.7	86.0	86.1	82.1	80.1	80.3	79.9	79.5	80.3	79.0	80.3	80.1	79.9	80.4	80.4	80.2	79.8	60.2	60.9	57.8	61.9	61.9	60.9	60.9	61.3	62.5
Fs	16.8	14.6	13.4	13.2	17.0	17.5	17.3	17.9	17.6	17.9	17.9	18.1	18.3	18.4	17.9	18.5	18.8	18.9	38.0	37.6	40.4	36.6	36.7	37.6	37.6	37.6	36.0

Sample	S-4	S-4	S-4	S-4	S-5	S-5	S-5	S-5	S-5	S-5	S-5	S-5	S-5	S-5	S-5	S-6	S-6	S-6	S-6	S-6	S-6	S-7	S-7	S-7	S-7	S-7	S-7	S-8
Metres	11.3	11.3	11.3	11.3	18.2	18.2	18.2	18.2	18.2	18.2	18.2	18.2	18.2	18.2	18.2	22.1	22.1	22.1	22.1	22.1	22.1	26.5	26.5	26.5	26.5	26.5	26.5	32.3
Position	c	c	c	c	c	c	c	c	c	m	m	m	m	m	m	c	c	c	m	m	m	c	c	c	m	m	m	c
Wt. %																												
SiO_2	53.04	52.77	52.46	52.57	54.09	56.06	55.35	55.71	55.38	55.88	55.88	55.47	55.66	55.61	56.02	55.88	55.68	55.94	56.15	56.07	55.38	55.53	55.62	55.32	55.72	55.45	55.96
TiO_2	0.15	0.14	0.15	0.12	0.15	0.13	0.13	0.13	0.12	0.08	0.10	0.14	0.13	0.12	0.17	0.11	0.16	0.17	0.15	0.14	0.15	0.15	0.18	0.17	0.17	0.16	0.13
Al_2O_3	0.71	0.58	0.63	0.56	3.15	0.87	0.89	0.96	1.14	0.85	0.78	1.01	0.76	0.89	0.95	1.12	0.99	0.87	0.81	0.80	1.03	0.98	0.91	0.96	0.85	0.98	1.01
Cr_2O_3	0.05	0.04	0.05	0.05	0.43	0.36	0.42	0.42	0.47	0.27	0.34	0.42	0.31	0.38	0.40	0.45	0.43	0.35	0.40	0.36	0.43	0.43	0.43	0.43	0.43	0.39	0.43
FeO	22.39	22.70	23.67	23.55	12.00	11.67	12.19	12.11	12.04	12.41	12.32	12.16	12.40	12.18	12.23	12.32	11.70	12.55	12.38	12.36	12.27	12.41	12.30	12.27	12.39	12.53	11.44
MnO	0.45	0.52	0.50	0.52	0.25	0.24	0.24	0.26	0.27	0.27	0.26	0.23	0.32	0.27	0.24	0.25	0.26	0.26	0.25	0.27	0.25	0.22	0.24	0.24	0.27	0.24	0.26
NiO	0.05	0.06	0.04	0.04	0.08	0.03	0.05	0.07	0.07	0.02	0.04	0.05	0.06	0.07	0.05	0.07	0.05	0.05	0.08	0.01	0.07	0.07	0.07	0.07	0.07	0.06	0.07
MgO	22.34	21.83	21.41	21.62	27.37	29.26	30.21	29.79	29.43	30.37	30.46	29.68	29.42	29.42	28.76	28.77	28.16	29.12	29.56	29.17	29.34	29.26	29.21	29.27	29.54	29.54	28.70
CaO	0.71	0.71	0.70	0.54	2.85	1.96	0.61	1.32	1.64	0.44	0.49	1.32	0.72	0.95	1.43	1.16	2.43	0.75	0.74	0.93	1.21	1.41	1.07	0.91	1.05	0.58	1.26
Na_2O	0.00	0.01	0.01	0.00	0.01	0.04	0.02	0.02	0.03	0.01	0.00	0.01	0.01	0.01	0.02	0.02	0.04	0.02	0.01	0.01	0.03	0.02	0.01	0.01	0.01	0.01	0.02
Total	99.89	99.35	99.62	99.57	100.37	100.61	100.09	100.79	100.59	100.60	100.67	100.49	99.78	99.91	100.27	100.14	99.93	100.09	100.51	100.13	100.15	100.47	100.03	99.65	100.49	99.94	99.28
Cations (based on 6 oxygens):																											
Si	1.9790	1.9840	1.9767	1.9796	1.9244	1.9785	1.9640	1.9656	1.9602	1.9713	1.9703	1.9634	1.9817	1.9768	1.9849	1.9821	1.9822	1.9851	1.9828	1.9877	1.9673	1.9682	1.9763	1.9731	1.9722	1.9719	1.9937
Ti	0.0041	0.0040	0.0043	0.0035	0.0040	0.0034	0.0033	0.0034	0.0032	0.0022	0.0027	0.0037	0.0034	0.0033	0.0044	0.0030	0.0043	0.0046	0.0040	0.0037	0.0039	0.0039	0.0047	0.0046	0.0044	0.0042	0.0036
Al	0.0310	0.0255	0.0279	0.0251	0.1321	0.0361	0.0374	0.0400	0.0476	0.0354	0.0324	0.0421	0.0318	0.0374	0.0396	0.0468	0.0417	0.0364	0.0339	0.0332	0.0430	0.0407	0.0380	0.0404	0.0353	0.0409	0.0423
Cr	0.0015	0.0012	0.0014	0.0014	0.0120	0.0100	0.0118	0.0117	0.0132	0.0076	0.0094	0.0118	0.0089	0.0106	0.0112	0.0126	0.0122	0.0098	0.0110	0.0102	0.0122	0.0121	0.0122	0.0122	0.0121	0.0110	0.0122
Fe	0.6987	0.7136	0.7458	0.7416	0.3570	0.3444	0.3618	0.3573	0.3564	0.3661	0.3633	0.3600	0.3691	0.3621	0.3625	0.3655	0.3481	0.3726	0.3655	0.3663	0.3646	0.3680	0.3654	0.3660	0.3666	0.3727	0.3408
Mn	0.0143	0.0166	0.0160	0.0166	0.0076	0.0071	0.0071	0.0077	0.0081	0.0081	0.0078	0.0068	0.0096	0.0082	0.0071	0.0076	0.0078	0.0079	0.0074	0.0082	0.0076	0.0067	0.0073	0.0072	0.0080	0.0071	0.0079
Ni	0.0015	0.0018	0.0013	0.0011	0.0022	0.0008	0.0014	0.0020	0.0020	0.0007	0.0012	0.0014	0.0017	0.0021	0.0019	0.0013	0.0020	0.0013	0.0022	0.0003	0.0020	0.0020	0.0020	0.0020	0.0020	0.0018	0.0020
Mg	1.2420	1.2230	1.2026	1.2134	1.4515	1.5392	1.5976	1.5669	1.5526	1.5969	1.6008	1.5661	1.5612	1.5587	1.5190	1.5212	1.4942	1.5402	1.5557	1.5414	1.5539	1.5457	1.5473	1.5556	1.5586	1.5657	1.5242
Ca	0.0285	0.0286	0.0281	0.0216	0.1086	0.0743	0.0231	0.0497	0.0622	0.0164	0.0183	0.0501	0.0273	0.0364	0.0542	0.0442	0.0927	0.0287	0.0280	0.0353	0.0459	0.0536	0.0406	0.0347	0.0399	0.0222	0.0482
Na	0.0000	0.0004	0.0005	0.0000	0.0006	0.0025	0.0012	0.0016	0.0018	0.0007	0.0000	0.0008	0.0004	0.0005	0.0011	0.0013	0.0026	0.0014	0.0005	0.0009	0.0018	0.0012	0.0008	0.0008	0.0009	0.0010	0.0012
Total	4.0006	3.9989	4.0046	4.0038	3.9998	3.9963	4.0087	4.0059	4.0072	4.0053	4.0062	4.0063	3.9949	3.9961	3.9858	3.9858	3.9879	3.9879	3.9910	3.9874	4.0021	4.0021	3.9944	3.9965	4.0001	3.9985	3.9761
MMF	0.6400	0.6315	0.6172	0.6206	0.8026	0.8171	0.8153	0.8143	0.8133	0.8135	0.8150	0.8131	0.8088	0.8115	0.8073	0.8063	0.8110	0.8052	0.8098	0.8080	0.8100	0.8077	0.8090	0.8095	0.8096	0.8077	0.8173
Wo	1.4	1.5	1.4	1.1	5.7	3.8	1.2	2.5	3.2	0.8	0.9	2.5	1.4	1.9	2.8	2.3	4.8	1.5	1.4	1.8	2.3	2.7	2.1	1.8	2.0	1.1	2.5
En	63.1	62.2	60.8	61.4	75.7	78.6	80.6	79.4	78.8	80.7	80.8	79.2	79.8	79.6	78.5	78.8	77.2	79.3	79.8	79.3	79.1	78.6	79.2	79.5	79.3	79.9	79.7
Fs	35.5	36.3	37.7	37.5	18.6	17.6	18.3	18.1	18.1	18.5	18.3	18.2	18.9	18.5	18.7	18.9	18.0	19.2	18.7	18.9	18.6	18.7	18.7	18.7	18.7	19.0	17.8

MICROPROBE DATA TABLE C5: Composition of **orthopyroxene** in the UG1 Footwall and MG3 Units - all **S** samples.
Metres given below base of UG1 chromitite.
c = core of grain m = grain margin.

Sample	S-8	S-8	S-8	S-8	S-8	S-9	S-9	S-9	S-9	S-9	S-9	S-10	S-10	S-10	S-10	S-10	S-10	S-10	S-10	S-10	S-10	S-10	S-10	S-10	S-11	S-11	S-11
Metres	32.3	32.3	32.3	32.3	32.3	37.8	37.8	37.8	37.8	37.8	37.8	42.5	42.5	42.5	42.5	42.5	42.5	42.5	42.5	42.5	42.5	42.5	42.5	42.5	49.8	49.8	49.8
Position	c	c	m	m	m	c	c	c	m	m	m	c	c	c	c	c	c	c	c	c	c	c	m	m	m	c	c	c
Wt. %																												
SiO_2	56.55	56.23	56.59	56.20	56.62	56.07	55.93	55.96	56.38	55.57	56.15	54.95	54.68	54.84	55.13	54.48	54.59	54.10	54.16	54.85	54.77	55.90	55.35	55.30	55.70	55.90	55.53
TiO_2	0.12	0.11	0.15	0.13	0.10	0.14	0.14	0.12	0.12	0.15	0.15	0.12	0.21	0.14	0.14	0.15	0.15	0.17	0.13	0.13	0.11	0.10	0.13	0.16	0.17	0.13	0.17
Al_2O_3	0.98	1.01	0.98	0.89	0.81	0.93	1.07	1.03	0.83	0.96	0.81	0.88	0.88	0.96	0.94	0.89	0.89	0.90	1.06	1.06	1.06	0.88	0.90	0.94	0.99	1.00	0.99
Cr_2O_3	0.43	0.43	0.43	0.43	0.43	0.43	0.43	0.43	0.43	0.43	0.43	0.38	0.38	0.37	0.36	0.34	0.36	0.37	0.40	0.42	0.41	0.38	0.34	0.35	0.40	0.40	0.37
FeO	11.76	11.65	11.72	11.49	11.53	12.53	12.02	12.41	12.69	12.62	12.52	12.31	12.26	12.38	11.83	12.17	12.07	11.49	11.99	11.82	11.78	12.30	12.64	12.32	12.56	12.70	12.65
MnO	0.26	0.28	0.27	0.25	0.22	0.30	0.30	0.28	0.30	0.30	0.29	0.29	0.26	0.29	0.25	0.29	0.27	0.21	0.25	0.22	0.26	0.25	0.24	0.29	0.24	0.25	0.28
NiO	0.07	0.07	0.07	0.07	0.07	0.07	0.07	0.07	0.07	0.07	0.07	0.09	0.06	0.04	0.08	0.09	0.08	0.11	0.12	0.10	0.10	0.06	0.06	0.06	0.09	0.11	0.14
MgO	29.46	28.93	29.11	29.01	29.58	28.95	28.08	28.83	29.49	29.14	29.33	29.58	29.93	30.11	29.69	30.18	29.97	29.16	29.47	29.04	28.98	29.80	29.50	28.91	28.45	28.60	28.58
CaO	1.15	1.26	1.21	1.05	0.61	1.21	2.78	1.58	0.51	0.67	0.69	1.44	1.27	1.01	1.70	0.74	1.26	2.77	1.73	2.22	2.69	0.43	0.70	1.27	1.51	1.49	1.56
Na_2O	0.03	0.02	0.03	0.03	0.01	0.01	0.04	0.02	0.00	0.01	0.01	0.02	0.02	0.02	0.02	0.01	0.02	0.03	0.03	0.02	0.03	0.00	0.00	0.00	0.02	0.02	0.03
Total	100.81	99.99	100.58	99.54	99.99	100.65	100.86	100.71	100.82	99.92	100.44	100.06	99.95	100.16	100.13	99.33	99.66	99.32	99.34	99.88	100.19	100.11	99.87	99.61	100.13	100.60	100.29
Cations (based on 6 oxygens):																											
Si	1.9864	1.9912	1.9919	1.9958	1.9988	1.9817	1.9774	1.9777	1.9859	1.9777	1.9853	1.9585	1.9508	1.9511	1.9593	1.9523	1.9516	1.9458	1.9457	1.9576	1.9523	1.9801	1.9716	1.9752	1.9809	1.9799	1.9746
Ti	0.0032	0.0028	0.0039	0.0034	0.0027	0.0037	0.0037	0.0031	0.0032	0.0040	0.0040	0.0031	0.0055	0.0038	0.0038	0.0041	0.0041	0.0045	0.0035	0.0036	0.0029	0.0027	0.0035	0.0043	0.0046	0.0035	0.0046
Al	0.0405	0.0420	0.0407	0.0372	0.0335	0.0388	0.0444	0.0428	0.0345	0.0402	0.0336	0.0371	0.0370	0.0404	0.0395	0.0375	0.0377	0.0383	0.0447	0.0446	0.0446	0.0368	0.0379	0.0397	0.0415	0.0417	0.0415
Cr	0.0121	0.0122	0.0121	0.0122	0.0121	0.0121	0.0121	0.0121	0.0120	0.0122	0.0121	0.0108	0.0107	0.0105	0.0100	0.0095	0.0101	0.0105	0.0114	0.0118	0.0116	0.0107	0.0097	0.0099	0.0113	0.0112	0.0105
Fe	0.3456	0.3451	0.3451	0.3412	0.3404	0.3705	0.3554	0.3670	0.3738	0.3755	0.3703	0.3670	0.3658	0.3684	0.3516	0.3646	0.3608	0.3456	0.3603	0.3528	0.3511	0.3642	0.3767	0.3679	0.3737	0.3762	0.3761
Mn	0.0078	0.0083	0.0082	0.0075	0.0067	0.0091	0.0090	0.0082	0.0090	0.0091	0.0086	0.0087	0.0077	0.0088	0.0076	0.0087	0.0082	0.0064	0.0077	0.0068	0.0078	0.0074	0.0072	0.0089	0.0071	0.0075	0.0086
Ni	0.0020	0.0020	0.0020	0.0020	0.0020	0.0020	0.0020	0.0020	0.0020	0.0020	0.0020	0.0026	0.0018	0.0011	0.0022	0.0025	0.0023	0.0031	0.0036	0.0028	0.0030	0.0018	0.0017	0.0017	0.0026	0.0031	0.0039
Mg	1.5424	1.5269	1.5272	1.5359	1.5562	1.5253	1.4798	1.5185	1.5482	1.5455	1.5457	1.5711	1.5913	1.5967	1.5729	1.6121	1.5970	1.5632	1.5782	1.5448	1.5398	1.5733	1.5662	1.5394	1.5082	1.5098	1.5149
Ca	0.0431	0.0476	0.0455	0.0398	0.0232	0.0457	0.1053	0.0597	0.0192	0.0257	0.0260	0.0551	0.0487	0.0384	0.0646	0.0285	0.0483	0.1066	0.0667	0.0850	0.1027	0.0164	0.0266	0.0486	0.0577	0.0565	0.0594
Na	0.0019	0.0012	0.0024	0.0018	0.0005	0.0007	0.0027	0.0012	0.0000	0.0006	0.0006	0.0013	0.0011	0.0012	0.0012	0.0006	0.0012	0.0024	0.0019	0.0017	0.0024	0.0000	0.0000	0.0000	0.0014	0.0014	0.0017
Total	3.9851	3.9794	3.9790	3.9770	3.9760	3.9895	3.9919	3.9923	3.9877	3.9924	3.9882	4.0151	4.0204	4.0203	4.0127	4.0204	4.0211	4.0265	4.0237	4.0114	4.0180	3.9934	4.0011	3.9957	3.9888	3.9909	3.9957
MMF	0.8170	0.8156	0.8157	0.8182	0.8205	0.8046	0.8064	0.8054	0.8055	0.8045	0.8068	0.8107	0.8131	0.8125	0.8173	0.8156	0.8157	0.8189	0.8141	0.8141	0.8143	0.8120	0.8061	0.8071	0.8014	0.8005	0.8011
Wo	2.2	2.5	2.4	2.1	1.2	2.4	5.4	3.1	1.0	1.3	1.3	2.8	2.4	1.9	3.2	1.4	2.4	5.3	3.3	4.3	5.2	0.8	1.3	2.5	3.0	2.9	3.0
En	79.9	79.5	79.6	80.1	81.1	78.6	76.3	78.1	79.8	79.4	79.6	78.8	79.3	79.7	79.1	80.4	79.6	77.6	78.7	77.9	77.2	80.5	79.5	78.7	77.8	77.7	77.7
Fs	17.9	18.0	18.0	17.8	17.7	19.1	18.3	18.9	19.3	19.3	19.1	18.4	18.2	18.4	17.7	18.2	18.0	17.1	18.0	17.8	17.6	18.6	19.1	18.8	19.3	19.4	19.3

Sample	S-11	S-11	S-11	S-12	S-12	S-12	S-12	S-12	S-12	S-12	S-12	S-12	S-12	S-12	S-12	S-12	S-13	S-13	S-13	S-13	S-13	S-13	S-13	S-13	S-13	S-13	S-14
Metres	49.8	49.8	49.8	57.1	57.1	57.1	57.1	57.1	57.1	57.1	57.1	57.1	57.1	57.1	57.1	57.1	67.9	67.9	67.9	67.9	67.9	67.9	67.9	67.9	67.9	67.9	75.2
Position	m	m	m	c	c	c	c	c	c	c	c	c	c	m	m	m	c	c	c	c	c	m	m	m	m	m	c
Wt. %																											
SiO_2	55.73	55.93	55.49	55.42	54.70	54.77	54.54	54.93	54.71	54.69	54.73	54.56	54.82	55.32	55.29	55.28	56.13	55.58	56.70	55.81	56.00	55.87	55.51	55.92	55.90	55.97	55.03
TiO_2	0.16	0.14	0.17	0.13	0.11	0.12	0.14	0.12	0.11	0.10	0.10	0.10	0.11	0.11	0.15	0.17	0.15	0.17	0.14	0.13	0.13	0.18	0.11	0.15	0.15	0.15	0.17
Al_2O_3	0.83	0.81	0.81	0.94	0.87	0.96	0.94	0.93	1.01	1.05	1.00	0.91	0.96	0.71	0.75	0.90	0.91	1.01	0.76	0.96	0.96	0.85	0.81	0.86	0.77	0.85	0.93
Cr_2O_3	0.35	0.34	0.31	0.37	0.32	0.36	0.38	0.37	0.39	0.39	0.37	0.38	0.40	0.32	0.34	0.36	0.40	0.40	0.31	0.40	0.41	0.32	0.36	0.36	0.31	0.34	0.39
FeO	12.69	12.63	13.04	12.75	12.61	12.35	12.75	12.42	12.38	12.40	12.48	12.51	12.32	12.71	12.82	12.85	12.30	13.02	12.67	12.99	13.00	12.78	13.22	13.24	12.77	12.85	13.17
MnO	0.29	0.28	0.26	0.27	0.26	0.29	0.26	0.27	0.25	0.26	0.27	0.26	0.27	0.27	0.27	0.28	0.24	0.31	0.25	0.26	0.30	0.23	0.30	0.29	0.23	0.26	0.29
NiO	0.15	0.13	0.11	0.09	0.09	0.05	0.09	0.09	0.09	0.06	0.08	0.08	0.03	0.12	0.12	0.12	0.08	0.07	0.03	0.07	0.08	0.08	0.08	0.06	0.06	0.09	0.11
MgO	28.93	28.94	28.98	29.79	29.53	29.56	29.69	29.63	29.39	29.34	29.11	29.61	29.30	29.33	29.08	28.25	27.28	28.44	27.80	28.69	28.88	28.59	28.83	28.81	28.54	28.50	29.19
CaO	0.99	0.91	0.75	0.85	1.19	1.28	0.95	1.11	1.28	1.51	1.86	1.18	1.57	0.64	0.54	1.15	2.15	0.91	1.43	1.00	0.90	0.85	0.77	0.79	0.57	0.52	0.84
Na_2O	0.02	0.00	0.01	0.01	0.00	0.01	0.01	0.02	0.01	0.03	0.02	0.01	0.03	0.01	0.00	0.00	0.03	0.02	0.01	0.00	0.00	0.00	0.01	0.00	0.00	0.01	0.01
Total	100.13	100.11	99.94	100.60	99.67	99.73	99.75	99.87	99.62	99.83	100.00	99.60	99.82	99.54	99.36	99.36	99.69	99.93	100.10	100.30	100.66	99.74	99.99	100.48	99.31	99.54	100.13
Cations (based on 6 oxygens):																											
Si	1.9816	1.9866	1.9786	1.9629	1.9582	1.9574	1.9520	1.9598	1.9579	1.9547	1.9555	1.9546	1.9587	1.9780	1.9805	1.9831	2.0031	1.9819	2.0115	1.9819	1.9814	1.9912	1.9800	1.9832	1.9983	1.9972	1.9631
Ti	0.0042	0.0037	0.0046	0.0034	0.0029	0.0032	0.0038	0.0032	0.0030	0.0027	0.0026	0.0026	0.0030	0.0030	0.0040	0.0046	0.0040	0.0046	0.0037	0.0035	0.0033	0.0047	0.0029	0.0041	0.0040	0.0039	0.0047
Al	0.0347	0.0341	0.0340	0.0391	0.0365	0.0404	0.0398	0.0389	0.0426	0.0442	0.0420	0.0385	0.0405	0.0299	0.0317	0.0381	0.0385	0.0424	0.0318	0.0403	0.0400	0.0355	0.0339	0.0361	0.0325	0.0357	0.0391
Cr	0.0098	0.0095	0.0087	0.0104	0.0092	0.0103	0.0107	0.0106	0.0109	0.0110	0.0103	0.0107	0.0114	0.0090	0.0096	0.0102	0.0113	0.0112	0.0086	0.0112	0.0115	0.0090	0.0100	0.0102	0.0089	0.0097	0.0110
Fe	0.3772	0.3753	0.3888	0.3777	0.3774	0.3690	0.3816	0.3706	0.3704	0.3706	0.3730	0.3749	0.3681	0.3801	0.3841	0.3855	0.3671	0.3883	0.3759	0.3857	0.3847	0.3808	0.3943	0.3926	0.3818	0.3834	0.3930
Mn	0.0086	0.0085	0.0078	0.0080	0.0078	0.0087	0.0078	0.0081	0.0076	0.0080	0.0081	0.0078	0.0083	0.0082	0.0082	0.0085	0.0073	0.0093	0.0077	0.0077	0.0090	0.0071	0.0090	0.0087	0.0070	0.0080	0.0087
Ni	0.0042	0.0036	0.0031	0.0025	0.0026	0.0013	0.0025	0.0025	0.0027	0.0017	0.0022	0.0024	0.0008	0.0035	0.0035	0.0036	0.0023	0.0020	0.0008	0.0021	0.0023	0.0022	0.0024	0.0016	0.0018	0.0025	0.0032
Mg	1.5332	1.5321	1.5404	1.5727	1.5757	1.5745	1.5840	1.5757	1.5677	1.5632	1.5501	1.5810	1.5604	1.5631	1.5526	1.5105	1.4511	1.5117	1.4701	1.5185	1.5231	1.5188	1.5326	1.5232	1.5207	1.5157	1.5523
Ca	0.0379	0.0346	0.0288	0.0321	0.0458	0.0490	0.0364	0.0424	0.0490	0.0579	0.0712	0.0452	0.0601	0.0246	0.0207	0.0442	0.0821	0.0346	0.0543	0.0379	0.0341	0.0324	0.0294	0.0298	0.0219	0.0199	0.0320
Na	0.0014	0.0002	0.0009	0.0004	0.0000	0.0005	0.0005	0.0013	0.0009	0.0020	0.0014	0.0007	0.0019	0.0003	0.0000	0.0000	0.0024	0.0017	0.0008	0.0001	0.0003	0.0000	0.0006	0.0001	0.0003	0.0004	0.0005
Total	3.9927	3.9881	3.9958	4.0092	4.0161	4.0143	4.0192	4.0129	4.0128	4.0160	4.0164	4.0186	4.0133	3.9997	3.9948	3.9882	3.9693	3.9876	3.9650	3.9890	3.9897	3.9818	3.9954	3.9896	3.9772	3.9764	4.0075
MMF	0.8025	0.8032	0.7985	0.8063	0.8068	0.8101	0.8058	0.8096	0.8089	0.8083	0.8061	0.8083	0.8091	0.8044	0.8017	0.7967	0.7981	0.7956	0.7964	0.7974	0.7984	0.7996	0.7954	0.7951	0.7993	0.7981	0.7980
Wo	1.9	1.8	1.5	1.6	2.3	2.5	1.8	2.1	2.5	2.9	3.6	2.3	3.0	1.3	1.1	2.3	4.3	1.8	2.9	2.0	1.8	1.7	1.5	1.5	1.1	1.0	1.6
En	78.7	78.9	78.7	79.3	78.8	79.0	79.1	79.2	78.9	78.5	77.7	79.0	78.5	79.4	79.3	77.9	76.4	78.1	77.4	78.2	78.4	78.6	78.3	78.3	79.0	79.0	78.5
Fs	19.4	19.3	19.9	19.1	18.9	18.5	19.1	18.6	18.6	18.6	18.7	18.7	18.5	19.3	19.6	19.9	19.3	20.1	19.8	19.9	19.8	19.7	20.2	20.2	19.8	20.0	19.9

MICROPROBE DATA TABLE C5: Composition of **orthopyroxene** in the UG1 Footwall and MG3 Units - all S samples.
Metres given below base of UG1 chromitite.
c = core of grain m = grain margin.

Sample	S-14	S-14	S-14	S-14	S-14	S-15	S-15	S-15	S-15	S-15	S-15	S-15	S-15	S-15	S-15	S-15	S-15	S-15	S-16	S-16	S-16	S-16	S-16	S-16	S-17	S-17	S-17
Metres	75.2	75.2	75.2	75.2	75.2	80.9	80.9	80.9	80.9	80.9	80.9	80.9	80.9	80.9	80.9	80.9	80.9	80.9	85.3	85.3	85.3	85.3	85.3	85.3	89.7	89.7	89.7
Position	c	c	m	m	m	c	c	c	c	c	c	c	c	c	c	m	m	m	c	c	c	m	m	m	c	c	c
Wt. %																											
SiO_2	54.99	55.14	55.27	55.37	55.10	54.77	54.86	54.88	54.88	54.99	54.75	54.73	54.69	54.96	54.74	55.23	55.56	55.66	55.47	55.40	55.28	55.27	55.38	55.35	55.57	55.06	55.65
TiO_2	0.19	0.15	0.17	0.17	0.17	0.17	0.17	0.16	0.19	0.17	0.14	0.18	0.18	0.17	0.17	0.18	0.19	0.16	0.12	0.12	0.13	0.14	0.13	0.14	0.19	0.21	0.20
Al_2O_3	0.86	1.08	0.86	0.83	0.86	0.86	0.84	0.79	0.82	0.85	0.92	0.85	0.83	0.88	0.93	0.92	0.89	0.94	0.99	1.14	0.95	0.86	0.88	0.85	0.94	0.95	0.92
Cr_2O_3	0.38	0.37	0.35	0.37	0.36	0.35	0.35	0.35	0.36	0.34	0.38	0.35	0.37	0.35	0.36	0.36	0.33	0.32	0.33	0.38	0.36	0.32	0.32	0.27	0.37	0.37	0.37
FeO	13.39	12.82	13.28	13.30	13.00	13.20	13.04	13.24	13.28	13.10	12.79	12.98	12.93	12.91	13.11	13.17	13.01	13.12	13.25	12.81	13.02	13.19	13.28	13.52	13.16	13.14	13.40
MnO	0.32	0.27	0.30	0.26	0.28	0.29	0.31	0.32	0.28	0.29	0.30	0.31	0.31	0.30	0.29	0.25	0.25	0.29	0.31	0.27	0.29	0.28	0.26	0.29	0.32	0.26	0.24
NiO	0.10	0.11	0.11	0.08	0.12	0.05	0.07	0.05	0.05	0.04	0.07	0.06	0.07	0.04	0.06	0.08	0.05	0.09	0.09	0.14	0.10	0.09	0.11	0.10	0.11	0.12	0.08
MgO	29.24	29.15	29.10	29.28	28.60	29.74	29.83	29.93	29.66	29.73	29.64	29.67	29.83	29.69	29.65	29.07	28.89	28.82	29.41	28.74	28.65	29.07	28.98	29.02	28.89	28.58	28.59
CaO	0.71	1.03	0.77	0.53	0.94	1.05	0.93	0.92	0.98	1.05	1.35	1.00	1.10	1.18	1.19	0.66	0.64	0.62	0.69	1.64	1.18	0.61	0.78	0.72	1.16	1.06	0.97
Na_2O	0.00	0.01	0.01	0.01	0.00	0.00	0.00	0.01	0.01	0.00	0.02	0.00	0.01	0.00	0.01	0.01	0.01	0.02	0.00	0.00	0.01	0.01	0.01	0.01	0.04	0.02	0.02
Total	100.19	100.12	100.22	100.20	99.43	100.50	100.40	100.65	100.50	100.57	100.34	100.13	100.32	100.47	100.50	99.94	99.81	100.01	100.65	100.62	99.99	99.84	100.13	100.26	100.76	99.77	100.42
Cations (based on 6 oxygens):																											
Si	1.9623	1.9640	1.9693	1.9713	1.9767	1.9500	1.9530	1.9506	1.9534	1.9544	1.9506	1.9535	1.9491	1.9542	1.9489	1.9708	1.9813	1.9819	1.9665	1.9660	1.9735	1.9741	1.9739	1.9721	1.9701	1.9711	1.9781
Ti	0.0051	0.0040	0.0046	0.0045	0.0046	0.0045	0.0044	0.0043	0.0050	0.0045	0.0037	0.0047	0.0049	0.0046	0.0045	0.0049	0.0050	0.0042	0.0031	0.0031	0.0035	0.0039	0.0034	0.0036	0.0050	0.0056	0.0053
Al	0.0361	0.0453	0.0363	0.0350	0.0364	0.0362	0.0351	0.0330	0.0344	0.0358	0.0384	0.0356	0.0350	0.0369	0.0389	0.0389	0.0374	0.0393	0.0413	0.0476	0.0401	0.0360	0.0370	0.0358	0.0394	0.0401	0.0384
Cr	0.0109	0.0103	0.0097	0.0104	0.0102	0.0099	0.0098	0.0098	0.0101	0.0096	0.0107	0.0099	0.0104	0.0098	0.0100	0.0102	0.0094	0.0089	0.0092	0.0106	0.0102	0.0089	0.0091	0.0077	0.0103	0.0105	0.0103
Fe	0.3997	0.3820	0.3957	0.3961	0.3900	0.3932	0.3882	0.3937	0.3952	0.3893	0.3811	0.3876	0.3854	0.3838	0.3903	0.3931	0.3879	0.3906	0.3928	0.3801	0.3886	0.3939	0.3959	0.4029	0.3902	0.3933	0.3982
Mn	0.0096	0.0080	0.0091	0.0077	0.0085	0.0089	0.0094	0.0096	0.0085	0.0089	0.0090	0.0093	0.0092	0.0090	0.0087	0.0077	0.0075	0.0086	0.0093	0.0081	0.0089	0.0085	0.0077	0.0089	0.0095	0.0079	0.0072
Ni	0.0029	0.0030	0.0031	0.0024	0.0035	0.0015	0.0020	0.0013	0.0015	0.0011	0.0019	0.0018	0.0021	0.0012	0.0018	0.0024	0.0014	0.0025	0.0026	0.0039	0.0030	0.0027	0.0030	0.0030	0.0031	0.0036	0.0022
Mg	1.5554	1.5478	1.5455	1.5536	1.5293	1.5782	1.5826	1.5858	1.5738	1.5750	1.5738	1.5784	1.5846	1.5736	1.5733	1.5461	1.5355	1.5297	1.5540	1.5202	1.5244	1.5478	1.5393	1.5411	1.5267	1.5247	1.5150
Ca	0.0272	0.0394	0.0295	0.0202	0.0362	0.0402	0.0355	0.0352	0.0373	0.0398	0.0515	0.0382	0.0420	0.0449	0.0454	0.0254	0.0246	0.0236	0.0262	0.0622	0.0453	0.0234	0.0298	0.0273	0.0442	0.0406	0.0371
Na	0.0001	0.0005	0.0007	0.0006	0.0001	0.0000	0.0000	0.0005	0.0004	0.0001	0.0010	0.0000	0.0007	0.0000	0.0006	0.0006	0.0005	0.0012	0.0000	0.0002	0.0009	0.0006	0.0010	0.0004	0.0028	0.0013	0.0012
Total	4.0092	4.0044	4.0035	4.0018	3.9955	4.0225	4.0202	4.0239	4.0196	4.0185	4.0217	4.0190	4.0236	4.0179	4.0224	4.0001	3.9905	3.9904	4.0051	4.0019	3.9983	3.9998	4.0001	4.0027	4.0015	3.9986	3.9929
MMF	0.7956	0.8020	0.7962	0.7968	0.7968	0.8006	0.8030	0.8011	0.7993	0.8018	0.8051	0.8029	0.8044	0.8039	0.8012	0.7973	0.7983	0.7966	0.7982	0.8000	0.7969	0.7971	0.7954	0.7928	0.7964	0.7949	0.7919
Wo	1.4	2.0	1.5	1.0	1.9	2.0	1.8	1.7	1.9	2.0	2.6	1.9	2.1	2.2	2.3	1.3	1.3	1.2	1.3	3.2	2.3	1.2	1.5	1.4	2.3	2.1	1.9
En	78.5	78.6	78.4	78.9	78.2	78.5	78.9	78.7	78.4	78.6	78.4	78.8	78.8	78.6	78.3	78.7	78.8	78.7	78.8	77.5	77.8	78.8	78.3	78.2	77.8	77.8	77.7
Fs	20.2	19.4	20.1	20.1	19.9	19.5	19.4	19.5	19.7	19.4	19.0	19.3	19.2	19.2	19.4	20.0	19.9	20.1	19.9	19.4	19.8	20.0	20.1	20.4	19.9	20.1	20.4

Sample	S-17	S-17	S-17	S-18	S-18	S-18	S-18	S-18	S-18	S-18	S-18	S-18	S-18	S-18	S-18	S-18	S-19	S-19	S-19	S-19	S-19	S-19	S-20	S-20	S-20	S-20	S-20
Metres	89.7	89.7	89.7	94.1	94.1	94.1	94.1	94.1	94.1	94.1	94.1	94.1	94.1	94.1	94.1	94.1	98.8	98.8	98.8	98.8	98.8	98.8	106.0	106.0	106.0	106.0	106.0
Position	m	m	m	c	c	c	c	c	c	c	c	c	c	m	m	m	c	c	c	m	m	m	c	c	c	c	c
Wt. %																											
SiO_2	55.51	55.49	55.56	55.45	54.90	54.98	55.20	55.42	54.84	55.27	55.20	55.30	55.69	55.40	55.39	55.30	55.29	55.68	55.07	55.15	55.80	55.00	54.82	54.96	55.30	55.18	55.20
TiO_2	0.17	0.18	0.17	0.08	0.10	0.12	0.12	0.13	0.14	0.14	0.10	0.14	0.08	0.14	0.14	0.14	0.14	0.12	0.14	0.12	0.14	0.14	0.12	0.11	0.08	0.10	0.12
Al_2O_3	0.83	0.90	0.90	0.97	1.06	0.98	0.98	0.95	0.99	0.96	1.04	0.99	1.00	0.92	0.91	0.92	0.91	0.86	0.99	0.83	0.85	0.89	0.99	0.96	0.95	0.94	0.89
Cr_2O_3	0.34	0.32	0.32	0.35	0.37	0.34	0.36	0.37	0.35	0.34	0.37	0.35	0.33	0.34	0.28	0.30	0.35	0.30	0.34	0.30	0.32	0.33	0.39	0.43	0.43	0.35	0.30
FeO	13.28	13.41	13.28	12.15	12.43	12.58	12.77	12.49	12.30	12.43	12.20	12.84	12.66	12.90	12.90	12.92	12.90	13.01	12.80	12.83	13.06	12.88	12.60	12.68	12.60	13.05	12.89
MnO	0.29	0.30	0.27	0.25	0.26	0.26	0.30	0.25	0.29	0.31	0.27	0.27	0.28	0.28	0.32	0.33	0.27	0.24	0.26	0.26	0.31	0.29	0.25	0.25	0.24	0.29	0.25
NiO	0.12	0.05	0.08	0.09	0.08	0.06	0.05	0.10	0.07	0.10	0.15	0.10	0.06	0.04	0.03	0.00	0.07	0.09	0.07	0.07	0.12	0.10	0.06	0.07	0.07	0.09	0.05
MgO	29.25	28.72	28.79	29.05	29.63	29.24	29.25	29.42	29.12	29.17	29.00	29.53	29.27	28.73	28.70	28.73	29.36	29.14	28.50	29.39	29.04	29.21	28.96	29.04	28.98	29.67	29.77
CaO	0.63	0.75	0.61	1.09	1.41	1.48	1.32	0.98	1.51	0.97	1.38	1.06	1.09	0.63	0.72	0.60	0.77	0.67	1.03	0.70	0.60	0.75	1.20	1.43	1.80	0.74	0.57
Na_2O	0.02	0.01	0.01	0.01	0.02	0.01	0.02	0.03	0.02	0.00	0.02	0.00	0.01	0.02	0.02	0.02	0.02	0.02	0.02	0.01	0.02	0.01	0.03	0.03	0.02	0.00	0.00
Total	100.45	100.13	100.00	99.50	100.25	100.06	100.38	100.13	99.64	99.69	99.73	100.59	100.46	99.40	99.41	99.26	100.08	100.14	99.23	99.67	100.25	99.62	99.40	99.97	100.47	100.41	100.05
Cations (based on 6 oxygens):																											
Si	1.9719	1.9776	1.9804	1.9794	1.9533	1.9607	1.9627	1.9697	1.9622	1.9725	1.9702	1.9613	1.9733	1.9831	1.9831	1.9825	1.9687	1.9796	1.9773	1.9710	1.9821	1.9685	1.9661	1.9628	1.9651	1.9610	1.9652
Ti	0.0046	0.0049	0.0046	0.0020	0.0027	0.0032	0.0031	0.0035	0.0037	0.0038	0.0027	0.0038	0.0022	0.0038	0.0038	0.0038	0.0038	0.0033	0.0039	0.0032	0.0037	0.0039	0.0031	0.0029	0.0021	0.0027	0.0033
Al	0.0347	0.0379	0.0376	0.0408	0.0443	0.0414	0.0411	0.0398	0.0419	0.0406	0.0439	0.0413	0.0416	0.0388	0.0384	0.0389	0.0382	0.0359	0.0421	0.0349	0.0354	0.0375	0.0417	0.0404	0.0398	0.0395	0.0371
Cr	0.0096	0.0090	0.0091	0.0099	0.0103	0.0097	0.0100	0.0105	0.0100	0.0097	0.0103	0.0099	0.0091	0.0096	0.0079	0.0085	0.0098	0.0085	0.0097	0.0085	0.0089	0.0094	0.0111	0.0122	0.0121	0.0097	0.0085
Fe	0.3945	0.3997	0.3959	0.3627	0.3700	0.3752	0.3797	0.3713	0.3681	0.3710	0.3640	0.3809	0.3751	0.3862	0.3863	0.3873	0.3841	0.3869	0.3844	0.3835	0.3881	0.3855	0.3779	0.3788	0.3744	0.3880	0.3837
Mn	0.0087	0.0090	0.0081	0.0075	0.0078	0.0078	0.0089	0.0075	0.0089	0.0092	0.0083	0.0081	0.0085	0.0085	0.0097	0.0101	0.0082	0.0072	0.0079	0.0079	0.0093	0.0089	0.0075	0.0075	0.0072	0.0087	0.0075
Ni	0.0035	0.0014	0.0024	0.0027	0.0022	0.0016	0.0016	0.0028	0.0019	0.0029	0.0043	0.0027	0.0018	0.0012	0.0009	0.0000	0.0021	0.0026	0.0020	0.0019	0.0034	0.0029	0.0018	0.0020	0.0020	0.0026	0.0015
Mg	1.5491	1.5256	1.5297	1.5457	1.5717	1.5543	1.5504	1.5585	1.5530	1.5519	1.5428	1.5608	1.5458	1.5329	1.5316	1.5352	1.5585	1.5445	1.5253	1.5658	1.5375	1.5583	1.5480	1.5456	1.5349	1.5714	1.5798
Ca	0.0240	0.0287	0.0234	0.0418	0.0537	0.0564	0.0504	0.0371	0.0579	0.0371	0.0527	0.0405	0.0413	0.0242	0.0276	0.0230	0.0293	0.0256	0.0396	0.0268	0.0229	0.0289	0.0462	0.0548	0.0685	0.0280	0.0217
Na	0.0014	0.0005	0.0007	0.0010	0.0011	0.0007	0.0015	0.0018	0.0012	0.0003	0.0015	0.0002	0.0007	0.0012	0.0013	0.0015	0.0015	0.0017	0.0016	0.0009	0.0013	0.0008	0.0018	0.0022	0.0013	0.0000	0.0003
Total	4.0020	3.9943	3.9920	3.9936	4.0172	4.0109	4.0094	4.0026	4.0088	3.9988	4.0007	4.0094	3.9995	3.9894	3.9906	3.9908	4.0042	3.9957	3.9937	4.0045	3.9926	4.0046	4.0053	4.0092	4.0075	4.0117	4.0088
MMF	0.7970	0.7924	0.7944	0.8099	0.8094	0.8055	0.8033	0.8076	0.8084	0.8071	0.8091	0.8038	0.8047	0.7988	0.7986	0.7985	0.8023	0.7997	0.7987	0.8033	0.7985	0.8017	0.8038	0.8031	0.8039	0.8020	0.8046
Wo	1.2	1.5	1.2	2.1	2.7	2.8	2.5	1.9	2.9	1.9	2.7	2.0	2.1	1.2	1.4	1.2	1.5	1.3	2.0	1.4	1.2	1.5	2.3	2.8	3.5	1.4	1.1
En	78.7	78.1	78.5	79.3	78.8	78.3	78.3	79.2	78.5	79.2	78.7	78.7	78.8	78.9	78.7	78.9	79.0	78.9	78.3	79.2	78.9	79.0	78.5	78.1	77.6	79.1	79.6
Fs	20.1	20.5	20.3	18.6	18.5	18.9	19.2	18.9	18.6	18.9	18.6	19.2	19.1	19.9	19.9	19.9	19.5	19.8	19.7	19.4	19.9	19.5	19.2	19.1	18.9	19.5	19.3

MICROPROBE DATA TABLE C5: Composition of **orthopyroxene** in the UG1 Footwall and MG3 Units - all **S** samples.
Metres given below base of UG1 chromitite.
c = core of grain m = grain margin.

Sample	S-20	S-20	S-20	S-20	S-20	S-20	S-20	S-20	S-20	S-20	S-20	S-20	S-20	S-20	S-20	S-21	S-21	S-21	S-21	S-21	S-21	S-22	S-22	S-22	S-22	S-22	S-22	S-23
Metres	106.0	106.0	106.0	106.0	106.0	106.0	106.0	106.0	106.0	106.0	106.0	106.0	106.0	106.0	106.0	110.7	110.7	110.7	110.7	110.7	110.7	115.1	115.1	115.1	115.1	115.1	115.1	120.4
Position	c	c	c	c	c	c	m	m	m	m	m	m	m	m	c	c	c	m	m	m	m	c	c	c	m	m	m	c
Wt. %																												
SiO_2	54.94	55.01	55.28	55.90	55.11	55.11	55.40	55.21	55.06	55.12	55.19	56.08	56.08	56.08	56.02	56.12	55.84	56.02	56.18	56.13	55.67	55.66	55.74	55.38	55.88	55.80	54.63	
TiO_2	0.12	0.11	0.11	0.13	0.13	0.13	0.10	0.11	0.11	0.13	0.12	0.14	0.14	0.14	0.10	0.09	0.11	0.10	0.09	0.10	0.13	0.15	0.14	0.12	0.13	0.13	0.11	
Al_2O_3	0.97	1.01	0.91	0.96	0.99	0.99	0.84	0.86	0.88	0.92	0.82	0.80	0.80	0.80	0.98	0.88	1.01	0.84	0.86	0.83	0.88	0.84	0.94	0.80	0.84	0.79	0.91	
Cr_2O_3	0.30	0.32	0.34	0.36	0.30	0.30	0.43	0.43	0.43	0.33	0.27	0.29	0.29	0.29	0.36	0.33	0.38	0.32	0.31	0.32	0.33	0.34	0.36	0.32	0.33	0.35	0.34	
FeO	12.66	12.54	12.86	12.62	12.58	12.58	12.95	12.80	12.94	12.75	12.67	12.87	12.87	12.87	12.56	12.11	12.41	12.52	12.50	12.67	12.79	12.87	12.99	12.98	12.81	13.00	12.63	
MnO	0.28	0.26	0.30	0.28	0.25	0.25	0.24	0.26	0.27	0.26	0.29	0.26	0.26	0.26	0.28	0.24	0.26	0.27	0.26	0.25	0.23	0.27	0.24	0.20	0.25	0.28	0.28	
NiO	0.08	0.08	0.04	0.08	0.09	0.09	0.07	0.07	0.07	0.08	0.10	0.07	0.07	0.07	0.08	0.08	0.09	0.05	0.11	0.10	0.07	0.07	0.06	0.08	0.04	0.07	0.09	
MgO	29.06	28.96	29.86	28.76	28.91	28.91	29.30	29.24	29.30	29.41	29.65	29.10	29.10	29.10	28.85	28.58	28.45	28.60	28.95	28.67	28.89	28.70	28.97	29.13	28.93	29.24	30.02	
CaO	1.28	1.47	0.67	1.15	1.18	1.18	1.03	1.17	1.12	0.63	0.50	0.50	0.50	0.50	0.78	1.28	1.01	1.01	0.74	0.68	1.10	0.94	0.99	0.54	0.66	0.57	1.24	
Na_2O	0.00	0.02	0.00	0.02	0.01	0.01	0.02	0.02	0.03	0.00	0.00	0.00	0.00	0.00	0.01	0.03	0.02	0.01	0.02	0.02	0.02	0.00	0.00	0.01	0.01	0.00	0.02	
Total	99.69	99.80	100.38	100.26	99.55	99.55	100.38	100.17	100.20	99.63	99.61	100.11	100.11	100.11	100.00	99.76	99.57	99.74	100.03	99.78	100.12	99.84	100.43	99.56	99.88	100.23	100.26	
Cations (based on 6 oxygens):																												
Si	1.9657	1.9658	1.9625	1.9836	1.9719	1.9719	1.9689	1.9664	1.9624	1.9695	1.9713	1.9901	1.9901	1.9901	1.9890	1.9956	1.9914	1.9946	1.9933	1.9970	1.9800	1.9848	1.9773	1.9799	1.9882	1.9815	1.9465	
Ti	0.0032	0.0029	0.0029	0.0033	0.0036	0.0036	0.0027	0.0030	0.0029	0.0034	0.0031	0.0036	0.0036	0.0036	0.0026	0.0024	0.0028	0.0027	0.0023	0.0028	0.0034	0.0040	0.0036	0.0031	0.0036	0.0035	0.0028	
Al	0.0408	0.0427	0.0382	0.0400	0.0416	0.0416	0.0352	0.0360	0.0371	0.0388	0.0344	0.0335	0.0335	0.0335	0.0411	0.0369	0.0423	0.0352	0.0359	0.0350	0.0370	0.0353	0.0391	0.0337	0.0352	0.0329	0.0381	
Cr	0.0084	0.0092	0.0096	0.0101	0.0085	0.0085	0.0121	0.0122	0.0122	0.0094	0.0077	0.0080	0.0080	0.0080	0.0100	0.0093	0.0107	0.0091	0.0088	0.0090	0.0092	0.0095	0.0102	0.0090	0.0093	0.0098	0.0097	
Fe	0.3788	0.3748	0.3817	0.3744	0.3763	0.3763	0.3849	0.3814	0.3855	0.3810	0.3784	0.3821	0.3821	0.3821	0.3729	0.3601	0.3701	0.3726	0.3709	0.3769	0.3805	0.3837	0.3855	0.3881	0.3811	0.3860	0.3762	
Mn	0.0085	0.0078	0.0091	0.0085	0.0075	0.0075	0.0072	0.0077	0.0081	0.0078	0.0087	0.0079	0.0079	0.0079	0.0083	0.0072	0.0080	0.0081	0.0079	0.0076	0.0068	0.0081	0.0073	0.0061	0.0076	0.0085	0.0085	
Ni	0.0023	0.0023	0.0012	0.0024	0.0027	0.0027	0.0020	0.0020	0.0020	0.0023	0.0028	0.0021	0.0021	0.0021	0.0022	0.0023	0.0025	0.0015	0.0031	0.0029	0.0019	0.0020	0.0018	0.0024	0.0012	0.0019	0.0026	
Mg	1.5495	1.5427	1.5799	1.5213	1.5417	1.5417	1.5521	1.5526	1.5563	1.5656	1.5788	1.5392	1.5392	1.5392	1.5268	1.5149	1.5121	1.5180	1.5309	1.5203	1.5317	1.5255	1.5318	1.5521	1.5344	1.5479	1.5945	
Ca	0.0492	0.0562	0.0254	0.0438	0.0452	0.0452	0.0392	0.0446	0.0427	0.0241	0.0193	0.0189	0.0189	0.0189	0.0297	0.0488	0.0385	0.0384	0.0281	0.0261	0.0421	0.0360	0.0375	0.0208	0.0252	0.0217	0.0472	
Na	0.0002	0.0017	0.0001	0.0011	0.0009	0.0009	0.0011	0.0012	0.0020	0.0000	0.0002	0.0000	0.0000	0.0000	0.0004	0.0024	0.0016	0.0009	0.0016	0.0012	0.0017	0.0000	0.0003	0.0007	0.0004	0.0001	0.0013	
Total	4.0066	4.0062	4.0107	3.9885	3.9999	3.9999	4.0054	4.0071	4.0111	4.0030	4.0046	3.9855	3.9855	3.9855	3.9831	3.9800	3.9800	3.9810	3.9828	3.9788	3.9943	3.9889	3.9945	3.9959	3.9862	3.9937	4.0274	
MMF	0.8036	0.8045	0.8054	0.8025	0.8038	0.8038	0.8013	0.8028	0.8015	0.8044	0.8067	0.8011	0.8011	0.8011	0.8037	0.8079	0.8034	0.8029	0.8050	0.8013	0.8010	0.7990	0.7989	0.8000	0.8010	0.8004	0.8091	
Wo	2.5	2.8	1.3	2.3	2.3	2.3	2.0	2.3	2.2	1.2	1.0	1.0	1.0	1.0	1.5	2.5	2.0	2.0	1.5	1.4	2.2	1.8	1.9	1.1	1.3	1.1	2.3	
En	78.4	78.2	79.5	78.4	78.5	78.5	78.5	78.5	78.4	79.5	79.9	79.3	79.3	79.3	79.1	78.7	78.7	78.7	79.3	79.0	78.4	78.4	78.4	79.2	79.1	79.2	79.0	
Fs	19.2	19.0	19.2	19.3	19.2	19.2	19.5	19.3	19.4	19.3	19.1	19.7	19.7	19.7	19.3	18.7	19.3	19.3	19.2	19.6	19.5	19.7	19.7	19.8	19.6	19.7	18.6	

Sample	S-23	S-23	S-23	S-23	S-23	S-23	S-23	S-23	S-23	S-23	S-23	S-23	S-24	S-24	S-24	S-24	S-24	S-24	S-24	S-24	S-24	S-24	S-24	S-24	S-24	S-25	S-25
Metres	120.4	120.4	120.4	120.4	120.4	120.4	120.4	120.4	120.4	120.4	120.4	120.4	124.8	124.8	124.8	124.8	124.8	124.8	124.8	124.8	124.8	124.8	124.8	124.8	124.8	129.1	129.1
Position	c	c	c	c	c	c	c	c	c	m	m	m	c	c	c	c	c	c	c	c	c	c	m	m	m	c	c
Wt. %																											
SiO_2	54.19	54.27	54.37	54.12	54.15	54.01	54.22	54.01	54.04	55.20	54.95	55.10	54.59	54.63	54.64	54.33	54.34	54.87	54.91	54.58	54.33	54.40	55.53	55.06	55.43	55.44	55.24
TiO_2	0.12	0.11	0.13	0.13	0.13	0.13	0.13	0.12	0.12	0.13	0.15	0.12	0.17	0.18	0.14	0.14	0.14	0.12	0.18	0.16	0.23	0.18	0.18	0.16	0.20	0.13	0.13
Al_2O_3	0.88	0.89	0.89	0.97	0.90	0.93	0.99	0.85	0.88	0.82	0.89	0.84	0.90	0.94	0.95	0.93	0.92	1.01	0.97	0.90	0.85	0.86	0.78	0.84	0.92	0.77	0.78
Cr_2O_3	0.36	0.34	0.37	0.40	0.36	0.38	0.36	0.39	0.35	0.32	0.34	0.32	0.36	0.31	0.34	0.34	0.34	0.38	0.36	0.35	0.30	0.32	0.24	0.27	0.33	0.31	0.35	
FeO	12.55	12.76	12.70	12.71	12.95	13.01	12.94	12.83	12.89	13.01	13.12	12.89	13.63	13.20	13.27	13.09	13.06	13.05	13.14	12.44	13.46	13.46	13.59	13.81	13.62	13.39	13.36	
MnO	0.30	0.25	0.30	0.28	0.27	0.28	0.30	0.29	0.22	0.27	0.25	0.29	0.26	0.28	0.30	0.31	0.29	0.30	0.30	0.29	0.26	0.24	0.28	0.33	0.28	0.30	0.30	
NiO	0.09	0.11	0.10	0.09	0.09	0.11	0.08	0.09	0.10	0.06	0.09	0.09	0.09	0.08	0.10	0.06	0.10	0.10	0.10	0.11	0.07	0.07	0.09	0.12	0.09	0.07	0.07	
MgO	29.94	30.18	30.01	29.79	29.84	30.07	30.10	30.27	30.27	29.37	28.99	29.11	29.10	28.77	28.86	28.69	28.73	28.49	28.58	27.92	29.12	29.09	28.53	28.65	28.54	29.03	29.05	
CaO	1.26	1.19	1.26	1.29	1.56	1.21	1.27	1.07	1.20	0.70	0.92	0.96	0.91	1.28	1.14	1.48	1.56	1.62	1.77	3.04	0.97	1.04	0.87	0.50	0.79	0.89	0.70	
Na_2O	0.01	0.02	0.01	0.02	0.01	0.02	0.01	0.02	0.01	0.00	0.00	0.00	0.03	0.02	0.01	0.03	0.03	0.03	0.03	0.05	0.00	0.02	0.02	0.02	0.01	0.02	0.01	
Total	99.69	100.13	100.14	99.81	100.25	100.14	100.39	99.94	100.10	99.88	99.71	99.73	100.05	99.68	99.75	99.39	99.52	99.96	100.33	99.85	99.58	99.68	100.12	99.77	100.19	100.36	99.99	
Cations (based on 6 oxygens):																											
Si	1.9429	1.9388	1.9419	1.9401	1.9364	1.9331	1.9345	1.9348	1.9334	1.9702	1.9676	1.9704	1.9552	1.9608	1.9602	1.9574	1.9557	1.9639	1.9602	1.9602	1.9539	1.9549	1.9814	1.9740	1.9768	1.9734	1.9728	
Ti	0.0031	0.0030	0.0034	0.0036	0.0034	0.0035	0.0036	0.0033	0.0032	0.0035	0.0041	0.0033	0.0047	0.0049	0.0037	0.0037	0.0039	0.0033	0.0047	0.0043	0.0062	0.0048	0.0050	0.0043	0.0052	0.0036	0.0034	
Al	0.0372	0.0376	0.0374	0.0410	0.0378	0.0391	0.0415	0.0358	0.0373	0.0346	0.0378	0.0354	0.0378	0.0398	0.0402	0.0396	0.0391	0.0427	0.0409	0.0381	0.0360	0.0364	0.0328	0.0356	0.0385	0.0324	0.0329	
Cr	0.0103	0.0096	0.0105	0.0114	0.0103	0.0106	0.0100	0.0110	0.0099	0.0090	0.0098	0.0092	0.0101	0.0087	0.0097	0.0096	0.0098	0.0106	0.0101	0.0101	0.0086	0.0091	0.0067	0.0077	0.0092	0.0087	0.0099	
Fe	0.3762	0.3812	0.3794	0.3810	0.3872	0.3893	0.3859	0.3845	0.3858	0.3883	0.3927	0.3856	0.4081	0.3961	0.3980	0.3943	0.3929	0.3905	0.3922	0.3737	0.4049	0.4045	0.4054	0.4141	0.4062	0.3987	0.3990	
Mn	0.0090	0.0077	0.0092	0.0086	0.0081	0.0086	0.0090	0.0089	0.0067	0.0083	0.0077	0.0088	0.0079	0.0084	0.0092	0.0095	0.0087	0.0091	0.0091	0.0086	0.0078	0.0073	0.0085	0.0101	0.0084	0.0091	0.0091	
Ni	0.0026	0.0032	0.0028	0.0026	0.0025	0.0032	0.0023	0.0025	0.0029	0.0018	0.0026	0.0025	0.0027	0.0023	0.0028	0.0017	0.0029	0.0029	0.0028	0.0032	0.0021	0.0020	0.0027	0.0033	0.0025	0.0019	0.0019	
Mg	1.6002	1.6072	1.5976	1.5919	1.5903	1.6041	1.6006	1.6161	1.6142	1.5623	1.5470	1.5519	1.5535	1.5391	1.5429	1.5407	1.5414	1.5198	1.5208	1.4943	1.5607	1.5580	1.5175	1.5308	1.5169	1.5399	1.5464	
Ca	0.0483	0.0457	0.0482	0.0494	0.0597	0.0464	0.0486	0.0411	0.0458	0.0266	0.0353	0.0368	0.0351	0.0493	0.0438	0.0570	0.0603	0.0623	0.0677	0.1170	0.0372	0.0401	0.0334	0.0194	0.0302	0.0341	0.0267	
Na	0.0007	0.0013	0.0007	0.0011	0.0008	0.0016	0.0004	0.0011	0.0007	0.0000	0.0000	0.0000	0.0022	0.0011	0.0009	0.0022	0.0023	0.0021	0.0021	0.0035	0.0001	0.0013	0.0015	0.0016	0.0006	0.0016	0.0008	
Total	4.0306	4.0353	4.0311	4.0307	4.0366	4.0394	4.0364	4.0391	4.0401	4.0045	4.0045	4.0040	4.0173	4.0106	4.0115	4.0155	4.0171	4.0072	4.0106	4.0132	4.0176	4.0183	3.9947	4.0008	3.9944	4.0033	4.0028	
MMF	0.8096	0.8083	0.8081	0.8069	0.8042	0.8047	0.8057	0.8078	0.8071	0.8009	0.7975	0.8010	0.7919	0.7953	0.7950	0.7962	0.7969	0.7956	0.7950	0.7999	0.7940	0.7939	0.7892	0.7871	0.7888	0.7944	0.7949	
Wo	2.4	2.2	2.4	2.4	2.9	2.3	2.4	2.0	2.2	1.3	1.8	1.9	1.8	2.5	2.2	2.9	3.0	3.2	3.4	5.9	1.9	2.0	1.7	1.0	1.5	1.7	1.4	
En	79.0	79.0	78.9	78.7	78.1	78.6	78.6	79.2	78.9	79.0	78.3	78.6	77.8	77.6	77.7	77.3	77.3	77.0	76.8	75.3	77.9	77.8	77.6	77.9	77.7	78.1	78.4	
Fs	18.6	18.7	18.7	18.8	19.0	19.1	19.0	18.8	18.9	19.6	19.9	19.5	20.4	20.0	20.1	19.8	19.7	19.8	19.8	18.8	20.2	20.2	20.7	21.1	20.8	20.2	20.2	

MICROPROBE DATA TABLE C5: Composition of **orthopyroxene** in the UG1 Footwall and MG3 Units - all **S** samples.
Metres given below base of UG1 chromitite.
c = core of grain m = grain margin.

Sample	S-25	S-25	S-25	S-25	S-26	S-26	S-26	S-26	S-26	S-26	S-26	S-26	S-26	S-26	S-26	S-26	S-26	S-26	S-26	S-26	S-27	S-27	S-27	S-27	S-27	S-27	S-28	S-28
Metres	129.1	129.1	129.1	129.1	133.5	133.5	133.5	133.5	133.5	133.5	133.5	133.5	133.5	133.5	133.5	133.5	133.5	133.5	133.5	133.5	137.9	137.9	137.9	137.9	137.9	137.9	142.5	142.5
Position	c	m	m	m	c	c	c	c	c	c	c	c	c	c	m	m	m	m	m	c	c	c	m	m	m	c	c
Wt. %																												
SiO_2	55.67	55.48	55.38	55.43	55.10	54.87	54.68	54.68	54.80	54.92	54.64	54.50	54.59	54.79	54.63	55.14	54.79	54.72	60.22	55.85	55.30	55.49	56.01	56.12	55.27	55.75	55.43
TiO_2	0.14	0.10	0.14	0.15	0.10	0.10	0.13	0.12	0.11	0.10	0.12	0.11	0.11	0.11	0.11	0.12	0.13	0.08	0.10	0.10	0.12	0.11	0.12	0.11	0.12	0.11	0.11
Al_2O_3	0.85	0.79	0.74	0.87	0.98	0.83	0.99	0.95	0.89	0.81	0.95	0.87	1.01	0.85	0.87	0.84	0.85	1.53	1.91	0.90	0.91	0.90	0.94	0.87	0.81	1.01	0.94
Cr_2O_3	0.33	0.27	0.31	0.32	0.37	0.34	0.38	0.42	0.37	0.35	0.36	0.37	0.40	0.38	0.35	0.32	0.35	0.34	0.29	0.39	0.36	0.39	0.36	0.39	0.34	0.45	0.39
FeO	13.30	13.58	13.14	13.57	13.02	13.27	12.93	13.06	13.35	13.23	13.22	13.23	13.30	13.09	13.38	13.32	13.54	13.22	11.21	12.68	13.29	13.19	13.01	13.23	13.32	13.45	13.29
MnO	0.28	0.30	0.27	0.32	0.23	0.28	0.26	0.24	0.26	0.29	0.27	0.26	0.25	0.25	0.31	0.28	0.30	0.29	0.26	0.29	0.30	0.28	0.29	0.30	0.23	0.32	0.31
NiO	0.12	0.12	0.09	0.06	0.02	0.05	0.06	0.02	0.04	0.05	0.06	0.06	0.07	0.04	0.08	0.09	0.12	0.08	0.09	0.12	0.08	0.11	0.11	0.10	0.09	0.10	0.10
MgO	29.13	29.27	29.12	28.93	29.49	30.09	29.29	29.48	29.89	29.78	29.54	29.83	29.44	29.86	28.96	29.41	29.26	29.09	24.68	27.76	28.61	28.54	28.34	28.39	28.51	28.45	28.73
CaO	0.73	0.46	0.65	0.77	1.28	0.76	1.65	1.34	0.87	0.92	1.12	1.00	1.20	0.78	0.94	0.68	0.70	0.74	0.87	1.74	0.83	1.44	1.21	0.66	1.00	0.97	0.70
Na_2O	0.01	0.00	0.01	0.00	0.02	0.01	0.04	0.02	0.01	0.02	0.02	0.02	0.02	0.02	0.01	0.00	0.00	0.05	0.07	0.03	0.01	0.04	0.02	0.01	0.02	0.01	0.00
Total	100.56	100.36	99.85	100.42	100.61	100.61	100.40	100.33	100.57	100.47	100.31	100.23	100.40	100.17	99.64	100.20	100.04	100.13	99.70	99.85	99.82	100.49	100.43	100.18	99.69	100.61	100.00
Cations (based on 6 oxygens):																												
Si	1.9752	1.9740	1.9773	1.9725	1.9566	1.9501	1.9496	1.9499	1.9492	1.9547	1.9496	1.9464	1.9474	1.9537	1.9619	1.9653	1.9600	1.9516	2.1035	1.9932	1.9773	1.9739	1.9877	1.9942	1.9794	1.9788	1.9775
Ti	0.0038	0.0026	0.0039	0.0039	0.0027	0.0028	0.0035	0.0031	0.0030	0.0026	0.0032	0.0029	0.0029	0.0030	0.0030	0.0031	0.0034	0.0020	0.0027	0.0025	0.0033	0.0030	0.0032	0.0030	0.0031	0.0029	0.0030
Al	0.0354	0.0330	0.0311	0.0363	0.0408	0.0350	0.0415	0.0399	0.0373	0.0341	0.0398	0.0366	0.0425	0.0357	0.0366	0.0354	0.0360	0.0643	0.0787	0.0380	0.0383	0.0379	0.0394	0.0364	0.0343	0.0423	0.0396
Cr	0.0093	0.0075	0.0087	0.0090	0.0105	0.0095	0.0108	0.0119	0.0103	0.0099	0.0102	0.0104	0.0113	0.0107	0.0101	0.0090	0.0098	0.0095	0.0081	0.0111	0.0103	0.0109	0.0100	0.0109	0.0096	0.0126	0.0109
Fe	0.3947	0.4041	0.3923	0.4040	0.3868	0.3944	0.3854	0.3896	0.3970	0.3939	0.3945	0.3950	0.3968	0.3905	0.4018	0.3970	0.4051	0.3943	0.3276	0.3784	0.3976	0.3922	0.3861	0.3932	0.3991	0.3992	0.3965
Mn	0.0083	0.0091	0.0080	0.0095	0.0068	0.0085	0.0077	0.0071	0.0078	0.0088	0.0083	0.0077	0.0076	0.0077	0.0095	0.0084	0.0091	0.0087	0.0076	0.0086	0.0092	0.0085	0.0089	0.0092	0.0069	0.0096	0.0094
Ni	0.0034	0.0034	0.0025	0.0018	0.0006	0.0016	0.0017	0.0007	0.0011	0.0013	0.0018	0.0016	0.0020	0.0010	0.0023	0.0026	0.0034	0.0024	0.0024	0.0033	0.0022	0.0032	0.0032	0.0028	0.0025	0.0027	0.0028
Mg	1.5403	1.5523	1.5497	1.5344	1.5609	1.5938	1.5562	1.5670	1.5851	1.5796	1.5713	1.5880	1.5656	1.5872	1.5503	1.5624	1.5602	1.5467	1.2851	1.4770	1.5249	1.5131	1.4991	1.5040	1.5218	1.5051	1.5277
Ca	0.0277	0.0174	0.0249	0.0294	0.0486	0.0289	0.0631	0.0511	0.0330	0.0351	0.0427	0.0381	0.0459	0.0298	0.0361	0.0260	0.0267	0.0282	0.0326	0.0665	0.0318	0.0548	0.0462	0.0252	0.0383	0.0369	0.0268
Na	0.0010	0.0000	0.0007	0.0000	0.0013	0.0009	0.0026	0.0014	0.0005	0.0015	0.0017	0.0013	0.0016	0.0012	0.0004	0.0001	0.0000	0.0033	0.0044	0.0021	0.0003	0.0027	0.0015	0.0008	0.0011	0.0009	0.0000
Total	3.9992	4.0032	3.9993	4.0009	4.0157	4.0254	4.0221	4.0218	4.0242	4.0215	4.0231	4.0279	4.0236	4.0206	4.0120	4.0094	4.0137	4.0111	3.8526	3.9808	3.9953	4.0001	3.9852	3.9796	3.9961	3.9912	3.9942
MMF	0.7960	0.7935	0.7980	0.7916	0.8014	0.8016	0.8015	0.8009	0.7997	0.8004	0.7993	0.8008	0.7978	0.8025	0.7942	0.7974	0.7939	0.7968	0.7969	0.7960	0.7932	0.7942	0.7952	0.7928	0.7922	0.7904	0.7939
Wo	1.4	0.9	1.3	1.5	2.4	1.4	3.1	2.5	1.6	1.7	2.1	1.9	2.3	1.5	1.8	1.3	1.3	1.4	2.0	3.5	1.6	2.8	2.4	1.3	2.0	1.9	1.4
En	78.5	78.6	78.8	78.0	78.2	79.0	77.6	78.0	78.7	78.6	78.2	78.6	78.0	79.1	78.0	78.7	78.3	78.5	78.1	76.9	78.0	77.2	77.6	78.2	77.7	77.5	78.3
Fs	20.1	20.5	19.9	20.5	19.4	19.6	19.2	19.4	19.7	19.6	19.6	19.5	19.8	19.5	20.2	20.0	20.3	20.0	19.9	19.7	20.3	20.0	20.0	20.5	20.4	20.6	20.3

Sample	S-28	S-28	S-28	S-28	S-29	S-29	S-29	S-29	S-29	S-29	S-29	S-29	S-29	S-29	S-29	S-29	S-29	S-29	S-30	S-30	S-30	S-30	S-30	S-30	S-31	S-31	S-31	S-31
Metres	142.5	142.5	142.5	142.5	146.9	146.9	146.9	146.9	146.9	146.9	146.9	146.9	146.9	146.9	146.9	146.9	146.9	146.9	151.6	151.6	151.6	151.6	151.6	151.6	156.3	156.3	156.3	156.3
Position	c	m	m	m	c	c	c	c	c	c	c	c	c	c	m	m	m	c	c	c	m	m	m	c	c	c	c
Wt. %																												
SiO_2	55.69	55.88	55.77	55.78	54.94	54.84	54.56	54.91	54.75	54.93	54.74	54.57	54.80	54.62	55.45	55.44	55.44	55.03	55.33	54.64	54.87	54.67	54.55	55.27	55.32	55.14	54.91
TiO_2	0.10	0.11	0.10	0.11	0.09	0.11	0.11	0.11	0.10	0.08	0.11	0.11	0.10	0.12	0.12	0.10	0.10	0.17	0.11	0.14	0.14	0.13	0.16	0.10	0.09	0.12	0.11
Al_2O_3	0.92	0.80	0.90	0.88	1.58	0.92	0.91	0.90	0.92	0.84	0.94	0.87	0.88	0.94	0.83	0.93	0.93	0.84	0.81	0.86	0.81	0.82	0.82	0.72	0.88	0.87	0.88
Cr_2O_3	0.36	0.36	0.37	0.34	0.35	0.38	0.35	0.36	0.37	0.36	0.37	0.37	0.35	0.37	0.33	0.38	0.38	0.36	0.30	0.31	0.31	0.30	0.31	0.27	0.31	0.30	0.31
FeO	13.69	13.25	13.33	13.34	12.91	13.22	13.17	13.18	13.18	13.18	13.08	13.18	13.40	13.05	13.21	13.19	13.19	13.58	13.23	13.51	13.77	13.37	13.47	13.19	13.10	13.16	12.99
MnO	0.31	0.27	0.28	0.27	0.28	0.29	0.32	0.26	0.25	0.26	0.24	0.32	0.27	0.29	0.32	0.30	0.30	0.28	0.29	0.25	0.29	0.26	0.29	0.31	0.29	0.30	0.29
NiO	0.06	0.11	0.10	0.08	0.11	0.08	0.09	0.09	0.08	0.08	0.08	0.10	0.09	0.05	0.07	0.06	0.06	0.12	0.08	0.06	0.10	0.06	0.04	0.08	0.07	0.10	0.06
MgO	28.69	28.66	28.53	28.96	28.97	29.36	29.70	29.74	29.63	29.74	29.65	29.38	29.71	29.47	28.58	28.64	28.64	28.87	28.96	28.79	28.85	28.76	28.94	29.57	29.58	29.65	29.70
CaO	0.81	0.56	0.79	0.66	1.25	0.98	0.78	0.96	1.16	0.94	1.08	1.14	0.87	1.05	0.57	0.61	0.61	1.19	0.78	1.35	0.82	0.97	1.19	1.07	1.39	1.21	0.91
Na_2O	0.00	0.01	0.02	0.01	0.05	0.00	0.00	0.01	0.00	0.01	0.01	0.01	0.01	0.01	0.00	0.00	0.00	0.00	0.00	0.01	0.00	0.01	0.01	0.01	0.01	0.00	0.01
Total	100.63	100.01	100.18	100.42	100.51	100.18	99.97	100.52	100.44	100.43	100.31	100.06	100.49	99.95	99.48	99.65	99.65	100.45	99.90	99.93	99.95	99.34	99.79	100.60	101.04	100.86	100.16
Cations (based on 6 oxygens):																												
Si	1.9775	1.9898	1.9852	1.9803	1.9517	1.9574	1.9514	1.9531	1.9505	1.9552	1.9513	1.9525	1.9519	1.9535	1.9860	1.9823	1.9823	1.9626	1.9762	1.9595	1.9660	1.9677	1.9582	1.9637	1.9577	1.9555	1.9573
Ti	0.0027	0.0028	0.0026	0.0029	0.0023	0.0029	0.0029	0.0030	0.0028	0.0023	0.0030	0.0029	0.0028	0.0031	0.0032	0.0027	0.0027	0.0046	0.0030	0.0039	0.0038	0.0034	0.0044	0.0027	0.0025	0.0031	0.0030
Al	0.0385	0.0337	0.0376	0.0368	0.0660	0.0388	0.0385	0.0376	0.0384	0.0354	0.0395	0.0367	0.0369	0.0395	0.0350	0.0393	0.0393	0.0355	0.0339	0.0365	0.0341	0.0347	0.0348	0.0303	0.0368	0.0363	0.0371
Cr	0.0101	0.0102	0.0103	0.0094	0.0099	0.0107	0.0098	0.0100	0.0103	0.0101	0.0105	0.0106	0.0098	0.0104	0.0094	0.0106	0.0106	0.0102	0.0086	0.0088	0.0087	0.0087	0.0087	0.0076	0.0085	0.0085	0.0088
Fe	0.4065	0.3946	0.3969	0.3961	0.3835	0.3948	0.3938	0.3919	0.3926	0.3924	0.3899	0.3944	0.3992	0.3903	0.3957	0.3944	0.3944	0.4051	0.3953	0.4051	0.4126	0.4024	0.4046	0.3920	0.3875	0.3903	0.3872
Mn	0.0093	0.0083	0.0084	0.0081	0.0085	0.0088	0.0096	0.0079	0.0076	0.0078	0.0073	0.0097	0.0082	0.0087	0.0096	0.0091	0.0091	0.0085	0.0087	0.0076	0.0087	0.0078	0.0090	0.0092	0.0086	0.0090	0.0088
Ni	0.0017	0.0031	0.0028	0.0023	0.0030	0.0023	0.0025	0.0026	0.0024	0.0023	0.0023	0.0028	0.0027	0.0016	0.0020	0.0016	0.0016	0.0035	0.0023	0.0016	0.0028	0.0018	0.0012	0.0022	0.0020	0.0028	0.0016
Mg	1.5184	1.5211	1.5137	1.5324	1.5341	1.5618	1.5832	1.5769	1.5733	1.5780	1.5753	1.5671	1.5769	1.5708	1.5257	1.5263	1.5263	1.5347	1.5418	1.5387	1.5407	1.5430	1.5486	1.5657	1.5603	1.5672	1.5779
Ca	0.0308	0.0213	0.0299	0.0251	0.0474	0.0373	0.0297	0.0367	0.0443	0.0359	0.0413	0.0438	0.0332	0.0402	0.0220	0.0235	0.0235	0.0454	0.0297	0.0519	0.0315	0.0374	0.0459	0.0407	0.0525	0.0461	0.0347
Na	0.0000	0.0008	0.0016	0.0005	0.0034	0.0002	0.0000	0.0005	0.0002	0.0007	0.0004	0.0009	0.0006	0.0005	0.0000	0.0002	0.0002	0.0000	0.0002	0.0008	0.0000	0.0007	0.0004	0.0007	0.0009	0.0003	0.0007
Total	3.9956	3.9857	3.9891	3.9939	4.0098	4.0150	4.0215	4.0203	4.0224	4.0202	4.0209	4.0214	4.0222	4.0187	3.9886	3.9901	3.9901	4.0101	3.9997	4.0144	4.0088	4.0075	4.0158	4.0149	4.0175	4.0191	4.0171
MMF	0.7888	0.7940	0.7923	0.7946	0.8000	0.7982	0.8008	0.8009	0.8003	0.8008	0.8016	0.7989	0.7980	0.8010	0.7940	0.7947	0.7947	0.7912	0.7959	0.7916	0.7888	0.7932	0.7929	0.7998	0.8010	0.8006	0.8030
Wo	1.6	1.1	1.5	1.3	2.4	1.9	1.5	1.8	2.2	1.8	2.1	2.2	1.7	2.0	1.1	1.2	1.2	2.3	1.5	2.6	1.6	1.9	2.3	2.0	2.6	2.3	1.7
En	77.6	78.5	78.0	78.4	78.1	78.3	78.9	78.6	78.3	78.6	78.5	78.1	78.5	78.5	78.5	78.5	78.5	77.3	78.4	77.1	77.6	77.8	77.5	78.3	78.0	78.2	78.9
Fs	20.8	20.4	20.5	20.3	19.5	19.8	19.6	19.5	19.5	19.6	19.4	19.7	19.9	19.5	20.4	20.3	20.3	20.4	20.1	20.3	20.8	20.3	20.2	19.6	19.4	19.5	19.4

MICROPROBE DATA TABLE C5: Composition of **orthopyroxene** in the UG1 Footwall and MG3 Units - all **S** samples.
Metres given below base of UG1 chromitite.
c = core of grain m = grain margin.

Sample	S-31	S-31	S-31	S-31	S-31	S-31	S-31	S-31	S-32	S-32	S-32	S-32	S-32	S-32	S-33	S-33	S-33	S-33	S-33	S-33	S-33	S-33	S-33	S-33	S-33	S-33
Metres	156.3	156.3	156.3	156.3	156.3	156.3	156.3	156.3	161.3	161.3	161.3	161.3	161.3	161.3	166.0	166.0	166.0	166.0	166.0	166.0	166.0	166.0	166.0	166.0	166.0	166.0
Position	c	c	c	c	c	m	m	m	c	c	c	m	m	m	c	c	c	c	c	c	c	c	c	c	m	m
Wt. %																										
SiO_2	54.71	54.52	54.99	54.76	54.78	55.34	55.64	55.54	55.74	55.74	55.30	55.38	55.40	55.85	54.75	54.74	54.76	54.81	54.53	54.67	54.82	54.73	54.62	54.88	54.49	54.79	54.82
TiO_2	0.12	0.13	0.11	0.11	0.12	0.12	0.14	0.13	0.11	0.14	0.12	0.14	0.11	0.14	0.15	0.14	0.14	0.16	0.16	0.15	0.16	0.14	0.18	0.14	0.12	0.15	0.12
Al_2O_3	0.90	1.09	0.87	0.85	0.88	0.88	0.78	0.83	0.93	0.79	0.88	0.79	0.79	0.79	0.81	0.82	0.83	0.87	0.84	0.80	0.83	0.77	0.90	0.81	0.76	0.76	0.61
Cr_2O_3	0.29	0.29	0.32	0.30	0.31	0.31	0.28	0.27	0.35	0.28	0.33	0.36	0.29	0.28	0.28	0.29	0.29	0.29	0.29	0.29	0.29	0.29	0.31	0.29	0.28	0.29	0.22
FeO	13.05	13.09	13.32	13.31	13.20	13.20	13.11	13.14	13.05	13.77	13.30	13.22	13.59	13.65	13.14	13.16	13.16	13.07	13.00	13.37	13.36	13.24	13.04	12.99	13.88	13.91	13.73
MnO	0.29	0.29	0.29	0.29	0.31	0.30	0.25	0.32	0.30	0.32	0.31	0.33	0.29	0.35	0.28	0.27	0.29	0.27	0.27	0.27	0.27	0.30	0.24	0.26	0.26	0.29	0.32
NiO	0.06	0.06	0.07	0.05	0.07	0.12	0.11	0.09	0.09	0.13	0.07	0.07	0.08	0.11	0.06	0.04	0.06	0.03	0.08	0.07	0.08	0.07	0.06	0.06	0.03	0.05	0.04
MgO	29.45	29.63	29.68	29.73	29.60	28.27	28.34	28.57	27.87	28.75	28.55	28.35	28.67	28.77	29.52	29.73	29.61	29.47	29.40	29.84	29.64	29.79	29.43	29.59	29.11	28.83	28.86
CaO	1.06	0.60	0.85	0.89	0.84	0.79	0.59	0.57	0.83	0.69	1.13	0.83	0.55	0.69	0.88	0.96	0.82	1.41	1.09	0.91	1.18	0.94	1.05	1.07	0.53	0.65	0.74
Na_2O	0.00	0.00	0.01	0.01	0.01	0.02	0.01	0.00	0.02	0.01	0.01	0.01	0.00	0.01	0.00	0.00	0.00	0.00	0.00	0.00	0.00	0.01	0.00	0.00	0.00	0.01	0.01
Total	99.94	99.68	100.50	100.30	100.11	99.35	99.25	99.46	99.31	100.61	99.99	99.47	99.78	100.64	99.88	100.14	99.98	100.39	99.65	100.37	100.62	100.28	99.83	100.09	99.47	99.73	99.47
Cations (based on 6 oxygens):																											
Si	1.9565	1.9525	1.9562	1.9530	1.9560	1.9862	1.9949	1.9884	1.9977	1.9801	1.9758	1.9859	1.9819	1.9819	1.9586	1.9541	1.9573	1.9533	1.9559	1.9497	1.9509	1.9527	1.9550	1.9585	1.9618	1.9675	1.9724
Ti	0.0031	0.0034	0.0029	0.0031	0.0032	0.0033	0.0038	0.0036	0.0031	0.0037	0.0033	0.0037	0.0029	0.0036	0.0041	0.0038	0.0039	0.0042	0.0043	0.0041	0.0042	0.0038	0.0050	0.0037	0.0032	0.0041	0.0033
Al	0.0379	0.0462	0.0366	0.0356	0.0369	0.0372	0.0330	0.0350	0.0393	0.0331	0.0368	0.0332	0.0333	0.0331	0.0343	0.0343	0.0350	0.0366	0.0353	0.0335	0.0348	0.0323	0.0380	0.0341	0.0323	0.0320	0.0259
Cr	0.0081	0.0081	0.0090	0.0084	0.0086	0.0088	0.0079	0.0077	0.0100	0.0078	0.0093	0.0101	0.0082	0.0080	0.0079	0.0082	0.0083	0.0083	0.0083	0.0081	0.0080	0.0081	0.0086	0.0082	0.0080	0.0081	0.0063
Fe	0.3904	0.3919	0.3962	0.3969	0.3942	0.3962	0.3931	0.3934	0.3911	0.4092	0.3974	0.3964	0.4065	0.4051	0.3932	0.3926	0.3934	0.3894	0.3898	0.3988	0.3976	0.3951	0.3903	0.3876	0.4177	0.4178	0.4131
Mn	0.0089	0.0088	0.0089	0.0088	0.0094	0.0091	0.0076	0.0097	0.0092	0.0095	0.0093	0.0101	0.0089	0.0105	0.0084	0.0081	0.0088	0.0082	0.0083	0.0082	0.0082	0.0091	0.0073	0.0080	0.0081	0.0090	0.0098
Ni	0.0018	0.0017	0.0019	0.0014	0.0019	0.0035	0.0032	0.0026	0.0027	0.0037	0.0019	0.0020	0.0024	0.0031	0.0018	0.0012	0.0018	0.0010	0.0023	0.0019	0.0024	0.0021	0.0018	0.0016	0.0009	0.0015	0.0012
Mg	1.5699	1.5814	1.5736	1.5804	1.5753	1.5123	1.5145	1.5245	1.4888	1.5221	1.5202	1.5153	1.5289	1.5219	1.5740	1.5820	1.5772	1.5652	1.5718	1.5864	1.5721	1.5841	1.5703	1.5738	1.5623	1.5430	1.5477
Ca	0.0407	0.0229	0.0324	0.0341	0.0321	0.0302	0.0227	0.0219	0.0320	0.0263	0.0433	0.0317	0.0211	0.0263	0.0338	0.0367	0.0315	0.0539	0.0418	0.0347	0.0449	0.0360	0.0404	0.0411	0.0204	0.0251	0.0285
Na	0.0003	0.0000	0.0007	0.0006	0.0009	0.0013	0.0006	0.0000	0.0014	0.0009	0.0009	0.0006	0.0003	0.0008	0.0000	0.0000	0.0000	0.0000	0.0000	0.0000	0.0000	0.0004	0.0000	0.0002	0.0000	0.0007	0.0005
Total	4.0175	4.0169	4.0184	4.0222	4.0185	3.9881	3.9812	3.9867	3.9753	3.9962	3.9982	3.9891	3.9946	3.9943	4.0162	4.0209	4.0172	4.0200	4.0179	4.0254	4.0234	4.0236	4.0167	4.0167	4.0148	4.0088	4.0085
MMF	0.8009	0.8014	0.7989	0.7993	0.7999	0.7924	0.7939	0.7949	0.7920	0.7881	0.7928	0.7927	0.7900	0.7898	0.8001	0.8012	0.8004	0.8008	0.8013	0.7991	0.7981	0.8004	0.8009	0.8024	0.7890	0.7869	0.7893
Wo	2.0	1.1	1.6	1.7	1.6	1.6	1.2	1.1	1.7	1.3	2.2	1.6	1.1	1.3	1.7	1.8	1.6	2.7	2.1	1.7	2.2	1.8	2.0	2.1	1.0	1.3	1.4
En	78.5	79.2	78.6	78.6	78.7	78.0	78.5	78.6	77.9	77.8	77.5	78.0	78.1	77.9	78.7	78.7	78.8	77.9	78.5	78.5	78.0	78.6	78.5	78.6	78.1	77.7	77.8
Fs	19.5	19.6	19.8	19.7	19.7	20.4	20.4	20.3	20.5	20.9	20.3	20.4	20.8	20.7	19.7	19.5	19.6	19.4	19.5	19.7	19.7	19.6	19.5	19.4	20.9	21.0	20.8

Sample	S-34	S-34	S-34	S-34	S-34	S-34	S-35	S-35	S-35	S-35	S-35	S-35	S-35	S-35	S-36	S-36	S-36	S-36	S-36	S-36	S-36	S-36	S-36	S-36	S-36	S-36	S-36
Metres	170.6	170.6	170.6	170.6	170.6	170.6	175.6	175.6	175.6	175.6	175.6	175.6	175.6	175.6	181.5	181.5	181.5	181.5	181.5	181.5	181.5	181.5	181.5	181.5	181.5	181.5	181.5
Position	m	m	m	c	c	c	c	c	c	c	c	m	m	m	c	c	c	c	c	c	c	c	c	c	m	m	m
Wt. %																											
SiO_2	55.31	55.24	55.26	55.33	55.33	55.10	55.66	55.55	55.64	55.53	55.39	55.72	55.93	55.75	54.63	54.72	54.50	54.77	54.59	54.50	54.56	54.25	54.81	54.22	55.50	55.36	55.12
TiO_2	0.16	0.13	0.15	0.15	0.13	0.17	0.13	0.13	0.12	0.12	0.10	0.13	0.14	0.14	0.21	0.27	0.20	0.17	0.21	0.16	0.16	0.15	0.15	0.20	0.14	0.18	0.19
Al_2O_3	0.84	0.83	0.90	0.99	1.00	0.93	0.89	0.96	0.92	0.95	1.08	0.86	0.88	0.82	0.98	0.86	0.80	0.87	0.87	0.87	0.90	0.89	0.86	0.85	0.77	0.89	0.89
Cr_2O_3	0.25	0.23	0.26	0.27	0.31	0.25	0.28	0.29	0.29	0.29	0.32	0.29	0.32	0.28	0.23	0.24	0.25	0.27	0.25	0.27	0.24	0.26	0.26	0.25	0.21	0.22	0.22
FeO	13.97	13.95	13.89	13.93	13.73	14.01	12.74	12.63	12.96	12.65	12.69	12.84	12.94	12.79	14.14	14.48	14.17	14.35	14.12	14.27	14.17	14.24	14.38	14.27	14.49	14.66	14.60
MnO	0.27	0.29	0.30	0.28	0.25	0.25	0.29	0.24	0.33	0.29	0.26	0.29	0.28	0.29	0.29	0.33	0.30	0.31	0.28	0.34	0.32	0.34	0.30	0.35	0.31	0.30	0.29
NiO	0.07	0.07	0.06	0.04	0.06	0.09	0.10	0.09	0.10	0.08	0.08	0.09	0.09	0.10	0.06	0.06	0.08	0.07	0.05	0.09	0.07	0.07	0.08	0.04	0.11	0.09	0.09
MgO	28.68	28.62	28.38	28.19	28.05	28.31	28.86	28.97	28.93	28.80	28.37	29.31	29.11	29.12	28.96	28.83	28.99	29.13	28.57	28.92	28.76	28.87	28.89	28.89	28.21	27.83	27.68
CaO	0.64	0.67	0.80	0.76	1.13	0.97	0.71	0.90	0.82	0.95	1.78	0.54	0.62	0.59	0.73	0.79	0.74	0.73	1.59	0.48	0.78	0.83	0.98	0.88	0.50	0.71	0.82
Na_2O	0.01	0.02	0.02	0.01	0.01	0.02	0.00	0.00	0.01	0.00	0.01	0.00	0.01	0.02	0.00	0.02	0.00	0.00	0.01	0.01	0.00	0.01	0.01	0.02	0.02	0.02	0.03
Total	100.21	100.04	100.01	99.94	99.99	100.10	99.66	99.76	100.11	99.65	100.07	100.07	100.33	99.90	100.22	100.60	100.04	100.67	100.53	99.91	99.96	99.90	100.71	99.97	100.26	100.26	99.93
Cations (based on 6 oxygens):																											
Si	1.9748	1.9756	1.9769	1.9795	1.9789	1.9719	1.9856	1.9803	1.9797	1.9822	1.9746	1.9804	1.9831	1.9844	1.9553	1.9553	1.9559	1.9541	1.9532	1.9578	1.9589	1.9516	1.9560	1.9500	1.9834	1.9809	1.9797
Ti	0.0042	0.0034	0.0040	0.0039	0.0034	0.0045	0.0034	0.0035	0.0031	0.0031	0.0026	0.0034	0.0038	0.0037	0.0058	0.0073	0.0055	0.0047	0.0056	0.0044	0.0044	0.0040	0.0041	0.0054	0.0039	0.0047	0.0050
Al	0.0352	0.0349	0.0378	0.0415	0.0423	0.0392	0.0376	0.0403	0.0384	0.0398	0.0452	0.0360	0.0370	0.0342	0.0412	0.0362	0.0337	0.0365	0.0366	0.0369	0.0381	0.0378	0.0362	0.0362	0.0322	0.0375	0.0377
Cr	0.0071	0.0065	0.0074	0.0077	0.0088	0.0071	0.0080	0.0081	0.0083	0.0082	0.0089	0.0081	0.0091	0.0079	0.0065	0.0067	0.0071	0.0075	0.0072	0.0075	0.0067	0.0075	0.0073	0.0072	0.0060	0.0064	0.0064
Fe	0.4171	0.4171	0.4154	0.4167	0.4106	0.4193	0.3801	0.3765	0.3857	0.3777	0.3784	0.3817	0.3836	0.3808	0.4233	0.4326	0.4252	0.4281	0.4223	0.4288	0.4255	0.4285	0.4290	0.4292	0.4330	0.4388	0.4387
Mn	0.0081	0.0088	0.0090	0.0085	0.0076	0.0077	0.0087	0.0074	0.0100	0.0087	0.0078	0.0087	0.0085	0.0087	0.0088	0.0099	0.0092	0.0095	0.0084	0.0104	0.0099	0.0103	0.0091	0.0106	0.0094	0.0090	0.0088
Ni	0.0021	0.0019	0.0016	0.0010	0.0017	0.0026	0.0029	0.0025	0.0030	0.0023	0.0023	0.0026	0.0025	0.0027	0.0016	0.0017	0.0024	0.0020	0.0015	0.0025	0.0020	0.0019	0.0023	0.0011	0.0031	0.0025	0.0025
Mg	1.5261	1.5255	1.5129	1.5034	1.4954	1.5103	1.5348	1.5390	1.5342	1.5322	1.5074	1.5528	1.5387	1.5450	1.5447	1.5352	1.5507	1.5488	1.5235	1.5483	1.5388	1.5479	1.5365	1.5486	1.5026	1.4845	1.4821
Ca	0.0246	0.0257	0.0306	0.0293	0.0431	0.0372	0.0271	0.0344	0.0311	0.0363	0.0681	0.0204	0.0236	0.0226	0.0279	0.0304	0.0286	0.0279	0.0608	0.0186	0.0301	0.0320	0.0374	0.0338	0.0193	0.0272	0.0314
Na	0.0008	0.0016	0.0015	0.0007	0.0004	0.0011	0.0000	0.0003	0.0006	0.0000	0.0010	0.0003	0.0005	0.0015	0.0000	0.0012	0.0001	0.0000	0.0004	0.0005	0.0000	0.0004	0.0005	0.0014	0.0017	0.0016	0.0018
Total	4.0002	4.0011	3.9972	3.9923	3.9923	4.0010	3.9882	3.9922	3.9941	3.9907	3.9962	3.9943	3.9903	3.9916	4.0151	4.0166	4.0183	4.0192	4.0195	4.0158	4.0143	4.0220	4.0184	4.0236	3.9945	3.9932	3.9941
MMF	0.7853	0.7853	0.7846	0.7830	0.7846	0.7827	0.8015	0.8035	0.7991	0.8022	0.7993	0.8027	0.8005	0.8023	0.7849	0.7802	0.7848	0.7834	0.7830	0.7831	0.7834	0.7832	0.7817	0.7830	0.7763	0.7718	0.7716
Wo	1.3	1.3	1.6	1.5	2.2	1.9	1.4	1.8	1.6	1.9	3.5	1.0	1.2	1.2	1.4	1.5	1.4	1.4	3.0	0.9	1.5	1.6	1.9	1.7	1.0	1.4	1.6
En	77.6	77.5	77.2	77.1	76.7	76.8	79.0	78.9	78.6	78.7	77.1	79.4	79.1	79.3	77.4	76.8	77.4	77.3	75.9	77.6	77.2	77.1	76.7	77.0	76.9	76.1	75.9
Fs	21.2	21.2	21.2	21.4	21.1	21.3	19.6	19.3	19.8	19.4	19.4	19.5	19.7	19.5	21.2	21.7	21.2	21.4	21.0	21.5	21.3	21.3	21.4	21.3	22.1	22.5	22.5

MICROPROBE DATA TABLE C5: Composition of **orthopyroxene** in the UG1 Footwall and MG3 Units - all **S** samples.
Metres given below base of UG1 chromitite.
c = core of grain m = grain margin.

Sample	S-36	S-36	S-38	S-38	S-38	S-38	S-38	S-38	S-38	S-38	S-38	S-38	S-40	S-40	S-40	S-40	S-40	S-40	S-40	S-40	S-42	S-42	S-42	S-42	S-42	S-42	S-42
Metres	181.5	181.5	190.3	190.3	190.3	190.3	190.3	190.3	190.3	190.3	190.3	190.3	199.3	199.3	199.3	199.3	199.3	199.3	199.3	199.3	208.1	208.1	208.1	208.1	208.1	208.1	208.1
Position	m	m	c	c	c	c	c	m	m	m	m	m	c	c	c	c	c	m	m	m	c	c	c	c	c	c	c
Wt. %																											
SiO_2	55.28	55.34	55.77	55.95	55.83	55.73	55.50	55.50	55.57	55.55	55.58	55.91	55.40	54.97	55.47	55.11	55.21	55.54	55.49	54.97	54.59	54.16	54.12	53.94	54.15	54.32	54.00
TiO_2	0.18	0.18	0.17	0.16	0.15	0.15	0.16	0.13	0.14	0.16	0.13	0.17	0.07	0.11	0.10	0.12	0.10	0.11	0.10	0.11	0.09	0.12	0.10	0.12	0.10	0.12	0.11
Al_2O_3	0.99	0.93	0.90	0.85	0.85	0.89	0.90	0.82	0.87	0.78	0.77	0.79	1.06	0.98	0.97	1.06	1.04	0.90	0.90	0.98	0.95	1.27	1.06	1.07	1.04	1.05	1.08
Cr_2O_3	0.23	0.23	0.32	0.28	0.31	0.32	0.35	0.25	0.26	0.25	0.24	0.28	0.37	0.31	0.35	0.32	0.39	0.30	0.28	0.31	0.31	0.36	0.37	0.38	0.37	0.35	0.38
FeO	14.20	14.57	13.25	12.71	13.04	13.46	13.25	13.30	13.50	13.28	13.19	13.34	12.78	13.05	12.97	12.99	13.18	12.61	12.81	13.05	12.98	12.79	12.90	12.92	13.21	13.04	13.03
MnO	0.28	0.28	0.29	0.26	0.29	0.30	0.24	0.26	0.29	0.29	0.26	0.28	0.25	0.26	0.32	0.28	0.29	0.30	0.26	0.26	0.29	0.27	0.28	0.30	0.32	0.26	0.29
NiO	0.09	0.09	0.06	0.11	0.10	0.07	0.07	0.04	0.04	0.06	0.06	0.08	0.07	0.14	0.09	0.12	0.10	0.03	0.13	0.14	0.05	0.04	0.04	0.07	0.08	0.07	0.08
MgO	27.72	28.13	28.66	28.40	28.64	28.28	28.12	28.62	28.56	28.72	28.59	28.80	28.50	28.71	28.60	28.51	28.84	28.92	28.69	28.71	30.58	30.19	30.30	30.50	30.29	30.65	30.51
CaO	0.77	0.64	0.71	0.63	0.77	0.77	0.87	0.54	0.61	0.62	0.56	0.48	0.90	0.85	0.62	0.89	0.69	0.49	0.61	0.85	0.82	1.14	0.96	0.85	0.89	0.84	0.79
Na_2O	0.03	0.02	0.00	0.01	0.02	0.03	0.01	0.00	0.00	0.01	0.00	0.02	0.01	0.02	0.00	0.00	0.01	0.01	0.01	0.02	0.01	0.02	0.01	0.00	0.00	0.01	0.00
Total	99.76	100.41	100.14	99.36	100.00	100.01	99.49	99.46	99.84	99.72	99.38	100.15	99.41	99.40	99.50	99.40	99.86	99.19	99.28	99.40	100.68	100.35	100.11	100.14	100.45	100.70	100.27
Cations (based on 6 oxygens):																											
Si	1.9837	1.9765	1.9842	1.9991	1.9878	1.9877	1.9886	1.9874	1.9848	1.9850	1.9906	1.9883	1.9830	1.9729	1.9845	1.9764	1.9723	1.9879	1.9875	1.9729	1.9383	1.9303	1.9336	1.9277	1.9316	1.9300	1.9280
Ti	0.0048	0.0047	0.0046	0.0043	0.0041	0.0040	0.0044	0.0034	0.0036	0.0043	0.0034	0.0046	0.0019	0.0029	0.0026	0.0033	0.0028	0.0029	0.0026	0.0029	0.0024	0.0031	0.0026	0.0032	0.0026	0.0031	0.0029
Al	0.0419	0.0392	0.0379	0.0358	0.0355	0.0375	0.0379	0.0347	0.0366	0.0330	0.0327	0.0331	0.0447	0.0416	0.0408	0.0449	0.0437	0.0378	0.0381	0.0416	0.0399	0.0531	0.0446	0.0449	0.0438	0.0442	0.0454
Cr	0.0066	0.0066	0.0090	0.0079	0.0087	0.0091	0.0099	0.0070	0.0073	0.0070	0.0069	0.0078	0.0105	0.0087	0.0100	0.0091	0.0111	0.0085	0.0081	0.0087	0.0088	0.0100	0.0103	0.0107	0.0105	0.0099	0.0107
Fe	0.4261	0.4352	0.3944	0.3797	0.3882	0.4015	0.3971	0.3983	0.4034	0.3970	0.3951	0.3968	0.3826	0.3916	0.3882	0.3896	0.3937	0.3773	0.3837	0.3916	0.3855	0.3812	0.3854	0.3862	0.3939	0.3874	0.3891
Mn	0.0085	0.0085	0.0087	0.0078	0.0087	0.0091	0.0074	0.0079	0.0087	0.0088	0.0078	0.0083	0.0077	0.0080	0.0098	0.0084	0.0089	0.0090	0.0078	0.0080	0.0087	0.0082	0.0084	0.0090	0.0096	0.0078	0.0089
Ni	0.0025	0.0026	0.0018	0.0031	0.0028	0.0019	0.0021	0.0010	0.0013	0.0017	0.0018	0.0024	0.0020	0.0041	0.0027	0.0034	0.0028	0.0009	0.0038	0.0041	0.0015	0.0013	0.0010	0.0020	0.0024	0.0020	0.0023
Mg	1.4826	1.4974	1.5198	1.5124	1.5200	1.5035	1.5018	1.5277	1.5205	1.5298	1.5265	1.5264	1.5203	1.5359	1.5251	1.5240	1.5354	1.5429	1.5317	1.5359	1.6183	1.6037	1.6135	1.6249	1.6102	1.6232	1.6236
Ca	0.0297	0.0245	0.0271	0.0241	0.0294	0.0295	0.0335	0.0208	0.0234	0.0236	0.0213	0.0184	0.0346	0.0328	0.0239	0.0341	0.0265	0.0186	0.0233	0.0328	0.0312	0.0436	0.0366	0.0327	0.0339	0.0321	0.0300
Na	0.0022	0.0014	0.0002	0.0009	0.0016	0.0021	0.0005	0.0002	0.0000	0.0008	0.0000	0.0013	0.0005	0.0012	0.0000	0.0000	0.0006	0.0005	0.0004	0.0012	0.0006	0.0012	0.0006	0.0002	0.0003	0.0006	0.0002
Total	3.9884	3.9966	3.9878	3.9752	3.9868	3.9860	3.9833	3.9885	3.9896	3.9910	3.9862	3.9873	3.9878	3.9996	3.9875	3.9933	3.9979	3.9864	3.9870	3.9996	4.0352	4.0356	4.0366	4.0415	4.0388	4.0402	4.0411
MMF	0.7768	0.7748	0.7940	0.7993	0.7965	0.7892	0.7909	0.7932	0.7903	0.7940	0.7944	0.7937	0.7989	0.7968	0.7971	0.7964	0.7959	0.8035	0.7997	0.7968	0.8076	0.8080	0.8072	0.8080	0.8034	0.8073	0.8067
Wo	1.5	1.2	1.4	1.3	1.5	1.5	1.7	1.1	1.2	1.2	1.1	0.9	1.8	1.7	1.2	1.8	1.4	1.0	1.2	1.7	1.5	2.2	1.8	1.6	1.7	1.6	1.5
En	76.5	76.5	78.3	78.9	78.4	77.7	77.7	78.5	78.1	78.4	78.6	78.6	78.5	78.4	78.7	78.2	78.5	79.6	79.0	78.4	79.5	79.1	79.3	79.5	79.0	79.5	79.5
Fs	22.0	22.2	20.3	19.8	20.0	20.8	20.6	20.5	20.7	20.4	20.3	20.4	19.7	20.0	20.0	20.0	20.1	19.5	19.8	20.0	18.9	18.8	18.9	18.9	19.3	19.0	19.0

Sample	S-42	S-42	S-42	S-42	S-42	S-42	S-43	S-43	S-43	S-43	S-43	S-43	S-43	S-43	S-43	S-43	S-45	S-45	S-45	S-45	S-45	S-45	S-45	S-45	S-45	S-45	S-49
Metres	208.1	208.1	208.1	208.1	208.1	208.1	213.2	213.2	213.2	213.2	213.2	213.2	213.2	213.2	213.2	213.2	221.9	221.9	221.9	221.9	221.9	221.9	221.9	221.9	221.9	221.9	238.9
Position	c	c	c	m	m	m	c	c	c	c	c	m	m	m	m	m	c	c	c	c	c	m	m	m	m	m	c
Wt. %																											
SiO_2	54.00	54.16	54.82	55.78	55.42	55.54	55.42	55.70	55.22	55.05	55.09	55.37	55.69	55.49	55.40	55.30	55.13	55.19	55.16	55.24	55.27	55.82	55.60	55.20	55.12	54.62	54.86
TiO_2	0.11	0.11	0.15	0.12	0.14	0.13	0.12	0.12	0.15	0.16	0.12	0.15	0.13	0.13	0.14	0.13	0.14	0.15	0.13	0.12	0.11	0.15	0.13	0.10	0.09	0.10	0.09
Al_2O_3	1.20	0.98	1.12	1.12	1.05	1.12	1.00	1.00	0.97	1.01	1.01	0.93	0.86	1.00	0.86	0.86	1.03	0.92	1.04	1.07	0.94	0.86	0.82	0.95	0.94	0.95	0.98
Cr_2O_3	0.37	0.33	0.33	0.33	0.34	0.31	0.36	0.33	0.36	0.31	0.32	0.28	0.30	0.34	0.31	0.35	0.29	0.23	0.35	0.35	0.31	0.27	0.25	0.34	0.29	0.31	0.27
FeO	12.66	12.64	12.72	12.88	13.00	12.93	12.69	13.43	13.18	13.24	13.27	12.80	13.13	13.06	13.01	13.28	12.93	13.25	13.33	13.15	13.21	13.38	13.19	13.26	13.15	13.29	13.82
MnO	0.27	0.31	0.24	0.21	0.24	0.24	0.29	0.31	0.25	0.23	0.30	0.28	0.24	0.26	0.25	0.25	0.29	0.28	0.30	0.30	0.26	0.27	0.23	0.22	0.27	0.23	0.32
NiO	0.09	0.06	0.05	0.06	0.11	0.06	0.06	0.08	0.11	0.08	0.09	0.10	0.09	0.07	0.09	0.10	0.05	0.06	0.09	0.05	0.06	0.05	0.05	0.06	0.06	0.04	0.10
MgO	30.29	30.58	30.31	29.09	28.84	29.18	28.17	28.85	28.44	28.47	28.39	28.57	28.70	28.64	28.67	28.65	28.65	28.89	28.69	28.66	28.98	28.89	28.94	28.67	28.75	28.88	28.85
CaO	0.84	0.91	0.98	0.59	0.79	0.67	1.71	0.77	0.92	0.69	0.73	0.69	0.55	0.87	0.60	0.77	0.81	0.60	0.83	0.78	0.65	0.65	0.66	0.67	0.81	0.68	0.42
Na_2O	0.01	0.00	0.00	0.00	0.01	0.00	0.00	0.00	0.01	0.00	0.00	0.00	0.02	0.01	0.01	0.01	0.00	0.01	0.01	0.01	0.00	0.02	0.00	0.01	0.01	0.01	0.00
Total	99.84	100.09	100.70	100.18	99.93	100.18	99.82	100.58	99.61	99.25	99.33	99.16	99.71	99.87	99.35	99.70	99.32	99.57	99.92	99.74	99.79	100.36	99.88	99.47	99.50	99.11	99.72
Cations (based on 6 oxygens):																											
Si	1.9325	1.9335	1.9427	1.9792	1.9757	1.9729	1.9798	1.9763	1.9778	1.9778	1.9786	1.9860	1.9878	1.9797	1.9850	1.9788	1.9771	1.9759	1.9714	1.9748	1.9747	1.9824	1.9828	1.9784	1.9756	1.9674	1.9677
Ti	0.0028	0.0030	0.0039	0.0031	0.0036	0.0034	0.0033	0.0032	0.0039	0.0043	0.0032	0.0042	0.0034	0.0034	0.0037	0.0036	0.0038	0.0040	0.0034	0.0033	0.0029	0.0041	0.0034	0.0026	0.0025	0.0028	0.0024
Al	0.0506	0.0414	0.0466	0.0467	0.0443	0.0470	0.0422	0.0416	0.0410	0.0427	0.0428	0.0392	0.0363	0.0422	0.0364	0.0364	0.0437	0.0389	0.0437	0.0452	0.0396	0.0359	0.0344	0.0401	0.0399	0.0404	0.0416
Cr	0.0104	0.0093	0.0092	0.0093	0.0095	0.0086	0.0102	0.0092	0.0101	0.0088	0.0092	0.0078	0.0085	0.0096	0.0088	0.0098	0.0081	0.0065	0.0098	0.0099	0.0088	0.0075	0.0071	0.0096	0.0083	0.0089	0.0078
Fe	0.3790	0.3775	0.3769	0.3822	0.3876	0.3842	0.3791	0.3985	0.3947	0.3979	0.3986	0.3838	0.3920	0.3895	0.3899	0.3973	0.3876	0.3966	0.3985	0.3931	0.3948	0.3973	0.3933	0.3974	0.3943	0.4002	0.4145
Mn	0.0083	0.0094	0.0072	0.0063	0.0073	0.0072	0.0088	0.0092	0.0077	0.0070	0.0092	0.0084	0.0074	0.0079	0.0076	0.0077	0.0088	0.0085	0.0091	0.0090	0.0078	0.0082	0.0070	0.0068	0.0081	0.0071	0.0097
Ni	0.0025	0.0018	0.0013	0.0017	0.0032	0.0018	0.0016	0.0023	0.0033	0.0024	0.0025	0.0027	0.0026	0.0020	0.0027	0.0030	0.0014	0.0018	0.0026	0.0015	0.0017	0.0015	0.0014	0.0016	0.0017	0.0013	0.0029
Mg	1.6155	1.6271	1.6007	1.5387	1.5323	1.5453	1.4999	1.5255	1.5183	1.5247	1.5200	1.5277	1.5270	1.5230	1.5313	1.5282	1.5315	1.5418	1.5281	1.5273	1.5430	1.5296	1.5384	1.5318	1.5357	1.5507	1.5422
Ca	0.0321	0.0350	0.0371	0.0225	0.0301	0.0254	0.0655	0.0293	0.0354	0.0265	0.0283	0.0263	0.0211	0.0332	0.0232	0.0294	0.0312	0.0230	0.0317	0.0300	0.0251	0.0247	0.0252	0.0257	0.0313	0.0261	0.0163
Na	0.0008	0.0003	0.0000	0.0000	0.0006	0.0001	0.0003	0.0000	0.0007	0.0002	0.0000	0.0001	0.0010	0.0007	0.0005	0.0005	0.0002	0.0007	0.0004	0.0007	0.0001	0.0011	0.0000	0.0007	0.0004	0.0005	0.0000
Total	4.0346	4.0383	4.0255	3.9896	3.9941	3.9959	3.9908	3.9951	3.9930	3.9923	3.9923	3.9864	3.9870	3.9914	3.9890	3.9947	3.9933	3.9977	3.9987	3.9947	3.9983	3.9923	3.9931	3.9946	3.9980	4.0054	4.0052
MMF	0.8100	0.8117	0.8094	0.8010	0.7981	0.8009	0.7982	0.7929	0.7937	0.7930	0.7922	0.7992	0.7957	0.7963	0.7971	0.7937	0.7980	0.7954	0.7931	0.7953	0.7963	0.7938	0.7964	0.7940	0.7957	0.7948	0.7882
Wo	1.6	1.7	1.8	1.2	1.5	1.3	3.4	1.5	1.8	1.4	1.5	1.4	1.1	1.7	1.2	1.5	1.6	1.2	1.6	1.5	1.3	1.3	1.3	1.3	1.6	1.3	0.8
En	79.7	79.8	79.5	79.2	78.6	79.0	77.1	78.1	77.9	78.2	78.1	78.8	78.7	78.3	78.8	78.2	78.5	78.6	78.0	78.3	78.6	78.4	78.6	78.4	78.3	78.4	78.2
Fs	18.7	18.5	18.7	19.7	19.9	19.7	19.5	20.4	20.3	20.4	20.5	19.8	20.2	20.0	20.1	20.3	19.9	20.2	20.4	20.2	20.1	20.4	20.1	20.3	20.1	20.2	21.0

MICROPROBE DATA TABLE C5: Composition of **orthopyroxene** in the UG1 Footwall and MG3 Units - all **S** samples.
Metres given below base of UG1 chromitite.
c = core of grain m = grain margin.

Sample	S-49	S-49	S-49	S-49	S-49	S-52	S-52	S-52	S-52	S-52	S-52	S-52	S-52	S-54	S-54	S-54	S-54	S-54	S-54	S-54	S-54	S-54	S-54	S-56	S-56	S-56	S-56
Metres	238.9	238.9	238.9	238.9	238.9	252.2	252.2	252.2	252.2	252.2	252.2	252.2	252.2	261.4	261.4	261.4	261.4	261.4	261.4	261.4	261.4	261.4	261.4	270.2	270.2	270.2	270.2
Position	c	c	m	m	m	c	c	c	c	c	m	m	m	c	c	c	c	c	m	m	m	m	m	c	c	c	c
Wt. %																											
SiO_2	54.72	54.83	54.89	55.04	54.48	55.68	55.65	55.70	55.54	55.78	55.05	54.47	54.92	55.27	55.03	55.44	55.19	54.90	55.53	55.39	55.39	55.33	55.20	55.51	55.32	55.32	55.33
TiO_2	0.16	0.17	0.16	0.14	0.17	0.14	0.15	0.14	0.15	0.14	0.11	0.10	0.09	0.13	0.13	0.16	0.13	0.14	0.13	0.11	0.17	0.14	0.14	0.10	0.11	0.13	0.14
Al_2O_3	1.02	1.00	0.90	0.89	1.01	0.92	0.96	0.89	0.97	0.87	0.79	0.81	0.85	0.95	0.93	1.01	0.87	0.98	0.96	0.83	0.93	0.79	0.88	1.00	1.04	1.05	0.92
Cr_2O_3	0.33	0.31	0.32	0.27	0.31	0.36	0.31	0.33	0.40	0.34	0.29	0.31	0.30	0.36	0.35	0.34	0.29	0.36	0.37	0.25	0.30	0.28	0.31	0.41	0.35	0.36	0.35
FeO	13.31	13.77	13.63	13.52	13.78	13.27	13.57	13.53	13.27	13.42	13.53	13.85	13.41	13.11	13.49	13.31	13.49	13.00	13.08	13.00	13.57	13.36	13.26	13.06	13.01	13.19	13.34
MnO	0.28	0.28	0.23	0.31	0.32	0.30	0.33	0.33	0.26	0.31	0.30	0.27	0.25	0.29	0.30	0.27	0.28	0.23	0.25	0.25	0.24	0.23	0.26	0.34	0.28	0.28	0.32
NiO	0.06	0.09	0.09	0.06	0.06	0.07	0.05	0.05	0.05	0.05	0.04	0.08	0.06	0.07	0.07	0.06	0.06	0.08	0.05	0.06	0.04	0.05	0.05	0.11	0.10	0.08	0.06
MgO	27.72	28.17	28.42	28.76	28.38	28.34	28.40	28.74	27.99	28.44	28.89	29.19	29.06	28.40	28.42	28.26	28.52	27.97	28.44	28.73	28.38	28.89	28.73	27.70	27.77	28.15	28.14
CaO	1.68	0.73	0.52	0.43	0.79	1.12	0.91	0.63	1.23	1.14	0.61	0.55	0.79	0.71	0.59	1.02	0.53	1.68	0.76	0.56	0.76	0.54	0.63	1.25	1.03	0.87	0.84
Na_2O	0.01	0.00	0.02	0.00	0.01	0.01	0.00	0.00	0.04	0.02	0.01	0.02	0.01	0.00	0.01	0.03	0.03	0.02	0.00	0.01	0.01	0.03	0.02	0.01	0.01	0.02	0.03
Total	99.29	99.35	99.18	99.42	99.31	100.23	100.32	100.35	99.90	100.51	99.62	99.64	99.73	99.28	99.31	99.89	99.39	99.36	99.56	99.19	99.80	99.65	99.48	99.50	99.03	99.44	99.46
Cations (based on 6 oxygens):																											
Si	1.9727	1.9740	1.9770	1.9760	1.9646	1.9828	1.9809	1.9805	1.9845	1.9817	1.9740	1.9584	1.9676	1.9834	1.9783	1.9807	1.9811	1.9747	1.9858	1.9868	1.9813	1.9797	1.9786	1.9901	1.9902	1.9834	1.9849
Ti	0.0043	0.0047	0.0043	0.0037	0.0047	0.0038	0.0041	0.0039	0.0039	0.0039	0.0029	0.0026	0.0024	0.0034	0.0036	0.0042	0.0036	0.0037	0.0035	0.0031	0.0045	0.0038	0.0037	0.0027	0.0031	0.0034	0.0038
Al	0.0435	0.0425	0.0381	0.0376	0.0431	0.0388	0.0401	0.0375	0.0407	0.0365	0.0334	0.0344	0.0361	0.0402	0.0394	0.0426	0.0370	0.0416	0.0405	0.0350	0.0391	0.0334	0.0370	0.0424	0.0441	0.0442	0.0389
Cr	0.0095	0.0089	0.0091	0.0077	0.0088	0.0101	0.0085	0.0094	0.0114	0.0096	0.0083	0.0089	0.0084	0.0101	0.0100	0.0097	0.0083	0.0102	0.0103	0.0070	0.0085	0.0078	0.0088	0.0116	0.0101	0.0101	0.0099
Fe	0.4014	0.4145	0.4106	0.4059	0.4156	0.3952	0.4039	0.4023	0.3965	0.3987	0.4056	0.4165	0.4017	0.3934	0.4055	0.3977	0.4048	0.3911	0.3912	0.3901	0.4059	0.3997	0.3976	0.3914	0.3914	0.3956	0.4001
Mn	0.0085	0.0084	0.0070	0.0095	0.0098	0.0089	0.0099	0.0099	0.0079	0.0092	0.0090	0.0081	0.0075	0.0087	0.0091	0.0081	0.0085	0.0071	0.0076	0.0075	0.0074	0.0071	0.0080	0.0103	0.0086	0.0086	0.0096
Ni	0.0018	0.0025	0.0025	0.0017	0.0017	0.0021	0.0014	0.0015	0.0014	0.0014	0.0013	0.0022	0.0018	0.0020	0.0019	0.0016	0.0016	0.0024	0.0016	0.0018	0.0011	0.0015	0.0014	0.0032	0.0029	0.0023	0.0016
Mg	1.4896	1.5118	1.5256	1.5390	1.5256	1.5039	1.5069	1.5234	1.4909	1.5062	1.5439	1.5644	1.5516	1.5194	1.5228	1.5046	1.5262	1.4996	1.5157	1.5362	1.5131	1.5409	1.5347	1.4802	1.4894	1.5044	1.5046
Ca	0.0648	0.0281	0.0202	0.0165	0.0305	0.0429	0.0346	0.0238	0.0471	0.0434	0.0236	0.0212	0.0303	0.0274	0.0226	0.0389	0.0204	0.0649	0.0292	0.0214	0.0291	0.0208	0.0243	0.0479	0.0398	0.0334	0.0324
Na	0.0010	0.0002	0.0011	0.0002	0.0008	0.0010	0.0000	0.0001	0.0024	0.0014	0.0008	0.0011	0.0007	0.0003	0.0004	0.0018	0.0019	0.0013	0.0000	0.0006	0.0010	0.0019	0.0016	0.0010	0.0005	0.0012	0.0020
Total	3.9970	3.9957	3.9956	3.9977	4.0052	3.9895	3.9906	3.9923	3.9868	3.9921	4.0027	4.0179	4.0081	3.9882	3.9936	3.9898	3.9935	3.9964	3.9853	3.9894	3.9909	3.9968	3.9956	3.9807	3.9799	3.9866	3.9879
MMF	0.7877	0.7848	0.7879	0.7913	0.7859	0.7919	0.7886	0.7911	0.7899	0.7907	0.7919	0.7897	0.7943	0.7943	0.7897	0.7910	0.7903	0.7931	0.7949	0.7975	0.7885	0.7940	0.7943	0.7909	0.7919	0.7918	0.7899
Wo	3.3	1.4	1.0	0.8	1.5	2.2	1.8	1.2	2.4	2.2	1.2	1.1	1.5	1.4	1.2	2.0	1.0	3.3	1.5	1.1	1.5	1.1	1.2	2.5	2.1	1.7	1.7
En	76.2	77.4	78.0	78.5	77.4	77.4	77.5	78.1	77.1	77.3	78.2	78.1	78.2	78.3	78.1	77.5	78.2	76.7	78.3	78.9	77.7	78.6	78.4	77.1	77.5	77.8	77.7
Fs	20.5	21.2	21.0	20.7	21.1	20.3	20.8	20.6	20.5	20.5	20.6	20.8	20.3	20.3	20.8	20.5	20.7	20.0	20.2	20.0	20.8	20.4	20.3	20.4	20.4	20.5	20.7

Sample	S-56	S-56	S-56	S-56	S-58	S-58	S-58	S-58	S-58	S-58	S-58	S-58	S-58	S-58	S-59	S-59	S-59	S-59	S-59	S-59	S-59	S-59	S-66	S-66	S-66	S-66	S-66
Metres	270.2	270.2	270.2	270.2	279.7	279.7	279.7	279.7	279.7	279.7	279.7	279.7	279.7	279.7	286.4	286.4	286.4	286.4	286.4	286.4	286.4	286.4	307.9	307.9	307.9	307.9	307.9
Position	c	m	m	m	c	c	c	c	c	m	m	m	m	m	c	c	c	c	c	m	m	m	c	c	c	c	c
Wt. %																											
SiO_2	55.27	55.30	55.58	54.69	55.32	55.32	55.41	55.20	55.30	55.55	55.40	55.09	55.70	55.09	56.02	55.93	55.84	55.77	55.83	55.52	55.46	55.63	55.21	54.80	55.13	55.18	55.21
TiO_2	0.12	0.11	0.12	0.10	0.12	0.11	0.13	0.11	0.10	0.13	0.11	0.08	0.11	0.08	0.14	0.14	0.16	0.16	0.17	0.14	0.12	0.11	0.09	0.11	0.11	0.11	0.09
Al_2O_3	1.00	0.95	0.90	1.38	0.96	0.93	0.99	0.98	0.96	0.89	0.83	0.87	0.91	0.87	0.92	0.99	0.98	0.93	0.99	0.94	0.93	0.86	1.14	1.23	1.31	1.25	1.08
Cr_2O_3	0.35	0.31	0.34	0.31	0.34	0.33	0.32	0.32	0.28	0.32	0.30	0.30	0.31	0.30	0.33	0.31	0.31	0.34	0.32	0.30	0.29	0.25	0.43	0.49	0.51	0.49	0.47
FeO	13.37	13.37	13.73	13.38	13.38	13.29	12.52	12.53	12.75	12.93	13.24	13.29	12.44	13.29	13.11	12.89	12.89	12.18	12.92	12.99	12.87	13.07	11.60	11.97	11.97	12.00	12.24
MnO	0.29	0.32	0.31	0.32	0.28	0.26	0.25	0.25	0.27	0.25	0.26	0.25	0.24	0.25	0.26	0.27	0.23	0.24	0.25	0.27	0.27	0.27	0.23	0.23	0.23	0.26	0.22
NiO	0.09	0.09	0.09	0.07	0.08	0.08	0.12	0.12	0.08	0.06	0.09	0.09	0.12	0.09	0.06	0.03	0.06	0.02	0.06	0.06	0.06	0.08	0.07	0.11	0.08	0.11	0.09
MgO	28.44	28.74	28.59	28.59	29.29	29.06	28.77	28.60	28.85	28.84	29.07	29.28	28.87	29.28	28.86	28.82	28.95	27.48	28.57	28.74	29.36	29.37	29.93	29.51	29.83	29.68	30.02
CaO	0.51	0.41	0.50	0.56	0.60	0.81	1.10	1.10	1.08	0.64	0.68	0.53	0.82	0.53	0.87	1.07	1.07	3.49	1.23	0.89	0.65	0.55	0.65	0.93	1.14	0.79	0.54
Na_2O	0.03	0.02	0.02	0.04	0.01	0.02	0.01	0.02	0.01	0.00	0.02	0.01	0.01	0.01	0.00	0.01	0.02	0.06	0.01	0.01	0.02	0.01	0.00	0.01	0.01	0.01	0.00
Total	99.47	99.63	100.19	99.45	100.39	100.22	99.63	99.22	99.67	99.63	100.00	99.80	99.53	99.80	100.56	100.46	100.52	100.65	100.34	99.86	100.03	100.21	99.36	99.38	100.32	99.88	99.95
Cations (based on 6 oxygens):																											
Si	1.9815	1.9792	1.9813	1.9635	1.9673	1.9704	1.9789	1.9799	1.9761	1.9839	1.9759	1.9695	1.9873	1.9695	1.9837	1.9818	1.9780	1.9803	1.9819	1.9805	1.9737	1.9768	1.9677	1.9595	1.9536	1.9619	1.9620
Ti	0.0032	0.0031	0.0031	0.0026	0.0033	0.0030	0.0034	0.0030	0.0026	0.0034	0.0030	0.0021	0.0030	0.0021	0.0037	0.0037	0.0043	0.0042	0.0044	0.0039	0.0031	0.0030	0.0025	0.0030	0.0030	0.0031	0.0024
Al	0.0422	0.0400	0.0376	0.0585	0.0403	0.0391	0.0418	0.0413	0.0405	0.0376	0.0347	0.0367	0.0384	0.0367	0.0385	0.0412	0.0410	0.0388	0.0414	0.0394	0.0391	0.0369	0.0478	0.0520	0.0549	0.0523	0.0454
Cr	0.0100	0.0089	0.0095	0.0089	0.0096	0.0094	0.0091	0.0090	0.0080	0.0092	0.0083	0.0086	0.0087	0.0086	0.0091	0.0086	0.0088	0.0095	0.0090	0.0085	0.0083	0.0071	0.0120	0.0139	0.0142	0.0136	0.0131
Fe	0.4010	0.4002	0.4094	0.4017	0.3978	0.3959	0.3740	0.3757	0.3811	0.3861	0.3949	0.3974	0.3713	0.3974	0.3882	0.3821	0.3819	0.3617	0.3834	0.3873	0.3832	0.3885	0.3459	0.3580	0.3546	0.3568	0.3637
Mn	0.0088	0.0096	0.0092	0.0098	0.0085	0.0079	0.0076	0.0076	0.0082	0.0076	0.0079	0.0077	0.0074	0.0077	0.0078	0.0082	0.0069	0.0071	0.0074	0.0082	0.0083	0.0082	0.0070	0.0068	0.0068	0.0078	0.0067
Ni	0.0025	0.0027	0.0026	0.0021	0.0022	0.0022	0.0035	0.0034	0.0022	0.0018	0.0027	0.0027	0.0035	0.0027	0.0017	0.0008	0.0017	0.0005	0.0018	0.0016	0.0016	0.0024	0.0020	0.0031	0.0023	0.0032	0.0024
Mg	1.5196	1.5332	1.5192	1.5301	1.5522	1.5426	1.5316	1.5290	1.5368	1.5351	1.5453	1.5604	1.5351	1.5604	1.5231	1.5221	1.5286	1.4545	1.5120	1.5281	1.5571	1.5553	1.5899	1.5726	1.5757	1.5728	1.5902
Ca	0.0196	0.0159	0.0192	0.0215	0.0228	0.0311	0.0420	0.0424	0.0413	0.0246	0.0260	0.0202	0.0312	0.0202	0.0329	0.0406	0.0406	0.1329	0.0468	0.0339	0.0246	0.0210	0.0250	0.0354	0.0433	0.0302	0.0205
Na	0.0020	0.0013	0.0016	0.0027	0.0009	0.0013	0.0009	0.0012	0.0007	0.0000	0.0013	0.0005	0.0007	0.0005	0.0000	0.0009	0.0017	0.0038	0.0009	0.0005	0.0012	0.0006	0.0000	0.0005	0.0008	0.0005	0.0000
Total	3.9902	3.9939	3.9928	4.0014	4.0049	4.0030	3.9928	3.9926	3.9973	3.9893	4.0002	4.0059	3.9865	4.0059	3.9888	3.9900	3.9936	3.9933	3.9890	3.9920	4.0001	3.9989	3.9998	4.0049	4.0092	4.0024	4.0064
MMF	0.7912	0.7930	0.7877	0.7921	0.7960	0.7958	0.8038	0.8027	0.8013	0.7990	0.7965	0.7970	0.8052	0.7970	0.7969	0.7993	0.8001	0.8008	0.7977	0.7978	0.8025	0.8001	0.8213	0.8146	0.8163	0.8151	0.8139
Wo	1.0	0.8	1.0	1.1	1.2	1.6	2.2	2.2	2.1	1.3	1.3	1.0	1.6	1.0	1.7	2.1	2.1	6.8	2.4	1.7	1.3	1.1	1.3	1.8	2.2	1.5	1.0
En	78.3	78.7	78.0	78.3	78.7	78.3	78.6	78.5	78.4	78.9	78.6	78.9	79.2	78.9	78.3	78.3	78.3	74.6	77.8	78.4	79.2	79.2	81.1	80.0	79.8	80.3	80.5
Fs	20.7	20.5	21.0	20.6	20.2	20.1	19.2	19.3	19.5	19.8	20.1	20.1	19.2	20.1	20.0	19.6	19.6	18.6	19.7	19.9	19.5	19.8	17.6	18.2	18.0	18.2	18.4

MICROPROBE DATA TABLE C5: Composition of **orthopyroxene** in the UG1 Footwall and MG3 Units - all **S** samples.
Metres given below base of UG1 chromitite.
c = core of grain m = grain margin.

Sample	S-66	S-66	S-66	S-66	S-66	S-68	S-68	S-68	S-68	S-68	S-68	S-68	S-68	S-71	S-71	S-71	S-71	S-71	S-71	S-71	S-71	S-81	S-81	S-81	S-81	S-81	S-81
Metres	307.9	307.9	307.9	307.9	307.9	310.2	310.2	310.2	310.2	310.2	310.2	310.2	310.2	325	325	325	325	325	325	325	325	344.9	344.9	344.9	344.9	344.9	344.9
Position	m	m	m	m	m	c	c	c	c	c	m	m	m	c	c	c	c	c	m	m	m	c	c	c	m	m	m
Wt. %																											
SiO_2	53.97	55.11	55.03	54.96	55.11	54.90	54.71	55.75	55.56	55.75	55.58	55.14	55.12	55.10	54.94	54.84	54.84	55.00	55.18	55.41	55.42	55.34	55.40	55.51	55.01	55.38	55.48
TiO_2	0.18	0.12	0.12	0.13	0.12	0.13	0.15	0.10	0.13	0.10	0.13	0.13	0.14	0.16	0.15	0.14	0.15	0.15	0.13	0.12	0.13	0.18	0.16	0.15	0.16	0.18	0.19
Al_2O_3	1.76	1.12	1.13	1.11	1.12	1.24	1.08	1.15	1.11	1.15	1.04	1.18	1.22	1.11	1.13	1.17	1.15	1.17	0.93	0.88	1.00	1.00	1.14	1.08	1.04	0.96	0.94
Cr_2O_3	0.62	0.43	0.44	0.42	0.43	0.53	0.50	0.48	0.49	0.48	0.47	0.51	0.46	0.51	0.50	0.51	0.53	0.54	0.41	0.41	0.43	0.31	0.38	0.39	0.33	0.35	0.33
FeO	11.75	11.89	11.91	11.91	11.89	11.94	12.06	11.90	11.72	11.90	12.03	11.93	11.92	11.81	11.87	12.03	12.27	12.04	11.92	11.97	12.07	12.76	12.87	12.99	12.80	12.99	12.73
MnO	0.18	0.23	0.20	0.19	0.23	0.30	0.32	0.23	0.26	0.23	0.30	0.33	0.29	0.23	0.22	0.25	0.25	0.26	0.25	0.25	0.23	0.28	0.30	0.30	0.24	0.29	0.24
NiO	0.10	0.09	0.11	0.09	0.09	0.13	0.11	0.10	0.15	0.10	0.09	0.12	0.11	0.05	0.02	0.04	0.03	0.05	0.07	0.08	0.04	0.06	0.08	0.09	0.10	0.09	0.09
MgO	28.82	30.30	30.10	29.91	30.30	28.99	29.50	29.19	29.00	29.19	29.13	29.56	29.32	30.10	29.57	29.36	29.35	29.65	30.53	30.49	30.15	29.35	29.24	28.97	28.93	29.15	29.01
CaO	1.78	0.45	0.54	0.71	0.45	0.94	0.66	0.86	0.97	0.86	0.64	0.66	0.62	0.80	0.89	0.96	0.77	0.71	0.46	0.50	0.58	0.52	0.82	0.97	0.58	0.63	0.70
Na_2O	0.02	0.00	0.00	0.01	0.00	0.00	0.00	0.01	0.00	0.01	0.00	0.00	0.00	0.01	0.01	0.00	0.01	0.01	0.00	0.01	0.01	0.01	0.03	0.02	0.02	0.02	0.03
Total	99.19	99.74	99.58	99.44	99.74	99.10	99.09	99.75	99.40	99.75	99.41	99.57	99.21	99.86	99.30	99.30	99.37	99.58	99.89	100.13	100.07	99.80	100.42	100.46	99.21	100.03	99.72
Cations (based on 6 oxygens):																											
Si	1.9390	1.9597	1.9604	1.9614	1.9597	1.9680	1.9626	1.9804	1.9810	1.9804	1.9822	1.9659	1.9706	1.9581	1.9636	1.9626	1.9626	1.9617	1.9598	1.9633	1.9651	1.9723	1.9659	1.9703	1.9735	1.9726	1.9789
Ti	0.0049	0.0032	0.0033	0.0035	0.0032	0.0035	0.0040	0.0028	0.0034	0.0028	0.0036	0.0034	0.0039	0.0043	0.0042	0.0038	0.0041	0.0041	0.0036	0.0033	0.0034	0.0047	0.0044	0.0040	0.0042	0.0049	0.0050
Al	0.0746	0.0468	0.0474	0.0466	0.0468	0.0523	0.0455	0.0481	0.0468	0.0481	0.0436	0.0496	0.0514	0.0464	0.0478	0.0494	0.0487	0.0490	0.0389	0.0368	0.0418	0.0419	0.0476	0.0452	0.0442	0.0401	0.0395
Cr	0.0176	0.0121	0.0124	0.0119	0.0121	0.0151	0.0142	0.0133	0.0139	0.0133	0.0132	0.0145	0.0130	0.0142	0.0142	0.0144	0.0151	0.0152	0.0116	0.0114	0.0121	0.0088	0.0107	0.0108	0.0095	0.0098	0.0092
Fe	0.3530	0.3537	0.3548	0.3553	0.3537	0.3579	0.3618	0.3535	0.3495	0.3535	0.3587	0.3559	0.3565	0.3509	0.3547	0.3599	0.3673	0.3592	0.3541	0.3546	0.3578	0.3802	0.3820	0.3855	0.3840	0.3870	0.3797
Mn	0.0055	0.0070	0.0062	0.0058	0.0070	0.0091	0.0096	0.0068	0.0079	0.0068	0.0090	0.0101	0.0088	0.0069	0.0066	0.0075	0.0076	0.0079	0.0076	0.0076	0.0069	0.0083	0.0091	0.0089	0.0073	0.0088	0.0071
Ni	0.0029	0.0025	0.0030	0.0025	0.0025	0.0038	0.0033	0.0029	0.0044	0.0029	0.0027	0.0036	0.0031	0.0013	0.0006	0.0012	0.0010	0.0014	0.0020	0.0022	0.0013	0.0018	0.0022	0.0026	0.0027	0.0025	0.0026
Mg	1.5433	1.6056	1.5984	1.5912	1.6056	1.5489	1.5771	1.5453	1.5411	1.5453	1.5486	1.5709	1.5623	1.5946	1.5752	1.5660	1.5653	1.5761	1.6161	1.6105	1.5936	1.5594	1.5465	1.5327	1.5468	1.5474	1.5420
Ca	0.0684	0.0173	0.0205	0.0271	0.0173	0.0362	0.0254	0.0327	0.0372	0.0327	0.0243	0.0250	0.0237	0.0303	0.0340	0.0368	0.0295	0.0270	0.0173	0.0191	0.0222	0.0199	0.0313	0.0368	0.0224	0.0239	0.0267
Na	0.0016	0.0000	0.0000	0.0008	0.0000	0.0000	0.0000	0.0006	0.0000	0.0006	0.0000	0.0000	0.0000	0.0005	0.0009	0.0000	0.0006	0.0010	0.0001	0.0008	0.0007	0.0004	0.0020	0.0016	0.0016	0.0011	0.0019
Total	4.0108	4.0077	4.0064	4.0062	4.0077	3.9948	4.0036	3.9864	3.9852	3.9864	3.9859	3.9987	3.9933	4.0075	4.0017	4.0016	4.0017	4.0026	4.0113	4.0097	4.0049	3.9978	4.0016	3.9985	3.9963	3.9981	3.9926
MMF	0.8138	0.8195	0.8183	0.8174	0.8195	0.8123	0.8134	0.8138	0.8151	0.8138	0.8119	0.8153	0.8142	0.8196	0.8162	0.8131	0.8100	0.8144	0.8203	0.8196	0.8166	0.8040	0.8019	0.7990	0.8011	0.7999	0.8024
Wo	3.5	0.9	1.0	1.4	0.9	1.9	1.3	1.7	1.9	1.7	1.3	1.3	1.2	1.5	1.7	1.9	1.5	1.4	0.9	1.0	1.1	1.0	1.6	1.9	1.1	1.2	1.4
En	78.5	81.2	81.0	80.6	81.2	79.7	80.3	80.0	79.9	80.0	80.2	80.5	80.4	80.7	80.2	79.8	79.8	80.3	81.3	81.2	80.7	79.6	78.9	78.4	79.2	79.0	79.1
Fs	18.0	17.9	18.0	18.0	17.9	18.4	18.4	18.3	18.1	18.3	18.6	18.2	18.4	17.8	18.1	18.3	18.7	18.3	17.8	17.9	18.1	19.4	19.5	19.7	19.7	19.8	19.5

MICROPROBE DATA TABLE C6: Composition of **clinopyroxene** in the UG1 Footwall Unit - S samples.
Metres given below base of UG1 chromitite.

Sample	S-35	S-35	S-35	S-42	S-42	S-42	S-52	S-52	S-52	S-59	S-59	S-59
Metres	175.6	175.6	175.6	208.1	208.1	208.1	252.2	252.2	252.2	286.4	286.4	286.4
Wt. %												
SiO_2	54.02	53.76	53.82	53.95	53.63	53.77	53.09	53.15	53.16	53.53	53.58	53.66
TiO_2	0.22	0.22	0.23	0.23	0.23	0.22	0.27	0.26	0.26	0.25	0.24	0.22
Al_2O_3	1.22	1.27	1.27	1.50	1.39	1.34	1.37	1.36	1.24	1.55	1.44	1.42
Cr_2O_3	0.54	0.51	0.50	0.74	0.63	0.66	0.70	0.71	0.63	0.66	0.62	0.63
FeO	4.39	4.58	4.66	4.45	4.17	4.24	4.51	4.61	5.35	4.56	4.29	4.50
MnO	0.12	0.11	0.11	0.11	0.13	0.12	0.14	0.12	0.13	0.08	0.10	0.09
NiO	0.07	0.06	0.03	0.06	0.04	0.08	0.06	0.07	0.08	0.03	0.05	0.07
MgO	16.96	17.18	16.97	16.83	16.77	16.70	16.73	16.86	17.10	16.90	17.00	16.90
CaO	21.90	22.08	22.03	22.24	22.42	22.58	22.49	22.50	21.49	22.54	22.66	22.51
Na_2O	0.29	0.30	0.29	0.30	0.31	0.28	0.33	0.35	0.27	0.30	0.30	0.31
Total	99.72	100.06	99.93	100.41	99.72	99.99	99.70	99.99	99.70	100.40	100.29	100.31
Cations (based on 6 oxygens):												
Si	1.9763	1.9642	1.9687	1.9636	1.9649	1.9663	1.9525	1.9500	1.9561	1.9527	1.9552	1.9583
Ti	0.0060	0.0061	0.0064	0.0063	0.0064	0.0060	0.0075	0.0071	0.0072	0.0068	0.0065	0.0061
Al	0.0525	0.0545	0.0549	0.0644	0.0599	0.0576	0.0593	0.0590	0.0536	0.0667	0.0619	0.0612
Cr	0.0155	0.0146	0.0144	0.0213	0.0184	0.0190	0.0204	0.0206	0.0184	0.0190	0.0178	0.0181
Fe	0.1343	0.1401	0.1426	0.1355	0.1277	0.1297	0.1388	0.1414	0.1645	0.1392	0.1310	0.1372
Mn	0.0038	0.0034	0.0035	0.0034	0.0041	0.0038	0.0042	0.0037	0.0040	0.0025	0.0032	0.0027
Ni	0.0020	0.0017	0.0009	0.0018	0.0011	0.0024	0.0018	0.0020	0.0022	0.0009	0.0016	0.0020
Mg	0.9247	0.9357	0.9251	0.9128	0.9160	0.9102	0.9174	0.9221	0.9376	0.9187	0.9248	0.9192
Ca	0.8584	0.8645	0.8634	0.8673	0.8802	0.8846	0.8863	0.8846	0.8473	0.8807	0.8858	0.8801
Na	0.0202	0.0209	0.0208	0.0215	0.0222	0.0197	0.0238	0.0250	0.0194	0.0211	0.0213	0.0217
Total	3.9938	4.0056	4.0006	3.9980	4.0007	3.9993	4.0121	4.0155	4.0104	4.0082	4.0091	4.0068
MMF	0.8731	0.8698	0.8665	0.8708	0.8777	0.8753	0.8686	0.8671	0.8507	0.8684	0.8760	0.8701
Wo	44.8	44.6	44.7	45.3	45.8	46.0	45.6	45.4	43.5	45.4	45.6	45.4
En	48.2	48.2	47.9	47.7	47.6	47.3	47.2	47.3	48.1	47.4	47.6	47.5
Fs	7.0	7.2	7.4	7.1	6.6	6.7	7.1	7.3	8.4	7.2	6.7	7.1

MICROPROBE DATA TABLE C7: Composition of **orthopyroxene** in the Bastard Unit - profile **LEF**.
Metres given above base of Unit.

Sample	H979.91	H979.91	H979.91	H979.91	H979.91	H984.48	H984.48	H984.48	H984.48	H984.48	H984.48	H984.48	H984.48	H992.8	H992.8	H992.8	H995.5	H995.5	H995.5	H995.5	H995.5	H997.11	H997.11	H997.11	H997.11	H997.11	H997.26
Metres	18.29	18.29	18.29	18.29	18.29	13.72	13.72	13.72	13.72	13.72	13.72	13.72	13.72	5.40	5.40	5.40	2.70	2.70	2.70	2.70	2.70	1.09	1.09	1.09	1.09	1.09	0.94
Position											m	m	m														
Wt. %											(m = margin)																
SiO_2	55.26	55.65	56.04	55.32	55.02	55.71	55.78	56.27	56.52	55.48	55.40	55.80	55.40	56.20	55.79	56.06	54.89	55.09	54.83	54.96	54.89	56.01	55.54	55.94	55.44	54.97	54.96
TiO_2	0.23	0.25	0.21	0.33	0.23	0.30	0.30	0.20	0.20	0.21	0.36	0.25	0.36	0.21	0.24	0.21	0.31	0.30	0.29	0.27	0.31	0.25	0.25	0.22	0.29	0.30	0.24
Al_2O_3	1.01	1.04	1.06	1.03	1.10	0.97	0.91	1.12	1.07	1.13	1.07	1.12	1.07	0.98	0.92	1.04	0.94	0.91	0.86	0.83	0.94	0.95	0.94	0.86	0.87	0.85	0.89
Cr_2O_3	0.33	0.35	0.33	0.34	0.38	0.30	0.26	0.41	0.40	0.40	0.35	0.38	0.35	0.37	0.35	0.39	0.33	0.30	0.26	0.24	0.33	0.22	0.22	0.24	0.25	0.21	0.29
FeO	13.18	13.15	13.02	13.24	12.91	13.78	13.90	12.85	13.46	13.32	13.58	13.43	13.58	13.07	12.92	12.41	15.48	15.82	15.97	16.98	15.48	15.62	15.49	15.50	15.66	15.55	16.47
MnO	0.27	0.30	0.28	0.27	0.27	0.27	0.27	0.25	0.28	0.26	0.28	0.28	0.28	0.24	0.23	0.24	0.30	0.31	0.39	0.33	0.30	0.35	0.35	0.30	0.33	0.33	0.30
NiO	0.05	0.00	0.09	0.07	0.08	0.07	0.10	0.04	0.05	0.07	0.10	0.09	0.10	0.08	0.11	0.08	0.09	0.08	0.07	0.02	0.09	0.10	0.10	0.09	0.06	0.05	0.14
MgO	28.98	29.12	29.02	28.84	28.99	27.93	28.16	28.10	28.69	28.69	28.57	28.51	28.57	28.80	28.86	28.77	26.57	26.64	26.42	26.21	26.57	25.82	25.60	26.98	26.99	27.21	26.36
CaO	1.28	1.14	1.31	1.12	1.49	1.12	0.96	1.50	0.83	1.02	0.91	0.93	0.91	1.40	1.07	1.63	0.99	1.00	1.07	0.91	0.99	2.01	1.99	1.22	1.21	1.00	1.02
Na_2O	0.02	0.02	0.00	0.00	0.01	0.03	0.01	0.02	0.01	0.03	0.03	0.02	0.03	0.02	0.00	0.02	0.03	0.02	0.05	0.04	0.03	0.03	0.03	0.00	0.02	0.02	0.00
Total	100.61	101.02	101.37	100.57	100.47	100.47	100.65	100.74	101.51	100.60	100.65	100.80	100.65	101.37	100.50	100.86	99.92	100.47	100.20	100.79	99.92	101.36	100.50	101.37	101.10	100.50	100.68
Cations (based on 6 oxygens):																											
Si	1.9630	1.9660	1.9717	1.9650	1.9572	1.9827	1.9820	1.9885	1.9844	1.9692	1.9680	1.9759	1.9680	1.9775	1.9779	1.9782	1.9811	1.9800	1.9790	1.9788	1.9811	1.9951	1.9951	1.9879	1.9789	1.9735	1.9777
Ti	0.0060	0.0067	0.0057	0.0088	0.0061	0.0081	0.0079	0.0052	0.0052	0.0055	0.0095	0.0067	0.0095	0.0056	0.0065	0.0056	0.0083	0.0080	0.0077	0.0073	0.0083	0.0067	0.0068	0.0060	0.0077	0.0082	0.0065
Al	0.0421	0.0435	0.0439	0.0433	0.0460	0.0405	0.0379	0.0466	0.0444	0.0471	0.0448	0.0467	0.0448	0.0405	0.0383	0.0433	0.0399	0.0387	0.0365	0.0353	0.0399	0.0398	0.0398	0.0361	0.0365	0.0361	0.0378
Cr	0.0092	0.0097	0.0092	0.0094	0.0107	0.0085	0.0074	0.0114	0.0111	0.0112	0.0097	0.0106	0.0097	0.0102	0.0099	0.0109	0.0093	0.0084	0.0075	0.0069	0.0093	0.0061	0.0062	0.0067	0.0070	0.0061	0.0084
Fe	0.3915	0.3886	0.3832	0.3933	0.3839	0.4101	0.4129	0.3796	0.3950	0.3953	0.4036	0.3976	0.4036	0.3845	0.3831	0.3662	0.4673	0.4755	0.4820	0.5112	0.4673	0.4653	0.4654	0.4607	0.4672	0.4668	0.4957
Mn	0.0081	0.0091	0.0083	0.0082	0.0082	0.0081	0.0082	0.0073	0.0083	0.0079	0.0083	0.0084	0.0083	0.0071	0.0070	0.0072	0.0091	0.0095	0.0119	0.0100	0.0091	0.0107	0.0106	0.0091	0.0098	0.0101	0.0090
Ni	0.0015	0.0001	0.0027	0.0020	0.0022	0.0019	0.0027	0.0010	0.0015	0.0020	0.0028	0.0026	0.0028	0.0022	0.0031	0.0023	0.0025	0.0023	0.0020	0.0007	0.0025	0.0029	0.0029	0.0025	0.0017	0.0014	0.0039
Mg	1.5343	1.5333	1.5222	1.5271	1.5369	1.4813	1.4913	1.4802	1.5014	1.5182	1.5128	1.5045	1.5128	1.5106	1.5248	1.5130	1.4290	1.4271	1.4213	1.4063	1.4290	1.3710	1.3707	1.4292	1.4361	1.4558	1.4140
Ca	0.0488	0.0432	0.0492	0.0426	0.0567	0.0427	0.0365	0.0566	0.0312	0.0387	0.0347	0.0354	0.0347	0.0528	0.0408	0.0616	0.0383	0.0384	0.0415	0.0351	0.0383	0.0767	0.0766	0.0464	0.0463	0.0385	0.0394
Na	0.0017	0.0011	0.0002	0.0003	0.0007	0.0020	0.0007	0.0015	0.0005	0.0022	0.0021	0.0012	0.0021	0.0012	0.0000	0.0011	0.0022	0.0011	0.0036	0.0026	0.0022	0.0018	0.0021	0.0002	0.0012	0.0013	0.0002
Total	4.0062	4.0013	3.9962	4.0000	4.0087	3.9857	3.9877	3.9780	3.9830	3.9973	3.9963	3.9894	3.9963	3.9922	3.9915	3.9896	3.9870	3.9890	3.9931	3.9942	3.9870	3.9761	3.9762	3.9848	3.9923	3.9978	3.9928
MMF	0.7967	0.7978	0.7989	0.7952	0.8001	0.7832	0.7832	0.7959	0.7917	0.7934	0.7894	0.7910	0.7894	0.7971	0.7992	0.8051	0.7536	0.7501	0.7467	0.7334	0.7536	0.7466	0.7466	0.7562	0.7545	0.7572	0.7404
Wo	2.5	2.2	2.5	2.2	2.9	2.2	1.9	3.0	1.6	2.0	1.8	1.8	1.8	2.7	2.1	3.2	2.0	2.0	2.1	1.8	2.0	4.0	4.0	2.4	2.4	2.0	2.0
En	77.7	78.0	77.9	77.8	77.7	76.6	76.8	77.2	77.9	77.8	77.5	77.7	77.5	77.5	78.2	78.0	73.9	73.5	73.1	72.0	73.9	71.7	71.7	73.8	73.7	74.2	72.5
Fs	19.8	19.8	19.6	20.0	19.4	21.2	21.3	19.8	20.5	20.2	20.7	20.5	20.7	19.7	19.7	18.9	24.2	24.5	24.8	26.2	24.2	24.3	24.3	23.8	24.0	23.8	25.4

Sample	H997.26	H997.26	H997.26	H997.26	H997.95	H997.95	H997.95	H998.1	H998.1	H998.1	H998.1	H998.1	H998.1	H998.1	H998.1	H998.1	H998.1
Metres	0.94	0.94	0.94	0.94	0.25	0.25	0.25	0.01	0.01	0.01	0.01	0.01	0.10	0.10	0.10	0.10	0.10
Position								c	c	c	c	c	t	t	t	t	t
Wt. %								(At basal contact = c)					(10cm above contact = t)				
SiO_2	55.05	54.92	54.34	54.34	55.21	54.92	54.76	55.86	55.20	55.36	55.68	55.52	55.82	56.04	55.99	55.87	56.02
TiO_2	0.25	0.21	0.30	0.30	0.30	0.28	0.32	0.09	0.09	0.11	0.12	0.15	0.17	0.14	0.23	0.11	0.11
Al_2O_3	0.91	0.86	0.93	0.93	0.78	0.70	0.81	1.46	1.65	1.80	1.19	1.44	1.47	1.26	0.99	1.64	1.54
Cr_2O_3	0.27	0.32	0.31	0.31	0.08	0.09	0.07	0.51	0.54	0.52	0.46	0.55	0.38	0.50	0.41	0.49	0.46
FeO	16.51	16.58	16.64	16.64	17.49	17.77	17.81	12.55	12.52	12.26	12.44	12.09	12.05	12.24	13.46	12.17	12.29
MnO	0.33	0.33	0.35	0.35	0.36	0.36	0.39	0.23	0.29	0.28	0.26	0.26	0.21	0.25	0.23	0.22	0.23
NiO	0.09	0.12	0.10	0.10	0.07	0.11	0.09	0.07	0.03	0.03	0.08	0.07	0.09	0.15	0.12	0.17	0.09
MgO	26.40	26.61	26.34	26.34	25.36	25.62	25.22	28.26	28.41	28.44	29.23	29.00	28.60	28.33	28.07	28.18	28.16
CaO	1.14	1.11	1.18	1.18	1.10	0.95	1.10	1.92	1.83	2.16	1.03	1.68	1.58	2.14	1.13	1.97	2.15
Na_2O	0.02	0.01	0.05	0.05	0.02	0.01	0.03	0.03	0.03	0.03	0.01	0.03	0.01	0.03	0.01	0.03	0.03
Total	100.98	101.06	100.54	100.54	100.77	100.81	100.61	100.97	100.61	100.99	100.50	100.80	100.38	101.07	100.65	100.85	101.08
Cations (based on 6 oxygens):																	
Si	1.9759	1.9714	1.9640	1.9640	1.9915	1.9840	1.9839	1.9719	1.9575	1.9547	1.9705	1.9606	1.9747	1.9755	1.9857	1.9716	1.9733
Ti	0.0069	0.0057	0.0081	0.0081	0.0081	0.0077	0.0087	0.0024	0.0023	0.0028	0.0031	0.0039	0.0045	0.0036	0.0062	0.0030	0.0029
Al	0.0386	0.0365	0.0398	0.0398	0.0333	0.0299	0.0347	0.0605	0.0691	0.0748	0.0494	0.0598	0.0612	0.0525	0.0412	0.0683	0.0640
Cr	0.0078	0.0090	0.0089	0.0089	0.0024	0.0025	0.0020	0.0142	0.0152	0.0147	0.0129	0.0153	0.0107	0.0138	0.0114	0.0137	0.0129
Fe	0.4955	0.4976	0.5029	0.5029	0.5277	0.5367	0.5395	0.3705	0.3713	0.3621	0.3682	0.3572	0.3564	0.3608	0.3993	0.3590	0.3621
Mn	0.0102	0.0100	0.0107	0.0107	0.0110	0.0110	0.0120	0.0067	0.0089	0.0083	0.0078	0.0079	0.0062	0.0075	0.0070	0.0066	0.0069
Ni	0.0026	0.0034	0.0029	0.0029	0.0020	0.0031	0.0027	0.0021	0.0008	0.0010	0.0023	0.0021	0.0026	0.0042	0.0035	0.0047	0.0025
Mg	1.4122	1.4235	1.4190	1.4190	1.3635	1.3798	1.3620	1.4866	1.5019	1.4965	1.5417	1.5265	1.5083	1.4882	1.4839	1.4819	1.4784
Ca	0.0437	0.0427	0.0456	0.0456	0.0425	0.0370	0.0427	0.0725	0.0697	0.0816	0.0391	0.0636	0.0600	0.0808	0.0431	0.0745	0.0812
Na	0.0012	0.0004	0.0032	0.0032	0.0015	0.0007	0.0020	0.0021	0.0023	0.0022	0.0006	0.0021	0.0005	0.0019	0.0005	0.0021	0.0023
Total	3.9946	4.0004	4.0051	4.0051	3.9834	3.9925	3.9901	3.9894	3.9991	3.9988	3.9956	3.9990	3.9851	3.9887	3.9820	3.9855	3.9865
MMF	0.7402	0.7410	0.7383	0.7383	0.7210	0.7199	0.7163	0.8005	0.8018	0.8052	0.8072	0.8104	0.8089	0.8049	0.7880	0.8050	0.8033
Wo	2.2	2.2	2.3	2.3	2.2	1.9	2.2	3.8	3.6	4.2	2.0	3.3	3.1	4.2	2.2	3.9	4.2
En	72.4	72.5	72.1	72.1	70.5	70.6	70.1	77.0	77.3	77.1	79.1	78.4	78.4	77.1	77.0	77.4	76.9
Fs	25.4	25.3	25.6	25.6	27.3	27.5	27.8	19.2	19.1	18.7	18.9	18.3	18.5	18.7	20.7	18.7	18.8

MICROPROBE DATA TABLE C8: Composition of **orthopyroxene** in the Bastard Unit - profile **RPM** (from Kruger, 1982). Metres given above base of Unit.

Sample	B-2	B-2	B-2	B-2	B-2	B-3	B-3	B-3	B-3	B-3	B-4	B-4	B-4	B-4	B-4	B-5	B-5	B-5	B-5	B-5	B-7	B-7	B-7	B-7	B-7	B-9	B-9
Metres	0.5	0.5	0.5	0.5	0.5	1.7	1.7	1.7	1.7	1.7	3.0	3.0	3.0	3.0	3.0	4.1	4.1	4.1	4.1	4.1	7.0	7.0	7.0	7.0	7.0	9.1	9.1
Wt. %																											
SiO_2	55.24	55.28	54.98	55.27	55.00	53.96	54.61	54.20	54.34	54.70	54.62	54.14	55.28	55.04	55.17	54.88	54.98	54.96	54.93	55.06	54.81	55.24	55.39	54.86	54.24	53.25	53.14
TiO_2	0.21	0.12	0.21	0.13	0.14	0.10	0.13	0.23	0.23	0.00	0.11	0.13	0.28	0.17	0.24	0.18	0.21	0.14	0.15	0.20	0.14	0.21	0.20	0.20	0.18	0.10	0.18
Al_2O_3	1.26	1.34	1.47	1.52	1.34	1.48	1.73	1.28	1.28	1.25	1.56	1.59	1.23	1.73	1.08	1.32	1.28	1.41	1.52	1.34	1.60	1.21	1.22	1.26	1.03	1.68	1.30
Cr_2O_3	0.39	0.43	0.43	0.47	0.46	0.48	0.51	0.41	0.37	0.41	0.50	0.53	0.44	0.48	0.31	0.46	0.51	0.45	0.45	0.43	0.54	0.48	0.46	0.43	0.33	0.51	0.38
FeO	13.02	12.33	12.08	12.36	12.68	12.05	11.91	12.31	12.19	12.04	11.64	11.36	12.07	12.09	12.56	12.59	12.01	12.60	12.60	12.11	11.48	11.78	11.66	11.57	12.37	15.52	15.22
MnO	0.27	0.27	0.31	0.24	0.28	0.27	0.24	0.26	0.25	0.25	0.27	0.26	0.25	0.25	0.26	0.30	0.28	0.27	0.23	0.27	0.24	0.27	0.23	0.26	0.26	0.31	0.32
NiO	0.09	0.07	0.09	0.07	0.10	0.12	0.12	0.13	0.09	0.09	0.11	0.12	0.11	0.13	0.10	0.12	0.08	0.08	0.09	0.07	0.07	0.09	0.08	0.08	0.08	0.06	0.05
MgO	29.30	29.15	27.82	28.40	28.83	30.40	29.80	29.54	29.54	30.54	30.00	29.69	30.89	30.96	31.07	28.28	28.96	30.10	28.67	28.23	28.99	29.33	29.43	29.43	29.60	27.67	27.95
CaO	1.02	1.48	2.65	2.30	1.55	1.33	1.55	1.35	1.73	1.13	1.59	2.04	0.84	0.79	0.84	1.22	1.01	0.89	1.79	2.28	1.95	1.03	1.02	1.05	1.09	0.81	1.29
Na_2O	0.00	0.00	0.00	0.00	0.00	0.00	0.00	0.00	0.00	0.00	0.00	0.00	0.00	0.00	0.00	0.00	0.00	0.00	0.00	0.00	0.00	0.00	0.00	0.00	0.00	0.00	0.00
Total	100.80	100.47	100.04	100.76	100.38	100.19	100.60	99.71	100.02	100.41	100.40	99.86	101.39	101.64	101.63	99.35	99.32	100.90	100.43	99.99	99.82	99.64	99.69	99.14	99.18	99.91	99.83
Cations (based on 6 oxygens):																											
Si	1.9561	1.9597	1.9621	1.9580	1.9564	1.9226	1.9340	1.9404	1.9397	1.9399	1.9366	1.9316	1.9395	1.9269	1.9359	1.9688	1.9667	1.9420	1.9529	1.9637	1.9522	1.9673	1.9694	1.9627	1.9502	1.9291	1.9279
Ti	0.0056	0.0032	0.0056	0.0035	0.0037	0.0027	0.0035	0.0062	0.0062	0.0000	0.0029	0.0035	0.0074	0.0045	0.0063	0.0049	0.0056	0.0037	0.0040	0.0054	0.0037	0.0056	0.0053	0.0054	0.0049	0.0027	0.0049
Al	0.0526	0.0560	0.0618	0.0635	0.0562	0.0621	0.0722	0.0540	0.0538	0.0522	0.0652	0.0669	0.0509	0.0714	0.0447	0.0558	0.0540	0.0587	0.0637	0.0563	0.0672	0.0508	0.0511	0.0531	0.0436	0.0717	0.0556
Cr	0.0109	0.0121	0.0121	0.0132	0.0129	0.0135	0.0143	0.0116	0.0104	0.0115	0.0140	0.0150	0.0122	0.0133	0.0086	0.0130	0.0144	0.0126	0.0126	0.0121	0.0152	0.0135	0.0129	0.0122	0.0094	0.0146	0.0109
Fe	0.3856	0.3655	0.3605	0.3662	0.3772	0.3591	0.3527	0.3686	0.3639	0.3571	0.3451	0.3389	0.3541	0.3540	0.3686	0.3777	0.3593	0.3723	0.3746	0.3612	0.3419	0.3508	0.3467	0.3462	0.3719	0.4702	0.4618
Mn	0.0081	0.0081	0.0094	0.0072	0.0084	0.0081	0.0072	0.0079	0.0076	0.0075	0.0081	0.0079	0.0074	0.0074	0.0077	0.0091	0.0085	0.0081	0.0069	0.0082	0.0072	0.0081	0.0069	0.0079	0.0079	0.0095	0.0098
Ni	0.0026	0.0020	0.0026	0.0020	0.0029	0.0034	0.0034	0.0037	0.0026	0.0026	0.0031	0.0034	0.0031	0.0037	0.0028	0.0035	0.0023	0.0023	0.0026	0.0020	0.0020	0.0026	0.0023	0.0023	0.0023	0.0017	0.0015
Mg	1.5465	1.5403	1.4798	1.4996	1.5285	1.6145	1.5731	1.5763	1.5717	1.6144	1.5854	1.5789	1.6154	1.6155	1.6250	1.5122	1.5440	1.5853	1.5193	1.5007	1.5390	1.5569	1.5597	1.5693	1.5863	1.4941	1.5114
Ca	0.0387	0.0562	0.1013	0.0873	0.0591	0.0508	0.0588	0.0518	0.0562	0.0429	0.0604	0.0780	0.0316	0.0296	0.0316	0.0469	0.0387	0.0337	0.0682	0.0871	0.0744	0.0393	0.0389	0.0402	0.0420	0.0314	0.0501
Na	0.0000	0.0000	0.0000	0.0000	0.0000	0.0000	0.0000	0.0000	0.0000	0.0000	0.0000	0.0000	0.0000	0.0000	0.0000	0.0000	0.0000	0.0000	0.0000	0.0000	0.0000	0.0000	0.0000	0.0000	0.0000	0.0000	0.0000
Total	4.0066	4.0031	3.9953	4.0003	4.0053	4.0369	4.0192	4.0206	4.0220	4.0282	4.0209	4.0240	4.0216	4.0263	4.0312	3.9919	3.9935	4.0186	4.0049	3.9967	4.0029	3.9950	3.9932	3.9993	4.0185	4.0251	4.0339
MMF	0.8004	0.8082	0.8041	0.8037	0.8021	0.8181	0.8168	0.8105	0.8120	0.8189	0.8212	0.8233	0.8202	0.8203	0.8151	0.8001	0.8112	0.8098	0.8022	0.8060	0.8182	0.8161	0.8181	0.8193	0.8101	0.7606	0.7660
Wo	2.0	2.9	5.2	4.5	3.0	2.5	3.0	2.6	3.3	2.1	3.0	3.9	1.6	1.5	1.6	2.4	2.0	1.7	3.5	4.5	3.8	2.0	2.0	2.1	2.1	1.6	2.5
En	78.5	78.5	76.2	76.8	77.8	79.8	79.3	78.9	78.5	80.1	79.6	79.1	80.7	80.8	80.2	78.1	79.5	79.6	77.4	77.0	78.7	80.0	80.2	80.2	79.3	74.9	74.7
Fs	19.6	18.6	18.6	18.7	19.2	17.7	17.8	18.5	18.2	17.7	17.3	17.0	17.7	17.7	18.2	19.5	18.5	18.7	19.1	18.5	17.5	18.0	17.8	17.7	18.6	23.6	22.8

Sample	B-9	B-9	B-9	B-10	B-10	B-10	B-10	B-10	B-13	B-13	B-13	B-13	B-13	B-15	B-15	B-15	B-15	B-15	B-19	B-19	B-19	B-19	B-19	B-20	B-20	B-20	B-20
Metres	9.1	9.1	9.1	10.4	10.4	10.4	10.4	10.4	11.20	11.20	11.20	11.20	11.20	12.7	12.7	12.7	12.7	12.7	15.0	15.0	15.0	15.0	15.0	18.6	18.6	18.6	18.6
Wt. %																											
SiO_2	53.73	53.95	54.25	55.27	54.71	54.82	53.85	54.10	54.58	54.57	54.55	54.31	54.49	53.61	52.93	52.62	53.50	52.35	53.31	53.38	53.55	53.12	53.38	52.95	53.12	52.77	52.82
TiO_2	0.21	0.22	0.18	0.21	0.25	0.17	0.27	0.28	0.24	0.26	0.22	0.26	0.24	0.18	0.24	0.39	0.19	0.33	0.19	0.17	0.16	0.31	0.17	0.25	0.19	0.21	0.23
Al_2O_3	1.13	1.16	1.28	1.10	1.02	1.11	1.13	1.02	1.10	1.13	1.09	1.11	0.97	1.45	0.94	0.93	1.26	0.93	1.51	1.12	1.07	0.96	1.12	0.86	0.70	0.91	1.36
Cr_2O_3	0.38	0.35	0.38	0.35	0.33	0.29	0.37	0.30	0.35	0.34	0.34	0.32	0.27	0.58	0.14	0.17	0.45	0.18	0.30	0.28	0.24	0.16	0.28	0.06	0.03	0.15	0.05
FeO	16.14	14.77	14.84	15.09	15.28	14.98	15.84	15.85	15.57	15.44	15.39	15.54	15.69	16.22	20.67	20.26	15.61	20.14	17.50	17.20	16.57	19.52	17.20	21.88	21.88	22.30	21.08
MnO	0.37	0.29	0.33	0.35	0.32	0.30	0.32	0.35	0.33	0.32	0.32	0.34	0.35	0.33	0.42	0.38	0.31	0.40	0.33	0.35	0.35	0.39	0.35	0.47	0.46	0.47	0.50
NiO	0.08	0.06	0.07	0.05	0.04	0.06	0.06	0.06	0.10	0.04	0.06	0.08	0.06	0.06	0.06	0.06	0.06	0.06	0.06	0.06	0.07	0.05	0.06	0.04	0.05	0.04	0.05
MgO	26.75	26.99	27.34	27.08	27.32	28.10	26.53	26.94	27.34	27.37	26.98	27.25	27.13	25.62	24.27	24.47	26.33	24.62	25.70	25.53	26.10	23.71	25.53	22.37	22.42	23.09	22.95
CaO	0.78	1.82	1.66	1.02	0.88	0.93	1.13	1.20	1.59	1.31	1.50	1.14	1.32	2.78	0.93	1.21	2.88	0.99	1.60	1.52	1.53	1.42	1.52	0.90	0.80	0.89	0.92
Na_2O	0.00	0.00	0.00	0.00	0.00	0.00	0.00	0.00	0.00	0.00	0.00	0.00	0.00	0.00	0.00	0.00	0.00	0.00	0.00	0.00	0.00	0.00	0.00	0.00	0.00	0.00	0.00
Total	99.57	99.61	100.33	100.52	100.15	100.76	99.50	100.10	101.20	100.78	100.45	100.35	100.52	100.83	100.60	100.49	100.49	100.00	100.50	99.61	99.64	99.64	99.61	99.78	99.65	100.83	99.96
Cations (based on 6 oxygens):																											
Si	1.9561	1.9556	1.9519	1.9783	1.9687	1.9589	1.9598	1.9575	1.9526	1.9565	1.9626	1.9567	1.9613	1.9401	1.9494	1.9399	1.9377	1.9384	1.9396	1.9561	1.9559	1.9656	1.9561	1.9745	1.9821	1.9533	1.9595
Ti	0.0057	0.0060	0.0049	0.0057	0.0068	0.0046	0.0074	0.0076	0.0065	0.0070	0.0060	0.0070	0.0065	0.0049	0.0066	0.0108	0.0052	0.0092	0.0052	0.0047	0.0044	0.0086	0.0047	0.0070	0.0053	0.0058	0.0064
Al	0.0485	0.0496	0.0543	0.0464	0.0433	0.0467	0.0485	0.0435	0.0464	0.0477	0.0462	0.0471	0.0411	0.0618	0.0408	0.0404	0.0538	0.0406	0.0647	0.0484	0.0461	0.0419	0.0484	0.0378	0.0308	0.0397	0.0595
Cr	0.0109	0.0100	0.0108	0.0099	0.0094	0.0082	0.0106	0.0086	0.0099	0.0096	0.0097	0.0091	0.0077	0.0166	0.0041	0.0050	0.0129	0.0053	0.0086	0.0081	0.0069	0.0047	0.0081	0.0018	0.0009	0.0044	0.0015
Fe	0.4914	0.4477	0.4465	0.4517	0.4598	0.4476	0.4821	0.4796	0.4658	0.4630	0.4630	0.4682	0.4723	0.4909	0.6366	0.6246	0.4698	0.6237	0.5325	0.5271	0.5061	0.6040	0.5271	0.6823	0.6828	0.6903	0.6540
Mn	0.0114	0.0089	0.0101	0.0106	0.0098	0.0091	0.0099	0.0107	0.0100	0.0097	0.0098	0.0104	0.0107	0.0101	0.0131	0.0119	0.0095	0.0125	0.0102	0.0109	0.0108	0.0122	0.0109	0.0148	0.0145	0.0147	0.0157
Ni	0.0023	0.0017	0.0020	0.0014	0.0012	0.0017	0.0018	0.0017	0.0029	0.0012	0.0017	0.0023	0.0017	0.0017	0.0018	0.0018	0.0017	0.0018	0.0018	0.0018	0.0021	0.0015	0.0018	0.0012	0.0015	0.0012	0.0015
Mg	1.4516	1.4583	1.4662	1.4447	1.4653	1.4966	1.4391	1.4529	1.4578	1.4627	1.4468	1.4633	1.4555	1.3819	1.3323	1.3446	1.4214	1.3588	1.3937	1.3944	1.4209	1.3077	1.3944	1.2433	1.2469	1.2739	1.2690
Ca	0.0304	0.0707	0.0640	0.0391	0.0339	0.0356	0.0441	0.0465	0.0609	0.0503	0.0578	0.0440	0.0509	0.1078	0.0367	0.0478	0.1118	0.0393	0.0624	0.0597	0.0599	0.0563	0.0597	0.0360	0.0320	0.0353	0.0366
Na	0.0000	0.0000	0.0000	0.0000	0.0000	0.0000	0.0000	0.0000	0.0000	0.0000	0.0000	0.0000	0.0000	0.0000	0.0000	0.0000	0.0000	0.0000	0.0000	0.0000	0.0000	0.0000	0.0000	0.0000	0.0000	0.0000	0.0000
Total	4.0084	4.0086	4.0107	3.9879	3.9982	4.0091	4.0032	4.0088	4.0128	4.0078	4.0035	4.0082	4.0078	4.0158	4.0215	4.0267	4.0238	4.0295	4.0186	4.0110	4.0132	4.0025	4.0110	3.9987	3.9968	4.0188	4.0036
MMF	0.7471	0.7651	0.7665	0.7618	0.7611	0.7698	0.7491	0.7518	0.7578	0.7596	0.7575	0.7576	0.7550	0.7379	0.6767	0.6828	0.7516	0.6854	0.7236	0.7257	0.7374	0.6840	0.7257	0.6457	0.6462	0.6486	0.6599
Wo	1.5	3.6	3.2	2.0	1.7	1.8	2.2	2.4	3.1	2.5	2.9	2.2	2.6	5.4	1.8	2.4	5.6	1.9	3.1	3.0	3.0	2.9	3.0	1.8	1.6	1.8	1.9
En	73.6	73.8	74.2	74.6	74.8	75.6	73.2	73.4	73.5	74.0	73.5	74.1	73.6	69.8	66.4	66.7	71.0	67.2	70.1	70.4	71.5	66.4	70.4	63.4	63.6	63.7	64.8
Fs	24.9	22.7	22.6	23.3	23.5	22.6	24.5	24.2	23.5	23.4	23.5	23.7	23.9	24.8	31.7	31.0	23.5	30.8	26.8	26.6	25.5	30.7	26.6	34.8	34.8	34.5	33.4

MICROPROBE DATA TABLE C8: Composition of **orthopyroxene** in the Bastard Unit - profile **RPM** (from Kruger, 1982).
Metres given above base of Unit.

Sample	B-20	B-21	B-21	B-21	B-21	B-21	B-22	B-22	B-22	B-22	B-22	B-23	B-23	B-23	B-23	B-23	B-25	B-25	B-25	B-25	B-25	B-26	B-26	B-26	B-26	B-26	B-26
Metres	18.6	23.2	23.2	23.2	23.2	23.2	27.7	27.7	27.7	27.7	27.7	32.3	32.3	32.3	32.3	32.3	41.9	41.9	41.9	41.9	41.9	46.3	46.3	46.3	46.3	46.3	46.3
Wt. %																											
SiO_2	52.82	53.70	54.01	53.82	53.75	53.69	54.49	54.21	53.87	54.23	53.87	52.55	52.73	53.72	53.01	53.26	53.54	53.24	53.79	53.11	53.54	52.71	53.34	51.92	52.36	51.75	52.01
TiO_2	0.23	0.18	0.12	0.18	0.17	0.14	0.17	0.30	0.31	0.12	0.31	0.19	0.31	0.26	0.32	0.16	0.17	0.27	0.17	0.18	0.17	0.16	0.15	0.33	0.23	0.38	0.32
Al_2O_3	1.36	1.15	1.31	1.10	1.10	1.29	1.12	0.83	0.93	1.39	0.93	1.07	0.83	0.96	0.86	1.08	1.11	0.84	0.98	0.99	1.11	1.31	1.16	1.08	0.94	0.71	0.75
Cr_2O_3	0.05	0.29	0.34	0.28	0.31	0.35	0.28	0.12	0.08	0.40	0.08	0.20	0.11	0.22	0.13	0.30	0.35	0.10	0.27	0.24	0.35	0.32	0.30	0.11	0.10	0.08	0.04
FeO	21.08	16.57	16.11	16.98	16.67	16.50	17.15	18.14	18.06	16.19	18.06	18.41	18.87	17.91	18.96	18.06	17.35	18.95	16.50	18.27	17.35	20.75	20.72	24.09	22.51	25.01	24.76
MnO	0.50	0.33	0.34	0.34	0.32	0.32	0.34	0.37	0.36	0.33	0.36	0.38	0.36	0.38	0.36	0.37	0.35	0.39	0.32	0.37	0.35	0.39	0.37	0.48	0.41	0.48	0.48
NiO	0.05	0.06	0.06	0.05	0.07	0.08	0.06	0.07	0.07	0.06	0.07	0.06	0.04	0.02	0.06	0.05	0.06	0.05	0.04	0.03	0.06	0.02	0.07	0.02	0.04	0.03	0.06
MgO	22.95	26.12	26.08	26.40	25.20	26.13	25.10	26.08	25.14	26.63	25.14	25.07	24.87	24.67	24.52	24.67	25.32	25.24	25.78	24.93	25.32	22.90	22.89	21.04	19.43	20.06	20.11
CaO	0.92	1.68	2.34	1.29	1.69	1.94	2.31	1.17	1.27	1.65	1.27	2.00	1.54	2.09	1.14	1.94	1.37	1.20	2.18	1.95	1.37	1.72	1.62	1.02	4.53	1.25	1.20
Na_2O	0.00	0.00	0.00	0.00	0.00	0.00	0.00	0.00	0.00	0.00	0.00	0.00	0.00	0.00	0.00	0.00	0.00	0.00	0.00	0.00	0.00	0.00	0.00	0.00	0.00	0.00	0.00
Total	99.96	100.08	100.71	100.44	99.28	100.44	101.02	101.29	100.09	101.00	100.09	99.93	99.66	100.23	99.36	99.89	99.62	100.28	100.03	100.07	99.62	100.28	100.62	100.09	100.55	99.75	99.73
Cations (based on 6 oxygens):																											
Si	1.9595	1.9531	1.9509	1.9518	1.9700	1.9471	1.9682	1.9577	1.9680	1.9496	1.9680	1.9368	1.9486	1.9640	1.9615	1.9555	1.9615	1.9524	1.9590	1.9503	1.9615	1.9518	1.9651	1.9544	1.9652	1.9651	1.9714
Ti	0.0064	0.0049	0.0033	0.0049	0.0047	0.0038	0.0046	0.0081	0.0085	0.0032	0.0085	0.0053	0.0086	0.0071	0.0089	0.0044	0.0047	0.0074	0.0047	0.0050	0.0047	0.0045	0.0042	0.0093	0.0065	0.0109	0.0091
Al	0.0595	0.0493	0.0558	0.0470	0.0475	0.0551	0.0477	0.0353	0.0400	0.0589	0.0400	0.0465	0.0361	0.0414	0.0375	0.0468	0.0479	0.0363	0.0421	0.0428	0.0479	0.0572	0.0504	0.0479	0.0416	0.0318	0.0335
Cr	0.0015	0.0083	0.0097	0.0080	0.0090	0.0100	0.0080	0.0034	0.0023	0.0114	0.0023	0.0058	0.0032	0.0064	0.0038	0.0087	0.0101	0.0029	0.0078	0.0070	0.0101	0.0094	0.0087	0.0033	0.0030	0.0024	0.0012
Fe	0.6540	0.5040	0.4866	0.5150	0.5109	0.5004	0.5180	0.5478	0.5517	0.4867	0.5517	0.5675	0.5832	0.5476	0.5867	0.5548	0.5316	0.5812	0.5025	0.5611	0.5316	0.6426	0.6384	0.7583	0.7065	0.7942	0.7849
Mn	0.0157	0.0102	0.0104	0.0104	0.0099	0.0098	0.0104	0.0113	0.0111	0.0100	0.0111	0.0119	0.0113	0.0118	0.0113	0.0115	0.0109	0.0121	0.0099	0.0115	0.0109	0.0122	0.0115	0.0153	0.0130	0.0154	0.0154
Ni	0.0015	0.0018	0.0017	0.0015	0.0021	0.0023	0.0017	0.0020	0.0021	0.0017	0.0021	0.0018	0.0012	0.0006	0.0018	0.0015	0.0018	0.0015	0.0012	0.0009	0.0018	0.0006	0.0021	0.0006	0.0012	0.0009	0.0018
Mg	1.2690	1.4160	1.4041	1.4270	1.3766	1.4124	1.3513	1.4038	1.3689	1.4269	1.3689	1.3772	1.3699	1.3443	1.3523	1.3508	1.3826	1.3795	1.3994	1.3645	1.3826	1.2639	1.2569	1.1805	1.0869	1.1354	1.1361
Ca	0.0366	0.0655	0.0906	0.0501	0.0664	0.0754	0.0894	0.0453	0.0497	0.0636	0.0497	0.0790	0.0610	0.0819	0.0452	0.0764	0.0538	0.0471	0.0851	0.0767	0.0538	0.0682	0.0639	0.0411	0.1822	0.0509	0.0487
Na	0.0000	0.0000	0.0000	0.0000	0.0000	0.0000	0.0000	0.0000	0.0000	0.0000	0.0000	0.0000	0.0000	0.0000	0.0000	0.0000	0.0000	0.0000	0.0000	0.0000	0.0000	0.0000	0.0000	0.0000	0.0000	0.0000	0.0000
Total	4.0036	4.0131	4.0131	4.0158	3.9971	4.0165	3.9994	4.0148	4.0024	4.0121	4.0024	4.0317	4.0231	4.0050	4.0090	4.0113	4.0048	4.0206	4.0115	4.0198	4.0048	4.0104	4.0012	4.0107	4.0061	4.0070	4.0022
MMF	0.6599	0.7375	0.7426	0.7348	0.7293	0.7384	0.7229	0.7193	0.7127	0.7457	0.7127	0.7082	0.7014	0.7106	0.6974	0.7088	0.7223	0.7036	0.7358	0.7086	0.7223	0.6630	0.6632	0.6089	0.6061	0.5884	0.5914
Wo	1.9	3.3	4.6	2.5	3.4	3.8	4.6	2.3	2.5	3.2	2.5	3.9	3.0	4.1	2.3	3.9	2.7	2.3	4.3	3.8	2.7	3.5	3.3	2.1	9.2	2.6	2.5
En	64.8	71.3	70.9	71.6	70.5	71.0	69.0	70.3	69.5	72.2	69.5	68.1	68.0	68.1	68.2	68.2	70.3	68.7	70.4	68.1	70.3	64.0	64.2	59.6	55.0	57.3	57.7
Fs	33.4	25.4	24.6	25.9	26.1	25.2	26.4	27.4	28.0	24.6	28.0	28.0	29.0	27.7	29.6	28.0	27.0	28.9	25.3	28.0	27.0	32.5	32.6	38.3	35.8	40.1	39.8

Sample	B-26	B-26	B-26	B-26	B-28	B-28	B-28	B-28	B-28	B30	B30	B30	B30	B30
Metres	46.3	46.3	46.3	46.3	51.9	51.9	51.9	51.9	51.9	60.1	60.1	60.1	60.1	60.1
Wt. %														
SiO_2	51.51	52.01	51.59	52.01	52.50	52.67	52.28	52.16	52.50	52.28	52.23	51.50	51.95	52.23
TiO_2	0.23	0.24	0.24	0.32	0.28	0.26	0.21	0.24	0.28	0.19	0.27	0.30	0.27	0.27
Al_2O_3	0.73	0.91	0.78	0.75	0.80	0.78	1.10	0.78	0.80	0.81	0.76	0.78	0.82	0.76
Cr_2O_3	0.04	0.07	0.02	0.04	0.10	0.10	0.08	0.08	0.10	0.09	0.07	0.07	0.11	0.07
FeO	26.10	22.17	25.82	24.76	23.97	24.53	24.01	25.03	23.97	24.66	24.87	24.85	24.10	24.87
MnO	0.48	0.41	0.51	0.48	0.44	0.44	0.47	0.51	0.44	0.47	0.45	0.46	0.44	0.45
NiO	0.06	0.02	0.04	0.06	0.02	0.05	0.09	0.04	0.02	0.06	0.04	0.04	0.06	0.04
MgO	19.73	19.30	18.95	20.11	21.10	20.81	20.90	20.97	21.10	20.73	19.85	20.23	19.34	19.85
CaO	0.84	4.37	2.25	1.20	1.36	1.10	1.60	0.99	1.36	1.37	1.44	1.31	2.39	1.44
Na_2O	0.00	0.00	0.00	0.00	0.00	0.00	0.00	0.00	0.00	0.00	0.00	0.00	0.00	0.00
Total	99.72	99.50	100.20	99.73	100.57	100.74	100.74	100.80	100.57	100.66	99.98	99.54	99.48	99.98
Cations (based on 6 oxygens):														
Si	1.9649	1.9698	1.9634	1.9714	1.9651	1.9708	1.9565	1.9576	1.9651	1.9627	1.9755	1.9597	1.9747	1.9755
Ti	0.0066	0.0068	0.0069	0.0091	0.0079	0.0073	0.0059	0.0068	0.0079	0.0054	0.0077	0.0086	0.0077	0.0077
Al	0.0328	0.0406	0.0350	0.0335	0.0353	0.0344	0.0485	0.0345	0.0353	0.0358	0.0339	0.0350	0.0367	0.0339
Cr	0.0012	0.0021	0.0006	0.0012	0.0030	0.0030	0.0024	0.0024	0.0030	0.0027	0.0021	0.0021	0.0033	0.0021
Fe	0.8326	0.7022	0.8218	0.7849	0.7503	0.7676	0.7514	0.7856	0.7503	0.7742	0.7867	0.7908	0.7661	0.7867
Mn	0.0155	0.0132	0.0164	0.0154	0.0139	0.0139	0.0149	0.0162	0.0139	0.0149	0.0144	0.0148	0.0142	0.0144
Ni	0.0018	0.0006	0.0012	0.0018	0.0006	0.0015	0.0027	0.0012	0.0006	0.0018	0.0012	0.0012	0.0018	0.0012
Mg	1.1218	1.0895	1.0749	1.1361	1.1772	1.1606	1.1658	1.1731	1.1772	1.1600	1.1191	1.1474	1.0957	1.1191
Ca	0.0343	0.1773	0.0917	0.0487	0.0545	0.0441	0.0642	0.0398	0.0545	0.0551	0.0584	0.0534	0.0973	0.0584
Na	0.0000	0.0000	0.0000	0.0000	0.0000	0.0000	0.0000	0.0000	0.0000	0.0000	0.0000	0.0000	0.0000	0.0000
Total	4.0115	4.0020	4.0120	4.0022	4.0079	4.0032	4.0122	4.0172	4.0079	4.0127	3.9988	4.0131	3.9976	3.9988
MMF	0.5740	0.6081	0.5667	0.5914	0.6107	0.6019	0.6081	0.5989	0.6107	0.5997	0.5872	0.5920	0.5885	0.5872
Wo	1.7	9.0	4.6	2.5	2.8	2.2	3.2	2.0	2.8	2.8	3.0	2.7	5.0	3.0
En	56.4	55.3	54.1	57.7	59.4	58.8	58.8	58.7	59.4	58.3	57.0	57.6	55.9	57.0
Fs	41.9	35.7	41.3	39.8	37.9	38.9	37.9	39.3	37.9	38.9	40.1	39.7	39.1	40.1

MICROPROBE DATA TABLE C9: Representative **clinopyroxene** analyses in the Bastard Unit - profile **RPM** (from Kruger, 1982). Metres given above base of Unit.

Sample	B-2	B-3	B-4	B-5	B-7	B-9	B-10	B-13	B-15	B-19	B-20	B-21	B-22	B-23	B-25	B-26	B-28	B-30
Metres	0.5	1.7	3.0	4.1	7.0	9.1	10.4	11.2000	12.7	15.0	18.6	23.2	27.7	32.3	41.9	46.3	51.9	60.1
Wt. %																		
SiO_2	53.08	52.08	52.18	52.42	52.38	52.08	52.82	52.67	53.30	52.54	51.99	52.41	52.58	52.36	51.79	51.50	51.88	51.60
TiO_2	0.70	0.65	0.39	0.39	0.38	0.37	0.38	0.52	0.37	0.37	0.39	0.28	0.47	0.48	0.33	0.57	0.37	0.48
Al_2O_3	2.10	1.86	2.87	2.37	1.77	1.98	1.89	1.66	1.70	1.94	1.46	1.50	1.45	1.45	1.59	1.47	1.63	1.64
Cr_2O_3	0.72	0.69	0.97	0.86	0.77	0.66	0.53	0.53	0.33	0.54	0.27	0.52	0.17	0.15	0.26	0.11	0.18	0.15
FeO	5.58	5.08	4.73	5.08	4.17	6.20	5.90	6.04	8.09	8.59	8.13	6.33	8.10	7.92	8.96	11.67	10.48	11.10
MnO	0.16	0.14	0.13	0.15	0.13	0.18	0.16	0.15	0.14	0.23	0.21	0.17	0.22	0.21	0.22	0.27	0.24	0.22
NiO	0.06	0.02	0.08	0.07	0.07	0.05	0.03	0.04	0.03	0.04	0.00	0.04	0.04	0.06	0.03	0.07	0.03	0.02
MgO	16.21	16.40	16.12	15.28	15.94	15.64	15.91	15.55	14.24	14.89	14.84	15.79	14.96	15.41	15.51	13.04	13.39	13.15
CaO	22.08	21.83	22.20	22.96	21.85	21.77	22.79	22.12	22.08	20.68	22.56	22.07	21.41	21.28	20.74	19.63	20.88	20.64
Na_2O	0.44	0.00	0.00	0.00	0.00	0.00	0.31	0.00	0.00	0.00	0.00	0.00	0.00	0.00	0.00	0.00	0.00	0.00
Total	101.13	98.75	99.67	99.58	97.46	98.93	100.72	99.28	100.28	99.82	99.85	99.11	99.40	99.32	99.43	98.33	99.08	99.00
Cations (based on 6 oxygens):																		
Si	1.9316	1.9353	1.9193	1.9361	1.9618	1.9406	1.9358	1.9534	1.9698	1.9523	1.9406	1.9512	1.9611	1.9536	1.9392	1.9668	1.9610	1.9570
Ti	0.0192	0.0182	0.0108	0.0108	0.0107	0.0104	0.0105	0.0145	0.0103	0.0103	0.0109	0.0078	0.0132	0.0135	0.0093	0.0164	0.0105	0.0137
Al	0.0901	0.0815	0.1244	0.1032	0.0781	0.0870	0.0816	0.0726	0.0741	0.0850	0.0642	0.0658	0.0637	0.0638	0.0702	0.0662	0.0726	0.0733
Cr	0.0207	0.0203	0.0282	0.0251	0.0228	0.0194	0.0154	0.0155	0.0096	0.0159	0.0080	0.0153	0.0050	0.0044	0.0077	0.0033	0.0054	0.0045
Fe	0.1698	0.1579	0.1455	0.1569	0.1306	0.1932	0.1808	0.1873	0.2500	0.2669	0.2538	0.1971	0.2527	0.2471	0.2806	0.3727	0.3313	0.3521
Mn	0.0049	0.0044	0.0041	0.0047	0.0041	0.0057	0.0050	0.0047	0.0044	0.0072	0.0066	0.0054	0.0070	0.0066	0.0070	0.0087	0.0077	0.0071
Ni	0.0018	0.0006	0.0024	0.0021	0.0021	0.0015	0.0009	0.0012	0.0009	0.0012	0.0000	0.0012	0.0012	0.0018	0.0009	0.0022	0.0009	0.0006
Mg	0.8793	0.9085	0.8839	0.8413	0.8899	0.8688	0.8692	0.8597	0.7845	0.8248	0.8258	0.8763	0.8318	0.8571	0.8657	0.7424	0.7545	0.7434
Ca	0.8609	0.8692	0.8750	0.9087	0.8769	0.8692	0.8950	0.8790	0.8744	0.8234	0.9023	0.8804	0.8556	0.8508	0.8321	0.8033	0.8457	0.8388
Na	0.0310	0.0000	0.0000	0.0000	0.0000	0.0000	0.0220	0.0000	0.0000	0.0000	0.0000	0.0000	0.0000	0.0000	0.0000	0.0000	0.0000	0.0000
Total	4.0094	3.9957	3.9936	3.9889	3.9771	3.9958	4.0162	3.9880	3.9780	3.9870	4.0123	4.0004	3.9913	3.9988	4.0126	3.9820	3.9895	3.9904
MMF	0.8381	0.8519	0.8586	0.8428	0.8720	0.8181	0.8278	0.8211	0.7583	0.7555	0.7649	0.8164	0.7670	0.7762	0.7552	0.6657	0.6949	0.6786
Wo	45.1	44.9	45.9	47.7	46.2	45.0	46.0	45.6	45.8	43.0	45.5	45.1	44.1	43.5	42.1	41.9	43.8	43.4
En	46.0	46.9	46.4	44.1	46.9	45.0	44.7	44.6	41.1	43.1	41.7	44.9	42.9	43.8	43.8	38.7	39.1	38.4
Fs	8.9	8.2	7.6	8.2	6.9	10.0	9.3	9.7	13.1	13.9	12.8	10.1	13.0	12.6	14.2	19.4	17.2	18.2

MICROPROBE DATA TABLE C10: Composition of **orthopyroxene** in the Bastard Unit - profile **Y**.
Metres given above base of Unit.

Sample	Y722.4	Y722.4	Y722.4	Y722.4	Y740.5	Y740.5	Y740.5	Y746.4	Y746.4	Y746.4	Y746.4	Y755.66	Y755.66	Y755.66	Y755.66	Y760.2	Y760.2	Y760.2	Y760.2	Y764.4	Y764.4	Y764.4	Y764.4	Y765.48	Y765.48	Y765.48	Y765.48
Metres	54.0	54.0	54.0	54.0	35.9	35.9	35.9	30.0	30.0	30.0	30.0	20.8	20.8	20.8	20.8	16.2	16.2	16.2	16.2	12.2	12.2	12.2	12.2	10.9	10.9	10.9	10.9
Wt. %																											
SiO_2	52.43	52.74	52.54	52.56	51.35	51.48	51.75	54.35	54.17	54.13	53.94	55.09	55.20	55.50	55.44	55.30	55.33	55.20	55.47	54.29	54.42	54.02	54.31	54.34	54.32	54.38	54.47
TiO_2	0.20	0.24	0.27	0.23	0.19	0.62	0.27	0.14	0.14	0.18	0.25	0.22	0.25	0.23	0.20	0.21	0.29	0.21	0.19	0.22	0.23	0.28	0.19	0.28	0.26	0.25	0.24
Al_2O_3	0.55	0.57	0.61	0.60	0.54	0.56	0.57	0.88	1.15	0.79	0.63	0.69	0.66	0.67	0.87	0.69	0.83	0.82	0.76	0.78	0.82	0.82	0.80	0.84	0.81	0.88	0.82
Cr_2O_3	0.02	0.01	0.03	0.02	0.00	0.03	0.02	0.23	0.21	0.14	0.11	0.09	0.08	0.09	0.11	0.17	0.08	0.09	0.11	0.26	0.23	0.25	0.25	0.12	0.10	0.14	0.10
FeO	25.97	26.09	26.81	27.24	27.92	26.73	26.57	17.47	17.70	18.51	19.02	15.95	16.05	15.37	15.27	15.66	16.11	15.52	15.82	16.75	17.01	16.74	16.53	18.29	18.62	19.17	18.66
MnO	0.52	0.50	0.61	0.57	0.57	0.48	0.53	0.36	0.33	0.39	0.42	0.30	0.32	0.28	0.29	0.28	0.34	0.28	0.29	0.30	0.32	0.32	0.30	0.34	0.35	0.35	0.34
NiO	0.06	0.06	0.06	0.10	0.01	0.03	0.00	0.13	0.09	0.09	0.08	0.10	0.11	0.06	0.07	0.04	0.01	0.03	0.04	0.04	0.06	0.03	0.03	0.02	0.02	0.01	0.04
MgO	18.89	19.14	18.38	18.34	18.09	18.90	18.77	25.35	24.70	25.04	24.58	26.40	26.77	27.37	27.11	27.20	26.24	26.46	26.77	26.56	26.62	26.32	26.55	24.39	24.33	24.58	24.64
CaO	1.21	1.06	1.42	1.03	0.98	1.19	1.30	1.38	2.01	1.01	0.90	1.19	0.81	0.84	1.08	0.75	1.16	1.27	1.15	0.74	0.72	0.92	1.08	0.92	0.98	0.84	0.83
Na_2O	0.00	0.00	0.02	0.01	0.01	0.00	0.00	0.01	0.05	0.01	0.00	0.02	0.02	0.01	0.01	0.02	0.02	0.02	0.02	0.02	0.01	0.00	0.02	0.02	0.00	0.00	0.01
Total	99.85	100.42	100.75	100.70	99.67	100.02	99.78	100.29	100.54	100.30	99.93	100.05	100.27	100.43	100.46	100.32	100.42	99.90	100.62	99.95	100.44	99.69	100.06	99.57	99.78	100.59	100.16
Cations (based on 6 oxygens):																											
Si	1.9932	1.9924	1.9886	1.9917	1.9774	1.9655	1.9780	1.9762	1.9699	1.9755	1.9804	1.9893	1.9879	1.9882	1.9859	1.9861	1.9903	1.9911	1.9887	1.9709	1.9679	1.9678	1.9694	1.9917	1.9900	1.9809	1.9878
Ti	0.0058	0.0069	0.0076	0.0066	0.0056	0.0178	0.0077	0.0038	0.0039	0.0049	0.0068	0.0061	0.0067	0.0061	0.0053	0.0056	0.0079	0.0056	0.0051	0.0059	0.0062	0.0076	0.0052	0.0078	0.0071	0.0068	0.0066
Al	0.0248	0.0253	0.0273	0.0269	0.0247	0.0251	0.0259	0.0379	0.0492	0.0341	0.0273	0.0293	0.0279	0.0285	0.0367	0.0292	0.0350	0.0349	0.0321	0.0333	0.0350	0.0352	0.0343	0.0361	0.0349	0.0377	0.0351
Cr	0.0006	0.0004	0.0009	0.0005	0.0000	0.0008	0.0005	0.0066	0.0060	0.0041	0.0031	0.0026	0.0023	0.0026	0.0030	0.0047	0.0024	0.0027	0.0031	0.0074	0.0066	0.0071	0.0072	0.0035	0.0030	0.0039	0.0030
Fe	0.8256	0.8243	0.8487	0.8632	0.8992	0.8536	0.8492	0.5310	0.5382	0.5650	0.5839	0.4816	0.4835	0.4604	0.4574	0.4703	0.4846	0.4682	0.4743	0.5086	0.5146	0.5099	0.5013	0.5608	0.5705	0.5840	0.5695
Mn	0.0167	0.0161	0.0195	0.0182	0.0186	0.0157	0.0171	0.0111	0.0102	0.0120	0.0131	0.0093	0.0099	0.0086	0.0088	0.0086	0.0103	0.0086	0.0089	0.0091	0.0098	0.0100	0.0093	0.0107	0.0107	0.0108	0.0106
Ni	0.0018	0.0020	0.0019	0.0030	0.0003	0.0010	0.0001	0.0038	0.0026	0.0027	0.0024	0.0029	0.0031	0.0018	0.0021	0.0012	0.0004	0.0008	0.0012	0.0012	0.0016	0.0009	0.0008	0.0005	0.0007	0.0003	0.0012
Mg	1.0707	1.0776	1.0368	1.0358	1.0382	1.0754	1.0693	1.3735	1.3387	1.3622	1.3452	1.4209	1.4371	1.4612	1.4476	1.4560	1.4066	1.4229	1.4303	1.4369	1.4350	1.4292	1.4348	1.3326	1.3284	1.3343	1.3401
Ca	0.0492	0.0430	0.0578	0.0417	0.0405	0.0486	0.0531	0.0536	0.0784	0.0395	0.0353	0.0460	0.0312	0.0323	0.0416	0.0290	0.0448	0.0491	0.0441	0.0288	0.0278	0.0358	0.0418	0.0362	0.0384	0.0327	0.0325
Na	0.0000	0.0000	0.0013	0.0007	0.0004	0.0002	0.0000	0.0006	0.0032	0.0010	0.0000	0.0014	0.0014	0.0010	0.0009	0.0011	0.0015	0.0011	0.0017	0.0011	0.0010	0.0000	0.0012	0.0015	0.0002	0.0002	0.0006
Total	3.9883	3.9879	3.9903	3.9884	4.0048	4.0038	4.0011	3.9981	4.0002	4.0010	3.9976	3.9893	3.9910	3.9907	3.9894	3.9919	3.9839	3.9850	3.9894	4.0034	4.0056	4.0035	4.0053	3.9814	3.9840	3.9917	3.9869
MMF	0.5646	0.5666	0.5499	0.5454	0.5359	0.5575	0.5574	0.7212	0.7133	0.7068	0.6973	0.7469	0.7483	0.7604	0.7599	0.7559	0.7437	0.7524	0.7510	0.7386	0.7361	0.7370	0.7411	0.7038	0.6996	0.6956	0.7018
Wo	2.5	2.2	3.0	2.1	2.0	2.5	2.7	2.7	4.0	2.0	1.8	2.4	1.6	1.7	2.1	1.5	2.3	2.5	2.3	1.5	1.4	1.8	2.1	1.9	2.0	1.7	1.7
En	55.0	55.4	53.4	53.4	52.5	54.4	54.2	70.1	68.5	69.3	68.5	72.9	73.6	74.8	74.4	74.5	72.7	73.3	73.4	72.8	72.6	72.4	72.5	69.1	68.6	68.4	69.0
Fs	42.4	42.4	43.7	44.5	45.5	43.2	43.1	27.1	27.5	28.7	29.7	24.7	24.8	23.6	23.5	24.1	25.0	24.1	24.3	25.8	26.0	25.8	25.3	29.1	29.4	29.9	29.3

Sample	Y770.58	Y770.58	Y770.58	Y770.58	Y775	Y775	Y775
Metres	5.8	5.8	5.8	5.8	1.4	1.4	1.4
Wt. %							
SiO_2	56.63	56.31	56.40	56.18	56.45	55.29	55.93
TiO_2	0.24	0.18	0.17	0.17	0.24	0.28	0.22
Al_2O_3	1.13	1.15	1.16	1.05	0.97	1.03	0.99
Cr_2O_3	0.45	0.44	0.42	0.45	0.27	0.30	0.33
FeO	11.92	12.11	12.02	12.30	12.16	12.32	11.92
MnO	0.24	0.30	0.26	0.31	0.26	0.28	0.29
NiO	0.10	0.06	0.10	0.08	0.10	0.06	0.12
MgO	29.26	29.44	29.44	29.52	29.78	29.20	29.63
CaO	1.10	0.80	1.00	0.94	0.70	1.03	1.06
Na_2O	0.01	0.00	0.01	0.00	0.01	0.02	0.01
Total	101.08	100.78	100.98	101.00	100.97	99.82	100.51
Cations (based on 6 oxygens):							
Si	1.9847	1.9804	1.9799	1.9756	1.9815	1.9697	1.9745
Ti	0.0062	0.0047	0.0045	0.0046	0.0064	0.0076	0.0059
Al	0.0468	0.0478	0.0480	0.0435	0.0403	0.0434	0.0412
Cr	0.0124	0.0122	0.0116	0.0124	0.0076	0.0085	0.0092
Fe	0.3494	0.3563	0.3527	0.3617	0.3571	0.3669	0.3519
Mn	0.0073	0.0089	0.0078	0.0091	0.0079	0.0084	0.0087
Ni	0.0029	0.0016	0.0027	0.0024	0.0028	0.0018	0.0033
Mg	1.5286	1.5430	1.5404	1.5473	1.5581	1.5504	1.5591
Ca	0.0411	0.0300	0.0377	0.0353	0.0263	0.0394	0.0402
Na	0.0004	0.0001	0.0010	0.0000	0.0008	0.0013	0.0008
Total	3.9797	3.9850	3.9863	3.9919	3.9886	3.9974	3.9948
MMF	0.8139	0.8124	0.8137	0.8105	0.8136	0.8086	0.8158
Wo	2.1	1.6	2.0	1.8	1.4	2.0	2.1
En	79.6	80.0	79.8	79.6	80.3	79.2	79.9
Fs	18.2	18.5	18.3	18.6	18.4	18.8	18.0

MICROPROBE DATA TABLE C11: Composition of **clinopyroxene** in the Bastard Unit - profile **Y**.
Metres given above base of Unit.

Sample	Y722.4	Y722.4	Y722.4	Y722.4	Y740.5	Y740.5	Y755.66	Y755.66	Y755.66	Y755.66	Y765.48	Y765.48	Y765.48	Y765.48
Metres	54.0	54.0	54.0	54.0	35.9	35.9	20.3	20.3	20.3	20.3	10.9	10.9	10.9	10.9
Wt. %														
SiO_2	52.33	52.82	52.60	52.34	51.18	51.49	53.22	49.69	52.99	52.95	52.62	52.37	52.48	52.63
TiO_2	0.31	0.28	0.27	0.26	0.40	0.27	0.34	0.01	0.53	0.49	0.51	0.44	0.41	0.29
Al_2O_3	1.28	1.28	1.08	1.33	1.30	1.20	1.35	31.18	1.48	1.44	1.57	1.61	1.47	1.44
Cr_2O_3	0.21	0.22	0.18	0.14	0.01	0.02	0.20	0.00	0.23	0.26	0.18	0.25	0.23	0.22
FeO	9.05	8.67	8.52	10.22	11.59	10.79	5.78	0.30	5.91	6.06	8.21	8.21	8.24	7.79
MnO	0.24	0.26	0.23	0.24	0.27	0.27	0.15	0.00	0.18	0.18	0.20	0.20	0.21	0.19
NiO	0.02	0.02	0.01	0.04	0.05	0.06	0.02	0.00	0.04	0.02	0.04	0.06	0.04	0.05
MgO	15.01	14.76	14.93	13.74	13.28	13.30	15.69	0.01	16.06	16.22	14.84	14.85	15.00	15.02
CaO	20.94	21.79	21.62	21.84	21.22	22.23	23.58	15.38	22.91	22.65	22.00	21.81	21.72	22.21
Na_2O	0.22	0.23	0.20	0.22	0.25	0.23	0.27	2.91	0.28	0.30	0.29	0.31	0.27	0.26
Total	99.59	100.33	99.63	100.39	99.55	99.86	100.60	99.49	100.60	100.58	100.46	100.11	100.07	100.09
Cations (based on 6 oxygens):														
Si	1.9570	1.9607	1.9643	1.9568	1.9435	1.9467	1.9536	1.7126	1.9443	1.9435	1.9484	1.9466	1.9504	1.9535
Ti	0.0087	0.0079	0.0076	0.0074	0.0113	0.0077	0.0093	0.0001	0.0146	0.0135	0.0143	0.0123	0.0115	0.0081
Al	0.0564	0.0559	0.0474	0.0584	0.0583	0.0535	0.0584	1.2664	0.0639	0.0622	0.0685	0.0704	0.0642	0.0629
Cr	0.0062	0.0064	0.0054	0.0042	0.0004	0.0005	0.0059	0.0000	0.0066	0.0075	0.0054	0.0073	0.0068	0.0065
Fe	0.2829	0.2691	0.2660	0.3197	0.3681	0.3411	0.1773	0.0088	0.1813	0.1861	0.2543	0.2550	0.2561	0.2417
Mn	0.0075	0.0083	0.0074	0.0077	0.0088	0.0086	0.0046	0.0000	0.0055	0.0055	0.0063	0.0064	0.0067	0.0058
Ni	0.0007	0.0007	0.0003	0.0013	0.0016	0.0018	0.0006	0.0000	0.0012	0.0007	0.0012	0.0019	0.0012	0.0015
Mg	0.8365	0.8165	0.8311	0.7658	0.7515	0.7497	0.8584	0.0007	0.8782	0.8876	0.8189	0.8224	0.8309	0.8310
Ca	0.8392	0.8667	0.8650	0.8750	0.8632	0.9005	0.9273	0.5681	0.9005	0.8908	0.8727	0.8686	0.8651	0.8833
Na	0.0156	0.0164	0.0143	0.0161	0.0182	0.0170	0.0191	0.1945	0.0196	0.0216	0.0206	0.0226	0.0194	0.0187
Total	4.0108	4.0085	4.0088	4.0125	4.0249	4.0271	4.0145	3.7513	4.0157	4.0189	4.0106	4.0136	4.0123	4.0131
MMF	0.7473	0.7521	0.7575	0.7055	0.6712	0.6873	0.8288	0.0766	0.8288	0.8267	0.7631	0.7633	0.7644	0.7747
Wo	42.8	44.4	44.1	44.6	43.5	45.2	47.2	98.4	45.9	45.3	44.8	44.6	44.3	45.2
En	42.7	41.8	42.4	39.1	37.9	37.6	43.7	0.1	44.8	45.2	42.1	42.3	42.6	42.5
Fs	14.4	13.8	13.6	16.3	18.6	17.1	9.0	1.5	9.3	9.5	13.1	13.1	13.1	12.4

MICROPROBE DATA TABLE C12: Composition of **orthopyroxene** in the Bastard Unit - profile **X**.
Metres given above base of Unit.

Sample	X735	X735	X735	X745.44	X745.44	X745.44	X763.95	X763.95	X763.95	X768.5	X768.5	X768.5	X768.5	X768.5	X776.5	X776.5	X776.5	X776.5	X776.5	X779.82	X779.82	X779.82	X779.82	X779.82	X782.7	X782.7	X782.7
Metres	57.9	57.9	57.9	47.5	47.5	47.5	29.0	29.0	29.0	24.4	24.4	24.4	24.4	24.4	16.4	16.4	16.4	16.4	16.4	13.1	13.1	13.1	13.1	13.1	10.2	10.2	10.2
Wt. %																											
SiO_2	53.57	53.59	53.79	54.19	54.23	54.02	52.86	52.98	53.01	54.38	54.06	53.65	54.18	53.65	54.21	54.06	54.02	53.96	53.78	54.91	54.64	54.53	54.48	54.53	55.91	55.74	55.48
TiO_2	0.26	0.12	0.15	0.19	0.25	0.24	0.16	0.15	0.18	0.18	0.22	0.19	0.22	0.19	0.19	0.21	0.17	0.06	0.18	0.20	0.19	0.19	0.18	0.19	0.21	0.19	0.21
Al_2O_3	0.58	0.62	0.54	0.62	0.74	0.63	0.59	0.56	0.61	0.57	0.71	0.66	0.59	0.66	0.58	0.63	0.59	0.56	0.72	0.83	0.98	1.11	0.92	1.11	1.02	1.07	1.03
Cr_2O_3	0.03	0.03	0.06	0.03	0.02	0.04	0.02	0.02	0.00	0.04	0.08	0.04	0.05	0.04	0.07	0.07	0.07	0.08	0.08	0.33	0.40	0.42	0.39	0.42	0.40	0.42	0.42
FeO	23.40	22.52	22.57	20.02	19.89	20.01	23.07	22.65	22.61	19.56	19.84	20.83	20.20	20.83	22.13	21.82	22.42	22.65	22.36	16.19	16.20	15.32	15.87	15.32	12.93	12.86	12.97
MnO	0.44	0.39	0.44	0.38	0.40	0.37	0.44	0.45	0.44	0.38	0.47	0.47	0.45	0.47	0.48	0.42	0.50	0.45	0.51	0.35	0.31	0.31	0.38	0.31	0.27	0.30	0.26
NiO	0.01	0.04	0.07	0.01	0.00	0.01	0.10	0.05	0.08	0.06	0.09	0.11	0.09	0.11	0.02	0.05	0.04	0.04	0.02	0.09	0.11	0.06	0.07	0.06	0.11	0.15	0.12
MgO	21.12	21.42	21.73	23.11	23.24	23.05	21.50	21.68	21.96	23.41	23.38	23.12	23.39	23.12	22.07	22.03	21.80	22.04	21.77	26.65	26.58	26.07	26.58	26.07	28.54	28.72	28.96
CaO	1.13	1.56	1.04	0.64	0.84	0.87	0.76	0.66	0.87	0.76	0.87	0.75	1.01	0.75	0.86	0.84	0.80	0.52	0.88	0.67	0.79	1.82	0.95	1.82	1.22	1.09	0.92
Na_2O	0.02	0.02	0.02	0.01	0.02	0.01	0.03	0.02	0.03	0.02	0.02	0.01	0.02	0.01	0.00	0.01	0.00	0.00	0.00	0.00	0.00	0.03	0.00	0.03	0.01	0.00	0.01
Total	100.55	100.33	100.41	99.19	99.63	99.27	99.51	99.22	99.80	99.38	99.75	99.82	100.20	99.82	100.61	100.13	100.40	100.36	100.30	100.21	100.20	99.86	99.83	99.86	100.62	100.54	100.38
Cations (based on 6 oxygens):																											
Si	1.9933	1.9931	1.9965	2.0070	1.9999	2.0015	1.9868	1.9917	1.9828	2.0073	1.9940	1.9873	1.9931	1.9873	2.0010	2.0020	2.0012	2.0002	1.9950	1.9808	1.9732	1.9736	1.9738	1.9736	1.9802	1.9759	1.9705
Ti	0.0072	0.0035	0.0042	0.0053	0.0069	0.0067	0.0044	0.0041	0.0050	0.0049	0.0062	0.0054	0.0061	0.0054	0.0054	0.0059	0.0046	0.0017	0.0050	0.0053	0.0053	0.0052	0.0048	0.0052	0.0055	0.0051	0.0057
Al	0.0255	0.0272	0.0234	0.0269	0.0322	0.0277	0.0261	0.0246	0.0270	0.0248	0.0309	0.0287	0.0255	0.0287	0.0251	0.0276	0.0256	0.0244	0.0314	0.0352	0.0417	0.0476	0.0393	0.0476	0.0426	0.0448	0.0431
Cr	0.0009	0.0009	0.0018	0.0007	0.0006	0.0013	0.0006	0.0005	0.0000	0.0013	0.0023	0.0012	0.0013	0.0012	0.0020	0.0019	0.0019	0.0025	0.0023	0.0095	0.0115	0.0119	0.0113	0.0119	0.0113	0.0118	0.0118
Fe	0.7281	0.7004	0.7005	0.6201	0.6135	0.6200	0.7252	0.7122	0.7074	0.6036	0.6120	0.6453	0.6214	0.6453	0.6830	0.6759	0.6948	0.7022	0.6936	0.4886	0.4891	0.4638	0.4807	0.4638	0.3831	0.3811	0.3853
Mn	0.0139	0.0124	0.0140	0.0119	0.0125	0.0117	0.0139	0.0143	0.0140	0.0119	0.0148	0.0147	0.0140	0.0147	0.0152	0.0131	0.0157	0.0142	0.0160	0.0107	0.0095	0.0095	0.0117	0.0095	0.0082	0.0091	0.0079
Ni	0.0002	0.0011	0.0020	0.0002	0.0000	0.0004	0.0029	0.0015	0.0026	0.0019	0.0025	0.0032	0.0028	0.0032	0.0006	0.0014	0.0012	0.0011	0.0007	0.0025	0.0032	0.0017	0.0022	0.0017	0.0031	0.0042	0.0036
Mg	1.1717	1.1877	1.2023	1.2758	1.2774	1.2729	1.2041	1.2151	1.2244	1.2880	1.2852	1.2764	1.2826	1.2764	1.2144	1.2160	1.2036	1.2176	1.2040	1.4329	1.4309	1.4064	1.4353	1.4064	1.5070	1.5175	1.5330
Ca	0.0450	0.0622	0.0414	0.0255	0.0333	0.0347	0.0305	0.0268	0.0348	0.0302	0.0344	0.0297	0.0400	0.0297	0.0337	0.0332	0.0317	0.0207	0.0350	0.0261	0.0305	0.0705	0.0370	0.0705	0.0462	0.0412	0.0350
Na	0.0011	0.0017	0.0012	0.0009	0.0012	0.0008	0.0020	0.0017	0.0020	0.0016	0.0017	0.0009	0.0013	0.0009	0.0000	0.0006	0.0000	0.0000	0.0000	0.0000	0.0000	0.0024	0.0000	0.0024	0.0005	0.0000	0.0007
Total	3.9869	3.9901	3.9872	3.9744	3.9774	3.9777	3.9965	3.9925	3.9998	3.9756	3.9840	3.9928	3.9880	3.9928	3.9802	3.9776	3.9804	3.9846	3.9831	3.9915	3.9949	3.9926	3.9961	3.9926	3.9876	3.9907	3.9966
MMF	0.6167	0.6290	0.6318	0.6729	0.6755	0.6725	0.6241	0.6304	0.6338	0.6809	0.6774	0.6642	0.6736	0.6642	0.6400	0.6427	0.6340	0.6342	0.6345	0.7457	0.7452	0.7520	0.7491	0.7520	0.7973	0.7993	0.7992
Wo	2.3	3.2	2.1	1.3	1.7	1.8	1.6	1.4	1.8	1.6	1.8	1.5	2.1	1.5	1.7	1.7	1.6	1.1	1.8	1.3	1.6	3.6	1.9	3.6	2.4	2.1	1.8
En	60.2	60.9	61.8	66.4	66.4	66.0	61.4	62.2	62.3	67.0	66.5	65.4	66.0	65.4	62.9	63.2	62.4	62.7	62.3	73.6	73.4	72.5	73.5	72.5	77.8	78.2	78.5
Fs	37.4	35.9	36.0	32.3	31.9	32.2	37.0	36.4	36.0	31.4	31.7	33.1	32.0	33.1	35.4	35.1	36.0	36.2	35.9	25.1	25.1	23.9	24.6	23.9	19.8	19.6	19.7

Sample	X782.7	X782.7	X788.41	X788.41	X788.41	X788.41	X788.41	X791.8	X791.8	X791.8	X791.8	X791.8
Metres	10.2	10.2	4.5	4.5	4.5	4.5	4.5	1.1	1.1	1.1	1.1	1.1
Wt. %												
SiO_2	55.93	55.48	56.25	56.15	56.11	55.56	56.11	55.80	55.76	55.57	55.53	56.15
TiO_2	0.19	0.21	0.18	0.15	0.16	0.16	0.16	0.16	0.21	0.20	0.12	0.12
Al_2O_3	0.96	1.03	1.15	1.15	1.06	1.21	1.06	0.68	0.74	0.89	0.94	0.61
Cr_2O_3	0.36	0.42	0.48	0.48	0.47	0.50	0.47	0.26	0.26	0.33	0.35	0.23
FeO	13.02	12.97	11.41	11.36	11.33	11.33	11.33	12.38	12.17	11.76	11.88	11.99
MnO	0.30	0.26	0.27	0.26	0.27	0.22	0.27	0.27	0.26	0.26	0.28	0.27
NiO	0.13	0.12	0.08	0.05	0.06	0.07	0.06	0.07	0.09	0.08	0.07	0.08
MgO	28.74	28.96	29.66	29.66	29.39	28.99	29.39	29.87	30.13	29.55	29.97	30.13
CaO	1.00	0.92	0.86	1.10	1.16	1.85	1.16	0.63	0.64	1.36	0.76	0.63
Na_2O	0.00	0.01	0.02	0.02	0.03	0.03	0.03	0.02	0.00	0.03	0.02	0.01
Total	100.62	100.38	100.37	100.39	100.04	99.91	100.04	100.15	100.26	100.03	99.91	100.22
Cations (based on 6 oxygens):												
Si	1.9809	1.9705	1.9811	1.9784	1.9836	1.9721	1.9836	1.9785	1.9737	1.9723	1.9710	1.9847
Ti	0.0049	0.0057	0.0047	0.0041	0.0043	0.0043	0.0043	0.0044	0.0056	0.0054	0.0032	0.0031
Al	0.0401	0.0431	0.0479	0.0476	0.0442	0.0507	0.0442	0.0286	0.0308	0.0371	0.0395	0.0254
Cr	0.0101	0.0118	0.0134	0.0135	0.0131	0.0139	0.0131	0.0072	0.0073	0.0093	0.0097	0.0064
Fe	0.3855	0.3853	0.3360	0.3346	0.3349	0.3363	0.3349	0.3670	0.3602	0.3490	0.3525	0.3545
Mn	0.0089	0.0079	0.0081	0.0078	0.0081	0.0067	0.0081	0.0081	0.0077	0.0077	0.0084	0.0079
Ni	0.0036	0.0036	0.0022	0.0014	0.0018	0.0021	0.0018	0.0020	0.0025	0.0023	0.0019	0.0022
Mg	1.5172	1.5330	1.5570	1.5573	1.5487	1.5339	1.5487	1.5789	1.5896	1.5632	1.5854	1.5875
Ca	0.0378	0.0350	0.0325	0.0416	0.0439	0.0702	0.0439	0.0241	0.0243	0.0519	0.0289	0.0240
Na	0.0002	0.0007	0.0016	0.0016	0.0018	0.0018	0.0018	0.0012	0.0000	0.0020	0.0013	0.0010
Total	3.9892	3.9966	3.9844	3.9878	3.9844	3.9921	3.9844	3.9999	4.0016	4.0002	4.0019	3.9968
MMF	0.7974	0.7992	0.8225	0.8231	0.8222	0.8202	0.8222	0.8114	0.8152	0.8175	0.8181	0.8174
Wo	1.9	1.8	1.7	2.2	2.3	3.6	2.3	1.2	1.2	2.6	1.5	1.2
En	78.2	78.5	80.9	80.5	80.4	79.1	80.4	80.1	80.5	79.6	80.6	80.7
Fs	19.9	19.7	17.4	17.3	17.4	17.3	17.4	18.6	18.2	17.8	17.9	18.0

MICROPROBE DATA TABLE C13: Composition of **orthopyroxene** in the Bastard Unit - profile **RD**.
Metres given above base of Unit.
clinopyroxene analyses for RD-6 included)

Sample	RD-3	RD-3	RD-3	RD-3	RD-3	RD-3	RD-4	RD-4	RD-4	RD-4	RD-6	RD-6	RD-6	RD-6	RD-6	RD-6	RD-6	RD-6	RD-13	RD-13	RD-13	RD-13	RD-15	RD-15	RD-15	RD-16	RD-16
Metres	31.0	31.0	31.0	31.0	31.0	31.0	29.4	29.4	29.4	29.4	22.5	22.5	22.5	22.5	22.5	22.5	22.5	22.5	10.6	10.6	10.6	10.6	8.3	8.3	8.3	5.9	5.9
Wt. %															cpx	cpx	cpx	cpx									
SiO_2	54.07	53.44	53.18	53.27	53.33	53.53	54.58	54.52	54.24	54.00	54.14	54.38	54.22	54.14	52.72	52.81	52.75	52.94	54.97	55.90	55.74	55.62	55.23	55.83	55.81	54.90	56.67
TiO_2	0.16	0.17	0.30	0.30	0.43	0.14	0.22	0.22	0.27	0.23	0.18	0.14	0.21	0.15	0.39	0.36	0.37	0.36	0.16	0.15	0.14	0.16	0.14	0.12	0.26	0.14	0.16
Al_2O_3	0.62	0.76	0.87	0.72	0.74	0.87	0.67	0.73	0.71	0.65	0.85	0.76	0.74	0.82	1.42	1.48	1.37	1.44	0.98	0.94	0.82	0.95	1.16	1.12	1.04	1.90	1.16
Cr_2O_3	0.10	0.08	0.15	0.12	0.10	0.19	0.14	0.21	0.16	0.11	0.21	0.19	0.15	0.19	0.43	0.42	0.44	0.51	0.35	0.30	0.30	0.35	0.44	0.39	0.39	0.51	0.50
FeO	19.64	19.42	19.30	19.24	19.74	18.68	17.67	17.66	18.06	18.00	18.34	18.71	18.04	19.01	6.90	7.90	6.79	6.19	12.46	12.38	12.30	12.32	11.96	12.60	12.51	11.03	11.15
MnO	0.41	0.41	0.37	0.43	0.37	0.32	0.32	0.33	0.36	0.38	0.38	0.39	0.40	0.39	0.23	0.23	0.23	0.22	0.25	0.23	0.25	0.30	0.28	0.29	0.27	0.24	0.23
NiO	0.05	0.04	0.02	0.08	0.05	0.00	0.05	0.05	0.06	0.02	0.06	0.05	0.02	0.04	0.05	0.00	0.01	0.01	0.12	0.10	0.09	0.10	0.13	0.11	0.11	0.08	0.06
MgO	24.51	24.50	23.81	23.99	24.27	24.09	25.01	25.42	25.39	25.12	24.85	24.87	25.08	24.18	15.87	16.64	15.76	15.71	29.01	29.66	29.63	29.41	28.21	28.94	28.71	29.50	30.06
CaO	0.63	0.66	1.49	1.61	1.01	2.05	1.43	1.09	0.69	1.15	0.75	0.73	1.00	0.98	21.79	19.92	22.34	22.86	0.93	0.85	1.12	1.33	1.61	0.89	1.06	1.55	1.05
Na_2O	0.01	0.02	0.02	0.02	0.02	0.04	0.03	0.02	0.02	0.02	0.02	0.02	0.02	0.03	0.31	0.34	0.34	0.30	0.03	0.02	0.02	0.04	0.04	0.04	0.03	0.31	0.02
Total	100.19	99.49	99.50	99.78	100.05	99.91	100.11	100.25	99.95	99.68	99.77	100.24	99.88	99.93	100.11	100.11	100.41	100.53	99.26	100.52	100.42	100.58	99.19	100.34	100.19	100.15	101.04
Cations (based on 6 oxygens):																											
Si	1.9828	1.9740	1.9683	1.9679	1.9647	1.9696	1.9877	1.9816	1.9798	1.9792	1.9824	1.9842	1.9818	1.9862	1.9483	1.9492	1.9461	1.9471	1.9713	1.9753	1.9736	1.9687	1.9797	1.9787	1.9809	1.9447	1.9799
Ti	0.0045	0.0046	0.0084	0.0084	0.0120	0.0038	0.0060	0.0061	0.0075	0.0062	0.0049	0.0039	0.0058	0.0042	0.0107	0.0100	0.0102	0.0099	0.0043	0.0039	0.0037	0.0044	0.0038	0.0032	0.0070	0.0036	0.0042
Al	0.0267	0.0330	0.0379	0.0312	0.0321	0.0379	0.0287	0.0311	0.0304	0.0281	0.0366	0.0328	0.0319	0.0354	0.0620	0.0646	0.0597	0.0623	0.0413	0.0391	0.0344	0.0395	0.0489	0.0468	0.0434	0.0792	0.0478
Cr	0.0028	0.0023	0.0045	0.0036	0.0028	0.0056	0.0039	0.0062	0.0046	0.0032	0.0062	0.0054	0.0042	0.0054	0.0127	0.0122	0.0130	0.0149	0.0099	0.0083	0.0085	0.0099	0.0124	0.0109	0.0109	0.0142	0.0138
Fe	0.6022	0.6000	0.5974	0.5944	0.6080	0.5747	0.5383	0.5368	0.5513	0.5518	0.5616	0.5708	0.5515	0.5831	0.2131	0.2437	0.2095	0.1905	0.3737	0.3657	0.3642	0.3646	0.3585	0.3734	0.3713	0.3269	0.3257
Mn	0.0126	0.0127	0.0117	0.0133	0.0115	0.0101	0.0098	0.0101	0.0111	0.0117	0.0118	0.0120	0.0124	0.0121	0.0072	0.0072	0.0073	0.0068	0.0075	0.0067	0.0075	0.0090	0.0085	0.0088	0.0082	0.0071	0.0067
Ni	0.0015	0.0011	0.0005	0.0023	0.0014	0.0000	0.0014	0.0013	0.0017	0.0007	0.0017	0.0015	0.0007	0.0012	0.0013	0.0000	0.0003	0.0003	0.0034	0.0028	0.0026	0.0029	0.0037	0.0032	0.0030	0.0022	0.0016
Mg	1.3395	1.3491	1.3139	1.3210	1.3327	1.3210	1.3574	1.3771	1.3812	1.3721	1.3560	1.3528	1.3662	1.3219	0.8742	0.9156	0.8663	0.8614	1.5506	1.5622	1.5637	1.5515	1.5070	1.5289	1.5186	1.5577	1.5655
Ca	0.0249	0.0261	0.0589	0.0637	0.0399	0.0806	0.0557	0.0424	0.0269	0.0453	0.0293	0.0287	0.0390	0.0383	0.8629	0.7879	0.8830	0.9007	0.0357	0.0322	0.0425	0.0505	0.0619	0.0338	0.0404	0.0587	0.0391
Na	0.0010	0.0018	0.0012	0.0012	0.0015	0.0030	0.0018	0.0017	0.0016	0.0012	0.0016	0.0013	0.0018	0.0023	0.0222	0.0240	0.0241	0.0211	0.0024	0.0012	0.0014	0.0027	0.0028	0.0030	0.0020	0.0215	0.0011
Total	3.9984	4.0046	4.0027	4.0069	4.0066	4.0064	3.9908	3.9945	3.9960	3.9995	3.9921	3.9934	3.9952	3.9903	4.0147	4.0145	4.0195	4.0149	4.0000	3.9976	4.0020	4.0037	3.9872	3.9907	3.9859	4.0158	3.9856
MMF	0.6899	0.6922	0.6875	0.6897	0.6867	0.6968	0.7161	0.7195	0.7147	0.7132	0.7071	0.7033	0.7124	0.6939	0.8040	0.7898	0.8052	0.8189	0.8058	0.8103	0.8111	0.8097	0.8078	0.8037	0.8035	0.8265	0.8278
Wo	1.3	1.3	3.0	3.2	2.0	4.1	2.9	2.2	1.4	2.3	1.5	1.5	2.0	2.0	44.2	40.5	45.1	46.1	1.8	1.6	2.2	2.6	3.2	1.7	2.1	3.0	2.0
En	68.1	68.3	66.7	66.7	67.3	65.8	69.6	70.4	70.5	69.7	69.7	69.3	69.8	68.0	44.8	47.0	44.2	44.1	79.1	79.7	79.4	78.9	78.2	79.0	78.7	80.2	81.1
Fs	30.6	30.4	30.3	30.0	30.7	29.1	27.6	27.4	28.1	28.0	28.8	29.2	28.2	30.0	10.9	12.5	10.7	9.8	19.1	18.7	18.5	18.5	18.6	19.3	19.2	16.8	16.9

Sample	RD-16	RD-16	RD-16	RD-17	RD-17	RD-17	RD-17	RD-18	RD-18	RD-18	RD-18	RD-19	RD-19	RD-19	RD-19
Metres	5.9	5.9	5.9	3.6	3.6	3.6	3.6	0.5	0.5	0.5	0.5	0.1	0.1	0.1	0.1
Wt. %															
SiO_2	55.89	56.23	55.86	54.89	54.62	54.97	55.16	55.51	55.27	54.73	55.28	56.14	55.87	55.69	55.72
TiO_2	0.15	0.14	0.18	0.12	0.10	0.11	0.17	0.17	0.17	0.19	0.19	0.10	0.18	0.17	0.20
Al_2O_3	1.21	1.24	1.25	1.19	1.27	1.12	0.95	1.15	1.05	1.13	1.15	1.16	1.27	1.18	1.14
Cr_2O_3	0.43	0.46	0.48	0.42	0.41	0.39	0.38	0.34	0.28	0.30	0.31	0.45	0.45	0.41	0.40
FeO	10.92	11.05	11.03	12.95	12.77	12.59	13.46	13.60	14.36	14.97	15.02	12.72	13.24	12.83	12.77
MnO	0.23	0.25	0.24	0.27	0.26	0.25	0.25	0.28	0.25	0.29	0.30	0.23	0.26	0.26	0.26
NiO	0.07	0.07	0.08	0.06	0.05	0.10	0.10	0.06	0.08	0.09	0.07	0.06	0.10	0.13	0.16
MgO	29.74	30.11	29.84	28.43	27.97	28.39	28.46	26.08	26.69	27.53	27.50	28.99	28.56	28.29	28.20
CaO	1.65	0.98	1.56	1.40	1.84	1.78	1.12	3.57	2.22	0.78	1.22	1.05	1.33	1.68	1.86
Na_2O	0.02	0.02	0.03	0.03	0.03	0.03	0.02	0.08	0.05	0.03	0.03	0.00	0.00	0.03	0.03
Total	100.30	100.55	100.55	99.75	99.31	99.74	100.07	100.85	100.42	100.04	101.06	100.92	101.27	100.67	100.74
Cations (based on 6 oxygens):															
Si	1.9708	1.9746	1.9665	1.9654	1.9655	1.9674	1.9712	1.9805	1.9801	1.9684	1.9692	1.9785	1.9700	1.9740	1.9744
Ti	0.0039	0.0036	0.0047	0.0031	0.0026	0.0031	0.0045	0.0046	0.0045	0.0051	0.0051	0.0027	0.0047	0.0046	0.0053
Al	0.0503	0.0514	0.0519	0.0500	0.0537	0.0472	0.0400	0.0485	0.0442	0.0479	0.0481	0.0483	0.0529	0.0495	0.0478
Cr	0.0120	0.0128	0.0133	0.0118	0.0116	0.0111	0.0109	0.0095	0.0079	0.0084	0.0086	0.0125	0.0126	0.0115	0.0113
Fe	0.3220	0.3244	0.3246	0.3878	0.3843	0.3768	0.4021	0.4058	0.4301	0.4503	0.4476	0.3749	0.3904	0.3804	0.3785
Mn	0.0069	0.0076	0.0072	0.0082	0.0080	0.0077	0.0075	0.0085	0.0076	0.0090	0.0091	0.0069	0.0076	0.0078	0.0077
Ni	0.0019	0.0019	0.0022	0.0017	0.0014	0.0028	0.0030	0.0018	0.0023	0.0026	0.0020	0.0017	0.0029	0.0036	0.0045
Mg	1.5633	1.5757	1.5659	1.5176	1.5000	1.5148	1.5159	1.3872	1.4254	1.4756	1.4601	1.5228	1.5010	1.4947	1.4896
Ca	0.0622	0.0370	0.0590	0.0537	0.0709	0.0684	0.0429	0.1366	0.0854	0.0299	0.0465	0.0398	0.0502	0.0640	0.0706
Na	0.0017	0.0013	0.0020	0.0020	0.0023	0.0023	0.0015	0.0055	0.0035	0.0022	0.0020	0.0002	0.0002	0.0020	0.0020
Total	3.9949	3.9903	3.9972	4.0015	4.0004	4.0015	3.9995	3.9886	3.9910	3.9994	3.9983	3.9885	3.9926	3.9920	3.9917
MMF	0.8292	0.8293	0.8283	0.7965	0.7960	0.8008	0.7903	0.7737	0.7682	0.7662	0.7654	0.8024	0.7936	0.7971	0.7974
Wo	3.2	1.9	3.0	2.7	3.6	3.5	2.2	7.1	4.4	1.5	2.4	2.1	2.6	3.3	3.6
En	80.3	81.3	80.3	77.5	76.7	77.3	77.3	71.9	73.4	75.4	74.7	78.6	77.3	77.1	76.8
Fs	16.5	16.7	16.7	19.8	19.7	19.2	20.5	21.0	22.2	23.0	22.9	19.3	20.1	19.6	19.5

MICROPROBE DATA TABLE C14: Composition of **orthopyroxene** in the Bastard Unit - profile **UA**.
Metres given above base of Unit.

Sample	UA-1	UA-1	UA-1	UA-1	UA-1	UA-2	UA-2	UA-2	UA-2	UA-2	UA-4	UA-4	UA-4	UA-4	UA-4	UA-6	UA-6	UA-6	UA-6	UA-6	UA-8	UA-8	UA-8	UA-8	UA-8	UA-9	UA-9
Metres	53.2	53.2	53.2	53.2	53.2	50.5	50.5	50.5	50.5	50.5	44.6	44.6	44.6	44.6	44.6	39.4	39.4	39.4	39.4	39.4	33.7	33.7	33.7	33.7	33.7	31.2	31.2
Wt. %																											
SiO_2	51.82	52.17	51.94	52.09	52.10	53.09	54.12	54.15	54.26	54.15	52.99	52.98	53.01	52.91	53.02	53.56	53.27	53.45	53.39	53.72	53.62	53.77	53.88	53.81	54.16	54.50	54.71
TiO_2	0.14	0.35	0.09	0.21	0.13	0.17	0.17	0.17	0.12	0.17	0.15	0.25	0.21	0.15	0.23	0.26	0.84	0.17	0.17	0.17	0.15	0.14	0.20	0.17	0.21	0.22	0.13
Al_2O_3	0.61	0.71	0.71	0.66	0.69	0.69	0.78	0.91	0.87	0.91	0.72	0.74	0.65	0.68	0.68	0.75	0.75	0.71	0.77	0.71	0.95	0.94	0.73	0.80	0.78	0.67	0.75
Cr_2O_3	0.00	0.07	0.09	0.07	0.05	0.03	0.18	0.22	0.20	0.22	0.08	0.12	0.09	0.11	0.11	0.12	0.12	0.12	0.11	0.11	0.25	0.25	0.15	0.18	0.16	0.04	0.13
FeO	25.03	21.20	23.91	23.42	23.76	22.27	18.85	17.75	18.18	17.75	20.04	19.15	19.40	18.68	19.58	19.39	19.09	18.86	19.11	19.45	15.99	16.25	17.20	16.64	16.94	17.79	17.16
MnO	0.50	0.37	0.45	0.44	0.44	0.48	0.37	0.37	0.30	0.37	0.48	0.40	0.36	0.37	0.39	0.37	0.37	0.38	0.36	0.37	0.39	0.34	0.39	0.33	0.33	0.36	0.36
NiO	0.06	0.06	0.05	0.07	0.03	0.07	0.02	0.02	0.04	0.02	0.08	0.03	0.05	0.05	0.04	0.06	0.09	0.07	0.03	0.04	0.04	0.01	0.04	0.04	0.01	0.05	0.08
MgO	19.85	22.81	20.94	21.27	20.98	21.68	23.91	23.69	24.38	23.69	23.94	24.75	24.88	24.23	24.77	23.97	24.03	23.66	23.85	24.00	25.50	25.46	25.87	25.50	26.03	24.25	24.63
CaO	1.27	1.13	0.74	0.87	0.68	0.92	1.14	2.38	1.58	2.38	0.83	0.84	0.60	2.08	0.72	1.17	1.54	1.60	1.21	0.87	1.80	2.17	0.88	1.54	0.96	1.28	1.89
Na_2O	0.02	0.03	0.01	0.00	0.00	0.00	0.01	0.02	0.02	0.02	0.02	0.02	0.01	0.02	0.00	0.01	0.04	0.00	0.00	0.01	0.03	0.04	0.02	0.03	0.01	0.00	0.01
Total	99.29	98.89	98.92	99.11	98.87	99.41	99.55	99.69	99.94	99.69	99.31	99.27	99.25	99.28	99.54	99.67	100.14	99.01	99.02	99.45	98.72	99.36	99.37	99.04	99.59	99.15	99.83
Cations (based on 6 oxygens):																											
Si	1.9767	1.9622	1.9750	1.9731	1.9791	1.9898	1.9915	1.9873	1.9850	1.9873	1.9701	1.9627	1.9647	1.9629	1.9618	1.9770	1.9593	1.9835	1.9810	1.9847	1.9720	1.9684	1.9734	1.9756	1.9754	2.0025	1.9950
Ti	0.0039	0.0098	0.0026	0.0060	0.0037	0.0049	0.0048	0.0046	0.0033	0.0046	0.0042	0.0071	0.0058	0.0042	0.0064	0.0072	0.0231	0.0048	0.0048	0.0047	0.0042	0.0039	0.0055	0.0047	0.0058	0.0060	0.0034
Al	0.0272	0.0314	0.0316	0.0296	0.0309	0.0306	0.0338	0.0395	0.0373	0.0395	0.0315	0.0322	0.0282	0.0299	0.0297	0.0326	0.0327	0.0311	0.0337	0.0307	0.0413	0.0406	0.0314	0.0348	0.0337	0.0289	0.0324
Cr	0.0000	0.0021	0.0026	0.0021	0.0016	0.0010	0.0053	0.0064	0.0057	0.0064	0.0023	0.0035	0.0025	0.0033	0.0033	0.0034	0.0035	0.0034	0.0032	0.0033	0.0073	0.0071	0.0043	0.0052	0.0046	0.0011	0.0037
Fe	0.7986	0.6669	0.7603	0.7418	0.7546	0.6980	0.5800	0.5448	0.5563	0.5448	0.6230	0.5934	0.6012	0.5794	0.6059	0.5984	0.5872	0.5853	0.5931	0.6008	0.4917	0.4973	0.5269	0.5109	0.5168	0.5465	0.5233
Mn	0.0160	0.0117	0.0143	0.0142	0.0140	0.0151	0.0116	0.0114	0.0094	0.0114	0.0151	0.0125	0.0112	0.0116	0.0122	0.0116	0.0115	0.0120	0.0115	0.0117	0.0120	0.0104	0.0122	0.0102	0.0102	0.0111	0.0111
Ni	0.0018	0.0019	0.0017	0.0022	0.0010	0.0022	0.0005	0.0005	0.0011	0.0005	0.0023	0.0008	0.0015	0.0016	0.0011	0.0018	0.0026	0.0019	0.0010	0.0013	0.0013	0.0004	0.0013	0.0011	0.0003	0.0013	0.0022
Mg	1.1285	1.2787	1.1867	1.2010	1.1880	1.2110	1.3117	1.2960	1.3295	1.2960	1.3267	1.3665	1.3747	1.3399	1.3662	1.3189	1.3175	1.3089	1.3192	1.3219	1.3977	1.3894	1.4126	1.3956	1.4150	1.3284	1.3385
Ca	0.0521	0.0454	0.0302	0.0351	0.0278	0.0370	0.0449	0.0936	0.0618	0.0936	0.0330	0.0331	0.0238	0.0828	0.0287	0.0464	0.0606	0.0637	0.0481	0.0343	0.0710	0.0850	0.0346	0.0605	0.0376	0.0505	0.0737
Na	0.0017	0.0022	0.0008	0.0000	0.0003	0.0000	0.0006	0.0017	0.0011	0.0017	0.0011	0.0013	0.0010	0.0012	0.0000	0.0009	0.0029	0.0001	0.0000	0.0005	0.0018	0.0028	0.0017	0.0021	0.0007	0.0000	0.0006
Total	4.0066	4.0123	4.0058	4.0050	4.0011	3.9895	3.9845	3.9860	3.9907	3.9860	4.0093	4.0131	4.0146	4.0169	4.0153	3.9983	4.0009	3.9946	3.9957	3.9938	4.0004	4.0053	4.0040	4.0007	4.0000	3.9765	3.9838
MMF	0.5856	0.6572	0.6095	0.6182	0.6116	0.6344	0.6934	0.7040	0.7050	0.7040	0.6805	0.6972	0.6957	0.6981	0.6928	0.6879	0.6917	0.6910	0.6899	0.6875	0.7398	0.7364	0.7283	0.7320	0.7325	0.7085	0.7189
Wo	2.6	2.3	1.5	1.8	1.4	1.9	2.3	4.8	3.2	4.8	1.7	1.7	1.2	4.1	1.4	2.4	3.1	3.3	2.5	1.8	3.6	4.3	1.8	3.1	1.9	2.6	3.8
En	57.0	64.2	60.0	60.7	60.3	62.2	67.7	67.0	68.3	67.0	66.9	68.6	68.7	66.9	68.3	67.2	67.0	66.9	67.3	67.5	71.3	70.5	71.6	71.0	71.9	69.0	69.2
Fs	40.4	33.5	38.5	37.5	38.3	35.9	29.9	28.2	28.6	28.2	31.4	29.8	30.1	28.9	30.3	30.5	29.9	29.9	30.3	30.7	25.1	25.2	26.7	26.0	26.2	28.4	27.0

Sample	UA-9	UA-9	UA-9	UA-11	UA-11	UA-11	UA-11	UA-11	UA-11	UA-12	UA-12	UA-12	UA-12	UA-12	UA-14	UA-14	UA-14	UA-16B	UA-16B	UA-16B	UA-16B	UA-16B	UA-17	UA-17	UA-17	UA-17	UA-17	UA-19
Metres	31.2	31.2	31.2	26.3	26.3	26.3	26.3	26.3	23.7	23.7	23.7	23.7	23.7	20.2	20.2	20.2	17.7	17.7	17.7	17.7	17.7	16.2	16.2	16.2	16.2	16.2	11.8
Wt. %																											
SiO_2	54.51	54.57	54.64	54.90	54.91	54.75	54.94	54.72	53.28	52.99	53.34	53.32	53.17	54.31	54.00	54.40	54.08	54.24	53.95	54.06	54.08	55.73	55.75	55.81	55.60	55.60	55.95
TiO_2	0.16	0.15	0.17	0.17	0.16	0.19	0.18	0.20	0.21	0.12	0.16	0.15	0.21	0.10	0.06	0.16	0.37	0.16	0.21	0.18	0.37	0.20	0.17	0.18	0.17	0.17	0.15
Al_2O_3	0.84	0.75	0.75	0.74	0.75	0.78	0.78	0.79	0.66	0.84	0.67	0.76	0.74	0.78	0.80	0.88	1.15	0.95	0.99	1.09	1.15	1.12	1.08	1.06	1.02	1.02	0.96
Cr_2O_3	0.17	0.15	0.11	0.16	0.16	0.16	0.16	0.15	0.11	0.11	0.13	0.11	0.13	0.15	0.14	0.18	0.38	0.29	0.32	0.34	0.38	0.38	0.38	0.36	0.34	0.34	0.38
FeO	16.86	17.35	17.32	17.10	17.27	17.54	16.82	17.12	19.59	20.71	19.69	19.40	20.05	18.73	19.00	18.27	14.52	15.20	15.12	14.96	14.52	12.78	13.00	13.08	13.10	13.10	12.17
MnO	0.39	0.40	0.42	0.33	0.36	0.41	0.37	0.34	0.41	0.48	0.44	0.39	0.45	0.44	0.45	0.43	0.28	0.30	0.28	0.32	0.28	0.25	0.31	0.28	0.28	0.28	0.27
NiO	0.08	0.05	0.06	0.11	0.07	0.03	0.02	0.02	0.03	0.03	0.04	0.03	0.04	0.05	0.03	0.01	0.08	0.05	0.08	0.08	0.08	0.15	0.09	0.10	0.09	0.09	0.12
MgO	24.77	25.29	24.90	25.37	25.60	25.45	25.46	25.00	24.14	23.65	24.17	23.67	24.02	24.93	24.86	25.31	27.25	27.94	27.25	27.27	27.25	28.64	28.56	28.78	28.30	28.30	29.19
CaO	2.05	1.00	1.33	1.09	0.70	0.95	0.99	1.60	0.56	0.55	1.27	1.78	0.79	0.36	0.37	0.46	1.69	0.79	1.33	1.58	1.69	0.69	0.95	0.70	1.32	1.32	0.45
Na_2O	0.01	0.01	0.01	0.00	0.02	0.00	0.00	0.01	0.01	0.01	0.02	0.04	0.00	0.00	0.00	0.00	0.04	0.02	0.04	0.04	0.04	0.03	0.03	0.01	0.03	0.03	0.00
Total	99.84	99.72	99.72	99.97	100.00	100.27	99.74	99.94	99.02	99.48	99.94	99.65	99.60	99.85	99.71	100.10	99.83	99.94	99.55	99.92	99.83	99.97	100.33	100.37	100.24	100.24	99.64
Cations (based on 6 oxygens):																											
Si	1.9874	1.9900	1.9936	1.9940	1.9930	1.9857	1.9962	1.9909	1.9790	1.9703	1.9691	1.9732	1.9699	1.9875	1.9825	1.9821	1.9535	1.9575	1.9576	1.9546	1.9535	1.9824	1.9800	1.9800	1.9793	1.9793	1.9890
Ti	0.0044	0.0040	0.0047	0.0047	0.0044	0.0052	0.0050	0.0053	0.0060	0.0034	0.0045	0.0040	0.0059	0.0027	0.0018	0.0044	0.0100	0.0044	0.0056	0.0050	0.0100	0.0053	0.0046	0.0048	0.0045	0.0045	0.0039
Al	0.0362	0.0323	0.0325	0.0317	0.0322	0.0333	0.0335	0.0337	0.0291	0.0369	0.0291	0.0332	0.0322	0.0338	0.0347	0.0378	0.0488	0.0403	0.0422	0.0465	0.0488	0.0471	0.0451	0.0445	0.0427	0.0427	0.0402
Cr	0.0050	0.0043	0.0032	0.0047	0.0046	0.0046	0.0047	0.0044	0.0033	0.0031	0.0038	0.0031	0.0037	0.0044	0.0041	0.0052	0.0108	0.0082	0.0091	0.0097	0.0108	0.0106	0.0107	0.0102	0.0096	0.0096	0.0107
Fe	0.5139	0.5291	0.5285	0.5195	0.5241	0.5324	0.5111	0.5208	0.6084	0.6439	0.6078	0.6003	0.6213	0.5731	0.5834	0.5566	0.4387	0.4587	0.4587	0.4522	0.4387	0.3803	0.3860	0.3880	0.3899	0.3899	0.3618
Mn	0.0121	0.0124	0.0129	0.0100	0.0110	0.0127	0.0114	0.0106	0.0130	0.0150	0.0139	0.0122	0.0142	0.0137	0.0140	0.0132	0.0086	0.0092	0.0085	0.0096	0.0086	0.0076	0.0093	0.0085	0.0084	0.0084	0.0082
Ni	0.0023	0.0015	0.0019	0.0031	0.0021	0.0008	0.0006	0.0007	0.0010	0.0009	0.0012	0.0009	0.0013	0.0015	0.0008	0.0003	0.0024	0.0013	0.0025	0.0023	0.0024	0.0042	0.0026	0.0028	0.0025	0.0025	0.0035
Mg	1.3460	1.3746	1.3544	1.3730	1.3849	1.3766	1.3786	1.3557	1.3362	1.3105	1.3297	1.3057	1.3267	1.3599	1.3606	1.3746	1.4672	1.5028	1.4738	1.4697	1.4672	1.5187	1.5120	1.5221	1.5018	1.5018	1.5470
Ca	0.0801	0.0390	0.0521	0.0425	0.0272	0.0368	0.0385	0.0623	0.0224	0.0217	0.0503	0.0707	0.0312	0.0140	0.0144	0.0179	0.0656	0.0306	0.0518	0.0614	0.0656	0.0262	0.0361	0.0266	0.0502	0.0502	0.0171
Na	0.0006	0.0008	0.0006	0.0000	0.0015	0.0001	0.0003	0.0004	0.0010	0.0010	0.0013	0.0027	0.0002	0.0000	0.0000	0.0000	0.0027	0.0017	0.0026	0.0028	0.0027	0.0021	0.0024	0.0009	0.0023	0.0023	0.0003
Total	3.9879	3.9880	3.9843	3.9831	3.9850	3.9892	3.9799	3.9849	3.9994	4.0068	4.0106	4.0060	4.0063	3.9907	3.9963	3.9920	4.0081	4.0147	4.0124	4.0138	4.0081	3.9845	3.9887	3.9883	3.9912	3.9912	3.9818
MMF	0.7237	0.7221	0.7193	0.7255	0.7255	0.7211	0.7295	0.7224	0.6871	0.6705	0.6863	0.6851	0.6811	0.7035	0.6999	0.7118	0.7698	0.7662	0.7626	0.7647	0.7698	0.7997	0.7966	0.7969	0.7939	0.7939	0.8105
Wo	4.1	2.0	2.7	2.2	1.4	1.9	2.0	3.2	1.1	1.1	2.5	3.6	1.6	0.7	0.7	0.9	3.3	1.5	2.6	3.1	3.3	1.4	1.9	1.4	2.6	2.6	0.9
En	69.4	70.8	70.0	71.0	71.5	70.7	71.5	69.9	67.9	66.3	66.9	66.1	67.0	69.8	69.5	70.5	74.4	75.4	74.3	74.1	74.4	78.9	78.2	78.6	77.3	77.3	80.3
Fs	26.5	27.2	27.3	26.8	27.1	27.4	26.5	26.9	30.9	32.6	30.6	30.4	31.4	29.4	29.8	28.6	22.3	23.0	23.1	22.8	22.3	19.8	20.0	20.0	20.1	20.1	18.8

MICROPROBE DATA TABLE C14: Composition of **orthopyroxene** in the Bastard Unit - profile **UA.**
Metres given above base of Unit.

Sample	UA-19	UA-19	UA-21	UA-21	UA-21	UA-23	UA-23	UA-23	UA-25	UA-25	UA-25	UA-27	UA-27	UA-27
Metres	11.8	11.8	8.5	8.5	8.5	5.1	5.1	5.1	1.9	1.9	1.9	0.05	0.05	0.05
Wt. %														
SiO_2	55.75	55.61	55.17	55.63	55.14	55.86	56.08	55.82	55.65	56.09	55.61	54.80	54.99	55.19
TiO_2	0.15	0.17	0.17	0.17	0.14	0.15	0.13	0.15	0.19	0.16	0.20	0.17	0.16	0.15
Al_2O_3	1.09	1.07	1.15	1.08	1.15	1.24	1.34	1.36	1.17	0.91	0.88	1.23	1.04	1.30
Cr_2O_3	0.45	0.45	0.50	0.42	0.47	0.46	0.50	0.54	0.36	0.34	0.30	0.41	0.31	0.43
FeO	12.29	11.81	11.21	11.52	11.43	11.13	11.61	11.44	12.14	12.05	12.28	12.28	12.86	12.94
MnO	0.27	0.25	0.19	0.25	0.27	0.23	0.23	0.25	0.26	0.25	0.24	0.20	0.22	0.25
NiO	0.06	0.09	0.17	0.09	0.13	0.09	0.11	0.07	0.15	0.08	0.11	0.09	0.08	0.10
MgO	28.95	28.81	29.23	30.08	29.68	29.13	29.97	29.27	28.57	28.95	29.20	28.42	29.24	29.09
CaO	0.59	1.00	1.85	0.77	0.97	1.26	0.58	1.33	1.02	1.23	0.58	1.89	0.54	0.62
Na_2O	0.00	0.01	0.04	0.03	0.02	0.01	0.01	0.03	0.04	0.04	0.02	0.03	0.02	0.00
Total	99.59	99.25	99.68	100.03	99.40	99.56	100.55	100.26	99.56	100.10	99.42	99.50	99.46	100.07
Cations (based on 6 oxygens):														
Si	1.9849	1.9853	1.9647	1.9690	1.9661	1.9829	1.9722	1.9721	1.9841	1.9881	1.9841	1.9638	1.9684	1.9648
Ti	0.0040	0.0045	0.0047	0.0045	0.0037	0.0039	0.0035	0.0040	0.0050	0.0041	0.0054	0.0047	0.0043	0.0040
Al	0.0457	0.0448	0.0482	0.0449	0.0485	0.0518	0.0554	0.0567	0.0491	0.0381	0.0370	0.0519	0.0440	0.0544
Cr	0.0128	0.0126	0.0141	0.0118	0.0132	0.0128	0.0138	0.0152	0.0103	0.0095	0.0084	0.0115	0.0088	0.0121
Fe	0.3659	0.3525	0.3340	0.3410	0.3408	0.3305	0.3415	0.3380	0.3618	0.3572	0.3665	0.3680	0.3851	0.3851
Mn	0.0080	0.0076	0.0058	0.0076	0.0080	0.0071	0.0068	0.0074	0.0079	0.0076	0.0073	0.0060	0.0068	0.0076
Ni	0.0018	0.0025	0.0048	0.0026	0.0038	0.0025	0.0030	0.0019	0.0044	0.0023	0.0033	0.0026	0.0023	0.0027
Mg	1.5362	1.5332	1.5516	1.5868	1.5775	1.5412	1.5711	1.5413	1.5182	1.5292	1.5529	1.5180	1.5604	1.5436
Ca	0.0225	0.0382	0.0704	0.0291	0.0370	0.0480	0.0219	0.0505	0.0391	0.0466	0.0221	0.0724	0.0206	0.0237
Na	0.0000	0.0005	0.0024	0.0017	0.0014	0.0006	0.0010	0.0017	0.0030	0.0025	0.0017	0.0019	0.0011	0.0000
Total	3.9818	3.9817	4.0007	3.9990	4.0000	3.9812	3.9902	3.9888	3.9828	3.9853	3.9887	4.0008	4.0015	3.9980
MMF	0.8076	0.8131	0.8229	0.8231	0.8224	0.8234	0.8214	0.8202	0.8075	0.8106	0.8091	0.8049	0.8021	0.8003
Wo	1.2	2.0	3.6	1.5	1.9	2.5	1.1	2.6	2.0	2.4	1.1	3.7	1.0	1.2
En	79.8	79.7	79.3	81.1	80.7	80.3	81.2	79.9	79.1	79.1	80.0	77.5	79.4	79.1
Fs	19.0	18.3	17.1	17.4	17.4	17.2	17.7	17.5	18.9	18.5	18.9	18.8	19.6	19.7

MICROPROBE DATA TABLE C15: Composition of **orthopyroxene** in the UG1 and UG2 Units - profile **UB**.
Metres given above the base of the UG1 chromitite.
c = core of grain m = grain margin.

Sample	235/31	235/31	235/31	235/31	235/31	235/34	235/34	235/34	235/34	235/34	235/34	235/34
Metres	18.7	18.7	18.7	18.7	18.7	12.5	12.5	12.5	12.5	12.5	12.5	12.5
Position	c	c	c	c	c	c	c	c	c	c	c	c
Wt.%												
SiO_2	55.99	55.31	56.26	55.73	55.97	55.15	54.56	54.96	54.88	55.42	55.47	55.39
TiO_2	0.13	0.12	0.08	0.12	0.12	0.17	0.17	0.14	0.16	0.15	0.17	0.19
Al_2O_3	1.18	1.30	0.75	1.20	1.21	1.26	1.20	1.19	1.10	0.92	0.97	0.86
Cr_2O_3	0.28	0.28	0.12	0.24	0.24	0.46	0.48	0.47	0.49	0.35	0.36	0.33
FeO	12.77	12.67	12.90	12.79	12.79	12.46	12.52	12.29	12.36	12.15	12.48	12.58
MnO	0.30	0.27	0.25	0.24	0.23	0.27	0.26	0.32	0.23	0.25	0.29	0.29
NiO	0.06	0.05	0.08	0.04	0.09	0.10	0.10	0.07	0.12	0.09	0.08	0.10
MgO	28.58	28.07	29.03	28.52	29.15	28.75	28.74	28.46	28.56	27.70	28.10	28.59
CaO	1.08	1.24	0.53	0.95	0.84	1.34	0.96	1.65	1.31	2.35	1.35	0.83
Na_2O	0.03	0.03	0.01	0.02	0.04	0.02	0.01	0.01	0.02	0.05	0.02	0.02
Total	100.38	99.34	100.00	99.85	100.69	99.98	98.99	99.56	99.23	99.43	99.29	99.17
Cations (based on 6 oxygens):												
Si	1.9836	1.9815	1.9972	1.9842	1.9765	1.9654	1.9638	1.9676	1.9700	1.9863	1.9877	1.9861
Ti	0.0035	0.0031	0.0021	0.0031	0.0033	0.0044	0.0047	0.0036	0.0043	0.0040	0.0047	0.0051
Al	0.0493	0.0549	0.0314	0.0505	0.0504	0.0530	0.0508	0.0501	0.0465	0.0388	0.0412	0.0364
Cr	0.0078	0.0081	0.0032	0.0067	0.0068	0.0131	0.0138	0.0133	0.0138	0.0099	0.0101	0.0093
Fe	0.3783	0.3795	0.3829	0.3809	0.3777	0.3714	0.3767	0.3680	0.3711	0.3643	0.3741	0.3773
Mn	0.0089	0.0083	0.0075	0.0071	0.0069	0.0081	0.0079	0.0096	0.0071	0.0076	0.0087	0.0088
Ni	0.0016	0.0013	0.0023	0.0012	0.0026	0.0028	0.0028	0.0021	0.0034	0.0026	0.0023	0.0028
Mg	1.5095	1.4987	1.5360	1.5136	1.5343	1.5272	1.5416	1.5189	1.5281	1.4800	1.5009	1.5279
Ca	0.0409	0.0475	0.0203	0.0362	0.0319	0.0510	0.0371	0.0632	0.0506	0.0901	0.0517	0.0318
Na	0.0017	0.0019	0.0009	0.0013	0.0026	0.0015	0.0004	0.0010	0.0013	0.0035	0.0015	0.0011
Total	3.9851	3.9849	3.9838	3.9847	3.9930	3.9979	3.9995	3.9975	3.9962	3.9871	3.9828	3.9865
MMF	0.7996	0.7979	0.8004	0.7989	0.8024	0.8044	0.8036	0.8050	0.8046	0.8025	0.8005	0.8020
Wo	2.1	2.5	1.0	1.9	1.6	2.6	1.9	3.2	2.6	4.7	2.7	1.6
En	78.3	77.8	79.2	78.4	78.9	78.3	78.8	77.9	78.4	76.5	77.9	78.9
Fs	19.6	19.7	19.7	19.7	19.4	19.1	19.3	18.9	19.0	18.8	19.4	19.5

Sample	235/37	235/37	235/37	235/37	235/37	235/37	235/37	235/37	235/37	235/37	235/37
Metres	1.5	1.5	1.5	1.5	1.5	1.5	1.5	1.5	1.5	1.5	1.5
Position	c	c	c	c	c	c	c	m	m	m	m
Wt.%											
SiO_2	55.48	55.62	55.36	54.52	54.91	55.04	54.42	54.39	54.68	54.90	54.65
TiO_2	0.13	0.11	0.08	0.18	0.21	0.17	0.15	0.20	0.20	0.21	0.19
Al_2O_3	1.15	0.74	1.46	1.18	0.91	0.97	1.22	0.84	0.95	0.84	0.86
Cr_2O_3	0.41	0.23	0.45	0.37	0.23	0.26	0.34	0.21	0.30	0.21	0.29
FeO	14.41	13.99	13.69	14.06	14.31	14.09	13.93	14.47	14.27	14.10	14.55
MnO	0.34	0.29	0.29	0.26	0.26	0.26	0.31	0.35	0.31	0.31	0.28
NiO	0.06	0.04	0.09	0.09	0.08	0.08	0.08	0.07	0.04	0.06	0.07
MgO	27.59	28.27	27.48	27.74	27.81	27.62	27.40	27.58	27.90	28.10	27.74
CaO	0.75	0.40	1.31	0.94	0.90	1.13	1.38	0.83	0.92	0.69	0.85
Na_2O	0.01	0.02	0.03	0.02	0.02	0.03	0.01	0.01	0.01	0.00	0.01
Total	100.33	99.72	100.23	99.37	99.65	99.66	99.24	98.94	99.57	99.43	99.49
Cations (based on 6 oxygens):											
Si	1.9814	1.9917	1.9760	1.9673	1.9764	1.9794	1.9678	1.9745	1.9704	1.9775	1.9732
Ti	0.0035	0.0029	0.0020	0.0050	0.0056	0.0047	0.0041	0.0054	0.0053	0.0056	0.0052
Al	0.0485	0.0313	0.0613	0.0503	0.0384	0.0411	0.0520	0.0359	0.0403	0.0356	0.0367
Cr	0.0117	0.0066	0.0126	0.0106	0.0065	0.0074	0.0097	0.0062	0.0085	0.0061	0.0082
Fe	0.4305	0.4189	0.4088	0.4243	0.4308	0.4238	0.4212	0.4392	0.4302	0.4248	0.4394
Mn	0.0101	0.0088	0.0086	0.0081	0.0080	0.0078	0.0095	0.0109	0.0096	0.0094	0.0085
Ni	0.0019	0.0011	0.0026	0.0026	0.0023	0.0023	0.0024	0.0019	0.0012	0.0018	0.0021
Mg	1.4686	1.5089	1.4620	1.4922	1.4921	1.4806	1.4767	1.4922	1.4987	1.5087	1.4928
Ca	0.0285	0.0154	0.0501	0.0364	0.0348	0.0436	0.0533	0.0324	0.0355	0.0265	0.0329
Na	0.0009	0.0016	0.0024	0.0013	0.0016	0.0022	0.0010	0.0008	0.0005	0.0002	0.0006
Total	3.9855	3.9872	3.9863	3.9980	3.9964	3.9928	3.9978	3.9994	4.0001	3.9962	3.9995
MMF	0.7733	0.7827	0.7815	0.7786	0.7760	0.7775	0.7781	0.7726	0.7770	0.7803	0.7726
Wo	1.5	0.8	2.6	1.9	1.8	2.2	2.7	1.7	1.8	1.4	1.7
En	76.2	77.6	76.1	76.4	76.2	76.0	75.7	76.0	76.3	77.0	76.0
Fs	22.3	21.6	21.3	21.7	22.0	21.8	21.6	22.4	21.9	21.7	22.4

MICROPROBE DATA TABLE C16: Composition of **orthopyroxene** in the Bastard Unit - profile **UC**.
Metres given above base of Unit.

Sample	UC-1	UC-1	UC-1	UC-1	UC-1	UC-3	UC-3	UC-3	UC-5	UC-5	UC-5	UC-7	UC-7	UC-7	UC-7	UC-7	UC-7	UC-7	UC-7	UC-11	UC-11	UC-11	UC-11	UC-11	UC-11	UC-11	UC-11	UC-12
Metres	30.8	30.8	30.8	30.8	30.8	28.5	28.5	28.5	24.0	24.0	24.0	21.5	21.5	21.5	21.5	21.5	21.5	21.5	21.5	14.7	14.7	14.7	14.7	14.7	14.7	14.7	14.7	13.3
Position	c = core	c	c	c	c	c	c	c	c	c	c	c	c	c	c	c	c	c	c	c	c	c	c	m = margin	m	m	m	c
Wt. %																												
SiO_2	53.20	52.98	52.81	52.72	52.62	53.32	52.91	52.84	53.98	54.40	53.81	54.24	54.01	53.64	53.84	54.10	54.01	54.27	55.89	56.02	56.22	56.27	56.14	55.71	55.92	56.16	56.05
TiO_2	0.17	0.21	0.21	0.20	0.22	0.17	0.16	0.22	0.06	0.14	0.11	0.14	0.12	0.15	0.10	0.12	0.09	0.11	0.08	0.06	0.08	0.07	0.07	0.06	0.07	0.08	0.08
Al_2O_3	0.95	0.85	0.87	0.80	0.96	0.90	0.93	0.88	0.66	0.68	0.72	0.90	0.85	0.82	0.77	0.87	0.87	0.82	1.33	1.35	1.28	1.25	1.37	1.44	1.37	1.39	1.26
Cr_2O_3	0.18	0.16	0.18	0.16	0.19	0.14	0.16	0.17	0.06	0.11	0.13	0.25	0.24	0.25	0.23	0.26	0.23	0.24	0.25	0.23	0.24	0.24	0.20	0.25	0.23	0.20	0.38
FeO	19.92	19.94	20.14	19.86	20.10	22.72	22.02	22.27	20.62	20.18	19.88	16.79	17.22	18.03	17.70	17.70	18.01	18.71	11.05	10.94	10.45	10.95	11.46	11.03	10.69	10.65	11.32
MnO	0.33	0.35	0.34	0.36	0.34	0.41	0.33	0.39	0.36	0.37	0.34	0.35	0.38	0.42	0.39	0.36	0.38	0.43	0.28	0.32	0.34	0.36	0.34	0.30	0.32	0.29	0.25
NiO	0.00	0.06	0.06	0.05	0.05	0.03	0.06	0.03	0.04	0.05	0.08	0.02	0.02	0.01	0.05	0.01	0.05	0.05	0.02	0.06	0.02	0.06	0.03	0.05	0.02	0.01	0.06
MgO	22.49	22.72	22.98	22.82	22.57	19.94	20.26	20.22	23.23	23.71	23.36	25.48	25.56	24.90	25.41	25.58	24.75	24.41	29.92	30.01	29.70	29.77	29.97	30.34	29.94	29.80	29.35
CaO	1.83	2.02	1.69	2.01	1.96	1.76	1.69	1.98	0.45	0.59	0.82	0.88	0.71	0.72	0.51	0.78	0.63	0.75	0.82	0.74	0.95	0.89	0.72	0.60	0.74	0.72	1.12
Na_2O	0.03	0.04	0.02	0.02	0.03	0.03	0.02	0.03	0.01	0.00	0.02	0.01	0.01	0.02	0.01	0.02	0.02	0.01	0.01	0.00	0.00	0.01	0.00	0.00	0.00	0.00	0.01
Total	99.10	99.32	99.30	99.01	99.04	99.43	98.55	99.03	99.46	100.24	99.26	99.05	99.13	98.96	99.01	99.79	99.04	99.80	99.65	99.74	99.27	99.86	100.31	99.76	99.30	99.30	99.88
Cations (based on 6 oxygens):																												
Si	1.9826	1.9739	1.9687	1.9708	1.9684	2.0036	2.0006	1.9937	1.9995	1.9958	1.9943	1.9862	1.9807	1.9793	1.9810	1.9755	1.9886	1.9893	1.9781	1.9795	1.9908	1.9862	1.9768	1.9694	1.9820	1.9881	1.9829
Ti	0.0048	0.0058	0.0059	0.0057	0.0061	0.0048	0.0046	0.0062	0.0017	0.0038	0.0031	0.0037	0.0034	0.0043	0.0029	0.0033	0.0025	0.0030	0.0021	0.0016	0.0021	0.0019	0.0020	0.0015	0.0018	0.0022	0.0022
Al	0.0417	0.0373	0.0383	0.0354	0.0424	0.0400	0.0415	0.0392	0.0289	0.0293	0.0313	0.0388	0.0370	0.0357	0.0335	0.0374	0.0375	0.0355	0.0556	0.0561	0.0536	0.0520	0.0567	0.0602	0.0574	0.0578	0.0527
Cr	0.0054	0.0046	0.0052	0.0049	0.0056	0.0042	0.0049	0.0051	0.0017	0.0032	0.0039	0.0072	0.0070	0.0072	0.0066	0.0074	0.0066	0.0069	0.0070	0.0065	0.0067	0.0067	0.0056	0.0069	0.0063	0.0057	0.0107
Fe	0.6207	0.6212	0.6279	0.6208	0.6287	0.7140	0.6965	0.7025	0.6388	0.6193	0.6162	0.5142	0.5282	0.5565	0.5446	0.5405	0.5546	0.5736	0.3271	0.3233	0.3094	0.3231	0.3375	0.3260	0.3169	0.3153	0.3350
Mn	0.0105	0.0109	0.0107	0.0114	0.0109	0.0132	0.0107	0.0124	0.0112	0.0114	0.0106	0.0107	0.0117	0.0132	0.0121	0.0111	0.0119	0.0134	0.0085	0.0095	0.0101	0.0106	0.0102	0.0089	0.0096	0.0088	0.0074
Ni	0.0000	0.0018	0.0019	0.0014	0.0016	0.0009	0.0017	0.0010	0.0013	0.0015	0.0022	0.0005	0.0005	0.0003	0.0014	0.0004	0.0016	0.0015	0.0006	0.0018	0.0006	0.0017	0.0009	0.0013	0.0005	0.0002	0.0016
Mg	1.2492	1.2618	1.2769	1.2714	1.2584	1.1169	1.1417	1.1369	1.2824	1.2966	1.2903	1.3905	1.3971	1.3695	1.3933	1.3921	1.3582	1.3338	1.5782	1.5809	1.5677	1.5661	1.5731	1.5988	1.5816	1.5726	1.5476
Ca	0.0730	0.0805	0.0676	0.0807	0.0784	0.0708	0.0686	0.0798	0.0177	0.0233	0.0325	0.0345	0.0280	0.0284	0.0203	0.0303	0.0248	0.0293	0.0310	0.0282	0.0360	0.0338	0.0273	0.0228	0.0282	0.0274	0.0426
Na	0.0023	0.0028	0.0012	0.0018	0.0019	0.0020	0.0012	0.0024	0.0004	0.0002	0.0012	0.0010	0.0007	0.0012	0.0007	0.0012	0.0012	0.0006	0.0006	0.0003	0.0000	0.0007	0.0003	0.0000	0.0000	0.0000	0.0007
Total	3.9902	4.0007	4.0042	4.0043	4.0025	3.9704	3.9721	3.9792	3.9837	3.9843	3.9856	3.9875	3.9943	3.9956	3.9964	3.9994	3.9875	3.9868	3.9888	3.9878	3.9770	3.9829	3.9903	3.9956	3.9843	3.9780	3.9835
MMF	0.6680	0.6701	0.6704	0.6719	0.6668	0.6100	0.6211	0.6181	0.6675	0.6768	0.6768	0.7301	0.7257	0.7111	0.7190	0.7203	0.7101	0.6993	0.8283	0.8302	0.8351	0.8290	0.8234	0.8306	0.8331	0.8330	0.8221
Wo	3.8	4.1	3.4	4.1	4.0	3.7	3.6	4.2	0.9	1.2	1.7	1.8	1.4	1.5	1.0	1.5	1.3	1.5	1.6	1.5	1.9	1.8	1.4	1.2	1.5	1.4	2.2
En	64.3	64.3	64.7	64.4	64.0	58.7	59.9	59.2	66.1	66.9	66.5	71.7	71.5	70.1	71.2	70.9	70.1	68.9	81.5	81.8	81.9	81.4	81.2	82.1	82.1	82.1	80.4
Fs	31.9	31.6	31.8	31.5	32.0	37.5	36.5	36.6	32.9	31.9	31.8	26.5	27.0	28.5	27.8	27.5	28.6	29.6	16.9	16.7	16.2	16.8	17.4	16.7	16.4	16.5	17.4

Sample	UC-12	UC-12	UC-12	UC-12	UC-12	UC-12	UC-13	UC-13	UC-13	UC-13	UC-13	UC-13	UC-13	UC-13	UC-13	UC-13	UC-13	UC-14	UC-14	UC-14	UC-14	UC-14	UC-14	UC-14	UC-14	UC-14	UC-14	UC-14	UC-14
Metres	13.3	13.3	13.3	13.3	13.3	13.3	11.1	11.1	11.1	11.1	11.1	11.1	11.1	11.1	11.1	11.1	11.1	9.0	9.0	9.0	9.0	9.0	9.0	9.0	9.0	9.0	9.0	9.0	9.0
Position	c	c	m	m	m	m	c	c	c	c	c	c	c	m	m	m	c	c	c	c	c	c	c	c	m	m	m	m	m
Wt. %																													
SiO_2	56.07	56.18	55.68	56.20	56.60	56.26	55.24	55.50	55.17	55.23	55.00	55.22	55.09	55.09	55.00	55.10	56.54	56.85	56.24	56.07	56.20	56.42	56.50	55.74	56.47	56.36	56.56
TiO_2	0.08	0.10	0.10	0.11	0.07	0.06	0.07	0.09	0.07	0.04	0.08	0.06	0.08	0.04	0.04	0.03	0.09	0.07	0.06	0.07	0.05	0.07	0.06	0.08	0.08	0.09	0.08
Al_2O_3	1.30	1.34	1.18	1.26	1.00	1.22	1.36	1.37	1.47	1.44	1.38	1.43	1.41	1.39	1.39	1.26	1.26	1.26	1.30	1.33	1.34	1.37	1.27	1.57	1.21	1.32	1.19
Cr_2O_3	0.38	0.39	0.37	0.40	0.31	0.38	0.22	0.26	0.20	0.24	0.22	0.22	0.24	0.18	0.16	0.16	0.35	0.36	0.40	0.40	0.36	0.36	0.36	0.35	0.41	0.39	0.41
FeO	11.37	11.28	11.62	11.75	11.56	11.56	11.55	11.85	11.48	11.83	11.71	11.84	11.86	11.93	11.68	12.05	11.08	11.03	11.00	10.91	10.91	10.89	10.66	11.10	10.91	11.17	10.99
MnO	0.28	0.25	0.29	0.28	0.29	0.27	0.21	0.24	0.23	0.20	0.23	0.27	0.23	0.21	0.23	0.29	0.28	0.24	0.23	0.24	0.27	0.27	0.21	0.24	0.26	0.26	0.27
NiO	0.06	0.10	0.09	0.09	0.06	0.06	0.06	0.07	0.05	0.06	0.04	0.00	0.04	0.08	0.10	0.03	0.08	0.09	0.08	0.06	0.07	0.04	0.05	0.07	0.04	0.04	0.05
MgO	29.56	29.43	29.57	29.48	29.73	29.69	29.79	29.96	30.05	30.16	29.88	30.02	29.81	29.98	30.06	30.12	29.84	30.14	30.01	30.02	29.97	30.06	29.51	30.14	30.37	30.13	30.49
CaO	0.83	1.16	0.71	0.86	0.52	0.58	0.84	0.88	0.60	0.60	0.76	0.74	0.87	0.56	0.66	0.55	1.06	1.06	0.79	1.11	0.96	1.02	1.69	0.76	0.54	0.55	0.66
Na_2O	0.00	0.00	0.01	0.01	0.02	0.00	0.02	0.03	0.03	0.01	0.03	0.02	0.02	0.02	0.02	0.04	0.01	0.02	0.02	0.02	0.01	0.02	0.02	0.00	0.01	0.02	0.02
Total	99.93	100.22	99.63	100.45	100.15	100.08	99.35	100.24	99.35	99.80	99.33	99.83	99.65	99.49	99.35	99.62	100.59	101.11	100.13	100.24	100.13	100.52	100.32	100.04	100.29	100.31	100.73
Cations (based on 6 oxygens):																												
Si	1.9818	1.9809	1.9777	1.9803	1.9944	1.9854	1.9677	1.9629	1.9638	1.9600	1.9618	1.9604	1.9604	1.9625	1.9608	1.9618	1.9831	1.9827	1.9802	1.9742	1.9791	1.9787	1.9859	1.9666	1.9824	1.9805	1.9790
Ti	0.0022	0.0025	0.0028	0.0028	0.0017	0.0017	0.0017	0.0024	0.0019	0.0010	0.0022	0.0016	0.0022	0.0011	0.0011	0.0007	0.0024	0.0019	0.0016	0.0019	0.0013	0.0019	0.0016	0.0021	0.0021	0.0023	0.0022
Al	0.0543	0.0558	0.0494	0.0524	0.0414	0.0505	0.0569	0.0571	0.0616	0.0604	0.0580	0.0598	0.0590	0.0582	0.0585	0.0528	0.0523	0.0519	0.0539	0.0552	0.0556	0.0566	0.0527	0.0652	0.0501	0.0546	0.0492
Cr	0.0106	0.0108	0.0105	0.0111	0.0087	0.0105	0.0061	0.0072	0.0056	0.0067	0.0061	0.0062	0.0066	0.0051	0.0046	0.0045	0.0097	0.0100	0.0111	0.0110	0.0101	0.0101	0.0101	0.0096	0.0113	0.0109	0.0114
Fe	0.3360	0.3325	0.3451	0.3462	0.3405	0.3411	0.3442	0.3504	0.3418	0.3510	0.3492	0.3515	0.3531	0.3555	0.3482	0.3588	0.3250	0.3217	0.3239	0.3212	0.3212	0.3193	0.3132	0.3276	0.3202	0.3283	0.3217
Mn	0.0083	0.0075	0.0088	0.0085	0.0088	0.0080	0.0062	0.0071	0.0070	0.0059	0.0071	0.0080	0.0069	0.0063	0.0070	0.0087	0.0083	0.0069	0.0069	0.0072	0.0081	0.0080	0.0062	0.0071	0.0077	0.0076	0.0079
Ni	0.0016	0.0029	0.0027	0.0026	0.0017	0.0016	0.0017	0.0020	0.0013	0.0017	0.0011	0.0001	0.0012	0.0024	0.0027	0.0008	0.0021	0.0025	0.0024	0.0017	0.0020	0.0013	0.0013	0.0020	0.0011	0.0010	0.0013
Mg	1.5574	1.5467	1.5654	1.5484	1.5614	1.5614	1.5817	1.5791	1.5942	1.5956	1.5884	1.5882	1.5810	1.5916	1.5975	1.5983	1.5600	1.5666	1.5753	1.5757	1.5729	1.5714	1.5459	1.5849	1.5892	1.5781	1.5900
Ca	0.0313	0.0437	0.0269	0.0325	0.0196	0.0221	0.0321	0.0333	0.0227	0.0228	0.0289	0.0283	0.0332	0.0215	0.0254	0.0211	0.0400	0.0395	0.0300	0.0421	0.0362	0.0384	0.0637	0.0287	0.0205	0.0207	0.0248
Na	0.0000	0.0000	0.0007	0.0008	0.0011	0.0002	0.0012	0.0023	0.0018	0.0008	0.0022	0.0015	0.0017	0.0017	0.0014	0.0026	0.0007	0.0014	0.0010	0.0013	0.0005	0.0011	0.0013	0.0003	0.0006	0.0013	0.0017
Total	3.9836	3.9833	3.9899	3.9855	3.9793	3.9825	3.9996	4.0037	4.0017	4.0059	4.0050	4.0057	4.0054	4.0057	4.0072	4.0102	3.9838	3.9851	3.9863	3.9914	3.9871	3.9867	3.9818	3.9940	3.9851	3.9852	3.9893
MMF	0.8225	0.8230	0.8194	0.8173	0.8210	0.8207	0.8213	0.8184	0.8234	0.8197	0.8198	0.8188	0.8174	0.8174	0.8211	0.8167	0.8276	0.8296	0.8294	0.8307	0.8304	0.8311	0.8315	0.8287	0.8323	0.8278	0.8317
Wo	1.6	2.3	1.4	1.7	1.0	1.1	1.6	1.7	1.2	1.2	1.5	1.4	1.7	1.1	1.3	1.1	2.1	2.0	1.6	2.2	1.9	2.0	3.3	1.5	1.1	1.1	1.3
En	80.9	80.4	80.8	80.3	81.3	81.1	80.8	80.5	81.4	81.0	80.8	80.7	80.4	80.8	81.0	80.8	81.0	81.3	81.7	81.3	81.5	81.5	80.4	81.6	82.3	81.9	82.1
Fs	17.5	17.3	17.8	18.0	17.7	17.7	17.6	17.9	17.5	17.8	17.8	17.9	17.9	18.1	17.7	18.1	16.9	16.7	16.8	16.6	16.6	16.6	16.3	16.9	16.6	17.0	16.6

MICROPROBE DATA TABLE C16: Composition of **orthopyroxene** in the Bastard Unit - profile UC.
Metres given above base of Unit.

Sample	UC-15	UC-15	UC-15	UC-15	UC-16	UC-16	UC-16	UC-16	UC-17	UC-17	UC-17	UC-17	UC-17	UC-17	UC-17	UC-17	UC-18	UC-18	UC-18	UC-18	UC-18	UC-18m	UC-18m	UC-18m	UC-19	UC-19	UC-19
Metres	7.4	7.4	7.4	7.4	5.3	5.3	5.3	5.3	4.1	4.1	4.1	4.1	4.1	4.1	4.1	4.1	2.3	2.3	2.3	2.3	2.3	2.3	2.3	2.3	0.6	0.6	0.6
Position	c	c	c	c	c	c	c	c	c	c	c	c	c	m	m	m	c	c	c	c	c	m	m	m	c	c	c
Wt. %																											
SiO_2	55.81	55.89	55.67	55.94	56.26	56.30	56.41	56.04	56.05	55.97	55.89	55.94	55.88	56.36	56.31	55.67	55.23	55.37	55.55	54.88	56.31	55.53	56.08	55.85	55.89	55.80	55.38
TiO_2	0.14	0.15	0.14	0.15	0.13	0.11	0.11	0.11	0.12	0.16	0.14	0.16	0.16	0.10	0.12	0.12	0.16	0.18	0.15	0.13	0.17	0.20	0.15	0.20	0.19	0.16	0.19
Al_2O_3	1.11	1.22	1.26	1.15	1.49	1.42	1.45	1.56	1.31	1.34	1.32	1.36	1.38	1.14	1.17	1.15	1.13	0.92	1.21	1.29	0.83	0.82	0.87	0.81	0.91	1.12	1.07
Cr_2O_3	0.41	0.39	0.44	0.44	0.38	0.38	0.42	0.39	0.44	0.43	0.35	0.42	0.42	0.37	0.34	0.38	0.44	0.26	0.39	0.41	0.26	0.29	0.30	0.30	0.27	0.35	0.34
FeO	11.22	11.51	11.63	11.33	11.00	11.06	10.81	10.83	10.55	10.96	11.31	11.27	11.42	11.18	11.43	11.46	11.93	12.42	12.04	12.46	12.24	13.25	12.79	12.46	12.70	12.32	12.13
MnO	0.23	0.21	0.23	0.28	0.25	0.24	0.24	0.24	0.20	0.24	0.24	0.28	0.24	0.24	0.24	0.25	0.25	0.26	0.25	0.30	0.29	0.29	0.28	0.27	0.30	0.25	0.29
NiO	0.06	0.06	0.08	0.07	0.05	0.07	0.03	0.01	0.08	0.08	0.08	0.10	0.10	0.06	0.07	0.08	0.11	0.12	0.10	0.12	0.07	0.05	0.09	0.05	0.12	0.10	0.07
MgO	30.13	30.41	30.36	30.32	29.78	29.93	29.97	29.82	29.24	29.38	29.48	29.29	29.25	30.11	30.08	29.33	27.94	28.32	28.06	27.94	28.91	27.98	28.47	28.24	28.78	28.56	28.61
CaO	1.11	1.08	0.69	1.02	1.00	0.86	1.02	0.97	1.43	1.01	0.91	1.12	1.13	0.66	0.59	0.50	1.90	1.37	1.95	1.12	0.56	0.65	0.49	0.60	0.42	0.92	1.08
Na_2O	0.01	0.01	0.00	0.00	0.01	0.02	0.01	0.02	0.01	0.01	0.00	0.02	0.00	0.02	0.00	0.00	0.02	0.02	0.04	0.00	0.01	0.00	0.00	0.01	0.00	0.00	0.02
Total	100.23	100.93	100.50	100.71	100.34	100.39	100.48	99.99	99.44	99.58	99.72	99.95	99.98	100.23	100.36	98.94	99.12	99.24	99.74	98.64	99.64	99.05	99.52	98.79	99.56	99.58	99.18
Cations (based on 6 oxygens):																											
Si	1.9695	1.9614	1.9616	1.9660	1.9774	1.9778	1.9783	1.9753	1.9864	1.9827	1.9799	1.9788	1.9769	1.9831	1.9808	1.9868	1.9819	1.9851	1.9812	1.9796	2.0005	1.9961	1.9999	2.0040	1.9925	1.9884	1.9825
Ti	0.0036	0.0039	0.0037	0.0040	0.0034	0.0029	0.0029	0.0028	0.0031	0.0042	0.0038	0.0041	0.0042	0.0026	0.0032	0.0032	0.0043	0.0048	0.0039	0.0035	0.0046	0.0053	0.0040	0.0054	0.0051	0.0043	0.0051
Al	0.0461	0.0506	0.0522	0.0476	0.0616	0.0590	0.0597	0.0646	0.0546	0.0558	0.0550	0.0567	0.0577	0.0473	0.0487	0.0485	0.0479	0.0388	0.0507	0.0547	0.0346	0.0347	0.0365	0.0341	0.0384	0.0469	0.0450
Cr	0.0116	0.0108	0.0123	0.0123	0.0105	0.0106	0.0117	0.0109	0.0123	0.0120	0.0099	0.0117	0.0117	0.0104	0.0094	0.0107	0.0125	0.0075	0.0110	0.0117	0.0073	0.0082	0.0084	0.0085	0.0075	0.0098	0.0097
Fe	0.3310	0.3378	0.3426	0.3331	0.3235	0.3249	0.3171	0.3192	0.3127	0.3247	0.3350	0.3335	0.3378	0.3289	0.3363	0.3419	0.3580	0.3723	0.3590	0.3760	0.3637	0.3983	0.3814	0.3739	0.3786	0.3670	0.3632
Mn	0.0070	0.0062	0.0069	0.0083	0.0074	0.0071	0.0071	0.0073	0.0061	0.0073	0.0072	0.0083	0.0073	0.0070	0.0071	0.0076	0.0075	0.0079	0.0075	0.0091	0.0086	0.0088	0.0084	0.0082	0.0089	0.0075	0.0087
Ni	0.0017	0.0016	0.0022	0.0020	0.0014	0.0020	0.0009	0.0003	0.0023	0.0021	0.0022	0.0028	0.0028	0.0016	0.0021	0.0022	0.0033	0.0035	0.0030	0.0035	0.0019	0.0015	0.0024	0.0015	0.0033	0.0029	0.0020
Mg	1.5850	1.5907	1.5947	1.5881	1.5600	1.5673	1.5666	1.5666	1.5446	1.5513	1.5563	1.5440	1.5427	1.5794	1.5770	1.5603	1.4945	1.5136	1.4918	1.5022	1.5311	1.4993	1.5135	1.5100	1.5292	1.5169	1.5266
Ca	0.0419	0.0405	0.0262	0.0386	0.0377	0.0323	0.0383	0.0365	0.0543	0.0385	0.0345	0.0423	0.0430	0.0248	0.0222	0.0192	0.0730	0.0528	0.0745	0.0431	0.0214	0.0249	0.0189	0.0231	0.0159	0.0353	0.0416
Na	0.0008	0.0009	0.0002	0.0003	0.0004	0.0010	0.0009	0.0013	0.0009	0.0008	0.0002	0.0010	0.0000	0.0010	0.0000	0.0000	0.0013	0.0011	0.0030	0.0002	0.0006	0.0000	0.0002	0.0008	0.0000	0.0000	0.0011
Total	3.9983	4.0044	4.0026	4.0002	3.9833	3.9850	3.9835	3.9848	3.9774	3.9795	3.9840	3.9834	3.9842	3.9860	3.9869	3.9804	3.9842	3.9874	3.9856	3.9838	3.9743	3.9771	3.9737	3.9697	3.9795	3.9789	3.9856
MMF	0.8272	0.8248	0.8232	0.8266	0.8283	0.8283	0.8316	0.8307	0.8317	0.8269	0.8229	0.8224	0.8203	0.8276	0.8242	0.8203	0.8067	0.8026	0.8060	0.7998	0.8080	0.7901	0.7987	0.8015	0.8015	0.8052	0.8078
Wo	2.1	2.1	1.3	2.0	2.0	1.7	2.0	1.9	2.8	2.0	1.8	2.2	2.2	1.3	1.1	1.0	3.8	2.7	3.9	2.2	1.1	1.3	1.0	1.2	0.8	1.8	2.2
En	81.0	80.8	81.2	81.0	81.2	81.4	81.5	81.5	80.8	81.0	80.8	80.4	80.2	81.7	81.5	81.2	77.6	78.1	77.5	78.2	79.9	78.0	79.1	79.2	79.5	79.0	79.0
Fs	16.9	17.2	17.4	17.0	16.8	16.9	16.5	16.6	16.4	17.0	17.4	17.4	17.6	17.0	17.4	17.8	18.6	19.2	18.6	19.6	19.0	20.7	19.9	19.6	19.7	19.1	18.8

Sample	UC-19	UC-19	UC-20	UC-20	UC-20	UC-20	UC-20	UC-20	UC-20	UC-20	UC-20	UC-20	UC-20	UC-20	UC-20
Metres	0.6	0.6	0.1	0.1	0.1	0.1	0.1	0.1	0.1	0.1	0.1	0.1	0.1	0.1	0.1
Position	c	c	c	c	c	c	c	c	c	c	m	m	m	m	m
Wt. %															
SiO_2	55.73	55.68	54.99	55.18	55.82	55.64	55.66	55.82	55.30	54.91	55.97	55.81	55.63	55.84	55.74
TiO_2	0.20	0.21	0.10	0.13	0.21	0.36	0.18	0.21	0.18	0.16	0.18	0.20	0.15	0.17	0.15
Al_2O_3	1.16	1.22	1.36	1.34	0.95	1.13	1.18	1.04	1.20	0.90	1.21	1.00	1.24	1.05	1.14
Cr_2O_3	0.34	0.34	0.43	0.37	0.40	0.47	0.51	0.39	0.40	0.37	0.44	0.41	0.39	0.41	0.36
FeO	11.98	12.22	12.43	11.56	12.38	11.77	11.16	12.17	12.05	12.44	12.84	12.53	12.66	12.40	12.04
MnO	0.29	0.24	0.27	0.26	0.30	0.29	0.21	0.27	0.24	0.18	0.26	0.32	0.24	0.28	0.26
NiO	0.09	0.13	0.10	0.09	0.11	0.11	0.13	0.11	0.08	0.08	0.05	0.07	0.06	0.06	0.07
MgO	28.15	28.46	28.92	27.27	29.29	28.58	27.58	29.10	28.87	29.24	28.99	28.93	28.66	29.19	29.20
CaO	1.21	0.96	0.58	3.22	0.72	1.64	3.33	0.95	0.70	0.51	0.70	0.66	0.88	0.55	0.55
Na_2O	0.01	0.01	0.00	0.07	0.01	0.03	0.05	0.02	0.02	0.01	0.01	0.01	0.01	0.01	0.02
Total	99.16	99.47	99.18	99.48	100.20	100.02	99.99	100.08	99.06	98.81	100.64	99.95	99.90	99.96	99.53
Cations (based on 6 oxygens):															
Si	1.9925	1.9860	1.9701	1.9768	1.9787	1.9760	1.9805	1.9798	1.9794	1.9746	1.9774	1.9835	1.9792	1.9819	1.9832
Ti	0.0055	0.0057	0.0027	0.0036	0.0057	0.0097	0.0048	0.0056	0.0048	0.0044	0.0048	0.0053	0.0040	0.0046	0.0041
Al	0.0489	0.0511	0.0576	0.0564	0.0398	0.0474	0.0496	0.0436	0.0506	0.0381	0.0505	0.0420	0.0519	0.0440	0.0480
Cr	0.0096	0.0096	0.0123	0.0104	0.0112	0.0133	0.0144	0.0111	0.0114	0.0105	0.0122	0.0116	0.0109	0.0116	0.0102
Fe	0.3582	0.3646	0.3725	0.3462	0.3672	0.3495	0.3320	0.3610	0.3607	0.3741	0.3793	0.3725	0.3766	0.3681	0.3583
Mn	0.0087	0.0072	0.0081	0.0079	0.0089	0.0087	0.0063	0.0081	0.0074	0.0054	0.0078	0.0096	0.0072	0.0083	0.0080
Ni	0.0027	0.0039	0.0028	0.0026	0.0030	0.0032	0.0039	0.0031	0.0024	0.0024	0.0013	0.0020	0.0019	0.0018	0.0019
Mg	1.5001	1.5132	1.5441	1.4562	1.5476	1.5128	1.4626	1.5381	1.5404	1.5671	1.5263	1.5325	1.5199	1.5444	1.5484
Ca	0.0464	0.0366	0.0222	0.1237	0.0275	0.0623	0.1270	0.0360	0.0269	0.0198	0.0263	0.0249	0.0335	0.0211	0.0209
Na	0.0006	0.0005	0.0000	0.0049	0.0007	0.0018	0.0035	0.0017	0.0016	0.0008	0.0010	0.0004	0.0003	0.0004	0.0013
Total	3.9731	3.9783	3.9922	3.9887	3.9904	3.9848	3.9844	3.9881	3.9856	3.9971	3.9869	3.9845	3.9855	3.9860	3.9843
MMF	0.8073	0.8058	0.8057	0.8079	0.8083	0.8123	0.8150	0.8099	0.8103	0.8073	0.8010	0.8045	0.8014	0.8075	0.8121
Wo	2.4	1.9	1.1	6.4	1.4	3.2	6.6	1.9	1.4	1.0	1.4	1.3	1.7	1.1	1.1
En	78.8	79.0	79.6	75.6	79.7	78.6	76.1	79.5	79.9	79.9	79.0	79.4	78.8	79.9	80.3
Fs	18.8	19.0	19.2	18.0	18.9	18.2	17.3	18.7	18.7	19.1	19.6	19.3	19.5	19.0	18.6

MICROPROBE DATA TABLE C17: Composition of **clinopyroxene** in the Bastard Unit - profile **UC**.
Metres given above base of Unit.

Sample	UC-1	UC-1	UC-1	UC-1	UC-3	UC-3	UC-5	UC-5	UC-5	UC-7	UC-7	UC-7	UC-13	UC-13	UC-13	UC-13	UC-20	UC-20	UC-20	UC-20
Metres	30.8	30.8	30.8	30.8	28.5	28.5	24.0	24.0	24.0	21.5	21.5	21.5	11.1	11.1	11.1	11.1	0.1	0.1	0.1	0.1
Wt. %																				
SiO_2	51.88	52.13	51.87	52.32	52.58	52.48	52.51	52.17	52.19	52.79	52.70	52.77	52.27	52.55	52.26	52.28	52.83	52.88	52.97	52.71
TiO_2	0.35	0.31	0.37	0.15	0.26	0.26	0.46	0.46	0.44	0.24	0.34	0.29	0.25	0.24	0.21	0.24	0.51	0.44	0.39	0.42
Al_2O_3	1.28	1.16	1.30	0.98	1.04	1.07	1.23	1.83	1.15	1.13	1.25	1.32	2.12	2.17	2.24	2.05	2.36	2.23	2.16	2.23
Cr_2O_3	0.29	0.26	0.30	0.24	0.08	0.07	0.16	0.19	0.07	0.32	0.32	0.31	0.70	0.73	0.81	0.68	0.86	0.81	0.80	0.81
FeO	7.84	7.43	7.87	7.41	9.23	10.14	7.36	7.41	7.58	5.65	5.84	6.11	4.42	4.51	4.61	4.69	5.38	6.15	5.87	5.49
MnO	0.18	0.20	0.21	0.16	0.23	0.26	0.19	0.17	0.16	0.23	0.21	0.21	0.14	0.12	0.11	0.16	0.15	0.23	0.18	0.22
NiO	0.01	0.03	0.02	0.04	0.05	0.00	0.02	0.06	0.07	0.03	0.00	0.00	0.04	0.05	0.09	0.03	0.10	0.09	0.11	0.09
MgO	14.50	14.56	14.67	14.90	13.69	13.44	14.86	14.59	14.53	15.53	15.50	15.59	16.73	16.77	16.60	17.17	16.95	17.98	18.07	17.15
CaO	22.57	22.77	22.46	23.13	22.50	21.46	22.95	22.50	22.75	23.05	22.86	22.48	22.78	22.46	22.56	22.09	20.88	19.15	19.55	20.67
Na_2O	0.27	0.26	0.26	0.24	0.24	0.25	0.27	0.28	0.22	0.24	0.26	0.29	0.30	0.30	0.31	0.25	0.40	0.33	0.38	0.37
Total	99.16	99.10	99.34	99.58	99.89	99.44	100.00	99.65	99.16	99.22	99.28	99.37	99.74	99.90	99.80	99.63	100.43	100.28	100.49	100.16
Cations (based on 6 oxygens):																				
Si	1.9498	1.9570	1.9461	1.9562	1.9695	1.9766	1.9521	1.9442	1.9579	1.9631	1.9590	1.9595	1.9245	1.9293	0.0218	0.0247	0.0529	0.0464	0.0409	0.0434
Ti	0.0098	0.0087	0.0105	0.0043	0.0072	0.0074	0.0128	0.0129	0.0123	0.0066	0.0094	0.0082	0.0068	0.0068	0.1729	0.1599	0.1829	0.1767	0.1708	0.1742
Al	0.0566	0.0512	0.0577	0.0431	0.0460	0.0476	0.0539	0.0805	0.0511	0.0496	0.0550	0.0576	0.0921	0.0937	0.0982	0.0836	0.1041	0.1004	0.0997	0.0996
Cr	0.0087	0.0076	0.0090	0.0070	0.0023	0.0020	0.0048	0.0055	0.0020	0.0095	0.0095	0.0091	0.0205	0.0212	0.3738	0.3848	0.4393	0.5128	0.4884	0.4519
Fe	0.2462	0.2333	0.2471	0.2318	0.2891	0.3193	0.2289	0.2309	0.2379	0.1757	0.1815	0.1897	0.1360	0.1385	0.0098	0.0141	0.0130	0.0202	0.0159	0.0193
Mn	0.0057	0.0062	0.0067	0.0052	0.0073	0.0084	0.0060	0.0054	0.0052	0.0073	0.0065	0.0066	0.0044	0.0037	0.0076	0.0023	0.0090	0.0082	0.0098	0.0081
Ni	0.0003	0.0008	0.0005	0.0013	0.0016	0.0000	0.0006	0.0018	0.0020	0.0009	0.0000	0.0000	0.0011	0.0015	1.3702	1.4343	1.4065	1.5259	1.5295	1.4346
Mg	0.8123	0.8147	0.8204	0.8301	0.7643	0.7545	0.8231	0.8105	0.8125	0.8608	0.8585	0.8632	0.9179	0.9175	3.4512	3.4193	3.2107	3.0116	3.0661	3.2045
Ca	0.9088	0.9159	0.9028	0.9266	0.9029	0.8661	0.9140	0.8984	0.9144	0.9185	0.9105	0.8945	0.8985	0.8836	0.0342	0.0284	0.0444	0.0378	0.0429	0.0412
Na	0.0193	0.0186	0.0189	0.0175	0.0177	0.0185	0.0191	0.0199	0.0162	0.0175	0.0187	0.0210	0.0212	0.0211	0.0591	0.0598	0.0594	0.0607	0.0606	0.0599
Total	4.0175	4.0141	4.0195	4.0231	4.0079	4.0005	4.0153	4.0099	4.0114	4.0095	4.0087	4.0094	4.0230	4.0170	5.5988	5.6111	5.5221	5.5007	5.5245	5.5366
MMF	0.7674	0.7774	0.7685	0.7817	0.7256	0.7027	0.7825	0.7783	0.7735	0.8305	0.8255	0.8198	0.8710	0.8688	0.9972	0.9959	0.9960	0.9934	0.9948	0.9940
Wo	46.2	46.6	45.8	46.6	46.2	44.6	46.5	46.3	46.5	47.0	46.7	45.9	46.0	45.6	1.0	0.8	1.4	1.2	1.4	1.3
En	41.3	41.5	41.6	41.7	39.1	38.9	41.9	41.8	41.4	44.0	44.0	44.3	47.0	47.3	98.7	98.8	98.2	98.1	98.1	98.1
Fs	12.5	11.9	12.5	11.7	14.8	16.5	11.6	11.9	12.1	9.0	9.3	9.7	7.0	7.1	0.3	0.4	0.4	0.7	0.5	0.6

TABLE C18: Average composition of **orthopyroxene** in the Bastard Unit.
Profile **AE** (from Field, 1987 p.51).
Metres given above base of Unit (n = number of analyses).

Sample	AE-1	AE-2	AE-5	AE-7	AE-9	AE-10	AE-12	AE-13	AE-15	AE-16
Metres	35.8	34.0	26.4	20.0	17.0	14.7	8.1	5.2	1.1	0.2
n	6	5	3	3	8	5	5	5	6	4
Wt. %										
SiO_2	53.75	53.89	53.84	54.16	54.62	55.07	55.58	55.51	55.40	54.76
TiO_2	0.36	0.28	0.28	0.26	0.31	0.28	0.19	0.25	0.25	0.19
Al_2O_3	0.73	0.83	0.70	0.85	1.01	1.09	1.24	1.28	1.16	1.30
Cr_2O_3	0.08	0.10	0.09	0.11	0.22	0.29	0.26	0.27	0.25	0.29
FeO	20.29	19.67	19.43	17.53	14.80	12.89	11.12	11.43	11.85	14.96
MnO	0.34	0.37	0.39	0.37	0.31	0.29	0.25	0.25	0.21	0.31
NiO	0.05	0.04	0.07	0.05	0.08	0.10	0.09	0.07	0.08	0.14
MgO	23.34	23.08	23.81	25.40	27.13	28.71	29.73	29.72	28.95	27.02
CaO	1.18	1.13	1.13	1.22	1.34	1.20	1.03	1.12	1.41	1.85
Na_2O	0.04	0.01	0.02	0.02	0.02	0.02	0.01	0.01	0.05	0.02
Total	100.16	99.40	99.76	99.97	99.84	99.94	99.50	99.91	99.61	100.84
Cations (based on 6 oxygens):										
Si	1.9808	1.9934	1.9843	1.9749	1.9701	1.9664	1.9738	1.9671	1.9740	1.9603
Ti	0.0100	0.0078	0.0078	0.0071	0.0084	0.0075	0.0051	0.0067	0.0067	0.0051
Al	0.0317	0.0362	0.0304	0.0365	0.0429	0.0459	0.0519	0.0535	0.0487	0.0548
Cr	0.0023	0.0029	0.0026	0.0032	0.0063	0.0082	0.0073	0.0076	0.0070	0.0082
Fe	0.6253	0.6085	0.5989	0.5346	0.4464	0.3849	0.3302	0.3387	0.3531	0.4479
Mn	0.0106	0.0116	0.0122	0.0114	0.0095	0.0088	0.0075	0.0075	0.0063	0.0094
Ni	0.0015	0.0012	0.0021	0.0015	0.0023	0.0029	0.0026	0.0020	0.0023	0.0040
Mg	1.2820	1.2725	1.3079	1.3805	1.4585	1.5280	1.5735	1.5698	1.5376	1.4417
Ca	0.0466	0.0448	0.0446	0.0477	0.0518	0.0459	0.0392	0.0425	0.0538	0.0710
Na	0.0029	0.0007	0.0014	0.0014	0.0014	0.0014	0.0007	0.0007	0.0035	0.0014
Total	3.9937	3.9796	3.9922	3.9988	3.9976	3.9998	3.9919	3.9960	3.9931	4.0038
MMF	0.6722	0.6765	0.6859	0.7209	0.7657	0.7988	0.8265	0.8225	0.8132	0.7630
Wo	2.4	2.3	2.3	2.4	2.6	2.3	2.0	2.2	2.8	3.6
En	65.6	66.1	67.0	70.3	74.5	78.0	81.0	80.5	79.1	73.5
Fs	32.0	31.6	30.7	27.2	22.8	19.7	17.0	17.4	18.2	22.8

TABLE C19: Average composition of **clinopyroxene** in the Bastard Unit.
Profile **AE** (from Field, 1987 p.58).
Metres given above base of Unit (n = number of analyses).

Sample	AE-2	AE-5	AE-7	AE-13	AE-15	AE-16
Metres	34.0	26.4	20.0	5.2	1.1	0.2
n	3	5	1	3	1	3
Wt. %						
SiO_2	52.65	52.51	52.35	53.06	52.86	52.95
TiO_2	0.50	0.49	0.47	0.48	0.60	0.50
Al_2O_3	1.50	1.23	1.72	2.23	2.08	1.80
Cr_2O_3	0.17	0.09	0.16	0.59	0.48	0.38
FeO	8.47	10.93	8.30	5.30	5.19	6.57
MnO	0.20	0.26	0.23	0.15	0.14	0.19
NiO	0.04	0.01	0.04	0.00	0.05	0.12
MgO	15.28	14.05	15.78	17.30	16.36	14.73
CaO	20.34	20.14	19.98	20.16	21.18	23.01
Na_2O	0.28	0.25	0.28	0.35	0.44	0.34
Total	99.43	99.96	99.31	99.62	99.38	100.59
Cations (based on 6 oxygens):						
Si	1.9617	1.9670	1.9508	1.9439	1.9472	1.9493
Ti	0.0140	0.0138	0.0132	0.0132	0.0166	0.0138
Al	0.0659	0.0543	0.0755	0.0963	0.0903	0.0781
Cr	0.0050	0.0027	0.0047	0.0171	0.0140	0.0111
Fe	0.2639	0.3424	0.2587	0.1624	0.1599	0.2023
Mn	0.0063	0.0082	0.0073	0.0047	0.0044	0.0059
Ni	0.0012	0.0003	0.0012	0.0000	0.0015	0.0036
Mg	0.8487	0.7846	0.8766	0.9448	0.8984	0.8084
Ca	0.8120	0.8084	0.7978	0.7914	0.8360	0.9077
Na	0.0202	0.0182	0.0202	0.0249	0.0314	0.0243
Total	3.9990	3.9998	4.0060	3.9986	3.9997	4.0044
MMF	0.7628	0.6962	0.7721	0.8533	0.8489	0.7998
Wo	42.2	41.8	41.3	41.7	44.1	47.3
En	44.1	40.5	45.3	49.8	47.4	42.1
Fs	13.7	17.7	13.4	8.6	8.4	10.5

MICROPROBE DATA TABLE C20: Composition of **plagioclase** in the UG1 Footwall and MG3 Units - all **S** samples.
Metres given below base of UG1 chromitite.
c = cumulus and intercumulus grains.
i = inclusions within cumulus orthopyroxene.

Sample	S-1	S-1	S-1	S-1	S-1	S-2	S-2	S-2	S-2	S-2	S-2	S-2	S-2	S-2	S-2	S-3	S-3	S-3	S-3	S-3	S-3	S-3	S-3	S-3	S-4	S-4
Metres	2.6	2.6	2.6	2.6	2.6	5.3	5.3	5.3	5.3	5.3	5.3	5.3	5.3	5.3	5.3	8.4	8.4	8.4	8.4	8.4	8.4	8.4	8.4	8.4	11.3	11.3
Position	c	c	c	c	c	c	c	c	c	c	c	c	c	c	c	c	c	c	c	c	c	c	c	c	c	c
Wt.%																										
SiO_2	48.71	48.61	48.02	47.83	48.78	47.53	48.04	49.29	49.55	47.98	48.58	47.71	47.52	47.70	48.71	48.65	48.92	49.33	49.20	48.85	49.85	49.79	48.20	48.85	48.92	50.25	50.21
Al_2O_3	32.18	32.44	32.70	32.77	32.38	33.60	33.42	31.49	32.15	33.45	33.02	33.82	33.91	33.63	32.88	32.70	32.62	32.06	32.36	32.72	31.83	32.08	32.75	32.58	32.49	31.83	31.98
Fe_2O_3	0.18	0.03	0.05	0.15	0.13	0.11	0.11	0.12	0.15	0.15	0.16	0.14	0.13	0.14	0.16	0.35	0.28	0.27	0.28	0.32	0.33	0.31	0.32	0.36	0.28	0.23	0.24
CaO	15.52	15.99	16.25	16.69	16.07	16.46	16.11	16.02	15.32	15.93	15.64	16.21	16.39	16.20	15.43	16.04	15.86	15.62	15.74	15.99	15.18	15.40	16.27	15.67	15.53	14.96	15.17
Na_2O	2.72	2.56	2.35	2.01	2.44	2.24	2.43	2.81	2.68	2.48	2.76	2.39	2.25	2.37	2.81	2.21	2.35	2.66	2.47	2.46	2.77	2.74	2.18	2.30	2.35	2.96	2.88
K_2O	0.10	0.09	0.07	0.02	0.02	0.00	0.00	0.10	0.02	0.01	0.01	0.01	0.02	0.01	0.02	0.01	0.00	0.00	0.02	0.00	0.00	0.00	0.01	0.02	0.01	0.02	0.01
Total	99.41	99.73	99.44	99.47	99.82	99.94	100.11	99.82	99.87	100.00	100.16	100.28	100.22	100.04	100.02	99.97	100.02	99.93	100.06	100.34	99.96	100.32	99.74	99.78	99.58	100.26	100.49
Cations (based on 32 oxygens):																											
Si	8.9675	8.9255	8.8501	8.8178	8.9437	8.7228	8.7896	9.0484	9.0542	8.7876	8.8764	8.7224	8.6956	8.7393	8.9078	8.9065	8.9418	9.0240	8.9884	8.9133	9.1023	9.0642	8.8553	8.9486	8.9712	9.1406	9.1164
Al	6.9822	7.0204	7.1028	7.1195	6.9969	7.2671	7.2068	6.8137	6.9236	7.2203	7.1108	7.2860	7.3141	7.2630	7.0869	7.0547	7.0287	6.9135	6.9668	7.0361	6.8495	6.8842	7.0918	7.0334	7.0231	6.8240	6.8425
Fe	0.0222	0.0040	0.0060	0.0187	0.0161	0.0139	0.0135	0.0144	0.0192	0.0190	0.0195	0.0174	0.0158	0.0168	0.0204	0.0439	0.0346	0.0331	0.0351	0.0392	0.0409	0.0387	0.0401	0.0442	0.0353	0.0283	0.0293
Ca	3.0613	3.1462	3.2088	3.2963	3.1568	3.2352	3.1584	3.1501	2.9999	3.1251	3.0624	3.1759	3.2132	3.1795	3.0235	3.1450	3.1057	3.0608	3.0811	3.1251	2.9697	3.0037	3.2020	3.0757	3.0506	2.9163	2.9517
Na	0.9706	0.9103	0.8395	0.7182	0.8671	0.7957	0.8631	0.9987	0.9510	0.8797	0.9767	0.8451	0.7979	0.8415	0.9959	0.7851	0.8314	0.9425	0.8747	0.8696	0.9805	0.9670	0.7778	0.8177	0.8358	1.0444	1.0132
K	0.0235	0.0221	0.0166	0.0035	0.0055	0.0000	0.0008	0.0232	0.0040	0.0019	0.0021	0.0032	0.0039	0.0029	0.0041	0.0028	0.0000	0.0000	0.0037	0.0011	0.0000	0.0003	0.0015	0.0039	0.0028	0.0038	0.0025
Total	20.0273	20.0285	20.0236	19.9740	19.9861	20.0346	20.0321	20.0485	19.9519	20.0336	20.0479	20.0500	20.0404	20.0430	20.0386	19.9381	19.9422	19.9739	19.9498	19.9844	19.9428	19.9580	19.9684	19.9234	19.9188	19.9574	19.9556
An	75.93	77.56	79.26	82.11	78.45	80.26	78.54	75.93	75.93	78.03	75.82	78.98	80.11	79.07	75.22	80.02	78.88	76.46	77.89	78.23	75.18	75.65	80.46	79.00	78.50	73.63	74.45

Sample	S-4	S-4	S-4	S-4	S-4	S-4	S-4	S-4	S-5	S-5	S-5	S-5	S-5	S-6	S-6	S-6	S-6	S-6	S-6	S-6	S-7	S-7	S-7	S-7	S-7	S-8	S-8
Metres	11.3	11.3	11.3	11.3	11.3	11.3	11.3	11.3	18.2	18.2	18.2	18.2	18.2	22.1	22.1	22.1	22.1	22.1	22.1	22.1	26.5	26.5	26.5	26.5	26.5	32.3	32.3
Position	c	c	c	c	c	c	c	c	c	c	c	c	c	c	c	c	c	c	c	i	i	c	c	c	c	c	c
Wt.%																											
SiO_2	49.58	48.54	50.04	48.98	48.68	48.18	49.72	49.26	48.43	49.14	48.06	49.29	48.98	49.37	49.60	49.76	49.44	49.25	50.07	50.42	49.25	48.93	48.93	49.72	49.67	49.37	49.43
Al_2O_3	32.46	32.91	31.85	32.47	32.59	32.72	31.92	32.41	32.68	32.41	33.19	32.57	32.71	31.94	31.77	31.36	31.97	31.79	31.20	31.20	31.74	32.51	32.51	31.53	31.80	31.85	31.73
Fe_2O_3	0.19	0.25	0.30	0.21	0.28	0.30	0.22	0.30	0.09	0.17	0.08	0.09	0.15	0.09	0.11	0.08	0.04	0.08	0.20	0.18	0.11	0.13	0.13	0.10	0.11	0.18	0.14
CaO	15.60	16.42	15.28	16.07	16.22	16.43	15.43	15.90	15.90	15.32	16.37	15.32	15.70	15.51	15.56	15.46	15.50	15.71	14.80	14.53	15.56	15.84	15.84	15.41	15.39	15.52	15.35
Na_2O	2.65	2.20	2.99	2.44	2.39	2.24	2.86	2.54	2.45	2.62	2.13	2.73	2.66	2.58	2.64	2.76	2.54	2.59	3.04	3.30	2.65	2.48	2.48	2.79	2.73	2.68	2.85
K_2O	0.00	0.01	0.02	0.02	0.02	0.01	0.03	0.03	0.08	0.09	0.07	0.09	0.11	0.01	0.01	0.02	0.01	0.01	0.03	0.03	0.01	0.02	0.02	0.02	0.02	0.01	0.02
Total	100.47	100.34	100.47	100.19	100.18	99.88	100.17	100.43	99.63	99.74	99.89	100.09	100.32	99.50	99.69	99.44	99.51	99.44	99.34	99.66	99.32	99.91	99.91	99.58	99.71	99.60	99.52
Cations (based on 32 oxygens):																											
Si	9.0144	8.8634	9.0995	8.9477	8.9035	8.8456	9.0711	8.9748	8.8971	8.9977	8.8128	8.9942	8.9356	9.0576	9.0845	9.1360	9.0649	9.0503	9.1912	9.2216	9.0590	8.9551	8.9551	9.1168	9.0928	9.0561	9.0741
Al	6.9550	7.0816	6.8263	6.9902	7.0245	7.0815	6.8623	6.9598	7.0760	6.9947	7.1718	7.0049	7.0330	6.9062	6.8579	6.7859	6.9091	6.8850	6.7500	6.7253	6.8808	7.0115	7.0115	6.8135	6.8603	6.8846	6.8650
Fe	0.0231	0.0313	0.0367	0.0264	0.0349	0.0367	0.0266	0.0365	0.0111	0.0207	0.0098	0.0111	0.0184	0.0110	0.0138	0.0097	0.0055	0.0104	0.0249	0.0220	0.0138	0.0158	0.0158	0.0129	0.0136	0.0221	0.0169
Ca	3.0377	3.2123	2.9779	3.1455	3.1782	3.2318	3.0151	3.1041	3.1296	3.0060	3.2157	2.9945	3.0684	3.0487	3.0534	3.0412	3.0449	3.0939	2.9108	2.8473	3.0665	3.1054	3.1054	3.0277	3.0181	3.0502	3.0191
Na	0.9321	0.7802	1.0536	0.8649	0.8473	0.7962	1.0114	0.8975	0.8729	0.9292	0.7563	0.9659	0.9417	0.9174	0.9372	0.9822	0.9034	0.9225	1.0816	1.1698	0.9448	0.8813	0.8813	0.9926	0.9673	0.9528	1.0148
K	0.0006	0.0030	0.0035	0.0038	0.0040	0.0035	0.0073	0.0062	0.0183	0.0220	0.0161	0.0203	0.0249	0.0033	0.0030	0.0047	0.0033	0.0023	0.0070	0.0070	0.0023	0.0055	0.0055	0.0055	0.0036	0.0023	0.0050
Total	19.9630	19.9718	19.9976	19.9784	19.9924	19.9952	19.9938	19.9789	20.0050	19.9702	19.9826	19.9908	20.0220	19.9442	19.9498	19.9597	19.9311	19.9644	19.9656	19.9931	19.9672	19.9746	19.9746	19.9690	19.9557	19.9682	19.9949
An	76.52	80.46	73.86	78.43	78.95	80.23	74.88	77.57	78.19	76.39	80.96	75.61	76.52	76.87	76.52	75.59	77.12	77.03	72.91	70.88	76.45	77.89	77.89	75.31	75.73	76.20	74.84

MICROPROBE DATA TABLE C20: Composition of **plagioclase** in the UG1 Footwall and MG3 Units - all S samples.
Metres given below base of UG1 chromitite.
c = cumulus and intercumulus grains.
i = inclusions within cumulus orthopyroxene.

Sample	S-8	S-8	S-8	S-8	S-8	S-8	S-8	S-8	S-10	S-10	S-10	S-10	S-10	S-10	S-10	S-10	S-10	S-10	S-10	S-10	S-10	S-10	S-10	S-10	S-10
Metres	32.3	32.3	32.3	32.3	32.3	32.3	32.3	32.3	42.5	42.5	42.5	42.5	42.5	42.5	42.5	42.5	42.5	42.5	42.5	42.5	42.5	42.5	42.5	42.5	42.5
Position	c	c	c	i	i	i	i	i	c	c	c	c	c	c	c	c	c	c	c	i	i	i	i	i	i
Wt.%																									
SiO_2	49.61	49.37	49.61	50.55	50.55	50.55	50.55	50.55	49.75	49.60	50.50	49.97	50.41	50.31	50.72	50.14	50.26	49.89	51.64	50.62	50.71	49.86	50.40	49.80	50.03	50.16	50.18
Al_2O_3	31.72	31.85	31.72	30.97	30.97	31.04	31.04	31.04	31.40	31.70	31.41	31.81	31.51	31.43	31.30	31.58	31.57	31.64	30.73	31.24	30.85	31.34	31.18	31.65	31.57	31.26	31.25
Fe_2O_3	0.20	0.18	0.20	0.37	0.37	0.30	0.30	0.30	0.21	0.18	0.15	0.19	0.21	0.28	0.19	0.18	0.20	0.14	0.21	0.15	0.33	0.35	0.38	0.26	0.34	0.31	0.51
CaO	15.33	15.52	15.33	14.48	14.48	14.70	14.70	14.70	15.26	15.46	15.27	15.16	14.20	14.41	14.72	15.40	15.29	15.21	14.24	14.76	14.47	14.86	14.80	15.26	15.23	14.89	15.04
Na_2O	2.86	2.68	2.86	3.33	3.33	3.27	3.27	3.27	2.94	2.76	2.76	2.71	3.12	3.01	2.98	2.75	2.81	2.76	3.40	3.22	3.26	3.08	3.07	2.76	2.95	3.15	3.05
K_2O	0.00	0.01	0.00	0.02	0.02	0.02	0.02	0.02	0.03	0.04	0.05	0.04	0.04	0.06	0.06	0.05	0.05	0.06	0.06	0.05	0.04	0.06	0.04	0.09	0.03	0.03	0.04
Total	99.73	99.60	99.73	99.72	99.72	99.88	99.88	99.88	99.59	99.73	100.13	99.89	99.49	99.49	99.96	100.10	100.18	99.70	100.28	100.04	99.67	99.55	99.87	99.82	100.17	99.80	100.06
Cations (based on 32 oxygens):																											
Si	9.0867	9.0561	9.0867	9.2444	9.2444	9.2322	9.2322	9.2322	9.1264	9.0864	9.1949	9.1232	9.2180	9.2067	9.2398	9.1431	9.1553	9.1296	9.3678	9.2257	9.2733	9.1478	9.2078	9.1120	9.1266	9.1763	9.1641
Al	6.8482	6.8846	6.8482	6.6754	6.6754	6.6813	6.6813	6.6813	6.7891	6.8432	6.7407	6.8452	6.7904	6.7789	6.7199	6.7862	6.7779	6.8241	6.5690	6.7105	6.6493	6.7763	6.7135	6.8241	6.7867	6.7400	6.7269
Fe	0.0253	0.0221	0.0253	0.0454	0.0454	0.0366	0.0366	0.0366	0.0258	0.0224	0.0186	0.0240	0.0264	0.0345	0.0231	0.0219	0.0251	0.0176	0.0262	0.0184	0.0408	0.0438	0.0469	0.0328	0.0423	0.0388	0.0629
Ca	3.0084	3.0502	3.0084	2.8371	2.8371	2.8773	2.8773	2.8773	2.9985	3.0348	2.9791	2.9651	2.7816	2.8260	2.8727	3.0094	2.9834	2.9828	2.7680	2.8811	2.8359	2.9199	2.8958	2.9904	2.9772	2.9180	2.9437
Na	1.0153	0.9528	1.0153	1.1803	1.1803	1.1576	1.1576	1.1576	1.0450	0.9796	0.9736	0.9599	1.1053	1.0680	1.0527	0.9731	0.9923	0.9776	1.1943	1.1364	1.1559	1.0949	1.0868	0.9799	1.0441	1.1155	1.0781
K	0.0008	0.0023	0.0008	0.0053	0.0053	0.0055	0.0055	0.0055	0.0080	0.0083	0.0107	0.0097	0.0090	0.0130	0.0139	0.0115	0.0108	0.0134	0.0127	0.0118	0.0087	0.0136	0.0094	0.0206	0.0078	0.0069	0.0088
Total	19.9846	19.9682	19.9846	19.9880	19.9880	19.9904	19.9904	19.9904	19.9927	19.9747	19.9176	19.9270	19.9307	19.9271	19.9220	19.9452	19.9448	19.9450	19.9381	19.9839	19.9639	19.9964	19.9601	19.9598	19.9848	19.9955	19.9845
An	74.77	76.20	74.77	70.62	70.62	71.31	71.31	71.31	74.16	75.60	75.37	75.54	71.56	72.57	73.18	75.56	75.04	75.32	69.86	71.71	71.04	72.73	72.71	75.32	74.04	72.34	73.19

Sample	S-10	S-12	S-12	S-12	S-12	S-12	S-12	S-12	S-12	S-12	S-12	S-12	S-12	S-12	S-12	S-12	S-12	S-12	S-12	S-12	S-12	S-12	S-15	S-15	S-15	S-15	S-15	S-15
Metres	42.5	57.1	57.1	57.1	57.1	57.1	57.1	57.1	57.1	57.1	57.1	57.1	57.1	57.1	57.1	57.1	57.1	57.1	57.1	57.1	57.1	57.1	80.9	80.9	80.9	80.9	80.9	80.9
Position	i	c	c	c	c	c	c	c	c	c	c	i	i	i	i	i	i	i	i	i	i	i	c	c	c	c	c	c
Wt.%																												
SiO_2	50.00	49.03	49.23	49.35	48.99	49.11	48.31	49.32	49.21	49.15	49.18	48.25	48.23	49.51	49.55	49.54	49.06	50.00	48.31	48.52	48.82	50.32	50.74	50.48	49.67	50.35	50.73
Al_2O_3	31.54	31.89	31.87	31.83	31.99	31.54	32.37	31.81	32.08	31.95	31.78	32.64	32.52	31.54	31.70	31.99	31.76	31.21	32.47	32.56	32.23	31.57	31.49	31.83	32.34	31.80	31.78
Fe_2O_3	0.38	0.11	0.10	0.07	0.05	0.08	0.08	0.09	0.09	0.11	0.10	0.08	0.08	0.25	0.18	0.12	0.26	0.30	0.23	0.09	0.13	0.20	0.14	0.17	0.19	0.22	0.27
CaO	14.98	15.74	15.62	15.48	15.62	15.80	16.11	15.46	15.84	15.92	15.75	16.44	16.44	15.49	15.49	15.31	15.60	15.10	16.14	16.35	16.12	15.41	15.08	15.35	15.76	15.16	15.01
Na_2O	2.93	2.89	2.85	2.95	2.85	2.92	2.67	2.98	2.87	2.84	2.86	2.50	2.56	3.06	3.11	2.98	3.03	3.35	2.73	2.39	2.77	2.83	3.04	2.88	2.59	2.92	2.97
K_2O	0.05	0.13	0.14	0.15	0.14	0.17	0.12	0.15	0.14	0.13	0.14	0.09	0.11	0.15	0.14	0.15	0.21	0.19	0.16	0.11	0.02	0.02	0.02	0.03	0.02	0.03	0.03
Total	99.89	99.79	99.81	99.83	99.64	99.63	99.65	99.81	100.23	100.10	99.81	99.99	99.94	99.99	100.17	100.09	99.92	100.14	100.05	100.03	100.08	100.35	100.52	100.74	100.57	100.47	100.78
Cations (based on 32 oxygens):																												
Si	9.1386	9.0023	9.0288	9.0454	9.0010	9.0351	8.8922	9.0442	8.9948	8.9982	9.0243	8.8547	8.8599	9.0696	9.0595	9.0510	9.0062	9.1421	8.8691	8.8917	8.9416	9.1524	9.2040	9.1440	9.0253	9.1427	9.1767
Al	6.7952	6.8994	6.8877	6.8752	6.9264	6.8388	7.0223	6.8741	6.9118	6.8940	6.8743	7.0592	7.0413	6.8095	6.8309	6.8888	6.8718	6.7248	7.0263	7.0337	6.9577	6.7686	6.7321	6.7950	6.9260	6.8057	6.7765
Fe	0.0469	0.0136	0.0128	0.0092	0.0057	0.0102	0.0103	0.0108	0.0116	0.0139	0.0124	0.0094	0.0103	0.0316	0.0219	0.0147	0.0328	0.0367	0.0290	0.0113	0.0158	0.0251	0.0172	0.0212	0.0234	0.0268	0.0332
Ca	2.9339	3.0966	3.0690	3.0408	3.0751	3.1149	3.1767	3.0364	3.1013	3.1219	3.0959	3.2326	3.2352	3.0393	3.0351	2.9966	3.0677	2.9585	3.1740	3.2107	3.1632	3.0035	2.9304	2.9789	3.0676	2.9491	2.9085
Na	1.0395	1.0280	1.0123	1.0478	1.0164	1.0422	0.9530	1.0603	1.0156	1.0091	1.0188	0.8882	0.9103	1.0855	1.1005	1.0563	1.0779	1.1862	0.9720	0.8500	0.9822	0.9983	1.0702	1.0108	0.9105	1.0265	1.0404
K	0.0120	0.0310	0.0331	0.0356	0.0330	0.0405	0.0274	0.0355	0.0326	0.0304	0.0320	0.0219	0.0248	0.0345	0.0329	0.0359	0.0485	0.0438	0.0375	0.0268	0.0049	0.0039	0.0051	0.0067	0.0051	0.0067	0.0062
Total	19.9660	20.0708	20.0437	20.0540	20.0577	20.0817	20.0818	20.0613	20.0676	20.0676	20.0577	20.0660	20.0819	20.0699	20.0808	20.0433	20.1047	20.0921	20.1080	20.0242	20.0653	19.9519	19.9590	19.9566	19.9578	19.9576	19.9417
An	73.84	75.08	75.20	74.37	75.16	74.93	76.92	74.12	75.33	75.57	75.24	78.44	78.04	73.68	73.39	73.94	74.00	71.38	76.56	79.07	76.31	75.05	73.25	74.66	77.11	74.18	73.65

MICROPROBE DATA TABLE C20: Composition of **plagioclase** in the UG1 Footwall and MG3 Units - all **S** samples.
Metres given below base of UG1 chromitite.
c = cumulus and intercumulus grains.
i = inclusions within cumulus orthopyroxene.

Sample	S-15	S-15	S-15	S-15	S-15	S-15	S-15	S-15	S-15	S-15	S-15	S-15	S-15	S-15	S-18	S-18	S-18	S-18	S-18	S-18	S-18	S-18	S-18	S-18	S-18	S-18
Metres	80.9	80.9	80.9	80.9	80.9	80.9	80.9	80.9	80.9	80.9	80.9	80.9	80.9	80.9	94.1	94.1	94.1	94.1	94.1	94.1	94.1	94.1	94.1	94.1	94.1	94.1
Position	c	c	c	c	i	i	i	i	i	i	i	i	i	i	c	c	c	c	c	c	c	c	c	c	i	i	i
Wt.%																											
SiO_2	50.66	50.88	50.04	49.77	51.17	50.63	50.57	50.18	50.06	50.31	50.54	50.59	50.40	50.52	49.23	48.68	48.96	49.28	49.48	49.54	50.00	50.11	49.55	49.51	50.51	50.12	49.96
Al_2O_3	31.72	31.35	31.73	31.80	30.96	30.82	30.74	31.00	31.03	31.52	31.70	31.63	31.88	31.70	32.18	32.34	32.00	31.87	32.02	31.80	31.46	31.84	31.86	31.58	31.71	31.93	31.74
Fe_2O_3	0.24	0.20	0.25	0.21	0.35	0.33	0.32	0.34	0.32	0.26	0.33	0.31	0.32	0.26	0.24	0.25	0.23	0.29	0.28	0.28	0.22	0.26	0.31	0.25	0.28	0.23	0.28
CaO	15.25	14.80	15.24	15.39	14.45	14.67	14.67	14.95	15.02	14.96	14.90	14.95	14.97	15.05	15.74	16.38	16.12	15.66	15.54	15.61	15.21	14.89	15.37	15.32	14.76	15.02	14.93
Na_2O	2.94	3.19	2.89	2.87	3.40	3.34	3.36	3.16	3.22	3.08	3.25	3.21	3.09	3.11	2.75	2.44	2.57	2.80	2.81	2.89	2.99	2.87	2.72	2.92	2.98	2.94	2.80
K_2O	0.02	0.02	0.03	0.03	0.01	0.01	0.02	0.01	0.02	0.03	0.01	0.02	0.02	0.02	0.16	0.12	0.10	0.15	0.14	0.13	0.00	0.00	0.01	0.13	0.02	0.02	0.06
Total	100.84	100.44	100.18	100.06	100.33	99.79	99.67	99.63	99.67	100.16	100.74	100.72	100.68	100.66	100.30	100.21	100.00	100.04	100.26	100.25	99.88	99.97	99.82	99.71	100.26	100.25	99.77
Cations (based on 32 oxygens):																											
Si	9.1668	9.2330	9.1206	9.0885	9.2926	9.2563	9.2582	9.1977	9.1783	9.1660	9.1587	9.1697	9.1360	9.1600	8.9906	8.9124	8.9755	9.0223	9.0322	9.0490	9.1412	9.1358	9.0680	9.0828	9.1802	9.1199	9.1322
Al	6.7647	6.7048	6.8158	6.8424	6.6259	6.6404	6.6324	6.6956	6.7056	6.7677	6.7704	6.7562	6.8104	6.7731	6.9256	6.9786	6.9137	6.8776	6.8878	6.8463	6.7780	6.8425	6.8723	6.8275	6.7917	6.8467	6.8374
Fe	0.0298	0.0240	0.0302	0.0254	0.0427	0.0406	0.0391	0.0425	0.0398	0.0327	0.0404	0.0384	0.0392	0.0323	0.0301	0.0316	0.0292	0.0361	0.0345	0.0342	0.0276	0.0327	0.0389	0.0316	0.0344	0.0288	0.0352
Ca	2.9565	2.8780	2.9764	3.0104	2.8116	2.8732	2.8780	2.9356	2.9506	2.9203	2.8936	2.9024	2.9081	2.9242	3.0796	3.2136	3.1660	3.0714	3.0390	3.0550	2.9786	2.9079	3.0144	3.0108	2.8733	2.9271	2.9239
Na	1.0315	1.1208	1.0207	1.0153	1.1983	1.1834	1.1915	1.1221	1.1449	1.0877	1.1429	1.1275	1.0854	1.0912	0.9752	0.8651	0.9136	0.9932	0.9935	1.0215	1.0602	1.0146	0.9638	1.0389	1.0490	1.0361	0.9909
K	0.0048	0.0050	0.0059	0.0065	0.0021	0.0023	0.0052	0.0015	0.0044	0.0068	0.0026	0.0050	0.0058	0.0038	0.0362	0.0278	0.0238	0.0340	0.0327	0.0309	0.0009	0.0009	0.0017	0.0310	0.0050	0.0035	0.0149
Total	19.9541	19.9655	19.9696	19.9886	19.9733	19.9961	20.0044	19.9950	20.0236	19.9811	20.0086	19.9993	19.9848	19.9848	20.0372	20.0290	20.0218	20.0345	20.0198	20.0370	19.9865	19.9343	19.9591	20.0226	19.9337	19.9621	19.9344
An	74.14	71.97	74.46	74.78	70.12	70.83	70.72	72.35	72.05	72.86	71.69	72.02	72.82	72.82	75.95	78.79	77.61	75.57	75.36	74.94	73.75	74.13	75.77	74.35	73.26	73.86	74.69

Sample	S-18	S-18	S-18	S-18	S-18	S-18	S-18	S-20	S-20	S-20	S-20	S-20	S-20	S-20	S-20	S-20	S-20	S-23	S-23	S-23	S-23	S-23	S-23	S-23	S-23	S-23	S-23
Metres	94.1	94.1	94.1	94.1	94.1	94.1	94.1	106.0	106.0	106.0	106.0	106.0	106.0	106.0	106.0	106.0	106.0	120.4	120.4	120.4	120.4	120.4	120.4	120.4	120.4	120.4	120.4
Position	i	i	i	i	i	i	i	i	i	i	i	i	c	c	c	c	c	c	c	c	c	c	c	c	c	c	c
Wt.%																											
SiO_2	50.45	49.74	53.62	49.58	49.76	49.19	49.20	50.14	49.96	50.25	49.61	48.88	49.56	49.90	49.67	49.81	49.70	50.83	50.33	50.18	49.72	50.39	50.64	50.87	50.15	50.49	50.21
Al_2O_3	31.28	31.90	28.45	31.75	31.74	31.98	32.08	31.19	32.19	32.06	32.05	32.41	32.50	31.83	31.85	32.15	32.17	31.14	31.17	31.21	31.38	31.11	31.25	31.04	31.10	31.26	31.49
Fe_2O_3	0.31	0.31	0.21	0.31	0.33	0.25	0.31	1.12	0.43	0.45	0.33	0.36	0.22	0.27	0.21	0.23	0.24	0.33	0.31	0.36	0.38	0.28	0.32	0.25	0.31	0.26	0.26
CaO	14.89	15.25	11.70	15.27	15.14	15.43	15.45	14.54	15.20	15.46	14.97	15.57	15.59	15.29	15.11	15.40	15.40	15.06	14.92	14.83	15.27	14.90	15.01	14.74	15.14	14.85	14.72
Na_2O	3.07	2.94	2.76	2.95	3.12	2.99	2.94	2.88	2.91	2.65	3.06	2.81	2.62	2.76	2.84	2.72	2.75	3.03	3.23	2.97	2.90	3.18	3.08	3.18	2.96	3.17	2.94
K_2O	0.05	0.17	3.12	0.13	0.14	0.11	0.12	0.01	0.02	0.02	0.02	0.03	0.01	0.02	0.02	0.02	0.02	0.02	0.03	0.02	0.02	0.02	0.03	0.03	0.01	0.02	0.01
Total	100.05	100.30	99.86	99.97	100.23	99.96	100.09	99.89	100.71	100.90	100.03	100.06	100.49	100.07	99.69	100.33	100.28	100.41	99.98	99.57	99.67	99.89	100.33	100.11	99.68	100.04	99.64
Cations (based on 32 oxygens):																											
Si	9.2003	9.0702	9.8086	9.0714	9.0838	9.0116	9.0013	9.1723	9.0633	9.0962	9.0602	8.9459	9.0086	9.1039	9.0929	9.0648	9.0520	9.2344	9.1921	9.1931	9.1189	9.2083	9.2106	9.2619	9.1861	9.2058	9.1826
Al	6.7227	6.8563	6.1326	6.8461	6.8281	6.9046	6.9172	6.7238	6.8830	6.8394	6.8973	6.9899	6.9627	6.8424	6.8710	6.8959	6.9058	6.6677	6.7093	6.7377	6.7821	6.6993	6.6990	6.6597	6.7149	6.7177	6.7871
Fe	0.0384	0.0377	0.0254	0.0382	0.0413	0.0313	0.0385	0.1387	0.0527	0.0551	0.0405	0.0448	0.0274	0.0336	0.0254	0.0289	0.0297	0.0407	0.0381	0.0442	0.0477	0.0342	0.0396	0.0314	0.0386	0.0325	0.0328
Ca	2.9100	2.9794	2.2925	2.9932	2.9606	3.0295	3.0290	2.8492	2.9554	2.9976	2.9282	3.0539	3.0360	2.9877	2.9636	3.0024	3.0059	2.9324	2.9200	2.9116	3.0001	2.9166	2.9258	2.8749	2.9713	2.9007	2.8831
Na	1.0836	1.0386	0.9773	1.0453	1.1023	1.0615	1.0412	1.0227	1.0246	0.9313	1.0838	0.9984	0.9218	0.9770	1.0072	0.9578	0.9695	1.0672	1.1423	1.0544	1.0302	1.1274	1.0846	1.1224	1.0494	1.1215	1.0409
K	0.0119	0.0396	0.7290	0.0300	0.0329	0.0256	0.0286	0.0021	0.0044	0.0051	0.0057	0.0059	0.0015	0.0039	0.0048	0.0042	0.0042	0.0048	0.0070	0.0043	0.0047	0.0057	0.0059	0.0069	0.0035	0.0037	0.0029
Total	19.9669	20.0218	19.9655	20.0241	20.0490	20.0640	20.0558	19.9088	19.9834	19.9248	20.0157	20.0389	19.9580	19.9486	19.9649	19.9538	19.9670	19.9473	20.0088	19.9453	19.9837	19.9915	19.9654	19.9572	19.9636	19.9818	19.9294
An	72.87	74.15	70.11	74.12	72.87	74.05	74.42	73.59	74.26	76.30	72.99	75.36	76.71	75.36	74.64	75.82	75.61	73.32	71.88	73.41	74.44	72.12	72.96	71.92	73.90	72.12	73.47

MICROPROBE DATA TABLE C20: Composition of **plagioclase** in the UG1 Footwall and MG3 Units - all **S** samples.
Metres given below base of UG1 chromitite.
c = cumulus and intercumulus grains.
i = inclusions within cumulus orthopyroxene.

Sample	S-23	S-23	S-23	S-23	S-23	S-23	S-23	S-23	S-23	S-23	S-24	S-24	S-24	S-24	S-24	S-24	S-24	S-24	S-24	S-24	S-24	S-24	S-24	S-24	S-24
Metres	120.4	120.4	120.4	120.4	120.4	120.4	120.4	120.4	120.4	120.4	124.8	124.8	124.8	124.8	124.8	124.8	124.8	124.8	124.8	124.8	124.8	124.8	124.8	124.8	124.8
Position	i	i	i	i	i	i	i	i	i	i	c	c	c	c	c	c	c	c	c	c	i	i	i	i	i
Wt.%																									
SiO_2	51.40	49.92	50.16	49.15	50.15	50.18	50.08	51.17	50.27	50.25	50.85	51.31	51.32	51.53	50.33	50.50	50.30	49.77	50.06	50.48	53.45	53.52	53.33	53.53	53.86	51.79	54.03
Al_2O_3	30.58	31.30	31.02	32.01	31.04	31.19	31.21	31.15	31.22	31.00	31.62	31.26	31.00	31.18	31.57	30.83	30.71	31.29	31.04	30.98	28.69	29.04	28.96	28.90	28.61	29.93	28.63
Fe_2O_3	0.33	0.47	0.53	0.76	0.36	0.49	0.42	0.44	0.50	0.41	0.24	0.27	0.25	0.25	0.29	0.25	0.29	0.26	0.26	0.31	0.51	0.50	0.48	0.47	0.79	0.29	0.48
CaO	14.39	14.85	14.79	15.25	14.83	14.80	14.76	14.17	14.74	15.06	14.29	14.00	13.74	13.93	14.88	14.86	14.85	15.28	15.03	14.84	12.36	12.46	12.58	12.61	11.86	13.87	12.16
Na_2O	2.98	3.21	3.18	2.66	3.19	3.16	3.25	3.35	3.13	3.03	3.37	3.41	3.52	3.43	3.10	3.44	3.42	3.24	3.21	3.46	4.69	4.70	4.68	4.65	4.77	3.98	4.77
K_2O	0.04	0.03	0.03	0.02	0.03	0.02	0.02	0.02	0.03	0.03	0.20	0.20	0.22	0.25	0.19	0.24	0.23	0.19	0.20	0.23	0.30	0.31	0.31	0.33	0.31	0.26	0.33
Total	99.73	99.78	99.70	99.84	99.59	99.85	99.75	100.29	99.89	99.78	100.57	100.47	100.05	100.58	100.36	100.11	99.79	100.04	99.79	100.31	99.99	100.53	100.32	100.48	100.21	100.12	100.39
Cations (based on 32 oxygens):																											
Si	9.3696	9.1439	9.1908	9.0088	9.1948	9.1793	9.1715	9.2883	9.1874	9.1985	9.2164	9.2974	9.3320	9.3245	9.1591	9.2260	9.2211	9.1138	9.1752	9.2073	9.7114	9.6761	9.6668	9.6857	9.7571	9.4346	9.7669
Al	6.5711	6.7580	6.6993	6.9141	6.7070	6.7246	6.7350	6.6635	6.7251	6.6877	6.7550	6.6762	6.6439	6.6484	6.7719	6.6385	6.6347	6.7531	6.7045	6.6600	6.1445	6.1892	6.1858	6.1628	6.1094	6.4253	6.0994
Fe	0.0413	0.0580	0.0654	0.0940	0.0452	0.0608	0.0525	0.0539	0.0616	0.0509	0.0296	0.0331	0.0310	0.0306	0.0357	0.0310	0.0364	0.0321	0.0324	0.0382	0.0621	0.0607	0.0586	0.0571	0.0966	0.0356	0.0584
Ca	2.8106	2.9155	2.9037	2.9956	2.9125	2.8999	2.8963	2.7556	2.8871	2.9538	2.7744	2.7180	2.6773	2.7010	2.9018	2.9077	2.9166	2.9979	2.9514	2.8991	2.4059	2.4144	2.4422	2.4457	2.3026	2.7067	2.3556
Na	1.0545	1.1389	1.1282	0.9451	1.1322	1.1213	1.1531	1.1780	1.1102	1.0754	1.1855	1.1992	1.2419	1.2043	1.0937	1.2172	1.2157	1.1484	1.1399	1.2246	1.6527	1.6463	1.6434	1.6304	1.6765	1.4063	1.6722
K	0.0089	0.0065	0.0070	0.0042	0.0069	0.0058	0.0056	0.0053	0.0059	0.0072	0.0461	0.0473	0.0510	0.0587	0.0435	0.0551	0.0534	0.0451	0.0457	0.0535	0.0700	0.0709	0.0715	0.0761	0.0719	0.0593	0.0755
Total	19.8559	20.0208	19.9945	19.9618	19.9986	19.9916	20.0141	19.9447	19.9773	19.9735	20.0070	19.9712	19.9771	19.9675	20.0057	20.0754	20.0779	20.0904	20.0491	20.0827	20.0466	20.0576	20.0684	20.0576	20.0141	20.0678	20.0280
An	72.72	71.91	72.02	76.02	72.01	72.12	71.52	70.05	72.23	73.31	70.06	69.39	68.31	69.16	72.63	70.49	70.58	72.30	72.14	70.30	59.28	59.46	59.78	60.00	57.87	65.81	58.48

Sample	S-24	S-24	S-24	S-26	S-26	S-26	S-26	S-26	S-26	S-26	S-26	S-26	S-26	S-26	S-26	S-26	S-26	S-26	S-26	S-26	S-26	S-26	S-26	S-29	S-29	S-29	S-29
Metres	124.8	124.8	124.8	133.5	133.5	133.5	133.5	133.5	133.5	133.5	133.5	133.5	133.5	133.5	133.5	133.5	133.5	133.5	133.5	133.5	133.5	133.5	133.5	146.9	146.9	146.9	146.9
Position	i	i	i	c	c	c	c	c	c	c	c	c	c	i	i	i	i	i	i	i	i	i	i	c	c	c	c
Wt.%																											
SiO_2	51.68	50.31	51.28	50.50	49.56	47.85	49.56	50.21	50.59	50.62	50.65	50.89	49.47	50.61	50.63	50.18	50.18	50.41	50.40	49.62	50.84	49.82	50.91	50.43	50.19	50.55	49.85
Al_2O_3	30.45	30.57	30.19	31.54	31.84	32.50	31.34	31.86	31.55	31.74	31.83	31.48	32.14	31.35	31.61	31.97	31.97	31.86	31.71	31.89	31.61	31.21	31.31	31.28	31.44	31.12	31.59
Fe_2O_3	0.23	0.34	0.28	0.20	0.26	0.26	0.27	0.32	0.26	0.32	0.26	0.28	0.25	0.39	0.35	0.53	0.41	0.53	0.46	0.46	0.43	0.49	0.52	0.22	0.26	0.23	0.22
CaO	14.29	15.10	14.25	15.17	15.26	16.52	15.01	15.08	14.93	15.27	15.20	14.82	15.39	14.87	14.77	15.09	15.18	15.01	15.16	15.27	14.70	15.76	14.76	14.77	14.85	14.44	15.47
Na_2O	3.62	3.24	3.61	2.97	2.90	2.25	2.95	2.86	2.96	2.95	2.83	3.11	2.53	3.09	3.06	2.83	2.94	2.94	2.91	2.72	3.06	2.76	3.21	2.86	2.83	2.94	2.79
K_2O	0.25	0.26	0.22	0.01	0.01	0.01	0.02	0.02	0.02	0.02	0.02	0.02	0.02	0.02	0.01	0.02	0.02	0.02	0.02	0.02	0.02	0.02	0.02	0.01	0.01	0.02	0.01
Total	100.51	99.82	99.84	100.39	99.82	99.38	99.16	100.35	100.31	100.92	100.79	100.60	99.79	100.31	100.44	100.61	100.71	100.77	100.65	99.98	100.66	100.06	100.72	99.57	99.58	99.30	99.93
Cations (based on 32 oxygens):																											
Si	9.3749	9.2256	9.3698	9.1766	9.0711	8.8357	9.1264	9.1290	9.1931	9.1568	9.1636	9.2205	9.0481	9.2040	9.1897	9.1064	9.1020	9.1329	9.1430	9.0682	9.2057	9.1159	9.2234	9.2222	9.1838	9.2603	9.1125
Al	6.5099	6.6081	6.5022	6.7544	6.8680	7.0724	6.8031	6.8266	6.7571	6.7661	6.7868	6.7212	6.9286	6.7184	6.7616	6.8375	6.8332	6.8033	6.7793	6.8693	6.7455	6.7303	6.6855	6.7418	6.7792	6.7198	6.8054
Fe	0.0287	0.0423	0.0341	0.0248	0.0321	0.0321	0.0341	0.0389	0.0320	0.0396	0.0317	0.0346	0.0304	0.0475	0.0435	0.0648	0.0506	0.0651	0.0567	0.0573	0.0531	0.0610	0.0633	0.0276	0.0324	0.0281	0.0275
Ca	2.7771	2.9672	2.7900	2.9543	2.9925	3.2684	2.9617	2.9378	2.9060	2.9584	2.9465	2.8775	3.0149	2.8967	2.8730	2.9338	2.9501	2.9132	2.9464	2.9905	2.8522	3.0890	2.8643	2.8933	2.9114	2.8338	3.0294
Na	1.2733	1.1521	1.2797	1.0443	1.0287	0.8042	1.0537	1.0069	1.0425	1.0339	0.9926	1.0911	0.8960	1.0891	1.0766	0.9947	1.0351	1.0319	1.0218	0.9623	1.0724	0.9803	1.1261	1.0135	1.0042	1.0434	0.9902
K	0.0570	0.0599	0.0520	0.0033	0.0016	0.0026	0.0056	0.0047	0.0057	0.0055	0.0045	0.0048	0.0047	0.0039	0.0032	0.0052	0.0052	0.0050	0.0054	0.0042	0.0046	0.0040	0.0054	0.0027	0.0031	0.0040	0.0026
Total	20.0209	20.0551	20.0279	19.9577	19.9940	20.0154	19.9846	19.9440	19.9365	19.9601	19.9257	19.9496	19.9228	19.9596	19.9476	19.9424	19.9762	19.9514	19.9526	19.9518	19.9335	19.9805	19.9680	19.9011	19.9141	19.8894	19.9675
An	68.56	72.03	68.56	73.88	74.42	80.25	73.76	74.47	73.60	74.10	74.80	72.51	77.09	72.68	72.74	74.68	74.03	73.84	74.25	75.66	72.68	75.91	71.78	74.06	74.35	73.09	75.37

MICROPROBE DATA TABLE C20: Composition of **plagioclase** in the UG1 Footwall and MG3 Units - all **S** samples.
Metres given below base of UG1 chromitite.
c = cumulus and intercumulus grains.
i = inclusions within cumulus orthopyroxene.

Sample	S-29	S-29	S-29	S-29	S-29	S-29	S-29	S-29	S-29	S-29	S-29	S-29	S-29	S-29	S-29	S-29	S-31	S-31	S-31	S-31	S-31	S-31	S-31	S-31	S-31	S-31	S-31
Metres	146.9	146.9	146.9	146.9	146.9	146.9	146.9	146.9	146.9	146.9	146.9	146.9	146.9	146.9	146.9	146.9	151.6	151.6	151.6	151.6	151.6	151.6	151.6	151.6	151.6	151.6	151.6
Position	c	c	c	c	c	c	i	i	i	i	i	i	i	i	i	i	c	c	c	c	c	c	c	c	c	c	i
Wt.%																											
SiO_2	49.92	49.53	49.36	50.84	50.20	50.05	50.15	49.74	50.58	50.52	49.20	50.67	49.64	50.65	49.85	50.71	51.00	50.93	51.82	52.48	52.07	50.82	50.80	50.02	49.69	50.79	51.59
Al_2O_3	31.31	30.81	31.40	30.99	31.37	31.55	31.77	32.00	31.27	31.84	32.65	31.65	32.40	31.56	32.11	31.58	31.12	31.44	30.67	30.42	30.26	31.02	30.83	31.49	31.78	31.25	30.79
Fe_2O_3	0.24	0.25	0.22	0.25	0.19	0.24	0.63	0.53	0.57	0.35	0.36	0.29	0.24	0.34	0.34	0.34	0.28	0.17	0.20	0.17	0.20	0.26	0.26	0.22	0.16	0.19	0.39
CaO	14.96	14.86	15.20	14.36	15.16	15.19	15.52	15.55	14.73	14.91	15.93	15.02	15.94	15.03	15.78	15.06	14.41	14.37	13.89	13.28	13.51	14.35	14.57	15.11	15.36	14.89	13.77
Na_2O	2.97	3.04	2.79	3.25	2.95	3.00	2.69	2.66	3.24	3.14	2.44	3.09	2.51	3.03	2.65	3.09	3.36	3.28	3.54	3.81	3.73	3.30	3.16	2.94	2.85	3.20	3.52
K_2O	0.03	0.01	0.00	0.01	0.01	0.01	0.00	0.00	0.00	0.01	0.01	0.01	0.01	0.01	0.01	0.00	0.02	0.01	0.02	0.03	0.03	0.02	0.02	0.06	0.08	0.08	0.01
Total	99.42	98.50	98.97	99.70	99.88	100.04	100.77	100.49	100.39	100.76	100.59	100.74	100.74	100.61	100.74	100.78	100.19	100.21	100.14	100.17	99.79	99.77	99.64	99.83	99.92	100.40	100.08
Cations (based on 32 oxygens):																											
Si	9.1621	9.1809	9.1062	9.2826	9.1714	9.1355	9.0996	9.0523	9.1993	9.1489	8.9491	9.1768	9.0094	9.1842	9.0489	9.1823	9.2721	9.2494	9.4008	9.4964	9.4704	9.2751	9.2866	9.1456	9.0869	9.2281	9.3702
Al	6.7722	6.7297	6.8284	6.6683	6.7539	6.7868	6.7953	6.8639	6.7032	6.7956	7.0002	6.7559	6.9301	6.7437	6.8684	6.7398	6.6683	6.7297	6.5587	6.4873	6.4859	6.6731	6.6416	6.7866	6.8493	6.6922	6.5910
Fe	0.0294	0.0308	0.0275	0.0309	0.0229	0.0295	0.0771	0.0650	0.0700	0.0424	0.0440	0.0361	0.0297	0.0420	0.0423	0.0411	0.0342	0.0214	0.0242	0.0211	0.0243	0.0322	0.0318	0.0275	0.0193	0.0238	0.0485
Ca	2.9415	2.9500	3.0046	2.8092	2.9683	2.9717	3.0179	3.0319	2.8702	2.8935	3.1052	2.9151	3.0995	2.9199	3.0687	2.9219	2.8067	2.7955	2.6998	2.5742	2.6337	2.8056	2.8537	2.9600	3.0086	2.8979	2.6796
Na	1.0573	1.0920	0.9976	1.1519	1.0452	1.0625	0.9475	0.9394	1.1419	1.1010	0.8589	1.0839	0.8821	1.0637	0.9324	1.0831	1.1848	1.1552	1.2443	1.3347	1.3147	1.1671	1.1202	1.0424	1.0114	1.1254	1.2387
K	0.0062	0.0033	0.0008	0.0015	0.0019	0.0032	0.0009	0.0005	0.0011	0.0024	0.0017	0.0026	0.0019	0.0025	0.0025	0.0007	0.0056	0.0030	0.0045	0.0059	0.0059	0.0053	0.0058	0.0130	0.0178	0.0180	0.0028
Total	19.9688	19.9865	19.9650	19.9445	19.9637	19.9892	19.9384	19.9531	19.9856	19.9838	19.9591	19.9704	19.9527	19.9560	19.9631	19.9691	19.9718	19.9542	19.9322	19.9197	19.9349	19.9584	19.9397	19.9751	19.9933	19.9855	19.9308
An	73.56	72.98	75.07	70.92	73.96	73.66	76.11	76.34	71.54	72.44	78.33	72.89	77.85	73.30	76.70	72.96	70.32	70.76	68.45	65.85	66.70	70.62	71.81	73.96	74.84	72.03	68.39

Sample	S-31	S-31	S-31	S-31	S-31	S-31	S-31	S-31	S-31	S-33	S-33	S-33	S-33	S-33	S-33	S-33	S-33	S-33	S-33	S-33	S-33	S-33	S-33	S-33	S-33	S-33	S-33
Metres	151.6	151.6	151.6	151.6	151.6	151.6	151.6	151.6	151.6	166.0	166.0	166.0	166.0	166.0	166.0	166.0	166.0	166.0	166.0	166.0	166.0	166.0	166.0	166.0	166.0	166.0	166.0
Position	i	i	i	i	i	i	i	i	i	c	c	c	c	c	c	c	c	c	c	i	i	i	i	i	i	i	i
Wt.%																											
SiO_2	50.63	50.83	51.11	50.95	51.02	51.03	50.85	51.03	51.02	50.72	50.97	50.53	50.38	49.71	50.61	49.14	49.02	50.97	49.32	51.79	50.76	51.14	50.97	50.48	50.95	50.79	50.74
Al_2O_3	31.05	30.92	30.77	30.89	30.74	31.17	31.10	31.36	31.15	31.04	31.13	30.97	31.06	31.55	31.36	31.80	32.00	31.05	31.97	30.71	30.93	30.93	30.72	31.20	31.01	30.99	31.28
Fe_2O_3	0.56	0.52	0.45	0.42	0.35	0.35	0.40	0.32	0.40	0.15	0.23	0.18	0.25	0.23	0.28	0.26	0.20	0.22	0.23	0.24	0.39	0.53	0.59	0.46	0.34	0.39	0.29
CaO	14.20	13.92	13.96	13.91	13.99	14.36	14.40	14.40	14.41	14.62	14.49	14.60	14.77	15.44	14.95	15.72	15.90	14.31	15.43	13.97	14.23	14.13	14.12	14.43	14.16	14.16	14.51
Na_2O	3.34	3.35	3.39	3.38	3.45	3.34	3.29	3.29	3.27	3.16	3.32	3.13	3.14	2.89	2.85	2.64	2.60	3.40	2.68	3.79	3.36	3.41	3.60	3.25	3.40	3.42	3.27
K_2O	0.01	0.01	0.01	0.01	0.01	0.01	0.00	0.00	0.01	0.02	0.02	0.03	0.02	0.01	0.00	0.01	0.01	0.02	0.00	0.04	0.01	0.03	0.03	0.03	0.02	0.02	0.03
Total	99.80	99.55	99.69	99.56	99.56	100.26	100.03	100.40	100.26	99.71	100.15	99.45	99.61	99.84	100.04	99.56	99.73	99.97	99.63	100.54	99.69	100.17	100.03	99.84	99.89	99.77	100.11
Cations (based on 32 oxygens):																											
Si	9.2482	9.2948	9.3279	9.3104	9.3258	9.2712	9.2613	9.2543	9.2704	9.2633	9.2697	9.2561	9.2234	9.1014	9.2171	9.0280	8.9956	9.2830	9.0431	9.3742	9.2757	9.3009	9.2943	9.2191	9.2873	9.2734	9.2361
Al	6.6848	6.6620	6.6190	6.6516	6.6222	6.6730	6.6751	6.7038	6.6693	6.6819	6.6716	6.6866	6.7010	6.8071	6.7301	6.8868	6.9205	6.6647	6.9092	6.5521	6.6615	6.6283	6.6020	6.7172	6.6624	6.6690	6.7095
Fe	0.0691	0.0647	0.0560	0.0523	0.0430	0.0430	0.0490	0.0390	0.0486	0.0186	0.0282	0.0229	0.0308	0.0290	0.0339	0.0327	0.0246	0.0267	0.0287	0.0295	0.0487	0.0653	0.0734	0.0564	0.0417	0.0479	0.0358
Ca	2.7793	2.7260	2.7308	2.7234	2.7392	2.7944	2.8094	2.7984	2.8051	2.8603	2.8239	2.8652	2.8971	3.0294	2.9163	3.0938	3.1270	2.7934	3.0306	2.7095	2.7868	2.7535	2.7587	2.8235	2.7655	2.7705	2.8292
Na	1.1838	1.1863	1.1999	1.1969	1.2213	1.1752	1.1631	1.1570	1.1513	1.1188	1.1702	1.1099	1.1129	1.0255	1.0064	0.9404	0.9265	1.2014	0.9524	1.3312	1.1897	1.2010	1.2725	1.1490	1.2029	1.2101	1.1536
K	0.0034	0.0024	0.0022	0.0031	0.0016	0.0030	0.0005	0.0004	0.0031	0.0058	0.0037	0.0071	0.0040	0.0015	0.0004	0.0014	0.0015	0.0055	0.0000	0.0081	0.0029	0.0078	0.0065	0.0068	0.0046	0.0046	0.0078
Total	19.9685	19.9362	19.9357	19.9377	19.9531	19.9599	19.9585	19.9529	19.9478	19.9488	19.9673	19.9477	19.9692	19.9940	19.9043	19.9831	19.9958	19.9747	19.9641	20.0046	19.9654	19.9567	20.0075	19.9719	19.9644	19.9755	19.9720
An	70.13	69.68	69.47	69.47	69.16	70.39	70.72	70.75	70.90	71.88	70.70	72.08	72.25	74.71	74.34	76.69	77.14	69.93	76.09	67.05	70.08	69.63	68.43	71.08	69.69	69.60	71.04

MICROPROBE DATA TABLE C20: Composition of **plagioclase** in the UG1 Footwall and MG3 Units - all **S** samples.
Metres given below base of UG1 chromitite.
c = cumulus and intercumulus grains.
i = inclusions within cumulus orthopyroxene.

Sample	S-33	S-33	S-35	S-35	S-35	S-35	S-35	S-35	S-35	S-35	S-35	S-35	S-36	S-36	S-36	S-36	S-36	S-36	S-36	S-36	S-36	S-36	S-38	S-38	S-38	S-38	S-38
Metres	166.0	166.0	175.6	175.6	175.6	175.6	175.6	175.6	175.6	175.6	175.6	175.6	181.5	181.5	181.5	181.5	181.5	181.5	181.5	181.5	181.5	181.5	190.3	190.3	190.3	190.3	190.3
Position	i	i	c	c	c	c	c	i	i	i	i	i	c	c	c	c	c	i	i	i	i	i	i	i	i	i	i
Wt.%																											
SiO_2	51.31	51.10	51.23	51.14	49.85	50.89	48.94	50.45	50.18	50.71	50.35	50.55	48.45	48.27	48.55	47.78	47.11	52.23	49.54	50.51	49.39	50.76	53.66	51.81	51.49	51.46	51.84
Al_2O_3	30.82	30.63	30.95	31.37	31.13	31.28	32.11	31.22	31.19	30.99	31.62	31.31	33.21	33.36	32.22	32.63	32.78	30.51	31.94	31.42	32.01	30.99	29.45	30.95	30.85	30.90	30.92
Fe_2O_3	0.27	0.28	0.49	0.18	0.22	0.49	0.19	0.40	0.37	0.42	0.44	0.33	0.12	0.10	0.18	0.15	0.15	0.54	0.42	0.46	0.34	0.59	0.48	0.38	0.34	0.26	0.27
CaO	14.23	14.28	13.90	14.72	15.67	14.30	15.83	14.62	14.51	15.12	15.26	15.05	16.94	16.88	16.42	16.87	17.11	13.84	15.50	14.79	15.79	14.58	12.57	13.65	13.75	13.82	13.80
Na_2O	3.52	3.43	3.27	3.21	2.89	3.35	2.56	3.18	3.09	3.13	2.84	3.20	2.01	2.05	2.26	2.04	1.96	3.21	2.88	3.23	2.74	3.35	4.51	3.68	3.58	3.51	3.56
K_2O	0.02	0.02	0.01	0.01	0.02	0.01	0.02	0.01	0.02	0.02	0.02	0.03	0.01	0.01	0.01	0.01	0.01	0.02	0.01	0.02	0.02	0.00	0.03	0.02	0.01	0.01	0.02
Total	100.19	99.72	99.87	100.63	99.78	100.32	99.65	99.87	99.36	100.40	100.53	100.47	100.75	100.66	99.64	99.47	99.12	100.35	100.29	100.43	100.29	100.27	100.71	100.48	100.01	99.96	100.39
Cations (based on 32 oxygens):																											
Si	9.3259	9.3302	9.3275	9.2552	9.1385	9.2450	8.9848	9.2124	9.2061	9.2255	9.1463	9.1895	8.8173	8.7914	8.9269	8.8154	8.7366	9.4486	9.0395	9.1831	9.0155	9.2408	9.6611	9.3708	9.3587	9.3552	9.3807
Al	6.6026	6.5911	6.6417	6.6917	6.7266	6.6969	6.9480	6.7183	6.7437	6.6455	6.7692	6.7078	7.1223	7.1620	6.9816	7.0942	7.1641	6.5042	6.8693	6.7308	6.8869	6.6490	6.2495	6.5972	6.6078	6.6200	6.5930
Fe	0.0335	0.0340	0.0609	0.0226	0.0269	0.0597	0.0238	0.0489	0.0465	0.0522	0.0544	0.0411	0.0152	0.0119	0.0225	0.0188	0.0185	0.0661	0.0513	0.0572	0.0423	0.0722	0.0591	0.0469	0.0413	0.0317	0.0325
Ca	2.7706	2.7932	2.7118	2.8538	3.0774	2.7832	3.1139	2.8608	2.8512	2.9470	2.9701	2.9311	3.3030	3.2936	3.2355	3.3342	3.3990	2.6822	3.0296	2.8811	3.0891	2.8443	2.4254	2.6460	2.6772	2.6922	2.6746
Na	1.2413	1.2123	1.1556	1.1255	1.0256	1.1804	0.9126	1.1255	1.0973	1.1051	1.0001	1.1266	0.7104	0.7246	0.8071	0.7290	0.7058	1.1246	1.0183	1.1376	0.9677	1.1836	1.5732	1.2887	1.2601	1.2369	1.2477
K	0.0054	0.0051	0.0028	0.0031	0.0050	0.0031	0.0053	0.0018	0.0052	0.0056	0.0036	0.0064	0.0023	0.0012	0.0021	0.0018	0.0022	0.0056	0.0028	0.0038	0.0047	0.0011	0.0059	0.0037	0.0034	0.0028	0.0036
Total	19.9794	19.9660	19.9004	19.9519	20.0000	19.9684	19.9883	19.9677	19.9501	19.9810	19.9437	20.0025	19.9703	19.9846	19.9757	19.9935	20.0261	19.8313	20.0108	19.9936	20.0061	19.9909	19.9742	19.9533	19.9485	19.9388	19.9321
An	69.06	69.73	70.12	71.72	75.00	70.22	77.33	71.76	72.21	72.73	74.81	72.24	82.30	81.97	80.03	82.06	82.80	70.46	74.84	71.69	76.15	70.62	60.66	67.25	68.00	68.52	68.19

Sample	S-38	S-38	S-38	S-38	S-38	S-40	S-40	S-40	S-40	S-40	S-40	S-40	S-40	S-40	S-40	S-40	S-40	S-40	S-40	S-40	S-40	S-42	S-42	S-42	S-42	S-42	S-42	S-42
Metres	190.3	190.3	190.3	190.3	190.3	199.3	199.3	199.3	199.3	199.3	199.3	199.3	199.3	199.3	199.3	199.3	199.3	199.3	199.3	199.3	199.3	208.1	208.1	208.1	208.1	208.1	208.1	208.1
Position	c	c	c	c	c	i	i	i	i	i	i	i	i	i	i	c	c	c	c	c	c	c	c	c	c	c	i	i
Wt.%																												
SiO_2	52.52	52.49	53.11	50.07	52.49	51.10	50.94	50.23	50.95	50.77	50.94	50.23	50.95	50.77	51.10	50.52	51.33	49.89	50.49	51.33	52.92	49.56	49.36	49.08	49.07	49.28	48.29
Al_2O_3	30.65	30.57	30.03	31.08	29.82	31.63	31.24	31.56	31.12	31.32	31.24	31.56	31.12	31.32	31.63	31.42	30.57	31.77	31.09	30.57	29.81	32.33	32.07	32.40	32.50	32.45	32.66
Fe_2O_3	0.19	0.16	0.17	0.14	0.19	0.31	0.12	0.34	0.38	0.32	0.12	0.34	0.38	0.32	0.31	0.06	0.10	0.10	0.14	0.10	0.15	0.19	0.34	0.25	0.23	0.31	0.27
CaO	13.84	13.90	13.25	14.16	12.75	14.39	14.14	14.47	14.11	14.32	14.14	14.47	14.11	14.32	14.39	14.77	14.12	15.34	14.84	14.12	12.76	15.76	15.12	15.48	15.98	15.94	16.21
Na_2O	3.47	3.69	3.73	3.56	4.42	3.16	3.27	2.99	3.41	3.22	3.27	2.99	3.41	3.22	3.16	3.21	3.54	2.89	3.18	3.54	4.39	2.73	2.72	2.62	2.51	2.47	2.35
K_2O	0.02	0.02	0.03	0.01	0.01	0.01	0.02	0.02	0.03	0.03	0.02	0.02	0.03	0.03	0.01	0.02	0.03	0.02	0.02	0.03	0.01	0.00	0.01	0.01	0.01	0.00	0.00
Total	100.68	100.83	100.33	99.02	99.69	100.62	99.74	99.61	100.00	99.98	99.73	99.61	100.00	99.98	100.62	99.98	99.69	100.00	99.76	99.69	100.04	100.58	99.62	99.84	100.31	100.46	99.78
Cations (based on 32 oxygens):																												
Si	9.4622	9.4537	9.5850	9.2162	9.5514	9.2418	9.2845	9.1844	9.2773	9.2460	9.2848	9.1844	9.2773	9.2460	9.2418	9.2069	9.3656	9.1077	9.2286	9.3656	9.5879	9.0097	9.0464	8.9838	8.9522	8.9737	8.8696
Al	6.5079	6.4892	6.3871	6.7422	6.3964	6.7427	6.7108	6.8003	6.6781	6.7223	6.7109	6.8003	6.6781	6.7223	6.7427	6.7486	6.5739	6.8350	6.6964	6.5739	6.3650	6.9286	6.9262	6.9890	6.9888	6.9648	7.0683
Fe	0.0230	0.0199	0.0202	0.0176	0.0237	0.0384	0.0150	0.0422	0.0472	0.0391	0.0151	0.0422	0.0472	0.0391	0.0384	0.0069	0.0121	0.0123	0.0169	0.0121	0.0187	0.0239	0.0420	0.0313	0.0287	0.0388	0.0338
Ca	2.6715	2.6831	2.5627	2.7918	2.4866	2.7887	2.7619	2.8350	2.7534	2.7943	2.7614	2.8350	2.7534	2.7943	2.7887	2.8839	2.7602	2.9998	2.9066	2.7602	2.4770	3.0705	2.9696	3.0356	3.1246	3.1106	3.1887
Na	1.2113	1.2882	1.3047	1.2687	1.5581	1.1093	1.1562	1.0600	1.2024	1.1357	1.1552	1.0600	1.2024	1.1357	1.1093	1.1345	1.2528	1.0229	1.1270	1.2528	1.5421	0.9627	0.9679	0.9307	0.8878	0.8730	0.8375
K	0.0039	0.0036	0.0079	0.0032	0.0027	0.0028	0.0045	0.0049	0.0059	0.0075	0.0047	0.0049	0.0059	0.0075	0.0028	0.0037	0.0062	0.0048	0.0053	0.0062	0.0013	0.0000	0.0025	0.0019	0.0016	0.0000	0.0000
Total	19.8799	19.9376	19.8676	20.0398	20.0189	19.9237	19.9329	19.9269	19.9642	19.9449	19.9321	19.9269	19.9642	19.9449	19.9237	19.9845	19.9709	19.9825	19.9809	19.9709	19.9920	19.9954	19.9547	19.9723	19.9837	19.9610	19.9980
An	68.80	67.56	66.26	68.76	61.48	71.54	70.49	72.79	69.60	71.10	70.50	72.79	69.60	71.10	71.54	71.77	68.78	74.57	72.06	68.78	61.63	76.13	75.42	76.53	77.87	78.09	79.20

MICROPROBE DATA TABLE C20: Composition of **plagioclase** in the UG1 Footwall and MG3 Units - all **S** samples.
Metres given below base of UG1 chromitite.
c = cumulus and intercumulus grains.
i = inclusions within cumulus orthopyroxene.

Sample	S-42	S-42	S-42	S-43	S-43	S-43	S-43	S-43	S-43	S-43	S-43	S-43	S-43	S-45	S-45	S-45	S-45	S-45	S-45	S-45	S-45	S-45	S-45	S-49	S-49	S-49	S-49
Metres	208.1	208.1	208.1	213.2	213.2	213.2	213.2	213.2	213.2	213.2	213.2	213.2	213.2	221.9	221.9	221.9	221.9	221.9	221.9	221.9	221.9	221.9	221.9	238.9	238.9	238.9	238.9
Position	i	i	i	i	i	i	i	i	i	c	c	c	c	c	i	i	i	i	i	i	c	c	c	c	c	c	c
Wt.%																											
SiO_2	49.30	48.86	49.51	49.21	49.62	50.37	49.76	49.46	50.01	49.42	49.94	49.50	49.65	50.08	50.91	51.02	51.00	50.56	49.64	49.42	49.57	49.23	49.48	47.61	48.37	48.61	46.72
Al_2O_3	32.25	32.52	32.40	31.38	31.31	30.46	30.82	31.34	30.93	31.29	30.77	31.19	31.20	31.52	31.37	31.32	31.19	31.51	31.85	31.97	31.53	32.07	31.88	32.90	32.20	32.14	33.39
Fe_2O_3	0.27	0.39	0.25	0.53	0.44	0.52	0.51	0.44	0.22	0.21	0.18	0.20	0.18	0.28	0.32	0.38	0.30	0.39	0.13	0.11	0.15	0.11	0.17	0.17	0.25	0.25	0.17
CaO	15.46	15.67	15.87	15.22	15.05	14.26	14.74	15.18	14.70	15.35	14.82	15.16	15.15	15.27	14.68	14.38	14.31	14.71	15.76	15.81	15.69	15.88	15.81	16.63	15.96	15.87	17.48
Na_2O	2.74	2.71	2.65	3.07	3.18	3.61	3.33	2.98	3.38	3.06	3.27	3.06	3.14	2.94	3.29	3.39	3.31	2.99	2.68	2.58	2.68	2.53	2.63	2.14	2.46	2.68	1.66
K_2O	0.01	0.01	0.02	0.01	0.00	0.00	0.02	0.02	0.02	0.02	0.03	0.02	0.01	0.01	0.03	0.02	0.02	0.03	0.01	0.00	0.01	0.01	0.01	0.01	0.01	0.02	0.00
Total	100.02	100.16	100.68	99.43	99.61	99.23	99.17	99.43	99.27	99.35	99.01	99.12	99.34	100.10	100.61	100.51	100.13	100.19	100.07	99.89	99.62	99.83	99.98	99.46	99.25	99.56	99.42
Cations (based on 32 oxygens):																											
Si	9.0092	8.9329	8.9953	9.0648	9.1125	9.2695	9.1751	9.0990	9.1992	9.0992	9.2096	9.1262	9.1348	9.1377	9.2277	9.2501	9.2730	9.1975	9.0661	9.0413	9.0931	9.0149	9.0491	8.7837	8.9259	8.9447	8.6432
Al	6.9457	7.0078	6.9374	6.8116	6.7762	6.6051	6.6969	6.7955	6.7049	6.7902	6.6878	6.7781	6.7653	6.7779	6.7022	6.6920	6.6841	6.7559	6.8565	6.8931	6.8168	6.9224	6.8709	7.1526	7.0032	6.9704	7.2795
Fe	0.0329	0.0485	0.0304	0.0667	0.0549	0.0643	0.0631	0.0553	0.0277	0.0262	0.0220	0.0245	0.0223	0.0344	0.0392	0.0461	0.0374	0.0483	0.0160	0.0142	0.0190	0.0137	0.0206	0.0210	0.0318	0.0314	0.0216
Ca	3.0279	3.0690	3.0896	3.0037	2.9611	2.8121	2.9114	2.9917	2.8972	3.0282	2.9285	2.9945	2.9871	2.9847	2.8511	2.7939	2.7869	2.8671	3.0835	3.0988	3.0831	3.1161	3.0975	3.2879	3.1556	3.1290	3.4640
Na	0.9692	0.9589	0.9321	1.0958	1.1335	1.2885	1.1910	1.0625	1.2057	1.0919	1.1687	1.0946	1.1206	1.0402	1.1569	1.1930	1.1656	1.0552	0.9500	0.9149	0.9517	0.8983	0.9317	0.7670	0.8789	0.9542	0.5959
K	0.0025	0.0024	0.0044	0.0030	0.0008	0.0009	0.0053	0.0055	0.0054	0.0055	0.0066	0.0041	0.0031	0.0025	0.0061	0.0045	0.0040	0.0076	0.0012	0.0008	0.0023	0.0017	0.0027	0.0015	0.0013	0.0036	0.0000
Total	19.9874	20.0196	19.9891	20.0455	20.0391	20.0405	20.0430	20.0095	20.0401	20.0412	20.0232	20.0219	20.0333	19.9775	19.9831	19.9796	19.9511	19.9317	19.9733	19.9630	19.9660	19.9671	19.9724	20.0137	19.9967	20.0333	20.0042
An	75.75	76.19	76.82	73.27	72.32	68.58	70.97	73.79	70.61	73.50	71.47	73.23	72.72	74.16	71.13	70.08	70.51	73.10	76.45	77.20	76.41	77.62	76.88	81.09	78.22	76.63	85.32

Sample	S-49	S-49	S-49	S-49	S-49	S-49	S-52	S-52	S-52	S-52	S-52	S-52	S-52	S-52	S-52	S-52	S-54	S-54	S-54	S-54	S-54	S-54	S-54	S-54	S-54	S-54	S-56
Metres	238.9	238.9	238.9	238.9	238.9	238.9	252.2	252.2	252.2	252.2	252.2	252.2	252.2	252.2	252.2	252.2	261.4	261.4	261.4	261.4	261.4	261.4	261.4	261.4	261.4	261.4	270.2
Position	c	i	i	i	i	i	c	c	c	c	c	i	i	i	i	i	i	i	i	i	i	c	c	c	c	c	c
Wt.%																											
SiO_2	47.08	49.43	48.62	49.26	48.86	50.08	53.00	52.70	51.55	51.95	51.61	53.07	53.18	54.41	51.38	53.37	52.19	52.47	52.68	51.62	52.30	51.40	51.97	52.11	52.13	52.33	50.83
Al_2O_3	33.25	32.21	32.04	31.71	31.93	31.11	29.46	29.97	30.36	30.30	30.55	29.43	29.47	28.64	30.52	29.39	30.10	30.31	30.47	31.11	30.82	30.94	30.73	30.63	30.60	30.39	31.60
Fe_2O_3	0.17	0.48	0.50	0.44	0.40	0.36	0.28	0.30	0.36	0.23	0.25	0.32	0.44	0.73	0.42	0.53	0.47	0.46	0.34	0.28	0.31	0.28	0.25	0.24	0.19	0.13	0.29
CaO	17.16	15.51	15.91	15.54	15.74	14.91	12.78	13.04	13.97	13.80	13.94	12.60	12.78	11.73	14.11	12.74	13.43	13.75	13.51	14.59	14.08	14.43	14.21	13.98	14.20	13.78	14.80
Na_2O	1.80	2.68	2.60	2.80	2.81	3.29	4.10	4.05	3.60	3.70	3.60	4.32	4.09	4.87	3.64	4.14	3.72	3.79	3.76	3.36	3.56	3.25	3.52	3.61	3.45	3.75	3.15
K_2O	0.00	0.01	0.03	0.00	0.01	0.01	0.04	0.03	0.03	0.05	0.02	0.04	0.04	0.03	0.02	0.04	0.04	0.03	0.04	0.03	0.04	0.04	0.04	0.03	0.04	0.06	0.01
Total	99.46	100.31	99.70	99.76	99.73	99.75	99.66	100.08	99.88	100.02	99.98	99.78	100.00	100.40	100.10	100.20	99.94	100.81	100.80	100.99	101.11	100.33	100.71	100.60	100.62	100.45	100.68
Cations (based on 32 oxygens):																											
Si	8.6960	9.0126	8.9429	9.0394	8.9775	9.1737	9.6334	9.5488	9.3933	9.4400	9.3874	9.6380	9.6362	9.8098	9.3522	9.6533	9.4847	9.4642	9.4853	9.3095	9.4048	9.3246	9.3864	9.4153	9.4176	9.4634	9.2031
Al	7.2385	6.9213	6.9463	6.8577	6.9146	6.7172	6.3116	6.4009	6.5194	6.4888	6.5500	6.2989	6.2943	6.0853	6.5469	6.2651	6.4470	6.4430	6.4664	6.6130	6.5306	6.6143	6.5407	6.5229	6.5148	6.4773	6.7432
Fe	0.0218	0.0592	0.0618	0.0542	0.0492	0.0448	0.0346	0.0363	0.0448	0.0287	0.0313	0.0391	0.0539	0.0891	0.0517	0.0649	0.0577	0.0566	0.0414	0.0347	0.0380	0.0342	0.0308	0.0291	0.0234	0.0161	0.0361
Ca	3.3958	3.0301	3.1361	3.0559	3.0982	2.9256	2.4884	2.5321	2.7273	2.6870	2.7158	2.4521	2.4817	2.2652	2.7523	2.4683	2.6146	2.6563	2.6061	2.8187	2.7125	2.8036	2.7493	2.7057	2.7486	2.6689	2.8707
Na	0.6427	0.9463	0.9254	0.9941	1.0007	1.1666	1.4428	1.4230	1.2717	1.3033	1.2697	1.5211	1.4381	1.7010	1.2858	1.4501	1.3097	1.3235	1.3131	1.1753	1.2400	1.1410	1.2321	1.2642	1.2077	1.3154	1.1067
K	0.0005	0.0015	0.0063	0.0010	0.0018	0.0018	0.0082	0.0061	0.0074	0.0105	0.0051	0.0084	0.0092	0.0064	0.0054	0.0101	0.0082	0.0080	0.0100	0.0063	0.0099	0.0081	0.0091	0.0074	0.0102	0.0130	0.0016
Total	19.9954	19.9710	20.0188	20.0023	20.0419	20.0295	19.9190	19.9472	19.9641	19.9582	19.9593	19.9577	19.9134	19.9567	19.9941	19.9118	19.9219	19.9517	19.9223	19.9575	19.9359	19.9258	19.9484	19.9445	19.9223	19.9542	19.9614
An	84.08	76.20	77.22	75.45	75.59	71.49	63.30	64.02	68.20	67.34	68.14	61.72	63.31	57.11	68.16	62.99	66.63	66.74	66.50	70.57	68.63	71.07	69.05	68.16	69.47	66.98	72.18

MICROPROBE DATA TABLE C20: Composition of **plagioclase** in the UG1 Footwall and MG3 Units - all **S** samples.
Metres given below base of UG1 chromitite.
c = cumulus and intercumulus grains.
i = inclusions within cumulus orthopyroxene.

Sample	S-56	S-56	S-56	S-56	S-56	S-56	S-56	S-56	S-56	S-58	S-58	S-58	S-58	S-58	S-58	S-58	S-58	S-58	S-58	S-59	S-59	S-59	S-59	S-59	S-59	S-59	S-59
Metres	270.2	270.2	270.2	270.2	270.2	270.2	270.2	270.2	270.2	279.7	279.7	279.7	279.7	279.7	279.7	279.7	279.7	279.7	279.7	286.4	286.4	286.4	286.4	286.4	286.4	286.4	286.4
Position	c	c	c	c	i	i	i	i	i	c	c	c	c	c	i	i	i	i	i	c	c	c	c	c	i	i	i
Wt.%																											
SiO_2	51.43	50.54	50.54	51.32	51.45	50.80	50.70	50.81	50.70	54.16	54.18	53.91	53.59	51.89	53.90	53.71	53.79	53.40	53.30	51.00	50.99	53.39	50.99	51.00	51.14	53.37	53.49
Al_2O_3	31.46	31.04	31.04	31.14	30.47	30.84	30.93	31.16	30.92	29.29	29.66	29.63	30.03	30.89	29.73	29.96	29.98	30.08	29.77	30.63	30.40	28.99	30.39	30.63	30.44	29.30	29.09
Fe_2O_3	0.26	0.18	0.18	0.23	0.38	0.32	0.33	0.41	0.40	0.27	0.29	0.21	0.26	0.23	0.40	0.44	0.40	0.43	0.36	0.23	0.16	0.28	0.17	0.23	0.17	0.38	0.47
CaO	14.73	14.49	14.49	14.55	14.23	14.79	14.87	14.72	14.71	12.02	11.93	12.27	12.48	13.71	12.09	12.25	12.32	12.53	12.35	14.34	14.08	12.47	14.10	14.34	14.26	12.22	12.03
Na_2O	3.31	3.29	3.29	3.40	3.34	3.07	3.09	3.24	3.26	4.63	4.53	4.42	4.34	3.63	4.40	4.40	4.23	4.15	4.33	3.38	3.74	4.60	3.73	3.38	3.69	4.59	4.59
K_2O	0.01	0.01	0.01	0.00	0.01	0.01	0.02	0.02	0.02	0.04	0.04	0.03	0.04	0.03	0.03	0.03	0.02	0.03	0.03	0.02	0.02	0.03	0.02	0.02	0.03	0.03	0.02
Total	101.20	99.55	99.55	100.65	99.89	99.84	99.93	100.36	100.01	100.40	100.63	100.46	100.74	100.39	100.56	100.79	100.75	100.62	100.13	99.60	99.39	99.76	99.41	99.60	99.73	99.89	99.71
Cations (based on 32 oxygens):																											
Si	9.2598	9.2487	9.2487	9.2884	9.3727	9.2744	9.2526	9.2356	9.2498	9.7493	9.7254	9.6995	9.6261	9.3889	9.6901	9.6433	9.6535	9.6070	9.6343	9.3239	9.3450	9.6988	9.3438	9.3239	9.3434	9.6771	9.7120
Al	6.6750	6.6952	6.6952	6.6423	6.5425	6.6358	6.6522	6.6762	6.6488	6.2140	6.2734	6.2830	6.3581	6.5867	6.2986	6.3397	6.3415	6.3770	6.3418	6.5991	6.5660	6.2072	6.5643	6.5991	6.5553	6.2606	6.2255
Fe	0.0317	0.0224	0.0224	0.0283	0.0473	0.0392	0.0404	0.0500	0.0493	0.0334	0.0358	0.0250	0.0321	0.0288	0.0485	0.0536	0.0488	0.0529	0.0443	0.0288	0.0195	0.0341	0.0215	0.0288	0.0212	0.0469	0.0583
Ca	2.8420	2.8404	2.8404	2.8212	2.7783	2.8932	2.9072	2.8662	2.8748	2.3188	2.2934	2.3652	2.4023	2.6585	2.3286	2.3554	2.3693	2.4146	2.3910	2.8094	2.7651	2.4267	2.7681	2.8094	2.7911	2.3740	2.3401
Na	1.1536	1.1686	1.1686	1.1911	1.1801	1.0879	1.0931	1.1411	1.1513	1.6150	1.5746	1.5404	1.5101	1.2733	1.5339	1.5300	1.4723	1.4460	1.5160	1.1975	1.3293	1.6201	1.3258	1.1975	1.3083	1.6142	1.6150
K	0.0030	0.0029	0.0029	0.0010	0.0033	0.0034	0.0042	0.0055	0.0056	0.0082	0.0094	0.0073	0.0103	0.0078	0.0070	0.0065	0.0040	0.0073	0.0067	0.0047	0.0041	0.0074	0.0056	0.0047	0.0060	0.0070	0.0053
Total	19.9651	19.9783	19.9783	19.9724	19.9242	19.9338	19.9498	19.9746	19.9796	19.9386	19.9120	19.9203	19.9389	19.9439	19.9068	19.9284	19.8895	19.9047	19.9340	19.9633	20.0290	19.9943	20.0290	19.9633	20.0254	19.9797	19.9563
An	71.13	70.85	70.85	70.31	70.19	72.67	72.67	71.52	71.40	58.95	59.29	60.56	61.40	67.62	60.29	60.62	61.67	62.55	61.20	70.11	67.53	59.97	67.62	70.11	68.09	59.53	59.17

Sample	S-59	S-59	S-62d	S-62d	S-62d	S-62d	S-66	S-66	S-66	S-66	S-66	S-66	S-66	S-66	S-66	S-66	S-68	S-68	S-68	S-68	S-68	S-68	S-68	S-68	S-68	S-71	S-71
Metres	286.4	286.4	296.0	296.0	296.0	296.0	307.9	307.9	307.9	307.9	307.9	307.9	307.9	307.9	307.9	307.9	310.2	310.2	310.2	310.2	310.2	310.2	310.2	310.2	310.2	325.0	325.0
Position	i	i	c	c	c	c	i	i	i	i	c	c	c	c	c	c	c	c	c	c	i	i	i	i	i	c	c
Wt.%																											
SiO_2	53.61	53.07	49.38	49.54	49.68	49.55	49.84	50.03	50.11	48.38	49.78	50.51	49.94	50.07	49.92	49.10	49.65	49.65	49.73	49.69	49.88	48.76	49.09	49.13	48.89	49.51	49.07
Al_2O_3	29.26	29.01	32.19	32.29	32.08	32.15	31.44	31.43	30.93	32.32	31.40	30.97	31.48	31.25	31.61	32.15	31.84	31.85	31.78	31.99	31.43	32.46	32.19	31.95	31.83	31.61	31.90
Fe_2O_3	0.33	0.46	0.16	0.16	0.19	0.14	0.48	0.38	0.76	0.59	0.27	0.25	0.38	0.29	0.22	0.25	0.29	0.26	0.24	0.20	0.37	0.54	0.47	0.45	0.50	0.24	0.31
CaO	12.27	12.33	15.83	15.55	15.69	15.42	14.65	14.71	13.98	15.48	14.59	13.88	14.64	14.33	14.71	15.71	15.46	15.46	15.66	15.52	15.03	16.02	15.89	15.83	15.84	15.67	16.03
Na_2O	4.59	4.63	2.81	2.82	2.80	2.81	3.07	3.07	3.36	2.42	2.95	3.30	2.92	3.00	2.95	2.65	2.64	2.63	2.65	2.73	2.77	2.40	2.46	2.58	2.51	2.69	2.55
K_2O	0.02	0.02	0.02	0.01	0.02	0.02	0.01	0.02	0.02	0.01	0.02	0.02	0.01	0.02	0.01	0.02	0.00	0.03	0.01	0.01	0.01	0.01	0.01	0.01	0.01	0.01	0.02
Total	100.09	99.52	100.39	100.37	100.46	100.09	99.49	99.64	99.16	99.20	99.01	98.95	99.37	98.96	99.42	99.87	99.88	99.88	100.07	100.15	99.48	100.18	100.11	99.95	99.58	99.74	99.87
Cations (based on 32 oxygens):																											
Si	9.6979	9.6708	9.0027	9.0216	9.0425	9.0437	9.1438	9.1615	9.2195	8.9264	9.1627	9.2831	9.1613	9.2111	9.1508	8.9939	9.0791	9.0791	9.0804	9.0642	9.1480	8.9196	8.9769	9.0006	8.9922	9.0766	8.9985
Al	6.2388	6.2305	6.9162	6.9297	6.8825	6.9148	6.7973	6.7825	6.7068	7.0280	6.8127	6.7086	6.8055	6.7745	6.8284	6.9398	6.8605	6.8640	6.8403	6.8778	6.7923	6.9974	6.9384	6.8984	6.9009	6.8295	6.8943
Fe	0.0408	0.0564	0.0203	0.0197	0.0230	0.0177	0.0600	0.0470	0.0947	0.0743	0.0334	0.0312	0.0473	0.0358	0.0274	0.0309	0.0364	0.0318	0.0298	0.0244	0.0459	0.0663	0.0581	0.0563	0.0628	0.0303	0.0388
Ca	2.3786	2.4070	3.0915	3.0340	3.0600	3.0151	2.8792	2.8856	2.7566	3.0593	2.8781	2.7333	2.8777	2.8251	2.8899	3.0840	3.0288	3.0295	3.0632	3.0333	2.9541	3.1392	3.1132	3.1074	3.1215	3.0785	3.1492
Na	1.6078	1.6362	0.9927	0.9945	0.9878	0.9933	1.0914	1.0903	1.1985	0.8663	1.0512	1.1759	1.0378	1.0706	1.0471	0.9399	0.9340	0.9307	0.9382	0.9667	0.9841	0.8503	0.8727	0.9158	0.8955	0.9545	0.9049
K	0.0046	0.0057	0.0040	0.0029	0.0057	0.0041	0.0030	0.0042	0.0058	0.0026	0.0035	0.0058	0.0028	0.0041	0.0025	0.0044	0.0010	0.0064	0.0034	0.0030	0.0012	0.0019	0.0034	0.0031	0.0016	0.0027	0.0035
Total	19.9685	20.0067	20.0273	20.0024	20.0015	19.9888	19.9747	19.9711	19.9819	19.9569	19.9416	19.9379	19.9325	19.9211	19.9461	19.9929	19.9399	19.9416	19.9553	19.9695	19.9256	19.9747	19.9628	19.9815	19.9746	19.9721	19.9892
An	59.67	59.53	75.69	75.31	75.60	75.22	72.51	72.58	69.70	77.93	73.25	69.92	73.50	72.52	73.40	76.64	76.43	76.50	76.55	75.83	75.01	78.69	78.11	77.24	77.71	76.33	77.68

MICROPROBE DATA TABLE C20: Composition of **plagioclase** in the UG1 Footwall and MG3 Units - all S samples.
Metres given below base of UG1 chromitite.
c = cumulus and intercumulus grains.
i = inclusions within cumulus orthopyroxene.

Sample	S-71	S-71	S-71	S-71	S-71	S-71	S-71	S-78b	S-78b	S-78b	S-78b	S-78b	S-81	S-81	S-81	S-81	S-81
Metres	325.0	325.0	325.0	325.0	325.0	325.0	325.0	340.7	340.7	340.7	340.7	340.7	344.9	344.9	344.9	344.9	344.9
Position	c	c	i	i	i	i	i	c	c	c	c	c	c	c	c	c	c
Wt.%																	
SiO_2	48.15	49.38	49.12	49.47	48.24	49.38	49.42	49.34	49.26	49.30	50.04	49.12	49.62	49.27	49.05	49.78	50.21
Al_2O_3	32.10	31.54	31.68	31.21	32.34	31.91	31.75	31.89	32.08	31.96	31.17	31.76	32.25	32.42	32.11	31.79	31.43
Fe_2O_3	0.28	0.31	0.40	0.45	0.61	0.48	0.32	0.39	0.36	0.39	0.45	0.47	0.25	0.24	0.27	0.30	0.16
CaO	16.29	15.39	15.77	15.21	16.10	15.53	15.58	15.98	15.66	15.78	15.26	15.71	16.08	15.83	15.99	15.45	14.98
Na_2O	2.40	2.90	2.63	2.87	2.34	2.77	2.74	2.59	2.52	2.53	2.91	2.60	2.51	2.52	2.55	2.75	3.09
K_2O	0.02	0.03	0.01	0.02	0.01	0.01	0.00	0.01	0.02	0.00	0.00	0.01	0.01	0.01	0.01	0.01	0.01
Total	99.24	99.55	99.60	99.22	99.64	100.07	99.81	100.20	99.88	99.97	99.84	99.67	100.72	100.30	100.00	100.09	99.88
Cations (based on 32 oxygens):																	
Si	8.9005	9.0732	9.0294	9.1165	8.8826	9.0302	9.0549	9.0185	9.0167	9.0213	9.1591	9.0220	9.0125	8.9833	8.9815	9.0863	9.1713
Al	6.9922	6.8308	6.8619	6.7783	7.0172	6.8766	6.8566	6.8681	6.9202	6.8937	6.7248	6.8748	6.9040	6.9670	6.9299	6.8403	6.7658
Fe	0.0352	0.0380	0.0494	0.0559	0.0759	0.0599	0.0400	0.0485	0.0440	0.0488	0.0558	0.0581	0.0310	0.0295	0.0337	0.0372	0.0199
Ca	3.2250	3.0302	3.1055	3.0021	3.1769	3.0434	3.0583	3.1294	3.0716	3.0945	2.9937	3.0917	3.1303	3.0924	3.1371	3.0225	2.9308
Na	0.8609	1.0340	0.9357	1.0236	0.8352	0.9816	0.9731	0.9157	0.8937	0.8970	1.0336	0.9265	0.8823	0.8894	0.9058	0.9746	1.0941
K	0.0048	0.0066	0.0016	0.0037	0.0014	0.0013	0.0011	0.0016	0.0036	0.0011	0.0007	0.0035	0.0021	0.0032	0.0035	0.0029	0.0025
Total	20.0186	20.0127	19.9836	19.9800	19.9892	19.9930	19.9839	19.9819	19.9499	19.9565	19.9678	19.9766	19.9622	19.9648	19.9914	19.9637	19.9842
An	78.93	74.56	76.85	74.57	79.18	75.61	75.86	77.36	77.46	77.53	74.34	76.94	78.01	77.66	77.59	75.62	72.82

MICROPROBE DATA TABLE C21: Composition of **plagioclase** in the Bastard Unit - profile **LEF**.
Metres given above base of Unit.

Sample	H979.91	H979.91	H979.91	H979.91	H984.48	H984.48	H984.48	H984.48	H984.48	H992.8	H992.8	H992.8	H992.8	H992.8	H995.5	H995.5	H995.5	H995.5	H995.5	H995.66	H995.66	H995.66	H995.66	H995.66	H997.11	H997.11	H997.11
Metres	18.29	18.29	18.29	18.29	13.72	13.72	13.72	13.72	13.72	5.40	5.40	5.40	5.40	5.40	2.70	2.70	2.70	2.70	2.70	2.50	2.50	2.50	2.50	2.50	1.09	1.09	1.09
Postition																											
Wt.%																											
SiO_2	49.51	49.72	49.06	48.66	49.75	49.00	49.48	49.62	49.15	49.86	49.25	49.23	49.27	49.82	49.27	49.01	48.99	48.60	48.87	49.38	49.73	49.65	49.22	49.23	49.29	49.81	49.70
Al_2O_3	31.99	31.95	31.91	32.10	32.07	32.26	32.73	32.09	32.86	32.22	32.38	32.54	32.11	32.30	31.78	32.06	32.23	32.50	32.34	32.23	32.03	31.64	32.29	32.00	32.98	32.41	32.46
Fe_2O_3	0.34	0.33	0.44	0.34	0.41	0.38	0.39	0.37	0.45	0.33	0.35	0.33	0.32	0.33	0.61	0.37	0.41	0.37	0.38	0.59	0.49	0.49	0.54	0.57	0.37	0.36	0.28
CaO	15.93	15.85	15.73	15.99	15.84	15.98	16.13	15.77	16.40	15.54	15.88	15.83	15.45	15.79	15.53	16.03	15.70	16.13	16.00	15.97	15.36	15.67	16.12	15.80	16.20	15.70	15.70
Na_2O	2.66	2.67	2.65	2.59	2.61	2.62	2.47	2.74	2.40	2.65	2.58	2.55	2.71	2.72	2.81	2.62	2.68	2.50	2.53	2.58	2.82	2.62	2.49	2.63	2.46	2.67	2.77
K_2O	0.18	0.16	0.14	0.14	0.14	0.12	0.10	0.12	0.12	0.13	0.12	0.12	0.13	0.13	0.20	0.13	0.10	0.11	0.09	0.12	0.16	0.17	0.14	0.15	0.10	0.15	0.13
Total	100.60	100.68	99.93	99.82	100.82	100.34	101.29	100.72	101.38	100.73	100.55	100.60	99.99	101.09	100.20	100.23	100.11	100.21	100.21	100.86	100.59	100.23	100.79	100.37	101.40	101.09	101.03
Cations (based on 32 oxygens):																											
Si	9.0185	9.0429	8.9971	8.9415	9.0353	8.9525	8.9483	9.0234	8.8944	9.0485	8.9704	8.9592	9.0147	9.0209	9.0180	8.9677	8.9655	8.8970	8.9385	8.9768	9.0481	9.0701	8.9568	8.9929	8.9077	9.0157	9.0031
Al	6.8671	6.8492	6.8965	6.9517	6.8636	6.9471	6.9755	6.8771	7.0092	6.8923	6.9519	6.9803	6.9250	6.8933	6.8560	6.9151	6.9509	7.0116	6.9716	6.9061	6.8684	6.8117	6.9252	6.8889	7.0250	6.9145	6.9299
Fe	0.0418	0.0405	0.0552	0.0424	0.0504	0.0467	0.0472	0.0456	0.0549	0.0411	0.0427	0.0402	0.0394	0.0405	0.0753	0.0460	0.0510	0.0455	0.0471	0.0721	0.0606	0.0610	0.0667	0.0707	0.0455	0.0445	0.0339
Ca	3.1093	3.0895	3.0905	3.1488	3.0826	3.1276	3.1252	3.0731	3.1807	3.0214	3.0993	3.0866	3.0281	3.0639	3.0454	3.1435	3.0782	3.1643	3.1362	3.1115	2.9943	3.0665	3.1439	3.0928	3.1366	3.0454	3.0476
Na	0.9388	0.9428	0.9425	0.9226	0.9186	0.9268	0.8657	0.9641	0.8406	0.9337	0.9095	0.9000	0.9623	0.9559	0.9970	0.9275	0.9513	0.8869	0.8959	0.9079	0.9941	0.9287	0.8779	0.9298	0.8619	0.9351	0.9721
K	0.0415	0.0376	0.0329	0.0318	0.0328	0.0269	0.0227	0.0281	0.0278	0.0295	0.0267	0.0286	0.0293	0.0311	0.0458	0.0314	0.0244	0.0253	0.0217	0.0273	0.0378	0.0399	0.0314	0.0343	0.0228	0.0342	0.0290
Total	20.0172	20.0025	20.0147	20.0387	19.9833	20.0275	19.9846	20.0114	20.0077	19.9664	20.0004	19.9949	19.9989	20.0057	20.0377	20.0312	20.0213	20.0305	20.0110	20.0017	20.0034	19.9779	20.0019	20.0093	19.9995	19.9894	20.0156
An	76.81	76.62	76.63	77.34	77.04	77.14	78.31	76.12	79.10	76.39	77.31	77.43	75.88	76.22	75.34	77.22	76.39	78.11	77.78	77.41	75.08	76.75	78.17	76.89	78.45	76.51	75.82

Sample	H997.11	H997.11	H997.26	H997.26	H997.26	H997.26	H997.26	H997.95	H997.95	H997.95	H997.95	H997.95	H998.1	H998.1	H998.1	H998.1	H998.1	H998.1	H998.1	H998.1	H998.1	H998.1	H998.1	H998.1	H998.1	H998.1	H998.1
Metres	1.09	1.09	0.94	0.94	0.94	0.94	0.94	0.25	0.25	0.25	0.25	0.25	0.10	0.10	0.10	0.10	0.10	0.01	0.01	0.01	0.01	0.01	-0.01	-0.01	-0.01	-0.01	-0.01
Postition													t	t	t	t	t	c	c	c	c	c					
Wt.%													(10cm above basal contact = t)					(At basal contact = c)									
SiO_2	48.91	49.37	48.59	48.07	47.01	48.57	48.03	48.74	49.34	49.24	49.42	49.10	50.44	50.20	49.82	49.77	49.71	48.35	48.47	48.73	49.36	48.97	47.19	47.27	48.47	47.33	47.92
Al_2O_3	32.43	32.36	32.06	32.19	32.69	32.30	32.32	32.75	32.39	32.67	32.72	32.67	31.94	31.55	31.59	31.48	31.35	31.66	31.90	31.87	32.02	32.39	33.36	33.42	32.62	33.15	31.85
Fe_2O_3	0.36	0.41	0.43	0.42	0.40	0.43	0.42	0.44	0.36	0.38	0.47	0.40	0.29	0.27	0.30	0.28	0.21	0.50	0.48	0.48	0.55	0.50	0.38	0.47	0.32	0.26	0.36
CaO	16.21	15.93	16.18	16.19	16.85	15.84	16.09	16.41	15.83	16.31	16.24	16.11	15.08	14.89	14.97	14.64	14.73	15.98	15.97	16.09	15.89	16.36	17.37	17.14	16.52	17.12	16.15
Na_2O	2.50	2.57	2.44	2.36	2.21	2.42	2.53	2.35	2.61	2.35	2.44	2.42	2.89	2.95	2.77	2.83	2.96	2.55	2.55	2.53	2.62	2.43	1.75	1.87	2.40	2.03	2.47
K_2O	0.14	0.12	0.13	0.11	0.09	0.14	0.11	0.13	0.14	0.14	0.13	0.22	0.22	0.20	0.18	0.20	0.18	0.15	0.16	0.13	0.14	0.13	0.05	0.08	0.05	0.03	0.12
Total	100.56	100.76	99.83	99.34	99.25	99.68	99.50	100.81	100.67	101.09	101.41	100.93	100.86	100.06	99.62	99.20	99.13	99.18	99.53	99.83	100.59	100.76	100.10	100.24	100.38	99.91	98.87
Cations (based on 32 oxygens):																											
Si	8.9224	8.9763	8.9326	8.8824	8.7226	8.9286	8.8644	8.8738	8.9768	8.9294	8.9348	8.9214	9.1324	9.1590	9.1294	9.1509	9.1511	8.9507	8.9394	8.9579	8.9969	8.9211	8.6742	8.6770	8.8631	8.7114	8.9003
Al	6.9736	6.9342	6.9451	7.0097	7.1480	6.9982	7.0307	7.0268	6.9451	6.9825	6.9710	6.9964	6.8156	6.7835	6.8223	6.8228	6.8030	6.9071	6.9337	6.9060	6.8797	6.9533	7.2277	7.2311	7.0305	7.1913	6.9725
Fe	0.0450	0.0500	0.0538	0.0531	0.0500	0.0531	0.0520	0.0541	0.0444	0.0465	0.0579	0.0498	0.0358	0.0332	0.0368	0.0348	0.0262	0.0627	0.0593	0.0595	0.0685	0.0617	0.0472	0.0578	0.0396	0.0326	0.0458
Ca	3.1692	3.1033	3.1858	3.2049	3.3493	3.1193	3.1821	3.2015	3.0853	3.1680	3.1453	3.1370	2.9257	2.9110	2.9392	2.8843	2.9047	3.1687	3.1568	3.1701	3.1043	3.1927	3.4210	3.3706	3.2370	3.3765	3.2133
Na	0.8824	0.9074	0.8699	0.8464	0.7960	0.8611	0.9047	0.8301	0.9205	0.8269	0.8538	0.8521	1.0146	1.0439	0.9842	1.0085	1.0567	0.9150	0.9123	0.9008	0.9266	0.8564	0.6240	0.6645	0.8517	0.7229	0.8898
K	0.0335	0.0281	0.0314	0.0256	0.0212	0.0318	0.0251	0.0291	0.0332	0.0326	0.0297	0.0499	0.0502	0.0476	0.0427	0.0466	0.0419	0.0354	0.0375	0.0309	0.0326	0.0291	0.0126	0.0194	0.0115	0.0067	0.0273
Total	20.0261	19.9993	20.0186	20.0222	20.0870	19.9922	20.0591	20.0154	20.0053	19.9859	19.9925	20.0065	19.9742	19.9784	19.9546	19.9479	19.9836	20.0396	20.0390	20.0252	20.0086	20.0143	20.0066	20.0205	20.0334	20.0415	20.0491
An	78.22	77.38	78.55	79.11	80.80	78.37	77.86	79.41	77.02	79.30	78.65	78.64	74.25	73.60	74.91	74.09	73.32	77.59	77.58	77.87	77.01	78.85	84.57	83.53	79.17	82.37	78.31

MICROPROBE DATA TABLE C22: Composition of **plagioclase** in the Bastard Unit - profile **RPM** (from Kruger, 1982).
Metres given above base of Unit.

Sample	B-10	B-13	B-13	B-13	B-13	B-13	B-13	B-13	B-13	B-15	B-15	B-15	B-15	B-15	B-15	B-15	B-15	B-19	B-19	B-19	B-19	B-19	B-19	B-19	B-19	B-20	B-20
Metres	10.4	11.2	11.2	11.2	11.2	11.2	11.2	11.2	11.2	12.7	12.7	12.7	12.7	12.7	12.7	12.7	12.7	15.0	15.0	15.0	15.0	15.0	15.0	15.0	15.0	18.6	18.6
Wt.%																											
SiO_2	49.51	48.76	48.74	49.52	49.32	48.92	48.32	48.74	48.99	49.51	48.94	48.93	48.46	48.29	48.42	48.08	48.54	50.91	49.59	48.82	50.12	49.08	47.47	49.85	50.09	50.56	49.97
Al_2O_3	32.10	32.17	32.43	31.69	32.20	32.15	32.41	32.56	32.01	31.72	32.05	31.84	31.85	32.36	31.95	32.37	32.50	30.59	31.73	32.30	31.33	32.04	32.95	31.36	31.42	31.96	32.03
Fe_2O_3	0.38	0.37	0.26	0.46	0.34	0.41	0.33	0.34	0.34	0.41	0.42	0.39	0.44	0.43	0.41	0.42	0.37	0.38	0.41	0.43	0.36	0.36	0.40	0.32	0.38	0.43	0.43
CaO	15.96	15.54	15.92	14.99	15.56	15.52	15.99	15.79	15.71	15.09	15.71	15.50	15.87	16.00	15.59	16.18	16.18	13.63	14.43	15.54	13.93	15.70	16.26	14.72	14.07	14.96	15.04
Na_2O	2.67	2.46	2.32	2.81	2.55	2.46	2.22	2.52	2.46	2.59	2.69	2.71	2.44	2.31	2.62	2.19	2.40	3.57	2.93	2.69	3.16	2.70	2.03	3.14	3.17	2.71	2.55
K_2O	0.08	0.13	0.11	0.19	0.16	0.14	0.14	0.15	0.17	0.13	0.13	0.13	0.14	0.12	0.14	0.11	0.10	0.16	0.12	0.08	0.20	0.20	0.10	0.19	0.17	0.18	0.20
Total	100.70	99.43	99.78	99.66	100.13	99.60	99.41	100.10	99.68	99.45	99.94	99.50	99.20	99.51	99.13	99.35	100.09	99.24	99.21	99.86	99.10	100.08	99.21	99.58	99.30	100.80	100.22
Cations (based on 32 oxygens):																											
Si	9.0074	8.9735	8.9407	9.0846	9.0103	8.9867	8.9045	8.9203	8.9971	9.0909	8.9752	9.0059	8.9567	8.8970	8.9526	8.8758	8.8945	9.3387	9.1164	8.9532	9.2120	8.9886	8.7781	9.1467	9.1927	9.1496	9.1001
Al	6.8828	6.9776	7.0112	6.8518	6.9331	6.9606	7.0391	7.0231	6.9284	6.8644	6.9273	6.9068	6.9379	7.0267	6.9622	7.0428	7.0188	6.6133	6.8747	6.9813	6.7867	6.9157	7.1811	6.7815	6.7960	6.8164	6.8746
Fe	0.0465	0.0457	0.0317	0.0566	0.0426	0.0511	0.0416	0.0427	0.0428	0.0511	0.0524	0.0485	0.0556	0.0541	0.0515	0.0528	0.0455	0.0469	0.0512	0.0538	0.0443	0.0441	0.0501	0.0400	0.0470	0.0531	0.0534
Ca	3.1110	3.0641	3.1289	2.9464	3.0457	3.0547	3.1571	3.0962	3.0912	2.9687	3.0868	3.0566	3.1427	3.1584	3.0884	3.2002	3.1766	2.6788	2.8422	3.0534	2.7432	3.0807	3.2215	2.8938	2.7666	2.9006	2.9346
Na	0.9415	0.8775	0.8249	0.9992	0.9029	0.8759	0.7929	0.8939	0.8757	0.9218	0.9562	0.9668	0.8741	0.8249	0.9389	0.7836	0.8524	1.2693	1.0440	0.9562	1.1257	0.9584	0.7276	1.1167	1.1276	0.9505	0.9001
K	0.0186	0.0305	0.0257	0.0445	0.0373	0.0328	0.0329	0.0350	0.0398	0.0304	0.0304	0.0305	0.0330	0.0282	0.0330	0.0259	0.0234	0.0374	0.0281	0.0187	0.0469	0.0467	0.0236	0.0445	0.0398	0.0416	0.0465
Total	20.0079	19.9689	19.9631	19.9830	19.9719	19.9618	19.9681	20.0113	19.9750	19.9274	20.0283	20.0151	20.0001	19.9892	20.0266	19.9811	20.0112	19.9845	19.9567	20.0167	19.9588	20.0341	19.9819	20.0231	19.9696	19.9117	19.9092
An	76.77	77.74	79.14	74.68	77.13	77.72	79.93	77.60	77.93	76.31	76.35	75.97	78.24	79.29	76.69	80.33	78.84	67.85	73.14	76.15	70.90	76.27	81.58	72.16	71.04	75.32	76.53

Sample	B-20	B-20	B-20	B-20	B-20	B-20	B-21	B-21	B-21	B-21	B-21	B-21	B-21	B-21	B-21	B-22	B-22	B-22	B-22	B-22	B-22	B-22	B-22	B-23	B-23	B-23	B-23
Metres	18.6	18.6	18.6	18.6	18.6	18.6	23.2	23.2	23.2	23.2	23.2	23.2	23.2	23.2	23.2	27.7	27.7	27.7	27.7	27.7	27.7	27.7	27.7	32.3	32.3	32.3	32.3
Wt.%																											
SiO_2	50.97	51.12	51.15	51.31	52.32	49.28	49.12	49.82	48.31	48.77	49.26	47.95	48.10	49.31	48.32	48.71	49.06	48.39	49.71	49.28	49.41	49.59	49.12	48.99	49.81	49.92	49.96
Al_2O_3	31.03	31.90	30.27	31.44	31.03	31.15	31.43	31.17	31.81	31.50	31.26	32.42	32.28	31.45	31.97	32.10	31.76	32.07	31.42	31.55	31.21	31.35	32.00	32.07	31.65	31.80	32.09
Fe_2O_3	0.59	0.39	0.33	0.39	0.53	0.43	0.38	0.39	0.40	0.34	0.41	0.34	0.29	0.34	0.33	0.31	0.31	0.33	0.37	0.42	0.38	0.30	0.31	0.36	0.33	0.31	0.37
CaO	14.36	14.91	14.66	14.59	14.21	16.08	14.69	14.15	14.96	15.16	14.79	16.00	15.84	14.65	15.64	15.50	15.00	15.50	14.58	14.92	14.79	14.42	15.35	15.56	14.77	14.99	15.27
Na_2O	2.88	2.72	2.98	2.91	2.71	2.71	2.87	3.16	2.58	2.64	2.77	2.24	2.36	2.89	2.46	2.48	2.81	2.45	2.97	2.94	2.87	2.82	2.56	2.61	2.91	2.76	2.77
K_2O	0.50	0.19	0.17	0.20	0.20	0.24	0.18	0.21	0.15	0.22	0.24	0.13	0.12	0.17	0.14	0.14	0.15	0.15	0.18	0.11	0.21	0.17	0.15	0.15	0.21	0.16	0.16
Total	100.33	101.23	99.56	100.84	101.00	99.89	98.67	98.90	98.21	98.63	98.73	99.08	98.99	98.81	98.86	99.24	99.09	98.89	99.23	99.22	98.87	98.65	99.49	99.74	99.68	99.94	100.62
Cations (based on 32 oxygens):																											
Si	9.2731	9.2024	9.3609	9.2672	9.4049	9.0590	9.0951	9.1889	8.9939	9.0462	9.1178	8.8714	8.9025	9.1117	8.9519	8.9796	9.0499	8.9564	9.1446	9.0802	9.1320	9.1622	9.0258	8.9925	9.1243	9.1172	9.0749
Al	6.6534	6.7680	6.5289	6.6924	6.5739	6.7487	6.8588	6.7757	6.9796	6.8862	6.8193	7.0692	7.0414	6.8492	6.9805	6.9743	6.9048	6.9957	6.8121	6.8514	6.7983	6.8265	6.9300	6.9379	6.8330	6.8449	6.8698
Fe	0.0726	0.0474	0.0413	0.0476	0.0649	0.0539	0.0474	0.0486	0.0504	0.0433	0.0515	0.0432	0.0362	0.0431	0.0418	0.0388	0.0389	0.0418	0.0457	0.0527	0.0473	0.0375	0.0387	0.0442	0.0414	0.0385	0.0451
Ca	2.7991	2.8757	2.8745	2.8233	2.7368	3.1670	2.9143	2.7962	2.9840	3.0128	2.9331	3.1716	3.1411	2.9004	3.1045	3.0615	2.9646	3.0738	2.8737	2.9455	2.9287	2.8545	3.0220	3.0601	2.8988	2.9332	2.9718
Na	1.0156	0.9490	1.0570	1.0187	0.9442	0.9656	1.0300	1.1297	0.9310	0.9491	0.9938	0.8033	0.8466	1.0351	0.8833	0.8861	1.0047	0.8789	1.0590	1.0500	1.0281	1.0099	0.9117	0.9286	1.0332	0.9770	0.9752
K	0.1160	0.0436	0.0397	0.0461	0.0459	0.0563	0.0425	0.0494	0.0356	0.0521	0.0567	0.0307	0.0283	0.0401	0.0331	0.0329	0.0353	0.0354	0.0422	0.0259	0.0495	0.0401	0.0352	0.0351	0.0491	0.0373	0.0371
Total	19.9298	19.8862	19.9024	19.8952	19.7707	20.0506	19.9881	19.9885	19.9744	19.9897	19.9720	19.9894	19.9962	19.9797	19.9951	19.9733	19.9982	19.9820	19.9772	20.0056	19.9840	19.9307	19.9633	19.9984	19.9797	19.9482	19.9738
An	73.38	75.19	73.11	73.49	74.35	76.64	73.89	71.23	76.22	76.04	74.69	79.79	78.77	73.70	77.85	77.55	74.69	77.76	73.07	73.72	74.02	73.87	76.82	76.72	73.72	75.01	75.29

MICROPROBE DATA TABLE C22: Composition of **plagioclase** in the Bastard Unit - profile **RPM** (from Kruger, 1982).
Metres given above base of Unit.

Sample	B-2	B-2	B-2	B-2	B-2	B-2	B-2	B-3	B-3	B-3	B-3	B-3	B-3	B-3	B-3	B-4	B-4	B-4	B-4	B-4	B-4	B-4	B-4	B-5a	B-5a	B-5a	B-5a
Metres	0.5	0.5	0.5	0.5	0.5	0.5	0.5	1.7	1.7	1.7	1.7	1.7	1.7	1.7	1.7	3.0	3.0	3.0	3.0	3.0	3.0	3.0	3.0	4.1	4.1	4.1	4.1
Wt.%																											
SiO_2	55.18	55.02	52.44	52.72	54.10	52.22	52.26	51.77	52.12	51.34	49.77	50.14	54.05	49.87	51.18	53.04	50.18	52.61	53.24	50.12	48.89	49.83	52.20	49.19	48.95	49.29	49.20
Al_2O_3	28.19	28.74	29.91	29.95	28.19	30.52	29.78	30.50	30.69	30.49	31.75	31.27	29.39	32.15	31.26	30.13	32.25	30.33	29.91	31.75	32.57	31.65	30.33	32.09	32.10	31.83	32.23
Fe_2O_3	0.21	0.18	0.23	0.24	0.18	0.27	0.24	0.20	0.21	0.27	0.26	0.23	0.21	0.27	0.22	0.19	0.21	0.28	0.26	0.28	0.37	0.36	0.28	0.32	0.32	0.29	0.33
CaO	11.44	11.53	13.62	13.13	11.81	13.48	13.23	12.96	13.05	13.60	14.06	13.98	11.19	15.30	14.22	12.47	14.90	12.62	12.05	14.60	15.26	14.33	12.67	16.00	15.99	15.50	15.77
Na_2O	5.01	5.01	3.84	3.92	4.95	3.79	3.73	3.72	3.50	3.21	2.92	3.13	4.39	2.64	3.27	4.54	3.07	4.28	4.74	3.21	2.62	3.13	4.00	2.59	2.67	3.03	2.84
K_2O	0.33	0.28	0.35	0.30	0.29	0.29	0.24	0.23	0.26	0.24	0.23	0.19	0.23	0.13	0.22	0.24	0.19	0.35	0.22	0.23	0.15	0.21	0.32	0.19	0.15	0.20	0.17
Total	100.36	100.76	100.39	100.26	99.52	100.57	99.48	99.38	99.83	99.15	98.99	98.94	99.46	100.36	100.37	100.61	100.80	100.47	100.42	100.19	99.86	99.51	99.80	100.38	100.18	100.14	100.54
Cations (based on 32 oxygens):																											
Si	9.9349	9.8682	9.5059	9.5478	9.8446	9.4427	9.5366	9.4503	9.4629	9.4047	9.1547	9.2248	9.7905	9.0734	9.2847	9.5648	9.0902	9.5107	9.6112	9.1360	8.9544	9.1382	9.4933	8.9839	8.9616	9.0226	8.9723
Al	5.9818	6.0752	6.3900	6.3927	6.0458	6.5043	6.4048	6.5618	6.5671	6.5826	6.8830	6.7804	6.2742	6.8939	6.6836	6.4036	6.8853	6.4621	6.3637	6.8209	7.0306	6.8406	6.5009	6.9074	6.9261	6.8669	6.9271
Fe	0.0257	0.0216	0.0286	0.0300	0.0219	0.0327	0.0302	0.0247	0.0260	0.0331	0.0318	0.0291	0.0259	0.0329	0.0273	0.0231	0.0259	0.0340	0.0312	0.0343	0.0455	0.0442	0.0342	0.0399	0.0400	0.0358	0.0412
Ca	2.2068	2.2157	2.6452	2.5477	2.3026	2.6116	2.5867	2.5347	2.5386	2.6692	2.7709	2.7557	2.1717	2.9825	2.7639	2.4093	2.8919	2.4443	2.3307	2.8514	2.9945	2.8156	2.4688	3.1309	3.1365	3.0399	3.0813
Na	1.7483	1.7416	1.3492	1.3760	1.7459	1.3283	1.3193	1.3162	1.2317	1.1397	1.0410	1.1161	1.5413	0.9310	1.1498	1.5868	1.0779	1.4997	1.6585	1.1341	0.9301	1.1125	1.4100	0.9168	0.9474	1.0750	1.0038
K	0.0758	0.0641	0.0809	0.0693	0.0673	0.0669	0.0559	0.0536	0.0602	0.0561	0.0540	0.0446	0.0531	0.0302	0.0509	0.0552	0.0439	0.0807	0.0507	0.0535	0.0350	0.0491	0.0742	0.0443	0.0350	0.0467	0.0395
Total	19.9734	19.9863	19.9999	19.9635	20.0281	19.9864	19.9335	19.9413	19.8865	19.8854	19.9354	19.9508	19.8567	19.9438	19.9602	20.0429	20.0151	20.0315	20.0460	20.0302	19.9901	20.0003	19.9813	20.0231	20.0466	20.0869	20.0652
An	55.80	55.99	66.22	64.93	56.88	66.29	66.22	65.82	67.33	70.08	72.69	71.17	58.49	76.21	70.62	60.29	72.85	61.98	58.42	71.54	76.30	71.68	63.65	77.35	76.80	73.88	75.43

Sample	B-5a	B-5a	B-5a	B-5a	B-7	B-7	B-7	B-7	B-7	B-7	B-7	B-7	B-9	B-9	B-9	B-9	B-9	B-9	B-9	B-9	B-10	B-10	B-10	B-10	B-10	B-10	B-10
Metres	4.1	4.1	4.1	4.1	7.0	7.0	7.0	7.0	7.0	7.0	7.0	7.0	9.1	9.1	9.1	9.1	9.1	9.1	9.1	9.1	10.4	10.4	10.4	10.4	10.4	10.4	10.4
Wt.%																											
SiO_2	48.34	50.15	49.63	48.34	48.87	49.04	48.40	49.26	48.99	49.17	48.68	48.81	47.66	48.24	47.97	47.92	48.45	48.74	47.39	47.68	48.60	48.81	49.36	48.61	49.32	49.45	48.84
Al_2O_3	32.27	31.47	32.15	32.34	32.53	31.76	31.83	32.04	31.85	31.90	32.26	32.03	33.00	32.59	33.00	32.88	32.88	32.57	33.17	32.99	31.84	32.28	32.06	31.53	31.95	31.84	32.13
Fe_2O_3	0.31	0.36	0.34	0.37	0.29	0.34	0.36	0.32	0.32	0.36	0.33	0.24	0.33	0.33	0.42	0.42	0.39	0.36	0.46	0.44	0.41	0.34	0.37	0.37	0.38	0.37	0.38
CaO	16.22	15.35	15.89	16.13	15.24	15.12	15.33	14.92	15.05	15.05	15.46	15.20	16.25	15.83	15.88	16.11	16.21	15.70	16.47	16.57	17.06	16.75	16.39	16.52	16.36	16.31	16.42
Na_2O	2.49	3.01	2.80	2.53	2.36	2.47	2.48	2.47	2.37	2.38	2.23	2.52	2.17	2.30	2.22	2.33	2.22	2.39	1.98	1.93	2.23	2.30	2.51	2.29	2.58	2.46	2.31
K_2O	0.17	0.22	0.16	0.15	0.07	0.14	0.16	0.13	0.11	0.15	0.14	0.14	0.11	0.14	0.11	0.13	0.20	0.14	0.16	0.10	0.14	0.13	0.16	0.12	0.11	0.17	0.11
Total	99.80	100.56	100.97	99.86	99.36	98.87	98.56	99.14	98.69	99.01	99.10	98.94	99.52	99.43	99.60	99.79	100.35	99.90	99.63	99.71	100.28	100.61	100.85	99.44	100.70	100.60	100.19
Cations (based on 32 oxygens):																											
Si	8.8929	9.1286	9.0090	8.8873	8.9772	9.0574	8.9857	9.0618	9.0562	9.0624	8.9762	9.0123	8.7862	8.8864	8.8249	8.8130	8.8560	8.9305	8.7380	8.7778	8.9156	8.9103	8.9814	8.9744	8.9874	9.0151	8.9427
Al	6.9967	6.7513	6.8781	7.0074	7.0426	6.9133	6.9647	6.9465	6.9391	6.9293	7.0107	6.9701	7.1699	7.0755	7.1550	7.1268	7.0832	7.0333	7.2082	7.1579	6.8841	6.9450	6.8753	6.8605	6.8618	6.8412	6.9336
Fe	0.0388	0.0438	0.0423	0.0457	0.0359	0.0431	0.0447	0.0401	0.0403	0.0444	0.0416	0.0306	0.0416	0.0416	0.0526	0.0526	0.0481	0.0441	0.0569	0.0554	0.0511	0.0426	0.0452	0.0458	0.0466	0.0453	0.0468
Ca	3.1970	2.9936	3.0904	3.1773	2.9994	2.9920	3.0494	2.9407	2.9808	2.9719	3.0543	3.0070	3.2097	3.1244	3.1300	3.1744	3.1746	3.0821	3.2537	3.2684	3.3532	3.2761	3.1953	3.2677	3.1941	3.1858	3.2212
Na	0.8879	1.0619	0.9851	0.9016	0.8403	0.8842	0.8924	0.8807	0.8492	0.8502	0.7970	0.9018	0.7754	0.8212	0.7916	0.8306	0.7865	0.8488	0.7076	0.6887	0.7929	0.8138	0.8852	0.8194	0.9112	0.8692	0.8198
K	0.0399	0.0511	0.0370	0.0352	0.0164	0.0330	0.0379	0.0305	0.0259	0.0353	0.0329	0.0330	0.0259	0.0329	0.0258	0.0305	0.0466	0.0327	0.0376	0.0235	0.0328	0.0303	0.0371	0.0283	0.0256	0.0395	0.0257
Total	20.0532	20.0304	20.0419	20.0545	19.9119	19.9230	19.9747	19.9004	19.8916	19.8935	19.9126	19.9548	20.0086	19.9820	19.9800	20.0278	19.9950	19.9715	20.0021	19.9716	20.0296	20.0180	20.0195	19.9963	20.0268	19.9961	19.9899
An	78.26	73.82	75.83	77.90	78.12	77.19	77.36	76.95	77.83	77.76	79.31	76.93	80.54	79.19	79.81	79.26	80.14	78.41	82.14	82.60	80.88	80.10	78.31	79.95	77.80	78.56	79.71

MICROPROBE DATA TABLE C22: Composition of **plagioclase** in the Bastard Unit - profile **RPM** (from Kruger, 1982).
Metres given above base of Unit.

Sample	B-23	B-23	B-23	B-23	B-25	B-25	B-25	B-25	B-25	B-25	B-25	B-25	B-26	B-26	B-26	B-26	B-26	B-26	B-26	B-26	B-28	B-28	B-28	B-28	B-28	B-28	B-28
Metres	32.3	32.3	32.3	32.3	41.9	41.9	41.9	41.9	41.9	41.9	41.9	41.9	46.3	46.3	46.3	46.3	46.3	46.3	46.3	46.3	51.9	51.9	51.9	51.9	51.9	51.9	51.9
Wt.%																											
SiO_2	49.29	50.18	49.53	50.32	49.10	48.48	50.47	49.31	50.18	49.85	49.06	50.04	49.69	49.60	50.25	49.47	50.97	48.54	49.07	51.03	49.93	51.44	50.44	51.31	50.32	51.50	50.97
Al_2O_3	32.51	31.63	32.36	31.74	32.15	31.88	31.26	31.94	31.30	31.11	32.25	31.37	31.59	31.61	31.04	31.62	30.57	32.32	31.68	30.54	31.46	30.65	31.36	30.96	31.55	30.48	30.93
Fe_2O_3	0.32	0.36	0.37	0.34	0.30	0.27	0.30	0.31	0.28	0.31	0.34	0.31	0.29	0.40	0.38	0.34	0.40	0.37	0.37	0.34	0.43	0.42	0.40	0.33	0.38	0.41	0.39
CaO	15.51	14.64	15.55	14.66	15.04	15.21	14.37	15.04	14.22	14.12	15.41	14.43	14.75	15.00	14.48	15.05	13.87	15.31	15.29	13.67	14.92	13.89	14.61	13.93	14.66	13.60	14.06
Na_2O	2.66	2.94	2.57	2.93	2.71	2.50	3.09	2.60	3.22	3.22	2.50	3.07	2.82	2.85	3.11	2.75	3.40	2.77	0.26	3.55	2.88	3.55	3.10	3.44	3.16	3.59	3.34
K_2O	0.13	0.21	0.18	0.18	0.18	0.13	0.24	0.17	0.24	0.19	0.16	0.20	0.12	0.14	0.19	0.14	0.21	0.09	0.19	0.20	0.22	0.25	0.23	0.20	0.15	0.32	0.29
Total	100.42	99.96	100.56	100.17	99.48	98.47	99.73	99.37	99.44	98.80	99.72	99.42	99.26	99.60	99.45	99.37	99.42	99.40	96.86	99.33	99.84	100.20	100.14	100.17	100.22	99.90	99.98
Cations (based on 32 oxygens):																											
Si	8.9792	9.1597	9.0103	9.1614	9.0197	8.9990	9.2261	9.0610	9.2028	9.2004	8.9957	9.1808	9.1314	9.1004	9.2198	9.0943	9.3374	8.9405	9.1680	9.3518	9.1387	9.3540	9.1954	9.3250	9.1666	9.3873	9.2936
Al	6.9799	6.8046	6.9380	6.8106	6.9606	6.9744	6.7348	6.9172	6.7654	6.7670	6.9694	6.7831	6.8419	6.8353	6.7122	6.8509	6.6002	7.0160	6.9759	6.5962	6.7864	6.5688	6.7380	6.6313	6.7736	6.5479	6.6467
Fe	0.0398	0.0440	0.0452	0.0425	0.0373	0.0335	0.0371	0.0387	0.0345	0.0389	0.0428	0.0387	0.0360	0.0497	0.0469	0.0429	0.0496	0.0457	0.0464	0.0428	0.0537	0.0520	0.0494	0.0410	0.0466	0.0508	0.0480
Ca	3.0273	2.8632	3.0308	2.8597	2.9602	3.0250	2.8145	2.9611	2.7941	2.7921	3.0274	2.8365	2.9042	2.9487	2.8465	2.9643	2.7224	3.0213	3.0607	2.6841	2.9259	2.7062	2.8537	2.7124	2.8613	2.6560	2.7467
Na	0.9392	1.0402	0.9062	1.0339	0.9649	0.8995	1.0948	0.9260	1.1446	1.1519	0.8885	1.0917	1.0044	1.0135	1.1060	0.9799	1.2072	0.9889	0.0942	1.2610	1.0217	1.2512	1.0954	1.2117	1.1157	1.2683	1.1804
K	0.0302	0.0489	0.0418	0.0418	0.0422	0.0308	0.0560	0.0398	0.0561	0.0447	0.0374	0.0468	0.0281	0.0328	0.0445	0.0328	0.0491	0.0211	0.0453	0.0468	0.0514	0.0580	0.0535	0.0464	0.0349	0.0744	0.0675
Total	19.9956	19.9605	19.9721	19.9499	19.9849	19.9621	19.9633	19.9439	19.9976	19.9950	19.9612	19.9776	19.9460	19.9803	19.9759	19.9651	19.9659	20.0336	19.3905	19.9826	19.9777	19.9902	19.9853	19.9679	19.9986	19.9847	19.9829
An	75.32	73.35	76.98	73.45	75.42	77.08	71.99	76.18	70.94	70.79	77.31	72.21	74.30	74.42	72.02	75.16	69.28	75.34	97.02	68.04	74.12	68.38	72.26	69.12	71.95	67.68	69.94

Sample	B-28	B-28	B-28	B-30	B-30	B-30	B-30	B-30	B-30	B-30	B-30	B-30	B-30
Metres	51.9	51.9	51.9	60.1	60.1	60.1	60.1	60.1	60.1	60.1	60.1	60.1	60.1
Wt.%													
SiO_2	51.45	50.76	51.68	49.48	51.02	51.01	51.42	50.84	52.19	51.63	48.84	51.32	51.40
Al_2O_3	30.76	31.07	30.54	31.85	30.97	31.47	30.37	31.12	30.25	30.61	31.75	30.59	30.99
Fe_2O_3	0.39	0.42	0.37	0.42	0.39	0.41	0.43	0.36	0.39	0.37	0.38	0.36	0.29
CaO	13.86	14.33	13.50	14.93	14.14	14.44	13.38	13.95	13.16	13.24	14.46	13.62	13.69
Na_2O	3.43	3.17	3.76	2.69	3.18	3.05	3.74	3.27	3.86	3.61	2.90	3.39	3.44
K_2O	0.18	0.21	0.24	0.17	0.27	0.21	0.27	0.25	0.24	0.30	0.21	0.25	0.20
Total	100.07	99.96	100.09	99.54	99.97	100.59	99.61	99.79	100.09	99.76	98.54	99.53	100.01
Cations (based on 32 oxygens):													
Si	9.3565	9.2588	9.3972	9.0786	9.2981	9.2413	9.3970	9.2789	9.4758	9.4075	9.0533	9.3779	9.3450
Al	6.5928	6.6793	6.5449	6.8873	6.6519	6.7194	6.5412	6.6940	6.4731	6.5734	6.9364	6.5880	6.6404
Fe	0.0479	0.0522	0.0452	0.0525	0.0480	0.0504	0.0536	0.0439	0.0478	0.0452	0.0474	0.0440	0.0356
Ca	2.7005	2.8005	2.6301	2.9350	2.7610	2.8029	2.6198	2.7279	2.5600	2.5847	2.8718	2.6666	2.6667
Na	1.2090	1.1207	1.3252	0.9566	1.1233	1.0710	1.3248	1.1568	1.3584	1.2749	1.0419	1.2007	1.2122
K	0.0418	0.0489	0.0557	0.0398	0.0628	0.0485	0.0629	0.0582	0.0556	0.0697	0.0497	0.0583	0.0464
Total	19.9485	19.9603	19.9982	19.9498	19.9450	19.9335	19.9994	19.9596	19.9707	19.9555	20.0006	19.9355	19.9463
An	69.08	71.42	66.50	75.42	71.08	72.35	66.42	70.22	65.33	66.97	73.38	68.95	68.75

MICROPROBE DATA TABLE C23: Composition of **plagioclase** in the Bastard Unit - profile **Y**.
Metres given above base of Unit.

Sample	Y722.4	Y722.4	Y722.4	Y722.4	Y740.5	Y740.5	Y740.5	Y740.5	Y740.5	Y746.4	Y746.4	Y746.4	Y746.4	Y746.4	Y746.4	Y755.56	Y755.56	Y755.56	Y755.56	Y755.56	Y760.2	Y760.2	Y760.2	Y760.2	Y760.2	Y764.4	Y764.4
Metres	54.0	54.0	54.0	54.0	35.9	35.9	35.9	35.9	35.9	30.0	30.0	30.0	30.0	30.0	30.0	20.8	20.8	20.8	20.8	20.8	16.2	16.2	16.2	16.2	16.2	12.2	12.2
Wt.%																											
SiO_2	51.76	50.72	50.81	50.10	51.13	50.57	50.50	49.27	51.69	50.47	49.42	49.72	49.41	48.89	49.15	49.47	49.98	49.35	49.64	49.38	50.21	50.22	49.58	49.86	49.39	48.86	48.22
Al_2O_3	29.97	30.57	31.28	31.37	31.57	31.70	31.69	32.57	31.25	31.85	32.68	32.36	32.46	32.63	32.39	32.79	32.82	32.76	32.41	32.48	32.88	32.37	32.60	32.35	32.59	32.67	33.30
Fe_2O_3	0.37	0.39	0.33	0.35	0.37	0.40	0.31	0.32	0.42	0.28	0.30	0.29	0.31	0.32	0.28	0.40	0.40	0.38	0.39	0.38	0.28	0.31	0.36	0.29	0.32	0.31	0.31
CaO	13.35	13.99	14.32	14.84	14.02	14.28	14.28	15.35	13.82	14.64	15.40	14.94	15.28	15.41	15.08	15.54	15.43	15.59	15.20	15.48	15.46	15.14	15.42	15.18	15.37	15.74	16.47
Na_2O	3.90	3.59	3.41	3.13	3.49	3.36	3.40	2.80	3.80	3.24	2.81	2.98	2.86	2.68	2.87	2.65	2.95	2.64	2.90	2.66	2.78	3.05	2.82	2.96	2.71	2.56	2.25
K_2O	0.01	0.03	0.02	0.02	0.01	0.01	0.00	0.00	0.00	0.01	0.00	0.00	0.02	0.00	0.01	0.01	0.01	0.02	0.01	0.02	0.00	0.00	0.00	0.01	0.01	0.00	0.02
Total	99.37	99.27	100.17	99.81	100.59	100.32	100.17	100.32	100.98	100.48	100.62	100.29	100.34	99.93	99.77	100.87	101.58	100.74	100.56	100.40	101.60	101.10	100.78	100.65	100.39	100.14	100.57
Cations (based on 32 oxygens):																											
Si	9.4659	9.3090	9.2419	9.1636	9.2516	9.1863	9.1852	8.9783	9.3161	9.1576	8.9775	9.0483	9.0007	8.9454	8.9978	8.9667	8.9961	8.9583	9.0220	8.9907	9.0218	9.0707	8.9941	9.0473	8.9887	8.9274	8.7942
Al	6.4605	6.6125	6.7065	6.7617	6.7321	6.7880	6.7933	6.9942	6.6394	6.8111	6.9974	6.9403	6.9681	7.0366	6.9897	7.0052	6.9626	7.0096	6.9411	6.9711	6.9634	6.8916	6.9697	6.9192	6.9918	7.0353	7.1567
Fe	0.0453	0.0479	0.0408	0.0436	0.0457	0.0489	0.0387	0.0399	0.0512	0.0339	0.0370	0.0359	0.0388	0.0396	0.0347	0.0488	0.0483	0.0473	0.0481	0.0471	0.0336	0.0381	0.0440	0.0353	0.0393	0.0384	0.0382
Ca	2.6166	2.7508	2.7908	2.9077	2.7179	2.7792	2.7823	2.9974	2.6682	2.8462	2.9977	2.9125	2.9816	3.0203	2.9574	3.0184	2.9756	3.0317	2.9599	3.0190	2.9767	2.9297	2.9961	2.9510	2.9968	3.0816	3.2189
Na	1.3823	1.2754	1.2034	1.1107	1.2227	1.1840	1.1984	0.9893	1.3268	1.1399	0.9908	1.0520	1.0096	0.9495	1.0194	0.9307	1.0284	0.9276	1.0214	0.9394	0.9680	1.0685	0.9897	1.0428	0.9563	0.9056	0.7967
K	0.0034	0.0059	0.0053	0.0038	0.0016	0.0019	0.0000	0.0003	0.0005	0.0024	0.0008	0.0011	0.0035	0.0000	0.0012	0.0033	0.0031	0.0051	0.0031	0.0053	0.0003	0.0000	0.0009	0.0022	0.0018	0.0006	0.0044
Total	19.9740	20.0015	19.9888	19.9911	19.9717	19.9882	19.9980	19.9994	20.0023	19.9910	20.0011	19.9901	20.0024	19.9913	20.0003	19.9732	20.0142	19.9796	19.9956	19.9726	19.9638	19.9986	19.9944	19.9979	19.9748	19.9889	20.0089
An	65.43	68.32	69.87	72.36	68.97	70.13	69.90	75.19	66.79	71.40	75.16	73.47	74.70	76.08	74.37	76.43	74.32	76.57	74.35	76.27	75.46	73.28	75.17	73.89	75.81	77.29	80.16

Sample	Y764.4	Y764.4	Y764.4	Y764.4	Y765.48	Y765.48	Y765.48	Y765.48	Y765.48	Y770.58	Y770.58	Y770.58	Y770.58	Y770.58	Y775	Y775	Y775	Y775	Y775
Metres	12.2	12.2	12.2	12.2	10.9	10.9	10.9	10.9	10.9	5.8	5.8	5.8	5.8	5.8	1.4	1.4	1.4	1.4	1.4
Wt.%																			
SiO_2	48.30	49.25	47.87	49.31	48.34	48.19	48.91	48.21	48.21	48.92	49.31	49.04	48.45	48.85	49.97	49.47	49.49	50.14	49.62
Al_2O_3	32.97	32.37	33.40	32.70	33.05	33.32	33.00	33.50	33.13	32.87	33.03	33.11	33.26	32.77	32.22	32.48	32.27	31.85	32.50
Fe_2O_3	0.26	0.20	0.24	0.22	0.45	0.46	0.44	0.39	0.42	0.18	0.20	0.25	0.24	0.25	0.15	0.14	0.10	0.14	0.16
CaO	16.30	15.60	16.64	15.65	15.64	15.95	15.80	16.40	15.96	15.73	15.50	15.70	15.98	15.64	14.94	15.32	15.09	14.53	15.29
Na_2O	2.35	2.78	2.09	2.71	2.39	2.35	2.55	2.29	2.47	2.55	2.65	2.48	2.30	2.54	3.24	3.02	3.08	3.38	2.97
K_2O	0.01	0.01	0.01	0.00	0.00	0.01	0.00	0.00	0.00	0.01	0.01	0.01	0.01	0.01	0.00	0.01	0.00	0.00	0.00
Total	100.18	100.21	100.25	100.59	99.87	100.29	100.70	100.78	100.19	100.26	100.70	100.59	100.25	100.06	100.53	100.44	100.04	100.03	100.53
Cations (based on 32 oxygens):																			
Si	8.8372	8.9888	8.7587	8.9627	8.8573	8.8054	8.8929	8.7740	8.8202	8.9215	8.9449	8.9114	8.8433	8.9267	9.0752	9.0017	9.0345	9.1387	9.0156
Al	7.1091	6.9620	7.2026	7.0050	7.1376	7.1756	7.0703	7.1862	7.1437	7.0656	7.0620	7.0904	7.1560	7.0579	6.8957	6.9663	6.9424	6.8416	6.9603
Fe	0.0319	0.0245	0.0299	0.0273	0.0555	0.0574	0.0541	0.0476	0.0526	0.0221	0.0244	0.0304	0.0296	0.0307	0.0187	0.0178	0.0129	0.0170	0.0193
Ca	3.1955	3.0510	3.2620	3.0487	3.0711	3.1226	3.0780	3.1980	3.1277	3.0743	3.0128	3.0578	3.1259	3.0620	2.9074	2.9866	2.9524	2.8381	2.9761
Na	0.8348	0.9819	0.7411	0.9543	0.8482	0.8314	0.8989	0.8062	0.8746	0.8998	0.9325	0.8737	0.8151	0.9005	1.1408	1.0664	1.0906	1.1934	1.0467
K	0.0021	0.0015	0.0026	0.0004	0.0008	0.0030	0.0005	0.0002	0.0000	0.0027	0.0033	0.0027	0.0031	0.0029	0.0006	0.0012	0.0006	0.0000	0.0000
Total	20.0107	20.0097	19.9969	19.9985	19.9706	19.9953	19.9946	20.0122	20.0189	19.9859	19.9799	19.9664	19.9730	19.9807	20.0383	20.0400	20.0334	20.0287	20.0180
An	79.29	75.65	81.49	76.16	78.36	78.97	77.40	79.87	78.15	77.36	76.36	77.78	79.32	77.27	71.82	73.69	73.02	70.40	73.98

MICROPROBE DATA TABLE C24: Composition of **plagioclase** in the Bastard Unit - profile **X**.
Metres given above the base of Unit.

Sample	X735.0	X735.0	X735.0	X735.0	X735.0	X745.44	X745.44	X745.44	X745.44	X745.44	X763.95	X763.95	X763.95	X763.95	X763.95	X768.5	X768.5	X768.5	X768.5	X768.5	X776.5	X776.5	X776.5	X776.5	X776.5	X779.82	X779.82
Metres	57.9	57.9	57.9	57.9	57.9	47.5	47.5	47.5	47.5	47.5	29.0	29.0	29.0	29.0	29.0	24.4	24.4	24.4	24.4	24.4	16.4	16.4	16.4	16.4	16.4	13.1	13.1
Wt.%																											
SiO_2	51.67	51.46	49.91	52.66	52.27	50.84	49.42	49.77	49.83	50.74	49.63	50.59	48.94	49.98	49.32	51.65	51.11	50.49	50.97	51.28	50.20	49.29	49.84	50.10	48.64	51.88	50.73
Al_2O_3	31.10	31.18	32.34	30.54	30.58	31.53	32.09	32.03	32.00	31.40	31.63	31.12	32.29	31.58	32.06	30.93	30.87	31.31	31.33	30.93	31.92	32.52	32.03	31.74	32.94	30.51	31.35
Fe_2O_3	0.27	0.24	0.19	0.20	0.26	0.32	0.33	0.34	0.32	0.35	0.45	0.38	0.39	0.39	0.38	0.25	0.26	0.23	0.20	0.24	0.36	0.34	0.35	0.34	0.34	0.19	0.21
CaO	14.24	14.11	15.54	13.42	13.83	14.90	15.83	15.47	15.58	14.87	15.38	14.74	16.02	15.10	15.89	14.39	14.57	14.95	14.73	14.46	14.99	15.60	15.34	15.00	16.27	14.04	14.49
Na_2O	3.47	3.56	2.79	4.02	3.76	3.12	2.50	2.74	2.72	3.19	2.85	3.34	2.55	3.02	2.64	3.34	3.21	3.00	3.24	3.30	2.85	2.75	2.91	3.10	2.36	3.67	3.38
K_2O	0.18	0.21	0.11	0.23	0.22	0.11	0.13	0.13	0.11	0.13	0.17	0.13	0.14	0.19	0.15	0.23	0.20	0.15	0.12	0.22	0.14	0.13	0.15	0.18	0.11	0.24	0.22
Total	100.94	100.76	100.87	101.06	100.92	100.82	100.30	100.47	100.56	100.68	100.11	100.30	100.33	100.27	100.44	100.79	100.23	100.13	100.58	100.41	100.47	100.62	100.62	100.46	100.65	100.53	100.37
Cations (based on 32 oxygens):																											
Si	9.3234	9.3045	9.0429	9.4707	9.4244	9.2008	9.0179	9.0582	9.0623	9.2013	9.0764	9.2138	8.9452	9.1171	8.9988	9.3355	9.2974	9.2017	9.2397	9.3075	9.1214	8.9684	9.0615	9.1169	8.8622	9.3984	9.2229
Al	6.6147	6.6445	6.9068	6.4737	6.4987	6.7268	6.9010	6.8708	6.8589	6.7115	6.8166	6.6806	6.9545	6.7897	6.8941	6.5891	6.6185	6.7245	6.6945	6.6159	6.8360	6.9730	6.8629	6.8073	7.0722	6.5141	6.7159
Fe	0.0327	0.0290	0.0231	0.0239	0.0323	0.0395	0.0404	0.0415	0.0390	0.0436	0.0552	0.0467	0.0485	0.0482	0.0471	0.0306	0.0325	0.0283	0.0240	0.0292	0.0441	0.0413	0.0435	0.0421	0.0417	0.0238	0.0253
Ca	2.7539	2.7331	3.0167	2.5857	2.6721	2.8902	3.0941	3.0168	3.0364	2.8888	3.0142	2.8761	3.1377	2.9516	3.1061	2.7872	2.8386	2.9200	2.8599	2.8125	2.9188	3.0412	2.9875	2.9245	3.1751	2.7254	2.8226
Na	1.2148	1.2474	0.9809	1.4011	1.3153	1.0929	0.8852	0.9676	0.9579	1.1228	1.0114	1.1800	0.9018	1.0691	0.9345	1.1716	1.1334	1.0604	1.1384	1.1596	1.0043	0.9711	1.0252	1.0924	0.8324	1.2869	1.1894
K	0.0419	0.0480	0.0246	0.0522	0.0501	0.0249	0.0308	0.0291	0.0263	0.0292	0.0394	0.0305	0.0329	0.0453	0.0347	0.0531	0.0469	0.0344	0.0274	0.0500	0.0321	0.0301	0.0345	0.0426	0.0267	0.0550	0.0503
Total	19.9813	20.0064	19.9950	20.0072	19.9928	19.9750	19.9694	19.9840	19.9808	19.9972	20.0131	20.0278	20.0206	20.0211	20.0153	19.9671	19.9672	19.9693	19.9840	19.9747	19.9567	20.0251	20.0151	20.0258	20.0104	20.0036	20.0263
An	69.39	68.66	75.46	64.86	67.01	72.56	77.76	75.71	76.02	72.01	74.88	70.91	77.68	73.41	76.87	70.41	71.47	73.36	71.53	70.81	74.40	75.80	74.45	72.81	79.23	67.93	70.35

Sample	X779.82	X779.82	X779.82	X782.7	X782.7	X782.7	X782.7	X782.7	X788.41	X788.41	X788.41	X788.41	X788.41	X791.8	X791.8	X791.8	X791.8	X791.8
Metres	13.1	13.1	13.1	10.2	10.2	10.2	10.2	10.2	4.5	4.5	4.5	4.5	4.5	1.1	1.1	1.1	1.1	1.1
Wt.%																		
SiO_2	51.60	50.83	50.27	48.63	49.29	48.89	49.33	49.27	49.39	49.29	49.29	49.58	48.81	54.49	51.37	50.97	50.87	51.05
Al_2O_3	30.69	31.16	31.42	32.78	32.49	32.64	32.44	32.23	32.14	31.75	31.82	31.91	32.32	28.40	30.48	30.91	30.95	30.84
Fe_2O_3	0.16	0.22	0.21	0.23	0.20	0.24	0.24	0.18	0.19	0.25	0.29	0.25	0.27	0.30	0.13	0.14	0.17	0.13
CaO	13.95	14.43	14.84	16.49	15.92	16.15	15.81	16.00	16.00	16.00	16.07	16.04	16.30	11.85	13.86	14.24	14.07	14.24
Na_2O	3.73	3.38	3.07	2.29	2.52	2.42	2.49	2.63	2.43	2.49	2.52	2.53	2.38	5.01	3.81	3.56	3.65	3.56
K_2O	0.26	0.19	0.21	0.12	0.13	0.12	0.15	0.15	0.15	0.14	0.10	0.12	0.11	0.13	0.18	0.15	0.15	0.11
Total	100.38	100.20	100.03	100.53	100.55	100.47	100.45	100.47	100.30	99.92	100.09	100.44	100.18	100.19	99.81	99.96	99.86	99.93
Cations (based on 32 oxygens):																		
Si	9.3638	9.2513	9.1760	8.8717	8.9721	8.9168	8.9846	8.9839	9.0114	9.0335	9.0211	9.0383	8.9320	9.8436	9.3717	9.2926	9.2843	9.3061
Al	6.5637	6.6833	6.7593	7.0483	6.9701	7.0165	6.9633	6.9265	6.9120	6.8581	6.8631	6.8551	6.9701	6.0476	6.5534	6.6408	6.6572	6.6272
Fe	0.0203	0.0266	0.0265	0.0282	0.0246	0.0294	0.0295	0.0224	0.0233	0.0306	0.0358	0.0308	0.0335	0.0368	0.0155	0.0175	0.0211	0.0165
Ca	2.7116	2.8146	2.9017	3.2233	3.1040	3.1548	3.0853	3.1265	3.1268	3.1410	3.1502	3.1331	3.1951	2.2943	2.7088	2.7807	2.7510	2.7806
Na	1.3104	1.1910	1.0871	0.8102	0.8884	0.8569	0.8780	0.9295	0.8607	0.8854	0.8949	0.8942	0.8454	1.7550	1.3478	1.2589	1.2918	1.2569
K	0.0594	0.0449	0.0483	0.0269	0.0311	0.0287	0.0345	0.0351	0.0341	0.0321	0.0236	0.0288	0.0254	0.0289	0.0410	0.0343	0.0343	0.0264
Total	20.0291	20.0117	19.9988	20.0086	19.9903	20.0031	19.9752	20.0239	19.9683	19.9809	19.9887	19.9803	20.0015	20.0061	20.0382	20.0248	20.0397	20.0137
An	67.42	70.27	72.75	79.91	77.75	78.64	77.85	77.08	78.42	78.01	77.88	77.80	79.08	56.66	66.78	68.84	68.05	68.87

MICROPROBE DATA TABLE C25: Composition of **plagioclase** in the Bastard Unit - profile **RD**.
Metres given above base of Unit.

Sample	RD-3	RD-3	RD-3	RD-3	RD-3	RD-4	RD-4	RD-4	RD-4	RD-4	RD-4	RD-6	RD-6	RD-6	RD-6	RD-6	RD-6	RD-13	RD-13	RD-13	RD-13	RD-13	RD-15	RD-15	RD-15	RD-15	RD-15
Metres	31.0	31.0	31.0	31.0	31.0	29.4	29.4	29.4	29.4	29.4	29.4	22.5	22.5	22.5	22.5	22.5	22.5	10.6	10.6	10.6	10.6	10.6	8.3	8.3	8.3	8.3	8.3
Wt.%																											
SiO_2	49.97	50.29	49.60	49.34	49.74	49.85	49.35	49.48	49.59	49.62	49.69	49.75	50.30	49.61	49.30	50.11	49.42	48.87	48.61	48.58	48.45	48.48	49.35	49.36	49.23	48.79	48.36
Al_2O_3	32.10	32.27	32.29	32.40	32.57	31.91	32.11	32.17	32.16	32.15	31.99	32.25	32.01	32.53	31.88	31.81	32.19	32.69	32.39	32.93	32.62	32.01	33.03	32.88	32.65	32.51	32.42
Fe_2O_3	0.32	0.27	0.31	0.32	0.27	0.37	0.34	0.29	0.29	0.35	0.34	0.36	0.33	0.36	0.38	0.36	0.27	0.28	0.27	0.21	0.22	0.27	0.29	0.26	0.34	0.31	0.31
CaO	15.15	15.06	15.33	15.46	15.32	14.71	14.95	15.01	14.97	14.94	14.74	14.86	14.69	15.35	14.92	14.87	14.96	15.83	15.77	15.78	15.88	15.43	15.70	15.69	15.63	15.37	15.35
Na_2O	2.88	2.95	2.78	2.74	2.92	3.01	2.88	3.03	2.95	2.89	3.04	2.86	3.05	2.76	2.82	2.93	2.87	2.46	2.56	2.56	2.49	2.80	2.47	2.51	2.56	2.59	2.50
K_2O	0.02	0.00	0.01	0.01	0.01	0.02	0.01	0.02	0.01	0.03	0.02	0.02	0.02	0.02	0.02	0.03	0.03	0.02	0.02	0.01	0.00	0.02	0.00	0.00	0.01	0.00	0.00
Total	100.44	100.84	100.33	100.28	100.82	99.87	99.66	99.99	99.97	99.98	99.82	100.11	100.41	100.63	99.32	100.09	99.74	100.16	99.62	100.06	99.66	99.00	100.84	100.71	100.41	99.56	98.94
Cations (based on 32 oxygens):																											
Si	9.0828	9.0968	9.0318	8.9960	9.0134	9.1071	9.0426	9.0398	9.0557	9.0595	9.0848	9.0665	9.1326	9.0084	9.0632	9.1321	9.0441	8.9267	8.9318	8.8843	8.8987	8.9637	8.9426	8.9561	8.9635	8.9551	8.9337
Al	6.8770	6.8796	6.9304	6.9623	6.9574	6.8692	6.9346	6.9270	6.9218	6.9188	6.8925	6.9274	6.8500	6.9610	6.9071	6.8313	6.9443	7.0383	7.0151	7.0977	7.0623	6.9745	7.0536	7.0317	7.0061	7.0325	7.0588
Fe	0.0392	0.0333	0.0379	0.0389	0.0325	0.0454	0.0425	0.0361	0.0364	0.0436	0.0418	0.0448	0.0408	0.0444	0.0469	0.0440	0.0337	0.0349	0.0342	0.0255	0.0279	0.0333	0.0355	0.0320	0.0414	0.0379	0.0388
Ca	2.9509	2.9188	2.9914	3.0202	2.9741	2.8781	2.9355	2.9377	2.9285	2.9230	2.8878	2.9021	2.8584	2.9868	2.9385	2.9025	2.9326	3.0986	3.1041	3.0922	3.1245	3.0575	3.0471	3.0502	3.0493	3.0234	3.0388
Na	1.0144	1.0357	0.9823	0.9687	1.0264	1.0658	1.0243	1.0717	1.0427	1.0211	1.0788	1.0093	1.0746	0.9725	1.0041	1.0347	1.0171	0.8723	0.9122	0.9070	0.8850	1.0025	0.8676	0.8832	0.9029	0.9207	0.8942
K	0.0041	0.0008	0.0028	0.0033	0.0022	0.0057	0.0030	0.0044	0.0028	0.0077	0.0037	0.0042	0.0057	0.0043	0.0038	0.0060	0.0069	0.0039	0.0042	0.0021	0.0008	0.0041	0.0005	0.0010	0.0020	0.0008	0.0005
Total	19.9684	19.9650	19.9767	19.9894	20.0059	19.9713	19.9826	20.0167	19.9880	19.9737	19.9893	19.9542	19.9622	19.9774	19.9637	19.9506	19.9788	19.9747	20.0017	20.0087	19.9992	20.0357	19.9469	19.9542	19.9652	19.9704	19.9648
An	74.42	73.81	75.28	75.72	74.34	72.98	74.13	73.27	73.74	74.11	72.80	74.20	72.68	75.44	74.53	73.72	74.25	78.03	77.29	77.32	77.93	75.31	77.84	77.55	77.15	76.66	77.27

Sample	RD-16	RD-16	RD-16	RD-16	RD-16	RD-17	RD-17	RD-17	RD-17	RD-17	RD-17	RD-18	RD-18	RD-18	RD-18	RD-18	RD-18	RD-19	RD-19	RD-19	RD-19	RD-19
Metres	5.9	5.9	5.9	5.9	5.9	3.6	3.6	3.6	3.6	3.6	3.6	0.5	0.5	0.5	0.5	0.5	0.5	0.1	0.1	0.1	0.1	0.1
Wt.%																						
SiO_2	49.58	49.01	49.22	48.70	49.40	51.46	51.43	52.63	52.65	51.37	52.01	50.08	50.02	49.83	50.56	50.51	52.13	50.97	51.41	51.18	50.62	
Al_2O_3	33.01	33.49	33.34	33.10	32.76	30.93	31.08	30.91	30.87	30.60	30.62	31.52	31.59	31.97	31.36	31.25	31.04	31.17	29.98	31.09	31.88	
Fe_2O_3	0.22	0.25	0.23	0.24	0.24	0.29	0.31	0.35	0.33	0.35	0.28	0.31	0.25	0.31	0.33	0.30	0.30	0.34	0.63	0.32	0.30	
CaO	15.45	15.89	15.68	15.58	15.13	13.44	13.70	12.83	13.15	13.05	12.91	14.23	14.51	14.96	14.18	13.93	13.41	13.93	13.22	13.72	14.46	
Na_2O	2.63	2.34	2.41	2.41	2.60	3.70	3.65	3.88	4.01	3.95	3.87	3.22	3.21	3.05	3.44	3.45	3.84	3.49	4.02	3.70	3.30	
K_2O	0.00	0.00	0.01	0.01	0.00	0.01	0.02	0.02	0.03	0.03	0.02	0.02	0.01	0.01	0.02	0.01	0.03	0.03	0.03	0.01	0.02	
Total	100.88	100.98	100.88	100.04	100.14	99.83	100.18	100.62	101.04	99.35	99.72	99.37	99.60	100.12	99.89	99.45	100.75	99.92	99.29	100.02	100.57	
Cations (based on 32 oxygens):																						
Si	8.9718	8.8727	8.9105	8.8950	8.9971	9.3624	9.3324	9.4724	9.4549	9.3914	9.4540	9.1807	9.1562	9.0873	9.2226	9.2438	9.3949	9.2828	9.4254	9.3086	9.1724	
Al	7.0399	7.1447	7.1148	7.1254	7.0329	6.6318	6.6464	6.5579	6.5325	6.5948	6.5601	6.8088	6.8153	6.8705	6.7409	6.7410	6.5939	6.6902	6.4782	6.6639	6.8080	
Fe	0.0274	0.0309	0.0277	0.0296	0.0300	0.0362	0.0379	0.0432	0.0403	0.0431	0.0350	0.0379	0.0310	0.0384	0.0413	0.0373	0.0371	0.0415	0.0781	0.0396	0.0362	
Ca	2.9947	3.0813	3.0413	3.0498	2.9517	2.6193	2.6641	2.4749	2.5297	2.5571	2.5145	2.7953	2.8466	2.9222	2.7709	2.7323	2.5893	2.7172	2.5967	2.6736	2.8080	
Na	0.9209	0.8193	0.8460	0.8538	0.9194	1.3052	1.2850	1.3533	1.3971	1.4005	1.3649	1.1429	1.1400	1.0785	1.2178	1.2227	1.3423	1.2325	1.4298	1.3047	1.1574	
K	0.0009	0.0006	0.0021	0.0021	0.0003	0.0028	0.0043	0.0039	0.0057	0.0059	0.0047	0.0038	0.0030	0.0013	0.0036	0.0022	0.0069	0.0067	0.0062	0.0033	0.0041	
Total	19.9555	19.9495	19.9423	19.9555	19.9313	19.9577	19.9701	19.9056	19.9601	19.9928	19.9332	19.9693	19.9922	19.9981	19.9971	19.9795	19.9643	19.9709	20.0145	19.9936	19.9862	
An	76.48	78.99	78.24	78.13	76.25	66.74	67.46	64.65	64.42	64.61	64.82	70.98	71.40	73.04	69.47	69.08	65.86	68.80	64.49	67.20	70.81	

MICROPROBE DATA TABLE C26: Composition of **plagioclase** in the Bastard Unit - profile **UA**.
Metres given above base of Unit.

Sample	UA-2	UA-2	UA-2	UA-2	UA-2	UA-6	UA-6	UA-6	UA-6	UA-6	UA-9	UA-9	UA-9	UA-9	UA-9	UA-11	UA-11	UA-11	UA-11	UA-11	UA-14	UA-14	UA-14	UA-14	UA-14	UA-17	UA-17
Metres	50.5	50.5	50.5	50.5	50.5	39.4	39.4	39.4	39.4	39.4	31.2	31.2	31.2	31.2	31.2	26.3	26.3	26.3	26.3	26.3	20.2	20.2	20.2	20.2	20.2	16.2	16.2
Wt.%																											
SiO_2	49.91	50.13	50.36	49.80	49.18	49.34	49.68	49.29	50.02	49.31	49.96	49.94	50.09	50.12	49.73	49.89	50.68	50.81	51.02	49.78	49.86	49.37	49.68	49.31	49.74	49.63	49.08
Al_2O_3	32.44	32.01	31.74	32.19	32.55	31.94	31.80	32.00	31.64	31.87	31.96	31.94	31.97	31.73	32.08	32.02	31.46	31.20	31.34	31.79	31.25	31.83	31.65	31.84	31.60	31.99	32.51
Fe_2O_3	0.29	0.27	0.38	0.32	0.37	0.33	0.34	0.32	0.31	0.32	0.30	0.26	0.32	0.31	0.35	0.29	0.30	0.31	0.30	0.28	0.34	0.36	0.39	0.38	0.37	0.27	0.25
CaO	15.49	15.28	14.85	15.45	15.88	15.35	15.26	15.63	15.15	15.36	15.09	15.06	15.41	15.18	15.39	15.45	14.80	14.91	14.77	15.22	15.02	15.61	15.21	15.44	15.21	15.88	16.37
Na_2O	2.68	2.92	3.00	2.73	2.63	2.77	2.94	2.76	2.98	2.75	2.85	2.73	2.85	2.92	2.75	2.62	3.07	3.01	3.19	2.70	3.14	2.80	3.05	2.78	2.97	2.61	2.40
K_2O	0.13	0.11	0.17	0.13	0.11	0.16	0.14	0.14	0.15	0.15	0.16	0.16	0.16	0.18	0.13	0.16	0.21	0.17	0.18	0.15	0.16	0.13	0.14	0.13	0.15	0.14	0.12
Total	100.95	100.73	100.49	100.61	100.72	99.88	100.17	100.13	100.23	99.76	100.33	100.09	100.80	100.43	100.42	100.42	100.52	100.42	100.80	99.93	99.78	100.10	100.11	99.87	100.04	100.53	100.73
Cations (based on 32 oxygens):																											
Si	9.0358	9.0938	9.1488	9.0482	8.9459	9.0376	9.0727	9.0144	9.1210	9.0416	9.0958	9.1068	9.0866	9.1203	9.0542	9.0774	9.2017	9.2326	9.2352	9.0991	9.1408	9.0327	9.0820	9.0367	9.0964	9.0378	8.9326
Al	6.9223	6.8437	6.7968	6.8942	6.9791	6.8940	6.8453	6.8963	6.7990	6.8886	6.8578	6.8637	6.8349	6.8059	6.8837	6.8664	6.7315	6.6822	6.6861	6.8488	6.7518	6.8639	6.8190	6.8766	6.8095	6.8660	6.9731
Fe	0.0356	0.0337	0.0466	0.0395	0.0454	0.0411	0.0423	0.0402	0.0380	0.0402	0.0371	0.0325	0.0396	0.0381	0.0426	0.0353	0.0374	0.0387	0.0371	0.0347	0.0426	0.0441	0.0480	0.0466	0.0460	0.0334	0.0309
Ca	3.0053	2.9696	2.8896	3.0079	3.0960	3.0125	2.9866	3.0617	2.9594	3.0186	2.9442	2.9414	2.9957	2.9590	3.0021	3.0116	2.8795	2.9035	2.8650	2.9809	2.9509	3.0605	2.9795	3.0326	2.9799	3.0989	3.1920
Na	0.9417	1.0265	1.0563	0.9606	0.9262	0.9828	1.0398	0.9771	1.0520	0.9758	1.0066	0.9643	1.0026	1.0282	0.9690	0.9241	1.0796	1.0599	1.1179	0.9558	1.1152	0.9946	1.0801	0.9880	1.0526	0.9203	0.8460
K	0.0310	0.0264	0.0390	0.0297	0.0248	0.0363	0.0336	0.0321	0.0340	0.0344	0.0370	0.0373	0.0359	0.0407	0.0308	0.0377	0.0476	0.0400	0.0416	0.0353	0.0366	0.0294	0.0319	0.0304	0.0353	0.0324	0.0276
Total	19.9716	19.9939	19.9772	19.9801	20.0174	20.0043	20.0202	20.0219	20.0035	19.9991	19.9785	19.9459	19.9954	19.9922	19.9825	19.9526	19.9774	19.9569	19.9829	19.9547	20.0379	20.0252	20.0405	20.0109	20.0198	19.9888	20.0022
An	76.14	74.31	73.23	75.79	76.97	75.40	74.18	75.81	73.77	75.57	74.52	75.31	74.92	74.21	75.60	76.52	72.73	73.26	71.93	75.72	72.57	75.47	73.39	75.43	73.90	77.10	79.05

Sample	UA-17	UA-17	UA-17	UA-19	UA-19	UA-19	UA-19	UA-19	UA-21	UA-21	UA-21	UA-21	UA-21	UA-23	UA-23	UA-23	UA-23	UA-23	UA-25	UA-25	UA-25	UA-25	UA-25	UA-27	UA-27	UA-27	UA-27	UA-27
Metres	16.2	16.2	16.2	11.8	11.8	11.8	11.8	11.8	8.5	8.5	8.5	8.5	8.5	5.1	5.1	5.1	5.1	5.1	1.9	1.9	1.9	1.9	1.9	0.5	0.5	0.5	0.5	0.5
Wt.%																												
SiO_2	49.11	49.34	49.38	48.10	48.92	48.91	48.60	48.50	47.98	48.11	48.38	48.46	48.01	49.29	49.63	50.38	50.16	49.70	53.24	54.62	54.35	49.84	54.59	53.26	53.27	54.84	53.38	53.26
Al_2O_3	32.16	32.14	31.91	33.52	32.69	32.69	32.81	32.70	32.51	32.33	32.56	32.39	32.37	32.23	31.98	31.34	31.47	32.02	29.36	28.73	28.79	31.71	28.50	29.28	29.60	28.48	29.36	29.28
Fe_2O_3	0.21	0.27	0.32	0.24	0.24	0.22	0.25	0.25	0.24	0.21	0.20	0.18	0.23	0.24	0.22	0.21	0.23	0.20	0.17	0.19	0.20	0.26	0.16	0.27	0.25	0.25	0.21	0.27
CaO	16.08	16.16	15.88	16.94	16.31	16.21	16.19	16.31	16.23	16.09	16.14	16.02	16.20	15.91	15.41	14.61	14.78	15.40	12.30	11.24	11.19	14.97	11.11	12.46	12.36	11.32	12.35	12.46
Na_2O	2.47	2.60	2.69	1.91	2.33	2.35	2.33	2.29	2.36	2.54	2.57	2.57	2.41	2.53	2.79	3.16	3.04	2.76	4.43	4.87	4.87	2.84	4.87	4.66	4.69	5.27	4.61	4.66
K_2O	0.12	0.11	0.11	0.07	0.13	0.13	0.13	0.11	0.10	0.14	0.12	0.13	0.12	0.12	0.13	0.16	0.17	0.14	0.33	0.41	0.33	0.18	0.45	0.27	0.29	0.43	0.37	0.27
Total	100.16	100.62	100.29	100.79	100.62	100.51	100.31	100.16	99.43	99.42	99.97	99.74	99.34	100.32	100.16	99.86	99.85	100.22	99.82	100.06	99.72	99.80	99.69	100.19	100.47	100.59	100.27	100.19
Cations (based on 32 oxygens):																												
Si	8.9809	8.9874	9.0202	8.7581	8.9104	8.9150	8.8802	8.8777	8.8534	8.8794	8.8786	8.9065	8.8678	8.9935	9.0590	9.2017	9.1685	9.0632	9.6671	9.8604	9.8425	9.1181	9.8885	9.6511	9.6251	9.8706	9.6616	9.6511
Al	6.9314	6.8988	6.8690	7.1924	7.0173	7.0220	7.0645	7.0538	7.0702	7.0334	7.0412	7.0171	7.0460	6.9312	6.8792	6.7467	6.7783	6.8827	6.2828	6.1138	6.1436	6.8371	6.0857	6.2530	6.3034	6.0418	6.2626	6.2530
Fe	0.0254	0.0339	0.0393	0.0295	0.0290	0.0270	0.0305	0.0307	0.0301	0.0265	0.0243	0.0223	0.0293	0.0295	0.0277	0.0266	0.0287	0.0249	0.0209	0.0231	0.0239	0.0322	0.0202	0.0334	0.0311	0.0303	0.0252	0.0334
Ca	3.1507	3.1544	3.1075	3.3047	3.1824	3.1661	3.1692	3.1990	3.2077	3.1818	3.1730	3.1552	3.2065	3.1105	3.0139	2.8589	2.8947	3.0086	2.3924	2.1748	2.1711	2.9353	2.1566	2.4198	2.3937	2.1822	2.3949	2.4198
Na	0.8761	0.9175	0.9535	0.6756	0.8242	0.8297	0.8256	0.8113	0.8456	0.9069	0.9147	0.9161	0.8616	0.8951	0.9855	1.1184	1.0761	0.9752	1.5580	1.7027	1.7095	1.0061	1.7103	1.6352	1.6432	1.8375	1.6155	1.6352
K	0.0286	0.0261	0.0257	0.0169	0.0304	0.0310	0.0303	0.0266	0.0245	0.0321	0.0285	0.0293	0.0284	0.0280	0.0300	0.0370	0.0393	0.0318	0.0773	0.0952	0.0758	0.0429	0.1047	0.0614	0.0658	0.0992	0.0853	0.0614
Total	19.9931	20.0181	20.0152	19.9772	19.9938	19.9909	20.0002	19.9990	20.0315	20.0601	20.0603	20.0465	20.0395	19.9877	19.9953	19.9893	19.9857	19.9865	19.9986	19.9701	19.9665	19.9717	19.9660	20.0540	20.0622	20.0617	20.0449	20.0540
An	78.24	77.47	76.52	83.03	79.43	79.24	79.33	79.77	79.14	77.82	77.62	77.50	78.82	77.65	75.36	71.88	72.90	75.52	60.56	56.09	55.95	74.47	55.77	59.67	59.30	54.29	59.72	59.67

MICROPROBE DATA TABLE C27: Composition of **plagioclase** in the Bastard Unit - profile **UC**.
Metres given above base of Unit.
cc = cumulus cores ic = intercumulus cores.
cm = cumulus margins im = intercumulus margins.

Sample	UC-1	UC-1	UC-1	UC-1	UC-1	UC-1	UC-1	UC-1	UC-1	UC-3	UC-3	UC-3	UC-3	UC-3	UC-3	UC-5	UC-5	UC-5	UC-5	UC-7	UC-11	UC-11	UC-11	UC-11	UC-11	UC-11	UC-11
Metres	30.75	30.75	30.75	30.75	30.75	30.75	30.75	30.75	30.75	28.51	28.51	28.51	28.51	28.51	28.51	23.99	23.99	23.99	23.99	21.46	14.71	14.71	14.71	14.71	14.71	14.71	14.71
Position	cc	cc	cc	cc	cc	cm	cm	cm	cm	cc	cc	cc	cc	cc	cc	cc	cc	cc	cc	cc	cc	cc	cc	cc	cc	cc	cc
Wt.%																											
SiO_2	49.26	49.20	49.48	49.62	49.85	48.48	48.04	48.54	48.28	50.12	48.81	50.39	49.84	49.20	50.20	49.47	48.84	50.12	48.83	48.41	47.07	46.44	47.09	47.16	47.28	47.90	47.32
Al_2O_3	32.22	32.42	32.16	31.94	31.86	32.92	33.41	33.07	32.78	32.36	33.31	32.39	32.70	32.73	32.30	32.80	32.46	32.18	32.72	32.42	34.86	34.82	34.80	34.76	34.73	34.50	34.77
Fe_2O_3	0.21	0.17	0.13	0.26	0.22	0.22	0.24	0.23	0.22	0.31	0.31	0.29	0.24	0.34	0.32	0.25	0.23	0.22	0.20	0.19	0.14	0.16	0.11	0.16	0.26	0.23	0.21
CaO	15.19	15.33	14.81	14.74	14.49	15.89	16.16	15.90	15.75	15.03	15.72	14.34	14.76	15.62	14.76	15.71	15.24	14.82	15.51	15.78	17.45	17.40	17.27	17.47	16.45	15.99	16.53
Na_2O	2.79	2.88	2.89	3.06	3.11	2.56	2.33	2.46	2.40	2.82	2.40	3.11	2.82	2.67	3.07	2.68	2.77	3.11	2.69	2.68	1.61	1.66	1.75	1.77	1.59	1.82	1.67
K_2O	0.01	0.01	0.01	0.01	0.02	0.01	0.00	0.01	0.01	0.01	0.01	0.01	0.02	0.00	0.01	0.02	0.02	0.01	0.02	0.01	0.00	0.00	0.00	0.00	0.00	0.00	0.00
Total	99.69	100.02	99.47	99.63	99.55	100.08	100.18	100.21	99.44	100.64	100.56	100.53	100.38	100.57	100.67	100.94	99.55	100.46	99.98	99.49	101.13	100.49	101.03	101.34	100.29	100.43	100.51
Cations (based on 32 oxygens):																											
Si	9.0241	8.9906	9.0680	9.0873	9.1256	8.8700	8.7866	8.8659	8.8819	9.0821	8.8755	9.1252	9.0473	8.9488	9.0947	8.9631	8.9663	9.0996	8.9308	8.9107	8.5500	8.4994	8.5605	8.5565	8.6270	8.7135	8.6206
Al	6.9570	6.9829	6.9459	6.8943	6.8744	7.0989	7.2015	7.1192	7.1081	6.9101	7.1375	6.9121	6.9954	7.0163	6.8975	7.0032	7.0226	6.8855	7.0543	7.0343	7.4627	7.5097	7.4563	7.4322	7.4684	7.3959	7.4650
Fe	0.0257	0.0212	0.0161	0.0320	0.0277	0.0269	0.0301	0.0280	0.0270	0.0376	0.0380	0.0352	0.0296	0.0421	0.0394	0.0305	0.0284	0.0275	0.0252	0.0236	0.0174	0.0202	0.0141	0.0198	0.0316	0.0280	0.0260
Ca	2.9816	3.0021	2.9073	2.8917	2.8420	3.1159	3.1659	3.1121	3.1041	2.9186	3.0615	2.7811	2.8696	3.0442	2.8650	3.0501	2.9971	2.8830	3.0399	3.1118	3.3963	3.4116	3.3646	3.3964	3.2153	3.1155	3.2272
Na	0.9894	1.0195	1.0249	1.0859	1.1026	0.9082	0.8261	0.8692	0.8558	0.9889	0.8456	1.0922	0.9921	0.9414	1.0769	0.9419	0.9838	1.0946	0.9528	0.9579	0.5667	0.5894	0.6170	0.6240	0.5615	0.6431	0.5902
K	0.0031	0.0017	0.0027	0.0026	0.0050	0.0029	0.0010	0.0013	0.0029	0.0024	0.0027	0.0030	0.0047	0.0000	0.0033	0.0046	0.0038	0.0022	0.0053	0.0023	0.0003	0.0003	0.0003	0.0010	0.0000	0.0002	0.0000
Total	19.9808	20.0180	19.9648	19.9938	19.9772	20.0227	20.0112	19.9957	19.9799	19.9397	19.9609	19.9488	19.9387	19.9927	19.9769	19.9933	20.0020	19.9924	20.0085	20.0405	19.9934	20.0305	20.0129	20.0300	19.9038	19.8962	19.9290
An	75.08	74.65	73.94	72.70	72.05	77.43	79.31	78.17	78.39	74.69	78.36	71.80	74.31	76.38	72.68	76.41	75.29	72.48	76.14	76.46	85.70	85.27	84.50	84.48	85.13	82.89	84.54

Sample	UC-11	UC-11	UC-11	UC-11	UC-11	UC-11	UC-11	UC-11	UC-11	UC-12	UC-12	UC-12	UC-12	UC-12	UC-13	UC-13	UC-13	UC-13	UC-13	UC-13	UC-13	UC-13	UC-13	UC-13	UC-14	UC-14	UC-14
Metres	14.71	14.71	14.71	14.71	14.71	14.71	14.71	14.71	14.71	13.30	13.30	13.30	13.30	13.30	11.13	11.13	11.13	11.13	11.13	11.13	11.13	11.13	11.13	11.13	9.00	9.00	9.00
Position	cm	cm	cm	cm	cm	cm	cm	cm	cm	cc	cc	cc	cc	cc	cc	cc	cc	cc	cc	cm	cm	cm	cm	cm	cc	cc	cc
Wt.%																											
SiO_2	46.68	46.34	46.70	46.33	46.47	46.21	45.09	45.98	44.59	47.66	47.41	47.22	47.42	47.51	46.40	46.26	46.00	46.60	46.09	45.29	44.07	45.71	45.78	45.33	47.62	47.47	46.82
Al_2O_3	35.54	35.98	35.57	35.12	35.23	35.15	35.58	35.57	35.50	34.30	34.53	34.49	33.92	34.21	34.11	34.14	34.36	33.60	33.74	34.34	33.57	34.35	33.60	33.67	34.52	34.56	34.78
Fe_2O_3	0.28	0.35	0.28	0.22	0.14	0.27	0.31	0.31	0.34	0.13	0.15	0.09	0.15	0.13	0.28	0.25	0.21	0.20	0.37	0.33	3.70	0.31	1.46	0.55	0.08	0.09	0.11
CaO	17.23	17.58	17.28	17.83	18.13	17.87	18.70	18.46	18.68	17.38	17.11	16.97	16.74	16.99	17.33	17.39	17.78	17.51	17.34	17.80	16.31	18.04	16.98	17.92	17.24	17.46	17.81
Na_2O	1.24	1.02	1.25	1.42	1.35	1.35	0.93	1.10	0.86	1.74	1.77	1.79	1.87	1.81	1.77	1.67	1.51	1.61	1.62	1.50	1.29	1.39	1.67	1.35	1.68	1.65	1.46
K_2O	0.00	0.01	0.00	0.00	0.00	0.00	0.00	0.00	0.00	0.00	0.00	0.00	0.00	0.00	0.00	0.01	0.00	0.00	0.00	0.00	0.00	0.00	0.00	0.00	0.00	0.01	0.01
Total	100.97	101.27	101.10	100.92	101.33	100.85	100.61	101.42	99.96	101.21	100.98	100.56	100.11	100.64	99.89	99.73	99.86	99.53	99.16	99.26	98.94	99.80	99.49	98.83	101.13	101.25	101.00
Cations (based on 32 oxygens):																											
Si	8.4812	8.4037	8.4765	8.4502	8.4441	8.4357	8.2766	8.3597	8.2419	8.6460	8.6168	8.6140	8.6855	8.6589	8.5488	8.5380	8.4859	8.6132	8.5575	8.4185	8.2977	8.4484	8.5051	8.4705	8.6361	8.6092	8.5254
Al	7.6099	7.6892	7.6094	7.5494	7.5446	7.5621	7.6978	7.6217	7.7338	7.3332	7.3959	7.4147	7.3217	7.3484	7.4081	7.4254	7.4705	7.3200	7.3832	7.5230	7.4489	7.4823	7.3555	7.4154	7.3789	7.3870	7.4638
Fe	0.0339	0.0427	0.0349	0.0271	0.0177	0.0340	0.0388	0.0384	0.0419	0.0154	0.0187	0.0111	0.0185	0.0156	0.0350	0.0316	0.0264	0.0246	0.0460	0.0412	0.4713	0.0391	0.1839	0.0695	0.0092	0.0112	0.0137
Ca	3.3532	3.4152	3.3600	3.4843	3.5300	3.4960	3.6771	3.5970	3.6992	3.3786	3.3325	3.3174	3.2857	3.3168	3.4214	3.4377	3.5137	3.4677	3.4489	3.5457	3.2894	3.5727	3.3796	3.5869	3.3507	3.3927	3.4741
Na	0.4375	0.3574	0.4402	0.5009	0.4764	0.4770	0.3294	0.3866	0.3067	0.6126	0.6241	0.6321	0.6650	0.6377	0.6325	0.5990	0.5386	0.5767	0.5845	0.5421	0.4698	0.4968	0.6016	0.4897	0.5896	0.5816	0.5168
K	0.0000	0.0019	0.0009	0.0000	0.0000	0.0000	0.0000	0.0000	0.0000	0.0004	0.0000	0.0000	0.0008	0.0007	0.0002	0.0025	0.0000	0.0010	0.0002	0.0001	0.0000	0.0000	0.0004	0.0000	0.0005	0.0016	0.0012
Total	19.9157	19.9101	19.9220	20.0120	20.0129	20.0047	20.0198	20.0035	20.0236	19.9863	19.9879	19.9892	19.9773	19.9782	20.0460	20.0342	20.0350	20.0032	20.0203	20.0705	19.9771	20.0393	20.0262	20.0320	19.9649	19.9833	19.9949
An	88.46	90.53	88.42	87.43	88.11	87.99	91.78	90.30	92.34	84.65	84.23	83.99	83.17	83.87	84.40	85.16	86.71	85.74	85.51	86.74	87.50	87.79	84.89	87.99	85.04	85.37	87.05

MICROPROBE DATA TABLE C27: Composition of **plagioclase** in the Bastard Unit - profile **UC**.
Metres given above base of Unit.
cc = cumulus cores ic = intercumulus cores.
cm = cumulus margins im = intercumulus margins.

Sample	UC-14	UC-14	UC-15	UC-15	UC-15	UC-15	UC-15	UC-16	UC-16	UC-16	UC-16	UC-16	UC-17	UC-17	UC-17	UC-17	UC-17	UC-17	UC-17	UC-17	UC-17	UC-17	UC-18	UC-18	UC-18	UC-18	UC-18
Metres	9.00	9.00	7.41	7.41	7.41	7.41	7.41	5.26	5.26	5.26	5.26	5.26	4.10	4.10	4.10	4.10	4.10	4.10	4.10	4.10	4.10	4.10	2.30	2.30	2.30	2.30	2.30
Position	cc	cc	cc	cc	cc	cc	cc	cc	cc	cc	cc	cc	ic	ic	ic	ic	ic	ic	ic	im	im	im	ic	ic	ic	ic	ic
Wt.%																											
SiO_2	47.55	47.11	46.43	47.22	47.23	47.80	47.78	47.14	47.30	47.30	47.47	47.68	50.58	50.18	49.67	50.31	48.35	48.52	48.49	48.38	48.42	48.38	54.39	52.34	49.82	49.35	51.80
Al_2O_3	34.47	34.58	34.37	33.92	33.62	33.29	33.67	33.70	34.16	34.39	34.26	34.33	32.00	32.53	32.47	31.39	33.12	33.77	33.45	33.86	33.89	32.88	29.92	31.13	33.00	33.19	31.31
Fe_2O_3	0.14	0.17	0.14	0.15	0.11	0.16	0.14	2.20	1.17	0.15	0.19	0.17	0.28	0.27	0.26	0.20	0.06	0.12	0.11	0.12	0.23	1.11	0.18	0.13	0.14	0.12	0.06
CaO	17.35	17.69	17.37	16.87	16.77	16.15	16.32	16.14	16.72	17.23	17.08	16.86	13.93	14.74	14.79	13.81	15.96	16.29	16.23	16.62	16.46	15.78	11.92	13.40	15.20	15.60	13.43
Na_2O	1.69	1.69	1.63	1.91	1.91	2.23	2.05	1.85	1.77	1.84	1.92	1.96	3.26	3.06	2.93	3.46	2.45	2.38	2.40	2.23	2.41	2.52	4.63	3.84	2.89	2.67	3.72
K_2O	0.00	0.01	0.00	0.00	0.00	0.00	0.01	0.00	0.00	0.00	0.00	0.00	0.01	0.02	0.01	0.02	0.01	0.00	0.01	0.01	0.01	0.01	0.01	0.01	0.01	0.01	0.00
Total	101.20	101.25	99.94	100.07	99.65	99.65	99.96	101.03	101.12	100.91	100.92	100.99	100.05	100.79	100.13	99.18	99.95	101.07	100.69	101.21	101.42	100.69	101.04	100.84	101.08	100.93	100.32
Cations (based on 32 oxygens):																											
Si	8.6264	8.5587	8.5410	8.6605	8.6946	8.7864	8.7519	8.6121	8.6089	8.6105	8.6377	8.6606	9.1908	9.0769	9.0463	9.2278	8.8515	8.7908	8.8189	8.7608	8.7558	8.8273	9.7168	9.4138	8.9954	8.9323	9.3647
Al	7.3688	7.4054	7.4518	7.3315	7.2945	7.2122	7.2684	7.2544	7.3290	7.3772	7.3468	7.3487	6.8531	6.9343	6.9699	6.7846	7.1459	7.2115	7.1708	7.2261	7.2223	7.0710	6.3003	6.5982	7.0229	7.0803	6.6710
Fe	0.0167	0.0214	0.0178	0.0183	0.0141	0.0201	0.0179	0.2721	0.1443	0.0184	0.0239	0.0204	0.0344	0.0336	0.0318	0.0245	0.0077	0.0142	0.0133	0.0145	0.0283	0.1368	0.0212	0.0152	0.0174	0.0142	0.0077
Ca	3.3716	3.4439	3.4231	3.3152	3.3076	3.1807	3.2022	3.1590	3.2607	3.3609	3.3303	3.2802	2.7126	2.8565	2.8862	2.7143	3.1304	3.1621	3.1623	3.2250	3.1893	3.0859	2.2815	2.5825	2.9411	3.0247	2.6008
Na	0.5948	0.5942	0.5812	0.6776	0.6807	0.7962	0.7275	0.6541	0.6234	0.6492	0.6767	0.6898	1.1467	1.0719	1.0342	1.2292	0.8702	0.8351	0.8457	0.7831	0.8431	0.8923	1.6025	1.3375	1.0125	0.9364	1.3021
K	0.0002	0.0025	0.0000	0.0007	0.0000	0.0000	0.0015	0.0000	0.0000	0.0002	0.0000	0.0000	0.0022	0.0037	0.0030	0.0037	0.0026	0.0004	0.0019	0.0018	0.0029	0.0034	0.0030	0.0023	0.0029	0.0014	0.0011
Total	19.9784	20.0262	20.0148	20.0037	19.9915	19.9955	19.9694	19.9517	19.9662	20.0164	20.0154	19.9997	19.9399	19.9769	19.9714	19.9841	20.0081	20.0141	20.0129	20.0113	20.0418	20.0166	19.9252	19.9494	19.9922	19.9893	19.9475
An	85.00	85.28	85.49	83.03	82.93	79.98	81.49	82.85	83.95	83.81	83.11	82.62	70.29	72.71	73.62	68.83	78.25	79.11	78.90	80.46	79.09	77.57	58.74	65.88	74.39	76.36	66.64

Sample	UC-18	UC-19	UC-19	UC-19	UC-19	UC-19	UC-19	UC-19	UC-19	UC-19	UC-19	UC-20	UC-20	UC-20	UC-20	UC-20	UC-20	UC-20	UC-20	UC-20	UC-20	UC-20
Metres	2.30	0.57	0.57	0.57	0.57	0.57	0.57	0.57	0.57	0.57	0.57	0.10	0.10	0.10	0.10	0.10	0.10	0.10	0.10	0.10	0.10	0.10
Position	ic	ic	ic	ic	ic	ic	ic	ic	ic	ic	ic	ic	ic	ic	ic	ic	ic	ic	ic	ic	ic	ic
Wt.%																						
SiO_2	49.09	56.52	53.55	52.07	53.20	49.32	49.39	48.08	51.12	50.05	50.49	53.01	52.42	50.16	53.10	54.72	55.03	55.35	53.72	53.88	51.81	
Al_2O_3	33.09	26.97	29.51	31.27	28.84	32.73	32.54	32.80	31.47	32.51	31.90	30.44	31.02	32.62	30.89	29.58	29.39	29.09	29.92	30.15	31.29	
Fe_2O_3	0.14	0.11	0.18	0.15	0.13	0.13	0.15	0.10	0.14	0.13	0.16	0.11	0.16	0.13	0.11	0.11	0.13	0.13	0.13	0.15	0.37	
CaO	15.65	9.38	11.85	13.01	12.07	14.91	14.77	15.28	13.95	14.93	14.21	12.90	12.63	14.77	12.79	11.51	11.14	11.10	12.11	12.04	13.57	
Na_2O	2.49	6.11	4.60	3.74	4.57	2.88	2.97	2.62	3.47	2.99	3.25	4.10	4.25	3.04	4.11	4.97	4.96	5.15	4.57	4.56	3.75	
K_2O	0.00	0.05	0.02	0.01	0.02	0.01	0.01	0.01	0.01	0.02	0.02	0.03	0.02	0.02	0.00	0.03	0.03	0.04	0.04	0.03	0.02	
Total	100.46	99.14	99.71	100.26	98.83	99.98	99.83	98.90	100.16	100.61	100.02	100.57	100.50	100.74	100.99	100.93	100.68	100.85	100.49	100.81	100.82	
Cations (based on 32 oxygens):																						
Si	8.9250	10.2271	9.7020	9.4050	9.7343	8.9971	9.0221	8.8848	9.2772	9.0694	9.1844	9.5434	9.4505	9.0741	9.5139	9.7811	9.8429	9.8862	9.6627	9.6570	9.3402	
Al	7.0904	5.7531	6.3020	6.6578	6.2200	7.0378	7.0055	7.1427	6.7301	6.9423	6.8388	6.4582	6.5900	6.9538	6.5224	6.2314	6.1947	6.1227	6.3435	6.3677	6.6481	
Fe	0.0173	0.0139	0.0220	0.0185	0.0155	0.0161	0.0191	0.0130	0.0173	0.0153	0.0199	0.0130	0.0200	0.0157	0.0133	0.0137	0.0160	0.0163	0.0157	0.0176	0.0457	
Ca	3.0486	1.8180	2.3011	2.5185	2.3662	2.9147	2.8919	3.0262	2.7132	2.8980	2.7689	2.4880	2.4390	2.8623	2.4554	2.2046	2.1345	2.1234	2.3344	2.3120	2.6218	
Na	0.8789	2.1442	1.6139	1.3111	1.6192	1.0169	1.0511	0.9386	1.2193	1.0496	1.1448	1.4296	1.4862	1.0667	1.4266	1.7236	1.7211	1.7832	1.5935	1.5840	1.3104	
K	0.0006	0.0105	0.0042	0.0028	0.0046	0.0034	0.0029	0.0029	0.0032	0.0038	0.0037	0.0075	0.0038	0.0037	0.0000	0.0076	0.0063	0.0083	0.0094	0.0080	0.0038	
Total	19.9609	19.9668	19.9451	19.9137	19.9598	19.9861	19.9926	20.0081	19.9603	19.9784	19.9605	19.9396	19.9895	19.9763	19.9316	19.9619	19.9155	19.9401	19.9592	19.9463	19.9700	
An	77.62	45.88	58.78	65.76	59.37	74.13	73.34	76.33	68.99	73.41	70.75	63.51	62.14	72.85	63.25	56.12	55.36	54.35	59.43	59.34	66.68	

MICROPROBE DATA TABLE C28: Representative **plagioclase** analyses in the Bastard Unit - profile **AE** (from Field, 1987 p.61)
Metres given above base of Unit.
r = rim of grain c = core of grain rs = restrained grain.

Sample	AE-1	AE-1	AE-2	AE-2	AE-2	AE-4	AE-4	AE-4	AE-5	AE-5	AE-5	AE-7	AE-7	AE-7	AE-9	AE-9	AE-9	AE-10	AE-10	AE-10	AE-12	AE-12	AE-12	AE-13	AE-13	AE-15	AE-15
Metres	35.8	35.8	34.0	34.0	34.0	29.8	29.8	29.8	26.4	26.4	26.4	20.0	20.0	20.0	17.0	17.0	17.0	14.7	14.7	14.7	8.1	8.1	8.1	5.2	5.2	1.1	1.0
Position	r	c	r	c	rs	r	c	rs	r	c	rs	r	c	rs	r	c	rs	r	c	rs	r	c	rs	r	c	r	c
Wt.%																											
SiO_2	49.94	49.22	49.95	51.76	50.99	47.26	50.28	49.29	48.26	49.23	48.43	49.71	48.44	47.98	48.55	48.79	49.02	47.78	48.40	48.65	47.99	48.95	48.68	52.23	49.15	54.38	50.06
Al_2O_3	30.43	31.98	31.79	30.29	30.65	32.28	30.80	31.50	32.00	31.39	31.09	31.24	32.14	32.69	32.30	31.82	31.79	32.72	31.93	32.16	32.15	31.82	31.73	29.95	31.87	27.75	30.79
Fe_2O_3	0.26	0.21	0.35	0.31	0.21	0.28	0.29	0.29	0.26	0.21	0.45	0.36	0.36	0.39	0.27	0.23	0.35	0.25	0.19	0.21	0.22	0.26	0.31	0.39	0.19	0.53	0.20
CaO	14.60	16.09	15.70	14.15	14.19	16.99	14.98	15.56	16.17	15.44	16.63	15.44	16.38	16.73	16.31	15.90	15.93	16.87	16.10	16.34	16.61	15.85	16.05	13.53	16.08	11.30	14.99
Na_2O	2.79	2.26	2.69	3.48	2.46	1.79	2.87	2.56	2.30	2.61	2.46	2.70	2.10	2.09	2.00	2.26	2.34	1.84	2.35	2.21	2.05	2.35	2.24	3.69	2.28	4.82	2.98
K_2O	0.23	0.14	0.16	0.21	1.56	0.09	0.19	0.17	0.09	0.18	0.16	0.14	0.12	0.06	0.11	0.14	0.13	0.12	0.17	0.18	0.13	0.18	0.19	0.30	0.14	0.31	0.16
Total	98.25	99.91	100.64	100.20	100.06	98.70	99.40	99.36	99.08	99.05	99.22	99.58	99.55	99.94	99.54	99.13	99.57	99.58	99.14	99.75	99.14	99.41	99.19	100.09	99.72	99.09	99.18
Cations (based on 32 oxygens):																											
Si	9.2679	9.0142	9.0819	9.4073	9.3260	8.7989	9.2334	9.0741	8.9281	9.0877	8.9794	9.1282	8.9219	8.8163	8.9299	9.0043	9.0135	8.8072	8.9491	8.9396	8.8814	9.0125	8.9907	9.4926	9.0193	9.9246	9.2168
Al	6.6565	6.9041	6.8131	6.4900	6.6077	7.0841	6.6659	6.8352	6.9779	6.8293	6.7948	6.7619	6.9779	7.0799	7.0033	6.9227	6.8902	7.1086	6.9576	6.9660	7.0140	6.9060	6.9076	6.4162	6.8944	5.9694	6.6810
Fe	0.0321	0.0260	0.0428	0.0380	0.0259	0.0357	0.0355	0.0357	0.0322	0.0260	0.0569	0.0444	0.0449	0.0490	0.0332	0.0289	0.0435	0.0318	0.0239	0.0266	0.0270	0.0326	0.0391	0.0475	0.0236	0.0655	0.0252
Ca	2.9028	3.1577	3.0593	2.7562	2.7798	3.3889	2.9485	3.0686	3.2058	3.0545	3.3036	3.0372	3.2327	3.2946	3.2153	3.1441	3.1389	3.3321	3.1891	3.2168	3.2936	3.1267	3.1760	2.6339	3.1620	2.2097	2.9570
Na	1.0034	0.8039	0.9483	1.2266	0.8722	0.6464	1.0214	0.9144	0.8235	0.9326	0.8824	0.9626	0.7513	0.7439	0.7136	0.8073	0.8356	0.6586	0.8420	0.7874	0.7341	0.8389	0.8007	1.3002	0.8115	1.7057	1.0636
K	0.0537	0.0334	0.0378	0.0478	0.3635	0.0209	0.0438	0.0390	0.0222	0.0419	0.0374	0.0316	0.0270	0.0150	0.0265	0.0325	0.0314	0.0270	0.0392	0.0431	0.0300	0.0420	0.0443	0.0705	0.0335	0.0717	0.0366
Total	19.9164	19.9393	19.9832	19.9659	19.9751	19.9749	19.9485	19.9671	19.9897	19.9719	20.0546	19.9658	19.9558	19.9987	19.9219	19.9398	19.9532	19.9654	20.0007	19.9794	19.9801	19.9586	19.9584	19.9609	19.9442	19.9466	19.9802
An	74.31	79.71	76.34	69.20	76.12	83.98	74.27	77.04	79.56	76.61	78.92	75.93	81.14	81.58	81.84	79.57	78.98	83.50	79.11	80.34	81.77	78.85	79.87	66.95	79.58	56.44	73.55

Sample	AE-16	AE-16	AE-16
Metres	0.1	0.1	0.1
Position	r	c	rs
Wt.%			
SiO_2	48.82	49.47	49.44
Al_2O_3	32.24	31.75	32.01
Fe_2O_3	0.46	0.30	0.45
CaO	16.15	15.53	15.81
Na_2O	2.00	2.55	2.37
K_2O	0.12	0.17	0.15
Total	99.78	99.76	100.23
Cations (based on 32 oxygens):			
Si	8.9571	9.0669	9.0269
Al	6.9715	6.8591	6.8889
Fe	0.0572	0.0375	0.0552
Ca	3.1738	3.0497	3.0936
Na	0.7106	0.9043	0.8385
K	0.0274	0.0388	0.0345
Total	19.8976	19.9563	19.9375
An	81.71	77.13	78.68

MICROPROBE DATA TABLE C29: Composition of **plagioclase** in zoned grains.

Sample - Y722.4 Profile 1.

Point	SiO_2	Al_2O_3	FeO	CaO	Na_2O	K_2O	Total	An%
Y722A1	51.07	30.78	0.30	13.45	3.58	0.13	99.31	67.52
Y722A2	51.28	30.76	0.27	13.33	3.74	0.13	99.50	66.36
Y722A2	51.58	30.58	0.31	13.56	3.79	0.16	99.98	66.42
Y722B1	51.25	30.55	0.28	13.61	3.73	0.15	99.58	66.86
Y722B3	50.45	30.86	0.34	14.03	3.44	0.13	99.25	69.31
Y722B4	50.48	30.90	0.32	14.22	3.50	0.14	99.56	69.16
Y722B5	50.91	30.64	0.26	13.97	3.63	0.15	99.56	68.01
Y722B6	50.97	30.61	0.26	13.70	3.64	0.16	99.35	67.54
Y722C1	51.05	30.89	0.30	14.12	3.43	0.15	99.94	69.45
Y722C2	50.39	30.79	0.34	14.07	3.37	0.14	99.10	69.74
Y722C3	50.56	30.96	0.31	14.13	3.37	0.14	99.47	69.85
Y722C4	50.57	30.62	0.34	13.98	3.53	0.17	99.21	68.62
Y722C5	50.83	30.91	0.31	13.97	3.48	0.17	99.67	68.94
Y722C6	50.69	30.86	0.30	14.01	3.51	0.18	99.56	68.78
Y722C7	50.31	30.79	0.99	13.94	3.51	0.15	99.69	68.70
Y722C8	50.50	30.78	0.37	14.06	3.52	0.17	99.40	68.80
Y722C9	50.69	30.73	0.32	14.01	3.45	0.16	99.36	69.19
Y722C10	50.67	30.79	0.30	13.83	3.55	0.19	99.35	68.27
Y722C11	50.54	30.17	0.34	14.15	3.33	0.17	98.70	70.14
Y722C12	50.02	30.44	0.26	14.06	3.46	0.18	98.42	69.17
Y722D1	50.52	31.23	0.29	14.21	3.40	0.16	99.80	69.81
Y722D2	50.50	30.46	0.29	13.89	3.56	0.16	98.86	68.33
Y722D3	50.72	30.71	0.35	13.97	3.53	0.18	99.45	68.62
Y722D4	50.67	31.16	0.32	14.21	3.42	0.15	99.94	69.64
Y722D5	50.44	31.10	0.31	14.08	3.49	0.16	99.57	69.06
Y722D6	50.65	30.91	0.31	14.15	3.48	0.17	99.68	69.19
Y722D7	50.71	30.82	0.34	13.99	3.53	0.16	99.55	68.69
Y722D8	50.75	30.96	0.35	14.11	3.45	0.18	99.81	69.30
Y722D9	50.80	31.01	0.28	14.27	3.51	0.19	100.07	69.21
Y722D10	51.01	30.87	0.28	14.10	3.53	0.19	99.98	68.83
Y722E1	51.28	30.85	0.30	14.02	3.54	0.17	100.17	68.65
Y722E4	50.62	30.54	0.31	13.97	3.48	0.19	99.13	68.93
Y722E5	50.31	30.30	0.32	14.31	3.37	0.15	98.76	70.12
Y722E6	50.05	30.51	0.28	14.46	3.27	0.15	98.71	70.97
Y722E7	49.90	30.98	0.31	14.82	3.17	0.12	99.31	72.08
Y722E8	50.05	30.54	0.28	14.43	3.31	0.16	98.77	70.69
Y722E9	50.38	30.63	0.39	14.26	3.39	0.14	99.19	69.94
Y722E10	50.80	30.69	0.31	14.36	3.42	0.17	99.74	69.90

Sample - Y722.4 Profile 2.

Y722I1	53.42	29.02	0.53	12.08	4.51	0.15	99.70	60.00
Y722I2	50.99	30.42	0.30	13.84	3.71	0.14	99.40	67.34
Y722I3	50.15	30.85	0.28	14.30	3.46	0.12	99.16	69.57
Y722I4	50.04	30.95	0.29	14.68	3.27	0.12	99.35	71.27
Y722I5	50.54	30.42	0.26	14.21	3.50	0.15	99.08	69.18
Y722I6	50.41	30.76	0.28	14.18	3.46	0.16	99.26	69.38
Y722I7	50.93	30.41	0.28	13.97	3.54	0.16	99.29	68.56
Y722I8	50.70	30.27	0.31	14.03	3.55	0.14	99.01	68.58
Y722I9	50.54	30.44	0.28	14.22	3.48	0.15	99.11	69.31
Y722I10	50.27	30.23	0.28	14.26	3.45	0.17	98.66	69.52
Y722J1	50.92	30.80	0.25	14.14	3.36	0.18	99.66	69.92
Y722J2	50.59	31.02	0.22	14.29	3.39	0.18	99.69	69.99
Y722J3	50.62	30.68	0.27	14.13	3.48	0.20	99.39	69.16
Y722J4	50.99	30.79	0.28	14.09	3.51	0.19	99.86	68.93
Y722J5	50.69	30.54	0.29	14.11	3.52	0.18	99.34	68.87
Y722J6	50.51	30.71	0.26	14.14	3.49	0.20	99.31	69.12
Y722J7	49.73	31.27	0.29	14.94	3.04	0.14	99.42	73.07
Y722J8	49.04	31.47	0.25	15.21	2.82	0.13	98.93	74.88
Y722J9	50.57	30.79	0.32	14.27	3.48	0.16	99.58	69.41
Y722J10	50.29	30.97	0.43	14.31	3.39	0.17	99.57	70.02

Sample - Y722.4 Profile 3.

Point	SiO_2	Al_2O_3	FeO	CaO	Na_2O	K_2O	Total	An%
Y722H9	52.55	30.80	0.32	13.38	3.72	0.13	100.90	66.54
Y722H8	51.58	30.49	0.26	13.54	3.74	0.14	99.76	66.68
Y722H7	51.53	30.58	0.24	13.47	3.75	0.14	99.70	66.52
Y722H6	49.67	29.15	1.82	13.14	3.44	0.12	97.34	67.88
Y722H5	49.73	31.53	0.28	14.91	3.02	0.08	99.55	73.18
Y722H4	50.25	31.53	0.33	14.77	3.18	0.13	100.19	72.00
Y722H3	50.97	30.87	0.22	14.07	3.55	0.15	99.83	68.67
Y722H2	50.54	30.32	0.30	13.64	3.52	0.16	98.49	68.15
Y722H1	49.87	32.07	0.15	14.97	2.96	0.05	100.08	73.65
Y722G6	51.13	30.39	0.31	13.67	3.87	0.14	99.52	66.10
Y722G4	50.67	30.87	0.31	13.61	3.61	0.17	99.24	67.56
Y722G3	51.11	30.85	0.33	13.99	3.54	0.15	99.97	68.57
Y722G1	51.09	30.92	0.34	13.74	3.57	0.17	99.83	68.01
Y722F20	50.96	31.01	0.35	13.95	3.46	0.19	99.91	69.01
Y722F19	50.43	31.05	0.31	13.96	3.48	0.16	99.38	68.91
Y722F18	50.74	30.86	0.60	13.60	3.40	0.25	99.44	68.83
Y722F17	52.07	31.52	0.28	13.74	3.04	0.20	100.84	71.43
Y722F16	50.57	30.82	0.31	13.89	3.49	0.20	99.27	68.78
Y722F15	50.85	30.65	0.32	13.83	3.57	0.18	99.40	68.16
Y722F14	51.12	30.62	0.34	13.86	3.50	0.19	99.63	68.66
Y722F13	51.03	30.71	0.31	13.94	3.55	0.19	99.74	68.47
Y722F12	50.71	30.56	0.33	13.85	3.49	0.21	99.15	68.72
Y722F11	50.96	30.83	0.31	13.69	3.42	0.19	99.40	68.90
Y722F10	51.06	30.59	0.33	13.91	3.55	0.19	99.64	68.40
Y722F9	50.80	30.74	0.26	14.18	3.55	0.20	99.72	68.86
Y722F8	50.08	31.29	0.35	14.77	3.19	0.15	99.82	71.88
Y722F7	49.47	31.62	0.31	14.83	3.06	0.15	99.44	72.82
Y722F6	49.59	31.94	0.28	15.33	2.79	0.13	100.06	75.23
Y722F5	50.32	31.07	0.27	14.37	3.31	0.13	99.46	70.58
Y722F4	50.66	30.72	0.30	14.02	3.59	0.16	99.44	68.35
Y722F3	51.47	30.37	0.26	13.78	3.80	0.17	99.84	66.75
Y722F2	52.07	29.98	0.27	13.19	4.03	0.21	99.75	64.38
Y722F1	52.41	30.03	0.40	12.96	4.06	0.21	100.08	63.83

Sample X768.5 Profile A.

X768D9	49.20	32.62	0.18	15.79	2.54	0.12	100.45	77.43
X768D10	49.82	32.35	0.23	15.47	2.78	0.17	100.81	75.47
X768D11	51.12	31.65	0.27	14.54	3.12	0.19	100.89	72.00
X768D12	50.95	31.61	0.20	14.46	3.21	0.21	100.65	71.35
X768D13	50.95	31.58	0.26	14.53	3.25	0.21	100.78	71.21
X768D14	50.89	31.45	0.26	14.42	3.20	0.20	100.42	71.35
X768D15	51.01	31.40	0.22	14.56	3.22	0.23	100.64	71.40
X768D16	50.49	31.49	0.27	14.55	3.08	0.22	100.10	72.30
X768D17	49.90	31.85	0.24	15.01	2.86	0.19	100.05	74.36
X768D18	49.79	32.13	0.27	15.39	2.72	0.16	100.47	75.76
X768D19	49.25	32.35	0.27	15.62	2.55	0.15	100.19	77.19
X768D20	49.56	32.33	0.23	15.80	2.64	0.12	100.67	76.70
X768E1	49.73	32.49	0.25	15.44	2.62	0.14	100.67	76.51
X768E2	49.03	32.00	0.19	15.33	2.60	0.13	99.27	76.55
X768E3	49.13	31.93	0.25	15.21	2.72	0.16	99.39	75.54
X768E4	50.39	31.55	0.24	14.56	3.11	0.19	100.03	72.12
X768E5	50.49	31.51	0.26	14.51	3.12	0.19	100.08	72.01
X768E6	50.32	31.48	0.26	14.63	3.11	0.19	99.98	72.25
X768E7	49.43	31.09	0.19	14.49	3.09	0.14	98.43	72.15
X768E8	48.95	31.66	0.25	14.87	2.81	0.12	98.66	74.55

Sample X768.5 Profile B.

X768F1	48.41	33.08	0.27	16.37	2.14	0.10	100.38	80.85
X768F2	48.80	32.19	0.26	15.22	2.65	0.16	99.28	76.05
X768F3	50.13	32.13	0.23	14.90	2.85	0.14	100.37	74.30
X768F4	49.91	31.87	0.23	14.71	2.89	0.16	99.77	73.80
X768F5	49.41	31.88	0.25	15.16	2.79	0.15	99.65	75.04
X768F6	49.71	32.24	0.30	15.05	2.76	0.15	100.21	75.08
X768F7	49.66	32.12	0.28	15.05	2.76	0.15	100.02	75.05
X768F8	49.60	32.17	0.24	15.24	2.74	0.14	100.12	75.49

Point	SiO_2	Al_2O_3	FeO	CaO	Na_2O	K_2O	Total	An%
X768F9	49.65	32.47	0.28	15.24	2.71	0.16	100.51	75.69
X768F10	50.47	31.87	0.24	14.72	2.96	0.19	100.45	73.33
X768F11	50.79	31.56	0.25	14.69	3.03	0.22	100.54	72.81
X768F12	50.70	31.39	0.26	14.44	3.23	0.22	100.24	71.21
X768F13	50.69	31.50	0.24	14.45	3.23	0.20	100.30	71.22
X768F14	50.67	31.41	0.25	14.40	3.28	0.22	100.22	70.81
X768F15	50.45	31.25	0.24	14.39	3.21	0.22	99.75	71.22
X768F16	50.61	31.30	0.25	14.53	3.15	0.21	100.04	71.84
X768F17	50.53	31.48	0.23	14.59	3.22	0.21	100.26	71.44
X768F18	50.42	31.29	0.26	14.48	3.23	0.23	99.91	71.22
X768F19	50.47	31.48	0.20	14.55	3.22	0.21	100.13	71.39
X768F20	50.33	31.10	0.24	14.46	3.22	0.23	99.58	71.28
Sample X768.5 Profile C.								
X768A1	49.13	32.08	0.21	15.33	2.75	0.13	99.63	75.47
X768A2	49.47	32.19	0.22	15.38	2.75	0.16	100.16	75.58
X768A2	49.52	32.23	0.28	15.44	2.66	0.16	100.29	76.22
X768A4	50.15	31.32	0.24	14.72	3.15	0.22	99.80	72.10
X768A5	50.36	30.98	0.26	14.25	3.18	0.21	99.24	71.24
X768A6	50.42	31.20	0.23	14.37	3.19	0.23	99.63	71.33
X768A7	50.68	31.26	0.21	14.52	3.28	0.22	100.17	70.97
X768A8	49.57	32.22	0.23	15.65	2.67	0.15	100.48	76.44
X768A9	49.69	31.93	0.25	15.42	2.78	0.15	100.22	75.38
X768A10	49.96	31.62	0.20	14.97	3.03	0.15	99.92	73.21
X768B1	50.12	31.94	0.24	14.91	2.83	0.14	100.17	74.46
X768B2	49.72	31.94	0.22	14.76	2.93	0.13	99.70	73.59
X768B3	50.41	31.65	0.25	14.38	3.16	0.14	99.98	71.57
X768B4	50.47	31.45	0.24	14.27	3.13	0.15	99.70	71.60
X768B5	48.51	32.63	0.24	15.77	2.40	0.09	99.65	78.41
X768B6	49.95	31.41	0.18	14.13	3.06	0.13	98.87	71.84
X768B7	49.73	31.45	0.19	14.39	3.01	0.15	98.91	72.52
X768B8	49.57	31.55	0.24	14.32	2.98	0.15	98.81	72.65
X768B9	49.45	31.64	0.19	14.66	2.90	0.13	98.97	73.67
X768B10	49.80	31.73	0.21	14.77	2.87	0.13	99.51	73.96
X768C1	50.05	32.01	0.19	15.15	2.93	0.12	100.44	74.10
X768C2	49.50	31.97	0.21	15.13	2.90	0.14	99.84	74.27
X768C3	49.49	31.90	0.20	15.06	2.94	0.13	99.72	73.91
X768C4	49.72	31.80	0.21	14.81	3.08	0.16	99.78	72.66
X768C5	49.90	31.70	0.20	14.72	3.17	0.13	99.83	71.94
X768C6	49.59	32.10	0.25	15.33	2.92	0.13	100.31	74.38
X768C7	49.34	32.20	0.24	15.30	2.82	0.15	100.06	74.98
X768C8	49.62	32.26	0.21	15.47	2.83	0.14	100.52	75.12
X768C9	49.60	31.98	0.20	15.13	2.99	0.13	100.02	73.67
X768C10	49.18	31.85	0.23	15.24	2.93	0.14	99.56	74.22
X768D1	49.70	32.41	0.19	15.60	2.69	0.13	100.73	76.21
X768D2	49.84	32.17	0.21	15.53	2.80	0.13	100.67	75.42
X768D3	49.95	32.01	0.24	15.17	2.94	0.17	100.49	74.05
X768D4	50.71	31.41	0.20	14.69	3.16	0.18	100.35	71.97
X768D5	50.03	31.64	0.25	15.00	2.95	0.17	100.05	73.74
X768D6	49.42	32.38	0.24	15.74	2.63	0.15	100.55	76.75
X768D7	49.56	32.33	0.23	15.80	2.64	0.12	100.67	76.82
X768D8	48.38	32.69	0.22	15.89	2.43	0.13	99.75	78.29
Sample X768.5 Profile D.								
X768E9	49.00	32.12	0.20	15.17	2.73	0.15	99.37	75.43
X768E10	49.02	31.70	0.21	14.98	2.93	0.17	99.00	73.87
X768E11	49.62	32.21	0.21	15.39	2.71	0.14	100.27	75.84
X768E12	49.43	32.18	0.25	15.13	2.74	0.14	99.87	75.30
X768E13	50.46	31.29	0.25	14.37	3.19	0.19	99.75	71.33
X768E14	50.44	31.18	0.24	14.27	3.04	0.20	99.37	72.17
X768E15	50.81	31.11	0.20	14.22	3.17	0.22	99.73	71.25
X768E16	50.59	31.35	0.23	14.55	3.13	0.21	100.06	72.01
X768E17	49.07	32.38	0.26	15.71	2.62	0.14	100.18	76.78
X768E18	49.08	32.17	0.22	15.31	2.67	0.15	99.61	76.01
X768E19	47.68	33.48	0.21	16.59	2.13	0.07	100.15	81.17
X768E20	49.01	32.22	0.24	15.38	2.72	0.15	99.72	75.79

MICROPROBE DATA TABLE C30: Composition of **chromite** at the base of the Bastard Unit - profile **LEF.**

LEF - Sample H998.1

Wt.%						
TiO_2	1.59	1.62	1.53	1.55	1.56	1.56
Al_2O_3	11.29	11.15	11.33	11.10	11.38	11.29
Cr_2O_3	42.90	42.73	42.79	41.40	42.99	41.98
FeO(P)	37.33	37.43	37.06	38.78	37.30	37.77
FeO(C)	25.69	25.72	25.56	25.77	25.72	25.65
Fe_2O_3	12.93	13.01	12.78	14.46	12.87	13.47
MnO	0.33	0.31	0.34	0.37	0.37	0.30
NiO	0.28	0.25	0.27	0.26	0.27	0.28
MgO	5.96	5.92	5.91	5.78	5.94	5.87
Total	99.68	99.41	99.24	99.24	99.81	99.04
Total(C)	100.98	100.72	100.52	100.69	101.10	100.39
Recalculated as cations per 32 oxygens.						
Ti	0.3229	0.3297	0.3106	0.3167	0.3154	0.3185
Fe^{2+}	0.3229	0.3297	0.3106	0.3167	0.3154	0.3185
Al	3.5881	3.5541	3.6162	3.5462	3.6113	3.6102
Cr	9.1429	9.1382	9.1589	8.8719	9.1510	9.0026
Fe^{3+}	2.6231	2.6483	2.6037	2.9485	2.6068	2.7503
Fe^{2+}	5.4688	5.4876	5.4764	5.5235	5.4743	5.5006
Mn	0.0754	0.0705	0.0783	0.0850	0.0833	0.0678
Ni	0.0598	0.0550	0.0597	0.0567	0.0583	0.0601
Mg	2.3960	2.3868	2.3855	2.3348	2.3840	2.3715
Cr/Al	2.5481	2.5712	2.5328	2.5018	2.5340	2.4937
MMF	0.3047	0.3031	0.3034	0.2971	0.3034	0.3013
FFE	0.3242	0.3255	0.3222	0.3480	0.3226	0.3333
Cr/(Cr+Al	0.7182	0.7200	0.7169	0.7144	0.7170	0.7138

APPENDIX D.

X-RAY FLUORESCENCE ANALYSIS OF WHOLE-ROCK SAMPLES

Whole-rock analysis for major elements employed the fusion-disk technique of Norrish and Hutton (1969). All samples were analysed in duplicate using a Philips PW1410 semi-automatic X-ray fluorescence spectrometer, employing the batch-processing system in general use at Rhodes University (Marsh, 1979). The machine was calibrated using a range of international and Rhodes internal standards. Where it was deemed necessary, analyses were repeated in triplicate. Sodium and trace elements were determined in 5g pressed powder briquettes, with corrections for background, spectral line interference, absorption and instrumental drift.

All calibrations were made using a variety of USGS, NIMROC and other international standards. Determinations of Ti were run in quadruplicate for 15 samples deemed to be of particular significance in the UG1 Footwall Unit. All counting on spectral-line peaks for trace elements was fixed at 200 seconds, and 100 seconds for backgrounds. Higher precision for Sr and Rb in samples from the UG1 Footwall Unit (**S** samples) was ensured by repeating the counting on peak for 400 seconds and 200 seconds on background in a second run using the Molybdenum Compton scatter method. The mean difference between samples in the two runs was 1.3ppm Sr for pyroxenites and 2.6ppm for norites and leuconorites.

The reliability of Sr and Rb values can be gauged by comparison of three different analytical techniques used on selected samples which were submitted for initial strontium isotope determinations. Three analytical runs were done up to 2 years apart. The results of this comparison are presented in Table D1.

TABLE D1: Comparison of results for Strontium and Rubidium using three different analytical methods. Two pressed disks were prepared for some samples (- = No analysis, nd = below detection limits).

1. Isotope dilution - Dr. JF Kruger BPI (Univ. of the Witwatersrand.)
2. XRF determination of the Rb short wavelength MAC and the Sr and Rb concentrations using the Molybdenum Compton scatter method - 400 cps on peak (method after Reynolds, 1967 and Nesbitt et al., 1976).
3. XRF determination in the analytical run for Rb, Sr, Y, Zr and Nb (200 cps on peak).

	1		2				3			
	Isotope Dilution		XRF Mo Compton method at 400 cps on peak				XRF Normal five element run with 200 cps on peak			
SAMPLE	Rb	Sr	Rb Disk 1	Rb Disk 2	Sr Disk 1	Sr Disk 2	Rb Disk 1	Rb Disk 2	Sr Disk 1	Sr Disk 2
B232/22	4.95	335.0	4.6	6.2	337.9	340.3	6.3	-	339.0	-
B235/3	0.47	139.0	0.4	0.5	135.7	133.2	nd	nd	137.9	132.0
B235/6	6.42	53.7	7.0	6.5	55.7	48.3	5.0	7.0	54.7	55.0
B235/8	5.23	395.0	5.3	6.0	398.8	400.0	8.0	5.4	433.0	412.0
B235/11	1.96	373.0	2.3	1.6	348.9	349.3	2.3	-	337.0	335.0
B235/14	3.82	57.7	4.1	3.4	53.8	53.7	5.0	3.0	52.0	52.0
B235/15a	3.69	65.5	3.0	-	72.0	-	3.4		71.5	
B235/18	1.77	455.6	2.6	2.5	457.7	451.6	2.3	3.0	470.0	458.0
B235/21	1.61	390.8	2.1	2.2	380.5	375.9	3.0	2.0	387.4	379.0
B235/23	1.09	176.0	0.8	0.4	180.5	166.6	0.7	-	174.0	186.0
B235/29	8.94	69.2	9.4	8.0	62.1	65.2	7.9	11.0	69.0	63.0
B235/31	0.74	72.8	1.4	1.5	72.6	65.5	1.0	1.0	73.0	63.0
B235/34	5.92	61.9	6.1	9.2	50.8	31.2	5.4	8.0	55.0	34.0
B235/35	6.31	52.2	6.0		50.0		6.0		51.0	
B235/37	0.50	66.6	0.6	nd	71.2	74.1	nd	nd	69.0	62.0
B235/39	0.88	413.0	1.2	0.4	365.7	365.5	1.4	-	370.0	364.0
S-9	0.76	163.0	0.2		163.4		0.8		161.7	
S-13	0.84	190.0	0.5	0.7	215.1	183.1	1.1		214.9	
S-19	1.27	326.0	1.6		325.1		2.0		325.0	
S-23	1.30	198.0	1.3		197.9		2.1		206.3	
S-30	0.81	174.0	0.7	0.6	178.2	176.9	0.4	-	178.2	180.1
S-33	0.81	97.2	0.3		97.2		0.3		100.2	
S-35	1.07	125.0	1.6		123.5		1.6		124.8	
S-36	1.57	70.3	2.3		70.4		2.3		73.7	
S-38	0.41	47.6	0.2		46.1		0.2		48.9	
S-40	0.34	70.9	nd		71.9		nd		72.8	
S-43	0.31	37.7	nd		36.8		nd		38.1	
S-49	1.14	44.6	2.6		44.0		1.8		45.7	
S-54	1.51	39.4	2.5		40.5		2.5		41.7	
S-58	0.60	36.8	0.8		37.3		0.7		37.8	
S-66	0.56	78.5	2.0		78.4		2.0		82.7	
S-71	0.78	254.0	0.6		256.0		0.6		262.4	

Mass absorption coefficients (MACs) were either determined using the Mo-Compton Fe-K-alpha method (Reynolds, 1967; Nesbitt et al., 1976) or calculated from major element data using Heinrich's (1966) values.

Standard calibration and data reduction was achieved by using computer programs available on XRFFILE on the Rhodes University Cyber main frame computer. These programs allow for corrections to be made for instrumental drift, dead-time, background, tube and spectral line interferences. For each trace element analysis counting error, lower limit of detection and lower limit of determination (LLD - defined as twice the detection limit) were calculated. Typical LLD and absolute errors of determination are presented below.

Element	LLD	sd	Error	sd
Rb	1.39	0.18	0.41	0.05
Sr	1.32	0.17	0.72	0.20
Y	1.53	0.20	0.45	0.06
Zr	1.31	0.17	0.39	0.05
Co	2.08	0.33	0.55	0.11
Cr	2.34	0.27	1.87	1.08
V	2.95	0.35	0.77	0.12
Zn	2.04	0.21	0.73	0.04
Cu	2.19	0.23	0.78	0.05
Ni	2.78	0.29	1.16	0.12
Sc	0.52	0.05	0.45	0.26

Calibration curves were determined from the following international and in-house standards.

Major elements	- NIM-N, BCR, GSP, AGV, DTS, G-2.
Na	- G-2, PCC, BCR, AGV, GSP, NIM-G.
MACs	- DTS, BHVO, GSP, BCR, G-2, AGV.
Rb, Sr, Zr, Y	- BCR, G-2, S-12, AGV, SDC.
Co, Cr, V	- QLO, PCC, SDC, BHVO, KRF-13, BCR.
Zn, Cu, Ni	- PCC, BHVO, DTS, BCR, AGV.
Sc	- BCR, AGV, GSP, NIM-N.

Typical running conditions for the XRF are listed in Table D2 below.

TABLE D2: X-Ray Fluorescence analytical conditions.
(Kα emission line with a kV of 55 and mA of 40)

Element	Tube	Crystal	Time (Secs)	Counter	Collimator	Specimen
Si	Cr	PET	40	flow	coarse	fusion disc
Ti	Cr	LiF(200)	10	flow	fine	fusion disc
Al	Cr	PET	40	flow	coarse	fusion disc
Fe	Cr	LiF(200)	20	flow	fine	fusion disc
Mn	Cr	LiF(200)	20	flow	coarse	fusion disc
Mg	Cr	TLAP	200	flow	fine	fusion disc
Ca	Cr	LiF(200)	10	flow	fine	fusion disc
Na	Cr	TLAP	100	flow	fine	powder pellet
K	Cr	LiF(200)	10	flow	fine	fusion disc
P	Cr	Ge	20	flow	coarse	fusion disc
Sr	W	LiF(220)	200	scint.	fine	powder pellet
Rb	W	LiF(220)	200	scint.	fine	powder pellet
Zr	W	LiF(220)	200	scint.	fine	powder pellet
Y	W	LiF(220)	200	scint.	fine	powder pellet
Co	W	LiF(220)	200	flow	fine	powder pellet
Cr	W	LiF(220)	200	flow	fine	powder pellet
V	W	LiF(220)	200	flow	fine	powder pellet
Zn	Mo	LiF(220)	200	flow+scint.	fine	powder pellet
Cu	Mo	LiF(220)	200	flow+scint.	fine	powder pellet
Ni	Mo	LiF(220)	200	flow+scint.	fine	powder pellet
Sc	Cr	LiF(220)	200	flow	fine	powder pellet

Analytical data were checked by re-analysing selected samples during successive runs to check consistency of the results. The repeat analysis of randomly selected samples gave results which were close to those of the original analyses. In one particular instance all samples in 4 Bastard Unit profiles (**LEF**, **Y**, **X** and **RD**) were re-run for Sr some two years after the initial results had been obtained and a marginal decrease in the Sr concentration was recorded (see comparison of the two sets of results Sr in Table D1). Full check analyses for Sr, Rb, Y, and Zr were also made on the pyroxenite samples of these profiles. Additional checks were also carried out for other elements.

TABLE D3: Comparison of Sr determinations made two years apart on the same powder discs. In some cases a third determination is given.

Profile	Sample	Sr ppm 1st result	Sr ppm 2nd result	ppm diff.	% diff.
LEF	H979.91	246.4	247.0	-0.60	-0.24
	H984.48	308.6	301.8	6.80	2.20
	H992.8	273.6	271.5	2.10	0.77
	H995.6	399.0	394.1	4.90	1.23
	H997.26	371.4	367.1	4.30	1.16
	H998.1	94.2	93.3/93.0	0.90	0.96
Y	Y722.4	335.1	332.4	2.70	0.81
	Y740.5	328.9	318.4	10.50	3.19
	Y746.4	333.0	323.7	9.30	2.79
	Y755.66	341.9	331.6	10.30	3.01
	Y760.2	372.1	357.9	14.20	3.82
	Y764.2	272.5	268.4	4.10	1.50
	Y765.48	375.5	367.5	8.00	2.13
	Y770.58	215.1	211.5	3.60	1.67
	Y775	67.5	63.0	4.40	6.52
X	X735	314.2	306.4	7.8	2.48
	X745.44	357.6	347.2	10.4	2.91
	X763.95	332.2	324.0	8.2	2.47
	X768.5	327.9	321.0	6.9	2.10
	X776.52	327.9	317.4	10.5	3.20
	X779.82	80.4	78.5	1.9	2.36
	X782.7	270.5	267.5	3.0	1.11
	X788.41	162.9	157.2	5.7	3.50
	X791.8	65.4	60.5/60.6	-2.7	-4.13
RD	RD-1	493.4	473.3	20.1	4.07
	RD-3	456.4	448.5	7.9	1.73
	RD-4	459.5	451.2	8.3	1.81
	RD-6	566.9	551.9	15.0	2.65
	RD-15	330.7	322.6	8.1	2.45
	RD-16	205.2	203.9	1.3	0.63
	RD-17	71.4	66.5	4.9	6.86
	RD-18	70.8	66.0/63.0	4.8	6.78

Major element data are quoted in two forms.

1. **Actual corrected analyses.** Here the best result of the two determinations is recorded with total Fe quoted as Fe_2O_3 and includes LOI and H_2O^- (Tables D1 - D7).
2. **Working analyses** have been normalised to 100% and are LOI and H_2O^- free. These results have been used throughout in the presentation of results and calculation of the norms. They represent either the best result or an average of the two normalised determinations (Table D8 - D14).

Note MMF_{WR} - Magnesium No. (also quoted as whole-rock MMF ratio).

MMF_{WR} = atomic ratio of Mg/(Mg + Fe)

$$\frac{\left(\frac{MgO}{40.32}\right)}{\left(\frac{(0.9 * Fe_2O_3) + FeO}{71.85}\right) + \left(\frac{MgO}{40.32}\right)}$$

Plagioclase mineral separates.

Two plagioclase separates were prepared from the Bastard pyroxenite samples of profile **Y** and **X** (samples Y775.0 and X791.8). The samples were crushed and sieved and the fraction between 63 and 180 microns was retained. This was then washed in distilled water to remove the fines and dried at 110°C before separation. An electromagnetic separator was used to separate the plagioclase from the sample. By trial and error the optimum inclination, sideways tilt and rate of feed of the separator was determined. After an initial pass the plagioclase fraction was sent through the separator two more times. The final plagioclase fraction was then cleaned by hand-picking under a binocular microscope and extremely pure separates were obtained (>99%). Because of the small volume of the separates a dilution with pure silica was needed to make up the 5gm XRF briquette.

WHOLE ROCK DATA TABLE D4: Major element analyses - UG1 Footwall Unit - S samples.
Including LOI and H_2O-. Total Fe expressed as Fe_2O_3.
* = average of two analyses.
Metres given below base of UG1 chromitite).

Sample	S-0	S-1	S-2	S-3	S-4	S-5	S-6*	S-7*	S-8	S-9	S-10	S-11	S-12	S-13	S-14	S-15	S-16	S-17	S-18	S-19	S-20	S-21	S-22	S-23	S-24	S-25	S-26
Metres	1.0	2.6	5.3	8.4	11.3	18.2	22.1	26.5	32.3	37.8	42.5	49.8	57.1	67.9	75.2	80.9	85.3	89.7	94.1	98.8	106.0	110.7	115.1	120.4	124.8	129.1	133.5
Wt.%																											
SiO_2	48.30	49.30	49.60	49.37	49.22	50.29	52.38	51.77	50.13	50.08	50.23	52.73	51.06	51.97	50.17	49.41	51.86	51.53	50.49	48.69	62.17	48.62	52.12	53.33	52.48	51.46	50.43
TiO_2	0.02	0.06	0.04	0.05	0.03	0.05	0.10	0.11	0.10	0.11	0.09	0.11	0.12	0.09	0.07	0.10	0.08	0.11	0.06	0.06	0.08	0.06	0.09	0.10	0.18	0.08	0.09
Al_2O_3	32.60	25.20	25.71	31.86	32.11	22.91	14.18	11.69	12.04	10.04	12.97	11.45	9.55	14.87	21.14	16.53	20.82	15.08	24.03	20.59	24.13	14.22	14.99	13.39	3.80	15.16	15.37
Fe_2O_3	1.05	3.83	3.40	1.06	0.90	4.50	8.41	9.35	8.63	8.91	8.17	9.69	10.31	8.09	5.35	6.55	5.78	8.02	4.66	4.84	7.17	7.59	7.94	9.16	13.15	8.34	8.65
MnO	0.02	0.05	0.07	0.02	0.03	0.07	0.15	0.18	0.17	0.17	0.16	0.18	0.17	0.15	0.08	0.13	0.12	0.15	0.09	0.09	0.13	0.13	0.14	0.15	0.22	0.14	0.15
MgO	0.50	6.40	6.18	0.90	0.75	8.72	16.70	18.22	17.11	19.07	19.98	19.11	19.00	15.34	9.84	12.56	10.29	15.00	7.92	8.87	14.32	14.17	14.67	16.60	22.79	14.46	14.24
CaO	15.40	12.20	12.83	15.22	14.52	11.63	7.48	6.15	6.27	5.84	6.65	6.16	5.76	7.51	10.71	8.14	10.02	7.66	11.83	9.77	11.52	7.70	8.03	7.32	3.48	8.27	8.75
Na_2O	2.20	1.80	2.05	2.22	2.23	1.81	1.14	1.02	1.05	1.19	1.24	1.20	0.99	1.37	1.48	1.54	1.68	1.43	2.18	1.84	1.63	1.43	1.43	1.37	0.43	1.46	1.43
K_2O	0.09	0.11	0.06	0.11	0.12	0.09	0.07	0.33	0.10	0.07	0.09	0.08	0.07	0.07	0.10	0.09	0.12	0.09	0.13	0.10	0.11	0.03	0.07	0.05	0.03	0.06	0.07
P_2O_5	0.05	0.06	0.02	0.00	0.01	0.00	0.00	0.02	0.01	0.00	0.00	0.02	0.01	0.00	0.05	0.00	0.01	0.02	0.01	0.01	0.02	0.01	0.00	0.03	0.00	0.00	0.04
LOI	0.12	0.65	0.11	0.49	0.15	0.08	-0.17	0.26	0.01	-0.29	-0.20	-0.29	-0.13	-0.25	-0.03	-0.15	0.01	-0.06	0.40	0.09	0.34	-0.21	-0.23	-0.28	-0.42	-0.23	-0.25
H_2O-	0.00	0.00	0.05	0.09	0.05	0.08	0.04	0.09	0.04	0.04	0.04	0.05	0.04	0.03	0.06	0.05	0.04	0.07	0.06	0.05	0.09	0.06	0.05	0.06	0.06	0.08	0.08
Total	100.35	99.66	100.12	101.38	100.11	100.21	100.48	99.20	95.66	95.22	99.42	100.47	96.94	99.24	99.02	94.96	100.83	99.08	101.85	94.99	121.71	93.80	99.29	101.27	96.20	99.28	99.04

Sample	S-27	S-28	S-29	S-30	S-31	S-32	S-33	S-34	S-35	S-36	S-37	S-38	S-39	S-40	S-41	S-42	S-43	S-44	S-45	S-46	S-47	S-48	S-49	S-50	S-51	S-52	S-53
Metres	137.9	142.5	146.9	151.6	156.3	161.3	166.0	170.6	175.6	181.5	185.9	190.3	194.9	199.3	203.7	208.1	213.2	217.2	221.9	226.8	230.4	234.8	238.9	243.6	247.8	252.2	256.7
Wt.%																											
SiO_2	50.49	48.80	52.32	49.81	53.93	53.80	51.99	53.88	53.30	53.86	54.09	54.20	53.64	54.35	52.75	53.96	54.15	54.00	54.22	53.68	53.30	53.99	53.34	54.03	54.70	54.39	52.82
TiO_2	0.07	0.08	0.09	0.08	0.13	0.14	0.19	0.21	0.15	0.18	0.16	0.17	0.14	0.13	0.12	0.13	0.14	0.15	0.15	0.18	0.13	0.14	0.19	0.17	0.16	0.16	0.14
Al_2O_3	14.56	12.73	11.50	11.43	5.30	4.70	6.97	4.24	10.02	5.29	3.85	3.84	3.84	5.08	4.02	3.54	3.35	3.20	3.10	3.40	4.90	2.83	4.31	3.98	3.70	2.58	3.92
Fe_2O_3	8.58	8.65	9.93	9.23	12.90	13.55	11.44	14.22	10.67	13.99	13.80	13.75	12.95	12.63	13.00	13.16	13.90	13.80	13.67	14.40	13.20	14.61	14.40	13.82	13.79	15.17	14.82
MnO	0.16	0.20	0.18	0.18	0.25	0.26	0.24	0.50	0.47	0.25	0.24	0.23	0.24	0.23	0.22	0.25	0.24	0.24	0.26	0.25	0.24	0.35	0.34	0.24	0.24	0.28	0.26
MgO	14.87	15.36	17.47	16.88	23.50	24.20	23.89	23.38	19.22	22.36	24.48	24.44	24.21	23.74	24.28	24.78	25.49	25.50	25.71	24.80	23.87	25.51	23.67	24.10	23.97	25.93	24.44
CaO	7.84	7.07	6.54	6.66	3.95	3.67	4.53	3.72	5.31	4.05	3.45	3.35	3.32	3.81	3.28	3.00	3.21	3.15	3.20	3.40	3.77	2.34	3.59	3.44	3.36	2.65	3.56
Na_2O	1.43	1.24	1.20	1.13	0.61	0.51	0.83	0.39	0.74	0.53	0.60	0.56	0.54	0.56	0.39	0.44	0.35	0.25	0.32	0.32	0.59	0.25	0.35	0.45	0.45	0.28	0.45
K_2O	0.03	0.04	0.04	0.03	0.01	0.02	0.26	0.00	0.04	0.02	0.06	0.00	0.01	0.00	0.00	0.00	0.00	0.00	0.00	0.00	0.00	0.00	0.00	0.07	0.07	0.01	0.03
P_2O_5	0.00	0.01	0.04	0.01	0.02	0.08	0.00	0.06	0.06	0.03	0.00	0.60	0.00	0.00	0.04	0.02	0.00	0.05	0.01	0.01	0.03	0.00	0.00	0.01	0.00	0.06	0.02
LOI	-0.27	-0.28	-0.40	-0.34	-0.59	-0.78	-0.34	-0.55	0.03	-0.56	-0.73	-0.63	-0.58	-0.56	0.28	-0.41	-0.86	-0.56	-0.70	-0.57	-0.56	-0.51	-0.48	-0.45	-0.50	-0.73	-0.57
H_2O-	0.06	0.05	0.07	0.05	0.05	0.06	0.06	0.06	0.06	0.05	0.05	0.04	0.08	0.00	0.05	0.04	0.00	0.02	0.00	0.00	0.00	0.00	0.00	0.00	0.01	0.02	0.03
Total	97.82	93.95	98.97	95.16	100.06	100.20	100.07	100.11	100.07	100.06	100.04	100.56	98.39	99.97	98.42	98.91	99.98	99.80	99.94	99.86	99.48	99.51	99.71	99.85	99.95	100.80	99.91

Sample	S-54	S-55	S-56	S-57	S-58	S-59	S-64	S-65	S-66	S-69	S-70	S-71	S-72	S-73*	S-74	S-75	S-76	S-77	S-79	S-81
Metres	261.4	265.7	270.2	274.4	279.7	286.4	299.1	302.9	307.9	314.6	320.2	325.0	328.1	329.9	332.1	334.1	335.1	337.8	341.8	344.9
Wt.%																				
SiO_2	54.93	51.83	53.59	53.94	54.18	53.16	54.27	54.12	53.22	47.38	51.39	51.28	51.32	51.33	49.77	50.05	49.31	52.94	53.31	55.66
TiO_2	0.13	0.14	0.13	0.16	0.15	0.15	0.16	0.16	0.13	0.09	0.10	0.09	0.09	0.11	0.10	0.12	0.10	0.12	0.21	0.18
Al_2O_3	3.65	3.62	3.69	3.60	3.40	2.39	4.14	4.19	3.66	10.87	12.77	17.28	17.47	16.19	17.32	15.42	17.14	12.21	7.86	4.23
Fe_2O_3	14.10	14.29	13.98	14.59	13.39	13.76	12.65	12.79	13.95	8.13	9.02	7.04	6.30	8.19	7.50	8.39	7.70	9.55	12.77	14.29
MnO	0.03	0.26	0.24	0.25	0.26	0.25	0.23	0.23	0.24	0.15	0.15	0.11	0.11	0.14	0.14	0.15	0.14	0.17	0.20	0.25
MgO	24.53	25.37	24.48	23.70	25.60	25.16	25.31	25.12	24.70	16.47	17.08	13.76	12.50	15.23	13.78	15.56	14.69	18.12	22.15	26.87
CaO	3.21	3.36	3.33	3.46	3.08	2.58	3.16	3.20	3.33	5.86	7.45	9.21	9.18	8.98	9.69	8.82	9.25	6.95	4.34	3.67
Na_2O	0.42	0.49	0.42	0.48	0.42	0.20	0.61	0.48	0.65	1.04	1.17	1.20	1.29	1.55	1.63	1.57	1.61	1.08	0.76	0.41
K_2O	0.01	0.25	0.00	0.05	0.01	0.00	0.04	0.04	0.00	0.02	0.06	0.05	0.08	0.04	0.07	0.08	0.13	0.05	0.05	0.01
P_2O_5	0.00	0.00	0.09	0.00	0.01	0.05	0.00	0.00	0.04	0.00	0.00	0.05	0.02	0.01	0.06	0.02	0.01	0.07	0.02	0.00
LOI	-0.51	0.57	0.02	-0.27	-0.58	1.08	-0.57	-0.35	0.00	9.90	-0.23	-0.09	1.75	-2.03	-0.07	-0.22	-0.12	-0.23	-0.42	-5.62
H_2O-	0.04	0.02	0.56	0.05	0.00	0.06	0.04	0.07	0.06	0.05	0.03	0.00	0.52	0.02	0.00	0.00	0.00	0.01	0.03	0.00
Total	100.54	100.20	100.52	100.01	99.91	98.83	100.04	100.05	99.98	99.96	99.01	99.98	100.63	99.76	99.98	99.96	99.96	101.03	101.28	99.96

WHOLE ROCK DATA TABLE D5: Major element analyses - Upper Critical Zone - profile **UA**.
Including LOI and H_2O-. Total Fe expressed as Fe_2O_3.
* = average of two analyses.
Metres given relative to the base of the Bastard Unit.

Sample	UA-1	UA-2	UA-3	UA-4	UA-5	UA-6	UA-7	UA-8	UA-9	UA-10	UA-11	UA-12	UA-13	UA-14	UA-15	UA-16a	UA-16b	UA-17	UA-18	UA-20	UA-21	UA-22
Metres	53.2	50.5	47.6	44.6	41.9	39.4	36.8	33.7	31.2	28.9	26.3	23.7	21.8	20.2	19.0	17.9	17.7	16.2	14.2	10.1	8.5	7.2
Wt.%	*	*												*	*		*	*		*		*
SiO_2	50.64	49.88	49.96	52.40	50.56	53.11	49.87	51.04	52.42	50.42	49.53	53.11	49.76	49.75	48.20	49.87	48.80	50.84	51.32	51.76	52.65	52.39
TiO_2	0.18	0.12	0.07	0.08	0.08	0.08	0.07	0.07	0.09	0.09	0.05	0.08	0.11	0.09	0.11	0.06	0.09	0.10	0.10	0.10	0.09	0.11
Al_2O_3	27.25	27.84	29.04	30.88	28.27	30.95	29.28	29.69	29.53	30.77	30.43	33.48	29.45	27.31	31.52	32.83	26.70	20.30	19.48	15.36	16.95	10.70
Fe_2O_3	3.01	2.79	2.22	2.13	2.51	2.42	2.36	2.11	2.35	1.58	1.59	1.30	2.38	2.73	0.93	1.21	3.15	5.61	5.89	7.39	6.88	8.74
MnO	0.04	0.03	0.02	0.03	0.04	0.03	0.03	0.03	0.03	0.03	0.02	0.01	0.03	0.04	0.01	0.01	0.05	0.10	0.10	0.13	0.12	0.16
MgO	2.30	2.37	2.29	2.21	2.83	2.41	2.20	2.49	2.84	1.63	1.50	0.83	2.11	3.09	0.70	1.13	4.47	10.44	11.90	15.49	15.36	19.88
CaO	13.55	13.90	14.64	15.37	14.57	15.37	14.45	14.27	14.38	14.74	14.84	16.08	14.19	14.13	15.63	15.97	13.62	10.60	10.05	8.35	8.90	6.28
Na_2O	2.31	2.37	2.25	2.22	2.18	2.18	2.30	2.31	2.21	2.35	2.38	2.52	2.40	2.24	2.29	2.08	1.93	1.62	1.52	1.18	1.21	1.09
K_2O	0.34	0.26	0.21	0.22	0.20	0.22	0.19	0.19	0.19	0.19	0.16	0.23	0.20	0.18	0.21	0.25	0.19	0.12	0.12	0.07	0.08	0.05
P_2O_5	0.04	0.03	0.03	0.03	0.07	0.03	0.04	0.06	0.04	0.07	0.06	0.04	0.04	0.04	0.03	0.08	0.02	0.08	0.06	0.03	0.01	0.01
LOI	0.21	0.23	0.23	0.36	0.23	0.25	0.23	0.25	0.22	0.28	0.46	0.31	0.37	0.59	0.41	0.47	0.32	0.39	-0.25	0.04	-0.01	0.14
H_2O-	0.04	0.06	0.04	0.02	0.06	0.05	0.05	0.05	0.04	0.07	0.07	0.05	0.04	0.07	0.05	0.01	0.00	0.00	0.00	0.01	0.01	0.00
Total	99.91	99.87	100.99	105.96	101.59	107.08	101.08	102.56	104.33	102.21	101.07	108.05	101.05	100.24	100.08	103.96	99.33	100.19	100.28	99.90	102.24	99.54

Sample	UA-23	UA-24	UA-25	UA-26	UA-28	UA-29	UA-30	UA-31	UA-32	UA-33	UA-34	UA-35	UA-36	UA-37	UA-38	UA-39	UA-40	UA-41	UA-42	UA-46	UA-47
Metres	5.1	3.2	1.9	0.8	-1.0	-1.9	-4.4	-5.2	-6.2	-7.9	-9.8	-11.7	-13.7	-16.2	-17.4	-18.7	-20.4	-21.9	-23.3	-26.9	-28.1
Wt.%													*								
SiO_2	53.00	53.57	53.73	52.96	47.03	46.48	46.32	47.05	48.00	49.03	50.55	49.90	49.37	50.35	49.96	53.23	53.19	53.83	52.15	47.76	47.90
TiO_2	0.14	0.18	0.20	0.20	0.04	0.04	0.04	0.04	0.04	0.07	0.12	0.08	0.09	0.08	0.09	0.11	0.24	0.27	0.23	0.05	0.07
Al_2O_3	6.50	5.07	5.12	5.14	29.31	30.47	29.91	30.71	31.19	26.17	27.82	27.28	26.87	22.01	19.38	16.99	5.13	5.49	4.37	31.28	29.60
Fe_2O_3	10.44	11.19	11.38	11.43	1.17	1.01	1.43	1.04	0.93	3.42	2.95	3.48	3.03	4.71	6.10	8.18	11.76	11.34	12.14	1.00	1.76
MnO	0.20	0.21	0.21	0.19	0.01	0.01	0.01	0.01	0.01	0.05	0.44	0.59	0.05	0.08	0.11	0.14	0.20	0.20	0.21	0.01	0.02
MgO	23.70	23.51	23.94	23.18	1.79	1.12	1.38	1.30	1.10	5.33	1.14	1.26	4.83	8.70	11.59	14.80	23.40	22.65	23.59	0.84	1.85
CaO	4.19	3.62	3.44	3.70	14.60	14.28	14.73	15.03	15.04	13.18	13.74	13.22	13.40	11.56	10.32	9.53	3.61	4.08	4.17	15.20	14.64
Na_2O	0.58	0.71	0.68	0.70	2.37	2.50	2.25	2.23	2.27	1.97	2.01	2.20	2.00	1.75	1.43	1.29	0.70	0.76	0.56	2.45	2.32
K_2O	0.05	0.07	0.08	0.15	0.19	0.57	0.21	0.20	0.28	0.13	0.16	0.14	0.16	0.11	0.10	0.10	0.18	0.21	0.08	0.16	0.14
P_2O_5	0.06	0.02	0.02	0.07	0.00	0.00	0.00	0.00	0.00	0.00	0.02	0.05	0.07	0.00	0.00	0.05	0.02	0.05	0.00	0.00	0.00
LOI	-0.05	0.05	0.11	0.45	0.81	1.52	0.76	0.48	0.46	0.35	0.45	0.36	0.13	0.26	0.07	-0.03	0.19	0.14	-0.08	0.37	0.25
H_2O-	0.01	0.07	0.10	0.07	0.07	0.07	0.03	0.06	0.05	0.05	0.05	0.09	0.11	0.13	0.10	0.09	0.13	0.08	0.09	0.09	0.09
Total	98.82	98.26	99.00	98.23	97.39	98.06	97.07	98.14	99.38	99.74	99.43	98.64	100.11	99.74	99.24	104.47	98.74	99.10	97.50	99.19	98.62

Sample	UA-48	UA-49	UA-50a	UA-50b	UA-51	UA-52	UA-53a	UA-53b	UA-53c	UA-54	UA-55	UA-56	UA-57	UA-63	UA-64	UA-65	UA-66	UA-67	UA-68	UA-69	UA-70
Metres	-29.8	-30.8	-31.8	-32.0	-33.5	-35.4	-36.4	-36.7	-37.0	-38.2	-39.0	-39.2	-40.2	-45.4	-46.8	-48.4	-49.8	-51.3	-53.0	-53.7	-54.3
Wt.%	*				*	*															
SiO_2	48.81	50.77	47.96	48.14	46.36	50.02	48.97	49.17	48.97	47.88	51.26	51.32	50.77	52.26	54.27	51.78	52.06	53.50	52.36	52.85	46.30
TiO_2	0.07	0.08	0.07	0.07	0.05	0.08	0.09	0.09	0.06	0.05	0.08	0.14	0.14	0.26	0.11	0.18	0.22	0.23	0.25	0.13	0.18
Al_2O_3	28.93	31.85	29.87	27.85	27.16	24.76	25.71	25.26	28.72	25.38	19.01	10.89	12.31	4.66	17.22	4.85	4.60	3.99	4.46	5.92	3.53
Fe_2O_3	1.99	2.05	1.27	2.11	2.05	3.57	3.46	3.49	2.16	2.98	5.59	8.29	7.70	11.76	7.88	11.87	11.85	12.25	12.52	11.53	14.65
MnO	0.03	0.03	0.02	0.03	0.03	0.06	0.05	0.05	0.03	0.05	0.10	0.14	0.15	0.21	0.13	0.22	0.23	0.21	0.22	0.20	0.21
MgO	1.67	1.94	1.68	3.76	3.33	7.21	6.20	6.12	3.30	6.20	12.64	19.02	17.81	23.83	15.14	23.92	23.95	23.89	23.37	24.10	26.85
CaO	14.93	14.99	14.96	13.79	13.12	12.33	13.05	12.95	13.87	12.76	9.66	6.36	7.43	3.71	9.29	3.53	4.19	3.59	3.56	4.14	2.40
Na_2O	2.31	2.28	2.29	2.18	2.06	1.88	1.85	2.24	2.09	1.97	1.42	1.07	1.27	0.63	0.72	0.65	0.75	0.58	0.65	0.53	0.34
K_2O	0.16	0.16	0.17	0.12	0.13	0.14	0.15	0.15	0.18	0.18	0.17	0.06	0.09	0.13	0.09	0.02	0.04	0.04	0.05	0.03	0.09
P_2O_5	0.06	0.03	0.01	0.00	0.02	0.06	0.03	0.03	0.06	0.00	0.02	0.02	0.00	0.01	0.01	0.04	0.00	0.00	0.06	0.02	0.01
LOI	0.45	0.32	0.39	0.41	0.26	0.43	0.39	0.43	0.52	0.43	0.51	0.22	0.54	-0.21	-0.15	-0.31	-0.12	-0.28	-0.27	0.88	2.60
H_2O-	0.09	0.03	0.07	0.06	5.61	0.05	0.00	0.00	0.00	0.04	0.10	0.04	0.07	0.04	0.00	0.02	0.04	0.07	0.05	0.05	0.10
Total	99.50	104.53	98.74	98.51	100.20	100.58	99.95	99.98	99.97	97.91	100.56	97.55	98.28	97.29	104.71	96.75	97.80	98.07	97.28	100.37	97.26

WHOLE ROCK DATA TABLE D6: Major element analyses - Upper Critical Zone - profile **UC**.
Including LOI and H_2O-. Total Fe expressed as Fe_2O_3.
* = average of two analyses.
Metres given relative to the base of the Bastard Unit.

Sample	UC UC-1	UC-2	UC-3	UC-4	UC-5	UC-6	UC-7	UC-8	UC-9	UC-10	UC-11	UC-12	UC-13	UC-14	UC-15	UC-16	UC-17	UC-18	UC-19	UC-20	UC-21	UC-22	UC-23	UC-24a	UC-24b	UC-25	UC-26	UC-27
Metres	30.75	29.76	28.51	26.50	23.99	22.13	21.46	19.59	17.27	15.95	14.71	13.30	11.13	9.00	7.41	5.26	4.10	2.30	0.57	0.10	-0.15	-0.43	-1.80	-2.50	-2.85	-4.10	-6.60	-7.96
Wt.%																												
SiO_2	50.25	49.08	48.70	49.37	49.53	48.46	48.99	45.83	44.67	43.71	41.97	48.11	43.55	52.65	51.81	54.22	52.79	53.88	54.72	54.13	48.42	48.67	48.48	47.91	48.74	47.85	48.24	49.97
TiO_2	0.11	0.09	0.05	0.06	0.06	0.04	0.04	0.02	0.01	0.03	0.03	0.07	0.05	0.17	0.31	0.16	0.16	0.17	0.19	0.18	0.05	0.04	0.05	0.05	0.06	0.07	0.06	0.08
Al_2O_3	26.02	27.70	29.10	28.29	29.72	30.22	30.06	31.71	31.87	25.20	19.36	16.77	16.18	6.37	8.22	3.56	2.40	5.69	5.06	5.40	29.63	31.11	30.95	31.19	28.10	26.83	27.14	24.51
Fe_2O_3	4.33	3.24	2.40	2.44	1.68	1.07	1.41	0.88	1.14	3.14	7.49	7.32	9.10	10.35	10.83	11.66	12.70	11.57	11.50	11.72	1.78	1.10	1.14	1.00	2.39	2.83	3.09	4.06
MnO	0.08	0.05	0.04	0.04	0.03	0.03	0.03	0.02	0.03	0.05	0.11	0.13	0.14	0.21	0.21	0.23	0.23	0.23	0.20	0.21	0.03	0.01	0.02	0.02	0.04	0.05	0.05	0.07
MgO	4.28	2.73	1.80	2.35	2.05	1.17	1.95	1.50	1.86	4.69	14.51	15.39	17.24	21.78	21.74	26.27	27.13	23.88	23.53	23.26	2.49	1.34	1.70	1.23	3.57	4.20	4.25	6.47
CaO	12.60	13.20	13.90	14.11	14.40	15.10	14.92	15.94	16.37	16.43	10.96	9.41	10.10	7.13	5.22	3.10	2.88	4.35	3.80	3.40	14.07	15.63	15.31	15.74	14.48	13.56	13.51	12.45
Na_2O	2.00	2.13	2.30	2.27	2.51	2.59	2.42	1.95	1.81	1.42	0.68	0.88	0.68	0.43	0.48	0.19	0.61	0.62	0.27	0.62	1.82	1.63	1.78	2 42	2.26	2.09	2.05	2.07
K_2O	0.16	0.20	0.18	0.13	0.13	0.11	0.09	0.07	0.05	0.10	0.02	0.01	0.03	0.07	0.03	0.00	0.00	0.03	0.12	0.12	0.27	0.15	0.15	0.12	0.10	0.12	0.14	0.10
P_2O_5	0.07	0.06	0.06	0.06	0.04	0.10	0.04	0.02	0.06	0.03	0.01	0.05	0.03	0.02	0.08	0.02	0.01	0.08	0.02	0.00	0.06	0.05	0.06	0.11	0.04	0.03	0.12	0.03
LOI	0.42	0.67	1.19	1.01	0.33	0.37	0.25	1.37	1.89	4.11	3.88	0.92	2.58	0.45	0.18	-0.03	0.20	0.11	-0.12	0.38	1.43	0.30	0.37	0.21	0.19	2.33	0.45	0.21
H_2O-	0.07	0.07	0.07	0.07	0.05	0.05	0.05	0.07	0.07	0.09	0.14	0.07	0.09	0.05	0.05	0.05	0.04	0.09	0.05	0.13	0.12	0.05	0.03	0.05	0.04	0.07	0.04	0.04
Total	100.36	99.22	99.79	100.18	100.54	99.29	100.25	99.37	99.82	99.00	99.16	99.12	99.76	99.68	99.15	99.43	99.16	100.69	99.34	99.56	100.17	100.08	100.03	100.04	100.03	100.02	99.13	100.04

Sample	UC-28	UC-29	UC-30	UC-31	UC-32	UC-33	UC-34	UC-35	UC-36	UC-37	UC-38	UC-39	UC-40	UC-41	UC-42	UC-43	UC-44	UC-45	UC-46	UC-47	UC-48a	UC-48b	UC-51	UC-52	UC-53	UC-54	UC-55	UC-56
Metres	-9.61	-11.61	-13.69	-15.97	-17.65	-19.31	-20.97	-22.39	-23.65	-24.63	-25.57	-26.80	-28.85	-31.12	-33.21	-34.47	-35.93	-37.29	-38.30	-39.39	-41.17	-41.55	-45.03	-46.85	-48.65	-50.15	-51.95	-53.20
Wt.%																												
SiO_2	50.11	48.89	49.40	50.51	50.97	50.87	51.61	53.07	54.27	52.94	48.23	48.65	48.66	49.05	48.76	48.45	48.52	48.14	48.19	48.09	51.68	47.57	53.27	53.21	54.40	54.06	54.15	54.62
TiO_2	0.09	0.07	0.08	0.09	0.11	0.12	0.13	0.19	0.21	0.19	0.05	0.05	0.06	0.06	0.07	0.07	0.05	0.05	0.04	0.08	0.11	0.08	0.24	0.27	0.24	0.22	0.27	0.25
Al_2O_3	22.90	25.58	24.46	18.98	17.11	15.48	13.65	8.61	5.56	5.82	29.51	29.75	29.90	29.47	30.07	29.35	30.54	29.28	30.87	28.98	12.15	30.20	4.14	2.19	4.87	4.71	3.60	4.26
Fe_2O_3	4.57	3.49	3.77	6.14	6.95	7.88	8.28	10.37	12.34	12.33	1.44	1.63	1.35	1.79	1.65	1.95	1.43	1.95	1.16	2.01	8.79	1.20	13.45	14.21	12.18	12.58	12.48	11.71
MnO	0.50	0.06	0.07	0.10	0.13	0.14	0.15	0.18	0.21	0.22	0.03	0.02	0.02	0.02	0.03	0.02	0.03	0.04	0.02	0.04	0.15	0.04	0.24	0.26	0.22	0.22	0.23	0.22
MgO	7.66	5.81	6.49	11.16	13.21	14.92	16.85	20.35	23.06	23.19	1.55	2.14	1.79	2.34	2.14	2.25	2.13	2.91	1.53	2.39	17.26	1.31	24.57	25.79	22.53	23.86	24.19	23.83
CaO	12.11	13.61	12.60	10.41	9.48	9.00	7.93	5.80	3.61	4.64	15.06	14.83	14.99	14.84	15.33	14.89	15.48	14.88	15.25	15.31	6.92	15.39	3.47	3.64	4.66	3.35	4.16	4.23
Na_2O	1.89	2.21	1.86	1.73	1.48	1.53	1.33	1.22	0.82	0.71	2.62	2.48	2.40	2.28	2.31	2.05	2.32	2.28	2.35	2.33	2.12	2.54	0.45	0.26	0.86	0.85	0.62	0.70
K_2O	0.09	0.11	0.10	0.08	0.06	0.07	0.07	0.10	0.13	0.06	0.28	0.11	0.11	0.12	0.12	0.20	0.11	0.12	0.13	0.12	0.06	0.33	0.07	0.10	0.16	0.18	0.22	0.25
P_2O_5	0.02	0.08	0.04	0.02	0.07	0.02	0.03	0.07	0.06	0.01	0.08	0.02	0.03	0.08	0.04	0.04	0.09	0.05	0.05	0.11	0.03	0.06	0.11	0.06	0.06	0.11	0.03	0.01
LOI	0.05	0.10	0.13	0.10	-0.08	-0.01	-0.01	0.04	-0.23	-0.09	1.08	0.31	0.21	0.32	0.19	0.75	0.25	0.26	0.42	0.52	0.58	1.25	0.08	0.03	-0.18	-0.13	-0.11	-0.08
H_2O-	0.05	0.08	0.36	0.05	0.03	0.05	0.06	0.17	0.05	0.07	0.11	0.05	0.42	0.05	0.04	0.07	0.05	0.05	0.05	0.07	0.06	0.10	0.09	0.09	0.08	0.08	0.06	0.05
Total	100.05	100.07	99.35	99.37	99.51	100.05	100.06	100.17	100.07	100.08	100.05	100.04	99.93	100.41	100.76	100.10	100.98	100.03	100.04	100.04	99.90	100.06	100.18	100.09	100.09	100.09	99.88	100.07

Sample	UC-57	UC-58	UC-59	UC-60	UC-61	UC-62	UC-63	UC-65	UC-66a	UC-66b	UC-67	UC-68	UC-69	UC-70	UC-71	UC-72	UC-73	UC-74	UC-75a	UC-75b	UC-76	UC-77	UC-78	UC-80	UC-81a	UC-81b	UC-84
Metres	-55.25	-57.25	-59.30	-60.75	-62.25	-62.85	-63.40	-65.80	-67.60	-68.10	-70.15	-73.15	-75.80	-77.95	-81.35	-82.60	-83.65	-85.05	-85.80	-86.00	-88.75	-91.30	-92.75	-96.00	-97.15	-97.35	-101.65
Wt.%																											
SiO_2	54.41	48.62	54.49	53.41	53.44	46.75	52.24	53.93	53.49	51.04	53.21	54.04	53.40	53.60	46.80	44.80	48.29	50.25	49.60	48.41	51.50	49.13	49.10	47.60	47.80	48.07	50.89
TiO_2	0.26	0.04	0.22	0.20	0.18	0.12	0.23	0.23	0.23	0.24	0.20	0.20	0.21	0.18	0.03	0.04	0.04	0.05	0.04	0.02	0.05	0.04	0.04	0.04	0.03	0.05	0.08
Al_2O_3	3.30	31.23	4.71	5.41	5.59	4.98	3.85	2.93	3.87	6.37	5.04	3.86	3.49	5.20	31.10	30.83	27.60	23.38	25.71	30.86	19.90	29.70	31.00	31.60	31.09	28.20	18.89
Fe_2O_3	12.99	1.19	12.40	12.11	11.66	14.03	13.06	13.57	13.72	13.55	13.17	13.02	13.30	13.00	1.32	1.64	2.42	4.20	3.40	1.32	5.74	1.70	0.95	0.89	1.13	2.54	6.31
MnO	0.22	0.03	0.22	0.21	0.21	0.21	0.22	0.25	0.27	0.25	0.23	0.24	0.26	0.24	0.03	0.05	0.05	0.08	0.07	0.02	0.10	0.01	0.00	0.03	0.03	0.05	0.17
MgO	24.78	1.83	23.38	23.42	23.10	26.82	25.18	25.49	24.62	24.11	22.61	23.90	23.60	23.00	1.09	1.31	3.55	8.20	6.18	1.59	10.88	2.00	0.52	1.24	1.41	3.69	11.82
CaO	3.44	15.42	3.75	4.00	4.32	3.91	3.72	2.47	3.30	3.98	3.82	3.70	3.59	4.00	14.30	14.22	12.87	11.70	12.83	15.02	10.42	14.80	15.27	15.72	15.36	13.94	9.88
Na_2O	0.45	0.81	0.88	0.78	0.62	0.44	0.31	0.34	0.58	0.66	1.91	0.47	0.40	0.72	2.14	2.34	2.55	1.70	2.05	2.39	1.61	2.20	2.29	2.40	2.49	2.41	1.97
K_2O	0.23	0.09	0.08	0.06	0.07	0.02	0.11	0.14	0.09	0.03	0.07	0.02	0.02	0.02	1.15	1.37	0.26	0.05	0.06	0.06	0.03	0.07	0.09	0.07	0.11	0.13	0.10
P_2O_5	0.08	0.03	0.00	0.06	0.00	0.00	0.06	0.05	0.04	0.17	0.01	0.01	0.00	0.03	0.06	0.04	0.08	0.03	0.02	0.08	0.03	0.00	0.03	0.05	0.09	0.07	0.06
LOI	-0.16	-0.38	-0.31	-0.40	0.15	2.61	0.97	-0.44	-0.19	-0.37	-0.25	0.40	0.79	-0.45	1.72	3.14	2.36	0.13	0.11	0.19	-0.04	0.14	0.16	0.15	0.48	0.46	-0.03
H_2O-	0.08	0.05	0.06	0.05	0.51	0.05	0.02	0.03	0.01	0.01	0.02	0.01	0.00	0.01	0.00	0.14	0.12	0.00	0.05	0.04	0.04	0.03	0.04	0.03	0.06	0.07	0.10
Total	100.08	98.96	99.87	99.31	99.84	99.94	99.97	98.99	100.02	100.03	100.04	99.87	99.05	99.55	99.74	99.92	100.19	99.77	100.13	100.00	100.27	99.82	99.50	99.82	100.08	99.69	100.23

WHOLE ROCK DATA: TABLE D7: Major element analyses - Bastard Unit profiles **LEF, Y, X, RD** and **AF**.
Including LOI and H_2O-. Total Fe expressed as Fe_2O_3.
* = average of two analyses.
Metres given above base of Unit.

	LEF						Y									X								
Sample	H979.91	H984.48	H992.8	H995.6	H997.26	H998.1	Y722.4	Y740.5	Y746.4	Y755.66	Y760.2	Y764.2	Y765.48	Y770.58	Y775.0	X735.0	X745.44	X763.95	X768.5	X776.5	X779.82	X782.7	X788.41	X791.8
Metres	18.29	13.72	5.40	2.54	0.94	0.10	54.0	35.9	30.0	20.8	16.2	12.2	10.9	5.8	1.4	57.94	47.50	28.99	24.44	16.44	13.12	10.24	4.53	1.14
Wt.%																								
SiO_2	50.65	49.81	49.38	48.17	48.65	51.85	51.41	50.14	50.08	50.22	48.84	50.09	47.79	51.20	52.89	51.56	49.66	49.50	51.01	50.12	52.19	49.92	53.33	53.83
TiO_2	0.15	0.12	0.11	0.06	0.05	0.12	0.21	0.20	0.12	0.09	0.08	0.18	0.07	0.10	0.22	0.19	0.07	0.09	0.07	0.05	0.18	0.07	0.09	0.21
Al_2O_3	18.73	23.02	20.89	30.53	28.72	8.05	24.80	25.12	27.29	27.63	27.63	21.59	30.49	17.42	5.51	23.45	27.01	26.78	26.60	26.32	7.02	22.25	13.66	5.35
Fe_2O_3	6.14	4.18	5.07	1.27	2.39	11.19	4.63	4.49	3.34	2.29	2.54	5.68	1.80	6.61	11.43	4.92	3.11	3.51	3.23	3.09	13.00	4.65	7.54	11.33
MnO	0.07	0.03	0.05	0.00	0.00	0.14	0.07	0.06	0.04	0.03	0.04	0.09	0.04	0.11	0.21	0.08	0.05	0.06	0.03	0.02	0.22	0.06	0.11	0.17
MgO	10.95	7.09	8.77	0.86	2.72	20.28	2.63	3.07	4.03	3.08	2.81	7.31	1.67	13.00	22.94	4.11	2.84	3.32	2.92	2.90	20.20	8.82	17.07	23.66
CaO	9.96	12.14	10.92	15.35	14.44	4.95	12.06	12.39	13.68	13.62	14.05	11.72	14.91	9.34	4.12	12.23	12.95	12.95	13.32	13.56	5.09	11.59	7.41	3.57
Na_2O	1.56	1.86	1.78	2.13	2.07	0.55	2.79	2.54	2.40	2.52	2.14	1.80	2.16	1.43	0.62	2.52	2.53	2.29	2.29	2.38	0.77	1.67	1.17	0.65
K_2O	0.18	0.19	0.19	0.22	0.15	0.08	0.51	0.37	0.22	0.11	0.12	0.01	0.05	0.00	0.06	0.29	0.07	0.15	0.08	0.04	0.00	0.02	0.00	0.05
P_2O_5	0.01	0.01	0.01	0.01	0.00	0.00	0.08	0.09	0.03	0.03	0.04	0.03	0.03	0.01	0.01	0.03	0.01	0.03	0.04	0.03	0.00	0.02	0.01	0.01
LOI	0.50	0.35	0.22	0.86	0.34	-0.09	0.30	0.38	0.28	0.47	0.90	0.00	0.12	0.28	0.09	0.21	0.30	0.14	0.01	0.10	-0.51	-0.03	-0.16	0.19
H_2O-	0.16	0.16	0.13	0.21	0.17	0.17	0.21	0.19	0.15	0.16	0.19	0.11	0.10	0.16	0.12	0.13	0.11	0.11	0.08	0.10	0.10	0.12	0.15	0.13
Total	99.04	98.95	97.51	99.66	99.68	97.30	99.68	99.05	101.66	100.24	99.37	98.62	99.23	99.67	98.21	99.71	98.71	98.92	99.68	98.70	98.25	99.16	100.38	99.15

	RD								AF															
Sample	RD-1	RD-3	RD-4	RD-6	RD-15	RD-16	RD-17	RD-18	AF-1	AF-2	AF-3	AF-4	AF-5	AF-6	AF-7	AF-8a	AF-8b	AF-9	AF-10	AF-11	AF-12	AF-13	AF-14	AF-15	AF-16
Metres	35.00	31.00	29.40	22.50	8.30	5.90	3.62	0.50	34.20	32.30	30.60	27.90	24.90	21.70	18.90	18.05	17.85	17.05	13.60	10.50	6.65	4.40	2.45	1.25	0.05
Wt.%																									
SiO_2	49.85	50.68	49.13	49.12	49.93	51.11	54.03	53.24	50.82	48.90	49.56	49.94	50.52	52.27	49.32	51.42	52.59	50.08	50.20	51.00	52.50	52.20	53.95	54.50	53.50
TiO_2	0.12	0.08	0.08	0.07	0.09	0.10	0.20	0.20	0.11	0.09	0.06	0.06	0.09	0.11	0.13	0.10	0.12	0.12	0.10	0.10	0.14	0.17	0.22	0.21	0.20
Al_2O_3	26.94	28.74	27.00	28.12	19.87	14.23	5.85	5.55	25.95	28.20	30.80	29.35	29.23	29.00	25.62	28.90	26.09	19.86	19.30	16.90	12.60	7.70	5.90	5.43	6.75
Fe_2O_3	2.63	2.27	3.50	2.43	5.66	7.33	12.91	12.76	3.94	2.56	1.25	1.91	1.92	2.93	4.14	3.23	4.68	6.66	5.94	6.90	8.10	11.00	11.00	11.14	11.30
MnO	0.04	0.05	0.03	0.04	0.10	0.15	0.21	0.20	0.05	0.03	0.02	0.03	0.03	0.04	0.06	0.06	0.07	0.12	0.11	0.12	0.15	0.21	0.20	0.22	0.20
MgO	2.25	1.91	3.51	2.28	10.74	16.72	21.39	21.86	4.09	2.44	1.14	2.07	1.80	2.60	4.84	3.70	5.85	10.92	12.20	14.65	18.50	22.60	23.10	23.40	22.60
CaO	13.02	13.56	12.99	13.94	9.81	7.54	4.52	4.47	12.99	13.75	14.30	14.03	13.81	14.14	14.07	14.25	12.96	10.60	9.60	8.85	6.90	5.40	4.30	4.01	4.05
Na_2O	2.81	2.72	2.52	2.59	1.60	1.23	0.79	0.84	2.01	2.50	2.46	2.37	2.42	2.45	1.78	2.04	1.95	1.25	1.50	1.05	0.85	0.73	0.59	0.78	0.61
K_2O	0.20	0.20	0.22	0.20	0.02	0.01	0.00	0.00	0.17	0.21	0.22	0.18	0.22	0.25	0.20	0.22	0.23	0.15	0.12	0.11	0.08	0.06	0.24	0.23	0.20
P_2O_5	0.04	0.04	0.03	0.04	0.02	0.02	0.00	0.00	0.01	0.01	0.02	0.00	0.02	0.02	0.01	0.04	0.03	0.01	0.01	0.01	0.00	0.00	0.01	0.01	0.02
LOI	1.34	0.92	0.92	1.38	1.86	1.06	-0.19	0.06	0.56	0.35	0.51	0.64	0.31	-4.66	0.71	-4.76	-4.71	0.11	0.05	0.15	-0.07	-0.24	0.25	-0.10	0.39
H_2O-	0.19	0.16	0.17	0.22	0.21	0.20	0.14	0.17	0.03	0.02	0.00	0.03	0.02	0.02	0.04	0.02	0.04	0.02	0.02	0.02	0.10	0.08	0.13	0.10	0.13
Total	99.42	101.31	100.08	100.41	99.89	99.69	99.84	99.34	100.72	99.05	100.33	100.60	100.38	99.16	100.92	99.21	99.88	99.90	99.13	99.85	99.85	99.91	99.88	99.92	99.95

WHOLE ROCK DATA TABLE D8: Major element analyses, trace element analyses & CIPW weight % norms - UG1 Footwall Unit - S samples.
Major element analyses are normalised to 100% and are LOI and H2O- free.
They are the average of either 2 or 3 determinations on separate discs.
An assumed oxidation ratio of Fe_2O_3/FeO = 0.1 is used.
Metres given below base of UG1 chromitite.

Sample	S-0	S-1	S-2	S-3	S-4	S-5	S-6	S-7	S-8	S-9	S-10	S-11	S-12	S-13	S-14	S-15	S-16	S-17	S-18	S-19	S-20	S-21	S-22	S-23	S-24	S-25	S-26
Metres	1.0	2.6	5.3	8.4	11.3	18.2	22.1	26.5	32.3	37.8	42.5	49.8	57.1	67.9	75.2	80.9	85.3	89.7	94.1	98.8	106.0	110.7	115.1	120.4	124.8	129.1	133.5
Wt.%																											
SiO_2	48.30	49.30	49.74	49.08	49.48	50.67	52.46	53.22	52.87	52.89	50.83	53.02	53.24	52.35	50.86	52.12	51.59	52.27	50.51	50.43	51.54	52.19	52.72	52.81	54.83	52.28	51.75
TiO_2	0.00	0.06	0.04	0.04	0.03	0.05	0.10	0.11	0.11	0.11	0.09	0.11	0.12	0.10	0.06	0.11	0.08	0.11	0.06	0.07	0.06	0.07	0.08	0.10	0.18	0.08	0.09
Al_2O_3	32.60	25.20	25.96	31.60	32.03	23.09	14.39	11.86	12.67	11.41	13.12	11.49	9.97	14.96	21.45	17.57	20.78	15.36	24.06	21.84	19.96	15.38	15.16	13.32	3.95	15.42	15.53
Fe_2O_3	0.08	0.32	0.28	0.09	0.08	0.37	0.69	0.77	0.76	0.78	0.68	0.80	0.87	0.69	0.45	0.58	0.47	0.68	0.37	0.45	0.50	0.68	0.67	0.74	1.15	0.69	0.70
FeO	0.88	3.20	2.77	0.88	0.75	3.67	6.85	7.72	7.56	7.76	6.82	8.03	8.72	6.89	4.51	5.78	4.71	6.80	3.66	4.52	4.97	6.78	6.69	7.44	11.52	6.88	7.03
MnO	0.02	0.05	0.07	0.02	0.02	0.07	0.15	0.16	0.18	0.18	0.16	0.18	0.19	0.15	0.09	0.13	0.12	0.15	0.08	0.11	0.11	0.14	0.14	0.15	0.24	0.14	0.14
MgO	0.50	6.40	6.20	0.91	0.75	8.64	16.57	18.43	18.03	19.38	20.22	18.83	19.98	15.61	10.04	13.21	10.40	15.44	7.73	9.58	11.88	15.07	14.84	16.61	23.95	14.59	14.53
CaO	15.40	12.20	12.81	15.09	14.56	11.57	7.59	6.37	6.60	6.18	6.73	6.19	5.80	7.78	10.87	8.77	10.00	7.78	11.43	10.94	9.57	8.31	8.14	7.34	3.68	8.36	8.66
Na_2O	2.20	1.80	2.05	2.20	2.17	1.79	1.14	0.97	1.11	1.25	1.25	1.23	1.03	1.40	1.52	1.63	1.73	1.30	1.96	1.96	1.31	1.33	1.48	1.41	0.46	1.49	1.49
K_2O	0.09	0.11	0.06	0.11	0.12	0.08	0.07	0.34	0.11	0.07	0.09	0.08	0.07	0.07	0.10	0.10	0.11	0.10	0.13	0.11	0.09	0.05	0.07	0.05	0.03	0.06	0.06
P_2O_5	0.05	0.06	0.03	0.00	0.01	0.00	0.00	0.06	0.01	0.00	0.00	0.03	0.01	0.00	0.05	0.00	0.01	0.02	0.01	0.00	0.02	0.01	0.00	0.03	0.00	0.00	0.03
Total	100.1	98.7	100.0	100.0	100.0	100.0	100.0	100.0	100.0	100.0	100.0	100.0	100.0	100.0	100.0	100.0	100.0	100.0	100.0	100.0	100.0	100.0	100.0	100.0	100.0	100.0	100.0
MMF	0.4835	0.7658	0.7856	0.6283	0.6210	0.7938	0.7981	0.7961	0.7959	0.8033	0.8290	0.7930	0.7893	0.7873	0.7846	0.7888	0.7831	0.7878	0.7754	0.7760	0.7962	0.7841	0.7839	0.7849	0.7726	0.7760	0.7718
Trace element values (ppm).																											
Sr	463.0	364.0	379.0	464.9	471.9	336.1	195.9	210.6	183.7	163.4	203.0	164.4	142.7	215.0	320.8	252.9	304.5	223.5	359.6	325.1	293.9	231.3	232.0	206.3	46.3	230.6	234.6
Rb	0.0	0.8	2.2	2.2	1.2	0.5	1.0	10.6	2.7	0.1	0.9	0.5	2.0	0.9	1.6	1.2	0.4	2.3	2.4	2.0	0.5	0.3	0.6	2.1	4.7	3.5	1.8
Y	2.8	2.7	2.3	0.0	1.2	0.0	2.6	2.4	2.7	4.0	2.0	3.2	3.6	3.1	1.8	3.2	6.1	2.8	1.4	2.7	2.0	2.6	3.4	1.8	2.1	3.0	3.2
Zr	0.0	2.0	3.8	0.0	1.5	0.8	5.1	5.8	5.3	4.9	3.9	6.7	6.7	2.7	2.1	5.8	2.1	5.3	1.5	3.3	3.4	1.2	3.2	3.4	13.8	3.9	3.1
Co	5.0	29.0	25.9	7.6	5.7	35.9	69.8	76.6	74.0	76.9	70.1	77.5	82.6	66.5	44.3	57.9	45.7	64.4	33.8	41.5	48.7	63.5	65.6	71.6	105.7	62.8	62.7
Cr	455	975	937	61	34	957	1982	2150	2040	2060	1783	1990	2267	1689	1090	1411	1086	1584	738	879	1075	1443	1548	1707	2725	1556	1593
V	111.0	40.0	40.3	11.9	9.0	54.0	110.4	125.8	118.5	121.6	105.1	119.4	137.4	104.5	64.2	92.1	71.0	101.6	50.7	62.1	72.5	88.9	94.4	104.3	181.0	95.8	97.2
Zn	5.0	21.0	21.7	9.9	12.1	27.8	50.7	68.9	56.9	59.9	62.8	58.9	64.0	58.2	32.6	46.3	41.3	50.9	25.6	39.4	32.3	49.2	59.3	57.8	94.9	58.2	50.2
Cu	8.0	14.0	8.7	7.6	8.6	10.5	9.5	17.6	10.4	9.9	11.7	11.9	12.7	12.5	10.5	11.1	32.0	13.3	8.3	12.1	10.1	5.2	11.6	11.3	11.4	11.3	15.7
Ni	8.5	141.0	124.4	13.8	14.4	174.7	335.0	436.5	386.7	392.7	388.0	390.1	428.0	347.8	204.2	281.1	222.3	310.7	149.4	200.0	231.8	308.4	340.5	354.1	549.3	332.5	313.9
Sc	5.7	12.4	9.1	3.4	3.8	11.8	21.7	24.4	23.6	24.4	21.5	24.3	25.7	13.1	13.7	18.2	14.2	20.3	9.5	11.4	13.8	17.6	22.1	21.0	34.8	18.8	19.8
CIPW weight percent norms.																											
ap	0.12	0.14	0.07	0.00	0.02	0.00	0.00	0.14	0.02	0.00	0.00	0.07	0.02	0.00	0.12	0.00	0.02	0.05	0.02	0.00	0.05	0.02	0.00	0.07	0.00	0.00	0.07
il	0.00	0.11	0.08	0.08	0.06	0.09	0.19	0.21	0.21	0.21	0.17	0.21	0.23	0.19	0.11	0.21	0.15	0.21	0.11	0.13	0.11	0.13	0.15	0.19	0.34	0.15	0.17
or	0.53	0.65	0.35	0.65	0.71	0.47	0.41	2.01	0.65	0.41	0.53	0.47	0.41	0.41	0.59	0.59	0.65	0.59	0.77	0.65	0.53	0.30	0.41	0.30	0.18	0.35	0.35
ab	18.61	15.23	17.34	18.61	18.36	15.14	9.65	8.21	9.39	10.58	10.58	10.41	8.71	11.85	12.86	13.79	14.64	11.00	16.58	16.58	11.08	11.25	12.52	11.93	3.89	12.61	12.61
an	76.07	60.13	61.46	74.86	72.17	54.74	33.94	27.01	29.27	25.32	29.92	25.60	22.38	34.33	51.41	40.33	48.61	35.78	56.47	50.47	47.35	35.85	34.52	29.87	8.63	35.21	35.51
c	1.00	0.08	0.00	0.43	1.88	0.00	0.00	0.00	0.00	0.00	0.00	0.00	0.00	0.00	0.00	0.00	0.00	0.00	0.00	0.00	0.36	0.00	0.00	0.00	0.00	0.00	0.00
mt	0.12	0.46	0.41	0.13	0.12	0.54	1.00	1.12	1.10	1.13	0.99	1.16	1.26	1.00	0.65	0.84	0.68	0.99	0.54	0.65	0.72	0.99	0.97	1.07	1.67	1.00	1.01
dien	0.00	0.00	0.55	0.00	0.00	0.78	1.09	1.24	1.00	1.58	1.06	1.44	1.85	1.24	0.64	0.93	0.27	0.78	0.05	1.09	0.00	1.54	1.70	1.84	2.76	1.80	2.08
difs	0.00	0.00	0.18	0.00	0.00	0.24	0.32	0.37	0.30	0.45	0.25	0.44	0.57	0.39	0.20	0.29	0.09	0.24	0.02	0.37	0.00	0.49	0.55	0.59	0.94	0.60	0.71
diwo	0.00	0.00	0.79	0.00	0.00	1.11	1.55	1.76	1.42	2.23	1.45	2.05	2.64	1.78	0.91	1.33	0.39	1.12	0.07	1.59	0.00	2.22	2.45	2.65	4.02	2.61	3.03
hy	1.25	15.94	12.60	2.27	1.87	20.48	39.84	44.66	42.90	41.49	32.04	42.44	45.56	35.93	24.37	31.47	25.63	37.13	18.45	17.59	29.59	35.15	35.26	37.88	56.88	33.26	30.47
hyfs	1.59	5.61	4.02	1.51	1.30	6.17	11.71	13.29	12.82	11.83	7.71	12.89	14.15	11.27	7.78	9.76	8.27	11.61	6.20	5.91	8.82	11.27	11.32	12.06	19.42	11.17	10.48
q	0.83	0.34	0.00	1.48	3.52	0.00	0.00	0.02	0.00	0.00	0.00	0.00	0.00	0.00	0.36	0.00	0.60	0.00	0.00	0.00	1.40	0.00	0.15	0.00	1.27	0.00	0.00
fo	0.00	0.00	1.61	0.00	0.00	0.18	0.23	0.00	0.70	3.63	12.10	2.11	1.64	1.19	0.00	0.35	0.00	0.38	0.53	3.63	0.00	0.59	0.00	1.15	0.00	0.89	2.55
fa	0.00	0.00	0.56	0.00	0.00	0.06	0.07	0.00	0.23	1.14	3.21	0.71	0.56	0.41	0.00	0.12	0.00	0.13	0.20	1.34	0.00	0.21	0.00	0.40	0.00	0.33	0.97

ap = apatite
ab = albite
mt = magnetite
diwo = diopside/wollastonite
q = quartz
il = ilmenite
an = anorthite
dien = diopside/enstatite
hyen = hypersthene/enstatite
fo = forsterite
or = orthoclase
c = corundum
difs = diopside/ferrosilite
hyfs = hypersthene//ferrosilite
fa = fayalite

WHOLE ROCK DATA TABLE D8: Major element analyses, trace element analyses & CIPW weight % norms - UG1 Footwall Unit - S samples.
Major element analyses are normalised to 100% and are LOI and H2O- free.
They are the average of either 2 or 3 determinations on separate discs.
An assumed oxidation ratio of $Fe_2O_3/FeO = 0.1$ is used.
Metres given below base of UG1 chromitite.

Sample	S-27	S-28	S-29	S-30	S-31	S-32	S-33	S-34	S-35	S-36	S-37	S-38	S-39	S-40	S-41	S-42	S-43	S-44	S-45	S-46	S-47	S-48	S-49	S-50	S-51	S-52	S-53
Metres	137.9	142.5	146.9	151.6	156.3	161.3	166.0	170.6	175.6	181.5	185.9	190.3	194.9	199.3	203.7	208.1	213.2	217.2	221.9	226.8	230.4	234.8	238.9	243.6	247.8	252.2	256.7
Wt.%																											
SiO_2	52.17	52.06	52.84	52.96	54.28	53.79	53.93	53.61	53.33	53.97	54.20	53.75	54.88	54.45	54.53	54.85	54.54	54.65	54.25	54.21	53.85	54.54	53.89	54.64	55.15	54.60	53.35
TiO_2	0.07	0.09	0.10	0.08	0.13	0.14	0.12	0.18	0.11	0.19	0.18	0.17	0.15	0.16	0.14	0.12	0.15	0.15	0.16	0.16	0.13	0.14	0.19	0.18	0.17	0.16	0.14
Al_2O_3	14.85	13.44	11.67	11.75	5.18	4.71	7.53	4.24	8.68	5.31	4.47	3.82	3.94	4.38	4.28	3.63	3.33	3.28	3.09	4.24	4.90	2.83	4.31	3.97	3.74	2.61	3.97
Fe_2O_3	0.71	0.78	0.84	0.80	1.08	1.13	1.03	1.21	0.95	1.17	1.13	1.18	1.10	1.11	1.10	1.13	1.15	1.15	1.16	1.14	1.11	1.25	1.22	1.15	1.15	1.23	1.21
FeO	7.13	7.81	8.41	8.03	10.78	11.28	10.27	12.14	9.46	11.67	11.30	11.78	11.03	11.14	10.99	11.26	11.52	11.53	11.63	11.38	11.11	12.46	12.15	11.51	11.47	12.28	12.12
MnO	0.16	0.18	0.18	0.19	0.27	0.25	0.29	0.36	0.30	0.26	0.24	0.30	0.24	0.24	0.24	0.25	0.24	0.25	0.27	0.25	0.24	0.35	0.34	0.25	0.25	0.26	0.26
MgO	15.34	16.60	17.96	17.94	23.65	24.39	21.15	24.06	20.90	22.72	24.20	24.86	24.64	24.29	24.85	25.28	25.51	25.52	25.84	24.65	24.17	25.81	23.91	24.28	24.16	25.90	24.85
CaO	8.02	7.63	6.69	6.99	4.00	3.71	4.83	3.83	5.35	4.14	3.63	3.49	3.45	3.64	3.43	3.07	3.21	3.18	3.26	3.64	3.85	2.36	3.63	3.48	3.39	2.65	3.58
Na_2O	1.50	1.35	1.23	1.20	0.60	0.52	0.83	0.38	0.88	0.54	0.62	0.59	0.55	0.57	0.40	0.40	0.35	0.25	0.33	0.33	0.60	0.25	0.36	0.46	0.46	0.26	0.48
K_2O	0.04	0.04	0.05	0.04	0.01	0.02	0.01	0.00	0.06	0.03	0.03	0.00	0.01	0.00	0.00	0.00	0.00	0.00	0.00	0.00	0.00	0.00	0.00	0.07	0.07	0.01	0.03
P_2O_5	0.01	0.01	0.04	0.01	0.02	0.08	0.00	0.00	0.00	0.02	0.00	0.06	0.01	0.01	0.04	0.02	0.00	0.04	0.01	0.00	0.03	0.00	0.00	0.02	0.00	0.04	0.01
Total	100.0	100.0	100.0	100.0	100.0	100.0	100.0	100.0	100.0	100.0	100.0	100.0	100.0	100.0	100.0	100.0	100.0	100.0	100.0	100.0	100.0	100.0	100.0	100.0	100.0	100.0	100.0
MMF	0.7785	0.7764	0.7773	0.7851	0.7819	0.7795	0.7711	0.7642	0.7832	0.7609	0.7778	0.7752	0.7851	0.7809	0.7870	0.7859	0.7836	0.7835	0.7841	0.7797	0.7806	0.7720	0.7628	0.7752	0.7749	0.7753	0.7702
Trace element values (ppm).																											
Sr	232.6	195.8	168.9	178.4	69.3	59.0	97.2	55.4	124.8	73.7	62.6	48.9	52.7	72.8	48.1	50.9	38.1	33.1	35.8	37.7	61.3	27.1	45.7	48.8	46.0	24.8	48.2
Rb	0.2	2.2	0.2	0.4	0.6	0.6	0.3	0.8	1.6	2.3	0.6	0.2	1.7	0.0	2.1	0.2	0.0	0.5	0.5	1.2	0.4	1.6	2.6	1.9	2.2	2.3	0.6
Y	3.2	2.3	3.6	2.6	3.4	4.6	3.9	6.3	2.2	3.6	6.0	4.7	3.6	1.9	1.3	3.1	4.1	3.7	4.9	4.2	2.2	2.6	5.6	6.6	5.6	2.5	5.4
Zr	0.0	2.6	3.9	2.2	4.6	5.1	5.0	7.0	3.2	6.2	5.4	5.4	6.0	2.0	1.7	1.8	5.5	3.1	4.0	4.4	4.7	4.1	6.6	10.2	10.9	7.0	6.2
Co	65.8	112.3	79.3	79.5	102.2	105.0	95.3	140.6	87.7	101.0	101.6	102.4	103.0	101.0	101.2	103.9	105.8	108.8	106.5	101.9	97.9	110.1	107.3	105.1	104.3	118.9	103.1
Cr	1668	1833	2074	1814	2288	2417	2090	3009	1900	1964	2053	2415	2611	2790	2924	3200	3120	3168	2985	2782	2952	3396	2803	2579	2690	2821	2634
V	99.8	111.0	120.1	116.5	154.6	170.3	158.6	192.5	139.9	158.0	165.3	163.6	160.5	152.7	156.8	169.1	191.1	185.1	173.3	163.4	156.7	177.5	170.9	173.2	172.6	175.1	166.5
Zn	52.7	63.3	63.5	62.0	92.2	88.5	76.1	102.7	77.2	93.0	96.6	87.4	87.8	92.0	83.9	89.1	98.5	87.7	91.1	107.7	83.0	94.1	116.2	95.1	96.5	111.4	86.3
Cu	8.0	13.0	10.6	7.6	12.8	12.6	11.2	15.7	13.6	15.5	20.0	12.0	11.0	12.9	9.5	9.0	15.2	11.3	12.2	13.2	13.6	8.4	19.0	17.3	15.0	14.4	16.5
Ni	333.5	374.3	393.5	375.3	525.3	517.4	452.6	541.0	421.4	464.7	531.0	529.1	550.6	555.0	553.8	567.7	602.9	567.2	569.3	581.8	517.8	574.5	605.9	552.5	552.8	608.0	521.3
Sc	20.1	21.7	22.8	22.7	30.0	31.1	27.9	30.4	25.4	30.8	30.0	30.7	30.9	29.2	31.1	31.1	32.1	32.3	33.1	33.2	31.5	32.2	33.2	31.2	33.0	32.7	31.8
CIPW weight percent norms.																											
ap	0.02	0.02	0.09	0.02	0.05	0.19	0.00	0.00	0.00	0.05	0.00	0.14	0.02	0.02	0.09	0.05	0.00	0.09	0.02	0.00	0.07	0.00	0.00	0.05	0.00	0.09	0.02
il	0.13	0.17	0.19	0.15	0.24	0.26	0.23	0.34	0.21	0.36	0.34	0.32	0.28	0.30	0.26	0.23	0.28	0.28	0.30	0.30	0.24	0.26	0.36	0.34	0.32	0.30	0.26
or	0.24	0.24	0.30	0.24	0.06	0.12	0.06	0.00	0.35	0.18	0.18	0.00	0.06	0.00	0.00	0.00	0.00	0.00	0.00	0.00	0.00	0.00	0.00	0.41	0.41	0.06	0.18
ab	12.69	11.42	10.41	10.15	5.08	4.40	7.02	3.22	7.45	4.57	5.25	4.99	4.65	4.82	3.38	3.38	2.96	2.12	2.79	2.79	5.08	2.12	3.05	3.89	3.89	2.20	4.06
an	33.67	30.50	26.18	26.56	11.41	10.46	16.79	9.86	19.56	11.98	9.33	7.78	8.25	9.39	9.88	8.11	7.52	7.83	6.95	10.09	10.68	6.60	10.15	8.56	7.93	5.93	8.59
c	0.00	0.00	0.00	0.00	0.00	0.00	0.00	0.00	0.00	0.00	0.00	0.00	0.00	0.00	0.00	0.00	0.00	0.00	0.00	0.00	0.00	0.00	0.00	0.00	0.00	0.00	0.00
mt	1.03	1.13	1.22	1.16	1.57	1.64	1.49	1.75	1.38	1.70	1.64	1.71	1.59	1.61	1.59	1.64	1.67	1.67	1.68	1.65	1.61	1.81	1.77	1.67	1.67	1.78	1.75
dien	1.74	2.10	1.94	2.34	2.40	2.14	2.05	2.59	2.02	2.38	2.50	2.63	2.56	2.49	2.00	2.03	2.44	2.23	2.66	2.30	2.38	1.46	2.22	2.46	2.55	2.00	2.60
difs	0.58	0.70	0.65	0.75	0.78	0.71	0.71	0.94	0.66	0.87	0.83	0.89	0.81	0.81	0.63	0.65	0.78	0.72	0.85	0.76	0.78	0.51	0.81	0.83	0.86	0.67	0.90
diwo	2.53	3.04	2.82	3.36	3.47	3.10	2.99	3.82	2.92	3.52	3.63	3.82	3.67	3.59	2.87	2.92	3.51	3.21	3.82	3.33	3.43	2.13	3.28	3.58	3.71	2.91	3.80
hy	33.26	34.57	40.56	40.63	56.50	56.20	50.63	55.86	47.75	54.20	56.20	55.02	58.81	58.00	59.88	60.92	61.09	61.32	60.19	59.09	55.05	62.82	57.32	58.00	57.62	62.50	53.82
hyfs	11.05	11.61	13.53	13.01	18.41	18.52	17.64	20.20	15.57	19.77	18.62	18.61	18.74	18.92	18.86	19.37	19.63	19.73	19.31	19.41	18.04	21.77	20.82	19.53	19.44	21.09	18.71
q	0.00	0.00	0.00	0.00	0.04	0.00	0.38	0.00	0.00	0.46	0.00	0.00	0.55	0.03	0.54	0.72	0.13	0.81	0.00	0.29	0.00	0.52	0.23	0.69	1.61	0.48	0.00
fo	2.24	3.28	1.56	1.20	0.00	1.68	0.00	1.03	1.60	0.00	1.10	2.98	0.00	0.00	0.00	0.00	0.00	0.00	1.06	0.00	1.93	0.00	0.00	0.00	0.00	0.00	3.83
fa	0.82	1.21	0.57	0.42	0.00	0.61	0.00	0.41	0.57	0.00	0.40	1.11	0.00	0.00	0.00	0.00	0.00	0.00	0.37	0.00	0.70	0.00	0.00	0.00	0.00	0.00	1.47

WHOLE ROCK DATA TABLE D8: Major element analyses, trace element analyses & CIPW weight % norms - UG1 Footwall Unit - S samples.
Major element analyses are normalised to 100% and are LOI and H2O- free.
They are the average of either 2 or 3 determinations on separate discs.
An assumed oxidation ratio of $Fe_2O_3/FeO = 0.1$ is used.
Metres given below base of UG1 chromitite.

Sample	S-54	S-55	S-56	S-57	S-58	S-59	S-64	S-65	S-66	S-69	S-70	S-71	S-72	S-73	S-74	S-75	S-76	S-77	S-79	S-81
Metres	261.4	265.7	270.2	274.4	279.7	286.4	299.1	302.9	307.9	314.6	320.2	325.0	328.1	329.9	332.1	334.1	335.1	337.8	341.8	344.9
Wt.%																				
SiO_2	54.93	53.81	53.64	54.63	54.49	55.00	54.78	54.46	54.05	52.95	51.49	51.31	52.06	50.81	51.27	50.02	49.01	52.03	52.76	52.61
TiO_2	0.13	0.14	0.13	0.17	0.15	0.15	0.17	0.17	0.13	0.10	0.11	0.09	0.09	0.10	0.10	0.12	0.10	0.13	0.22	0.18
Al_2O_3	3.69	3.68	3.92	3.68	3.44	2.46	4.17	4.18	5.07	12.05	13.20	17.40	18.07	16.03	17.26	15.27	16.67	12.25	7.92	4.12
Fe_2O_3	1.15	1.16	1.18	1.19	1.13	1.18	1.05	1.07	1.08	0.76	0.76	0.63	0.54	0.67	0.61	0.71	0.67	0.80	1.05	1.19
FeO	11.51	11.64	11.80	11.93	11.29	11.78	10.54	10.70	10.84	7.56	7.61	6.29	5.39	6.69	6.13	7.08	6.74	7.99	10.54	11.94
MnO	0.34	0.26	0.36	0.25	0.26	0.26	0.24	0.24	0.23	0.16	0.16	0.11	0.11	0.14	0.13	0.15	0.14	0.17	0.22	0.26
MgO	24.62	25.45	25.20	24.18	25.68	26.26	25.18	25.36	24.18	18.59	17.67	13.62	12.88	15.08	13.55	15.79	15.01	18.41	21.97	25.50
CaO	3.21	3.36	3.38	3.46	3.11	2.68	3.21	3.28	3.70	6.60	7.66	9.25	9.45	8.89	9.33	9.11	9.69	7.02	4.46	3.75
Na_2O	0.42	0.46	0.39	0.46	0.44	0.19	0.61	0.49	0.67	1.20	1.27	1.21	1.32	1.54	1.50	1.66	1.84	1.10	0.79	0.43
K_2O	0.01	0.03	0.02	0.05	0.01	0.00	0.05	0.05	0.00	0.02	0.06	0.05	0.08	0.04	0.07	0.08	0.11	0.04	0.06	0.01
P_2O_5	0.00	0.00	0.00	0.01	0.00	0.04	0.01	0.01	0.04	0.01	0.01	0.05	0.01	0.01	0.06	0.01	0.01	0.06	0.03	0.00
Total	100.0	100.0	100.0	100.0	100.0	100.0	100.0	100.0	100.0	100.0	100.0	100.0	100.0	100.0	100.0	100.0	100.0	100.0	100.0	100.0
MMF	0.7777	0.7813	0.7774	0.7681	0.7881	0.7846	0.7962	0.7948	0.7848	0.8007	0.7914	0.7796	0.7962	0.7865	0.7833	0.7848	0.7846	0.7903	0.7731	0.7773
Trace element values (ppm).																				
Sr	41.7	42.8	40.5	47.9	37.8	15.8	51.0	50.6	82.6	168.1	185.6	262.4	242.6	266.2	254.3	225.0	242.9	158.6	83.3	47.5
Rb	2.5	1.7	1.8	2.8	0.8	2.8	3.2	2.0	2.0	1.5	0.9	0.6	0.6	1.9	0.8	1.3	1.9	0.3	2.9	0.9
Y	3.2	3.7	3.2	4.9	4.6	3.8	5.4	4.0	4.4	2.2	3.6	3.3	4.1	2.7	3.7	2.4	3.1	3.7	6.8	4.0
Zr	5.4	6.8	5.2	13.1	8.3	6.3	13.0	11.2	3.5	1.8	3.3	2.9	4.4	6.2	4.2	5.0	6.1	4.9	11.2	6.8
Co	104.4	106.1	104.6	103.1	107.6	108.7	101.1	99.8	95.1	73.8	70.9	54.9	61.7	52.3	56.8	62.7	58.0	74.4	95.5	101.1
Cr	2766	2795	2837	2309	2583	2682	2941	4284	5444	2556	2344	2032	2434	11617	2183	2606	2313	4048	18126	3804
V	165.9	175.2	170.0	178.6	174.6	172.7	146.2	146.1	132.8	87.7	85.2	69.0	82.9	65.1	72.1	82.3	77.8	102.2	248.1	164.0
Zn	89.5	103.5	84.5	81.3	95.2	80.9	87.8	84.6	73.7	55.4	60.1	42.8	44.8	48.9	43.5	47.9	56.4	54.3	87.3	90.9
Cu	10.1	20.8	14.7	8.7	15.5	11.2	5.9	13.0	15.6	4.7	15.7	14.3	13.2	16.2	12.5	12.8	18.1	12.8	21.2	17.9
Ni	537.0	569.4	521.4	557.4	563.7	548.2	549.9	567.8	488.8	343.4	378.5	261.5	296.5	269.8	277.6	305.4	300.9	371.9	481.9	530.0
Sc	32.3	31.5	32.3	32.2	31.9	33.5	30.2	31.3	28.8	22.3	20.0	16.4	17.5	15.6	16.3	18.7	18.0	25.2	30.8	33.0
CIPW weight percent norms.																				
ap	0.00	0.00	0.00	0.02	0.00	0.09	0.02	0.02	0.09	0.02	0.02	0.12	0.02	0.02	0.14	0.02	0.02	0.14	0.07	0.00
il	0.24	0.26	0.24	0.32	0.28	0.28	0.32	0.32	0.24	0.19	0.21	0.17	0.17	0.19	0.19	0.23	0.19	0.24	0.41	0.34
or	0.06	0.18	0.12	0.30	0.06	0.00	0.30	0.30	0.00	0.12	0.35	0.30	0.47	0.24	0.41	0.47	0.65	0.24	0.35	0.06
ab	3.55	3.89	3.30	3.89	3.72	1.61	5.16	4.15	5.67	10.15	10.75	10.24	11.17	13.03	12.69	14.05	15.57	9.31	6.68	3.64
an	8.15	7.89	8.89	7.83	7.38	5.86	8.49	9.06	10.83	27.44	30.14	41.90	43.15	36.71	40.16	33.98	36.90	28.37	17.89	9.28
c	0.00	0.00	0.00	0.00	0.00	0.00	0.00	0.00	0.00	0.00	0.00	0.00	0.00	0.00	0.00	0.00	0.00	0.00	0.00	0.00
mt	1.67	1.68	1.71	1.73	1.64	1.71	1.52	1.55	1.57	1.10	1.10	0.91	0.78	0.97	0.88	1.03	0.97	1.16	1.52	1.73
dien	2.23	2.54	2.26	2.64	2.34	2.08	2.17	2.10	2.11	1.55	2.28	1.06	1.08	2.13	1.66	3.24	3.22	1.77	1.16	2.68
difs	0.75	0.83	0.76	0.93	0.73	0.67	0.65	0.63	0.67	0.45	0.70	0.35	0.32	0.67	0.53	1.03	1.03	0.55	0.39	0.89
diwo	3.24	3.67	3.29	3.87	3.36	3.00	3.08	2.98	3.03	2.19	3.25	1.53	1.53	3.06	2.40	4.66	4.64	2.53	1.69	3.89
hy	59.08	56.48	56.67	57.58	60.44	63.31	59.87	59.81	55.72	42.30	32.78	32.44	30.99	25.71	28.22	19.26	11.96	38.79	48.63	51.27
hyfs	19.86	18.42	19.10	20.19	18.94	20.23	17.82	17.93	17.80	12.23	10.03	10.60	9.19	8.10	9.06	6.12	3.82	11.94	16.48	17.06
q	1.17	0.00	0.00	0.73	0.00	1.16	0.00	0.00	0.00	0.00	0.00	0.00	1.12	0.00	0.00	0.00	0.00	0.00	0.00	0.00
fo	0.00	3.06	2.68	0.00	0.82	0.00	0.47	0.87	1.67	1.71	6.26	0.30	0.00	6.81	2.70	11.79	15.55	3.70	3.45	6.69
fa	0.00	1.10	0.99	0.00	0.28	0.00	0.15	0.29	0.59	0.55	2.11	0.11	0.00	2.36	0.96	4.13	5.47	1.26	1.29	2.45

WHOLE ROCK DATA: TABLE D9: Major element analyses, trace element analyses and weight C.I.P.W. norms - Bastard Unit profiles **LEF**, **Y** and **X**
Major element analyses are normalised to 100% and are LOI and H_2O- free.
They are the average of either 2 or 3 determinations on separate discs.
An assumed oxidation ratio of $Fe_2O_3/FeO = 0.1$ is used.
Metres given above base of Bastard Unit.

	LEF						Y									X								
Sample	H979.91	H984.48	H992.8	H995.6	H997.26	H998.1	Y722.4	Y740.5	Y746.4	Y755.66	Y760.2	Y764.2	Y765.48	Y770.58	Y775	X735	X745.44	X763.95	X768.5	X776.52	X779.82	X782.7	X788.41	X791.8
Metres	18.29	13.72	5.40	2.54	0.94	0.10	54.01	35.91	30.01	20.75	16.21	12.21	10.93	5.83	1.41	57.94	47.50	28.99	24.44	16.44	13.12	10.24	4.53	1.14
Wt.%																								
SiO_2	51.85	50.69	51.01	48.95	48.92	53.89	51.78	50.86	49.81	50.66	49.69	50.47	48.94	52.93	56.00	52.01	50.66	50.21	50.78	50.75	53.89	50.76	53.26	55.09
TiO_2	0.15	0.12	0.11	0.06	0.05	0.13	0.21	0.20	0.11	0.10	0.08	0.14	0.07	0.10	0.24	0.19	0.06	0.09	0.07	0.05	0.16	0.07	0.09	0.22
Al_2O_3	19.07	23.40	21.77	31.02	29.19	8.30	24.90	25.46	26.67	27.62	28.33	22.26	30.59	18.12	5.67	23.63	27.54	27.34	26.95	26.64	7.34	22.81	13.90	5.47
Fe_2O_3	0.52	0.36	0.42	0.11	0.20	0.97	0.37	0.37	0.24	0.19	0.20	0.49	0.15	0.55	1.00	0.41	0.25	0.28	0.29	0.27	1.09	0.40	0.64	0.96
FeO	5.20	3.56	4.24	1.06	1.99	9.73	3.71	3.67	2.38	1.92	1.98	4.87	1.47	5.53	10.01	4.10	2.55	2.79	2.86	2.71	10.94	3.97	6.40	9.61
MnO	0.07	0.03	0.05	0.00	0.00	0.14	0.06	0.06	0.05	0.03	0.03	0.10	0.03	0.11	0.21	0.08	0.05	0.05	0.05	0.05	0.22	0.06	0.11	0.17
MgO	11.17	7.31	9.06	0.87	2.70	21.08	3.42	3.80	4.38	3.17	2.94	7.69	1.37	11.51	21.86	4.17	2.89	3.38	3.09	3.20	20.29	8.55	16.75	23.95
CaO	10.19	12.43	11.25	15.55	14.70	5.11	12.18	12.57	13.79	13.65	14.30	12.09	15.11	9.66	4.27	12.53	13.29	13.35	13.48	13.82	5.26	11.65	7.65	3.73
Na_2O	1.59	1.91	1.88	2.16	2.10	0.57	2.78	2.55	2.35	2.52	2.20	1.85	2.20	1.47	0.66	2.56	2.60	2.34	2.33	2.44	0.80	1.70	1.20	0.68
K_2O	0.19	0.19	0.19	0.22	0.15	0.08	0.51	0.38	0.20	0.12	0.10	0.01	0.05	0.01	0.07	0.29	0.08	0.15	0.08	0.05	0.00	0.02	0.00	0.11
P_2O_5	0.01	0.01	0.01	0.01	0.00	0.00	0.07	0.08	0.03	0.03	0.03	0.04	0.03	0.01	0.01	0.03	0.02	0.03	0.03	0.02	0.01	0.03	0.01	0.01
Total	100.0	100.0	100.0	100.0	100.0	100.0	100.0	100.0	100.0	100.0	99.9	100.0	100.0	100.0	100.0	100.0	100.0	100.0	100.0	100.0	100.0	100.0	100.0	100.0
MMF	0.7765	0.7707	0.7773	0.5726	0.6894	0.7798	0.6015	0.6288	0.7507	0.7300	0.7075	0.7209	0.6027	0.7730	0.7812	0.6247	0.6497	0.6645	0.6383	0.6591	0.7519	0.7768	0.8105	0.8029
Trace element values (ppm).																								
Sr	246.4	308.6	273.6	399.0	371.4	94.2	335.1	328.9	333.0	341.9	372.1	272.5	375.5	215.1	67.5	314.2	357.6	332.2	327.9	327.9	80.4	270.5	162.9	65.4
Rb	6.1	4.1	2.8	5.0	2.0	1.5	16.6	9.8	3.7	1.3	2.4	0.0	1.0	0.9	5.4	7.0	0.9	2.3	0.6	0.0	0.0	0.7	0.0	4.0
Y	2.8	2.8	4.2	0.1	1.4	0.0	8.0	7.6	4.5	3.4	3.1	3.6	2.2	2.6	8.1	7.3	1.4	2.5	3.6	2.5	5.6	2.2	2.8	6.5
Zr	15.9	11.0	8.7	4.2	2.0	5.9	38.6	21.0	13.0	7.9	2.8	6.2	1.0	3.8	13.4	20.9	1.8	5.7	4.4	1.6	4.9	3.6	4.2	19.1
Co	45.0	32.7	36.2	7.6	20.1	87.9	20.6	21.4	18.6	15.4	8.8	39.0	11.0	50.1	84.4	27.3	17.6	20.1	22.0	20.4	86.7	38.0	62.5	86.9
Cr	1271	823	1012	65	297	3141	148	141	199	201	208	704	169	1608	2452	256	139	218	206	78	2653	1105	2151	2653
V	73.2	50.2	51.3	13.8	22.1	116.6	59.5	60.8	66.6	33.4	36.4	71.2	20.9	65.4	126.7	82.5	42.0	38.7	50.9	54.5	136.1	52.5	83.1	119.8
Zn	45.7	27.7	31.8	10.1	33.8	79.1	26.4	29.3	12.2	14.0	10.0	31.9	7.7	38.9	95.1	25.9	18.4	19.7	18.9	14.8	89.3	29.1	52.2	66.2
Cu	20.2	16.6	18.5	11.3	102.2	214.2	20.8	14.4	11.5	6.9	13.5	28.0	12.0	18.7	166.3	24.4	14.7	8.6	7.1	9.4	73.4	16.8	19.7	178.3
Ni	239.6	148.3	203.1	23.8	231.9	889.3	44.4	46.9	46.4	47.5	54.4	140.6	30.1	271.1	749.5	84.1	42.1	55.6	58.2	46.7	460.2	174.6	353.5	796.5
Sc	14.8	10.7	11.4	3.4	4.9	27.0	9.3	9.5	9.0	5.9	6.0	13.4	3.7	16.3	31.0	11.1	6.8	5.8	6.9	7.8	30.3	11.8	19.3	29.6
CIPW weight percent norms.																								
ap	0.02	0.02	0.02	0.02	0.00	0.00	0.17	0.19	0.07	0.07	0.07	0.09	0.07	0.02	0.02	0.07	0.05	0.07	0.07	0.05	0.02	0.07	0.02	0.02
il	0.28	0.23	0.21	0.11	0.09	0.24	0.39	0.38	0.21	0.19	0.15	0.26	0.13	0.19	0.45	0.36	0.11	0.17	0.13	0.09	0.30	0.13	0.17	0.41
or	1.12	1.12	1.12	1.30	0.89	0.47	3.01	2.25	1.18	0.71	0.59	0.06	0.30	0.06	0.41	1.71	0.47	0.89	0.47	0.30	0.00	0.12	0.00	0.65
ab	13.45	16.16	15.91	18.28	17.77	4.82	23.52	21.58	19.88	21.32	18.61	15.65	18.61	12.44	5.58	21.66	22.00	19.80	19.71	20.64	6.77	14.38	10.15	5.75
an	44.34	54.72	50.41	74.30	69.78	19.85	53.96	56.91	61.64	63.70	67.14	52.41	73.45	42.82	12.30	52.13	63.24	63.66	62.85	61.59	16.44	54.55	32.54	11.55
c	0.00	0.00	0.00	0.00	0.00	0.00	0.00	0.00	0.00	0.00	0.00	0.00	0.00	0.00	0.00	0.00	0.00	0.00	0.00	0.00	0.00	0.00	0.00	0.00
mt	0.75	0.52	0.61	0.16	0.29	1.41	0.54	0.54	0.35	0.28	0.29	0.71	0.22	0.80	1.45	0.59	0.36	0.41	0.42	0.39	1.58	0.58	0.93	1.39
dien	1.78	1.98	1.54	0.62	0.82	1.59	1.39	1.19	1.85	1.05	0.96	1.97	0.30	1.45	2.55	2.34	0.63	0.60	0.93	1.70	2.68	0.88	1.60	2.05
difs	0.58	0.66	0.50	0.50	0.42	0.52	1.02	0.78	0.69	0.43	0.45	0.88	0.22	0.49	0.82	1.59	0.39	0.34	0.60	1.01	1.03	0.29	0.43	0.58
diwo	2.57	2.87	2.23	1.16	1.31	2.30	2.51	2.06	2.75	1.60	1.51	3.05	0.55	2.11	3.68	4.11	1.07	0.99	1.60	2.86	4.01	1.27	2.23	2.88
hyen	26.04	16.23	19.87	1.55	5.26	50.91	7.13	8.28	6.31	6.85	6.36	17.18	3.11	27.22	51.88	8.04	6.57	7.82	6.77	6.27	47.85	20.41	40.11	57.60
hyfs	8.43	5.44	6.48	1.26	2.67	16.60	5.26	5.44	2.36	2.83	2.95	7.62	2.29	9.25	16.74	5.45	4.08	4.50	4.39	3.75	18.31	6.67	10.85	16.24
q	0.64	0.06	0.00	0.75	0.00	1.29	1.10	0.43	0.00	0.99	0.80	0.12	0.75	3.17	4.10	1.95	1.02	0.77	2.07	1.34	1.02	0.66	0.97	0.89
fo	0.00	0.00	0.81	0.00	0.45	0.00	0.00	0.00	1.93	0.00	0.00	0.00	0.00	0.00	0.00	0.00	0.00	0.00	0.00	0.00	0.00	0.00	0.00	0.00
fa	0.00	0.00	0.29	0.00	0.25	0.00	0.00	0.00	0.80	0.00	0.00	0.00	0.00	0.00	0.00	0.00	0.00	0.00	0.00	0.00	0.00	0.00	0.00	0.00

WHOLE ROCK DATA: TBALE D10: Major element analyses, trace element analyses and weight C.I.P.W. norms - Bastard Unit profiles **RD** and **AE**.
Major element analyses are normalised to 100% and are LOI and H_2O- free.
They are the average of either 2 or 3 determinations on separate discs.
An assumed oxidation ratio of $Fe_2O_3/FeO = 0.1$ is used.
Metres given above base of Bastard Unit.

	RD								AE													
Sample	RD-1	RD-3	RD-4	RD-6	RD-15	RD-16	RD-17	RD-18	AE-1	AE-2	AE-3	AE-4	AE-5	AE-6	AE-7	AE-8	AE-9	AE-10	AE-11	AE-12	AE-13	AE-14	AE-15
Metres	35.00	31.00	29.40	22.50	8.30	5.90	3.62	0.50	35.80	34.00	32.40	29.80	26.40	23.60	19.95	18.42	17.00	14.70	10.75	8.05	5.15	3.15	1.05
Wt.%																							
SiO_2	50.73	50.03	49.94	49.72	51.17	51.96	54.23	53.92	50.08	50.54	50.34	50.40	50.29	50.08	49.35	49.62	50.35	51.40	51.60	52.83	54.10	55.01	54.84
TiO_2	0.11	0.08	0.08	0.08	0.09	0.11	0.20	0.20	0.10	0.13	0.07	0.08	0.10	0.10	0.12	0.12	0.13	0.12	0.12	0.10	0.26	0.25	0.21
Al_2O_3	27.85	28.90	27.18	28.34	20.40	15.28	5.89	5.79	28.70	26.68	28.89	29.56	28.92	28.87	29.12	26.18	23.33	19.70	17.30	13.40	7.15	6.18	5.83
Fe_2O_3	0.23	0.21	0.29	0.19	0.46	0.61	1.06	1.09	0.22	0.27	0.17	0.16	0.17	0.22	0.19	0.32	0.43	0.50	0.56	0.67	0.87	0.89	0.95
FeO	2.27	2.07	2.86	1.89	4.62	6.14	10.56	10.93	2.15	2.65	1.69	1.55	1.65	2.19	1.86	3.23	4.25	5.01	5.63	6.66	8.68	8.93	9.47
MnO	0.04	0.03	0.05	0.06	0.11	0.15	0.21	0.22	0.03	0.04	0.03	0.03	0.03	0.04	0.03	0.06	0.09	0.11	0.11	0.14	0.20	0.20	0.21
MgO	2.44	2.03	3.55	2.34	11.43	16.70	22.12	22.35	2.50	3.42	2.15	1.79	1.58	2.35	2.81	5.04	7.83	11.36	14.28	17.90	23.20	22.92	23.40
CaO	13.22	13.62	13.21	14.40	10.04	7.75	4.91	4.63	13.20	13.83	14.15	13.91	14.65	13.56	14.32	13.30	11.68	10.13	9.08	7.14	4.87	4.57	3.98
Na_2O	2.82	2.74	2.59	2.73	1.61	1.25	0.80	0.86	2.33	2.13	2.25	2.24	2.29	2.30	1.95	1.86	1.66	1.45	1.17	1.10	0.56	0.75	0.73
K_2O	0.23	0.24	0.19	0.20	0.03	0.01	0.00	0.00	0.25	0.26	0.20	0.23	0.25	0.25	0.20	0.22	0.21	0.17	0.09	0.06	0.08	0.24	0.22
P_2O_5	0.05	0.05	0.06	0.05	0.04	0.04	0.01	0.01	0.03	0.06	0.06	0.06	0.06	0.05	0.05	0.06	0.05	0.05	0.05	0.00	0.05	0.05	0.17
Total	100.0	100.0	100.0	100.0	100.0	100.0	100.0	100.0	99.6	100.0	100.0	100.0	100.0	100.0	100.0	100.0	100.0	100.0	100.0	100.0	100.0	100.0	100.0
MMF	0.6374	0.6153	0.6693	0.6690	0.8016	0.8164	0.7739	0.7697	0.6549	0.6781	0.6752	0.6531	0.6096	0.6368	0.7114	0.7185	0.7506	0.7876	0.8058	0.8145	0.8137	0.8076	0.8015
Trace element values (ppm).																							
Sr	493.4	456.4	459.5	566.9	330.7	205.2	71.4	70.8	346.0	321.0	353.0	363.0	353.0	351.0	329.0	312.0	273.0	237.0	191.0	228.0	56.7	65.3	63.3
Rb	5.1	4.2	3.5	4.7	1.8	1.2	1.4	1.0	6.3	5.8	2.7	4.6	3.7	2.6	4.4	6.9	6.3	3.8	1.4	4.1	3.2	7.1	4.1
Y	4.9	1.6	3.3	4.6	3.3	2.9	7.8	7.1	1.6	4.5	5.6	3.5	5.4	3.1	2.7	3.2	3.7	4.6	5.4	5.8	4.5	4.1	7.2
Zr	12.9	10.0	8.6	7.1	7.1	5.5	11.7	11.0	10.8	13.6	7.2	8.9	11.2	9.5	8.5	15.2	12.3	11.1	5.8	8.3	9.8	17.9	18.2
Co	11.9	14.7	15.0	70.4	42.4	69.3	87.1	94.3	16.6	20.6	23.6	12.0	11.4	15.2	15.5	25.4	37.1	38.1	56.2	66.7	90.6	107.0	95.5
Cr	180	135	202	2617	1309	2466	2689	2818	131	229	141	106	84	114	193	410	827	1287	1817	2331	3459	2717	2878
V	56.8	34.7	44.1	96.3	63.6	91.4	138.1	142.1	35.4	63.9	33.5	29.0	44.6	37.5	35.4	46.0	61.7	64.9	73.6	83.9	125.1	126.3	124.5
Zn	16.5	10.2	13.9	7.4	32.2	44.0	94.4	97.4	20.1	23.3	16.9	15.4	15.3	19.3	16.3	23.9	40.9	45.0	45.2	51.7	76.0	79.6	77.3
Cu	16.7	16.0	33.0	19.2	20.3	20.8	102.9	208.0	15.6	15.4	15.3	12.2	12.3	19.1	17.8	27.5	37.1	22.8	20.3	22.4	32.9	101.6	239.0
Ni	50.0	30.8	62.3	46.8	227.1	374.5	603.8	824.2	46.0	63.6	42.7	35.7	32.0	42.1	52.6	105.0	177.0	239.0	314.0	386.5	553.0	647.0	871.0
Sc	10.2	5.8	8.4	6.3	14.9	20.2	34.7	33.3	6.8	10.2	6.9	6.0	7.2	7.6	6.8	9.6	12.1	14.5	15.7	19.2	27.4	28.1	26.8
CIPW weight percent norms.																							
ap	0.12	0.12	0.14	0.12	0.09	0.09	0.02	0.02	0.07	0.14	0.14	0.14	0.14	0.12	0.12	0.14	0.12	0.12	0.12	0.00	0.12	0.12	0.40
il	0.21	0.15	0.15	0.15	0.17	0.21	0.38	0.38	0.19	0.24	0.13	0.15	0.19	0.19	0.23	0.23	0.24	0.23	0.23	0.19	0.49	0.47	0.39
or	1.36	1.42	1.12	1.18	0.18	0.06	0.00	0.00	1.48	1.54	1.18	1.36	1.48	1.48	1.18	1.30	1.24	1.00	0.53	0.35	0.47	1.42	1.30
ab	23.86	23.18	21.91	23.10	13.62	10.58	6.77	7.28	19.71	18.02	19.04	18.95	19.38	19.46	16.50	15.74	14.05	12.27	9.90	9.31	4.74	6.35	6.18
an	62.66	65.85	61.98	64.49	48.35	36.06	12.48	11.94	65.29	62.47	68.14	68.62	67.90	66.95	70.12	62.44	55.59	46.75	41.69	31.45	16.76	12.79	11.98
c	0.00	0.00	0.00	0.00	0.00	0.00	0.00	0.00	0.67	0.00	0.00	0.48	0.00	0.28	0.00	0.00	0.00	0.00	0.00	0.00	0.00	0.00	0.00
mt	0.33	0.30	0.42	0.28	0.67	0.88	1.54	1.58	0.32	0.39	0.25	0.23	0.25	0.32	0.28	0.46	0.62	0.72	0.81	0.97	1.26	1.29	1.38
dien	0.63	0.33	0.80	1.67	0.35	0.64	3.39	3.13	0.00	1.48	0.43	0.00	1.03	0.00	0.16	0.85	0.57	0.93	0.90	1.19	2.13	2.85	1.97
difs	0.40	0.23	0.45	0.95	0.10	0.17	1.14	1.08	0.00	0.78	0.23	0.00	0.73	0.00	0.07	0.38	0.22	0.29	0.25	0.32	0.56	0.78	0.56
diwo	1.09	0.58	1.32	2.77	0.50	0.89	4.93	4.58	0.00	2.40	0.69	0.00	1.83	0.00	0.25	1.32	0.85	1.33	1.27	1.66	2.95	3.99	2.78
hyen	5.44	4.26	6.02	1.35	27.55	37.54	51.69	50.71	6.23	7.04	4.93	4.46	2.90	5.85	6.84	11.70	18.93	27.36	34.66	42.60	55.65	54.22	56.30
hyfs	3.47	3.00	3.39	0.77	7.90	9.81	17.44	17.55	3.66	3.73	2.68	2.64	2.06	3.75	3.05	5.21	7.19	8.51	9.64	11.25	14.61	14.85	16.09
q	0.42	0.00	0.00	0.00	0.00	0.00	0.20	0.00	1.98	1.78	2.17	2.98	2.11	1.62	1.22	0.25	0.40	0.50	0.00	0.00	0.28	0.86	0.68
fo	0.00	0.33	1.42	1.96	0.39	2.39	0.00	1.27	0.00	0.00	0.00	0.00	0.00	0.00	0.00	0.00	0.00	0.00	0.00	0.55	0.00	0.00	0.00
fa	0.00	0.25	0.88	1.22	0.12	0.69	0.00	0.49	0.00	0.00	0.00	0.00	0.00	0.00	0.00	0.00	0.00	0.00	0.00	0.16	0.00	0.00	0.00

WHOLE ROCK DATA: TABLE D11: Major element analyses, trace element analyses and weight C.I.P.W. norms - Bastard Unit profile **AF**.
Major element analyses are normalised to 100% and are LOI and H_2O- free.
They are the average of either 2 or 3 determinations on separate discs.
An assumed oxidation ratio of $Fe_2O_3/FeO = 0.1$ is used.
Metres given above base of Bastard Unit.

	AF																
Sample	AF-1	AF-2	AF-3	AF-4	AF-5	AF-6	AF-7	AF-8a	AF-8b	AF-9	AF-10	AF-11	AF-12	AF-13	AF-14	AF-15	AF-16
Metres	34.20	32.30	30.60	27.90	24.90	21.70	18.90	18.05	17.85	17.05	13.60	10.50	6.65	4.40	2.45	1.25	0.05
Wt.%																	
SiO_2	50.94	49.65	49.82	50.06	50.58	50.47	49.44	49.60	50.50	50.34	50.99	51.41	52.87	52.54	54.59	55.10	54.29
TiO_2	0.11	0.09	0.06	0.06	0.09	0.10	0.13	0.09	0.12	0.12	0.10	0.10	0.15	0.18	0.23	0.21	0.20
Al_2O_3	26.01	28.68	30.95	29.42	29.27	28.01	25.66	27.89	25.05	20.13	19.59	17.05	12.72	7.81	6.07	5.48	6.86
Fe_2O_3	0.33	0.21	0.10	0.16	0.16	0.23	0.34	0.26	0.37	0.56	0.49	0.58	0.68	0.92	0.92	0.93	0.95
FeO	3.26	2.13	1.02	1.58	1.59	2.33	3.41	2.58	3.71	5.63	4.93	5.78	6.75	9.20	9.18	9.31	9.46
MnO	0.05	0.03	0.02	0.03	0.03	0.04	0.06	0.06	0.07	0.12	0.11	0.12	0.15	0.21	0.20	0.22	0.20
MgO	4.10	2.50	1.12	2.08	1.80	2.51	4.85	3.57	5.62	10.96	12.35	14.82	18.73	22.85	23.53	23.69	22.99
CaO	13.02	13.94	14.17	14.07	13.83	13.66	14.10	13.74	12.45	10.74	9.77	8.95	7.00	5.49	4.44	4.03	4.19
Na_2O	2.02	2.55	2.51	2.38	2.42	2.37	1.79	1.96	1.87	1.23	1.54	1.07	0.86	0.74	0.60	0.79	0.63
K_2O	0.17	0.21	0.22	0.18	0.22	0.24	0.20	0.21	0.22	0.16	0.12	0.11	0.09	0.06	0.24	0.23	0.21
P_2O_5	0.01	0.01	0.02	0.00	0.02	0.02	0.01	0.04	0.03	0.01	0.01	0.01	0.00	0.00	0.01	0.01	0.02
Total	100.0	100.0	100.0	100.0	100.0	100.0	100.0	100.0	100.0	100.0	100.0	100.0	100.0	100.0	100.0	100.0	100.0
FMF	0.6727	0.6570	0.6414	0.6825	0.6500	0.6379	0.6992	0.6940	0.7124	0.7608	0.8038	0.8075	0.8193	0.8024	0.8073	0.8062	0.7989
Trace element values (ppm).																	
Sr	329.0	352.0	369.0	343.0	353.0	352.0	0.0	330.0	306.0	243.0	228.0	195.0	145.0	92.0	92.0	65.0	77.0
Rb	2.6	2.6	2.8	1.7	4.9	3.3	0.0	4.5	6.5	1.8	2.4	0.9	1.8	1.3	11.2	8.0	6.6
Y	3.4	1.8	1.8	0.6	2.5	3.7	0.0	2.4	3.3	3.9	2.5	2.7	1.1	4.6	8.0	5.7	0.1
Zr	8.5	7.9	5.7	3.9	9.4	14.7	0.0	15.7	17.3	10.8	6.8	5.2	3.3	5.2	27.8	22.1	17.6
Co	25.4	15.8	8.4	13.5	12.1	126.1	25.0	19.5	39.6	48.1	48.4	56.4	70.5	82.9	90.8	84.1	97.4
Cr	174	136	58	146	87	129	372	278	549	1207	1398	1803	2383	3109	2676	2911	3572
V	65.4	32.3	20.6	30.5	33.4	41.3	57.7	33.4	66.4	69.3	64.6	70.4	84.5	113.0	125.0	126.9	121.5
Zn	26.6	23.8	10.7	15.0	20.4	71.6	24.9	25.7	29.0	43.7	46.4	44.3	52.9	81.0	76.2	76.3	81.8
Cu	8.6	13.9	9.9	8.4	14.2	16.4	30.1	15.5	18.0	14.5	20.0	47.9	18.1	28.0	103.7	135.0	165.3
Ni	78.0	51.0	20.0	40.0	37.0	41.0	81.0	72.0	108.0	215.0	267.0	301.0	393.0	503.0	669.0	728.0	1155.0
Sc	11.2	6.5	5.4	5.4	6.3	8.1	10.9	7.1	9.6	15.5	14.3	15.8	17.8	23.9	25.9	26.5	23.8
CIPW weight percent norms.																	
ap	0.02	0.02	0.05	0.00	0.05	0.05	0.02	0.09	0.07	0.02	0.02	0.02	0.00	0.00	0.02	0.02	0.05
il	0.21	0.17	0.11	0.11	0.17	0.19	0.24	0.17	0.23	0.23	0.19	0.19	0.28	0.34	0.43	0.39	0.38
or	1.00	1.24	1.30	1.06	1.30	1.42	1.18	1.24	1.30	0.95	0.71	0.65	0.53	0.35	1.42	1.36	1.24
ab	17.09	21.58	21.24	20.14	20.48	20.05	15.14	16.58	15.82	10.41	13.03	9.05	7.28	6.26	5.08	6.68	5.33
an	61.41	66.19	70.17	69.07	68.36	65.09	61.39	66.69	59.31	48.94	46.19	41.40	30.58	17.81	13.16	10.73	15.27
c	0.00	0.00	0.87	0.00	0.00	0.00	0.00	0.00	0.00	0.00	0.00	0.00	0.00	0.00	0.00	0.00	0.00
mt	0.48	0.30	0.14	0.23	0.23	0.33	0.49	0.38	0.54	0.81	0.71	0.84	0.99	1.33	1.33	1.35	1.38
dien	0.79	0.72	0.00	0.19	0.03	0.62	2.24	0.32	0.60	1.21	0.66	0.88	1.25	2.79	2.63	2.74	1.59
difs	0.44	0.42	0.00	0.10	0.02	0.40	1.09	0.16	0.28	0.44	0.19	0.24	0.32	0.80	0.72	0.76	0.46
diwo	1.30	1.21	0.00	0.31	0.05	1.07	3.55	0.51	0.94	1.79	0.93	1.23	1.73	3.93	3.67	3.84	2.25
hyen	9.42	4.14	2.79	4.99	4.45	5.63	9.84	8.57	13.39	25.21	26.74	34.70	45.39	45.40	55.97	56.26	55.66
hyfs	5.19	2.42	1.73	2.63	2.68	3.61	4.79	4.33	6.17	9.15	7.56	9.59	11.55	12.95	15.38	15.64	16.17
q	2.67	0.00	1.61	1.19	2.20	1.54	0.00	0.96	1.36	0.00	0.00	0.00	0.10	0.00	0.20	0.23	0.22
fo	0.00	0.96	0.00	0.00	0.00	0.00	0.00	0.00	0.00	0.61	2.35	0.93	0.00	6.10	0.00	0.00	0.00
fa	0.00	0.62	0.00	0.00	0.00	0.00	0.00	0.00	0.00	0.25	0.73	0.28	0.00	1.92	0.00	0.00	0.00

WHOLE ROCK DATA TABLE D12: Major element analyses, trace element analyses & CIPW weight % norms - profile **UA**.
Major element analyses are normalised to 100% and are LOI and H_2O- free.
They are the average of either 2 or 3 determinations on separate discs.
An assumed oxidation ratio of Fe_2O_3/FeO = 0.1 is used.
Metres given relative to the base of the Bastard Unit.

	UA																							
Sample	UA-1	UA-2	UA-3	UA-4	UA-5	UA-6	UA-7	UA-8	UA-9	UA-10	UA-11	UA-12	UA-13	UA-14	UA-15	UA-16a	UA-16b	UA-17	UA-18	UA-19	UA-20	UA-21	UA-22	UA-23	UA-24
Metres	53.2	50.5	47.6	44.6	41.9	39.4	36.8	33.7	31.2	28.9	26.3	23.7	21.8	20.2	19.0	17.9	17.7	16.2	14.2	11.8	10.1	8.5	7.2	5.1	3.2
Wt.%																									
SiO_2	50.96	50.22	49.75	49.90	50.07	49.87	50.15	50.15	50.56	49.57	49.46	49.26	49.70	50.08	48.42	48.62	49.43	51.21	51.16	51.60	52.19	52.08	53.13	54.30	54.98
TiO_2	0.18	0.12	0.07	0.07	0.08	0.07	0.07	0.07	0.09	0.09	0.05	0.07	0.11	0.09	0.11	0.06	0.09	0.11	0.10	0.10	0.10	0.09	0.11	0.14	0.18
Al_2O_3	27.42	28.04	28.88	29.32	27.85	29.02	28.86	28.87	28.30	30.25	30.31	30.74	29.25	27.49	31.66	31.61	27.04	20.44	19.68	17.10	15.49	16.73	10.85	6.54	5.24
Fe_2O_3	0.25	0.23	0.18	0.15	0.21	0.19	0.17	0.18	0.19	0.13	0.13	0.10	0.19	0.23	0.08	0.09	0.26	0.47	0.49	0.54	0.61	0.56	0.73	0.87	0.96
FeO	2.50	2.32	1.83	1.52	2.07	1.87	1.75	1.76	1.89	1.28	1.30	0.99	1.94	2.27	0.77	0.92	2.64	4.66	4.86	5.40	6.15	5.62	7.32	8.75	9.57
MnO	0.04	0.03	0.02	0.03	0.04	0.03	0.03	0.03	0.03	0.03	0.01	0.01	0.03	0.04	0.01	0.01	0.05	0.10	0.10	0.11	0.13	0.12	0.16	0.19	0.21
MgO	2.31	2.38	2.30	2.09	2.83	2.27	2.15	2.43	2.74	1.60	1.45	1.53	2.05	3.11	0.70	1.06	4.53	10.51	11.85	14.50	15.62	14.72	20.17	24.27	24.28
CaO	13.63	14.00	14.52	14.58	14.44	14.43	14.35	14.09	13.87	14.49	14.75	14.72	14.11	14.23	15.71	15.33	13.80	10.67	10.12	9.20	8.42	8.84	6.37	4.28	3.74
Na_2O	2.33	2.38	2.22	2.11	2.15	2.03	2.26	2.18	2.12	2.31	2.32	2.34	2.38	2.25	2.30	1.99	1.95	1.63	1.47	1.31	1.19	1.17	1.10	0.60	0.74
K_2O	0.34	0.26	0.21	0.21	0.20	0.20	0.19	0.19	0.19	0.19	0.16	0.21	0.20	0.18	0.21	0.23	0.19	0.12	0.12	0.10	0.07	0.08	0.05	0.00	0.09
P_2O_5	0.04	0.03	0.02	0.02	0.06	0.03	0.03	0.05	0.04	0.07	0.06	0.03	0.03	0.04	0.02	0.07	0.02	0.08	0.05	0.04	0.03	0.01	0.01	0.04	0.01
Total	100.0	100.0	100.0	100.0	100.0	100.0	100.0	100.0	100.0	100.0	100.0	100.0	100.0	100.0	100.0	100.0	100.0	100.0	100.0	100.0	100.0	100.0	100.0	100.0	100.0
MMF	0.6023	0.6270	0.6729	0.6911	0.6915	0.6654	0.6683	0.6932	0.7032	0.6717	0.6453	0.7164	0.6340	0.6916	0.5968	0.6531	0.7375	0.7866	0.7994	0.8145	0.8060	0.8108	0.8184	0.8194	0.8057
Trace element values (ppm).																									
Sr	329.3	340.5	341.5	357.0	268.7	343.4	346.0	350.5	347.3	361.4	361.7	345.3	375.4	334.9	377.3	364.2	323.8	248.2	234.8	218.7	181.4	174.91	134.9	68.4	59.2
Rb	9.2	3.1	3.2	5.0	1.4	0.0	1.4	3.4	2.5	1.7	1.2	3.8	2.0	6.0	1.0	4.6	4.9	1.6	3.4	3.4	3.2	0.00	0.0	0.0	0.0
Y	5.5	6.2	3.9	3.0	4.0	3.2	4.6	1.8	2.5	0.0	2.0	2.8	9.5	18.9	3.3	0.0	5.6	5.5	2.0	1.9	5.00	5.8	3.1	6.9	7.2
Zr	19.9	14.6	15.0	7.1	7.6	8.8	5.0	7.5	7.1	2.7	5.0	6.5	13.1	8.3	10.1	9.4	13.6	11.0	9.7	4.2	5.3	1.5	2.4	10.6	14.0
Co	15.8	15.6	14.6	14.4	16.0	15.0	13.8	13.6	15.4	9.4	9.1	5.7	12.8	15.6	4.3	5.9	22.7	43.2	44.74	45.6	59.6	54.7	43.6	51.8	61.6
Cr	111	118	139	127	220	139	151	145	173	101	79	22	97	172	40	79	544	1183	1380	1424	1967	1819	2372	2546	2432
V	51.2	40.0	38.6	31.8	49.8	36.3	36.9	34.4	38.7	23.9	18.7	15.2	31.0	41.9	10.1	13.6	39.1	57.0	61.1	55.8	73.7	66.5	52.9	92.9	89.1
Zn	23.5	21.1	15.5	14.5	16.9	14.5	15.0	13.8	16.2	12.2	10.6	9.6	16.5	16.7	7.4	7.4	21.6	36.4	35.8	36.3	46.4	43.5	55.8	69.7	76.0
Cu	18.3	18.5	12.1	9.2	10.0	11.5	11.7	10.1	10.2	11.1	10.6	11.3	16.8	19.2	13.5	10.6	19.5	20.1	16.2	16.5	15.9	17.1	21.3	22.6	109.9
Ni	42.1	39.2	45.3	38.3	54.2	40.1	40.0	46.9	46.3	29.7	23.2	14.7	36.2	53.0	18.9	24.0	104.1	223.1	219.9	259.2	337.6	315.9	436.0	537.8	670.4
Sc	7.4	5.6	6.5	5.6	7.3	5.2	6.0	4.8	6.0	2.6	3.9	2.63	5.1	7.7	1.7	3.4	8.4	14.0	15.5	14.5	19.1	19.9	22.3	27.9	30.4
CIPW weight percent norms.																									
ap	0.09	0.07	0.05	0.05	0.14	0.07	0.07	0.12	0.09	0.17	0.14	0.07	0.07	0.09	0.05	0.17	0.05	0.19	0.12	0.09	0.07	0.02	0.02	0.09	0.02
il	0.34	0.23	0.13	0.13	0.15	0.13	0.13	0.13	0.17	0.17	0.09	0.13	0.21	0.17	0.21	0.11	0.17	0.21	0.19	0.19	0.19	0.17	0.21	0.26	0.34
or	2.01	1.54	1.24	1.24	1.18	1.18	1.12	1.12	1.12	1.12	0.95	1.24	1.18	1.06	1.24	1.36	1.12	0.71	0.71	0.59	0.41	0.47	0.30	0.00	0.53
ab	19.71	20.14	18.78	17.85	18.19	17.18	19.12	18.44	17.94	19.54	19.63	19.80	20.14	19.04	19.46	16.84	16.50	13.79	12.44	11.08	10.07	9.90	9.31	5.08	6.26
an	63.36	65.06	68.22	69.92	65.75	69.49	68.05	68.43	67.15	71.43	71.82	72.76	68.54	64.38	75.45	75.60	64.47	48.10	46.75	40.49	36.72	40.16	24.52	15.15	10.71
c	0.00	0.00	0.00	0.00	0.00	0.00	0.00	0.00	0.00	0.07	0.00	0.00	0.00	0.00	0.00	0.38	0.00	0.00	0.00	0.00	0.00	0.00	0.00	0.00	0.00
mt	0.36	0.33	0.26	0.22	0.30	0.28	0.25	0.26	0.28	0.19	0.19	0.14	0.28	0.33	0.12	0.13	0.38	0.68	0.71	0.78	0.88	0.81	1.06	1.26	1.39
dien	0.93	1.01	0.94	0.60	1.43	0.48	0.75	0.30	0.37	0.00	0.24	0.02	0.31	1.55	0.56	0.00	1.06	1.26	0.93	1.47	1.45	1.09	2.12	1.76	2.32
difs	0.67	0.67	0.51	0.30	0.73	0.27	0.42	0.15	0.18	0.00	0.15	0.01	0.20	0.78	0.38	0.00	0.43	0.39	0.27	0.39	0.40	0.29	0.55	0.45	0.65
diwo	1.67	1.75	1.54	0.95	2.29	0.80	1.23	0.48	0.59	0.00	0.40	0.03	0.53	2.49	0.99	0.00	1.61	1.80	1.31	2.04	2.03	1.51	2.93	2.43	3.25
hyen	4.82	4.92	4.79	4.61	5.62	5.17	4.61	5.75	6.45	3.98	3.37	3.79	4.80	6.19	0.20	2.64	9.81	24.92	27.84	32.16	37.07	35.57	43.84	58.09	58.15
hyfs	3.49	3.27	2.62	2.31	2.85	2.95	2.60	2.88	3.05	2.15	2.07	1.63	3.09	3.12	0.14	1.54	3.98	7.79	8.06	8.47	10.36	9.64	11.31	14.88	16.23
q	2.53	1.03	0.91	1.83	1.37	2.02	1.67	1.94	2.64	1.19	0.95	0.37	0.66	0.79	0.00	1.23	0.00	0.17	0.00	0.00	0.00	0.37	0.00	0.00	0.15
fo	0.00	0.00	0.00	0.00	0.00	0.00	0.00	0.00	0.00	0.00	0.00	0.00	0.00	0.00	0.69	0.00	0.28	0.00	0.52	1.74	0.27	0.00	2.99	0.41	0.00
fa	0.00	0.00	0.00	0.00	0.00	0.00	0.00	0.00	0.00	0.00	0.00	0.00	0.00	0.00	0.52	0.00	0.13	0.00	0.17	0.50	0.08	0.00	0.85	0.12	0.00

WHOLE ROCK DATA TABLE D12: Major element analyses, trace element analyses & CIPW weight % norms - profile **UA**.
Major element analyses are normalised to 100% and are LOI and H_2O- free.
They are the average of either 2 or 3 determinations on separate discs.
An assumed oxidation ratio of Fe_2O_3/FeO = 0.1 is used.
Metres given relative to the base of the Bastard Unit.

	UA																							
Sample	UA-25	UA-26	UA-28	UA-29	UA-30	UA-31	UA-32	UA-33	UA-34	UA-35	UA-36	UA-37	UA-38	UA-39	UA-40	UA-41	UA-42	UA-46	UA-47	UA-48	UA-49	UA-50a	UA-50b	UA-51	UA-52
Metres	1.9	0.8	-1.0	-1.9	-4.4	-5.2	-6.2	-7.9	-9.8	-11.7	-13.7	-16.2	-17.4	-18.7	-20.4	-21.9	-23.3	-26.9	-28.1	-29.8	-30.8	-31.8	-32.0	-33.5	-35.4
Wt.%																									
SiO_2	54.92	54.70	48.81	48.47	48.44	48.20	48.43	49.51	51.23	51.36	49.57	50.41	50.82	51.35	54.45	54.62	54.07	48.43	49.00	49.41	49.14	48.65	49.23	49.24	50.12
TiO_2	0.20	0.21	0.04	0.04	0.04	0.04	0.04	0.07	0.12	0.08	0.09	0.08	0.09	0.11	0.24	0.26	0.23	0.05	0.07	0.07	0.08	0.08	0.07	0.06	0.08
Al_2O_3	5.30	5.35	30.45	31.29	30.86	31.66	31.49	26.47	28.20	27.38	26.98	22.57	19.66	16.39	5.32	5.68	4.44	31.71	30.05	29.29	30.25	30.67	28.32	28.86	24.83
Fe_2O_3	0.97	0.98	0.10	0.08	0.13	0.09	0.08	0.28	0.25	0.31	0.25	0.41	0.51	0.65	1.01	0.96	1.05	0.08	0.15	0.17	0.16	0.11	0.19	0.18	0.30
FeO	9.67	9.78	1.04	0.83	1.29	0.86	0.81	2.83	2.47	3.05	2.51	4.07	5.14	6.52	10.10	9.57	10.48	0.79	1.52	1.66	1.65	1.11	1.85	1.80	2.95
MnO	0.21	0.20	0.01	0.01	0.01	0.01	0.01	0.05	0.44	0.61	0.05	0.08	0.11	0.14	0.21	0.20	0.21	0.01	0.03	0.03	0.02	0.02	0.03	0.03	0.06
MgO	24.33	24.06	1.83	1.13	1.40	1.25	1.21	5.35	1.15	1.28	4.85	8.71	11.74	14.28	23.96	23.47	24.65	0.83	1.87	1.70	1.85	1.64	3.75	3.54	7.22
CaO	3.59	3.81	15.05	14.87	15.44	15.41	15.33	13.32	13.92	13.50	13.46	11.76	10.39	9.19	3.76	4.19	4.22	15.43	14.78	15.11	14.56	15.19	14.20	13.94	12.36
Na_2O	0.70	0.73	2.46	2.67	2.18	2.29	2.31	1.99	2.04	2.24	2.01	1.80	1.45	1.24	0.73	0.79	0.57	2.51	2.40	2.34	2.10	2.36	2.24	2.19	1.89
K_2O	0.10	0.16	0.20	0.61	0.22	0.20	0.29	0.12	0.16	0.15	0.16	0.12	0.09	0.10	0.19	0.22	0.09	0.16	0.14	0.16	0.16	0.17	0.12	0.14	0.14
P_2O_5	0.01	0.04	0.00	0.00	0.00	0.00	0.01	0.00	0.02	0.05	0.07	0.00	0.00	0.05	0.02	0.05	0.00	0.00	0.00	0.06	0.03	0.00	0.00	0.02	0.06
Total	100.0	100.0	100.0	100.0	100.0	100.0	100.0	100.0	100.0	100.0	100.0	100.0	100.0	100.0	100.0	100.0	100.0	100.0	100.0	100.0	100.0	100.0	100.0	100.0	100.0
MMF	0.8044	0.8009	0.7415	0.6904	0.6394	0.7046	0.7087	0.7554	0.4334	0.4076	0.7598	0.7777	0.7889	0.7818	0.7950	0.8003	0.7937	0.6305	0.6670	0.6261	0.6471	0.7062	0.7685	0.7627	0.7998
Trace element values (ppm).																									
Sr	74.3	60.2	383.4	356.9	395.1	397.1	399.8	347.7	350.1	334.7	347.5	297.7	252.1	217.5	60.6	65.8	38.5	354.3	458.0	463.8	452.4	453.8	425.9	424.8	367.55
Rb	17.6	3.9	0.0	0.0	10.73	3.5	16.8	2.9	4.5	2.1	4.3	3.0	2.6	1.6	8.0	7.9	3.0	1.1	2.0	5.0	5.1	4.9	1.6	0.0	3.2
Y	3.5	2.8	1.3	10.1	2.3	0.0	4.4	3.0	2.2	1.8	3.0	0.0	6.3	5.1	6.6	8.9	5.2	0.0	1.4	1.9	1.1	1.8	0.0	1.5	3.8
Zr	17.3	19.9	2.1	0.0	3.4	3.9	11.3	8.7	7.3	5.0	5.7	4.0	5.4	4.6	18.6	22.1	12.8	2.4	6.8	9.4	8.1	8.1	8.4	3.2	5.9
Co	88.4	87.7	5.2	3.9	11.1	4.5	6.3	21.9	18.2	21.7	18.9	32.3	43.9	52.5	92.2	83.8	102.1	4.0	9.0	6.2	8.7	7.5	13.7	13.8	25.3
Cr	2678	2827	167	48	86	49	59	539	454	584	499	917	1372	1766	3083	2929	3018	19	58	66	75	90	356	379	766
V	107.8	109.3	10.1	8.9	14.2	10.5	8.4	31.4	29.6	31.5	27.4	39.9	55.8	52.7	116.5	115.7	115.2	8.2	35.8	18.6	20.3	12.7	22.1	20.2	32.7
Zn	78.1	75.8	9.4	7.2	9.7	6.8	8.6	23.8	21.0	23.0	19.2	31.4	41.6	50.8	81.5	77.1	84.2	6.6	13.5	12.7	13.3	9.7	15.4	14.9	23.1
Cu	216.3	207.6	58.2	27.7	185.6	39.3	42.8	55.3	52.1	47.1	51.6	70.5	77.4	110.1	371.1	151.3	817.2	12.0	8.6	13.3	9.7	9.6	13.4	14.9	12.5
Ni	845.1	790.3	64.1	42.7	468.0	54.9	68.1	167.9	141.3	163.9	159.3	280.2	336.0	442.8	1128.2	735.9	1871.2	11.0	25.5	29.0	28.4	27.7	74.9	77.5	152.9
Sc	29.1	28.7	2.7	1.1	2.3	1.1	2.3	8.7	7.7	9.3	5.1	13.1	16.8	18.6	31.3	31.5	30.6	2.1	8.1	4.2	4.4	3.4	5.6	5.2	9.1
CIPW weight percent norms.																									
ap	0.02	0.09	0.00	0.00	0.00	0.00	0.02	0.00	0.05	0.12	0.17	0.00	0.00	0.12	0.05	0.12	0.00	0.00	0.00	0.14	0.07	0.00	0.00	0.05	0.14
il	0.38	0.39	0.08	0.08	0.08	0.08	0.08	0.13	0.23	0.15	0.17	0.15	0.17	0.21	0.45	0.49	0.43	0.09	0.13	0.13	0.15	0.15	0.13	0.11	0.15
or	0.59	0.95	1.18	3.60	1.30	1.18	1.71	0.71	0.95	0.89	0.95	0.71	0.53	0.59	1.12	1.30	0.53	0.95	0.83	0.95	0.95	1.00	0.71	0.83	0.83
ab	5.92	6.18	20.81	17.81	18.44	19.22	19.51	16.84	17.26	18.95	17.01	15.23	12.27	10.49	6.18	6.68	4.82	19.98	20.31	19.80	17.77	19.97	18.95	18.53	15.99
an	11.03	10.85	71.46	71.60	73.77	75.52	74.70	62.94	67.32	64.22	64.13	53.15	46.87	38.86	10.68	11.30	9.29	74.79	70.81	68.95	72.04	72.60	66.87	68.51	58.86
c	0.00	0.00	0.00	0.00	0.00	0.00	0.00	0.00	0.00	0.00	0.00	0.00	0.00	0.00	0.00	0.00	0.00	0.00	0.00	0.00	0.22	0.00	0.00	0.00	0.00
mt	1.41	1.42	0.14	0.12	0.19	0.13	0.12	0.41	0.36	0.45	0.36	0.59	0.74	0.94	1.46	1.39	1.52	0.12	0.22	0.25	0.23	0.16	0.28	0.26	0.43
dien	2.00	2.31	0.89	0.57	0.69	0.25	0.34	0.88	0.25	0.35	0.62	1.50	1.36	1.85	2.31	2.71	3.42	0.43	0.64	1.34	0.00	0.74	1.03	0.15	0.61
difs	0.56	0.66	0.35	0.29	0.44	0.12	0.16	0.33	0.43	0.70	0.22	0.49	0.42	0.60	0.69	0.78	1.03	0.27	0.36	0.90	0.00	0.34	0.35	0.05	0.18
diwo	2.81	3.25	1.34	0.91	1.18	0.39	0.54	1.31	0.67	1.02	0.92	2.17	1.95	2.67	3.28	3.82	4.86	0.74	1.05	2.35	0.00	1.15	1.49	0.22	0.86
hyen	58.59	57.03	0.16	0.00	1.33	0.00	0.00	10.83	2.61	2.84	11.15	17.95	25.59	31.18	55.70	54.98	54.61	0.00	2.61	2.89	4.61	0.93	5.78	7.53	16.31
hyfs	16.46	16.36	0.06	0.00	0.84	0.00	0.00	4.02	4.52	5.66	4.02	5.92	7.94	10.10	16.54	15.74	16.37	0.00	1.46	1.95	2.81	0.42	1.97	2.66	4.67
q	0.24	0.00	0.00	0.00	0.00	0.00	0.00	0.00	5.36	4.69	0.00	0.00	0.00	0.00	0.00	0.00	0.00	0.00	0.00	0.36	1.16	0.00	0.00	0.00	0.00
fo	0.00	0.40	2.46	1.57	1.03	2.01	1.87	1.12	0.00	0.00	0.21	1.57	1.60	1.77	1.16	0.53	2.35	1.15	0.99	0.00	0.00	1.69	1.77	0.80	0.74
fa	0.00	0.13	1.06	0.87	0.72	1.04	0.94	0.46	0.00	0.00	0.08	0.57	0.55	0.63	0.38	0.17	0.78	0.81	0.61	0.00	0.00	0.85	0.67	0.31	0.23

WHOLE ROCK DATA TABLE D12: Major element analyses, trace element analyses & CIPW weight % norms - profile **UA**.
Major element analyses are normalised to 100% and are LOI and H_2O- free.
They are the average of either 2 or 3 determinations on separate discs.
An assumed oxidation ratio of Fe_2O_3/FeO = 0.1 is used.
Metres given relative to the base of the Bastard Unit.

	UA														
Sample	UA-53a	UA-53b	UA-53c	UA-54	UA-55	UA-56	UA-57	UA-63	UA-64	UA-65	UA-66	UA-67	UA-68	UA-69	UA-70
Metres	-36.4	-36.7	-37.0	-38.2	-39.0	-39.2	-40.2	-45.4	-46.8	-48.4	-49.8	-51.3	-53.0	-53.7	-54.3
Wt.%															
SiO_2	49.51	49.55	49.31	49.49	51.55	52.94	52.19	54.65	52.11	54.27	54.16	55.22	54.24	53.87	50.05
TiO_2	0.09	0.09	0.06	0.05	0.08	0.15	0.14	0.28	0.10	0.19	0.22	0.24	0.26	0.13	0.20
Al_2O_3	25.72	25.45	28.87	25.98	19.12	11.15	12.75	4.70	16.54	5.03	4.77	4.12	4.65	6.11	3.98
Fe_2O_3	0.29	0.29	0.18	0.26	0.46	0.71	0.66	1.00	0.63	1.02	1.01	1.05	1.07	0.97	1.29
FeO	2.90	2.91	1.81	2.56	4.64	7.11	6.61	9.97	6.25	10.23	10.10	10.47	10.67	9.68	12.94
MnO	0.05	0.05	0.03	0.05	0.10	0.15	0.16	0.21	0.12	0.22	0.23	0.22	0.22	0.21	0.22
MgO	6.22	6.17	3.31	6.37	12.71	20.04	18.41	24.50	14.54	24.59	24.35	24.36	24.36	24.23	28.27
CaO	13.12	13.05	14.01	13.06	9.72	6.56	7.68	3.87	8.92	3.69	4.34	3.69	3.73	4.24	2.57
Na_2O	1.92	2.26	2.12	2.03	1.43	1.11	1.32	0.66	0.69	0.68	0.78	0.60	0.67	0.54	0.37
K_2O	0.16	0.15	0.27	0.14	0.17	0.07	0.09	0.15	0.09	0.03	0.04	0.04	0.06	0.02	0.10
P_2O_5	0.03	0.03	0.03	0.00	0.02	0.02	0.00	0.01	0.01	0.04	0.00	0.00	0.07	0.01	0.00
Total	100.0	100.0	100.0	100.0	100.0	100.0	100.0	100.0	100.0	100.0	100.0	100.0	100.0	100.0	100.0
MMF	0.7782	0.7764	0.7489	0.8024	0.8175	0.8217	0.8200	0.8007	0.7919	0.7971	0.7976	0.7918	0.7888	0.8036	0.7813
Trace element values (ppm).															
Sr	386.9	445.6	429.5	400.3	317.2	178.1	247.2	54.1	67.2	73.0	67.7	58.3	55.6	80.3	42.8
Rb	3.3	3.5	5.0	4.0	3.9	2.4	0.0	5.8	3.1	2.0	2.9	2.0	3.6	0.0	6.2
Y	4.5	1.9	1.7	1.5	1.3	2.9	5.3	6.5	5.1	5.6	9.7	7.4	5.8	3.8	4.3
Zr	8.6	3.0	5.7	3.8	2.4	8.5	7.8	13.1	6.0	6.6	7.5	10.5	8.5	5.3	13.0
Co	20.6	8.2	12.2	20.3	43.1	58.6	55.4	85.8	81.7	81.6	89.6	88.0	87.4	91.9	121.9
Cr	625	144	289	652	1466	2412	2320	3574	3447	3139	3553	3590	6523	4759	4190
V	31.8	15.6	21.1	25.6	45.9	76.2	71.8	116.9	105.1	102.3	126.4	124.8	142.3	98.9	91.2
Zn	22.3	10.4	15.2	21.4	32.8	53.3	49.9	79.9	78.8	84.1	77.3	163.7	158.5	68.8	88.1
Cu	16.5	12.2	10.0	12.7	27.9	38.2	55.0	29.2	32.6	36.1	33.1	58.2	75.1	23.4	29.8
Ni	148.5	41.0	72.4	135.2	278.0	480.9	455.0	635.6	601.4	602.7	542.9	1171.0	1209.5	742.6	1242.2
Sc	8.6	4.0	5.9	8.9	14.7	22.7	21.7	31.4	33.4	28.9	31.6	31.7	30.6	26.5	21.9
CIPW weight percent norms.															
ap	0.07	0.00	0.07	0.00	0.05	0.05	0.00	0.02	0.02	0.09	0.00	0.00	0.17	0.02	0.00
il	0.17	0.11	0.11	0.09	0.15	0.28	0.26	0.53	0.19	0.36	0.41	0.45	0.49	0.24	0.38
or	0.95	2.19	1.60	0.83	1.00	0.41	0.53	0.89	0.53	0.18	0.24	0.24	0.35	0.12	0.59
ab	16.24	17.43	17.94	17.18	12.10	9.39	11.17	5.58	5.84	5.75	6.60	5.08	5.67	4.57	3.13
an	61.09	71.52	68.47	61.37	45.25	25.24	28.60	9.42	41.77	10.58	9.40	8.43	9.50	14.19	8.90
c	0.00	0.00	0.00	0.00	0.00	0.00	0.00	0.00	0.00	0.00	0.00	0.00	0.00	0.00	0.00
mt	0.42	0.20	0.26	0.38	0.67	1.03	0.96	1.45	0.91	1.48	1.46	1.52	1.55	1.41	1.87
dien	1.10	0.44	0.24	1.02	0.86	2.18	2.87	2.88	0.71	2.20	3.58	2.90	2.50	2.01	1.11
difs	0.36	0.21	0.09	0.29	0.22	0.55	0.73	0.82	0.22	0.65	1.05	0.88	0.77	0.57	0.36
diwo	1.59	0.69	0.35	1.43	1.19	3.00	3.97	4.06	1.01	3.12	5.07	4.12	3.57	2.83	1.61
hyen	11.60	4.49	7.56	10.33	30.09	42.69	34.61	57.10	35.50	56.72	52.69	57.77	56.39	55.95	43.36
hyfs	3.77	2.12	2.88	2.93	7.79	10.70	8.81	16.30	10.80	16.71	15.45	17.50	17.38	15.91	14.03
q	0.00	0.60	0.00	0.00	0.00	0.00	0.00	0.00	2.50	0.00	0.00	1.13	0.00	0.00	0.00
fo	1.96	0.00	0.31	3.16	0.50	3.54	5.86	0.73	0.00	1.62	3.06	0.00	1.25	1.67	18.17
fa	0.70	0.00	0.13	0.99	0.14	0.98	1.64	0.23	0.00	0.53	0.99	0.00	0.42	0.52	6.48

WHOLE ROCK DATA: TABLE D13: Major element analyses, trace element analyses and weight C.I.P.W. norms - profile **UB**.
Major element analyses are normalised to 100% and are LOI and H_2O- free.
They are the average of 2 determinations on separate discs.
An assumed oxidation ratio of Fe_2O_3/FeO = 0.1 is used.
Metres given relative to the base of Bastard Unit. * = Majors from De Klerk (1982)

	UB																									
Sample	232/23	232/22	232/21	232/20	232/19	235/1	235/2	235/3	235/4	235/5	232/13	235/6	232/12	235/7	232/10	235/8	232/9	235/9	235/10	235/11	235/12	235/13	235/14	232/2	235/15	235/15A	235/16
Metres	27.6	25.1	22.8	22.1	18.2	16.7	13.4	10.4	8.2	4.4	3.0	0.5	0.5	-0.6	-0.6	-2.1	-2.1	-3.1	-6.9	-11.2	-14.7	-18.5	-22.0	-22.0	-22.6	-23.2	-23.9
Wt.%						*	*	*	*	*	*	*	*	*	*	*	*	*	*	*	*	*	*	*	*	*	*
SiO_2	50.23	49.67	49.11	50.16	50.94	50.40	51.19	51.68	52.58	54.31	54.13	54.01	54.38	48.05	48.64	47.99	48.57	48.48	49.46	49.62	50.49	52.64	53.42	53.07	47.33	43.85	45.66
TiO_2	0.26	0.13	0.13	0.12	0.13	0.10	0.12	0.13	0.14	0.22	0.22	0.24	0.22	0.06	0.06	0.06	0.05	0.07	0.09	0.08	0.11	0.19	0.25	0.23	0.15	0.16	0.16
Al_2O_3	28.62	28.64	28.77	23.80	20.26	19.41	17.00	11.91	10.37	5.43	5.67	5.42	4.97	31.62	31.79	31.45	31.85	30.31	26.71	27.40	19.00	9.15	4.81	4.85	7.11	4.94	4.45
Fe_2O_3	0.20	0.23	0.21	0.38	0.46	0.49	0.55	0.70	0.73	0.92	0.94	0.96	0.90	0.21	0.21	0.26	0.16	0.34	0.53	0.38	1.01	1.59	1.89	1.90	2.21	2.99	2.61
FeO	1.99	2.27	2.08	3.79	4.65	4.91	5.54	7.00	7.29	9.22	9.35	9.60	9.06	1.09	1.07	1.31	0.81	1.73	2.65	1.86	5.02	7.91	9.45	9.48	11.06	14.94	13.07
MnO	0.03	0.04	0.04	0.07	0.10	0.08	0.13	0.15	0.16	0.19	0.22	0.19	0.24	0.00	0.03	0.00	0.03	0.02	0.06	0.03	0.07	0.16	0.21	0.22	0.21	0.21	0.21
MgO	2.37	2.64	2.93	7.62	11.21	12.70	14.86	20.49	21.56	24.90	24.64	24.45	25.40	1.22	0.21	1.22	0.60	1.71	4.98	4.67	12.19	20.83	25.07	25.27	27.26	29.89	30.47
CaO	13.87	14.12	14.59	12.19	10.59	10.06	9.06	6.76	6.10	3.79	3.84	4.09	3.88	14.89	15.54	14.91	15.62	14.85	13.41	13.70	10.36	6.00	3.96	4.04	3.93	2.47	2.84
Na_2O	2.13	2.00	1.86	1.66	1.49	1.63	1.32	1.11	1.02	0.82	0.82	0.92	0.82	2.35	2.22	2.54	2.10	2.31	1.93	2.13	1.63	1.42	0.82	0.81	0.64	0.43	0.43
K_2O	0.26	0.24	0.23	0.19	0.14	0.22	0.23	0.07	0.04	0.19	0.15	0.12	0.13	0.50	0.17	0.25	0.14	0.17	0.15	0.14	0.11	0.12	0.09	0.11	0.10	0.12	0.10
P_2O_5	0.03	0.02	0.04	0.02	0.02	0.00	0.00	0.00	0.00	0.00	0.01	0.00	0.00	0.00	0.06	0.00	0.06	0.01	0.03	0.00	0.02	0.00	0.02	0.00	0.00	0.00	0.00
Total	100.0	100.0	100.0	100.0	100.0	100.0	100.0	100.0	100.0	100.0	100.0	100.0	100.0	100.0	100.0	100.0	100.0	100.0	100.0	100.0	100.0	100.0	100.0	100.0	100.0	100.0	100.0
MMI	0.6606	0.6551	0.6964	0.7669	0.7975	0.8089	0.8145	0.8271	0.8285	0.8153	0.8116	0.8064	0.8209	0.6294	0.2305	0.5839	0.5285	0.5992	0.7394	0.7912	0.7857	0.7991	0.8003	0.8009	0.7883	0.7513	0.7788
Trace element values (ppm):																											
Sr	349.0	339.1	336.0	276.0	240.0	223.0	183.0	135.0	114.0	61.0	62.0	54.0	57.0	371.0	407.0	412.0	415.0	390.0	331.0	335.0	244.0	123.0	52.0	59.0	85.0	72.0	54.0
Rb	6.0	6.3	5.1	4.7	2.1	1.3	1.0	0.5	0.0	7.6	5.0	7.0	5.0	13.9	0.0	5.4	0.0	0.0	1.0	2.0	3.0	3.0	3.0	4.0	1.5	3.0	4.0
Y	ND	ND	ND	ND	ND	3.0	4.0	4.0	3.5	6.7	7.0	7.2	7.0	1.5	4.0	2.3	3.0	3.0	2.0	4.0	4.0	6.6	7.9	9.0	3.8	0.0	3.0
Zr	ND	ND	ND	ND	ND	7.0	5.0	4.0	4.0	24.0	19.0	23.0	16.0	4.0	2.0	5.5	4.0	5.5	8.5	8.5	6.5	17.0	21.0	15.0	8.5	8.0	9.0
Co	15.2	17.6	17.1	34.9	50.8	50.0	57.0	72.0	79.0	94.0	99.0	101.0	99.0	8.5	4.0	9.0	5.0	13.0	24.0	23.0	49.0	84.0	100.0	106.0	122.0	201.0	168.0
Cr	95	119	315	851	1324	1475	1795	2490	2765	2710	2736	3130	3009	208	55	74	73	216	582	600	1405	2595	2850	2843	3525	3523	4890
V	36.5	40.2	36.8	55.3	60.9	65.0	72.0	93.0	101.0	131.0	127.0	138.0	129.0	15.5	9.0	14.0	10.0	21.5	37.0	36.0	65.0	119.0	137.0	143.0	68.0	58.0	73.0
Zn	14.8	20.0	15.9	32.2	38.9	38.0	41.0	55.0	53.0	84.0	ND	79.0	ND	8.0	ND	8.0	ND	11.0	19.0	17.0	38.0	63.0	77.0	ND	58.0	ND	81.0
Cu	12.8	17.3	18.2	18.7	17.3	19.0	19.0	24.0	4.0	101.0	80.0	278.0	300.0	55.0	30.0	44.0	40.0	55.0	46.0	52.0	76.0	244.0	391.0	370.0	290.0	600.0	317.0
Ni	37.0	57.0	57.0	161.0	245.0	266.0	316.0	422.0	453.0	636.0	870.0	912.0	1100.0	69.0	90.0	77.0	180.0	105.0	154.0	167.0	325.0	777.0	1164.0	1630.0	1274.0	3100.0	2435.0
Sc	5.9	6.9	6.7	10.7	13.5	18.4	22.2	24.7	26.7	33.9	ND	34.7	ND	6.8	ND	6.7	ND	7.5	11.6	11.5	19.1	29.7	34.0	ND	15.0	11.1	14.2
Ba	ND	ND	ND	ND	ND	42.8	42.8	27.4	21.6	77.4	ND	56.4	ND	130.0	ND	72.4	ND	58.1	59.5	71.4	46.6	65.8	45.0	ND	38.0	ND	24.0
CIPW weight percent norms.																											
ap	0.07	0.05	0.09	0.05	0.05	0.00	0.00	0.00	0.00	0.00	0.02	0.00	0.00	0.00	0.14	0.00	0.14	0.02	0.07	0.00	0.05	0.00	0.05	0.00	0.00	0.00	0.00
il	0.49	0.24	0.24	0.23	0.24	0.19	0.23	0.24	0.26	0.41	0.41	0.45	0.41	0.11	0.11	0.11	0.09	0.13	0.17	0.15	0.21	0.36	0.47	0.43	0.28	0.30	0.30
or	1.54	1.42	1.36	1.12	0.83	1.30	1.36	0.41	0.24	1.12	0.89	0.71	0.77	2.95	1.00	1.48	0.83	1.00	0.89	0.83	0.65	0.71	0.53	0.65	0.59	0.71	0.59
ab	18.02	16.92	15.74	14.05	12.61	13.79	11.17	9.39	8.63	6.94	6.94	7.78	6.94	18.26	18.78	19.21	17.77	19.54	16.33	18.02	13.79	12.01	6.94	6.85	5.41	3.64	3.64
an	67.77	68.47	69.48	56.93	48.18	45.00	39.78	27.31	23.60	10.58	11.35	10.31	9.50	73.87	76.28	73.68	77.07	71.84	63.78	64.79	44.21	18.24	9.18	9.27	16.23	11.20	9.92
c	0.00	0.00	0.00	0.00	0.00	0.00	0.00	0.00	0.00	0.00	0.00	0.00	0.00	0.14	0.00	0.00	0.00	0.00	0.00	0.00	0.00	0.00	0.00	0.00	0.00	0.00	0.00
mt	0.29	0.33	0.30	0.55	0.67	0.71	0.80	1.01	1.06	1.33	1.36	1.39	1.30	0.30	0.30	0.38	0.23	0.49	0.77	0.55	1.46	2.31	2.74	2.75	3.20	4.34	3.78
dien	0.22	0.36	0.70	0.97	1.25	1.47	1.55	1.90	2.03	2.48	2.29	2.98	2.95	0.00	0.04	0.07	0.01	0.42	0.73	0.96	2.11	3.48	3.13	3.26	0.97	0.30	1.23
difs	0.12	0.21	0.34	0.34	0.36	0.40	0.41	0.46	0.49	0.65	0.61	0.82	0.75	0.00	0.14	0.05	0.01	0.28	0.26	0.25	0.58	0.89	0.79	0.82	0.27	0.10	0.36
diwo	0.35	0.61	1.10	1.43	1.76	2.05	2.16	2.60	2.78	3.44	3.19	4.17	4.07	0.00	0.18	0.12	0.01	0.74	1.07	1.33	2.95	4.81	4.32	4.50	1.36	0.44	1.74
hyen	5.68	6.21	6.60	18.00	25.58	21.12	29.16	36.87	42.82	53.94	53.58	51.03	54.05	0.00	0.48	0.00	1.49	1.94	11.68	9.79	22.73	38.58	52.46	50.46	29.30	20.54	25.83
hyfs	3.01	3.63	3.18	6.24	7.45	5.74	7.70	8.92	10.25	14.07	14.36	14.07	13.66	0.00	1.61	0.00	1.32	1.29	4.14	2.55	6.24	9.82	13.26	12.73	8.04	6.93	7.48
q	2.43	1.55	0.86	0.09	0.00	0.00	0.00	0.00	0.00	0.00	0.00	0.00	0.00	0.00	0.93	0.00	1.02	0.00	0.14	0.00	0.00	0.00	0.00	0.00	0.00	0.00	0.00
fo	0.00	0.00	0.00	0.00	0.76	6.33	4.41	8.59	6.19	3.92	3.85	4.82	4.38	2.13	0.00	2.08	0.00	1.33	0.00	0.62	3.86	6.87	4.79	6.46	26.36	37.56	34.21
fa	0.00	0.00	0.00	0.00	0.25	1.90	1.28	2.29	1.63	1.13	1.14	1.46	1.22	1.34	0.00	1.58	0.00	0.97	0.00	0.18	1.17	1.93	1.34	1.79	7.97	13.95	10.92

WHOLE ROCK DATA: TABLE D13: Major element analyses, trace element analyses and weight C.I.P.W. norms - profile **UB**.
Major element analyses are normalised to 100% and are LOI and H_2O- free.
They are the average of 2 determinations on separate discs.
An assumed oxidation ratio of Fe_2O_3/FeO = 0.1 is used.
Metres given relative to the base of Bastard Unit. * = Majors from De Klerk (1982)

	UB																						
Sample	235/17	235/18	235/19	235/20	235/21	235/22	235/23	235/24	235/25	235/26	235/27	222/19	235/28	235/29	235/30	235/31	235/32	235/33	235/34	235/35	235/36	235/37	235/38	235/39
Metres	-24.4	-27.4	-30.5	-31.1	-34.4	-37.2	-39.8	-40.4	-41.1	-44.4	-45.9	-45.9	-47.2	-50.2	-54.1	-58.8	-61.1	-61.6	-64.4	-68.7	-72.3	-76.0	-79.0	-80.5
Wt.%	*	*	*	*	*	*	*	*	*	*	*	*	*	*	*	*	*	*	*	*	*	*	*	*
SiO_2	48.28	48.56	48.77	49.33	49.02	49.71	51.57	51.86	44.19	41.27	46.92	49.09	52.84	53.76	53.08	47.59	54.02	53.91	53.56	53.56	53.22	51.42	48.20	49.79
TiO_2	0.07	0.08	0.08	0.08	0.08	0.11	0.13	0.19	0.10	0.09	0.15	0.17	0.16	0.23	0.22	0.13	0.28	0.27	0.21	0.22	0.18	0.21	0.00	0.06
Al_2O_3	31.99	30.29	30.55	26.64	25.61	21.30	13.50	5.33	4.34	4.72	6.78	6.95	5.54	4.84	4.15	5.06	4.08	3.24	4.37	4.14	4.87	5.86	32.53	25.45
Fe_2O_3	0.18	0.36	0.33	0.51	0.53	0.85	1.15	1.86	2.20	2.39	2.12	1.98	1.72	1.91	1.90	2.28	2.02	2.13	1.98	2.00	1.98	2.24	0.17	0.65
FeO	0.89	1.84	1.66	2.52	2.67	4.24	5.75	9.30	11.01	11.98	10.57	9.91	8.60	9.54	9.50	11.42	10.10	10.64	9.92	10.02	9.89	11.22	0.87	3.22
MnO	0.00	0.02	0.00	0.03	0.05	0.09	0.12	0.23	0.25	0.18	0.18	0.19	0.21	0.20	0.21	0.25	0.24	0.27	0.27	0.26	0.26	0.24	0.02	0.05
MgO	0.30	1.72	1.11	5.57	6.70	10.75	18.84	26.86	34.96	36.22	28.67	26.90	25.87	25.22	25.73	29.63	25.07	25.18	25.51	25.57	25.04	24.37	0.50	6.46
CaO	15.59	14.74	14.97	13.27	13.11	10.96	7.57	3.79	2.42	2.74	3.86	3.89	4.93	3.24	4.36	3.51	3.06	3.64	3.30	3.34	3.75	3.70	15.37	12.32
Na_2O	2.51	2.22	2.33	1.92	2.00	1.83	1.31	0.52	0.43	0.33	0.63	0.72	0.08	0.81	0.71	0.06	0.51	0.51	0.71	0.71	0.71	0.72	2.20	1.82
K_2O	0.16	0.14	0.14	0.10	0.16	0.11	0.04	0.04	0.08	0.07	0.11	0.15	0.04	0.22	0.11	0.05	0.59	0.15	0.13	0.13	0.09	0.02	0.09	0.11
P_2O_5	0.02	0.03	0.05	0.03	0.06	0.05	0.02	0.02	0.01	0.01	0.02	0.04	0.02	0.03	0.02	0.01	0.03	0.05	0.02	0.05	0.01	0.00	0.05	0.06
Total	100.0	100.0	100.0	100.0	100.0	100.0	100.0	100.0	100.0	100.0	100.0	100.0	100.0	100.0	100.0	100.0	100.0	100.0	100.0	100.0	100.0	100.0	100.0	100.0
MMF	0.3391	0.5856	0.5030	0.7692	0.7914	0.7928	0.8318	0.8135	0.8274	0.8204	0.8037	0.8039	0.8196	0.7997	0.8035	0.7967	0.7894	0.7813	0.7953	0.7941	0.7926	0.7664	0.4655	0.7518
Trace element values (ppm):																								
Sr	459.0	458.0	452.0	388.0	379.0	319.0	177.0	84.0	59.0	61.0	99.0	85.0	76.0	65.0	57.0	68.5	32.0	32.0	42.8	51.0	55.0	69.0	463.0	366.0
Rb	3.0	3.0	2.0	2.0	2.0	3.5	0.6	2.0	1.0	0.0	3.5	2.0	3.0	9.0	5.0	1.0	13.5	6.0	7.1	4.0	0.0	0.6	0.0	0.8
Y	3.5	3.0	2.5	3.0	2.0	3.0	4.0	5.0	3.0	4.0	5.0	4.0	5.0	10.5	9.7	5.0	8.3	9.3	8.0	5.8	6.3	5.2	2.8	2.7
Zr	6.5	8.0	10.0	6.0	5.5	12.5	7.0	10.0	5.0	5.0	13.5	11.0	5.0	22.0	14.5	6.5	55.0	13.0	24.0	15.0	8.0	5.0	0.0	2.0
Co	6.0	10.5	10.5	24.0	26.0	39.0	62.0	112.0	141.0	116.0	125.0	130.0	96.0	97.0	100.0	137.0	106.0	105.0	100.0	100.0	100.0	100.0	5.0	29.0
Cr	18	72	96	618	695	1130	2270	3700	750	1910	4055	4297	3860	3385	3560	3880	4805	3685	7520	3380	3310	14555	455	975
V	13.5	20.0	18.5	30.0	34.0	47.0	78.0	106.0	30.0	35.0	81.0	97.0	123.0	138.0	146.0	95.0	151.0	165.0	180.0	144.0	151.0	251.0	11.0	40.0
Zn	6.0	11.0	11.0	19.0	19.0	28.0	45.0	67.0	68.0	55.0	76.0	ND	74.0	80.0	83.0	64.0	80.0	84.0	85.0	84.0	82.0	98.0	5.0	21.0
Cu	46.0	18.0	15.0	15.0	19.0	15.0	24.0	490.0	41.0	14.0	71.0	24.0	51.0	35.0	40.0	31.0	21.0	30.0	23.0	22.0	24.0	19.0	8.0	14.0
Ni	17.0	27.0	29.0	118.0	137.0	222.0	397.0	1820.0	1720.0	1780.0	1285.0	1540.0	600.0	570.0	575.0	1205.0	805.0	678.0	605.0	588.0	572.0	602.0	8.5	141.0
Sc	6.9	8.2	8.9	10.8	6.6	15.5	23.4	28.8	12.6	9.7	18.2	ND	32.6	32.1	37.3	21.7	33.9	40.5	35.5	35.3	34.5	33.3	5.7	12.4
Ba	64.5	64.0	62.6	53.0	49.0	58.0	54.0	36.5	27.0	22.8	52.0	ND	24.6	82.0	39.0	34.0	111.0	36.0	65.0	34.0	29.7	11.6	53.6	32.5
CIPW weight percent norms.																								
ap	0.05	0.07	0.12	0.07	0.14	0.12	0.05	0.05	0.02	0.02	0.05	0.09	0.05	0.07	0.05	0.02	0.07	0.12	0.05	0.12	0.02	0.00	0.12	0.14
il	0.13	0.15	0.15	0.15	0.15	0.21	0.24	0.36	0.19	0.17	0.28	0.32	0.30	0.43	0.41	0.24	0.53	0.51	0.39	0.41	0.34	0.39	0.00	0.11
or	0.95	0.83	0.83	0.59	0.95	0.65	0.24	0.24	0.47	0.41	0.65	0.89	0.24	1.30	0.65	0.30	3.49	0.89	0.77	0.77	0.53	0.12	0.53	0.65
ab	19.84	18.78	19.71	16.24	16.92	15.48	11.08	4.40	3.64	2.79	5.33	6.09	0.68	6.85	6.01	0.51	4.32	4.32	6.01	6.01	6.01	6.09	18.61	15.40
an	75.55	72.28	72.49	63.78	60.43	49.58	30.84	12.09	9.68	11.19	15.35	15.29	14.64	8.92	7.81	13.39	7.10	6.11	8.35	7.73	9.84	12.70	75.93	60.73
c	0.00	0.00	0.00	0.00	0.00	0.00	0.00	0.00	0.00	0.00	0.00	0.00	0.00	0.00	0.00	0.00	0.00	0.00	0.00	0.00	0.00	0.00	0.99	0.08
mt	0.26	0.52	0.48	0.74	0.77	1.23	1.67	2.70	3.19	3.47	3.07	2.87	2.49	2.77	2.75	3.31	2.93	3.09	2.87	2.90	2.87	3.25	0.25	0.94
dien	0.25	0.15	0.30	0.55	1.27	1.34	2.06	2.02	0.70	0.72	1.11	1.14	2.98	2.10	4.15	1.19	2.36	3.45	2.37	2.56	2.61	1.65	0.00	0.00
difs	0.46	0.11	0.29	0.16	0.34	0.35	0.42	0.47	0.15	0.16	0.28	0.28	0.67	0.53	1.03	0.31	0.64	0.98	0.62	0.68	0.70	0.51	0.00	0.00
diwo	0.69	0.27	0.61	0.78	1.76	1.86	2.75	2.75	0.95	0.98	1.53	1.56	4.05	2.90	5.72	1.65	3.29	4.85	3.29	3.56	3.63	2.36	0.00	0.00
hyen	0.00	3.75	2.46	12.36	9.19	17.14	35.02	50.34	17.69	5.42	27.01	35.62	57.57	55.11	50.38	37.61	57.24	58.07	55.53	55.45	53.32	46.98	1.25	16.09
hyfs	0.00	2.62	2.36	3.68	2.44	4.53	7.18	11.79	3.80	1.21	6.71	8.85	12.96	13.99	12.51	9.86	15.47	16.53	14.64	14.70	14.30	14.60	1.49	5.37
q	0.00	0.00	0.20	0.00	0.00	0.00	0.00	0.00	0.00	0.00	0.00	0.00	0.00	0.00	0.00	0.00	0.00	0.00	0.00	0.00	0.00	0.00	0.84	0.48
fo	0.35	0.27	0.00	0.68	4.37	5.81	6.90	10.19	48.12	58.91	30.33	21.18	2.71	3.92	6.69	24.52	1.98	0.83	3.95	3.97	4.50	8.45	0.00	0.00
fa	0.71	0.21	0.00	0.22	1.28	1.69	1.56	2.63	11.39	14.55	8.31	5.80	0.67	1.10	1.83	7.08	0.59	0.26	1.15	1.16	1.33	2.89	0.00	0.00

WHOLE ROCK DATA TABLE D14: Major element analyses, trace element analyses & CIPW weight % norms - profile UC.
Major element analyses are normalised to 100% and are LOI and H_2O- free.
They are the average of either 2 or 3 determinations on separate discs.
An assumed oxidation ratio of $Fe_2O_3/FeO = 0.1$ is used.
Metres given relative to the base of the Bastard Unit.

	UC																				
Sample	UC-1	UC-2	UC-3	UC-4	UC-5	UC-6	UC-7	UC-8	UC-9	UC-10	UC-11	UC-12	UC-13	UC-14	UC-15	UC-16	UC-17	UC-18	UC-19	UC-20	UC-21	UC-22
Metres	30.8	29.8	28.5	26.5	24.0	22.1	21.5	19.6	17.3	15.9	14.7	13.3	11.1	9.0	7.4	5.3	4.1	2.3	0.6	0.1	-0.2	-0.4
Wt.%																						
SiO_2	50.44	49.89	49.47	49.17	49.54	49.07	49.35	46.38	45.75	46.00	44.16	49.47	45.13	53.66	52.70	54.92	54.34	54.26	55.35	54.79	49.17	48.80
TiO_2	0.10	0.09	0.06	0.08	0.06	0.04	0.04	0.02	0.01	0.03	0.03	0.07	0.05	0.18	0.32	0.16	0.16	0.17	0.20	0.19	0.05	0.04
Al_2O_3	26.08	28.16	29.79	29.52	29.71	30.52	29.56	33.00	32.44	26.74	20.09	17.07	16.82	6.47	8.49	3.59	2.48	5.69	5.16	5.48	30.04	31.32
Fe_2O_3	0.36	0.28	0.20	0.20	0.14	0.09	0.12	0.07	0.09	0.27	0.66	0.63	0.78	0.87	0.92	0.99	1.05	0.98	0.98	1.01	0.15	0.09
FeO	3.64	2.84	2.00	2.03	1.39	0.90	1.17	0.73	0.94	2.74	6.62	6.27	7.81	8.71	9.19	9.90	10.53	9.76	9.83	10.07	1.49	0.90
MnO	0.08	0.06	0.05	0.06	0.03	0.03	0.03	0.02	0.03	0.08	0.11	0.13	0.14	0.21	0.22	0.23	0.24	0.22	0.21	0.22	0.03	0.01
MgO	4.34	2.83	1.83	2.35	2.05	1.22	1.94	1.56	1.93	4.97	15.96	15.78	18.02	22.13	22.19	26.84	27.61	23.78	23.94	23.97	2.63	1.33
CaO	12.71	13.42	14.07	14.14	14.40	15.24	15.17	16.14	16.84	17.54	11.59	9.61	10.48	7.24	5.38	3.16	2.95	4.41	3.91	3.49	14.24	15.68
Na_2O	2.02	2.17	2.30	2.26	2.52	2.61	2.46	1.97	1.85	1.51	0.74	0.90	0.72	0.45	0.49	0.20	0.62	0.63	0.28	0.64	1.85	1.62
K_2O	0.16	0.20	0.18	0.15	0.13	0.11	0.11	0.07	0.04	0.10	0.02	0.01	0.03	0.07	0.03	0.00	0.00	0.03	0.12	0.13	0.28	0.15
P_2O_5	0.07	0.06	0.06	0.05	0.04	0.17	0.05	0.03	0.08	0.03	0.01	0.06	0.03	0.02	0.08	0.02	0.02	0.07	0.03	0.01	0.08	0.06
Total	100.0	100.0	100.0	100.0	100.0	100.0	100.0	100.0	100.0	100.0	100.0	100.0	100.0	100.0	100.0	100.0	100.0	100.0	100.0	100.0	100.0	100.0
MMF	0.6613	0.6194	0.5991	0.6542	0.7067	0.6891	0.7309	0.7778	0.7704	0.7476	0.7976	0.8044	0.7905	0.8059	0.7980	0.8160	0.8109	0.7993	0.7993	0.7956	0.7419	0.7085
Trace element values (ppm).																						
Sr	330.6	357.1	370.6	361.0	362.0	373.1	364.6	426.3	416.7	292.1	221.8	194.4	187.5	77.3	103.6	29.5	21.7	80.6	60.1	58.8	365.0	402.1
Rb	2.7	2.5	3.0	0.0	0.0	0.0	0.0	0.0	2.6	2.6	4.7	0.0	0.0	0.0	0.0	0.0	3.2	3.1	7.2	4.4	5.9	0.0
Y	7.2	8.0	5.4	6.3	2.1	1.6	2.7	2.7	3.0	5.4	0.0	0.0	2.3	10.4	4.9	3.4	3.4	8.0	10.3	6.8	4.6	0.0
Zr	4.9	6.7	3.2	2.0	0.0	0.0	7.1	0.0	1.8	3.0	1.7	2.7	2.2	10.8	6.0	2.3	8.2	7.9	11.3	6.9	4.3	0.0
Co	26.0	18.2	13.7	14.7	11.0	7.6	10.5	7.5	12.4	32.9	61.2	65.3	91.6	74.8	83.9	95.1	101.4	90.0	93.6	94.6	12.6	7.3
Cr	264	137	104	151	109	74	103	94	43	340	1627	1777	1957	3190	2933	3806	3677	2871	2998	3060	524	110
V	51.7	37.3	22.1	32.9	25.3	16.9	25.2	10.1	5.9	29.1	44.9	71.2	57.2	190.3	115.6	127.4	124.5	122.0	128.0	122.6	22.7	12.4
Zn	24.2	35.3	23.3	23.1	16.9	8.9	14.4	12.1	11.4	15.5	37.8	44.2	49.4	78.0	85.4	79.2	88.6	84.5	77.3	77.7	12.5	8.2
Cu	38.8	23.9	6.2	9.5	9.6	15.6	8.2	8.8	10.6	257.8	8.2	12.8	8.2	16.1	28.8	12.4	16.1	102.7	238.9	293.3	174.1	43.6
Ni	34.7	50.8	35.0	41.9	35.5	23.4	30.2	36.1	66.8	129.8	396.2	429.6	725.8	445.8	491.5	615.1	730.0	640.1	881.8	1001.4	146.8	54.5
Sc	10.6	8.0	4.8	7.5	4.2	3.6	4.1	2.2	1.4	4.90	8.1	17.9	9.2	29.9	26.1	29.2	28.4	29.5	29.4	29.1	5.9	3.3
CIPW weight percent norms.																						
ap	0.17	0.14	0.12	0.09	0.40	0.12	0.07	0.19	0.07	0.02	0.14	0.07	0.05	0.19	0.05	0.05	0.17	0.07	0.02	0.19	0.14
il	0.19	0.17	0.11	0.15	0.11	0.08	0.08	0.04	0.02	0.06	0.06	0.13	0.09	0.34	0.60	0.30	0.30	0.32	0.38	0.36	0.09	0.08
or	0.95	1.18	1.06	0.89	0.77	0.65	0.65	0.41	0.24	0.59	0.12	0.06	0.18	0.41	0.18	0.00	0.00	0.18	0.71	0.77	1.65	0.89
ab	17.09	18.36	19.46	19.12	21.32	22.08	20.81	13.82	10.13	5.73	6.26	7.61	6.09	3.81	4.15	1.69	5.25	5.33	2.37	5.41	15.65	13.71
an	61.63	66.19	69.41	69.82	69.38	71.24	69.30	79.88	80.10	65.89	51.44	42.51	42.58	15.43	20.88	8.90	3.98	12.61	12.47	11.70	70.12	77.40
c	0.00	0.12	0.37	0.05	0.00	0.00	0.00	0.41	0.00	0.00	0.00	0.00	0.00	0.00	0.00	0.00	0.00	0.00	0.00	0.00	1.00	0.13
mt	0.52	0.41	0.29	0.29	0.20	0.13	0.17	0.10	0.13	0.39	0.96	0.91	1.13	1.26	1.33	1.44	1.52	1.42	1.42	1.46	0.22	0.13
dien	0.24	0.00	0.00	0.00	0.48	0.84	1.54	0.00	0.83	5.80	1.77	1.42	2.69	6.06	1.56	2.00	3.15	2.60	1.99	1.63	0.00	0.00
difs	0.14	0.00	0.00	0.00	0.22	0.44	0.65	0.00	0.29	2.30	0.52	0.40	0.83	1.69	0.45	0.52	0.85	0.76	0.58	0.49	0.00	0.00
diwo	0.41	0.00	0.00	0.00	0.75	1.36	2.35	0.00	1.22	8.74	2.50	1.99	3.85	8.50	2.21	2.78	4.39	3.68	2.81	2.32	0.00	0.00
hyen	10.57	7.05	4.56	5.85	4.34	0.90	2.41	0.00	0.00	0.00	2.85	27.49	7.74	48.30	51.54	64.84	57.57	56.17	57.63	58.06	6.55	3.31
hyfs	6.23	4.95	3.50	3.55	2.04	0.46	1.02	0.00	0.00	0.00	0.84	7.78	2.39	13.48	14.93	17.01	15.62	16.36	16.73	17.27	2.59	1.53
q	1.88	1.44	1.10	0.17	0.00	0.00	0.00	0.00	0.00	0.00	0.00	0.00	0.00	0.00	0.00	0.49	0.00	0.00	2.86	0.51	1.95	2.69
fo	0.00	0.00	0.00	0.00	0.20	0.91	0.62	2.72	2.78	4.61	24.62	7.28	24.14	0.52	1.51	0.00	5.64	0.32	0.00	0.00	0.00	0.00
fa	0.00	0.00	0.00	0.00	0.10	0.52	0.29	0.99	1.08	2.01	8.03	2.27	8.23	0.16	0.48	0.00	1.69	0.10	0.00	0.00	0.00	0.00

WHOLE ROCK DATA TABLE D14: Major element analyses, trace element analyses & CIPW weight % norms - profile **UC**.
Major element analyses are normalised to 100% and are LOI and H_2O- free.
They are the average of either 2 or 3 determinations on separate discs.
An assumed oxidation ratio of Fe_2O_3/FeO = 0.1 is used.
Metres given relative to the base of the Bastard Unit.

	UC																					
Sample	UC-23	UC-24a	UC-24b	UC-25	UC-26	UC-27	UC-28	UC-29	UC-30	UC-31	UC-32	UC-33	UC-34	UC-35	UC-36	UC-37	UC-38	UC-39	UC-40	UC-41	UC-42	UC-43
Metres	-1.8	-2.5	-2.8	-4.1	-6.6	-8.0	-9.6	-11.6	-13.7	-16.0	-17.7	-19.3	-21.0	-22.4	-23.7	-24.6	-25.6	-26.8	-28.9	-31.1	-33.2	-34.5
Wt.%																						
SiO_2	48.66	48.07	48.99	49.20	49.15	50.36	50.59	49.61	50.12	50.57	51.13	51.39	51.86	52.51	53.92	53.44	48.82	49.28	48.80	49.10	48.58	48.60
TiO_2	0.05	0.05	0.06	0.07	0.06	0.08	0.09	0.07	0.08	0.10	0.11	0.12	0.13	0.19	0.22	0.19	0.05	0.05	0.06	0.06	0.07	0.07
Al_2O_3	31.11	31.31	28.14	27.59	27.33	24.68	23.03	25.63	24.87	19.51	17.56	15.55	13.80	8.48	5.64	5.84	29.81	29.79	30.16	29.51	29.96	29.82
Fe_2O_3	0.09	0.08	0.20	0.24	0.26	0.34	0.38	0.28	0.32	0.52	0.59	0.65	0.70	0.90	1.05	1.02	0.12	0.14	0.11	0.15	0.14	0.16
FeO	0.94	0.81	2.00	2.35	2.62	3.35	3.79	2.78	3.22	5.22	5.89	6.45	6.98	8.98	10.53	10.22	1.21	1.37	1.13	1.48	1.36	1.55
MnO	0.02	0.02	0.04	0.05	0.06	0.06	0.29	0.05	0.06	0.10	0.12	0.14	0.15	0.19	0.23	0.22	0.03	0.02	0.01	0.02	0.03	0.03
MgO	1.71	1.31	3.59	4.31	4.29	6.47	7.72	5.65	6.74	11.52	13.48	15.13	16.86	21.12	23.60	23.42	1.64	2.08	1.80	2.34	2.13	2.27
CaO	15.43	15.68	14.55	13.98	13.84	12.66	12.08	13.47	12.56	10.54	9.61	8.94	8.04	5.99	3.77	4.85	15.29	14.89	15.21	14.85	15.27	15.10
Na_2O	1.79	2.44	2.28	2.06	2.15	1.86	1.91	2.24	1.90	1.82	1.37	1.56	1.37	1.36	0.86	0.72	2.66	2.24	2.52	2.28	2.31	2.17
K_2O	0.15	0.12	0.11	0.12	0.13	0.11	0.09	0.11	0.11	0.08	0.06	0.06	0.07	0.10	0.13	0.05	0.29	0.12	0.16	0.12	0.12	0.20
P_2O_5	0.05	0.11	0.05	0.03	0.11	0.03	0.02	0.09	0.04	0.02	0.07	0.03	0.03	0.18	0.05	0.02	0.08	0.03	0.04	0.08	0.04	0.04
Total	100.0	100.0	100.0	100.0	100.0	100.0	100.0	100.0	100.0	100.0	100.0	100.0	100.0	100.0	100.0	100.0	100.0	100.0	100.0	100.0	100.0	100.0
MMF	0.7473	0.7254	0.7462	0.7497	0.7281	0.7595	0.7689	0.7685	0.7739	0.7830	0.7891	0.7932	0.7978	0.7936	0.7856	0.7892	0.6890	0.7129	0.7231	0.7213	0.7197	0.7055
Trace element values (ppm).																						
Sr	387.7	404.6	358.3	354.0	360.9	320.7	298.6	338.7	326.9	247.7	218.7	191.7	169.2	118.6	73.1	74.5	452.3	463.1	464.9	450.3	455.0	443.7
Rb	3.7	0.0	0.0	2.5	0.0	0.0	2.6	1.5	2.0	2.8	0.0	0.0	0.0	0.0	4.0	2.9	5.4	3.6	0.0	0.0	4.5	6.8
Y	1.9	3.6	4.3	2.9	4.2	7.0	5.0	3.4	3.1	2.8	4.0	3.1	6.0	8.5	8.7	5.0	3.6	2.4	3.0	3.2	2.2	3.6
Zr	2.9	3.0	3.5	5.3	5.2	6.1	5.1	6.0	5.9	5.3	3.9	4.9	5.1	12.5	15.4	7.8	5.5	5.6	5.2	3.2	7.1	5.1
Co	8.6	7.6	17.8	21.1	20.3	29.3	32.9	24.2	30.0	46.7	54.4	59.3	66.0	81.9	96.1	100.7	8.6	10.3	9.5	12.2	10.7	11.2
Cr	151	167	514	524	482	770	976	673	802	1398	1709	1907	2153	2673	3042	3257	69	76	68	116	106	172
V	14.7	13.4	28.7	32.6	25.6	42.3	49.5	36.2	42.5	61.4	74.1	80.1	91.7	120.0	125.7	126.6	17.8	17.1	18.0	22.4	19.5	21.7
Zn	12.9	6.2	19.9	19.7	25.3	26.6	31.5	22.3	25.5	40.9	45.1	47.9	56.5	67.4	84.8	79.3	21.2	10.4	12.1	12.3	12.5	14.0
Cu	53.0	45.1	63.4	54.4	52.9	50.6	47.8	51.6	66.3	72.0	78.6	101.7	118.9	207.6	246.1	493.0	17.1	18.8	16.4	13.1	8.6	18.4
Ni	85.3	75.0	154.4	155.9	135.2	180.3	194.6	172.8	228.2	313.9	377.1	443.9	511.9	711.7	941.4	1358.6	36.5	29.4	24.5	32.5	28.9	33.0
Sc	3.2	3.2	6.4	7.1	7.7	11.3	12.1	8.9	9.9	15.5	18.9	20.0	28.7	22.5	30.4	32.1	6.3	5.5	4.4	5.7	3.8	5.1
CIPW weight percent norms.																						
ap	0.12	0.26	0.12	0.07	0.26	0.07	0.05	0.21	0.09	0.05	0.17	0.07	0.07	0.43	0.12	0.05	0.19	0.07	0.09	0.19	0.09	0.09
il	0.09	0.09	0.11	0.13	0.11	0.15	0.17	0.13	0.15	0.19	0.21	0.23	0.24	0.36	0.41	0.36	0.09	0.09	0.11	0.11	0.13	0.13
or	0.89	0.71	0.65	0.71	0.77	0.65	0.53	0.65	0.65	0.47	0.35	0.35	0.41	0.59	0.77	0.30	1.71	0.71	0.95	0.71	0.71	1.18
ab	15.14	18.80	19.29	17.43	18.19	15.74	16.16	18.95	16.08	15.40	11.59	13.20	11.59	11.51	7.28	6.09	19.74	18.95	20.84	19.29	19.54	18.36
an	76.22	74.13	66.23	65.69	64.54	58.67	54.00	59.56	59.01	44.83	41.59	35.25	31.30	16.74	11.15	12.56	68.55	70.88	70.52	69.94	71.03	71.04
c	0.07	0.00	0.00	0.00	0.00	0.00	0.00	0.00	0.00	0.00	0.00	0.00	0.00	0.00	0.00	0.00	0.00	0.00	0.00	0.00	0.00	0.00
mt	0.13	0.12	0.29	0.35	0.38	0.49	0.55	0.41	0.46	0.75	0.86	0.94	1.01	1.30	1.52	1.48	0.17	0.20	0.16	0.22	0.20	0.23
dien	0.00	0.80	1.57	0.97	0.92	1.11	1.64	1.91	0.87	2.13	1.64	2.61	2.48	3.47	2.10	3.32	1.76	0.75	1.28	0.87	1.21	0.96
difs	0.00	0.34	0.61	0.37	0.40	0.40	0.60	0.66	0.29	0.68	0.51	0.79	0.73	1.04	0.66	1.03	0.90	0.34	0.54	0.38	0.53	0.45
diwo	0.00	1.23	2.35	1.45	1.42	1.65	2.42	2.79	1.27	3.06	2.35	3.72	3.50	4.93	3.02	4.75	2.83	1.17	1.95	1.34	1.86	1.51
hyen	4.26	0.00	3.63	8.07	7.34	15.00	17.19	7.82	15.62	19.52	29.05	27.48	32.84	37.62	52.43	49.77	0.00	4.43	0.00	4.54	1.10	2.61
hyfs	1.61	0.00	1.41	3.08	3.17	5.45	6.29	2.70	5.24	6.25	8.98	8.29	9.63	11.30	16.54	15.38	0.00	2.02	0.00	1.97	0.48	1.23
q	1.47	0.00	0.00	0.00	0.00	0.62	0.00	0.00	0.00	0.00	0.00	0.00	0.00	0.00	0.00	0.00	0.00	0.40	0.00	0.00	0.00	0.00
fo	0.00	1.72	2.62	1.19	1.69	0.00	0.28	3.04	0.20	4.93	2.02	5.32	4.68	8.07	2.97	3.67	1.63	0.00	2.25	0.29	2.10	1.46
fa	0.00	0.80	1.13	0.50	0.81	0.00	0.11	1.16	0.07	1.74	0.69	1.77	1.51	2.67	1.03	1.25	0.92	0.00	1.05	0.14	1.01	0.76

WHOLE ROCK DATA TABLE D14: Major element analyses, trace element analyses & CIPW weight % norms - profile UC.
Major element analyses are normalised to 100% and are LOI and H_2O- free.
They are the average of either 2 or 3 determinations on separate discs.
An assumed oxidation ratio of $Fe_2O_3/FeO = 0.1$ is used.
Metres given relative to the base of the Bastard Unit.

	UC																				
Sample	UC-44	UC-45	UC-46	UC-47	UC-48a	UC-48b	UC-51	UC-52	UC-53	UC-54	UC-55	UC-56	UC-57	UC-58	UC-59	UC-60	UC-61	UC-62	UC-63	UC-65	UC-66a	UC-66b
Metres	-35.9	-37.3	-38.3	-39.4	-41.2	-41.6	-45.0	-46.9	-48.7	-50.2	-52.0	-53.2	-55.3	-57.3	-59.3	-60.8	-62.3	-62.9	-63.4	-65.8	-67.6	-68.1
Wt.%																						
SiO_2	48.25	48.37	48.44	48.44	52.49	48.39	53.85	53.92	54.93	54.72	54.95	55.73	55.15	54.49	54.39	54.12	53.79	49.41	53.08	55.16	53.93	51.77
TiO_2	0.05	0.05	0.04	0.08	0.11	0.08	0.24	0.28	0.24	0.22	0.27	0.26	0.27	0.18	0.22	0.20	0.18	0.12	0.24	0.22	0.23	0.24
Al_2O_3	30.37	29.42	31.03	29.19	12.34	30.84	4.20	2.26	4.85	4.85	3.64	4.23	3.20	5.42	5.63	5.37	5.76	5.15	3.88	3.01	3.99	6.41
Fe_2O_3	0.12	0.16	0.10	0.17	0.74	0.10	1.13	1.19	1.02	1.05	1.05	1.01	1.08	1.00	1.03	1.02	1.01	1.22	1.12	1.16	1.15	1.13
FeO	1.17	1.62	0.96	1.67	7.37	1.02	11.29	11.91	10.19	10.45	10.47	10.06	10.83	9.95	10.30	10.18	10.10	12.21	11.15	11.58	11.49	11.29
MnO	0.03	0.04	0.02	0.04	0.15	0.03	0.24	0.25	0.22	0.22	0.23	0.22	0.23	0.22	0.22	0.22	0.22	0.22	0.23	0.24	0.27	0.25
MgO	2.12	2.92	1.53	2.41	17.53	1.31	24.89	26.09	22.74	23.93	24.24	23.23	25.02	23.42	23.44	23.84	23.93	27.13	25.96	25.54	24.89	24.06
CaO	15.39	14.95	15.33	15.43	7.02	15.57	3.53	3.67	4.72	3.42	4.27	4.31	3.45	4.41	3.77	4.12	4.30	4.07	3.85	2.53	3.33	4.04
Na_2O	2.31	2.29	2.36	2.35	2.15	2.26	0.44	0.26	0.87	0.86	0.64	0.71	0.47	0.83	0.91	0.80	0.64	0.46	0.32	0.36	0.59	0.66
K_2O	0.10	0.12	0.14	0.12	0.06	0.34	0.07	0.11	0.16	0.19	0.22	0.24	0.23	0.08	0.09	0.07	0.07	0.02	0.11	0.14	0.09	0.02
P_2O_5	0.09	0.05	0.05	0.11	0.03	0.06	0.11	0.07	0.06	0.10	0.03	0.01	0.07	0.01	0.00	0.06	0.00	0.00	0.06	0.06	0.06	0.13
Total	100.0	100.0	100.0	100.0	100.0	100.0	100.0	100.0	100.0	100.0	100.0	100.0	100.0	100.0	100.0	100.0	100.0	100.0	100.0	100.0	100.0	100.0
MMF	0.7482	0.7468	0.7228	0.7025	0.7954	0.6777	0.7828	0.7817	0.7848	0.7891	0.7911	0.7906	0.7907	0.7938	0.7881	0.7929	0.7948	0.7842	0.7920	0.7829	0.7797	0.7770
Trace element values (ppm).																						
Sr	462.7	448.0	468.4	455.1	402.7	559.6	45.3	15.8	72.7	67.6	42.6	51.7	28.5	73.6	63.8	70.4	73.6	66.7	39.0	27.8	51.8	73.7
Rb	5.4	3.7	2.1	3.5	0.0	8.6	2.6	3.9	5.3	9.3	10.1	9.3	8.9	3.2	6.1	2.9	3.5	4.6	4.1	9.0	4.0	5.4
Y	2.8	3.1	3.4	2.0	5.2	3.7	7.3	11.0	9.6	7.1	9.0	9.8	10.4	2.7	2.9	5.9	5.0	3.7	7.4	6.6	7.4	2.3
Zr	3.1	2.2	2.1	2.1	5.0	0.0	13.9	14.3	16.2	25.9	27.0	35.3	20.2	9.7	12.1	11.4	13.5	6.5	20.8	11.4	12.1	8.3
Co	10.2	14.5	11.6	11.6	17.4	7.8	95.6	101.7	89.8	92.7	92.3	92.4	95.8	90.7	91.4	90.2	99.6	127.1	102.7	100.9	97.8	98.9
Cr	239	441	132	212	525	537	3745	2883	3330	3243	3393	3449	3450	3421	3527	3808	4885	4063	5694	3965	5578	22393
V	14.5	20.4	12.3	15.2	30.3	25.1	131.3	147.3	135.0	127.1	149.4	145.6	152.8	128.7	134.6	132.1	118.4	92.3	144.2	137.6	146.4	289.5
Zn	15.2	12.4	9.5	12.6	19.8	27.7	89.6	105.6	85.4	84.4	66.1	83.8	80.4	78.8	81.9	79.1	79.3	77.7	79.3	95.1	90.8	104.1
Cu	15.4	16.7	13.9	16.3	12.2	30.6	50.0	98.9	29.4	40.4	35.5	42.5	30.6	31.9	33.0	32.6	28.7	33.3	44.8	11.9	24.3	22.2
Ni	37.7	58.8	27.6	51.4	101.6	47.1	630.5	814.6	560.1	553.6	579.9	573.8	596.0	561.5	562.6	535.2	767.0	1218.1	786.7	698.7	605.0	581.9
Sc	4.0	4.7	2.9	4.8	8.0	5.2	30.3	35.7	32.7	28.9	35.1	33.4	34.6	30.5	30.6	31.7	28.2	20.7	32.2	32.4	32.7	32.6
CIPW weight percent norms.																						
ap	0.21	0.12	0.12	0.26	0.07	0.14	0.26	0.17	0.14	0.24	0.07	0.02	0.17	0.02	0.00	0.14	0.00	0.00	0.14	0.14	0.14	0.31
il	0.09	0.09	0.08	0.15	0.21	0.15	0.45	0.53	0.45	0.41	0.51	0.49	0.51	0.34	0.41	0.38	0.34	0.23	0.45	0.41	0.43	0.45
or	0.59	0.71	0.83	0.71	0.35	2.01	0.41	0.65	0.95	1.12	1.30	1.42	1.36	0.47	0.53	0.41	0.41	0.12	0.65	0.83	0.53	0.12
ab	19.54	19.38	19.97	19.60	18.19	18.67	3.72	2.20	7.36	7.28	5.41	6.01	3.98	7.02	7.70	6.77	5.41	3.89	2.71	3.05	4.99	5.58
an	72.21	69.65	73.67	68.75	23.85	73.01	9.28	4.68	8.86	8.81	6.41	7.65	5.94	10.83	11.01	10.86	12.64	11.93	8.83	6.18	7.97	14.47
c	0.00	0.00	0.00	0.00	0.00	0.00	0.00	0.00	0.00	0.00	0.00	0.00	0.00	0.00	0.00	0.00	0.00	0.00	0.00	0.00	0.00	0.00
mt	0.17	0.23	0.14	0.25	1.07	0.14	1.64	1.73	1.48	1.52	1.52	1.46	1.57	1.45	1.49	1.48	1.46	1.77	1.62	1.68	1.67	1.64
dien	0.99	1.17	0.56	1.87	3.17	0.99	2.18	3.79	4.12	2.19	4.27	4.00	3.14	3.23	2.25	2.70	2.56	2.40	2.90	1.73	2.36	1.36
difs	0.38	0.46	0.24	0.90	0.95	0.52	0.70	1.22	1.30	0.68	1.30	1.22	0.96	0.97	0.70	0.81	0.76	0.77	0.88	0.56	0.77	0.45
diwo	1.48	1.75	0.86	2.96	4.50	1.61	3.14	5.46	5.92	3.13	6.09	5.71	4.47	4.59	3.21	3.84	3.63	3.45	4.13	2.50	3.41	1.97
hyen	0.13	0.84	0.43	0.00	27.05	0.00	57.80	57.80	52.51	56.13	56.05	53.85	59.17	53.48	53.83	53.48	53.44	36.78	54.25	61.87	55.93	47.01
hyfs	0.05	0.33	0.19	0.00	8.07	0.00	18.52	18.60	16.59	17.31	17.04	16.41	18.03	16.10	16.71	16.16	15.99	11.77	16.44	19.84	18.30	15.60
q	0.00	0.00	0.00	0.00	0.00	0.00	0.00	0.00	0.33	0.00	0.00	1.78	0.72	0.00	0.00	0.00	0.00	0.00	0.00	1.22	0.00	0.00
fo	2.92	3.69	1.97	2.89	9.41	1.59	1.41	2.37	0.00	0.89	0.03	0.00	0.00	1.14	1.61	2.24	2.52	19.89	5.25	0.00	2.59	8.09
fa	1.23	1.59	0.94	1.53	3.09	0.92	0.50	0.84	0.00	0.30	0.01	0.00	0.00	0.38	0.55	0.74	0.83	7.02	1.75	0.00	0.93	2.96

WHOLE ROCK DATA TABLE D14: Major element analyses, trace element analyses & CIPW weight % norms - profile **UC**.
Major element analyses are normalised to 100% and are LOI and H_2O- free.
They are the average of either 2 or 3 determinations on separate discs.
An assumed oxidation ratio of $Fe_2O_3/FeO = 0.1$ is used.
Metres given relative to the base of the Bastard Unit.

	UC																			
Sample	UC-67	UC-68	UC-69	UC-70	UC-71	UC-72	UC-73	UC-74	UC-75a	UC-75b	UC-76	UC-77	UC-78	UC-79	UC-80	UC-81a	UC-81b	UC-82a	UC-82b	UC-84	UC-85
Metres	-70.2	-73.2	-75.8	-78.0	-81.4	-82.6	-83.7	-85.1	-85.8	-86.0	-88.8	-91.3	-92.8	-94.5	-96.0	-97.2	-97.4	-98.6	-98.7	-101.7	-104.6
Wt.%																					
SiO_2	53.71	54.93	54.94	54.06	47.83	47.44	49.52	50.60	49.74	48.79	51.62	49.43	49.28	48.35	47.90	48.29	48.86			51.11	
TiO_2	0.20	0.21	0.22	0.19	0.03	0.04	0.04	0.05	0.04	0.05	0.06	0.04	0.04	0.04	0.03	0.03	0.05			0.08	
Al_2O_3	5.09	3.97	3.58	5.25	31.73	31.37	28.29	23.52	25.96	29.17	20.10	29.42	30.95	31.00	31.70	31.13	28.40			18.97	
Fe_2O_3	1.10	1.10	1.13	1.09	0.11	0.13	0.21	0.35	0.28	0.17	0.47	0.14	0.08	0.06	0.07	0.10	0.21			0.52	
FeO	10.98	10.95	11.26	10.88	1.14	1.30	2.06	3.54	2.77	1.68	4.72	1.42	0.81	0.58	0.74	0.98	2.07			5.24	
MnO	0.23	0.26	0.27	0.24	0.04	0.04	0.05	0.08	0.07	0.04	0.10	0.02	0.01	0.04	0.03	0.03	0.05			0.17	
MgO	22.82	24.24	24.53	23.43	1.04	1.40	3.65	8.20	6.20	2.80	10.78	2.27	0.82	1.26	1.16	1.35	3.67			11.87	
CaO	3.86	3.83	3.65	4.03	14.64	15.15	13.22	11.92	12.81	14.77	10.49	14.88	15.54	15.40	15.79	15.44	14.06			9.92	
Na_2O	1.93	0.49	0.41	0.78	2.19	2.33	2.62	1.63	2.05	2.38	1.63	2.29	2.33	3.16	2.43	2.46	2.42			1.98	
K_2O	0.07	0.02	0.02	0.02	1.22	0.77	0.26	0.06	0.06	0.07	0.03	0.07	0.09	0.06	0.08	0.11	0.13			0.10	
P_2O_5	0.01	0.01	0.00	0.04	0.05	0.04	0.08	0.04	0.03	0.07	0.01	0.01	0.05	0.07	0.06	0.09	0.07			0.06	
Total	100.0	100.0	100.0	100.0	100.0	100.0	100.0	100.0	100.0	100.0	100.0	100.0	100.0	100.0	100.0	100.0	100.0			100.0	
MMF	0.7726	0.7835	0.7808	0.7789	0.5987	0.6376	0.7435	0.7912	0.7856	0.7313	0.7888	0.7237	0.6217	0.7815	0.7196	0.6923	0.7430			0.7875	
Trace element values (ppm).																					
Sr	66.4	58.4	51.1	64.3	438.9	467.6	412.1	343.1	379.0	457.7	287.6	441.6	453.0	466.9	473.0	471.7	424.0	414.2	459.4	278.9	178.3
Rb	0.0	0.0	0.0	3.3	38.2	53.5	13.5	0.0	2.2	0.0	2.3	2.1	2.0	3.8	2.8	3.3	3.0	2.0	2.6	0.0	2.7
Y	7.4	5.6	6.3	6.2	2.0	0.0	0.0	4.4	2.3	2.1	3.3	2.4	3.2	0.0	2.8	3.3	2.7	2.1	0.0	6.1	14.4
Zr	13.3	8.7	10.1	12.7	1.7	2.2	2.5	4.9	3.8	3.5	6.5	3.9	4.3	5.5	5.6	4.5	4.1	4.0	3.9	5.2	8.5
Co	93.2	96.9	98.8	98.1	7.8	12.5	17.0	35.5	25.9	8.3	46.4	14.2	7.2	5.9	5.7	7.3	17.2	18.8	9.2	51.9	71.2
Cr	3272	3378	3354	6511	5206	10494	1165	1287	937	231	1513	248	63	37	38	74	372	420	120	1406	2119
V	129.6	142.4	150.2	164.3	54.5	110.1	38.7	55.3	40.3	19.7	67.5	21.7	13.1	11.5	11.9	14.5	29.1	31.0	15.8	76.8	115.8
Zn	90.7	95.0	94.0	86.0	18.2	26.1	9.3	28.5	21.7	9.8	36.2	13.6	10.0	9.0	8.9	7.1	16.0	18.2	10.9	40.0	57.6
Cu	15.6	15.6	17.4	25.5	7.5	6.4	7.4	10.9	8.7	5.4	11.9	8.0	8.0	9.9	8.8	8.2	12.9	8.7	9.9	12.4	9.0
Ni	538.0	576.6	577.0	598.8	23.2	34.3	84.1	180.5	124.4	76.3	247.3	48.6	15.3	11.5	13.5	18.1	64.8	72.9	28.1	253.5	403.9
Sc	32.4	33.8	34.0	33.0	3.5	3.1	8.3	10.6	9.1	3.9	15.6	5.5	4.2	8.8	4.0	4.4	7.5	7.0	4.9	17.2	22.4
CIPW weight percent norms.																					
ap	0.02	0.02	0.00	0.09	0.12	0.09	0.19	0.09	0.07	0.17	0.02	0.02	0.12	0.17	0.14	0.21	0.17			0.14	
il	0.38	0.39	0.41	0.36	0.06	0.08	0.08	0.09	0.08	0.09	0.11	0.08	0.08	0.08	0.06	0.06	0.09			0.15	
or	0.41	0.12	0.12	0.12	7.21	4.55	1.54	0.35	0.35	0.41	0.18	0.41	0.53	0.35	0.47	0.65	0.77			0.59	
ab	16.33	4.15	3.47	6.60	14.07	13.70	22.17	13.79	17.34	20.14	13.79	19.38	19.71	18.84	18.18	19.92	20.48			16.75	
an	5.02	8.57	7.87	10.77	72.30	72.87	64.67	56.69	61.46	68.71	47.44	69.79	73.73	70.23	75.36	73.58	66.25			42.58	
c	0.00	0.00	0.00	0.00	0.31	0.00	0.00	0.00	0.00	0.00	0.00	0.00	0.00	0.00	0.00	0.00	0.00			0.00	
mt	1.59	1.59	1.64	1.58	0.16	0.19	0.30	0.51	0.41	0.25	0.68	0.20	0.12	0.09	0.10	0.14	0.30			0.75	
dien	4.03	3.01	2.96	2.59	0.00	0.49	0.11	0.64	0.55	1.12	1.32	1.07	0.73	1.65	0.69	0.63	0.84			1.81	
difs	1.37	0.96	0.96	0.85	0.00	0.32	0.04	0.20	0.18	0.47	0.41	0.47	0.49	0.54	0.31	0.32	0.34			0.58	
diwo	5.87	4.33	4.28	3.74	0.00	0.85	0.16	0.91	0.79	1.72	1.89	1.65	1.27	2.39	1.08	1.02	1.27			2.61	
hyen	37.36	57.36	58.13	53.59	0.00	0.00	4.29	19.78	12.60	2.31	25.52	4.58	1.32	0.00	0.00	0.00	2.92			21.04	
hyfs	12.73	18.38	18.93	17.65	0.00	0.00	1.72	6.08	4.02	0.97	7.96	2.00	0.89	0.00	0.00	0.00	1.16			6.68	
q	0.00	1.13	1.25	0.00	0.00	0.00	0.00	0.85	0.00	0.00	0.68	0.33	1.03	0.00	0.00	0.00	0.00			0.00	
fo	10.82	0.00	0.00	1.52	1.81	2.10	3.28	0.00	1.61	2.48	0.00	0.00	0.00	1.04	1.54	1.91	3.77			4.70	
fa	4.06	0.00	0.00	0.55	1.57	1.52	1.45	0.00	0.56	1.15	0.00	0.00	0.00	0.38	0.77	1.08	1.65			1.64	

WHOLE ROCK DATA TABLE D15: Trace element analyses - Bastard Unit profiles **B** and **C** at Amandelbult Section. Apart from Sc, all analyses were done by Mr. B Walters. Metres given above base of Unit.

	B												
Sample	B1	B2	B3	B4	B5	B6	B7	B8	B9	B10	B11	B12	B13
Metres	32.6	31.4	30.4	29.4	28.4	27.4	26.4	25.4	24.4	23.4	22.4	21.4	20.4
Trace element values (ppm)													
Co	22.3	18.7	19.1	16.4	13.3	17.3	14.1	16.1	15.4	12.6	16.1	19.3	19.9
Cr	132	92	115	65	55	79	54	66	73	46	64	94	90
V	40.5	38.6	42.6	33.8	27.0	35.6	29.3	34.4	33.1	23.6	30.1	39.3	32.7
Zn	13.4	16.1	16.6	13.7	14.2	9.0	11.9	15.6	17.2	11.6	15.6	18.0	22.3
Cu	29.6	15.7	21.5	22.3	14.5	12.2	16.5	24.2	19.4	15.7	25.4	42.8	25.9
Ni	106.3	62.5	77.6	57.1	42.0	51.4	42.4	49.7	56.0	37.1	47.8	70.4	69.8
Sc	-	5.8	-	5.0	-	5.8	-	5.6	-	3.9	-	7.1	-

Sample	B14	B15	B16	B17	B18	B19	B20	B21	B22	B23	B24	B25	B26
Metres	19.4	18.5	17.5	16.4	15.4	14.4	13.4	12.4	11.4	10.4	9.4	8.5	7.5
Trace element values (ppm)													
Co	17.6	34.6	46.9	46.5	45.4	43.5	44.4	45.3	45.8	50.6	60.7	58.1	21.4
Cr	127	359	728	760	744	718	690	741	793	912	1177	1104	204
V	28.0	48.8	62.6	61.1	60.2	53.3	50.3	53.5	54.0	55.6	69.0	68.6	30.7
Zn	12.8	27.5	39.3	38.4	37.8	37.4	34.9	34.5	36.2	41.6	48.1	46.9	18.2
Cu	28.7	30.4	27.6	27.3	26.2	30.9	24.5	21.0	17.3	23.6	21.4	23.1	62.6
Ni	75.6	163.9	246.8	255.1	243.9	257.4	249.5	256.7	262.3	297.1	357.3	348.8	149.4
Sc	5.2	-	16.2	-	14.3	-	12.9	-	14.9	-	18.6	-	8.4

							C						
Sample	B27	B28	B29	B30	B31	B32	C1	C2	C3	C4	C5	C6	C7
Metres	6.1	4.6	3.5	2.5	1.4	0.5	23.3	22.4	21.5	20.0	18.5	17.4	16.4
Trace element values (ppm)													
Co	72.6	81.0	92.9	94.8	93.7	101.0	17.0	31.1	17.8	18.0	17.8	20.6	19.3
Cr	1679	2157	2491	2075	2027	2262	82	345	80	85	80	90	73
V	85.4	96.6	119.1	118.1	116.7	115.9	32.2	38.0	39.3	39.7	39.0	39.1	61.1
Zn	55.4	63.7	74.6	76.4	75.3	74.0	19.8	24.0	15.5	15.9	17.1	19.0	20.0
Cu	34.5	35.5	78.0	112.0	207.1	460.9	28.2	71.0	16.4	17.1	26.5	24.4	25.0
Ni	452.6	498.5	848.5	701.7	881.1	1457.4	62.4	234.7	61.7	56.7	72.0	75.4	73.8
Sc	22.6	25.0	31.1	30.4	29.6	28.2	5.2	-	6.1	-	7.5	-	8.4

Sample	C8	C9	C11	C12	C13	C14	C15	C15a	C16	C17	C18	C19	C21
Metres	15.3	14.3	11.8	10.4	9.0	8.1	7.4	6.4	5.4	4.4	3.4	2.3	0.7
Trace element values (ppm)													
Co	19.8	39.5	37.5	44.1	52.3	57.7	54.3	54.8	61.4	79.4	86.9	89.8	94.6
Cr	89	264	554	628	974	1055	1055	1077	1316	1789	2068	1850	1990
V	36.1	66.1	55.4	60.8	66.9	72.9	69.3	68.4	74.5	110.0	118.8	116.8	117.2
Zn	17.0	37.7	38.0	40.5	41.9	44.8	44.8	43.8	124.4	72.0	130.7	85.1	81.3
Cu	19.9	22.8	40.0	37.6	36.5	38.5	36.3	34.1	31.0	50.2	153.4	190.8	285.7
Ni	65.2	153.6	184.2	220.7	292.8	323.5	314.0	326.7	373.0	451.7	719.0	808.3	1033.0
Sc	-	13.3	13.0	-	17.0	-	17.7	-	19.3	29.6	30.4	30.9	29.9

APPENDIX E.

The cyclic unit beneath the UG1 chromitite (UG1FW unit) at RPM Union Section Platinum Mine—Rosetta Stone of the Bushveld Upper Critical Zone?

H. V. EALES, W. J. DE KLERK, A. R. BUTCHER

Department of Geology, Rhodes University, Grahamstown, South Africa

AND

F.J. KRUGER

Bernard Price Institute, University of the Witwatersrand, Johannesburg, South Africa

Abstract

The UG1 Footwall unit is a layered pyroxenite–norite–leuconorite–anorthosite sequence between the Middle Group 4 and Upper Group 1 chromitites of the Upper Critical Zone, and is *c.* 300 m thick at Rustenburg Platinum Mines, Union Section, where it shows an oscillatory fluctuation in whole-rock Mg/(Mg + Fe), Cr/Co, Ni/V and Fe/Ti ratios with stratigraphic height. This permits subdivision into 8 sub-cycles which match a subdivision based on cyclical variations in orthopyroxene and feldspar compositions. Constituent pyroxene grains of pyroxenites, norites and leuconorites alike contain rounded and embayed plagioclase inclusions in abundance. Sr-isotope disequilibrium prevails in some samples between the orthopyroxene and feldspar populations. Chemical and isotopic data support a model of pulsatory injection of limited volumes of a more primitive, mafic liquid into a resident column of depleted residua, from which sodic labradorite and Mg-poor bronzite were crystallizing. The depleted liquid is equated with the supernatant liquid residuum of buried cumulates (Sr_i *c.* 0.7054) and the primitive liquid with magma parental to the UG1–UG2 lineage ($Sr_i \geq 0.7068$). The increase in leucocratic character of the 300 m column, with height, is attributed to the rising of low-density liquids enriched in the components of feldspar during separation of the pyroxenites. Deposition of the UG1 chromitite layers is attributed to mixing of a major influx of primitive liquid with a feldspathic residuum at the top of the UG1 Footwall unit. There is no evidence to indicate the participation of a discrete A-type liquid (Irvine and Sharpe, 1982) in this process.

KEYWORDS: Bushveld complex, magma mixing, chromitite, compositional convection.

Introduction

IN comparison with the Eastern Bushveld Complex, where outcrops of the layered sequence are generally good, the succession in Western Bushveld is not at all well exposed, and, in the case of the Critical Zone, a flat and rather featureless plain veneered by a black turf soil is all that is seen at the surface. Although considerable underground mining activity in the area for the exploitation of the platinum-bearing horizons—Merensky Reef and Upper Group Chromitite Layer 2 (UG2)—has exposed the uppermost parts of the Critical Zone (between the Upper Group Chromitite Layer 1 (UG1) and the Merensky-Bastard Units), relatively little is known about the cumulate sequences below the normal mineable limits, which are only exposed in the tramming and ventilation crosscuts from production shafts.

This paper presents textural and geochemical data pertaining to a suite of samples taken from one such crosscut, which has enabled documentation of a section extending approximately 350 m beneath the UG1 chromitites—including the

Mineralogical Magazine, March 1990, Vol. 54, pp. 23–43

so-called UG1 Footwall Unit (UG1FW)—in the Rustenburg Platinum Mines (R.P.M.) Union Section area, north-western Bushveld Complex. The aim is to build on the existing data base for the Upper Critical Zone and to provide further evidence and support for a model already proposed by Eales *et al.*, (1986, 1988). In this model it is argued that geochemical differences between successive units represent evidence for repeated injections of fresh, primitive magma into a column of partially depleted liquid resident above the crystalline floor of the chamber. The more mafic rocks, constituting the lower parts of cyclic units, are taken to have crystallized from such new inputs of liquid, whereas the more evolved or more leucocratic upper members have crystallized from hybrid liquids resulting from the mixing of the old and the new magmas.

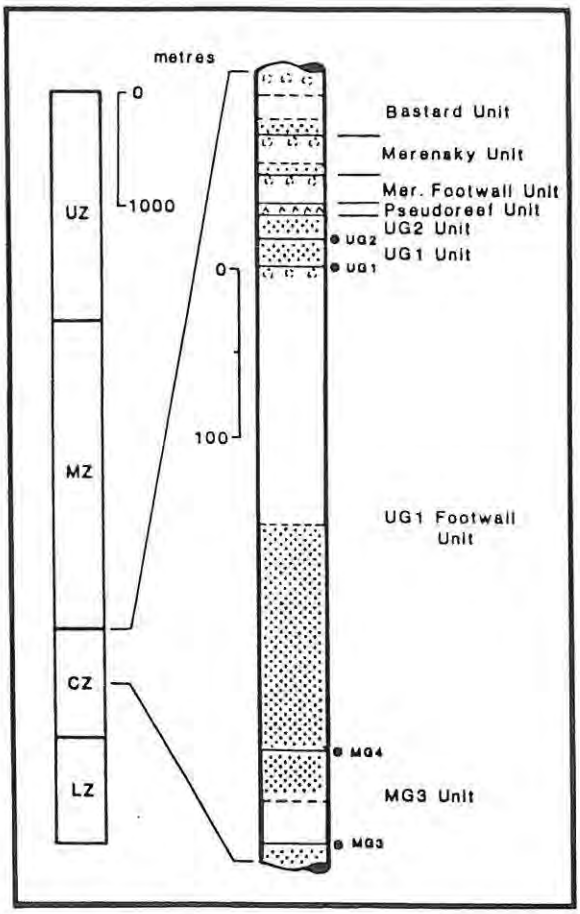

FIG. 1. Generalised stratigraphic succession through Western Bushveld with detail for the Upper Critical Zone at Union Section. Significant chromitite layers at bases of units are indicated by filled circles. Stipple—pyroxenites; unshaded—norites and leuconorites; circles—anorthosites; cone ornament—harzburgite. LZ—Lower Zone; CZ—Critical Zone; MZ—Main Zone; UZ—Upper Zone.

The stratigraphic succession

The Bushveld Complex is broadly divisible into Marginal, Lower, Critical, Main and Upper Zones, the combined thickness of which is some 7000 m in the Western limb. The first appearance of cumulus plagioclase feldspar within the column is used to segregate the ultramafic dunites, harzburgites, pyroxenites and chromitites of the Lower Critical and Lower Zones from rocks of the Upper Critical Zone (harzburgites, pyroxenites, norites, chromitites and minor anorthosites), the Main Zone (gabbronorites and anorthosites) and the Upper Zone (magnetite gabbros, magnetites, and evolved gabbros containing fayalitic olivine and cumulus apatite).

Detailed descriptions of the succession through the Upper Critical Zone in the northwestern part of the complex are available in the literature (Eales, 1987; Eales, *et al.*, 1986, 1988; Viljoen *et al.*, 1986*a,b*), and no more than a summary is necessary here (see Fig. 1). The Bastard and Merensky Units are ostensibly 'complete' cyclic units, comprising ultramafic members (feldspathic pyroxenites, with or without accompanying feldspathic harzburgites) at the base, grading upwards through melanorites, norites and leuconorites to anorthosites at the top. Plagioclase is of intercumulus habit within the ultramafic members, but adopts cumulus habits and becomes more calcic within and above the melanorites of each unit. The Merensky Footwall Unit forms the floor upon which the economically important, P.G.M.-enriched Merensky Reef rests, and may be characterized as a largely leucocratic sequence with trivial development of an ultramafic facies at its base. The Pseudoreef Multicyclic Unit beneath the Footwall Unit is largely an association of leuconorites and norites with feldspathic harzburgites (the Pseudoreefs), and is well developed at Amandelbult Section, but reduced to no more than two harzburgite layers at Union Section. The underlying UG2 and UG1 units are composed essentially of feldspathic pyroxenites floored by well developed chromitite layers up to 1 m thick.

The contact between the UG1 and the underlying UG1FW Unit is one of the more spectacular features of the Complex. In some parts of Union Section mine, an upper chromitite layer (50–60 cm thick) is separated from a lower layer (*c.* 30 cm) by *c.* 30 cm of pyroxenite, and this package rests concordantly upon snowy-white anorthosite constituting the top of the UG1FW unit. Elsewhere, the contact shows the same complexities as

are displayed at the well-known Dwars River exposures in the Eastern Bushveld Complex (Figs 196–201, Wager and Brown, 1968). An upper group of regular chromitite layers overlies 3–4 m of anorthosite within which thin chromitite layers (commonly 1–200 mm thick) converge and diverge to yield an anastomosing system. This may in turn give way to an irregular system of contorted, discontinuous stringers, lenses and pods of chromitite. Lenticular chromitite pods with an oblate-spheroid shape, and diameters up to 0.5 m, appear to have subsided within the anorthosite, depressing and disrupting the layering beneath and around the pods (Fig. 2*a*). These structures have been variously attributed to intrusion into the anorthosite of a chromitite-bearing residual magma (Sampson, 1932), intrusion of anorthosite into chromitite (Coertze, 1958), deposition of chromitite accompanied by turbulent mixing with plagioclase crystals (Vermaak, 1976), and emplacement of a chromitite mush as a result of fracturing (Cameron, 1964) or a process akin to that which produces sandstone dykes and sills in sediments (Lee, 1981).

The upper half of the UG1FW unit comprises a leucocratic suite. An upper layer of chromitiferous anorthosite (2–3 m thick) rests upon *c.* 5 m of what is locally known as the 'Streaky Norite', displaying mm-scale layering (Fig. 2*a*). Beneath this is a second couplet of Cr-poor anorthosite and leuconorite resting upon *c.* 130 m of norite alternating with leuconorite and minor pyroxenite. This grades downwards, via some 20 m of pyroxenite alternating with melanorite to a 115 m pyroxenite member floored by the MG4 chromitite. The total thickness of this unit (*c.* 285 m) is thus appreciably greater than that of other cyclic units in the northwestern exposures of the Upper Critical Zone, such as the Merensky and Bastard Units (20–30 m; Eales *et al.*, 1986, 1988). Justification for treating it as a single unit lies in (i) correspondence with the sequence chromitite–pyroxenite–melanorite–norite–leuconorite–anorthosite, characterising cyclic units elsewhere, and (ii) internal coherence of geochemical parameters (described later) which distinguish it from units above and below.

Between the MG4 and MG3 chromitites, the sequence is essentially an upward gradation from norite to pyroxenite, followed by an abrupt transition to anorthosite within the uppermost 1.5 m constituting the immediate footwall to the MG4 chromitite. A similar transition occurs immediately beneath the MG3 chromitite.

Some of the field characteristics of this sequence are implicit in the variations in whole-rock Al_2O_3 and normative minerals shown in Fig. 3. These are (i) the existence of a continuum of compositions between pyroxenite and anorthosite, but with a dominance of pyroxenites (<6.5% Al_2O_3) and norites (11–21% Al_2O_3), (ii) gradations from one horizon to another, as from pyroxenite to norite (160 m to 130 m), pyroxenite to leuconorite (125 m to 94 m) and melanorite to anorthosite (57 m to 8 m), and (iii) gradual but sustained increases in proportions of pyroxenes with stratigraphic height within parts of the sequence, as between 330 m (norite) and 300 m (pyroxenite), or 94 m (leuconorite) and 57 m (melanorite).

Petrography of the UG1 Footwall Unit

The UG1 Footwall Unit comprises orthopyroxene, plagioclase feldspar, clinopyroxene, chromite and magnesian biotite in various modal proportions. Following Eales *et al.* (1986) rocks with <6.5% Al_2O_3 and intercumulus feldspar only are termed pyroxenites; melanorites fall within the range 6.5–11% Al_2O_3, norites 11–21%, and leuconorites 21–28%. In pyroxenites, poikilitic clinopyroxene may form oikocrysts up to 0.5 cm in diameter, enclosing all older phases. Within norites, clinopyroxene may rim orthopyroxene and be optically continuous with exsolved blebs within the latter. Mica is invariably interstitial. Chromite is a rare accessory phase, in contrast with its ubiquitous occurrence in the overlying UG1, UG2, Merensky Footwall and Merensky Units. Only between 210 m and 250 m, and immediately above the MG4 chromite, are traces (*c.* 0.1%) of this phase found.

Grain-size indices plotted in Fig. 3 represent the mean value of the longer intercept of 30–60 orthopyroxene grains intersected, on a rectilinear grid, in each thin section. There is no obvious orientation of grains within the samples examined. A range of 0.63–2.65 mm is displayed. The rocks of finest grain size (0.6–1.25 mm) are pyroxenite adcumulates with well developed 120° triple junctions and low feldspar contents. The overlying noritic rocks are distinctly coarser (1.15–2.65 mm) with poorly developed crystal shapes—at best, a minority of grains are subhedral.

The uppermost 20 m of the unit includes leuconorites and anorthosites. Cumulus orthopyroxene is macroscopically visible in leuconorites ('spotted anorthosites') but true anorthosites with >28% Al_2O_3 bear only trivial amounts of intercumulus pyroxene. A poikilitic habit adopted by pyroxene yields 'mottled anorthosite'. Grain size of these rocks is normally 0.5–3 mm, and preferred orientation of feldspar laths, parallel to the layering, may be adopted.

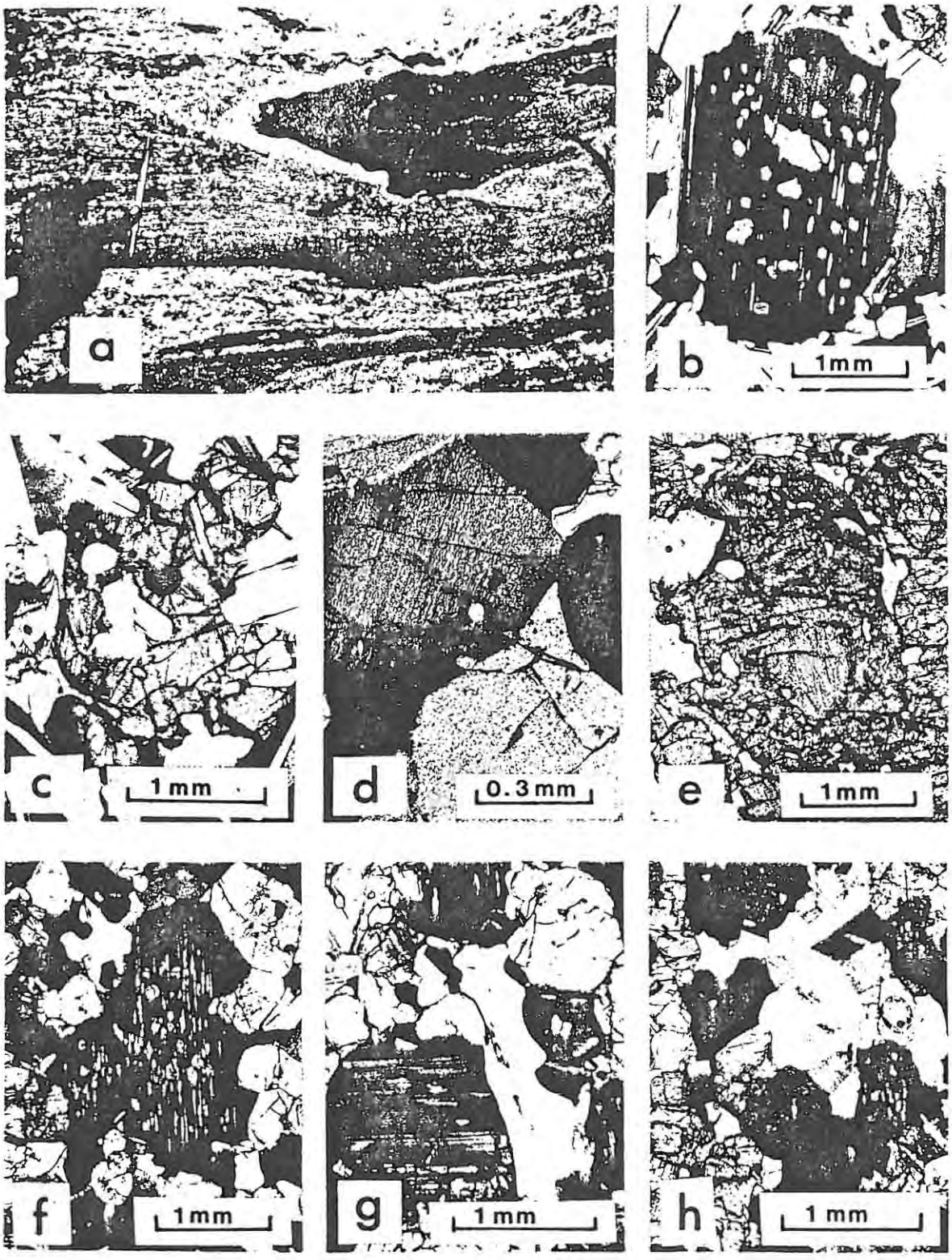
a
b
1mm
c
1mm
d
0.3mm
e
1mm
f
1mm
g
1mm
h
1mm

A significant and distinctive feature of the sampled section of the UG1FW unit is the abundance of small plagioclase inclusions within pyroxenes of norites (Fig. 2 *b–c*) and pyroxenites (Fig. 2 *d–f*) alike. These inclusions are commonly 0.02–0.25 mm in diameter, and spheroidal, ovoid or irregularly embayed. Some form clusters. Their frequency is variable, up to 20 particles being quite commonly seen per host grain, but no sample is free of them. Their distribution and orientation are random within their hosts. Their shapes are wholly atypical of cumulus plagioclase within noritic rocks, and the intergrowth is in no sense comparable with ophitic texture or of the fabric adopted by intercumulus pyroxenes within anorthosites. A further variety of plagioclase occurs as sparse laths up to 1.5 mm in length (Fig. 2*g*) or clusters up to 2.5 mm (Fig. 2*h*) embedded in some pyroxenites. Isotopic evidence, presented later, establishes beyond question that these are xenocrysts. In summary, therefore, these pyroxenites are characterised by the presence of intragranular, intergranular, and intercumulus varieties of plagioclase. We interpret the texture as unequivocal evidence for nucleation of pyroxenes within melts containing partially resorbed, earlier-generation feldspar. In the case of norites, plagioclase occurs both as partially resorbed inclusions within orthopyroxene host grains, and as a cumulus phase.

Mineral compositions of feldspars and pyroxenes in the UG1FW unit

Plagioclase feldspar. Microprobe analyses of the cores of 407 feldspar grains, summarized in Fig. 4, show that the range of composition is An_{57-85}. Neither the spheroidal inclusions within orthopyroxene nor grains surrounding pyroxenes constitute a discrete, identifiable population, but some bias is shown insofar as in 20 samples out of 25 (Fig. 4) the more sodic average compositions are yielded by the inclusions. It is also evident that inclusions and non-included feldspar do not vary independently in composition—samples with notably sodic inclusions show the surrounding grains shifted also to more sodic compositions.

The statement of Eales *et al.* (1986, 1988) that feldspar of anorthosites and norites at the tops of cyclic units are more calcic than both cumulus and intercumulus species in underlying rocks, is equally valid here (see Fig. 5). Mean compositions of feldspar cores are $An_{76.5-78.5}$ within the uppermost 25 m of the unit, and $An_{73.5-75.6}$ within underlying norites. Intercumulus grains of pyroxenites are commonly a further 5–10% richer in *ab* molecule.

Fig. 5 displays the compositional trends followed, respectively, by plagioclase included by, and that external to, orthopyroxene. The sympathetic variation established in Fig. 4 is seen to be followed at all stratigraphic levels, and a clear cyclicity is apparent. Within pyroxenites, subcycles show an upward decline of anorthite content, but above the level where cumulus feldspar enters the paragenesis (at 150 m) the trends followed by felsic and mafic phases vary sympathetically. A narrow outer rim may encircle each inclusion. At the base of cycles, where feldspars are calcic, this rim displays reversed zoning, but where more sodic compositions dominate at higher levels, zoning is either of normal type, or absent.

The origin of the inclusions is of critical importance in interpreting the UG1FW unit. The following possibilities exist: (*a*) inclusions are the crystallization products of a paragenetic sequence inverted by spatial shifts of primary phase volumes, under the influence of pressure, f_{O2} or concentration of volatiles, (*b*) inclusions represent feldspar nucleated within a bottom layer enriched in the components of feldspar, following on *in situ* bottom growth of pyroxenites upon the floor, (*c*) inclusions represent undigested remnants of fragmented or eroded, older, anorthositic or noritic layers, or (*d*) inclusions depict partial crystallization of residual melts saturated in feldspar, prior to their re-heating and mixing with later pulses of more primitive, mafic liquid.

FIG. 2. (*a*) Chromitite pod (black, upper right) fringed by anorthosite (white) disrupting and truncating cm-scale layering of uppermost norite in footwall of UG1 chromitite layer in Union Section Mine. (*b*) Bronzite grain hosting numerous ovoid and embayed plagioclase inclusions in leuconorite (Sample S-16). Vertical streaks are exsolved clinopyroxene. (*c*) Bronzite grain in norite (S-27) where feldspar inclusions retain vestiges of lath shapes, typical of upper parts of sub-cycles. (*d*) Pyroxenite adcumulate (S-43) showing advanced resorption of relict plagioclase feldspar. Inclusions are small and, in adcumulates, single inclusions may indent two contiguous bronzite grains. (*e*) Unusual type of zoned bronzite grain with clear core surrounded by mantle containing *c.* 80 partially resorbed feldspar inclusions of various sizes (pyroxenite S-37; 1 nicol). (*f*) Orthocumulus pyroxenite showing typical high density of plagioclase inclusions and exsolved clinopyroxene lamellae in core of bronzite grains, surrounded by clear mantle devoid of inclusions (S-41). (*g*) Pyroxenite (S-40) enclosing cumulus feldspar crystal (white, vertical orientation, right side of frame) and (*h*) cluster of cumulus feldspar grains (centre to upper right) yielding Sr-isotope signatures different to each other and to pyroxene fraction.

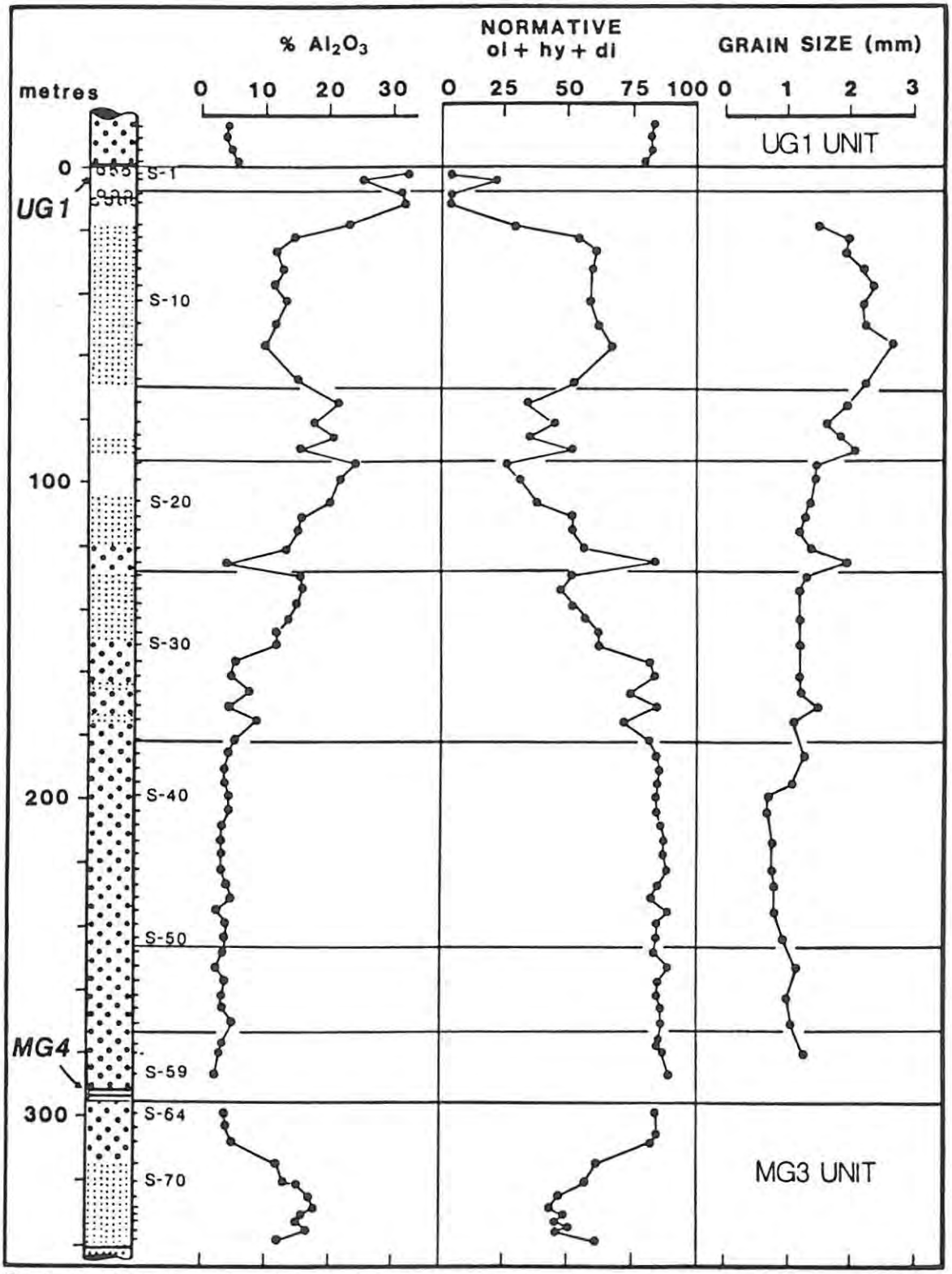

FIG. 3. Variations in wt.% Al_2O_3, normative *ol + hy + di*, and grain size of orthopyroxene through the MG3, UG1FW and base of UG1 units. Coarse stipple—pyroxenites; fine stipple—norites; unshaded—leuconorites; circles—anorthosites; heavy lines—chromitites. Sample positions are shown as S-1 to S-77. Subdivisions of UG1FW unit are based on data presented later (see Fig. 5).

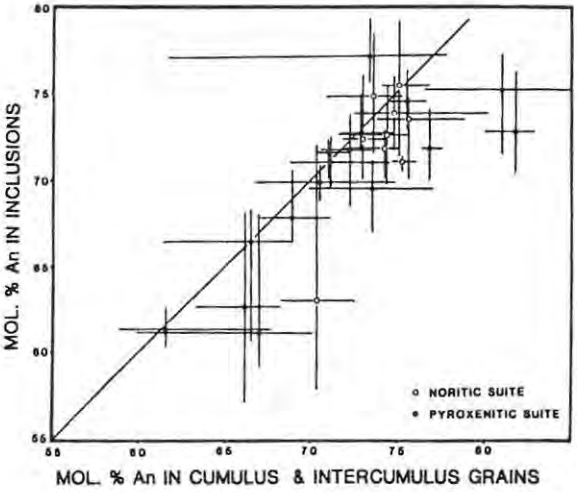

FIG. 4. Compositions (by microprobe analysis) of cores of partially resorbed plagioclase inclusions within orthopyroxene hosts, plotted against compositions of intercumulus and cumulus plagioclase grains in same sample. Bars represent apparent range in composition.

Alternatives (*a*) and (*b*) above ignore the variations in Sr-isotope data (described later) which argue against the texture arising merely out of aberrations in the crystallization of single liquids. Alternatives (*c*) and (*d*) are acceptable *prima facie* models, as they would accommodate the isotopic data, the rounded or embayed habit of the inclusions, and their encapsulation by orthopyroxenes. Inherent properties of the feldspar lattice render volume diffusion and compositional readjustment sluggish processes (Smith, 1974), but optimum conditions for the modification of grain compositions would be yielded by the small size of the inclusions, and super-liquidus conditions implied by resorption. Consequently, the present composition of the inclusions is probably not definitive of provenance, and the sympathetic variations in composition of feldspar inclusions and intercumulus feldspars are attributed to reaction between the inclusions and surrounding liquid.

Orthopyroxenes. 403 microprobe analyses show (Fig. 5) that orthopyroxenes of the UG1FW Unit do not follow the normal evolutionary sequence of magnesian species at the base of a unit giving way to Fe-enriched species towards the top (Eales *et al.*, 1986, 1988). The pattern is one of cyclical variations between a minimum $Mg/(Mg+Fe^2)$ atomic ratio (hereafter abbreviated to MMF ratio) of 0.783 and a maximum value of *c.*0.83. The mean MMF ratio in norites is 0.800 ± 0.007, and 0.794 ± 0.007 in the underlying pyroxenites. Zonal decline in MMF ratios towards crystal margins is muted in norites, never exceeding 1%; significant reversed zoning is absent in norites but not uncommon in pyroxenites. Cr_2O_3 levels in orthopyroxene (Fig. 5) increase from 0.25% at the 180 m level to 0.43% near the top of the norite column. The average in noritic pyroxenes is $0.347 \pm 0.043\%$, and $0.310 \pm 0.028\%$ in pyroxenites. Zonal decline in Cr towards crystal margins is evident in most cases. Absolute Cr-depletion, upward increase in MMF ratios and Cr levels, and good correspondence between MMF ratios and Cr levels in orthopyroxenes thus characterise the major part of the unit.

Fig. 6 shows a plot of Cr_2O_3 against MMF ratios for all samples of the UG1FW unit, together with data points for the Upper Group Chromitite 2 (UG2) pyroxenite and a section above the Lower Group Chromitite Layer 6 (LG6) for which abundant microprobe data are presently available. No discontinuity in trend is apparent. Irrespective of whether the trend is due to fractionation, or crystallization from hybridized liquids, Figs. 5–6 emphasize the anomalous increase in both Cr and Mg through the norites, towards the top of the unit.

A significant drop in MMF ratio to 0.62 and Cr_2O_3 levels averaging 0.02% occurs within the first anorthosite capping the noritic sequence (sub-cycle 7, Fig. 5). This follows the trends typifying anorthosites of the Merensky Footwall, Merensky and Bastard Units (Eales *et al,* 1986). The uppermost leuconorite–anorthosite couplet is, however, remarkable in that MMF ratios are uniquely high (0.82 and 0.85, respectively; see Fig. 5) while Cr_2O_3 in orthopyroxene exceeds 0.5% in the leuconorite and 0.25% in the anorthosite. The uppermost leuconorite is thus anomalously Cr-rich but contains no accessory chromite; the overlying anorthosite contains chromite as a major modal phase. We suggest that this is a contamination effect heralding the development of the overlying Cr-rich UG1 unit.

Whole-rock chemical data

All samples shown in Figs. 3 and 5 have been analysed for major and eleven trace elements. Representative data are presented in Table 1. Whole-rock Al_2O_3 levels (Fig. 3) provide a measure of normative plagioclase in norites and pyroxenites, where $or + ab + an = 3.03\ Al_2O_3 + 0.73$ (correlation coefficient 0.9996, $n = 56$ samples) but over-estimate normative plagioclase in anorthosites where feldspars are more anorthitic. The ratios MMF, Ni/V, Cr/Co and FeO/TiO_2 plotted in Fig. 5 utilise a dividend of higher, and divisor of lower, bulk distribution coefficient and

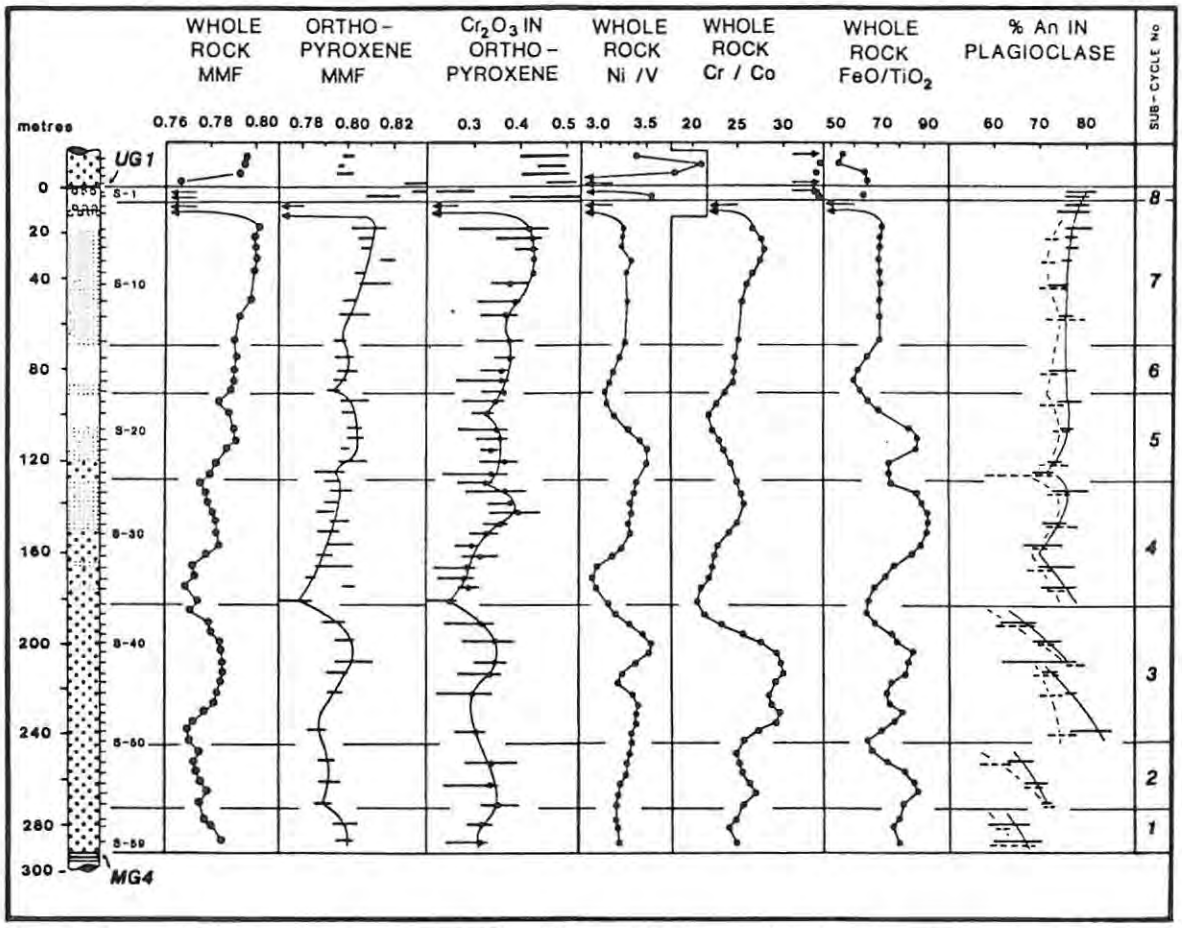

FIG. 5. Compositional trends through UG1FW and base of UG1 units. Whole-rock data smoothed in part by employing three-point moving averages. Bars indicate range of compositions found by microprobe analysis of orthopyroxenes (cores and margins; 403 analyses) and plagioclase feldspars (cores only; 407 analyses). Standard deviation yielded by multiple analyses of single grains was 0.30% An for plagioclase, and 0.002 and 0.019% for MMF and Cr_2O_3, respectively, in orthopyroxene. Filled circles on bars indicate average Cr_2O_3 levels in orthopyroxene cores. For plagioclase, solid bars indicate cumulus and intercumulus grains; dashed bars indicate partially resorbed inclusions. Arrows indicate data points off scale.

accordingly measure the chemical 'primitiveness' of the rock.

The sequence extending for 350 m beneath the UG1 chromitite displays the following features. (*a*) The most evolved rock in terms of MMF ratios is the lower of the two anorthosites within the uppermost 20 m but this ratio is decoupled from feldspar compositions, insofar as the most calcic plagioclase occurs in anorthosites. (*b*) There is no simple trend of cryptic variations within the column beneath the anorthosite roof. The highest (most primitive) MMF ratios are encountered immediately beneath the leucocratic roof, and the lowest at 50 m and 120 m above the MG4 chromitite. (*c*) Variations in Al_2O_3 show that total feldspar may either increase (160–130 m; 125–94 m; 57–0 m in Fig. 2) or decrease (335–30 m; 94–57 m) with height within the section. (*d*) Chemical trends through the Footwall, Merensky and Bastard Units in the northwestern limb of the complex display a saw-tooth pattern (Eales *et al.*, 1986, 1988) because rocks with primitive chemical signatures at the base of units abruptly overlie more evolved rocks at the top of previous cycles. No such pattern exists within the sub-cycles of the UG1FW unit; it is, rather, one of superimposed partial or complete sub-cycles showing a gradual increase in primitive character, followed by gradual decline. Eight such sub-cycles are identified in Figs 2 and 5. Sub-cycles 2–5 are ostensibly complete, with the rise and fall in MMF ratios (whole-rock and microprobe data) being matched to varying degrees of perfection by trends in Ni/V, Cr/Co and FeO/TiO_2 ratios, and Cr_2O_3 levels in

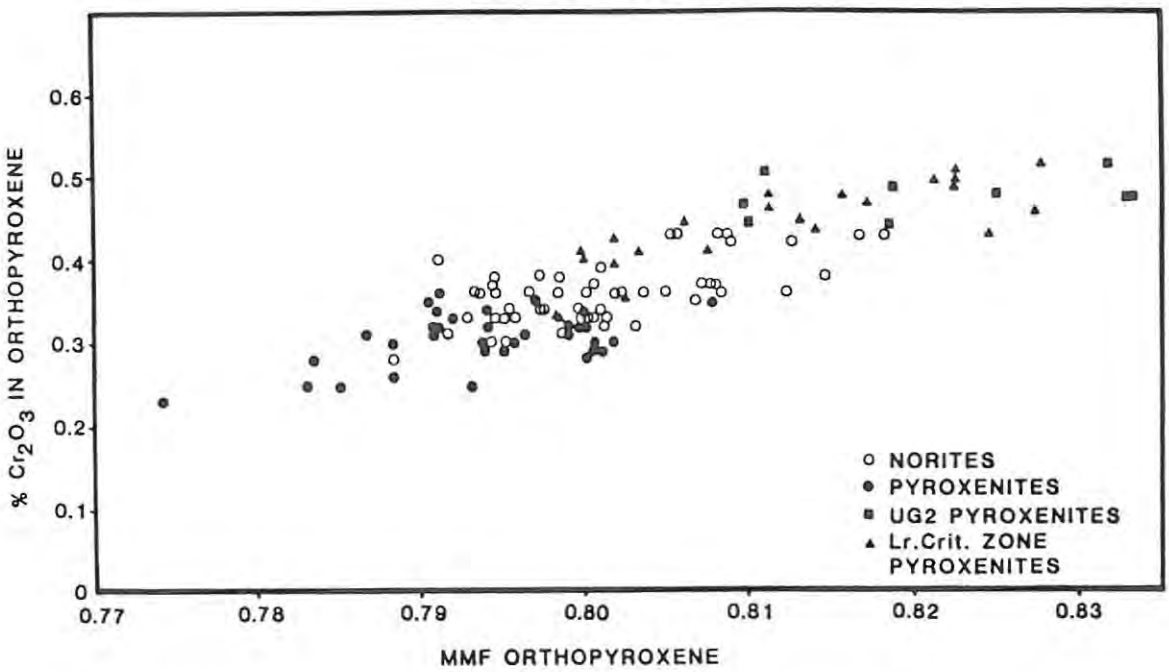

FIG. 6. Cr_2O_3 levels in orthopyroxenes at Union Section, based on averages compiled for UG1FW unit (403 analyses), UG2 unit (220 analyses) and 80 m section above LG6 chromitite of Lower Critical Zone (93 analyses by B. Teigler).

orthopyroxene. This subdivision of the UG1FW unit conforms with that indicated by cyclic variations in feldspar compositions described earlier, but Ni/V, Cr/Co and FeO/TiO_2 ratios, and feldspar data, suggest that sub-cycle 3 is composite. (*e*) Justification for treating the entire sequence between the MG4 and UG1 chromitites as a single unit, despite its great thickness of 285 m, is provided in Fig. 7. Here, the plotting of Sr against V yields a single regression line (Sr = 483.5–2.604 V; corr. coeff. = −0.995; n = 54 samples) which is significantly different to that for samples between the MG3 and MG4 chromitites (Sr = 443–2.743 V). As similar plots of Sr against Al_2O_3 fail to segregate these populations, it is clear that the discrete regression lines in Fig. 7 arise out of relative V-depletion below the MG4 chromitite. Marked inflections in trends of Ni/V and Cr/Co ratios also occur across the MG4 chromitite horizon.

Sr-isotope data

Variations of unexpected magnitude in $^{87}Sr/^{86}Sr$ initial (Sr_i) ratios of four samples were established during an early, exploratory survey, and this led to completion of a further 34 determinations. All results are given in Table 2, incorporating whole-rock and mineral-separate data.

Fig. 8 shows the frequency distribution of Sr_i ratios within the full range from 0.7056 to 0.7075; 60% of values lie between 0.7058 and 0.7064. There is no clear distinction between values for pyroxenites and members of the noritic suite (the subsidiary peak at 0.7070–0.7075 is yielded by five determinations of the isotopically discrete sample S-40). The data are also plotted in Fig. 9 against stratigraphic height, together with unpublished data for the Lower Critical zone and the MG3, UG1 and UG2 units, and published data for the Footwall, Merensky and Bastard units (Eales *et al.*, 1986; Kruger, 1988). Variations with stratigraphic height are seen to approximate a trend of regular increase through the noritic suite, but to follow a non-systematic and unpredictable pattern in the pyroxenites.

Where whole-rock and mineral-separate determinations are available, agreement is good in some samples (S-38 and S-43) but significantly different in others (S-40 and S-49). Results for sample S-40 are instructive. This is a bronzitite, with patchy development of adcumulus texture, analysing 4.4% Al_2O_3 (14% normative plagioclase). Bronzite grains bear spheroidal and embayed feldspar inclusions in the size range 20–125 μm,

TABLE 1 Representative Analyses of Rocks in UG1FW Unit

	1	2	3	4	5	6
SiO_2	54.56	54.36	52.68	52.06	50.67	49.28
TiO_2	0.14	0.16	0.11	0.08	0.05	0.03
Al_2O_3	3.52	3.57	11.75	14.81	23.09	31.81
Fe_2O_3	1.14	1.20	0.78	0.72	0.37	0.08
FeO	11.39	12.00	7.77	7.21	3.67	0.81
MnO	0.25	0.29	0.17	0.16	0.07	0.02
MgO	25.40	24.82	19.14	15.27	8.64	0.83
CaO	3.23	3.18	6.31	8.17	11.57	14.83
Na_2O	0.35	0.38	1.14	1.46	1.79	2.19
K_2O	tr.	0.03	0.13	0.05	0.08	0.11
P_2O_5	0.02	0.01	0.02	0.01	tr.	0.01
Rb	<1	1.9	1.2	1.9	<1	1.7
Sr	41	40	178	223	336	468
Y	3.4	4.7	3.0	2.9	<1	<1
Zr	3.2	7.5	5.6	3.2	<1	<1
Co	105	106	75	64	36	7
Cr	3030	2820	2005	1665	957	48
V	175	173	118	101	54	11
Sc	34	34	23	22	11	9
Ni	572	569	404	339	175	14
Cu	11	15	12	12	11	8
Zn	90	100	62	56	28	11

1. Average of 5 more primitive pyroxenites (S41 - S45).
2. Average of 6 less primitive pyroxenites (S48 - S53).
3. Average of 6 norites near top of unit (S7 - S12).
4. Average of 4 norites at base of noritic suite (S25 - S28).
5. Leuconorite, 18m below top of unit (S5).
6. Average of 2 anorthosites, 8 - 12 m below top of unit (S3-S4).

Major-element data normalised to 100%, L.O.I.- and H_2O-free. Ratio Fe_2O_3/FeO of 0.1 assumed. Trace-element data in ppm.

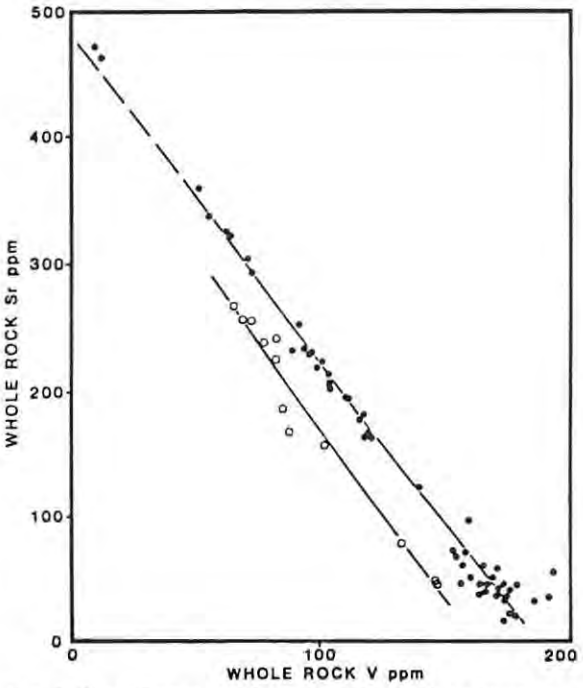

FIG. 7. Plot of whole-rock levels of Sr *vs.* V, to illustrate consistent difference between UG1FW unit (filled circles) and underlying MG3 unit (unfilled circles).

while intercumulus feldspar forms patches up to 0.5 mm. Sparse crystals of apparently cumulus or xenocrystic feldspar up to 1.5 mm long are entangled with the orthopyroxene (Fig. 2 *g–h*). The average of two whole-rock Sr_i ratios is 0.7072 ± 2, within error of the average of two values returned for the orthopyroxene fraction. Values for plagioclase are 0.7061 ± 2 and 0.7075 ± 2, respectively, for two xenocrysts hand-picked from the sample, and 0.7065 ± 2 for a composite plagioclase fraction that should contain all three textural types.

From this it is clear that isotopic disequilibrium may prevail between the phases in some samples, but not in others. Observation suggests that isotopic disequilibrium is maintained where the feldspars are large grains, whereas isotopic and major-element compositional equilibrium with liquid are approached when all inclusions are small. Particularly significant is the confirmation that the feldspar population is a mixed one. Further research is necessary to establish whether this is a general property of the Bushveld complex, as predicted by Eales *et al.* (1986) and Eales (1987).

Plagioclase mineral separates average *c.* 500ppm Sr (Table 2), and orthopyroxenes 3.5–6.5ppm Sr, with no guarantee that, even in −250 mesh fractions, all plagioclase inclusions have been removed. Mass balance calculations using whole-rock Al_2O_3 levels, and Al_2O_3 levels in orthopyroxenes from microprobe analysis, show that even in the more extreme adcumulates, >90% of the total Sr is resident in the plagioclase. The Sr-isotope signature is thus dominated by the feldspar fraction, and the effects of even small amounts of feldspar, not in equilibrium with the host rock, will be pronounced in pyroxenites. This accounts for the contrast between the irregular fluctuations displayed by the feldspar-poor pyroxenitic suite, and more regular trends in the norite suite, illustrated in Fig. 9. It is to be noted that the irregular fluctuations persist into the MG3 unit.

A model involving mixing of liquids, indicated by other geochemical data presented earlier, receives some support from the isotopic data, despite the potentially confusing effects arising

TABLE 2

Isotopic Data

Number	Description	Rb	Sr	$^{87}Rb/^{86}Sr$	$^{87}Sr/^{86}Sr_p$	Sr_i
232/22	Bastard Anorth.	4.95	335.0	0.0427	0.70906 ± 8	0.7078 ± 1
235/3	Bastard Norite	0.47	139.0	0.0098	0.70794 ± 8	0.7076 ± 1
235/6	Bastard Pyrox.	6.42	53.7	0.3462	0.71748 ± 6	0.7073 ± 2
235/8	Merensky Anorth.	5.23	395.0	0.0383	0.70854 ± 6	0.7074 ± 1
235/11	Merensky Norite	1.96	373.0	0.0152	0.70771 ± 8	0.7073 ± 1
235/14	Merensky Pyrox.	3.82	57.7	0.2098	0.71309 ± 6	0.7069 ± 1
235/15a	Merensky Reef	3.69	65.47	0.1631	0.71121 ± 6	0.7064 ± 1
235/18	Footwall Norite	1.77	455.6	0.0112	0.70677 ± 8	0.7064 ± 1
235/21	Footwall Norite	1.61	390.8	0.0119	0.70677 ± 8	0.7064 ± 1
235/23	Footwall Norite	1.09	176.0	0.0179	0.70685 ± 8	0.7063 ± 1
235/25	Pseudoreef Harz.	6.03	543.0	0.0321	0.70710 ± 2	0.7062 ± 1
235/29	UG2 Pyroxenite	8.94	69.2	0.3742	0.71802 ± 6	0.7070 ± 2
235/29	Repeat	9.19	71.0	0.3749	0.71783 ± 7	0.7068 ± 2
235/30	UG2 Pyroxenite	3.69	62.9	0.1698	0.71192 ± 1	0.7069 ± 1
235/31	UG2 Pyroxenite	0.74	72.8	0.0294	0.70719 ± 7	0.7063 ± 1
H235/8	UG2 Chr. Matrix	12.4	372.0	0.0965	0.70958 ± 1	0.7067 ± 1
H235/8	Repeat	13.4	386.0	0.1005	0.70974 ± 2	0.7068 ± 1
235/34	UG1 Proxenite	5.92	61.9	0.2769	0.71453 ± 7	0.7064 ± 2
235/35	UG1 Pyroxenite	6.31	52.2	0.3500	0.71665 ± 1	0.7063 ± 2
235/37	UG1 Pyroxenite	0.504	66.6	0.0219	0.70732 ± 7	0.7067 ± 1
235/39	UG1FW Leuconorite	0.88	413.0	0.0062	0.70647 ± 6	0.7063 ± 1
S-9	UG1FW Norite	0.76	163.0	0.0135	0.70656 ± 1	0.7062 ± 1
S-13	UG1FW Norite	0.84	190.0	0.0128	0.70643 ± 6	0.7061 ± 1
S-19	UG1FW Leuconorite	1.27	326.0	0.0113	0.70644 ± 5	0.7061 ± 1
S-23	UG1FW Norite	1.30	198.0	0.0190	0.70665 ± 3	0.7061 ± 1
S-25	UG1FW Norite	1.16	227.0	0.0148	0.70637 ± 2	0.7059 ± 1
S-30	UG1FW Norite	0.81	174.0	0.0135	0.70615 ± 1	0.7058 ± 1
S-33	UG1FW Melanorite	0.812	97.2	0.0242	0.70671 ± 6	0.7060 ± 1
S-35	UG1FW Melanorite	1.07	125.0	0.0248	0.70685 ± 1	0.7061 ± 1
S-36	UG1FW Pyroxenite	1.57	70.30	0.0646	0.70811 ± 3	0.7062 ± 1
S-38	UG1FW Pyroxenite	0.406	47.6	0.0247	0.70665 ± 1	0.7059 ± 1
S-38	UG1FW Pyrox.(Plg)	1.63	498.0	0.0095	0.70624 ± 1	0.7060 ± 1
S-38	UG1FW Pyrox.(Opx)	0.153	6.07	0.0729	0.70808 ± 3	0.7059 ± 1
S-40	UG1FW Pyroxenite	0.335	70.9	0.0137	0.70770 ± 5	0.7073 ± 1
S-40	Repeat	0.332	75.0	0.0128	0.70760 ± 1	0.7072 ± 1
S-40	UG1FW (Opx -125#)	0.087	6.59	0.0382	0.70845 ± 2	0.7073 ± 1
S-40	UG1FW (Opx +125#)	0.067	6.55	0.0296	0.70801 ± 2	0.7071 ± 1
S-40	UG1FW (Plg)	0.45	513.0	0.0025	0.70655 ± 1	0.7065 ± 1
S-40	UG1FW (Plg Xen.1)	0.828	464.0	0.0052	0.70624 ± 2	0.7061 ± 1
S-40	UG1FW (Plg Xen.2)	0.366	453.0	0.0023	0.70754 ± 2	0.7075 ± 1
S-43	UG1FW Pyroxenite	0.306	37.7	0.0235	0.70681 ± 1	0.7061 ± 1
S-43	UG1FW (Plg)	1.09	513.0	0.0061	0.70630 ± 1	0.7061 ± 1
S-49	UG1FW Pyroxenite	1.14	44.6	0.0740	0.70792 ± 6	0.7057 ± 1
S-49	UG1FW (Plg)	3.79	573.0	0.0191	0.70660 ± 2	0.7060 ± 1
S-54	UG1FW Pyroxenite	1.51	39.4	0.1109	0.70894 ± 8	0.7057 ± 1
S-58	UG1FW Pyroxenite	0.596	36.8	0.0469	0.70756 ± 4	0.7062 ± 1
S-58	Repeat	0.592	37.0	0.0463	0.70768 ± 8	0.7063 ± 1
S-62d	MG3 Norite	0.854	131.0	0.0189	0.70645 ± 1	0.7059 ± 1
S-66	MG3 Pyroxenite	0.563	78.5	0.0207	0.70684 ± 1	0.7062 ± 1
S-68	MG3 Norite	2.13	337.0	0.0183	0.70754 ± 1	0.7070 ± 1
S-71	MG3 Norite	0.784	254.0	0.0089	0.70629 ± 1	0.7060 ± 1
S-78b	MG2 Leuconorite	4.28	406.0	0.0305	0.70649 ± 1	0.7056 ± 1
Lower Critical Zone NG1 Borehole						
NG1-25	Pyroxenite	2.38	34.8	0.1979	0.71142 ± 3	0.7056 ± 1
NG1-49.75	Pyroxenite	1.76	31.9	0.1597	0.71024 ± 2	0.7055 ± 1
NG1-152.2	Pyroxenite	1.97	18.4	0.3099	0.71404 ± 1	0.7049 ± 2
NG1-163.27	Pyroxenite	2.71	39.6	0.1981	0.71110 ± 2	0.7052 ± 1
NG1-204.50	Pyroxenite	2.80	46.5	0.1743	0.71041 ± 1	0.7053 ± 1

Whole-rock and mineral separate Rb-Sr isotopic data for a 600m-section beneath the Bastard Unit. Data are plotted in Fig. 9 against stratigraphic height. Rb and Sr in ppm $^{87}Sr/^{86}Sr_p$ is present-day $^{87}Sr/^{86}Sr$ recovered from spiked sample; uncertainty is 2 standard errors of the mean. Sr_i is initial $^{87}Sr/^{86}Sr$ calculated for an age of 2050 million years; errors are given at the 1σ level. See appendix for further details. NG1 samples refer to a deep borehole drilled in the footwall of RPM Union Section Mine.

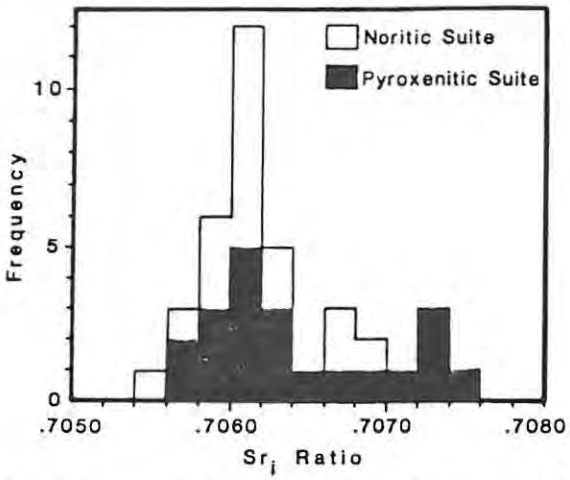

FIG. 8. Histogram showing frequency of occurrence of Sr_i ratios returned by 38 analyses of whole-rock samples and mineral separates, UG1FW, UG1 and UG2 units.

out of fractionation, compositional convection and isotopic disequilibrium. Fig. 10 displays the correlation between MMF ratios of orthopyroxenes (as determined by microprobe analysis) and Sr_i ratios. Included also are four data points representing Lower Critical Zone pyroxenites above the LG6 chromite layer at Union Section (Teigler, 1989) and six olivine- and chromite-poor UG1 and UG2 pyroxenites overlying the UG1FW unit. Despite scattering, 87% of UG1FW unit, and the six UG1–UG2 data points, define a regression line $MMF_{opx} = 20.758\ Sr_i - 13.8542$ (corr. coeff. 0.914). A plot of Cr_2O_3 levels in orthopyroxene against Sr_i ratios yields a distribution similar to that of Fig. 10, but with more scatter.

Fig. 10 therefore supports a model in which crystallization of Mg- and Cr-rich cumulates lower in the stratigraphic section (Sr_i *c.* 0.7054) generated an Fe-enriched, Cr-poor supernatant liquid residuum maintaining the same isotopic signature. This was then mixed in different proportions with liquid similar to that which was parental to the overlying UG1 and UG2 units (Mg- and Cr-enriched, Sr_i 0.7067–0.7070) during deposition of the UG1FW unit.

Sample S-36 is significantly displaced below the regression line of Fig. 10. This is almost certainly a result of crystal fractionation, as the sample represents the top of the pyroxenite suite immediately beneath the first melanorite layer, where the lowest values of MMF, Ni/V, Cr/Co and Fe/Ti in the UG1FW unit are encountered. Sample S-40 is wholly anomalous; the presence within it of xenocrystic plagioclase with Sr_i ratios of 0.7075

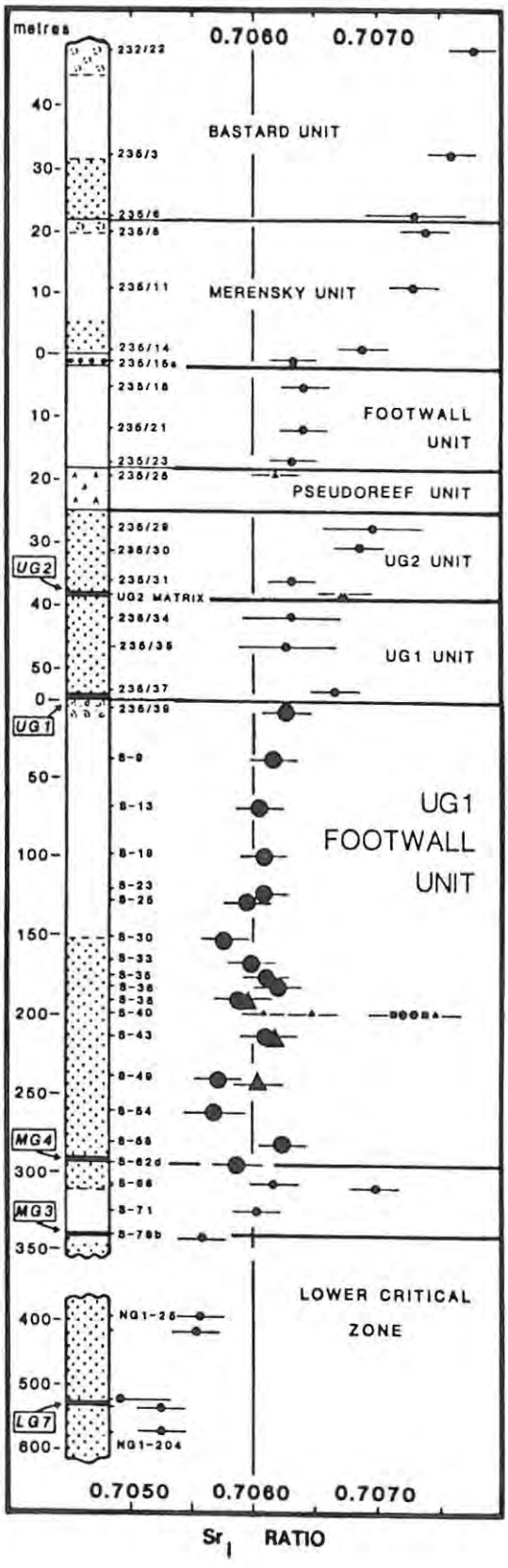

raises several alternative explanations, but these are little better than speculation at present.

Summary of the more relevant diagnostic data

Seven features of particular genetic significance may be isolated after excision of the finer details in the foregoing presentation.

(*a*) The UG1FW Footwall Unit is of exceptional thickness (285 m), but is geochemically coherent, and distinguishable from the units above and beneath it. Pyroxenite overlying chromitite is dominant within the lowermost 135 m, while norites of varying colour index constitute the succeeding 130 m section. The unit is capped by a lower leuconorite–anorthosite couplet displaying evolved attributes (low MMF ratios and Cr levels in orthopyroxene), which is overlain by a second leuconorite–anorthosite couplet in which MMF ratios of orthopyroxenes are higher than in any underlying member of the unit (Fig. 5) and in which Cr contents are anomalously high for rocks of leucocratic affinity. Chromite appears in abundance within the uppermost anorthosite, which is overlain by the robust UG1 chromitite layer and UG1 pyroxenites.

(*b*) A distinctive texture characterizes almost the entire column extending for 350 m below the UG1 chromite. Spheroidal or embayed inclusions of partially resorbed plagioclase feldspar are found entrapped in abundance within orthopyroxene hosts. Rare grains of cumulus or xenocrystic feldspar are entrapped within some pyroxenites. Intragranular, cumulus and late intercumulus feldspar species thus exist within pyroxenites, as well as norites. Microprobe analysis shows that anorthite contents of included and non-included grains vary in sympathy, with the inclusions being generally more sodic.

(*c*) Sr_i ratios vary in an unpredictable manner from one sample to another. This indicates that the UG1FW unit could not have been the derivative of a single, homogeneous column of liquid within which phase or modal layering was controlled by purely physical parameters such as temperature, pressure, rhythmic nucleation or the sorting of crystals settling under gravity, or under the influence of currents.

(*d*) Sr_i ratios vary independently of stratigraphic height and petrographic features. Separate analysis of feldspar and pyroxene fractions shows that, within the same sample, isotopic signatures may be significantly different in these two fractions. Non-systematic whole-rock Sr_i variations can best be attributed to the feldspar population being a mixed one.

(*e*) The plotting of peak MMF ratios of orthopyroxenes of the UG1FW, UG1 and UG2 units, as determined by microprobe analysis, against whole-rock Sr_i ratios (Fig. 10) reveals that >80% of the available data points can be regressed. The derivation of this suite of rocks by some form of mixing between end members S ($Sr_i = 0.7054$; MMF = 0.78–0.79) and P ($Sr_i = 0.7068$; MMF = 0.82) is thus a viable hypothesis.

(*f*) Whole-rock major- and trace-element data indicate at least 8 sub-cycles between the MG4 and UG1 chromitite layers (Figs 3, 5 and 11). These sub-cycles are not demarcated by abrupt reversals of trends such as mark the transition from one full unit to another in the uppermost part of the Upper Critical Zone (as shown by Eales *et al.*, 1986). The pattern is, rather, one of gradational change to rocks of more, or of less, primitive type with stratigraphic height.

(*g*) The unit as a whole shows chemically evolved traits when compared with overlying cyclic units. It is depleted in Cr. Apart from a thin interval immediately above the MG4 chromitite layer, chromite is either absent or present as minute traces only, in contrast with its common occurrence as an accessory phase in norites and pyroxenites of the UG1, UG2, Merensky and Bastard units. The orthopyroxenes average 0.336% Cr_2O_3 (std. dev. = 0.045%; 43 samples; 393 analyses). By contrast, four union Section borehole intersections of the UG2 pyroxenite show average Cr_2O_3 levels to be 0.492%, 0.463%, 0.417% and 0.412% Cr_2O_3, respectively (averages drawn from 240 microprobe analyses). Similar Cr depletion is noted in Cameron's (1982, Table 2) data pertaining to the equivalent M unit in the eastern lobe of the complex. Moderate but consistent Ni depletion is also evident in our data insofar as 26 whole-rock pyroxenite samples yield an average $(Ni/MgO) \times 10^4$ ratio of 22.23 ± 0.80, within the range of 20.7–23.6. The average value is 24.0 ± 1.5 (range 22.8–27.2) within the overlying UG1 and UG2 units at Union Section, and 24.20 ± 0.85 (range 23.4–25.9) at Amandelbult Section. A further indication of chemically evolved traits is given by MMF ratios of the orthopyroxenes. A mean value of 0.798 for the entire

FIG. 9. Variations in $^{87}Sr/^{86}Sr$ at 2050 ± 25 (2 sigma) Ma (Sr_i) plotted against stratigraphic height for a 600 m-section beneath the Bastard Unit (note changes of vertical scale above base of UG1 unit and below UG1FW unit). Filled circles—whole-rock data; triangles—plagioclase separates; squares—orthopyroxene separates. Stipple indicates pyroxenites, circles anorthosites, unshaded areas norites and cone symbols harzburgites of Pseudoreefs. Error bars are given at the 2 sigma level (see Appendix for details).

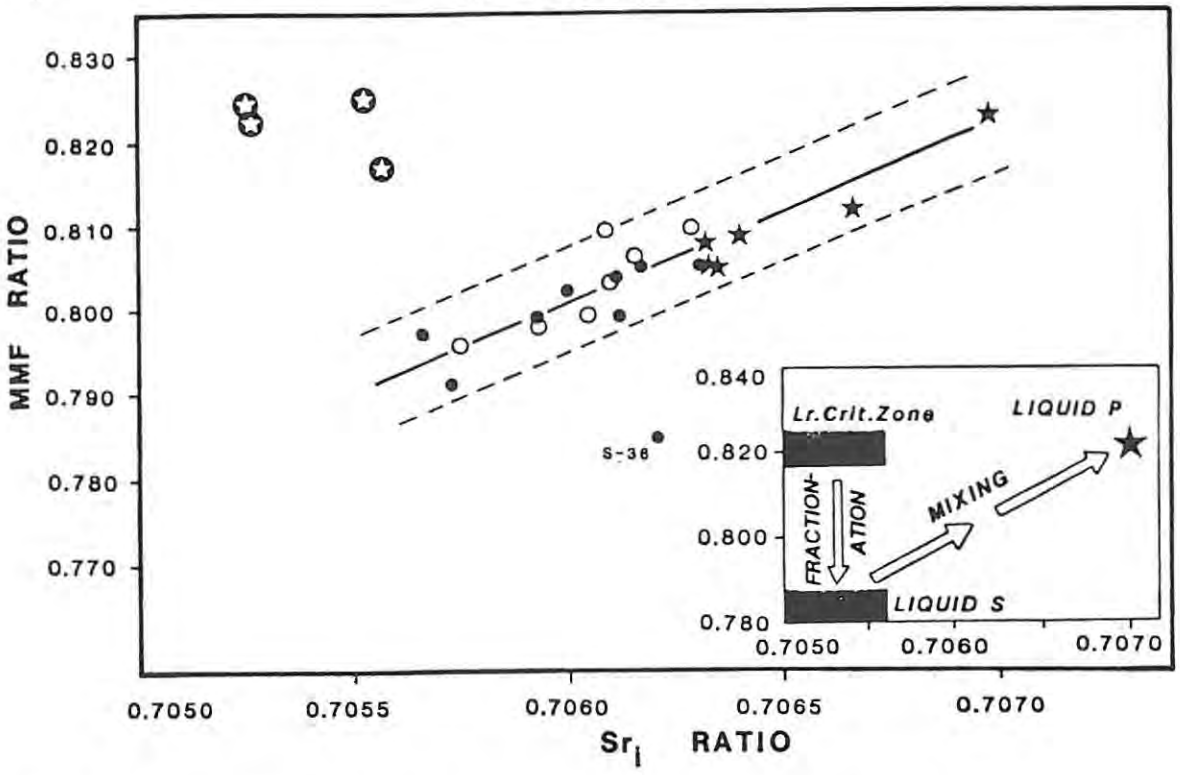

FIG. 10. Regression of peak MMF ratios detected by microprobe analysis of orthopyroxene population, against whole-rock Sr_i ratios for UG1FW norites (unfilled circles) and pyroxenites (filled circles), and UG1 and UG2 pyroxenites (stars). Also shown are 4 Lower Critical Zone pyroxenites (circled stars) and fractionated UG1FW unit pyroxenite sample S-36. Inset shows interpretation based on derivation of supernatant liquid S (liquid residuum of deeper-level cumulates) and subsequent mixing with primitive liquid P of UG1–UG2 lineage.

unit is suggestively lower than values of 0.822 ± 0.005, 0.817 ± 0.009, 0.814 ± 0.009 and 0.805 ± 0.007 determined in four separate intersections through the stratigraphically higher UG2 unit (24 samples; 240 analyses) at Union Section.

Discussion

Genetic models that are viable within the context of features (*a*)–(*g*) above are limited in number. Constraints imposed by the isotopic, petrographic, and gross chemical characteristics, and patterns of cryptic variations, leave little doubt about the operation of some process of mixing of a more primitive liquid with one bearing plagioclase in suspension. Hybridization apparently shifted the liquid composition into the primary phase volume of orthopyroxene, and led to compositional modification and partial resorption of the feldspar population. The muted internal cyclicity within the unit suggests that the process of hybridization was not a catastrophic event, but an ongoing one that waxed and waned in intensity. Accordingly, MMF, Ni/V and Cr/Co ratios define sub-cycles within the unit, without displaying a saw-tooth pattern, or marked discontinuities in trends.

The rôle which compositional convection (Tait *et al.*, 1984; Sparks *et al.*, 1984) might have played in influencing cryptic variations is uncertain. The concept recognises that changes in melt density, resulting from partial crystallization, may be more potent than temperature in promoting convection. Low-density residua may rise, in the earlier stages of crystallization, from a partially crystalline floor with high primary porosity, to be replaced by chemically undepleted melt drawn down into the crystal pile. Ostensibly, this provides a plausible mechanism for adcumulus growth. Such rocks should (*a*) exhibit extended growth of primocrysts into the void space that previously imparted high primary porosity, (*b*) show the most primitive chemical attributes where adcumulus traits are most extreme, and (*c*) yield fractionated residua in higher parts of the unit, to which low-density residua convect while phases

of high density are crystallizing. The general validity of this model is not under review here, but its applicability to the UG1FW unit is.

Our data on adcumulus bronzitites do not comply with the constraints. (*a*) Adcumulus growth by the mechanism of Tait *et al.* (1984) should yield overgrowth zones on pyroxene grains that are devoid of the abundant spheroidal feldspar inclusions. These inclusions are in reality as abundant close to grain margins as in cores of crystals in adcumulates (Fig. 2*d*). Rocks with more strongly orthocumulus affinities do display pyroxenes with marginal zones free of inclusions (Fig. 2*f*). This implies that adcumulus texture here is the result of compaction rather than grain enlargement. The fine grain size of the more extreme adcumulates of the UG1FW unit supports this argument. (*b*) If compositional convection governed the growth of adcumulates, samples with the highest MMF ratios should display the lowest degrees of residual porosity and, therefore, the lowest levels of incompatible elements (Henderson, 1968; Campbell. 1987). Conversely, entrapment of depleted residua should lower both whole-rock MMF ratios and, by reaction, those of ferromagnesian primocrysts (the trapped liquid shift of Barnes, 1986). Evidence here is unconvincing insofar as correlation coefficients between MMF ratios of pyroxenites (29 samples) and levels of incompatible elements Zr, Y and Ti are statistically weak (-0.36, -0.42 and -0.58, respectively). (*c*) Deposition of the UG1FW unit under a regime dominated by compositional convection, or crystal fractionation, should have led to accumulation of more evolved derivatives in the upper (noritic) half of the unit. Major- and trace-element whole-rock chemistry, and microprobe analysis of both pyroxenes and feldspars, prove conclusively that most of the upper half of the unit, although decidedly more feldspathic than the lower half, retains geochemically primitive traits. Averaged MMF ratios of norites are, in fact, higher than in pyroxenites. We conclude, therefore, that the totality of evidence requires periodic additions of primitive (Mg- and Cr-enriched) liquid to a resident column of evolved, supernatant liquid above the crystalline floor. Such a conclusion would accept the rising of low-density liquids, enriched in plagioclase component by compositional convection, and subsequent mixing with more primitive liquids.

The emplacement of an anorthositic (A-type) liquid within or beneath resident mafic (U-type) liquid, and subsequent mixing, has been cited as a fundamental process within the Bushveld complex (Irvine *et al.*, 1983; Sharpe, 1985; Harmer and Sharpe, 1985; Hatton, 1986). The A-type liquids of Sharpe (1985, Table 1) have higher Sr_i ratios (*c.* 0.7068) than U-type (*c.* 0.7030) and are, by definition, more feldspathic. The overall increase in Sr_i ratio, concomitant with a generalized increase in modal plagioclase with height in the UG1FW unit, therefore renders this a superficially attractive hypothesis. Other criteria refute the hypothesis. The upward increase in plagioclase in the UG1FW unit is accompanied by an increase in both MMF ratio and Cr content of the pyroxenes, which is the reverse of what an increasing proportion of A-type liquid would demand. Sr/Al_2O_3 ratios of Sharpe's putative A-type liquid (19.7×10^{-4}) are appreciably higher than ratios in U-type liquid (15.2×10^{-4}), whereas the noritic suite of the UG1FW unit maintains a remarkably constant ratio of $(14.8 \pm 0.7) \times 10^{-4}$ throughout. Cr/Ni and Cr/MgO ratios are, respectively, two and three times higher in U-type than in A-type liquids, but averaged values in the pyroxenitic and noritic suites of the UG1FW unit are indistinguishable (Cr/Ni of norites is 5.00 ± 0.33 and of pyroxenites 4.91 ± 0.50; Cr/MgO of norites is $(106 \pm 7) \times 10^{-4}$ and of pyroxenites $(108 \pm 11) \times 10^{-4}$). We find, therefore, no support for derivation of the norite–leuconorite suite by hybridization with discrete A-type liquid.

Some parallels may be drawn between the UG1FW unit and the Gabbronorite I–Olivine-bearing subzone I (OBZI)–Norite II sequence in the Lower Banded Series of the Stillwater complex (Barnes and Naldrett, 1986). In both, reversals of the normal fractionation trend are implicit in increased proportions of mafic phases, and enrichment in Mg, Ni and Cr. Rounded feldspar inclusions showing reversed zoning are enclosed in both (olivine in the OBZI and bronzite in the UG1FW unit) and imply a mixing of liquids resulting in partial resorption. Barnes and Naldrett postulate three end-member liquids—a primitive (P) liquid, an evolved resident liquid (G), and a feldspar-enriched (A) liquid yielded by high-pressure fractionation of P at depth. They argue that mixing took place within a thermal plume which spread laterally within resident G-type liquid, at some distance above the crystalline floor. Olivine bearing entrapped feldspar sank from the plume, through a column of resident G-type liquid before settling on the floor. Several paradoxes emerge when the Barnes–Naldrett model is applied to the UG1FW unit. Calling upon admixture with A-type liquid to account for the leucocratic nature of the upper part of the noritic suite does not explain the relative Cr- and Mg-enrichment characterizing the orthopyroxenes found there. By virtue of their evolution by extensive high-pressure fractionation of P-type liquids, A-type liquids

should be intrinsically Cr- and Mg-depleted. Furthermore, the composition of plagioclase inclusions becomes more sodic with height within subcycles of the UG1FW unit, in parallel with intercumulus plagioclase, while MMF ratios increase. The plume model offers no plausible reason for this.

Conclusions and synthesis

We adopt a model in which a hotter, more primitive liquid (P) is periodically added to and blended with a cooler, more evolved, supernatant liquid (S) resting upon the crystal pile. Sub-cycles developed within the unit include more primitive mafic cumulates deposited from hybrid liquids with a higher proportion of P component, whereas cumulates with more evolved traits reflect supernatant liquid fractions that experienced a lesser degree of rejuvenation, or evolved by subsequent fractionation. Extrapolation of the data embodied in Figs 5, 6 and 10 indicates the potential of these liquids to deposit cumulates with the following attributes:

Liquid S : Sr_i ratio *c.* 0.7054,
MMF of orthopyroxene *c.* 0.785,
Cr_2O_3 in pyroxene *c.* 0.25%,
Plagioclase *c.* An_{70},
Whole-rock Ni/V *c.* 2.9 and Cr/Co *c.* 20.

Liquid P : Sr_i ratio *c.* 0.7068,
MMF of orthopyroxene *c.* 0.82,
Cr_2O_3 in orthopyroxene *c.* 0.5%,
Plagioclase *c.* An_{81-85},
Whole-rock Ni/V *c.* 3.5 and Cr/Co *c.* 30.

The anorthositic tops of sub-cycles 7 and 8 (Fig. 5) introduce *c.* 3% anorthosite into the UG1FW unit. Our data offer no chemical or isotopic evidence to suggest that there was periodic influx of a discrete (A-type) magma from which these anorthosites crystallized. Even if the specific process that operated remains uncertain, we retain the view that liquids parental to the UG1FW unit anorthosites were generated within the magma chamber.

The more important variations in trends shown in Figs 3 and 5 are simplified in Fig. 11, to emphasize the cyclicity within the UG1FW unit, and a cartoon illustrating our synthesis is given in Fig. 12. Our synthesis to account for this cyclicity begins with (*a*) existence of a supernatant column of residual liquid, S, above the prevailing crystalline floor (Fig. 12*b*). Insofar as it was a liquid residuum generated during the separation of earlier cumulates, it was Cr-, Ni- and Mg-depleted, the Sr_i ratio was *c.* 0.7054 (Fig. 10), and it was nucleating sodic labradorite and Mg-poor bronzite in cotectic equilibrium. It is assumed that the liquid column was stratified, with the lowermost layer designated S representing the most dense liquid.

(*b*) Emplacement of a hot, primitive magma, P, with $Sr_i \geq 0.7068$ was then effected under conditions appropriate to jetting or fountaining (i.e. the intrusive liquid had a higher density than resident liquid; Campbell *et al.*, 1983; Campbell and Turner, 1986) rather than pluming. A hybrid layer consisting of P liquid, with entrained S liquid and suspended primocrysts, was formed immediately above the crystalline floor.

(*c*) Resorption, partial equilibration and reverse zoning of suspended, relict crystals inherited from the S liquid were initiated within the hybrid layer, and relative enrichment in the anorthite molecule was achieved in the small, severely corroded feldspar grains. A more limited temperature rise within the S liquid above the hybrid layer inhibited resorption and re-equilibration there, and plagioclase grains maintained a greater size and albite content than in the hotter hybrid layer.

(*d*) The addition of P liquid to S liquid in the hybrid layer shifted the system into the primary phase volume of bronzite (Fig. 12*c*), and subsequent nucleation and growth of bronzite primocrysts encapsulated relict feldspar grains. Compaction by sintering of the lower part of the crystallizing hybrid layer appears to have controlled the formation of adcumulate-textured pyroxenite with a low content of small, calcic feldspar inclusions. Above this, progressive crystallization of bronzite led to decline of the MMF ratio with height in some sub-cycles (1 and 2, Fig. 11). In others (sub-cycles 3 and 4 of Fig. 11), the P:S liquid ratio increased with time as more P liquid was injected, and earlier cumulates were covered by cumulates with increasingly higher Cr levels and MMF ratios (Fig. 12*d*). Reverse-zoned bronzite grains are commonly found here, but the earlier encapsulation of feldspar inclusions appears to have protected them from further reaction.

(*e*) All sub-cycles in the pyroxenite suite grade to Mg- and Cr-poor cumulates in their uppermost parts. This suggests fractionation through crystallization, but late-stage blending with evolved, supernatant (S) liquid overlying the hybrid layer was probably important (Fig. 12 *e–f*). The latter process would have been stimulated by the decline in density contrast between the two liquid layers, leading to breakdown of the interface as low-density residua migrated upwards by compositional convection during the separation of pyroxe-

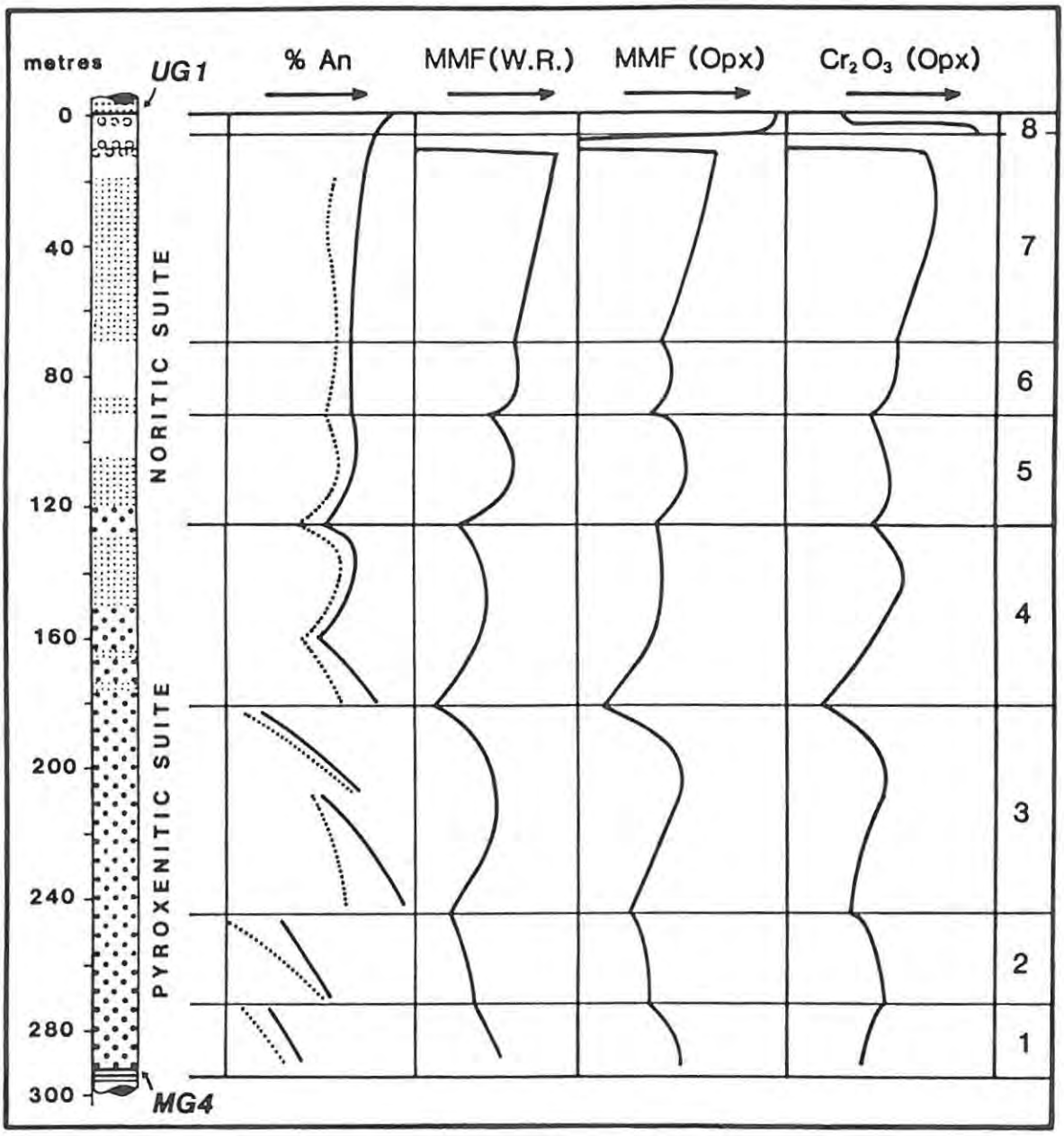

FIG. 11. Simplified representation of compositional trends depicted in Fig. 5, showing subdivision of sequence into sub-cycles 1–8. Dotted-line trends for feldspars represent inclusions in bronzite, and solid lines cumulus and intercumulus feldspars.

nites. The plagioclase inclusions trapped within pyroxene grains at this stage would, accordingly, have been relatively large, and sodic, reflecting their growth mainly in S-type liquid.

(*f*) Throughout accumulation of the pyroxenitic suite, the hybrid liquid was held within the primary phase volume of orthopyroxene by additions of P liquid, but there was substantial upward migration of low-density residua enriched in plagioclase components, as pyroxenite crystallized.

(*g*) Initiation of crystallization of intercumulus liquid lagged behind that of primocrysts. More calcic intercumulus feldspar would initially have nucleated at the base of the crystal pile, but concurrent compaction and reduction in primary porosity would have displaced sodic, intercumulus

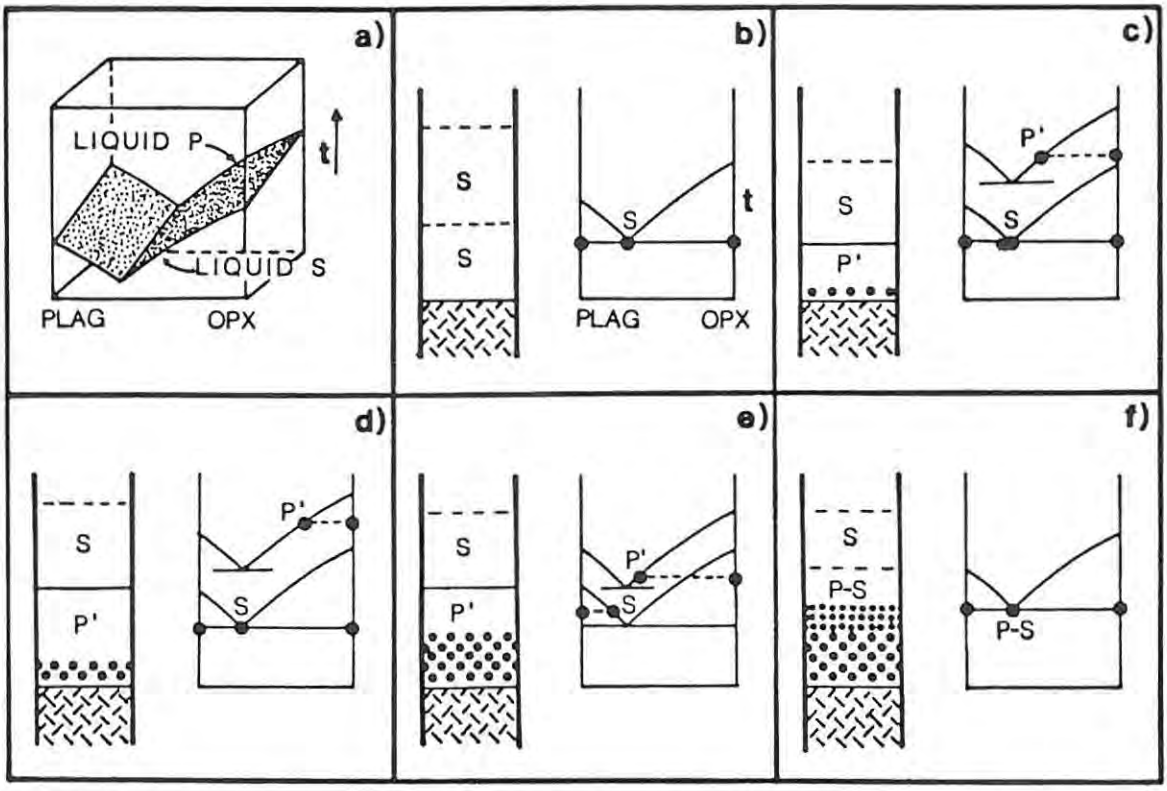

FIG. 12. Cartoon depicting sequence within an idealized sub-cycle. (*a*) Liquidus curves of evolved supernatant liquid S and more primitive inputs of liquid P. (*b*) Column of supernatant liquid S (probably stratified) resting upon existing floor (hatched). Qualitative phase diagram shows cotectic crystallization of plagioclase and orthopyroxene from liquid S. (*c*) Input of liquid P′ (P mixed with entrained S) beneath liquid layer S. P′ lies within primary phase volume of orthopyroxene; partially resorbed, relict plagioclase crystals suspended within liquid become entrapped within growing orthopyroxene grains. Preferential settling of orthopyroxene occurs within S, leaving it enriched in suspended plagioclase phenocrysts. Pyroxenite (stippled pattern) accumulates upon floor. (*d*) Continued input of P-type liquid leads to deposition of most magnesian orthopyroxene within sub-cycle. (*e*) Liquid P′ undergoes fractionation while liquid S (enriched in plagioclase due to settling of orthopyroxene) undergoes heating from below. Ultimately, liquid S enters primary phase volume of plagioclase as plagioclase is resorbed. (*f*) On subsequent cooling, advanced fractionation of low-volume residuum of P′ leads to conditions permitting mixing of P′ and S, forming hybrid P–S. Norite, leuconorite (finer stipple) and, in extreme cases, small volumes of anorthosite may be deposited from liquid P–S.

liquid residua upwards. Each subcycle therefore displays a trend towards sodic intercumulus feldspar with stratigraphic height (Fig. 11). Partitioning of Ca into late intercumulus clinopyroxene also has the potential to accelerate the shift towards sodic plagioclase (the augite effect of Morse, 1979).

(*h*) Periodic repetition of stages (*a*)–(*g*) above yielded sub-cycles 1–4 (Fig. 11). While the composition of successive pulses of intrusive P liquid remained sensibly constant (Figs 6, 7 and 10), the cumulative effects of repeated additions of P liquid to the system are evident. Fig. 11 shows that the starting compositions of both plagioclase inclusions and intercumulus plagioclase become systematically more calcic through sub-cycles 1 to 4.

(*i*) The slopes of the profiles depicting cryptic variations (Figs 5 and 11) are thus held to be a function of the volume and frequency of inputs of P-type liquid during the filling of the magma chamber. A low average volume and frequency of inputs per unit time resulted in sub-cycles of limited thickness (e.g. nos. 1 and 2 in Fig. 11) without pronounced reversals in the trend of cryptic variations; larger inputs of P liquid yielded thick sub-cycles within which significant increases in MMF ratio and Cr contents of orthopyroxene are seen (Fig. 11, sub-cycle 3).

(*j*) A significant change occurs within sub-cycle

4. Cumulus plagioclase joins the paragenesis ephemerally within thin layers of melanorite (7–10% Al_2O_3) at 175 m and 166 m depth; between 152 and 126 m the sequence becomes wholly noritic (11–16% Al_2O_3). The base of succeeding sub-cycle 5 exposes only 3 m of pyroxenite (5% Al_2O_3) before giving way to a noritic suite constituting the remainder of the UG1FW unit. The upper part of sub-cycle 4 thus marks the stage at which the hybrid liquid reached the bronzite–plagioclase cotectic. At this level, the decoupling of cryptic variations in bronzite and intercumulus plagioclase gives way to coupled variations between cumulus phases (see Fig. 11, sub-cycles 4–7). Several factors may have contributed towards the capacity of the hybrid liquid to crystallize primocrystal plagioclase. Upward movement and accumulation of low-density residua during protracted deposition of pyroxenites would have been important. Another factor might have been the preferential sinking of orthopyroxene out of the supernatant liquid layer S, followed by reheating of the layer as fresh influxes of primitive liquid were emplaced beneath it. This process would have had the capacity to generate a reservoir of liquid within the primary phase volume of plagioclase (Fig. 12 *e*).

(*k*) It is generally accepted (Campbell *et al.*, 1983; Sparks *et al.*, 1984) that the nucleation of plagioclase marks the evolutionary stage at which liquid residua will become more dense than the parent liquids. It is thus perhaps significant that the lowest MMF ratios in the UG1FW unit pyroxenites and lowest Cr contents of their orthopyroxenes, are encountered within the basal portion of sub-cycle 4, beneath the first norites (Figs 5 and 11). The implication is that fractionated residua no longer rose within the column above this point, but remained trapped as intercumulus liquid, or became ponded. Zonal decline of MMF ratios and Cr contents towards the margins of individual bronzite grains becomes the norm within the noritic suite. Oscillatory zoned feldspar primocrysts entangled within normally zoned (single-cycle) grains indicate the mixed nature of the population.

(*l*) A general trend towards increasing MMF ratios (whole-rock and microprobe data; Fig. 5 and 11) and increasing Cr in bronzite is maintained to within 20 m of the top of the UG1FW unit. Superimposed upon this is a muted cyclicity defining sub-cycles 5–7, suggesting minor, periodic influxes of primitive liquid. The apparent paradox of upward increase in MMF ratios and Cr levels in orthopyroxenes, as the sequence becomes more leucocratic, can be resolved in terms of mass balance. Additions of relatively small proportions of P liquid to a felsic liquid with a low content of ferromagnesian components would have increased MMF ratios without greatly increasing the absolute modal proportions of mafic phases.

(*m*) Sr_i ratios of norites and leuconorites (0.7058–0.7063) are within the range expected of a mixing of putative S liquids (*c.* 0.7054) and P liquids ($\geq$0.7068) in varying proportions. This range of values is well below that arising out of later emplacement of Main Zone liquids (*c.* 0.7087; Eales *et al.*, 1986) which might be equated with the A-type liquids of Sharpe, 1985). Fluctuations in Sr_i ratio are seen to be more conservative in norites (Fig. 9) than in pyroxenites because variations in the ratio S-type:P-type feldspars are more effectively buffered in norites, where feldspars are a major modal constituent.

(*n*) The band of leuconorite near the top of sub-cycle 7 (Fig. 5, 12–20 m) retains the chemical traits of the underlying norites, but the succeeding 6 m layer of anorthosite (32% Al_2O_3) at the top of sub-cycle 7 is strongly evolved. MMF ratios determined by both whole-rock and microprobe analysis of anorthosite samples drop to 0.62, Cr_2O_3 in orthopyroxene is <0.1%, and Ni/V, Cr/Co and Fe/Ti ratios are strongly depressed.

(*o*) The leuconorite at 4–6 m below the UG1 chromite (sub-cycle 8, Figs 5 and 11) shows higher MMF ratios and Cr contents of orthopyroxenes, and higher whole-rock Cr/Co ratios, than in subcycle 7 or in any underlying norites or pyroxenites of the UG1FW unit, but chromite does not yet appear as a phase. In the overlying 4 m anorthosite layer (the footwall of the UG1 chromitite layer) abundant chromite appears as disseminated grains, discontinuous layers, and pods. Microprobe data confirm that Cr contents are anomalously high for orthopyroxene found in anorthosites, and MMF ratios now match those of pyroxenes in the overlying UG1 unit. It is within the upper part of this anorthosite that the renowned system of anastomosing layers, and oblate spheroidal masses of chromitite that disrupt the layering (cf. Sampson, 1932; Lee, 1981; Viljoen *et al.*, 1986*a*) make their appearance. All these features point to interaction between a feldspathic residue at the top of the UG1FW unit, and the liquid parent of the overlying UG1 unit. The mixing of a chromiferous mafic liquid with feldspathic liquid has the potential to bring hybrids within the primary phase volume of Cr-spinel (Irvine *et al.*, 1983; Hatton and von Gruenewaldt, 1987) and the occurrence of the robust, if structurally complex, UG1 chromitite at this position is not in conflict with theory. We do not, however, subscribe to the view that the anorth-

ositic liquid need be derived as discrete injections of A-type liquid, as advocated by these authors. Indeed, the geochemical and isotopic data in this paper argue against the emplacement of a significant batch of A-type liquid at this level of the banded sequence.

Some conclusions of a broader nature emerge from this study. Firstly, Sr-isotope ratios are not reliable indices of either stratigraphic height or rock type within the complex, except in the broadest sense. Secondly, if the synthesis offered in this and two related papers (Eales *et al.*, 1986, 1988) is deemed valid, the broad thesis of Campbell *et al.* (1983) receives support. That is, the filling of a magma chamber to its full volume is accomplished in the early stages by injection of fresh magma pulses that intrude near the crystalline floor prevailing at that time. Jetting may be important. In the later stages, as within the uppermost part of the Critical Zone and the lower Main Zone, emplacement by pluming may become dominant. Thirdly, hybridization by partial resorption of earlier cumulates, or mingling of new liquids with older residual liquids may be a more general process than is commonly appreciated. It is only in specific sequences, as within the UG1FW unit, that this evidence is preserved in textural and chemical attributes.

Acknowledgements

Funding for this project was granted by the Foundation for Research Development of the C.S.I.R., for which our appreciation is recorded. The assistance of Claudia Schulte, Michelle Ellis, Andrea Wood and M. J. Aphane in sample preparation and analysis is acknowledged. Bernd Teigler is thanked for allowing us to incorporate his data on the Lower Critical Zone. Above all, the Management of R.P.M. Union Section Mine, and Dr Chris Lee, are thanked for allowing us access to mine workings, and for their goodwill and logistic support.

References

Barnes, S. J. (1986) *Contrib. Mineral. Petrol.* **93**, 524–31.

—— and Naldrett, A. J. (1986) *J. Petrol.* **27**, 791–825.

Cameron, E. N. (1964) In *Geology of some ore deposits in southern Africa*, **2**, Geol. Soc. S. Africa, 131–68.

—— (1982) *Econ. Geol.* **77**, 1307–27.

Campbell, I. H. (1987) *J. Geol.* **95**, 35–54.

—— and Turner, J. S. (1986) In *Short course in silicate melts* (C. M. Scarfe, ed.) Min. Assoc. Canada, 236–78.

—— Naldrett, A. J. and Barnes, S. J. (1983) *J. Petrol.* **24**, 133–65.

Coertze, F. J. (1958) *Geol. Soc. S. Africa Trans.* **61**, 387–92.

Eales, H. V. (1987) In *Evolution of chromium ore fields*, (C. W. Stowe, ed.) Van Nostrand Reinhold Co., New York, 144–68.

—— Marsh, J. S., Mitchell, A. A., de Klerk, W. J., Kruger, F. J. and Field, M. (1986) *Mineral. Mag.* **50**, 567–82.

—— Field, M., de Klerk, W. J. and Scoon, R. N. (1988) Ibid. **52**, 63–80.

Harmer, R. E. and Sharpe, M. R. (1985) *Econ. Geol.* **80**, 813–37.

Hatton, C. J. (1986) *Abstr. Geocongress Geol. Soc. S. Africa*, 595–98.

—— and von Gruenewaldt, G. (1987) In *In Evolution of chromium ore fields* (C. W. Stowe, ed.) Van Nostrand Reinhold Co., New York, 109–43.

Henderson, P. (1968) *Geochim. Cosmochim. Acta* **32**, 897–911.

Irvine, T. N. and Sharpe, M. R. (1982) *Carnegie Inst. Washington Ybk* **81**, 294–303.

Keith, D. W. and Todd, S. G. (1983) *Econ. Geol.* **78**, 1287–334.

Kruger, F. J. (1988) *Nuclear Active* **38**, 30–2.

Lee, C. A. (1981) *J. Geol. Soc. London*, **138**, 327–41.

Morse, S. A. (1979) *J. Geol.* **87**, 202–8.

Norrish, K. and Hutton, J. T. (1969) *Geochim. Cosmichim. Acta*, **33**, 431–53.

Sampson, E. (1932) *Econ. Geol.* **27**, 113–44.

Sharpe, M. R. (1985) *Nature*, **316**, 119–26.

Sparks, R. S. J., Huppert, H. E. and Turner, J. S. (1984) *Phil. Trans. Roy. Soc. London*, **A310**, 511–34.

Smith, J. V. (1974) *Feldspar Minerals*, **2**, Springer-Verlag, New York.

Tait, S. R., Huppert H. E. and Sparks, R. S. J. (1984) *Lithos*, **17**, 139–46.

Teigler, B. (1989) Ph.D. thesis, Rhodes University (in prep.).

Vermaak, C. F. (1976) *Econ. Geol.* **71**, 1270–98.

Viljoen, M. J., de Klerk, W. J., Coetzer, P. M., Hatch, N. P., Kinloch, E. and Peyerl, W. (1986a) in *Mineral deposits of Southern Africa* (C. R. Anhaeusser and S. Maske, Eds.) Geol. Soc. S. Africa, 1061–90.

—— Theron, J., Underwood, B., Walters, B. M., Weaver, J. and Peyerl, W. (1986b) Ibid. 1041–60.

Wager, L. R. and Brown, G. M. (1968) *Layered Igneous Rocks*, Oliver and Boyd, Edinburgh.

[*Manuscript received 12 July 1988; revised 11 July 1989.*]

Appendix–experimental methods

Sampling of the sequence was carried out along 20 Level Crosscut in the Spud Shaft Section of R.P.M. Union Section Mine, which affords excellent exposures with the layering dipping at 21° south-east. The MG4 chromitite horizon is here exposed at 1030 m below surface. Seventy-two samples of several kg each were taken at an average stratigraphic interval of 5m.

Isotope analysis. Sr and Rb concentrations were determined by isotope dilution mass spectrometry, and the $^{87}Sr/^{86}Sr$ ratio determined on the spiked sample. Approximately 100 mg of the sample powder was dissolved with ^{87}Rb and ^{84}Sr spikes in open Teflon beakers

using an HF–HNO_3 mixture on a hot plate. The sample was then dried and attacked with aqua regia to dissolve any precipitates. Cation exchange was carried out using 2.50M HCl and only the Sr fraction was collected. Sr was then loaded onto single outgassed Ta filaments using H_3PO_4; Rb was loaded onto double Ta filaments as a chloride without prior ion exchange separation. Total method blanks were less than 5 ng for Sr and *c.* 200 pg for Rb. In general, these amounts were not significant, with respect to the sample concentrations, and thus were largely ignored—with the exception of a Rb blank correction on the two plagioclase crystals of 3 mg, each from sample S-40. Both a VG-354 and a VG MM30 mass spectrometer were used to determine the isotopic ratios of Sr, whereas Rb was analysed using only the MM-30. During the period of this study, 19 replicates of the SRM-987 Sr standard were run on both machines. The results show that the machines are indistinguishable for that standard (VG 354—0.71022 ± 6 (2 std. dev.); MM-30—0.71025 ± 52). Replicate analyses of selected samples show that a one sigma precision of 1.5% in the ratio $^{87}Rb/^{86}Sr$ is a realistic estimate; uncertainties in $^{87}Sr/^{86}Sr$ present-day are 0.01% (1 sigma). Initial Sr ratios (Sr_i) are calculated at 2050 ± 25 Ma using the ^{87}Rb decay constant of 1.42×10^{-11} yr^{-1}. The total error quoted for Sr_i is based on analytical errors in $^{87}Rb/^{86}Sr$, $^{87}Sr/^{86}Sr$, and error in age, and was calculated with the isotope regression package, GEODATE, developed at the Council for Scientific and Industrial Research, Pretoria.

X-ray fluorescence spectrometry. Whole-rock analysis for major elements employed the fusion-disc technique of Norish and Hutton (1969). All samples were analysed in duplicate using a Philips PW 1410 XRF spectrometer and, where deemed necessary, analyses repeated in duplicate. Na_2O and trace elements were determined in 5g pressed powder briquettes, with corrections for background, spectral line interference, absorption and instrumental drift. All calibrations were made using a variety of USGS, NIMROC and other international standards. Determinations of Ti were run in quadruplicate for 15 samples of particular significance. All counting on spectral-line peaks for trace elements was fixed at 200secs, and 100secs for backgrounds. High precision for Sr and Rb was ensured by repeating the counting on peak for 400secs and 200secs on the background in a second run. The mean difference between samples in the two runs was 1.3ppm Sr for pyroxenites and 2.6 ppm for norites and leuconorites.

Electron microprobe. An automated JEOL CXA–733 electron microprobe was used for all mineral analyses, using well tested international standards and pure synthetic crystals for calibration. Most work was done with a defocussed 10 μm beam.